Entropy Theory in Hydraulic Engineering

An Introduction

Vijay P. Singh, Ph.D., P.E.

ASCE PRESS

Entropy Theory in Hydraulic Engineering

Other Titles of Interest

***Artificial Neural Networks in Water Supply Engineering*, edited by Srinivasa Lingireddy, P.E.; Gail M. Brion** (ASCE Technical Report, 2005). Examines the application of artificial neural network (ANN) technology to water supply engineering problems.

***Curve Number Hydrology: State of the Practice*, edited by Richard H. Hawkins; Timothy J. Ward; Donald E. Woodward; Joseph A. Van Mullem.** (ASCE Technical Report, 2009). Investigates the origin, development, role, application, and current status of the curve number method for estimating the runoff response from rainstorms.

***Risk and Reliability Analysis: A Handbook for Civil and Environmental Engineers*, by Vijay P. Singh, Ph.D., P.E.; Sharad K. Jain, Ph.D.; Aditya Tyagi, Ph.D., P.E.** (ASCE Press, 2007). Presents the key concepts of risk and reliability that apply to a wide array of problems in civil and environmental engineering.

***Sediment Dynamics upon Dam Removal*, edited by Athanasios (Thanos) N. Papanicolaou, Ph.D.; Brian D. Barkdoll, Ph.D., P.E.** (ASCE Manual of Practice No. 122, 2011). Provides guidance, documentation, and field results for the numerical and physical modeling of sediment movement when dams are removed from waterways.

***Treatment System Hydraulics*, by John Bergendahl, Ph.D., P.E.** (ASCE Press, 2008). Addresses the nuts-and-bolts of treatment systems, examining typical variables and describing methods for solving the problems faced by practitioners on a daily basis.

***Verification and Validation of 3D Free-Surface Flow Models*, edited by Sam S. Y. Wang, Ph.D., P.E.; Partick J. Roache, Ph.D.; Richard A. Schmalz Jr., Ph.D.; Yafei Jia, Ph.D.; Peter E. Smith, Ph.D., P.E.** (ASCE Technical Report, 2009). Describes in detail a new rigorous and systematic verification and validation process for computational models for simulating free surface flows.

***Water Resources Systems Analysis through Case Studies: Data and Models for Decision Making*, edited by David W. Watkins, Jr., Ph.D.** (ASCE Technical Report, 2013). Contains 10 case studies suitable for classroom use to demonstrate engineers' use of widely available modeling software in evaluating complex environmental and water resources systems.

Entropy Theory in Hydraulic Engineering

An Introduction

Vijay P. Singh, Ph.D., D.Sc., P.E., P.H., Hon. D. WRE

ASCE PRESS

Library of Congress Cataloging-in-Publication Data

Singh, V. P. (Vijay P.)
Entropy theory in hydraulic engineering: an introduction / Vijay P. Singh, Ph.D., P.E.
pages cm
Includes bibliographical references and index.
ISBN 978-0-7844-1272-5 (print: alk. paper) – ISBN 978-0-7844-7825-7 (ebook)
1. Hydrodynamics. 2. Hydraulics–Mathematics. 3. Entropy. I. Title.
TC171.S57 2014
627′.042–dc23

2013047646

Published by American Society of Civil Engineers
1801 Alexander Bell Drive
Reston, Virginia, 20191-4382
www.asce.org/bookstore | ascelibrary.org

Errata: Errata, if any, can be found at http://dx.doi.org/10.1061/9780784412725.

ISBN 978-0-7844-1272-5 (paper)
ISBN 978-0-7844-7825-7 (PDF)
Manufactured in the United States of America.

Dedicated to my family:

wife Anita,

daughter Arti,

son Vinay,

daughter-in-law Sonali,

and grandson Ronin

This page intentionally left blank

Contents

Part 5: Water Flow and Level Monitoring

Part 6: Water Distribution Systems

Preface

In the late 1940s Claude Shannon laid the foundation for the pioneering development of informational entropy. Then, Kullback and Leibler did their groundbreaking work in 1951 that led to the principle of minimum cross-entropy. Lindley in 1956 made a seminal contribution by introducing the concept of transinfomation. Then followed the landmark contributions of Jaynes in 1957 and 1958 leading to the development of the principle of maximum entropy and theorem of concentration. During the past five decades, entropy theory has been widely applied to a wide spectrum of areas, including biology, chemistry, economics, ecology, electronics and communication engineering, data acquisition and storage and retrieval, fluid mechanics, genetics, geology and geomorphology, geophysics, geography, geotechnical engineering, hydraulics, hydrology, image processing, management sciences, operations research, pattern recognition and identification, photogrammetry, psychology, physics and quantum mechanics, reliability analysis, reservoir engineering, social sciences, statistical mechanics, thermodynamics, topology, transportation engineering, and turbulence modeling. New areas finding applications of entropy have since continued to unfold. Entropy theory is indeed versatile, and its application is widespread.

In the area of hydraulics and hydraulic engineering, a range of applications of entropy have been reported during the past two decades, and new topics applying entropy are emerging each year. There are many books on entropy written in the fields of statistics, communication engineering, economics, biology, and reliability analysis. However, these books have been written with different objectives in mind and for addressing different kinds of problems from what is encountered in hydraulics and hydraulic engineering. Application of concepts and techniques discussed in these books to hydraulic problems is not always straightforward. Therefore, there exists a need for a book that deals with basic concepts of entropy theory from a hydraulic perspective and that deals with applications of these concepts to a range of hydraulic problems. Currently there is no book devoted to covering the application of entropy theory in hydraulics and hydraulic engineering. This book attempts to fill this need.

Much of the material in the book is derived from lecture notes prepared for a course on entropy theory and its application in water engineering taught to graduate students in biological and agricultural engineering, civil and environmental engineering, geoscience, and hydrologic science and water management at Texas A & M University, College Station, Texas. Comments, critiques, and

discussions offered by students have significantly influenced the content and style of presentation in the book.

The subject matter of this book is divided into 17 chapters. The first chapter introduces entropy theory as applied to hydraulic engineering. The remaining chapters are divided into six sections. The first part, encompassing five chapters, deals with the use of entropy for deriving velocity distributions. One-dimensional velocity distributions are discussed in Chapter 2, which presents velocity distributions based on different constraints, or the specification of information. Chapter 3 presents two-dimensional velocity distributions in rectangular as well as arbitrary domains. Chapter 4 presents other well-known velocity distributions. Applications of velocity distributions are illustrated in Chapter 5. Velocity distributions in pipe flow are treated in Chapter 6.

Part 2, which contains three chapters, discusses sediment concentration and discharge. Chapter 7 treats grain size analysis and distribution. Sediment concentration and discharge in rivers and streams constitute the subject matter of Chapter 8. Sediment concentration in debris flow is presented in Chapter 9.

Hydraulic geometry constitutes the subject matter of Part 3, which contains two chapters. Combining entropy theory with the theory of minimum energy dissipation rate, Chapter 10 presents downstream hydraulic geometry. Chapter 11 presents at-a-station hydraulic geometry.

Part 4 deals with stable channel design. Derivation of longitudinal channel profiles is given in Chapter 12. There is a vast network of channels in alluvial plains around the world. Design of alluvial channels takes on an added significance and is discussed in Chapter 13.

Water flow and level monitoring constitute the subject matter of Part 5. Chapter 14 presents water level monitoring and evaluation. Rating curves are dealt with in Chapter 15.

Water distribution systems are presented in Part 6. Reliability of water distribution systems is analyzed in Chapter 16. The concluding chapter, Chapter 17, deals with the evaluation of water quality and wastewater treatment systems.

Acknowledgments

The subject matter discussed in the book draws from works of hundreds of investigators who have developed and applied entropy-related concepts in hydraulics and hydraulic engineering. Without their contributions, this book would not have been possible. I have tried to make my acknowledgments as specific as possible, and any omission on my part has been entirely inadvertent and I offer my apologies in advance. Over the years I have worked with a number of colleagues and students on entropy-based modeling in hydrology, hydraulics, and water resources engineering, and I have learned much from them. Several of my colleagues helped in different ways, including supplying

data and example problems. They are too many to mention by name. Nevertheless, I would particularly like to acknowledge Gustavo Marini from the University of Sannio, Benevento, Italy, for help with the 2-D velocity distributions discussed in Chapters 3 and 4; Tommaso Moramarco from the Institute of Hydrogeological Protection Research, National Research Council, Perugia, Italy, for help with applications in Chapter 5; Emoke Imre from Szent Istvan University, Budapest, Hungary, for help with Chapter 7 on grain size distributions; S. Y. Cao from Sichuan University, Chengdu, China, for help with Chapter 13 on channel design; and J. L. Alfonso Segura from UNESCO-IHE Institute for Water Education, Delft, Netherlands, for help with Chapter 14 on water level monitoring. Many of my graduate students, especially Huijuan Cui, Li Chao, and C. P. Khedun, helped with example problems and constructing figures and tables. I am grateful to each of them.

My brothers and sisters in India have been a continuous source of inspiration. My wife Anita, son Vinay, daughter-in-law Sonali, daughter Arti, and grandson Ronin have been most supportive and allowed me to work during nights, weekends, and holidays, often away from them. They provided encouragement, showed patience, and helped in myriad ways. Most importantly, they were always there whenever I needed them, and I am deeply grateful. Without their support and affection, this book would not have come to fruition.

Vijay P. Singh
College Station, Texas

This page intentionally left blank

Chapter 1

Entropy Theory

In 1948, Claude Shannon formulated the concept of entropy as a measure of information or uncertainty. Almost a decade later, Jaynes (1957a, 1957b, 1958, 1982, 2003) developed the principle of maximum entropy (POME) for deriving the least biased probability distributions subject to given information in terms of constraints, as well as the theorem of concentration for hypothesis testing. Kullback and Leibler (1951) introduced the concept of cross-entropy, which specializes in the Shannon entropy theory, and Kullback (1959) introduced the principle of minimum cross-entropy (POMCE), which includes POME as a special case. Lindley (1956, 1961) presented mutual information that is fundamental to multivariate analyses, selection of variables, flow of information, and design of networks. Together these concepts constitute what can now be referred to as the *entropy theory*. Entropy has since been extensively applied in environmental and water engineering, including geomorphology, hydrology, and hydraulics. Harmancioglu et al. (1992) and Singh and Fiorentino (1992) surveyed applications of entropy in water resources. Singh (1997, 2011) discussed the use of entropy in hydrology and water resources. New applications of entropy continue to unfold. This chapter introduces the concept of entropy and entropy theory and provides a snapshot of applications of the theory in hydraulic engineering.

1.1 Overview of This Volume

The concept of entropy and entropy theory is introduced in this chapter, and the subject matter of this book is organized into six main topics: flow velocity, sediment concentration and discharge, hydraulic geometry, channel design, water flow and monitoring, and water distribution systems. These topics illustrate the power and usefulness of the entropy concept and entropy theory. Chapters on velocity distributions, channel cross-section, longitudinal slope and profile, sediment concentration and sediment discharge, channel design, and flow rating curves use entropy theory. Chapters on hydraulic geometry use only the principle of maximum entropy, and the chapter on reliability analysis of water distribution systems uses only the entropy concept. Likewise, the chapter on water level monitoring networks uses different types of entropies. The chapter on water quality and wastewater treatment systems uses diversity index, Shannon entropy, and thermodynamic entropy.

1.2 Entropy Concept

Entropy is regarded as a measure of uncertainty or surprise (or sometimes even disorder or chaos), since these are different shades of information. Consider, for example, a discrete random variable X that takes on values $x_1, x_2, \ldots, x_N$ with probabilities $p_1, p_2, \ldots, p_N$, respectively; i.e., each value of X, x_i, represents an event with a corresponding probability of occurrence, p_i, where $i = 1, 2, \ldots, N$. The occurrence of an event x_i provides a measure of information about the likelihood of that probability p_i being correct (Batty 2010). If p_i is very low, say 0.01, and if x_i actually occurs, then there is a great deal of surprise as to the occurrence of x_i with $p_i = 0.01$ because our anticipation of it would be highly uncertain. Conversely, if p_i is very high, say, at 0.99, and if x_i does actually occur, then there is hardly any surprise about the occurrence of x_i where $p_i = 0.99$ because our anticipation of it is quite certain.

Uncertainty about the occurrence of an event suggests that the random variable may take on different values. Information is gained by observing it only if there is uncertainty about the event. If an event occurs with a high probability, it conveys less information, and vice versa. Conversely, more information is needed to characterize less probable or more uncertain events or to reduce uncertainty about the occurrence of such an event. In a similar vein, if an event is more certain to occur, its occurrence or observation conveys less information, and less information is needed to characterize it. This phenomenon suggests that the more uncertain the event, the more information it transmits or the more information is needed to characterize it. This means that there is a connection among entropy, information, uncertainty, and surprise.

Example 1.1 Suppose that an event occurs with probability 1. Is there any uncertainty about this event? What is the degree of surprise about the event? If there is another event whose probability of occurrence is close to 0 but it does actually occur, then what can be said about the uncertainty and degree of surprise about this event?

Solution If an event occurs with probability 1, then it is a certain event, and there is no uncertainty associated with it. It does not correspond to a random value or it is not a manifestation of a random process. The degree of surprise in this case is zero. Conversely, the event whose probability of occurrence is close to 0 but it does occur, then the degree of surprise is enormously high because this is a highly uncertain event, i.e., its uncertainty is enormously high, and its occurrence provides enormously high information. If the probability of the event is indeed 0, then that means that it cannot occur and it does not correspond to a random value or is not an outcome of a random process.

Consider as an example a random variable representing dam breaching. The dam breaching can take on many values. Consider an average return period of a breach as T years. If, say, $T = 100$ years, then the breach has a probability of occurrence as $1/T = 0.01$. If this breach occurred, its occurrence would be a surprise because it was not anticipated and was a highly uncertain event. To model such an event, a lot of observations or information are needed to reduce anticipatory uncertainty. This kind of event contains a lot more uncertainty, and a lot more information is needed to reduce uncertainty. This phenomenon suggests that the anticipatory uncertainty of x_i before the observation is a decreasing function of increasing probability $p(x_i)$ of its occurrence. Thus, it seems that information varies inversely with probability p, i.e., $1/p$.

Now the question arises: What can be said about the information when two independent events x and y occur with probability p_x and p_y? The probability of the joint occurrence of x and y is $p_x p_y$. It would seem logical that the information to be gained from their joint occurrence would be the inverse of the probability of their occurrence, i.e., $1/(p_x p_y)$. This information, however, does not equal the sum of information gained from the occurrence of event x, $1/p_x$, and the information gained from the occurrence of event y, $1/p_y$, i.e.,

$$\frac{1}{p_x p_y} \neq \frac{1}{p_x} + \frac{1}{p_y} \tag{1.1a}$$

Let there be a function $g(.)$. Then the left side of equation (1.1a) can be written as $g(1/(p_x p_y))$, and likewise the right side can be written as $g((1/p_x) + (1/p_y))$. Thus, this inequality of equation (1.a) can be expressed as

$$g\left(\frac{1}{p_x p_y}\right) = g\left(\frac{1}{p_x} + \frac{1}{p_y}\right) \tag{1.1b}$$

It is possible to choose the function g such that equation (1.1b) can be mathematically expressed as

$$g\left(\frac{1}{p_x p_y}\right) = g\left(\frac{1}{p_x}\right) + g\left(\frac{1}{p_y}\right) \tag{1.1c}$$

The only solution that seems to satisfy equation (1.1c) is the logarithmic function. Therefore, equation (1.1c) can be expressed as

$$\log\left(\frac{1}{p_x p_y}\right) = \log\left(\frac{1}{p_x}\right) + \log\left(\frac{1}{p_y}\right) \tag{1.2}$$

Thus, one can summarize that the information gained from the occurrence of any event with probability p is $\log(1/p) = -\log p$. Tribus (1969) regarded $-\log p$ as a measure of uncertainty of the event occurring with probability p or a measure of surprise of the event occurring. This concept can be extended to a series of N events occurring with probabilities $p_1, p_2, \ldots, p_N$, which then leads to the Shannon entropy, which is described in this chapter.

1.3 Entropy Theory

Entropy theory is comprised of four parts: (1) Shannon entropy, (2) the principle of maximum entropy (POME), (3) concentration theorem, and (4) the principle of minimum cross-entropy (POMCE). Each of these parts is now briefly discussed.

1.3.1 Shannon Entropy

Consider a discrete random variable X that takes on values $x_1, x_2, \ldots, x_N$ with probabilities $p_1, p_2, \ldots, p_N$, respectively, i.e., each value corresponds to an event. Then, equation (1.2) can be extended as

$$\log\left(\frac{1}{p_1 p_2 \ldots p_N}\right) = \log\left(\frac{1}{p_1}\right) + \log\left(\frac{1}{p_2}\right) + \cdots + \log\left(\frac{1}{p_N}\right) = -\sum_{i=1}^{N} \log p_i \tag{1.3}$$

Equation (1.3) expresses the information gained by the joint occurrence of N events. One can write the average information as the expected value (or weighted average) of this series as

$$H = -\sum_{i=1}^{N} p_i \log p_i \tag{1.4}$$

where H is termed as entropy, defined by Shannon (1948).

The concept of entropy is central to statistical physics and can actually be traced to Rudolf Clausius in the early nineteenth century. Later, Boltzmann and then Gibbs provided statistical interpretations of H as a measure of thermodynamic entropy. Some investigators, therefore, designate H as Shannon–Boltzmann–Gibbs entropy (see Papalexiou and Koutsoyiannis 2012). In this text, we will call it Shannon entropy. Shannon (1948) generalized equation (1.4), defining entropy, H, as

$$H(X) = H(P) = -K\sum_{i=1}^{N} p(x_i)\log[p(x_i)] \tag{1.5}$$

where $H(X)$ is the entropy of X:$\{x_1, x_2, \ldots, x_N\}$, P:$\{p_1, p_2, \ldots, p_N\}$is the probability distribution of X, N is the sample size, and K is a parameter whose value depends on the base of the logarithm used. If different units of entropy are used, then the base of the logarithm changes. For example, one uses bits for base 2, Napier for base e, and decibels for base 10.

In general, K can be taken as unity, and equation (1.5), therefore, becomes

$$H(X) = H(P) = -\sum_{i=1}^{N} p(x_i)\log[p(x_i)] \tag{1.6}$$

$H(X)$, given by equation (1.6), represents the information content of random variable X or its probability distribution $P(x)$. It is a measure of the amount of uncertainty or indirectly the average amount of information content of a single value of X. Equation (1.6) satisfies a number of desiderata, such as continuity, symmetry, additivity, expansibility, and recursivity. Shannon and Weaver (1949), Kapur (1989), and Singh (2013) have given a full account of these properties and are, therefore, not repeated here.

If X is a deterministic variable, then the probability that it will take on a certain value is 1, and the probabilities of all other alternative values are zero. Then, equation (1.6) shows that $H(X) = 0$, which can be viewed as the lower limit of the values that the entropy function may assume. This notion corresponds to the absolute certainty, i.e., that there is no uncertainty and that the system is completely ordered. Conversely, when all instances of x_i are equally likely, i.e., the variable is uniformly distributed ($p_i = 1/N$, $i = 1, 2, \ldots, N$), then equation (1.6) yields

$$H(X) = H_{\max}(X) = \log N \tag{1.7}$$

This result shows that the entropy function attains a maximum, and equation (1.7) thus defines the upper limit. This result also reveals that the outcome has the maximum uncertainty. Equation (1.4) and in turn equation (1.7) show that the larger the number of events, the larger the entropy measure. This notion is intuitively appealing because more information is gained from the occurrence of more events, unless, of course, events have zero probability of occurrence. The maximum entropy occurs when the uncertainty is maximum or the disorder is maximum.

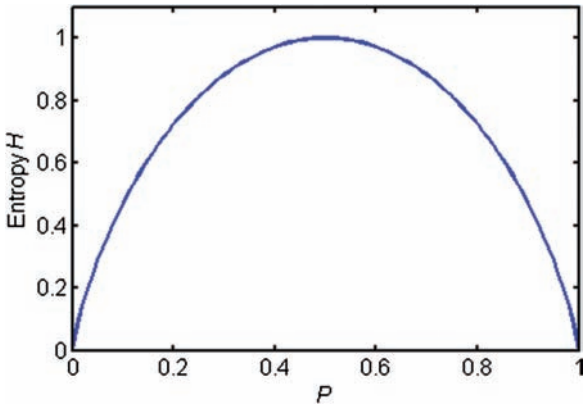

Figure 1-1 *Entropy as a function of probability.*

One can now state that entropy of any variable always assumes positive values within limits defined as

$$0 \le H(x) \le \log N \tag{1.8a}$$

It is logical to say that many probability distributions lie between these two extremes and their entropies between these two limits. For the special case of $N = 2$, the entropy measured in bits is

$$0 \le H(p) \le 1 \tag{1.8b}$$

As an example, consider a random variable X, which takes on a value of 1 with a probability p and 0 with a probability $q = 1 - p$. Taking different values of p, one can plot $H(p)$ as a function of p, as shown in Fig. 1-1. It is seen that for $p = ½$, $H(p) = 1$ bit is the maximum.

Example 1.2 Consider a random variable X taking on three values with probabilities p_1, p_2, and p_3. Using different combinations of these probabilities, as shown in Table 1-1, compute entropy and determine the combination for which the entropy is maximum. Tabulate the entropy values for different combinations of probabilities and plot entropy as a function of p_1, p_2, and p_3.

Solution For three events, the Shannon entropy can be written as

$$H(X) = H(P) = -\sum_{i=1}^{3} p(x_i)\log[p(x_i)]$$

For different combinations of the values of p_1, p_2, and p_3, the Shannon entropy is computed as shown in Table 1-1, and then it is plotted as shown in Fig. 1-2.

Table 1-1 *Values of probabilities p_1, p_2, and p_3 of values x_1, x_2, and x_3 that a random variable takes on, and corresponding entropy values.*

p_1	p_2	p_3	$H(X)$ [Decibels]
0.05	0.05	0.9	0.171
0.1	0.1	0.8	0.278
0.1	0.2	0.7	0.348
0.1	0.3	0.6	0.390
0.2	0.2	0.6	0.413
0.2	0.3	0.5	0.447
0.3	0.3	0.4	0.473
0.333	0.333	0.333	0.477
0.4	0.3	0.3	0.473
0.5	0.3	0.2	0.447
0.6	0.2	0.2	0.413
0.7	0.2	0.1	0.348
0.8	0.1	0.1	0.278
0.9	0.05	0.05	0.171

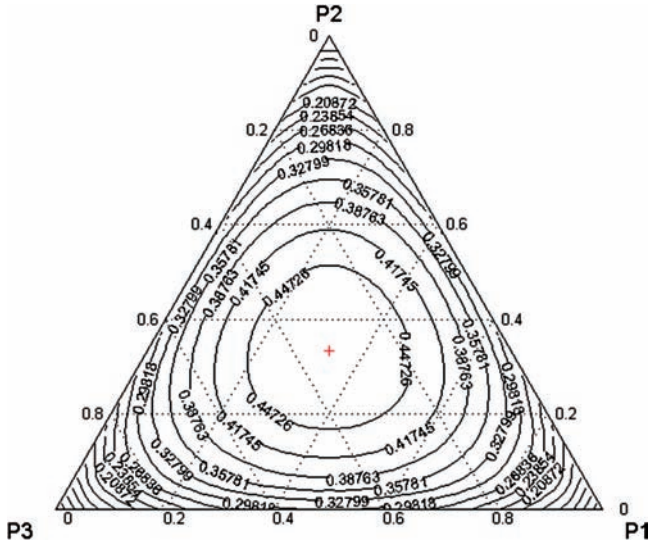

Figure 1-2 *Entropy of a distribution* P: {p_1, p_2, p_3} *as a function of probabilities. Note:* $p_1 + p_2 + p_3 = 1$.

The next question is, What happens to entropy if the random variable is continuous? Let X be a continuous random variable within a certain range and a probability density function $f(x)$. Then, the range within which the continuous variable assumes values can be divided into N intervals of width Δx. One can then express the probability that a value of X is within the nth interval as

$$p_n = P\left(x_n - \frac{\Delta x}{2} \le X \le x_n + \frac{\Delta x}{2}\right) = \int_{x_n-(\Delta x/2)}^{x_n+(\Delta x/2)} f(x)\,dx \tag{1.9}$$

For relatively small values of Δx, probability p_n can be approximated as

$$p_n \cong f(x_n)\Delta x \tag{1.10}$$

The marginal entropy of X expressed by equation (1.6) for a given class interval Δx can be written as

$$H(X;\Delta x) \cong -\sum_{n=1}^{N} p_n \log p_n = -\sum_{n=1}^{N} f(x_n)\log[f(x_n)\Delta x]\Delta x \tag{1.11}$$

This approximation would have an error whose sign would depend on the form of the function $-f(x)\log f(x)$. To reduce this approximation error, the Δx interval is chosen to be as small as possible. Let $p_i = p(x_i)\Delta x$. Let the interval size Δx tend to zero. Then, equation (1.11) can be expressed as

$$H(X;\Delta x) = -\lim_{\Delta x\to 0}\sum_{i=1}^{N} p(x_i)\Delta x \log[p(x_i)\Delta x] \tag{1.12}$$

Equation (1.12) can be written as

$$H(X;\Delta x) = -\lim_{\Delta x\to 0}\sum_{i=1}^{N} p(x_i)\Delta x \log[p(x_i)] - \lim_{\Delta x\to 0}\sum_{i=1}^{N} p(x_i)\ln(\Delta x)\Delta x \tag{1.13a}$$

Equation (1.13a) can also be extended to the case where Δx_i varies with i, and it shows that the discrete entropy of equation (1.13a) increases without bound. Equation (1.13a) is also written as

$$H(X;\Delta x) = -\sum_{i=1}^{N} p(x_i)\Delta x \log[p(x_i)] - \sum_{i=1}^{N} p(x_i)\ln(\Delta x)\Delta x \tag{1.13b}$$

For small values of Δx, equation (1.13a) converges to

$$H(X;\Delta x) = -\int_0^{\infty} f(x)\ln f(x)dx - \lim_{\Delta x\to 0}\sum_{i=1}^{N} p(x_i)\ln(\Delta x)\Delta x \tag{1.14}$$

Equation (1.14) yields

$$H(X;\Delta x) = -\int_0^{\infty} f(x)\ln f(x)\,dx - \lim_{\Delta x\to 0}\ln\Delta x \tag{1.15}$$

Equation (1.15) is also written as

$$H(X;\Delta x) = -\int_0^\infty f(x)\log f(x)\,dx - \log \Delta x \tag{1.16}$$

When we move $-\log\Delta x$ on the right side, equation (1.16) can, upon discretization, be written as

$$H(X;\Delta x) + \log \Delta x \cong -\sum_{n=1}^{N} p_n \log\left(\frac{p_n}{\Delta x}\right) = -\sum_{n=1}^{N} f(x_n)\log f(x_n)\Delta x \tag{1.17}$$

The right side of equation (1.17) can be written as

$$H(X) = -\int_0^\infty f(x)\log f(x)\,dx = -\int_0^\infty \log[f(x)]\,dF(x) = E[-\log f(x)] \tag{1.18}$$

Equation (1.17) is also referred to as spatial entropy if X is a space dimension and equation (1.18) is the commonly used expression for continuous Shannon entropy. Here $F(x)$ is the cumulative probability distribution function of X, $E[.]$ is the expectation of [.], and $H(X)$ is a measure of the uncertainty of random variable X of the system. It can also be understood as a measure of the amount of information required, on average, to describe the random variable. Thus, entropy is a measure of the amount of uncertainty represented by the probability distribution or of the lack of information about a system represented by the probability distribution. Sometimes it is referred to as a measure of the amount of chaos characterized by the random variable. If complete information is available, entropy = 0, that is, there is no uncertainty; otherwise, it is greater than zero. Thus, the uncertainty can be quantified using entropy taking into account all different kinds of available information.

Example 1.3 Consider a random variable $X \in (0, \infty)$, which is described by a gamma distribution whose probability density function (PDF) can be expressed as $f(x) = (x/\theta)^{k-1}\exp(-x/\theta)\{1/[\theta\Gamma(k)]\}$, where k and θ are parameters, and $\Gamma(k) = (k-1)!$. For illustrative purposes, take $k = 5$, $\theta = 1$, $X = (0, 10)$. The entropy theory shows that the gamma distribution can be derived by specifying the constraints $E[x]$ and $E[\log x]$, where E denotes the expectation, which are obtained from the data. It also shows that $k\theta = \overline{x}$ and $\Psi(k) - \ln(k) = \overline{\ln x}$, where $\Psi(k)$ is the digamma function, which is defined as the logarithmic derivative of the gamma function, as

$$\Psi(k) = \frac{d}{dk}\log\Gamma(k) = \frac{\Gamma'(k)}{\Gamma(k)}$$

and can be approximated as

$$\Psi(k) = \log(k) - \frac{1}{2k} - \frac{1}{12k^2} + \frac{1}{120k^4} - \frac{1}{252k^6} + O\left(\frac{1}{k^8}\right)$$

Table 1-2 *Values of entropy for different interval sizes.*

Δx	N	$H(x)$ [Napier]
1	10	2.046
0.1	100	4.313
0.01	1,000	6.571
0.005	2,000	7.251
0.001	10,000	8.830

Select an interval size for discrete approximation and compute entropy using the discrete approximation as well as the continuous form. Then, use different interval sizes and repeat the calculations; determine the effect of the choice of interval size.

Solution First, consider the continuous form. Then, substituting the gamma PDF $f(x) = (x/\theta)^{k-1}\exp(-x/\theta)\{1/[\theta\Gamma(k)]\}$ in the continuous form of entropy, $H(X) = -\int_{-\infty}^{+\infty} f(x)\log[f(x)]dx$, one obtains $H(X) = k\ln\theta + \ln\Gamma(k) + (1-k)\overline{\ln x} + (\bar{x}/\theta)$.

Substituting $\bar{x} = k\theta$ and $\overline{\ln x} = \Psi(k) - \ln(k)$, the entropy equation becomes the following:

$$H(X) = k + k\ln\theta + \ln\Gamma(k) + (1-k)[\Psi(k) - \ln k]$$
$$= 5 + 0 + \ln(24) - (1-5)(1.506 - 1.609) = 7.766 \text{ Napier}$$

Now consider discrete entropy, with interval Δx. The continuous entropy can be written as

$$H(X) = -\int_0^{\infty} f(x)\log f(x)dx = -\sum_{i=1}^{N} f(x_i)\Delta x \ln\left[f(x_i)\frac{\Delta x}{\Delta x}\right] = -\sum_{i=1}^{N} p_i \ln\left[\frac{p_i}{\Delta x}\right]$$

which can also be written as

$$H(x) = -\sum_{i=1}^{N} p_i \ln p_i + \ln\Delta x$$

Using this equation, entropy is computed for different interval sizes, as given in Table 1-2, which shows that the entropy value significantly depends on the interval size.

1.3.2 Principle of Maximum Entropy

It is common that some information is available on the random variable X. The question arises, What should be the probability density function of X that is consistent with the given information? The chosen probability distribution should then be consistent with the given information. Laplace's principle

of insufficient reason says that all outcomes of an experiment on the random variable are equally likely unless there is information to the contrary. The principle of maximum entropy (POME) states that the probability distribution should be selected in such a way that it maximizes entropy subject to the given information, i.e., POME takes into account all of the given information and at the same time avoids consideration of any information that is not given. This principle is consistent with Laplace's principle. In other words, for given information, the best possible distribution that fits the data would be the one with the maximum entropy, because it contains the most reliable assignment of probabilities. Because the POME-based distribution is favored over those with less entropy among those that satisfy the given constraints, according to the Shannon entropy as an information measure, entropy defines a kind of measure of the space of probability distributions. Intuitively, distributions of higher entropy represent more disorder, are smoother, are more probable, are less predictable, or assume less. The POME-based distribution is maximally noncommittal with regard to the missing information and is least biased. Maximizing the entropy given by equation (1.4) leads to the Boltzmann–Gibbs distribution (Papalexiou and Koutsoyiannis 2012) for describing the distribution of particles in a physical context.

1.3.3 Concentration Theorem

Entropy theory permits us to derive a probability density function (PDF) of any variable for specified constraints, but more than one PDF may satisfy the given constraints. POME states that the PDF that has the maximum entropy must be chosen. To measure the bias in this choice, the concentration theorem, formulated by Jaynes (1958), can be used. Consider a random variable X:$\{x_1, x_2, \ldots, x_n\}$ that has a probability mass function (PMF) P:$\{p_1, p_2, \ldots, p_n\}$. Each x_i is a possible outcome. As an illustration, consider a die that has six faces, any one of which can show up when it is thrown. In a random experiment involving N trials, there are only $n = 6$ possible outcomes. The probability of any face appearing is determined by the number of times (say m) that that face appears divided by the total number of trials N, that is $p_i = m_i / N$ where i denotes the ith outcome or face. In hydraulic terms, the random variable can be, say, mudslides in a given area in the month of January. It is assumed that mudslides are categorized, based on size and intensity, into four types (say, small, medium, large, and very large). For an area susceptible to mudslides, if we have 50 years of record with 50 mudslides in months of January, then $\boldsymbol{N} = 50$, $n = 4$, and m_i is computed by counting the number of mudslides of a given type, and p_i by dividing m_i by the total number of mudslides. Using entropy theory, one can determine the probability distribution of mudslides, subject to given constraints.

The concentration theorem states that the entropy $H(X)$ of X or the entropy of its PMF is in the range given as

$$H_{\max} - \Delta H \le H(x) \le H_{\max} \tag{1.19}$$

where ΔH is the change in entropy, and $H_{\max}$ is the maximum entropy that can be obtained by using POME as

$$H_{\max} = \log(Z) + \sum_{k=1}^{K} \lambda_k a_k \tag{1.20}$$

where K is the number of constraints; a_k is the kth constraint function specified to obtain $f(x)$; λ_k, $k = 0, 1, 2, \ldots, K$, are the Lagrange multipliers; Z is the potential function, which is a function of the Lagrange multipliers; and $Z = \exp(\lambda_0)$, $\lambda_0 = \lambda_0(\lambda_1, \lambda_2, \ldots, \lambda_K)$. Jaynes (1982) showed that twice the product of the number of trials and the entropy change, $2N\Delta H$, is asymptotically distributed as chi-square (χ^2) with $N - K - 1$ degrees of freedom, independently of the nature of constraints.

For the random experiment where there are n possible outcomes, meaning n probabilities of their occurrence, and N different realizations or trials, one can determine the concentration of these probabilities near the upper bound $H_{\max}$ with the use of the concentration theorem. Denoting the critical value of χ^2 for $N - K - 1$ degrees of freedom at the specified significance level (α) as $\chi_c^2(\alpha)$, $2N\Delta H$ is given in terms of the upper tail area $1 - F$ as

$$2N\Delta H = \chi_c^2(1 - F) \tag{1.21}$$

where F corresponds to the tail area of the PMF. If $F = 0.95$, then $\alpha = 1 - 0.95 = 0.05$. Equation (1.21) yields the percentage chance that the observed probability distribution will have an entropy outside the interval obtained from equation (1.19). Jaynes (1982) showed that for large N, the overwhelming majority of all possible distributions possess entropy values that would be near $H_{\max}$. One can compute $H_{\max}$ for a known PMF and the value of χ^2 for a given significance level (say, 5%) from χ^2 tables. Then, one computes the value of $2N\Delta H$ from equation (1.21), which yields ΔH. Using equation (1.19), one determines the range in which 95% of the values lie, and if they do then this would mean that the vast majority of realizations would follow the PDF known from the use of POME.

1.3.4 The Principle of Minimum Cross-Entropy

On the basis of intuition, experience, or theory, a random variable may be assumed to have an a priori probability distribution. Then, the Shannon entropy is maximum when the probability distribution of the random variable is the one that is as close to the a priori distribution as possible. This principle is referred to as the principle of minimum cross-entropy (POMCE), which minimizes the Bayesian entropy (Kullback and Leibler 1951). This method is equivalent to maximizing the Shannon entropy.

The Laplace principle of insufficient reason states that all outcomes of an experiment should be considered equally likely unless there is information to the contrary. A random variable has a probability distribution, called an a priori probability distribution, which, on the basis of intuition, experience, or theory,

may be determined. If some information on the random variable is available that can be encoded in the form of constraints, then the probability distribution of the random variable can be derived by maximizing the Shannon entropy subject to these constraints. The a priori probability distribution has an entropy, and the derived distribution has an entropy. Then the objective is to make these two entropy values as close as possible. This phenomenon suggests that the derived probability distribution of the random variable should be the one that is as close to the a priori distribution as possible. This principle is referred to as the principle of minimum cross-entropy (POMCE), which minimizes the Bayesian entropy (Kullback and Leibler 1951). This method is equivalent to maximizing the Shannon entropy.

1.4 Types of Entropy

1.4.1 Information

The entropy of a probability distribution can be regarded as a measure of information or a measure of uncertainty. The amount of information obtained when observing the result of an experiment can be considered numerically equal to the amount of uncertainty as regards the outcome of the experiment before conducting it. There are different types of entropy or measures of information: marginal entropy, conditional entropy, joint entropy, transinformation, and interaction information. The marginal entropy is the entropy of a single variable and is defined by equation (1.18) if the variable is continuous or equation (1.6) if the variable is discrete. Other types of entropy are defined when more than one variable is considered.

Entropy $H(X)$ permits us to measure information, and for that reason, it is also referred to as informational entropy. Intuitively, uncertainty can be considered as a measure of surprise, and information reduces uncertainty, or surprise, for that matter. Consider a set of values of a random variable. If nothing is known about the variable, then its entropy can be computed, assuming that all values are equally likely. Let this entropy be denoted as H_I. Then some information becomes available about the random variable. Then its probability distribution is derived using POME and its entropy is computed and it is denoted as H_O. The difference between these two entropy values is equal to the reduction in uncertainty $H(X)$ or information I, which can be expressed as

$$I = H_I - H_O \tag{1.22}$$

If an input–output channel or transmission conduit is considered, then H_I is the entropy (or uncertainty) of input (or message sent through a channel), and H_O is the entropy (or uncertainty) of output (or message received). Were there no noise in the channel, the output (the message received by the receiver or receptor) would be certain as soon as the input (message sent by the emitter)

was known. This situation means that the uncertainty in output H_O would be 0 and I would be equal to H_I.

1.4.2 Relative Entropy and Relative Redundancy

Relative entropy H^*, also called dimensionless entropy, can be defined as the ratio of entropy H to the maximum entropy $H_{\max}$:

$$H_* = \frac{H}{H_{\max}} \tag{1.23}$$

Comparing H with $H_{\max}$, a measure of information can be constructed as

$$I = H_{\max} - H = \log N + \sum_{i=1}^{N} p_i \log p_i \tag{1.24a}$$

Recalling that $H_{\max}$ is obtained when all probabilities are of the same value, i.e., all events occur with the same probability, equation (1.24a) can be written as

$$I = \sum_{i=1}^{N} p_i \log\left[\frac{p_i}{1/N}\right] = \sum_{i=1}^{N} p_i \log\left(\frac{p_i}{q_i}\right) \tag{1.24b}$$

where $q_i = 1/N$. In equation (1.24b), $\{q_i\}$ can be considered as a prior distribution, and $\{p_i\}$ as a posterior distribution. Normalizing I by $H_{\max}$, equation (1.24a) becomes

$$R = \frac{I}{H_{\max}} = 1 - \frac{H}{H_{\max}} \tag{1.25}$$

where R is designated as relative redundancy varying between 0 and 1.

1.4.3 Multivariate Entropy

Now consider two random variables X and Y that are not independent. Then, the marginal entropy, $H(X)$, given by equation (1.6), can be defined as the potential information of variable X; this is also the information of its underlying probability distribution. For two variables, the joint entropy $H(X, Y)$ is the total information content contained in both X and Y, i.e., it is the sum of marginal entropy of one of the variables and the uncertainty that remains in the other variable when a certain amount of information that it can convey is already present in the first variable, as shown in Fig. 1-3. Mathematically, the joint entropy of X and Y can be defined as

$$H(X, Y) = -\sum_{i=1}^{N}\sum_{j=1}^{M} p(x_i, y_j)\log p(x_i, y_j) \tag{1.26a}$$

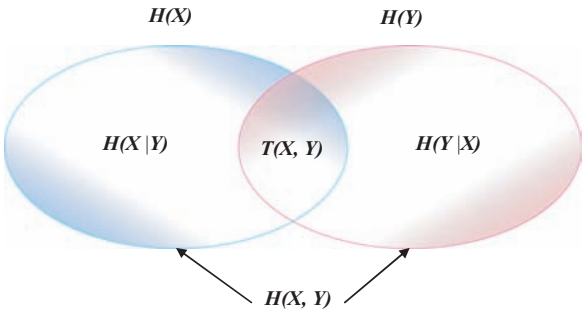

Figure 1-3 H(X)*: Marginal entropy of* X*;* H(Y)*: marginal entropy of* Y*;* T(X, Y)*: information common to* X *and* Y*;* H(X | Y)*: conditional entropy or information only in* X*;* H(Y | X)*: conditional entropy or information only in* Y*; and* H(X, Y)*: total information in* X *and* Y *together.*

where $p(x_i, y_j)$ is the joint probability of $X = x_i$ and $Y = y_j$; N is the number of values that X takes on; and M is the number of values that Y takes on. Equation (1.26a) can be generalized to any number of variables as

$$H(X_1, X_2, \ldots, X_n) = -\sum_{i=1}^{n_1}\sum_{j=1}^{n_2}\ldots\sum_{n=1}^{n_n} p(_{1i}, p_{2j}, \ldots, p_{nn}) \log p(p_{1i}, p_{2j}, \ldots, p_{nn}) \tag{1.26b}$$

1.4.4 Conditional Entropy

Now consider the conditional entropy for two variables denoted as $H(X|Y)$, as shown in Fig. 1-3. This is a measure of the information content of X that is not contained in Y, or entropy of X given the knowledge of Y or the amount of information that still remains in X even if Y is known. Similarly, one can define $H(X|Y)$. The conditional entropy $H(X|Y)$ can be expressed mathematically as

$$H(X|Y) = -\sum_{i=1}^{N}\sum_{j=1}^{M} p(x_i, y_j) \log p(x_i|y_j) \tag{1.27}$$

where $p(x_i|y_j)$ is the conditional probability of $X = x_i$ conditional on $Y = y_j$. Equation (1.27) can be easily generalized to any number of variables. Consider n variables denoted as (X_1, X_2, …, X_n). Then the conditional entropy can be written as

$$H[(X_1, X_2, \ldots, X_{n-1})|X_n] = -\sum_{1_i}^{N_1}\ldots\sum_{n_{i-1}}^{N_{n-1}} p(x_{1i}, x_{2i}, \ldots, x_{(n-1)_i}) \log[p(x_{1_i}, x_{2_i.}, \ldots, x_{(n-1)_i}|x_n)] \tag{1.28}$$

or

$$H[(X_1, X_2, \ldots, X_{n-1})|X_n] = H(X_1, X_2, \ldots, X_{n-1}, X_n) - H(X_n) \tag{1.29}$$

where N_i is the number of values X_i takes on.

It may be noted that conditional entropy $H(X|Y)$ can also be used as an indicator of the amount of information loss during transmission, meaning the part of X that never reaches Y. Conversely, $H(X|Y)$ represents the amount of information received as noise, that is, this part was never sent by X but was received by Y. Clearly, both of these quantities must be positive.

1.4.5 Transinformation

The mutual entropy (information) between X and Y, also called *transinformation*, $T(X, Y)$, can be defined as the information content of X that is contained in Y. In other words, it is the difference between the total entropy of X and Y and the sum of entropy of X and entropy of Y. This is the information repeated in both X and Y, and it defines the amount of uncertainty that can be reduced in one of the variables when the other variable is known. It is also interpreted as the reduction in the original uncertainty of X, due to the knowledge of Y.

The information transmitted from variable X to variable Y is represented by the mutual information $T(X, Y)$ and is given (Lathi 1969) as

$$T(X, Y) = H(X) - H(X|Y) \tag{1.30}$$

Equation (1.30) can be generalized as

$$T[(X_1, X_2, \ldots, X_{n-1}); X_n] = H(X_1, X_2, \ldots, X_{n-1}) - H[(X_1, X_2, \ldots, X_{n-1})|X_n] \tag{1.31}$$

For computing, equation (1.30) can be expressed as

$$T(X, Y) = \sum_i \sum_j p(x_i, y_j) \log \frac{p(x_i|y_j)}{p(x_i)} \tag{1.32a}$$

or as the expected value

$$T(X, Y) = E\left[\log \frac{p(x_i, y_j)}{p(x_i)p(y_j)}\right] = \sum_i \sum_j p(x_i, y_j) \log \frac{p(x_i, y_j)}{p(x_i)p(y_j)} \tag{1.32b}$$

$T(X, Y)$ is symmetric, i.e., $T(X, Y) = T(Y, X)$, and is nonnegative. A zero value occurs when two variables are statistically independent so that no information is mutually transferred, that is,$T(X, Y) = 0$ if X and Y are independent. When two variables are functionally dependent, the information in one variable can be fully transmitted to another variable with no loss of information at all. Subsequently, $T(X, Y) = T(X) = T(Y)$. For any other case, $0 \le T(X, Y) \le H(X) = H(Y)$. Larger values of T correspond to greater amounts of information transferred. Thus, T is an indicator of the capability of the information transmission and the degree of dependency of two variables. Transinformation or mutual information measures information transferred among information emitters (predictor variables) and the information receivers (predicted variables). This fact means that the information contained in different variables can be inferred, to some extent, from the

information in other variables. Mutual information is used for measuring the inferred information or, equivalently, for information transmission. Entropy and mutual information have advantages over other measures of information, for they provide a quantitative measure of (a) the information in a variable, (b) the information transferred and information lost during transmission, and (c) a description of the relationship among variables based on their information transmission characteristics.

Example 1.4 Consider data on monthly mean stream flow at three stations (say *A*, *B*, and *C*) for a river in Texas. The data are given in Table 1-3. Compute marginal entropies of stations *A*, *B*, and *C*. Then, compute conditional entropies, $H(A \mid B)$, $(B \mid C)$, and $(A \mid C)$. Then, compute joint entropies $H(A, B)$, $H(B, C)$, and $H(A, C)$. Also, compute transinformation $T(A, B)$, $T(B, C)$, and $T(A, C)$.

Solution Different entropies are computed as follows.

(1) Computation of marginal entropy

To illustrate the steps for computaion, take station *A* as an example. By dividing the range of stream flow into five equal-sized intervals, the contigency table can be constructued as shown in Table 1-4.

Then the marginal entropy for station *A* can be computed as

$$\begin{aligned} H(A) &= -\sum_{i=1}^{N} p(x_i)\log_2[p(x_i)] \\ &= -0.383 \times \log_2 0.383 - 0.433 \times \log_2 0.433 - \ldots - 0.033 \times \log_2 0.033 \\ &= 1.7418 \text{ bits} \end{aligned}$$

Similarly, for station *B* the contigency table can be constructed as shown in Table 1-5.

The marginal entropy for station *B* can be obtained as

$$\begin{aligned} H(B) &= -\sum_{i=1}^{N} p(x_i)\log_2[p(x_i)] \\ &= -0.467 \times \log_2 0.467 - 0.300 \times \log_2 0.300 - \ldots - 0.050 \times \log_2 0.050 \\ &= 1.8812 \text{ bits} \end{aligned}$$

The contigency table for station *C* is shown in Table 1-6. From the contingency table, the marginal entropy for station *C* is obtained as

$$\begin{aligned} H(C) &= -\sum_{i=1}^{N} p(x_i)\log_2[p(x_i)] \\ &= -0.750 \times \log_2 0.750 - 0.150 \times \log_2 0.150 - \ldots - 0.017 \times \log_2 0.017 \\ &= 1.1190 \text{ bits} \end{aligned}$$

Table 1-3 *Streamflow observations.*

Year	Month	*A*	*B*	*C*	Year	Month	*A*	*B*	*C*
2000	1	61.21	2.54	6.86	2002	7	90.68	73.15	416.56
2000	2	40.64	8.13	45.97	2002	8	25.65	16.00	17.27
2000	3	122.68	22.10	15.75	2002	9	29.72	32.78	144.78
2000	4	97.54	18.80	26.16	2002	10	140.72	124.71	198.12
2000	5	179.83	23.88	80.52	2002	11	99.82	13.21	23.88
2000	6	110.49	120.65	109.22	2002	12	125.22	26.16	37.34
2000	7	12.45	12.45	7.87	2003	1	18.54	4.06	19.05
2000	8	4.06	0.51	7.11	2003	2	189.23	42.16	45.21
2000	9	62.23	16.51	48.00	2003	3	51.56	35.31	41.15
2000	10	59.69	109.47	185.67	2003	4	30.48	11.68	4.06
2000	11	347.98	84.07	140.46	2003	5	56.64	38.86	23.62
2000	12	137.16	14.73	34.54	2003	6	123.95	148.34	112.27
2001	1	120.14	30.48	64.77	2003	7	111.25	16.00	182.12
2001	2	104.90	36.83	30.73	2003	8	39.37	59.18	46.23
2001	3	175.01	33.27	59.44	2003	9	90.17	68.83	119.38
2001	4	14.48	14.73	39.62	2003	10	93.47	91.69	66.29
2001	5	89.15	60.20	72.39	2003	11	116.33	20.57	23.11
2001	6	336.55	5.84	22.61	2003	12	58.93	0	1.52
2001	7	41.66	12.45	25.15	2004	1	110.24	35.81	57.91
2001	8	117.35	70.10	92.71	2004	2	156.97	48.51	44.70
2001	9	168.66	52.32	67.31	2004	3	75.95	48.26	95.25
2001	10	103.89	21.84	43.43	2004	4	131.06	61.21	176.53
2001	11	72.39	77.98	126.49	2004	5	105.16	22.86	31.24
2001	12	144.53	4.83	34.80	2004	6	212.34	105.41	232.16
2002	1	49.78	10.67	6.60	2004	7	54.10	62.23	32.26
2002	2	57.91	30.23	6.10	2004	8	105.66	119.38	59.44
2002	3	82.55	41.91	27.69	2004	9	50.04	37.08	76.20
2002	4	59.44	9.40	60.45	2004	10	179.07	150.37	77.72
2002	5	101.85	32.00	50.55	2004	11	249.68	159.00	142.24
2002	6	104.65	41.15	50.29	2004	12	66.80	10.41	5.84

Table 1-4 *Contingency table for station* A *in Example 1.4.*

	Station *A*				
Interval	4.06 ~ 72.84	72.84 ~ 141.62	141.62 ~ 210.40	210.40 ~ 279.18	279.18 ~ 347.96
Counts	23	26	7	2	2
Probability	0.383	0.433	0.117	0.033	0.033

Table 1-5 *Contingency table for station* B *in Example 1.4.*

	Station *B*				
Interval	0 ~ 31.80	31.80 ~ 63.60	63.60 ~ 95.40	95.40 ~ 127.20	127.20 ~ 159.00
Counts	28	18	6	5	3
Probability	0.467	0.300	0.100	0.083	0.050

Table 1-6 *Contingency table for station* C *in Example 1.4.*

	Station *C*				
Interval	1.52 ~ 84.53	84.53 ~ 167.54	167.54 ~ 250.55	250.55 ~ 333.56	333.56 ~ 416.57
Counts	45	9	5	0	1
Probability	0.750	0.150	0.083	0.000	0.017

(2) Computation of conditional entropy

For illustraton, $H(A \mid B)$ is taken as an example. First, the joint contigency table is constructed as shown in Table 1-7.

From the definition of conditional entropy

$$H(A|B) = -\sum_{i=1}^{N}\sum_{j=1}^{M} p(A_i, B_j)\log_2 \frac{p(A_i, B_j)}{p(B_j)}$$

It can be seen that the marginal distribution of streamflow at station B is required. The marginal probability distribution of streamflow at station B can be obtained by marginalizing out the marginal probability distribution of streamflow at station A from the bivariate contingency table. The results are shown in Table 1-8.

The last row corresponds to the marginal probability distribution of streamflow at station B. Take the first entry in the shaded row as an example. It is obtained by summing up all elements of the first column in the bivariate contingency table, i.e.,

$$0.467 = 0.250 + 0.167 + 0.033 + 0.000 + 0.017$$

Table 1-7 *Joint contingency table for stations* A *and* B *in Example 1.4.*

Contingency Table of Counts						
		Station *B*				
		0 ~ 31.80	31.80 ~ 63.60	63.60 ~ 95.40	95.40 ~ 127.20	127.20 ~ 159.00
Station *A*	4.06 ~ 72.84	15	6	1	1	0
	72.84 ~ 141.62	10	8	4	3	1
	141.62 ~ 210.40	2	4	0	0	1
	210.40 ~ 279.18	0	0	0	1	1
	279.18 ~ 347.96	1	0	1	0	0
Contingency Table of Probability						
		Station *B*				
		0 ~ 31.80	31.80 ~ 63.60	63.60 ~ 95.40	95.40 ~ 127.20	127.20 ~ 159.00
Station *A*	4.06 ~ 72.84	0.520	0.100	0.017	0.017	0.000
	72.84 ~ 141.62	0.167	0.133	0.067	0.050	0.017
	141.62 ~ 210.40	0.033	0.067	0.000	0.000	0.017
	210.40 ~ 279.18	0.000	0.000	0.000	0.017	0.017
	279.18 ~ 347.96	0.017	0.000	0.017	0.000	0.000

Using the definition of conditional entropy, $H(A \mid B)$ can be computed as

$$
\begin{aligned}
H(A|B) &= -\sum_{i=1}^{N}\sum_{j=1}^{M} p(A_i, B_j)\log_2 \frac{p(A_i, B_j)}{p(B_j)} \\
&= -0.250 \times \log_2 \frac{0.250}{0.467} - 0.167 \times \log_2 \frac{0.167}{0.467} - \ldots - 0.017 \times \log_2 \frac{0.017}{0.467} \\
&\quad \cdots \\
&\quad - 0.000 \times \log_2 \frac{0.000}{0.050} - 0.017 \times \log_2 \frac{0.017}{0.050} - \ldots - 0.000 \times \log_2 \frac{0.000}{0.050} \\
&= 1.4575 \text{ bits}
\end{aligned}
$$

Similarly, the joint contingency table for stations *B* and *C* is constructed as shown in Table 1-9.

The marginal probability distribution of streamflow at station *C* can be obtained by marginalizing out the probability distribution of streamflow at station *B*. The results are presented in the last row of Table 1-10.

Table 1-8 *Joint probability of stations* A *and* B *and marginal probability of station* B *in Example 1.4.*

		Station *B*				
		0 ~ 31.80	31.80 ~ 63.60	63.60 ~ 95.40	95.40 ~ 127.20	127.20 ~ 159.00
Station *A*	4.06 ~ 72.84	0.250	0.100	0.017	0.017	0.000
	72.84 ~ 141.62	0.167	0.133	0.067	0.050	0.017
	141.62 ~ 210.40	0.033	0.067	0.000	0.000	0.017
	210.40 ~ 279.18	0.000	0.000	0.000	0.017	0.017
	279.18 ~ 347.96	0.017	0.000	0.017	0.000	0.000
		0.467	0.300	0.100	0.083	0.050

Table 1-9 *Joint contingency table for stations* B *and* C *in Example 1.4.*

Contingency Table of Counts						
		Station *C*				
		1.52 ~ 84.53	84.53 ~ 167.54	167.54 ~ 250.55	250.55 ~ 333.56	333.56 ~ 416.57
Station *B*	0 ~ 31.80	27	0	1	0	0
	31.80 ~ 63.60	15	2	1	0	0
	63.60 ~ 95.40	1	4	0	0	1
	95.40 ~ 127.20	1	1	3	0	0
	127.20 ~ 159.00	1	2	0	0	0
Contingency Table of Probability						
		Station *C*				
		1.52 ~ 84.53	84.53 ~ 167.54	167.54 ~ 250.55	250.55 ~ 333.56	333.56 ~ 416.57
Station *B*	0 ~ 31.80	0.450	0.000	0.017	0.000	0.000
	31.80 ~ 63.60	0.250	0.033	0.017	0.000	0.000
	63.60 ~ 95.40	0.017	0.067	0.000	0.000	0.017
	95.40 ~ 127.20	0.017	0.017	0.050	0.000	0.000
	127.20 ~ 159.00	0.017	0.033	0.000	0.000	0.000

Table 1-10 *Joint probability of stations* B *and* C *and marginal probability of station* C *in Example 1.4.*

		Station *C*				
		1.52 ~ 84.53	84.53 ~ 167.54	167.54 ~ 250.55	250.55 ~ 333.56	333.56 ~ 416.57
Station *B*	0 ~ 31.80	0.450	0.000	0.017	0.000	0.000
	31.80 ~ 63.60	0.250	0.033	0.017	0.000	0.000
	63.60 ~ 95.40	0.017	0.067	0.000	0.000	0.017
	95.40 ~ 127.20	0.017	0.017	0.050	0.000	0.000
	127.20 ~ 159.00	0.017	0.033	0.000	0.000	0.000
		0.750	0.150	0.083	0.000	0.017

The conditional entropy $H(B \mid C)$ can be computed as

$$
\begin{aligned}
H(B \mid C) &= -\sum_{i=1}^{N}\sum_{j=1}^{M} p(B_i, C_j)\log_2 \frac{p(B_i, C_j)}{p(C_j)} \\
&= -0.450 \times \log_2 \frac{0.450}{0.750} - 0.250 \times \log_2 \frac{0.250}{0.750} - \ldots - 0.017 \times \log_2 \frac{0.017}{0.750} \\
&\quad \cdots \\
&\quad - 0.000 \times \log_2 \frac{0.000}{0.017} - 0.000 \times \log_2 \frac{0.000}{0.017} - \ldots - 0.000 \times \log_2 \frac{0.000}{0.017} \\
&= 1.3922 \text{ bits}
\end{aligned}
$$

The joint contingency table for stations A and C is constructed as shown in Table 1-11.

The marginal probability distribution of streamflow at station C can be obtained as shown in Table 1-12. Similarly,

$$
\begin{aligned}
H(C \mid A) &= -\sum_{i=1}^{N}\sum_{j=1}^{M} p(C_i, A_j)\log_2 \frac{p(C_i, A_j)}{p(A_j)} \\
&= -0.333 \times \log_2 \frac{0.333}{0.383} - 0.250 \times \log_2 \frac{0.033}{0.383} - \ldots - 0.000 \times \log_2 \frac{0.000}{0.383} \\
&\quad \cdots\cdots \\
&\quad - 0.017 \times \log_2 \frac{0.017}{0.033} - 0.017 \times \log_2 \frac{0.017}{0.033} - \ldots - 0.000 \times \log_2 \frac{0.000}{0.033} \\
&= 0.9327 \text{ bits}
\end{aligned}
$$

Table 1-11 *Joint contingency table for stations* A *and* C *in Example 1.4.*

Contingency Table of Counts						
		Station *A*				
		4.06 ~ 72.84	72.84 ~ 141.62	141.62 ~ 210.40	210.40 ~ 279.18	279.18 ~ 347.96
Station *C*	1.52 ~ 84.53	20	17	7	0	1
	84.53 ~ 167.54	2	5	0	1	1
	167.54 ~ 250.55	1	3	0	1	0
	250.55 ~ 333.56	0	0	0	0	0
	333.56 ~ 416.57	0	1	0	0	0
Contingency Table of Probability						
		Station *A*				
		4.06 ~ 72.84	72.84 ~ 141.62	141.62 ~ 210.40	210.40 ~ 279.18	279.18 ~ 347.96
Station *C*	1.52 ~ 84.53	0.333	0.283	0.117	0.000	0.017
	84.53 ~ 167.54	0.033	0.083	0.000	0.017	0.017
	167.54 ~ 250.55	0.017	0.050	0.000	0.017	0.000
	250.55 ~ 333.56	0.000	0.000	0.000	0.000	0.000
	333.56 ~ 416.57	0.000	0.017	0.000	0.000	0.000

Table 1-12 *Joint probability of stations* C *and* A *and marginal probability of station* A *in Example 1.4.*

		Station *A*				
		4.06 ~ 72.84	72.84 ~ 141.62	141.62 ~ 210.40	210.40 ~ 279.18	279.18 ~ 347.96
Station *C*	1.52 ~ 84.53	0.333	0.283	0.117	0.000	0.017
	84.53 ~ 167.54	0.033	0.083	0.000	0.017	0.017
	167.54 ~ 250.55	0.017	0.050	0.000	0.017	0.000
	250.55 ~ 333.56	0.000	0.000	0.000	0.000	0.000
	333.56 ~ 416.57	0.000	0.017	0.000	0.000	0.000
		0.383	0.433	0.117	0.033	0.033

(3) Computation of joint entropy

From the joint contingency table of stations A and B, the joint entropy $H(A, B)$ can be computed as

$$\begin{aligned} H(A,B) &= -\sum_{i=1}^{N}\sum_{j=1}^{M} p(A_i, B_j)\log_2 p(A_i, B_j) \\ &= -0.250\times\log_2 0.250 - 0.167\times\log_2 0.167 - \ldots - 0.017\times\log_2 0.017 \\ &\quad \ldots\ldots \\ &\quad - 0.000\times\log_2 0.000 - 0.017\times\log_2 0.017 - \ldots - 0.000\times\log_2 0.000 \\ &= 3.3388 \text{ bits} \end{aligned}$$

From the joint contingency table of stations B and C, the joint entropy $H(B, C)$ can be computed as

$$\begin{aligned} H(B,C) &= -\sum_{i=1}^{N}\sum_{j=1}^{M} p(B_i, C_j)\log_2 p(B_i, C_j) \\ &= -0.450\times\log_2 0.450 - 0.250\times\log_2 0.250 - \ldots - 0.017\times\log_2 0.017 \\ &\quad \ldots\ldots \\ &\quad - 0.000\times\log_2 0.000 - 0.000\times\log_2 0.000 - \ldots - 0.000\times\log_2 0.000 \\ &= 2.5112 \text{ bits} \end{aligned}$$

Similarly, from the joint contingency table of stations B and C, the joint entropy $H(B, C)$ can be computed as

$$\begin{aligned} H(A,C) &= -\sum_{i=1}^{N}\sum_{j=1}^{M} p(A_i, C_j)\log_2 p(A_i, C_j) \\ &= -0.333\times\log_2 0.333 - 0.283\times\log_2 0.283 - \ldots - 0.017\times\log_2 0.017 \\ &\quad \ldots\ldots \\ &\quad - 0.000\times\log_2 0.000 - 0.017\times\log_2 0.017 - \ldots - 0.000\times\log_2 0.000 \\ &= 2.6745 \text{ bits} \end{aligned}$$

(4) Computation of transinformation

There are three different approaches to compute the transinformation.

Approach 1

$$T(A,B) = H(A) - H(A|B) = 1.7418 - 1.4575 = 0.2843 \text{ bits}$$

$$T(B,C) = H(B) - H(B|C) = 1.8812 - 1.3922 = 0.4890 \text{ bits}$$

$$T(A,C) = H(C) - H(C|A) = 1.1190 - 0.9327 = 0.1863 \text{ bits}$$

Table 1-13 *Joint and marginal probabilities of stations* A *and* B *in Example 1.4.*

		Station *B*					
		0 ~ 31.80	31.80 ~ 63.60	63.60 ~ 95.40	95.40 ~ 127.20	127.20 ~ 159.00	
Station *A*	4.06 ~ 72.84	0.250	0.100	0.017	0.017	0.000	0.383
	72.84 ~ 141.62	0.167	0.133	0.067	0.050	0.017	0.433
	141.62 ~ 210.40	0.033	0.067	0.000	0.000	0.017	0.117
	210.40 ~ 279.18	0.000	0.000	0.000	0.017	0.017	0.033
	279.18 ~ 347.96	0.017	0.000	0.017	0.000	0.000	0.033
		0.467	0.300	0.100	0.083	0.050	

Approach 2

$$T(A,B) = H(A) + H(B) - H(A,B) = 1.7418 + 1.8812 - 3.3388 = 0.2843 \text{ bits}$$

$$T(B,C) = H(B) + H(C) - H(B,C) = 1.8812 + 1.1190 - 2.5112 = 0.4890 \text{ bits}$$

$$T(A,C) = H(A) + H(C) - H(A,C) = 1.7418 + 1.1190 - 2.6745 = 0.1863 \text{ bits}$$

Approach 3

The third method is to compute transinformation directly from its definition rather than using shortcut formulas, as in approach 1 and approach 2. Let us compute the transinformation between stations A and B first. The bivariate contingency table between stations A and B has already been shown when computing their joint entropy. From the joint contingency table, we can compute the marginal probability distribution of streamflow at stations A and B by marginalizing out the probability distribution of streamflow of one of the stations. The results are shown in Table 1-13.

The marginal probability distributions of streamflow at stations A and B are shown in the last column and last row of Table 1-13. According to the definition of transinformation, we have

$$\begin{aligned}
T(A,B) &= \sum_i \sum_j p(A_i, B_j) \log \frac{p(A_i, B_j)}{p(A_i)p(B_j)} \\
&= 0.250 \times \log_2 \frac{0.250}{0.467 \times 0.383} + 0.167 \log_2 \frac{0.167}{0.467 \times 0.433} \\
&\quad + \ldots + 0.017 \times \log_2 \frac{0.017}{0.467 \times 0.117} \\
&\quad \ldots\ldots \\
&\quad + 0.000 \times \log_2 \frac{0.000}{0.050 \times 0.383} + 0.017 \times \log_2 \frac{0.017}{0.050 \times 0.433} \\
&\quad + \ldots + 0.000 \log_2 \frac{0.000}{0.050 \times 0.033} \\
&= 0.2843 \text{ bits}
\end{aligned}$$

Table 1-14 *Joint and marginal probabilities of Stations* B *and* C *in Example 1.4.*

		Station *C*					
		1.52 ~ 84.53	84.53 ~ 167.54	167.54 ~ 250.55	250.55 ~ 333.56	333.56 ~ 416.57	
Station *B*	0 ~ 31.80	0.450	0.000	0.017	0.000	0.000	0.467
	31.80 ~ 63.60	0.250	0.033	0.017	0.000	0.000	0.300
	63.60 ~ 95.40	0.017	0.067	0.000	0.000	0.017	0.100
	95.40 ~ 127.20	0.017	0.017	0.050	0.000	0.000	0.083
	127.20 ~ 159.00	0.017	0.033	0.000	0.000	0.000	0.050
		0.750	0.150	0.083	0.000	0.017	

Similarly, the transinformation between stations B and C, $H(B, C)$, can be computed. From their joint contingency table, we can compute the marginal probability distributions of streamflow at stations B and C by marginalizing out the probability distributions of streamflow at one of the stations. The results are shown in Table 1-14.

The marginal probability distributions of streamflow at B and C are shown in the last column and last row of Table 1-14. From the definition of transinformation, we have

$$
\begin{aligned}
T(B,C) &= \sum_i \sum_j p(B_i, C_j) \log \frac{p(B_i, C_j)}{p(B_i)p(C_j)} \\
&= 0.450 \times \log_2 \frac{0.450}{0.750 \times 0.467} + 0.250 \log_2 \frac{0.250}{0.750 \times 0.300} \\
&\quad + \ldots + 0.017 \times \log_2 \frac{0.017}{0.750 \times 0.050} \\
&\quad \ldots\ldots \\
&\quad + 0.000 \times \log_2 \frac{0.000}{0.017 \times 0.467} + 0.000 \times \log_2 \frac{0.000}{0.017 \times 0.300} \\
&\quad + \ldots + 0.000 \log_2 \frac{0.000}{0.017 \times 0.050} \\
&= 0.4890 \text{ bits}
\end{aligned}
$$

Similarly, the transinformation between stations A and C, $H(A, C)$, can be computed. From their joint contingency table, we can compute the marginal probability distributions of streamflow at stations A and C by marginalizing the probability distribution of streamflow at one of the stations out. The results are shown in Table 1-15.

Table 1-15 *Joint and marginal probabilities of Stations* A *and* C *in Example 1.4.*

		Station *C*					
		1.52 ~ 84.53	84.53 ~ 167.54	167.54 ~ 250.55	250.55 ~ 333.56	333.56 ~ 416.57	
Station *A*	4.06 ~ 72.84	0.333	0.033	0.017	0.000	0.000	0.383
	72.84 ~ 141.62	0.283	0.083	0.050	0.000	0.017	0.433
	141.62 ~ 210.40	0.117	0.000	0.000	0.000	0.000	0.117
	210.40 ~ 279.18	0.000	0.017	0.017	0.000	0.000	0.033
	279.18 ~ 347.96	0.017	0.017	0.000	0.000	0.000	0.033
		0.750	0.150	0.083	0.000	0.017	

The marginal probability distributions of streamflow at stations A and C are shown in the last column and last row of Table 1-15. From the definition of transinformation, we have

$$\begin{aligned} T(A,C) &= \sum_i \sum_j p(A_i, C_j) \log \frac{p(A_i, C_j)}{p(A_i)p(C_j)} \\ &= 0.333 \times \log_2 \frac{0.333}{0.750 \times 0.383} + 0.283 \log_2 \frac{0.283}{0.750 \times 0.433} \\ &\quad + \ldots + 0.017 \times \log_2 \frac{0.017}{0.750 \times 0.033} \\ &\quad \ldots\ldots \\ &\quad + 0.000 \times \log_2 \frac{0.000}{0.017 \times 0.383} + 0.017 \times \log_2 \frac{0.017}{0.017 \times 0.433} \\ &\quad + \ldots + 0.000 \log_2 \frac{0.000}{0.017 \times 0.033} \\ &= 0.1863 \text{ bits} \end{aligned}$$

1.4.6 Interaction Information

When more than two variables are under consideration, it is likely that they are interactive. For three variables X, Y, and Z, McGill (1954) defined interaction information (or co-information), denoted by $I(X, Y, Z)$, as

$$\begin{aligned} I(X,Y,Z) &= H(X) + H(Y) + H(Z) - [H(X,Y) + H(Y,Z) + H(X,Z)] + H(X,Y,Z) \\ &= I(\boldsymbol{X}, Y; Z) - I(X,Y) - I(Y,Z) \end{aligned} \tag{1.33}$$

Equation (1.33) can be extended to n variables (Fano 1949, Han 1980) as

$$I(X_1; X_2; \ldots; X_n) = I(X_1; X_2; \ldots, X_{n-1}) - I(X_1; X_2; \ldots; X_{n-1} | X_n) \tag{1.34}$$

Interaction information has been interpreted differently in the literature. To illustrate these interpretations, consider three variables X, Y, and Z. Jakulin and Bratko (2003) interpret interaction information as a measure of the amount of information common to X, Y, and Z (all variables) but is not present in either of these three variables. The interaction information can be positive or negative, because the dependency among variables (say X and Y) can increase or decrease with the knowledge of a new variable (say Z). Jakulin and Bratko (2004) interpret a positive interaction information value as a synergy between X, Y, and Z, whereas a negative value is a redundancy among these variables.

Interaction information is interpreted by Srinivasa (2005) as a gain or loss in the information transmitted between a set of variables (say X and Y) because of the knowledge of a new variable (say Z). The interpretation by Fass (2006) is as the name suggests. Accordingly, it reflects the influence of one variable (say, X) on the amount of information shared between the remainder of variables (say, Y and Z). Fass goes on to state that with the knowledge of the third variable (say, Z) a positive interaction information strengthens the correlation between the two variables (say, X and Y). Conversely, a negative value diminishes the correlation between X and Y.

Example 1.5 Compute interaction information between the three stations A, B, and C using the data in Example 1.4.

Solution The interaction information can be computed by equation (1.33), i.e.,

$$I(A,B,C) = H(A) + H(B) + H(C) - [H(A,B) + H(B,C) + H(A,C)] + H(A,B,C)$$

All the components, except for the trivariate joint entropy $H(A, B, C)$ in this equation, have been obtained in Example 1.4. Now we need to compute the $H(A, B, C)$. By dividing the ranges of streamflow values at station A, B, and C into 5 equal-sized intervals, the trivariate contingency table can be constructed as shown in Table 1-16.

Accordingly,

$$\begin{aligned}
H(A,B,C) &= -\sum_i \sum_j \sum_k p(A_i, B_j, C_k) \log_2 p(A_i, B_j, C_k) \\
&= -0.233 \times \log_2 0.233 - 0.117 \times \log_2 0.117 - \ldots - 0.000 \times \log_2 0.000 \\
&\quad - 0.033 \times \log_2 0.033 - 0.000 \times \log_2 0.000 - \ldots - 0.000 \times \log_2 0.000 \\
&\quad - 0.000 \times \log_2 0.000 - 0.017 \times \log_2 0.017 - \ldots - 0.017 \times \log_2 0.017 \\
&\quad - 0.000 \times \log_2 0.000 - 0.000 \times \log_2 0.000 - \ldots - 0.000 \times \log_2 0.000 \\
&\quad - 0.000 \times \log_2 0.000 - 0.000 \times \log_2 0.000 - \ldots - 0.000 \times \log_2 0.000 \\
&= 3.9264 \text{ bits}
\end{aligned}$$

Table 1-16 *Trivariate contingency table for Example 1.5.*

Station C: 1.5 ~ 84.53						
Contingency Table of Counts						
				Station *B*		
	Interval	0 ~ 31.80	31.80 ~ 63.60	63.60 ~ 95.40	95.40 ~ 127.20	127.20 ~ 159.00
Station *A*	4.06 ~ 72.84	14	5	1	0	0
	72.84 ~ 141.62	7	6	1	2	0
	141.62 ~ 210.40	3	4	0	0	1
	210.40 ~ 279.18	0	0	0	0	0
	279.18 ~ 347.96	1	0	0	0	0
Contingency Table of Probability						
				Station *B*		
	Interval	0 ~ 31.80	31.80 ~ 63.60	63.60 ~ 95.40	95.40 ~ 127.20	127.20 ~ 159.00
Station *A*	1.52 ~ 84.53	0.233	0.083	0.017	0.000	0.000
	84.53 ~ 167.54	0.117	0.100	0.017	0.033	0.000
	167.54 ~ 250.55	0.050	0.067	0.000	0.000	0.017
	250.55 ~ 333.56	0.000	0.000	0.000	0.000	0.000
	333.56 ~ 416.57	0.017	0.000	0.000	0.000	0.000
Station C: 84.53 ~ 167.53						
Contingency Table of Counts						
				Station *B*		
	Interval	0 ~ 31.80	31.80 ~ 63.60	63.60 ~ 95.40	95.40 ~ 127.20	127.20 ~ 159.00
Station *A*	4.06 ~ 72.84	2	2	0	0	0
	72.84 ~ 141.62	0	1	0	1	1
	141.62 ~ 210.40	0	0	0	0	0
	210.40 ~ 279.18	0	0	0	0	1
	279.18 ~ 347.96	0	0	1	0	0

Continued

Table 1-16 *Trivariate contingency table for Example 1.5. (Continued)*

Station C: 84.53 ~ 167.53						
Contingency Table of Probability						
				Station *B*		
		0 ~ 31.80	31.80 ~ 63.60	63.60 ~ 95.40	95.40 ~ 127.20	127.20 ~ 159.00
Station *A*	1.52 ~ 84.53	0.033	0.033	0.000	0.000	0.000
	84.53 ~ 167.54	0.000	0.017	0.000	0.017	0.017
	167.54 ~ 250.55	0.000	0.000	0.000	0.000	0.000
	250.55 ~ 333.56	0.000	0.000	0.000	0.000	0.017
	333.56 ~ 416.57	0.000	0.000	0.017	0.000	0.000
Station C: 167.53 ~ 250.54						
Contingency Table of Counts						
				Station *B*		
	Interval	0 ~ 31.80	31.80 ~ 63.60	63.60 ~ 95.40	95.40 ~ 127.20	127.20 ~ 159.00
Station *A*	4.06 ~ 72.84	0	0	0	0	1
	72.84 ~ 141.62	1	0	0	0	0
	141.62 ~ 210.40	0	0	1	0	1
	210.40 ~ 279.18	0	0	0	0	0
	279.18 ~ 347.96	0	0	0	0	1
Contingency Table of Probability						
				Station *B*		
	Interval	0 ~ 31.80	31.80 ~ 63.60	63.60 ~ 95.40	95.40 ~ 127.20	127.20 ~ 159.00
Station *A*	1.52 ~ 84.53	0.000	0.000	0.000	0.000	0.017
	84.53 ~ 167.54	0.017	0.000	0.000	0.000	0.000
	167.54 ~ 250.55	0.000	0.000	0.017	0.000	0.017
	250.55 ~ 333.56	0.000	0.000	0.000	0.000	0.000
	333.56 ~ 416.57	0.000	0.000	0.000	0.000	0.017

Table 1-16 *Trivariate contingency table for Example 1.5.(Continued)*

Station C: 250.54 ~ 333.55						
Contingency Table of Counts						
				Station *B*		
	Interval	0 ~ 31.80	31.80 ~ 63.60	63.60 ~ 95.40	95.40 ~ 127.20	127.20 ~ 159.00
Station *A*	4.06 ~ 72.84	0	0	0	0	0
	72.84 ~ 141.62	0	0	0	0	0
	141.62 ~ 210.40	0	0	0	0	0
	210.40 ~ 279.18	0	0	0	0	0
	279.18 ~ 347.96	0	0	0	0	0
Contingency Table of Probability						
				Station *B*		
	Interval	0 ~ 31.80	31.80 ~ 63.60	63.60 ~ 95.40	95.40 ~ 127.20	127.20 ~ 159.00
Station *A*	1.52 ~ 84.53	0.000	0.000	0.000	0.000	0.000
	84.53 ~ 167.54	0.000	0.000	0.000	0.000	0.000
	167.54 ~ 250.55	0.000	0.000	0.000	0.000	0.000
	250.55 ~ 333.56	0.000	0.000	0.000	0.000	0.000
	333.56 ~ 416.57	0.000	0.000	0.000	0.000	0.000
Station C: 333.55 ~ 416						
Contingency Table of Counts						
				Station *B*		
	Interval	0 ~ 31.80	31.80 ~ 63.60	63.60 ~ 95.40	95.40 ~ 127.20	127.20 ~ 159.00
Station *A*	4.06 ~ 72.84	0	0	0	0	0
	72.84 ~ 141.62	0	0	0	0	0
	141.62 ~ 210.40	0	0	1	0	0
	210.40 ~ 279.18	0	0	0	0	0
	279.18 ~ 347.96	0	0	0	0	0
Contingency Table of Probability						
				Station *B*		
	Interval	0 ~ 31.80	31.80 ~ 63.60	63.60 ~ 95.40	95.40 ~ 127.20	127.20 ~ 159.00
Station *A*	1.52 ~ 84.53	0.000	0.000	0.000	0.000	0.000
	84.53 ~ 167.54	0.000	0.000	0.000	0.000	0.000
	167.54 ~ 250.55	0.000	0.000	0.017	0.000	0.000
	250.55 ~ 333.56	0.000	0.000	0.000	0.000	0.000
	333.56 ~ 416.57	0.000	0.000	0.000	0.000	0.000

Now the interaction information is computed as

$$\begin{aligned} I(A;,B,C) &= H(A)+H(B)+H(C)-[H(A,B)+H(B,C)+H(A,C)]+H(A,B,C) \\ &= 1.7418+1.8812+1.1190-(3.3388+2.5112+2.6745)+3.9264 \\ &= 1.1439 \text{ bits} \end{aligned}$$

1.4.7 Calculation of Transinformation

From the point of view of calculating T, variables are either discrete or are discretized if they are continuous. For two variables, X taking on values $i = 1, 2, 3, \ldots, N$, and Y taking on values $j = 1, 2, 3, \ldots, M$, let n be the total number observations of events (i, j) and let n_{ij} denote the number of times i occurred and j was caused, i.e., it is assumed that when i occurs, j is caused. Contingency tables are used to compute relative frequencies, wherein XY would represent cells and n_{ij} would be entries. The relative frequencies would be: $p(i) = n_i/n$, $p(j) = n_j/n$, and $p(i, j) = n_{ij}/n$. Thus, one can think of a joint event (i, j) as having a relative frequency $p(i, j)$. Rather than using relative frequencies, one can also use a simpler notation for computing entropies in terms of absolute frequencies, and this phenomenon is explained here. See Appendix 1.1 at the end of the chapter for further explanation of symbols.

One can write the summations as

$$n_i = \sum_j n_{ij};\ n_j = \sum_i n_{ij};\ n = \sum_{i,j} n_{ij} \tag{1.35}$$

Then, one can express

$$s_{ij} = \frac{1}{n}\sum_{i,j} n_{ij}\log_2 n_{ij};\ s_i = \frac{1}{n}\sum_i n_i \log_2 n_i;\ s_j = \frac{1}{n}\sum_j n_j \log_2 n_j;\ s = \log_2 n \tag{1.36}$$

Now the transinformation can be expressed in terms of these summations as

$$T(X,Y) = s - s_i - s_j + s_{ij} \tag{1.37}$$

The two-dimensional case of the amount of information transmitted can be extended to three or more dimensional cases (McGill 1953, 1954). Consider three random variables: U, V, and Y, where U and V can be interpreted to constitute sources, and Y, the effect. In this case, X of the two-dimensional case has been replaced by U and V. Then, as shown in Fig. 1-4, transinformation can be written as

$$T(U,V;Y) = H(U,V) + H(Y) - H(U,V,Y) \tag{1.38}$$

Here X is divided into two classes, U and V, with values of U as $k = 1, 2, 3, \ldots, K$ and values of V as $w = 1, 2, 3, \ldots, W$. The subdivision of X is made such that the range of values of U and V jointly constitute the values of X, with the implication that the input event i can be replaced by the joint event (k, w). This replacement means that $n_i = n_{kw}$.

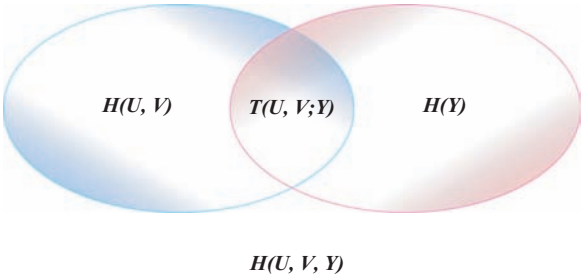

Figure 1-4 *Schematic of the components of three-dimensional transmitted information.*

Here $T(U, V; Y)$ measures the amount of information transmission that U and V transmit to Y. It can be shown that the direction of transmission is irrelevant because

$$T(U, V; Y) = T(Y; U, V) \tag{1.39}$$

This irrelevance also implies that distinguishing sources from effect or transmitters from receivers does not gain anything, because the amount of information transmitted measures the association between variables, and, hence, the direction in which information travels is immaterial. However, it is important to note that symbols cannot be permuted at will, because

$$T(U, Y; V) = H(U, Y) + H(V) - H(U, Y; V) \tag{1.40}$$

and it is not necessarily equal to $T(U, V; Y)$.

For computation, $T(U, V; Y)$ can be expressed as a function of bivariate transmission between U and Y, and V and Y. Observations of the joint event (k, w, j) can be organized into a three-dimensional contingency table with UVY cells with n_{kwj} entries. Then one can compute the terms of

$$T(U, V; Y) = s - s_j - s_{kw} + s_{kwj} \tag{1.41}$$

where

$$s_{kwj} = \frac{1}{n} \sum_{k,w,j} n_{kwj} \log_2 n_{kwj} \tag{1.42}$$

Other terms can be expressed in a similar manner.

One can investigate transmission between U and Y. This step would involve eliminating V, which can be done in two ways. First, the three-dimensional contingency table can be reduced to two dimensions by summing over V, resulting in the entries of the reduced table as

$$n_{kj} = \sum_{w} n_{kwj} \tag{1.43}$$

The transmitted information between U and Y can be expressed as

$$T(U;Y) = s - s_k - s_j + s_{kj} \tag{1.44}$$

The second way to eliminate V is to compute the transmission between U and Y separately for each value of V and then average the transmitted values together. Designating $T_w(U;Y)$ as the information transmitted between U and Y for a single value of V, namely w, one can write the transmitted information $T_v(U;Y)$ as

$$T_v(U;Y) = \sum_w \frac{n_w}{n}[T_w(U;Y)] \tag{1.45}$$

It can be shown that

$$T_v(U;Y) = s_w - s_{kw} - s_{wj} + s_{kwj} \tag{1.46}$$

In a three-dimensional contingency table, three different pairs of variables occur. For transmission between V and Y, one can write

$$T(V;Y) = s - s_w - s_j + s_{wj} \tag{1.47}$$

$$T_u(V;Y) = s_k - s_{kw} - s_{kj} + s_{kwj} \tag{1.48}$$

The transmission between U and V can be expressed as

$$T(U;V) = s - s_k - s_w + s_{kw} \tag{1.49}$$

$$T_y(U;V) = s_j - s_{kj} - s_{wj} + s_{kwj} \tag{1.50}$$

Now, the information transmitted between U and Y can be reconsidered. If V affects the transmission between U and Y, i.e., U and V are related, then $T_v(U;Y) \neq T(U;Y)$. This effect can be measured as

$$A(UVY) = T_v(U;Y) - T(U;Y) \tag{1.51}$$

$$A(UVY) = -s + s_k + s_w + s_j - s_{kw} - s_{wj} - s_{kj} + s_{kwj} \tag{1.52}$$

A little algebra shows that

$$A(UVY) = T_v(U;Y) - T(U;Y) = T_u(V;Y) - T(V;Y) = T_y(U;V) - T(U;V) \tag{1.53}$$

Keeping this symmetry in mind, $A(UVY)$ can be regarded as the $U.V.Y$ interaction information and is the gain (or loss) in information transmitted between any two of the variables because of the knowledge of the third variable.

Now the three-dimensional information transmitted from U, V to Y, i.e., $T(U, V; Y)$, can be expressed as a function of its bivariate components:

$$T(U,V;Y) = T(U;Y) + T(V;Y) + A(UVY) \tag{1.54}$$

$$T(U,V;Y) = T_v(U;Y) + T_u(V;Y) - A(UVY) \tag{1.55}$$

Following these two equations, taken together, $T(U, V; Y)$ can be shown as in Fig. 1-4 with overlapping circles. This figure assumes that there is a positive interaction between U, V, and Y, meaning that when one of the interacting variables is held constant, the amount of association between the remaining two increases, i.e., $T_v(U; Y) > T(U; Y)$, and $T_u(V; Y) > T(V; Y)$.

For the three-dimensional case, one can write

$$H(Y) = H_{uv}(Y) + T(U; Y) + T(V; Y) + A(UVY) \tag{1.56}$$

where $H(Y) = s - s_j$ and $H_{uv}(Y) = s_{kwj} - s_{kw}$. This equation shows that the marginal information is partitioned into an error term and a set of correlation terms because of input variables. The error term is $H_{uv}(Y)$, and it denotes the unexplained or residual variance in the output Y after the information caused by inputs U and V has been removed. For the two-dimensional case, one can write

$$H(Y) = H_u(Y) + T(U; Y) \tag{1.57}$$

In this case, H_u is the error term, because there is only one input variable U. Shannon (1948) has shown that

$$H_u(Y) \geq H_{uv}(Y) \tag{1.58}$$

This notion shows that if only U is controlled, the error term cannot be increased if V is also controlled. It can be shown that

$$H_u(Y) = H_{uv}(y) + T_{uv}(V; Y) \tag{1.59}$$

Now the issue of independence in three-dimensional transmission is considered. If the output is independent of the joint input, then $T(U, V; Y) = 0$, i.e.,

$$n_{kwj} = \frac{n_{kw} n_j}{n} \tag{1.60}$$

Then it can be shown that

$$s_{kwj} = s_{kw} + s_j - s \tag{1.61}$$

This equation can be used to show that $T(U, V; Y) = 0$.

Now assume that $T(U, V; Y) > 0$, but V and Y are independent, i.e.,

$$n_{wj} = \frac{n_w n_j}{n} \tag{1.62}$$

This variation results in

$$s_{wj} = s_w + s_j - s \tag{1.63}$$

If s_{wj} from equation (1.47) is used in equation (1.63), then $T(V; Y) = 0$. Equation (1.63) does not lead to a unique condition for independence between V and Y.

If the input variables are correlated, then the question arises: How is the transmitted information affected? The three-dimensional transmitted information $T(U, V; Y)$ would account for only part of the total association in a three-dimensional contingency table. Let $C(U, V; Y)$ be the correlated information. Then one can write

$$C(U,V;Y) = H(U) + H(V) + H(Y) - H(U,V;Y) \tag{1.64}$$

Adding to and subtracting from equation (1.64) $H(U, V)$, one obtains

$$C(U,V;Y) = T(U;V) + T(U,V;Y) \tag{1.65}$$

$$C(U,V;Y) = T(U;V) + T(U;Y) + T(V;Y) + A(UVY) \tag{1.66}$$

It is seen that $C(U, V; Y)$ can be used to generate all possible components of the three correlated sources of information U, V, and Y.

Example 1.6 Using the s-notation method, compute transinformation $T(A, B)$, $T(B, C)$, $T(A, C)$ and the interaction information $A(A, B, C)$ using the data from Example 1.5.

Solution

Calculation of transinformation

Let us compute $T(A, B)$ first. From equation (1.37), we know that we need to compute s, s_i, s_j, and s_{ij}. All of the components can be obtained from equation (1.36). In the following list, by taking transinformation $T(A, B)$ as an example, we compute all the components one by one.

1. Computation of s: Dividing the ranges of streamflow values at stations A and B into 5 equal-sized intervals and counting the number of occurrences in all combinations of these subintervals, the contingency table can be computed as shown in Table 1-17.
2. From equation (1.35), we have

   $$n = \sum_{i,j} n_{ij} = 15+10+2+0+1+6+8+4+0+0+\ldots+0+1+1+1+0 = 60$$

   From equation (1.36), we have

   $$s = \log_2 n = 5.9069$$
3. Computation of s_i and s_j: Marginalizing out one of the two sets of streamflow values, the contingency table of stations A and B can be obtained from Table 1-17.

   From equation (1.35), we have

   $$n_i(1) = \sum_j n_{1j} = 15+6+1+1+1 = 23$$

   $$n_i(2) = \sum_j n_{2j} = 10+8+4+3+1 = 26$$

   ……

   $$n_i(5) = \sum_j n_{5j} = 1+0+1+0+0 = 2$$

Table 1-17 n *Table for Stations* A *and* B *in Example 1.6.*

	Interval	0 ~ 31.80	31.80 ~ 63.60	63.60 ~ 95.40	95.40 ~ 127.20	127.20 ~ 159.00
Station *A*	4.06 ~ 72.84	15	6	1	1	0
	72.84 ~ 141.62	10	8	4	3	1
	141.62 ~ 210.40	2	4	0	0	1
	210.40 ~ 279.18	0	0	0	1	1
	279.18 ~ 347.96	1	0	1	0	0

Table 1-18 n *and marginal* n *tables for Stations* A *and* B *in Example 1.6.*

		Station *B*					
	Interval	0 ~ 31.80	31.80 ~ 63.60	63.60 ~ 95.40	95.40 ~ 127.20	127.20 ~ 159.00	
Station *A*	4.06 ~ 72.84	15	6	1	1	0	23
	72.84 ~ 141.62	10	8	4	3	1	26
	141.62 ~ 210.40	2	4	0	0	1	7
	210.40 ~ 279.18	0	0	0	1	1	2
	279.18 ~ 347.96	1	0	1	0	0	2
		28	18	6	5	3	

The results (contingency table for station *A*) are shown in the last column in Table 1-18. Similarly, we also have

$$n_j(1) = \sum_i n_{i1} = 15 + 10 + 2 + 0 + 1 = 28$$

$$n_j(2) = \sum_i n_{i2} = 6 + 8 + 4 + 0 + 0 = 18$$

……

$$n_j(5) = \sum_i n_{i5} = 0 + 1 + 1 + 1 + 0 = 3$$

as shown in Table 1-18.

Finally, from equation (1.36), we have

$$\begin{aligned} s_i &= \frac{1}{n}\sum_i n_i \log_2 n_i \\ &= \frac{1}{60}(23 \times \log_2 23 + 26 \times \log_2 26 + 7 \times \log_2 7 + 2 \times \log_2 2 + 2 \times \log_2 2) \\ &= 4.1651 \text{ bits} \end{aligned}$$

Also we have

$$s_j = \frac{1}{n}\sum_j n_j \log_2 n_j$$
$$= \frac{1}{60}(28\times\log_2 28 + 18\times\log_2 18 + 6\times\log_2 6 + 5\times\log_2 5 + 3\times\log_2 3)$$
$$= 4.0256 \text{ bits}$$

4. Compute s_{ij}: From the joint contingency table and equation (1.36), we can also compute s_{ij},

$$s_{ij} = \frac{1}{n}\sum_{i,j} n_{ij} \log_2 n_{ij}$$
$$= \frac{1}{60}(15\times\log_2 15 + 10\times\log_2 10 + 2\times\log_2 2$$
$$+ \ldots + 0\times\log_2 0 + 1\times\log_2 1 + \ldots + 0\times\log_2 0)$$
$$= 2.5681 \text{ bits}$$

Finally,

$$T(A, B) = s - s_i - s_j + s_{ij} = 5.9069 - 4.1651 - 4.0256 + 2.5681$$
$$= 0.2843 \text{ bits}$$

Similarly, $T(B, C)$ and $T(C, A)$ can be computed as

$$T(B, C) = 0.4890 \text{ bits}$$

$$T(C, A) = 0.1863 \text{ bits}$$

Interaction information calculation

Dividing the ranges of streamfow values at stations A, B, and C into five equal-sized intervals can be used to create the trivariate contingency table. The resulting contingency tables are shown in Tables 1-19 to 1-23.

Summing up all the elements in the above trivariate joint contingency tables, we have $n = 60$. Therefore, $s = \log_2 60 = 5.9069$ bits. The marginal contingency table can be obtained in the following way:

- The marginal contingency table of stations A and B given $C \in (1.5, 84.53]$ is shown in Table 1-24.
- The marginal contingency table of stations A and B given $C \in (84.53, 167.53]$ is shown in Table 1-25.
- The marginal contingency table of stations A and B given $C \in (167.53, 250.54]$ is shown in Table 1-26.

Table 1-19 n *Table for Station* C*: 1.5 ~ 84.53 in Example 1.6.*

		Station *B*				
	Interval	0 ~ 31.80	31.80 ~ 63.60	63.60 ~ 95.40	95.40 ~ 127.20	127.20 ~ 159.00
Station *A*	4.06 ~ 72.84	14	5	1	0	0
	72.84 ~ 141.62	7	6	1	2	0
	141.62 ~ 210.40	3	4	0	0	1
	210.40 ~ 279.18	0	0	0	0	0
	279.18 ~ 347.96	1	0	0	0	0

Table 1-20 *Contingency table of counts for Station* C*: 84.53 ~ 167.53 in Example 1.6.*

		Station *B*				
	Interval	0 ~ 31.80	31.80 ~ 63.60	63.60 ~ 95.40	95.40 ~ 127.20	127.20 ~ 159.00
Station *A*	4.06 ~ 72.84	2	2	0	0	0
	72.84 ~ 141.62	0	1	0	1	1
	141.62 ~ 210.40	0	0	0	0	0
	210.40 ~ 279.18	0	0	0	0	1
	279.18 ~ 347.96	0	0	1	0	0

Table 1-21 *Contingency table of counts for Station* C*: 167.53 ~ 250.54 in Example 1.6.*

		Station *B*				
	Interval	0 ~ 31.80	31.80 ~ 63.60	63.60 ~ 95.40	95.40 ~ 127.20	127.20 ~ 159.00
Station *A*	4.06 ~ 72.84	0	0	0	0	1
	72.84 ~ 141.62	1	0	0	0	0
	141.62 ~ 210.40	0	0	1	0	1
	210.40 ~ 279.18	0	0	0	0	0
	279.18 ~ 347.96	0	0	0	0	1

Table 1-22 *Contingency table of counts for Station* C*: 250.54 ~ 333.55 in Example 1.6.*

		Station *B*				
	Interval	0 ~ 31.80	31.80 ~ 63.60	63.60 ~ 95.40	95.40 ~ 127.20	127.20 ~ 159.00
Station *A*	4.06 ~ 72.84	0	0	0	0	0
	72.84 ~ 141.62	0	0	0	0	0
	141.62 ~ 210.40	0	0	0	0	0
	210.40 ~ 279.18	0	0	0	0	0
	279.18 ~ 347.96	0	0	0	0	0

Table 1-23 *Contingency table of counts for Station* C*: 333.55 ~ 416 in Example 1.6.*

		Station *B*				
	Interval	0 ~ 31.80	31.80 ~ 63.60	63.60 ~ 95.40	95.40 ~ 127.20	127.20 ~ 159.00
Station *A*	4.06 ~ 72.84	0	0	0	0	0
	72.84 ~ 141.62	0	0	0	0	0
	141.62 ~ 210.40	0	0	1	0	0
	210.40 ~ 279.18	0	0	0	0	0
	279.18 ~ 347.96	0	0	0	0	0

Table 1-24 n *Table for Station* C*: 1.5 ~ 84.53 in Example 1.6.*

		Station *B*					
	Interval	0 ~ 31.80	31.80 ~ 63.60	63.60 ~ 95.40	95.40 ~ 127.20	127.20 ~ 159.00	
Station *A*	4.06 ~ 72.84	14	5	1	0	0	20
	72.84 ~ 141.62	7	6	1	2	0	16
	141.62 ~ 210.40	3	4	0	0	1	8
	210.40 ~ 279.18	0	0	0	0	0	0
	279.18 ~ 347.96	1	0	0	0	0	1
		25	15	2	2	1	

Table 1-25 n *Table for Station* C*: 84.53 ~ 167.53 in Example 1.6.*

		Station *B*					
	Interval	0 ~ 31.80	31.80 ~ 63.60	63.60 ~ 95.40	95.40 ~ 127.20	127.20 ~ 159.00	
Station *A*	4.06 ~ 72.84	2	2	0	0	0	4
	72.84 ~ 141.62	0	1	0	1	1	3
	141.62 ~ 210.40	0	0	0	0	0	0
	210.40 ~ 279.18	0	0	0	0	1	1
	279.18 ~ 347.96	0	0	1	0	0	1
		2	3	1	1	2	

Table 1-26 n *Table for Station* C*: 167.53 ~ 250.54 in Example 1.6.*

		Station *B*					
	Interval	0 ~ 31.80	31.80 ~ 63.60	63.60 ~ 95.40	95.40 ~ 127.20	127.20 ~ 159.00	
Station *A*	4.06 ~ 72.84	0	0	0	0	1	1
	72.84 ~ 141.62	1	0	0	0	0	1
	141.62 ~ 210.40	0	0	1	0	1	2
	210.40 ~ 279.18	0	0	0	0	0	0
	279.18 ~ 347.96	0	0	0	0	1	1
		1	0	1	0	3	

- The marginal contingency table of stations A and B given $C \in$ (250.54, 333.55] is shown in Table 1-27.
- The marginal contingency table of stations A and B given $C \in$ (333.55, 416] is shown in Table 1-28.

Then the marginal contingency table for station A can be obtained by summing up the last columns of Tables 1-24 to 1-28 in an element-by-element way:

$$n_k(1) = \sum_{w,j} n_{1wj} = 20 + 4 + 1 + 0 + 0 = 25$$

$$n_k(2) = \sum_{w,j} n_{2wj} = 16 + 3 + 1 + 0 + 0 = 20$$

$$n_k(3) = \sum_{w,j} n_{3wj} = 8 + 0 + 2 + 0 + 1 = 11$$

$$n_k(4) = \sum_{w,j} n_{4wj} = 0 + 1 + 0 + 0 + 0 = 1$$

$$n_k(5) = \sum_{w,j} n_{5wj} = 1 + 1 + 1 + 0 + 0 = 3$$

Table 1-27 n *Table for Station* C*: 250.54 ~ 333.55 in Example 1.6.*

		Station *B*					
	Interval	0 ~ 31.80	31.80 ~ 63.60	63.60 ~ 95.40	95.40 ~ 127.20	127.20 ~ 159.00	
Station *A*	4.06 ~ 72.84	0	0	0	0	0	0
	72.84 ~ 141.62	0	0	0	0	0	0
	141.62 ~ 210.40	0	0	0	0	0	0
	210.40 ~ 279.18	0	0	0	0	0	0
	279.18 ~ 347.96	0	0	0	0	0	0
		0	0	0	0	0	

Table 1-28 n *Table for Station* C*: 333.55 ~ 416 in Example 1.6.*

		Station *B*					
	Interval	0 ~ 31.80	31.80 ~ 63.60	63.60 ~ 95.40	95.40 ~ 127.20	127.20 ~ 159.00	
Station *A*	4.06 ~ 72.84	0	0	0	0	0	0
	72.84 ~ 141.62	0	0	0	0	0	0
	141.62 ~ 210.40	0	0	1	0	0	1
	210.40 ~ 279.18	0	0	0	0	0	0
	279.18 ~ 347.96	0	0	0	0	0	0
		0	0	1	0	0	

Tabulate the results as shown in Table 1-29, and the marginal contingency table for station *B* can be obtained by summing up the last rows and last columns of Tables 1-24 to 1-28 in an element-by-element way

$$n_j(1) = \sum_{k,w} n_{kw1} = 25 + 2 + 1 + 0 + 0 = 28$$

$$n_j(2) = \sum_{k,w} n_{kw2} = 15 + 3 + 0 + 0 + 0 = 18$$

$$n_j(3) = \sum_{k,w} n_{kw3} = 2 + 1 + 1 + 0 + 1 = 5$$

$$n_j(4) = \sum_{k,w} n_{kw4} = 2 + 1 + 0 + 0 + 0 = 3$$

$$n_j(5) = \sum_{k,w} n_{kw5} = 1 + 2 + 3 + 0 + 0 = 6$$

Tabulate the results as shown in Table 1-30.

Table 1-29 *Marginal contingency table for Station* A *in Example 1.6.*

	n_k				
	4.06 ~ 72.84	72.84 ~ 141.62	141.62 ~ 210.40	210.40 ~ 279.18	279.18 ~ 347.96
Station *A*	25	30	11	1	3

Table 1-30 *Marginal contingency table for Station* B *in Example 1.6.*

	n_j				
	0 ~ 31.80	31.80 ~ 63.60	63.60 ~ 95.40	95.40 ~ 127.20	127.20 ~ 159.00
Station *B*	28	18	5	3	6

Table 1-31 *Marginal contingency table for Station* C *in Example 1.6.*

	n_w				
	1.5 ~ 84.53	84.53 ~ 167.53	167.53 ~ 250.54	250.54 ~ 333.55	333.55 ~ 416
Station *C*	45	9	5	0	1

The marginal contingency table for station *C* can be computed by summing up all elements of Tables 1-24 to 1-28:

$$
\begin{aligned}
n_w(1) &= 25+15+2+2+1 = 20+16+8+0+1 = 45\\
n_w(2) &= 2+3+1+1+2 = 4+3+0+1+1 = 9\\
n_w(3) &= 1+0+1+0+3 = 1+1+2+0+1 = 5\\
n_w(4) &= 0+0+0+0+0 = 0+0+0+0+0 = 0\\
n_w(5) &= 0+0+1+0+0 = 0+0+1+0+0 = 1
\end{aligned}
$$

Tabulate the results as shown in Table 1-31.

Therefore, we can have

$$
\begin{aligned}
s_k &= \frac{1}{60}(25\times\log_2 25+20\times\log_2 20+11\times\log_2 11+1\times\log_2 1+3\times\log_2 3)\\
&= 4.0891 \text{ bits}
\end{aligned}
$$

$$
\begin{aligned}
s_j &= \frac{1}{60}(28\times\log_2 28+18\times\log_2 18+5\times\log_2 5+3\times\log_2 3+6\times\log_2 6)\\
&= 4.0256 \text{ bits}
\end{aligned}
$$

$$
s_w = \frac{1}{60}(45\times\log_2 45+9\times\log_2 9+5\times\log_2 5+0\times\log_2 0+1\times\log_2 1) = 4.7879 \text{ bits}
$$

Table 1-32 n_{kj} *Table for Station* A *in Example 1.6.*

	Interval	0 ~ 31.80	31.80 ~ 63.60	63.60 ~ 95.40	95.40 ~ 127.20	127.20 ~ 159.00
Station *A*	4.06 ~ 72.84	16	7	1	0	1
	72.84 ~ 141.62	8	7	1	3	1
	141.62 ~ 210.40	3	4	2	0	2
	210.40 ~ 279.18	0	0	0	0	1
	279.18 ~ 347.96	1	0	1	0	1

Table 1-33 n_{wj} *Table for Station* B *in Example 1.6.*

	Interval	1.5 ~ 84.53	84.53 ~ 167.53	167.53 ~ 250.54	250.54 ~ 333.55	333.55 ~ 416
Station *B*	0 ~ 31.80	25	2	1	0	0
	31.80 ~ 63.60	15	3	0	0	0
	63.60 ~ 95.40	2	1	1	0	1
	95.40 ~ 127.20	2	1	0	0	0
	127.20 ~ 159.00	1	2	3	0	0

Now we compute s_{kw}, s_{wj}, and s_{kj}. The bivariate contingency table can also be obtained from the trivariate contingency by marginalizing out one of the three sets of streamflow values. Using equation (1.43), we can have the bivariate joint contingency table of stations *A* and *B* as shown in Table 1-32. Therefore, s_{kj} in bits can be computed as

$$S_{kj} = \frac{1}{60}(16\times\log_2 16 + 8\times\log_2 8 + 3\times\log_2 3 + \ldots + 1\times\log_2 1 + 1\times\log_2 1)$$
$$= 2.4802$$

Similarly, the bivariate joint contingency table of *B* and *C* is shown in Table 1-33, and s_{wj} in bits can be computed as

$$S_{kj} = \frac{1}{60}(25\times\log_2 25 + 15\times\log_2 15 + 2\times\log_2 2 + \ldots + 0\times\log_2 0 + 0\times\log_2 0)$$
$$= 3.2035$$

The bivariate joint contingency table of stations *A* and *C* is shown in Table 1-34, and s_{kw} in bits is computed as

$$s_{kw} = \frac{1}{60}(20\times\log_2 20 + 16\times\log_2 16 + 8\times\log_2 8 + \ldots + 0\times\log_2 0 + 0\times\log_2 0)$$
$$= 3.1532$$

Table 1-34 n_{wj} *Table for Station C in Example 1.6.*

	Interval	1.5 ~ 84.53	84.53 ~ 167.53	167.53 ~ 250.54	250.54 ~ 333.55	333.55 ~ 416
Station *B*	4.06 ~ 72.84	20	4	1	0	0
	72.84 ~ 141.62	16	3	1	0	0
	141.62 ~ 210.40	8	0	2	0	1
	210.40 ~ 279.18	0	1	0	0	0
	279.18 ~ 347.96	1	1	1	0	0

Using the trivariate contingency table and equation (1.42), s_{kwj} can be computed as

$$\begin{aligned}
s_{kwj} &= \frac{1}{n}\sum_{k,w,j} n_{kwj}\log_2 n_{kwj} \\
&= \frac{1}{60}(14\times\log_2 14 + 7\times\log_2 7 + 3\times\log_2 3 + \ldots + 0\times\log_2 0 + 0\times\log_2 0 \\
&\quad + 2\times\log_2 2 + 0\times\log_2 0 + 0\times\log_2 0 + \ldots + 1\times\log_2 1 + 0\times\log_2 0 \\
&\quad + 0\times\log_2 0 + 1\times\log_2 1 + 0\times\log_2 0 + \ldots + 0\times\log_2 0 + 1\times\log_2 1 \\
&\quad + 0\times\log_2 0 + 0\times\log_2 0 + 0\times\log_2 0 + \ldots + 0\times\log_2 0 + 0\times\log_2 0 \\
&\quad + 0\times\log_2 0 + 0\times\log_2 0 + 0\times\log_2 0 + \ldots + 0\times\log_2 0 + 0\times\log_2 0) \\
&= 1.9805 \text{ bits}
\end{aligned}$$

So far, we can use equation (1.52) to compute the interaction information

$$\begin{aligned}
A(A,B,C) &= -s + s_k + s_w + s_j - s_{kw} - s_{wj} - s_{kj} + s_{kwj} \\
&= -5.9069 + 4.0891 + 4.7879 + 4.0256 - 3.1532 - 3.2035 - 2.4802 + 1.9805 \\
&= 0.1393 \text{ bits}
\end{aligned}$$

1.4.8 Informational Correlation Coefficient

The informational correlation coefficient R_0 is a measure of transferable information and measures the mutual dependence between random variables X and Y and does not assume any type of relationship between them. It is a dimensional quantity and is expressed in terms of transinformation as

$$R_0 = \sqrt{1-\exp(-2T_0)} \tag{1.67}$$

where T_0 is transinformation or mutual information representing the upper limit of transferable information between two variables X and Y. If the values of probabilities are computed from the corresponding sample frequencies (Harmancioglu et al. 1992), then the transinformation so obtained represents the upper limit

of transferable information between the two variables. When X and Y are normally distributed and linearly correlated, R_0 reduces to the classical Pearson correlation coefficient between X and Y, r_{xy}:

$$r_0 = r_{xy} = \frac{\text{Cov}(x, y)}{\sigma_x \sigma_y} \tag{1.68}$$

where $Cov(x, y)$ is the covariance between X and Y, σ_x is the standard deviation of X, and σ_y is the standard deviation of Y. These quantities can be computed from sample data as follows:

$$\text{Cov}(x, y) = \frac{1}{N}\sum_{i=1}^{N}(x_i - \bar{x})(y_i - \bar{y}) \tag{1.69}$$

where $\bar{x}$ is the mean of X, $\bar{y}$ is the mean of Y, and N is the sample size. The standard deviations are computed as

$$\sigma_x = \sqrt{\frac{1}{N-1}\sum_{i=1}^{N}(x_i - \bar{x})^2}, \sigma_y = \sqrt{\frac{1}{N-1}\sum_{i=1}^{N}(y_i - \bar{y})^2} \tag{1.70}$$

1.5 Application of Entropy Theory to Hydraulic Engineering Problems

The entropy concept has been applied to a wide range of problems in hydraulics. These problems can be classified into three groups: (1) statistical, (2) physical, and (3) mixed. In the first group, problems are entirely statistical and do not invoke any physical laws. Examples of such problems are derivation of frequency distributions for given constraints, estimation of frequency distribution parameters in terms of given constraints, evaluation of monitoring networks in space and/or time, flow forecasting, spatial and inverse spatial analysis, complexity analysis, clustering analysis, and so on.

In the second group, problems involve a kind of physical law in the form of a flux-concentration relation and a hypothesis on the cumulative probability distribution of either flux or concentration, depending on the problem at hand. Examples of such problems are distribution of velocity in water courses, hydraulic geometry, channel cross section, sediment concentration, sediment yield, and river longitudinal profile.

The third group involves problems wherein relations are derived between entropy and design variables and then relations between design variables and system characteristics are established. Examples of such problems include geomorphologic relations for elevation, slope, and fall and evaluation of water distribution systems. In hydraulics, the entropy theory has been applied to address problems from the second and third groups.

1.6 Hypothesis on the Cumulative Distribution Function

The second concept deals with the formulation of a hypothesis on the cumulative distribution function (CDF) of flux in terms of concentration, as for example, the CDF of velocity of flow in open channels in terms of depth of flow, the CDF of discharge in terms of flow stage or depth, the CDF of sediment concentration in terms of flow depth, and so on. Now, depending on the problem at hand, the cumulative distribution function (CDF) of X, say flux, can be hypothesized as

$$F(x) = a + b\left(\frac{h}{D}\right)^c \tag{1.71}$$

where D is the maximum value of h, say concentration, and a, b, and c are constants. A frequently used form of equation (1.71) is such that $a = 0$, $b = c = 1$; or $a = 1$, $b = -1$, and $c = 1$; or $a = 0$, $b = -1$ and $c = 1$. In the first case, equation (1.71) expresses the notion that the probability of flux X, which is less than or equal to a given value x, is equal to the concentration h at $X = x$ divided by the maximum concentration, D. From a sampling standpoint, all values of h are equally likely to be sampled; in other words, h follows a uniform distribution. This is a simple hypothesis and may not be entirely true. There is little physical justification for equation (1.71), except that it has been found to be adequate for several hydraulic problems (Cui and Singh 2012).

Example 1.7 Using field measurements of velocity as shown in Table 1-35, plot equation (1.71) and show values of parameters a, b, and c.

Table 1-35 *Field measurements of velocity.*

y/D	F	u (m/s)	y/D	F	u (m/s)
0	0.05	0	0.3704	0.50	0.266
0.0925	0.07	0.232	0.4444	0.53	0.281
0.1111	0.10	0.229	0.5185	0.58	0.343
0.1296	0.11	0.203	0.6111	0.65	0.399
0.1481	0.14	0.189	0.7037	0.70	0.358
0.1667	0.17	0.222	0.7963	0.825	0.388
0.1852	0.20	0.270	0.8889	0.825	0.388
0.2222	0.30	0.248	0.9444	0.95	0.406
0.2593	0.35	0.240	1	1	0.377
0.3148	0.37	0.222			

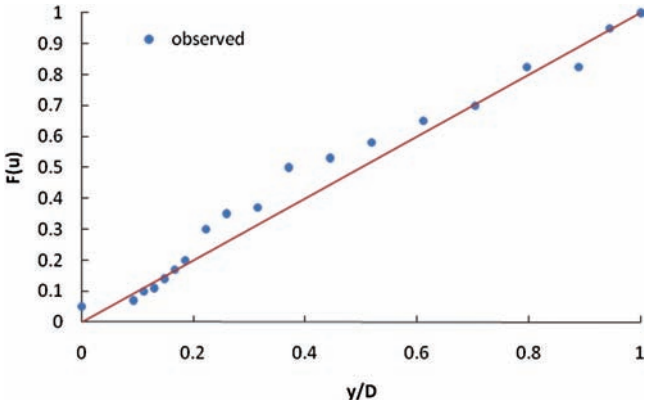

Figure 1-5 *Relation between* F(u) *and* y/D.

Solution The velocity data were obtained for a cross section at Ghamasiab River in Iran. For this data set, using the least-squares method, parameters were found to be $a = 0$, $b = 1$, and $c = 1$. Equation (1.71) is plotted, as shown in Fig. 1-5.

1.7 Methodology for Application of Entropy Theory

The methodology for application of the entropy theory as outlined involves the following steps:

1. Expression of the random variable and then its Shannon entropy.
2. Specification of constraints.
3. Maximization of entropy using the method of Lagrange multipliers.
4. Determination of the entropy-based PDF and determination of entropy in terms of constraints.
5. Determination of the Lagrange multipliers in terms of constraints.
6. Formulation of CDF hypothesis.
7. Derivation of desired relations.

Step 6 is described in the preceding section, Step 7 is obtained with the use of Step 6, and the remainder of these steps are briefly discussed in what follows.

1.7.1 Defining the Random Variable

If flux is the design variable, then time-averaged or space-averaged flux is assumed as a random variable. Let X be flux and h be the associated concentration. In many problems, the time-averaged flux can be considered as a random

variable. For example, in open channel flow, the time-averaged velocity at a given cross section can be considered as a random variable. If X is space-averaged, it can be considered as a random variable. For example, space-averaged capacity rate of seepage through a dam can be considered as a random variable. Likewise, space-averaged soil moisture can be considered as a random variable. This assumption is fundamental to the next step and is the basis of entropy-based analysis. How valid this assumption is may depend on the problem at hand. What is interesting, however, is that the final result does not seem to be greatly affected by the perfect or less than perfect validity of this assumption—a marvelous attribute of the entropy theory.

1.7.2 Specification of Constraints

The second concept involves specification of constraints in terms of the laws of mathematical physics—mass conservation, momentum conservation, and energy conservation—or constitutive laws. These three concepts link statistical analysis based on entropy with physical concepts in hydraulic engineering.

The information on a random variable can be expressed in many different ways, but it is more convenient to express it in terms of moments, such as mean, variance, covariance, cross covariance, and linear combinations of these statistics. Thus, constraints encode relevant information. If observations are available, then one way to express information on the random variable is in terms of constraints C_r, $r = 0, 1, 2, \ldots, n$, defined as

$$C_0 = \int_a^b f(x)\,dx = 1 \tag{1.72}$$

$$C_r = \int_a^b g_r(x) f(x)\,dx = \overline{g_r(x)},\ r = 1, 2, \ldots, n \tag{1.73}$$

where $g_r(x)$, $r = 1, 2, \ldots, n$ represent some functions of x, n denotes the number of constraints, and $\overline{g_r(x)}$ is the expectation of $g_r(x)$. Equation (1.72) states that the PDF must satisfy the total probability. Other constraints, defined by equation (1.73), have physical meaning. For example, if $r = 1$ and $g_1(x) = x$, equation (1.73) would correspond to the mean $\bar{x}$; likewise, for $r = 2$ and $g_2(x) = (x - \bar{x})^2$, it would denote the variance of x. For most hydraulic engineering problems, more than two or three constraints are not needed.

1.7.3 Maximization of Entropy

To obtain the least-biased $f(x)$, the entropy given by equation (1.18) is maximized, subject to equations (1.72) and (1.73), and one simple way to achieve the

maximization is the use of the method of Lagrange multipliers. To that end, the Lagrangian function L can be constructed as

$$L = -\int_a^b f(x)\ln f(x)dx - (\lambda_0 - 1)\left[\int_a^b f(x)dx - C_0\right] - \sum_{r=1}^{n}\lambda_r\left[\int_a^b f(x)g_r(x)dx - C_r\right] \tag{1.74}$$

where $\lambda_1, \lambda_2, \ldots, \lambda_n$ are the Lagrange multipliers. To obtain an $f(x)$ that maximizes L, one may recall the Euler–Lagrange calculus of variation, and, therefore, one differentiates L with respect to $f(x)$ (noting X as a parameter and f as a variable), equates the derivative to zero, and obtains the following:

$$\frac{\partial L}{\partial f} = 0 \Rightarrow -[1 + \ln f(x)] - (\lambda_0 - 1) - \sum_{r=1}^{n}\lambda_r g_r(x) = 0 \tag{1.75}$$

1.7.4 Probability Distribution

Equation (1.75) leads to the probability density function of X in terms of the given constraints:

$$f(x) = \exp\left[-\lambda_0 - \sum_{r=1}^{n}\lambda_r g_r(x)\right] \tag{1.76}$$

where the Lagrange multipliers λ_r, $r = 0, 1, 2, \ldots, n$, can be determined with the use of equations (1.72) and (1.73). Equation (1.76) is also written as

$$f(x) = \frac{1}{Z(\lambda_1, \lambda_2, \ldots, \lambda_n)}\exp\left[-\sum_{r=1}^{n}\lambda_r g_r(x)\right] \tag{1.77}$$

where $Z = \exp(\lambda_0)$ is called the partition function. Integration of equation (1.76) leads to the cumulative distribution function or simply the probability distribution of X, $F(x)$ as

$$F(x) = \int_a^x \exp\left[-\lambda_0 - \sum_{r=1}^{n}\lambda_r g_r(x)\right]dx \tag{1.78}$$

Substitution of equation (1.76) in equation (1.18) results in the maximum entropy of $f(x)$ or X as

$$H = \lambda_0 + \sum_{r=1}^{n}\lambda_r\overline{g_r(x)} = \lambda_0 + \sum_{r=1}^{n}\lambda_1 E[g_r(x)] = \lambda_0 + \sum_{r=1}^{n}\lambda_r C_r \tag{1.79}$$

where $E[g(x)]$ is the expectation of $g(x)$. Equation (1.79) shows that the entropy of the probability distribution of X depends only on the specified constraints,

since the Lagrange multipliers themselves can be expressed in terms of the specified constraints. Equations (1.18), (1.72), (1.73), (1.76), and (1.79) constitute the building blocks for application of the entropy theory. Entropy maximization results in the probability distribution that is most conservative and hence most informative. If a distribution with lower entropy were chosen, then it would mean the assumption of information that is not available. Conversely, a distribution with higher entropy would violate the known constraints. Thus, it can be stated that the maximum entropy leads to a probability distribution of a particular macro state among all possible configurations of events under consideration.

1.7.5 Determination of Lagrange Multipliers

Equation (1.76) is the POME-based probability distribution containing Lagrange multipliers λ_0, λ_1, λ_2, …, λ_n as parameters that can be determined by inserting equation (1.76) in equations (1.72) and (1. 73):

$$\exp(\lambda_0) = \int_a^b \exp\left[-\sum_{r=1}^{n} \lambda_r g_r(x)\right] dx, \quad r = 1, 2, \ldots, n \tag{1.80}$$

and

$$C_r = \int_a^b g_r(x) \exp\left[-\sum_{r=1}^{n} \lambda_r g_r(x)\right] dx, r = 1, 2, \ldots, n \tag{1.81}$$

Equation (1.80) can be written for the zeroth Lagrange multiplier as

$$\lambda_0 = \ln \int_a^b \exp\left[-\sum_{r=1}^{n} \lambda_r g_r(x)\right] dx, r = 1, 2, \ldots, n \tag{1.82}$$

Equation (1.82) expresses the partition function Z as

$$Z(\lambda_1, \lambda_2, \ldots, \lambda_m) = \int_a^b \exp\left[-\sum_{r=1}^{m} \lambda_r g_r(x)\right] dx \tag{1.83}$$

Differentiating equation (1.83) with respect to λ_r, one gets

$$\frac{\partial \lambda_0}{\partial \lambda_r} = -\frac{\int_a^b g_r(x) \exp\left[-\sum_{r=1}^{n} \lambda_r g_r(x)\right] dx}{\int_a^b \exp\left[-\sum_{r=1}^{n} \lambda_r g_r(x)\right] dx}, r = 1, 2, \ldots, n \tag{1.84}$$

Multiplying the numerator as well as the denominator of equation (1.84) by $\exp(-\lambda_0)$, one obtains

$$\frac{\partial \lambda_0}{\partial \lambda_r} = -\frac{\int_a^b g_r(x)\exp\left[-\lambda_0 - \sum_{r=1}^{n}\lambda_r g_r(x)\right]dx}{\int_a^b \exp\left[-\lambda_0 - \sum_{r=1}^{n}\lambda_r g_r(x)\right]dx}, r = 1, 2, \ldots, n \tag{1.85}$$

The denominator in equation (1.85) equals unity by virtue of equation (1.72). Therefore, equation (1.85) becomes

$$\frac{\partial \lambda_0}{\partial \lambda_r} = -\int_a^b g_r(x)\exp\left[-\lambda_0 - \sum_{r=1}^{n}\lambda_r g_r(x)\right]dx, r = 1, 2, \ldots, n \tag{1.86}$$

Note that substitution of equation (1.76) in equation (1.73) yields

$$C_r = \int_a^b g_r(x)\exp\left[-\lambda_0 - \sum_{r=1}^{n}\lambda_r g_r(x)\right]dx, r = 1, 2, \ldots, n \tag{1.87}$$

Therefore, equations (1.86) and (1.87) yield

$$\frac{\partial \lambda_0}{\partial \lambda_r} = -C_r, r = 1, 2, \ldots, n \tag{1.88}$$

Likewise, equation (1.83) can be written analytically as

$$\lambda_0 = \lambda_0(\lambda_1, \lambda_2, \ldots, \lambda_n) \tag{1.89}$$

Equation (1.89) can be differentiated with respect to λ_r, $r = 1, 2, \ldots, n$, and each derivative can be equated to the corresponding derivative in equation (1.88). This correspondence would lead to a system of $n - 1$ equations with $n - 1$ unknowns, whose solution would lead to the expression of Lagrange multipliers in terms of constraints.

Example 1.8 Assume a discrete random variable X, which takes on values x_1, x_2, x_3, …, x_N with probabilities p_1, p_2, p_3, …, p_N. The expected value or the average value of the variable is known from observations. What should be its probability distribution?

Solution The expected value of the variable is known:

$$p_1x_1 + p_2x_2 + \ldots + p_Nx_N = \sum_{i=1}^{N} x_i p_i = \bar{x} \tag{1.90}$$

Of course, the total probability law holds

$$\sum_{i=1}^{N} p_i = 1, \quad p_i \geq 0, i = 1, 2, \ldots, N \tag{1.91}$$

The objective is to derive the POME-based distribution $P = \{p_1, p_2, \ldots, p_N\}$, subject to equations (1.90) and (1.91). In other words, one maximizes the Shannon entropy given by equation (1.4), subject to equations (1.90) and (1.91).

Following the POME formalism, one constructs the Lagrangian L:

$$L = -\sum_{i=1}^{N} p_i \ln p_i - (\lambda_0 - 1)\left(\sum_{i=1}^{N} p_i - 1\right) - \lambda_1\left(\sum_{i=1}^{N} p_i x_i - \bar{x}\right) \tag{1.92}$$

Differentiating equation (1.92) with respect to p_i, $i = 1, 2, \ldots, N$, and equating each derivative to zero, one obtains:

$$\frac{\partial L}{\partial p_i} = 0 \Rightarrow -\ln p_i - \lambda_0 - \lambda_i x_i = 0, \; i = 1, 2, \ldots, N \tag{1.93}$$

Equation (1.93) yields

$$p_i = \exp[-\lambda_0 - \lambda_1 x_i], \; i = 1, 2, \ldots, N \tag{1.94}$$

Equation (1.94) contains parameters λ_0 and λ_1, which are determined with the use of equations (1.90) and (1.91). Inserting equation (1.94) in equation (1.91), one gets

$$\exp(-\lambda_0) = \left[\sum_{i=1}^{N} \exp(-\lambda_1 x_i)\right]^{-1} \tag{1.95}$$

When equation (1.95) is substituted in equation (1.94), the result is

$$p_i = \frac{\exp(-\lambda_i x_i)}{\sum_{i=1}^{N} \exp(-\lambda_1 x_i)} \tag{1.96}$$

Equation (1.96) is called the Maxwell–Boltzmann (M–B) distribution, which is used in statistical mechanics.

Now its parameter, λ_1, must be determined in terms of constraint $\bar{x}$. Inserting equation (1.94) in equation (1.90), one gets

$$\sum_{i=1}^{N} x_i \exp(-\lambda_0 - \lambda_1 x_i) = \bar{x} \tag{1.97}$$

Taking advantage of equation (1.95), equation (1.97) yields

$$\frac{\sum_{i=1}^{N} x_i \exp(-\lambda_i x_i)}{\sum_{i=1}^{N} \exp(-\lambda_1 x_i)} = \bar{x} \tag{1.98}$$

Equation (1.98) permits the estimation of λ_1 in terms of $\bar{x}$. Note that if $\lambda_1 = 0$, clearly equation (1.96) would be a rectangular distribution with $p_i = 1/N$. If λ_1 is negative, then the probability increases as x_i increases, and if $\lambda_1 > 0$, then the

probability decreases as x_i increases. In physics, the M–B distribution has been used to derive the microstates of a system on the basis of some knowledge about macroscopic data. For example, if a system had a large number of particles, each with an energy level, then the M–B distribution would be used to determine the probability distribution of energy levels of particles, provided that the expected energy of the system was somehow known. Fiorentino et al. (1993) used the M–B distribution to describe the probability distribution of elevations of links in a river basin if the mean basin elevation was known.

Example 1.9 Consider a random variable X varying over a semi-infinite interval $(0, \infty)$ and having a probability density function (PDF) $f(x)$. From observations, the expected value of X, $E[x]$, is known. Derive the PDF $f(x)$ of X.

Solution In this case, the constraint equation is given as

$$\int_0^\infty xf(x)dx = E[x] = \bar{x} = k \tag{1.99}$$

The Shannon entropy is given by equation (1.18), where

$$\int_0^\infty f(x)dx = 1 \tag{1.100}$$

The least-biased $f(x)$ is determined by maximizing equation (1.18), subject to equations (1.99) and (1.100). To that end, the Lagrangean L is constructed as

$$L = -\int_0^\infty f(x)\ln f(x)dx - (\lambda_0 - 1)\left[\int_0^\infty f(x)dx - 1\right] - \lambda_1\left[\int_0^\infty xf(x)dx - k\right] \tag{1.101}$$

Taking the derivative of L with respect to $f(x)$ and equating it to 0, one obtains

$$\frac{\partial L}{\partial f(x)} = 0 \Rightarrow -[1 + \ln f(x)] - (\lambda_0 - 1) - \lambda_1 x = 0 \tag{1.102}$$

Therefore,

$$f(x) = \exp(-\lambda_0 - \lambda_1 x) \tag{1.103}$$

Equation (1.103) is the POME-based distribution with λ_0 and λ_1 as parameters.

Substituting equation (1.103) in equation (1.100), one obtains

$$\int_0^\infty \exp(-\lambda_0 - \lambda_1 x)dx = \lambda_1 \exp(\lambda_0) = 1 \tag{1.104}$$

Substituting equation (1.104) in equation (1.103), one gets

$$f(x) = \lambda_1 \exp(-\lambda_1 x) \tag{1.105}$$

Inserting equation (1.105) in equation (1.100), one gets

$$\int_0^\infty \lambda_1 x \exp(-\lambda_1 x) dx = k \quad or\ \lambda_1 = \frac{1}{k} \tag{1.106}$$

Thus equation (1.106) becomes

$$f(x) = \frac{1}{k} \exp\left(-\frac{x}{k}\right), \quad k = \bar{x} \tag{1.107}$$

which is the exponential distribution.

The entropy-based method of deriving a probability distribution can also be used for estimating parameters of a distribution. In that case, first the constraints for the distribution must be derived. Then, distribution parameters can be expressed in terms of these constraints.

Appendix 1.1

Counts of Event Occurrences

n_i, n_j, n_k: the counts of event $X = x_i$, $Y = y_j$, and $Z = z_k$ occurrences, respectively.
n_{ij}, n_{ik}, n_{jk}: the counts of joint event $[X = x_i, Y = y_j]$, $[X = x_i, Z = z_k]$, $[Y = y_j, Z = z_k]$ occurrences, respectively.
n_{ijk}: the counts of joint event $[X = x_i, Y = y_j,$ and $Z = z_k]$ occurrences.
n: the total number of events.

S-Notation

$$s_X = \frac{1}{n} \sum_i n_i \log_2 n_i$$

$$s_Y = \frac{1}{n} \sum_j n_j \log_2 n_j$$

$$s_Z = \frac{1}{n} \sum_k n_k \log_2 n_k$$

$$s_{XY} = \frac{1}{n} \sum_i \sum_j n_{ij} \log_2 n_{ij}$$

$$s_{YZ} = \frac{1}{n} \sum_j \sum_k n_{jk} \log_2 n_{jk}$$

$$s_{XZ} = \frac{1}{n} \sum_i \sum_k n_{ik} \log_2 n_{ik}$$

$$s_{XYZ} = \frac{1}{n} \sum_i \sum_j \sum_k n_{ijk} \log_2 n_{ijk}$$

$$s = \log_2 n$$

S-Notation for Bivariate and Trivariate Transinformation

$$T(X;Y) = s - s_X - s_Y + s_{XY}$$
$$T(X;Z) = s - s_X - s_Z + s_{XZ}$$
$$T(Y;Z) = s - s_Y - s_Z + s_{YZ}$$
$$T(Y,Z;X) = s - s_X - s_{YZ} + s_{XYZ}$$
$$T(X,Z;Y) = s - s_Y - s_{XZ} + s_{XYZ}$$
$$T(X,Y;Z) = s - s_Z - s_{XY} + s_{XYZ}$$
$$T_Z(X;Y) = s_Z - s_{XZ} - s_{YZ} + s_{XYZ}$$
$$T_X(Y;Z) = s_X - s_{YX} - s_{ZX} + s_{XYZ}$$
$$T_Y(X;Z) = s_Y - s_{XY} - s_{ZY} + s_{XYZ}$$

S-Notation for Interaction Information

$$A(X,Y,Z) = -s + s_X + s_Y + s_Z - s_{XY} - s_{YZ} - s_{XZ} + s_{XYZ}$$

Relationship between Trivariate Transinformation and Its Bivariate Component

$$T(X,Z;Y) = T(X;Y) + T(Z;Y) + A(X,Y,Z)$$
$$T(X,Z;Y) = T_Z(X;Y) + T_X(Z;Y) - A(X,Y,Z)$$
$$T(X,Y;Z) = T(X;Z) + T(Y;Z) + A(X,Y,Z)$$
$$T(X,Y;Z) = T_Y(X;Z) + T_X(Y;Z) - A(X,Y,Z)$$
$$T(Y,Z;X) = T(Y;X) + T(Z;X) + A(X,Y,Z)$$
$$T(Y,Z;X) = T_Z(Y;X) + T_Y(Z;X) + A(X,Y,Z)$$

Questions

Q1.1 If an event occurs with a probability $p_1 = 0.1$, then compute its entropy. Likewise, if six different events occur with probabilities, respectively, of $p_2 = 0.2$, $p_3 = 0.4$, $p_4 = 0.5$, $p_5 = 0.6$, $p_6 = 0.8$, and $p_7 = 0.9$, then compute entropy for each value of p. What can be said about the uncertainty, degree of surprise, and information with respect to each event?

Q1.2 Compute the value of information reduction. Table 1-36 shows discharge values for two stations, A and B, for 30 years.

Q1.3 Compute joint entropy using discharge values in Q1.2.

Q1.4 Compute conditional entropy using the data in Q1.2.

Table 1-36 *Discharge values at two stations, A and B.*

A (m^3/s)			B (m^3/s)		
78.7	57.1	142	73.2	51.8	140
79.2	127	31.9	54.5	165	116
87.8	360	150	55.6	1210	194
33.9	156	144	56.8	2270	322
10	178	60.9	67.6	234	225
7.45	340	138	59	354	242
20.7	434	160	52.6	953	137
62.7	610	168	119	1280	286
25.6	229	132	89	3250	258
15.9	246	1200	93.3	1340	6860
77.3	739	1440	99.9	865	2350
19.7	459	1440	103	1220	2650
166	507	1440	130	2730	2000
124	597	2330	154	917	2030
17.6	606	3660	124	1690	6700
33.6	574	5550	153	1690	7060
18.9	852	7780	144	1900	5200

Q1.5 Compute transinformation using the data in Q1.2.

Q1.6 Compute the CDF for velocity as a function of flow depth for the data on velocity and depth given in Table 1-37.

Q1.7 Consider data in Table 1-38 on flow discharge at three stations (A, B, and C) for a river in Texas. Compute marginal entropies of stations A, B, and C. Then compute conditional entropies of $A \mid B$, $B \mid C$, $A \mid C$. Then compute joint entropies $H(A, B)$, $H(B, C)$, $H(A, C)$. Also, compute transinformation $T(A, B)$, $T(B, C)$, $T(A, C)$.

Q1.8 Using the entropy theory, compute the probability density function of a random variable whose mean and variance are known. Compute the Lagrange multipliers and the partition function and provide their physical interpretations.

Q1.9 Using the entropy theory, compute the probability density function of a random variable whose mean and the mean of logarithmic values of the variable are known. Compute the Lagrange multipliers and the partition function, and provide their physical interpretations.

Table 1-37 *Velocity measurements.*

Depth (ft)	Velocity (ft/s)	Depth (ft)	Velocity (ft/s)
0.006	2.221	0.045	5.075
0.009	2.497	0.050	5.298
0.011	2.720	0.054	5.522
0.011	2.858	0.064	5.806
0.015	2.964	0.074	6.090
0.017	3.329	0.084	6.293
0.019	3.573	0.095	6.516
0.024	3.898	0.104	6.699
0.034	4.519	0.124	7.113
0.040	4.831		

Table 1-38 *Discharge values (m^3/s) (arranged in seven class intervals) from 1980 to 2009 at stations* A, B, *and* C, *and their relative frequencies.*

Discharge Values (m^3/s)	*A*		*B*		*C*	
	Frequency	Relative Frequency	Frequency	Relative Frequency	Frequency	Relative Frequency
0–5,000	224	0.95	216	0.92	215	0.91
5,000–10,000	7	0.03	7	0.03	2	0.01
10,000–15,000	2	0.01	5	0.02	5	0.02
15,000–20,000	1	0.005	0	0	2	0.01
20,000–25,000	0	0	5	0.02	2	0.01
25,000–30,000	1	0.005	0	0	7	0.03
30,000–35,000	0	0	2	0.01	2	0.01
Sum	235	1.00	235	1.00	235	1.00

Q1.10 Using the entropy theory, compute the probability density function of a random variable where nothing is known about the variable. The variable takes on values over a finite interval. Compute the Lagrange multipliers and the partition function, and provide their physical interpretations.

Q1.11 Using the entropy theory, compute the probability density function of a random variable whose mean and variance are known. However, the variable takes on values over the semi-infinite domain, i.e., 0 to infinity. Compute the Lagrange multipliers and the partition function, and provide their physical interpretations.

References

Batty, M. (2010). "Space, scale, and scaling in entropy maximizing." *Geograph. Anal.*, 42, 395–421.

Cui, H., and Singh, V. P. (2012). "On the cumulative distribution function for entropy-based hydrologic modeling." *Trans. ASABE*, 55(2), 429–438.

Fano, R.M. (1949). "The transmission of information." *MIT Research Laboratory of Electronics Technical Report No. 65,* Cambridge, MA.

Fass, D. M. (2006). *Human sensitivity to mutual information*. Rutgers, New Brunswick, NJ.

Fiorentino, M., Claps, P., and Singh, V. P. (1993). "An entropy-based morphological analysis of river-basin networks." *Water Resour. Res.*, 29(4), 1215–1224.

Han, T. S. (1980). Multiple mutual informations and multiple interactions in frequency data. *Inform. Contr.*, 46, 26–45.

Harmancioglu, N. B., Singh, V. P., and Alpaslan, N. (1992). "Versatile uses of the entropy concept in water resources." *Entropy and energy dissipation in water resources*, V. P. Singh and M. Fiorentino, eds., Kluwer Academic, Dordrecht, The Netherlands, 91–118.

Jakulin, A., and Bratko, I. (2003). *Quantifying and visualizing attribute interactions*. ArXiv preprint cs.AI/0308002.

Jakulin, A., and Bratko, I. (2004). *Testing the significance of attribute interactions*. ACM Int. Conf. Proc. Series, Banff, Canada.

Jaynes, E. T. (1957a). "Information theory and statistical mechanics, I." *Phys. Rev.*, 106, 620–630.

Jaynes, E. T. (1957b). "Information theory and statistical mechanics, II." *Phys. Rev.*, 108, 171–190.

Jaynes, E. T. (1958). "Probability theory in science and engineering." *Colloquium lectures in pure and applied science*, 4, Socony Mobil Oil Co., Dallas, TX.

Jaynes, E. T. (1982). "On the rationale of maximum entropy methods." *Proc., IEEE*, 70, 939–952.

Jaynes, E. T. (2003). *Probability theory*. Cambridge University Press, Cambridge, UK.

Kapur, J. N. (1989). *Maximum entropy models in science and engineering*. Wiley Eastern, New Delhi.

Kullback, S. (1959). *Information theory and statistics*. Wiley, New York.

Kullback, S., and Leibler, R.A. (1951). On information and sufficiency. *Ann. Math. Stat.*, 22, 79–86.

Lathi, B. P. (1969). *An introduction to random signals and communication theory*. International Textbook, Scranton, PA.

Lindley, D.V. (1956). On a measure of the information provided by an experiment. *Ann. Math. Stat.*, 22, 79–86.

Lindley, D.V. (1961). The use of prior probability distributions in statistical inference and decision. *Proc., 4th Berkeley Symposium on Math., Stat., Probabil.*, 1, 895–904, University of California, Berkeley, CA.

McGill, W. J. (1953). Multivariate transmission of information and its relation to analysis of variance. *Human Factors Operations Research Laboratories Report 32*, MIT Press, Cambridge, MA.
McGill, W. J. (1954). "Multivariate information transmission." *Psychometrica*, 19(2), 97–116.
Papalexiou, S. M., and Koutsoyiannis, D. (2012). "A worldwide investigation of the probability distribution of daily rainfall." *Adva. Water Resour.*, 45, 51–57.
Shannon, C. E. (1948). "The mathematical theory of communications, I and II." *Bell Sys. Tech. J.*, 27, 379–423.
Shannon, C. E., and Weaver, W. (1949). *The mathematical theory of communication*. University of Illinois Press, Urbana, IL.
Singh, V. P. (1997). "The use of entropy in hydrology and water resources." *Hydrol. Proc.*, 11, 587–626.
Singh, V. P. (2011). "Hydrologic synthesis using entropy theory: Review." *J. of Hydrol. Eng.*, 16(5), 421–433.
Singh, V. P., and Fiorentino, M. (1992). "A historical perspective of entropy applications in water resources." *Entropy and energy dissipation in water resources*, V. P. Singh and M. Fiorentino, eds., Kluwer Academic, Dordrecht, The Netherlands, 21–61.
Srinivasa, S. (2005). *A review on multivariate mutual information*. www3.nd.edu/~jnl/ee80653/Fall2005/tutorials/sunil.pdf, University of Notre Dame, South Bend, IN.
Tribus, M. (1969). *Rational descriptions, decisions and designs*, Pergamon Press, New York.

Additional Reading

Brillouin, L. (1956). *Science and information theory*. Academic Press, New York.
Denbigh, K. G. (1989). "Note on entropy, disorder and disorganization." *Brit. J. Philos. Sci.*, 40, 323–332.
Fast, J. D. (1968). *Entropy: The significance of the concept of entropy and its application in science and technology*. Gordon and Breach, New York.
Fisher, R. A. (1920). "On mathematical foundations of theoretical statistics." *Philos. Trans. Royal Society of London, Series A*, 222, 309–368.
Gull, S. F. (1991). "Some misconceptions about entropy." *Maximum entropy in action*, B. Buck and V. A. McCauley, eds., Oxford Science, 171–186.
Hartley, R. V. L. (1928). "Transmission of information." *Bell Sys. Tech. J.*, 7(3), 535–563.
Kaplan, S., and Garrick, B. J. (1981). "On the quantitative definition of risk." *Risk Anal.*, 1(1), 11–27.
Klir, G. J. (2006). *Uncertainty and information: Foundations of generalized information theory*. Wiley, New York.

Levine, R. D., and Tribus, M., eds. (1978). *The maximum entropy formalism*, MIT Press, Cambridge, MA.

Luce, R. D. (1960). "The theory of selective information and source of its behavioral applications." *Developments in mathematical psychology*, R. D. Luce, ed., Free Press, Glencoe, IL.

Marchand, B. (1972). "Information theory and geography." *Geograph. Anal.*, 4, 234–257.

Ng, S. K. (1996). "Information and system modeling." *Math. Comput. Model.*, 23(5), 1–15.

Pal, N. R., and Pal, S. K. (1991). "Entropy: A new definition and its applications." *IEEE: Trans. Syst., Man, Cybernet.*, 21(5), 1260–1270.

Prigogine, I. (1989). "What is entropy?" *Naturwissenschaften*, 76, 1–8 (in German).

Renyi, A. (1961). "On measures of entropy and information." *Proc., 4th Berkeley Symp. Math., Stat., Prob.*, 1, 547–561.

Rosenthal, H., and Binia, J. (1988). "On the epsilon entropy of mixed random variables." *IEEE Trans. Inform. Theory*, 34(5), 1110–1114.

Singh, V. P. (1998). *Entropy-based parameter estimation in hydrology*, Kluwer Academic, Boston, MA.

Singh, V. P. (2010). "Entropy theory for earth system science modeling." *J. of Indian Geol. Cong.*, 2(2), 5–40, 2010.

Singh, V. P. (2013). *Entropy theory and its application in environmental and water engineering*. Wiley, Chichester, UK.

Sugawara, M. (1971). "Water resources and negentropy." *Proc. Warsaw Symp. Math. Models Hydrol.*, 2, 876–878, IAHS-UNESCO-WM, Warsaw, Poland.

Tsallis, C. (1988). "Possible generalization of Boltzmann–Gibbs statistics." *J. Stat. Phys.*, 52(1/2), 479–487.

Watanabe, S. (1985). *Knowing and guessing*. Wiley, New York.

White, H. (1965). "The entropy of a continuous distribution." *Bull. Math. Biophys.*, 27, 135–143.

Zurek, W. H. (1989). "Algorithmic randomness and physical entropy." *Phys. Rev.*, 40(8), 4731–4751.

This page intentionally left blank

Part 1

Velocity Distributions

This page intentionally left blank

Chapter 2

One-Dimensional Velocity Distributions

Fundamental to hydraulic modeling of flow propagation, sediment transport, pollutant transport, and river behavior is the velocity distribution in river cross sections. The velocity distribution is influenced by the hydraulics of flow, which entails three classes of variables relating to (1) geometry, (2) flow, and (3) fluid. Geometry-related variables include the depth of flow, hydraulic depth, stage, top width, bottom width, cross-sectional area, wetted perimeter, hydraulic radius, bed roughness, and bed slope. The bed forms, side slope, and vegetation in the channel also influence the velocity distribution. The variables in the flow class are discharge, velocity, shear force (stress), drag, lift force, water surface slope, and energy grade line slope. The fluid-related variables are density, specific weight (or weight density), specific gravity, viscosity, compressibility, and temperature. The water flowing in the channel is laden with sediment and may also be carrying pollutants, including biological, physical, and chemical—organic and inorganic. The velocity distribution of clear-water flow is not the same as that of mixed-water flow. Furthermore, flow in open channels can be characterized by nondimensional parameters defined by grouping some of these variables. The most commonly used nondimensional parameters are the relative roughness, the Reynolds number (R_n) (the ratio of the inertial force to the viscous force), Froude number (F_r) (the ratio of inertial force to the gravitational force), Euler number (the ratio of kinetic to potential energy difference or the ratio of pressure and gravity force difference to the inertial force), Weber number (the ratio of inertial force to the surface tension force),

Richardson number (the ratio of gravitational acceleration times the gradient of density in vertical direction to the density times the square of the gradient of velocity in the vertical direction), Mach number (the ratio of the inertial force to the compression force), and the Cauchy number (the square of the Mach number) (Cruise et al. 2007).

The flow in an open channel at a given time and location can be laminar, turbulent, or mixed (transitional). Based on the value of the Reynolds number, this classification of flows is laminar ($R_n \leq 500$), transient ($500 \leq R_n \leq 2000$), and turbulent ($R_n \geq 2000$) in pipe flow. However, in open-channel flow where the characteristic length may be defined by hydraulic mean depth, the classification of flows is laminar ($R_n \leq 1000$), transient ($1000 \leq R_n \leq 12500$), and turbulent ($R_n \geq 12500$). For both pipe and channel flows, these ranges of R_n are only approximate. Likewise, flows can be classified into subcritical (tranquil) ($F_r < 1$), critical ($F_r = 1$), and supercritical ($F_r > 1$), depending on the value of the Froude number. Further classification of open-channel flow can be based on the variability of velocity (or flow depth) in time as steady or unsteady flow and in space as uniform or varied (nonuniform) flow. Thus, steady flow can be uniform—a rare occurrence—or nonuniform—a usual occurrence that itself can be gradually varied or rapidly varied. Likewise, unsteady flow can be uniform or nonuniform—again gradually varied or rapidly varied (Chow 1959; Henderson 1966; Singh 1996).

The velocity distribution varies from one class of flow to another. Fundamental to the flow and its velocity distribution is the flow resistance. For example, the flow in open channels on alluvial sand beds is generally hydraulically rough, and, therefore, turbulent flow prevails for most natural conditions. If the flow is laminar, then velocity can be defined accurately. However, in turbulent flow, the velocity vector is not constant, and the velocity fluctuates both spatially and temporally. The discussion in this chapter is restricted to time-averaged velocity at a given location.

Chiu (1987) was probably the first to use entropy and the principle of maximum entropy (POME) to derive the probability density function of velocity, subject to mass conservation. He then derived the one-dimensional (1-D) velocity distribution as a function of depth. Barbé et al. (1991) extended Chiu's work by incorporating constraints based on the conservation of mass, momentum, and energy. Chiu and his associates have since extended Chiu's work to a variety of issues related to open-channel flow and sediment and pollutant concentration (Chiu 1988, 1989, 1991; Chiu and Murray 1992; Chiu and Said 1995; Chiu et al. 2000; Chiu and Tung 2002; Chiu and Chen 2003; Chen and Chiu 2004; Chiu et al. 2005). Chiu's work has been used by Xia (1997) for establishing the relation between mean and maximum velocities, Moramarco et al. (2004) for estimating mean velocity, Greco (1999) for velocity distribution in a river, Choo (2000) for sediment discharge measurements, and Moramarco and Singh (2001) for estimation of discharge at remote locations. We closely follow Chiu's work and ensuing works by others here. Before deriving velocity distributions, we briefly review concepts of mass, momentum, and energy conservation.

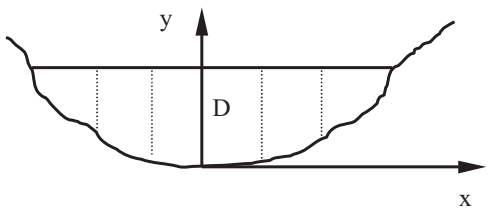

Figure 2-1 *A typical channel cross section.*

2.1 Preliminaries

Consider a typical channel cross section, as shown in Fig. 2.1. For purposes of deriving 1-D velocity distribution, we assume that the flow in an open channel is uniform with a flow depth D, and the velocity u (time-averaged) at a given location monotonically increases with depth y from zero at the channel bed to a maximum value u_D, at the water surface. Thus, the velocity u at any distance y from the bed is less than the velocity u_1 at another distance, say y_1, greater than y. The velocity is assumed to be zero at the bed because of the maximum boundary shear and maximum at the water surface because of the minimum boundary shear and when the water–air interface is neglected. Thus, the maximum velocity at the water surface is an assumption. In reality, the maximum velocity occurs somewhere between 10% and 40% of the flow depth below the water surface, depending on the channel aspect ratio (width/depth).

First, recall the flux of mass, momentum, and energy passing through an elemental area $dA = dyB$, where A is the cross-sectional area (L^2) (here L is the length), B is the flow width (L), and y is the flow depth (L). The mass of fluid m (kg) passing through this elemental area dA (L^2) at a velocity u (L/T) in a time dt (T) is $m = \rho(udt)(dA)$, where ρ is the mass density (kg/L^3) or the mass (kg) per unit volume (L^3), and udt is the distance (L) traversed by the mass of water m in time dt. Similarly, the momentum (kg-L/T) in time dt equals $mu = \rho u^2(dt)(dA)$, and the kinetic energy (kg-L^2/T^2) is represented as $(1/2)mu^2 = (1/2)\rho u^3(dt)(dA)$. Integrating over the elemental area and dividing by dt, one gets the expressions for the fluxes of mass, momentum, and energy, respectively, as follows:

$$\text{mass/time} = \text{mass flux} = \rho\int_A udA = \rho KAu_m = \rho KQ \tag{2.1}$$

$$\text{Momentum/time} = \text{momentum flux} = \rho\int_A u^2 dA = \rho\beta Au_m^2 = \rho\beta Qu_m \tag{2.2}$$

$$\text{Kinetic energy/time} = \text{kinetic energy flux} = \frac{1}{2}\rho\int_A u^3 dA = \frac{1}{2}\rho\alpha Au_m^3 = \frac{1}{2}\rho\alpha Qu_m^2 \tag{2.3}$$

where u_m is the cross-sectional average velocity (L/T) over the cross-sectional area, $Q = Au_m$ is discharge, K is the mass distribution factor (dimensionless), β is the momentum distribution factor (dimensionless), and α is the energy distribution factor (dimensionless).

By definition, one can write the cross-sectional average velocity as

$$u_m = \frac{1}{A}\int_A u dA \tag{2.4}$$

The volume per unit time is defined as discharge or quantity of flow per unit time:

$$Q = \int_A u\, dA = Au_m \tag{2.5}$$

Distribution factors, K, β and α, can be evaluated from, respectively, equations (2.1), (2.2), and (2.3) by noting equations (2.4) and (2.5) as

$$K = \frac{1}{A}\int\left(\frac{u}{u_m}\right)dA = \frac{1}{Q}\int u\, dA = 1 \tag{2.6}$$

$$\beta = \frac{1}{A}\int\left(\frac{u}{u_m}\right)^2 dA = \frac{A}{Q^2}\int u^2 dA \tag{2.7}$$

$$\alpha = \frac{1}{A}\int\left(\frac{u}{u_m}\right)^3 dA = \frac{A^2}{Q^3}\int u^3 dA \tag{2.8}$$

It may also be noted that

$$\alpha > \beta > K = 1 \tag{2.9}$$

From 62 current-meter measurements in natural trapezoidal-shaped channels without overbank flow and with no bridge piers or other human-made structures, Franz and Melching (1996) found that 36 of 62 values of β were significantly greater than unity. These channels were compact, and yet β was greater than 1.1 in more than half of the channel measurements and greater than 1.2 for 8 of them. Likewise, α was greater than 1.3 in 30 and greater than 1.5 in 13 channel measurements, respectively. The average values of β and α were found to be 1.12 and 1.36 for the 62 measurements. It seems logical that these values would be much higher for channels with overbank flow, as is frequently the case in nature. This phenomenon suggests that it may be necessary to include the effect of velocity distribution in equations governing channel flow (Singh 1996).

Xia and Yen (1994) evaluated the effect of flow nonuniformity and approximation of β on computed water surface profiles by conducting a series of experiments on flow routing subject to a variety of downstream boundary conditions. Experiments included routing a sinusoidal stage hydrograph with a peak 2.25 times the base stage through a 54-mile (86.9-km) long channel of rectangular, wide, or trapezoidal geometry. The maximum error in the computed depth was

found to be 0.36% for $\beta = 1.33$, and 1.11% for $\beta = 2$ for a channel with bed slope of 0.00019 and downstream backwater ranging from 0 to 2.53 times the base stage. This result indicates that a reasonable approximation of β should be acceptable for computation of water surface profiles.

Example 2.1 For a rectangular channel cross section with $B = 1.006$ ft, $D = 0.194$ ft, and $Q = 1.139\,\text{ft}^3/\text{s}$, flow measurements are given in Table 2-1. Compute the values of β and α.

Solution For $B = 1.006$ ft, $D = 0.194$ ft, $A = 1.006\,\text{ft}^2$, and $Q = 1.139\,\text{ft}^3/\text{s}$,

$$\beta = \frac{A}{Q^2}\int u^2 dA = \frac{A}{Q^2}\int u^2 B\,dy = \frac{AB}{Q^2}\int u^2 dy = \frac{1.006^2 \times 0.194}{1.139^2}\sum u^2 \Delta y$$

$$\alpha = \frac{A^2}{Q^3}\int u^3 dA = \frac{A^2}{Q^3}\int u^3 B\,dy = \frac{A^2 B}{Q^3}\int u^3 dy = \frac{1.006^3 \times 0.194^2}{1.139^3}\sum u^3 \Delta y$$

To perform numerical integration, set Δy as 0.01 ft. The resulting computation is shown in Table 2-2.

$$\sum u^2 \Delta y = 741.011 \times 0.01 = 7.41$$

$$\sum u^3 \Delta y = 4810.383 \times 0.01 = 48.1$$

$$\beta = \frac{1.006^2 \times 0.194}{1.139^2}\sum u^2 \Delta y = 1.12$$

$$\alpha = \frac{1.006^3 \times 0.194^2}{1.139^3}\sum u^3 \Delta y = 1.25$$

Both β and α are significantly greater than unity; this fact suggests that the momentum distribution and the energy distribution are not uniform in the vertical plane, i.e., there is a lot of turbulence in the flow.

Table 2-1 *Velocity data from experiment S8 of Einstein and Chien (1955) in Example 2.1.*

y (ft)	0.006	0.007	0.008	0.036	0.01	0.014	0.017	0.019	0.029
obs. u (ft/s)	2.467	2.7	2.807	2.983	3.105	3.586	3.941	4.094	4.774
y (ft)	0.034	0.044	0.064	0.079	0.094	0.119	0.144	0.169	0.194
obs. u (ft/s)	5.041	5.423	5.92	6.16	6.37	6.718	6.951	7.195	7.409

Note: obs. = observed.

Table 2-2 *Computation of values for Example 2.1.*

y (ft)	u (ft/s)	u^2 (ft/s)^2	u^3 (ft/s)^3
0	0.000	0.000	0.000
0.01	3.104	9.633	29.898
0.02	4.161	17.311	72.025
0.03	4.826	23.292	112.411
0.04	5.271	27.778	146.406
0.05	5.573	31.054	173.049
0.06	5.822	33.892	197.311
0.07	6.017	36.203	217.825
0.08	6.175	38.130	235.455
0.09	6.315	39.883	251.874
0.1	6.454	41.652	268.815
0.11	6.591	43.444	286.349
0.12	6.725	45.229	304.173
0.13	6.820	46.513	317.220
0.14	6.915	47.815	330.635
0.15	7.011	49.160	344.686
0.16	7.109	50.540	359.292
0.17	7.205	51.917	374.077
0.18	7.291	53.156	387.547
0.19	7.376	54.409	401.335
Sum		741.011	4810.383

2.2 Derivation of One-Dimensional Velocity Distributions

Derivation of a velocity distribution using the entropy theory entails (1) formulation of a hypothesis on the cumulative distribution function (CDF) of velocity in terms of flow depth, (2) expression of the Shannon entropy, (3) specification of constraints, (4) maximization of entropy, (5) derivation of the probability density function (PDF) of velocity, (6) determination of the Lagrange multipliers, and (7) entropy of the velocity distribution. These steps are described in the next sections.

2.2.1 Hypothesis on the Cumulative Distribution Function of Velocity in Terms of Flow Depth

Let the time-averaged velocity be considered as a random variable. It is assumed that all values of y between 0 and D are equally likely to be sampled; in reality, that is not entirely true. Then the probability of velocity being equal to or less than u is y/D; thus the cumulative distribution function (CDF) of velocity, $F(u) = P$(velocity $\leq$ a given value of u), $P =$ probability, can be expressed as

$$F(u) = \frac{y}{D} \tag{2.10}$$

Note that on the right side of equation (2.10) the variable is y, not u. Differentiation of $F(u)$ in equation (2.10) yields the probability density function (PDF) of u, $f(u)$, as

$$f(u) = \frac{dF(u)}{du} = \frac{1}{D}\frac{dy}{du} \quad or \quad f(u) = \left(D\frac{du}{dy}\right)^{-1} \tag{2.11}$$

The term $f(u)du = F(u + du) - F(u)$ denotes the probability of velocity being between u and $u + du$, where du represents a small change in velocity. Equation (2.10) constitutes the fundamental hypothesis that is used for deriving 1-D velocity distributions in this chapter.

Example 2.2 Consider velocity measurements in a river cross section, presented in Table 2-3. Compute the CDF of velocity for these measurements. Verify if the hypothesis expressed by equation (2.10) holds.

Solution Data on flow velocity and the corresponding flow depth are obtained for a cross section of the Ghamasiab River where the maximum flow depth is

Table 2-3 *Velocity measurements in a cross section of the Ghamasiab River, Iran.*

Depth (m)	Velocity (m/s)	Depth (m)	Velocity (m/s)
0.05	0.2	0.2	0.369
0.06	0.229	0.24	0.424
0.07	0.277	0.29	0.41
0.08	0.288	0.34	0.447
0.09	0.299	0.4	0.458
0.11	0.314	0.47	0.483
0.13	0.347	0.55	0.506
0.16	0.366	0.59	0.535

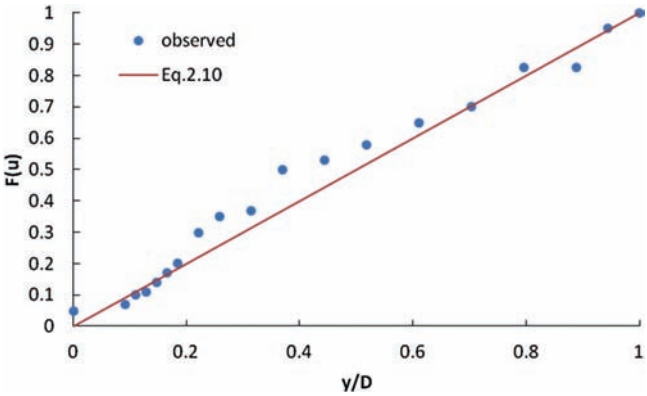

Figure 2-2 *Cumulative (probability) distribution function of velocity as a function of dimensionless flow depth.*

0.59 m. The flow depth is first nondimensionalized by diving by the maximum flow depth $D = 0.59$ m. Then, the cumulative probability distribution of velocity is computed, as shown in Fig. 2-2, which validates equation (2.10) reasonably well.

2.2.2 Expression of the Shannon Entropy

In practice, u is measured discretely. For N discrete measurements of u, the Shannon entropy can be written as

$$H(u) = -k\sum_{i=1}^{N} p(u_i)\log p(u_i) = -\sum_{i=1}^{N} p_i \log p_i \tag{2.12}$$

where $p_i = p(u_i)$ is the probability of $u = u_i$, $i = 1, 2, \ldots, N$; log is the logarithm, usually taken to the base of 2, 10, or e, thus yielding the units of H in bits, decibels, or Napier, respectively; and k is a constant that depends on the base of the logarithm; often it is taken as unity. Here the probability distribution of velocity $U = \{u_1, u_2, \ldots, u_N\}$ can be expressed as $P = \{p_1, p_2, \ldots, p_N\}$. Equation (2.12) can be written for continuous u by noting that $p(u) = f(u)\Delta u$, where Δu is a small quantity and can be represented as du, and the velocity range, $0 \le u \le u_D$, u_D being the upper limit of u, can be divided into N intervals where N is large. Then equation (2.12) becomes

$$H(u) = -k\int_0^{u_D} f(u)\log f(u)\,du + k\log\Delta u \tag{2.13}$$

where k is also taken as unity.

The second term on the right side of equation (2.13), $\log\Delta u$, is either considered small and is, hence, neglected or is considered as base reference above, which $H(u)$ is measured. Thus, equation (2.13) is normally written [with the base e of log] as

$$H(u) = -\int_0^{u_D} f(u) \ln f(u)\, du \tag{2.14a}$$

More generally, equation (2.14a) is expressed as

$$H(u) = -k\int_0^{u_D} f(u) \ln\left[\frac{f(u)}{m(u)}\right] du \tag{2.14b}$$

where $m(u)$ is the invariance measure that ensures the invariance of entropy regardless of the coordinate system and is often taken as unity. It will have the same dimension as $f(u)$.

Thus, equation (2.14a) expresses the relative Shannon entropy for continuous velocity. It may be noted here that it is more convenient to use the continuous form of the Shannon entropy, for the algebra is much simpler, and, hence, equation (2.14a) in place of equation (2.12) will be used henceforth. Equation (2.14a) expresses a measure of uncertainty about $f(u)$ or the average information content of sampled u.

To derive the velocity distribution, the first step is to determine the probability density function of u, $f(u)$. This determination is accomplished by maximizing the Shannon entropy of velocity, $H(u)$. Maximizing $H(u)$ is equivalent to maximizing $[f(u)\ \ln f(u)]$. To maximize $H(u)$, certain constraints need to be satisfied.

2.2.3 Specification of Constraints

For velocity, one can now state the constraints based on hydraulic considerations. The first constraint, C_1, is the total probability:

$$C_1 = \int_0^{u_D} f(u)\, du = 1 = b_1 \tag{2.15}$$

In actuality, C_1 is not a constraint, because $f(u)$ must always satisfy the total probability. Nevertheless, it is treated as a constraint for the sake of discussion.

Flow in open channels satisfies the laws of conservation of mass, momentum, and energy. These laws constitute additional constraints to which entropy maximization can be subjected. According to Fig. 2-3, the conservation of mass in open-channel flow can be expressed as

$$q = \int_0^D u\, dy = u_m D \tag{2.16}$$

where q is the specific discharge (discharge per unit width $= Q/B$, $B =$ channel width) (L^2/T), and u_m is the cross-sectional mean velocity. Substitution of dy from equation (2.11) in equation (2.16) yields

$$\int_0^{u_D} uDf(u)\, du = u_m D \tag{2.17}$$

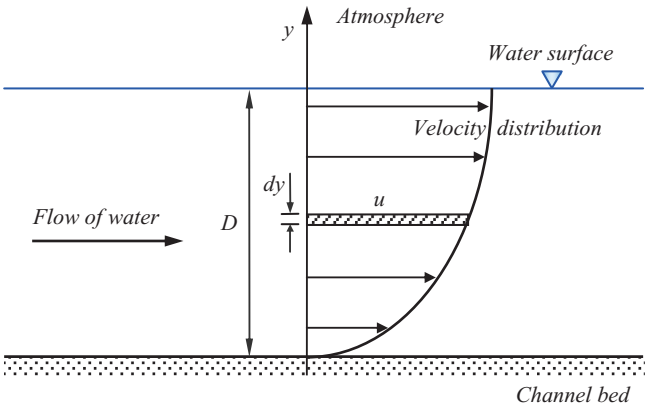

Figure 2-3 *Schematic for mass conservation in open-channel flow.*

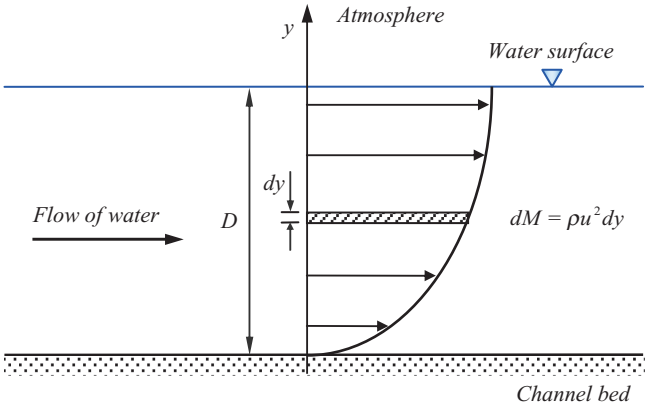

Figure 2-4 *Schematic for momentum conservation in open-channel flow.*

Thus, the second constraint, C_2, can be expressed as

$$C_2 = \int_0^{uD} uf(u)du = u_m = b_2 \tag{2.18}$$

Equation (2.18) can be interpreted as the first moment of random variable u about the origin, which is the mean velocity, and defines the mass conservation-based constraint.

On a unit width basis, the momentum through the elemental area ($dA = dy$) can be stated, according to Fig. 2-4, as

$$dM = \rho u^2 dy \tag{2.19}$$

Integrating equation (2.19) over the cross section, one obtains the momentum transfer M:

$$\rho \int_0^D u^2 dy = M \tag{2.20}$$

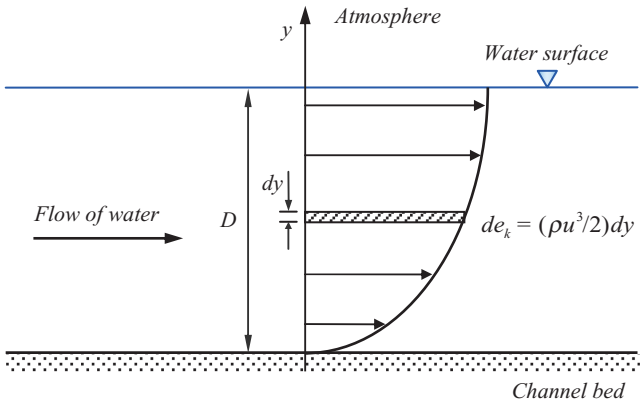

Figure 2-5 *Schematic for energy conservation in open-channel flow.*

where M is the momentum transferred across a section per unit width of the channel, and ρ is the mass density or mass per unit volume. Substitution of dy from equation (2.11) in equation (2.20) results in

$$\int_0^{uD} u^2 D f(u)\,du = \frac{M}{\rho} \tag{2.21}$$

The third constraint, C_3, can be expressed from equation (2.21) as

$$C_3 = \int_0^{uD} u^2 f(u)\,du = \overline{u^2} = \beta u_m^2 = \frac{M}{\rho D} = K_1 = b_3 \tag{2.22}$$

where $K_1 = M/(\rho D)$, $\overline{u^2}$ is the mean of u^2, and β is the momentum distribution coefficient $= \overline{u^2} / u_m^2$, often referred to as the Boussinesq coefficient. Equation (2.22) can be interpreted as the second moment of random variable u about the origin and defines the momentum conservation-based constraint and is a measure of the variability of velocity distribution.

Referring to Fig. 2-5, the transport of kinetic energy (KE) through the elemental cross section is

$$\Delta \mathrm{KE} = \frac{\rho}{2} u^3 dA \tag{2.23}$$

Integrating equation (2.23) over the cross section, one gets the kinetic energy transfer:

$$\int \frac{\rho}{2} u^3 dA = \frac{\rho}{2} \overline{u^3} A = \alpha \frac{\rho}{2} u_m^3 A = \rho Q \left(\alpha \frac{u_m^2}{2g} \right) \tag{2.24}$$

where α is the energy distribution coefficient $= \overline{u^3} / u_m^3$, often referred to as Coriolis coefficient, in which $\overline{u^3}$ is the cross section mean of u^3, and g is the acceleration caused by gravity.

Frequently energy in open channels is expressed in terms of head. Then, the specific energy in open channels in terms of head is composed of pressure head and the kinetic energy head:

$$D + \frac{\int_0^{E_k} de_k}{2g\int_0^D u\,dy} = D + E_k \tag{2.25}$$

where de_k is the incremental kinetic energy given by equation (2.23), and E_k is the kinetic energy head. As in equation (2.24), the conservation of energy in open-channel flow can be stated in terms of head over the cross section, according to Fig. 2-5, as

$$D + \frac{\int_0^D u^3 dy}{2g\int_0^D u\,dy} = E \tag{2.26}$$

where E is the specific energy head per unit width of the channel in a section. Substitution of dy from equation (2.11) in equation (2.26) yields

$$D\int_0^{u_D} u^3 f(u)\,du = (E-D)\left[D(2g)\int_0^{u_D} uf(u)\,du\right] \tag{2.27}$$

Thus, the fourth constraint, C_4, can be expressed as

$$C_4 = \int_0^{u_D} u^3 f(u)\,du = \overline{u^3} = \alpha u_m^3 = (E-D)2gu_m = K_2 = b_4 \tag{2.28}$$

where $K_2 = b_4 = (E - D)2gu_m$, and $\overline{u^3}$ is the mean of u^3. Equation (2.28) can be interpreted as the third moment of random variable u about the origin and measures the skewness of the probability distribution of u, $f(u)$. It defines the energy conservation-based constraint.

The momentum and energy coefficients in equations (2.22) and (2.28) can also be interpreted statistically. Recall the definition of variance σ^2 of u:

$$\sigma^2 = E[u^2] - (E[u])^2 = \overline{u^2} - u_m^2 \tag{2.29}$$

where E is the expectation operator. Equation (2.29) can be expressed as

$$\sigma^2 = \beta u_m^2 - u_m^2 = (\beta - 1)u_m^2 \tag{2.30}$$

Defining the coefficient of variation of velocity, CV,

$$CV = \frac{\sigma}{u_m} \tag{2.31}$$

equation (2.30) yields the momentum coefficient as

$$\beta = 1 + CV^2, \quad CV = \frac{\sigma}{u_m} \tag{2.32}$$

where σ is the standard deviation of velocity u.

In a similar vein, the energy coefficient can be expressed as

$$\alpha = 1 + 3CV^2 + \gamma CV^3 \tag{2.33}$$

where γ is the coefficient of skewness defined as

$$\gamma = \frac{\mu^3}{\sigma^3} \tag{2.34}$$

where μ^3 is the third central moment of u about the centroid or mean.

In open-channel flow, coefficients β and σ, for simplicity, are often assumed to equal 1 (Chow 1959). Equations (2.31) and (2.33) show that if the coefficient of variation of velocity is very small as compared with unity, coefficients β and α would tend to unity.

Example 2.3 Consider the values of CV as 0.0, 0.25, 0.5, 0.75, 1.0, 1.25, 1.5, 1.75, 2.0, 2.25, 2.50, 2.75, and 3.0; and the values of γ as 0.5, 0.5, 2.0, 2.5, and 3.0. Then, compute the values of α and β. What do these values say about channel flow characteristics? Plot β as function of CV and α as a function of CV, for various values of γ.

Solution Recall equation (2.32): $\beta = 1 + CV^2$. Values of β are calculated for given values of CV as shown in Table 2-4. Similarly, recall equation (2.33): $\alpha = 1 + 3CV^2$

Table 2-4 *Values of β and α for given values of CV and γ.*

CV	β	α(γ = 0.5)	α(γ = 1)	α(γ = 1.5)	α(γ = 2)	α(γ = 2.5)	α(γ = 3)
0	1	1	1	1	1	1	1
0.25	1.063	1.195	1.203	1.211	1.219	1.227	1.234
0.5	1.25	1.813	1.875	1.938	2	2.063	2.125
0.75	1.563	2.898	3.109	3.320	3.531	3.742	3.953
1	2	4.5	5	5.5	6	6.5	7
1.25	2.563	6.664	7.641	8.617	9.594	10.570	11.547
1.5	3.25	9.438	11.125	12.813	14.5	16.188	17.875
1.75	4.063	12.867	15.547	18.227	20.906	23.586	26.266
2	5	17	21	25	29	33	37
2.25	6.063	21.883	27.578	33.273	38.969	44.664	50.359
2.5	7.25	27.563	35.375	43.188	51	58.813	66.625
2.75	8.563	34.086	44.484	54.883	65.281	75.680	86.078
3	10	41.5	55	68.5	82	95.5	109

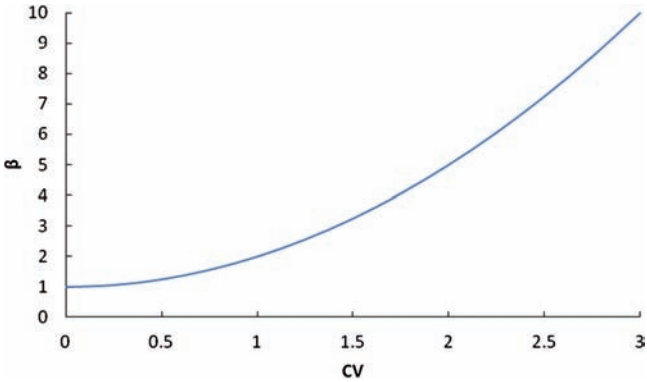

Figure 2-6 *Plot of β as a function of* CV.

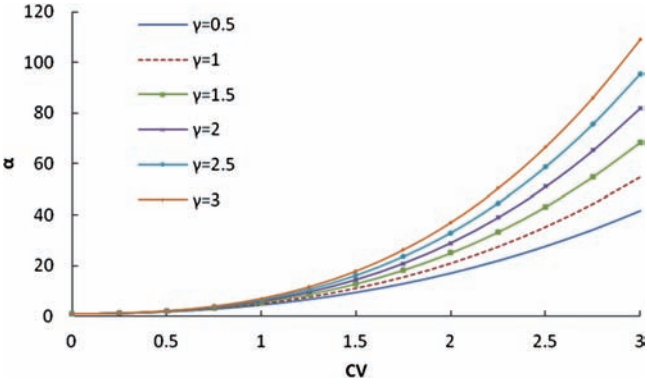

Figure 2-7 *Plot of α as a function of* CV *for various values of γ.*

$+ \gamma CV^3$, where values of α are computed for given values of CV and γ, as shown in Table 2-4. Fig. 2-6 plots β as a function of CV, and Fig. 2-7 plots α as a function of CV for various values of γ. It is seen that depending on the variability of flow velocity, the values of α and β can be greatly different from unity. With increasing CV, α and β increase. Likewise, α increases with increasing γ. Thus, only for CV equal to zero do these coefficients become unity. Increasing values of β and α indicate high turbulence.

2.2.4 Maximization of Entropy

The velocity entropy given by equation (2.14a) is to be maximized subject to the constraints given by equations (2.15), (2.18), (2.22), and (2.28). To that end, the

method of Lagrange multipliers is used. Then the Lagrangian function L can be expressed as

$$L = -\int_0^{u_D} f(u)\ln f(u)du + \lambda_1\left(\int_0^{u_D} f(u)dy - 1\right) + \lambda_2\left(\int_0^{u_D} uf(u)du - u_m\right) + \lambda_3\left(\int_0^{u_D} u^2 f(u)du - \overline{u^2}\right) + \lambda_4\left(\int_0^{u_D} u^3 f(u)du - \overline{u^3}\right) \tag{2.35}$$

where λ_1, λ_2, λ_3, and λ_4 are the Lagrange multipliers. Recalling the Euler–Lagrange equation of calculus of variation, differentiating equation (2.35) with respect to $f(u)$, noting f as variable and u as parameter, and equating the derivative to zero, one gets

$$\frac{\partial L}{\partial f} = 0 \Rightarrow -[1 + \ln f(u)] + \lambda_1 + \lambda_2 u + \lambda_3 u^2 + \lambda_4 u^3 \tag{2.36}$$

Details of the method of Lagrange multipliers are given in Appendix 2.1.

2.2.5 Derivation of the Probability Density Function of Velocity

The probability density function of velocity for which the entropy is maximum can be expressed from equation (2.36) as

$$f(u) = \exp[(\lambda_1 - 1) + \lambda_2 u + \lambda_3 u^2 + \lambda_4 u^3] \tag{2.37}$$

Equation (2.37) expresses the entropy-based probability density function of velocity. In this equation, the Lagrange multipliers λ_i, $i = 1, 2, 3$, and 4 are unknown. Denoting $\lambda_1 - 1$ by λ_0, equation (2.37) can be cast as

$$f(u) = \exp[\lambda_0 + \lambda_2 u + \lambda_3 u^2 + \lambda_4 u^3] \tag{2.38}$$

The CDF of u follows from integration of equation (2.38):

$$F(u) = \int_0^{u_D} \exp(\lambda_0 + \lambda_2 u + \lambda_3 u^2 + \lambda_4 u^3)du \tag{2.39}$$

2.2.6 Determination of the Lagrange Multipliers

Equation (2.38) is a general expression of PDF of velocity with four parameters: Lagrange multipliers λ_i, $i = 0, 2, 3$, and 4, which can be estimated using constraint equations (2.15), (2.18), (2.22), and (2.28). The method of estimation involves the following steps:

1. Substitute equation (2.38) in equation (2.15):

$$\int_0^{u_D} \exp(\lambda_0 + \lambda_2 u + \lambda_3 u^2 + \lambda_4 u^3)du = 1 \tag{2.40}$$

Equation (2.40) can be written as

$$\lambda_0 = -\ln \int_0^{u_D} \exp(\lambda_2 u + \lambda_3 u^2 + \lambda_4 u^3)\, du \tag{2.41}$$

2. Differentiate equation (2.41) with respect to λ_2, λ_3, and λ_4, multiply the numerator and the denominator of the derivative by $\exp(\lambda_0)$, and recall constraint equations (2.18), (2.22), and (2.28):

$$\frac{\partial \lambda_0}{\partial \lambda_i} = -\frac{\int_0^{u_D} u^i \exp(\lambda_0 + \lambda_2 u + \lambda_3 u^2 + \lambda_4 u^3)\, du}{\int_0^{u_D} \exp(\lambda_0 + \lambda_2 u + \lambda_3 u^2 + \lambda_4 u^3)\, du} = -C_i,\ i = 2, 3, 4 \tag{2.42}$$

3. Equation (2.41) does not have an analytical solution, but it can also be expressed as

$$\lambda_0 = \xi(\lambda_2, \lambda_3, \lambda_4) \tag{2.43}$$

where ξ is some function. It may be possible to analytically express equation (2.43).

4. Differentiate equation (2.43) with respect to λ_i, $i = 2, 3, 4$:

$$\frac{\partial \lambda_0}{\partial \lambda_i} = \xi(\lambda_2, \lambda_3, \lambda_4), \quad i = 2, 3, 4 \tag{2.44}$$

For simple cases, equation (2.44) results in explicit equations.

5. Equating equation (2.42) to equation (2.44), one gets three equations with three unknowns (λ_2, λ_3, and λ_4), which are then solved for the unknowns. In this manner, the unknown Lagrange multipliers are expressed in terms of constraints.

2.2.7 Entropy of Velocity Density Function

Substitution of equation (2.38) in equation (2.14) yields

$$\begin{aligned} H(u) &= -\int \exp[\lambda_0 + \lambda_2 u + \lambda_3 u^2 + \lambda_4 u^3][\lambda_0 + \lambda_2 u + \lambda_3 u^2 + \lambda_4 u^3]\, du \\ &= -[\lambda_0 + \lambda_2 u_m + \lambda_3 \overline{u^2} + \lambda_4 \overline{u^3}] \end{aligned} \tag{2.45}$$

Equation (2.45) shows that the entropy of velocity is expressed in terms of the Lagrange multipliers and constraints. Because the Lagrange multipliers themselves are expressed in terms of constraints, the entropy is determined in terms of constraints alone.

2.2.8 General Velocity Distribution

Substitution of equation (2.38) in equation (2.11) and integrating gives the velocity distribution as

$$\int_0^u \exp[\lambda_0 + \lambda_2 u + \lambda_3 u^2 + \lambda_4 u^3]\,du = \frac{y}{D} + c \tag{2.46}$$

where c is a constant of integration evaluated using $u = 0$ at $y = 0$. Because of its highly nonlinear nature, equation (2.46) does not lend itself to a simple expression. The method of parameter estimation for the general velocity distribution becomes cumbersome and hence is not presented here. Rather, estimation of parameters for simplified velocity distributions are discussed at appropriate places in the chapter. Simple velocity distributions can be derived depending on the constraints to be used. Now velocity distributions are derived for different constraints.

2.3 One-Dimensional Velocity Distribution with No Physical Constraint

In this case, there are no physical constraints, i.e., $\lambda_2 = \lambda_3 = \lambda_4 = 0$, and the only constraint is the total probability equation (2.15). Then, equation (2.38) becomes

$$f(u) = \exp[\lambda_0] \tag{2.47}$$

The PDF of u given by equation (2.47) is uniform. The CDF of u is expressed by integrating equation (2.47) as

$$F(u) = \int_0^u f(u)\,du = \int_0^u \exp(\lambda_0)\,du = \exp(\lambda_0)u \tag{2.48}$$

The value of λ_0 can be obtained by substituting equation (2.47) in equation (2.15) and solving:

$$\exp[-\lambda_0] = u_D \tag{2.49}$$

Equation (2.49) shows a unique relation between λ_0 and u_D:

$$\lambda_0 = -\ln u_D \tag{2.50}$$

Thus, the PDF and CDF of u are obtained by substituting equation (2.50) in equation (2.47) and equation (2.48), respectively, as

$$f(u) = \frac{1}{u_D} \tag{2.51}$$

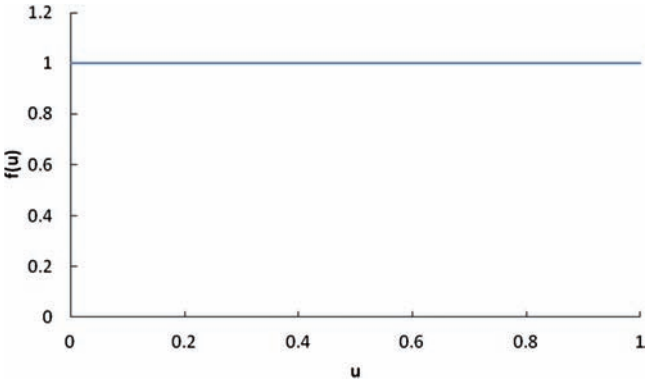

Figure 2-8 *PDF of* u.

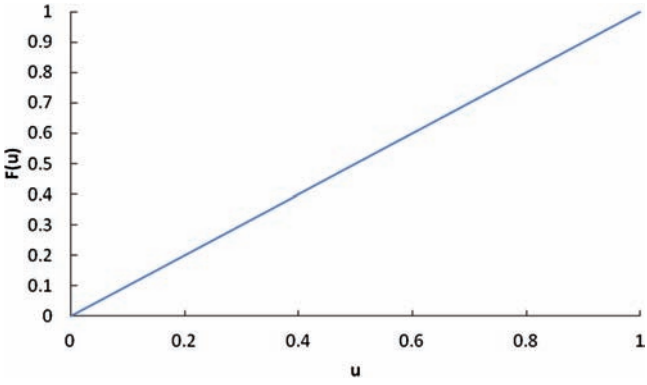

Figure 2-9 *CDF of* u.

and

$$F(u) = \frac{u}{u_D} \tag{2.52}$$

Fig. 2-8 shows the PDF of u, and Fig. 2-9, the CDF of u.

The velocity distribution from equation (2.46) then becomes

$$u = \exp(-\lambda_0)\frac{y}{D} \tag{2.53}$$

which, with the use of equation (2.50), becomes

$$u = u_D \frac{y}{D} \quad or \quad \frac{u}{u_D} = \frac{y}{D} \tag{2.54}$$

Equation (2.54) shows that if there are no constraints, then velocity increases linearly with distance from the bed, attaining the maximum value of u as u_D at the water surface $y = D$.

Example 2.4 Consider a 10-m-wide open channel with a flow depth of 2.5 m. The velocity at the surface is about 1 m/s. Plot the velocity as a function of flow depth, assuming zero velocity at the bottom. What is the average flow velocity? Comment on this velocity distribution. How realistic is it?

Solution Here the cross-sectional area $A = 10\,\text{m} \times 2.5\,\text{m} = 25\,\text{m}^2$. $u_D = 1\,\text{m/s}$. With the velocity at the water surface denoted by u_D, the velocity distribution is expressed as

$$u = u_D \frac{y}{D} = \frac{y}{D} = \frac{y}{2.5}$$

Substituting u in the mass conservation expressed by equation (2.16) and solving for u_m

$$q = \int_0^{2.5} \frac{y}{2.50} dy = \frac{y^2}{5}\bigg|_0^{2.5} = \frac{(2.5)^2}{5} = \frac{6.25}{5} = 1.25\,\text{m}^2/\text{s}$$

Therefore,

$$u_m = \frac{1.25\,\text{m}^2/\text{s}}{2.5\,\text{m}} = 0.5\,\text{m/s}$$

One can also arrive at

$$u_m = \frac{u_D}{2} = 0.5\,\text{m/s}$$

The velocity distribution is sketched in Fig. 2-10. The velocity distribution shown in the figure is linear, i.e., the flow velocity increases linearly from a value of

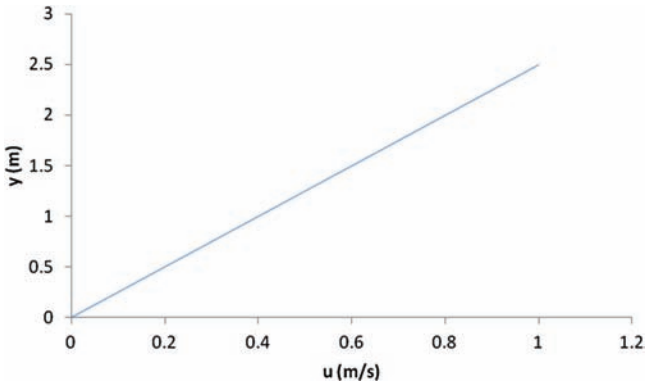

Figure 2-10 *Velocity as a function of depth.*

zero at the channel bed to a maximum of 2.5 m/s at the water surface. In the real world, the velocity distribution is significantly different from linear, and, therefore, the linear velocity distribution is not realistic.

Example 2.5 Construct the PDF and CDF of u with no physical constraints using the data from Example 2.4.

Solution The PDF $f(u) = \dfrac{1}{u_D} = 1$ is uniform, as shown in Fig. 2-11.

The CDF $F(u) = \dfrac{u}{u_D} = \dfrac{u}{1} = u$ is linear, as shown in Fig. 2-12.

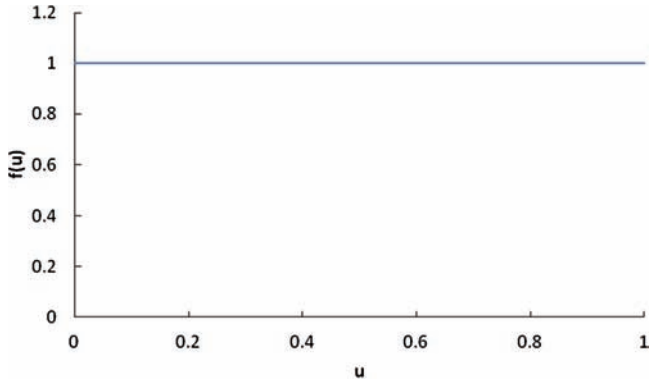

Figure 2-11 *PDF of* u.

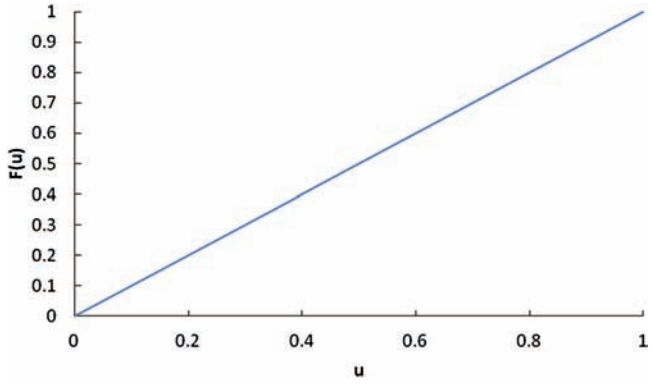

Figure 2-12 *CDF of* u.

2.4 One-Dimensional Velocity Distribution with One Physical Constraint

In this case, there is only one physical constraint—mass conservation—given by equation (2.18). Of course, equation (2.15) must be satisfied. Thus, $\lambda_3 = \lambda_4 = 0$. Then the PDF of u from equation (2.38) becomes

$$f(u) = \exp[\lambda_0 + \lambda_2 u] \quad or \quad f(u) = \exp[\lambda_1 - 1 + \lambda_2 u] \tag{2.55}$$

which is the entropy-based probability density function of velocity with Lagrange multipliers as its parameters. The CDF of u follows from the integration of equation (2.55):

$$F(u) = \frac{\exp(\lambda_0)}{\lambda_2}[\exp(\lambda_2 u) - 1] \tag{2.56}$$

If $u = 0$, $f(u) = \exp(\lambda_0)$, and $F(u) = 0$, from equations (2.55) and (2.56), respectively.

2.4.1 Determination of Lagrange Multipliers

The Lagrange multipliers can be determined following the procedure outlined earlier. Substituting equation (2.55) in equation (2.15), one obtains

$$\int_0^{u_D} \exp(\lambda_1 - 1 + \lambda_2 u)\, du = 1 \tag{2.57}$$

or

$$\exp(\lambda_1 - 1)[\exp(\lambda_2 u_D) - 1] = \lambda_2 \tag{2.58}$$

Equation (2.58) yields

$$\lambda_1 = 1 + \ln \lambda_2 - \ln[\exp(\lambda_2 u_D) - 1] \tag{2.59}$$

Differentiating equation (2.59) with respect to λ_2, one gets

$$\frac{\partial \lambda_1}{\partial \lambda_2} = \frac{1}{\lambda_2} - \frac{u_D \exp(\lambda_2 u_D)}{\exp(\lambda_2 u_D) - 1} \tag{2.60}$$

Equation (2.57) can also be written as

$$\lambda_1 = -\ln \int_0^{u_D} \exp(-1 + \lambda_2 u)\, du \tag{2.61}$$

Differentiating equation (2.61) with respect to λ_2, one gets

$$\frac{\partial \lambda_1}{\partial \lambda_2} = -\frac{\int_0^{u_D} u \exp(-1+\lambda_2 u)\,du}{\int_0^{u_D} \exp(-1+\lambda_2 u)\,du} \tag{2.62}$$

Multiplying and dividing equation (2.62) by $\exp(\lambda_1)$ and recalling equation (2.18), one obtains

$$\frac{\partial \lambda_1}{\partial \lambda_2} = -\frac{\int_0^{u_D} u \exp(\lambda_1 - 1+\lambda_2 u)\,du}{\int_0^{u_D} \exp(\lambda_1 - 1+\lambda_2 u)\,du} = -C_2 = -u_m \tag{2.63}$$

Equating equation (2.60) to equation (2.63), one gets

$$u_m = \frac{u_D \exp(\lambda_2 u_D)}{\exp(\lambda_2 u_D) - 1} - \frac{1}{\lambda_2} \tag{2.64}$$

Equation (2.64) is implicit in terms of the Lagrange multiplier λ_2 and, therefore, cannot be solved explicitly for the Lagrange multiplier.

One can also arrive at equation (2.64) as follows. Substitution of equation (2.55) in equation (2.18) yields

$$u_m = [\exp(\lambda_1) - 1]\left[\frac{u_D \exp(\lambda_2 u_D)}{\lambda_2} - \frac{\exp(\lambda_2 u_D)}{\lambda_2^2} + \frac{1}{\lambda_2^2}\right] \tag{2.65a}$$

Eliminating λ_1 by inserting equation (2.59) in equation (2.65a), the result is

$$u_m[\exp(\lambda_2 u_D) - 1] = u_D \exp(\lambda_2 u_D) - \frac{1}{\lambda_2}[\exp(\lambda_2 u_D) - 1] \tag{2.65b}$$

or

$$u_m = \frac{u_D \exp(\lambda_2 u_D)}{\exp(\lambda_2 u_D) - 1} - \frac{1}{\lambda_2}$$

which is the same as equation (2.64). It expresses λ_2 in terms of u_m and u_D, which can be obtained from observations.

2.4.2 Velocity Distribution

To obtain the velocity as a function of y, one combines equations (2.11) and (2.55):

$$\exp(\lambda_2 u)\,du = \frac{1}{D}\exp(1-\lambda_1)\,dy \tag{2.66}$$

Integration of equation (2.66) with the boundary condition that $u = 0$ when $y = 0$ yields

$$u = \frac{1}{\lambda_2} \ln\left[1 + \frac{\lambda_2}{\exp(\lambda_1 - 1)} \frac{y}{D}\right] \tag{2.67}$$

Eliminating λ_1 by substituting equation (2.59) in equation (2.67), the velocity distribution becomes

$$u = \frac{1}{\lambda_2} \ln\left[1 + \{\exp(\lambda_2 u_D) - 1\} \frac{y}{D}\right] \tag{2.68}$$

This is a one-physical constraint velocity distribution in which the Lagrange multiplier λ_2 remains yet to be determined.

2.4.3 Estimation of Lagrange Multiplier λ_2

Using empirical evidence, Chiu (1987) related λ_2 to shear velocity denoted by u^* as

$$\lambda_2 = \frac{k_1}{u^*} \tag{2.69}$$

where k_1 is a parameter, and u^* is equal to $\sqrt{gDS}$ in which g is the acceleration caused by gravity, D is the channel flow depth, and S is the channel bed slope. Introducing equation (2.69) in equation (2.68), one obtains

$$u = \frac{u^*}{k_1} \ln\left[1 + \left\{\exp\left(k_1 \frac{u_D}{u^*}\right) - 1\right\} \frac{y}{D}\right] \tag{2.70}$$

The corresponding PDF and CDF of u then becomes

$$f(u) = \frac{\lambda_2 \exp(\lambda_2 u)}{\exp(\lambda_2 u_D) - 1} \tag{2.71}$$

and

$$F(u) = \frac{\exp(\lambda_2 u) - 1}{\exp(\lambda_2 u_D) - 1} \tag{2.72}$$

Substitution of equation (2.69) in equations (2.71) and (2.72) leads to

$$f(u) = \frac{k_1}{u^*} \frac{\exp(k_1 u / u^*)}{\exp(k_1 u_D / u^*) - 1} \tag{2.73}$$

and

$$F(u) = \frac{\exp(k_1 u / u^*) - 1}{\exp(k_1 u_D / u^*) - 1} \tag{2.74}$$

It should now be noted that parameters k_1, u_D, and u_m are related through equations (2.64) and (2.69). To determine λ_1, one can use equation (2.59), provided that k_1 and u_D or u_m are known. Recognizing that $u = 0$ at the channel bottom ($y = 0$) and setting $u = 0$ in equation (2.55), one gets

$$\lambda_1 = 1 + \ln f(u) \tag{2.75}$$

and likewise setting $u = 0$ in equation (2.66), one gets

$$\lambda_1 = \ln\left(1 - D\frac{du}{dy}\right) \tag{2.76}$$

Equations (2.75) and (2.76) are expressions for λ_1, but it is not certain if they are more useful than equation (2.59) or equation (2.65a), which can be used in conjunction with k_1 and u_D or u_m.

2.4.4 Entropy of Velocity Probability Distribution

The entropy of the velocity distribution can be obtained by inserting equation (2.55) in equation (2.14) as

$$H(u) = -\ln\lambda_0 + \lambda_2 u_m \tag{2.77}$$

In equation (2.77), λ_0 can be expressed in terms of λ_2 using equation (2.59). Taking advantage of equations (2.59) and (2.69), equation (2.77) becomes

$$H(u) = -\ln k_1 + \ln u^* + \frac{k_1}{u^*}u_m + \ln[\exp(k_1 u_D / u^*) - 1] \tag{2.78}$$

Example 2.6 Consider the channel of Example 2.4. Taking the mean flow velocity as a constraint, compute the velocity distribution, plot it, and compare it with the velocity distribution plotted in Example 2.3.

Solution Taking $S = 0.0014$, and $D = 2.5\,\text{m}$, the shear velocity is

$$u^* = \sqrt{gDS} = 0.185\,\text{m/s}$$

With $k_1 = 0.4$, and $u_D = 1\,\text{m/s}$, the velocity distribution from equation (2.70) is determined as

$$u = \frac{0.185}{0.4}\ln\left[1 + \left\{\exp\left(\frac{0.4}{0.185}\right) - 1\right\}\frac{y}{2.5}\right]$$

Note that $\lambda_2 = 0.4/0.185\,\text{s/m}$. The velocity distribution is plotted in Fig. 2-13. Clearly the velocity distribution given by equation (2.70) is significantly different from the velocity distribution given by equation (2.54), and it seems more realistic.

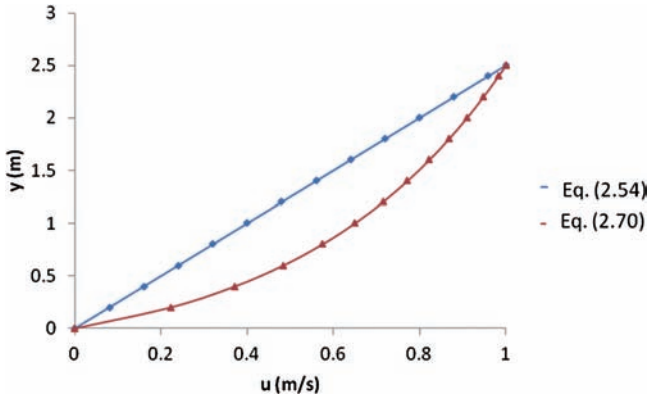

Figure 2-13 *Velocity distributions.*

2.5 Testing of One-Physical-Constraint Velocity Distribution

Chiu (1987) tested equation (2.70) using 29 sets of experimental velocity and sediment data collected by Einstein and Chien (1955) for flows ranging from zero to heavy sediment concentration over coarse, medium, and fine-grained sand bed channels. In the experiments, velocity was measured close to the bed. Chiu also compared the velocity distribution with the Prandtl–von Karman universal velocity distribution (Prandtl 1925; von Karman 1935), which is discussed in Chapter 4. The velocity at the water surface can be either measured or estimated from equation (2.64) with the knowledge of u_m, u^*, and k_1. For heavy sediment concentration over coarse sand beds, equation (2.70) was found to predict the velocity distribution quite accurately, whereas the Prandtl–von Karman velocity distribution equation did not when y/D was below 0.05. Chiu (1987) also noted that the fit of equation (2.70) could be further improved by estimating, adjusting, and selecting the mean velocity value, u_m, which relates u_D to λ_2 and, hence, to k_1. This relationship means that u_m can be estimated along with u_D and k_1. Equation (2.70) covers the full depth from $y = 0$ to $y = D$.

Using velocity profile measurements made by Davoren (1985), who measured flow velocity downstream from a hydropower plant, which enabled flow to be uniform for several hours, Barbé et al. (1991) compared equation (2.70), Prandtl–von Karman velocity distribution, and power law velocity distribution with observed velocity profiles. They found that the Prandtl–von Karman velocity distribution was good close to the water surface but deviated significantly as y tended to approach the bed. Hence, it would not be suitable for modeling near-the-bed processes, such as scour. The power law velocity distribution with exponent close to 1/6 was satisfactory. Near the bed, it was better than the Prandtl–von Karman distribution. The entropy-based velocity distribution was found to be superior, and the most improvement was near the bed.

Plotting the dimensionless velocity ($u^* = u/u^*$) against the argument of logarithmic function in equation (2.70), Chiu (1987) expressed the probability distribution function of dimensionless velocity as

$$f\left(\frac{u}{u^*}\right) = u^* f(u) \tag{2.79}$$

where $f(u)$, given by equation (2.55), has the same parameters as equation (2.70).

Example 2.7 Considering equation (2.70) and using the data from Einstein and Chien (1955) given in Table 2-5, plot the following: (1) y/D on the log scale and u/u^* on the arithmetic scale; (2) $\left[1+\{\exp(k_1 u_D / u^*)-1\}\frac{y}{D}\right]$ on the y-axis (log scale) and u/u^* on the x-axis; and (3) $f(u/u^*)$ versus observed velocity values divided by u^*. For the second case, the slope of the line is the value of k_1. Determine the value of k_1. Note that the velocity probability distribution is based on one physical constraint (mean) and is given by equation (2.70). What can one conclude from the plot? For the laboratory channel, $D = 0.378$ ft, $u^* = 0.406$ ft/s, $u_D = 9.094$ ft/s, and $k_1 = 0.205$.

Solution For the data from experiment S4 (Einstein and Chien 1955), a plot of u/u^* versus y/D is constructed, as shown in Fig. 2-14. It is seen that the computed dimensionless velocity values are in close agreement with observed values, with slight deviations close to the bed for y/D below 0.05. Fig. 2-15 plots $\left[1+\{\exp(k_1 u_D / u^*)-1\}\frac{y}{D}\right]$ versus u/u^*. The agreement between computed and observed values is quite close. Fig. 2-16 is a plot of $f(u/u^*)$ versus u/u^*. The PDF increases hyperbolically with increasing dimensionless velocity.

Table 2-5 *Velocity measurements for experiment S4 from Einstein and Chien (1955).*

y (ft)	Observed u (ft/s)	y (ft)	Observed u (ft/s)
0.000	0.000	0.040	4.831
0.006	2.221	0.045	5.075
0.009	2.497	0.050	5.298
0.011	2.720	0.054	5.522
0.011	2.858	0.064	5.806
0.015	2.964	0.074	6.090
0.017	3.329	0.084	6.293
0.019	3.573	0.095	6.516
0.024	3.898	0.104	6.699
0.034	4.519	0.124	7.133
0.040	4.831	0.378	9.094

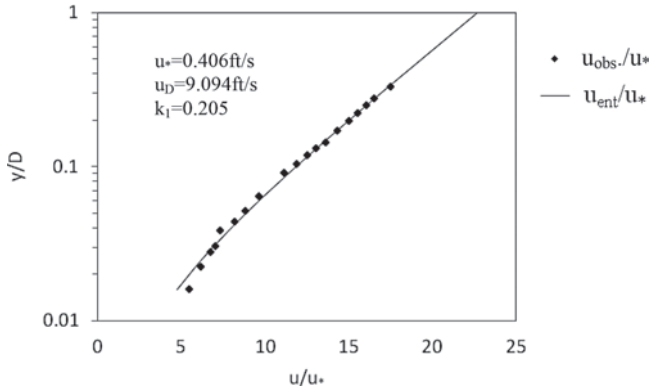

Figure 2-14 *Plot of* u/u* *versus* y/D.
Note: $u_{obs.}$ *= observed* u*; and* u_{ent} *=* u *computed by the entropy method.*

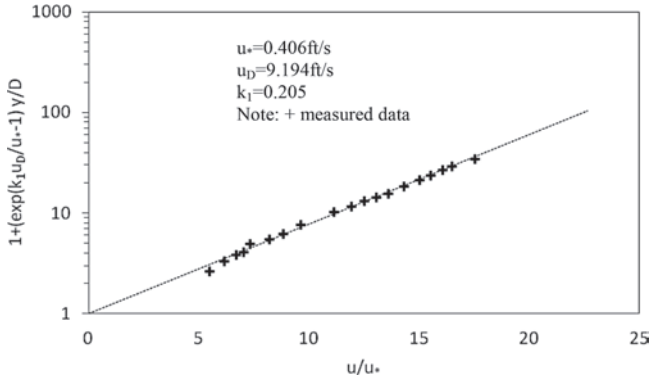

Figure 2-15 *Plot of* $1+\left\{exp\left(k_1\frac{u_D}{u^*}\right)-1\right\}\frac{y}{D}$ *versus* u/u*.

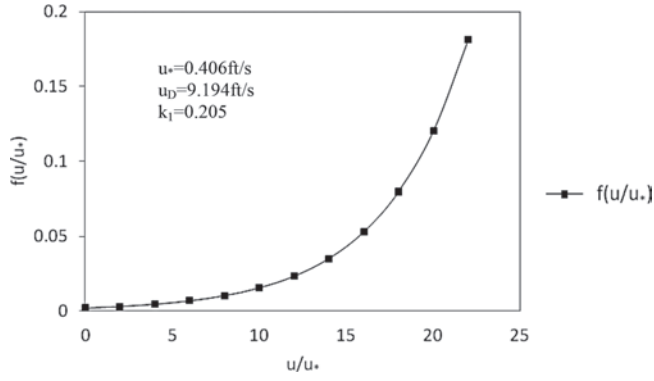

Figure 2-16 *Plot of* f(u/u*) *versus* u/u*.

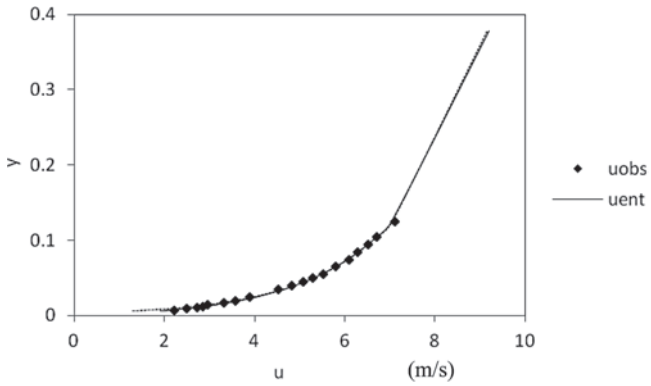

Figure 2-17 *Comparison of entropy-based velocity distribution equation (2.55) and observations.*
Note: uobs = observed velocity, and uent = velocity computed using the entropy-based velocity distribution.

Example 2.8 Plot on rectangular graph paper y/D on the y-axis and u/u^* on the axis, using observed values near the bed and an entropy-based velocity distribution equation. What can one conclude from this plot?

Solution The velocity distribution is plotted in Fig. 2-17. It is seen that the entropy-based velocity distribution predicts the velocity well near the bed as well as in the middle portion. There are no observed values beyond what is shown in the figure.

2.6 One-Dimensional Velocity Distribution with Two Physical Constraints

If in equation (2.38), $\lambda_4 = 0$, then the velocity distribution with two constraints is obtained:

$$f(u) = \exp[\lambda_0 + \lambda_2 u + \lambda_3 u^2] \tag{2.80}$$

The constraints for equation (2.80) are given by equations (2.15), (2.18), and (2.22). An exact analytical solution of these equations and equation (2.11) for velocity is not tractable and hence an approximate solution is obtained by expanding the term involving the third parameter λ_3 (Barbé et al. 1991). Equation (2.80) can be expressed as

$$f(u) = \exp[\lambda_0 + \lambda_2 u]\exp[\lambda_3 u^2] \tag{2.81}$$

Recall that for a function $f(x) = \exp[g(x)]$, the Maclaurin series expansion can be obtained as

$$f(x) = 1 + g(x) + \frac{1}{2!}[g(x)]^2 + \frac{1}{3!}[g(x)]^3 + \ldots \tag{2.82}$$

In equation (2.81), the quadratic term can be expressed as

$$\exp[\lambda_3 u^2] = 1 + \lambda_3 u^2 + \frac{1}{2!}[\lambda_3 u^2]^2 + \frac{1}{3!}[\lambda_3 u^2]^3 + \ldots \tag{2.83}$$

Equation (2.83) can be approximated by retaining only the first two terms:

$$\exp[\lambda_3 u^2] \cong 1 + \lambda_3 u^2 \tag{2.84}$$

Thus, equation (2.80) or (2.81) becomes

$$f(u) = (1 + \lambda_3 u^2)\exp[\lambda_0 + \lambda_2 u] \tag{2.85}$$

Using equation (2.85) in equation (2.15), one obtains

$$\int_0^{u_D} (1 + \lambda_3 u^2)\exp(\lambda_0 + \lambda_1 u)\, du = C_1 = 1 \tag{2.86}$$

Integration of equation (2.86) leads to

$$\lambda_2 \exp(-\lambda_0) = [\exp(\lambda_2 u_D) - 1] + \lambda_3 \left\{ \exp(\lambda_2 u_D)\left[u_D^2 - \frac{2u_D}{\lambda_2} + \frac{2}{\lambda_2^2} \right] - \frac{2}{\lambda_2^2} \right\} \tag{2.87}$$

Substituting equation (2.87) in equation (2.18) and simplifying yields

$$\begin{aligned} \lambda_2 u_m \exp(-\lambda_0) = {} & \left\{ \exp(\lambda_2 u_D)\left[u_D - \frac{1}{\lambda_2} \right] + \frac{1}{\lambda_2} \right\} \\ & + \lambda_3 \left\{ \exp(\lambda_2 u_D)\left[u_D^3 - \frac{3u_D^2}{\lambda_2} + \frac{6u_D}{\lambda_2^2} - \frac{6}{\lambda_2^3} \right] + \frac{6}{\lambda_2^3} \right\} \end{aligned} \tag{2.88}$$

Substituting equation (2.85) in equation (2.22) and simplifying, one obtains

$$\begin{aligned} \lambda_2 u_m K_1 \exp(-\lambda_0) = {} & \left\{ \exp(\lambda_2 u_D)\left[u_D^2 - \frac{2u_D}{\lambda_2} + \frac{2}{\lambda_2^2} \right] - \frac{2}{\lambda_2^2} \right\} \\ & + \lambda_3 \left\{ \exp(\lambda_2 u_D)\left[u_D^4 - \frac{4u_D^3}{\lambda_2} + \frac{12u_D^2}{\lambda_2^2} - \frac{24u_D}{\lambda_2^3} + \frac{24}{\lambda_2^4} \right] - \frac{24}{\lambda_2^4} \right\} \end{aligned} \tag{2.89}$$

Equations (2.87) to (2.89) can be solved simultaneously for λ_0, λ_2, and λ_3, and their substitution in equation (2.85) yields the velocity distribution.

Example 2.9 Consider the velocity observations on the Tiber River given in Table 2-6. Compute the velocity distribution using two physical constraints and plot it. Compare it with the one-physical-constraint velocity distribution.

Solution $D = 6.07\,\text{m}$, $u_D = 2.26\,\text{m/s}$. Solving Equations (2.87) to (2.89) numerically, $\lambda_0 = 2.29$, $\lambda_2 = 0.75$, and $\lambda_3 = 0.43$. Up to a height of about 3 m, the velocity is predicted well. For depths greater than 3 m, the observed velocity is not predicted well at all, as shown in Figure 2-18.

Table 2-6a *Velocity observations at Ponte Nuovo at the Tiber River, Italy, June 3, 1997.*

Vertical 1		Vertical 2		Vertical 3		Vertical 4	
y (m)	u (m/s)	y (m)	u (m/s)	y (m)	u (m/s)	y (m)	u (m/s)
4.71	0.52	6.31	0.99	6.21	1.54	6.09	1.98
4.65	0.52	6.25	0.99	6.15	1.54	6.03	1.98
4.35	0.63	5.95	1.25	5.85	1.74	5.73	2.15
3.65	0.92	5.25	1.51	5.15	1.87	5.03	2.32
2.65	1.02	4.25	1.81	4.15	2.13	4.06	2.34
1.85	0.97	3.25	1.83	3.15	2.08	3.09	2.48
1.15	0.74	1.25	1.65	2.18	2.06	2.09	2.32
0.45	0.67	0.45	0.97	1.18	1.92	1.09	1.97
0.15	0.34	0.15	0.81	0.48	1.47	0.39	1.78
0	0	0	0	0.15	1.28	0.15	1.37
				0	0	0	0

Vertical 5		Vertical 6		Vertical 7		Vertical 8		Vertical 9	
y (m)	u (m/s)	y (m)	u (m/s)	y (m)	u (m/s)	y (m)	u (m/s)	y (m)	u (m/s)
6.07	2.66	5.89	2.37	5.76	1.97	5.66	1.42	5.36	0.88
6.01	2.66	5.83	2.37	5.7	1.97	5.6	1.42	5.3	0.88
5.71	2.58	1.89	2.41	5.4	2.03	5.3	1.4	5	0.87
5.04	2.61	0.89	1.91	4.7	1.98	4.6	1.63	4.3	1.16
4.07	2.66	0.39	1.53	3.7	2.39	3.6	1.97	3.3	1.49
3.13	2.72	0.15	1.49	2.7	2.22	2.6	1.92	2.3	1.71
2.13	2.61	0	0	1.9	2.37	1.8	1.81	1.3	1.19
1.1	2.32			1.2	2.06	1.1	1.73	0.4	0.91
0.37	1.92			0.5	1.51	0.5	1.36	0.15	0.8
0.15	1.47			0.15	1.42	0.15	0.71	0	0
0	0			0	0	0	0		

Table 2-6b *Velocity observations at Ponte Nuovo at the Tiber River, Italy, June 3, 1997.*

Vertical	*D* (m)	Maximum *u* (m/s)	*h* (m)	*Z* (m)
1	4.71	1.02	2.7	–20.2
2	6.31	1.83	2.7	–2.64
3	6.21	2.13	2.7	–11.44
4	6.09	2.48	2.7	–6.24
5	6.07	2.72	2.7	0
6	5.89	2.41	2.7	6.24
7	5.76	2.39	2.7	11.44
8	5.66	1.97	2.7	15.6
9	5.36	1.72	2.7	19.76

Note: *y* = vertical distance (m) of each sampled point from the channel bed; *u* = observed velocity (m/s); *D* = water depth (m) along the vertical; maximum *u* = maximum sampled velocity (m/s) along the vertical; *h* = vertical distance (m) below the water surface where the maximum velocity occurs; *z* = horizontal distance from the vertical where the maximum velocity is sampled.]

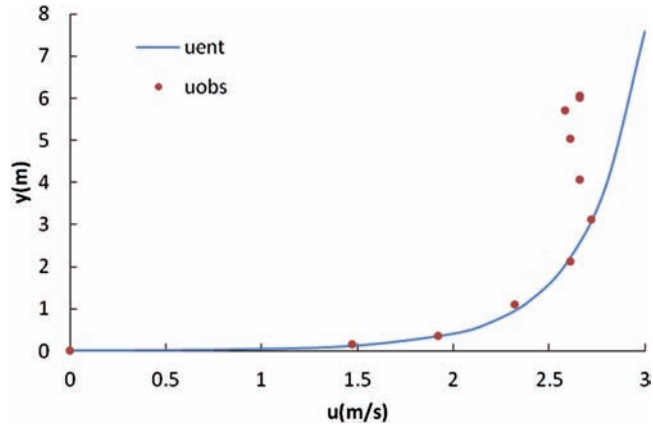

Figure 2-18 *Two-physical-constraint velocity distribution. Note: uobs = observed velocity and uent = velocity computed using the entropy equation.*

2.7 One-Dimensional Velocity Distribution with Three Physical Constraints

The velocity distribution for the three-physical-constraint case is given as

$$\exp(\lambda_0)\left\{\exp(\lambda_2 u)+\lambda_3\left[\exp(\lambda_2 u)\left(u^2-\frac{2u}{\lambda_2}+\frac{2}{\lambda_2^2}\right)\right]\right\}=\frac{y}{D}+C \tag{2.90}$$

where C is the constant of integration. Using the boundary condition $u = 0$ at $y = 0$, C becomes

$$C=\exp(\lambda_0)\left[\frac{1}{\lambda_2}+\frac{2\lambda_3}{\lambda_2^3}\right] \tag{2.91}$$

The velocity distribution now becomes

$$\exp(\lambda_0)\left\{\exp(\lambda_2 u)+\lambda_3\left[\exp(\lambda_2 u)\left(u^2-\frac{2u}{\lambda_2}+\frac{2}{\lambda_2^2}\right)\right]\right\}=\frac{y}{D}+\exp(\lambda_0)\left[\frac{1}{\lambda_2}+\frac{2\lambda_3}{\lambda_2^3}\right] \tag{2.92}$$

The Lagrange multipliers are determined numerically.

Example 2.10 Consider the velocity observations on the Tiber River given in Table 2-6. Compute the velocity distribution using three physical constraints and plot it.

Solution The PDF of the velocity distribution with three physical constraints can be written as

$$f(u)=\exp(\lambda_0+\lambda_2 u+\lambda_3 u^2+\lambda_4 u^3)=\exp(\lambda_0+\lambda_2 u)\exp(\lambda_3 u^2+\lambda_4 u^3) \tag{2.93}$$

According to the Maclaurin series expansion, in equation (2.93) the second term can be expressed as

$$\exp[\lambda_3 u^2+\lambda_4 u^3]=1+\lambda_3 u^2+\lambda_4 u^3+\frac{1}{2!}[\lambda_3 u^2+\lambda_4 u^3]^2+\frac{1}{3!}[\lambda_3 u^2+\lambda_4 u^3]^3+\ldots \tag{2.94}$$

Equation (2.94) can be approximated by retaining only the first three terms:

$$\exp[\lambda_3 u^2+\lambda_4 u^3]\cong 1+\lambda_3 u^2+\lambda_4 u^3 \tag{2.95}$$

Thus, equation (2.93) becomes

$$f(u)=(1+\lambda_3 u^2+\lambda_4 u^3)\exp[\lambda_0+\lambda_2 u] \tag{2.96}$$

Using equation (2.96) in equation (2.15), one obtains

$$\int_0^{u_D}(1+\lambda_3 u^2+\lambda_4 u^3)\exp(\lambda_0+\lambda_1 u)\,du=C_1=1 \tag{2.97}$$

Integration of equation (2.97) leads to

$$\lambda_2 \exp(-\lambda_0) = \exp(\lambda_2 u_D)\left[1 + \lambda_4 u_D^3 + \left(\lambda_3 - \frac{3\lambda_4}{\lambda_2}\right)u_D^2 - \left(\frac{2\lambda_2\lambda_3 - 6\lambda_4}{\lambda_2^2}\right)u_D + \frac{2\lambda_2\lambda_3 - 6\lambda_4}{\lambda_2^3}\right] - \left(1 + \frac{2\lambda_2\lambda_3 - 6\lambda_4}{\lambda_2^3}\right) \tag{2.98}$$

Substituting equation (2.96) in equation (2.18) and simplifying yields

$$\lambda_2 u_m \exp(-\lambda_0) = -\left(\frac{\lambda_2^3 + 6\lambda_2\lambda_3 - 6\lambda_4}{\lambda_2^4}\right) + \exp(\lambda_2 u_D)\left[\lambda_4 u_D^4 + \left(\lambda_3 - \frac{4\lambda_4}{\lambda_2}\right)u_D^3 - \left(\frac{3\lambda_2\lambda_3 - 12\lambda_4}{\lambda_2^2}\right)u_D^2 + \left(\frac{\lambda_2^2 + 6\lambda_2\lambda_3 - 24\lambda_4}{\lambda_2^3}\right)u_D - \frac{\lambda_2^3 + 6\lambda_2\lambda_3 - 6\lambda_4}{\lambda_2^4}\right] \tag{2.99}$$

Substituting equation (2.96) in equation (2.22) and simplifying, the result is

$$\lambda_2 u_m^2 K_1 \exp(-\lambda_0) = \exp(\lambda_2 u_D)\left[\lambda_4 u_D^5 + \left(\lambda_3 - \frac{5\lambda_4}{\lambda_2}\right)u_D^4 - \left(\frac{4\lambda_2\lambda_3 - 20\lambda_4}{{\lambda_2}^2}\right)u_D^3 + \left(\frac{\lambda_2^3 + 12\lambda_2\lambda_3 - 60\lambda_4}{\lambda_2^3}\right)u_D^2 - \left(\frac{2\lambda_2^3 + 24\lambda_2\lambda_3 - 120\lambda_4}{\lambda_2^4}\right)u_D + \frac{2\lambda_2^3 + 24\lambda_2\lambda_3 - 120\lambda_4}{\lambda_2^5}\right] - \left(\frac{2\lambda_2^3 + 24\lambda_2\lambda_3 - 120\lambda_4}{{\lambda_2}^5}\right) \tag{2.100}$$

Substituting equation (2.96) in equation (2.28) and simplifying, one gets

$$\lambda_2 u_m^3 K_2 \exp(-\lambda_0) = \exp(\lambda_2 u_D)\left[\lambda_4 u_D^6 + \left(\lambda_3 - \frac{6\lambda_4}{\lambda_2}\right)u_D^5 - \left(\frac{5\lambda_2\lambda_3 - 30\lambda_4}{\lambda_2^2}\right)u_D^4 + \left(\frac{\lambda_2^3 + 20\lambda_2\lambda_3 - 120\lambda_4}{\lambda_2^3}\right)u_D^3 - \left(\frac{3\lambda_2^3 + 60\lambda_2\lambda_3 - 360\lambda_4}{\lambda_2^4}\right)u_D^2 + \left(\frac{6\lambda_2^3 + 120\lambda_2\lambda_3 - 720\lambda_4}{\lambda_2^5}\right)u_D \times \left(\frac{6\lambda_2^3 + 120\lambda_2\lambda_3 - 720\lambda_4}{\lambda_2^5}\right)\right] - \left(\frac{6\lambda_2^3 + 120\lambda_2\lambda_3 - 720\lambda_4}{\lambda_2^5}\right) \tag{2.101}$$

For $D = 6.07\,\text{m}$, $u_D = 2.26\,\text{m/s}$, the Lagrange multipliers using equations (2.98) to (2.101) are obtained as $\lambda_0 = 2.56$, $\lambda_2 = 0.46$, $\lambda_3 = 0.13$, and $\lambda_4 = 0.05$. With the use of these multipliers in equation (2.92), the velocity distribution is computed as shown in Fig. 2-19. Comparing with observations, it seems that the

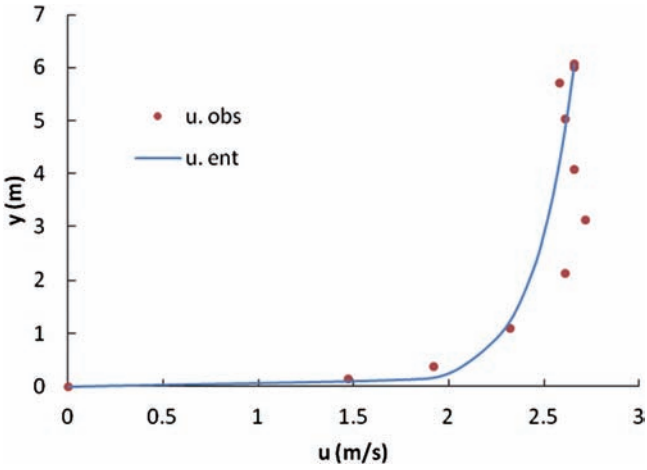

Figure 2-19 *Three-constraint velocity distribution.*

three-constraint velocity distribution does not reproduce observed values well. This result suggests that the approximation by the Maclaurin series expansion is not good.

Appendix 2.1: Method of Lagrange Multipliers

The function to be maximized is the Shannon entropy of velocity given by equation (2.14), which is rewritten as

$$H(u) = -\int_0^{u_D} f(u) \ln f(u) du \tag{2.102}$$

Let $R(f) = -f(u) \ln f(u)$. Then equation (2.102) can be written as

$$H(f) = \int_0^{u_D} R[f(u)] du \tag{2.103}$$

The Lagrange function, L, can be formulated as

$$L(f; \lambda_1, \lambda_2, \lambda_3, \lambda_4) = H(f) - \sum_{i=1}^{4} \lambda_i [\phi_i(u) - C_i] \tag{2.104}$$

where λ_i, $i = 1, 2, 3$, and 4, are the Lagrange multipliers; ϕ_i, $i = 1, 2, 3$, and 4, are functions of u for expressing constraints; and C_i constraints are expressed as

$$E[\phi_i(u)] = \int_0^{u_D} \phi_i(u) f(u) du = C_i,\ i = 1, 2, \ldots, 4;\ E[\phi_1(u)] = 1.$$

$$C_1 = 1; C_2 = u_m; C_3 = K_1; C_4 = K_2 \text{ or } C_i = b_i,\ i = 1, 2, 3, 4 \tag{2.105}$$

Note that for permissible values of u, $C_i - b_i = 0$, $i = 1, 2, 3$, and 4. The Lagrange function can also be cast as

$$L(f; \lambda_1, \lambda_2, \lambda_3, \lambda_4) = R(f) - \sum_{i=1}^{4} \lambda_i [u^{i-1} f(u) - C_i] \tag{2.106}$$

Thus, $L(f; \lambda_1, \lambda_2, \lambda_3, \lambda_4) = R(f)$. To achieve the maximum entropy,

$$\frac{\partial L}{\partial f} = \frac{\partial R}{\partial f} - \sum_{i=1}^{4} \lambda_i \frac{\partial [u^{i-1} f(u)]}{\partial f} = 0 \tag{2.107}$$

$$\frac{\partial L}{\partial \lambda_i} = -[u^i f(u)] = 0 \tag{2.108}$$

Equations (2.107) and (2.108) are to be solved for f and λ_i, $i = 1, 2, 3$, and 4. First, the first part of equation (2.107) on the right side is obtained:

$$\frac{\partial R(f)}{\partial f} = \frac{\partial [-f(u) \ln f(u)]}{\partial f} = -1 - \ln f(u) \tag{2.109}$$

Second, for $f(u)$,

$$\frac{\partial \psi_1(f)}{\partial f} = \frac{\partial f(u)}{\partial f} = 1 \tag{2.110}$$

Third, for $uf(u)$,

$$\frac{\partial \psi_2(f)}{\partial f} = \frac{\partial (uf(u))}{\partial f} = u \frac{\partial f(u)}{\partial f} = u \tag{2.111}$$

For $u^2 f(u)$,

$$\frac{\partial \psi_3(f)}{\partial f} = \frac{\partial [u^2 f(u)]}{\partial f} = u^2 \frac{\partial f(u)}{\partial f} = u^2 \tag{2.112}$$

For $u^3 f(u)$,

$$\frac{\partial \psi_4(f)}{\partial f} = \frac{\partial [u^3 f(u)]}{\partial f} = u^3 \frac{\partial f(u)}{\partial f} = u^3 \tag{2.113}$$

The task is to solve for $f(u)$. Therefore, inserting equations (2.109)–(2.113) in equation (2.107), one obtains

$$-1 - \ln f(u) + \lambda_1 + \lambda_2 u + \lambda_3 u^2 + \lambda_4 u^3 = 0 \tag{2.114}$$

This insertion results in

$$f(u) = \exp[(\lambda_1 - 1) + \lambda_2 u + \lambda_3 u^2 + \lambda_4 u^3] \tag{2.115}$$

Denoting $\lambda_1 - 1$ by λ_0, equation (2.115) leads to the entropy-based probability distribution of velocity as

$$f(u) = \exp[\lambda_0 + \lambda_2 u + \lambda_3 u^2 + \lambda_4 u^3] \tag{2.116}$$

The constraints for maximization are given by equations (2.15), (2.18), (2.22), and (2.28).

Questions

Q2.1 Consider a set of velocity observations for a river cross section, given in Table 2-7. Compute the mean, standard deviation, coefficient of variation, and coefficient of skewness of velocity from these observations. Then, compute the momentum distribution coefficient and the energy distribution coefficient. How much do these coefficients deviate from unity?

Q2.2 Check if the hypothesis on the cumulative distribution function of velocity given by equation (2.10) is valid for velocity observations in Q2.1.

Q2.3 Compute the flow cross-sectional area, discharge, specific discharge, and shear velocity for the cross section in Q2.1. Then compute the PDF and CDF of velocity.

Table 2-7 *Velocity data from experiment C13.*

y (ft)	u (ft/s)	y (ft)	u (ft/s)
0.003	2.471	0.038	4.485
0.004	2.457	0.046	4.746
0.005	2.925	0.056	4.834
0.006	2.869	0.066	5.113
0.008	3.270	0.045	5.113
0.010	3.427	0.076	5.113
0.013	3.699	0.091	5.479
0.016	3.884	0.106	5.514
0.020	4.066	0.126	5.835
0.025	4.212	0.151	5.849
0.030	4.415	0.176	6.073

Source: Data from Einstein and Chien (1955).

Q2.4 Using the data in Q2.1, compute the velocity distribution assuming that there are no physical constraints known. Also, compute the PDF and CDF of velocity and plot them. Then compute the velocity entropy. Compute the Lagrange multipliers.

Q2.5 Using the data in Q2.1, compute the velocity distribution assuming that there is only one physical constraint based on the mass conservation. Also, compute the PDF and CDF of velocity and plot them. Then, compute the velocity entropy. Compute the Lagrange multipliers.

Q2.6 Using the data in Q2.1, compute the velocity distribution assuming that there are two physical constraints known. These constraints are based on the conservation of mass and momentum. Also, compute the PDF and CDF of velocity and plot them. Then compute the velocity entropy. Compute the Lagrange multipliers.

Q2.7 Using the data in Q2.1, compute the velocity distribution assuming that there are three physical constraints known. These constraints are based on the conservation of mass, momentum, and energy. Also, compute the PDF and CDF of velocity and plot them. Then compute the velocity entropy. Compute the Lagrange multipliers.

Q2.8 What is the probability density value of velocity at the bed for the data in Q2.1? What is the probability of zero velocity at the bed?

References

Barbé, D. E., Cruise, J. F., and Singh, V. P. (1991). "Solution of three-constraint entropy-based velocity distribution." *J. Hydraul. Eng.*, 117(10), 1389–1396.

Chen, Y.-C., and Chiu, C.-L. (2004). "A fast method of flood discharge estimation." *Hydrol. Proc.*, 18, 1671–1684.

Chiu, C.-L. (1987). "Entropy and probability concepts in hydraulics." *J. Hydraul. Eng.*, 113(5), 583–600.

Chiu, C.-L. (1988). "Entropy and 2-D velocity distribution in open channels." *J. Hydraul. Eng.*, 114(7), 738–756.

Chiu, C.-L. (1989). "Velocity distribution in open channel flow." *J. Hydraul. Eng.*, 115(5), 576–594.

Chiu, C.-L. (1991). "Application of entropy concept in open-channel flow study." *J. Hydraul. Eng.*, 117(5), 615–628.

Chiu, C.-L., and Chen, Y.-C. (2003). "An efficient method of discharge estimation based on probability concept." *J. Hydraul. Res.*, 41(6), 589–596.

Chiu, C.-L., Hsu, S. M., and Tung, N.-C. (2005). "Efficient methods of discharge measurements in rivers and streams based on the probability concept." *Hydrol. Proc.*, 19, 3935–3946.

Chiu, C.-L., Jin, W., and Chen, Y.-C. (2000). "Mathematical models of distribution of sediment concentration." *J. Hydraul. Eng.*, 126(1), 16–23.

Chiu, C.-L., and Murray, D. W. (1992). "Variation of velocity distribution along nonuniform open-channel flow." *J. Hydraul. Eng.*, 118(7), 989–1001.

Chiu, C.-L., and Said, C. A. A. (1995). "Maximum and mean velocities and entropy in open-channel flow." *J. Hydraul. Eng.*, 121(1), 26–35.

Chiu, C.-L., and Tung, N.-C. (2002). "Maximum velocity and regularities in open-channel flow." *J. Hydraul. Eng.*, 128(4), 390–398.

Choo, T. H. (2000). "An efficient method of the suspended sediment-discharge measurement using entropy concept." *Water Eng. Res.*, 1(2), 95–105.

Chow, V. T. (1959). *Open-channel hydraulics*, McGraw-Hill, New York.

Cruise, J. F., Sherif, M. M., and Singh, V. P. (2007). *Elementary hydraulics*, Thomson-Nelson, Toronto.

Davoren, A. (1985). *Local scour around a cylindrical bridge pier*, Publication No. 3 of the Hydrology Center, National Water and Soil Conservation Authority, Ministry of Works and development, Christchurch, New Zealand.

Einstein, H. A., and Chien, N. (1955). "*Effects of heavy sediment concentration near the bed on velocity and sediment distribution*." Report No. 8, M.R.D. Sediment Series, U.S. Army Corps of Engineers, Omaha, NE.

Franz, D. D., and Melching, C. S. (1996). "Full equations (FEQ) model for the solution of the full dynamic equations of motion for one-dimensional unsteady flow in open channels and through control structures." U.S. Geological Survey Water Resources Investigations Report 96-4240, U.S. Geological Survey, Branch of Information Services, Federal Center, Denver.

Greco, M. (1999). "Entropy velocity distribution in a river." *Proc. Int. Assoc. of Hydraul. Res. (IAHR) Symp. River, Coastal and Estuarine Morphodyn.*, Vol. II, 121–130.

Henderson, F. M. (1966). *Open channel flow*, Macmillan, New York.

Moramarco, T., and Singh, V. P. (2001). "Simple method for relating local stage and remote discharge." *J. Hydrol. Eng.* 6(1), 78–81.

Moramarco, T., Saltalippi, C., and Singh, V. P. (2004). "Estimation of mean velocity in natural channels based on Chiu's velocity distribution." *J. Hydrol. Eng.*, 9(1), 42–50.

Prandtl, L. (1925). "Bericht uber unter suchugen zur ausgebildeten turbulenz." *Zeitschrift fur Angewanate Mathematik und Mechanik*, 5(2), 136 (in German).

Singh, V. P. (1996). *Kinematic wave modeling in water resources: Surface water hydrology*. Wiley, New York.

von Karman, T. (1935). "Some aspects of the turbulent problem." *Mech. Eng.*, 57(7), 407–412.

Xia, R. (1997). "Relation between mean and maximum velocities in a natural river." *J. Hydraul. Eng.*, 123(8), 720–723.

Xia, R., and Yen, B. C. (1994). "Significance of averaging coefficients in open-channel flow equations." *J. Hydraul. Eng.*, 120(2), 169–190.

Additional Reading

Ammari, A., and Remini, B. (2009). "Estimation of Algerian river discharges based on Chiu's equation." *Arab J. Geosci.*, DOI 10.1007/s12517-009-0056-y, 1–7.

Ardiclioglu, M., Araujo, J. C. D., and Senturk, A. I. (2005). "Applicability of velocity distribution equations in rough-bed open channel flow." *La Houille Blanche*, 4-2005, 73–79.

Chiu, C. L. (1990). "Velocity distribution equations for pen channel flows." *Encyclopedia of fluid mechanics*, Vol. 10, N. P. Cheremisinoff, ed., Gulf Publishing, Houston, 69–98.

Coleman, N. L. (1986). "Effects of suspended sediment on open-channel velocity distribution." *Water Resour. Res.*, 22(10), 1377–1384.

Daugherty, R. L., and Franzini, J. B. (1977). *Fluid mechanics with engineering applications*, McGraw-Hill, New York.

Ferro, V. (2003). "ADV measurements of velocity distribution in a gravel-bed flume." *Earth Surf. Proc. Land.*, 28, 707–722.

Gray, W. G., and Ghidaoui, M. S. (2009). "Thermodynamic analysis of stream flow hydrodynamics." *J. Hydraul. Res.*, 47(4), 403–417.

Rajaratnam, N., and Muralidhar, D. (1969). "Boundary shear stress distribution in rectangular open channels." *La Houille Blanche*, 6, 603–609.

Song, T., and Graf, W. H. (1996). "Velocity and turbulence distribution in unsteady open-channel flows." *J. Hydraul. Eng.*, 122(3), 141–154.

Tang, X., and Knight, D. W. (2009). "Analytical models for velocity distribution in open channel flows." *J. Hydraul. Res.*, 47(4), 418–428.

Yang, K., Cao, S., and Knight, D. W. (2007). "Flow patterns in compound channels with vegetated floodplains." *J. Hydraul. Eng.*, 133(2), 148–159.

Yang, C. T., and Song, C. C. S. (1988). "Theory of minimum energy and energy dissipation rate." *Encyclopedia of fluid mechanics*, Vol. 1, N. P. Cheremisinoff, ed., Gulf Publishing, Houston, TX, 353–395.

This page intentionally left blank

Chapter 3

Two-Dimensional Velocity Distributions

The distribution of velocity is influenced by flow properties, such as shear stress distribution, secondary currents, and sediment and pollutant transport; channel geometry, such as width, cross-sectional area and shape, depth, slope, aspect ratio, roughness, meandering, and braiding; vegetation; geological material properties; and boundary conditions. Flow in channels belongs to the general class of bounded shear flows. For purposes of describing the distribution of velocity in such flows, the boundary layer above the viscous sublayer can be divided into two regions: (1) the near-boundary inertial region, and (2) the outer (or wake) region (Landweber 1953; Coles 1956).

In the inertial region, the velocity profile can be closely approximated by a logarithmic equation, but in the secondary region the velocity deviates such that the velocities are actually higher than those predicted by the logarithmic equation. The deviation of velocity from the logarithmic law is linearly proportional to the logarithmic distance $\log(1 - y/D)$ from the surface, where y is the distance normal to the boundary and D is the flow depth. In the inner region, the controlling variables are the inner variables, such as kinematic viscosity, local shear velocity, and the distance normal to the boundary (Montes 1998).

The outer region is dominated by the flow depth. The relative thicknesses of these two regions depend on the level of turbulence in the outer part of the boundary layer and in the free stream (Landweber 1953). In an experimental study, Coleman (1986) found that the thickness of the logarithmic region (inertial) was reduced by suspended sediment and that this effect was greater for

smaller sediment sizes. Velocity profile was found to be more sensitive to the suspension of finer sediment particle sizes than to coarse particles.

In the outer region, the maximum velocity occurs, but its location depends on the aspect ratio. The maximum velocity occurs below the water surface if the channel aspect ratio is less than a certain value. The occurrence of the maximum velocity below the water surface is often referred to as the *dip phenomenon* and has been of interest for more than a century (Stearns 1883; Murphy 1904). This phenomenon can occur near side walls even if the aspect ratio is large. The mechanism of the dip phenomenon is explained in terms of secondary currents. Nezu and Nakagawa (1993) reasoned that low-momentum fluids are transported by secondary motion from near the bank to the center and high-momentum fluids are transported by this motion from the free surface toward the bed. Yang et al. (2004) derived a velocity distribution incorporating the dip phenomenon.

In narrow channels, the time-averaged velocity varies in both the vertical direction (y) and the transverse direction (z). In other words, velocity is two-dimensional (2-D). When contours of equal velocity lines, called *isovels*, are plotted, they tend to curve up the water surface because of the effect of channel boundaries, among other things. Velocity observations show that the maximum velocity is not at the water surface because of the air–water interaction at the water surface but is below the surface, meaning that there can be two depths where velocity is the same.

Chiu (1988) was the first to use entropy for determining two-dimensional (2-D) velocity distributions. Chiu and his associates have since extended Chiu's work to a variety of issues related to open-channel flow and sediment and pollutant concentration (Chiu 1989, 1991; Chiu and Murray 1992; Chiu et al. 2000, 2005; Chiu and Tung 2002; Chiu and Chen 2003; Chen and Chiu 2004). Choo (2000) extended Chiu's work to sediment discharge measurements, Moramarco and Singh (2001) to estimation of discharge at remote locations, and Moramarco et al. (2004) to estimation of mean cross-sectional velocity. The discussion in this chapter is heavily drawn from Chiu's work.

3.1 Derivation of Velocity Distributions

Derivation of velocity distributions entails a number of steps, including (1) defining a coordinate system, (2) formulation of a hypothesis on the cumulative distribution of velocity in terms of space coordinates, (3) expression of the Shannon entropy, (4) specification of constraints, (5) maximization of entropy, (6) derivation of entropy-based probability distribution of velocity, (7) determination of the Lagrange multipliers, (8) determination of velocity distribution, (9) definition of entropy parameter, (10) velocity distribution in terms of entropy parameter, (11) testing of velocity distribution, (12) PDF, CDF, and entropy of velocity distribution in terms of entropy parameter, (13) measures of homogeneity of velocity distribution, (14) entropy of velocity distribution, (15) significance of entropy

parameter, and (16) estimation of entropy parameter. Each of these steps is described in the next 16 sections.

3.1.1 Defining a Coordinate System

It is convenient to transform the Cartesian coordinates (y, z) into another system of coordinates (r, s), in which r has a unique one-to-one relation with velocity (Chiu and Chiou 1986), where y is the vertical coordinate and z is the transverse horizontal coordinate; in other words, one value of r corresponds to one velocity value. Fig. 3-1 depicts patterns of two-dimensional velocity distributions, wherein isovels are represented by r-coordinate curves, and s-coordinate curves are their orthogonal trajectories. Thus, r is a function of y and z. The orthogonality of r and s suggests that if r is determined, then s can be determined. The idea of using the (r, s) coordinates seems analogous to using curvilinear coordinates for flow in pipes. The time-averaged velocity u is bounded, and its time-invariant value, $0 \le u \le u_{max}$, is on an isovel that corresponds to a value of r, $r_0 \le r \le r_{max}$. Here u_{max} is the maximum velocity at $r = r_{max}$, which may occur on or below the water surface. The velocity u is zero along an isovel that corresponds to $r = r_0$, where r_0 represents the channel bed, including boundaries, and has a small value. It is implied that u increases monotonically with r from $r = r_0$ to $r = r_{max}$. It should be emphasized that u may not increase monotonically with y, the vertical distance from the channel bed, all the way up to the water surface.

3.1.2 Formulation of a Hypothesis

It is hypothesized that there exists a deterministic relation between u and r expressed as

$$u = W(r) \text{ or } r = W^{-1}(u) \tag{3.1}$$

where W is some function. Both u and r are considered random variables with probability density functions as $f(u)$ and $g(r)$, respectively. If it is assumed that all values of r between r_0 and r_{max} are equally likely to be sampled, then the probability density function of r, $g(r)$, will be uniform on the interval $0 \le r \le r_{max}$:

$$g(r) = \frac{1}{r_{max} - r_0} \tag{3.2}$$

The cumulative distribution function (i.e., the probability of velocity being less than or equal to u), $F(u)$, can be expressed as

$$F(u) = \int_0^u f(u)du = \int_0^u f[W(r)]du = \int_{r_0}^{W^{-1}(u)=r} g(r)dr = \frac{r - r_0}{r_{max} - r_0} \tag{3.3}$$

where $f(u)$ is the probability density function (PDF) of velocity u. Equation (3.3) states that if r is sampled between r_0 and r_{max} and the corresponding velocity

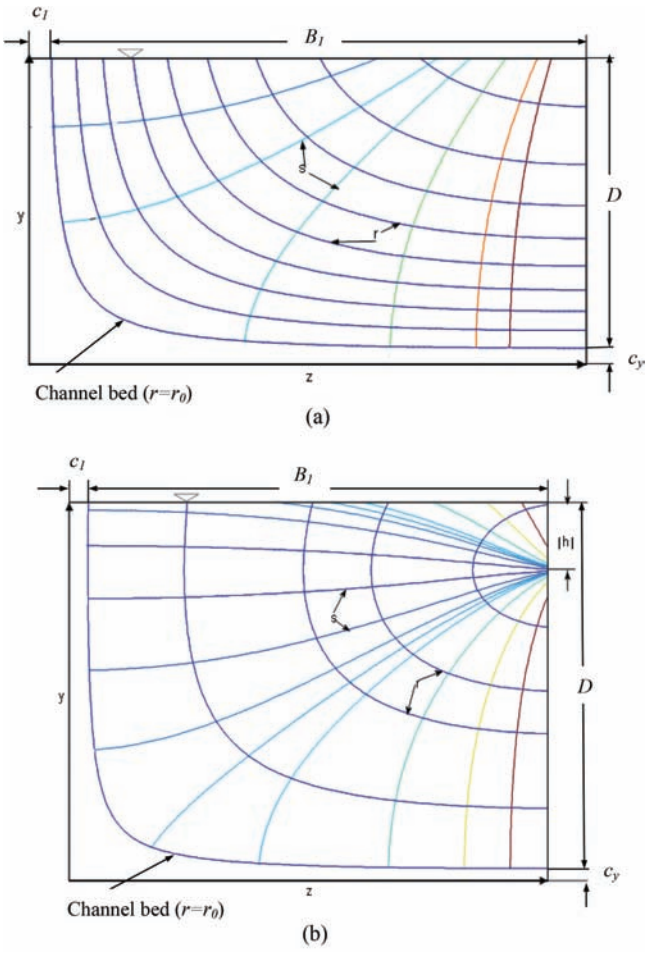

Figure 3-1 *Velocity distribution and curvilinear coordinate system: (a)* $h > 0$ *and (b)* $h < 0$.

Note: Here D = *channel flow depth,* B_1 = *half channel width,* h = *the distance from the water surface to the maximum velocity,* y = *vertical coordinate,* z = *transverse coordinate,* c_1 = *distance from the* y*-coordinate to the channel boundary,* c_y = *distance from the* z*-coordinate to the channel bed, and* c_1 *and* c_y *are also considered as coefficients.*

$u = W(r)$ is obtained, then the probability of velocity being between u and $u + du$ is $f(u)du$. Chiu and Chiou (1986) showed that $(r - r_0)/(r_{max} - r_0)$ in equation (3.3) is equal to the ratio of the area between the isovel r and the channel bed to the total area of the channel cross section.

Differentiation of equation (3.3) yields

$$f(u) = \frac{dF(u)}{du} = \frac{dF(u)}{dr}\frac{dr}{du} = \left[(r_{max} - r_0)\frac{du}{dr}\right]^{-1} \tag{3.4}$$

Equations (3.3) and (3.4) show that if $f(u)$ and r are determined, then the velocity distribution as a function of y and z coordinates can be determined. Fundamental to deriving the velocity distribution is the derivation of $f(u)$, which can be obtained by maximizing the Shannon entropy, subject to given constraints, in accordance with the principle of maximum entropy.

3.1.3 Expression of the Shannon Entropy

The Shannon entropy of the PDF of u can be expressed as

$$H(u) = -\int_0^{u_{\max}} f(u)\log f(u)du \tag{3.5}$$

Equation (3.5) can be interpreted as the average information content per sampled value of u and can, therefore, be used as a measure of uncertainty about u or $f(u)$. The base of the logarithm log can be 2 for H in bits or e for H in Napiers. The objective is to derive $f(u)$ using the principle of maximum entropy (POME). Thus, one maximizes entropy $H(u)$ subject to specified constraints.

3.1.4 Specification of Constraints

The PDF of u must satisfy

$$\int_0^{u_{\max}} f(u)du = 1 \tag{3.6}$$

For simplicity, one can use just one constraint based on mass conservation:

$$\int_0^{u_{\max}} uf(u)du = u_m \tag{3.7}$$

where $u_{\max}$ is the maximum velocity, and u_m is the cross section mean velocity defined as Q/A, where Q is the discharge and A is the cross-sectional area. Equation (3.7) states that u must be distributed over the entire cross-sectional area or over the entire domain of the PDF $f(u)$.

3.1.5 Maximization of Entropy

Entropy, given by equation (3.5), can be maximized, subject to equations (3.6) and (3.7), following POME. This can be accomplished by using the method of Lagrange multipliers. To that end, the Lagrangian function L, using equations (3.6) and (3.7), can be expressed as

$$L = -\int_0^{u_{\max}} f(u)\ln f(u)du + \lambda_1\left(\int_0^{u_{\max}} f(u)dy - 1\right) + \lambda_2\left(\int_0^{u_{\max}} uf(u)du - u_m\right) \tag{3.8}$$

where λ_1 and λ_2 are the Lagrange multipliers. Recalling the Euler–Lagrange equation of calculus of variation, differentiating equation (3.8) with respect to $f(u)$ noting that u is parameter and f is a variable, and equating the derivative to zero, one gets

$$\frac{\partial L}{\partial f} = 0 \Rightarrow -[1 + \ln f(u)] + \lambda_1 + \lambda_2 u \tag{3.9}$$

3.1.6 Derivation of Entropy-Based Probability Distribution of Velocity

The entropy-based probability density function of velocity is obtained from equation (3.9) as

$$f(u) = \exp[(\lambda_1 - 1) + \lambda_2 u] \tag{3.10}$$

Equation (3.10) can be expressed as

$$f(u) = b_1 \exp(\lambda_2 u), \quad b_1 = \exp(\lambda_1 - 1) \tag{3.11}$$

The CDF of u becomes

$$F(u) = \frac{1}{\lambda_2} \exp(\lambda_1 - 1)[\exp(\lambda_2 u) - 1] \tag{3.12}$$

or

$$F(u) = \frac{b_1}{\lambda_2}[\exp(\lambda_2 u) - 1] \tag{3.13}$$

3.1.7 Determination of the Lagrange Multipliers

Equation (3.10) contains two Lagrange multipliers λ_1 and λ_2, which can be determined with the aid of equations (3.6) and (3.7). Substituting equation (3.10) in equation (3.6), one obtains

$$\int_0^{u_{\max}} \exp(\lambda_1 - 1 + \lambda_2 u)\, du = \exp(\lambda_1 - 1)\frac{1}{\lambda_2}[\exp(\lambda_2 u_{\max}) - 1] = 1 \tag{3.14}$$

Equation (3.14) can be written as

$$\exp(\lambda_1 - 1) = \lambda_2 [\exp(\lambda_2 u_{\max}) - 1]^{-1} \tag{3.15}$$

or

$$\lambda_1 = 1 + \ln \lambda_2 - \ln[\exp(\lambda_2 u_{\max}) - 1] \tag{3.16}$$

Equation (3.16) expresses a relation between λ_1 and λ_2.

Differentiating equation (3.16) with respect to λ_2, the result is

$$\frac{\partial \lambda_1}{\partial \lambda_2} = \frac{1}{\lambda_2} - \frac{u_{\max} \exp(\lambda_2 u_{\max})}{\exp(\lambda_2 u_{\max}) - 1} \tag{3.17}$$

Conversely, equation (3.14) can also be written as

$$\lambda_1 = -\ln \int_0^{u_{\max}} \exp(-1 + \lambda_2 u) du \tag{3.18}$$

When we differentiate equation (3.18) with respect to λ_2, the result is

$$\frac{\partial \lambda_1}{\partial \lambda_2} = -\frac{\int_0^{u_{\max}} u \exp(-1 + \lambda_2 u) du}{\int_0^{u_{\max}} \exp(-1 + \lambda_2 u) du} \tag{3.19}$$

By multiplying and dividing equation (3.19) by $\exp(\lambda_1)$ and recalling equation (3.7), one obtains

$$\frac{\partial \lambda_1}{\partial \lambda_2} = -\frac{\int_0^{u_{\max}} u \exp(\lambda_1 - 1 + \lambda_2 u) du}{\int_0^{u_{\max}} \exp(\lambda_1 - 1 + \lambda_2 u) du} = -u_m \tag{3.20}$$

Equating equation (3.17) to equation (3.20) leads to

$$u_m = \frac{u_{\max} \exp(\lambda_2 u_{\max})}{\exp(\lambda_2 u_{\max}) - 1} - \frac{1}{\lambda_2} \tag{3.21}$$

Equation (3.21) implicitly expresses λ_2 in terms of $u_{\max}$ but can be solved numerically.

Equation (3.21) can also be derived as follows. Substituting equation (3.10) in equation (3.7), one obtains

$$\int_0^{u_{\max}} u \exp(\lambda_1 - 1 + \lambda_2 u) du = u_m \tag{3.22a}$$

When we insert equation (3.15) in equation (3.22a), the result is

$$u_m = u_{\max} \exp(\lambda_2 u_{\max}) [\exp(\lambda_2 u_{\max}) - 1]^{-1} - \frac{1}{\lambda_2} \tag{3.22b}$$

which is the same as equation (3.21).

The Lagrange multipliers λ_1 and λ_2 can be determined from equations (3.16) and (3.21) where u_m and $u_{\max}$ are measurable quantities or parameters from observations and can be determined by applying the least-squares method to velocity observations.

Now the PDF and CDF of u can be expressed from equations (3.10) and (3.12) by eliminating λ_1 with the use of equation (3.16) as

$$f(u) = \frac{\lambda_2 \exp(\lambda_2 u)}{\exp(\lambda_2 u_{\max}) - 1} \tag{3.23}$$

and

$$F(u) = \frac{\exp(\lambda_2 u) - 1}{\exp(\lambda_2 u_{\max}) - 1} \tag{3.24}$$

Note that at $u = 0$ (corresponding to r_0), $f(u) = \exp(\lambda_1 - 1)$ = value of the probability density function at $u = 0$ and is related to λ_2 and $u_{\max}$ through equation (3.15). Likewise, $F(u)\,|_{u\to 0} = -[\exp(\lambda_2 u_{\max}) - 1]^{-1}$.

Also the entropy of the velocity distribution can be expressed as

$$H(u) = \ln \lambda_2 + \lambda_2 u_m + \ln[\exp(\lambda_2 u_{\max}) - 1] \tag{3.25}$$

Example 3.1 Construct a plot of λ_1 as a function of λ_2 for various values of $u_{\max}$. Discuss the plot and its implications.

Solution Fig. 3-2 plots λ_1 as a function of λ_2 for $u_{\max} = 0.1$, 0.5, 1, 2, 5, and 10 m/s. For $\lambda_2 > 0$, λ_1 is negative. It is interesting to note that the relation between λ_1 and λ_2 is more or less linear but is sensitive to the value of $u_{\max}$, with $\partial\lambda_1/\partial\lambda_2$ increasing with increasing $u_{\max}$.

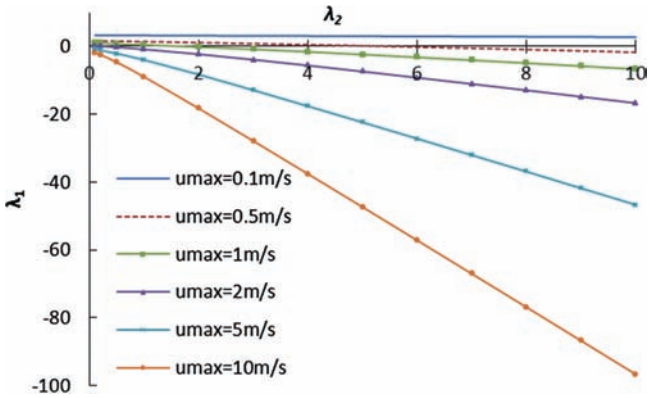

Figure 3-2 *Plot of λ_1 as a function of λ_2 for various values of u_{max} (m/s).*

Example 3.2 Construct a plot of λ_2 as a function of u_m for various values of u_{max}. Discuss the plot and its implications.

Solution Using equation (3.21), a plot of λ_2 versus u_m (m/s) is constructed for $u_{max} = 0.1$, 0.5, 1, 2, 5, and 10 m/s, as shown in Fig. 3-3. It is seen that λ_2 increases sharply with increasing u_m, such that a small change in u_m causes a huge change in λ_2. This difference indicates that u_m should be correctly determined.

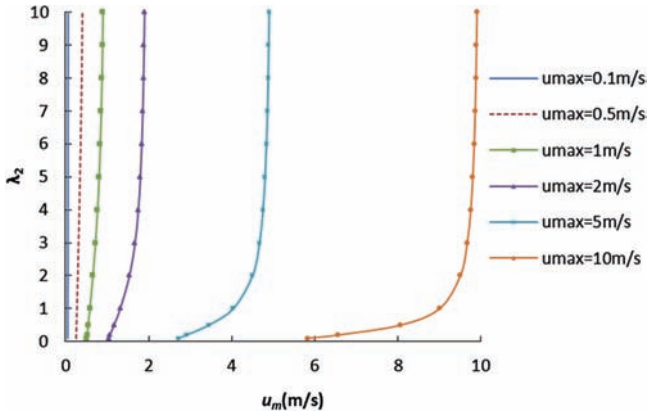

Figure 3-3 *Plot of λ_2 as a function of u_m (m/s) for various values of u_{max} (m/s).*

3.1.8 Determination of Velocity Distribution

From equations (3.10) and (3.4), one gets

$$\exp(\lambda_1 - 1 + \lambda_2 u)\frac{du}{dr} = \frac{1}{r_{max} - r_0} \tag{3.26a}$$

or

$$\frac{du}{dr} = \frac{\exp(1 - \lambda_1 - \lambda_2 u)}{r_{max} - r} \tag{3.26b}$$

Integration of equation (3.26b) with the condition that $u = 0$ at $r = r_0$, one obtains

$$u = \frac{1}{\lambda_2}\ln\left[1 + \frac{\lambda_2}{\exp(\lambda_1 - 1)}\frac{r - r_0}{r_{max} - r_0}\right] \tag{3.27}$$

Equation (3.27) can be recast with the substitution of λ_1 by equation (3.16) as

$$u = \frac{1}{\lambda_2}\ln\left[1 + \{\exp(\lambda_2 u_{max}) - 1\}\frac{r - r_0}{r_{max} - r_0}\right] \tag{3.28}$$

Equation (3.28) is the entropy-based velocity distribution. Chiu (1988) defined a dimensionless parameter, M, as $M = \lambda_2 u_{max}$, which is called entropy number. Equation (3.28) can be expressed in terms of M as

$$\frac{u}{u_{max}} = \frac{1}{M}\ln\left[1 + \{\exp(M) - 1\}\frac{r - r_0}{r_{max} - r_0}\right] \tag{3.29}$$

3.1.9 Definition and Meaning of Entropy Number *M*

Parameter M can be determined as follows. From equation (3.10), one can write

$$f(u_{max}) = \exp(\lambda_1 - 1)\exp(\lambda_2 u_{max}) \tag{3.30}$$

For $u_{max} = 0$, equation (3.30) becomes

$$f(0) = \exp(\lambda_1 - 1) \tag{3.31}$$

Equation (3.31) shows that the PDF has a finite value at the bed. Dividing equation (3.30) by equation (3.31), one gets

$$\frac{f(u_{max})}{f(0)} = \exp(\lambda_2 u_{max}) = \exp(M) \tag{3.32}$$

Therefore,

$$M = \ln\left[\frac{f(u_{max})}{f(0)}\right] \tag{3.33}$$

Equation (3.33) shows that M is the logarithm of the ratio of the PDF of u evaluated at $u = u_{max}$ to the PDF of u evaluated at the bed, i.e., $u = 0$.

Using equation (3.33) and (3.4), one obtains

$$M = \ln\frac{f(u_{max})}{f(0)} = \ln\left[\frac{\left(\frac{du}{dr}\right)_{r=r_0}}{\left(\frac{du}{dr}\right)_{r=r_{max}}}\right] \tag{3.34}$$

where $(du/dr)|_{r=r_0}$ is du/dr evaluated at $r = r_0$. Equation (3.34) shows that M is the logarithm of the ratio of the derivative of u with respect to r evaluated at $r = r_0$ to the derivative of u evaluated at $u = u_{max}$. Thus, entropy number M can be determined.

3.1.10 Velocity Distribution in Terms of Entropy Number

With the use of parameter M, equation (3.29) can be expressed as

$$\frac{u}{u_{max}} = \frac{1}{M}\ln\left[1 + \{\exp(M) - 1\}\frac{r - r_0}{r_{max} - r_0}\right] \tag{3.35a}$$

Equation (3.35a) is a 2-D velocity distribution equation and has a parameter M, which consists of two parameters: λ_2 and u_{max}. It describes the velocity spatially. For wide channels, Chiu (1988) showed that $(r - r_0)/(r_{max} - r_0)$ equals y/D. Thus, equation (3.35a) can be cast as

$$\frac{u}{u_{max}} = \frac{1}{M}\ln\left\{1 + \left[\exp(M) - 1\right]\frac{y}{D}\right\} \tag{3.35b}$$

By taking the derivative of equation (3.35b), we can express the velocity gradient as

$$\frac{du}{dy} = \frac{u_{max}}{DM}[\exp(M) - 1]\left\{1 + [\exp(M) - 1]\frac{y}{D}\right\}^{-1} \tag{3.36}$$

Example 3.3 Construct a plot of u/u_{max} as a function of $(r - r_0)/(r_{max} - r_0)$ for various values of M. Discuss the plot and its implications.

Solution Using equation (3.35a), a plot of u/u_{max} versus $(r - r_0)/(r_m - r_0)$ is constructed for various values of M (0.1, 0.5, 1.0, 2.0, 5.0, and 10.0), as shown in Fig. 3-4. The relation between u/u_{max} and $(r - r_0)/(r_{max} - r_0)$ is sensitive to the value of M. Interestingly, when M is very small (say, 0.1), the velocity distribution becomes linear. The larger the value of M, the more nonlinear the velocity distribution, which is also seen from its distribution. This fact means that M can be used as a parameter to characterize the influence of channel geometry and boundary conditions that cause the velocity distribution nonlinear.

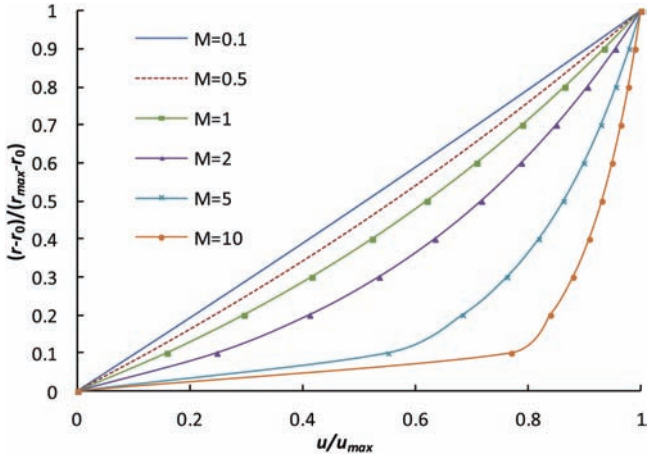

Figure 3-4 *Plot of* u/u_{max} *as a function of* $(r - r_0)/(r_{max} - r_0)$ *for various values of* M.

Example 3.4 Construct a plot of du/dy as a function of y/D for various values of M. Discuss the plot and its implications.

Solution Using equation (3.36), we see that a plot of du/dy versus y/D is constructed for various values of M (0.1, 0.5, 1.0, 2.0, 5.0, 10.0), as shown in Fig. 3-5. It is interesting to note that du/dy becomes almost independent of y/D for very small values of M.

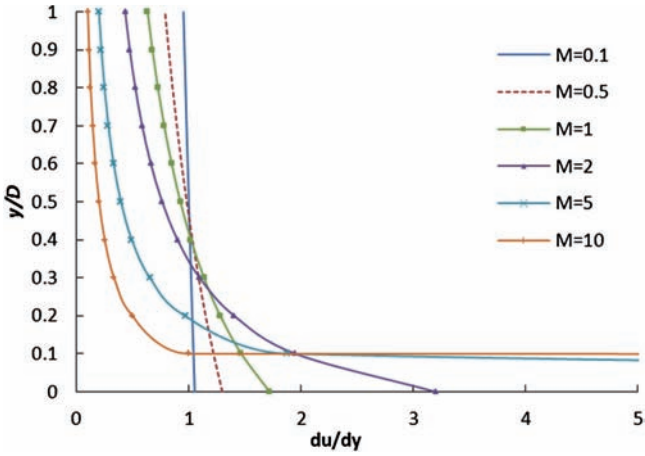

Figure 3-5 *Plot of* du/dy *as a function of* y/D *for various values of* M.

3.1.11 Testing of Velocity Distribution

Araújo and Chaudhry (1998) tested equation (3.35a) and compared it with the Prandtl–von Karman velocity distribution using 1,832 velocity measurements obtained using laser–Doppler velocimetry in five experiments on rectangular smooth wall flumes. They found equation (3.35a) to be superior in practically all flow regions, especially in those near the channel bed. Moramarco et al. (2004) applied equation (3.35a) for reconstructing velocity profiles sampled in four flow cross-sectional areas (at P. Nuovo, Rosciano, P. Felcino, and S. Lucia) during seven flood events in the upper Tiber River basin for which the depth varied from 0.9 to 6.7 m, discharge from 1.5 to 537 m^3/s, and the number of observations at cross sections from 34 to 51, as given in Table 3-1. For each event, the M value adopted was constant, $u_m = 0.665u_{max}$, $M = 2.13$, whereas u_{max} was assumed as the maximum value of the velocity points sampled during each event. Fig. 3-6 shows the velocity profiles estimated by the two-dimensional velocity distribution, with the velocity points observed along three different verticals sampled during the flood event that occurred in June 1997 at the Ponte Nuovo section: $z = 19.7$ m and $z = -3.6$ m represent the horizontal distance of the other verticals from $z = 0$. This figure shows that equation (3.35a) performed better in the middle portion of the flow area, whereas in the regions close to the side walls the velocity was poorly estimated (Araújo and Chaudhry 1998). Equation (3.35a) involves several parameters (Chiu 1989) that need to be estimated.

Table 3-1 *Velocity observations at Ponte Nuovo at the Tiber River, Italy, June 3, 1997.*

Vertical 1		Vertical 2		Vertical 3		Vertical 4	
y **(m)**	***u*** **(m/s)**	***y*** **(m)**	***u*** **(m/s)**	***y*** **(m)**	***u*** **(m/s)**	***y*** **(m)**	***u*** **(m/s)**
4.71	0.52	6.31	0.99	6.21	1.54	6.09	1.98
4.65	0.52	6.25	0.99	6.15	1.54	6.03	1.98
4.35	0.63	5.95	1.25	5.85	1.74	5.73	2.15
3.65	0.92	5.25	1.51	5.15	1.87	5.03	2.32
2.65	1.02	4.25	1.81	4.15	2.13	4.06	2.34
1.85	0.97	3.25	1.83	3.15	2.08	3.09	2.48
1.15	0.74	1.25	1.65	2.18	2.06	2.09	2.32
0.45	0.67	0.45	0.97	1.18	1.92	1.09	1.97
0.15	0.34	0.15	0.81	0.48	1.47	0.39	1.78
0	0	0	0	0.15	1.28	0.15	1.37
				0	0	0	0

Vertical 5		Vertical 6		Vertical 7		Vertical 8		Vertical 9	
y **(m)**	***u*** **(m/s)**	***y*** **(m)**	***u*** **(m/s)**	***y*** **(m)**	***u*** **(m/s)**	***y*** **(m)**	***u*** **(m/s)**	***y*** **(m)**	***u*** **(m/s)**
6.07	2.66	5.89	2.37	5.76	1.97	5.66	1.42	5.36	0.88
6.01	2.66	5.83	2.37	5.7	1.97	5.6	1.42	5.3	0.88
5.71	2.58	1.89	2.41	5.4	2.03	5.3	1.4	5	0.87
5.04	2.61	0.89	1.91	4.7	1.98	4.6	1.63	4.3	1.16
4.07	2.66	0.39	1.53	3.7	2.39	3.6	1.97	3.3	1.49
3.13	2.72	0.15	1.49	2.7	2.22	2.6	1.92	2.3	1.71
2.13	2.61	0	0	1.9	2.37	1.8	1.81	1.3	1.19
1.1	2.32			1.2	2.06	1.1	1.73	0.4	0.91
0.37	1.92			0.5	1.51	0.5	1.36	0.15	0.8
0.15	1.47			0.15	1.42	0.15	0.71	0	0
0	0			0	0	0	0		

Vertical	***D*** **(m)**	**Maximum** ***u*** **(m/s)**	***h*** **(m)**	***z*** **(m)**
1	4.71	1.02	2.7	–20.2
2	6.31	1.83	2.7	–4.64
3	6.21	2.13	2.7	–11.44
4	6.09	2.48	2.7	–6.24
5	6.07	2.72	2.7	0
6	5.89	2.41	2.7	6.24
7	5.76	2.39	2.7	11.44
8	5.66	1.97	2.7	15.6
9	5.36	1.72	2.7	19.76

Note: ***Y*** = vertical distance (m) of each sampled point from the channel bed; ***u*** = observed velocity (m/s); ***D*** = water depth (m) along the vertical; maximum ***u*** = maximum sampled velocity (m/s) along the vertical; ***h*** = vertical distance (m) below the water surface where the maximum velocity occurs; ***z*** = horizontal distance from the vertical where the maximum velocity is sampled.

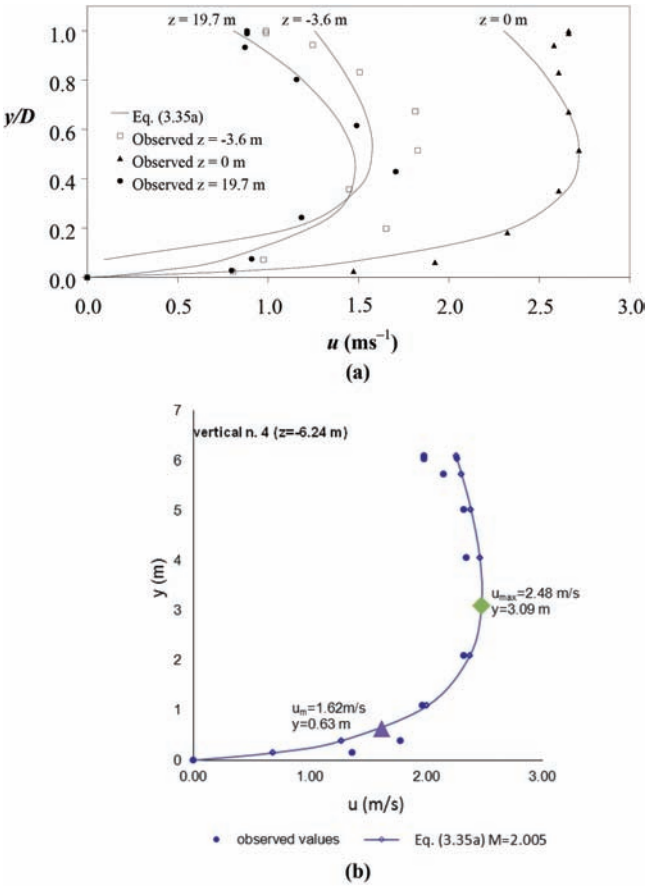

Figure 3-6 *(a) Velocity distribution, and (b) the velocity profile at vertical 4 and the location of maximum and mean velocity at the Ponte Nuovo section of the Tiber River, Italy, June 1997.*

3.1.12 PDF, CDF, and Entropy of Velocity in Terms of Entropy Parameter

The probability density function of velocity can be written in terms of M as

$$f(u) = \frac{M}{u_{\max}[\exp(M)-1]} \exp\left[M\frac{u}{u_{\max}}\right], \quad 0 \le u \le u_{\max} \tag{3.37}$$

and the CDF of u as

$$F(u) = \frac{\exp(Mu/u_{\max})}{\exp(M)-1} \tag{3.38}$$

The velocity entropy becomes

$$H(u) = -\ln\left\{\frac{M}{u_{\max}[\exp(M)-1]}\right\} - \frac{Mu_m}{u_{\max}} \tag{3.39}$$

The Lagrange multipliers can be expressed in terms of M as

$$\lambda_0 = \frac{M}{u_{\max}[\exp(M)-1]} \tag{3.40}$$

and

$$\lambda_2 = \frac{M}{u_{\max}} \tag{3.41}$$

Thus, M plays an important role in the description of velocity distribution and associated characteristics.

3.1.13 Measures of Homogeneity of Velocity Distribution

Equation (3.34) shows that parameter M can be considered as a measure of the uniformity or homogeneity of the probability distribution of velocity, as well as velocity distribution. Uniformity implies that the distribution remains the same from one location to another for the same value of M and channel geometry. In other words, it suggests that flow characteristics remain the same. For wide channels $(r - r_0)/(r_{\max} - r_0)$ can be replaced by y/D. In equation (3.35b), the point of maximum velocity can be below the water surface. Now the uniformity of the velocity distribution can be evaluated.

On an isovel with $r = \bar{r}$ and $u = u_m$, equation (3.35a) becomes

$$\frac{u_m}{u_{\max}} = \frac{1}{M}\ln\left\{1 + [\exp(M)-1]\frac{\bar{r} - r_0}{r_{\max} - r_0}\right\} \tag{3.42}$$

With the use of M, equation (3.21), when divided by $u_{\max}$, yields

$$\frac{u_m}{u_{\max}} = \exp(M)[\exp(M)-1]^{-1} - \frac{1}{M} \tag{3.43}$$

The left side of equation (3.43), given by term $u_m/u_{\max}$, describes the uniformity or homogeneity of the spatial velocity distribution. Equating equation (3.42) to equation (3.43), one obtains

$$\frac{\bar{r} - r_0}{r_{\max} - r_0} = \frac{\exp\{M\exp(M)[\exp(M)-1]^{-1} - 1\} - 1}{\exp(M) - 1} \tag{3.44}$$

The term $(\bar{r} - r_0)/(r_{\max} - r_0)$, given by equation (3.44), is another measure of uniformity or homogeneity of the velocity distribution.

Equations (3.43) and (3.44), expressing $u_m/u_{\max}$ and $(\overline{r}-r_0)/(r_{\max}-r_0)$, respectively, have M as a common parameter and represent different ways of describing the homogeneity of velocity distribution in a channel cross section. Equation (3.35a) describes the velocity distribution in space, whereas $u_m/u_{\max}$, given by equation (3.43) and $(\overline{r}-r_0)/(r_{\max}-r_0)$, given by equation (3.44), can be regarded as measures of homogeneity or uniformity of the velocity distribution.

The probability density function of dimensionless velocity, $u^* = u/u_{\max}$, $f(u/u_{\max})$, can also be written in terms of the M parameter as

$$f\left(\frac{u}{u_{\max}}\right) = f(u^*) = u_{\max} f(u) = M[\exp(M)-1]^{-1}\exp\left(\frac{Mu}{u_{\max}}\right) = M[\exp(M)-1]^{-1}\exp(Mu^*) \tag{3.45}$$

The CDF of $u^* = u/u_{\max}$ can be written as

$$F\left(\frac{u}{u_{\max}}\right) = F(u^*) = u_{\max} F(u) = \frac{\exp\left(\frac{Mu}{u_{\max}}\right)-1}{\exp(M)-1} = \frac{\exp(Mu^*)-1}{\exp(M)-1} \tag{3.46}$$

3.1.14 Entropy of Velocity Distribution

The entropy from equation (3.5) can be expressed with the aid of equations (3.10), (3.15), and (3.33) as

$$H(u) = H\left(\frac{u}{u_{\max}}\right) + \ln u_{\max} \tag{3.47}$$

where $H(u/u_{\max})$ is also an entropy function expressed as

$$H\left(\frac{u}{u_{\max}}\right) = \phi(M) - \ln M \tag{3.48}$$

where

$$\phi(M) = 1 + \ln[\exp(M)-1] - M\exp(M)[\exp(M)-1]^{-1} \tag{3.49}$$

$H(u/u_{\max})$ is also a measure of uniformity of the spatial velocity distribution.

Equations (3.48), (3.45), and (3.49), expressing $H(u/u_{\max})$ and $f(u/u_{\max})$, $\phi(M)$, respectively, have M as a common parameter and represent different ways of describing the homogeneity of velocity distribution in a channel cross section. $H(u/u_{\max})$ given by equation (3.48), can be regarded as a measure of homogeneity or uniformity of the PDF of velocity.

3.1.15 More on Significance of Parameter *M*

One can now examine the dependence of velocity distribution on parameter M. Fig. 3-7 shows a family of curves of $(r - r_0)/(r_{\max} - r_0)$ versus u/u_m, and Fig. 3-8

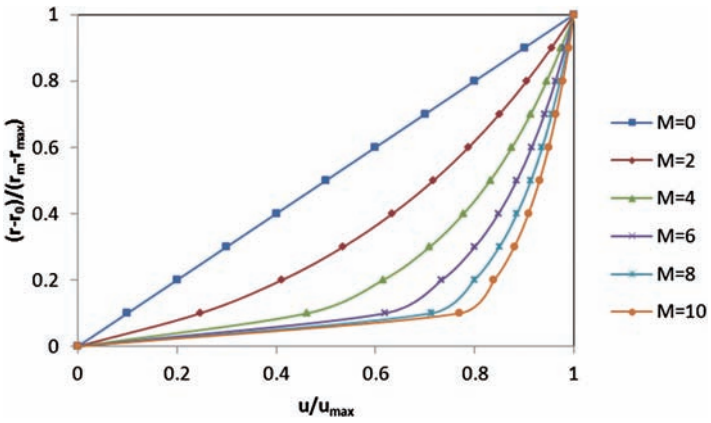

Figure 3-7 *Dimensionless velocity* u/u_{max} *versus dimensionless space coordinate* $(r - r_0)/(r_{max} - r_0)$.

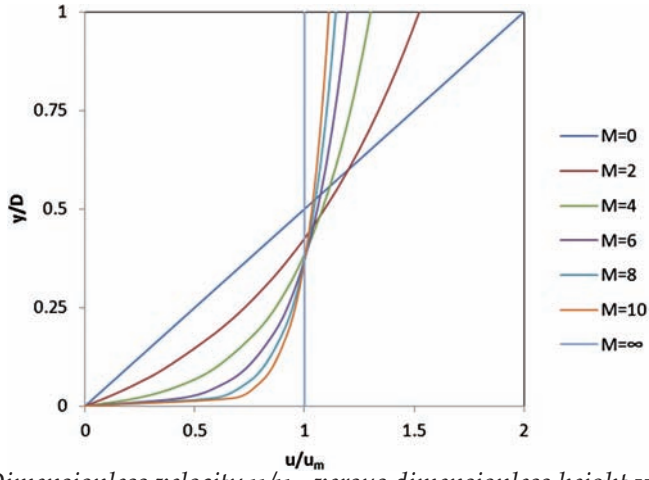

Figure 3-8 *Dimensionless velocity* u/u_m *versus dimensionless height* y/D *for various values of* M.

shows a family of curves of y/D versus u/u_m for various values of M, including $M = 0$ and $M \to \infty$, obtained from equations (3.35a) and (3.35b), respectively. Quantity $(r - r_0)/(r_{\max} - r_0)$ in equation (3.35a) can be approximated by y/D. Referring to Fig. 3-7, the linear velocity distribution in which $u = 0$ at the bed and $u = u_{\max}$ at the water surface corresponds to $M = 0$. The constant velocity distribution is represented by the value of $M \to \infty$. It should be noted that the mean velocity for $M = 0$ and $M \to \infty$ is about the same as for equation (3.42). For $M > 6$, the velocity distribution curves intersect at about $y/D = 0.37$, and

u/u_m is unity. This phenomenon shows that the mean velocity in wide channels occurs at about $y/D = 0.37$ if M exceeds 6. Additional insights into the role of M is obtained by plotting equation (3.43), (3.44), (3.47), and (3.49) as functions of M.

Example 3.5 Plot $f(u/u_{\max})$ versus $u/u_{\max}$ for various values of parameter M, $M = 0$, 2, 4, 6, 8, 10, and 12. What do you conclude from this plot?

Solution Using equation (3.45), a plot of the PDF $f(u^*)$ versus $u/u_{\max}$ is constructed for various values of M (0, 2, 4, 6, 8, and 10), as shown in Fig. 3-9. For $M = 0$, $f(u/u_{\max})$ becomes constant equal to unity, i.e., it becomes a uniform distribution and corresponds to the maximum (theoretical) value of entropy function $H(u/u_{\max})$, which is equal to zero in this case. When $M \to \infty$, $f(u/u_{\max})$ becomes zero, except at the point $u/u_{\max} = 1$, where $f(u/u_{\max})$ tends to infinity, and this case corresponds to the entropy function that has the minimum value.

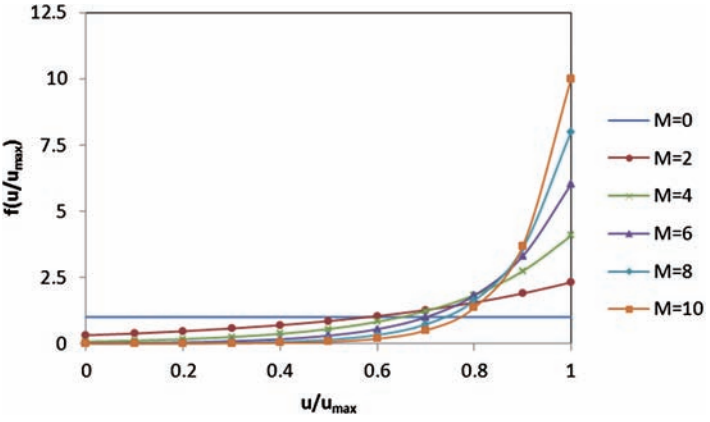

Figure 3-9 *Probability density function* f(u/u$_{max}$) *versus* u/u$_{max}$ *for various values of* M.

Example 3.6 Plot $u_m/u_{\max}$, $\phi(M)$, $H(u/u_{\max})$, and $(\bar{r} - r_0)/(r_m - r_0)$ as functions of parameter M. One may want to take M on the log scale and values of M as 1 to 100 or perhaps 1,000. Discuss the graphs.

Solution Quantity $u_m/u_{\max}$ from equation (3.43), as a function of M, is graphed in Fig. 3-10. It is seen from the figure that $u_m/u_{\max}$ increases with M as a deformed S curve, with the point of inflection around M equal to 8. When M becomes large, $u_m/u_{\max}$ tends to unity.

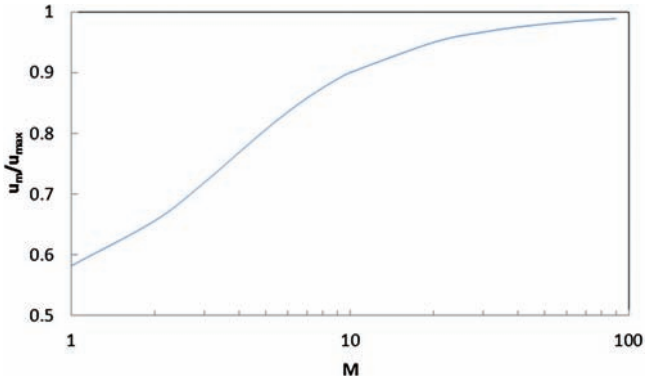

Figure 3-10 u_m/u_{max} *versus* M.

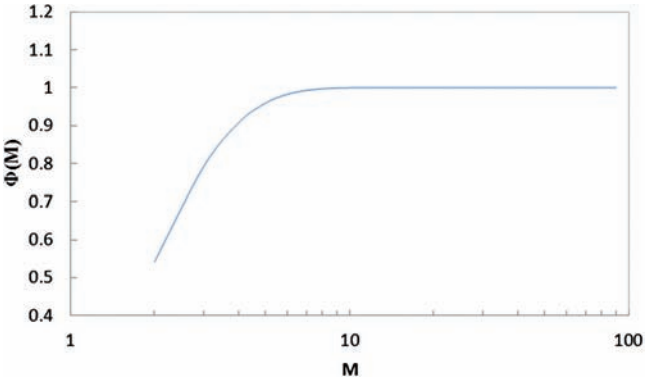

Figure 3-11 ϕ(M) *versus* M.

Quantity $\phi(M)$ as a function of M from equation (3.49), $\phi(M) = 1 + \ln[\exp(M) - 1] - M\exp(M)[\exp(M) - 1]^{-1}$, is graphed in Fig. 3-11. The $\phi(M)$ function increases with M as a quadratic function but tends to approach one as M approaches around 8, as seen from the figure.

Quantity $H(u/u_{\max})$ as a function of M given by equation (3.48) expressed as $H\left(\frac{u}{u_{\max}}\right) = \phi(M) - \ln M$ is graphed in Fig. 3-12. The value of $H(u/u_{\max})$ decreases with increasing M. As $M = 8$, it approximates a value of –1.1, as seen in the figure.

The quantity $(\overline{r} - r_0)/(r_{\max} - r_0)$ as a function of M given by equation (3.44) as $\frac{\overline{r} - r_0}{r_{\max} - r_0} = \frac{\exp\{M\exp(M)[\exp(M) - 1]^{-1} - 1\} - 1}{\exp(M) - 1}$ is graphed in Fig. 3-13. As seen in the figure, as M approaches 8, $(\overline{r} - r_0)/(r_{\max} - r_0)$ approaches 0.368.

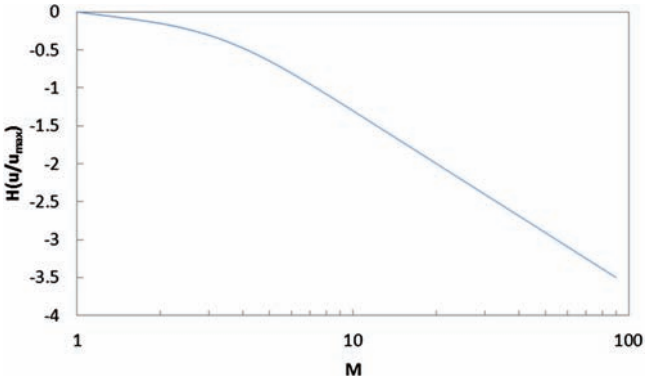

Figure 3-12 $H(u/u_{max})$ *versus* M.

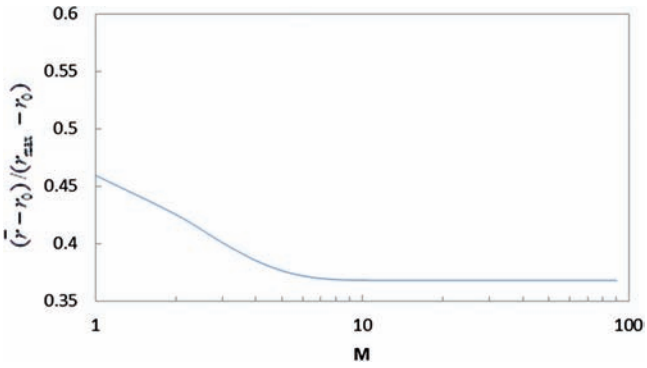

Figure 3-13 $(\overline{r} - r_0)/(r_{max} - r_0)$ *as a function of* M.

3.1.16 Estimation of Parameter *M*

Chiu (1988) empirically found a relation between $H(u/u_{\max})$ and u_m/u^* and between $u_m/u_{\max}$ and u_m/u^*, where u^* is the shear velocity, as

$$H\left(\frac{u}{u_{\max}}\right) = -0.730 - 0.0251\frac{u_m}{u^*} \tag{3.50}$$

and

$$\frac{u_m}{u_{\max}} = 0.832 + 0.00298\frac{u_m}{u^*} \tag{3.51}$$

Also,

$$\frac{u_m}{u_{\max}} = 1.283\left(\frac{u_m}{u^*}\right)^{0.956} \tag{3.52}$$

Equations (3.50) to (3.52) are based on a large set of velocity data that Chiu and Chiou (1986) generated by simulation using 176 rectangular channels with clear-water flow having width to depth (aspect) ratios ranging from 1 to 100, slopes from 2×10^{-5} to 2×10^{-2}, and Manning's n from 0.012 to 0.03.

It may be noted that u_m/u^* is related to the friction factor (Darcy–Weisbach's f_l, Chezy's C, or Manning's n) as

$$\frac{u_m}{u^*} = \sqrt{\frac{8}{f_l}} = \frac{C}{\sqrt{g}} = \frac{aR_h^{1/6}}{n\sqrt{g}} \tag{3.53}$$

where $u^* = \sqrt{\tau_0/\rho}$ is the shear velocity, τ_0 = mean boundary shear, u_m is the cross-sectional mean velocity, R_h is the hydraulic radius, and a is a factor equal to 1 if SI units are used and 1.49 if foot-pound-second units are used.

As $H(u/u_{\max})$ and $u_m/u_{\max}$ are functions of M only, as shown by equations (3.48) and (3.43), respectively, the M values are shown alongside the values of the two functions, as shown in Figs. 3-14a and 3-14b. In Fig. 3-14a, besides the linear relationship between $H(u/u_{\max})$ and u_m/u^*, every value of u_m/u^* corresponds to one value of f_l with respect to equation (3.53) and every value of $H(u/u_{\max})$ corresponds to one M value, as shown in equation (3.48). Fig. 3-14b shows a linear relationship between $u_m/u_{\max}$ and u_m/u^*, where every value of u_m/u^* corresponds to one value of f_l with respect to equation (3.53) and every value of $u_m/u_{\max}$ corresponds to one M value with respect to equation (3.43). These graphs illustrate that each point on the line corresponds to a unique value of M and f_l.

The friction factor f_l can be expressed using equations (3.53) and (3.43) as

$$f_l = 8\left[\phi(M)\frac{u_{\max}}{u^*}\right]^{-2} \tag{3.54}$$

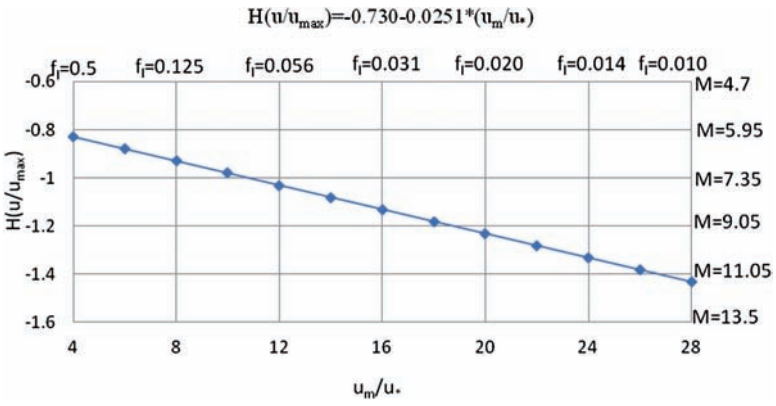

Figure 3-14a *Relation of* u_m/u^* *to* $H(u/u_{max})$, M, *and* f_l.

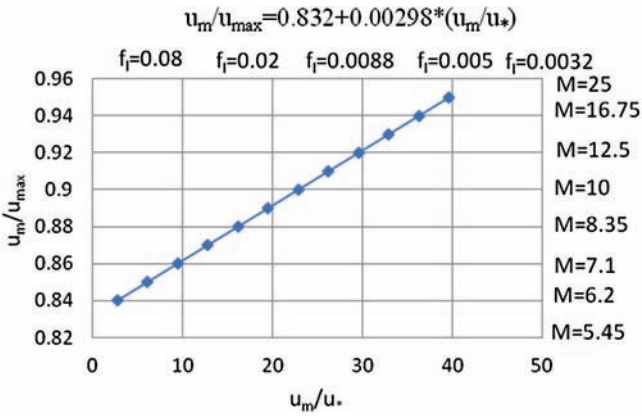

Figure 3-14b *Relation of* u_m/u^* *to* u_m/u_{max}, M, *and* f_l.

Thus, the M values can be determined from u_m/u^*, f_l, C, and n, or directly from equation (3.43) or from the Reynolds number:

$$R_n = \frac{u_m R_h}{\upsilon} \tag{3.55}$$

where υ is the kinematic viscosity. From the Moody diagram in open-channel flow hydraulics, it is normally seen that when R_n is between 500 and 2,000, the flow is in transition between laminar flow and turbulent flow. For the transitional range, the value of f_l is found to be 0.04 for smooth channels and between 0.04 and 0.08 for rough channels. The value of $f_l = 0.04$ corresponds to u_m/u^* of about 14 from equation (3.53) and the M value of about 8 in Chiu's data from Fig. 3-14b. Likewise, the value of $f_l = 0.08$ corresponds to $u_m/u^* = 10$ and $M = 7.35$. This result means that the M value between 7 and 8 corresponds to the transitional range between laminar flow and turbulent flow and $M > 8$ in the turbulent flow ($f_l < 0.04$). In other words, M can be used for classification of flow types. It is not clear if this would be true if the flow is sediment laden.

In open channels, the flow would tend to be turbulent, because entropy $H(u/u_{\max})$ would tend to be maximum as M would be between 7 and 8, and f_l would be about 0.03. For erodible channels, the maximum entropy is achieved by the adjustment of hydraulic geometry parameters (width, depth, and shape), friction, slope, alignment, velocity distribution, and perhaps sediment transport. Chiu's data show that for M in the neighborhood of 8, channels have greater width-to-depth (aspect) ratios and roughness and smaller slopes. Erodible channels tend to shape the channel cross section and velocity distribution such that $u_m/u_{\max}$ may lie between 0.85 and 0.9 for M between 6 and 10 (Blaney 1937). For nonerodible channels, $H(u/u_{\max})$ is maximized by adjusting velocity distribution and flow depth and, hence, has a wider range of M values.

To summarize, dimensionless parameter M can be regarded as entropy number or parameter. This definition relates to a multitude of interesting

hydraulic characteristics: (1) velocity distribution; (2) locations of mean and maximum velocities; (3) $H(u/u_{max})$; (4) $u_m/u^*, f_l, C$, and n; (5) u_m/u_{max}; (6) $f(u_m/u_{max})$; (7) $(\bar{r} - r_0)/(r_{max} - r_0)$; and (8) the state of flow—laminar, transitional, or turbulent. Essentially M is the logarithm of the ratio of $f(u)$, or du/dr, evaluated at r_{max} and r_0 as shown by equation (3.34).

It may also be noted that the energy and momentum distribution coefficients can be related to M. For wide rectangular channels, when $M \to \infty$ and, hence, entropy is minimum, the velocity is uniform everywhere, i.e., $u = u_m$; then both α and β equal unity. Conversely, when $M = 0$, and entropy is maximum, u increases linearly from zero at $y = 0$ to $u_{max} = 2u_m$ at $y = 2D$, then $\alpha = 2$ and $\beta = 1.33$. For other values of M between these two extremes, α is between 1 and 2, and β is between 1 and 1.33. Actual values of α and β can be determined for a given value of M.

3.2 Construction of Isovels and Relation between (x, y) Coordinates and (r, s) Coordinates

The velocity pattern in open-channel flow can be graphed using contours of equal velocity, called isovels. Clearly, along an isovel the velocity is constant. These isovels can help determine the maximum and mean velocities, as well as their locations and axes. Furthermore, they help describe the variation of velocity in the vertical and transverse directions. They graph the spatial variability of velocity, that is, isovels are a 2-D mapping of the velocity field.

Chiu and Lin (1983) and Chiu and Chiou (1986) provided equations for transforming the (y, z) coordinates into orthogonal curvilinear coordinates (r, s), which seem capable of representing different features of isovels. The curvilinear coordinates are expressed in terms of dimensionless coordinates Y and Z, which are expressed as

$$Y = \frac{y + c_y}{D + c_y + h} \tag{3.56}$$

$$Z = \frac{2|\zeta|}{B + 2c_i} \tag{3.57}$$

$$\zeta = \frac{B}{2} - z \tag{3.58}$$

Here D is the depth of water at the y-axis; B is the transverse distance on the water surface between the y-axis and either the left or the right bank of a channel cross section (with $2B$ denoting the top width); z is the transverse coordinate direction; y is the vertical coordinate direction (y is selected such that it passes through the point of maximum velocity); and h, c_y, and c_i are coefficients characterizing the isovel geometry (shape) and reflecting the influence of channel cross

section and the isovels near the bed and sides. Coefficients, c_y and c_i, are zero for rectangular cross sections and increase with the deviation of cross section from the rectangular shape. Coefficient c_y is the distance between the horizontal axis and the channel bed, and c_i is the distance between the channel side and the vertical axis. Coefficient h controls the slope and, hence, the shape of isovels at and near the water surface, particularly near the y-axis and near the point of maximum velocity.

The physical meaning of h can be explained as follows. When h is less than or equal to zero (between $-D$ and 0), its absolute magnitude $|h|$ signifies that the actual depth of the maximum velocity $u_{\max}$ is below the water surface. When it is greater than 0, h simply shapes the isovel pattern but loses its physical significance.

The curvilinear coordinates are expressed by Chiu (1989) as

$$r = Y(1-Z)^{b_i} \exp[b_i Z - Y + 1] \tag{3.59}$$

$$s = \pm \frac{1}{Z}[|1-Y|]^{a_i} \exp[Z + a_i Y] \tag{3.60}$$

where b_i is parameter, and

$$a_i = b_i \frac{4(D + c_y + h)^2}{(B + 2c_i)^2} \tag{3.61}$$

Note that $h < 0$ represents the case when the maximum velocity is below the water surface, and for $h \geq 0$ the maximum velocity is considered to occur at the water surface.

The two-dimensional velocity distribution, given by equation (3.35a), and the curvilinear coordinates have seven parameters: c_y, c_i, b_i, h, r_0, M, and $u_{\max}$. Using the geometry of flow and mass conservation, Araújo and Chaudhry (1998) derived equations for estimating these parameters where measured data are not needed. Their equations are given here. Let r_{0e} be an estimate of the null velocity isovel r_0. Then, from equations (3.56) and (3.59), one can write

$$r_0 \approx r_{0e} = \frac{c_y}{D + c_y}\left(1 - \frac{B}{B + 2c_i}\right)^{b_i} \tag{3.62}$$

$$A = 2\left(\frac{B}{2} + c_i\right)(D + c_y)\left[1 + \frac{1}{b_i - 1}(r_{0e} - b_i r_{0e}^{1/b_i})\right] \tag{3.63}$$

The channel cross-sectional area A can be expressed as

$$A = 2\int_{z=0}^{B/2}\int_{y(z)}^{D} dy\, dz \tag{3.64}$$

Recall the continuity equation:

$$Q = 2\int_{z=0}^{B/2}\int_{y(z)}^{D} u(y,z)\,dy\,dz \tag{3.65}$$

Integration of equation (3.65) leads to

$$Q = 2\int_{s_0=0}^{\infty}\int_{r_0}^{r_{\max}(s)} uh_r h_s\,dr\,ds \tag{3.66}$$

where h_r and h_s are scale factors defined as

$$h_r = \frac{(D + c_y + h)Y(1-Z)}{r\sqrt{T}} \tag{3.67}$$

$$h_s = \frac{(B + 2c_i)Z(1-Y)}{2s\sqrt{T}} \tag{3.68}$$

in which

$$T = [(1-Y)(1-Z)]^2 + a_i b_i Y^2 Z^2 \tag{3.69}$$

Equation (3.63) results from equations (3.66) through (3.69). The isovel for the null velocity r_0 can be evaluated as

$$r_0 = \frac{c_y}{D + c_y + h}\exp\left(1 - \frac{c_y}{D + c_y + h}\right) \tag{3.70}$$

Using the velocity profile data of Nezu and Rodi (1986), Araujo (1994) proposed for the surface maximum velocity

$$\frac{u_{\max}}{u^*} = 5.91\log\left(\frac{u^* D}{\upsilon}\right) + 4.81 \tag{3.71}$$

where u^* is the mean shear velocity, and υ is the kinematic viscosity. The mean shear stress on the solid boundary $\overline{\tau_0}$ can be expressed in curvilinear coordinates as

$$\overline{\tau_0} = \frac{2}{P}\int_{s_0}^{\infty} \tau_0(s) h_s\,ds \quad ; \quad s_0 = s_0(r_0) \tag{3.72}$$

where P is the wetted perimeter. Function $\overline{\tau_0}(s)$ was also given by Chiu and Chiou (1986). Here,

$$P = 2\int_{s_0}^{\infty} h_s\,ds \quad ; \quad s_0 = s_0(r_0) \tag{3.73}$$

$$\overline{\tau_0} = \rho g R_h S_f \tag{3.74}$$

where R_h is the hydraulic radius. Thus, equations (3.64) through (3.71) constitute a system of eight nonlinear equations with eight unknowns. These parameters can be estimated iteratively without requiring measurements. Steps involved in the iterative method are the following:

1. Estimate a value of h.
2. Estimate a value of c_y.
3. Compute r_0 using equation (3.70).
4. Compute $u_{\max}$ (u_D for $h \geq 0$) using equation (3.71) and M using equation (3.43).
5. Compute a_i and b_i using equations (3.59) and (3.61), taking r ($\zeta = B/2$, $y + D) = r_0$.
6. Compute values of $\overline{\tau_0}$ using equations (3.73) and (3.74) and verify the value of c_y.
7. Using equation (3.66), check h. If the difference between the estimated and computed values of Q is acceptable, then the iteration is terminated; otherwise start again from step 1.

The procedure for parameter estimation is a numerical iteration. The inputs are flow cross-sectional area, channel width, flow depth, slope of the energy line, kinematic viscosity, shear velocity, and density of water. The output includes parameter values, mean boundary shear stress, and maximum velocity.

The slope of an isovel, s_r, can be expressed by differentiating equation (3.60) (Chiu 1988) as

$$s_r = \frac{dy}{d|z|} = b_i \frac{D + c_y + h}{B + c_i} \frac{YZ}{(1-Y)(1-Z)} \tag{3.75}$$

In equation (3.75), quantities Y, Z, and $(1 - Z)$ have positive values. For $h > 0$, $y < D + h$, $(1 - Y) > 0$ as $Y < 1$, so that isovel slopes are greater than or equal to zero with increasing z. If $h < 0$, meaning that the maximum velocity occurs below the water surface, $Y > 1$ in the region $D + h < y < D$. Then, s_r is less than or equal to 0 so that isovels tend to curve in toward the y-axis. If $h = 0$, the isovels are perpendicular to the water surface. The isovel parameters of equations (3.56) through (3.58) can be determined from velocity observations or from observations of discharge, slope, roughness, and cross section. Based on analysis of simulated data, Chiu (1988) found that h can be significantly greater than zero only if M is between 6 and 9. When the width-to-depth ratio (aspect ratio) and roughness are large, h can be zero, smaller, or greater than zero if M is between 6 and 9; then isovels may or may not be perpendicular to the water surface. If M is outside this range, h can only be zero or slightly less than zero; then isovels tend to be perpendicular to the water surface. If flow is turbulent and f_l is less

than 0.04 (or $u_m/u^* > 14$), then the h value can only be zero or slightly less than zero, and, hence, isovels are perpendicular to the water surface. Streams and rivers usually have values greater than zero, and they have a tendency to attain a value of M between 6 and 9.

Araújo and Chaudhry (1998) also used 2-D entropy-based velocity distribution. Using velocimetry in five experiments with rectangular smooth wall flumes, they found the entropy-based velocity distribution equation to be more accurate than the logarithmic velocity distribution in all flow regimes, especially near the channel wall. Because secondary flow is disregarded, velocity predictions in the upper region of near side walls are relatively less accurate.

Example 3.7 Consider a small rectangular channel with a flow depth of 0.145 m, width of 1.1 m and discharge of 0.04 m^3/s. The shear velocity is 0.013 m/s. Determine the curvilinear coordinates, and compute the two-dimensional velocity distribution in the channel. Construct isovels and determine the slope of isovels.

Solution Assume that $h = 0.1$ m and $c_y = 0.1$ m. Then,

$$r_0 = \frac{c_y}{D + c_y + h} \exp\left(1 - \frac{c_y}{D + c_y + h}\right) = 0.590$$

$$u_{\max} = u^*\left[5.91 \log\left(\frac{u^* D}{\upsilon}\right) + 4.81\right] = 0.203 \text{ m/s}$$

If $u_m = 1.12$ m/s, M can be computed from equation (3.43) and obtains $M = 1.1$.

Taking r ($z = B/2$, $y = D$) = r_0, b_i can be computed from equation (3.59) as 2.35. Taking $c_i = 0.1$, a_i can be computed from equation (3.61):

$$a_i = b_i \frac{4(D + c_y + h)^2}{(B + 2c_i)^2} = -0.66$$

Checking Q with equation (3.65), one gets 0.036 m^3/s, and the assumption seems appropriate.

With $r_0 = 0.59$, the curvilinear coordinate can be determined as

$$r = Y(1 - Z)^{-2.35} \exp[-2.35Z - Y + 1]$$

$$s = \pm\frac{1}{Z}[|1 - Y|]^{-0.66} \exp[Z + -0.66Y]$$

These results can be plotted as shown in Fig. 3-15a. The slope of isovels s can be computed from equation (3.75), and one obtains a contour as in Fig. 3-15b.

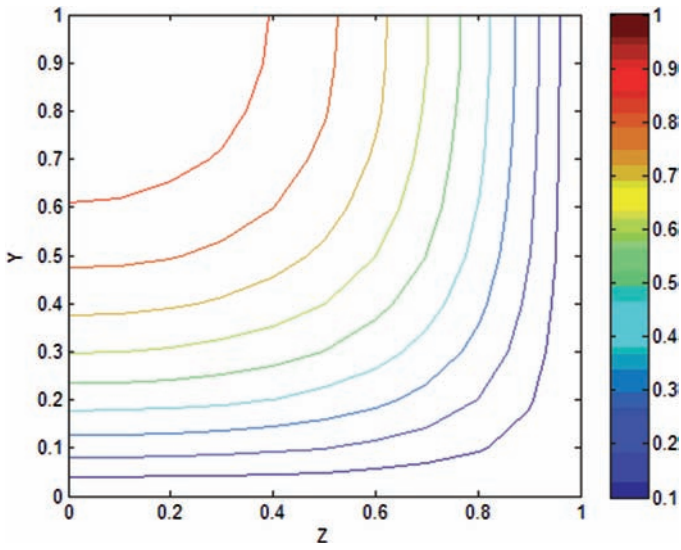

Figure 3-15a *Isovels of velocity.*

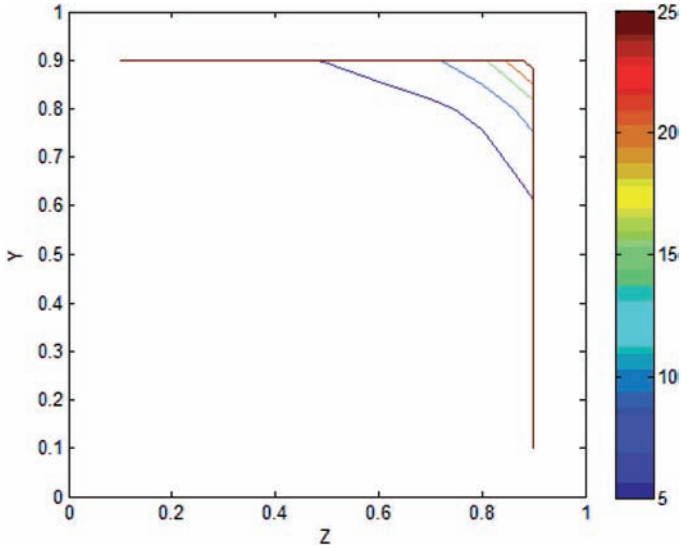

Figure 3-15b *Slope of isovels.*

Example 3.8 Consider a channel 1.5 m wide that has a flow depth of 0.25 m, shear velocity of 0.032, kinematic viscosity of $\upsilon = 1.003 \times 10^{-6}\,m^2/s$, density of 1,000 kg/m^3, and slope of 0.001. Compute the mean velocity, mean boundary shear stress, and maximum velocity.

Solution Take Manning's $n = 0.012$, $R = h = 0.25\,m$, $u^* = 0.032\,m/s$, $\upsilon = 1.003 \times 10^{-6}\,m^2/s$. Thus,

$$u_m = u^* \frac{aR^{1/6}}{n\sqrt{g}} = 0.032 \times \frac{0.25^{1/6}}{0.012\sqrt{9.81}} = 0.676 \text{ m/s}$$

$$u_{\max} = u^* 5.91 \log\left(\frac{u^* D}{\upsilon}\right) + 4.81 = 0.032 \times 5.91 \times \log\left(\frac{0.032 \times 0.25}{1.003 \times 10^{-6}}\right) + 4.81 = 5.548 \text{ m/s}$$

$$\overline{\tau_0} = \rho g R_h S_f = 1{,}000 \times 9.81 \times 0.25 \times 0.001 = 2.453 \text{ kg/(ms}^2\text{)}$$

Field observations show that the velocity does not always increase monotonically with the vertical distance from the bed ($y = 0$) to the water surface ($y = D$), meaning that a unique relation between y and u may not exist. Therefore, it is advisable to transform y to r such that there is a unique relation between u and r. Along the y-axis where $z = 0$, equations (3.56) and (3.59) yield

$$r = \frac{y}{D+h} \exp\left[1 - \frac{y}{D+h}\right] \tag{3.76}$$

Equation (3.76) can be used to characterize the spatial variation of velocity. Clearly, when $y = 0$, $r = 0$, and when $y = D$, $r = r_{\max}$. When $h < 0$, the value of h represents the actual depth of the point below the water surface and then r increases with y from $y = 0$ to $y = D + h$, where the maximum velocity occurs at $r = r_{\max} = 1$ and decreases from $D + h$ to D (water surface), as shown in Fig. 3-16.

It is seen that $r/r_{\max}$ converges to y/D for h/D exceeding unity. Differentiating equation (3.76), one obtains

$$dr = \frac{1}{D+h}\left[1 - \frac{y}{D}\right] \exp\left[1 - \frac{y}{D+h}\right] dy \tag{3.77}$$

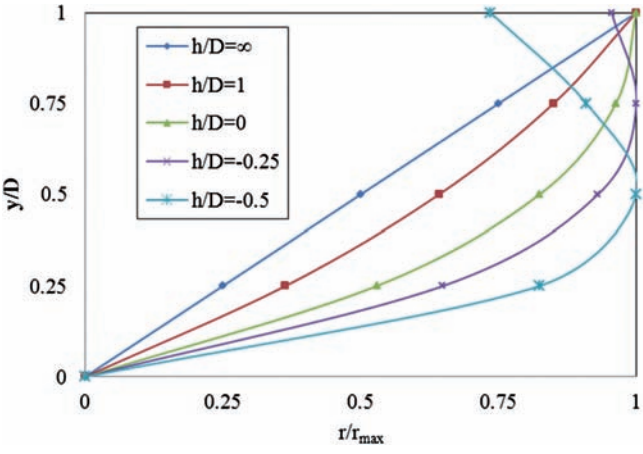

Figure 3-16 y/D *versus* r/r$_{max}$ *for various values of* h/D *from* ∞ *to –0.5.*

or

$$(D+h)\left\{\left[1-\frac{y}{D}\right]\exp\left[1-\frac{y}{D+h}\right]\right\}^{-1}dr=dy \tag{3.78}$$

which can be simply written as

$$h_r dr = dy \tag{3.79}$$

where

$$h_r=(D+h)\left\{\left[1-\frac{y}{D}\right]\exp\left[1-\frac{y}{D+h}\right]\right\}^{-1} \tag{3.80}$$

Coefficient h_r is a scale factor required for coordinate transformation between y and r systems. This transformation allows h_r and dr to have the same length dimension as dy. Using equations (3.75) and (3.80), h_r is obtained as

$$h_r=\frac{(D+c_y+h)Y(1-Z)}{r\sqrt{[(1-Y)(1-Z)]^2+\left(b_i\dfrac{D+c_y+h}{b_i+c_i}YZ\right)^2}} \tag{3.81}$$

Note that dr is dimensionless, but $h_r dr$ is an arc length on an s-curve, corresponding to an s-curve when the center of the arc is (Y, Z). Along the y-axis, $z = 0$, $c_y = 0$, then equation (3.59) is the same as equation (3.76). For narrow channels, c_y may be significantly different from 0, and, hence, the minimum value of c_y may not be zero.

The s-curves shown in Fig. 3-1 are orthogonal to r-curves that can be derived from equation (3.60) (Chiu and Said 1995):

$$s=\pm\frac{1}{Z}(|1-Z|)^{b_i[|(D+c_y-h)/(B_i-c_i)|]^2}\exp\left[Z+b_i\left(\frac{D+c_y-h}{B_i+c_i}\right)^2Y\right] \tag{3.82}$$

where s takes on a negative sign, provided that $y > D - h$ and $h > 0$; otherwise s is positive. The isovel for null velocity r_0 can be expressed as

$$r_0=\frac{c_y}{D+c_y+h}\exp\left[1-\frac{c_y}{D+c_y+h}\right] \tag{3.83}$$

The velocity gradient is

$$\frac{du}{dy}=\frac{1}{h_r}\frac{du}{dr}=[h_r r_{\max} f(u)]^{-1} \tag{3.84}$$

For calculating the longitudinal velocity at a given point (y, z) in the cross section, six parameters (c_i, c_y, b_i, h, r_0, and k) are needed. Following Chiu and Chiou (1986), these parameters can be estimated using equations (3.56) to (3.58) and (3.75) without measured data, given the geometric and flow parameters: flow discharge Q, flow cross-sectional area A, flow depth D, wetted perimeter P, mean

shear velocity u^*, slope of the energy grade line S_f, fluid kinematic viscosity υ, and density ρ.

Example 3.9 Plot patterns of isovels for M, B/D ratio, and Manning's n. Consider z as 0 to 4 m to the right of the vertical divide. Take two sets of isovels. In the first set, construct two patterns. (1) Take $u_{max} = 5\,m/s$, $h/D = -0.15$, $B/D = 1.0$, Manning's $n = 0.015$, $M = 11.25$, and $u_m = 3.50\,m/s$. (2) Take $u_{max} = 2\,m/s$, $h/D = 0.5$, $B/D = 10$, Manning's $n = 0.015$, $M = 9$, and $u_m = 1.85\,m/s$. In the second set, construct another set of four graphs.

1. Take $u_{max} = 2.85\,m/s$, $h/D = -0.01$, $B/D = 1.0$, Manning's $n = 0.03$, $M = 6.0$, and $u_m = 2.50\,m/s$.
2. Take $u_{max} = 2.15\,m/s$, $h/D = 0.00$, $B/D = 2.0$, Manning's $n = 0.03$, $M = 5.85$, and $u_m = 1.85\,m/s$.
3. Take $u_{max} = 1.75\,m/s$, $h/D = 0.20$, $B/D = 3.0$, Manning's $n = 0.03$, $M = 8.75$, and $u_m = 1.70\,m/s$.
4. Take $u_{max} = 1.15\,m/s$, $h/D = 2.20$, $B/D = 10$, Manning's $n = 0.03$, $M = 7.25$, and $u_m = 0.90\,m/s$.

What do you conclude from these two sets of isovel patterns?

Solution These curves are shown in Figs. 3-17 to 3-22. In Fig. 3-17, the maximum velocity occurs below the water surface, when h/D is positive, then velocity

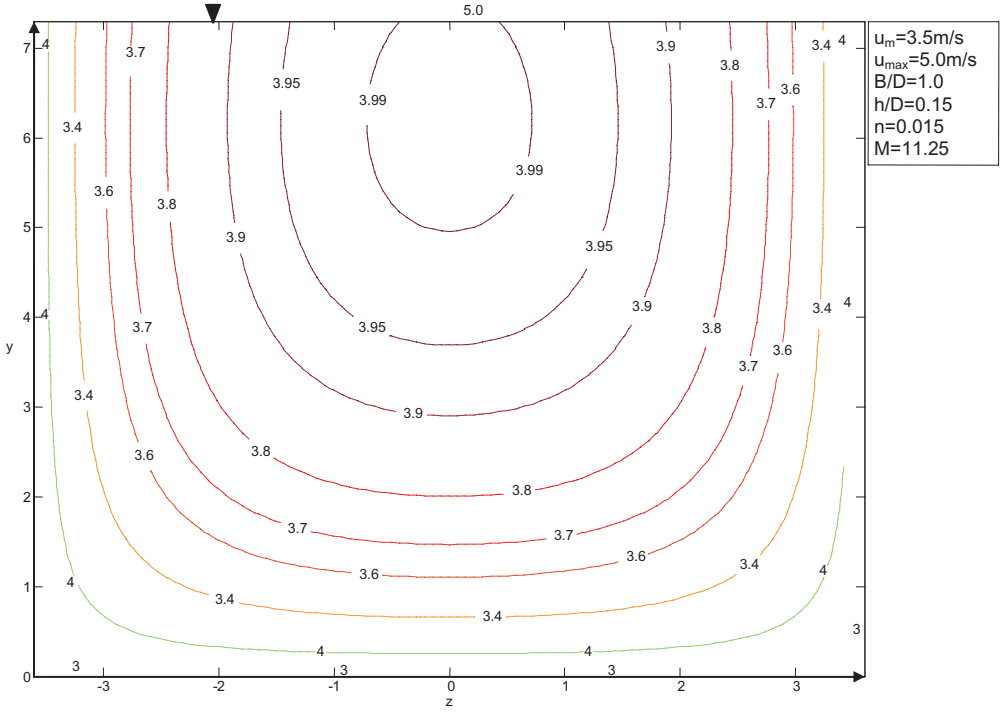

Figure 3-17 *Velocity distribution for* $u_m = 3.5\,m/s$, $u_{max} = 5\,m/s$, M = *11.25*, B/D *ratio = 1.0*, h/D = *0.15, and Manning's* n = *0.015.*

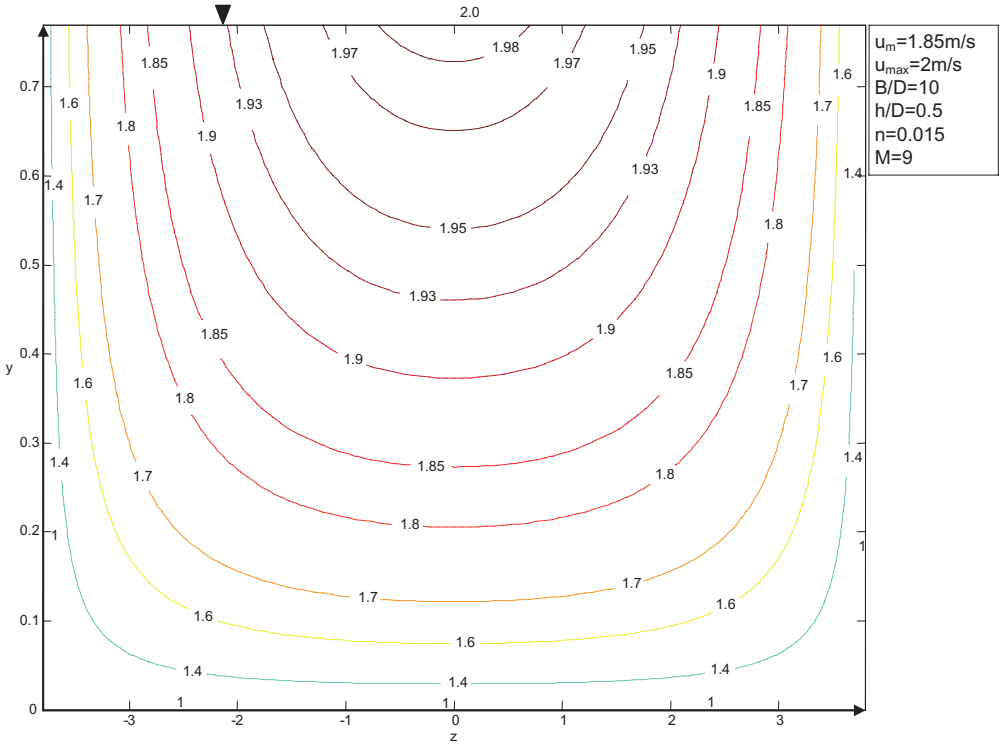

Figure 3-18 *Velocity distribution for various values of velocity distribution for* u_m = *1.85 m/s,* u_{max} = *2.0 m/s,* M = *9.0,* B/D *ratio = 10,* h/D = *0.5, and Manning's* n = *0.015.*

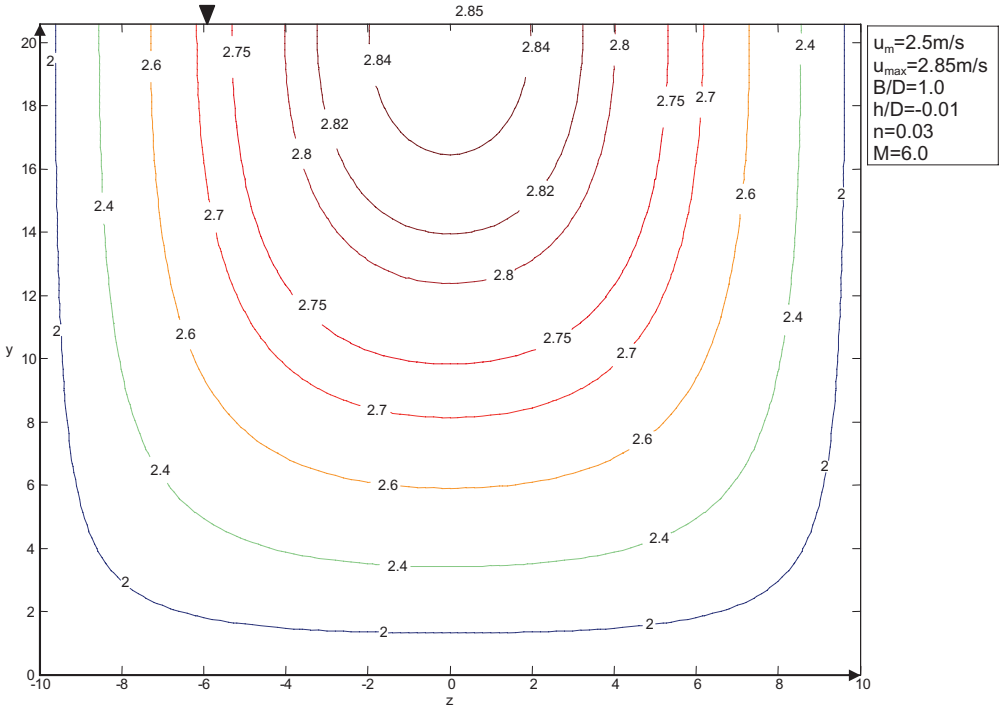

Figure 3-19 *Velocity distribution for* u_m = *2.5 m/s,* u_{max} = *2.85 m/s,* M = *6.0,* B/D *ratio = 1.0,* h/D = *0.01, and Manning's* n = *0.03.*

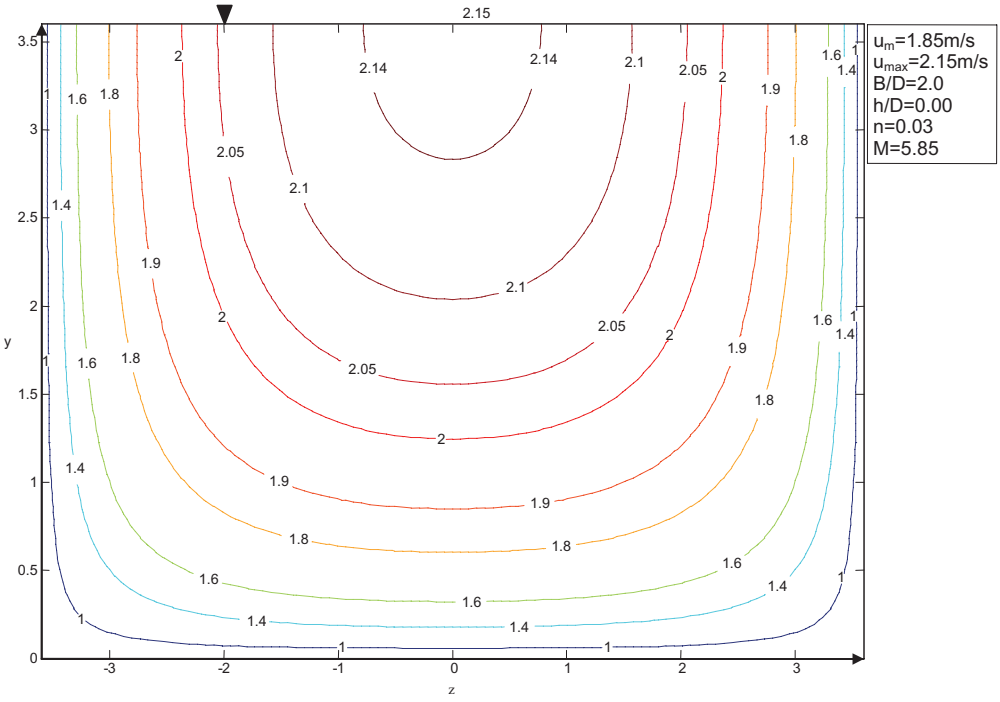

Figure 3-20 *Velocity distribution for* $u_m = 1.85\,m/s$, $u_{max} = 2.15\,m/s$, $M = 5.850$, B/D *ratio* $= 1.0$, $h/D = 0.00$, *and Manning's* $n = 0.03$.

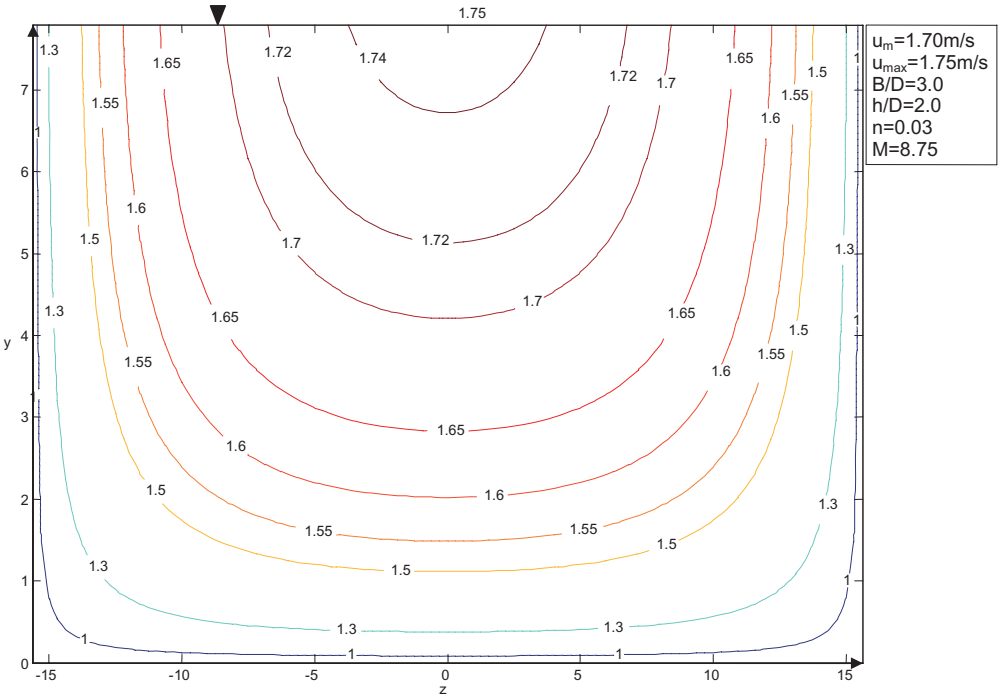

Figure 3-21 *Velocity distribution for* $u_m = 1.7\,m/s$, $u_{max} = 1.75\,m/s$, $M = 8.75$, B/D *ratio* $= 3.0$, $h/D = 2.0$, *and Manning's* $n = 0.03$.

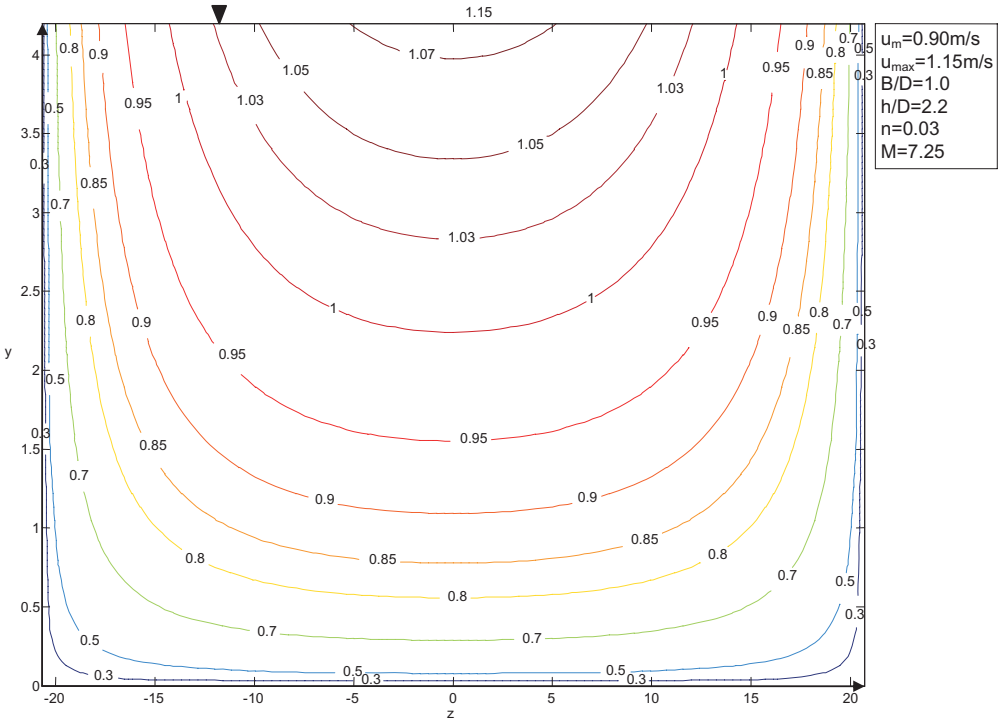

Figure 3-22 *Velocity distribution for* $u_m = 0.9\,m/s$, $u_{max} = 1.15\,m/s$, M = *7.25,* B/D *ratio* = *1.0,* h/D = *2.2, and Manning's* n = *0.03.*

decreases, expanding to the channel boundary. If h/D is nonpositive, as in Figs. 3-18 and 3-19, then the maximum velocity occurs at the water surface. When h/D is zero, the maximum velocity occurs at the surface, as shown in Fig. 3.20, and the same is true when h/D is positive as shown in Figs. 3-21 and 3-22.

3.3 Estimation of Parameters of Velocity Distribution

If $u_{\max}$ and the statistical moments of u are known, the Lagrange multipliers can be easily determined in terms of the known moments. Another simple procedure, described by Chiu (1989), is briefly outlined here.

On the channel bed $u = 0$, $y = 0$, and $h_r = (D + h)e^{-1}$, and $f(u) = \exp(\lambda_0)$. Then

$$\frac{du}{dy} = \{r_{\max}(D+h)\exp[\lambda_0 - 1]\}^{-1} \tag{3.85}$$

The velocity distribution near the bed can be assumed to be in the laminar sublayer. Hence, the velocity gradient at the channel bed can be expressed as

$$\frac{du}{dy} = \frac{\tau_0}{\mu} = \frac{u^{*2}}{\upsilon} \tag{3.86}$$

where τ_0 is the shear stress at the channel bed, $\mu = \upsilon g$ is the dynamic viscosity of the fluid, u^* is the shear velocity, g is the acceleration because of gravity, and υ is the kinematic viscosity. From equations (3.85) and (3.86), parameter λ_0 can be determined as

$$\lambda_0 = 1 + \ln\left[\frac{\upsilon}{u^{*2}(D+h)r_{\max}}\right] \tag{3.87}$$

in which $r_{\max} = 1$ if $h \le 0$; $r_{\max} = (D/h)\exp[h/(D+h)]$ if $h > 0$.

For wide channels $r/r_{\max} \approx y/D$, and, hence, $h_r = D$, $r_{\max} = 1$, so that

$$\lambda_0 = \ln\left(\frac{\upsilon}{u^{*2}D}\right) \tag{3.88}$$

For flow with isovels perpendicular to the water surface, parameter λ_0 can be obtained with the use of $h = 0$ and $r_{\max} = 1$ in equation (3.87). Now λ_0 and u_m can be used in equations (3.10) and (3.21) to obtain λ_1 and $u_{\max}$. It may be noted that for clear-water flow the viscosity can be obtained for a given temperature, but for sediment-laden flow it varies with sediment concentration. Equations (3.87) and (3.88) can, therefore, be used to obtain λ_0 and υ, and can, in turn, yield sediment concentration at the bed.

3.4 Maximum and Mean Velocities

3.4.1 Location of Maximum Velocity

Equation (3.35a) with $r_0 = 0$ can be expressed as

$$u = \frac{u_{\max}}{M}\ln\left\{1 - [\exp(M) - 1]\frac{r}{r_{\max}}\right\} \tag{3.89}$$

where $u_{\max}$ occurs and corresponds to $r = r_{\max}$, the maximum value of r; r is constant along an isovel where velocity is u. The ratio $r/r_{\max}$ is equal to the probability of velocity, randomly sampled, being less than or equal to u:

$$\int_0^u f(u)du = \frac{r}{r_{\max}} \tag{3.90}$$

On the vertical axis where $u_{\max}$ occurs, designated as y-axis, r can be expressed from equation (3.76) as

$$r = \frac{y}{D+h}\exp\left[1 - \frac{y}{D+h}\right] = \frac{\frac{y}{D}}{1+\frac{h}{D}}\exp\left[1 - \frac{\frac{y}{D}}{1+\frac{h}{D}}\right] \tag{3.91}$$

where y is the vertical distance from the bed and h can take on negative, positive, and zero values. Here, three cases can be distinguished.

Case 1

The maximum velocity occurs not at the water surface but at a vertical distance h below. In this case, h takes on a negative value, because it is measured downward from the water surface. If h is assigned a positive value, then $y = D - h$. This situation means that u decreases from this point upward to the water surface and $du/dy < 0$ at $y = D$. This situation means that $h < 0$, and r_{max} and u_{max} occur at $y = D + h$, i.e., the upper limit of $|h/D|$, h/D, is one. In that case, equation (3.91) yields $r_{max} = 1$, and

$$\frac{r}{r_{max}} = r = \frac{y}{D+h}\exp\left[1-\frac{y}{D+h}\right] = \int_0^u f(u)du \tag{3.92}$$

$$\frac{du}{dy} = \frac{1}{h_r}\frac{du}{dr} = [h_r r_{max} f(u)]^{-1} \tag{3.93}$$

in which r_{max} and $f(u)$ are positive; h_r is positive for $0 \le y \le D + h$ but equals $D + h$ and becomes negative for $D + h \le y \le D$ if $h < 0$.

One can express the location of the mean velocity as

$$\frac{\bar{r} - r_0}{r_m - r_0} = \frac{\frac{y_m}{D}}{1+\frac{h}{D}}\exp\left(1-\frac{\frac{y_m}{D}}{1+\frac{h}{D}}\right) \tag{3.94}$$

where y_m is the vertical distance from the channel bed where velocity is the mean velocity. This equation shows that y_m/D and h/D are indicators of the locations where u_m and u_{max} occur on the y-axis.

Case 2

u_{max} occurs at the water surface, i.e., $h = 0$, $r_{max} = 1$, and equation (3.91) becomes

$$\frac{r}{r_{max}} = r = \frac{y}{D}\exp\left[1-\frac{y}{D}\right] \tag{3.95}$$

In this case, $du/dy = 0$ at the water surface, and the velocity curve intersects the water surface at a right angle.

Case 3

u_{max} occurs at the water surface and $du/dy > 0$ at the surface, and $h > 0$. The maximum value of r is

$$r_{max} = \frac{D}{D+h}\exp\left[1-\frac{D}{D+h}\right] \tag{3.96}$$

Thus,

$$\frac{r}{r_{\max}} = \frac{y}{D}\exp\left[1-\frac{D+y}{D+h}\right] \text{ or } \frac{r}{r_{\max}} = \frac{y}{D}\exp\left[\frac{D-y}{D+h}\right] \tag{3.97}$$

As $h \to \infty$,

$$r/r_{\max} \to y/D \tag{3.98}$$

One can also write

$$\frac{\bar{r}-r_0}{r_{\max}-r_0} = \frac{y_m}{D}\exp\left(\frac{1-\frac{y_m}{D}}{1+\frac{h}{D}}\right) \tag{3.99}$$

In this case, h does not have the same physical meaning as in cases 1 and 2. Equations (3.92), (3.95), and (3.97) show that various patterns of velocity distributions can be obtained from equation (3.89) by varying $r/r_{\max}$.

Plotting equations (3.94) and (3.99) for various values of M, it can be seen from Figs. 3-23 and 3-24 that the relation between y_m/D and h/D becomes independent of M for $M > 8$ or y_m/D, where y_m is the value of y from the channel bed corresponding to mean velocity, becomes independent of h/D when $h/D > 30$, and for $M > 6$, it becomes $e^{-1} = 0.368$. For smaller values of h/D (less than 1), y_m/D increases rapidly with h/D. y_m/D becomes 0.16 at $h = 0$. When the maximum velocity occurs below the water surface, i.e., $h < 0$, y_m/D decreases below 0.3. Equation (3.94) or (3.99) expresses the relation between y_m/D and h/D.

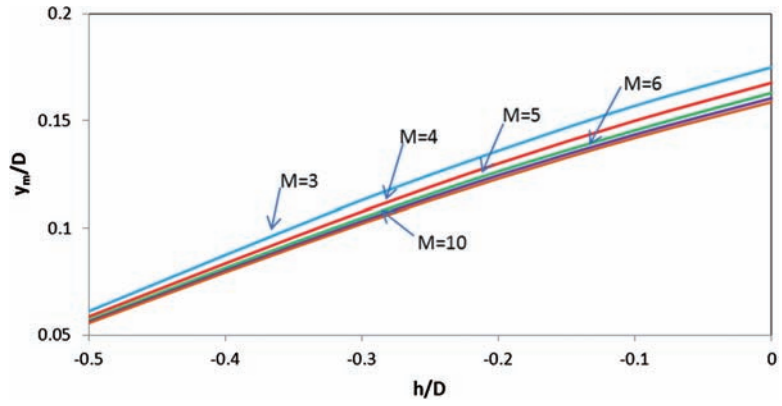

Figure 3-23 *Relation between* h/D *and* y_m/D *for various values of* M *with* h > 0.

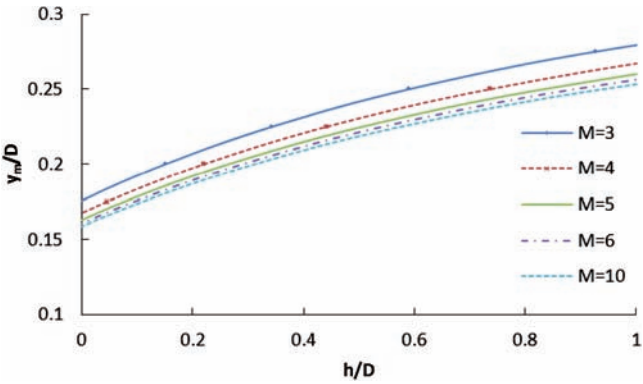

Figure 3-24 *Relation between* h/D *and* y_m/D *for various values of* M *with* h < 0.

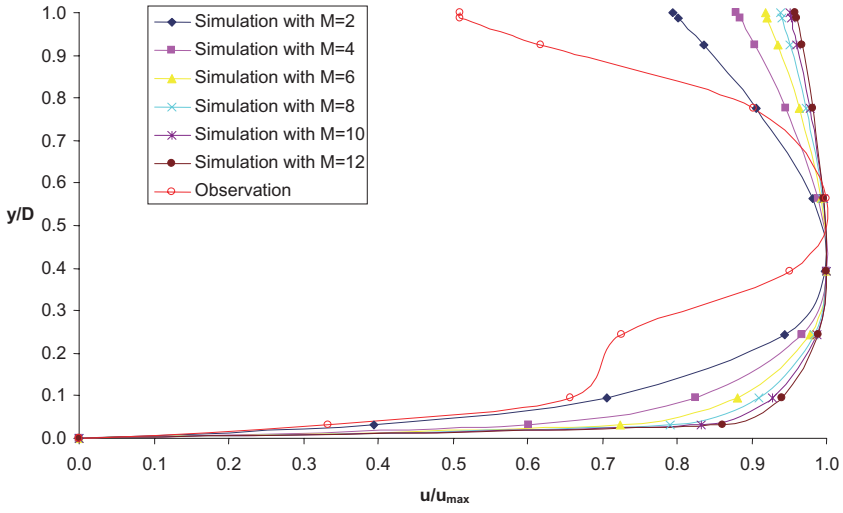

Figure 3-25 *Velocity* (u/u_{max}) *versus* y/D *for various values of* M.

Example 3.10 Plot y/D versus u/u_{max} for various values of parameter M, $M = 0$, 2, 4, 6, 8, 10, and 12. What do you conclude from this plot?

Solution The 2-D velocity distribution equation is given by equation (3.35a). When u_{max} occurs, r can be expressed as a function of y in equation (3.91). The maximum velocity u_{max} occurs at a vertical distance h below the water surface ($y = D - h$), thus $du/dy < 0$ at the water surface. In this case, $h < 0$ and r_{max} and u_{max} occur at $y = D - h$. Combining equations (3.35a) and (3.91) with $r = r_{max}$, one obtains a plot of y/D versus u/u_{max} for various values of M, as shown in Fig. 3-25.

Example 3.11 Yen (1965) reported a set of velocity data in a cross section at the entrance to a bend of a trapezoidal channel. The mean velocity through the cross section was 3.15 ft/s (0.96 m/s). The maximum value for velocity in the data was 3.737 ft/s (1.14 m/s), although the maximum velocity was not known or reported. Check if the mean velocity reported is in accord with what one would obtain from the procedure outlined here.

Solution Assume that the maximum velocity is the same as the maximum value as given: $u_{\max} = 3.15\,\text{ft/s}$. Then $u_m/u_{\max} = 3.15\,\text{ft/s}/3.737\,\text{ft/s} = 0.83$. This equation yields an M value of 6 (approximately) from Fig. 3-8. The isovels constructed with the data set seem perpendicular to the water surface; h/D is about 0. Then y_m/D from Fig. 3-23 is 0.16. On the y axis ($z = 0$), the vertical passing through the point of maximum velocity, the $y = 0.16D$ should have velocity = 3.15 ft/s, mean velocity. This result confirms the mean velocity reported by Yen (1965).

3.4.2 Determination of Maximum Velocity

If velocity is measured at two points $y = 0.2D$ and $y = 0.8D$, i.e., $u_{0.2}$ and $u_{0.8}$, between the water surface, then $u_{\max}$ from $u_{0.2}$ and $u_{0.8}$ is computed from equation (3.35a) as follows:

$$u_{0.2} = \frac{u_{\max}}{M_1}\ln\left\{1 + [\exp(M_1) - 1]\frac{r_{0.2}}{r_{\max}}\right\} \tag{3.100}$$

$$u_{0.8} = \frac{u_{\max}}{M_1}\ln\left\{1 + [\exp(M_1) - 1]\frac{r_{0.8}}{r_{\max}}\right\} \tag{3.101}$$

$$\overline{u}_y = \frac{u_{0.2} + u_{0.8}}{2} = \frac{u_{\max}}{MD}\int_0^D \ln\left\{1 + [\exp(M_1) - 1]\frac{r}{r_{\max}}\right\} dy \tag{3.102}$$

$$r_{0.2} = \frac{0.8D}{D-h}\exp\left(1 - \frac{0.8D}{D-h}\right) \tag{3.103a}$$

$$r_{0.2} = \frac{0.2D}{D+h}\exp\left(1 - \frac{0.2D}{D+h}\right) \tag{3.103b}$$

$$r_{0.8} = \frac{0.2D}{D-h}\exp\left(1 - \frac{0.2D}{D-h}\right) \tag{3.104a}$$

$$r_{0.8} = \frac{0.8D}{D+h}\exp\left(1 - \frac{0.8D}{D+h}\right) \tag{3.104b}$$

$$r_{\max} = 1 \quad \text{if} \quad h \geq 0 \tag{3.105}$$

$$r_{\max} = 1 \quad \text{if} \quad h \leq 0 \tag{3.106}$$

$$r_{\max} = \frac{D}{D-h}\exp\left(1-\frac{D}{D-h}\right) \quad \text{if} \quad h<0 \tag{3.107}$$

$$r_{\max} = \frac{D}{D+h}\exp\left(1-\frac{D}{D+h}\right) \quad \text{if} \quad h>0 \tag{3.108}$$

where M_1 is the value of local M of a flow event on the y-axis. Values of $u_{\max}$, M_1, and h can be obtained from the solution of equations (3.100), (3.101), and (3.103b) to (3.107).

3.4.3 Location of the Maximum Velocity Axis

It is not easy to determine the location of the axis of maximum velocity in open-channel flow. Velocity observations can be used to ascertain the location of the y-axis on which the maximum velocity occurs. If a channel is straight and regular as are human-made canals, the y-axis usually occurs at the center of the cross section. Field observations taken on rivers under a variety of flow conditions indicate that the position of the y-axis is quite stable and is almost invariant with discharge, gauge height, and time, provided that the channel bed does not change significantly (Chen 1998). Conversely, when the channel overflows, its banks are topped and water spreads in the floodplain, and the location of the y-axis changes. The maximum cross-sectional velocity is close to the maximum velocity on the y-axis. During floods, the maximum velocity on the water surface can reasonably indicate the location of the y-axis. The maximum velocities can be estimated from the mean location of the y-axis.

3.4.4 Relation of the Location of Maximum Velocity to M and ϕ

One can gain insight into the mechanism that determines the location of maximum velocity below the water surface from consideration of the bed shear at the y-axis expressed as

$$\rho g S_f (D-h) = \rho \varepsilon_0 \frac{du}{dy}\Big|_{y=0} \tag{3.109}$$

$$\frac{du}{dy}\Big|_{y=0} = \frac{u_{\max}}{DM}\frac{\exp(M)-1}{\left\{1+[\exp(M)-1]\frac{y}{D}\right\}\Big|_{y=0}} = \frac{u_{\max}}{DM}[\exp(M)-1] \tag{3.110}$$

where ρ is the mass density of water, g is the acceleration caused by gravity, S_f is the friction slope, and ε_0 is the momentum transfer coefficient at the channel bed and equals the kinematic viscosity of the fluid if flow is laminar or has a viscous sublayer at the channel bed. The bed shear at the y-axis may be assumed to equal the mean boundary shear (Chiu and Lin 1983; Chiu and Chiou 1986). One can invoke the Darcy–Weisbach relation between shear velocity u^* and friction factor f_l, which is given by equation (3.53).

The gradient of velocity in equation (3.109) can be obtained from equation (3.35a), with r defined by equation (3.1), and then combining equations (3.109) and (3.53), one obtains

$$\left(1-\frac{h}{D}\right)^2=\frac{\varepsilon_0}{\upsilon}\left(\frac{R_h}{D}\right)^2\frac{8\rho}{f_l R_n}G(M) \tag{3.111}$$

where R_h is the hydraulic radius, R_n is the Reynolds number defined by equation (3.55), and

$$G(M)=\frac{\exp(M)-1}{M\phi} \tag{3.112}$$

in which ϕ is expressed in terms of M defined by equation (3.49). Equation (3.112) sheds some light on the location of maximum velocity.

Consider a wide channel in which $u_{\max}$ occurs at the water surface so that r/r_m in equation (3.35a) is y/D and $\tau_0 = \rho g D S_f$. Then

$$\frac{\varepsilon_0}{\upsilon}\frac{8}{f_l R_n}G(M)=1 \tag{3.113}$$

The quantity $\varepsilon_0/\upsilon = 1$ in flows with a viscous sublayer. Then equation (3.113) becomes

$$G(M)=\frac{fR_n}{8} \tag{3.114a}$$

Therefore,

$$\rho g S_f(D-h)=\rho\varepsilon_0\frac{u_{\max}}{DM}[\exp(M)-1] \tag{3.114b}$$

This equation means that $G(M)$ and, hence, M vary with the product of $f_l R_n$. For laminar flow, $f_l R_n$ is constant, and, hence, $G(M)$ and, in turn, M are constant for a channel cross section. Conversely, $f_l R_n$ varies with M, ϕ, or $u_m/u_{\max}$. One can interpret the idea that ϕ and M are constant for a channel cross section and, hence, control ε_0/υ, f_l, R_n, R_h, and h. Therefore, a relation between h/D and $G(M)$ must exist. Chiu and Tung (2002), using regression analysis, found

$$\frac{h}{D}=-0.2\ln\frac{G(M)}{58.3} \tag{3.115}$$

for the data range $1.0 \le M \le 5.6$ and $0 \le h/D \le 0.61$. Equation (3.115) can be converted into an $h/(D - M)$ relation.

For the South Esk River at Bridge 4 (Bridge and Jarvis 1985), Chiu and Tung (2002) found that h increased with $u_{\max}$, but h/D was invariant with $u_{\max}$ or discharge. The average h/D value was 0.48. In general, the average h/D and M are constant at a channel cross section. This means that in equation (3.110), (ε_0/υ) (), (R_h/D), and $(f_l R_n)^{-1}$ are also constant at a channel cross section.

3.4.5 Relative Locations of u_{max} and u_m

If u_{max} occurs at the water surface and M is greater than 6, r/r_{max} in equation (3.35a) can be represented by y/D. The location of the point where $u = u_m$ is $\bar{y}/D = \bar{r}/r_{max} = 0.368$, where $\bar{y}$ and $\bar{r}$ are the values of y and r, respectively, where $u = u_m$. To determine the point where $u = u_m$ on the y axis and u_{max} occurs below the water surface, one can write

$$\frac{u_m}{u_{max}} = \Phi = \frac{\exp(M)}{\exp(M)-1} - \frac{1}{M} = \frac{1}{M}\ln\left\{1+[\exp(M)-1]\frac{\bar{r}}{r_{max}}\right\} \tag{3.116}$$

in which $\bar{r}/r_{max}$ can be expressed as

$$\frac{\bar{r}}{r_{max}} = \frac{\frac{\bar{y}}{D}}{1+\frac{h}{D}}\exp\left[1-\frac{\frac{\bar{y}}{D}}{1+\frac{h}{D}}\right] = \Omega(M) \tag{3.117}$$

$\bar{y}$ is the location of the point on the y-axis where the velocity is equal to the cross-sectional mean velocity $u_m = Q/A$; it is not the location of the point where the velocity equals the vertical mean on the y-axis. The value of $\bar{y}/D$ is not $e^{-1} = 0.368$ if u_{max} occurs below the water surface. Equation (3.117) yields $\bar{y}/D = 0.16$ or smaller (Chiu 1988), even though $M > 6$ if $h \le 0$ or u_{max} occurs below the water surface.

3.4.6 Determination of Mean Velocity

In hydraulics, a relation between the mean velocity and the maximum velocity in pipe flow is often expressed as

$$\frac{u_m}{u_{max}} = c \tag{3.118}$$

where c is a constant = 0.8167 (Streeter and Wylie 1979). This relation can be obtained from Prandtl's (1925) one-seventh power law velocity distribution:

$$\frac{u}{u_{max}} = \left(\frac{y}{r_0}\right)^{1/m} \tag{3.119}$$

where y is the distance from the pipe wall, r_0 is the pipe radius, and m is an exponent equal to 7.

In contrast with the cross-sectional mean velocity, the maximum velocity in a channel has received little attention. In the two-dimensional velocity distribution, the mean velocity, u_m, can be expressed as a linear function of the maximum velocity, u_{max}, through a dimensionless entropy parameter M (Chiu 1991). The M parameter is a fundamental measure of information about the characteristics of the channel section, such as changes in bed form, slope, and geometric shape

(Chiu and Murray 1992), and it can be derived from the pairs of u_{max} and u_m measured at a channel cross section. Xia (1997) investigated the relation between mean and maximum velocities by using the velocity data collected in some cross sections of the Mississippi River. He found that the relation was perfectly linear along both straight reaches and river bends and that the M value was constant and equal to 2.45 and 5, respectively. Although Xia's results were preliminary because of the limited amount of data, the relation between the mean and maximum velocities, as introduced by Chiu (1991), if tested on other natural channels, can be useful for investigating the flood characteristics in rivers (Moramarco and Singh 2001).

Another efficient method for estimating the mean flow velocity was proposed by Chiu and Said (1995). They estimated the location of the mean velocity on the vertical passing through the point of the maximum velocity. On the same profile, more recently Chiu and Tung (2002) also investigated the location of the maximum velocity as a function of M. If h = location of maximum velocity below the water surface; D = water depth on the vertical passing through the point of maximum velocity; and $\bar{y}$ = location of mean velocity above the bed on the same vertical, they showed that at a river site, h/D and $\bar{y}/D$ were constant and depended on the M value. However, for new river sites, M cannot be estimated accurately because of limited velocity data. Moramarco et al. (2004) evaluated the accuracy of the linear relation between the mean and maximum velocities by using the data collected during a period of 20 years for four gauged sections in the upper Tiber River basin in central Italy. They also evaluated the velocity profiles at different verticals estimated through the spatial velocity distribution proposed by Chiu (1987, 1988, 1989) and those given by two simple approaches and based on the same Chiu velocity distribution, by using the velocity data collected during seven flood events. They developed a practical method, both for new and historical river sites, for estimating the cross-sectional mean velocity also when, because of high floods, it is difficult to carry out velocity measurements in the lower portion of the flow area.

The relation between the mean velocity, u_m, and the maximum velocity, u_{max}, can be expressed as (Chiu and Said 1995)

$$u_m = \phi(M) u_{max} \tag{3.120}$$

in which

$$\phi(M) = \frac{u_m}{u_{max}} = \frac{e^M}{e^M - 1} - \frac{1}{M} \tag{3.121}$$

and M is the entropy parameter. Equation (3.120) shows that if a sample of pairs (u_m, u_{max}) is given, $\Phi(M)$ can be estimated and then so can the entropy parameter M.

Using the velocity data collected during a period of 20 years at four gauged sections, three of them located along the Tiber River at 68 km (Santa Lucia), at 109.2 km (Ponte Felcino), and at 137.4 km (Ponte Nuovo) and one section along the Chiascio River, a tributary of the Tiber River, at 85 km (Rosciano), Moramarco

et al. (2004) tested the relationship between the mean velocity and the maximum velocity in a channel cross section. The selected sections were equipped with a remote ultrasonic water-level gauge, and the velocity measurements were made by current meter from cableways. Depending on the cross-sectional flow area, the number of verticals carried out changed from 4 up to 10, and for each vertical at least 5 velocity points were sampled. Comparing the velocity points sampled along different verticals and applying the well-known velocity–area method (Herschy 1985), the maximum and mean velocities were estimated (Chiu and Said 1995; Xia 1997). Generally, the true maximum velocity is unknown, but for each vertical, the maximum value in the data set of velocity points sampled can be assumed for it (Chiu 1988).

Using pairs of u_m and $u_{\max}$ collected at the four gauged sections, the best-fit mean velocity, u_{bf}, was calculated. The values of $\Phi(M)$ were estimated, as shown in Fig. 3-26. Therefore, $\Phi(M)$ can be assumed to be constant for the four gauged sections, confirming the results obtained by Xia (1997) for the Mississippi River. The best-fit line relative to the mean and maximum velocity data set of the four gauged sections was as shown in Fig. 3-27. As can be seen, the linear relationship based on equation (3.120)

$$u_{bf} = b\, u_{\max}, \quad b = 0.665 \tag{3.122}$$

has a high correlation coefficient showing that parameter $\Phi(M) = 0.665$ and then $M = 2.13$ can be assumed to be constant within the two river reaches investigated. The accuracy of this linear relationship for the four gauged sections was investigated by evaluating the errors ε and ε(%), which are defined as follows:

$$u_m = u_{bf} + \varepsilon \tag{3.123}$$

$$\varepsilon(\%) = 100 \cdot \frac{u_{bf} - u_m}{u_m} \tag{3.124}$$

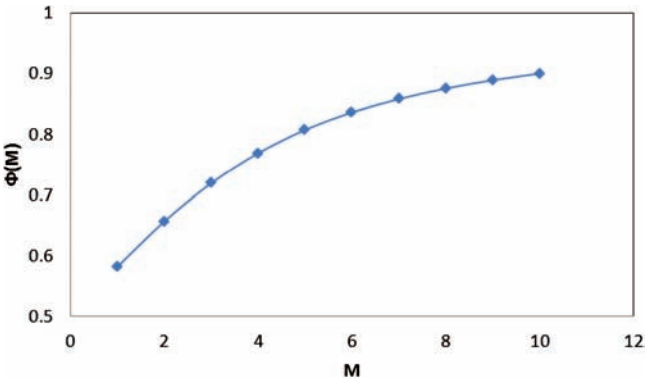

Figure 3-26 *Estimated values of ϕ(M).*

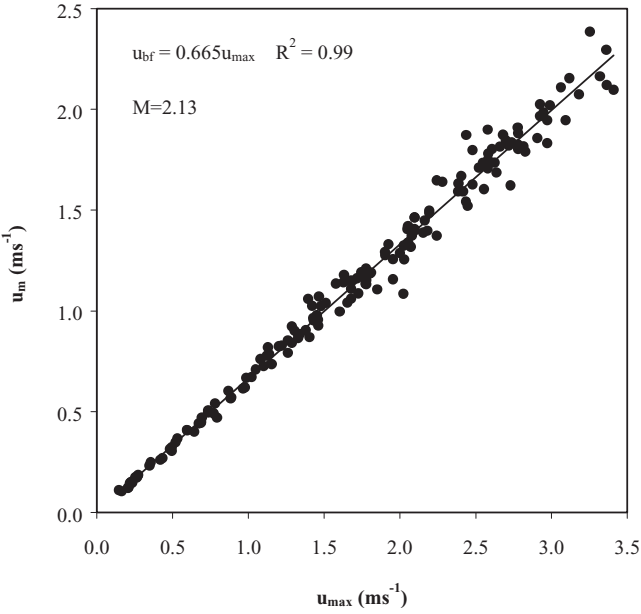

Figure 3-27 *Mean and maximum velocity data set of four gauged sections.*

in which u_{bf} is the mean velocity calculated by equation (3.122). Based on error analysis, Moramarco et al. (2004) concluded that M can be considered as an intrinsic parameter of a river reach.

Equation (3.122) is applicable to straight as well as curved reaches. However, the value of $\Phi(M)$ increases slightly with increasing value of r_c/B, where r_c is loop radius at channel center, and B is the channel surface width. Xia (1997) reasoned that a relation between b and r_c/B would be useful. One can easily obtain a value of r_c/B from a map. Then, with r_c/B thus obtained, one can obtain b from the relation; then one can obtain the relation between u^* and $u_{\max}$. Since the variation in the value with increasing r_c/B is only small, it can be argued that the relations between the cross-sectional mean and maximum velocities for different river bends would be similar. The implication is that a relation between the two velocities for one river bend could be used for another river bend.

Comparing the relations between $u_{\max}$ and u_m for straight and curved reaches, $u_{\max}$ on a straight reach is greater than that on a river bend for the same cross-sectional mean velocity u_m. Bhowmik (1979), for example, found under three flow discharges (29.5, 40.2, and 113.3 m^3/s) that the average ratio $u_{\max}/u_m$ values in a straight reach were 1.75, 1.5, and 1.5, respectively. In a river bend with r_c/B = 1.90, the measured ratios were 1.50, 1.23, and 1.35, respectively.

To develop a practical and simple method for estimating discharge, also during high floods, Moramarco et al. (2004) assumed that equation (3.35a), written for the vertical where the maximum velocity occurs (x = 0), can be

applied to other verticals in the following form (Chiu 1988, 1989; Chiu and Murray 1992; Chiu and Said 1995; Greco 1999):

$$u_i = \frac{u_{\max_i}}{M_i}\ln\left(1+\left(e^{M_i}-1\right)\frac{y}{D_i-h_i}\exp\left(1-\frac{y}{D_i-h_i}\right)\right) i=1,2,\ldots,N_v \quad (3.125)$$

where u_i and D_i are the velocity and water depth along the ith vertical, respectively; y is the vertical distance measured from the channel bed; N_v is the number of verticals sampled in the cross-sectional flow area; M_i, h_i, and $u_{\max_i}$, in this case, are parameters. For applying equation (3.125), two scenarios were tested. First, parameter M_i was assumed to be constant along all verticals and its value was equal to 2.13; $u_{\max_i}$, D_i, and h_i are the maximum velocity, water depth, and depth of $u_{\max_i}$ below the water surface, respectively, on each vertical. Second, the M_i parameter value changed along each vertical as

$$\frac{e^{M_i}}{e^{M_i}-1}-\frac{1}{M_i}=\frac{u_{m_i}}{u_{\max}} \quad (3.126)$$

where u_{m_i} is the mean velocity along the ith vertical, and $u_{\max}$ is the maximum velocity sampled in the cross-sectional flow area. It was found that for the data collected during the flood events of June 1997 and November 1996 at the Ponte Nuovo section, equation (3.125) improved the accuracy of the velocity profile estimation, also in the portions close to the side walls, as shown in Fig. 3-28. It was thus suggested that parameter M could be considered a signal of the boundary effects on the velocity distribution (Chiu and Said 1995).

Xia (1997) investigated the relation between the maximum velocity and the cross-sectional mean velocity. Using the velocity data collected from the Mississippi River at five gauging stations (three were on bends and two on almost straight reaches), he found

$$u_{\max} = bu_m \quad (3.127)$$

where the value of b varied from 1.2386 to 1.2433 for bends and 1.458 to 1.46 for straight reaches. He reported that b varied a little bit with r_c/B, a measure of meandering of a river bed, r_c = loop radius at the channel centerline. The value of the maximum velocity in a straight reach is greater than in a river bend for the same cross-sectional mean velocity.

3.4.7 Estimation of Mean Velocity from Velocity Profile along the y-Axis

The maximum velocity on the y-axis is the cross-sectional maximum. The ratio of the cross-sectional mean velocity u_m to the vertical mean u_{my} on the y-axis can be expressed as

$$\frac{u_m}{u_{my}} = \frac{M\phi(M)}{I\left(M,\frac{h}{D}\right)} = b\left(M,\frac{h}{D}\right) \quad (3.128)$$

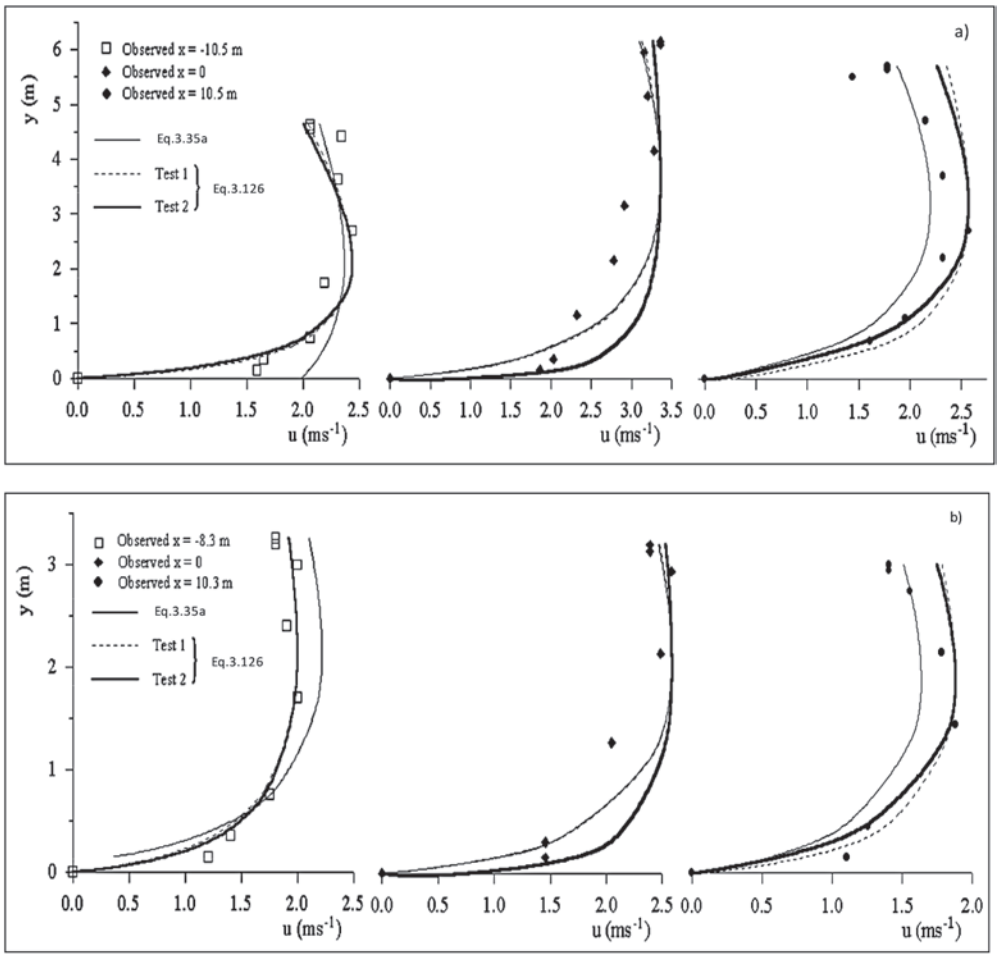

Figure 3-28 *A comparison of the velocity profiles obtained by equations (3.35a) and (3.125) for the data collected during the flood events of June 1997 and November 1996 at the Ponte Nuovo section.*

where for $h \le 0$,

$$I\left(M, \frac{h}{D}\right) = \int_0^1 \ln\{1 + [\exp(M) - 1]\frac{D}{1 + \frac{h}{D}} \exp\left[1 - \frac{\frac{y}{D}}{1 + \frac{h}{D}}\right] d\left(\frac{y}{D}\right) \qquad (3.129)$$

and for $h \ge 0$,

$$I\left(M, \frac{h}{D}\right) = \int_0^1 \ln\{1 + [\exp(M) - 1]\frac{D}{1 + \frac{h}{D}} \exp\left[\frac{1 + \frac{y}{D}}{1 + \frac{h}{D}}\right] d\left(\frac{y}{D}\right) \qquad (3.130)$$

For small magnitudes of M and h/D, equation (3.128) is not stable.

3.5 Comparison of Mean Velocity Estimates

It may be interesting to compare the error in estimating the mean velocity along each sampled vertical by using Chiu's two-dimensional velocity distribution (equation (3.35a)) and the scenario tests. For 45 verticals sampled during the selected flood events, the mean velocity was estimated with an error less than 10% for 82% of the verticals, and equation (3.35a) for 78% of the verticals. Once the mean velocity is estimated along each vertical, the cross sectional mean velocity can be calculated by applying the velocity–area method. Then, comparison of the errors in estimating the mean velocity of the flow through equation (3.35a) and the two scenarios was made. Both scenarios were fairly accurate for most of the selected events with a percentage error of less than 10%. Therefore, the experimental evidence showed that equation (3.125) can be applied locally at each vertical. This result is useful in practical engineering concerning flood estimation through velocity measurements. In fact, in addition to the drastic reduction of the number of parameters, equation (3.125) can also be conveniently adopted during high floods, when it is not possible to collect direct velocity measurements, especially in the lower portion of the flow area. If a topographical survey of the gauged section is available and the location of the maximum velocity is sampled, equation (3.125) can be easily used for reconstructing the velocity profile along each vertical of the flow area.

In the case that M is known (historical gauged sections), scenario 1 is more suitable for this analysis, whereas scenario 2 should be applied for new river sites where the velocity data are limited for estimating an accurate best-fit line. The results obtained for scenario 1 point out that the velocity profile for each vertical can be estimated by only sampling the maximum velocity along each vertical, $u_{\max_i}$. Since maximum velocities occur in the upper portion of the flow area, their sampling, for instance, by a current meter through cableways, can be carried out more easily, even during high floods. Once the velocity profiles are known, the cross-sectional mean velocity can be calculated.

For scenario 2, if the local parameter M_i can be estimated, considering the ratio between the mean velocity occurring along each vertical and the maximum velocity sampled, it permits us to overcome the gap in the velocity data for new river sites where M is unknown. However, the mean velocity along each vertical must be known, and during high floods it is possible to sample the maximum velocity, $u_{\max}$, but the sampling of the velocity points in any portion of the flow area cannot always be easily carried out. Furthermore, sometimes the velocity profiles reconstructed for scenario 2 are not quite accurate in the flow area close to side walls. For this reason, a practical method for estimating the behavior of the mean velocity in the different portions of the flow area is proposed in the next section.

3.6 Alternative Method for Estimation of the Cross-Sectional Area Mean Velocity for New River Sites

Equation (3.127) permits the estimation of the mean velocity, once the maximum velocity is sampled; if the flow area is known, the discharge can also be calculated. However, in some cases the estimated discharge can have substantial errors. Besides, for newly gauged river sections, where there is a limited amount of velocity data for determining the M value, a simple technique for estimating discharge by the single velocity profile passing through the point of maximum velocity occurring at $x = 0$ was proposed by Chiu and Said (1995). If $u_{\max}$ and h are determined from the velocity profile sampled at $x = 0$, then substituting in equation (3.121), the M value can be determined through the least-squares method (Chiu and Said 1995). Once M is estimated, on the same profile the location at which the velocity is equal to the cross-sectional mean, u_m, is given (Chiu and Said 1995) by

$$\bar{r} = \frac{y_m}{D-h}\exp\left(1-\frac{y_m}{D-h}\right) \tag{3.131}$$

where

$$\bar{r} = \frac{\exp\left[Me^M\left(e^M-1\right)^{-1}-1\right]-1}{e^M-1} \tag{3.132}$$

and y_m, on the profile investigated, is the distance from the channel bed where $u = u_m$, $\bar{r}$ is the location at which the velocity is equal to the cross-sectional mean velocity.

This approach overcomes the lack of velocity data for new sites, but it does not substantially improve the accuracy of the linear relationship. Therefore, in order to have a more accurate estimate of the cross-sectional mean velocity when velocity point data are limited, an alternative and practical approach is as follows. The mean velocity along the verticals sampled in the cross-sectional flow area can be surmised as a parabolic curve:

$$u_{m_i}(x) = \alpha x^2 + \beta x + \gamma \tag{3.133}$$

where α, β, and γ are parameters; and $u_{m_i}(x)$ is the mean velocity along the vertical located at the x coordinate in the transverse direction.

Parameters of the parabolic curve can be estimated by two simple conditions. The first condition assumes that the maximum value of the mean velocity along the vertical occurs at $x = 0$, yielding

$$\left.\frac{du_{m_i}(x)}{dx}\right|_{x=0} = 0 \tag{3.134}$$

and

$$u_{m_i}(0) = \gamma \tag{3.135}$$

Equation (3.134) gives $\beta = 0$. Quantity $u_{m_i}(0)$ can be obtained through the velocity points sampled along the vertical or by using the velocity profile at $x = 0$ expressed by equation (3.125). The second condition allows an estimated α setting in which at the banks (left side, $x = x_L$, and right side, $x = x_R$), the flow velocity is zero:

$$u_{m_i}(x)\big|_{x=x_L;x=x_R} = \alpha x^2 + u_{m_i}(0) = 0 \tag{3.136}$$

A similar condition might be used also if velocity points are sampled along a vertical line close to the bank, in this case, the x coordinate referring to the location where the vertical is sampled, thus permitting a more accurate estimate of the parabolic shape. Obviously, if the flow area section is asymmetric with respect to $x = 0$, the α value for the right flow portion is different from that on the left.

The method was applied to the velocity data collected during the selected flood events. The mean velocity along the vertical at $x = 0$ was estimated through Chiu's velocity distribution, equation (3.125), once $u_{\max}$ and h were derived from the velocity points collected and considering $M = 2.13$.

Fig. 3-29 compares the observed mean velocity along each vertical and that estimated by equation (3.116) for the flood events that occurred in June 1997 at Ponte Nuovo. The parabolic shape adequately represented the distribution of the mean velocity in different portions of the flow area. Analogous results were also obtained for other events. Therefore, the parabolic shape implicitly takes into

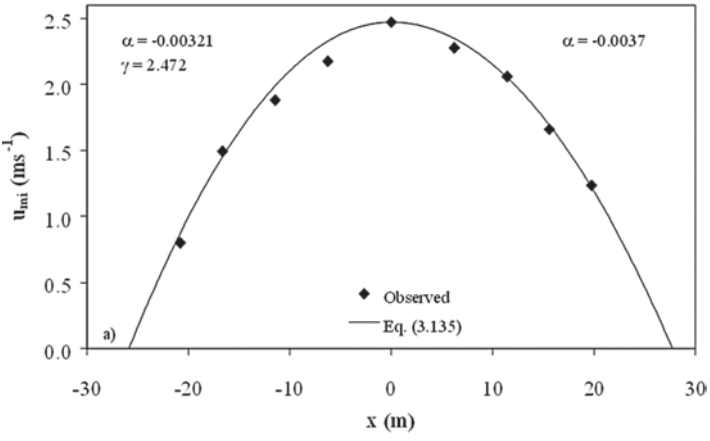

Figure 3-29 *Comparison of observed mean velocity along each vertical and that estimated by equation (3.133) for the flood events that occurred in June 1997 at Ponte Nuovo.*

account the effects of side walls on the velocity distribution in the cross-sectional flow area. Once the mean velocity along each vertical is estimated, the cross-sectional mean velocity can be derived by applying the velocity–area method.

The Chiu and Said technique, as defined by equations (3.125) and (3.127), was also applied to the seven selected flood events and then the cross-sectional mean velocity was estimated for each of them, considering the gauged sections both at historical sites (where $M = 2.13$) and new sites (where M was unknown). The depth below the water surface where u_{max} was collected, h, was defined through the velocity points sampled on vertical at $x = 0$, whereas for the hypothesis of new sites, the M value was determined by the least-squares method applied to the velocity profile at $x = 0$, equation (3.125), as proposed by Chiu and Said (1995).

Comparison of the mean flow velocity estimated by this technique and that obtained by the parabolic method showed that the parabolic approach significantly improved the estimate of the cross-sectional mean velocity. The Chiu and Said technique applied to historical sites had the same accuracy as that of the linear relationship, equation (3.127), whereas for new sites it was found to be less accurate.

To summarize, the linear relationship between the mean and the maximum flow velocities is found to be accurate and the value of parameter M can be surmised to be constant at any site. The percentage error in estimating the mean velocity by the linear relationship is nearly normally distributed. The simple method developed for reconstructing the velocity profiles at a river section, which is based on the assumption that Chiu's velocity distribution can be applied locally, is found capable of estimating with reasonable accuracy the shape of the observed velocity profiles, even for high flood events. Finally, the practical approach, based on the hypothesis that the behavior of the mean velocity within different portions of the flow area follows a parabolic shape, is suitable for estimating the cross-sectional mean velocity even during high floods.

3.7 Derivation of 2-D Velocity Distribution Using a Mathematically Sound Coordinate System

Although the 2-D velocity distribution as discussed has been used in a number of theoretical investigations, its practical usefulness is inhibited by the many parameters it contains. Furthermore, its basis for defining the coordinate system is less than rigorous. Therefore, according to the method of Marini et al. (2011), the discussion here presents a coordinate system that is mathematically sound, which is then applied to derive a 2-D velocity distribution that is parsimonious and whose parameters can be interpreted in terms of hydraulic characteristics. To that end, consider a 2-D domain as (x, y), where x represents the transverse direction and y the vertical direction (measured from the bed-upward positive). Thus, one can write $u = u(x, y)$, and its PDF, $f(u)$, as $f(u(x, y))$, and a cumulative distribution function (CDF), $(F(u))$, as $F(u(x, y))$.

3.7.1 2-D Probability Distributions

Taking the partial derivatives of $F(u)$ with respect to x and y, one obtains

$$\frac{\partial F(u)}{\partial x} = \frac{\mathrm{d}F(u)}{\mathrm{d}u}\frac{\partial u}{\partial x} = f(u)\frac{\partial u}{\partial x} \tag{3.137a}$$

$$\frac{\partial F(u)}{\partial y} = \frac{\mathrm{d}F(u)}{\mathrm{d}u}\frac{\partial u}{\partial y} = f(u)\frac{\partial u}{\partial y} \tag{3.137b}$$

Applying equation (3.10), equations (3.137a) and (3.137b) can be rewritten as

$$\frac{\partial F(u)}{\partial x} = \frac{\mathrm{d}F(u)}{\mathrm{d}u}\frac{\partial u}{\partial x} = \exp(\lambda_1 + \lambda_2 u - 1)\frac{\partial u}{\partial x} \tag{3.138a}$$

$$\frac{\partial F(u)}{\partial y} = \frac{\mathrm{d}F(u)}{\mathrm{d}u}\frac{\partial u}{\partial y} = \exp(\lambda_1 + \lambda_2 u - 1)\frac{\partial u}{\partial y} \tag{3.138b}$$

Equations (3.138a) and (3.138b) can be rearranged as

$$\exp(\lambda_2 u)\frac{\partial u}{\partial x} = \exp(1-\lambda_1)\frac{\partial F(u)}{\partial x} \tag{3.139a}$$

$$\exp(\lambda_2 u)\frac{\partial u}{\partial y} = \exp(1-\lambda_1)\frac{\partial F(u)}{\partial y} \tag{3.139b}$$

Before proceeding further, it is convenient to denote quantity $\exp(\lambda_2 u)$ by w and then calculate the partial derivative of w with respect to x and y as follows:

$$\frac{\partial w}{\partial x} = \frac{\partial \exp(\lambda_2 u)}{\partial x} = \lambda_2 \exp(\lambda_2 u)\frac{\partial u}{\partial x} \tag{3.140a}$$

$$\frac{\partial w}{\partial y} = \frac{\partial \exp(\lambda_2 u)}{\partial y} = \lambda_2 \exp(\lambda_2 u)\frac{\partial u}{\partial y} \tag{3.140b}$$

Substituting equations (3.140a) and (3.140b) into equations (3.139a) and (3.139b), the following system of equations is obtained:

$$\frac{\partial w}{\partial x} = \lambda_2 \exp(1-\lambda_1)\frac{\partial F(u)}{\partial x} \tag{3.141a}$$

$$\frac{\partial w}{\partial y} = \lambda_2 \exp(1-\lambda_1)\frac{\partial F(u)}{\partial y} \tag{3.141b}$$

Equations (3.141a) and (3.141b) can be integrated using the theory of differential forms (or the Leibnitz rule), which states

$$\int_{0,0}^{(x,y)} \frac{\partial w}{\partial x} dx + \frac{\partial w}{\partial y} dy = w(x, y) - w(0, 0) \tag{3.142}$$

Because the point with coordinates (0, 0) lies on the solution domain's contour, u at this point is therefore equal to 0, and the right side of equation (3.142) becomes

$$w(x, y) - w(0, 0) = w(x, y) - \exp(\lambda_2 u) = w(x, y) - \exp(0) = w(x, y) - 1 \tag{3.143}$$

The definite integral of the first part of equation (3.142) can be calculated at a generic point of coordinates $(\bar{x}, \bar{y})$ which is identified by means of a polygonal curve that starts from the origin of axes (0, 0), passes across the point $(\bar{x}, 0)$ and ends at $(\bar{x}, \bar{y})$ (Fig. 3-30). The calculation yields

$$\int_{0,0}^{(\bar{x},\bar{y})} \frac{\partial F(u)}{\partial y} \lambda_2 e^{1-\lambda_1} dy + \frac{\partial F(u)}{\partial x} \lambda_2 e^{1-\lambda_1} dx = \int_0^{\bar{y}} \frac{\partial F(u)}{\partial y} \lambda_2 e^{1-\lambda_1} dy = \lambda_2 e^{1-\lambda_1} F(u) \tag{3.144}$$

in which $(\bar{x}, \bar{y})$ represents a point defined in the domain.

3.7.2 2-D Velocity Distribution

The right side of equation (3.144) can be equated to the right side of equation (3.143) to obtain the following expression of $w(x, y)$:

$$w(x, y) = 1 + \lambda_2 e^{1-\lambda_1} F(u) \tag{3.145}$$

Remembering that $w(x, y)$ is equal to $\exp(\lambda_2 u)$, equation (3.145) can be rewritten as

$$e^{\lambda_2 u(x,y)} = 1 + \lambda_2 e^{1-\lambda_1} F(u(x, y)) \tag{3.146}$$

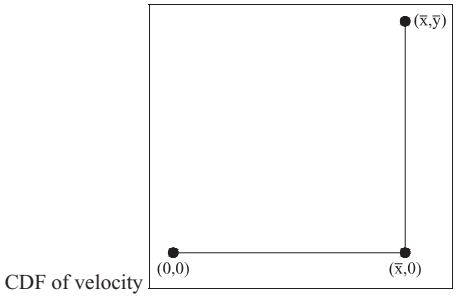

Figure 3-30 *Polygonal curve for integration of equation (3.142).*

and then the expression of $u(x, y)$ can be obtained as follows:

$$u(x,y)=\frac{1}{\lambda_2}\ln\left[1+\lambda_2 e^{1-\lambda_1}F(u(x,y))\right] \tag{3.147}$$

Integration of constraint equation (3.6) yields

$$\int_0^{u_{\max}} e^{\lambda_1-1+\lambda_2 u}\,\mathrm{d}u=1\Rightarrow\lambda_2 e^{1-\lambda_1}=e^{\lambda_2 u_{\max}}-1 \tag{3.148}$$

Considering equation (3.148) and denoting $\lambda_2 u_{\max}$ by G, henceforth called the *entropic parameter* (Chiu 1988), equation (3.147) can be rewritten as

$$u(x,y)=\frac{u_{\max}}{G}\ln\left[1+\left(e^{G}-1\right)F(u(x,y))\right] \tag{3.149}$$

in which parameter G can be calculated considering the constraint expressed by equation (3.7). Equation (3.149) is the 2-D velocity distribution in terms of $u_{\max}$, parameter G, and 2-D CDF.

3.7.3 Mean and Maximum Velocities

Using the probability density function $f(u)$ defined by equation (3.10), the ratio between the mean velocity and the maximum velocity can be derived as an exponential function of G only. Parameter G is a measure of the uniformity of velocity distribution, and statistically speaking, the mean value of G is constant at a channel section, implying that the probability density function $f(u/u_{\max})$ is resilient and that the various flow patterns observable at a channel section are governed by the same probability distribution (Chiu 1989). It also shows the stability and reliability of equation (3.149) as a velocity distribution equation for various types of flows at a channel section.

A constraint equation used for deriving velocity distributions, for example, equation (3.7), is often referred to as the *average value of velocity*, which means the average velocity in the geometric space (u_{av}). This average value is, however, different from the probabilistic value ($\bar{u}$) defined by equation (3.7), a point often overlooked in the hydraulics literature. That means that for cross-sectional average velocity, one cannot use equation (3.7) but must use the following equation, which defines u_{av}:

$$u_{av}=\frac{1}{A}\int_A\frac{u_{\max}}{G}\ln\left[1+\left(e^{G}-1\right)F(u)\right]dA \tag{3.150}$$

where A is the total area of the two-dimensional domain. Equation (3.150) can be solved to obtain the value of G. However, because the expression of $F(u)$ can be complex, the integration in equation (3.150) cannot be performed explicitly, as we will see later, and, therefore, a closed-form expression for u_{av} does not seem easily handled.

Finally, referring to a geometric domain, if u_{av} and u_{max} are known, then one can determine first the value of G by means of equation (3.150), as we explain later, and consequently calculate the velocity distribution by means of equation (3.149). To do so, one must define the CDF in the two-dimensional case. This method is discussed in the next section.

3.7.4 Probability Distributions in Dimensionless Form

The cumulative probability distribution function depends on the geometry of the domain. When defining CDF, it must have certain properties: (1) It must be defined between 0 and 1; (2) it must be continuous and differentiable; and (3) its value on the borders must be 0, and it must have just one point at which it reaches the value of 1. For illustration, consider the case of a rectangular channel in which the distribution of velocity is symmetrical with respect to the vertical axis, as shown in Fig. 3-31. The figure can distinguish the position of coordinates; the location of u_{max}, which can occur on or below the water surface (depending on the value of y_0); and the size of domain H (height) and $B/2$ (half width).

It is convenient to convert this domain in a dimensionless form using the normalizing quantities, B and H, as follows:

$$\psi = y/H, \xi = 2x/B, \psi_0 = y_0/H \tag{3.151}$$

in which one considers the ratio u/u_{max} instead of u. A sketch of this dimensionless domain is shown in Fig. 3-32. Using the variables as defined and

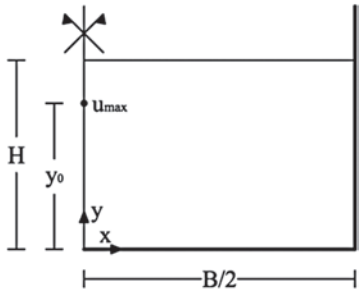

Figure 3-31 *Symmetrical rectangular domain.*

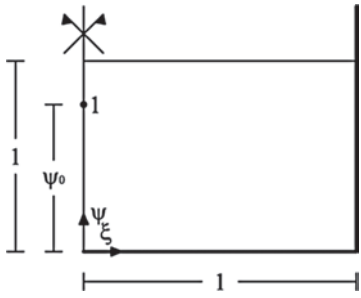

Figure 3-32 *Symmetrical rectangular dimensionless domain.*

through geometrical considerations explained in Appendix 3.1, one can write $F(u)$ as

$$F(u) = 4\left(1-\xi^2\right)^{\frac{H}{B}}\left[\left(\frac{\psi}{2}\right)^{\frac{\ln 2}{\ln 2-\ln(\psi_0)}} - \left(\frac{\psi}{2}\right)^{\frac{2\ln 2}{\ln 2-\ln(\psi_0)}}\right] \tag{3.152}$$

Equation (3.152) satisfies all the aforementioned properties: It is continuous and differentiable, it varies between 0 and 1, and it reaches the value 1 when ξ is equal to 0 and ψ is equal to ψ_0.

The probability density function is now defined as the partial derivative of the CDF given by equation (3.152) with respect to both independent variables, ξ and ψ, as

$$f(u) = \frac{\partial^2 F(u)}{\partial\xi\,\partial\psi} = -8\frac{H}{B}a\xi\left(1-\xi^2\right)^{\frac{H}{B}-1}\left(2^{-a}\psi^{a-1} - 2^{1-2a}\psi^{2a-1}\right) \tag{3.153}$$

where

$$a = \frac{\ln 2}{\ln 2 - \ln(\psi_0)}$$

A three-dimensional sketch of $F(u)$ is shown in Fig. 3-33 for $H/B = 0.5$ and $\psi_0 = 0.8$. The same function is represented by means of contours in Fig. 3-34. Analogous sketches, related to the PDF calculated by means of equation (3.153), are in shown in Figs. 3-35 and 3-36.

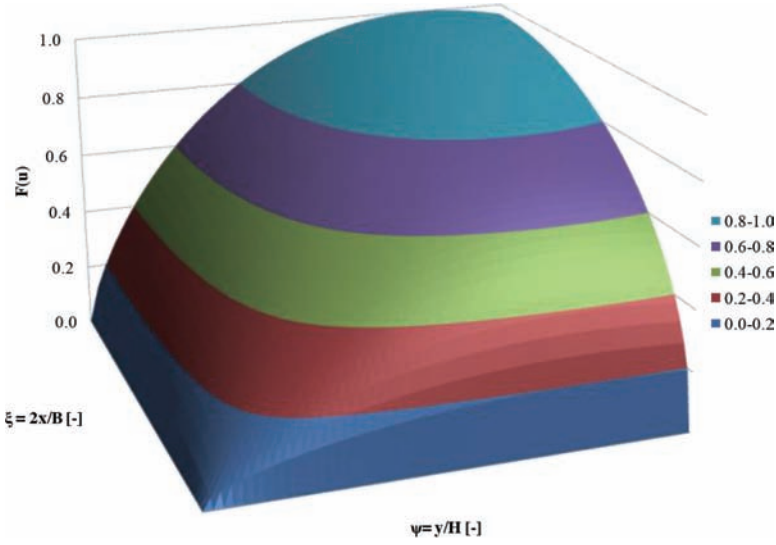

Figure 3-33 *Three-dimensional sketch of CDF* F(u) *(*H/B *= 0.5 and* $\psi_0 = 0.8$*).*

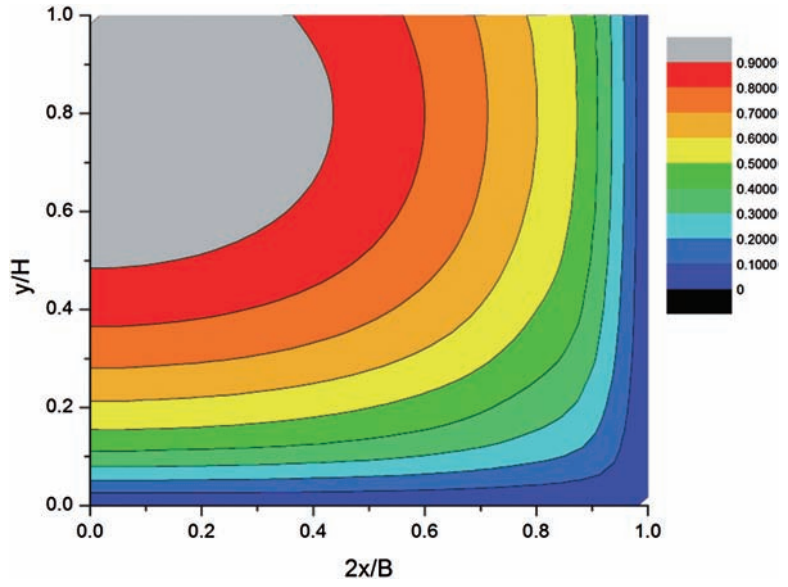

Figure 3-34 *Contour sketch of CDF* F(u) *(*H/B *= 0.5 and* $\psi_0 = 0.8$*).*

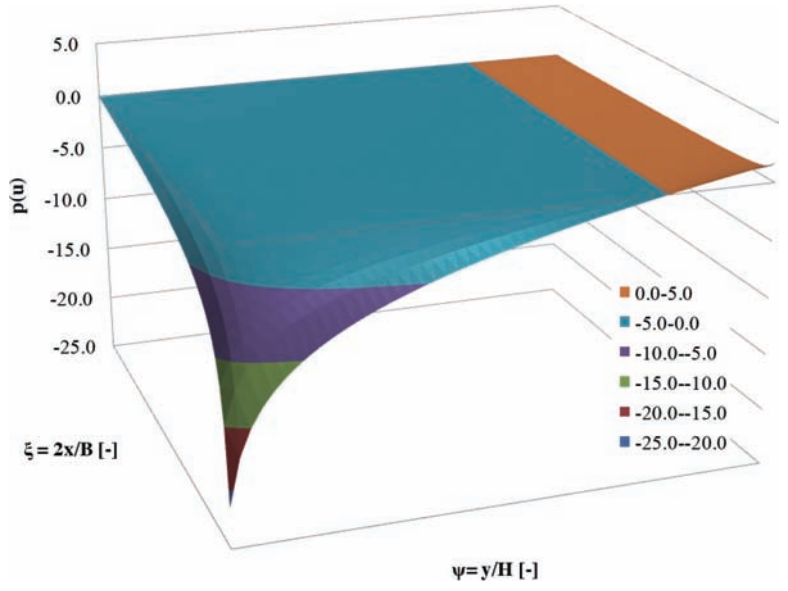

Figure 3-35 *Three-dimensional sketch of PDF* f(u) *(*H/B *= 0.5 and* $\psi_0 = 0.8$*).*

The CDF $F(u)$, given by equation (3.152), has two parts: the first one, $(1 - \xi^2)^{H/B}$, expresses the dependence on ξ, and the second part expresses the dependence on ψ. In the first part, the ratio H/B appears as an exponent, meaning that when the domain is very wide and consequently the ratio H/B tends to 0, the

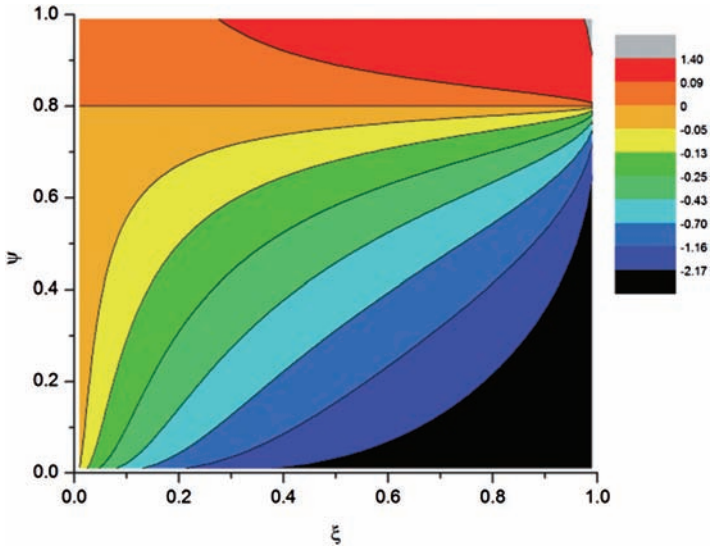

Figure 3-36 *Contour sketch of PDF* f(u) *(*H/B *= 0.5 and* $\psi_0 = 0.8$*).*

first part of $F(u)$ tends to 1 and so $F(u)$ depends only on ψ. Therefore, when the domain becomes very wide, the physical intuition, that $F(u)$ must depend just on the ψ variable, is confirmed. In this case (wide channel), equation (3.152) becomes

$$F(u) = 4\left[\left(\frac{\psi}{2}\right)^{\frac{\ln 2}{\ln 2 - \ln(\psi_0)}} - \left(\frac{\psi}{2}\right)^{\frac{2\ln 2}{\ln 2 - \ln(\psi_0)}}\right] \tag{3.154}$$

Equation (3.154) allows us to estimate the velocity distribution in the one-dimensional case when the maximum velocity occurs on or below the water surface. This same one-dimensional case was discussed by Chiu (1988) and Chiu and Hsu (2006), who proposed the following expression for $F(u)$:

$$F(u) = \frac{\psi}{\psi_0}\exp\left(1 - \frac{\psi}{\psi_0}\right) \tag{3.155}$$

Fig. 3-37 compares $F(u)$ given by equations (3.154) and $F(u)$ given by equation (3.155) from Chiu (1988) for a ψ_0 value of 0.8. This figure shows that both curves of $F(u)$ are quite comparable, suggesting that the two-dimensional theory, presented here, when applied to a one-dimensional case, represents approximately the formulation proposed by Chiu (1988).

3.7.5 Parameter *G*

To apply the two-dimensional velocity distribution equation given by equation (3.149), parameter G must be evaluated by means of equation (3.150). Using equation (3.152) for $F(u)$, one can express equation (3.150) as

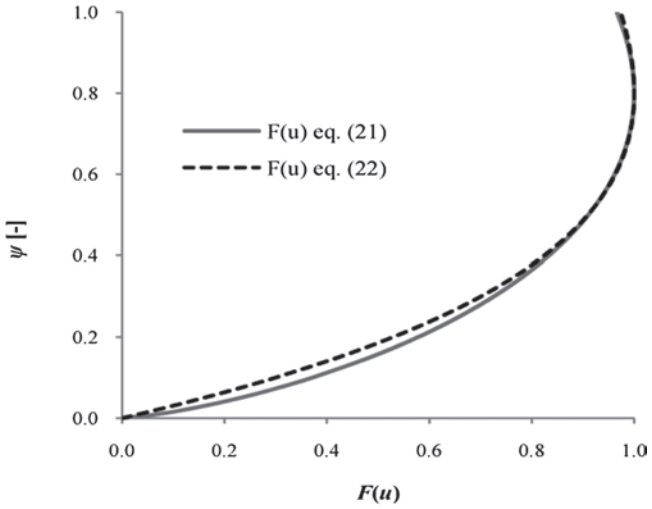

Figure 3-37 F(u) *curves corresponding to equations (3.154) and (3.155).*

$$\frac{u_{av}}{u_{\max}} = \int_0^1 d\psi \int_0^1 \frac{1}{G} \ln\left\{1 + \left(e^G - 1\right)\left(1 - \xi^2\right)^{\frac{H}{B}} 4\left[\left(\frac{\psi}{2}\right)^{\frac{\ln 2}{\ln 2 - \ln(\psi_0)}} - \left(\frac{\psi}{2}\right)^{\frac{2\ln 2}{\ln 2 - \ln(\psi_0)}}\right]\right\} d\xi \qquad (3.156)$$

To obtain G, equation (3.156) needs to be solved numerically because of its implicit form. This solution depends on the ratio H/B and the parameter ψ_0, as well as the ratio $u_{av}/u_{\max}$. Results of integration of equation (3.156) for the case of a wide channel ($H/B = 0$) with varying $u_{av}/u_{\max}$ and ψ_0 between 0.6 and 1 are shown in Fig. 3-38. In the same way, charts analogous to Fig. 3-38 for different values of H/B can be easily constructed. The entropic parameter tends to be invariant at a channel section, regardless of whether the flow is steady or unsteady (Chiu et al. 2005). Recently, by means of theoretical and experimental analysis, Moramarco and Singh (2010) showed that the entropic parameter is also independent of energy or water surface slope.

3.7.6 Application to Experimental Measurements on a Rectangular Channel

Now the method as explained is applied to a real rectangular channel with measured velocity data. Bortz (1989) reported data on a rectangular channel 121.9 cm wide with the water level as 18.3 cm, average velocity as 71.6 cm/s, and maximum velocity as 78.3 cm/s. The maximum velocity occurred approximately 1 cm below water surface, so the value of ψ_0 is 0.95. Data are shown in Table 3-2. To compute velocity distribution in this channel, using equation (3.152) for $F(u)$ in equation (3.150), the following equation is obtained:

$$u(x,y) = \frac{u_{\max}}{G} \ln\left[1 + \left(e^G - 1\right)\left(1 - \xi^2\right)^{\frac{H}{B}} 4\left[\left(\frac{\psi}{2}\right)^{\frac{\ln 2}{\ln 2 - \ln(\psi_0)}} - \left(\frac{\psi}{2}\right)^{\frac{2\ln 2}{\ln 2 - \ln(\psi_0)}}\right]\right] \qquad (3.157)$$

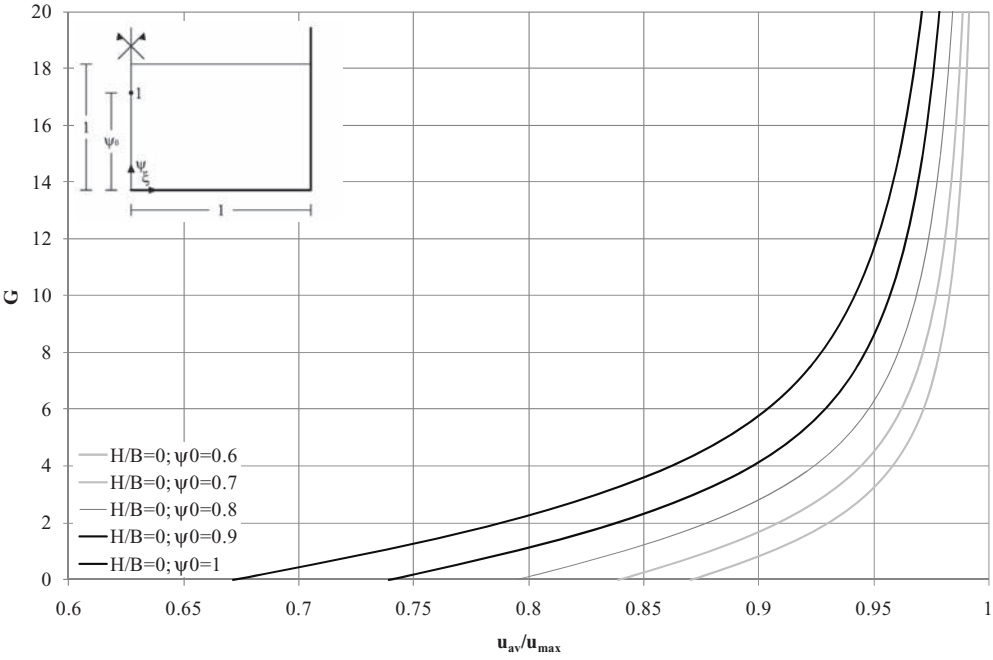

Figure 3-38 *The relation of* G *and* u_{av}/u_{max} *for wide channel* (H/B = *0) and varying* ψ_0.

The values of u_{max}, H, B, and ψ_0 are known, but the value of G needs to be calculated. Knowing the value of average velocity (u_{av} or u_m), equation (3.156) is integrated numerically to yield $G = 7.03$. Then, equation (3.157) is applied to calculate the velocity for those points where measurements are available and results are shown in the last two columns of Table 3-2. Results are also plotted in Fig. 3-39, which shows small differences between measured data and calculated profiles with smaller values approaching the axis of symmetry. The bigger differences are related to boundary areas, particularly near the banks. These differences can be explained by considering two aspects.

First, experimental measurements near the boundary suffer from greater uncertainty compared with other areas. Thus, it is likely that the measurements are not as precise. Second, the banks and channel bottom significantly influence the velocity, and the stated 2-D velocity distribution, as well as other entropy methods, are based on only one constraint in the mass conservation and do not explicitly account for boundary effects. Nevertheless, Marini et al. (2011) showed that the proposed 2-D velocity distribution is remarkably accurate and is superior to the Chiu distribution.

3.7.7 Cumulative Probability Distribution Function in 2-D Arbitrary Geometry Domains

The CDF adequate for generic shapes must respect the same properties explained before. To that end, we need to consider the fact that whatever contour

Table 3-2 *Velocity measurements (based on Bortz 1989) and calculated velocities.*

x (cm)	y (cm)	u (cm/s)	ξ (–)	ψ (–)	u/u_{max} (–)	u_m (cm/s)	u_m/u_{max} (–)
0.00	0.63	56.4	0.000	0.034	0.720	51.5	0.658
0.00	0.95	57.3	0.000	0.052	0.732	55.6	0.709
0.00	1.58	59.1	0.000	0.086	0.755	60.6	0.774
0.00	1.89	63.1	0.000	0.103	0.805	62.4	0.796
0.00	3.15	64.6	0.000	0.172	0.825	67.2	0.858
0.00	3.78	67.1	0.000	0.207	0.856	68.8	0.879
0.00	6.94	72.2	0.000	0.379	0.922	73.9	0.943
0.00	11.04	74.1	0.000	0.603	0.946	76.9	0.982
0.00	14.50	76.2	0.000	0.793	0.973	78.1	0.997
0.00	15.13	76.8	0.000	0.828	0.981	78.2	0.998
0.00	15.77	77.4	0.000	0.862	0.988	78.3	0.999
0.00	16.40	78.3	0.000	0.897	1.000	78.3	1.000
0.00	17.34	78.3	0.000	0.948	1.000	78.3	1.000
0.00	18.29	78.3	0.000	1.000	1.000	78.3	1.000
19.72	0.95	54.6	0.324	0.052	0.696	55.4	0.707
19.72	2.84	63.1	0.324	0.155	0.805	66.0	0.843
19.72	6.62	69.8	0.324	0.362	0.891	73.3	0.936
19.72	14.50	72.2	0.324	0.793	0.922	77.9	0.994
19.72	16.40	74.1	0.324	0.897	0.946	78.1	0.997
19.72	18.29	75.6	0.324	1.000	0.965	78.1	0.997
39.90	0.95	50.0	0.655	0.052	0.638	54.6	0.697
39.90	2.84	61.6	0.655	0.155	0.786	65.3	0.833
39.90	6.62	66.1	0.655	0.362	0.844	72.6	0.927
39.90	14.50	67.7	0.655	0.793	0.864	77.1	0.985
39.90	18.29	67.7	0.655	1.000	0.864	77.4	0.988
51.30	0.95	46.9	0.842	0.052	0.599	53.5	0.683
51.30	2.84	56.4	0.842	0.155	0.720	64.1	0.819
51.30	6.62	62.5	0.842	0.362	0.798	71.5	0.912
51.30	14.50	62.5	0.842	0.793	0.798	76.0	0.970

of arbitrary geometry domain we see is defined by a simple equation (e.g., polynomial). Such a domain is shown in Fig. 3-40, which can distinguish the position of coordinates (x_0, y_0), the location of u_{max} that can occur on or below the water surface (depending on the value of y_0), the size of domain H (height) and B (top

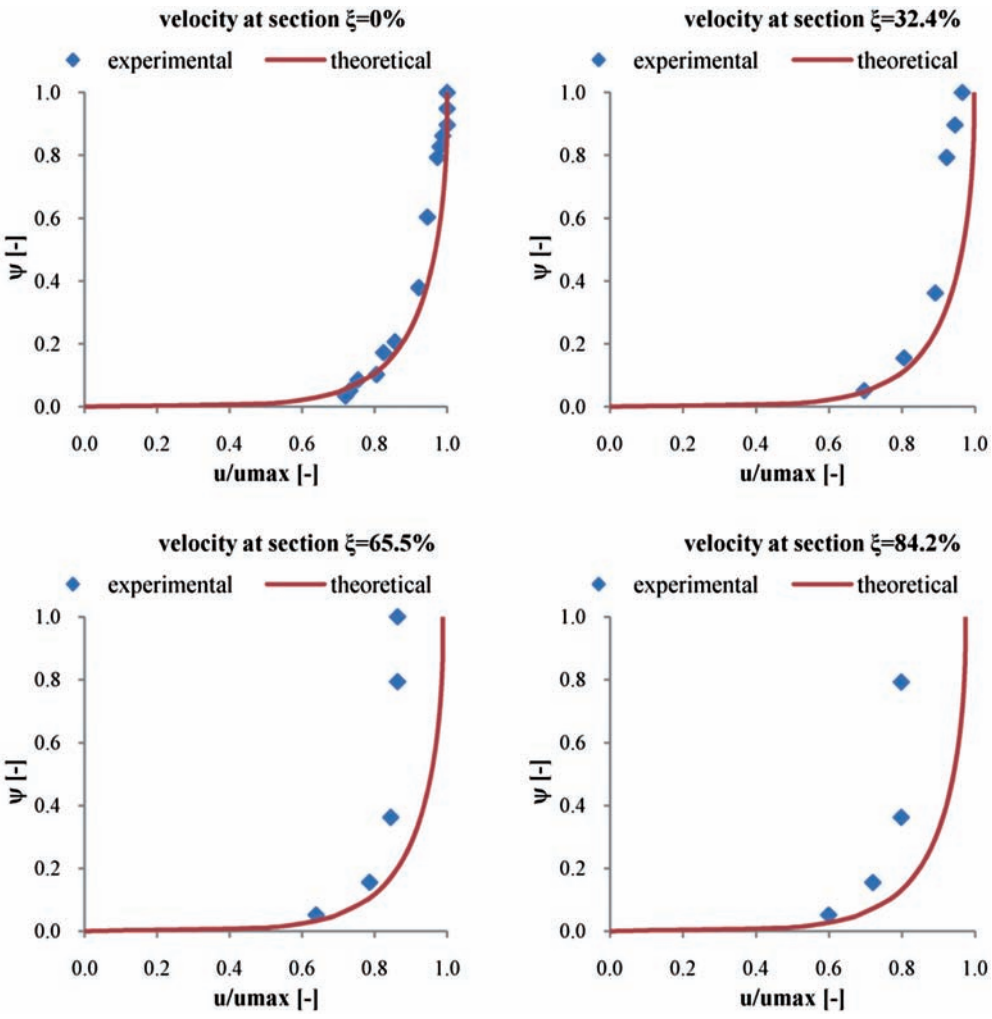

Figure 3-39 *Comparison between velocity data by Bortz (1989) and velocity profiles calculated using the 2-D velocity distribution.*

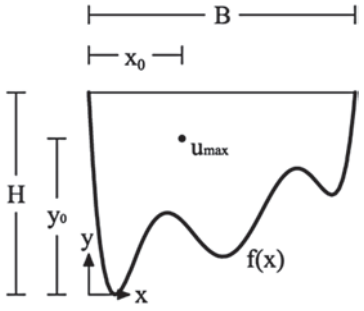

Figure 3-40 *Arbitrary geometry domain.*

water-surface width), and the contour with equation $f(x)$. It is convenient to convert this domain in a dimensionless form using the normalizing quantities as follows:

$$\xi = x/B;\ \psi = y/H;$$

$$\xi_0 = x_0/B;\ \psi_0 = y_0/H \tag{3.158}$$

in which one considers the ratio $u/u_{\max}$ instead of u. A sketch of this dimensionless domain is shown in Fig. 3-41.

Using the variables as defined and through geometrical considerations explained in Appendix 3.1, one can write $F(u)$ as

$$F(u) = \left\{4\left[\xi^a - \xi^{2a}\right]\right\}^m \left\{4\left[\left(\frac{\psi - f(\xi)}{2}\right)^{\frac{\ln 2}{\ln 2 - \ln|\psi_0 - f(\xi)|}} - \left(\frac{\psi - f(\xi)}{2}\right)^{\frac{2\ln 2}{\ln 2 - \ln|\psi_0 - f(\xi)|}}\right]\right\} \tag{3.159}$$

where

$$a = -\frac{\ln 2}{\ln \xi_0};\ m = \frac{H}{B}\left(\frac{Ar}{A}\right)^{13} \tag{3.160}$$

Equation (3.159) satisfies all the aforementioned properties: It is continuous and differentiable, it varies between 0 and 1, and it reaches the value 1 when ξ is equal to ξ_0 and ψ is equal to ψ_0 at the same time and null value when ψ is equal to $f(\xi)$, for any ξ.

The CDF $F(u)$, given by equation (3.159), has two parts: The first one expresses the dependence on ξ, and the second part expresses the dependence on ψ. In the first part, exponent m, which is equal to H/B in the rectangular domain CDF, is modified here to take into account differences in geometry. Exponent m is equal to $H/B \cdot (Ar/A)^{13}$ where Ar/A is the ratio between two areas: Ar is the area (equal to $H \times B$) of the circumscribed rectangle of the considered domain, and A is the area of the considered domain. This parameter can be derived by fitting some

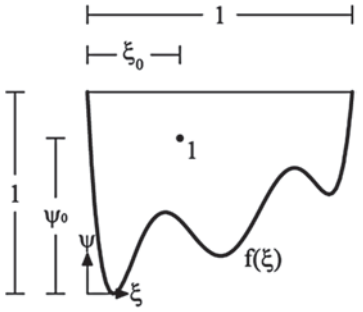

Figure 3-41 *Arbitrary geometry dimensionless domain.*

experimental data (Marini et al. 2013). A more detailed study should be carried out to find the physical meaning underlying this equation. Parameter m appears as a form factor because if the domain tends to a rectangle, m tends to H/B as well as in a rectangle domain. Therefore, when the domain becomes a rectangle, $f(\xi)$ is null and equation (3.159) becomes

$$F(u) = \left\{4\left[\xi^{a} - \xi^{2a}\right]\right\}^{m}\left\{4\left[\left(\frac{\psi}{2}\right)^{\frac{\ln 2}{\ln 2 - \ln|\psi_0 - f(\xi)|}} - \left(\frac{\psi}{2}\right)^{\frac{2\ln 2}{\ln 2 - \ln|\psi_0 - f(\xi)|}}\right]\right\} \tag{3.161}$$

where

$$a = \frac{\ln 2}{\ln \xi_0};\ m = \frac{H}{B} \tag{3.162}$$

Equation (3.161) represents the CDF for a rectangular domain where the velocity distribution is not symmetrical with respect to the vertical axis; the maximum velocity is reached at the ξ_0, ψ_0 coordinate point. The case of ξ_0 equal to 0.5 means that the distribution is symmetric with respect to the vertical axis, so equation (3.159) becomes equal to equation (3.152), when we keep in mind the change in the system of coordinates that is in the middle of the rectangular domain.

Equation (3.159) is flexible because it is valid for any shape; for its application, just the equation of the contour is necessary. Precisely for this general validity and for strict dependence on $f(\xi)$, it is not possible to produce generalized diagrams useful to evaluate the CDF in a generic channel as well as Fig. 3-42. For this reason, the case of a domain defined by a polynomial equation is explained in the next section.

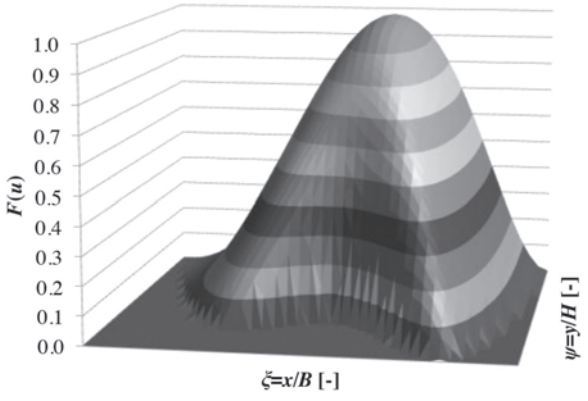

Figure 3-42 *CDF of domain with contour equation (3.163) and* m = *2,* $\xi_0 = 0.6$, $\psi_0 = 0.8$.

Let it be assumed that the domain contour is defined in dimensionless coordinates, the value of exponent m is 2, and the velocity reaches the maximum for $\xi_0 = 0.6$ and $\psi_0 = 0.8$:

$$f(\xi) = -21.604\xi^6 + 110.658\xi^5 - 159.492\xi^4 + 83.797\xi^3 - 9.503\xi^2 - 3.856\xi + 1 \quad (3.163)$$

The CDF derived by equation (3.159) for this case is plotted in Fig. 3-42.

To obtain the velocity distribution, for the given CDF, definition of entropy parameter G is necessary. This point is explained in the next section.

Parameter G for generic geometry domain

It is assumed that the contour domain has equation (3.163). Using equation (3.159) for $F(u)$, one can specify equation (3.156) as

$$\frac{u_{av}}{u_{\max}} = \int_{\xi=0}^{1}\int_{\psi=f(\xi)}^{1} \frac{1}{G}\ln\left\{1+(\exp(G)-1)\left[4\left(\xi^{\frac{-\ln 2}{\ln\xi_0}} - \xi^{\frac{-2\ln 2}{\ln\xi_0}}\right)\right]^m 4\left[\left(\frac{\psi - f(\xi)}{2}\right)^{\frac{\ln 2}{\ln 2 - \ln|\psi_0 - p(\xi)|}} - \left(\frac{\psi - f(\xi)}{2}\right)^{\frac{2\ln 2}{\ln 2 - \ln|\psi_0 - p(\xi)|}}\right]\right\} d\psi\, d\xi \quad (3.164)$$

To obtain G, equation (3.164) needs to be solved numerically because of its implicit form. This solution depends on exponent m, contour equation $f(\xi)$, parameters ξ_0, ψ_0, and ratio $u_{av}/u_{\max}$. Results of integration of equation (3.164) with varying $u_{av}/u_{\max}$ and contour equation (3.162), $\xi_0 = 0.6$, $\psi_0 = 0.8$, $m = 2$, are shown in Fig. 3-43. In the same way, charts analogous to Fig. 3-43 for different contour equations, as well as values of parameters m, ξ_0, and ψ_0, can be easily constructed. The velocity distribution can be derived if the G value is known using equation (3.149) where $F(u)$ is defined by equation (3.159).

3.7.8 Application to Experimental Measurements on River Cross Sections

Now the 2-D method is applied to the velocity measurements in the cross section at Ponte Nuovo in the Upper Tiber River basin, Italy. Here the top water surface is equal to 58.3 m, maximum depth is equal to 6.71 m, average velocity is equal to 1.706 m/s, and the maximum velocity is equal to 2.597 m/s, which occurs approximately at the point with coordinate $\xi_0 = 0.54$ and $\psi_0 = 0.70$. The cross-sectional contour was measured and data are shown in Table 3-3. It was interpolated by means of a polynomial equation expressed as

$$f(\xi) = -1.147\xi^8 - 0.543\xi^7 + 98.044\xi^6 - 275.672\xi^5 + 321.058\xi^4 - 197.524\xi^3 + 68.589\xi^2 - 12.805 + 1 \quad (3.165)$$

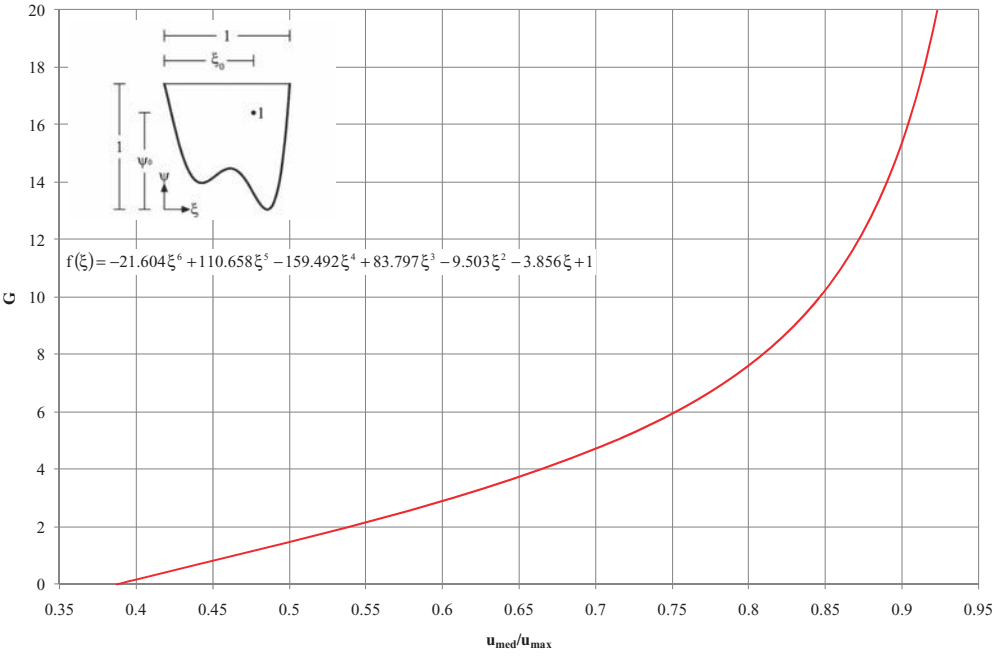

Figure 3-43 *The relation of* G *and* u_{av}/u_{max} *for channel with contour equation (3.162),* $m = 2$, $\xi_0 = 0.6$, $\psi_0 = 0.8$.

Table 3-3 *Real contour coordinates.*

x (m)	y (m)	ξ (–)	Ψ (–)
0.00	6.71	0.000	1.000
8.35	1.60	0.143	0.239
10.43	0.00	0.179	0.000
14.59	0.13	0.250	0.019
18.75	0.07	0.322	0.010
31.23	0.07	0.536	0.010
37.43	0.53	0.642	0.079
42.67	0.50	0.732	0.075
47.87	0.70	0.821	0.104
49.95	0.95	0.857	0.142
58.30	6.71	1.000	1.000

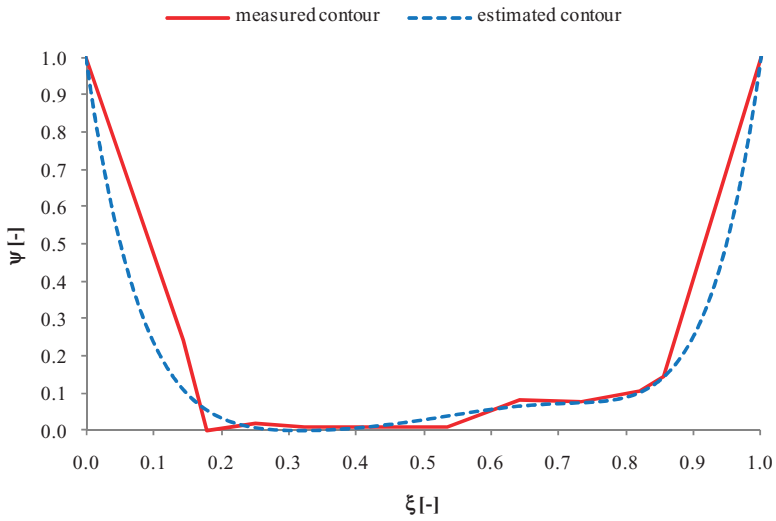

Figure 3-44 *Comparison between measured contour and estimated one by means of a polynomial equation. The sketch is in dimensionless coordinates.*

Fig. 3-44 shows the real contour and interpolated contour. Nine velocity profiles were measured at different verticals. Data are shown in Table 3-4. To compute the velocity distribution in this river cross section, we have to apply equation (3.149), in which $F(u)$ is expressed by equation (3.159). All parameters are known, except G, which is calculated by integrating equation (3.164) knowing the function $f(\xi)$ expressed by equation (3.165) and knowing the value of u_{av}. The result is $G = 2.47$. Calculated velocity is shown in the last two columns of Table 3-4. Results are also plotted in Fig. 3-45, which shows small differences between data and calculated profiles with smaller values approaching the middle of the cross section. Comments about these differences are the same as for the rectangular channel.

3.8 Trapezoidal Domain

Many natural channels approximately resemble a trapezoidal shape. It is, therefore, no surprise that a trapezoidal cross section is commonly used in human-made channels. Hence, it is useful to define an appropriate CDF for the case of trapezoidal sections. It may be noted that the rectangular domain is a special case of the trapezoidal domain, where sides are vertical. The CDF for the trapezoidal domain, sketched in Fig. 3-46, can be defined from equation (3.161) by simple geometrical considerations and must have the same properties as stated earlier. In assessing the CDF, the part of equation (3.161) that depends on ψ remains unchanged, and the part that depends on ξ should be modified because the geometry is different. The abscissa ξ for each value of ψ must be reduced by

Table 3-4 *Velocity data for Ponte Nuovo River section and velocity estimated by means of 2-D method.*

x (m)	y (m)	u (m/s)	ξ (–)	ψ (–)	u/u_{max} (–)	u_m (m/s)	u_m/u_{max} (–)
8.35	6.71	0.72	0.143	1.000	0.276	0.932	0.359
8.35	6.65	0.72	0.143	0.991	0.276	0.934	0.360
8.35	6.45	0.67	0.143	0.961	0.257	0.942	0.363
8.35	5.65	0.74	0.143	0.842	0.286	0.965	0.372
8.35	4.15	0.86	0.143	0.618	0.331	0.971	0.374
8.35	3.15	0.81	0.143	0.469	0.311	0.935	0.360
8.35	2.15	0.73	0.143	0.320	0.281	0.840	0.323
8.35	1.75	0.39	0.143	0.261	0.149	0.768	0.296
10.43	6.71	0.68	0.179	1.000	0.263	1.241	0.478
10.43	6.65	0.68	0.179	0.991	0.263	1.244	0.479
10.43	6.45	0.97	0.179	0.961	0.375	1.253	0.482
10.43	5.65	1.09	0.179	0.842	0.420	1.281	0.493
10.43	4.65	1.50	0.179	0.693	0.576	1.292	0.498
10.43	4.15	1.36	0.179	0.618	0.524	1.287	0.496
10.43	3.65	1.55	0.179	0.544	0.595	1.273	0.490
10.43	3.15	1.81	0.179	0.469	0.698	1.248	0.481
10.43	2.65	1.46	0.179	0.395	0.563	1.209	0.466
10.43	2.15	1.11	0.179	0.320	0.427	1.150	0.443
10.43	1.65	0.96	0.179	0.246	0.368	1.061	0.408
10.43	0.65	0.55	0.179	0.097	0.211	0.626	0.241
10.43	0.35	0.72	0.179	0.052	0.276	0.000	0.000
10.43	0.15	1.01	0.179	0.022	0.388	0.000	0.000
14.59	6.71	1.56	0.250	1.000	0.601	1.745	0.672
14.59	6.65	1.56	0.250	0.991	0.601	1.749	0.673
14.59	6.45	1.44	0.250	0.961	0.556	1.760	0.678
14.59	5.68	1.81	0.250	0.846	0.698	1.791	0.690
14.59	4.72	1.91	0.250	0.703	0.736	1.806	0.696
14.59	3.74	1.98	0.250	0.557	0.762	1.788	0.689
14.59	2.74	1.85	0.250	0.408	0.710	1.723	0.664
14.59	2.04	1.60	0.250	0.304	0.614	1.634	0.629
14.59	1.72	1.70	0.250	0.256	0.653	1.574	0.606
14.59	1.22	1.26	0.250	0.182	0.486	1.442	0.555

Table 3-4 *Velocity data for Ponte Nuovo River section and velocity estimated by means of 2-D method. (Continued)*

x (m)	y (m)	u (m/s)	ξ (–)	ψ (–)	u/u_{max} (–)	u_m (m/s)	u_m/u_{max} (–)
14.59	0.52	1.29	0.250	0.077	0.498	1.081	0.416
14.59	0.28	0.97	0.250	0.042	0.375	0.814	0.313
18.75	6.71	1.83	0.322	1.000	0.704	2.105	0.811
18.75	6.65	1.83	0.322	0.991	0.704	2.109	0.812
18.75	6.45	1.93	0.322	0.961	0.743	2.121	0.817
18.75	5.68	1.86	0.322	0.846	0.717	2.155	0.830
18.75	4.72	2.10	0.322	0.703	0.807	2.170	0.836
18.75	3.74	2.10	0.322	0.557	0.807	2.151	0.828
18.75	2.74	2.13	0.322	0.408	0.820	2.083	0.802
18.75	1.74	1.86	0.322	0.259	0.717	1.930	0.743
18.75	0.74	1.80	0.322	0.110	0.691	1.566	0.603
18.75	0.42	1.39	0.322	0.063	0.537	1.313	0.506
18.75	0.22	1.23	0.322	0.033	0.472	1.037	0.399
31.23	6.71	2.53	0.536	1.000	0.974	2.529	0.974
31.23	6.65	2.53	0.536	0.991	0.974	2.533	0.975
31.23	6.45	2.53	0.536	0.961	0.974	2.545	0.980
31.23	5.68	2.50	0.536	0.846	0.961	2.580	0.994
31.23	4.72	2.60	0.536	0.703	1.000	2.597	1.000
31.23	3.74	2.55	0.536	0.557	0.981	2.577	0.992
31.23	2.77	2.56	0.536	0.413	0.987	2.504	0.964
31.23	1.77	2.53	0.536	0.264	0.974	2.331	0.897
31.23	0.72	1.83	0.536	0.107	0.704	1.803	0.694
31.23	0.42	1.23	0.536	0.063	0.472	1.313	0.505
31.23	0.22	1.28	0.536	0.033	0.492	0.000	0.000
37.43	6.71	2.25	0.642	1.000	0.865	2.424	0.933
37.43	6.65	2.25	0.642	0.991	0.865	2.427	0.935
37.43	6.45	2.20	0.642	0.961	0.846	2.439	0.939
37.43	5.65	2.36	0.642	0.842	0.910	2.475	0.953
37.43	4.68	2.45	0.642	0.697	0.942	2.490	0.959
37.43	3.72	2.38	0.642	0.554	0.916	2.469	0.951
37.43	2.72	2.33	0.642	0.405	0.897	2.390	0.920
37.43	1.72	2.05	0.642	0.256	0.788	2.196	0.846

Continued

Table 3-4 *Velocity data for Ponte Nuovo River section and velocity estimated by means of 2-D method. (Continued)*

x (m)	y (m)	u (m/s)	ξ (–)	ψ (–)	u/u_{max} (–)	u_m (m/s)	u_m/u_{max} (–)
37.43	0.88	1.61	0.642	0.131	0.621	1.746	0.672
37.43	0.68	1.39	0.642	0.101	0.537	1.479	0.569
42.67	6.71	1.86	0.732	1.000	0.717	2.144	0.825
42.67	6.65	1.86	0.732	0.991	0.717	2.147	0.827
42.67	6.45	1.75	0.732	0.961	0.672	2.159	0.831
42.67	5.65	1.91	0.732	0.842	0.736	2.193	0.845
42.67	4.68	2.10	0.732	0.697	0.807	2.208	0.850
42.67	3.72	2.10	0.732	0.554	0.807	2.187	0.842
42.67	2.68	1.70	0.732	0.399	0.653	2.105	0.810
42.67	1.68	1.68	0.732	0.250	0.646	1.905	0.734
42.67	0.85	1.26	0.732	0.127	0.486	1.421	0.547
42.67	0.65	1.14	0.732	0.097	0.440	1.086	0.418
47.87	6.71	0.99	0.821	1.000	0.381	1.626	0.626
47.87	6.65	0.99	0.821	0.991	0.381	1.629	0.627
47.87	6.45	1.29	0.821	0.961	0.498	1.639	0.631
47.87	5.65	1.23	0.821	0.842	0.472	1.670	0.643
47.87	4.65	1.71	0.821	0.693	0.659	1.684	0.648
47.87	3.65	1.70	0.821	0.544	0.653	1.662	0.640
47.87	2.65	1.56	0.821	0.395	0.601	1.582	0.609
47.87	1.65	1.14	0.821	0.246	0.440	1.378	0.531
47.87	1.05	1.01	0.821	0.156	0.388	1.055	0.406
47.87	0.85	0.72	0.821	0.127	0.276	0.801	0.308
49.95	6.71	0.84	0.857	1.000	0.322	1.326	0.511
49.95	6.65	0.84	0.857	0.991	0.322	1.329	0.512
49.95	6.45	0.96	0.857	0.961	0.370	1.338	0.515
49.95	5.65	1.23	0.857	0.842	0.472	1.367	0.526
49.95	4.65	1.49	0.857	0.693	0.574	1.379	0.531
49.95	3.65	1.35	0.857	0.544	0.521	1.358	0.523
49.95	2.65	1.30	0.857	0.395	0.502	1.278	0.492
49.95	2.15	0.80	0.857	0.320	0.306	1.197	0.461
49.95	1.65	0.64	0.857	0.246	0.247	1.051	0.405
49.95	1.30	0.54	0.857	0.194	0.208	0.851	0.328
49.95	1.10	0.44	0.857	0.164	0.169	0.610	0.235

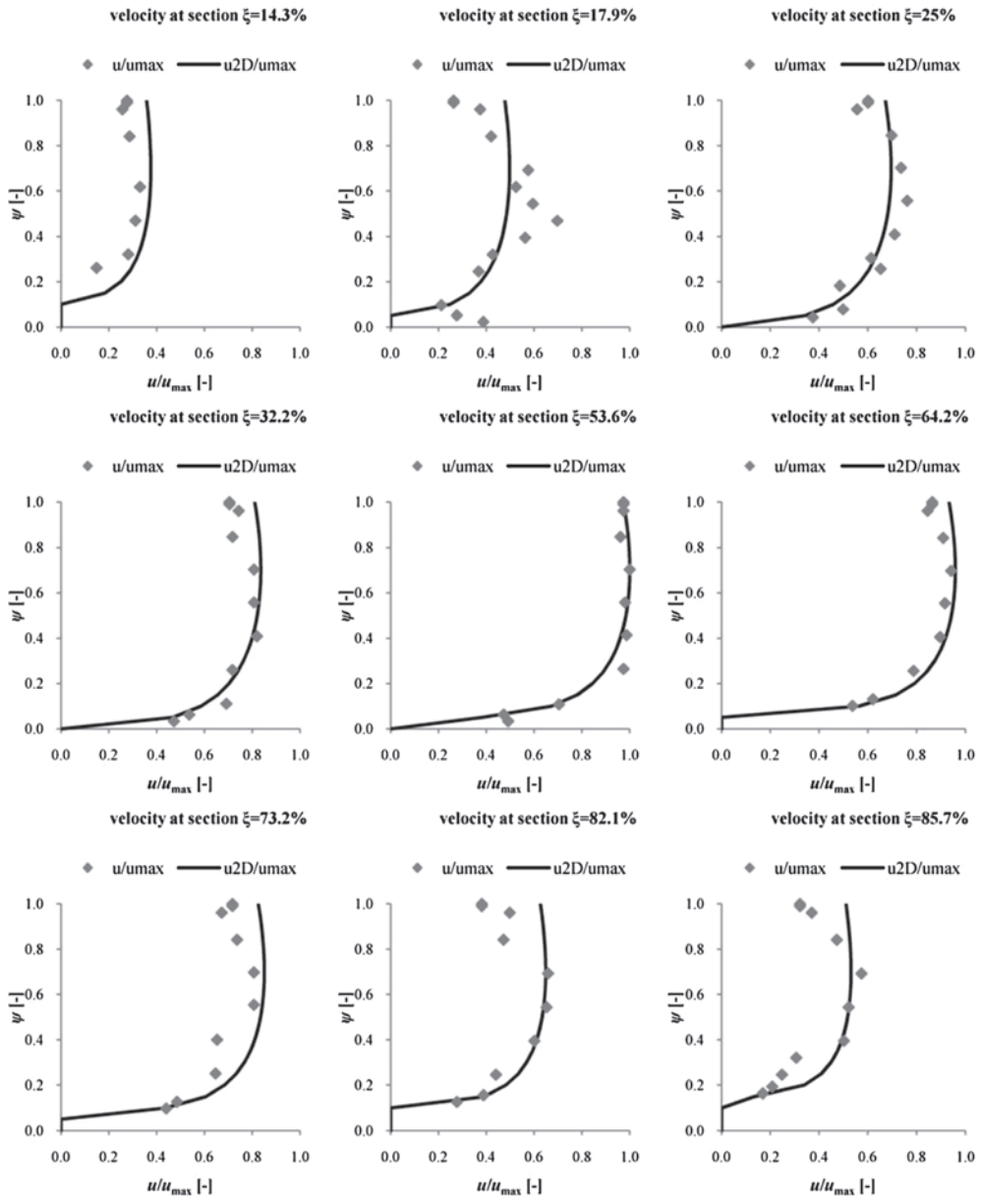

Figure 3-45 *Comparison between measured velocity at Ponte Nuovo and velocity profiles calculated by the 2-D method.*

the horizontal distance between the origin and the left side of the trapeze. In this way, ξ starts from the boundary of the cross section at every height. This distance is equal to $(1 - \psi) \cdot d \cdot \tan \alpha_1$, where d is the ratio H/B. Furthermore, since the width of the channel is not constant with ψ, the abscissa reduced by that distance must be divided by the width itself. The width depends on ψ, and it is equal to

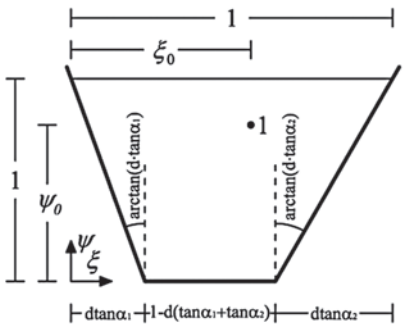

Figure 3-46 *Trapezoidal domains. Velocities are dimensionless with respect to maximum velocity.*

$1 - (1 - \psi)\cdot d\cdot(\tan\alpha_1 + \tan\alpha_2)$. Parameter a, which depends again on ξ_0, must be transformed following the same guidelines. Also the exponent of the part that depends on ξ needs to account for the differences in geometry. We call this exponent m, and we assume it to equal $H/B\cdot(Ar/A)^{19}$, where Ar/A is the ratio between the area of the circumscribing rectangle ($Ar = H\cdot B$) and the area of the cross section A. Marini et al. (2013) obtained the value of the exponent by fitting the data. Accordingly, the CDF is

$$F(u) = \left\{4\left[\left(\frac{\xi-(1-\psi)d\tan\alpha_1}{1-(1-\psi)d(\tan\alpha_1+\tan\alpha_2)}\right)^{a} - \left(\frac{\xi-(1-\xi)d\tan\alpha_1}{1-(1-\psi)d(\tan\alpha_1+\tan\alpha_2)}\right)^{2a}\right]\right\}^{m}$$
$$\times\left\{4\left[\left(\frac{\psi}{2}\right)^{\frac{\ln 2}{\ln 2-\ln\psi_0}} - \left(\frac{\psi}{2}\right)^{2\frac{\ln 2}{\ln 2-\ln\psi_0}}\right]\right\}$$

$$a = -\frac{\ln 2}{\ln\left[\dfrac{\xi_0-(1-\psi)d\tan\alpha_1}{1-(1-\psi)d(\tan\alpha_1+\tan\alpha_2)}\right]}; \quad m = \frac{H}{B}\left(\frac{Ar}{A}\right)^{19} \tag{3.166}$$

Equation (3.166) can be used also for a rectangular section ($\alpha_1 = \alpha_2 = 0$ and $Ar/A = 1$), in which case it coincides with equation (3.161).

Appendix 3.1

In the case where we consider a rectangular channel (where the y axis is the axis of symmetry), the cumulative probability distribution $F(u(x, y))$ to be searched must have the following properties: (1) It must be defined between 0 and 1; (2) it must be continuous and differentiable; and (3) its value on the borders must be 0, and it must have just one point along the y-axis (with the 0, y_0 coordinate)

at which it reaches the value of 1. Many functions can fit these conditions. A good CDF should be addressed following simple steps, and a simple equation should be derived, as Chiu (1987, 1989) suggested. A step-by-step explanation as to how equation (3.152) can be obtained using the system of coordinates (ξ, ψ) is given. The equation must depend on ξ and ψ, and the simplest way to do this is to assume a first part depending on ξ and a second part on ψ; each part must vary from 0 to 1 in order for their product to yield 0 on the border and 1 in the point with the 0, ψ_0 coordinate.

The first part has to depend only on ξ and must be symmetrical on the ψ axis, and the derivative has to be null. The simplest equation that satisfies these properties is the parabolic equation, which is written as follows:

$$1-\xi^2 \tag{3.167}$$

If the rectangular domain is very wide ($H << B$), F should not depend on ξ, but only on ψ and, hence, the first part should be equal to 1. This can be done by considering an exponent equal to H/B to obtain

$$\left(1-\xi^2\right)^{H/B} \tag{3.168}$$

Equation (3.168) represents the first part of $F(u)$ that depends only on ξ.

The second part of $F(u)$ must depend only on ψ, the value for $\psi = 0$ must be 0, and for $\psi = \psi_0$ must be 1. Starting from the simple case of $\psi_0 = 1$, we can use the parabola equation written in this form:

$$a_1\psi^2 + a_2\psi \tag{3.169}$$

where coefficients a_1 and a_2 can be determined by imposing that for $\psi = \psi_0 = 1$ the equation is equal to 1 and the derivative is equal to 0. Equation (3.169) can be rewritten as follows:

$$2\psi - \psi^2 \tag{3.170}$$

or in analogous form as

$$4\left[\frac{\psi}{2} - \left(\frac{\psi}{2}\right)^2\right] \tag{3.171}$$

To consider that ψ_0 can be less than 1, equation (3.171) can be modified, introducing the same exponent a for each term (the linear and quadratic one), as

$$4\left[\frac{\psi}{2}^a - \left(\frac{\psi}{2}\right)^{2\cdot a}\right] \tag{3.172}$$

where a must be a function of ψ_0. Considering that $a(\psi_0)$ must have the following properties—it must be less than 1 for ψ_0 varying between 0 and 1; it must become equal to 1 when $\psi_0 = 1$; and when ψ is equal to ψ_0, equation (3.172) must yield

1—we can determine the equation of $a(\psi_0)$ solving the following equation (3.173) obtained from the third property of a:

$$\left[\frac{\psi_0}{2}^{a} - \left(\frac{\psi_0}{2}\right)^{2\cdot a}\right] = \frac{1}{4} \tag{3.173}$$

The solution of equation (3.173) gives the following expression for a:

$$a = \frac{\ln(2)}{\ln(2) - \ln(\psi_0)} \tag{3.174}$$

Consequently, the second part, which depends on ψ, has the following equation:

$$4\left[\frac{\psi}{2}^{\frac{\ln(2)}{\ln(2)-\ln(\psi_0)}} - \left(\frac{\psi}{2}\right)^{\frac{2\ln(2)}{\ln(2)-\ln(\psi_0)}}\right] \tag{3.175}$$

The product of equations (3.168) and (3.175) gives equation (3.152).

Appendix 3.2

The generic domain CDF can be defined from the CDF equation derived for rectangular symmetric domain, which is the same as equation (3.152) but with another system of coordinates for abscissa:

$$F(u) = \left(1-\kappa^2\right)^{\frac{H}{B}} \cdot 4 \cdot \left[\left(\frac{\psi}{2}\right)^{\frac{\ln 2}{\ln 2-\ln(\psi_0)}} - \left(\frac{\psi}{2}\right)^{\frac{2\ln 2}{\ln 2-\ln(\psi_0)}}\right] \tag{3.176}$$

where κ is the ξ coordinate in a system of coordinates on the axis of symmetry and the other symbols have the same meaning as explained in the text. In this domain, there is no axis of symmetry; therefore, putting the system of coordinates in the corner, as shown in Fig. 3-30, is better. Changing the system of coordinates and rescaling the domain to have the width equal to 1, the first part of equation (3.176) becomes

$$\left(1-\kappa^2\right)^{\frac{H}{B}} \rightarrow \left[4\cdot\left(\xi-\xi^2\right)\right]^{\frac{H}{B}} \tag{3.177}$$

Equation (3.177) must give 1 if $\xi = \xi_0$, where ξ_0 can be equal to or less than 1, so the equation can be modified by introducing for each term the same exponent a, which is a function of ξ_0 to obtain $4(\xi^a - \xi^{2a})$.

Considering that $a(\xi_0)$ must have the following properties—it must be less than 1 for ξ_0 varying between 0 and 1; it must become equal to 1 when $\xi_0 = 1$; and when ξ is equal to ξ_0, it must yield 1—we can determine the equation of $a(\xi_0)$

by applying the third property of a: $4(\xi^a - \xi^{2a}) = 1$. The solution gives the expression for a that can be substituted in equation (3.177) to obtain

$$\left[4 \cdot \left(\xi^{-\frac{\ln 2}{\ln \xi_0}} - \xi^{-2\frac{\ln 2}{\ln \xi_0}}\right)\right]^{\frac{H}{B}} \tag{3.178}$$

Exponent H/B is a form factor that allows us to take into account the variability of the shape of a rectangular domain; to consider the variability of the river shape equation (3.178) needs a form factor that in case of rectangular domain again becomes H/B. By fitting velocity data, Marini et al. (2011) introduced a form factor that modifies equation (3.178) as

$$\left[4 \cdot \left(\xi^{-\frac{\ln 2}{\ln \xi_0}} - \xi^{-2\frac{\ln 2}{\ln \xi_0}}\right)\right]^{\frac{H}{B}\left(\frac{Ar}{A}\right)^{13}} \tag{3.179}$$

where Ar/A is the ratio between two areas: Ar is the area (equal to $H \times B$) of the circumscribed rectangle of the considered domain, and A is the area of considered domain. When this equation is applied to the rectangular domain, Ar/A is equal to 1 and equation (3.179) becomes equation (3.178).

The second part of equation (3.176), which depends on ψ, has to be changed because the bottom of the domain is not a straight line, as in the rectangular domain but follows a curve defined by equation $f(\xi)$. Considering this aspect equation (3.179) becomes

$$\begin{aligned} &4\left[\left(\frac{\psi}{2}\right)^{\frac{\ln 2}{\ln 2 - \ln(\psi_0)}} - \left(\frac{\psi}{2}\right)^{\frac{2\ln 2}{\ln 2 - \ln(\psi_0)}}\right] \rightarrow \\ &4\left[\left(\frac{\psi - f(\xi)}{2}\right)^{\frac{\ln 2}{\ln 2 - \ln|\psi_0 - f(\xi)|}} - \left(\frac{\psi - f(\xi)}{2}\right)^{2\frac{\ln 2}{\ln 2 - \ln|\psi_0 - f(\xi)|}}\right] \end{aligned} \tag{3.180}$$

The product of equations (3.179) and (3.180) gives equation (3.159).

Questions

Q3.1 For a set of velocity observations given in Table 3-1, verify the hypothesis expressed by equation (3.3). For a wide channel $(r - r_0)/(r_{max} - r_0)$ can be approximated as y/D. How good is this approximation?

Q3.2 For velocity data in Q3.1, compute the PDF and CDF of velocity and plot them.

Q3.3 For the data in Q3.1, compute the Lagrange multipliers λ_1 and λ_2. Plot λ_1 as a function of λ_2 for various values of u_{max}. Discuss the plot.

Q3.4 Compute λ_2 as a function of u_m, plot it, and discuss the plot.

Q3.5 Compute λ_1 as a function of λ_2 for various values of u_{max}, plot it, and discuss the plot.

Q3.6 Compute entropy as a function of λ_2 for various values of u_{max}, plot them, and discuss the plot.

Q3.7 Compute the PDF of velocity as a function of λ_2 for various values of u_{max} and u_m, plot them, and discuss the plot.

Q3.8 Compute the CDF of velocity as a function of λ_2 for various values of u_{max}, plot them, and discuss the plot.

Q3.9 Compute the value of M for the data in Q3.1.

Q3.10 Compute the two-dimensional velocity distribution using the entropy-based equation and compare it with observations in Q3.1. How good is the entropy-based equation?

Q3.11 Compute different measures of uniformity of the velocity distribution for the data in Q3.1. Based on these measures, comment on the velocity distribution.

Q3.12 Compute entropy of the velocity for data in Q3.1.

Q3.13 Construct isovels for the data in Q3.1. Also construct isovels using the entropy-based velocity equation and compare them.

Q3.14 Compute the location of maximum velocity and compare it with the observed location for the data in Q3.1.

References

Araujo, J. C. (1994). "*2-dimensional velocity distribution in open channels—A principal of maximum entropy approach*." Ph.D. dissertation, Sao Carlos School of Engineering, University of Sao Paulo, Sao Carlos, Brazil (in Portuguese).

Araújo, J. C., and Chaudhry, F. H. (1998). "Experimental evaluation of 2-D entropy model for open-channel flow." *J. Hydraul. Eng.*, 124(10), 1064–1067.

Bhowmik, N. G. (1979). "*Hydraulics of flow in the Kaskaskia River, Illinois*." Illinois State Water Survey Contract Report 91, Champaign, IL.

Blaney, H. F. (1937). Discussion of "Stable channels in erodible materials," by E. W. Lane. Transactions of ASCE, 102, 152–153.

Bortz, K. M. (1989). "*Parameter estimation for velocity distribution in open channel flow*." M.S. thesis, Department of Civil Engineering, University of Pittsburgh, Pittsburgh, PA.

Bridge, J. S., and Jarvis, J. (1985). "*Flow and sediment transport data: River South Esk, Glen Glova, Scotland*." Report, Department of Geological Sciences, State University of New York, Binghamton.

Chen, Y.-C., and Chiu, C.-L. (2004). "A fast method of flood discharge estimation." *Hydrol. Proc.*, 18, 1671–1683.

Chen, Y. S. (1998). "*An efficient method of discharge measurement*." Ph.D. dissertation, University of Pittsburgh, Pittsburgh, PA.

Chiu, C.-L. (1987). "Entropy and probability concepts in hydraulics." *J. Hydraul. Eng.*, 113(5), 583–600.

Chiu, C.-L. (1988). "Entropy and 2-D velocity distribution in open channels." *J. Hydraul. Eng.*, 114(7), 738–756.

Chiu, C.-L. (1989). "Velocity distribution in open channel flow." *J. Hydraul. Eng.*, 115(5), 576–594.

Chiu, C.-L. (1991). "Application of entropy concept in open-channel flow study." *J. Hydraul. Eng.*, 117(5), 615–628.

Chiu, C.-L., and Chen, Y.-C. (2003). "An efficient method of discharge estimation based on probability concept." *J. Hydraul. Res.*, 41(6), 589–596.

Chiu, C.-L., and Chiou, J.-D. (1986). "Structure of 3-D flow in rectangular open channels." *J. Hydraul. Eng.*, 112(11), 1050–1068.

Chiu, C.-L., and Hsu, S. H. (2006). "Probabilistic approach to modeling of velocity distributions in fluid flows." *J. Hydrol.*, 316, 28–42.

Chiu, C.-L., Hsu, S. M., and Tung, N.-C. (2005). "Efficient methods of discharge measurements in rivers and streams based on the probability concept." *Hydrolog. Proc.*, 19, 3935–3946.

Chiu, C.-L., Jin, W., and Chen, Y.-C. (2000). "Mathematical models of distribution of sediment concentration." *J. Hydraul. Eng.*, 126(1), 16–23.

Chiu, C.-L., and Lin, G.-F. (1983). "Computation of 3-D flow and shear in open channels." *J. Hydraul. Eng.*, 109(11), 1424–1440.

Chiu, C.-L., and Murray, D. W. (1992). "Variation of velocity distribution along nonuniform open channel flow." *J. Hydraul. Eng.*, 118(7), 989–1001.

Chiu, C.-L., and Said, C. A. A. (1995). "Maximum and mean velocities and entropy in open-channel flow." *J. Hydraul. Eng.*, 121(1), 26–35.

Chiu, C.-L., and Tung, N.-C. (2002). "Maximum velocity and regularities in open-channel flow." *J. Hydraul. Eng.*, 128(4), 390–398.

Choo, T. H. (2000). "An efficient method of the suspended sediment-discharge measurement using entropy concept." *Water Eng. Res.*, 1(2), 95–105.

Coleman, N. L. (1986). "Effects of suspended sediment on the open channel velocity distribution." *Water Resour. Res.*, 22(10), 1377–1384.

Coles, D. (1956). "The law of the wake in the turbulent boundary layer." *J. Fluid Mech.*, 1, 191–226.

Greco, M. (1999). "Entropy velocity distribution in a river." *Proc., IAHR. Symp. on Ri.*

Herschy, R. W. (1985). *Streamflow measurement*, Elsevier, London.

Landweber, L. (1953). "The frictional resistance of flat plates in zero pressure gradient." *Trans., Soc. Naval Arch. Marine Eng.*, 61, 5–22.

Marini, G., De Martino, G., Fontana, N., Fiorentino, M., and Singh, V. P. (2011). "Derivation of 2D velocity distribution in open channel flow using entropy." *J. Hydraul. Res.*, 49(6), 784–790.

Marini, G., De Martino, G., Fontana, N., Fiorentino, M., and Singh, V. P. (2013). "Derivation of 2D velocity distribution in watercourses using entropy." *J. Hydraul. Res.*, under review.

Montes, S. (1998). *Hydraulics of open channel flow*, ASCE Press, Reston, VA.

Moramarco, T., and Singh, V. P. (2001). "Simple method for relating local stage and remote discharge." *J. Hydrol. Eng.*, 6(1), 78–81.

Moramarco, T., and Singh, V. P. (2010). "Formulation of the entropy parameter based on hydraulic and geometric characteristics of river cross sections." *J. Hydrol. Eng.*, 15(10), 852–858.

Moramarco, T., Saltalippi, C., and Singh, V. P. (2004). "Estimation of mean velocity in natural channels based on Chiu's velocity distribution equation." *J. Hydrol. Eng.*, 9(1), 42–50.

Murphy, C. (1904). "Accuracy of stream measurements." *Water Supply and Irrigation Paper* 95, 111–112.

Nezu, I., and Nakagawa, H. (1993). *Turbulence in open channel flows*, Balkema, Rotterdam, Netherlands.

Nezu, I., and Rodi, W. (1986). "Open-channel flow measurements with a laser Doppler anemometer." *J. Hydraul. Eng.*, 112(5), 335–355.

Prandtl, L. (1925). "Bericht uber unter suchugen zur ausgebildeten turbulenz." *Zeitschrift fur Angewandte Mathematik und Mechanik*, 5(2), 136 (in German).

Stearns, F. P. (1883). "On the current-meter: Together with a reason why the maximum velocity of water flowing in open channels is below the surface." *Trans., ASCE*, 12(1), 301–338.

Streeter, V. L., and Wylie, E. B. (1979). *Fluid mechanics*. McGraw-Hill, New York.

Xia, R. (1997). "Relation between mean and maximum velocities in a natural river." *J. Hydraul. Eng.*, 123(8), 720–723.

Yang, S.-Q., Tan, S.-K., and Lim, S.-Y. (2004). "Velocity distribution and dip-phenomenon in smooth uniform open channel flows." *J. Hydraul. Eng.*, 130(12), 1179–1186.

Yen, B. C. (1965). "*Characteristics of subcritical flow in a meandering channel*." Technical Report, Iowa Institute of Hydraulic Research, University of Iowa, Iowa City, IA.

Additional Reading

Barbé, D. E, Cruise, J. F., and Singh, V. P. (1991). "Solution of three-constraint entropy-based velocity distribution." *J. Hydraul. Eng.*, 117(10), 1389–1396.

Daugherty, R. L., and Franzini, J. B. (1977). *Fluid mechanics with engineering applications*, McGraw-Hill, New York.

Davoren, A. (1985). "*Local scour around a cylindrical bridge pier*." Publication No. 3 of the Hydrology Center, National Water and Soil Conservation Authority, Ministry of Works and Development, Christchurch, New Zealand.

Einstein, H. A., and Chien, N. (1955). "*Effects of heavy sediment concentration near the bed on velocity and sediment distribution*." Report No. 8, M.R.D. Sediment Sever, U.S. Army Corps of Engineers, Omaha, NE.

Gray, W. G., and Ghidaoui, M. S. (2009). "Thermodynamic analysis of stream flow hydrodynamics." *J. Hydraul. Res.*, 47(4), 403–417.

Karim, M. F., and Kennedy, J. F. (1987). "Velocity and sediment–concentration profiles in river flows." *J. Hydraul. Eng.*, 113(2), 159–178.

Sarma, K. V. N., Lakshminarayana, P., and Lakshmana Rao, N. S. (1983). "Velocity distribution in smooth rectangular open channels." *J. Hydraul. Eng.*, 109(2), 270–289.

Shione, K., and Knight, D. W. (1991). "Turbulent open channel flows with variable depth across the channel." *J. Fluid Mech.*, 222, 617–646.

Tang, X., and Knight, D. W. (2009). "Analytical models for velocity distributions in open channel flows." *J. Hydraul. Res.*, 47(4), 418–428.

von Karman, T. (1935). "Some aspects of the turbulent problem." *Mech. Eng.*, 57(7), 407–412.

Yang, K., Cao, S., and Knight, D. W. (2007). "Flow patterns in compound channels with vegetated floodplains." *J. Hydraul. Eng.*, 133(2), 148–159.

This page intentionally left blank

Chapter 4

Power Law and Logarithmic Velocity Distributions

The preceding two chapters present one-dimensional and two-dimensional velocity distributions in open-channel flow based on the entropy theory. This discussion is now extended to the power law and the Prandtl–von Karman universal (or logarithmic) velocity distribution equations that have been commonly used in hydraulic engineering. Recall that the power law velocity distribution can be expressed as

$$\frac{u}{u_D} = \left(\frac{y}{D}\right)^{1/n} \tag{4.1}$$

and the Prandtl–von Karman universal velocity distribution as

$$u = \frac{u^*}{k} \ln\left(\frac{y}{y_0}\right) \tag{4.2}$$

where u is the velocity (m/s), y is the distance from the bed (m), D is the flow depth (m), k is von Karman's universal constant, u^* is the shear velocity, y_0 is a parameter—a very small value of y at which the velocity becomes almost zero, and $(1/n)$ is the exponent. The value of k is equal to 0.42 for clear water, and it can be as low as 0.2 for sediment-laden water (Daugherty and Franzini 1977). There is some evidence that k may vary over a range of values as a function of

the Reynolds number. The term y_0 is of the same order of magnitude as the viscous sublayer thickness, and its value depends on whether the boundary is hydraulically rough or smooth. For smooth boundary, it solely depends on kinematic viscosity and shear velocity, and for rough boundary, it depends on roughness height.

The power law velocity distribution expresses the ratio of local to maximum velocity as a function of position where n is a constant on the order of 6 to 10. The value of n changes, to some extent, with the Reynolds number of flow. In many cases, the power law has been found to adequately represent the velocity distribution over smooth and rough surfaces. The universal velocity distribution is also referred to as log law velocity distribution and has been found to represent the velocity distribution within a turbulent boundary layer.

4.1 Preliminaries

The velocity of flow in an open channel varies along a vertical from zero at the bed to a maximum value, which may or may not occur at the water surface. At any point in space or in any cross section, the flow velocity varies with time, but this time variation does not follow a particular pattern and depends on the water and sediment influx. A number of investigators (Chiu 1987; Barbé et al. 1991; Xia 1997; Araújo and Chaudhry 1998; Choo 2000; Chen and Chiu 2004) have assumed that the time-averaged velocity at any point along a vertical is a random variable and, therefore, has a probability distribution. This same assumption is used in this chapter. The velocity values along the vertical are values of the random variable: velocity.

4.1.1 Hypothesis on Cumulative Probability Distribution of Velocity

Beginning with Chiu (1987) and his associates (Chiu and Murray 1992; Chiu and Said 1995; Chiu and Tung 2002; Chiu and Hsu 2006), Barbé et al. (1991), Xia (1997), Araújo and Chaudhry (1998), and Choo (2000), among others assumed that all values of flow depth y measured from the bed to any point between 0 and D were equally likely to occur, where D is the flow depth. In reality, this is not highly unlikely, because at different times different values of flow depth do occur. According to these investigators, the cumulative probability distribution of velocity can be expressed as the ratio of flow depth to the point where velocity is to be considered and the depth up to the water surface. Then the probability of velocity being equal to or less than u is y/D; at any depth (measured from the bed) less than y, the velocity is less than, say, u; thus the cumulative distribution function (CDF) of velocity, $F(u) = P(\text{velocity} \leq \text{a given value of } u)$, P = probability, can be expressed as

$$F(u) = \frac{y}{D} \tag{4.3a}$$

$F(u)$ denotes the CDF of velocity, u = velocity (m/s), y = distance from the bed, and D = flow depth. The probability density function (PDF) of u is obtained by differentiating equation (4.3a) with respect to u as

$$f(u) = \frac{dF(u)}{du} = \frac{1}{D}\frac{dy}{du} \quad or \quad f(u) = \left(D\frac{du}{dy}\right)^{-1} \tag{4.3b}$$

The term $f(u)du = F(u + du) - F(u)$ denotes the probability of velocity being between u and $u + du$. As equation (4.3b) constitutes the fundamental hypothesis used by the cited investigators, as well as used in this chapter for deriving velocity distributions that use the entropy theory, it will be useful to evaluate the validity of this hypothesis. This hypothesis (i.e., the relation between the cumulative probability $F(u)$ and the ratio y/D) has been tested for a number of natural rivers and found to be approximately true, as was shown in Chapter 2.

4.1.2 Shannon Entropy

The objective here is to determine the PDF of u, $f(u)$. This determination is accomplished by maximizing the Shannon entropy (Shannon 1948) of velocity, $H(u)$, expressed as

$$H(u) = -\int_0^{u_D} f(u)\ln f(u)du \tag{4.4}$$

Equation (4.4) expresses a measure of uncertainty about $f(u)$ or the average information content of sampled u. Maximizing $H(u)$ is equivalent to maximizing $f(u)$ ln $f(u)$. To determine an $f(u)$ that is the least biased toward what is not known about velocity, the principle of maximum entropy (POME), developed by Jaynes (1957a, 1957b, 1982), is invoked, which requires specification of certain information, called constraints, on velocity. According to POME, the most appropriate probability distribution is the one that has the maximum entropy or uncertainty, subject to these constraints.

The flow in a channel satisfies the laws of conservation of mass, momentum, and energy, and these laws can be used to define constraints that the velocity distribution must obey. For deriving the power law and logarithmic velocity distributions, only the law of mass conservation is found to be sufficient.

4.2 One-Dimensional Power Law Velocity Distribution

The power law velocity distribution has an exponent that is usually determined by calibration, and its determination from physically measurable quantities has been elusive.

4.2.1 Specification of Constraints

For the power law velocity distribution, according to Singh (1998), the first constraint to be specified is the total probability law, which must always be satisfied. Therefore, the first constraint, C_1, on the PDF of velocity can be written as

$$C_1 = \int_0^{u_D} f(u)du = 1 \tag{4.5a}$$

The second constraint is based on mass conservation:

$$C_2 = \int_0^{u_D} \ln u f(u)du = \overline{\ln u} \tag{4.5b}$$

Equation (4.5b) is the mean of the logarithmic velocity values and is the second constraint, C_2.

4.2.2 Maximization of Entropy

To obtain the least-biased probability distribution of u, $f(u)$, the Shannon entropy, given by equation (4.4), is maximized according to POME, subject to equations (4.5a) and (4.5b). To that end, the method of Lagrange multipliers is used. The Lagrangian function L then becomes

$$L = -\int_0^{u_D} f(u)\ln f(u)du - (\lambda_0 - 1)\left(\int_0^{u_D} f(u)du - C_1\right) - \lambda_1\left(\int_0^{u_D} \ln(u) f(u)du - C_2\right) \tag{4.6}$$

where λ_0 and λ_1 are the Lagrange multipliers. Recalling the Euler–Lagrange equation of calculus of variation, noting f as a variable and u as a parameter, differentiating equation (4.6) with respect to f, and equating the derivative to zero, one obtains

$$\frac{\partial L}{\partial f} = 0 = -\ln f(u) - \lambda_0 - \lambda_1 \ln u \tag{4.7}$$

4.2.3 Probability Distribution of Velocity

Equation (4.7) leads to the entropy-based PDF of velocity as

$$f(u) = \exp[-\lambda_0 - \lambda_1 \ln u] \quad \text{or} \quad f(u) = \exp(-\lambda_0)u^{-\lambda_1} \tag{4.8}$$

The PDF of u contains the Lagrange multipliers λ_0 and λ_1, which can be determined using equations (4.5a) and (4.5b).

4.2.4 Determination of Lagrange Multipliers

The Lagrange multipliers can be determined by substituting equation (4.8) in constraint equations (4.5a) and (4.5b). Substitution of equation (4.8) in equation (4.4) yields

$$\exp(\lambda_0) = \frac{u_D^{-\lambda_1+1}}{-\lambda_1+1} \quad \text{or} \quad \lambda_0 = -\ln(-\lambda_1+1) + (-\lambda_1+1)\ln(u_D) \tag{4.9}$$

where u_D is the velocity at $y = D$. Let $n = -\lambda_1 + 1$. Then substitution of equation (4.9) in equation (4.8) yields

$$f(u) = n\frac{u^{n-1}}{u_D^n} \tag{4.10}$$

Equation (4.10) is the PDF underlying the power law velocity distribution. For $n > 1$, the PDF monotonically increases from 0 to n/u_D. The PDF, given by equation (4.10), was also presented by Dingman (1989) without derivation. The cumulative probability distribution of velocity becomes

$$F(u) = \frac{u^n}{u_D^n} \tag{4.11}$$

Differentiating equation (4.9) with respect to λ_1, one obtains

$$\frac{\partial\lambda_0}{\partial\lambda_1} = -\ln u_D + \frac{1}{-\lambda_1+1} \tag{4.12}$$

On substituting equation (4.8) in equation (4.4a), one can also write

$$\lambda_0 = \ln \int_0^{u_D} u^{-\lambda_1} du \tag{4.13}$$

Differentiating equation (4.13) with respect to λ_1, recalling equation (4.5b), and simplifying, one obtains

$$\frac{\partial\lambda_0}{\partial\lambda_1} = -\overline{\ln u} \tag{4.14}$$

Equating equation (4.12) to equation (4.14) leads to an estimate of λ_1:

$$\lambda_1 = 1 - \frac{1}{\ln u_D - \overline{\ln u}} \tag{4.15}$$

Therefore, the power law velocity distribution exponent n becomes

$$n = \frac{1}{\ln u_D - \overline{\ln u}} \tag{4.16}$$

Equation (4.16) shows that exponent, n, of the power law velocity distribution can be estimated from the values of the logarithm of velocity at the water surface and the average of the logarithmic values of velocity. The higher the difference between these logarithm values, the lower the exponent will be.

4.2.5 Velocity Distribution

Substituting equation (4.10) in equation (4.3b) and integrating, one obtains

$$\frac{u}{u_D} = \left(\frac{y}{D}\right)^{1/n} \tag{4.17}$$

Equation (4.17) gives the power law velocity distribution used in hydraulics. It has an exponent $(1/n)$ that can be determined using equation (4.16).

4.2.6 Entropy of Velocity Distribution

The entropy (in Napiers) of the velocity distribution can be obtained by substituting equation (4.10) in equation (4.4) and using equation (4.16):

$$H = n(\ln u_D - \overline{\ln u}) + \overline{\ln u} - \ln n \tag{4.18}$$

Equation (4.18) shows that for a given value of n, the uncertainty increases as the difference between logarithm of the maximum velocity and the average of the logarithmically transformed values of the velocity increases. Taking advantage of equation (4.16), equation (4.18) becomes

$$H = 1 + \overline{\ln u} - \ln n \tag{4.19}$$

Equation (4.19) shows that higher average logarithmic velocity leads to higher uncertainty. In such situations, it is desirable that velocity is sampled more frequently along the vertical.

4.2.7 Testing

One can now examine if the exponent n yielded by equation (4.16) can be a good approximation. To that end, eight velocity data sets are used. These data sets were collected by Einstein and Chien (1955). Five of these data sets (designated by Einstein and Chien as S-1, S-4, S-5, S-6, and S-10) are for sediment-laden flows, and three data sets (designated as C-3, C-5, and C-8) are for clear-water flows. For these eight data sets, the value of n is computed using equation (4.16), and the computed n values, respectively, are found to be 2.43, 2.03, 1.81, 2.50, 1.86, 3.22, 3.34, and 3.20. The values of u_D for these data sets are 6.25, 9.19, 11.42, 7.15, 7.52, 6.58, 5.19, and 7.07 m/s. To assess the goodness of these n values, they are also obtained by fitting the power law velocity distribution, given by equation (4.17), to these data sets by the least-squares method. The n values so obtained are, respectively, 3.46, 2.61, 2.26, 3.51, 2.67, 4.18, 5.02, and 4.18. Fig. 4-1 compares for a sample data set S-1 velocity values obtained by the power law with n computed using equation (4.16) and n obtained by fitting observed values of velocity. The n values obtained in the two ways are not the same but are comparable, which is remarkable. The velocity values computed in the two ways are in good agreement. It is observed that the n value obtained using equation (4.16) is underestimated. Fig. 4-2 shows the relation between n_2 from equation (4.16) and n_1 from calibration or fitting, which is found to be

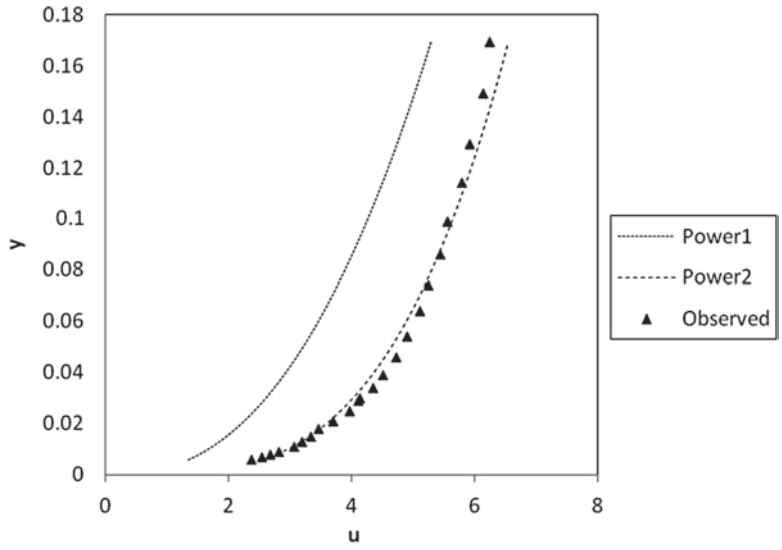

Figure 4-1 *Dimensionless velocity* (u/u_D) *versus dimensionless depth* (y/D) *for data set S-1.*
Note: Power 1 corresponds to velocity values with exponent n *obtained from equation (4.16) and Power 2 corresponds to velocity values obtained by fitting.*
Source: Data from Einstein and Chien (1955).

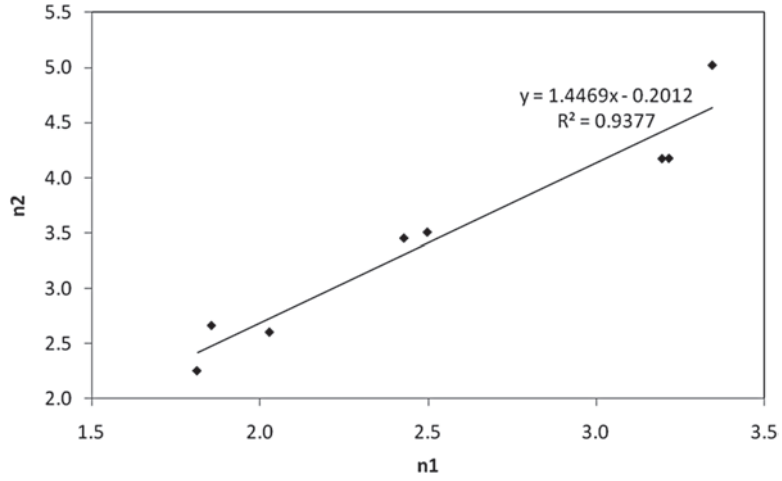

Figure 4-2 *Relation between* n *obtained from equation (4.16),* $x = n_1$, *and* n *obtained by fitting,* $y = n_2$, *for the eight data sets of Einstein and Chien (1955).*

$$n_2 = 1.45n_1 - 0.2 \tag{4.20}$$

with an R^2 (coefficient of determination) value of 0.94. This result shows that equation (4.16) provides a good first approximation of n, which can then be corrected using equation (4.20). In this manner, fitting or calibration can be entirely avoided.

Example 4.1 Compute and graph the probability density function underlying the power law velocity distribution for different values of n (2, 4, 6, 8, and 10).

Solution Assume that $u_D = 2\,\text{m/s}$. Using equation (4.10), a plot of $f(u)$ is constructed for various values of n, as shown in Fig. 4-3. It is clear that for $n = 2$, the PDF of u becomes linear with the slope as $2/(u_D)^2$.

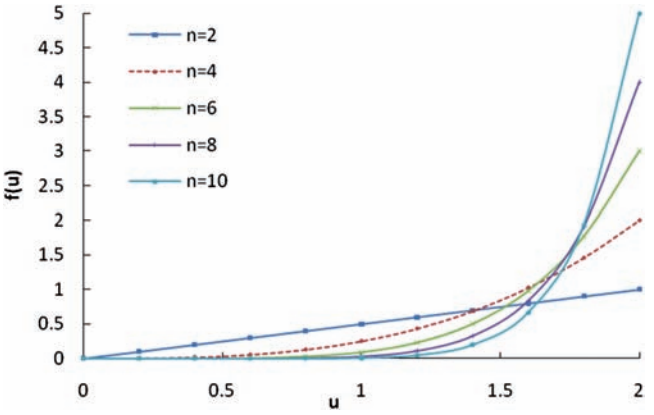

Figure 4-3 *The probability density function underlying the power law velocity distribution.*

Example 4.2 Compute and graph the cumulative probability distribution underlying the power law velocity.

Solution Using equation (4.11), a plot of $F(u)$ is constructed for various values of n as shown in Fig. 4-4. It is clear that for $n = 2$, the CDF of u is nonlinear but becomes linear for $n = 1$ with the slope as $1/u_D$.

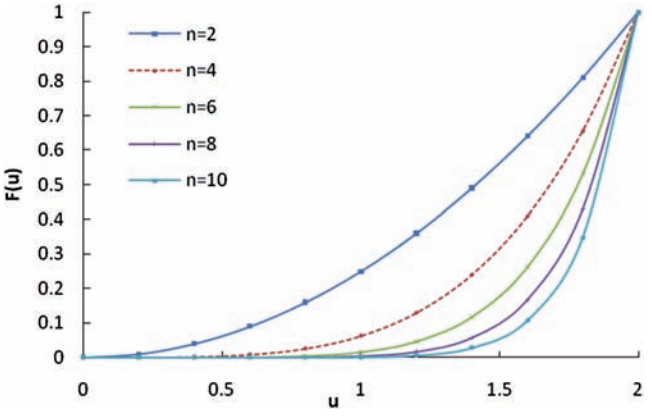

Figure 4-4 *The cumulative probability distribution underlying power law velocity.*

Example 4.3 Compute entropy, plot it as a function of n, and discuss the plot.

Solution Here $\overline{\ln u} = 1.469$ and from equation (4.18), $H = 1 + \overline{\ln u} - \ln n = 2.469 - \ln n$. A plot of $H(u)$ versus n is constructed, as shown in Fig. 4-5. It is clear that as n increases, the entropy of u decreases.

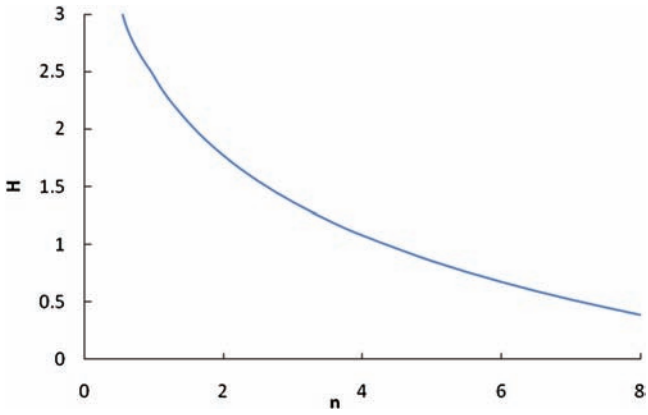

Figure 4-5 *Entropy as a function of* n.

Example 4.4 Plot the entropy of the power law velocity distribution as a function of average log velocity for a given n.

Solution When entropy is plotted as a function of the average of log velocity for different values of n, as shown in Fig. 4-6, it is seen that entropy is higher for smaller values of n. This phenomenon is understandable, because higher values of n make the power law velocity distribution less nonlinear and the probability distribution less variable.

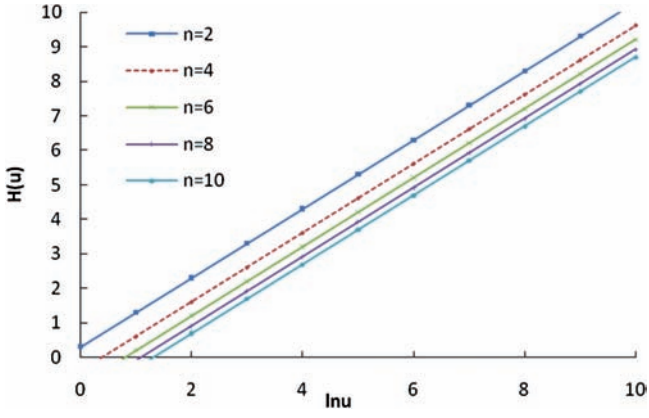

Figure 4-6 *Entropy of the power law velocity distribution as a function of average logarithmic velocity for a given* n.

Example 4.5 Consider a set of measurements of velocity in a river given in Table 4-1. Estimate the power law exponent for this data set using equation (4.16). Using this exponent, compute the velocity using the power law distribution and compare it with the observed velocity distribution. How good is the match?

Solution For the given data set, $D = 0.124\,\text{ft}$, $u_D = 7.11\,\text{ft/s}$, and $\overline{\ln u} = 2.469\,\text{ft/s}$. Then from equation (4.16), the value of n is obtained as

$$n = \frac{1}{\ln u_D - \overline{\ln u}} = \frac{1}{\ln 7.11 - 2.469} = 2.031$$

With this value of n, equation (4.17) is used to compute velocity, which is plotted in Fig. 4-7. Also plotted in the figure are observed velocity values.

Table 4-1 *Observed velocity values.*

y (ft)	u (ft/s)	y (ft)	u (ft/s)
0.006	2.22	0.04	4.83
0.009	2.5	0.045	5.08
0.011	2.72	0.05	5.3
0.011	2.86	0.054	5.52
0.015	2.96	0.064	5.81
0.017	3.33	0.074	6.09
0.019	3.57	0.084	6.29
0.024	3.9	0.095	6.52
0.034	4.52	0.104	6.7
		0.124	7.11

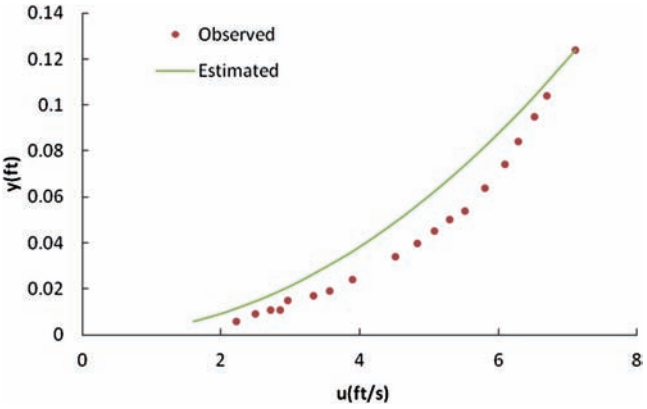

Figure 4-7 *Comparison of computed and observed velocity distributions.*

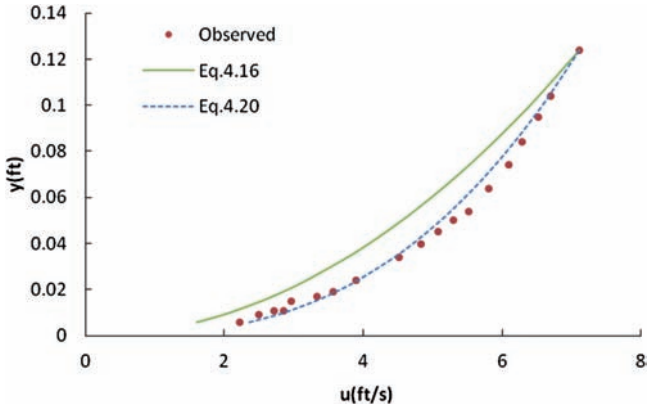

Figure 4-8 *Comparison of computed and observed velocity distributions.*

Example 4.6 For the data set in Example 4.5, compute the power law exponent using equation (4.20). Then compute the velocity using the power law distribution and compare it with the observed velocity distribution. How good is the match? Is there an improvement over the velocity distribution obtained in Example 4.5, and if there is, then how much?

Solution With the value of n obtained using equation (4.20), velocity is computed and is plotted in Fig. 4-8. Also plotted in the figure are computed velocities with n obtained from equation (4.16) and observed velocity values. Clearly, velocity values computed with n obtained using equation (4.20) are closer to observed values than the computed values with n from equation (4.16).

4.2.8 Another Way to Estimate Power Law Velocity Distribution Parameters

The power law velocity distribution in open channels, given by equation (4.17), can be expressed as

$$u = ay^b \tag{4.21a}$$

or

$$\frac{u}{u_D} = \left(\frac{y}{D}\right)^m \tag{4.21b}$$

where a, b, and m are parameters. The value of m is usually in the range of 6 to 7 (Karim and Kennedy 1987). It is usually determined by the frictional resistance at the bed and is, in practice, not known but can be determined using the least-squares method, if observed velocity values are available.

The average and mean velocities from the power law velocity distribution can be written as

$$u_m = a(\overline{y})^b \tag{4.22}$$

$$u_{\max} = a(D)^b \tag{4.23}$$

Let $\frac{\overline{y}}{D} = e^{-1}$. Therefore,

$$\frac{u_m}{u_{\max}} = \left(\frac{\overline{y}}{D}\right)^b = \exp(-b) \tag{4.24}$$

Using equation (4.24), we see that parameter b as a function of $M = \lambda_1 u_{\max}$, defined in Chapter 3, is obtained as

$$b = -\ln\frac{u_m}{u_{\max}} = -\ln\psi(M), \quad \psi(M) = \frac{u_m}{u_{\max}} \tag{4.25}$$

where ψ is some function. Then, parameter a is obtained as

$$a = \frac{u_m}{(\overline{y})^b} = \frac{u_m}{\left(\frac{\overline{y}}{D}\right)^b D^b} = \frac{u_m}{(De^{-1})^b} \tag{4.26}$$

which is also a function of M.

It may be noted that when $u_m/u_{\max} = 0.8$, or M between 7 and 8, equation (4.25) yields $b = 1/7$, a commonly used value. An increase in the value of b corresponds to a decrease in $u_m/u_{\max}$ or M, and would lead to an increase in entropy $H(u_m/u_{\max})$.

4.3 One-Dimensional Prandtl–von Karman Universal Velocity Distribution

From boundary shear considerations, the classical method for describing the velocity profile in wide channels entails relating velocity to flow depth (von Karman 1935). Thus, the well-known Prandtl–von Karman universal logarithmic velocity distribution can be written as

$$u = \frac{u^*}{k}\ln\frac{y}{y_0} \tag{4.27a}$$

where k is von Karman's universal constant, u^* is the shear velocity, and y_0 is a parameter. The Prandtl–von Karman velocity equation is also expressed (Daugherty and Franzini 1977) as

$$u = u_D + \frac{u^*}{k}\ln\left(\frac{y}{D}\right) \tag{4.27b}$$

Here $u^* = \sqrt{gDS}$, where S is the slope of the energy grade line. Equation (4.27a) hypothesizes that the shear stress distribution is uniform between the channel bed and water surface, which is not entirely realistic. The form of equation (4.27a) is similar to equation (2.70) (in Chapter 2), where both equations contain two parameters. It is also interesting to note that parameter k, defined as $\lambda_1 u^*$ in equation (2.69) (in Chapter 2), is similar to the von Karman constant. In practice, the values of k and S are not known. One can approximate S for uniform flow by the bed slope.

Example 4.7 Velocity observations were made by Einstein and Chien (1955) in sediment-laden flow. These observations are given in Table 4-2. Plot the Prandtl–von Karman velocity distribution (y/D on the y-axis (log-scale) and u/u^* on the x-axis). One can take a very small value of y_0 as 3.03×10^{-3} ft. Also plot observed values on this graph. What can one conclude from this plot?

Solution The Prandtl–von Karman universal velocity distribution is given by equation (4.27a), in which $k = 0.214$, and y_0 is taken as 3.02×10^{-3} ft, $u^* = \sqrt{gDS} = 0.406$ ft/s, and the channel bed slope $S = 0.014$. Calculated values are given in Table 4-2. The observed velocity distribution and the Prandtl–von Karman velocity distribution are shown in Fig. 4-9. It is seen that the Prandtl–von

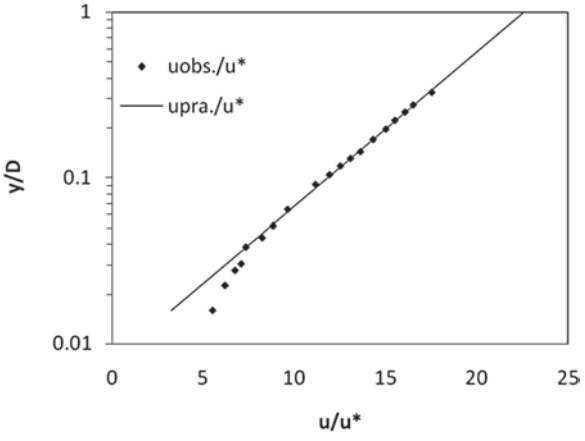

Figure 4-9 *Dimensionless velocity distribution (*y/D *versus* u/u**) based on measured data and Prandtl–von Karman velocity distribution equation.*
Note: uobs. = observed velocity, and upra. = velocity computed using the Prandtl–von Karman equation.

Table 4-2 *Observed and calculated values of velocity.*

y (ft)	y/D	u_{obs} (ft/s)	u_{obs}/u^*	$u_{pra.}$ (ft/s)	$u_{pra.}/u^*$
0.006	0.0159	2.22	5.47	1.31	3.22
0.009	0.0225	2.5	6.15	1.96	4.84
0.011	0.0278	2.72	6.7	2.37	5.83
0.011	0.0304	2.86	7.04	2.54	6.24
0.015	0.0384	2.96	7.3	2.98	7.34
0.017	0.0437	3.33	8.2	3.22	7.94
0.019	0.0515	3.57	8.8	3.54	8.71
0.024	0.0645	3.9	9.6	3.96	9.76
0.034	0.0912	4.52	11.13	4.62	11.4
0.04	0.1045	4.83	11.9	4.88	12
0.045	0.118	5.08	12.5	5.11	12.6
0.05	0.131	5.3	13.05	5.31	13.1
0.054	0.144	5.52	13.6	5.49	13.5
0.064	0.1705	5.81	14.3	5.81	14.3
0.074	0.197	6.09	15	6.08	15
0.084	0.223	6.29	15.5	6.32	15.6
0.095	0.25	6.52	16.05	6.53	16.1
0.104	0.276	6.7	16.5	6.72	16.6
0.124	0.329	7.11	17.52	7.05	17.4

Note: y (ft) = vertical distance measured from the channel bed for each sampled velocity; u_{obs} = observed velocity (ft/s); $u_{pra.}$ = velocity points values (ft/s) estimated by Prandtl–von Karman equation; and D = water depth (ft) along the vertical.

Karman velocity distribution significantly deviates from the observed velocity distribution near the bed, and, hence, it may not be suitable for representing the velocity profile close to the bed.

Example 4.8 Plot on a rectangular graph y/D on the y-axis and u/u^* on the x-axis using observed values in Table 4-1 near the bed, Prandtl–von Karman velocity distribution, and entropy-based velocity distribution developed in Chapter 2. What can one conclude from this plot?

Solution Observed velocity and velocity computed by the Prandtl–von Karman velocity distribution and entropy-based velocity distribution derived in Chapter 2 are plotted as shown in Fig. 4-10. It is seen that near the bed the entropy-based

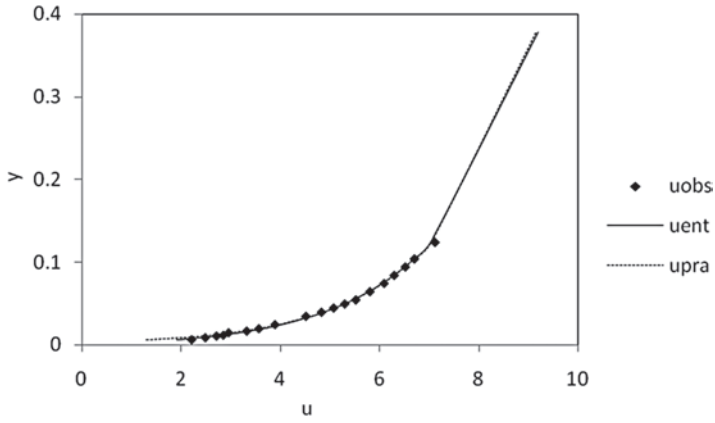

Figure 4-10 *Comparison of entropy-based velocity distribution (equations [2.70] and [4.27a]).*

velocity distribution does better. In the middle portion, both the Prandtl–von Karman and the entropy-based velocity distribution predict the velocity well.

The Prandtl–von Karman velocity distribution has a value of flow depth (y_0) that corresponds to the shear velocity. Determination of y_0 has been subjective and is frequently determined by calibration. Other limitations of these velocity distributions have been discussed by Chiu (1987) and Singh (1996), among others.

4.3.1 Specification of Constraints

For the Prandtl–von Karman universal velocity distribution, the constraints to be specified are equation (4.4) and

$$C_2 = \int_0^{u_D} uf(u)du = \overline{u} = u_m \tag{4.28}$$

where u_m is the mean of velocity values or the cross-sectional mean velocity, Q/A, where Q is discharge passing through a cross-sectional area A, and u_D is the velocity at $y = D$ (flow depth D or water surface).

4.3.2 Probability Distribution

In this case, the Shannon entropy, given by equation (4.3), is maximized, subject to equations (4.4) and (4.28), for obtaining the least-biased probability distribution of u, $f(u)$. Using the method of Lagrange multipliers as before, the entropy-based probability density function (PDF) of velocity becomes

$$f(u) = \exp[-\lambda_0 - \lambda_1 u] \tag{4.29}$$

where λ_0 and λ_1 are Lagrange multipliers. The CDF of u is expressed as

$$F(u) = \frac{1}{\lambda_1}\exp(-\lambda_0)[\exp(-\lambda_1 u^*) - \exp(-\lambda_1 u)] \tag{4.30}$$

4.3.3 Determination of Lagrange Multipliers

Substituting equation (4.29) in equation (4.5a) and integrating over $u^* \le u \le u_D$, where u^* is shear velocity, one obtains

$$\exp(-\lambda_0) = \frac{\lambda_1}{\exp(-\lambda_1 u^*) - \exp(-\lambda_1 u_D)} \tag{4.31}$$

Equation (4.31) can be written as

$$\lambda_0 = \ln[\exp(-\lambda_1 u^*) - \exp(-\lambda_1 u_D)] - \ln\lambda_1 \tag{4.32}$$

Differentiating equation (4.32) with respect to λ_1, one obtains

$$\frac{\partial\lambda_0}{\partial\lambda_1} = \frac{\exp(-\lambda_1 u_D) - u^*\exp(-\lambda_1 u^*)}{\exp(-\lambda_1 u^*) - \exp(-\lambda_1 u_D)} - \frac{1}{\lambda_1} \tag{4.33}$$

Conversely, substitution of equation (4.29) in equation (4.5a) yields

$$\lambda_0 = \ln\left[\int_0^{u_D} \exp(-\lambda_1 u)\right] du \tag{4.34}$$

Differentiating equation (4.34) with respect to λ_1, one obtains

$$\frac{\partial\lambda_0}{\partial\lambda_1} = -\frac{\int_0^{u_D} u\exp(-\lambda_1 u_D)du}{\int_0^{u_D} \exp(-\lambda_1 u)du} \tag{4.35}$$

Multiplying and dividing equation (4.35) by $\exp(-\lambda_0)$, and recalling equation (4.28), the result is

$$\frac{\partial\lambda_0}{\partial\lambda_1} = -\frac{\int_0^{u_D} u\exp(-\lambda_0 - \lambda_1 u_D)du}{\int_0^{u_D} \exp(-\lambda_0 - \lambda_1 u)du} = -u_m \tag{4.36}$$

Equating equation (4.33) to equation (4.36), one obtains

$$u_m = \frac{1}{\lambda_1} - \frac{u_D \exp(-\lambda_1 u_D) - u^* \exp(-\lambda_1 u^*)}{\exp(-\lambda_1 u^*) - \exp(-\lambda_1 u_D)} \tag{4.37}$$

Equation (4.37) expresses λ_1 implicitly in terms of u_m. It can also be derived as follows.

Substituting equation (4.29) in equation (4.28) and using equation (4.31), one obtains

$$\frac{\lambda_1}{b}\left[-u_D \exp(-\lambda_1 u_D + u^* \exp(-\lambda_1 u^*) - \frac{\exp(-\lambda_1 u_D)}{\lambda_1} + \frac{\exp(-\lambda_1 u^*)}{\lambda_1}\right] = u_m \tag{4.38a}$$

where b is defined as

$$b = \exp(-\lambda_1 u^*) - \exp(-\lambda_1 u_D) \tag{4.38b}$$

Equation (4.38a) is the same as equation (4.37). Equations (4.31) and (4.37) can be used to determine the Lagrange parameters λ_0 and λ_1.

The shear velocity is defined as $u^* = \sqrt{gDS}$, where g is acceleration caused by gravity, and S is channel slope. Combining equations (4.31) and (4.29), the result is the probability density function of velocity u as

$$f(u) = \frac{\lambda_1}{\exp(-\lambda_1 u^*) - \exp(-\lambda_1 u_D)} \exp(-\lambda_1 u) = \frac{\lambda_1}{b} \exp(-\lambda_1 u) \tag{4.39a}$$

and then the cumulative probability distribution function can be expressed as

$$F(u) = \frac{\lambda_1}{\exp(-\lambda_1 u^*) - \exp(-\lambda_1 u_D)} [\exp(-\lambda_1 u^*) - \exp(-\lambda_1 u)] \tag{4.39b}$$

Equation (4.39a) shows that the PDF of the Prandtl–von Karman universal velocity distribution is negative exponential with parameter λ_1 determined as discussed.

Example 4.9 Plot λ_0 as a function of λ_1 for a given u^* and u_D. Let $u_D = 7.11$ ft/s and $u^* = \sqrt{gDS} = 0.406$ ft/s.

Solution Using equation (4.32), we see that λ_0 is computed as a function of λ_1 and is plotted, as shown in Fig. 4-11. Clearly, λ_0 is negative for λ_1 greater than 0.4, and for λ_1 greater than 2.5 the variation becomes almost linear.

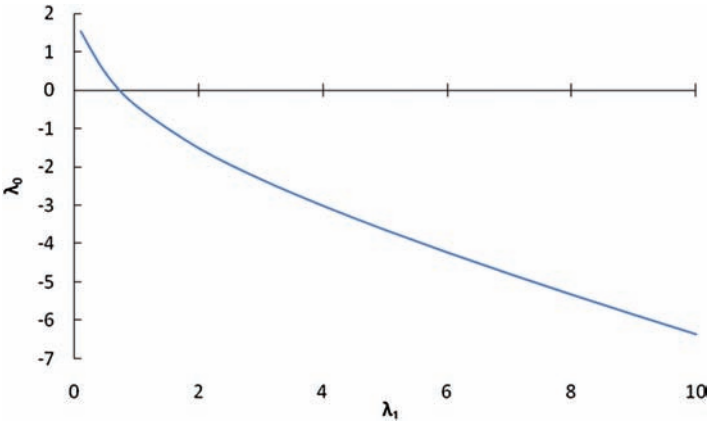

Figure 4-11 *Plot of λ_0 as a function of λ_1 for a given* u* *and* u_D.

It may be noted that if u^* is taken as a small quantity tending to 0, then equation (4.39a) simplifies to

$$f(u) = \frac{\lambda_1 \exp(-\lambda_1 u)}{1 - \exp(-\lambda_1 u_D)} = \frac{k \exp(ku / u^*)}{u^*[\exp(ku_D / u^*) - 1]} \tag{4.40}$$

and the cumulative PDF equation (4.39b) simplifies to

$$F(u) = \frac{\exp(ku / u^*) - 1}{[\exp(ku_D / u^*) - 1]} \tag{4.41}$$

where

$$\lambda_1 = -\frac{k}{u^*} \tag{4.42}$$

in which k is the von Karman constant. Equations (4.40) and (4.41) were given, without derivation, by Dingman (1989) for the Prandtl–von Karman universal velocity distribution.

Equation (4.39a) can be written in terms of k and u^* as

$$f(u) = \frac{k \exp(-ku / u^*)}{u^*[\exp(k) - \exp(-ku_D / u^*)]} \tag{4.43}$$

Example 4.10 Compute and graph the PDF underlying the Prandtl–von Karman velocity distribution. Take $k = 0.214$, $u^* = 0.406$ ft/s, $u_D = 7.11$ ft/s.

Solution Using equation (4.43), $f(u)$ is computed as a function of u, as shown in Fig. 4-12.

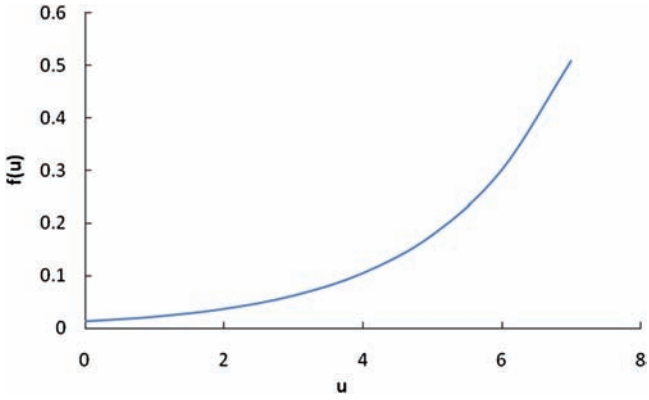

Figure 4-12 *Probability density function underlying the Prandtl–von Karman velocity distribution.*

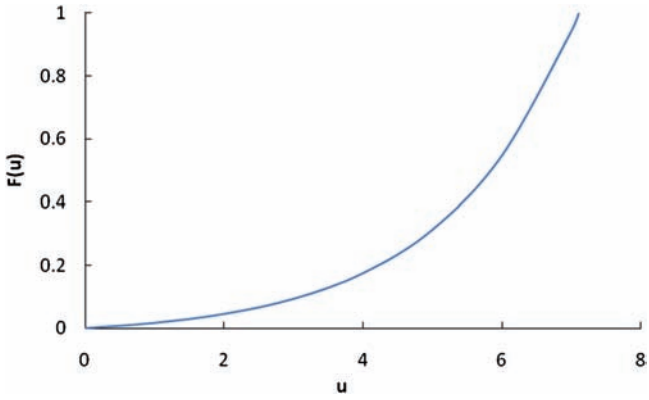

Figure 4-13 *Cumulative probability distribution underlying the Prandtl–von Karman velocity distribution.*

Example 4.11 Compute and graph the cumulative probability distribution underlying the Prandtl–von Karman velocity distribution. Take $k = 0.214$, $u^* = 0.406\,\text{ft/s}$, $u_D = 7.11\,\text{ft/s}$.

Solution Using equation (4.41), we see that $F(u)$ is computed as a function of u, as shown in Fig. 4-13.

4.3.4 Entropy of Velocity Distribution

The entropy of the Prandtl–von Karman velocity distribution can be obtained by inserting equation (4.43) in equation (4.4) as

$$H = -\ln[\exp(k) - \exp(-ku_D / u^*)] + \frac{k}{u^*}\bar{u} - \ln\left(\frac{k}{u^*}\right) \tag{4.44}$$

Equation (4.44) shows that the uncertainty of the velocity distribution is heavily influenced by the average velocity and the shear velocity. This influence means

that velocity should be sampled more frequently along the vertical, where the average velocity is high.

Example 4.12 Plot the entropy of the Prandtl–von Karman velocity distribution as a function of parameters in equation (4.44), varying one parameter and keeping others constant. Compute the entropy for the data in Example 4.5.

Solution Using equation (4.44), $H(u)$ is computed as a function of k, as shown in Fig. 4-14, as a function of u_m in Fig. 4-15, as a function of u_D in Fig. 4-16, and as a function of u^* in Fig. 4-17. Except for k less than 0.2, H increases linearly with k. For all values of u_m, H increases linearly. Conversely, H decreases with u_D rapidly and then becomes almost constant, whereas it declines exponentially with u^*.

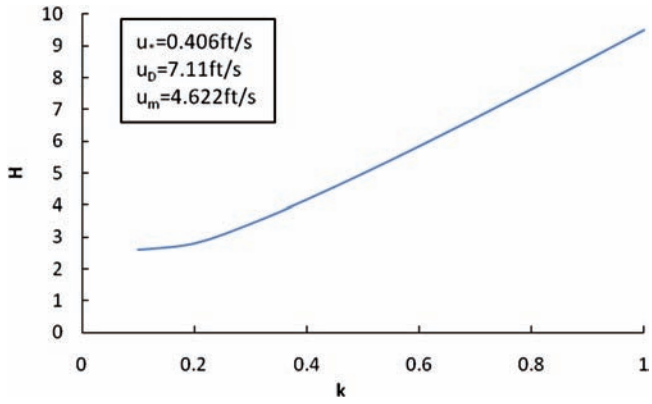

Figure 4-14 *Entropy as a function of* k.

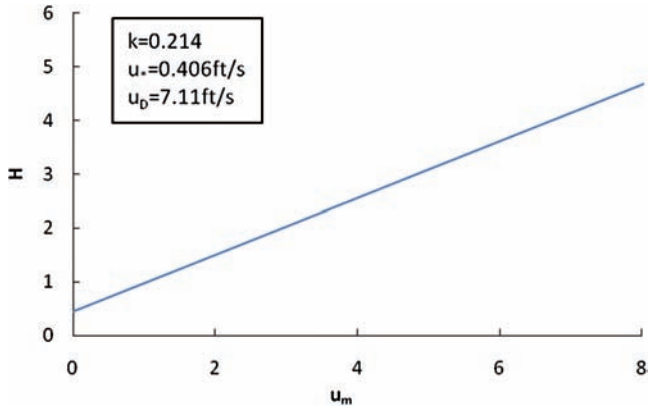

Figure 4-15 *Entropy as a function of* u_m *(ft/s).*

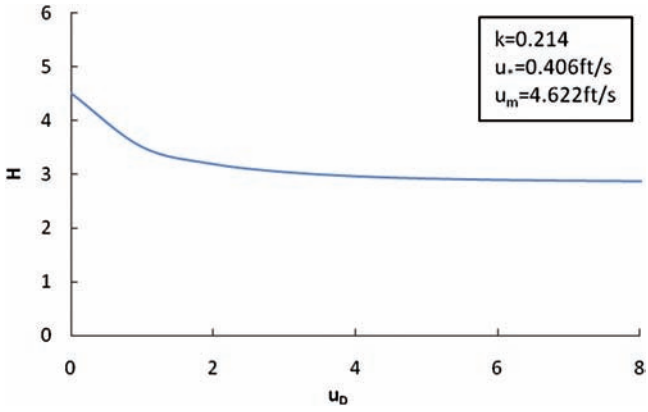

Figure 4-16 *Entropy as a function of* u_D *(ft/s).*

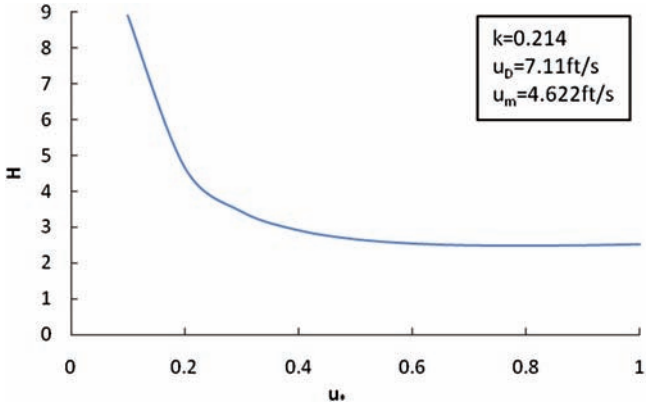

Figure 4-17 *Entropy as a function of* u*.

4.3.5 Velocity Distribution

Substitution of equation (4.39a) in equation (4.4a) and then integration with the condition that $u = u^*$ when $y = y_0$ yields the relation between velocity and depth:

$$\frac{1}{b}[\exp(-\lambda_1 u^*) - \exp(-\lambda_1 u) = \frac{y - y_0}{D - y_0} \tag{4.45}$$

Here y_0 represents the depth of shear flow or height corresponding to shear velocity. Equation (4.45) becomes

$$u = \frac{u^*}{k} \ln\left[\exp(k) - b\frac{y - y_0}{D - y_0}\right] \tag{4.46}$$

Clearly, equation (4.46) is similar to but not the same as the Prandtl–von Karman universal velocity distribution. However, a little algebraic simplification can lead to the same velocity distribution equation.

Assuming that the exponential term [exp(*k*)] is much smaller than exp(ku_D/u^*) and, hence, can be neglected, equation (4.38b) can be approximated as

$$b \approx \exp(ku_D / u^*) \tag{4.47}$$

Equation (4.46) then becomes

$$u = \frac{u^*}{k} \ln\left[\exp(k) + \exp\left(k \frac{u_D}{u^*} \right) \frac{y - y_0}{D - y_0} \right] \tag{4.48}$$

which can be approximated as

$$u = \frac{u^*}{k} \ln\left[\exp\left(k \frac{u_D}{u^*} \right) \frac{y - y_0}{D - y_0} \right] \tag{4.49}$$

Equation (4.49) is based on the assumption that $\exp(ku_D/u^*) >> \exp(k)$, which is quite reasonable.

If it is assumed that

$$y_0 \exp(ku_D / u^*) \approx D \tag{4.50}$$

then equation (4.49) reduces to

$$u = \frac{u^*}{k} \ln\left(\frac{y}{y_0} \right) \tag{4.51}$$

which is the Prandtl–von Karman universal velocity distribution.

If equation (4.50) is approximately true, then this provides an explicit relation between y_0 and k, u_D and D. Determination of y_0 has been pesky. Hydraulically, equation (4.50) states that for any flow with a depth of D and the corresponding velocity u_D, the channel has a particular value of y_0 for a given k and u^*. In other words, these parameter values must be compatible with each other, and, hence, equation (4.50) can be of great significance.

4.3.6 Testing

For verifying equation (4.50), the observed flow depth values are, respectively, 0.45, 0.38, 0.36, 0.76, 0.43, 0.40, 0.58, and 0.40 m, whereas the D values obtained from equation (4.50) are found to be 0.62, 0.23, 0.24, 0.36, 0.34, 0.48, 0.50, and 0.38. The two sets of values are not exactly the same but are in reasonable agreement, as shown in Fig. 4-18. The shear velocity is computed by $\sqrt{gDS}$, and the von Karman constant k varies from 0.2 to 0.4, according to different flow status. No consistent pattern of either overestimation or underestimation is found either for clear-water flow or sediment-laden flow. Of course, more data need to be

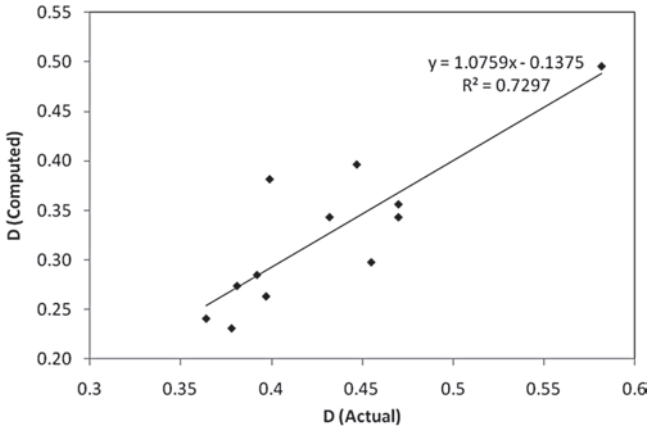

Figure 4-18 *Relation between observed flow depth and depth computed from equation (4.50).*

analyzed to determine the conditions under which equation (4.50) would apply and the amount of error that can be expected with the use of equation (4.50). An important implication of equation (4.50) that seems to hold is that it can provide an estimate of y_0 for given values of D, u_D, and u^*.

Example 4.13 Consider the measurements of velocity in a river as given in Example 4.5. Estimate y_0 for the log law velocity distribution for this data set. Using this y_0 value, compute the velocity using the Prandtl–von Karman velocity distribution and compare it with the observed velocity distribution. How good is the match?

Solution Take $k = 0.214$, $y_0 = 3.02 \times 10^{-3}$ ft, $u^* = \sqrt{gDS} = 0.406$ ft/s. The velocity computed using the Prandtl–von Karman velocity distribution compares well with the observed velocity, except near the bed, as shown in Fig. 4-19.

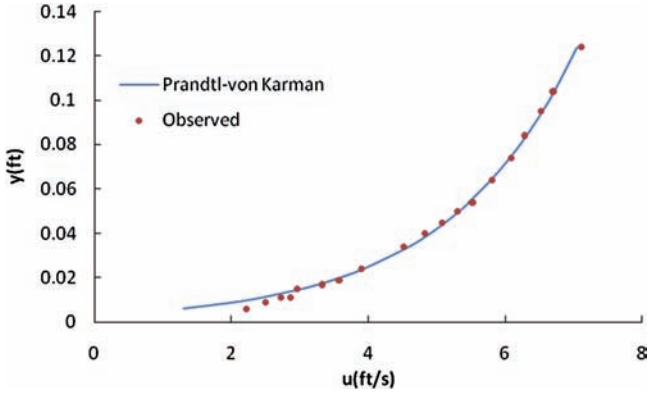

Figure 4-19 *Comparison of computed and observed velocity values.*

Example 4.14 For data set in Example 4.5, compute the value of D using equation (4.50). Then compute the velocity using the log law velocity distribution and compare it with the observed velocity distribution. How good is the match? Is there a decline in the accuracy of the velocity distribution obtained in Example 4.13, and if there is, then how much?

Solution

$$D = y_0 \exp(ku_D / u^*) = 0.00302 \times \exp(0.214 \times 7.11 / 0.406) = 0.128\, ft.$$

Take $k = 0.214$, $y_0 = 3.02 \times 10^{-3}$ ft, $u^* = \sqrt{gDS} = 0.406$ ft/s.

Computed and observed velocities are shown in Table 4-3 and plotted in Fig. 4-20. Both types of velocity distributions compare reasonably well.

Table 4-3 *Observed and computed velocity values.*

y (ft)	$u_{obs.}$ (ft/s)	$u_{pra.}$ (ft/s)	$u_{log.}$ (ft/s)	y (ft)	$u_{obs.}$ (ft/s)	$u_{pra.}$ (ft/s)	$u_{log.}$ (ft/s)
0.006	2.22	1.302	1.539	0.045	5.08	5.125	5.198
0.009	2.5	2.072	2.247	0.05	5.3	5.325	5.396
0.011	2.72	2.452	2.605	0.054	5.52	5.471	5.540
0.011	2.86	2.452	2.605	0.064	5.81	5.793	5.859
0.015	2.96	3.041	3.166	0.074	6.09	6.069	6.132
0.017	3.33	3.278	3.394	0.084	6.29	6.309	6.370
0.019	3.57	3.489	3.598	0.095	6.52	6.543	6.602
0.024	3.9	3.933	4.029	0.104	6.7	6.714	6.773
0.034	4.52	4.593	4.675	0.124	7.11	7.048	7.105
0.04	4.83	4.902	4.978				

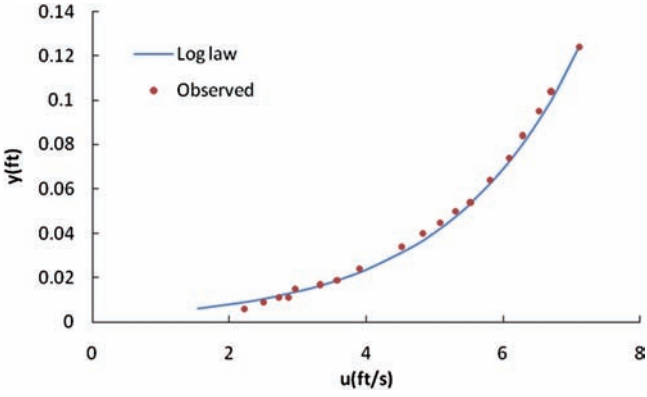

Figure 4-20 *Comparison of log-law computed velocity distribution and observed velocity values.*

In a manner similar to that in the case of the power law velocity distribution, the two parameters of the logarithmic law can be expressed in terms of M as follows. Let $y_m/D = e^{-1}$. Then, parameters of equation (4.51) can be written as

$$y_0 = D\exp\left[-\left(1-\frac{u_m}{u_{\max}}\right)^{-1}\right] = D\exp[\psi(M)-1]^{-1} \tag{4.52}$$

and

$$k = \left(\frac{u_m}{u^*}\right)^{-1}\left(\frac{u_m}{u_{\max}}\right)\left(1-\frac{u_m}{u_{\max}}\right)^{-1} = \left(\frac{u_m}{u^*}\right)^{-1}\psi(M)[1-\psi(M)]^{-1} \tag{4.53}$$

where

$$\frac{u_m}{u^*} = \frac{q}{Du^*} = \sqrt{\frac{8}{f_l}} = \frac{CD^{1/6}}{n\sqrt{g}} \tag{4.54}$$

where q is the specific discharge (i.e., discharge per unit width), f_l is the head loss, and C is 1.49 if the English system of units is used and is unity if the SI system is used.

The von Karman constant k is normally assumed as 0.40 or 0.42. If M is between 7 and 8, $u_m/u_{\max}$ is between 0.86 and 0.87, the aforementioned equations yield f_l between 0.03 and 0.035, which corresponds to the Reynolds number equal to 2,000, which is the lower limit for turbulent flow in open channels. For turbulent flow, the Reynolds number is greater than 2,000, and f_l is less than 0.035 (Chow 1959). From equation (4.54), if k = 0.4, $u_m/u_{\max}$ is greater than 0.86, and, hence, M is greater than 7. A higher value of $u_m/u_{\max}$ means a more uniform distribution, a greater value of M, and, hence, a lower value of entropy. A lower value of M below 7 and, hence, $u_m/u_{\max}$ below 0.86 would increase entropy and reduce k from 0.3 in alluvial channels with sediment concentration in flow. Einstein and Chien (1955) found lower values of k in sediment-laden flow.

4.4 Two-Dimensional Power Law Velocity Distribution

Following the discussion in Chapter 3, the one-dimensional (1-D) power law velocity distribution discussed earlier can be extended to two dimensions. Let the Cartesian coordinates be y and z, where y is the vertical coordinate and z is

the transverse coordinate. Let these coordinates be transformed into another system of coordinates (r, s), in which r is uniquely related to velocity (Chiu and Chiou 1986); i.e., each isovel corresponds to one value of r and isovels are represented by r-coordinate curves, and s-coordinate curves are their orthogonal trajectories. Thus, r is a function of y and z.

The orthogonality of r and s suggests that if r is determined, then s can be determined. Here, r varies as $r_0 \le r \le r_{max}$, where r_{max} is the maximum value of r, and the time averaged velocity u is bounded by $0 \le u \le u_{max}$. Here $u = 0$ occurs along an isovel corresponding to $r = r_0$, where r_0 represents the channel bed, including boundaries, and has a small value. Likewise, the maximum velocity u_{max}, which may occur on or below the water surface, occurs along the isovel corresponding to $r = r_{max}$. Thus, it is assumed that

$$u = W(r) \text{ or } r = W^{-1}(u) \tag{4.55}$$

where W is some function.

4.4.1 Hypothesis

As both u and r are considered random variables with probability density functions (PDFs) as $f(u)$ and $g(r)$, respectively, it is assumed that all values of r between r_0 and r_{max} are equally likely to be sampled. This phenomenon means that the PDF of r, $g(r)$, can be hypothesized to be uniform on the interval $r_0 \le r \le r_{max}$:

$$g(r) = \frac{1}{r_{max} - r_0} \tag{4.56}$$

Now the cumulative distribution function (CDF) of velocity (i.e., the probability of velocity being less than or equal to a given value of u), $F(u)$, can be expressed as

$$F(u) = \int_0^u f(u)du = \int_{r_0}^{W^{-1}(u)=r} f[W(r)]d[W(r)] = \int_{r_0}^{r} g(r)dr = \frac{r - r_0}{r_{max} - r_0} \tag{4.57}$$

where $f(u)$ is the PDF of velocity u and can be expressed as

$$f(u) = \frac{dF(u)}{du} = \frac{dF(u)}{dr}\frac{dr}{du} = \left[(r_{max} - r_0)\frac{du}{dr}\right]^{-1} \tag{4.58}$$

The hypothesis expressed by equation (4.56) needs to be tested.

4.4.2 Specification of Constraints

The constraints for the one-dimensional case expressed by equations (4.4) and (4.5) can be modified for the two-dimensional case as

$$\int_0^{u_{\max}} f(u)du = 1 \tag{4.59}$$

and

$$\int_0^{u_{\max}} \ln u f(u)du = \overline{\ln u} \tag{4.60}$$

where the maximum velocity $u_{\max}$ may no longer occur at $y = D$ (flow depth) or water surface.

4.4.3 Entropy-Based Probability Distribution

Equations (4.6) through (4.17) hold, except that u_D is replaced by $u_{\max}$. To avoid confusion, the following is expressed. Equation (4.8) holds, but equation (4.9) is modified as

$$\exp(\lambda_0) = \frac{u_{\max}^{-\lambda_1+1}}{-\lambda_1+1} \text{ or } \lambda_0 = -\ln(-\lambda_1+1) + (-\lambda_1+1)\ln u_{\max} \tag{4.61}$$

where λ_0 and λ_1 are the Lagrange multipliers. Differentiating equation (4.61) with respect to λ_1, one obtains

$$\frac{\partial \lambda_0}{\partial \lambda_1} = \frac{1}{-\lambda_1+1} - \ln u_{\max} \tag{4.62}$$

Likewise, equation (4.13) modifies to

$$\lambda_0 = \ln \int_0^{u_{\max}} u^{-\lambda_1} du \tag{4.63}$$

Example 4.15 Construct a plot of λ_0 as a function of λ_1 for various values of $u_{\max}$. Discuss the plot and its implications.

Solution A plot of λ_0 as a function of λ_1 for various values of $u_{\max}$ (2, 4, 6, and 8 m/s) is constructed as shown in Fig. 4-21. It is seen that λ_0 decreases with λ_1 for increasing $u_{\max}$. For a given λ_1 value, λ_0 increases with increasing $u_{\max}$.

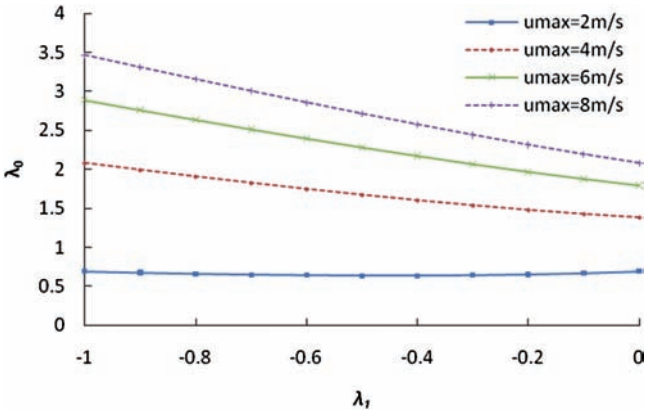

Figure 4-21 *Plot of λ_0 as a function of λ_1 for various values of* u_{max} *(m/s).*

Differentiating equation (4.63) with respect to λ_1, the result is

$$\frac{\partial \lambda_1}{\partial \lambda_2} = -\overline{\ln u} \tag{4.64}$$

Equating equation (4.64) to equation (4.62) leads to

$$\lambda_1 = 1 - \frac{1}{\ln u_{\max} - \overline{\ln u}} \tag{4.65}$$

Substitution of equation (4.65) in equation (4.61) yields

$$\lambda_0 = \ln[-\overline{\ln u} + \ln u_{\max}] + \frac{\ln u_{\max}}{-\overline{\ln u} + \ln u_{\max}} \tag{4.66}$$

The Lagrange multipliers λ_0 and λ_1 are expressed by equations (4.65) and (4.66) explicitly in terms of $\overline{\ln u}$ and $u_{\max}$.

Example 4.16 Construct a plot of λ_1 as a function of $\overline{\ln u}$ for various values of $u_{\max}$. Discuss the plot and its implications.

Solution Using equation (4.65), λ_1 is plotted as a function of $\overline{\ln u}$ for various values of $u_{\max}$ (2, 4, 6, and 8 m/s), as shown in Fig. 4-22. For a given u_{max}, λ_1 decreases with increasing $\overline{\ln u}$.

$$f(u) = n\frac{u^{n-1}}{u_{\max}^n} \tag{4.67}$$

and the CDF as

$$F(u) = \frac{u^n}{u_{\max}^n} \tag{4.68}$$

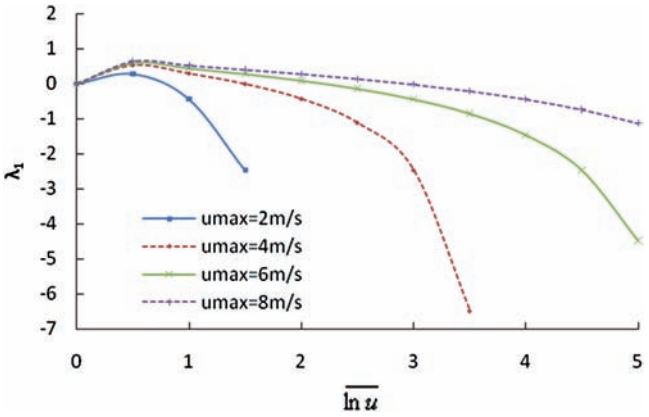

Figure 4-22 *Plot of λ_1 as a function of $\overline{\ln u}$ for various values of* u_{max} *(2, 4, 6, and 8 m/s).*

4.4.4 Velocity Distribution

Substituting equation (4.67) in equation (4.58), one obtains

$$\frac{nu^{n-1}}{u_{\max}^{n}}\frac{du}{dr}=\frac{1}{r_{\max}-r_0} \tag{4.69}$$

Integrating equation (4.69) with the condition that $u = 0$ at $r = r_0$, one gets

$$u=u_{\max}\left(\frac{r-r_0}{r_{\max}-r_0}\right)^{\frac{1}{n}} \tag{4.70}$$

The mean velocity u_m can be obtained from equation (4.70) as

$$u_m=u_{\max}\left(\frac{\overline{r}-r_0}{r_{\max}-r_0}\right)^{\frac{1}{n}} \tag{4.71}$$

Equation (4.71) can also be cast as

$$\frac{u_m}{u_{\max}}=\left(\frac{\overline{r}-r_0}{r_{\max}-r_0}\right)^{\frac{1}{n}} \tag{4.72}$$

For wide rectangular channels $(r - r_0)/(r_{\max} - r_0)$ can be approximated as y/D. Therefore, equation (4.70) can be written as

$$u=u_{\max}\left(\frac{y}{D}\right)^{\frac{1}{n}} \text{ or } \frac{u}{u_{\max}}=\left(\frac{y}{D}\right)^{\frac{1}{n}} \tag{4.73}$$

It may be noted from equation (4.16) that

$$n = \frac{1}{\ln u_{\max} - \overline{\ln u}} \text{ or } \frac{1}{n} = m = \ln u_{\max} - \overline{\ln u} \tag{4.74}$$

Thus, exponent n is expressed in terms of measurable physical quantities.

Equation (4.70) or (4.73) is a 2-D power law velocity distribution. Taking the derivative of equation (4.73), the velocity gradient can be expressed as

$$\frac{du}{dy} = u_{\max} m \left(\frac{1}{D}\right)^m y^{m-1} \tag{4.75}$$

Defining $N = mu_{\max}$, equation (4.75) can be written as

$$\frac{du}{dy} = N\left(\frac{1}{D}\right)^m y^{m-1} = \frac{N}{D}\left(\frac{y}{D}\right)^{m-1} \tag{4.76}$$

Likewise, one can also write from equation (4.70):

$$\frac{du}{dr} = u_{\max} \frac{1}{n} \frac{1}{(r_{\max} - r_0)} \left(\frac{r - r_0}{r_{\max} - r_0}\right)^{\frac{1}{n}-1} \tag{4.77}$$

Equation (4.72) can be cast as

$$\left(\frac{\overline{r} - r_0}{r_{\max} - r_0}\right) = \left(\frac{u_m}{u_{\max}}\right)^n \tag{4.78}$$

which can be used as a measure of uniformity or homogeneity of the velocity distribution.

Substituting equation (4.67) in equation (4.3) with u_D replaced by $u_{\max}$, one gets

$$H(u) = -\ln n - (n-1)\overline{\ln u} + n \ln u_{\max} \tag{4.79}$$

4.4.5 Construction of Isovels and Relation between (y, z) Coordinates and (r, s) Coordinates

The discussion in Chapter 3 provides the relations between the (y, z) and (r, s) coordinate systems (equations (3.56)–(3.61)), and along the y-axis where $z = 0$, it shows a relation between r and y (equation (3.76)):

$$r = \frac{y}{D+h}\exp\left[1-\frac{y}{D+h}\right] \tag{4.80}$$

When $y = 0$, $r = 0$, and when $y = D$, $r = r_{max}$. When $h < 0$, the value of h represents the actual depth of the point below the water surface and then r increases with y from $y = 0$ to $y = D + h$, where the maximum velocity occurs at $r = r_{max} = 1$ and decreases from $D + h$ to D (water surface). Differentiation of equation (4.80) yields

$$dr = \frac{1}{D+h}\left[1-\frac{y}{D}\right]\exp\left[1-\frac{y}{D+h}\right]dy \tag{4.81}$$

which can be simply written as

$$h_r dr = dy \tag{4.82}$$

where

$$h_r = (D+h)\left\{\left[1-\frac{y}{D}\right]\exp\left[1-\frac{y}{D+h}\right]\right\}^{-1} \tag{4.83}$$

Coefficient h_r is a scale factor required for coordinate transformation between y and r systems. This situation allows h_r and dr to have the same length dimension as dy.

The isovel for null velocity along r_0 can be expressed as

$$r_0 = \frac{c_y}{D+c_y+h}\exp\left[1-\frac{c_y}{D+c_y+h}\right] \tag{4.84}$$

The velocity gradient is

$$\frac{du}{dy} = \frac{1}{h_r}\frac{du}{dr} = \frac{u_{max}}{nh_r(r_{max}-r_0)}(r-r_0)^{\frac{1-n}{n}} = [h_r(r_{max}-r_0)f(u)]^{-1} \tag{4.85}$$

For calculating the longitudinal velocity at a given point (y, z) in the cross section, six parameters (c_i, c_y, b_i, h, r_0, and k) (see Chapter 3) are needed. According to Chiu and Chiou (1986), these parameters can be estimated using equations (3.56) through (3.61) of Chapter 3 without measured data, given the geometric and flow parameters: flow discharge Q, flow cross-sectional area A, flow depth D, wetted perimeter P, mean shear velocity u^*, slope of the energy grade line S_f, fluid kinematic viscosity υ, and density ρ.

Example 4.17 Construct a plot of u/u_{max} as a function of $(r - r_0)/(r_m - r_0)$ for various values of n. Discuss the plot and its implications.

Solution A plot of u/u_{max} as a function of $(r - r_0)/(r_m - r_0)$ is constructed for various values of $1/n$, as shown in Fig. 4-23. The function is nonlinear but tends toward linearity for smaller values of n.

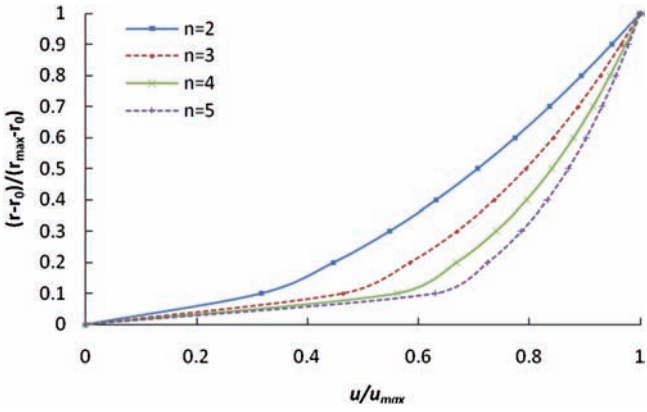

Figure 4-23 *A plot of* u/u_{max} *as a function of* $(r - r_0)/(r_m - r_0)$ *is constructed for various values of* n.

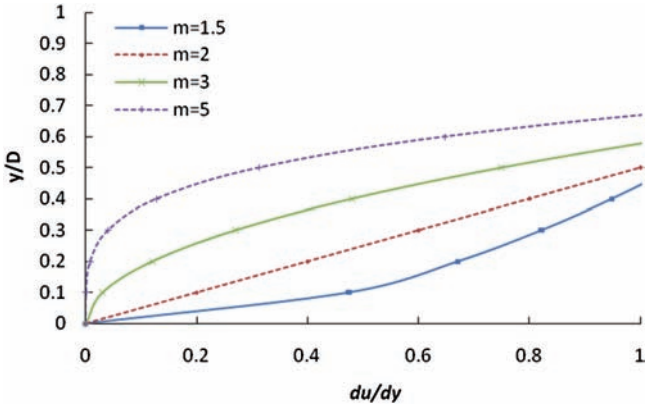

Figure 4-24 *Plot of* du/dy *as a function of* y/D *for various values of* m.

Example 4.18 Construct a plot of du/dy as a function of y/D for various values of n. Discuss the plot and its implications.

Solution Using equation (4.85), a plot of du/dy as a function of y/D for various values of m (1.5, 2.0, 3.0, and 5.0) is constructed, as shown in Fig. 4-24. The shape of the function changes from concave to convex as m increases.

Example 4.19 Plot $u_m/u_{\max}$ versus $(\overline{r} - r_0)/(r_m - r_0)$ for various values of n. Discuss the graph.

Solution Using equation (4.71), a plot of $u_m/u_{\max}$ versus $(\overline{r} - r_0)/(r_m - r_0)$ for various values of n (2.0, 3.0, 4.0, and 5.0) is constructed, as shown in Fig. 4-25. The shape of the function is convex. As n tends to a small value, the function tends to become linear.

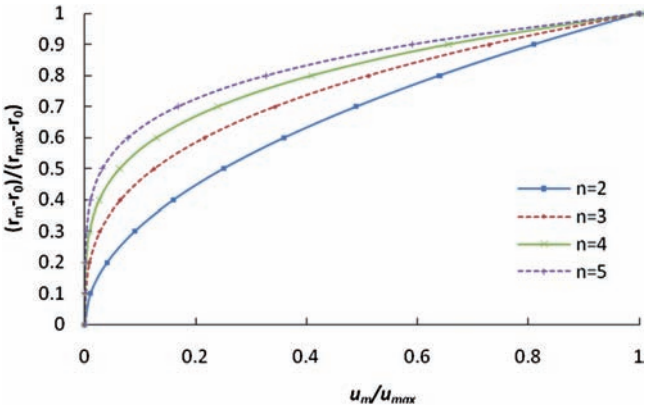

Figure 4-25 *A plot of* u_m/u_{max} *versus* $(\bar{r} - r_0) / (r_m - r_0)$ *for various values of* n.

Example 4.20 Plot patterns of isovels for various values of the B/D ratio and Manning's n. Consider z as 0 to 4 m to the right of the vertical divide. Take two sets of isovels. In the first set, construct four patterns:

- Take $u_{max} = 5\,m/s$, $h/D = -0.15$, $B/D = 1.0$, Manning's $n = 0.015$, and $u_m = 3.50\,m/s$.
- Take $u_{max} = 2\,m/s$, $h/D = 0.5$, $B/D = 10$, Manning's $n = 0.015$, and $u_m = 1.85\,m/s$.

In the second set, construct another set of graphs.

- Take $u_{max} = 2.85\,m/s$, $h/D = -0.01$, $B/D = 1.0$, Manning's $n = 0.03$, and $u_m = 2.50\,m/s$.
- Take $u_{max} = 2.15\,m/s$, $h/D = 0.00$, $B/D = 2.0$, Manning's $n = 0.03$, and $u_m = 1.85\,m/s$.
- Take $u_{max} = 1.75\,m/s$, $h/D = 0.20$, $B/D = 3.0$, Manning's $n = 0.03$, and $u_m = 1.70\,m/s$.
- Take $u_{max} = 1.15\,m/s$, $h/D = 2.20$, $B/D = 10$, Manning's $n = 0.03$, and $u_m = 0.90\,m/s$.

What do you conclude from these two sets of isovel patterns?

Solution Patterns of isovels for various values of the B/D ratio and Manning's n are constructed. These are shown in the following figures:

- Fig. 4-26 for $u_{max} = 5\,m/s$, $h/D = -0.15$, $B/D = 1.0$, Manning's $n = 0.015$, and $u_m = 3.50\,m/s$;
- Fig. 4-27 for $u_{max} = 2\,m/s$, $h/D = 0.5$, $B/D = 10$, Manning's $n = 0.015$, and $u_m = 1.85\,m/s$;
- Fig. 4-28 for $u_{max} = 2.85\,m/s$, $h/D = -0.01$, $B/D = 1.0$, Manning's $n = 0.03$, and $u_m = 2.50\,m/s$;
- Fig. 4-29 for $u_{max} = 2.15\,m/s$, $h/D = -0.00$, $B/D = 2.0$, Manning's $n = 0.03$, and $u_m = 1.85\,m/s$

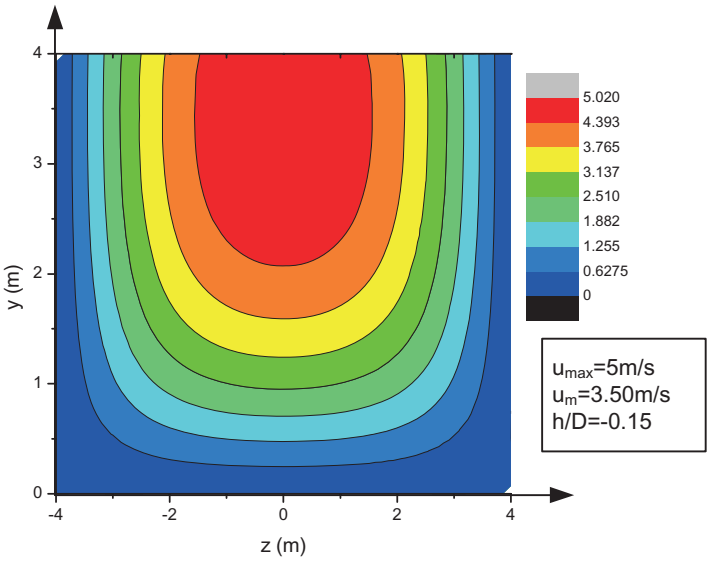

Figure 4-26 *Isovels for* $u_{max} = 5$ *m/s,* h/D = *–0.15,* B/D = *1.0, Manning's* n = *0.015, and* $u_m = 3.50$ *m/s.*

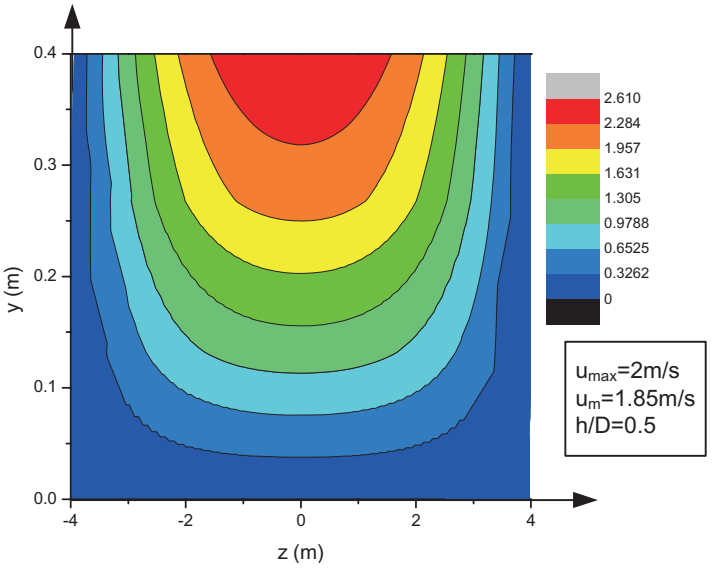

Figure 4-27 *Isovels for* $u_{max} = 2$ *m/s,* h/D = *0.5,* B/D = *10, Manning's* n = *0.015, and* $u_m = 1.85$ *m/s.*

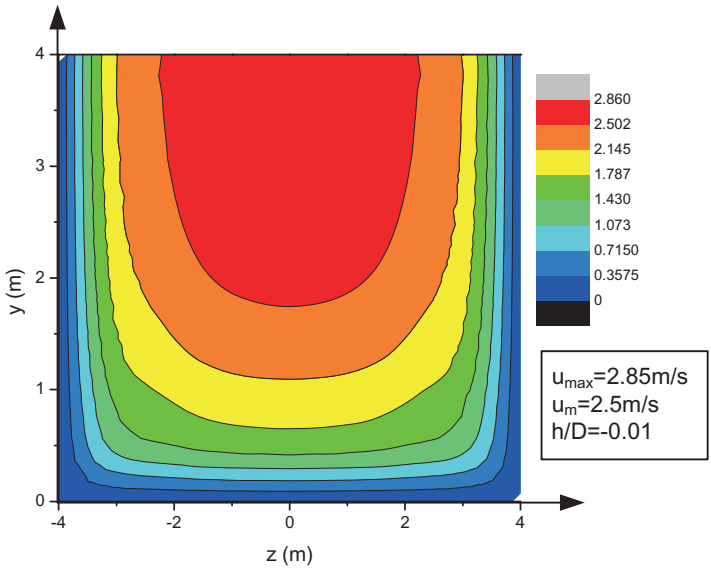

Figure 4-28 *Isovels for* $u_{max} = 2.85\,m/s$, $h/D = -0.01$, $B/D = 1.0$, *Manning's* $n = 0.03$, *and* $u_m = 2.50\,m/s$.

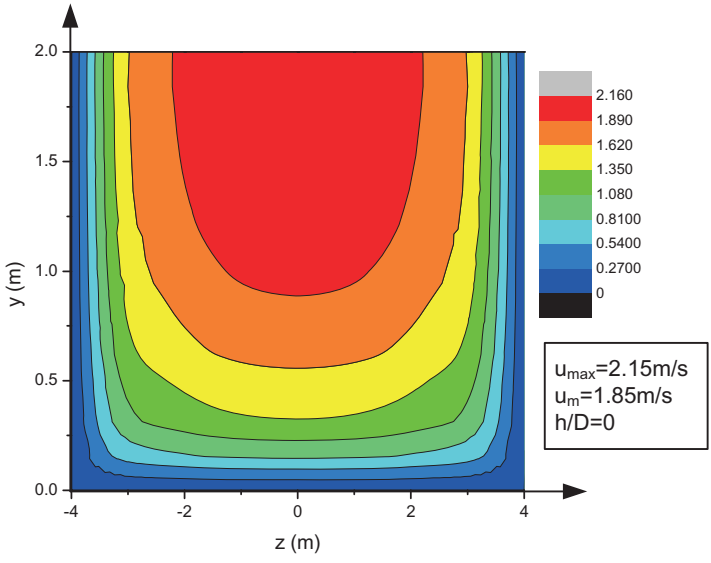

Figure 4-29 *Isovels for* $u_{max} = 2.15\,m/s$, $h/D = -0.00$, $B/D = 2.0$, *Manning's* $n = 0.03$, *and* $u_m = 1.85\,m/s$.

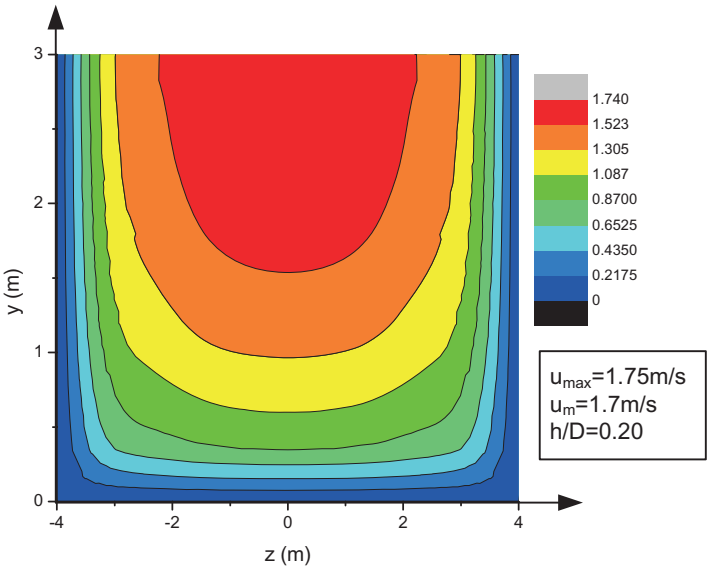

Figure 4-30 *Isovels with* $u_{max} = 1.75\,m/s$, h/D = *0.20*, B/D = *3.0*, *Manning's* n = *0.03*, *and* $u_m = 1.70\,m/s$.

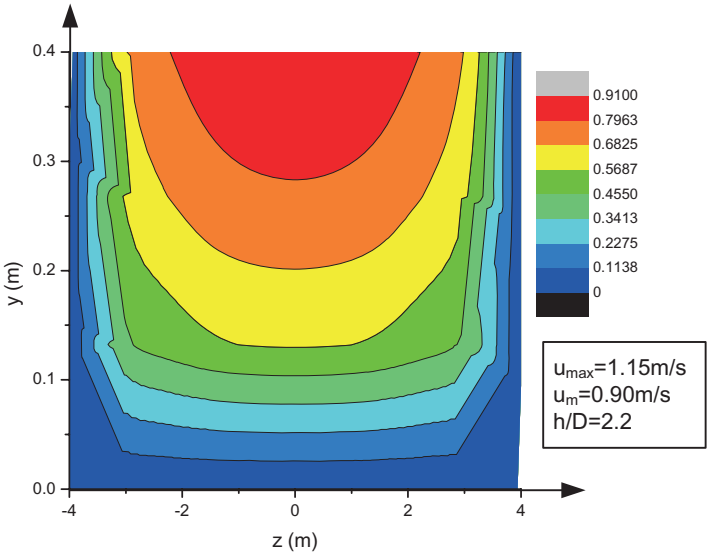

Figure 4-31 *Isovels with* $u_{max} = 1.15\,m/s$, h/D = *2.20*, B/D = *10*, *Manning's* n = *0.03*, *and* $u_m = 0.90\,m/s$.

- Fig. 4-30 for $u_{max} = 1.75\,m/s$, $h/D = 0.20$, $B/D = 3.0$, Manning's $n = 0.03$, and $u_m = 1.70\,m/s$; and
- Fig. 4-31 for $u_{max} = 1.15\,m/s$, $h/D = 2.20$, $B/D = 10$, Manning's $n = 0.03$, and $u_m = 0.90\,m/s$.

It is clear that the isovel pattern is significantly affected by the changes in these parameters, as shown by Figs. 4-26–4-31.

4.5 Two-Dimensional Prandtl–von Karman Velocity Distribution

Following the same procedure as in the previous section, the two-dimensional universal velocity distribution can be derived.

4.5.1 Specification of Constraints

The constraints for the two-dimensional case are expressed by equation (4.59) and

$$\int_0^{u_{\max}} uf(u)du = u_m \tag{4.86}$$

where the maximum velocity $u_{\max}$ may no longer occur at $y = D$ (flow depth) or water surface.

4.5.2 Determination of Lagrange Multipliers

In this case, the entropy-based PDF and CDF of velocity are the same as in the 1-D case. Substitution of equation (4.29) in equation (4.4) and integrating over $u^* \le u \le u_{\max}$, where u^* is shear velocity, one obtains

$$\exp(-\lambda_0) = \frac{\lambda_1}{\exp(-\lambda_1 u^*) - \exp(-\lambda_1 u_{\max})} \tag{4.87}$$

Equation (4.87) can be written as

$$\lambda_0 = \ln[\exp(-\lambda_1 u^*) - \exp(-\lambda_1 u_{\max})] - \ln\lambda_1 \tag{4.88}$$

Differentiating equation (4.88) with respect to λ_1, one obtains

$$\frac{\partial\lambda_0}{\partial\lambda_1} = \frac{\exp(-\lambda_1 u_{\max}) - u^*\exp(-\lambda_1 u^*)}{\exp(-\lambda_1 u^*) - \exp(-\lambda_1 u_{\max})} - \frac{1}{\lambda_1} \tag{4.89}$$

Conversely, substitution of equation (4.29) in equation (4.4) yields

$$\lambda_0 = \ln\left[\int_0^{u_{\max}} \exp(-\lambda_1 u)\right]du \tag{4.90}$$

Differentiating equation (4.90) with respect to λ_1, one obtains

$$\frac{\partial\lambda_0}{\partial\lambda_1} = -\frac{\int_0^{u_{\max}} u\exp(-\lambda_1 u_{\max})du}{\int_0^{u_{\max}} \exp(-\lambda_1 u)du} \tag{4.91}$$

Multiplying and dividing equation (4.91) by $\exp(-\lambda_0)$ and recalling equation (4.86), the result is

$$\frac{\partial \lambda_0}{\partial \lambda_1} = -\frac{\int_0^{u_{\max}} u \exp(-\lambda_0 - \lambda_1 u_D) du}{\int_0^{u_{\max}} \exp(-\lambda_0 - \lambda_1 u) du} = -u_m \tag{4.92}$$

Equating equation (4.91) to equation (4.92), one obtains

$$u_m = \frac{1}{\lambda_1} - \frac{u_{\max} \exp(-\lambda_1 u_{\max}) - u^* \exp(-\lambda_1 u^*)}{\exp(-\lambda_1 u^*) - \exp(-\lambda_1 u_{\max})} \tag{4.93}$$

Equation (4.93) expresses λ_1 implicitly in terms of u_m. It can also be derived as follows.

Substituting equation (4.29) in equation (4.5) and using equation (4.88), one obtains

$$\frac{\lambda_1}{b}\left[-u_{\max} \exp(-\lambda_1 u_{\max} + u^* \exp(-\lambda_1 u^*) - \frac{\exp(-\lambda_1 u_{\max})}{\lambda_1} + \frac{\exp(-\lambda_1 u^*)}{\lambda_1}\right] = u_m \tag{4.94a}$$

where b is defined as

$$b = \exp(-\lambda_1 u^*) - \exp(-\lambda_1 u_{\max}) \tag{4.94b}$$

Equation (4.94a) is the same as equation (4.93). Equations (4.88) and (4.93) can be used to determine the Lagrange parameters λ_0 and λ_1.

The shear velocity is defined as $u^* = \sqrt{gDS}$, where g is acceleration caused by gravity, and S is the channel slope. When we combine equations (4.31) and (4.29), the result is the probability density function (PDF) of velocity u as

$$f(u) = \frac{\lambda_1}{\exp(-\lambda_1 u^*) - \exp(-\lambda_1 u_{\max})} \exp(-\lambda_1 u) = \frac{\lambda_1}{b} \exp(-\lambda_1 u) \tag{4.95}$$

and then the cumulative PDF can be expressed as

$$F(u) = \frac{\lambda_1}{\exp(-\lambda_1 u^*) - \exp(-\lambda_1 u_{\max})} [\exp(-\lambda_1 u^*) - \exp(-\lambda_1 u)] \tag{4.96}$$

Equation (4.95) shows that the PDF of the Prandtl–von Karman universal velocity distribution is negative exponential with parameter λ_1, determined as shown.

It may be noted that if u^* is taken as a small quantity tending to 0, then equation (4.95) simplifies to

$$f(u) = \frac{\lambda_1 \exp(-\lambda_1 u)}{1 - \exp(-\lambda_1 u_{\max})} = \frac{k \exp(ku / u^*)}{u^*[\exp(k u_{\max} / u^*) - 1]} \tag{4.97}$$

and the cumulative PDF equation (4.96) to

$$F(u) = \frac{\exp(ku / u^*) - 1}{[\exp(ku_{\max} / u^*) - 1]} \tag{4.98}$$

where $\lambda_1 = -k/u^*$, in which k is the von Karman constant.

Equation (4.95) can be written in terms of k and u^* as

$$f(u) = \frac{k \exp(-ku / u^*)}{u^*[\exp(k) - \exp(-ku_{\max} / u^*)]} \tag{4.99}$$

4.5.3 Entropy of Velocity Distribution

Entropy of the Prandtl–von Karman velocity distribution can be obtained by inserting equation (4.99) in equation (4.3) as

$$H = -\ln[\exp(k) - \exp(-ku_{\max} / u^*)] + \frac{k}{u^*}\overline{u} - \ln\left(\frac{k}{u^*}\right) \tag{4.100}$$

Equation (4.100) shows that the uncertainty of the velocity distribution is heavily influenced by the average velocity and the shear velocity. This result means that velocity should be sampled more frequently along the vertical where the average velocity is high.

4.5.4 Velocity Distribution

Substitution of equation (4.95) in equation (4.2) and then integration with the condition that $u = u^*$ when $r = r_0$ yields the relation between velocity and depth:

$$\frac{1}{b}[\exp(-\lambda_1 u^*) - \exp(-\lambda_1 u) = \frac{r - r_0}{r_{\max} - r_0} \tag{4.101}$$

Here, r_0 represents the depth of shear flow or height corresponding to shear velocity. Equation (4.101) becomes

$$u = \frac{u^*}{k}\ln\left[\exp(k) - b\frac{r - r_0}{r_{\max} - r_0}\right] \tag{4.102}$$

Clearly, equation (4.102) is similar to but not the same as the Prandtl–von Karman universal velocity distribution. However, a little algebraic simplification can lead to the same velocity distribution.

Assuming that the exponential term $[\exp(k)]$ is much smaller than $\exp(ku_{\max}/u^*)$ and, hence, can be neglected, equation (4.94b) can be approximated as

$$b \approx \exp(ku_{\max} / u^*) \tag{4.103}$$

Equation (4.102) then becomes

$$u = \frac{u^*}{k}\ln\left[\exp(k) + \exp(ku_{\max}/u^*)\frac{r - r_0}{r_{\max} - r_0}\right] \tag{4.104}$$

which can be approximated as

$$u = \frac{u^*}{k}\ln\left[\exp(ku_{\max}/u^*)\frac{r - r_0}{r_{\max} - r_0}\right] \tag{4.105a}$$

If $M = ku_{\max}/u^*$, equation (4.105a) can be written as

$$\frac{u}{u_{\max}} = \frac{1}{M}\ln\left[\exp(M)\frac{r - r_0}{r_{\max} - r_0}\right] \tag{4.105b}$$

Equation (4.105a) is based on the assumption that $\exp(ku_{\max}/u^*) >> \exp(k)$, which is quite reasonable. If it is assumed that

$$r_0 \exp(ku_{\max}/u^*) \approx r_{\max} \tag{4.106}$$

then equation (4.105a) reduces to

$$u = \frac{u^*}{k}\ln\left(\frac{r}{r_0}\right) \tag{4.107}$$

which is the 2-D Prandtl–von Karman universal velocity distribution in the r, s coordinates.

Taking the derivative of equation (4.107), the velocity gradient can be expressed as

$$\frac{du}{dr} = \frac{u^*}{k}\left[\frac{1}{r} - \ln(r_0)\right] \tag{4.108}$$

4.5.5 Construction of Isovels and Relation between (y, z) Coordinates and (r, s) Coordinates

The discussion in Chapter 3 provides the relations between the (y, z) and (r, s) coordinate systems (equations [3.56] through [3.61]), and along the y-axis where $z = 0$, it shows a relation between r and y (equation (3.76)):

$$r = \frac{y}{D + h}\exp\left[1 - \frac{y}{D + h}\right] \tag{4.109}$$

When $y = 0$, $r = 0$, and when $y = D$, $r = r_{\max}$. When $h < 0$, the value of h represents the actual depth of the point below the water surface, and then r increases with y from $y = 0$ to $y = D + h$, where the maximum velocity occurs at $r = r_{\max} = 1$ and decreases from $D + h$ to D (water surface). Differentiation of equation (4.109) yields

$$dr = \frac{1}{D + h}\left[1 - \frac{y}{D}\right]\exp\left[1 - \frac{y}{D + h}\right]dy \tag{4.110}$$

which can be simply written as

$$h_r dr = dy \tag{4.111}$$

where

$$h_r = (D+h)\left\{\left[1-\frac{y}{D}\right]\exp\left[1-\frac{y}{D+h}\right]\right\}^{-1} \tag{4.112}$$

Coefficient h_r is a scale factor required for coordinate transformation between y and r systems. This factor allows h_r and dr to have the same length dimension as dy.

The isovel for null velocity along r_0 can be expressed as

$$r_0 = \frac{c_y}{D+c_y+h}\exp\left[1-\frac{c_y}{D+c_y+h}\right] \tag{4.113}$$

The velocity gradient is

$$\frac{du}{dy} = \frac{1}{h_r}\frac{du}{dr} = \frac{u_{\max}}{nh_r(r_{\max}-r_0)}(r-r_0)^{\frac{1-n}{n}} = [h_r(r_{\max}-r_0)f(u)]^{-1} \tag{4.114}$$

For calculating the longitudinal velocity at a given point (y, z) in the cross section, six parameters (c_i, c_y, b_i, h, r_0, and k) (see Chapter 3) are needed. According to Chiu and Chiou (1986), these parameters can be estimated using equations (3.56) through (3.61) without measured data, given the geometric and flow parameters: flow discharge Q, flow cross-sectional area A, flow depth D, wetted perimeter P, mean shear velocity u^*, slope of the energy grade line S_f, fluid kinematic viscosity υ, and density ρ.

Example 4.21 Construct a plot of λ_0 as a function of λ_1 for various values of $u_{\max}$. Discuss the plot and its implications.

Solution Using equation (4.88), a plot of λ_0 as a function of λ_1 is constructed for various values of $u_{\max}$, as shown in Fig. 4-32. Depending on the values of λ_1 and $u_{\max}$, the value of λ_0 goes from positive to negative.

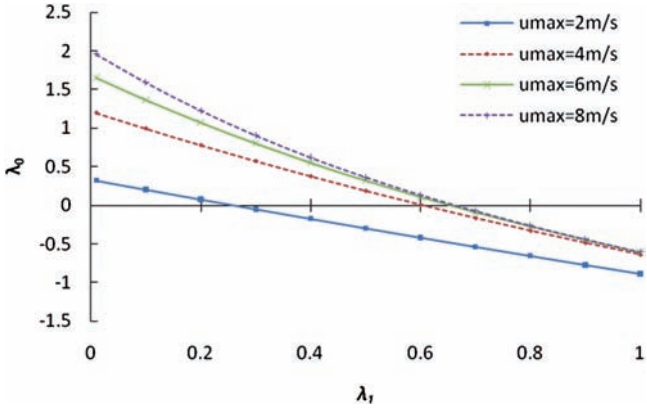

Figure 4-32 *Plot of λ_0 as a function of λ_1 is constructed for various values of u_{max} (m/s).*

Example 4.22 Construct a plot of λ_1 as a function of u_m for various values of u_{max}. Discuss the plot and its implications.

Solution A plot of λ_1 as a function of u_m for various values of u_{max} is constructed, as shown in Fig. 4-33. The graph shows that for a given value of u_{max}, λ_1 increases gradually with increasing u_m, reaches a value, and then increases sharply with decreasing u_m.

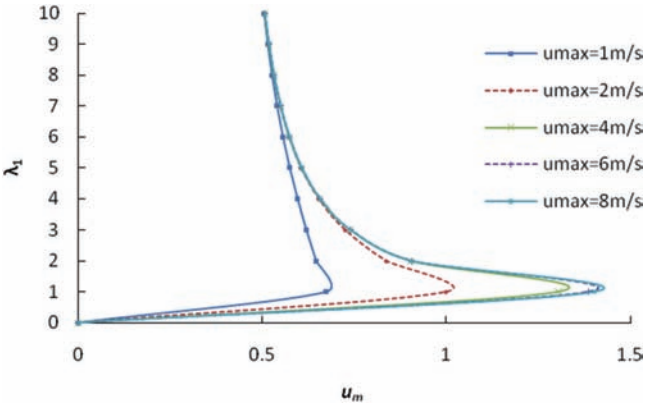

Figure 4-33 *Plot of* λ_1 *as a function of* u_m *for various values of* u_{max} *(m/s).*

Example 4.23 Construct a plot of u/u_{max} as a function of $(r - r_0)/(r_m - r_0)$ for various values of M. Discuss the plot and its implications.

Solution Recall that $\frac{u}{u_{max}} = \frac{1}{M}\ln\left[\exp(M)\frac{r - r_0}{r_{max} - r_0}\right]$. Then, a plot of u/u_{max} as a function of $(r - r_0)/(r_m - r_0)$ is constructed for various values of M, as shown in Fig. 4-34. The plot shows that for a given value of u/u_{max}, $(r - r_0)/(r_m - r_0)$ increases with decreasing value of M. For a given value of M, u/u_{max} increases with increasing $(r - r_0)/(r_m - r_0)$.

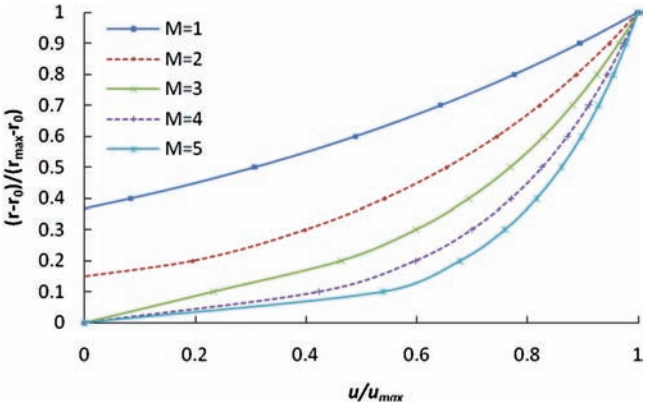

Figure 4-34 *Plot of* u/u_{max} *as a function of* $(r - r_0)/(r_m - r_0)$ *constructed for various values of* M.

Example 4.24 Construct a plot of du/dy as a function of y/D for various values of M.

Solution Using equation (4.114), a plot of du/dy as a function of y/D is constructed for various values of M, as shown in Fig. 4-35.

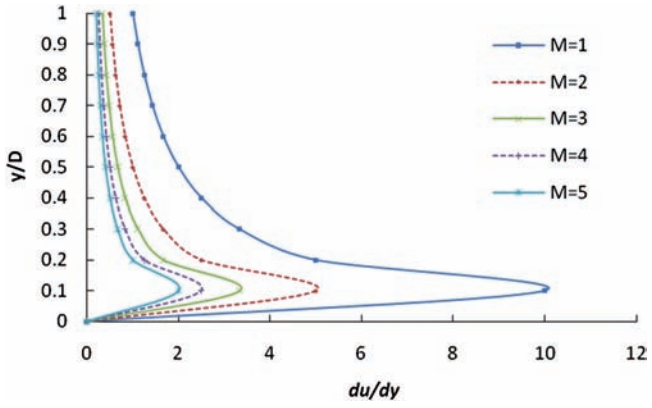

Figure 4-35 *Plot of* du/dy *as a function of* y/D *is constructed for various values of* M.

Example 4.25 Plot $u_m/u_{\max}$ versus $(\overline{r}-r_0)/(r_m-r_0)$ for various values of parameter M.

Solution Recall that $\dfrac{u_m}{u_{\max}}=\dfrac{1}{M}\ln\left[\exp(M)\dfrac{\overline{r}-r_0}{r_{\max}-r_0}\right]$. Plot of $u_m/u_{\max}$ versus $(\overline{r}-r_0)/(r_m-r_0)$ is constructed for various values of parameter M, as shown in Fig. 4-36.

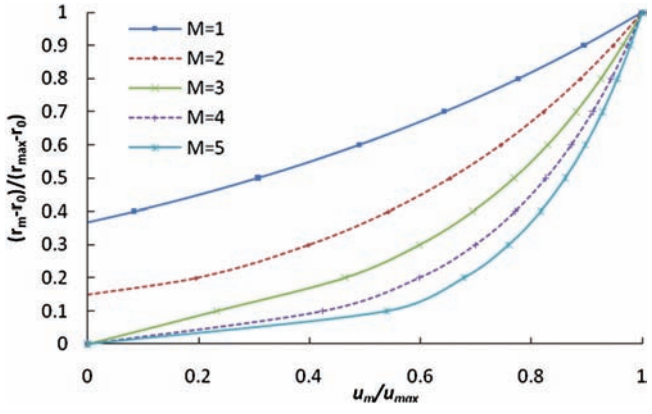

Figure 4-36 *Plot* u_m/u_{max} *versus* $(\overline{r}-r_0)/(r_m-r_0)$ *constructed for various values of parameter* M.

Example 4.26 Plot patterns of isovels for M, B/D ratio, and Manning's n. Consider z as 0 to 4 m to the right of the vertical divide. Take two sets of isovels. In the first set, construct two graphs of isovel patterns.

- Take $u_{max} = 5\,m/s$, $h/D = -0.15$, $B/D = 1.0$, Manning's $n = 0.015$, $M = 11.25$, and $u_m = 3.50\,m/s$.
- Take $u_{max} = 2\,m/s$, $h/D = 0.5$, $B/D = 10$, Manning's $n = 0.015$, $M = 9$, and $u_m = 1.85\,m/s$.

In the second set, construct another set of four graphs.

- Take $u_{max} = 2.85\,m/s$, $h/D = -0.01$, $B/D = 1.0$, Manning's $n = 0.03$, $M = 6.0$, and $u_m = 2.50\,m/s$.
- Take $u_{max} = 2.15\,m/s$, $h/D = 0.00$, $B/D = 2.0$, Manning's $n = 0.03$, $M = 5.85$, and $u_m = 1.85\,m/s$.
- Take $u_{max} = 1.75\,m/s$, $h/D = 0.20$, $B/D = 3.0$, Manning's $n = 0.03$, $M = 8.75$, and $u_m = 1.70\,m/s$.
- Take $u_{max} = 1.15\,m/s$, $h/D = 2.20$, $B/D = 10$, Manning's $n = 0.03$, $M = 7.25$, and $u_m = 0.90\,m/s$.

What do you conclude from these two sets of isovel patterns?

Solution Patterns of isovels are constructed for two data sets that have different values of M, B/D ratio, and Manning's n and z as 0 to 4 m to the right of the vertical divide. Isovels are shown in these figures:

- Fig. 4-37 for $u_{max} = 5\,m/s$, $h/D = -0.15$, $B/D = 1.0$, Manning's $n = 0.015$, $M = 11.25$, and $u_m = 3.50\,m/s$;

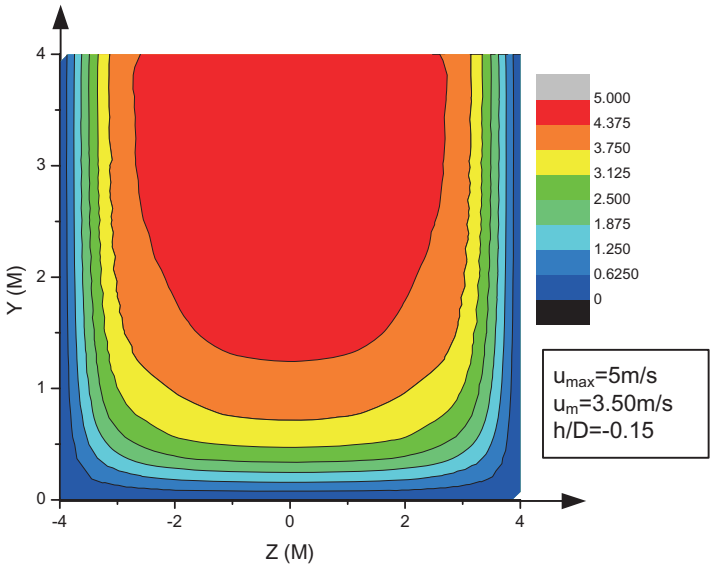

Figure 4-37 *Isovels for* $u_{max} = 5\,m/s$, $h/D = -0.15$, $B/D = 1.0$, *Manning's* $n = 0.015$, $M = 11.25$, *and* $u_m = 3.50\,m/s$.

- Fig. 4-38 for $u_{max} = 2\,m/s$, $h/D = 0.5$, $B/D = 10$, Manning's $n = 0.015$, $M = 9$, and $u_m = 1.85\,m/s$;
- Fig. 4-39 for $u_{max} = 2.85\,m/s$, $h/D = -0.01$, $B/D = 1.0$, Manning's $n = 0.03$, $M = 6.0$, and $u_m = 2.50\,m/s$;

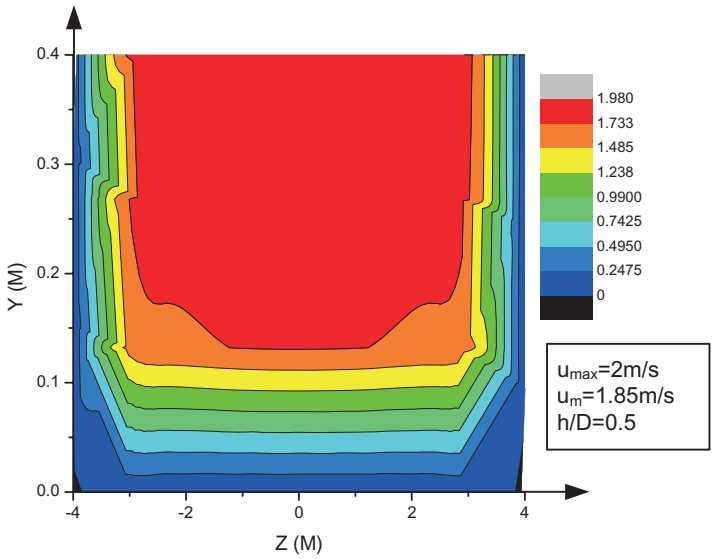

Figure 4-38 *Isovels for* $u_{max} = 2\,m/s$, $h/D = 0.5$, $B/D = 10$, *Manning's* $n = 0.015$, $M = 9$, *and* $u_m = 1.85\,m/s$.

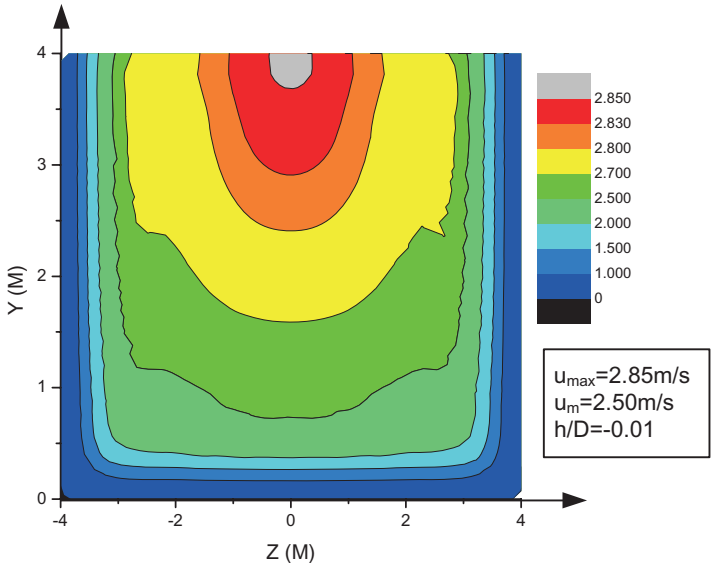

Figure 4-39 *Isovels for* $u_{max} = 2.85\,m/s$, $h/D = -0.01$, $B/D = 1.0$, *Manning's* $n = 0.03$, $M = 6.0$, *and* $u_m = 2.50\,m/s$.

- Fig. 4-40 for $u_{max} = 2.15\,m/s$, $h/D = -0.00$, $B/D = 2.0$, Manning's $n = 0.03$, $M = 5.85$, and $u_m = 1.85\,m/s$;
- Fig. 4-41 for $u_{max} = 1.75\,m/s$, $h/D = 0.20$, $B/D = 3.0$, Manning's $n = 0.03$, $M = 8.75$, and $u_m = 1.70\,m/s$; and

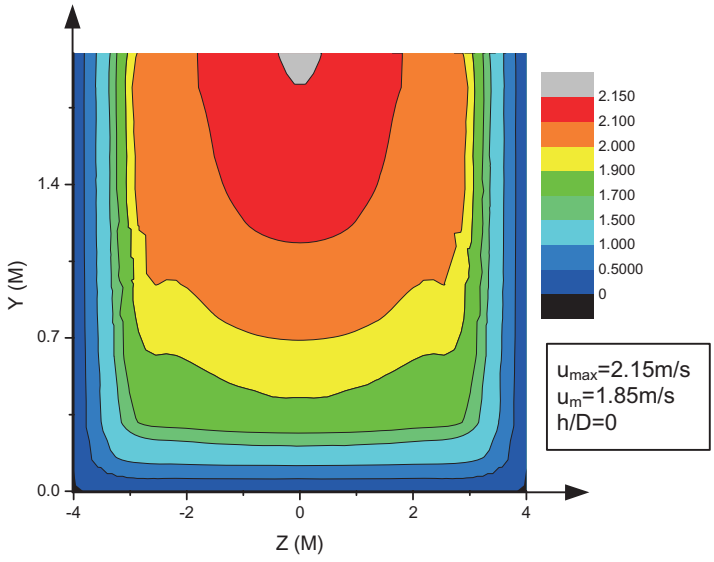

Figure 4-40 *Isovels for* $u_{max} = 2.15\,m/s$, $h/D = -0.00$, $B/D = 2.0$, *Manning's* $n = 0.03$, $M = 5.85$, *and* $u_m = 1.85\,m/s$.

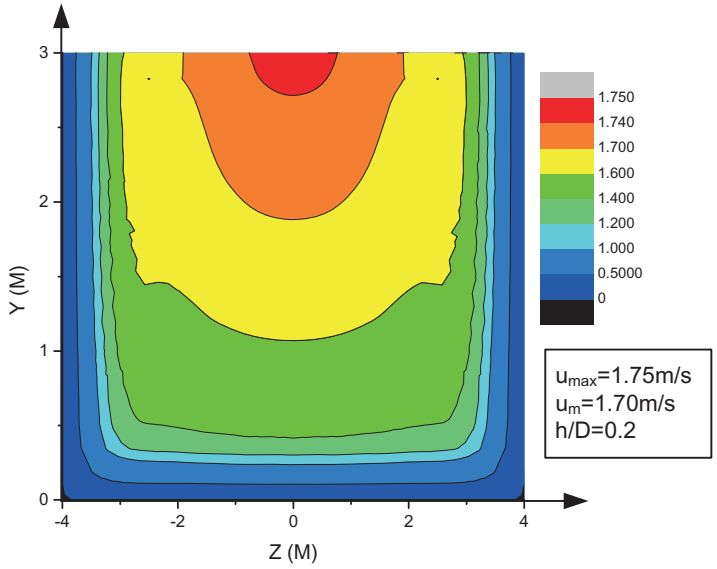

Figure 4-41 *Isovels for* $u_{max} = 1.75\,m/s$, $h/D = 0.20$, $B/D = 3.0$, *Manning's* $n = 0.03$, $M = 8.75$, *and* $u_m = 1.70\,m/s$.

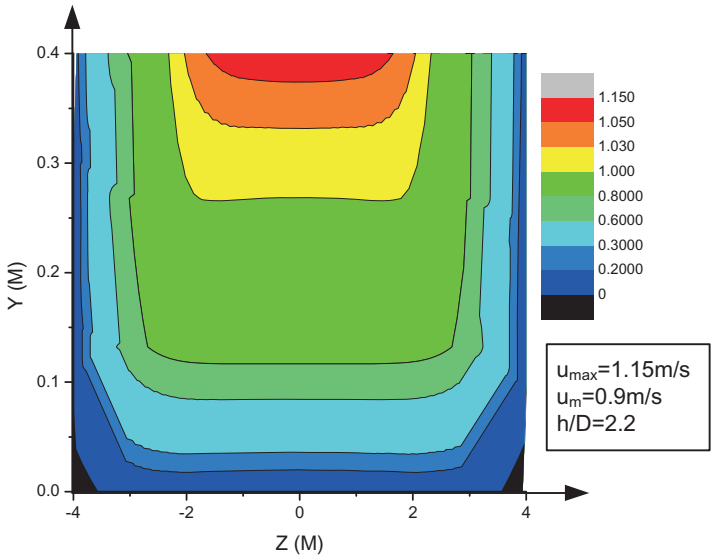

Figure 4-42 *Isovels for* $u_{max} = 1.15\,m/s$, $h/D = 2.20$, $B/D = 10$, *Manning's* $n = 0.03$, $M = 7.25$, *and* $u_m = 0.90\,m/s$.

- Fig. 4-42 for $u_{max} = 1.15\,m/s$, $h/D = 2.20$, $B/D = 10$, Manning's $n = 0.03$, $M = 7.25$, and $u_m = 0.90\,m/s$.

The isovel patterns vary with changes in these parameters.

Example 4.27 Plot y/D versus u/u_{max} for various values of parameter M, $M = 0$, 2, 4, 6, 8, 10, and 12. What do you conclude from this plot?

Solution Using equation (4.10), a plot of y/D versus u/u_{max} is constructed for various values of parameter M, as shown in Fig. 4-43.

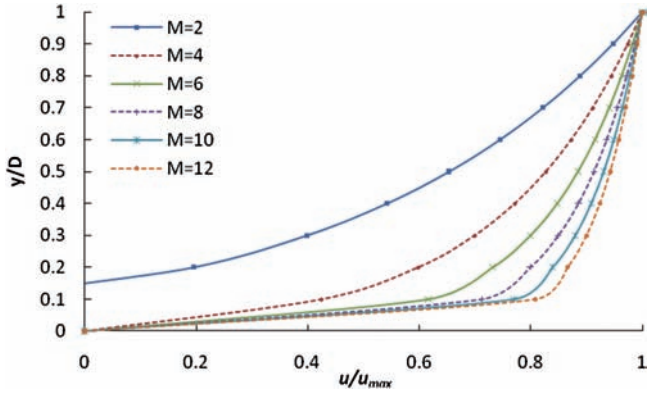

Figure 4-43 *Plot* y/D *versus* u/u_{max} *for various values of parameter* M.

4.6 Two-Dimensional Representation of Velocity Using a General Framework

In Chapter 3, a general framework is presented for describing the entropy-based velocity distribution in two dimensions. However, in that framework any velocity distribution can be used. The framework involves (1) specification of the geometric domain, (2) specification of the CDF of velocity in two dimensions, and (3) derivation of the velocity in two dimensions. The geometric domain can be arbitrary, including rectangular and trapezoidal as special cases. The methodology is now illustrated for the power law velocity distribution and universal velocity distribution using the rectangular geometric domain.

4.6.1 Power Law Velocity Distribution in Two Dimensions

Singh et al. (2013) derived 2-D power law velocity distribution, and their work is followed here. The procedure is the same as already discussed, and the 2-D domain (x, y), with x denoting the transverse direction and y the vertical direction measured from the bed, upward positive, is considered. To derive the 2-D velocity distribution, let $u = u(x, y)$ be the velocity distribution, $f[u(x, y)]$ the PDF, and $F[u(x, y)]$ the CDF. It is convenient to assume $v = \ln(u)$ (i.e., $u = \exp(v)$). Following the methodology developed by Marini et al. (2011) and taking the partial derivatives of $F(u)$ with respect to x and y, we obtain

$$\frac{\partial F(u)}{\partial x} = \frac{\partial F\left(e^v\right)}{\partial x} = \frac{\mathrm{d}F\left(e^v\right)}{\mathrm{d}e^v}\frac{\mathrm{d}\left(e^v\right)}{\mathrm{d}v}\frac{\partial v}{\partial x} = f\left(e^v\right)e^v\frac{\partial v}{\partial x} \tag{4.115a}$$

$$\frac{\partial F(u)}{\partial y} = \frac{\partial F\left(e^v\right)}{\partial y} = \frac{\mathrm{d}F\left(e^v\right)}{\mathrm{d}e^v}\frac{\mathrm{d}\left(e^v\right)}{\mathrm{d}v}\frac{\partial v}{\partial y} = f\left(e^v\right)e^v\frac{\partial v}{\partial y} \tag{4.115b}$$

Using equations (4.115a) and (4.115b), we can rewrite equations (4.8) as

$$\frac{\partial F(u)}{\partial x} = \exp(-\lambda_0 - \lambda_1 v)e^v\frac{\partial v}{\partial x} = \exp[-\lambda_0 - (\lambda_1 - 1)v]\frac{\partial v}{\partial x} \tag{4.116a}$$

$$\frac{\partial F(u)}{\partial y} = \exp(-\lambda_0 - \lambda_1 v)e^v\frac{\partial v}{\partial y} = \exp[-\lambda_0 - (\lambda_1 - 1)v]\frac{\partial v}{\partial y} \tag{4.116b}$$

Denoting $-\lambda_1 + 1 = n$, we can rewrite equations (4.116a) and (4.116b) as

$$\frac{\partial F(u)}{\partial x}\exp(\lambda_0) = \exp(nv)\frac{\partial v}{\partial x} \tag{4.117a}$$

$$\frac{\partial F(u)}{\partial y}\exp(\lambda_0) = \exp(nv)\frac{\partial v}{\partial y} \tag{4.117b}$$

Denoting $\exp(nv) = w$, we can express the partial derivatives of w with respect to x and y as

$$\frac{\partial w}{\partial x} = n\exp(nv)\frac{\partial v}{\partial x} \tag{4.118a}$$

$$\frac{\partial w}{\partial y} = n\exp(nv)\frac{\partial v}{\partial y} \tag{4.118b}$$

Substitution of equations (4.118a) and (4.118b) into equations (4.117a) and (4.117b) yields the following system of equations:

$$\frac{\partial w}{\partial x} = n\exp(\lambda_0)\frac{\partial F(u)}{\partial x} \tag{4.119a}$$

$$\frac{\partial w}{\partial y} = n\exp(\lambda_0)\frac{\partial F(u)}{\partial y} \tag{4.119b}$$

Equations (4.119a) and (4.119b) can be integrated using the Leibniz rule:

$$\int_{0,0}^{(x,y)} \frac{\partial w}{\partial x}\mathrm{d}x + \frac{\partial w}{\partial y}\mathrm{d}y = w(x, y) - w(0, 0) \tag{4.120}$$

Because the point with coordinates (0, 0) lies on a contour in the solution domain; u at this point is equal to 0 and $v = \ln(u) = -\infty$. Consequently, the right-hand side of equation (4.120) becomes

$$w(x, y) - w(0, 0) = w(x, y) - e^{nv} = w(x, y) - e^{n\ln(u)} = w(x, y) + u^n = w(x, y) - 0 \tag{4.121}$$

With the use of equations (4.119a) and (4.119b), the definite integral on the left side of equation (4.120) is calculated at a generic point $(\bar{x}, \bar{y})$ identified by the mean of a polygonal curve that starts from (0, 0), passes across $(\bar{x}, 0)$ and ends at $(\bar{x}, \bar{y})$, so that

$$\int_{0,0}^{(\bar{x},\bar{y})} \frac{\partial F(u)}{\partial x} ne^{\lambda_0}\mathrm{d}x + \frac{\partial F(u)}{\partial y} ne^{\lambda_0}\mathrm{d}y = \int_0^{\bar{y}} \frac{\partial F(u)}{\partial y} ne^{\lambda_0}\mathrm{d}y = ne^{\lambda_0}F(u) \tag{4.122}$$

in which coordinates $(\bar{x}, \bar{y})$ represent a point in the solution domain. Equating the right-hand side of equation (4.122) to the right-hand side of equation (4.121), one obtains

$$w(x, y) = ne^{\lambda_0}F(u) \tag{4.123}$$

Because $w(x, y) = \exp(n\, v)$, equation (4.123) can be recast as

$$e^{nv} = ne^{\lambda_0}F[u(x, y)] \tag{4.124}$$

and recalling that $v = \ln(u)$, the expression for $u(x, y)$ is obtained as

$$u(x, y) = \left[ne^{\lambda_0} F(u(x, y))\right]^{1/n} \tag{4.125}$$

Equation (4.125) contains two Lagrange multipliers λ_0 and λ_1, which can be calculated using equations (4.5a) and (4.5b). Equation (4.13) shows that

$$u_{\max}^n = n \cdot e^{\lambda_0} \tag{4.126}$$

Therefore, combining equation (4.126) and (4.125), we see that the result is the 2-D velocity distribution:

$$u(x, y) = u_{\max} \cdot F^{1/n} \tag{4.127}$$

Equation (4.127) is the 2-D power law velocity distribution, which depends on $u_{\max}$, n, and the 2-D CDF. The derived equation formally coincides with the equation obtained by Singh (2011) for 1-D domain, although in this case F is a function of x and y.

Parameter n can be calculated by using the constraint given by equation (4.5a), which results in equation (4.16), which is derived by Singh (2011). In that case, the PDF is given by the power law equation (4.8). One can also use the approach proposed by Marini et al. (2011) for estimating n. In that case, n can be calculated from the definition of average channel velocity u_{av}:

$$u_{av} = \frac{1}{A}\int_A u dA = \frac{1}{A}\int_A u_{\max} F^{1/n} dA \tag{4.128}$$

where A is the channel cross section. As pointed out in the literature, equation (4.16) refers to the mean of the logarithmic velocity distribution, whereas equation (4.128) includes the average logarithmic velocity in the channel cross section. Unlike $\bar{u}$, the average channel velocity has a straightforward physical meaning, and, consequently, it can be more effective for calculating parameter n.

4.6.2 Comparison with Entropy-Based Logarithmic 2-D Velocity Distribution

Equation (4.127) represents an effective way to estimate velocity distribution in a generic 2-D domain if the CDF is properly defined. Starting from the same hypothesis but using a different constraint equation than equation (5b), Marini et al. (2011) obtained the following equation (logarithmic model) (given by equation (3.149) in Chapter 3):

$$u(x, y) = \frac{u_{\max}}{G}\ln\left[1 + F\left(e^G - 1\right)\right] \tag{4.129}$$

Similar to equation (4.129), equation (4.127) depends only on $u_{\max}$, an entropic parameter (here called G), and the 2-D CDF. Parameter G can be calculated using

the following equation, depending on the mean of velocity distribution and the maximum velocity (Chiu 1987):

$$\frac{\bar{u}}{u_{\max}} = \frac{\exp(G)}{\exp(G)-1} - \frac{1}{G} \tag{4.130}$$

or considering again the definition of average channel velocity (as given by equation (3.150) in Chapter 3). For both equations (4.128) and (3.150), 1-D and 2-D domains can be considered, depending on the assumed CDF.

Singh et al. (2013) analyzed both 1-D and 2-D velocity distributions for different configurations and compared them for a data set. They found that the velocity profiles obtained from the power law velocity distribution and the entropy-based logarithmic law velocity distribution were almost the same.

4.6.3 Universal Velocity Distribution in Two Dimensions

The same procedure as already described for the power law velocity distribution is followed. Denoting a 2-D domain as (x, y), where x represents the transverse direction and y the vertical direction (measured from the bed-upward positive), one can write $u = u(x, y)$, and its PDF, $f(u)$, as $f(u(x, y))$ and cumulative probability distribution function [CDF ($F(u)$), as $F(u(x, y))$]. Then, partial differentiation of $F(u)$ with respect to x and y yields

$$\frac{\partial F(u)}{\partial x} = \frac{dF(u)}{du}\frac{\partial u}{\partial x} = f(u)\frac{\partial u}{\partial x} \tag{4.131a}$$

$$\frac{\partial F(u)}{\partial y} = \frac{dF(u)}{du}\frac{\partial u}{\partial y} = f(u)\frac{\partial u}{\partial y} \tag{4.131b}$$

Inserting equation (4.29), equations (4.131a) and (4.131b) can be rewritten as

$$\frac{\partial F(u)}{\partial x} = \frac{\mathrm{d}F(u)}{\mathrm{d}u}\frac{\partial u}{\partial x} = \exp(-\lambda_0 - \lambda_1 u)\frac{\partial u}{\partial x} \tag{4.132a}$$

$$\frac{\partial F(u)}{\partial y} = \frac{\mathrm{d}F(u)}{\mathrm{d}u}\frac{\partial u}{\partial y} = \exp(-\lambda_0 - \lambda_1 u)\frac{\partial u}{\partial y} \tag{4.132b}$$

Equations (4.132a) and (4.132b) can be recast as

$$\exp(-\lambda_1 u)\frac{\partial u}{\partial x} = \exp(\lambda_0)\frac{\partial F(u)}{\partial x} \tag{4.133a}$$

$$\exp(-\lambda_1 u)\frac{\partial u}{\partial y} = \exp(\lambda_0)\frac{\partial F(u)}{\partial y} \tag{4.133b}$$

It may be convenient to denote quantity $\exp(-\lambda_1 u)$ by w and then calculate the partial derivative of w with respect to x and y as follows:

$$\frac{\partial w}{\partial x} = \frac{\partial \exp(-\lambda_1 u)}{\partial x} = -\lambda_1 \exp(-\lambda_1 u)\frac{\partial u}{\partial x} \tag{4.134a}$$

$$\frac{\partial w}{\partial y} = \frac{\partial \exp(-\lambda_1 u)}{\partial y} = -\lambda_1 \exp(-\lambda_1 u)\frac{\partial u}{\partial y} \tag{4.134b}$$

Substitution of equations (4.133a) and (4.133b) into equations (4.134a) and (4.134b) results in the following system of equations:

$$\frac{\partial w}{\partial x} = -\exp(\lambda_0)\lambda_1 \frac{\partial F(u)}{\partial x} \tag{4.135a}$$

$$\frac{\partial w}{\partial y} = -\exp(\lambda_0)\lambda_1 \frac{\partial F(u)}{\partial y} \tag{4.135b}$$

Equations (4.135a) and (4.135b) can be integrated using the theory of differential forms that states

$$\int_{0,0}^{(x,y)} \frac{\partial w}{\partial x}\mathrm{d}x + \frac{\partial w}{\partial y}\mathrm{d}y = w(x, y) - w(0, 0) \tag{4.136}$$

The point with coordinates (0, 0) lies on the solution domain's contour; therefore, u at this point is equal to 0; and the right side of equation (4.136) becomes

$$w(x, y) - w(0, 0) = w(x, y) - \exp(-\lambda_1 u) = w(x, y) - \exp(0) = w(x, y) - 1 \tag{4.137}$$

Consider a generic point with coordinates $(\bar{x}, \bar{y})$, which can be identified by means of a polygonal curve starting from the origin of axes (0, 0), passing across the point $(\bar{x}, 0)$ and ending at $(\bar{x}, \bar{y})$ (see Fig. 3-28). At this point, the definite integral of the first part of equation (4.136) can be calculated as

$$\begin{aligned}\int_{0,0}^{(\bar{x},\bar{y})} -\frac{\partial F(u)}{\partial y}\lambda_1 \exp(\lambda_0)\mathrm{d}y - \frac{\partial F(u)}{\partial x}\lambda_1 \exp(\lambda_0)\mathrm{d}x \\ = -\int_0^{\bar{y}} \frac{\partial F(u)}{\partial y}\lambda_1 \exp(\lambda_0)\mathrm{d}y = -\lambda_1 \exp(\lambda_0)F(u)\end{aligned} \tag{4.138}$$

Equating the right side of equation (4.138) to the right side of equation (4.137), one obtains the expression of $w(x, y)$ as

$$w(x, y) = 1 - \lambda_1 \exp(\lambda_0)F(u) \tag{4.139}$$

Recalling that $w(x, y)$ is equal to $\exp(-\lambda_1 u)$, equation (4.139) can be rewritten as

$$\exp[-\lambda_1 u(x, y)] = 1 - \lambda_1 \exp(\lambda_0)F(u(x, y)) \tag{4.140}$$

Hence, the expression of $u(x, y)$ can be obtained as

$$u(x,y) = -\frac{1}{\lambda_1}\ln\left[1-\lambda_1 \exp(\lambda_0)F(u(x,y))\right] \tag{4.141}$$

Integration of constraint equation (4.4) yields

$$\int_0^{u_{max}} \exp(-\lambda_0 - \lambda_1 u)\,du = 1 \quad \Rightarrow \quad \lambda_1 \exp(\lambda_0) = 1 - \exp(-\lambda_1 u_{max}) \tag{4.142}$$

Denoting $\lambda_1 u_{max}$ by G and inserting equation (4.142), equation (4.141) can be rewritten as

$$u(x,y) = \frac{u_{max}}{G}\frac{1}{\ln\left[1-(1-\exp(G))\cdot F(u(x,y))\right]} \tag{4.143}$$

in which parameter G can be calculated considering the constraint expressed by equation (4.6). Equation (4.143) is the 2-D universal velocity distribution in terms of u_{max}, parameter G, and 2-D CDF. One can now determine properties of the 2-D velocity distribution as discussed in Chapter 3.

Questions

Q4.1 Considering different values of exponent n (n = 1, 2, 3, 4, 5, 6, 7, 8, 9, and 10), plot the power law velocity distribution. Which value of n seems most appropriate? Take flow depth as 0.5 m and u_{max} as 1.5 m/s.

Q4.2 Consider a set of velocity measurements as given in Table 4-4, where D = 0.122 ft and u_{max} = 8.796 ft/s. Fit the power law velocity distribution to the data, and determine the value of the exponent n using the least-squares method. How good is the fit?

Q4.3 For the data in Table 4-4, determine the value of exponent n by using the entropy method and also obtain the improved value of n by using the correction. Compute the power law velocity distribution with n computed by using the entropy method, and compare it with the observed velocity distribution.

Q4.4 Determine and plot the PDF of velocity by using the n values estimated in Q4.2 and Q4.3. Interpret the plots.

Q4.5 Determine and plot the CDF of velocity by using the n values estimated in Q4.2 and Q4.3. Interpret the plots.

Q4.6 Determine the entropy of velocity distribution by using the n values estimated in Q4.2 and Q4.3. Interpret the entropy values.

Table 4-4 *Velocity measurement of Einstein and Chien (1955).*

y (ft)	u (ft/s)	y (ft)	u (ft/s)
0.006	2.370	0.048	6.007
0.007	2.404	0.053	6.283
0.009	2.628	0.063	6.759
0.011	2.804	0.073	7.116
0.013	3.094	0.082	7.449
0.018	3.594	0.093	7.759
0.023	4.070	0.097	7.925
0.028	4.522	0.102	8.044
0.033	4.950	0.112	8.354
0.038	5.355	0.122	8.796
0.043	5.674		

Q4.7 For the data in Table 4-4, determine the value of exponent n by using the method that involves entropy parameter M. Now compute the power law velocity distribution with n computed as aforementioned, and compare it with the observed velocity distribution.

Q4.8 Determine and plot the PDF of velocity by using the n value estimated in Q4.7. Interpret the plot and compare it with that obtained in Q4.4.

Q4.9 Determine and plot the CDF of velocity by using the n value estimated in Q4.7. Interpret the plot and compare it with that obtained in Q4.5.

Q4.10 Determine the entropy of velocity distribution by using the n value estimated in Q4.7. Interpret the entropy value and compare it with that obtained in Q4.6.

Q4.11 Considering different values of exponent n (n = 1, 2, 3, 4, 5, 6, 7, 8, 9, and 10), plot the power law velocity distribution. Which value of n seems most appropriate? Take flow depth as 0.5 m and u_{max} as 1.5 m/s.

Q4.12 Consider the velocity measurements given in Table 4-4, fit the log law or Prandtl–von Karman velocity distribution to the data, and determine the parameter values using the least-squares method. How good is the fit?

Q4.13 For the data in Table 4-4, determine the log law velocity distribution parameter values by using the entropy method and also the simplification. Now compute the log law velocity distribution and compare it with the observed velocity distribution.

Q4.14 Determine and plot the PDF of velocity by using parameters estimated in Q4.12 and Q4.13. Interpret the plots.

Q4.15 Determine and plot the CDF of velocity by using parameters estimated in Q4.12 and Q4.13. Interpret the plots.

Q4.16 Determine the entropy of velocity by using the parameters estimated in Q4.12 and Q4.13. Interpret the entropy values.

Q4.17 For the data in Table 4-4, determine the log law velocity distribution parameters by using the method involving entropy parameter M. Now compute the log law velocity distribution with parameters computed as stated and compare it with the observed velocity distribution.

Q4.18 Determine and plot the PDF of velocity by using parameters estimated in Q4.17. Interpret the plot and compare it with that obtained in Q4.14.

Q4.19 Determine and plot the CDF of velocity by using parameters estimated in Q4.17. Interpret the plot and compare it with that obtained in Q4.15.

Q4.20 Determine the entropy of velocity by using parameters estimated in Q4.17. Interpret the entropy value and compare it with those obtained in Q4.16.

References

Araújo, J. C., and Chaudhry, F. H. (1998). "Experimental evaluation of 2-D entropy model for open-channel flow." *J. Hydraul. Eng.*, 124(10), 1064–1067.

Barbé, D. E., Cruise, J. F., and Singh, V. P. (1991). "Solution of three-constraint entropy-based velocity distribution." *J. Hydraul. Eng.*, 117(10), 1389–1396.

Chen, Y.-C., and Chiu, C.-L. (2004). "A fast method of flood discharge estimation." *Hydrol. Proc.*, 18(4), 1671–1684.

Chiu, C.-L. (1987). "Entropy and probability concepts in hydraulics." *J. Hydraul. Eng.*, 113(5), 583–600.

Chiu, C.-L., and Chiou, J.-D. (1986). "Structure of 3-D flow in rectangular open channels." *J. Hydraul. Eng.*, 112(11), 1050–1068.

Chiu, C.-L., and Hsu, S. M. (2006). "Probabilistic approach to modeling of velocity distributions in fluid flows." *J. Hydrol.*, 316, 28–42.

Chiu, C.-L., and Murray, D. W. (1992). "Variation of velocity distribution along nonuniform open-channel flow." *J. Hydraul. Eng.*, 118(7), 989–1001.

Chiu, C.-L., and Said, C. A. A. (1995). "Maximum and mean velocities and entropy in open-channel flow." *J. Hydraul. Eng.*, 121(1), 26–35.

Chiu, C.-L., and Tung, N.-C. (2002). "Maximum velocity and regularities in open-channel flow." *J. Hydraul. Eng.*, 128(4), 390–398.

Choo, T. H. (2000). "An efficient method of the suspended sediment-discharge measurement using entropy concept." *Water Eng. Res.*, 1(2), 95–105.

Chow, V. T. (1959). *Open-channel hydraulics*, McGraw-Hill, New York.

Daugherty, R. L., and Franzini, J. B. (1977). *Fluid mechanics with engineering applications*, McGraw-Hill, New York.

Dingman, S. L. (1989). "Probability distribution of velocity in natural channel cross sections." *Water Resour. Res.*, 25(3), 509–518.
Einstein, H. A., and Chien, N. (1955). "*Effects of heavy sediment concentration near the bed on velocity and sediment distribution*." Report No. 8, M.R.D. Sediment Series, U.S. Army Corps of Engineers, Omaha, NE.
Jaynes, E. T. (1957a). "Information theory and statistical mechanics, I." *Phys. Rev.*, 106, 620–630.
Jaynes, E. T. (1957b). "Information theory and statistical mechanics, II." *Phys. Rev.*, 108, 171–190.
Jaynes, E. T. (1982). "On the rationale of maximum entropy methods." *Proc. IEEE*, 70, 939–952.
Karim, M. F., and Kennedy, J. F. (1987). "Velocity and sediment-concentration profiles in river flows." *J. Hydraul. Eng.*, 113(2), 159–178.
Marini, G., de Martino, G., Fontana, N., Fiorentino, M., and Singh, V. P. (2011). "Entropy approach for 2D velocity distribution in open channels." *J. Hydraul. Res.*, 49, 784–790.
Shannon, C. E. (1948). "A mathematical theory of communications, I and II." *Bell Syst. Tech. J.*, 27, 379–443.
Singh, V. P. (1996). *Kinematic wave modeling in water resources: Surface water hydrology*, Wiley, New York.
Singh, V. P. (1998). *Entropy-based parameter estimation in hydrology*, Kluwer Academic, Dordrecht, The Netherlands.
Singh, V. P. (2011). "Derivation of power law and logarithmic velocity distributions using the Shannon entropy." *J. Hydrol. Eng.*, 16(5), 478–483.
Singh, V. P., Marini, G., and Fontana, N. (2013). "Derivation of 2D velocity distribution using entropy theory." *Entropy*, 15(4), 1221–1231, doi: 10.3390/e15041221.
von Karman, T. (1935). "Some aspects of the turbulent problem." *Mech. Eng.*, 57(7), 407–412.
Xia, R. (1997). "Relation between mean and maximum velocities in a natural channel." *J. Hydraul. Eng.*, 123(8), 720–723.

Additional Reading

Chow, V. T. (1959). *Open-channel hydraulics*, McGraw-Hill, New York.
French, R. H. (1985). *Open-channel hydraulics*, McGraw-Hill, New York.
Henderson, F. M. (1966). *Open channel flow*, Macmillan, New York.

Chapter 5

Applications of Velocity Distributions

In Chapters 2, 3, and 4, velocity distributions in one and two dimensions are derived using the principle of maximum entropy (POME). These velocity distributions are found to be useful in a variety of applications. This chapter discusses a sample of such applications.

5.1 Sampling Velocity Measurements

The one-dimensional velocity distribution based on the mass conservation constraint from Chapter 2 [given by equation (2.70)] is rewritten as

$$\begin{aligned} u &= \frac{1}{\lambda_2}\ln\left\{1+\frac{\lambda_2}{[\exp(\lambda_1-1)-1]}\frac{y}{D}\right\} = \frac{1}{\lambda_2}\ln\left\{1+[\exp(\lambda_2 u_D)-1]\frac{y}{D}\right\} \\ &= \frac{u^*}{k_1}\ln\left\{1+\left[\exp\left(\frac{k_1}{u^*}u_D\right)-1\right]\frac{y}{D}\right\} \end{aligned} \tag{5.1}$$

where u is the flow velocity at a distance y from the bed; D is the flow depth, $0 \le y \le D$; λ_1 is the Lagrange multiplier associated with the total probability; λ_2 is the Lagrange multiplier associated with mass conservation constraint; u_D is the flow velocity at $y = D$ and is the maximum velocity; u^* is the shear velocity, $u^* = \sqrt{gDS}$, g is the acceleration caused by gravity, S is the bed slope;

and $k_1 = u^*\lambda_2$ is a parameter related to shear velocity. The mean velocity u_m can be obtained from equation (5.1) as

$$u_m = u_D \exp(\lambda_2 u_D)[\exp(\lambda_2 u_D) - 1]^{-1} - \frac{1}{\lambda_2} \tag{5.2}$$

Equation (5.1) is obtained from one-physical-constraint (mass conservation based), entropy-based probability density function $f(u)$, which can be rewritten (see Chapter 2) as

$$f(u) = \exp[\lambda_1 - 1 + \lambda_2 u] \tag{5.3a}$$

where λ_1 and λ_2 are the Lagrange multipliers that have been expressed in terms of entropy number M in Chapter 3 as

$$\lambda_2 = \frac{M}{u_{\max}} \tag{5.3b}$$

and

$$\lambda_0 = \lambda_1 - 1 = \ln\left\{\frac{M}{[\exp(M) - 1]u_{\max}}\right\} \tag{5.4}$$

where $u_{\max}$ is the maximum velocity, which may or may not occur at $y = D$ (water surface) and may therefore not equal u_D. Substitution of equation (5.3a) into the total probability constraint:

$$\int_0^{u_D} f(u)du = 1$$

yields

$$\exp(\lambda_1 - 1)[\exp(\lambda_2 u_D) - 1] = \lambda_2 \tag{5.5}$$

Chiu (1987) commented on the usefulness of equation (5.1) for sampling velocity measurements. Because this equation is based on the uniform probability density function $f(y) = 1/D$, and $F(y) = y/D$, i.e., the velocity in each distance interval dy has an equal probability of being measured, velocity measurements between the channel bed and the water surface should lead to a set of data points distributed according to equation (5.3a). This result shows that higher velocity values have a higher probability density of being measured. If the entire range of velocity has equal probability of being measured, i.e., $f(u) = 1/u_D$, then the sampling method can be formulated as follows:

From the discussion in Chapter 2 (or equations (5.1) and (5.3a) here) and noting that $Df(u) = dy/du$, equation (5.5) can be written as

$$Df(u) = D\exp(u\lambda_2)\exp(\lambda_1 - 1) = D\exp(\lambda_1 - 1) + \lambda_2 y \tag{5.6}$$

Recalling that $f(y) = 1/D$, equation (5.6) can be used to write it as

$$f(y) = \frac{1}{D} = \frac{f(u)}{D\exp(\lambda_1 - 1) + \lambda_2 y} \tag{5.7}$$

Recalling that $f(u) = 1/u_D$, equation (5.7) can be written as

$$f(y) = [u_D\{D\exp(\lambda_1 - 1) + \lambda_2 y\}]^{-1} \tag{5.8}$$

Therefore, integration of equation (5.8) leads to

$$\begin{aligned} F(y) &= \int_0^y f(y)dy \\ &= \int_0^y \frac{1}{u_D[D\exp(\lambda_1 - 1) + \lambda_2 y]}dy \\ &= \frac{1}{u_D}\frac{1}{\lambda_2}\{\ln[D\exp(\lambda_1 - 1) + \lambda_2 y] - (\lambda_1 - 1)\} \end{aligned} \tag{5.9}$$

Equation (5.8) or (5.9) can constitute a basis for sampling. Equation (5.8) shows that sampling frequency increases with decreasing y. This result is reasonable because the fit of the Prandtl–von Karman universal velocity distribution (see Chapter 4, given by equation (4.27a) becomes less accurate as y and mean velocity u_m decrease. In general, one would concentrate on the measurement of maximum velocity u_D. The knowledge of maximum velocity allows us to determine the mean velocity through equation (3.118) (in Chapter 3), which yields k_1. Equation (5.1) has an advantage because it applies over the full range of y from zero to D, including the point where $u = 0$ and $y = 0$, even in sediment-laden flows. Thus, equation (5.1) can help greatly simplify velocity measurement or sampling.

Example 5.1 Plot the probability density function (PDF) of y given by equation (5.8) and the cumulative distribution function (CDF) given by equation (5.9). Assume that 100 observations of velocity have been taken at $y = 0.05$, 0.1, 0.2, 0.3, 0.4, 0.5, 0.6, 0.7, 0.8, 0.9, and 1.0 times D, where $D = 2$ m. The sampling frequency at each of these flow depths is given in Table 5-1.

Table 5-1 *Flow depth and probability distribution.*

y/D	y (m)	obs. $f(y)$	est. $f(y)$	obs. $F(y)$	est. $F(y)$
0.05	0.1	0.592	0.625	0.054	0.072
0.1	0.2	0.618	0.606	0.103	0.14
0.2	0.4	0.526	0.572	0.285	0.265
0.3	0.6	0.551	0.542	0.388	0.378
0.4	0.8	0.518	0.515	0.461	0.481
0.5	1	0.5	0.49	0.558	0.576
0.6	1.2	0.443	0.468	0.694	0.664
0.7	1.4	0.428	0.448	0.735	0.746
0.8	1.6	0.482	0.429	0.801	0.823
0.9	1.8	0.389	0.412	0.904	0.894
1	2	0.382	0.396	0.998	0.962

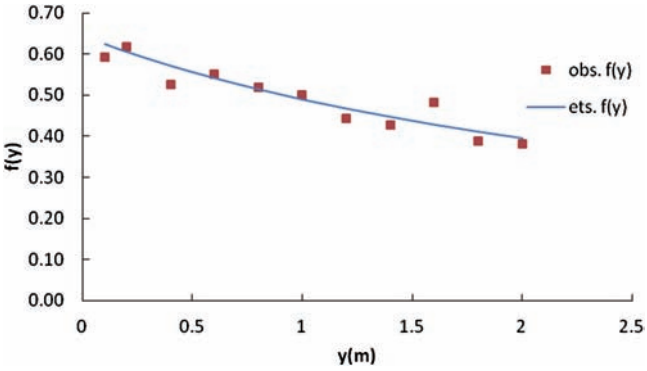

Figure 5-1 *PDF of* y *(m).*

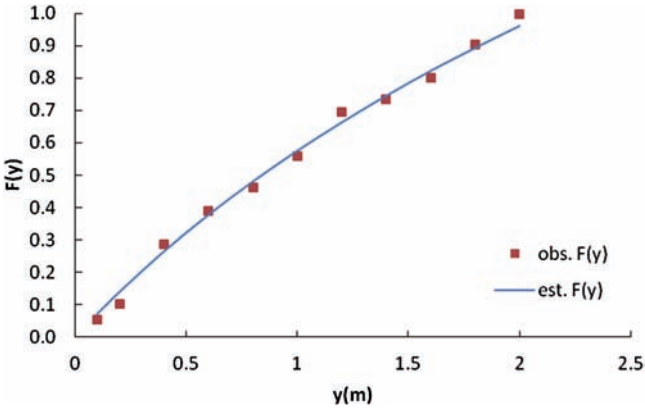

Figure 5-2 *CDF of* y *(m).*

Solution Take $u_D = 2.27\,\text{m/s}$, $D = 2\,\text{m}$. From equation (5.8) and (5.9), $f(y)$ and $F(y)$ can be computed as shown in Table 5-1. The PDF of velocity is plotted in Fig. 5-1 and the CDF in Fig. 5-2.

5.2 Use of k_1–Entropy Relation for Characterizing Open-Channel Flows

Entropy of the probability density function given by equations (5.3a) and (5.5) is expressed as

$$H(u) = -\lambda_1 + 1 - u_m \exp(\lambda_1 - 1)[\exp(\lambda_2 u_D) - 1] \tag{5.10}$$

For a large set of data, Chiu (1987) related parameter k_1 ($u^*\lambda_2$) to entropy (given by equations (3.40) and (3.41) in Chapter 3), written as

$$H\left(\frac{u}{u^*}\right) = H(u) - \ln u^* \tag{5.11}$$

$$\log k_1 = 0.48 - 0.46H\left(\frac{u}{u^*}\right) \tag{5.12}$$

Lower values of k_1 and hence higher values of entropy would be for flows over coarser channel beds and/or higher sediment concentration. Parameter k_1 can be used as a criterion to classify open-channel flows under the influence of both the coarseness of bed material and the sediment concentration. Equations (3.16) and (3.21) of Chapter 3 and equation (5.1), when solved simultaneously, yield k_1 and u_D, without measuring u at any point. Thus, the entropy function $H(u/u^*)$ plays a key role in this manner of parameter estimation.

Example 5.2 Consider the data given in Table 3-1 in Chapter 3 for the fourth vertical. Determine the values of k_1 and plot them as a function of entropy. Characterize flows, based on the values of k_1.

Solution First, determine the shear velocity $u^* = \sqrt{gDS}$.

$$u^* = \sqrt{gDS} = \sqrt{9.81 \times 6.07 \times 0.001} = 0.244$$

Now determine parameters λ_1 and λ_2.

$$\lambda_1 = 0.254 \text{ and } \lambda_2 = 0.179$$

Now determine $H(u)$ and $H(u/u^*)$. Plot k_1 as a function of $H(u/u^*)$ from equation (5.12).

$$\begin{aligned} H(u) &= -\lambda_1 + 2 - u_D \exp[\lambda_1 - 1 + \lambda_2 u_D] \\ &= 0.254 + 2 - 2.72 \times \exp[-0.254 - 1 + 0.487] \\ &= 0.991 \text{ Napier} \end{aligned}$$

$$H\left(\frac{u}{u^*}\right) = H(u) - \ln u^* = 0.991 - \ln(0.224) = 2.487 \text{ Napier}$$

Finally, characterize flows.

$$k_1 = \exp\left(0.48 - 0.46H\left(\frac{u}{u^*}\right)\right) = \exp(0.48 - 0.46 \times 2.487) = 0.514.$$

The value of k_1 is higher than the normal value, and, hence, it may suggest a coarse bed. Fig. 5-3 plots k_1 as against $H(u/u^*)$.

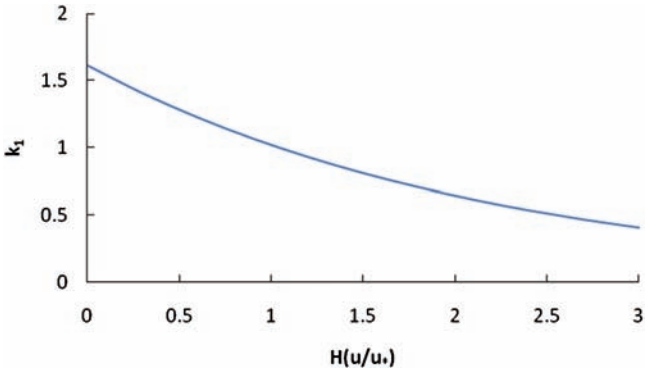

Figure 5-3 *Plot of* k_1 *as a function of entropy.*

5.3 Energy and Momentum Coefficients

The energy coefficient α is defined as

$$\alpha = \frac{\overline{u^3}}{\overline{u}^3} \tag{5.13}$$

and the momentum coefficient β as

$$\beta = \frac{\overline{u^2}}{u_m^2} \tag{5.14}$$

where $\overline{u^3}$ and $\overline{u^2}$ are the mean values of the cube of velocity (u^3) and square of velocity (u^2), respectively. In irregular channels, it is always difficult to obtain cross-sectional average velocities. As the PDF of u is derived using POME (equation [5.3a]), one can determine these expected values using equation (5.1) and the relation between mean and maximum velocities and express them in terms of entropy parameter M as

$$\alpha = \frac{[\exp(M)-1]^2\{\exp(M)[M^3-3M^2+6M-6]+6\}}{[\exp(M)(M-1)+1]^3} \tag{5.15}$$

$$\beta = \frac{[\exp(M)-1][\exp(M)(M^2-2M+2)-2]}{[\exp(M)(M-1)+1]^2} \tag{5.16}$$

Thus, if M ($\lambda_2 u_{\max}$) is known, α and β can be computed and would be constant for a channel section. Fig. 5-4 shows the variation of α and β with M.

If the flow in an open channel is nonuniform, then the energy coefficient tends to vary with the flow depth and discharge, and, hence, from section to section. The total energy head H at a section can be written as

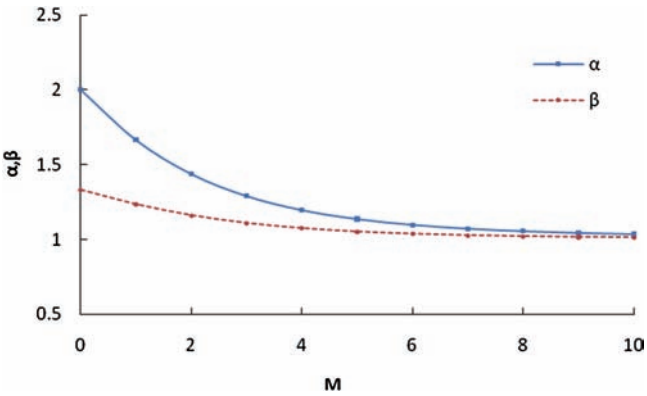

Figure 5-4 *Variation of* α *and* β *with* M.

$$H = Z + \alpha \frac{u_m^2}{2g} = Z + \alpha \frac{Q^2}{2gA^2} \tag{5.17}$$

where Z is the water surface elevation. Differentiating equation (5.17) with respect to x (the coordinate in the longitudinal direction), one obtains

$$\frac{d\alpha}{dx} = -\left(\frac{2B}{A}\frac{dD}{dx}\right)\alpha = \frac{2gA^2(S_w - S_f)}{Q^2} \tag{5.18}$$

where B is the flow width of the cross section at the water surface, and S_w is the slope of the water surface:

$$S_w = -\frac{dZ}{dx} \tag{5.19}$$

where S_f is the slope of the energy grade line:

$$S_f = -\frac{dH}{dx} = \left(\frac{Qn}{CAR^{2/3}}\right) \tag{5.20}$$

where n is Manning's roughness coefficient, R is the hydraulic radius, and C = 1.49 if the British system of units is used and is unity in the SI system.

Equation (5.18) can be integrated as

$$\alpha(x) = \frac{2gA^2}{Q^2}\int_0^x (S_w - S_f)dx + \alpha_0\left(\frac{A}{A_0}\right)^2 \tag{5.21}$$

where α_0 is α at $x = 0$, and A is A at $x = 0$. The $(S_w - S_f)$ term is the slope of the kinetic energy line in the x-direction over distance dx. The integral, therefore, represents the total change (net increase or decrease) in the flow kinetic energy between the channel section at $x = 0$ and a downstream channel section at a distance x.

Example 5.3 Consider two profiles: M-1, in which the flow depth increases in the flow direction, and S-1, in which the flow depth (or flow cross section) decreases in the flow direction. How do the two terms on the right side of equation (5.21) vary and consequently how does α vary with x?

Solution The first term includes the integral term, which decreases for the M-1 profile where A increases and increases for the S-1 profile in which A decreases. The second term increases for the M-1 profile and decreases for the S-1 profile. Thus, the gradient of the kinetic energy may change irregularly from one section to another, positive or negative, depending on whether the channel is narrowing or widening. Because α can be expressed in terms of entropy parameter M, its value can shed light on the homogeneity of the velocity distribution.

Example 5.4 Consider a test section 180 cm long and 10 cm wide of a rectangular channel with a slope of 0.00156. The discharge is 669 cm^3/s. The flow at the downstream end is a free fall; this means that it has a drawdown profile. The critical section occurs at about 10 cm upstream from the brink. The flow is an uprising profile at and near the upstream boundary of the test section. Around the middle of the test section, the flow is almost uniform. The water surface elevations are given in Table 5-2.

Compute the energy grade line. Compute α using equation (5.21) and velocity distribution. Also compute S_w and S_f. Plot these quantities as functions of distance. What is the value of α at $x = 100$ cm? S_f can be computed using Manning's equation with $n = 0.00891$ (Chiu and Murray 1992).

Solution Given $S_w = 0.00156$,

$$S_f = -\frac{dH}{dx} = \left(\frac{Qn}{CAR^{2/3}}\right) = \frac{669 \times 0.00891}{22 \times 1.528^{2/3}} = 0.204$$

Taking $\alpha_0 = 1.2$, α can be computed using equation (5.21), as see in Table 5-3. This result can be plotted as in Fig. 5-5.

Table 5-2 *Water surface elevation.*

x *(cm)*	h *(cm)*	x *(cm)*	h *(cm)*
180	2.2	80	2.21
160	2.25	60	2.1
140	2.3	40	1.8
120	2.35	20	1.7
100	2.27	0	1.3

Table 5-3 *Computed energy grade line in Example 5.4.*

x (cm)	a
140	1.35
120	1.21
100	1.11
80	1.2
60	1.19
40	1.21
20	1.18

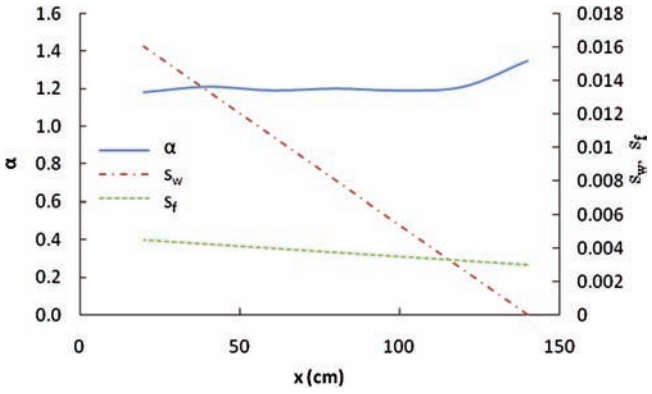

Figure 5-5 *Plot of α as a function of S_w and S_f, for x = 100 cm, $\alpha = 1.11$.*

5.4 Shear Stress Distribution

In steady uniform open-channel flow, shear stress τ is maximum at the bed, minimum or zero at the water surface, and the decrease from the bed to the water surface is monotonic. The maximum value is given as $\tau 0 = \rho gDS = \gamma DS$; $\gamma = \rho g$; $\tau = \tau_0$ at $y = 0$; $0 \le \tau \le \tau_0$; ρ is the fluid mass density. The probability of shear stress equal to or less than a particular value τ can be expressed as

$$F(\tau) = \frac{D - y}{D} \tag{5.22}$$

which is the cumulative probability distribution of τ. Differentiation of equation (5.22) leads to the probability density function of τ as

$$f(\tau) = -\frac{1}{D}\frac{dy}{d\tau} = -\left(D\frac{d\tau}{dy}\right)^{-1} \tag{5.23}$$

The objective is to determine $f(\tau)$ using the principle of maximum entropy (POME). This involves maximization of entropy

$$H(\tau) = -\int_0^{\tau_0} f(\tau) \ln f(\tau) d\tau \tag{5.24}$$

subject to

$$\int_0^{\tau_0} f(\tau) d\tau = 1 \tag{5.25}$$

and other constraints, such as the mean shear stress value and the variance of shear stress. However, for simplicity, other constraints are not used, as was done by Chiu (1987). Then, one obtains

$$f(\tau) = \exp[-\lambda_0 - 1] \tag{5.26}$$

where λ_0 is the zeroth Lagrange multiplier corresponding to equation (5.25). Substitution of equation (5.26) into equation (5.25) yields

$$f(\tau) = \exp[-\lambda_0 - 1] = \frac{1}{\tau_0} \tag{5.27}$$

Equation (5.27) is a uniform probability density function of τ. Measurement of τ between $y = 0$ and $y = D$ is done according to a uniform probability distribution $1/D$; the shear stress data exhibit a uniform probability density function as equation (5.27). Equating equation (5.27) to equation (5.23), one gets the relation between τ and y as

$$\tau = \tau_0 \left(1 - \frac{y}{D}\right) \tag{5.28}$$

Going from planar coordinates (y, z) to curvilinear coordinates (r, s), equation (5.28) can be written as

$$\tau = \tau_0 \left[1 - \frac{r - r_0}{r_{\max} - r_0}\right] \tag{5.29}$$

Equation (5.29) is widely used in hydraulics and is derived by using the equation of motion or momentum conservation for steady, uniform, one-dimensional flow.

A shear stress distribution compatible with the velocity as a function of r given by equation (5.28) may now be expressed in power series as

$$\frac{\tau}{\tau_0} = \frac{h}{D}\left(1 - \frac{y}{D+h}\right) + \left(1 + \frac{h}{D}\right)\left(1 - \frac{y}{D+h}\right)^2 \tag{5.30}$$

which satisfies the condition that $\tau = \tau_0$ at $y = 0$; $\tau = 0$ at $y = D + h$, where $u = u_{\max}$ and also at $y = D$ (water surface). Equation (5.30) becomes equation (5.28) as h/D tends to negative infinity. It can be shown, using L'Hospital's rule, that equation (5.30) is an approximate form of the polynomial shear stress distribution:

$$\tau = \alpha_0 + \alpha_1 (r_{\max} - r) + \alpha_2 (r_{\max} - r)^2 \tag{5.31}$$

where α_0, α_1, and α_2 are constants that can be evaluated using boundary conditions, and $r_{\max}$ is r when u is $u_{\max}$.

The shear stress can also be expressed as

$$\tau = \rho\varepsilon_0 \frac{du}{dy} = \rho\varepsilon_0 \frac{du}{drh_r} = \tau_0\left(1 - \frac{y}{D}\right) \tag{5.32}$$

where h_r is the scale factor or metric coefficient needed in the coordinate transformation between the y and r systems. The velocity gradient can be expressed using equations (3.36) and (3.84) as

$$\frac{du}{dy} = \frac{du}{drh_r} = \frac{u_{\max}}{M}\frac{[\exp(M)-1]}{(r_{\max}-r_0)}\left\{1+[\exp(M)-1]\frac{r-r_0}{r_{\max}-r_0}\right\}^{-1} h_r \tag{5.33}$$

The shear stress at the channel bed for a wide channel can be expressed as

$$\tau_0 = \rho g D S_f = \rho\varepsilon_0 \left.\frac{du}{dy}\right|_{y=0} \tag{5.34}$$

where ε_0 is the momentum transfer coefficient at the channel bed; it is equal to the kinematic viscosity of fluid in a smooth channel with the viscous sublayer likely to exist, and

$$\left.\frac{du}{dy}\right|_{y=0} = \frac{u_{\max}[\exp(M)-1]}{DM} \tag{5.35}$$

Substitution of equation (5.27) in equation (5.24) yields the maximum entropy of shear stress:

$$H(\tau) = \ln \tau_0 \tag{5.36}$$

Example 5.5 Construct the shear stress distribution τ/τ_0 versus y/D for h/D = 0.5, 0.2, 0.1, 0, –0.2, –0.4, –0.6, and –0.8, assuming $M = 2$.

Solution The relation between shear stress distribution τ/τ_0 as a function of y/D for various values of h/D is given in Fig. 5-6. Assume D = 1 m. Using equation (5.30), the ratio τ/τ_0 is computed, as shown in Table 5-4.

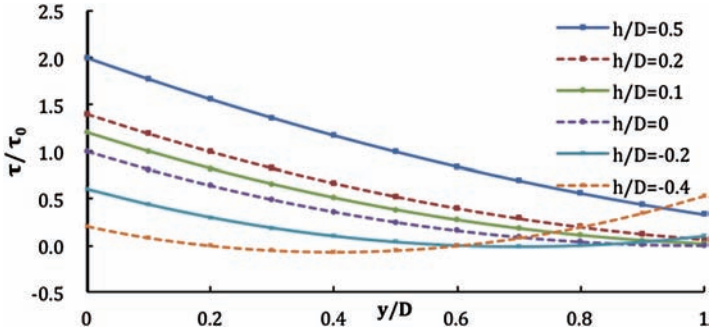

Figure 5-6 *Shear stress distribution* τ/τ_0 *versus* y/D *for* h/D.

Table 5-4 *Values of* τ/τ_0 *as a function of* y/D *for various values of* h/D.

y/D	*h/D* = 0.5	*h/D* = 0.2	*h/D* = 0.1	*h/D* = 0	*h/D* = –0.2	*h/D* = –0.4
0	2.000	1.400	1.200	1.000	0.600	0.200
0.1	1.773	1.192	1.000	0.810	0.438	0.083
0.2	1.560	1.000	0.818	0.640	0.300	0.000
0.3	1.360	0.825	0.655	0.490	0.188	–0.050
0.4	1.173	0.667	0.509	0.360	0.100	–0.067
0.5	1.000	0.525	0.382	0.250	0.038	–0.050
0.6	0.840	0.400	0.273	0.160	0.000	0.000
0.7	0.693	0.292	0.182	0.090	–0.013	0.083
0.8	0.560	0.200	0.109	0.040	0.000	0.200
0.9	0.440	0.125	0.055	0.010	0.038	0.350
1	0.333	0.067	0.018	0.000	0.100	0.533

5.5 Relation between Maximum Velocity, Darcy's Friction Factor, and Entropy Number

For wide rectangular channels, the shear stress can be written as

$$\tau_0 = \rho g D S_f = \rho \varepsilon_0 \left.\frac{du}{dy}\right|_{y=0} \tag{5.37}$$

where ε_0 is the momentum transfer coefficient at the channel bed. Here it is implied that the velocity gradient in equation (5.37) remains finite at the channel bed. ε_0 equals the kinematic viscosity if the channel bed is smooth such that the viscous sublayer exists. From equation (3.33) with $r = y/D$, then

$$\left.\frac{du}{dy}\right|_{y=0} = \frac{u_{\max}[\exp(M)]}{DM} \tag{5.38}$$

Thus, with the use of the right side of equation (5.38), equation (5.37) can be expressed as $\frac{\varepsilon_0}{\upsilon} = \frac{gD^2 S_f M}{u_{\max}\exp(M)}$, and $u_{\max}$ is replaced with $u_m/u_{\max}$ and u_m/u^* using equations (3.43) and (3.53). According to the Darcy–Weisbach equation, S_f can be expressed as $S_f = f_l \frac{1}{D}\frac{u_m^2}{2g}$. Summarizing the above relations, $\frac{\varepsilon_0}{\upsilon}$ can be expressed as

$$\frac{\varepsilon_0}{\upsilon} = \left(\frac{u_m}{u^*}\right)^{-2} \frac{R_n}{F_m(M)} = \frac{f_l R_n}{8F_m(M)} \tag{5.39}$$

where f_l is the friction factor, R_n is the Reynolds number, υ is the kinematic viscosity, and

$$F_m(M) = \frac{\exp(M) - 1}{M\phi(M)} \tag{5.40}$$

For a smooth channel, $\varepsilon_0/\upsilon = 1$. When R_n increases, f_l decreases, and, hence, M and $f_l R_n$ remain constant. Thus, M can be determined from the product of R_n and f_l or u_m/u^*. If a channel is rough, then it adjusts ε_0/υ beside f_l to keep M constant when R_n changes.

Example 5.6 Compute the shear stress for a wide rectangular channel where $u_{\max} = 2.72\,\text{m/s}$, $D = 6.07\,\text{m}$, and $M = 0.478$.

Solution Here,

$$\left.\frac{du}{dy}\right|_{y=0} = \frac{u_{\max}[\exp(M)]}{DM} = \frac{2.72 \times \exp(0.487)}{6.07 \times 0.487} = 1.497\ \text{s}^{-1}$$

$$\tau_0 = \rho g D S_f = \rho \varepsilon_0 \left.\frac{du}{dy}\right|_{y=0} = 2.05 \times 10^{-3}\ \text{kgm/s}^2$$

5.6 Discharge Measurements

During high flows, such as floods, reliable discharge data are often lacking. It is, therefore, desirable to have a method that requires only velocity sampling. Discharge involves mean velocity and cross-sectional area. The cross-sectional area can be determined from its relation to water level. In unsteady flow, the rating curve or the relation between discharge and water level is looped, which complicates discharge estimation.

Chiu et al. (2005) presented methods for discharge measurements using the entropy-based velocity equations derived in Chapter 3. Following their work here, a general form of velocity distribution (given by equation [3.35a]) can be written as

$$\frac{u_m}{u_{\max}} = \frac{1}{M}\ln\left\{1 + [\exp(M) - 1]\frac{\bar{r} - r_0}{r_{\max} - r_0}\right\} \tag{5.41}$$

where M is the dimensionless parameter, u_m is the mean velocity, $\bar{r}$ is the value of r where $u = u_m$, u_{max} is the maximum velocity in the channel cross section, $r_{\max}$ is the value of r, where $u = u_{\max}$, r_0 is the value of r where $u = 0$. The curvilinear coordinate r is related to y as

$$r = \frac{y}{D + h}\exp\left[1 - \frac{y}{D + h}\right] \tag{5.42}$$

where h is a parameter related to the shape and slope of the isovels.

The cumulative probability distribution function $F(u)$ (CDF) of velocity u, $0 \le u \le u_{max}$, corresponding to equation (5.41), can be written as

$$F(u) = \frac{1}{\exp(M)-1}\left[\exp\left(M\frac{u}{u_{max}}\right)-1\right] \tag{5.43}$$

Differentiating equation (5.43) and noting that the PDF of u/u_{max}, $f(u/u_{max}) = u_{max}f(u)$, one obtains

$$f\left(\frac{u}{u_{max}}\right) = u_{max}f(u) = \frac{M}{[\exp(M)-1]}\exp\left(\frac{Mu}{u_{max}}\right) \tag{5.44}$$

Equation (5.44) has only one parameter M. The mean value of u/u_{max} can be obtained from equation (5.41) as

$$\frac{u_m}{u_{max}} = \phi = \frac{\exp(M)}{\exp(M)-1} - \frac{1}{M} \tag{5.45}$$

Equation (5.45) has been found to be stable under a variety of flow types—steady or unsteady.

The question arises as to the invariance of M or ϕ under various flow conditions. For velocity data collected by the U.S. Geological Survey for the Alleghany River at Natrona, near Pittsburgh, Pennsylvania, during 1974–1994, Chiu et al. (2005) found ϕ to be 0.79 with u_{max} obtained at the mean distance from the reference point, and 0.81 if u_{max} was obtained at one standard deviation plus or minus of the mean distance.

Chiu (1988, 1991), Chiu and Said (1995), and Chiu and Tung (2002) related the following quantities to M: (1) u_m/u_{max} or ϕ; (2) h/D or ϕ_1, where h is the distance below the water surface at which maximum velocity occurs; (3) u_m/u_D or ϕ_2, u_D is the velocity at the water surface; (4) $u_m/\overline{u_y}$ or ϕ_3, $\overline{u_y}$ is the mean value of u on the $\underline{y}$-axis; (5) y_m/D, y_m or ϕ_4, y_m is the mean value of y on the y-axis where $u = u_m$; (6) $\overline{y_u}/D$ or ϕ_5, $\overline{y_u}$ is the value of y where $u = u_m$; and (7) the energy and momentum coefficients. The relationships of these equations with M are shown in Fig. 5-7.

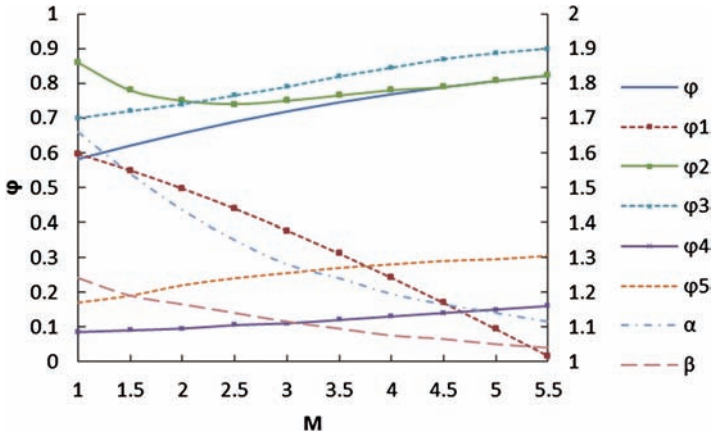

Figure 5-7 *Relations of different quantities with* M.

Leopold et al. (1995) discussed the notion that the maximum point velocity is usually about 25 to 50% higher than the average point velocity for the cross section. This observation translates into an M value between 2 and 5. Chiu and Tung (2005) showed that in this range $u_{\max}$ occurs below the water surface. In that case, ϕ_4 and ϕ_5 quickly approach 0.368, and $F(u)$ can be represented by y/D. Once M is determined, the seven quantities listed can be obtained, or vice versa. Since M is constant for a cross section, these quantities are also constant. Thus, in sampling velocity on the y-axis, the following methods for discharge measurements are suggested:

1. $u_{\max}$: By measuring or estimating $u_{\max}$, the cross-sectional mean velocity can be determined as

$$u_m = u_{\max}\phi \tag{5.46}$$

because ϕ is regarded as invariant. Given the cross-sectional area, discharge for known u_m can be determined.

2. Velocity at a single point on the water surface: The velocity measured at the water surface can be used to estimate $u_{\max}$ as

$$u_{\max} = (u_D M) \div \ln\left\{1 + [\exp(M) - 1]\frac{1}{1 + \dfrac{h}{D}}\exp\left[1 - \frac{1}{1 + \dfrac{h}{D}}\right]\right\} \tag{5.47}$$

Equation (5.47) is equivalent to equation (5.41). Chiu and Tung (2002) related h/D in equation (5.47) to M:

$$\frac{h}{D} = 0.2\ln\frac{58.3M\phi}{\exp(M) - 1} = \phi_1 \tag{5.48}$$

Noting that $u_{\max} = u_m/\phi$, equation (5.47) becomes

$$\frac{u_m}{u_D} = M\phi \div \ln\left\{1 + [\exp(M) - 1]\frac{1}{1 - \dfrac{h}{D}}\exp\left[1 - \frac{1}{1 - \dfrac{h}{D}}\right]\right\} = \phi_2 \tag{5.49}$$

Since both ϕ and h/D are functions of M, the u_m/u_D ratio is also a function of time, and this ratio is constant for a given cross section. Therefore,

$$u_m = \phi_2 u_D \tag{5.50}$$

3. $\overline{u_y}$: The cross-sectional mean velocity can be written as

$$u_m = \phi_3 \overline{u_y} \tag{5.51}$$

$\overline{u_y}$ can be determined by taking a couple of velocity observations on the y-axis. If just one observation is taken, then it should be at $y = \phi_5 D$, where

$u = \overline{u_y}$. For two observations, velocities $u_{0.2}$ and $u_{0.8}$, should be sampled at $y = 0.8D$ and $y = 0.2D$. Then the average velocity should be estimated.

4. Single velocity sampling: The cross-sectional mean velocity u_m can be measured by observing velocity at $y = \phi_4 D$ on the y-axis.

Now the location of the y-axis (vertical) on which the maximum velocity occurs needs to be found. In natural channels, it may not occur in the middle of the cross section, but its average location does not seem to change with discharge and water level for flows confined within the main channel. Both the maximum velocity on the water surface and the maximum velocity within the entire channel cross section tend to occur on the same y-axis. The velocity distribution tends to be quite uniform in the vicinity of the point at which $u_{\max}$ occurs. The y-axis therefore is highly informative in that it yields the magnitude and location of $u_{\max}$, which are required to estimate ϕ, M, h/D, and other constants at the channel cross section. Furthermore, the correlation between u_m and $u_{\max}$ and $\overline{u_y}$ on the y-axis is maximum. This phenomenon means that the cross-sectional mean velocity u_m can be estimated from $u_{\max}$ or $\overline{u_y}$ without sampling velocity on other verticals. For the data collected in the channel cross section of South Esk River at Bridge 2 (Bridge and Jarvis 1985) over a four month period from December 14, 1978, to April 14, 1979, Chiu et al. (2005) found ϕ_3 to be 0.86. The correlation was high near the y-axis but decreased toward the channel banks.

Example 5.7 The U.S. Geological Survey collected data during 1986 to 2000 at Skagit River at Mount Vernon, Washington, DC. The cross-sectional area, observed by acoustic Doppler current profiler (ACDP), was 578 m^2. From a plot of the observed mean and maximum velocities, it was found that $\phi = 0.64$, and $M = 1.80$ from equation (5.48). Compute ϕ_1, ϕ_2, ϕ_3, ϕ_4, ϕ_5, α, and β using Fig. 5-7. Compute u_m and Q.

Solution With the aid of Fig. 5-7, $\phi_1 = 0.51$, $\phi_2 = 0.76$, $\phi_3 = 0.73$, $\phi_4 = 0.09$, $\phi_5 = 0.21$, $\alpha = 1.475$, and $\beta = 1.5$. The velocity distribution was determined by regression, which yielded $u_{\max} = 1.41$ m/s. The mean velocity $u_m = u_{\max}\phi = 0.9$ m/s. Therefore, discharge $Q = 520$ m^3/s, which is only 1% less than the observed value of 525 m^3/s.

When $M = 1.80$, $h/D = \phi_1 = 0.51$ and a single velocity sample u_D is used in equation (5.47), the maximum velocity below the water surface, $u_{\max} = 1.43$ m/s. The mean velocity $u_m = 0.64\ u_{\max} = 0.915$ m/s. Then, $Q = 529$ m^3/s, which is only 0.8% greater than the observed value.

The mean velocity and discharge can also be estimated using ϕ_2. For $\phi_2 = 0.76$ at $M = 1.8$, $u_D = 1.20$ m/s, $u_m = 0.91$ m/s from multiplication of 0.76 and 1.20 m/s. Alternatively, $\phi_4 = y_m/D = 0.09$ at $M = 1.8$, u_m occurs at $y = 0.09D = 0.31$ m, since $D = 3.4$ m. At $y = 0.31$ m, $u_m = 0.9$ m/s from Fig. 5-8, which is about the same. For April 21, 1999, u_D in equation (5.47) gives $u_{\max} = 1.44$ m/s, and $u_m = 0.92$ m/s. For $A = 560$ m^3/s and observed $Q = 520$ m^3/s; both values are quite comparable.

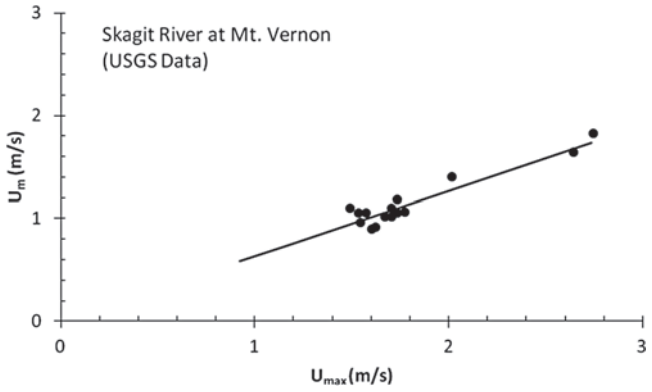

Figure 5-8 *Relation between mean and maximum velocities.*

5.7 Determination of Discharge at Remote Locations

Discharge estimation depends on local hydraulic conditions, which are defined by recording the water level at a gauged section. Local stage monitoring is fairly straightforward and relatively inexpensive compared with the cost to carry out both flow velocity measurements and topographic surveys of river cross sections, especially for remote sites or with unsuitable access. Therefore, it seems logical to convert stage records into discharge values through a reliable rating curve; however, the water level–discharge relationship may be unknown for some hydrometric sites. Moreover, if unsteady flow effects occur, a value of stage does not correspond to a single value of discharge (Herschy 1985). This difference is represented as a loop in the rating curve whose amplitude depends on how much the inertial and pressure forces influence the flood propagation (Moramarco and Singh 2000). In addition, velocity measurements are often available for low flows, so the rating curve extrapolation for higher stages cannot be reliable because of changes that occur in hydraulic and geometric characteristics of the river where the gauged cross section is located. The local discharge estimation from observed stages has also been approached by considering the hydraulic conditions observed at some distance away.

A simpler and more practical method was developed by Moramarco and Singh (2001), which, without adopting a flood routing procedure and using only the water levels observed at a local site, allows for a quick estimation of flow conditions through the assessment of two parameters linked to the discharge values recorded at a hydrometric section some distance away. However, the method investigated only the case of translation and attenuation of the peak flow, and thus it cannot be applied for reaches where the tributaries produce large contributions. This work was extended by Moramarco et al. (2004) by relating the stage recorded at a site of interest to discharge values observed some distance upstream. Also, they considered the case when significant lateral inflows occur

that affect an increase of both the peak flow and the volume at the downstream section.

Following the entropy-based relation between mean and maximum velocities expressed by equation (5.46), and recalling that $\phi(M)$ remains more or less constant (Xia 1997), Moramarco and Singh (2001) surmised a direct proportionality between upstream and downstream velocities as

$$\frac{u_{mU}}{u_{\max U}} \propto \frac{u_{mD}}{u_{\max D}} \tag{5.52}$$

where subscripts U and D represent quantities for the upstream and downstream sections, respectively. This, then, suggests a link between upstream and downstream discharges expressed as

$$Q_D(t) = \alpha \frac{A_D(t)}{A_U(t)} Q_U(t) \tag{5.53}$$

Equation (5.53), under the assumption that the contribution of lateral inflows is negligible, was verified using several flood events of different magnitudes recorded at two gauged sections of the Upper Tiber River, Italy, where the rating curve was unknown at the downstream section (Moramarco and Singh 2001).

Discrepancies between observed values and those computed by equation (5.53) were modified to take account of the wave travel time (Moramarco and Singh 2001). For a river reach where the stage and the surveyed stage–area relation are given at the two ends, where the discharge is known at the upstream section, for the case without lateral inflows, the discharge at the downstream end can be determined as

$$Q_D(t) = \alpha \frac{A_D(t)}{A_U(t - T_L)} Q_U(t - T_L) + \beta \tag{5.54}$$

where Q_D and Q_U are the downstream and upstream discharges, respectively; A_D and A_U are the effective downstream and upstream cross-sectional flow areas, respectively; T_L is the wave travel time depending on the wave celerity, c, that is referred to as the peak discharge velocity; and α and β are parameters. The effective flow area can be different from the surveyed area, both because of the particular morphologic characteristics of the river reach and the presence of a hydraulic structure close to the gauged section. In fact, around the zones of the river next to a weir or a bridge, there are areas of the cross section in which the water accumulates but is not being actively conveyed; hence, only a portion of the flow area contributes to the conveyance of water in the downstream direction (U.S. Army Corps of Engineers 1995, 2001). Equation (5.54) is based on the formulation by Chiu (1991) where the cross-sectional mean flow velocity, u_m, is expressed as a function of maximum velocity, $u_{\max}$, through a dimensionless parameter M, as equation (5.45). The method allows a quick estimation of the flow conditions at the site of interest, even if the rating curve is unknown and only the stage is monitored. Although equation (5.54) appears to be adequate for relating the discharges at local and remote sites, it needs to be further verified on sites where lateral inflows can be significant.

5.7.1 Accounting for Wave Travel Time

Moramarco and Singh (2001) assessed the relationship using five flood events of different magnitudes and durations. The relative stage data were recorded with a time interval of 0.5 h at the gauged sections of Santa Lucia and Ponte Felcino, along the Tiber River, Italy, which subtend drainage areas of 935 km^2 and 2,035 km^2, respectively. The peak discharge received a significant contribution of lateral inflow ranging from 13% to 53%.

Example 5.8 Obtain data for flood events for a drainage basin. Compute the contribution of lateral inflow as percentage of peak flow.

Solution Assume that the increase in discharge downstream from that upstream is all contributed by lateral flow. Thus, the lateral inflow is computed by $Q_d - Q_u$, as shown in Table 5-5.

Table 5-5 *The percentage of lateral inflow.*

	Q_u (m^3/s)	Q_d (m^3/s)	q_p (%)
December 1990	349.17	439.61	20.57
February 1991	276.13	600.28	54.00
January 1994	107.89	270.79	60.16
December 1995	407.08	418.50	2.73
December 1998	62.84	113.80	44.78

5.7.2 Estimation of Travel Time

The estimation of the wave travel time, T_L, was based on the stage hydrographs observed at the upstream (Santa Lucia) and downstream (Ponte Felcino) sections. Because of lateral inflows, the shape of the downstream hydrograph can change significantly from the upstream one. For this reason, T_L can be assumed as the time shift necessary to overlap the rising limb and the peak region of the two dimensionless stage hydrographs. At a gauged section of the dimensionless stage, $h^*(t)$, is given by

$$h^*(t) = \frac{h(t) - h^b}{h^p - h^b} \tag{5.55}$$

where h^b and h^p represent the minimum and the maximum values of the observed stage hydrograph, respectively. Specifically, T_L is estimated by minimizing the mean square of the residuals, $h_d^*(t) - h_u^*(t - T_L)$, in the rising limb and the peak region.

Parameters α and β can be obtained by linear regression. Equation (5.54) has been found suitable for all the events examined independently from the lateral inflow contribution. Therefore, α and β can be considered as characteristic parameters of the flood event; they are constant during the event but change from one event to another.

Table 5-6 *Computed time of travel for each flood event.*

	h_u^p (m)	h_u^b (m)	h_d^p (m)	h_d^b (m)	T_L **(hr)**
December 1990	349.17	8.23	439.61	4.38	2
February 1991	276.13	22.74	600.28	23.00	4
January 1994	107.89	35.65	270.79	47.81	3
December 1995	407.08	16.28	418.50	22.56	3
December 1998	62.84	16.66	113.80	29.87	4.5

Example 5.9 Compute the time of travel for flood events on a drainage basin.

Solution The maximum and minimum observed stages upstream and downstream are given in Table 5-6. The dimensionless stages $h_d^*(t)$ and $h_u^*(t)$ are computed using equation (5.55). By the trial and error method, the time of travel T_L is computed by minimizing $h_d^*(t) - h_u^*(t - T_L)$, and the results are shown in Table 5-6.

5.7.3 Estimation of Parameters α and β

When the downstream rating curve is unknown, for estimating α and β two particular flow conditions are considered: base flow and peak discharge (Moramarco and Singh 2001). To that end, because of the linear relationship, one can write the following:

$$Q_d(t_b) = \alpha \frac{A_d(t_b)}{A_u(t_b - T_L)} Q_u(t_b - T_L) + \beta \tag{5.56a}$$

$$Q_d(t_p) = \alpha \frac{A_d(t_p)}{A_u(t_p - T_L)} Q_u(t_p - T_L) + \beta \tag{5.56b}$$

where t_p and t_b are, respectively, the time when peak stage and base flow occur at the downstream section. In particular, t_b is assumed as the time just before the hydrograph rising limb. Therefore, once Q_d (t_b) and Q_d (t_p) are known, α and β can be obtained as

$$\alpha = \frac{Q_d(t_p) - Q_d(t_b)}{\left[\frac{A_d(t_p)}{A_u(t_p - T_L)} Q_u(t_p - T_L) - \frac{A_d(t_b)}{A_u(t_b - T_L)} Q_u(t_b - T_L)\right]} \tag{5.57}$$

$$\beta = Q_d(t_b) - \alpha \frac{A_d(t_b)}{A_u(t_b - T_L)} Q_u(t_b - T_L) \tag{5.58}$$

Base flow can be computed easily if the downstream gauged section, although not equipped for velocity measurements during high flood events, allows workers to carry out wading measurements. Otherwise, assuming that the mean

velocity is unchanged between the upstream and downstream sections, Q_d (t_b) can be computed as the product between the upstream mean velocity, estimated through Q_u ($t_b - T_L$), and the downstream flow area A_d (t_b). This assumption can result in significant errors in the computed base flow, but, as shown later, this value has a negligible influence on reconstructing the downstream discharge hydrograph for high stages, which are of the most interest in the hydrological practice. Finally, if a control structure, like a weir, identifies the downstream section, the hydraulic laws can be used to determine Q_d (t_b). The value of base flow can be assumed to be known.

Example 5.10 Compute parameters α and β for a number of flood events for a drainage basin.

Solution To compute parameters α and β, t_p and t_b are first obtained from the flow hydrograph. The value of T_L is taken from Example 5.9. The flow and area are shown in Table 5-7 for each corresponding time. Then, coefficients α and β can be computed using equations (5.57) and (5.58). For example, using the event of December 1990, $t_p = 29.5$ h, $t_b = 80$ h, and

$$\alpha = \frac{Q_d(t_p) - Q_d(t_b)}{\left[\frac{A_d(t_p)}{A_u(t_p - T_L)} Q_u(t_p - T_L) - \frac{A_d(t_b)}{A_u(t_b - T_L)} Q_u(t_b - T_L)\right]}$$

$$= \frac{400.94 - 54.54}{\left[\frac{142.25}{128.74} 349.2 - \frac{27.68}{22.36} 41.8\right]} = 1.15$$

$$\beta = Q_d(t_b) - \alpha \frac{A_d(t_b)}{A_u(t_b - T_L)} Q_u(t_b - T_L)$$

$$= 54.54 - 1.15 \times \frac{27.68}{22.36} 41.8 = -9.0$$

Computations for other events are shown in Table 5-7.

Table 5-7 *Estimation of parameters α and β.*

	t_p (hr)	t_b (hr)	$Q_d(t_p)$ (m^3/s)	$Q_d(t_b)$ (m^3/s)	$Q_u(t_p - T_L)$ (m^3/s)	$Q_u(t_b - T_L)$ (m^3/s)
December 1990	29.50	80.00	400.94	54.54	349.20	41.80
February 1991	81.00	123.00	593.82	76.61	276.1	45.00
January,1994	33.00	85.00	240.72	67.26	107.9	46.1
December 1995	32.50	96.00	424.16	41.54	407.10	27.60
December 1998	13.00	48.00	120.62	43.92	62.8	25.80

Continued

Table 5-7 Estimation of parameters α and β. (Continued)

	$A_d(t_p)$ (km^2)	$A_d(t_b)$ (km^2)	$A_u(t_p - T_L)$ (km^2)	$A_u(t_b - T_L)$ (km^2)	α	β
December 1990	142.25	27.68	128.74	22.36	1.15	–9.00
February 1991	209.89	35.12	105.11	27.72	1.09	–2.10
January 1994	84.5	31.99	48.04	24.18	1.50	–23.90
December 1995	150.29	23.16	147.27	15.99	1.00	–0.20
December 1998	49.65	23.65	31.03	15.14	1.19	–5.60

5.7.4 Consideration for Lateral Flow

The downstream peak discharge, $Q_d(t_p)$, can be surmised as the contribution of two main elements: (a) the upstream discharge delayed for the wave travel time T_L, $Q_u(t_p - T_L)$, with its attenuation caused by flood routing along the reach of length L; and (b) the lateral inflow, q_pL, during the time interval $(t_p - T_L, t_p)$. Therefore, the following relationship can be assumed for $Q_d(t_p)$ (Moramarco and Singh 2001):

$$Q_d(t_p) = [Q_u(t_p - T_L) - Q^*] + q_pL \tag{5.59}$$

It is clear that equation (5.59) is a simplification but is found suitable for estimating $Q_d(t_p)$. The upstream peak discharge attenuation, Q^*, can be estimated by the Price formula (Price 1973):

$$Q^* = \frac{K}{(L/T_L)^3} Q_u^p \left| \frac{Q_1 + Q_{-1} - 2Q_u^p}{(\Delta t^*)^2} \right| \tag{5.60}$$

where Δt^* is time interval, $K = L/2BS_0$ is the attenuation parameter for peak discharge at the downstream end, and S_0 and B are the bed slope and the mean river width, respectively. The last factor on the right-hand side of equation (5.60) is the curvature at the peak of the upstream hydrograph, Q_u^p; Q_1 and Q_{-1} are the discharges at Δt^* to either side of the peak, with Δt^* equal to one fifth of the time to peak of the inflow hydrograph (Raudkivi 1979). Equation (5.60) yields satisfactory results when the flood hydrograph is sufficiently symmetrical about the peak, and this condition often occurs in natural channels (Raudkivi 1979).

Example 5.11 Compute the upstream peak discharge using the Price formula. Then compute the downstream peak discharge as a sum of two main components.

Solution We are given that $L = 44.61$ km, $B = 35$ m, $S_0 = 0.002$, and $K = L/2BS_0 = 318$. T_L is given in Example 5.9.

Table 5-8 *Computation of upstream and downstream peak discharge using the Price formula.*

	Q_u^p (m^3/s)	Δt^* (hr)	Q_1 (m^3/s)	Q_{-1} (m^3/s)	Q^* (m^3/s)	Q_d (m^3/s)
December 1990	349.17	5.9	371.89	383.08	16.3	423.31
February 1991	276.13	16.2	82.81	211.11	62.4	537.88
January 1994	107.89	6.6	94.81	203.66	19.8	250.99
December 1995	407.08	6.5	351.49	412.48	46.8	371.70
December 1998	62.84	2.6	110.42	119.58	31.7	82.10

Using the Price formula, the upstream peak discharge can be computed as

$$Q^* = \frac{K}{(L/T_L)^3} Q_u^p \left| \frac{Q_1 + Q_{-1} - 2Q_u^p}{(\Delta t^*)^2} \right|$$
$$= \frac{318}{(44.61/2)^3} 349.17 \left| \frac{371.89 + 383.08 - 2 * 349.17}{6^2} \right| = 16.3$$

and using equation (5.59), the downstream peak discharge is

$$Q_d(t_p) = [Q_u(t_p - T_L) - Q^*] + q_p L = [349.2 - 16.3] + 90.41 = 423.31 \text{ m}^3/\text{s}$$

$$Q_d(t_p) = [Q_u(t_p - T_L) - Q^*] + q_p L$$
$$= [349.2 - 16.3] + 90.41 = 423.31 \, m^3/s$$

Computations for other events are shown in Table 5-8.

To estimate $q_p L$, the continuity equation is considered:

$$\frac{\partial Q}{\partial x} + \frac{\partial A}{\partial t} = q \tag{5.61}$$

where q_p is the lateral inflow per unit channel length. Equation (5.61) can be expressed in the characteristic form as

$$\frac{dA}{dt} = q \tag{5.62a}$$

$$\frac{dx}{dt} = c = \frac{\partial Q}{\partial A} \tag{5.62b}$$

where c is the kinematic celerity, the characteristic path in the space-time. Based on the assumption that T_L is the time to match the rising limb, the peak

region of the upstream and downstream dimensionless hydrographs c can be assumed as

$$c = \frac{L}{T_L} \tag{5.63}$$

Therefore, along the characteristic corresponding to the downstream stage peak (Moramarco and Singh 2000), the following relationship holds:

$$\frac{A_D(t_p) - A_U(t_p - T_L)}{T_L} = q_p \tag{5.64}$$

Moramarco and Singh (2001) considered 12 floods for the Tiber River and for the Timia River reach and 8 for the Chiascio River, all in Italy, including the Tiber River reach between the Santa Lucia and Ponte Felcino sections, the Timia River between the Azzano and Cantalupo sections, and the Chiascio River between the Branca and La Chiusa sites. The selected river reaches present very different characteristics, both for the drainage interbasin and for the branch itself. The annual average precipitation is practically invariant for the subtended basins and ranges from 700 to 1,600 mm. Floods are normally caused by widespread precipitation in the form of rain occurring in the November–May period. For these equipped river reaches, flood events with different lateral inflow contributions were selected.

To test the reliability of the discharge estimation method, the discharge hydrographs of all selected events observed at the downstream end of the investigated river reaches were considered as a benchmark. Assuming that the rating curve is unknown at each downstream section, the discharge hydrographs of the selected flood events were estimated starting from the monitored local stages, and the discharges and water levels were sampled at its upstream end, that is, Santa Lucia for the Tiber River, Azzano for the Timia River, and Branca for the Chiascio River.

The flow hydrographs for all events were simulated by the model, and the accuracy did not depend on the magnitude of the contribution of lateral inflows. The α parameter was found to range from 0.62 to 1.55 and was similar to that obtained by the flood events used to test equation (5.54). The absolute percentage error in peak discharge was found not to exceed 10%, except for two events where the error was less than 9%. The percentage error in the time to peak was nonzero for only 2 of the 12 events simulated. The discharge hydrograph shape was well reproduced for all selected events.

The cross-sectional area A may be estimated in three ways:

1. In terms of gauge height:

$$A = a_1(G - b_1)^{c_1} \tag{5.65}$$

where G is the gauge height and a_1, b_1, and c_1 are coefficients. Equation (5.65) is suitable for stable channel beds that are free of scour and deposition.

2. In terms of flow depth on the y-axis:

$$A = a_2(d - b_2)^{c_2} \tag{5.66}$$

where d is the water depth on the y axis and a_2, b_2, and c_2 are coefficients. Equation (5.66) is suitable for erodible channels subject to scour or sediment deposition.

3. In terms of width:

$$A = a_3(Bd - b_3)^{c_3} \tag{5.67}$$

where B is the channel width at the water surface, and a_3, b_3, and c_3 are coefficients. Equation (5.67) is suitable for frequently changing main channels. Parameters a_3, b_3, and c_3 are used to adjust the zero of the staff gauge to low flow. Chiu and Chen (2003) argue that equation (5.67) is superior to equation (5.65) or (5.66).

Example 5.12 Consider a 23-km-long reach of the Tiber River in central Italy between the upstream section at Ponte Felcino and the downstream section at Torgiano. The reach has a slope of 0.0014 and the average width $B = 45\,\text{m}$. The flow cross-sectional area for the upstream section is 2,035 km^2 and for the downstream section is 2,170.2 km^2. Determine flow cross-sectional area in three ways: in terms of (1) gauge height, (2) flow depth, and (3) flow width. Which way yields the cross-sectional area closer to the observed value?

Solution Given that $B = 45\,\text{m}$ and $d = 1.68\,\text{m}$, take $G = 10\,\text{m}$,

- Using equation (5.65), $A = a_1(G - b_1)^{c_1} = 143(10 - 4.3)^{1.52} = 2{,}069\ \text{km}^2$,
- Using equation (5.66), $A = a_2(d - b_2)^{c_2} = 143(1.68 + 1.5)^{2.3} = 2{,}046\ \text{km}^2$, and
- Using equation (5.67), $A = a_3(Bd - b_3)^{c_3} = 151(45 \times 1.68 + 126)^{0.5} = 2{,}144\ \text{km}^2$.

The solution using equation (5.67) is closer to the observation than the solutions from equation (5.65) or (5.66).

5.8 Determination of Flow Depth Distribution

One of the main problems in flow monitoring is the difficulty of carrying out velocity measurements for high stages that are, however, fundamental to achieve a reliable rating curve at a river gauging site. The difficulty in the real world is twofold. First, sampling velocity points in the lower portion of flow area may entail serious dangers for the operator during measurement. Second, there is a need for a rapid and simple measurement method when hydraulic conditions are changing rapidly. Velocity sampling during floods can be achieved by monitoring the maximum flow velocity, u_{max}, which can be easily sampled for high

stages, because its location occurs in the upper portion of the flow area (Moramarco et al. 2004; Fulton and Ostrowski 2008). Additionally, this information can be an index to depth distribution in the cross section. Moramarco et al. (2011) show that there is a strong relationship between mean velocity u_m and mean velocity and that this relationship holds for different river geometric and hydraulic characteristics (Corato et al. 2011; Moramarco et al. 2011). Since monitoring of the maximum velocity, which often coincides with the maximum flow velocity, can be done by using noncontact survey technology as fixed radar sensors or handheld radar units (Lee et al. 2002; Costa et al. 2006; Fulton and Ostrowski 2008; Plant et al. 2009), this relationship has much potential in hydrologic practice.

It is known that the estimation of flood discharge, based on entropy-based velocity profiles, is sensitive to the accuracy in estimating the flow cross-sectional area and the changes occurring therein during floods. During high floods, the geometric characteristics of river sections may change because of sediment deposition and degradation and transport. From the point of view of hydrologic practice, it would be desirable to determine if there exists a nexus between surface-water velocity distribution and water depths in the flow cross-sectional area. The nexus would permit flow monitoring during high floods through the sampling of surface flow velocities from which the cross-sectional geometry of the river site might be determined. Lee et al. (2002) estimated water depths from recorded surface velocities by using a noncontact radar sensor, but their method requires the knowledge of hydraulic quantities, such as energy slope and Manning's roughness. Moramarco et al. (2013) used POME for estimating the PDF of water depth as a function of the cumulative probability distribution function of the surface maximum flow velocity, and the discussion here follows their work.

5.8.1 Probability Distribution of Flow Depth

It is assumed that the flow depth monotonously increases from zero at the banks to a maximum value D in the middle of the channel and the maximum flow velocity is at the water surface denoted as $u_{\max\ S}$. Let the flow depth from the bank be denoted by h where the surface-water velocity is denoted by u_s. It is hypothesized that the probability of flow depth being less than or equal to h is $u_S/u_{\max S}$ so that the cumulative probability distribution (CDF) is

$$F(h) = \frac{u_S}{u_{\max S}} \tag{5.68}$$

The probability density function (PDF) $f(h)$ can be written as

$$f(h) = \frac{dF(h)}{dh} = \frac{dF(h)}{du_S}\frac{du_S}{dh} = \frac{1}{u_{\max S}}\frac{du_S}{dh} \tag{5.69}$$

For deriving $f(h)$, two constraints are considered for simplicity:

$$\int_0^D f(h)dh = 1 \tag{5.70}$$

and

$$\int_0^D hf(h)dh = h_m \tag{5.71}$$

where h_m is the mean flow depth in the river cross section. Maximizing entropy using the method of Lagrange multipliers discussed in the preceding Chapters 2, 3, and 4, the PDF of h is

$$f(h) = \exp(-\lambda_0 - \lambda_1 h) \tag{5.72}$$

where λ_0 and λ_1 are the Lagrange multipliers.

Substitution of equation (5.72) in equation (5.70) yields

$$\exp(\lambda_0) = \frac{1}{\lambda_1}[1 - \exp(-\lambda_1 D)] \tag{5.73}$$

It can be shown that

$$h_m = \frac{D\exp(-\lambda_1 D)}{\exp(-\lambda_1 D) - 1} + \frac{1}{\lambda_1} \tag{5.74}$$

5.8.2 Depth Distribution

Using equation (5.72) in equation (5.69), the result is

$$\frac{dh}{du_S} = \frac{1 - \exp(-\lambda_1 D)}{\lambda_1 \exp(-\lambda_1 h) u_{\max S}} \tag{5.75}$$

Integrating equation (5.75) between [0, D] for h and [0, $u_{\max\ S}$] for u, one obtains

$$h = \frac{1}{\lambda_1} \ln\left[\frac{\exp(-\lambda_1 D) - 1}{u_{\max S}} u_S + 1\right]^{-1} \tag{5.76}$$

Denoting $W = \lambda_1 D$, which can be considered anentropy flow depth parameter, equation (5.76) becomes

$$h(x) = \frac{D}{W} \ln\left[\frac{\exp(-\lambda_1 D) - 1}{u_{\max S}} u_S(x) + 1\right]^{-1} \tag{5.77}$$

which represents an entropy-based flow depth distribution in natural channels, where W is a parameter and x is the left and right horizontal distance from the y-axis ($x = 0$). Equation (5.77) is similar in form to that obtained by Chiu (1988) for the flow velocity profile along the y-axis for a wide channel. Therefore, if the surface velocity distribution is known, it is possible to have information about the cross-sectional bathymetry by using equation (5.77), which allows for estimating the flow depth distribution across the river site.

An important insight can be obtained from equation (5.74), i.e., the relationship between D and h_m:

$$\frac{h_m}{D} = \frac{\exp(-W)}{\exp(-W)-1} - \frac{1}{W} = \theta(W) \tag{5.78}$$

The cross-sectional flow area, A, can be computed by integrating equation (5.77) along the river cross section. For a speedy estimation of the flow area, the following relationship can be applied:

$$A = h_m w_T = \theta(W) D w_T \tag{5.79}$$

where w_T is the top channel width.

Equation (5.78) shows that observations of (H_m, D) allow us to determine $\theta(W)$ and, hence, the flow depth entropy parameter W. For estimation of $\theta(W)$, equation (5.77) can be integrated across the whole flow area. For ease of practical applications, integration can be done in discrete form as

$$\begin{aligned} h_m &= \frac{1}{w_T}\int_0^{w_T} \frac{D}{W}\ln\left[\frac{\exp(-W)-1}{u_{\max S}}u_S(x)+1\right]^{-1} \\ &= \frac{D}{w_T W}\sum_{j=1}^{N}\ln\left[\frac{\exp(-W)-1}{u_{\max S}}+1\right]_j^{-1}\Delta x_j \end{aligned} \tag{5.80}$$

Coupling equation (5.78) and equation (5.80), a little algebraic manipulations yields

$$\begin{aligned} \frac{1}{w_T W}\sum_{j=1}^{N}\ln\left[\frac{\exp(-W)-1}{u_{\max S}}+1\right]_j^{-1}\Delta x_j &= [\theta(W)]^{-1} \\ &= \left[\frac{\exp(-W)}{\exp(-W)-1}+\frac{1}{W}\right]^{-1} \end{aligned} \tag{5.81}$$

which can be evaluated numerically, once all water-surface velocities are known. If the channel width, w_T, can be directly measured or obtained from satellite imagery (Bjerklie et al. 2005), no assumption about channel geometry is necessary for estimating $\theta(W)$.

To significantly reduce the sampling period during measurement, Moramarco et al. (2011) assumed that the use of equation (5.77) requires only sampling of the maximum surface velocity point, $u_{\max\ S}$, and approximated the behavior of the maximum velocity by representing the cross-sectional flow area by an elliptical or parabolic profile shape:

$$u_S(x) = u_{\max S}\left[1-\left(\frac{x}{x_S}\right)^2\right]^{\alpha} \text{ with } \begin{cases} \alpha = 1 & \textit{parabolic} \\ \alpha = 0.5 & \textit{elliptic} \end{cases} \tag{5.82}$$

where $x_S = x_{LS}$ or $x_S = x_{RS}$ represents the distance from the left or right sidewall of the vertical, respectively, with reference to the y-axis ($x = 0$), along which the maximum surface velocity, $u_{\max\ S}$, is sampled. As shown by Moramarco et al.

(2011), the parabolic profile should be used for narrow river sections. This configuration results from Chezy's formula, wherein it is assumed that the friction slope remains constant over all vertical subsections in which the overall section is divided (Chow 1959). Therefore, surmising that the relation between mean velocities of subsections is the same, one gets $(u_S / u_{\max}) = \sqrt{h/D}$. Considering equation (5.82), the depth distribution implicitly assumed is a power-law relation:

$$\frac{h}{D} = 1 - \left|\frac{x}{x_S}\right|^b \tag{5.83}$$

with $b = 2$. It is noted that equation (5.83) is similar to the power law relation for channel cross sections proposed by Dingman and Bjerklei (2006) for hydrological applications of remote sensing, i.e.,

$$\frac{h}{D} = 1 - Y^* \left|\frac{x}{w_T^* / 2}\right|^b \tag{5.84}$$

where the bank at full width, w_T^*, and the corresponding maximum depth, Y^*, are considered along with exponent b, which might also assume values as high as 5 for some cases. With the use of equation (5.78), exponent b in equation (5.83) as well as in the power law relation of channel cross section in equation (5.84) can be expressed in terms of $\theta(W)$ as

$$b = \frac{\theta(W)}{1 - \theta(W)} \tag{5.85}$$

5.8.3 Discharge Estimation

It was shown in the preceding section that the mean flow velocity, u_m, can be estimated by sampling the maximum velocity, $u_{\max}$, using a linear entropic relationship. Therefore, discharge, Q, can be estimated by the product $u_m A$, with A estimated by integrating equation (5.77) along the river cross section.

5.9 Determination of Entropy Parameter from Hydraulic and Geometric Characteristics

It was shown in Chapter 2 that there exists a linear relationship between mean flow velocity and maximum velocity through what is termed an entropic parameter M. As shown in the preceding sections, parameter M represents an intrinsic river characteristic and is used in a number of hydraulic applications. Therefore, the knowledge of M can be fundamental to overcoming the problem of making velocity measurements during high floods. Moramarco and Singh (2010) investigated the entropic linear relation by expressing the M value in terms of hydraulic and geometric characteristics, and the discussion here is based on their work.

The relation between mean velocity, u_m or $\bar{u}$, and maximum velocity, u_{max}, sampled at a river cross section is given by equation (5.45):

$$\phi(M) = \frac{\bar{u}}{u_{max}} \tag{5.86}$$

Equation (5.86) shows that u_m and u_{max} together can determine $\phi(M)$ and then the entropy parameter M. To determine the dependence of $\phi(M)$ and, hence, of M on hydraulic and geometric characteristics, $\bar{u}$ and u_{max} should be expressed through these characteristics. The mean velocity $\bar{u}$ can be expressed using Manning's equation as

$$\bar{u} = \frac{1}{n} R^{2/3} \sqrt{S_f} \tag{5.87}$$

where n is the Manning roughness, R is the hydraulic radius, and S_f is the energy slope.

To determine u_{max} along the y-axis, the dip-modified logarithmic law for the velocity distribution in smooth, uniform, open-channel flow, proposed by Yang et al. (2004), is considered. Whatever the velocity distribution to be applied for the analysis proposed here, the choice of the distribution should be based both on its simplicity in application and its ability to take account of the likelihood that u_{max} may occur below the water surface. The distribution used here is based on two logarithmic depths, one from the bed, $\ln(y/y_0)$, and the other one from the water surface, $\ln(1 - y/D)$:

$$u(y) = u^* \left[\frac{1}{k} \ln \frac{y}{y_0} + \frac{\alpha}{k} \ln\left(1 - \frac{y}{D}\right) \right] \tag{5.88}$$

where y is the distance from the bottom; u^* is the shear velocity, $u^* = (gRS_f)^{0.5}$ (g is the gravitation acceleration, R is the hydraulic radius, and S_f is the energy slope); k is the von Karman constant, whose value is typically 0.41; α (dimensionless) is the dip-correction factor, depending only on the relative distance of the maximum velocity location from the river bottom, y_{max}, to the water depth, D, along the y-axis where u_{max} is sampled; and y_0 represents the location where the log velocity profile predicts the zero-velocity.

To obtain a formulation for u_{max}, equation (5.88) is differentiated with respect to y and the derivative is equated to 0, $\left.\frac{du}{dy}\right|_{u=u_{max}} = 0$, thus obtaining for the y-axis

$$\left.\frac{du}{dy}\right|_{u=u_{max}} = \frac{u^*}{k}\left(\frac{1}{y} - \frac{\alpha}{D-y}\right) = 0 \tag{5.89}$$

Equation (5.89) yields the location from the bottom where the maximum velocity occurs, y_{max}, as

$$y_{max} = \frac{D}{1+\alpha} \tag{5.90}$$

Substitution of equation (5.90) in equation (5.88) and a little algebraic manipulation yields an expression for the maximum flow velocity as

$$u_{\max} = \frac{u^*}{k}\ln\left(\frac{D}{y_0(1+\alpha)}\right) + \frac{\alpha}{k}u^*\ln\left(1-\frac{1}{1+\alpha}\right) \tag{5.91}$$

Now inserting equations (5.87) and (5.91) in equation (5.88), $\phi(M)$ can be expressed in terms of hydraulic and geometric characteristics of a river site as

$$\begin{aligned}\phi(M) &= \frac{\frac{1}{n}R^{2/3}\sqrt{S_f}}{\frac{\sqrt{gRS_f}}{k}\left[\ln\left(\frac{D}{y_0(1+\alpha)}\right)+\alpha\ln\left(1-\frac{1}{1+\alpha}\right)\right]} \\ &= \frac{\frac{1}{n}R^{1/6}/\sqrt{g}}{\frac{1}{k}\left[\ln\left(\frac{D}{y_0(1+\alpha)}\right)+\alpha\ln\left(1-\frac{1}{a+\alpha}\right)\right]}\end{aligned} \tag{5.92}$$

Equation (5.92) shows that $\phi(M)$ is independent of the flood dynamic represented by the energy slope, S_f. This observation may be the key to the understanding why $\phi(M)$ is always found more or less constant at gauged river sites. That is, whatever the flood condition (kinematic, diffusive, or dynamic) happening along the river, it does not seem to influence $\phi(M)$.

From equation (5.88), α can be expressed as

$$\alpha = \frac{D - y_{\max}}{y_{\max}} = \frac{h_a}{y_{\max}} \tag{5.93}$$

which is the ratio of two depths, with h_a representing the location of $u_{\max}$ below the water surface. Introducing equation (5.93) in equation (5.92), one gets

$$\phi(M) = \left(\frac{e^M}{e^M-1}-\frac{1}{M}\right) = \frac{\frac{1}{n}R^{1/6}\Big/\sqrt{g}}{\frac{1}{k}\left[\ln\left(\frac{y_{\max}}{y_0}\right)+\frac{h}{y_{\max}}\ln\left(\frac{h}{D}\right)\right]} \tag{5.94}$$

For large rivers, $u_{\max}$ can be assumed to occur at the water surface, $h_a = 0$, or just below it. Then, equation (5.94) becomes

$$\phi(M) = \left(\frac{e^M}{e^M-1}-\frac{1}{M}\right) = \frac{\frac{1}{n}R^{1/6}\Big/\sqrt{g}}{\frac{1}{k}\left[\ln\left(\frac{y_{\max}}{y_0}\right)\right]} \tag{5.95}$$

Depending on the location of $u_{\max}$, equation (5.94) or (5.95) expresses a direct relationship between the entropic parameter M and the hydraulic and geometric

characteristics of the river section. A similar expression can be obtained if $\overline{u}$ is expressed by Chezy's equation in that the term $R^{1/6}/n$ is replaced by Chezy's coefficient, C.

Questions

Q5.1 Determine the frequency of sampling velocity at a distance from the bed equal to 0.1, 0.2, 0.3, 0.4, 0.5, 0.6, 0.7, 0.8, 0.9, and 1.0 times flow depth. Assume that the channel flow is 2.5 m deep.

Q5.2 For a given set of flow measurements given in Table 5-9, determine the Lagrange multipliers λ_1 and λ_2 appearing in the velocity equation and then determine the entropy of velocity.

Q5.3 For a specified value of u^*, determine $H(u/u^*)$.

Q5.4 For M = 4, 6, 8, and 10, determine the energy distribution coefficient α and the momentum distribution coefficient β.

Q5.5 For a given Q, determine S_w and S_f.

Q5.6 For a given Q, S_w, and S_f, determine $d\alpha/dx$.

Table 5-9 *Velocity data from experiment.*

y (ft)	u (ft/s)	y (ft)	u (ft)
0.003	2.471	0.038	4.485
0.004	2.457	0.046	4.746
0.005	2.925	0.056	4.834
0.006	2.869	0.066	5.113
0.008	3.270	0.045	5.113
0.010	3.427	0.076	5.113
0.013	3.699	0.091	5.479
0.016	3.884	0.106	5.514
0.020	4.066	0.126	5.835
0.025	4.212	0.151	5.849
0.030	4.415	0.176	6.073

Source: Data from Einstein and Chien 1955.

Q5.7 Determine τ_0 as a function of D for a given S_f.

Q5.8 Determine τ as a function of r for given τ_0, r_0, and r_{max}.

Q5.9 For given discharge measurements, plot u_m and u_{max} and determine M.

References

Bjerklie, D. M., Moller, D., Smith, L., and Dingman, L. S. (2005). "Estimating discharge in rivers using remotely sensed hydraulic information." *J. Hydrol.*, 309, 191–209.

Bridge, J. S., and Jarvis, J. (1985). "*Flow and sediment transport data, River South Esk, Glen Glova, Scotland*." Report, Department of Geological Sciences, State University of New York, Binghampton.

Chiu, C.-L. (1987). "Entropy and probability concepts in hydraulics." *J. Hydraul. Eng.*, 113(5), 583–600.

Chiu, C.-L. (1988). Entropy and 2-D velocity distribution in open channels. *J. Hydraul. Eng.*, 114(7), 738–756.

Chiu, C.-L. (1991). "Application of entropy concept in open-channel flow study." *J. Hydraul. Eng.*, 117(5), 615–628.

Chiu, C.-L., and Chen, Y.-C. (2003). "An efficient method of discharge estimation based on probability concept." *J. Hydraul. Res.*, 41(6), 589–596.

Chiu, C.-L., Hsu, S. M., and Tung, N.-C. (2005). "Efficient methods of discharge measurements in rivers and streams based on the probability concept." *Hydrol. Proc.*, 19, 3935–3946.

Chiu, C.-L., and Murray, D. W. (1992). "Variation of velocity distribution along nonuniform open channel flow." *J. Hydraul. Eng.*, 118(7), 989–1001.

Chiu, C.-L., and Said, C. A. A. (1995). "Maximum and mean velocities and entropy in open-channel flow. *J. Hydraul. Eng.*, 121(1), 26–35.

Chiu, C.-L., and Tung, N.-C. (2002). "Maximum velocity and regularities in open-channel flow." *J. Hydraul. Eng.*, 128(4), 390–398.

Chow, V. T. (1959). *Open channel hydraulics*, McGraw-Hill, New York.

Corato, G., Moramarco, T., and Tucciarelli, T. (2011). "Discharge estimation combining flow routing and occasional measurements of velocity." *Hydrol. Earth Sys. Sci.*, 15, 2979–2994.

Costa, J. E., Cheng, R. T., Haeni, F. P., Melcher, N., Spicer, K. R., Hayes, E., Plant, W. J., Hayes, K., Teague, C., and Barrick, D. (2006). "Use of radars to monitor stream discharge by noncontact methods." *Water Resour. Res.*, 42, W07422, doi:10.1029/2005WR004430.

Dingman, S. L., and Bjerklie, D. M. (2006). "Hydrological application of remote sensing: Surface fluxes and other derived variables-river discharge." *Encyclopedia of hydrological sciences.* Wiley, New York.

Einstein, H. A., and Chien, N. (1955), "Effects of heavy sediment concentration near the bed on velocity and sediment distribution," Report No. 8, M.R.D. Sediment Series, U.S. Army Corps of Engineers, Omaha, NE.

Fulton, J., and Ostrowski, J. (2008). "Measuring real-time streamflow using emerging technologies: Radar, hydroacoustics and the probability concepts." *J. Hydrol.*, 357, 1–10.

Herschy, R. W. (1985). *Streamflow measurement*, Elsevier, London.

Lee, M. C., Lai, C. J., Leu, J. M., Plant, W. J., Keller, W. C., and Hayes, K. (2002). "Non-contact flood discharge measurements using an X-band pulse radar (I) theory." *Flow Meas. Instr.*, 13, 265–270.

Leopold, L. B., Wolman, M. G., and Miller, J. P. (1995). *Fluvial processes in geomorphology*, Dover, New York.

Moramarco, T., Corato, G., Melone, F., and Singh, V. P. (2013). "An entropy-based method for determining the flow depth distribution in natural channels." *J. Hydrol.*, 497, 176–188.

Moramarco, T., Saltalippi, C., and Singh, V. P. (2004). "Estimation of mean velocity in natural channels based on Chiu's velocity distribution." *J. Hydrol. Eng.*, 9(1), 42–50.

Moramarco, T., Saltalippi, C., and Singh, V. P. (2011). "Velocity profiles assessment in natural channel during high floods." *Hydrol. Res.*, 42, 162–170.

Moramarco, T., and Singh, V. P. (2000). "A practical method for analysis or river waves and for kinematic wave routing in natural channel networks." *Hydrol. Proc.*, 14, 51–62.

Moramarco, T., and Singh, V. P. (2001). "Simple method for relating local stage and remote discharge." *J. Hydrol. Eng.*, 6(1), 78–81.

Moramarco, T., and Singh, V. P. (2010). "A formulation of the entropy parameter based on hydraulic and geometric characteristics of river cross sections." *J. Hydrol. Eng.*, 15(10), 852-858.

Plant, W. J., Branch, R., Chatham, G., Chickadel, C. C., Hayes, K., Hayworth, B., Horner-Devine, A., Jessup, A., Fong, D. A., Fringer, O. B., Giddings, S. N., Monismith, S., and Wang, B. (2009). "Remotely sensed river surface features compared with modeling and in situ measurements." *J. Geophys. Res.*, 114, C11002.

Price, R. K. (1973). "Flood routing methods for British rivers." *Proc., Inst. Civil Eng.*, 55(12), 913–930.

Raudkivi, A. J. (1979). *Hydrology: An advanced introduction to hydrological processes and modeling*, Pergamon Press, New York.

U.S. Army Corps of Engineers. (1995). *Flow transitions in bridge backwater analysis*, RD-42, Hydraulic Engineering Center, Davis, CA.

U.S. Army Corps of Engineers. (2001). *HEC-RAS, River analysis system, hydraulic reference manual*, CPD-69, Hydraulic Engineering Center, Davis, CA.

Xia, R. (1997). "Relation between mean and maximum velocities in a natural river." *J. Hydraul. Eng.*, 123(8), 720–723.

Yang, S. Q., Tan, S. K., and Lim, S. Y. (2004). "Velocity distribution and dip-phenomenon in smooth uniform open channel flows." *J. Hydraul. Eng.*, 130(12), 1179–1186.

Additional Reading

Chiu, C.-L., and Chiou, J.-D. (1986).” Structure of 3-D flow in rectangular open channels.” *J. Hydraul. Eng.*, 112(11), 1050–1068.

Chiu, C.-L., Jin, W., and Chen, Y.-C. (2000). “Mathematical models of distribution of sediment concentration.” *J. Hydraul. Eng.*, 126(1), 16–23.

Choo, T. H. (2000). “An efficient method of the suspended sediment-discharge measurement using entropy concept.” *Water Eng. Res.*, 1(2), 95–105.

Vanoni, V. A. (1975). *Sedimentation engineering*, ASCE Press, New York.

This page intentionally left blank

Chapter 6

Velocity Distribution in Pipe Flow

Full flow in pipes is treated differently from flow in open channels because of the absence of a free water surface in full pipe flows. Pipes are usually circular, and, hence, their geometry is analytically expressed in simple form. Pipes are manufactured and are much smoother than natural channels. The flow in pipes is usually axially symmetric. In pipes, the velocity is zero at the pipe wall, and the velocity gradient has a finite value. The maximum velocity u_{max} occurs at the center of pipe, where the velocity gradient is zero. Chapters 2 to 5 discuss velocity distributions in natural channels and their application, and this chapter focuses on velocity distributions in pipes.

6.1 Derivation of Velocity Distribution

After the discussion in Chapter 2 on 1-D velocity distribution and in Chapter 3 on 2-D velocity distribution in open channel flow, the velocity (u) distribution in pipe flow can be described in a similar manner. Let ξ denote the distance from the wall, ξ_0 the distance from the boundary where u is minimum = 0, and ξ_{max} the distance from the boundary where u is maximum = u_{max}. It is assumed that the time-averaged velocity is a random variable. Then, the cumulative probability distribution (CDF) of velocity (i.e., the probability of velocity being less than or equal to a given value of u), $F(u)$, can be expressed (Chiu et al. 1993) as

$$F(u) = \frac{\xi - \xi_0}{\xi_{\max} - \xi_0} = \int_0^u f(u)du \tag{6.1}$$

and the probability density function (PDF) of u, $f(u)$, as

$$f(u) = \frac{\left(\frac{du}{d\xi}\right)^{-1}}{\xi_{\max} - \xi_0} \tag{6.2}$$

Thus, u ($0 \le u \le u_{\max}$) monotonically increases with ξ ($0 \le \xi_0 \le \xi_{\max}$), which is a dimensionless independent variable—a function of cylindrical or Cartesian coordinates in the physical plane.

The Shannon entropy of the PDF of u can be expressed as

$$H(u) = -\int_0^{u_{\max}} f(u)\ln f(u)du \tag{6.3}$$

To derive $f(u)$ using the principle of maximum entropy (POME), one maximizes entropy $H(u)$ subject to specified constraints. The first constraint is taken as the total probability:

$$\int_0^{u_{\max}} f(u)du = 1 \tag{6.4}$$

and the second constraint is based on mass conservation:

$$\int_0^{u_{\max}} uf(u)du = \overline{u} = u_m \tag{6.5}$$

where $\overline{u}$ or u_m is the cross section mean velocity defined as Q/A, Q is the discharge, and A is the cross-sectional area.

Maximization of entropy given by equation (6.3), subject to equations (6.4) and (6.5), using the method of Lagrange multipliers, results in $f(u)$:

$$f(u) = \exp[\lambda_1 - 1 + \lambda_2 u] \tag{6.6a}$$

where λ_1 and λ_2 are the Lagrange multipliers. The CDF of u becomes

$$F(u) = \frac{1}{\lambda_2}\exp(\lambda_1 - 1)[\exp(\lambda_2 u) - 1] \tag{6.6b}$$

Following the discussion in Chapter 3, the Lagrange multipliers are defined as

$$\exp(\lambda_1 - 1) = \lambda_2[\exp(\lambda_2 u_{\max}) - 1]^{-1} \tag{6.7a}$$

and

$$u_m = u_{\max}\exp(\lambda_2 u_{\max})[\exp(\lambda_2 u_{\max})-1]^{-1} - \frac{1}{\lambda_2} \tag{6.7b}$$

where u_m is the mean velocity. Defining $M = \lambda_2 u_{\max}$, which is called the entropy number, and coupling equation (6.6a) with equation (6.2), the velocity distribution is obtained as

$$\frac{u}{u_{\max}} = \frac{1}{M}\ln\left\{1+[\exp(M)-1]\frac{\xi-\xi_0}{\xi_{\max}-\xi_0}\right\} \tag{6.7c}$$

Equation (6.7c) is a 2-D velocity distribution equation.

The quantity $f(u)du$ defines the probability of velocity being between u and $u + du$, which can be obtained from velocity measurements. If ξ is generated by random sampling and then substituted in equation (6.7c), then values of u can be obtained for determining $f(u)du$. It should be noted that equation (6.6a) is an exponential PDF of u within the range $(0, u_{\max})$, whereas equation (6.1) relates to the uniform PDF of ξ in the range $(\xi_0, \xi_{\max})$. Equation (6.1), with the value of $(\xi - \xi_0)/(\xi_{\max} - \xi_0)$, gives the probability of velocity as equal to or less than u. Thus, it can guide in the selection of a suitable expression for ξ to fit a particular flow system. In pipe flow, isovels are concentric circles. Therefore, ξ should be

$$\xi = \frac{\pi R^2 - \pi r^2}{\pi R^2} = 1 - \left(\frac{r}{R}\right)^2 \tag{6.8}$$

where r is the radial distance from the center of the pipe cross section, and R is the radius of the pipe. Therefore, it is hypothesized that the CDF of u in pipe flow can be expressed as

$$F(u) = 1 - \left(\frac{r}{R}\right)^2 \tag{6.9}$$

and

$$f(u)du = -\frac{2r}{R^2}dr \tag{6.10}$$

Combining equation (6.8) with equation (6.7c), the velocity distribution becomes

$$u = \frac{u_{\max}}{M}\ln\left\{1+[\exp(M)-1]\left[1-\left(\frac{r}{R}\right)^2\right]\right\} \tag{6.11}$$

Equation (6.11) is the velocity distribution for flow in circular pipes.

Equation (6.8) is the ratio of area in which velocity is equal to or less than $u(\xi)$ to the total area of the pipe cross section, and defines the ξ-coordinate in terms of the r-coordinate. With $\xi_0 = 0$ and $\xi_{\max} = 1$, equation (6.7c) yields u at the wall ($\xi = 0$) or $r = R$ as $u = 0$. Thus, it satisfies this boundary condition.

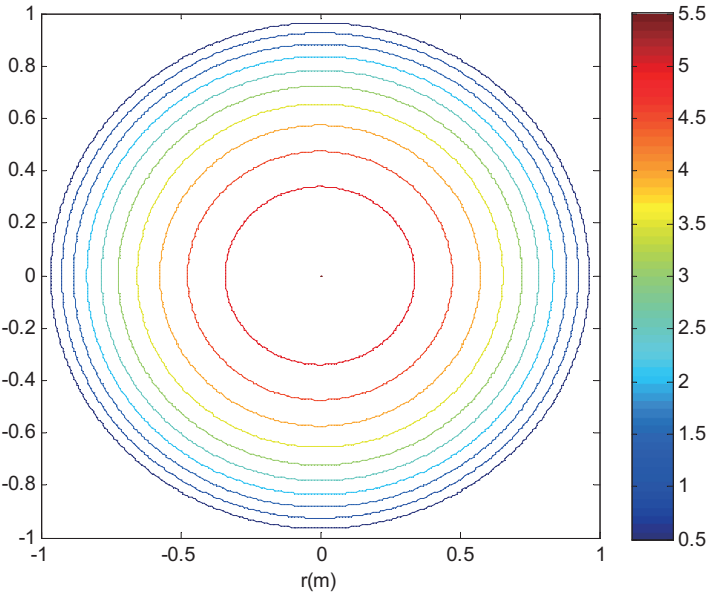

Figure 6-1 *Isovels of flow in a pipe.*

Example 6.1 Construct isovels for flow in a pipe, taking $R = 1\,\text{m}$, maximum velocity $u_{\max} = 5.5\,\text{m/s}$, and mean velocity $u_m = 3\,\text{m/s}$.

Solution For given values of mean and maximum velocities, $M(\lambda_2 u_{\max})$ can be solved for equation (6.7b): $M = 0.548$. Using equation (6.11), u is computed for each value of r. As shown in Fig. 6-1, isovels are circular.

Example 6.2 Take different values of r and compute probabilities of corresponding velocities.

Solution Assume that $R = 1$, and let r change from 0 to 1. Then, $f(u)$ can be computed from equation (6.10) as

$$f(u)du = -\frac{2r}{R^2}dr$$

with the results shown in Table 6-1.

Differentiating equation (6.7c) with respect to ξ, one gets

$$\frac{du}{d\xi} = \frac{u_{\max}}{M}\left\{1 + [\exp(M) - 1]\frac{\xi - \xi_0}{\xi_m - \xi_0}\right\}^{-1}\frac{[\exp(M) - 1]}{\xi_{\max} - \xi_0} \tag{6.12}$$

Table 6-1 *Computed probabilities of corresponding velocities for Example 6.2.*

r	f(u)	r	f(u)
0	0	0.5	1
0.1	0.2	0.6	1.2
0.2	0.4	0.7	1.4
0.3	0.6	0.8	1.6
0.4	0.8	0.9	1.8
		1	2

or

$$\frac{du}{dr} = -\frac{u_{\max}}{M} \frac{\frac{2r}{R^2}[\exp(M)-1]}{1+[\exp(M)-1]\left[\left[1-\left(\frac{r}{R}\right)^2\right]\right.} \tag{6.13}$$

Now, using $\xi_0 = 0$ and ξ_{max}, $du/d\xi$ at $\xi = 1(r = 0)$ yields $du/d\xi = 0$. Thus, equation (6.12) satisfies both boundary conditions. Equation (6.13) shows that $du/dr = 0$ at $r = 0$. At $r = R$ (pipe wall), Equation (6.8) shows that ξ varies with $1 - (r/R)^2$, not $1 - (r/R)$. Hence, the velocity in pipe flow of axial symmetry given by equation (6.7c) varies with $1 - (r/R)^2$. This is seen from Figs. 6-2 and 6-3. At the wall, $r = R$, equation (6.13) becomes

$$\left(\frac{du}{dr}\right)\Big|_{r=R} = -\frac{2u_{\max}[\exp(M)-1]}{MR} \tag{6.14}$$

which is finite. Applying L'Hospital's rule, M approaches 0, equation (6.13) becomes $-2u_{max}r/R^2$, and equation (6.14) becomes $-2u_{max}/R$.

With the use of equations (6.7a) and (6.7b), equation (6.6a) can be written as

$$f(u) = \frac{M}{u_{\max}[\exp(M)-1]} \exp\left[M\frac{u}{u_{\max}}\right], \quad 0 \le u \le u_{\max} \tag{6.15}$$

The mean velocity u_m can be written as

$$\frac{u_m}{u_{\max}} = \frac{\exp(M)}{\exp(M)-1} - \frac{1}{M} \tag{6.16}$$

Fig. 6-3 plots u/u_{max} versus $1 - (r/R)$ for various values of M (0, 2, 4, 6, 8, and 10).

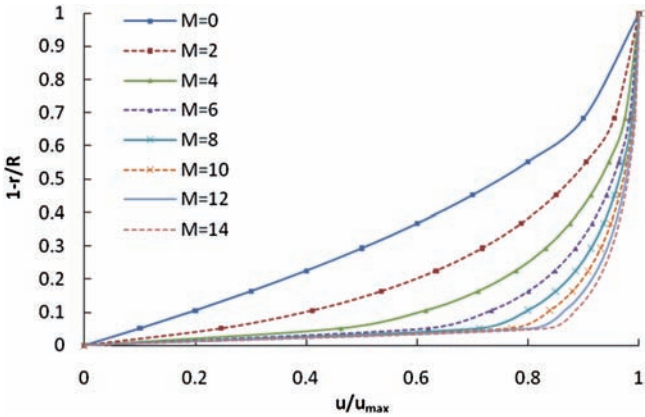

Figure 6-2 *Velocity distribution* u/u_{max} *versus* $1 - (r/R)$ *in a physical plane for* $M = 0, 2, 4, 6, 8, 10, 12,$ *and* 14.

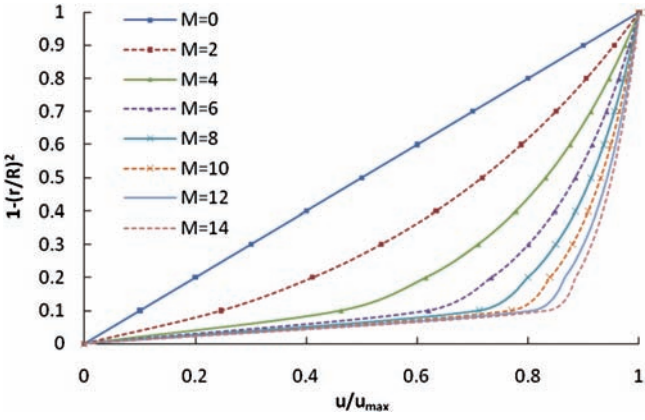

Figure 6-3 *Velocity distribution* u/u_{max} *versus* $\xi\,(1 - (r/R)^2)$ *in a physical plane for* $M = 0, 2, 4, 6, 8, 10, 12,$ *and* 14.

6.2 Comparison with Prandtl–von Karman Velocity Distribution

The Prandtl–von Karman universal velocity distribution in pipe flow of axial symmetry can be expressed as

$$\frac{u_{\max} - u}{u^*} = -\frac{1}{k}\ln\left(1 - \frac{r}{R}\right) \tag{6.17}$$

where u^* is the shear velocity, and k is the von Karman constant (0.4). Equation (6.17) does not fulfill the condition that $u = 0$ at $r = R$, indicating that it is not

valid at or near the wall. Furthermore, differentiating equation (6.17) with respect to r, one gets

$$\frac{du}{dr} = \frac{u^*}{k} \frac{\frac{1}{R}}{\left(1 - \frac{r}{R}\right)} = \frac{u^*}{k} \frac{1}{(R - r)} \tag{6.18}$$

Equation (6.18) shows that du/dr is not equal to 0 when $r = 0$ and does not fulfill this boundary condition either. This situation means that this equation is not accurate at the pipe center either.

Equation (6.17) does not apply at walls ($r = R$). This phenomenon may be true because the velocity is assumed to vary with distance ratio r/R, but in the entropy-based formulation, the velocity varies with the area ratio $(r/R)^2$. Applying L'Hospital's rule to equations (6.13) and (6.14) at $M = 0$, one obtains du/dr is $-2u_{max}/R$ at $r = R$, respectively. Also, from equation (6.11), one gets

$$u = u_{max}\left[1 - \left(\frac{r}{R}\right)^2\right] \tag{6.19}$$

Thus, equation (6.19) shows that the velocity in pipe is maximum when $r = 0$, that is, at the center, and decreases from this maximum value, reaching zero at the boundary, that is, $r = R$.

Example 6.3 Calculate and plot du/dr as a function of r/R. What do you conclude from this graph?

Solution Equation (6.13) states the relationship between du/dr and r/R. Assume that $R = 1$ m, and $u_{max} = 1$ m/s. Thus, du/dr can be computed from equation (6.13) for different M values. A plot du/dr as a function of r/R is shown in Fig. 6-4.

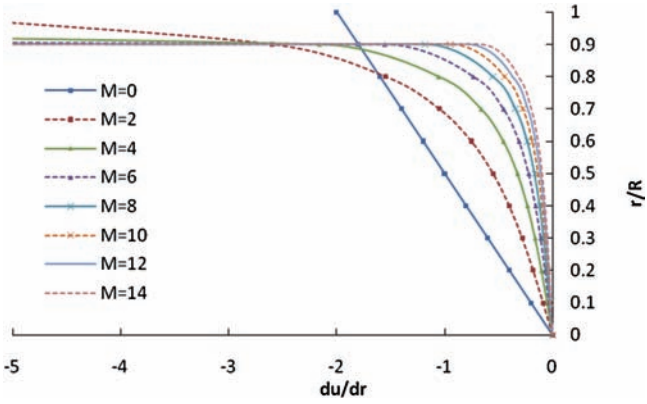

Figure 6-4 *Plot of* du/dr *as a function of* r/R.

6.3 Darcy–Weisbach Equation

The head loss in pipe flow caused by friction is often evaluated by the Darcy–Weisbach equation:

$$h_f = f_l \frac{L}{D} \frac{u_m^2}{2g} \tag{6.20}$$

where h_f is the head loss caused by friction, f_l is the friction factor, L is the pipe length, D is the pipe diameter, and g is the acceleration caused by gravity. For applying equation (6.20), an estimate of f_l is needed. For smooth pipes, the Moody diagram, as shown in Fig. 6-5, gives a unique relation between f_l and the Reynolds number:

$$N_R = \frac{u_m D}{\upsilon} \tag{6.21}$$

where υ is the kinematic viscosity. For rough pipes,the diagram relates f_l to N_R for each value of the relative roughness k_s/D, k_s = roughness height, as shown in Fig. 6-5. However, tables available for k_s do not encompass the wide range of roughness height values for pipe materials. This lack makes the estimation of f_l and hence h_f by the Moody diagram difficult.

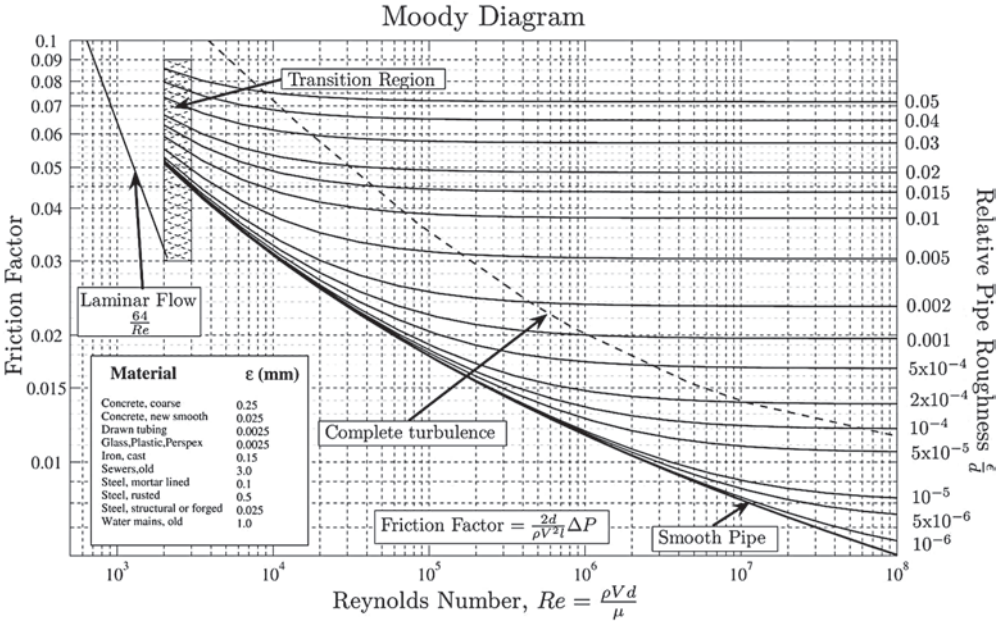

Figure 6-5 *Moody diagram.*
Source: http://en.wikipedia.org/wiki/File:Moody_diagram.jpg (accessed November 13, 2013). Created by S Beck and R Collins, University of Sheffield.

6.4 Head Loss and Friction Factor

Recall that the wall shear can be obtained by equating the sum of pressure and gravity forces to the frictional resistance as

$$\tau_0 = \gamma R_h S_f = \rho u^{*2} = \gamma R_h \frac{h_f}{L}, \quad \gamma = \rho g \tag{6.22}$$

where ρ is the mass density of water, γ is the weight density of water, R_h is the hydraulic radius equal to $D/4$, D is the pipe diameter, u^* is the shear velocity equal to

$$u^* = (gR_h S_f)^{0.5} \tag{6.23}$$

and S_f is the energy gradient expressed as h_f/L. Balancing the shear force with the diffusion of momentum at the pipe wall, one can write

$$\tau_0 = \rho \varepsilon_0 \left(-\frac{du}{dr} \right)\Bigg|_{r=R} \tag{6.24}$$

where ε_0 is the momentum transfer coefficient at the wall, which equals the kinematic viscosity for laminar flow or turbulent flow with a viscous sublayer (i.e., the pipe is hydraulically smooth). If the pipe is rough, then in turbulent flow ε_0 is greater than υ and depends on the pipe roughness and flow turbulence. Using equation (6.14) in equation (6.24), one gets

$$\tau_0 = \rho \varepsilon_0 \frac{2u_{\max}[\exp(M) - 1]}{MR} \tag{6.25}$$

Substituting equation (6.25) in equation (6.22), one obtains the head loss caused by friction over the pipe length as

$$h_f = 32 \frac{[\exp(M) - 1]}{M} \left(\frac{u_m}{u_{\max}} \right)^{-1} \left(\frac{Du_m}{\upsilon} \right)^{-1} \left(\frac{\varepsilon_0}{\upsilon} \right) \left(\frac{L}{D} \right) \frac{u_m^2}{2g} \tag{6.26}$$

Comparing equation (6.26) with equation (6.20), and using equation (6.16), one obtains

$$f_l = 32 \frac{[\exp(M) - 1]}{M} \left(\frac{u_m}{u_{\max}} \right)^{-1} \left(\frac{Du_m}{\upsilon} \right)^{-1} \left(\frac{\varepsilon_0}{\upsilon} \right) = 32 \frac{F_m(M)}{N_R} \left(\frac{\varepsilon_0}{\upsilon} \right) \tag{6.27}$$

where

$$F_m(M) = \frac{\exp(M) - 1}{\dfrac{M \exp(M)}{\exp(M) - 1} - 1} \tag{6.28}$$

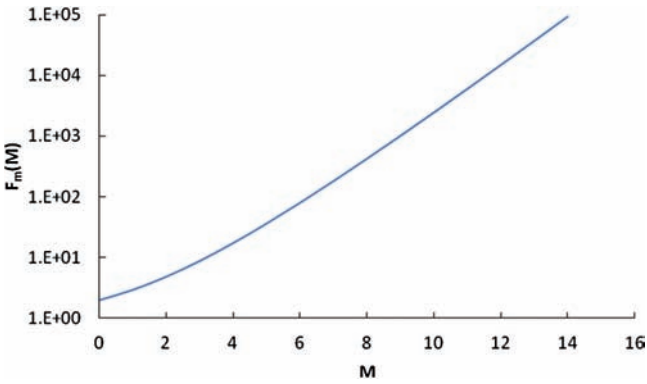

Figure 6-6 $F_m(M)$ *versus* M.

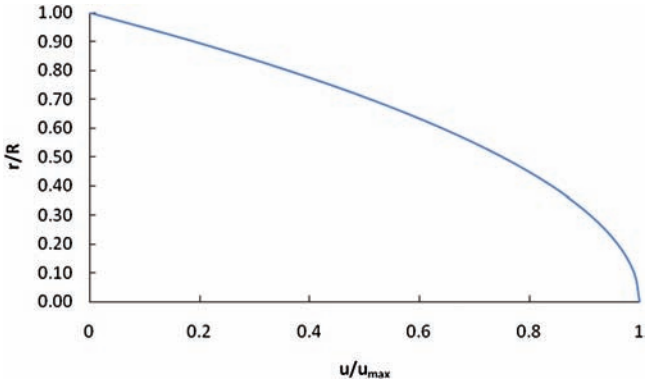

Figure 6-7 u/u_{max} *versus* r/R.

Equation (6.28) shows that $F_m(M)$ increases with M, as shown in Fig. 6-6.

Equation (6.27) yields the friction factor in terms of M, N_R, and (ε_0/υ) for turbulent flow in rough pipes. The entropy parameter is reflective of the velocity patterns and, in turn, of the rates of energy and momentum transport. In flow in smooth pipes, there exists a viscous sublayer at the wall and, hence, $\varepsilon_0 = \upsilon$.

For laminar flow, $\varepsilon_0 = \upsilon$ and $f_l = 64/N_R$; equation (6.27) yields $F_m(M) = 2$ or from equation (6.28), $M = 0$. As M tends to 0, equation (6.16), with the use of L'Hospital's rule, gives $u_{\max} = 2u_m$. Then, equation (6.7c), with ξ defined by equation (6.8), yields

$$\frac{u}{u_{\max}} = 1 - \left(\frac{r}{R}\right)^2 \tag{6.29}$$

which is the same as the parabolic velocity distribution derived by applying the momentum equation to a viscous Newtonian fluid, as shown in Fig. 6-7. Equating equation (6.25) to equation (6.22), one gets

$$u_{\max} = \frac{gS_f R^2}{4\upsilon} \tag{6.30}$$

Equation (6.30) expresses $u_{\max}$ in terms of γ, S_f, and R.

6.5 Relation of Mean Velocity, Maximum Velocity, and Friction Coefficient to *M*

From experimental measurements, Nikuradse (1932) empirically derived

$$\frac{u_m}{u_{\max}} = 1.17\left[1 + 9.02\left(\frac{u_m}{u^*}\right)^{-1}\right]^{-1} \tag{6.31}$$

where the ratio u_m/u^* can be written in terms of friction factor f_l as

$$\frac{u_m}{u^*} = \sqrt{\frac{8}{f_l}} \tag{6.32}$$

Combining equations (6.31) and (6.32), one obtains an expression for the friction factor f_l as

$$f_l = 0.0983\left[1.17\left(\frac{u_m}{u_{\max}}\right)^{-1} - 1\right]^2 \tag{6.33}$$

or

$$f_l = 0.0983\left[\frac{0.17M\exp(M) + \exp(M) - 1.17M - 1}{M\exp(M) - \exp(M) + 1}\right]^2 \tag{6.34}$$

Equation (6.34) is graphed in Fig. 6-8 and shows that f_l decreases as M increases and M is obtained as $u_m/u_{\max}$ from equation (6.33). For a given Q and pipe diameter D, u_m can be obtained. If $u_{\max}$ is measured at the center, M and then f_l can be determined. From equations (6.34) and (6.27), one gets ε_0/υ as

$$\frac{\varepsilon_0}{\upsilon} = 0.00307N_R\frac{1}{F_m(M)}\left[\frac{0.17M\exp(M) + \exp(M) - 1.17M - 1}{M\exp(M) - \exp(M) + 1}\right)\Bigg]^2 \tag{6.35}$$

Equation (6.35) is plotted in Fig. 6-9 for different values of the Reynolds number N_R.

In smooth pipe flow, $\varepsilon_0/\upsilon = 1$. Then equation (6.35) yields a relation between M and N_R as shown in Fig. 6-10. Then equation (6.34) yields a relation between f_l and N_R as shown in Fig. 6-9. Recall Prandtl's relation:

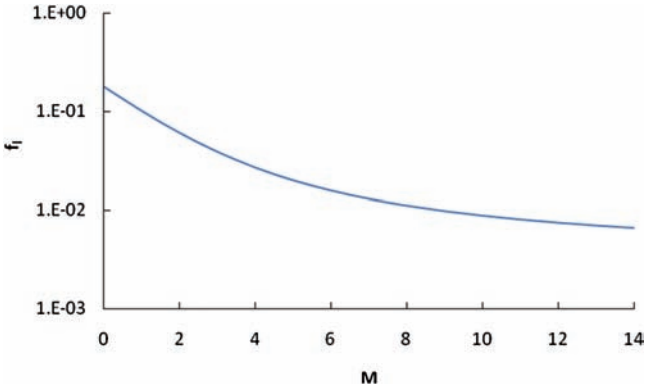

Figure 6-8 f_1 *as a function of* M.

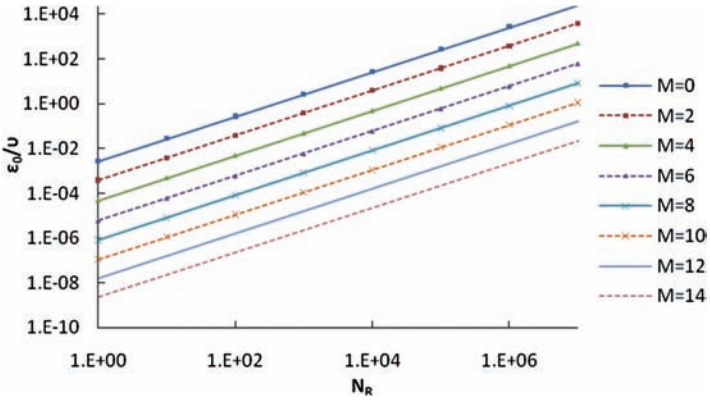

Figure 6-9 ε_0/υ *as function of* N_R *for various values of* M.

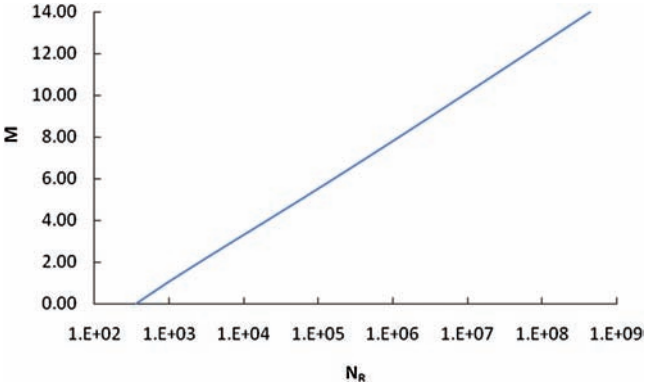

Figure 6-10 *Relation between* M *and* N_R.

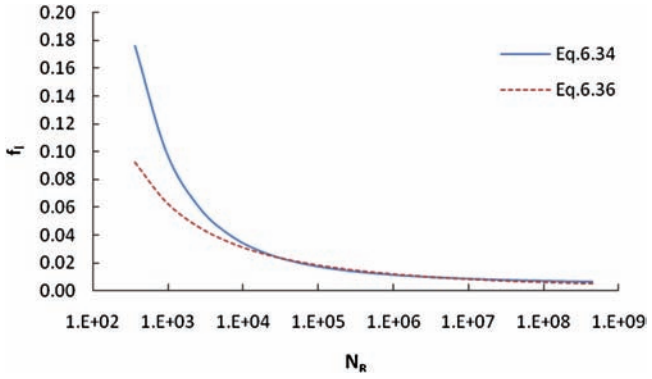

Figure 6-11 *Relation between* f_l *and* N_R.

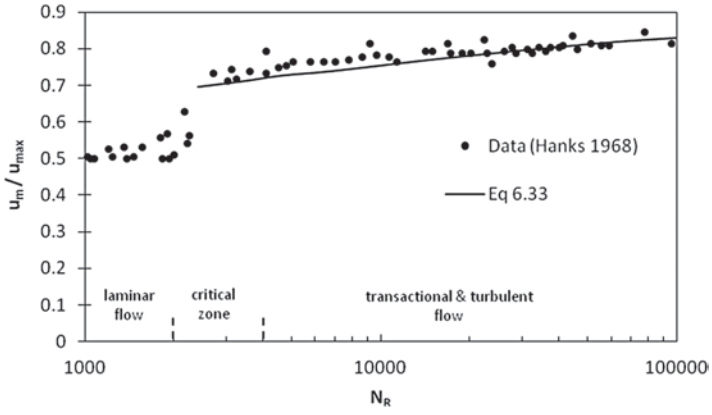

Figure 6-12 *Relation between* u_m/u_{max} *and* N_R.

$$\frac{1}{\sqrt{f_l}} = 2\log(N_R\sqrt{f_l}) - 0.8 \tag{6.36}$$

Equation (6.36) is also plotted in Fig. 6-11. The agreement with f_l obtained from equation (6.29) with ε_0/υ is close.

Conversely, if M is expressed as a function of N_R from equation (6.35), then equation (6.33) yields the relation between $u_m/u_{\max}$ and N_R, as shown in Fig. 6-12. Also plotted in this figure are data from Hanks (1968) indicating a good agreement for flows in turbulent flow. This agreement suggests that for turbulent flow in smooth pipes, M and $u_{\max}$ and, therefore, the velocity distribution can be derived from N_R and Q/A using Figs. 6-11 and 6-12.

For rough pipes, ε_0/υ increases with N_R for a given M value, or decreases with M for a given value of N_R, as shown in Fig. 6-13. Thus, it is essential to determine M for evaluating f_l for a given N_R. One way to accomplish this determination is to measure $u_{\max}$, obtain $u_m = Q/A$, and then determine using equation (6.16).

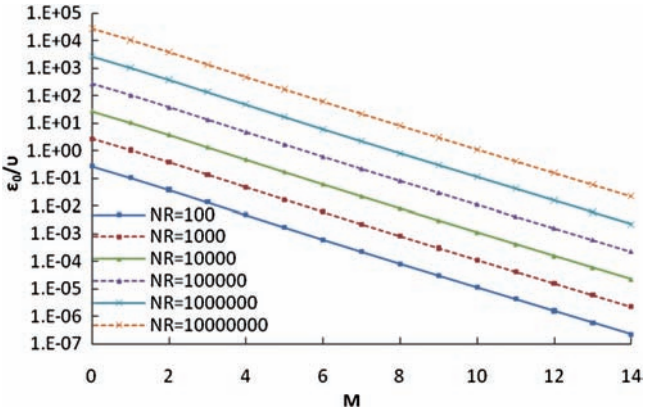

Figure 6-13 ε_0/υ *versus* M *for various values of* N_R.

6.6 Relation of Friction Coefficient, Manning's *n*, and *M*

Equation (6.33) relates f_l to M. This relation means that M can be estimated given f_l, which may be determined using Manning's equation:

$$u_m = \frac{\beta}{n} R_h^{2/3} S_f^{1/2}, \quad R_h = D/4, \quad S_f = h_f / L \tag{6.37}$$

where $\beta = 1$ if length is measured in meters (MKS system) and 1.49 if measured in feet (British system). Combining equation (6.37) with the Darcy–Weisbach equation, one obtains

$$f_l = 12.7 g n^2 \beta^{-2} D^{-1/3} \tag{6.38}$$

where n is Manning's roughness coefficient. Substitution of equation (6.38) in equation (6.34) yields M. Then this value of M and $u_m = Q/A$ can be inserted in equation (6.11) to give u_{max}. With M and u_{max} so obtained, equation (6.7c) can be used to describe the velocity distribution in flow in pipes whether smooth or rough. The value of M achieved from equation (6.27) can also be used to determine ε_0/υ from equation (6.35) for a given R_N.

For rough pipes, the velocity distribution given by equation (6.7c) with u/u_m versus $[1 - (r/R)]$ is plotted in Fig. 6-14. Also plotted are Nikuradse's (1932) data and the Prandtl–von Karman velocity distribution. The difference between the two equations is near the wall and in the center. Fig. 6-15 plots the velocity gradient versus r/R for equations (6.13) and (6.18). The main difference again is near the wall and the center. To further evaluate equation (6.7c), Fig. 6-16 plots the velocity distribution and a set of experimental data. The agreement between computed and measured values is quite close.

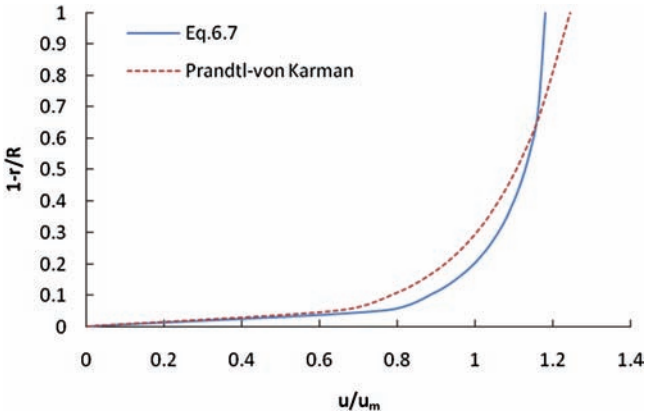

Figure 6-14 u/u_m *versus* $[1 - (r/R)]$.

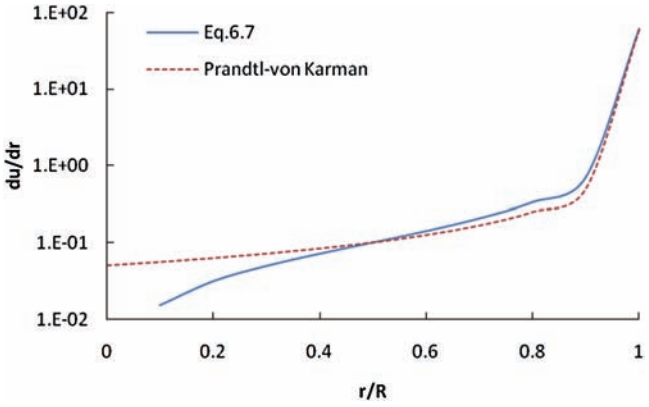

Figure 6-15 *Velocity gradient versus* r/R.

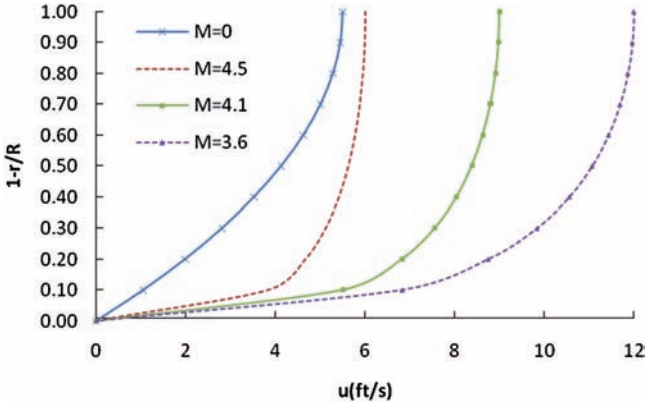

Figure 6-16 *Velocity distribution and a set of experimental data.*

6.7 Uncertainty in M, f_l, n, and Velocity Distribution

Parameters M and $u_{\max}$ may be subject to uncertainty and, in turn, the velocity distribution given by equation (6.7c). Since u_m is reasonably accurately determined by $u_m = Q/A$, $u_{\max}$ can be obtained from a given M and u_m using equation (6.16). Thus, the uncertainty in the velocity distribution depends on the uncertainty in M, unless $u_{\max}$ is measured independently. Using equations (6.7c) and (6.16), the velocity u at distance r from the pipe center can be written as

$$u = u_m \frac{\ln\left\{1+[\exp(M)-1]\left[1-\left(\frac{r}{R}\right)^2\right]\right\}}{M\exp(M)[\exp(M)-1]^{-1}-1} \tag{6.39}$$

For evaluating the uncertainty in the velocity distribution, let M be a random variable and, hence, also u can be a random variable. The first-order approximation of the conditional mean of u at r is

$$U = u_m \frac{\ln\left\{1+[\exp(\bar{M})-1]\left[1-\left(\frac{r}{R}\right)^2\right]\right\}}{\bar{M}\exp(\bar{M})[\exp(\bar{M})-1]^{-1}-1} \tag{6.40}$$

where $\bar{M}$ is the mean of M, which is independent of r, and U is the approximation of mean u_m. U is an effective measure of uncertainty and can be expressed in terms of mean and variance of M as

$$\frac{s_u^2}{s_M^2} = \frac{P_1 \times P_2 + P_3}{P_4} - \frac{P_5}{P_6} \tag{6.41}$$

where

$$P_1 = \left\{\exp(\bar{M}) + [\exp(2\bar{M}) - \exp(\bar{M})]\left[\left(1-\left(\frac{r}{R}\right)^2\right]\right\}\right.$$

$$P_2 = \ln\left\{1+[\exp(\bar{M})-1]\left[1-\left(\frac{r}{R}\right)^2\right]\right\}$$

$$P_3 = \left[\exp(2\bar{M}) - \exp(\bar{M})\left[\left(1-\left(\frac{r}{R}\right)^2\right]\right.\right.$$

$$P_4 = [\bar{M}\exp(\bar{M}) - \exp(\bar{M}) + 1][\bar{M}\exp(2\bar{M}) - \exp(2\bar{M}) - \bar{M}\exp(\bar{M}) + 2\exp(\bar{M}) - 1]\left[1-\left(\frac{r}{R}\right)^2\right]$$

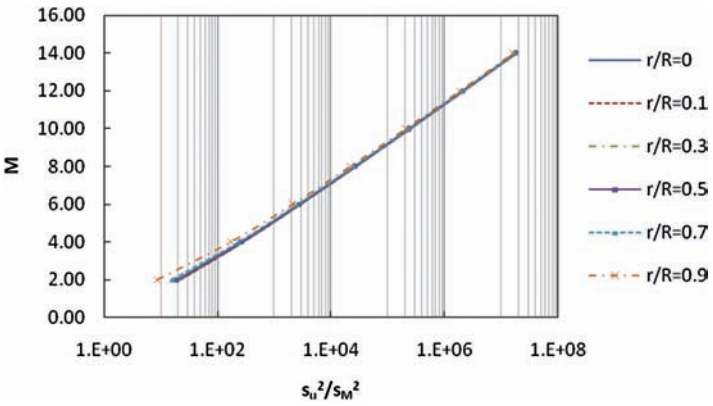

Figure 6-17 s_u^2/s_M^2 *against* r/R *for various values of* $\bar{M}$.

$$P_5 = \left[\bar{M}\exp(2\bar{M}) - \bar{M}\exp(\bar{M})\ln\left\{1+[\exp(\bar{M})-1]\left(1-\left(\frac{r}{R}\right)^2\right)\right\}\right]$$

$$P_6 = [\bar{M}\exp(\bar{M}) - \exp(\bar{M}) + 1]^2$$

where s_M^2 is the variance of M. Equation (6.41) is plotted against r/R for various values of $\bar{M}$. As $\bar{M}$ increases, s_u^2/s_M^2 tends to have the same order of magnitude and to be almost independent of $\bar{M}$ and r/R. With decreasing $\bar{M}$, s_u^2/s_M^2 changes rapidly, as shown in Fig. 6-17.

If M is evaluated from f_l, its mean and variance can be determined from f_l. Using equation (6.31), the first-order approximation of the mean and variance of f_l can be expressed as

$$\overline{f_l} = 0.0983\left[1.17\left(\frac{0.17\bar{M}\exp(\bar{M}) + \exp(\bar{M}) - 1.17\bar{M} - 1}{\bar{M}\exp(\bar{M}) - \exp(\bar{M}) + 1}\right)\right]^2 \tag{6.42}$$

$$\frac{s_{fl}^2}{s_M^2} = 0.053\left(\frac{\bar{M}\exp(\bar{M}) - \exp(\bar{M}) + 1}{[\overline{M^2}\exp(\bar{M}) - \exp(2\bar{M}) + 2\exp(\bar{M}) - 1] \times [0.17\bar{M}\exp(\bar{M}) + \exp(\bar{M}) - 1.17\bar{M} - 1]}\right)^2 \tag{6.43}$$

If f_l is determined from Manning's n, then the mean and the variance of f_l can be determined from equation (6.38) as

$$\overline{f_l} = 12.7(\overline{n})^2\beta^{-2}D^{-1/3} \tag{6.44}$$

$$s_{fl}^2 = s_u^2(25.4g\overline{n}\beta^{-2}D^{-1/3}) \tag{6.45}$$

where $\overline{n}$ and s_n^2 are the mean and variance of Manning's n. For a particular pipe material, a range of Manning's n can be obtained from tables (Chow 1959), and these tables can be used to obtain $\overline{n}$ and s_n^2. Then, $\overline{f_l}$ and s_{fl}^2 can be determined from equation (6.44) and (6.45). Then from equation (6.42) and (6.43), $\overline{M}$ and s_M^2 can be obtained. Equation (6.36) can be used to determine the uncertainty in u obtained from equation (6.7c).

Questions

Q6.1 Plot the cumulative probability distribution function of velocity as a function of distance from the wall. Compare the plot with observations given in Table 6-2.

Q6.2 Plot the probability density function of velocity as a function of distance from the wall. Compare the plot with observations given in Table 6-2.

Q6.3 Given the pipe diameter $R = 1\,\text{m}$, plot the CDF as a function of radius from the center of the plot and compare it with observations.

Q6.4 For the pipe in Q6.3, plot the PDF of velocity as a function of distance from the wall. Compare the plot with observations.

Q6.5 Plot u_m versus $u_{\max}$ and compute the entropic parameter M.

Q6.6 Compute u as a function of distance from the center using the Prandtl–von Karman velocity equation and compare it with observations.

Q6.7 Plot h_f as a function of u_m. Interpret the plot.

Q6.8 Plot $u_m/u_{\max}$ versus u_m/u^*. Interpret the plot.

Q6.9 Plot f_l as a function of $u_m/u_{\max}$. Interpret the plot.

Table 6-2 *Velocity distribution.*

(1 – r)/R	u (m/s)	(1 – r)/R	u (m/s)
0.03	0.51	0.33	1.12
0.05	0.65	0.4	1.13
0.06	0.73	0.47	1.16
0.07	0.79	0.59	1.19
0.11	0.83	0.69	1.2
0.13	0.89	0.82	1.21
0.17	0.94	0.91	1.2
0.21	0.99	1	1.19

Q6.10 Plot U as a function of r/R for different values of u_m and M. Interpret the plot.

Q6.11 Plot the ratio of the variance of velocity to the variance of M as a function of r/R for various values of mean M. Interpret the plot.

Q6.12 Plot the mean of f_l as a function of mean M.

Q6.13 Plot the variance of f_l as a function of mean M.

References

Chiu, C.-L., Lin, G.-F., and Lu, J.-M. (1993). "Application of probability and entropy concepts in pipe-flow study." *J. Hydraul. Eng.,* 119(6), 742–756.

Chow, V. T. (1959). *Open-channel hydraulics,* McGraw-Hill, New York, 110–111.

Hanks, R. W. (1968). "On the theoretical calculation of friction factors for laminar, transitional, and turbulent flow of Newtonian fluids in pipes and between parallel plane walls." *AICH J.,* 14(5), 691–695.

Nikuradse, J. (1932). *Gesetzmabigkeit der turbulenten Stromung in glatten Rohren.* Forschungsheft, Berlin, 356 (in German).

Additional Reading

American Iron, and Steel Institute. (1971). *Handbook of steel drainage & highway construction products,* American Iron and Steel Institute, Washington, DC.

Chadwick, A., and Morfett, J. (1986). *Hydraulics in civil engineering,* Allen and Unwin, Winchester, MA.

Clark, J. W., Viessman, W., and Hammer, M. J. (1977). *Water supply and pollution control,* Harper & Row Publishers, New York.

Morris, H. M., and Wiggert, J. M. (1972). *Applied hydraulics in engineering,* Wiley, New York.

Roberson, J. A., Cassidy, J. J., and Chaudhry, M. H. (1998). *Hydraulic engineering,* 2nd Ed., Wiley, New York.

Simon, A. L. (1976). *Practical hydraulics,* Wiley, New York.

Walski, T. M., Gessler, J., and Sjostrom, J. W. (1990). *Water distribution systems: Simulation and sizing*, Lewis Publishers, Chelsea, MI.

This page intentionally left blank

Part 2

Sediment Concentration and Discharge

This page intentionally left blank

Chapter 7

Grain Size Analysis and Distribution

Grain size analysis has many practical applications in geotechnical engineering, fluvial geomorphology, and hydraulic engineering. For example, it is used to characterize depositional processes within sedimentary environments (Swan et al. 1979a, 1979b). The analysis can lead to describing the grain size distribution and its properties, such as mean grain size, median, mode, standard deviation (SD), skewness, and kurtosis. Each property can be used as a measure of different aspects of depositional environments (Blatt et al. 1980) and in turn fluvial processes. Full et al. (1983) used entropy to define the aggregate properties of grain size distribution. This chapter discusses grain size analysis, distribution, and grading.

7.1 Grain Size Distribution

In grain size analysis, the range of grain sizes is divided into class intervals, and for each interval the relative frequency or proportion is determined. A plot of relative frequency versus grain size is the grain size distribution. The grain size distribution is a statistical distribution in which the cumulative relative frequency or probability is expressed as a function of diameter (d) of particles. The cumulative relative frequency is the fraction or percentage of particles finer than a given diameter. The grain size distribution is often referred to as the grading curve.

7.1.1 Class Intervals for Frequency Analysis

Discrete data are often grouped in classes and analyzed in the form of frequency histograms or cumulative frequency distributions. When we are constructing histograms, we need to answer two questions. The first is the number of class intervals to be used for constructing a histogram, and the second is the class interval size. The answers to these two questions influence the quality of information or data extracted for subsequent analysis, such as estimation of moments, discriminant functions, factor analysis, and determination of quantiles. To illustrate this point, consider two extreme cases. In the first case, all data are grouped in one class and the class interval clearly is too wide. The second case involves too many class intervals, with the result that class intervals have vanishingly sparse data. Folk (1966), Swan et al. (1979a), Full et al. (1983), and others have discussed the effect of class interval size. Furthermore, it frequently happens, even when the number of class intervals is appropriate, that some class intervals have too many data and others too few. Random perturbations may significantly affect the low class frequency portion of the distribution but not so much the high-frequency portion.

Conversely, high-frequency class intervals may contain more data than needed in terms of precision and meaning loss of information, and it may be worthwhile to subdivide the class intervals for testing for polymodality. When different data sets are compared, the issues of class intervals with too many frequencies and those with too few become even more important. One way to address these issues and remedy the underlying difficulties is to use variable class interval sizes. Examples of variable class interval sizes include percentile-based size measures (Inman 1952; Folk and Ward 1957), or graphic mean (Folk and Ward 1957). The objective of using unequal width class intervals is to maximize the amount of information that can be extracted from the data and its frequency distribution. The entropy theory provides a way to determine class intervals that will maximize information.

Entropy gives a measure of the degree of contrast among class intervals in the frequency histogram. If the class interval frequencies are considerably different, the entropy value is low. Conversely, a high entropy value characterizes the histogram with small differences among interval frequencies. Thus, the entropy method can be used to define the optimal interval width to best characterize the histogram.

Traditional methods of generating class intervals include arithmetic (A), phi (TP), log-arithmetic (LA), *Z*-scores (ZS), and log *Z*-scores (LZS) methods. In the arithmetic method, intervals are of equal width. In grain size analysis, the scale is in millimeters and, therefore, the width is also in millimeters. The phi method, which is frequently used in geology and sedimentology, scales as $(-\log_2 \text{mm})$, containing intervals each quarter-phi unit wide. In the $\log_2$ domain, the intervals are of equal width. In the log-arithmetic method, the arithmetic scale is transformed to the $\log_{10}$ space, and in the log space (i.e., log millimeter), the intervals are of equal width. The *Z*-score method (Mazzullo and Ehrlich 1980) assumes that pooled data have a higher density near the mean and that the data are

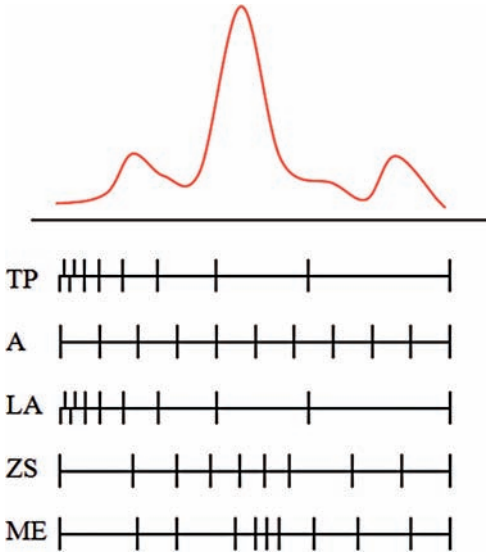

Figure 7-1 *Example of the partition of an arbitrary pooled collection of distributions using the traditional phi (TP), arithmetic (A), log (base 10) arithmetic (LA), Z-scores (ZS), and maximum entropy (ME) methods.*

normally distributed. In this method, intervals are defined such that each interval has the same frequency. This difference means that intervals would be narrower near the mean and progressively wider away from the mean. In the log-Z scores method, data are first logarithmically transformed by taking the base of logarithm as 10, and then the ZS method is applied. Fig. 7-1 shows these methods. It may be noted that the maximum entropy method is independent of most common transformations (e.g., log, square, or square root).

7.1.2 Feature Extraction

It may be worthwhile to compare different data sets and compare different methods of interval sizing. In this manner, the entropy of the total system can be computed using different methods, and by comparing total system entropies, the method of interval sizing can be identified. The information contained within a particular data set can be quantified by entropy. Consider data sets consisting of observations on different characteristics, such as size, shape, hydrologic analyses, or chemical analyses, which may have similar geologic information. The question arises: Which variable(s) are best suited for a clear and unambiguous analysis? To answer this question, one can use entropy as a numerical measure, and this criterion is termed *feature extractor*.

For feature extractor, the concept of relative entropy is defined as the ratio of the sample entropy to the maximum possible entropy, which is obtained when class intervals in the sample have equal frequencies or is equal to the natural logarithm of the number of class intervals. Thus, the relative entropy of the entire

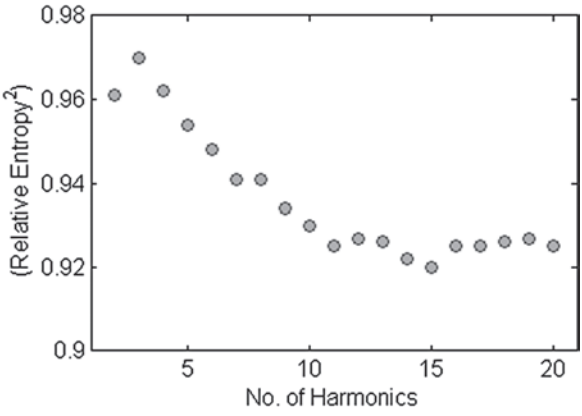

Figure 7-2 *Relative entropy versus number of harmonics.*

data set consisting of a number of samples is the sum of calculated sample entropies divided by the maximum possible sample entropy and the number of samples. Consider two sets of samples (data). For one set, the relative entropy is low, and for the other, it is high. The lowest relative entropy can be zero, and the highest can be one. Lower values of relative entropy reflect data with greater contrasts among samples, and higher values reflect smaller variation among samples. This, then, suggests that the set containing the lowest relative entropy has the greatest potential for a clear, unambiguous analysis. In this manner, the data set with the highest potential can be identified. Now, the question is: How can we maximize the information contained in that data set?

Consider a data set consisting of stream sediment samples from drainage basins. One may quantify the sediment size by using Fourier series containing harmonics. A greater magnitude of the harmonic implies greater contribution to the total size. In this manner, each sample can be represented by a set of harmonic amplitudes. Each harmonic represents a different scale of size variability, and hence different harmonics correspond to different amounts and types of information, as shown in Fig. 7-2. (The first harmonic represents an error measurement.) Thus, the problem is to determine a few harmonics that are likely to carry the most information. One can then use class frequencies of these harmonic amplitudes and compute relative entropy. A plot of relative entropy versus harmonics indicates the harmonic with the lowest entropy.

7.1.3 Sorting Index

Grain size analysis often involves sorting sediment particles and then deriving sediment characteristics, such as sediment grain size distribution, moments, and depositional features. Sorting qualitatively means that the way the mass of sediment particles is arranged among classes is defined somewhat arbitrarily. Frequently used terms are *poorly sorted* and *well sorted*. When most of the material is sorted in one class, the distribution is considered well sorted, and when the

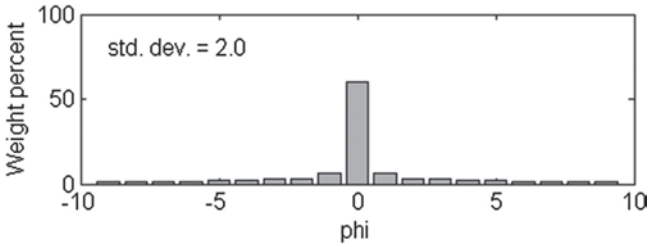

Figure 7-3 *Histogram of the hypothetical size analysis (standard deviation: 2.0).*

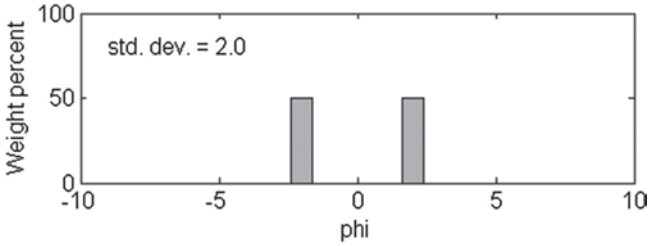

Figure 7-4 *Histogram of the hypothetical size analysis (standard deviation: 2.0).*

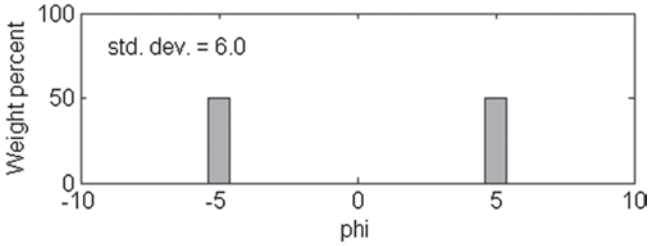

Figure 7-5 *Histogram of the hypothetical size analysis (standard deviation: 6.0).*

material is evenly distributed, it is considered poorly sorted. The arrangement of particles among classes reflects two properties: (1) evenness in the distribution of sediment mass and (2) spread of sediment size distribution. The standard deviation, as a measure of spread, can describe both these properties if the grain size distribution is normal but cannot if the distribution is not normal. Consider, for example, three cases shown in Figs. 7-3 to 7-5. In Figs. 7-3 and 7-4, the standard deviation is the same but the evenness with which the material is distributed is quite different. Likewise, in Figs. 7-4 and 7-5, the evenness is the same but the standard deviation is quite different. Thus, the standard deviation measures the spread but not the evenness.

The *standard deviation* (SD) can be considered a measure of sorting. A higher value of SD indicates poor sorting. However, it does not distinguish between a fine-grained distribution and a coarse-grained distribution because the two distributions may have equal degrees of sorting.

Although *skewness* is a measure of asymmetry of the distribution, it cannot be used to identify like distributions. Consider two very different distributions. One of the distributions belongs to fine- to medium-grained sands, and a substantial very fine and mud fraction, and the other distribution belongs to medium- to very coarse-grained sands with less important fine grains. It is not uncommon to see that these distributions have the same value of skewness. Fig. 7-6 illustrates this distribution characteristic.

Kurtosis is a measure of the distribution peakedness or flatness, as shown in Fig. 7-6. Friedman (1962) showed that most sand grain distributions were leptokurtic as a result of mixing of a predominant grain size with small amounts of coarse and finer material. However, two distributions may have the same kurtosis, but one may be more leptokurtic than the other. That is, one may be more concentrated in the fine sand to mud range than the other, which may be more platykurtic and multimodal. Another example is that the one distribution is less peaked and medium- to coarse-grained, and the other is highly peaked and bimodal in the sand and clay (mud) parts of the size range.

There are several sorting indexes, such as Udden's index of sorting (Udden 1914), Baker's grading factor (Baker 1920), Trask's measure of sorting (Trask 1932), and Niggli's index of sorting (Niggli 1935). However, these indexes essentially measure the spread of the grain size distribution, as pointed out by Krumbein and Pettijohn (1938). Sharp and Fan (1963) proposed a sorting index based on the entropy concept, which captures the evenness of the distribution and is described here.

Let f_i be the fraction observed in the ith class, and let N be the number of classes. We define a constant k, which depends on the scale specified. The sorting index, S_i, expressed in percentage is defined as

$$S_i = 100 + k\sum_{i=1}^{N} f_i \log_{10} f_i, \quad \sum_{i=1}^{N} f_i = 1 \tag{7.1}$$

This index equals 100 when all f_i are equal to either 1 or 0. It becomes 0 if all f_i have the same value given the maximum number of allowable classes and the properly adjusted k value. Clearly, the term $\sum_{i=1}^{N} f_i \log_{10} f_i$ is equal to the negative of the Shannon entropy or negentropy and becomes maximum when all f_i are equal. S_i is independent of the position of classes and uses all the data.

For any size scale split into arbitrary classes, the value of k can be computed as follows. Let N be the allowed number of classes. For $f_i = 1/N$, S_i can be set equal to 0. Then,

$$0 = 100 + k\sum_{i=1}^{N} f_i \log_{10}\left(\frac{1}{N}\right) \tag{7.2}$$

which yields

$$k = \frac{100}{\log_{10} N} \tag{7.3}$$

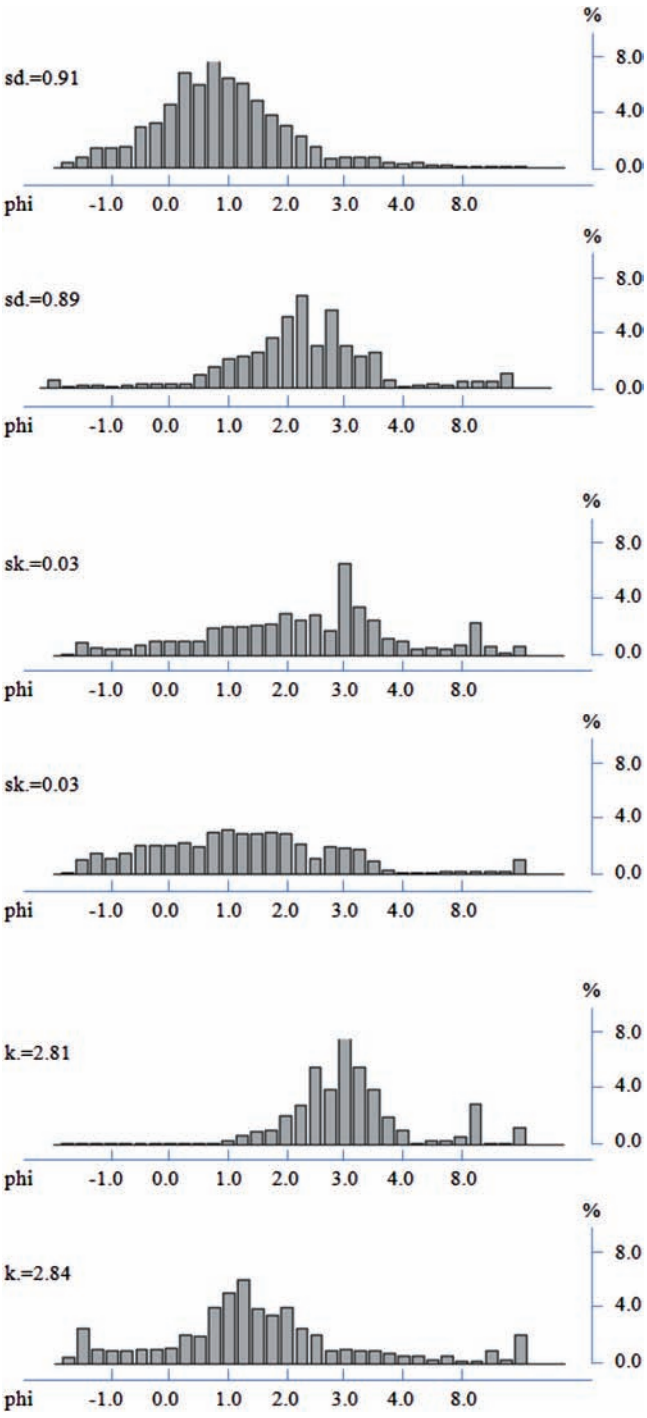

Figure 7-6 *Pairs of grain size distribution profiles with the same or similar standard deviation (sd.), skewness (sk.) and kurtosis (k.) values.*

As an example, consider setting up a sorting scale for sediment on the Wentworth scale in units on the ϕ scale, which is a logarithmic expression of the Wentworth scale. Consider a ϕ range of –10 to +10, thus giving classes of $N = 20$. In this case, $f_i = 1/20 = 0.05$, corresponding to the poorest sorted sediment. Then, constant k for this scale is

$$k = \frac{100}{\log_{10} 20} = \frac{100}{1.301} = 76.862$$

Thus, the sorting index is

$$S_i = 100 + 76.862 \times \sum_{i=1}^{N} f_i \log_{10} f_i = 0.0002325$$

This sorting index is for scales ranging from –10 to 10ϕ at class intervals of 1ϕ. The sorting index can be used to make inferences about the nature of ancient sediment deposits or to investigate variations in sedimentary rocks.

7.1.4 Characterizing Grain Size Distribution

Granulometric analysis of sediments is used to determine environment-diagnostic descriptors of grain size distributions. Some of the descriptors include mean grain size, phi-standard deviation, phi-skewness, and phi-kurtosis of the distribution. Each parameter measures different aspects of depositional environments. It has been frequently assumed that the grain size distributions are approximately normal or lognormal. These summary measures are relevant under this assumption but do not provide a complete summary of data for each grain size distribution. The question is the loss of information involved in the use of these statistics. Full et al. (1983) used entropy to define the aggregate properties of each grain size distribution. Forrest and Clark (1989) used variate analysis to characterize grain size distributions.

7.1.4.1 Univariate Case

Let X be the random variable defining the grain size and let the grain size population be divided into N (phi) classes or class interval sizes Δx_i, $i = 1, 2, \ldots, N$, i.e., X takes on values $X = \{x_i, i = 1, 2, \ldots, N\}$. For simplicity, a constant class interval size is often used, i.e., $\Delta x_i = \Delta x$, $i = 1, 2, \ldots, N$. Let p_i be the proportion of grains in the ith phi class interval. Thus, the probability distribution P of grain size X is $P = \{p_i, i = 1, 2, \ldots, N\}$. The Shannon entropy $H(X) = H(P)$ can be defined as

$$H(X) = -\sum_{i=1}^{N} p_i \log p_i \tag{7.4}$$

$H(X)$ is a measure of the grain size distribution over N intervals. The maximum value of $H(X)$ is $\log N$. Then, the more equally distributed the instances of p_i are,

the closer $H(X)$ would be to the maximum entropy $\log N$. The difference between the maximum entropy and the distribution entropy is

$$\begin{aligned} I(X) &= \log N - H(X) = \log N + \sum_{i=1}^{N} p_i \log p_i \\ &= \sum_{i=1}^{N} p_i \log N + \sum_{i=1}^{N} p_i \log p_i = \sum_{i=1}^{N} p_i \log(N p_i) \end{aligned} \tag{7.5}$$

where $I(X)$ is a measure of inequality or regularity of the distribution and is so called.

Using the regularity or inequality statistic, it is possible to determine an optimum number of categories, M, $M < N$. This determination is accomplished by maximizing between-class regularity and minimizing within-class regularity, yielding an optimal classification into M categories. For example, if for a sample there are $N = 20$ phi intervals, then a classification into, say, $M = 5$ categories would produce the optimal classification of intervals resulting in the maximum entropy histogram.

In the univariate characterization, all samples are classified into the same number of class intervals. The choice of M categories or classes is also the same for all samples. Full et al. (1983) reasoned that the same M value may not be optimal for individual samples. Forrest and Clark (1989) addressed this problem using multivariate analysis.

7.1.4.2 Multivariate Case

Let there be K samples and N phi class intervals. If p_{ij} defines the proportion of the total grains (of all K samples) in row i (sample i) and column j (class interval); $i = 1, 2, \ldots, K$ (number of samples); $j = 1, 2, \ldots, N$ (number of class intervals); p_j is the frequency value (of grains) in phi class interval j, p_i is the frequency value (of sand grains) in the phi class interval j that is in sample row i, such that $p_i = p_{ij}/p_j$; p_{ij} is the proportion of the total population (of all K samples) in row i and column j. The inequality statistic can be expressed as

$$I(X) = \sum_{j=1}^{N} p_j \sum_{i=1}^{K} p_i \log_2 K p_i \tag{7.6}$$

Here

$$\sum_{i=1}^{K} p_i = 1; \sum_{j=1}^{N} p_j = 1 \tag{7.7}$$

Here $I(X)$ denotes the inequality in the distribution of class interval values across all samples weighted by the frequency of sand grains in each phi category.

The weighted inter-row inequality value permits us to calculate between-group (of samples) inequality $I_B(X)$ as

$$I_B(X) = \sum_{j=1}^{N} p_j \sum_{r=1}^{R} p_{jr} \log_2 \frac{p_{jr}}{K_r / K} \tag{7.8}$$

where r is the number of groupings, and $I_B(X)$ is the between-group inequality.

All samples are allocated to a group based on the shared grain size distribution characteristics. Thus, K samples are grouped into R classes by maximizing between-class entropy and minimizing within-class entropy. The optimum number of groups is achieved when the between-class entropy starts to grow at a significantly decreasing rate with the addition of more classes.

7.1.5 Derivation of Grain Size Distributions

7.1.5.1 Normal Distribution

The normal distribution is frequently used for describing the grain size distribution. To derive this distribution using entropy, let the grain size be represented by a random variable X with probability density function $f(x)$, where x is a specific value of X. In this case, the constraint equations are

$$E[x] = m \tag{7.9}$$

$$E[x^2] = \sigma^2 + m^2 \quad or \quad E[(x-m)^2] = \sigma^2 \tag{7.10}$$

where m is the mean of X, and σ^2 is the variance of X. Furthermore,

$$\int_{-\infty}^{\infty} f(x)dx = 1 \tag{7.11}$$

The Shannon entropy is expressed as

$$H = -\int_{-\infty}^{\infty} f(x) \ln f(x) dx \tag{7.12}$$

Equation (7.12) is maximized, subject to equations (7.9), (7.10), and (7.11), in order to obtain the least biased f(x). Hence the Lagrangian L is expressed as

$$\begin{aligned} L = &-\int_{-\infty}^{\infty} f(x) \ln f(x) dx - (\lambda_0 - 1)\left[\int_{-\infty}^{\infty} f(x)dx - 1\right] - \lambda_1\left[\int_{-\infty}^{\infty} xf(x)dx - m\right] \\ &- \lambda_2\left[\int_{0}^{\infty} x^2 f(x)dx - \sigma^2 - m^2\right] \end{aligned} \tag{7.13}$$

Differentiating equation (7.13) with respect to $f(x)$ and equating the derivative to 0, one gets

$$\frac{\partial L}{\partial f(x)} = 0 \Rightarrow f(x) = \exp(-\lambda_0 - \lambda_1 x - \lambda_2 x^2) \tag{7.14}$$

Equation (7.14) is the distribution based on the principle of maximum entropy (POME) with λ_0, λ_1, and λ_2 as parameters. These parameters are determined using equations (7.9) through (7.11) as

$$\int_{-\infty}^{\infty} \exp(-\lambda_0 - \lambda_1 x - \lambda_2 x^2)dx = 1 \tag{7.15}$$

$$\int_{-\infty}^{\infty} x\exp(-\lambda_0 - \lambda_1 x - \lambda_2 x^2)dx = m \tag{7.16}$$

$$\int_{-\infty}^{\infty} x^2 \exp(-\lambda_0 - \lambda_1 x - \lambda_2 x^2)dx = \sigma^2 + m^2 \tag{7.17}$$

Equation (7.15) can be expressed as

$$\exp(\lambda_0) = \int_{-\infty}^{\infty} \exp(-\lambda_1 x - \lambda_2 x^2)dx = \exp\left(\frac{\lambda_1^2}{4\lambda_2}\right)\int_{-\infty}^{\infty} \exp-\left[\sqrt{\lambda_2 x} + \frac{\lambda_1}{2\sqrt{\lambda_2}}\right]^2 dx \tag{7.18}$$

Taking $t = \sqrt{\lambda_2 x} + \dfrac{\lambda_1}{2\sqrt{\lambda_2}}$, equation (7.18) can be written as

$$\exp(\lambda_0) = \frac{2\exp\left(\dfrac{\lambda_1^2}{4\lambda_2}\right)}{\sqrt{\lambda_2}}\int_{-\infty}^{\infty} \exp(-t^2)dt = \frac{\exp\left(\dfrac{\lambda_1^2}{4\lambda_2}\right)}{\sqrt{\lambda_2}}\sqrt{\pi} \tag{7.19}$$

A little algebraic manipulation yields the following:

$$\lambda_1 = -\frac{m}{\sigma^2}; \quad \lambda_2 = \frac{1}{2\sigma^2} \tag{7.20}$$

Substituting equation (7.17) in equation (7.11), one obtains

$$f(x) = \frac{1}{\sqrt{2\pi}\sigma}\exp\left[-\frac{1}{2}\left(\frac{x-m}{\sigma}\right)^2\right] \tag{7.21}$$

which is the probability density function of the normal distribution and corresponds to the case when mean and variance of grain sizes are known. It may be remarked that normal distribution can also be derived using only the variance as a constraint, because variance includes mean (Krstanovic and Singh 1988).

7.1.5.2 Lognormal Distribution

Let there be a normal random variable Y over the interval $(-\infty, \infty)$ and another random variable X related to Y as $Y = \ln X$. If Y is normally distributed, then X would be lognormally distributed over the interval $(0, \infty)$. The constraint equations are equation (7.11) and

$$E[y] = m_y \text{ or } E[x] = E[\exp(y)] = m_x \tag{7.22}$$

$$E[y^2] = \sigma^2 + m_y^2 \text{ or } E[x^2] = E[(\ln x - m_y^2)] \tag{7.23}$$

Equation (7.12) is maximized, subject to equations (7.11), (7.22), and (7.23), to obtain the least biased f(x). Hence the Lagrangian L is expressed as

$$\begin{aligned} L = &-\int_{-\infty}^{\infty} f(x)\ln f(x)dx - (\lambda_0 - 1)\left[\int_{-\infty}^{\infty} f(x)dx - 1\right] - \lambda_1\left[\int_{-\infty}^{\infty} (\ln x)f(x)dx - m_x\right] \\ &- \lambda_2\left[\int_0^{\infty} (\ln x)^2 f(x)dx - \sigma_y^2 - m_y^2\right] \end{aligned} \tag{7.24}$$

Differentiating equation (7.24) with respect to $f(x)$ and equating the derivative to 0, one gets

$$\frac{\partial L}{\partial f(x)} = 0 \Rightarrow f(x) = \exp[-\lambda_0 - \lambda_1 \ln x - \lambda_2 (\ln x)^2] \tag{7.25a}$$

or

$$f(x) = \exp(-\lambda_0) x^{-\lambda_1} \exp(-\lambda_2 \log x \log x) = \exp(-\lambda_0) x^{-\lambda_1} x^{-\lambda_2 \log x} \tag{7.25b}$$

Equation (7.25b) is the POME-based distribution with λ_0, λ_1, and λ_2 as parameters, which can be determined by substitution of equation (7.25b) in equations (7.9), (7.22), and (7.23) as

$$\int_0^{\infty} \exp[-\lambda_0 - \lambda_1 \ln x - \lambda_2 (\ln x)^2 dx = 1 \tag{7.26}$$

$$\int_0^{\infty} \ln x \exp[-\lambda_0 - \lambda_1 \ln x - \lambda_2 (\ln x)^2 dx = m_y \tag{7.27}$$

$$\int_0^{\infty} (\ln x)^2 \exp[-\lambda_0 - \lambda_1 \ln x - \lambda_2 (\ln x)^2] dx = \sigma_y^2 + m_y^2 \tag{7.28}$$

A little algebraic manipulation yields (Singh 1998):

$$\lambda_0 = \frac{1}{2}\ln \pi - \frac{1}{2}\ln \lambda_2 + \frac{(\lambda_1 - 1)^2}{4\lambda_2} \tag{7.29}$$

$$\lambda_1 = 1 - \frac{m_y}{\sigma_y^2} \tag{7.30}$$

$$\lambda_2 = \frac{1}{2\sigma_y^2} \tag{7.31}$$

Substituting equation (7.29) to (7.31) in equation (7.25a), one obtains

$$f(x) = \frac{1}{x\sqrt{2\pi}\sigma_y} \exp\left[-\frac{1}{2}\left(\frac{\ln x - m_y}{\sigma_y^2} \right)^2 \right] \tag{7.32}$$

which is the probability density function of the lognormal distribution and corresponds to the case when mean and variance of logarithmic values are known.

7.2 Soil Characteristics Using Grading Entropy

Lorincz (1986) derived the grading curve entropy and investigated different soil characteristics using the curve entropy. He established a relation between grading entropy and dry bulk density of granular materials (Lorincz 1990), investigated segregation of granular media and filter properties (Lorincz 1993a), and characterized piping and suffusion phenomena. Building on this work, Lorincz and his associates (Lorincz et al. 2005) quantified grading entropy caused by soil crushing, Lorincz et al. (2008) presented entropy criteria for granular filters, Lorincz et al. (2005) discussed particle breakage, Imre et al. (2008) characterized sand mixtures, and Imre et al. (2009) developed a general dry density law for sands. The discussion here draws from the investigations of Lorincz and his associates. The grading entropy theory has been used to define particle migration criteria (Lorincz 1993b; Lorincz et al. 2008), explain the particle breakage process (Lorincz et al. 2009), and construct the transfer function between soil physical properties and the grading curve (Imre et al. 2009).

7.2.1 Background and Definitions

In the traditional method of determining the grain size distribution of a soil, sieve analysis is done to construct the grading curve of the soil sample. In other words, a grading curve is measured by sieving, in which the hole diameters have a multiplier of two. Thus, a particular sieve mesh is characterized by a specific diameter, and the next sieve mesh diameter is twice as much, and so on. Usually the sieve mesh diameters are incremented by a multiplication factor of two when going upward. For example, if one sieve mesh diameter is 0.05mm, then the next higher mesh diameter is 0.1 mm, the next higher is 0.2 mm, the next higher is 0.4 mm, and so on. The mesh diameter may vary over several orders of magnitude (Lorincz et al. 2005). For purposes of discussion here, the minimum diameter, denoted as $d_{\min}$, is taken as the height of the silicon–oxygen (SiO_4) tetrahedron (2^{-22} mm) (Imre 1995).

When sieve analysis is done, the soil sample particles are divided into fractions by sieves. Let there be N fractions (also equal to the number of sieves); N is the number of fractions between the finest and the coarsest, and the fractions are numbered by increasing integers. A fraction is defined as a set of particles

passing through one sieve but retained by the next sieve. For convenience, fractions are indexed by increasing integers, as shown in Fig. 7-6. It may be noted that for a particular soil sample the particles may fall in one of the sieves rather than all of them. If the serial number of the coarsest fraction is denoted as i_{max} and the serial number of the finest fraction is i_{min}, the total number of fractions N of the soil sample can be expressed as

$$N = i_{max} - i_{min} + 1 \tag{7.33}$$

The smallest fraction can be between grain diameter $d = d_1$ and $d = d_2$; say $d_1 = 0.05$ and $d_2 = 0.1$. The ith fraction can be expressed in terms of its relative frequency, denoted as x_i. Note this is a measured quantity equal to the weight of particles of the ith fraction divided by the total weight of the soil sample. The relative frequencies, x_i, $i = 1, 2, \ldots, N$, are independent. Thus,

$$\sum_{i=1}^{N} x_i = 1, \quad x_i \geq 0, \quad N \geq 1 \tag{7.34}$$

Here the number of fractions, N, is between the coarsest fraction and the finest one. It is convenient to number the fractions by increasing integers and to index them by a serial number $i = 1, 2, \ldots, 27$.

With this convention, the diameter range of the ith fraction, d_i, can be defined as

$$2^i d_0 \leq d \leq 2^{i+1} d_0 \tag{7.35}$$

where d_0 is the elementary cell width (or diameter), which can be an arbitrary value and is usually taken as the height of the SiO_4 tetrahedron ($d_0 = 2^{-22}$) (Imre 1995). Equation (7.35) allows us to specify the diameter of different fractions or cells that can be expressed in terms of the minimum grain diameter $d_{min} = 2^{i-1} d_0$, as shown in Table 7-1 (from bottom to top in ascending order).

Lorincz (1990) tested soil fractions with a sieve test that had the following mesh sizes: $d_{min} = 0.063, 0.125, 0.25, 0.5, 1, 2, 4, 8, \ldots$ mm; each subsequent fraction had a double width or diameter of the immediately lower diameter fraction. He suggested and applied the width of the elementary cell as $d_0 = 2^{-17}$ mm.

Statistical cell systems are defined as primary and secondary, also known as real and imaginary, respectively. The reason for defining two cell (fraction) systems is that statistical cells or fractions are not uniform, but a uniform cell system is needed for the statistical entropy of a discrete distribution, thus invoking a double cell system. In this notion, probabilities are computed exclusively from fraction information, with the assumption of a uniform distribution in a

Table 7-1 *Fraction properties.*

Fraction	0	1	2	22	23	24
Diameter ***d*** (mm)	2^{-22}–2^{-21}	…	…	1–2	2–4	4–8

fraction. A primary statistical cell system is analogous to a sieve and is enumerated by the fraction of soil grains retained by its mesh. That is why it is called a real cell system and is so used henceforth. Thus, a real cell system is defined by successive multiplication with a factor of 2, the same as the base of logarithm in the entropy definition. Each cell system is assumed to have a uniform width, i.e., its mesh size or diameter remains the same. If the width of the elementary cell can be taken as d_0, the mesh diameter of the ith cell system (or sieve) can be determined by

$$d_i = 2^{i-1} d_0, \quad i = 1, 2, \ldots, N \tag{7.36}$$

In this sense, the real cell system can be generalized as a geometric progression with a factor of 2, defining the pattern that classical sieve hole diameters would follow. The definition of real cell system is illustrated in Fig. 7-7.

If the fractions are numbered by a serial number i (i = 1 2, …, N) then equation (7.36) applies, and its diameter range is defined by equation (7.35). Thus, there is a fraction grid, and within each fraction or cell system, there is an elementary cell grid, as shown in Fig. 7-7. The corresponding fraction is embedded in its grid system or elementary system.

A secondary or imaginary cell system does not really exist or is not visible as the real cell system. Here is also the reason why "imaginary" is adopted rather than "secondary." As an example, consider an ith fraction, and let us imagine that there exists a set of cells whose mesh size is linearly increased from d_i to d_{i+1} with an increment of d_0. The mesh diameter of the jth imaginary cell within the i—the real cell, d_{ij}, can be expressed as

$$d_{ij} = d_i + (j - i)d_0, \quad j = 1, 2, \ldots C_i \tag{7.37a}$$

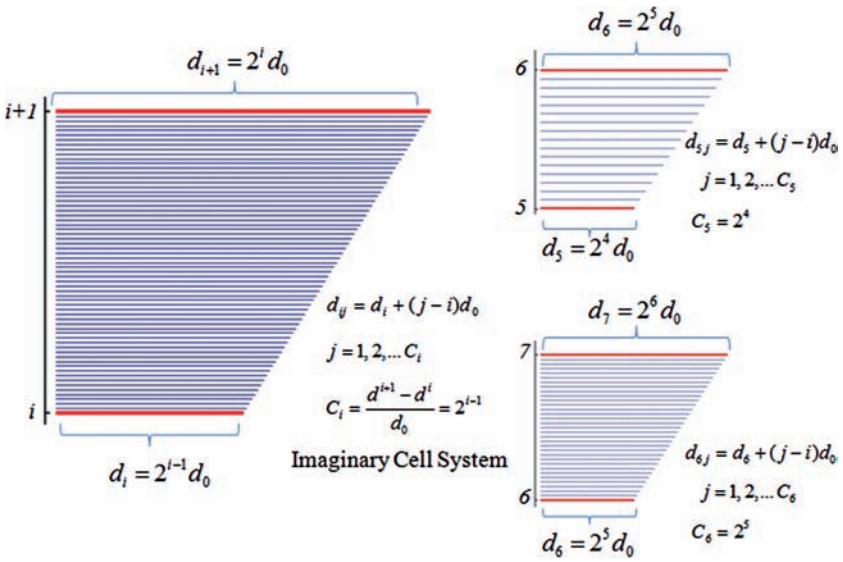

Figure 7-7 *Definition of an imaginary (secondary) cell system.*

where d_{ij} represents the diameter of the jth imaginary cell within the ith real cell and C_i is the number of elementary cells of width d_0 between d_i and d_{i+1}, which can be computed as

$$C_i = \frac{d^{i+1} - d^i}{d_0} = \frac{2^i d_0 - 2^{i-1} d_0}{d_0} = 2^{i-1} \tag{7.37b}$$

Just as the real cell system is generalized as a geometric progression, the imaginary cell system can be generalized as an arithmetic progression with an increment of d_0. Another important assumption associated with the imaginary cell system is that the soil particles within each fraction are uniformly distributed among the corresponding imaginary cells.

Once the real and imaginary cell systems are defined, the concept of a grading curve set is defined as a set of possible distribution functions where the grain distribution is uniform within each of the N fractions given the minimum cell width $d_{\min}$ (Imre et al. 2008). Let us assume that a sieve analysis is done and the soil sample is divided into N different fractions, the total weight of the soil sample is M, and the weight associated with the ith fraction is M_i. Then the relative frequency of the ith fraction can be expressed as

$$x_i = \frac{M_i}{M} \tag{7.38}$$

Furthermore, as grains are assumed to be uniformly distributed within each fraction, the relative frequency of the jth imaginary cell within the ith real fraction, p_{ij}, is

$$p_{ij} = \frac{x_i}{C_i}, \quad j = 1, 2, \ldots, C_i \tag{7.39}$$

With appropriate modification, equation (7.39) can be defined over all integers from 1 to N for i and from 1 to C_N for j. Thus,

$$p_{ij} = \begin{cases} \dfrac{x_i}{C_i} & 1 \le j \le C_i \\ 0 & C_i \le j \le C_N \end{cases} \tag{7.40}$$

As $\sum_{i,j} p_{ij} = 1$, equation (7.40) can be considered as a bivariate probability mass function accounting for weight as well as diameter of sediment particles. When sieve analysis is done, a contingency table can be filled easily whose entries are p_{ij} computed using equation (7.40), as shown in Table 7-2.

7.2.2 Grading Entropy

The concept of grading entropy, proposed by Lorincz (1986), is actually a specific application of statistical entropy to the grading curve. Let (X, Y) be a joint

Table 7-2 *Contingency table of bivariate probability mass function.*

Real Cell System (*i*)	Imaginary Cell System (*j*)					
	1	**2**	**3**	**…**	C_{N-1}	C_N
1	$\frac{x_1}{C_1}$	0	0	…	0	0
2	$\frac{x_2}{C_2}$	$\frac{x_2}{C_2}$	0	…	0	0
3	$\frac{x_3}{C_3}$	$\frac{x_3}{C_3}$	$\frac{x_3}{C_3}$	…	0	0
…	…	…	…	…	0	0
$N-1$	$\frac{x_{N-1}}{C_{N-1}}$	$\frac{x_{N-1}}{C_{N-1}}$	$\frac{x_{N-1}}{C_{N-1}}$	…	$\frac{x_{N-1}}{C_{N-1}}$	0
N	$\frac{x_N}{C_N}$	$\frac{x_N}{C_N}$	$\frac{x_N}{C_N}$	…	$\frac{x_N}{C_N}$	$\frac{x_N}{C_N}$

Note: $C_i = 2^{i-1}$, $x_i = \frac{M_i}{M}$, $\sum x_i = 1$.

distributed random vector with probability mass function $p(x, y)$, and marginals $p_X(x)$, $p_Y(y)$ of X and Y, respectively. The Shannon entropy $S(X)$ of random variable X measuring the uncertainty of X or the amount of information contained in it is defined as

$$S(X) = -\sum_x p(x)\log p(x) \tag{7.41a}$$

Likewise, for random variable Y, the Shannon entropy is

$$S(Y) = -\sum_y p(y)\log p(y) \tag{7.41b}$$

and the joint entropy $S(X, Y)$ of random vector (X, Y) measuring the joint uncertainty or the total amount of information conveyed by the vector (X, Y) is defined as

$$S(X, Y) = -\sum_x \sum_y p(x, y)\log p(x, y) \tag{7.42}$$

As stated previously, with an appropriate extension the relative frequency of the jth imaginary cell within each fraction in sieve analysis can be considered as a bivariate joint distribution whose probability mass function is given by equation (7.40) and also in Table 7-2. Applying this bivariate distribution to the joint

Shannon entropy (equation [7.42]), the grading entropy (Lorincz 1986) can be derived as

$$\begin{aligned} S &= -\sum_{i=1}^{N}\sum_{j=1}^{C_N} p_{ij}\log_2 p_{ij} = -\sum_{i=1}^{N}\sum_{j=1}^{C_i} p_{ij}\log_2 p_{ij} = -\sum_{i=1}^{N} p_{i\cdot}\log_2 p_{i\cdot} \\ &= -\sum \frac{x_i}{C_i}\log_2\frac{x_i}{C_i} + \frac{x_i}{C_i}\log_2\frac{x_i}{C_i} + \ldots + \frac{x_i}{C_i}\log_2\frac{x_i}{C_i} \\ &= -\sum_{i=1}^{N} C_i\frac{x_i}{C_i}\log_2\frac{x_i}{C_i} \end{aligned} \tag{7.43}$$

Now consider a special case where the soil is composed of a single fraction, say, $x_i = 1$ and $x_j = 0$ for all $j \neq i$. Then the grading entropy of this soil is

$$S = -C_i\frac{1}{C_i}\log_2\frac{1}{C_i} = \log_2 C_i$$

Since $C_i = 2^{i-1}$, equation (7.43) becomes

$$S_{0i} := S = \log_2 2^{i-1} = i - 1$$

This kind of grading entropy is also referred to as the eigen-entropy of fraction i and can be denoted as $S = S_{0i}$. The eigen-entropies of different fractions computed by equation (7.43) are listed in the last row of Table 7-2. One point that should be noted is that because the base of logarithm in equation (7.43) is selected as 2, the eigen-entropy can be expressed by a very simple function, $i - 1$, and i is just the index of the fraction. This is one of the reasons for selecting 2 as the base. Another reason is that if we consider a binary distributed random variable, the Shannon entropy (equation [7.41]) has a maximum value of 1 when the base is 2.

Equation (7.43) is a concave function of relative frequency x_i, and its concavity can be confirmed by the negative definite Hessian matrix of the second-order partial derivatives of S with respect to x_i, as shown:

$$\begin{bmatrix} -\frac{1}{x_1\log 2} & \cdot & \cdot & \cdot & \cdot \\ \cdot & -\frac{1}{x_2\log 2} & \cdot & \cdot & \cdot \\ \vdots & \cdot & -\frac{1}{x_3\log 2} & \cdots & \cdot \\ \cdot & \cdot & \cdot & \ddots & \cdot \\ \cdot & \cdot & \cdot & \cdots & -\frac{1}{x_N\log 2} \end{bmatrix}$$

Example 7.1 Compute the eigen-entropy of the fraction between sieves of 1-mm and 2-mm sizes.

Solution First, the number of elementary cells is computed (with $d_0 = 2^{-17}$ mm):

$$C = \frac{2\,\text{mm} - 1\,\text{mm}}{2^{-17}\,\text{mm}} = 2^{17}$$

Then, the eigen-entropy can be written as

$$S_0^{1-2} = \frac{\log 2^{17}}{\log 2} = 17$$

In a similar manner, the eigen-entropy of fraction 2–4 mm is 18, and so forth.

Example 7.2 Compute eigen-entropy values of the fractions from 0 to 24.

Solution

$$S_{0i} = \frac{\ln C_i}{\ln 2} = i$$

The results are shown in Table 7-3. It is independent of the cell width.

Table 7-3 *Eigen-entropy values in Example 7.2.*

Fraction	0	1	2	.	.	.	24
S_0	0	1	2	.	.	.	24

The grading entropy has a maximum value whose local maximum is also the global maximum. Now let us maximize the grading entropy with respect to the relative frequency x_i corresponding to the real (or primary) cell system. Considering the total probability constraint, $\sum_{i=1}^{N} x_i = 1$, this maximization problem can be formulated as

$$\text{maximize } S = -\sum_{i=1}^{N} C_i \frac{x_i}{C_i} \log_2 \frac{x_i}{C_i} \tag{7.44}$$

subject to the constraint

$$\sum_{i=1}^{N} x_i = 1 \tag{7.45}$$

The maximization can be achieved using the method of Lagrange multipliers where the Lagrange function L is expressed as

$$L = S + \lambda \times \text{constraint} = -\sum_{i=1}^{N} C_i \frac{x_i}{C_i} \log_2 \frac{x_i}{C_i} + \lambda \left(\sum_{i=1}^{N} x_i - 1 \right) \tag{7.46}$$

where λ is the Lagrange multiplier corresponding to the total probability constraint. Now differentiating the Lagrange function L with respect to the relative frequencies, x_i, and equating the derivative to zero, one obtains

$$\frac{\partial L}{\partial x_i} = -\left[\log_2 \frac{x_i}{C_i} + x_i \frac{1}{(x_i / C_i)\log_2} \frac{1}{C_i}\right] + \lambda = -\log_2 \frac{x_i}{C_i} - \frac{1}{\log_2 2} + \lambda = 0 \quad (7.47)$$

It is known that the relative frequency of the imaginary cells within a fraction is a constant, (x_i/C_i), but may vary among different fractions. Equation (7.47) shows that the grading entropy can be maximized if the frequency of each imaginary cell regardless of fractions corresponding to the real cell system is constant, that is,

$$\frac{x_i}{C_i} = \text{cons} \quad (7.48)$$

where cons = constant. Considering $C_i = 2^{i-1}$ equation (7.48) can be rewritten as

$$\frac{x_1}{1} = \frac{x_2}{2} = \frac{x_3}{2^2} = \ldots = \frac{x_N}{2^{N-1}} \quad (7.49)$$

Equation (7.49) can be further generalized as

$$x_i = 2^{i-1} x_1 \quad (7.50)$$

Equation (7.50) indicates that the grading entropy is maximized under the condition that grains are uniformly distributed among different imaginary cells and that they double the relative frequency x_i of each real cell from the bottom to the top of the sieve system. Substituting x_i into the total probability constraint (equation [7.45]), one obtains

$$\sum_{i=1}^{N} 2^{i-1} x_1 = x_1 \sum_{i=1}^{N} 2^{i-1} = x_1 \frac{1 - 2^{N-1} \times 2}{1 - 2} = 1 \quad (7.51)$$

The second equality in equation (7.51) is based on the formula for the sum of geometric progression. Solving for x_1, one gets

$$x_1 = \frac{1}{2^N - 1} \quad (7.52)$$

The above derivation concludes that the maximum point of the grading entropy is $[x_1\ x_2\ \ldots\ x_N]$, whose coordinates can be computed from equation (7.50) and (7.52).

Example 7.3 Assume that a soil system is mixed with two neighboring fractions. Compute the relative frequency for each fraction leading to the maximum grading entropy.

Solution For the two neighboring fractions 1 and 2, let x_1 and x_2 denote their relative frequencies, respectively. Since there are only two fractions, we have

$$x_1 + x_2 = 1$$

Using equation (7.50), we can further have

$$x_2 = 2x_1$$

It is easy to obtain $x_1 = 1/3$ and $x_2 = 2/3$. This result shows that in the case of two neighboring fractions, the proportions of fractions leading to the maximum grading entropy are 2/3 coarser and 1/3 finer fractions.

7.2.3 Simplex for Characterization of Grading Entropy

The concept of grading entropy can be explained from a geometric point of view in terms of the concept of simplex. In geometry, a *simplex* is a generalization of the notion of a triangle or tetrahedron to an arbitrary dimension. A single point may be regarded as 0-simplex. In one dimension, a line may be regarded as simplex; in two dimensions, a simplex is a triangle, referred to as 2-simplex; in three dimensions, it is a tetrahedron, referred to as 3-simplex; and in four dimensions, it is a *pentachoron*, referred to as 4-simplex. Thus, an n-dimensional *polytope* is a convex hull of $n + 1$ vertices. Thus, a simplex may be defined as the smallest convex set composing the given vertices. A regular n-simplex can be constructed from a regular $(n - 1)$ simplex by connecting a new vertex to all original vertices by common edge length. If any point in the simplex is assumed as the origin, then the other n points define vector directions that span the n-dimensional vector space. A simplex is a geometric figure comprising n points (or vertexes) in $(n - 1)$ dimensions, and all their interconnections.

Consider n points $p_1, p_2, \ldots, p_n$. The standard $n - 1$ dimensional simplex is a subset of R^n given by

$$\Delta^{n-1} = \left\{ [p_1 \quad p_2 \quad p_3 \quad \cdots \quad p_n] \in R^n \left| \sum_{i=1}^{n} p_i = 1, p_i \geq 0 \text{ for all } i \right. \right\}$$

where R^n represents the n-dimensional real space and $[p_1, p_2, \ldots, p_n]$ represents a point in R^n.

Specifically, the standard 0-, 1-, 2-, and 3-simplexes are point, unit line segment, equilateral triangle, and tetrahedron, respectively. The geometrical images of simplexes with dimension less than 3 are presented in Fig. 7-8. The dimension of a simplex is defined as its degree of freedom. Taking the equilateral triangle as an example, there are in total of three variables (or points). Among them, two are free variables (points), so its dimension is 2.

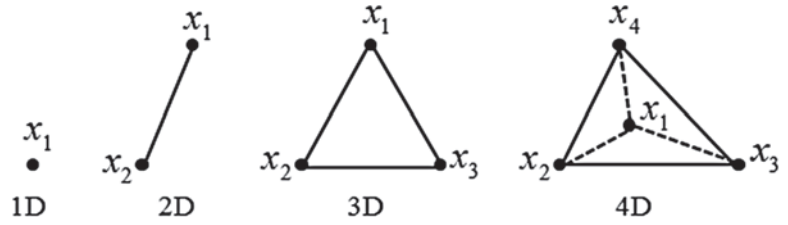

Figure 7-8 *Standard simplex images with dimension less than three. Note: The dimension of a simplex is defined as its degree of freedom.*

The vertices of a standard $n-1$ simplex are $e_1, e_2, \ldots, e_n$, which are given as

$$\begin{aligned} e_1 &= [1 \quad 0 \quad 0 \quad \cdots \quad 0] \\ e_2 &= [0 \quad 1 \quad 0 \quad \cdots \quad 0] \\ e_3 &= [0 \quad 0 \quad 1 \quad \cdots \quad 0] \\ &\cdots \\ e_n &= [0 \quad 0 \quad 0 \quad \cdots \quad 1] \end{aligned} \tag{7.53}$$

Since vertexes $e_1, e_2, \ldots, e_n$ also compose the usual basis of R^n, any point in R^n can be represented by $e_1, e_2, \ldots, e_n$, of course, including points within the $n-1$ standard simplex. An arbitrary point P of the $n-1$ standard simplex can be represented by a linear combination of $e_1, e_2, \ldots, e_n$ as

$$P = p_1 e_1 + p_2 e_2 + p_3 e_3 \tag{7.54}$$

The n scalars $p_1, p_2, p_3, \ldots, p_n$ are called the rectangular coordinates of point P relative to the usual basis of R^n, which are also the barycenter coordinates of P with respect to the vertexes of the $n-1$ standard simplex.

Recalling that the sum of nonnegative relative frequencies x_i of fractions corresponding to the real cell system is also equal to unity, it can be found that there exists a one-to-one relationship between grading curves with N fractions and points of $N-1$ standard simplex. Furthermore, the relative frequencies x_i are identified with the barycenter coordinates of the standard simplex points with respect to the vertexes of the simplex.

Among all the faces of a standard simplex, the vertexes (0-faces) and edges (1-faces) play an important role in the concept of grading entropy, as is explained in what follows. For an $n-1$ standard simplex, there are in total n vertexes and $\binom{n}{2}$ edges, which can be expressed as

$$i\text{-vertex} \quad P \in \{[p_1 \quad p_2 \quad p_3 \quad \ldots \quad p_n] \in R^n \,|\, p_i = 1, p_j = 0 \quad \text{for all } j \neq i \tag{7.55}$$

$$ij\text{-edge} \quad P \in \{[p_1 \quad p_2 \quad p_3 \quad \ldots \quad p_n] \in R^n \,|\, p_i + p_j = 1, p_k = 0 \quad \text{for all } k \neq i \text{ or } j \tag{7.56}$$

Consider a subset of $n+1$ points that define an n-simplex. Then the convex hull of the subset is called a face of the simplex. Faces are simplexes (simplices)

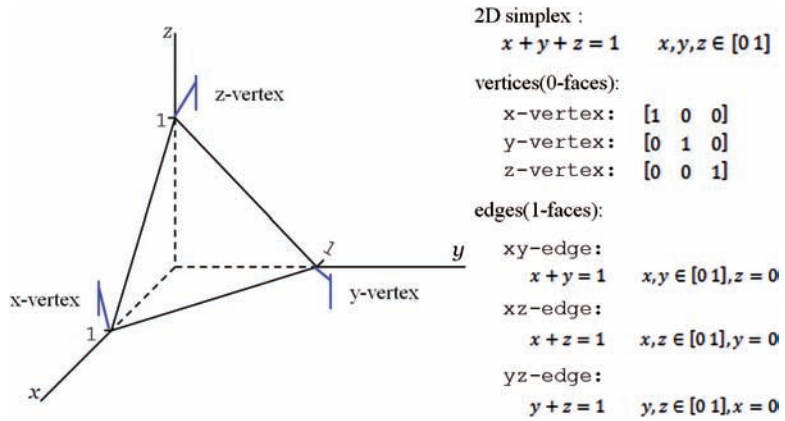

Figure 7-9 *Standard 2-simplex and its vertexes (vertices) and edges.*

themselves. For example, the convex hull of a subset of size (m + 1) of the (n + 1) defining points is an m-simplex and is referred to as an m-face of the n-simplex. The 0-faces are called vertexes (vertices), the 1-faces are called edges, the (n − 1) faces are called facets, and the sole n-face is the entire simplex itself. In general, the number of m faces is equal to the binomial coefficient $\binom{n+1}{m+1}$.

Taking the standard 2-simplex as an example, it represents a segment of the plane $x + y + z = 1$ intersected by a triangle prism as shown in Fig. 7-9. There are in total three vertexes and three edges whose functions can be derived from equation (7.55), together with equation (7.56), and are also shown on the right side of Fig. 7-9.

As illustrated previously, only the simplex with a dimension less than three can be visualized in a two or three Cartesian rectangular plane. In practice, points of standard 2- and 3-simplexes are plotted in ternary and quaternary diagrams as illustrated in Fig. 7-10. The advantage of so doing is twofold. First, it is much more readable as compared to displaying them directly in the Cartesian rectangular plane. Second, the quaternary diagram can display the 3-simplex, which is intractable directly in the Cartesian rectangular plane.

Now an explicit description about how to read the barycenter coordinates of a point within the ternary and quaternary diagrams is given. In a ternary diagram, the values of each vertex, denoted by A, B and C, without loss of generality, increase from 0 to 100% (or 1) when moving in the counterclockwise (or clockwise) direction. To get the barycenter coordinates of any point within the ternary diagram, draw lines passing through the point and parallel to each side of the triangle, and then extend these lines to meet the triangle sides. Two intersection points are obtained on each side; the intersection point, which gives the smaller value (the first intersection point along the increasing direction), along that side is selected. Hence, this method gives the three barycenter coordinates corresponding to the point.

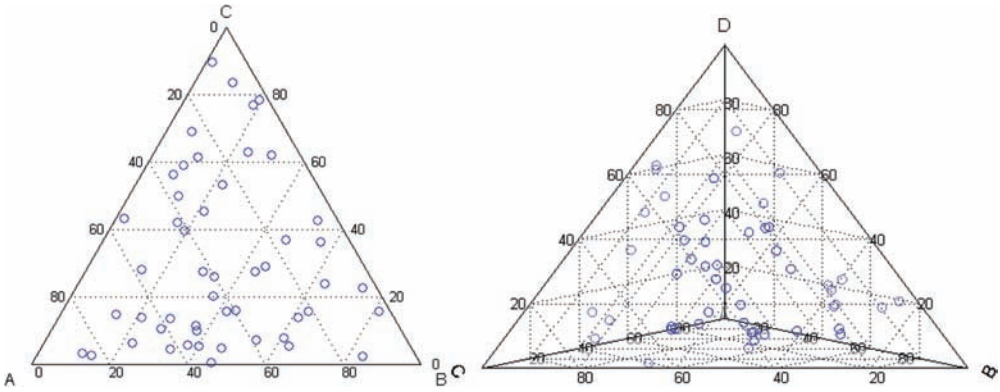

Figure 7-10 *Ternary and quaternary diagrams displaying 2- (left) and 3- (right) simplexes.*

In a quaternary diagram, using A, B, C, and D to denote the vertexes of the tetrahedron, the same procedure can be extended to obtain coordinates of a point within it with only a little modification. Here a fourth vertex, D, is added above the bottom face consisting of A, B, and C, such that the values of D coordinates increase from 0 to 100% (or 1) as we move from A, B, C to D. Now, to get the D coordinates of the point, take the values at which the plane containing the point and parallel to the bottom face ABC cuts the faces DAC, DAB, and DCB. This step invariably gives the same value at different edges, i.e., edges DA, DB, and DC. This value is just the D coordinates for which we are searching. Then, to get the coordinates corresponding to A, B, and C, draw planes passing through the point and parallel to all the other faces except the bottom one. These planes meet at two points, with each side of the bottom triangle. Then one uses the same method to get the coordinates of A, B, and C as that in the ternary diagram.

If one wants to plot the ternary and quaternary diagram in the Cartesian rectangular plane, all the coordinates corresponding to the ternary and quaternary diagram system should be projected to 2-D and 3-D Cartesian planes, respectively. After defining ternary and quaternary diagrams, which can be generated from the procedure of obtaining coordinates from them, we can project the coordinates. In the ternary diagram case, it is assumed that $[T_A\ T_B\ T_C]$ represent the barycenter coordinates of the point within the ternary diagram, and $[C_X\ C_Y]$ represent the corresponding Cartesian rectangular coordinates, as shown in Fig. 7-11.

The projection from the ternary coordinates to the rectangular coordinates can be expressed as

$$C_X = T_A + T_B \cos 60° \tag{7.57a}$$

$$C_Y = T_B \sin 60° \tag{7.57b}$$

However, the projection from the quaternary coordinates to the Cartesian rectangular coordinates is much more complicated than that from ternary to

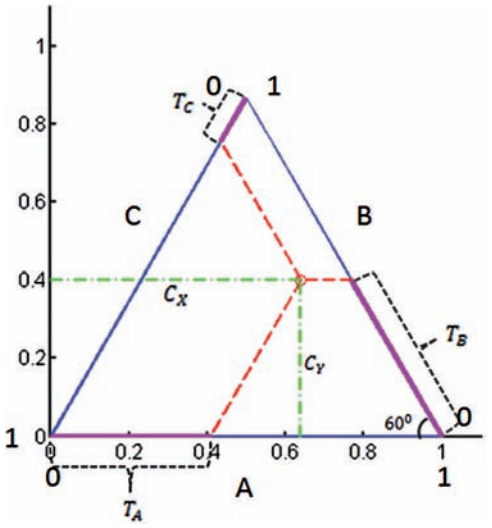

Figure 7-11 *Projection from ternary coordinates to Cartesian coordinates.*

Cartesian. For simplicity, an illustrative graph is shown in Fig. 7-11 and a detailed derivation is omitted, and only the projection relationship function is given here. Using [Q_A Q_B Q_C Q_D] to represent the quaternary coordinates and [C_X C_Y C_Z] to denote the corresponding Cartesian coordinates, the projection is represented [not shown] by

$$C_X = Q_B + Q_A \cos 60° + Q_D W \cos 30° \tag{7.58a}$$

$$C_Y = Q_A \sin 60° + Q_D W \sin 30° \tag{7.58b}$$

$$C_Z = Q_D \sin^2 60° \tag{7.58c}$$

where W can be computed as

$$W = \sqrt{\left(\frac{1}{2}\tan 30°\right)^2 + \left(\frac{1}{2}\right)^2}$$

Example 7.4 Assume a point [0.6, 0.4] in the Cartesian rectangular coordinates system. Project this point into the ternary coordinates system.

Solution From equation (7.57a) and (7.57b), one can have

$$\begin{cases} T_A + T_B \cos 60° = 0.6 \\ T_B \sin 60° = 0.4 \end{cases}$$

Solving these equations, one obtains

$$T_A = 0.4619, T_B = 0.3691$$

Therefore,

$$T_C = 1 - T_A - T_B = 1 - 0.4619 - 0.3691 = 0.1690$$

7.2.4 Grading Entropy Coordinates

The grain size distribution entails the integrated cell system, which couples the real cell system with the imaginary cell system. In other words, the imaginary cell system is built in the real cell system or the real cell system includes the imaginary cell system. The grading entropy defined by equation (7.43) contains two different terms, x_i and C_i, corresponding to the real cell system and the imaginary cell system, respectively. It is, therefore, intuitive to split the grading entropy into two parts, which leads to the grading entropy coordinates. Expanding equation (7.43), one obtains

$$\begin{aligned} S &= -\sum_{i=1}^{N} C_i \frac{x_i}{C_i} \log_2 \frac{x_i}{C_i} = -\sum_{i=1}^{N} x_i [\log_2 x_i - \log_2 C_i] \\ &= -\sum_{i=1}^{N} x_i \log_2 x_i + \sum_{i=1}^{N} x_i \log_2 C_i \\ &= \Delta S + S_0 \end{aligned} \tag{7.59}$$

where ΔS and S_0 are called entropy increment and base entropy, respectively.

Properties of entropy increment and base entropy are now discussed. First, the entropy increment ΔS is given by

$$\Delta S = -\sum_{i=1}^{N} x_i \log_2 x_i \tag{7.60}$$

Equation (7.60) shows that entropy increment is the statistical entropy of the grading curve in terms of fractions (real cell system). Thus, it possesses all the properties of the Shannon entropy, including symmetry and concavity. The symmetric property of ΔS is apparent, as it remains invariant for any permutation of $x_1, x_2, \ldots, x_n$. The concavity can be confirmed by its negative definite Hessian matrix, which is the same as that for the grading entropy. Usually the range of entropy increment ΔS is of interest.

Consider the extreme case where the soil is composed of a single fraction, say $x_i = 1$ and $x_j = 0$ for all $j \neq i$. Then, the entropy increment ΔS of this soil is

$$\Delta S = -1 \log_2 1 = 0 \tag{7.61}$$

Equation (7.61) shows that the entropy increment ΔS disappears at the vertexes of the standard $N - 1$ simplex, which is related to the soil mixture consisting of only a single fraction. In this case, the entropy increment ΔS disappears and the grading entropy S reduces to the base entropy. The maximum value of entropy increment ΔS, subject to equation (7.45), can be determined using the method of

Lagrange multipliers. For maximization of equation (7.60), the Lagrangian function L is constructed as

$$L = -\sum_{i=1}^{N} x_i \log_2 x_i + \lambda\left(\sum_{i=1}^{N} x_i - 1\right) \tag{7.62}$$

where λ is the Lagrange multiplier corresponding to the total probability constraint. Differentiating the Lagrange function L with respect to the relative frequencies, x_i, and equating the derivative to zero, one obtains

$$\frac{\partial L}{\partial x_i} = -\left(\log_2 x_i + \frac{1}{\log_2 2}\right) + \lambda = 0 \tag{7.63}$$

Equation (7.63) yields that the maximum of ΔS is reached when

$$x_i = 2^{\lambda - \frac{1}{\log_2 2}} = \text{cons} \tag{7.64}$$

where cons = constant. Substituting equation (7.64) into the total probability constraint equation (7.45), one obtains

$$\sum_{i=1}^{N} x_i = N x_i = 1 \tag{7.65a}$$

Therefore,

$$x_i = \frac{1}{N} \tag{7.65b}$$

Substituting equation (7.65b) in equation (7.60) yields the maximum entropy increment ΔS as

$$\Delta S = -\sum_{i=1}^{N} x_i \log_2 x_i = -\sum_{i=1}^{N} \frac{1}{N} \log_2 \frac{1}{N} = \log_2 N \tag{7.66}$$

Therefore, the maximum value of entropy increment ΔS is $\log_2 N$, which is also referred to as the global maximum of ΔS over the whole simplex, in the sense that there is no additional constraint but only the total probability constraint. The global maximum entropy increment ΔS is obtained at the point where all relative frequencies x_i of real cell fractions are equal to $1/N$. In other words, the entropy increment ΔS is maximized when the grains are uniformly distributed among all fractions. This result is different from the maximum point of grading entropy S, where grains are uniformly distributed among different imaginary cells leading to doubled relative frequency x_i of each fraction (corresponding to the real cell system) from the bottom to the top of the sieve system. This discussion also suggests that the range of ΔS is from 0 to $\log_2 N$. Obviously the range of entropy increment ΔS depends on N, the total number of fractions.

The base entropy S_0 is given as

$$S_0 = -\sum_{i=1}^{N} x_i \log_2 C_i \tag{7.67a}$$

Recalling the definition of eigen-entropy given by equation (7.43), equation (7.67a) can be rewritten as

$$S_0 = \sum_{i=1}^{N} x_i S_{0i} \tag{7.67b}$$

It can be seen from equation (7.67b) that the base entropy S_0 is the arithmetic mean of the eigen-entropies weighted by the relative frequencies x_i of the real cell fractions. One can find the range of base entropy S_0 by rewriting equation (7.67b) as

$$S_0 = \sum_{i=1}^{N} x_i S_{0i} = x_1 S_{0\min} + x_2 S_{0\min+1} + \ldots + x_N S_{0\max} \tag{7.68}$$

where $S_{0\min}$ and $S_{0\max}$ are the eigen-entropies of the finest and coarsest fractions of the soil mixture, respectively. One should note that $S_{0\min}$ and $S_{0\max}$ are not always equal to S_{01} and, S_{0N}, respectively. They assume the same values if and only if the grading curve set is defined over the integral cell system where the minimum sieve mesh diameter $d_{\min}$ and maximum sieve mesh diameter $d_{\max}$ are d_0 and d_N, respectively.

Equation (7.68) satisfies the following inequalities:

$$x_1 S_{0\min} + x_2 S_{0\min} + \ldots + x_N S_{0\min} = S_{0\min} \le S_0 \tag{7.69a}$$

$$x_1 S_{0\max} + x_2 S_{0\max} + \ldots + x_N S_{0\max} = S_{0\max} \ge S_0 \tag{7.69b}$$

Thus, the range of base entropy S_0 is from $S_{0\min}$ to $S_{0\max}$.

Graphs of grading entropy S and its two ingredients, entropy increment ΔS and base entropy S_0, help explain their properties. For 2-simplex corresponding to the soil mixed by no more than three fractions, graphs of grading entropy S, entropy increment ΔS and base entropy S_0 are shown in Fig. 7-12, where several points are worthy of note. First, the maximum points of the grading entropy S and entropy increment ΔS do not coincide with each other. The contour map of the entropy increment ΔS indicates that its maximum value is reached at the center of the 2-simplex. This situation is consistent with the conclusion derived theoretically that the entropy increment ΔS is maximized when grains are uniformly distributed among all fractions x_i.

Conversely, the contour map of the grading entropy S shows that its maximum value is reached at the point close to the vertexes with large indexes and far away from those with small indexes. This result is also consistent with the previous observation that grading entropy S has a maximum value when the relative

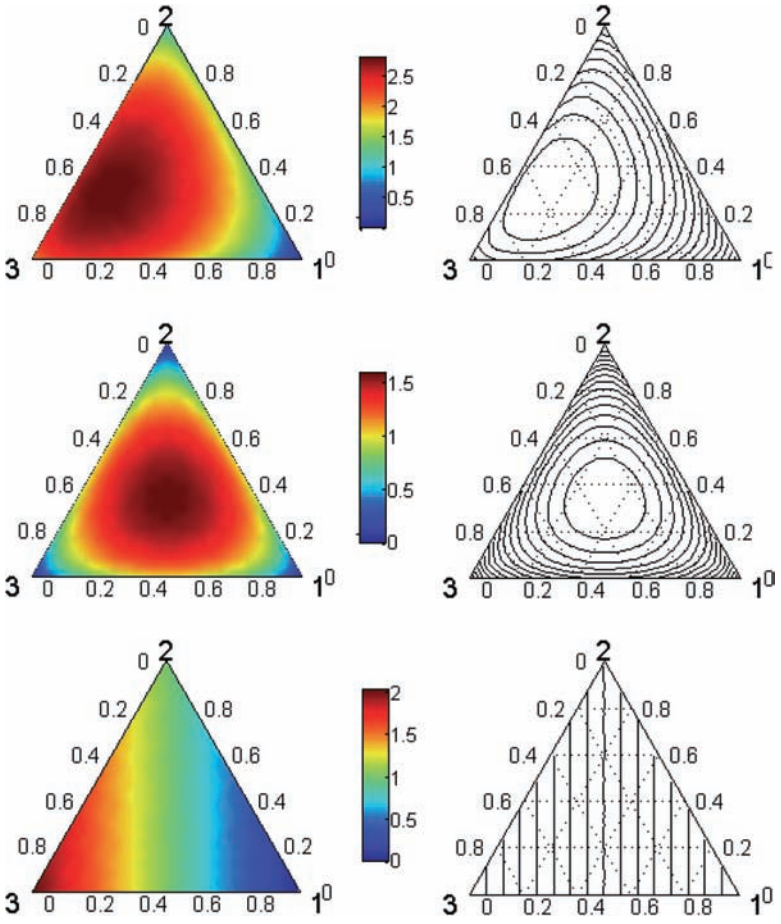

Figure 7-12 *Grading entropy* S *(1st row) and its two components (2nd row for* ΔS *and 3rd row for* S_0*) of standard 2-simplex.*

frequency x_i of each fraction is doubled successively from bottom to top. Second, the symmetry and concavity of entropy increment ΔS can be visualized in the second graph of the last column in Fig. 7-12. From this graph, one can also see that the lower boundary of ΔS appears at the edges of the simplex. Third, the eigen-entropy S_{0i} increases from the first vertex to the last one as shown in the graph located at the bottom right corner of Fig. 7-12, which corresponds to the finest and coarsest fractions, respectively.

As already shown, the entropy increment ΔS is dependent on the total number of fractions N, whereas the maximum value of base entropy S_0 is S_{0max}, which is also determined by N. It becomes much more convenient if the entropy increment ΔS can be normalized to be independent of N and the base entropy S_0 can be constrained to a fixed interval for a different number of fractions. This situation is discussed now.

The base entropy S_0 is normalized as

$$A = \frac{S_0 - S_{0\min}}{S_{0\max} - S_{0\min}} = \frac{\sum_{i=1}^{N} x_i S_{0i} - 0}{N - 1 - 0} = \frac{1}{N-1}\sum_{i=1}^{N} x_i (i-1) \tag{7.70}$$

where A is the normalized base entropy, also known as the relative base entropy.

The entropy increment ΔS can also be normalized as

$$B = \frac{\Delta S}{\log N} = -\frac{1}{\log N}\sum_{i=1}^{N} x_i \log_2 x_i \tag{7.71}$$

Actually, one can also normalize the entropy increment ΔS by $\log_2 N$ as

$$B' = -\frac{1}{\log_2 N}\sum_{i=1}^{N} x_i \log_2 x_i \tag{7.72}$$

After normalization, the range of normalized base entropy A is constrained between 0 and 1 and the normalized entropy increment B is independent of N and assumes values between 0 and $\log_2 N / \log N = 1/\log 2$ (or B' between 0 and 1 for the second normalization strategy). It can be seen that the normalized entropy coordinates do not change their shape and properties but only the range, as illustrated in Fig. 7-13. Comparison of Fig. 7-12 with Fig. 7-13 shows that the shapes of images for base entropy S_0 and entropy increment ΔS are invariant, but the range is not.

Example 7.5

Consider a grading curve of a soil consisting of four fractions, $N = 4$. Let the smallest fraction be between grain diameter of $d = 0.0625$ mm and $d = 0.125$ mm. Compute grading entropy A and B.

Solution

The relative frequencies of fractions are equal to $x_i = 1/4$. The base entropy S_0 is now computed as

$$S_0 = \sum_{i=1}^{N} x_i (i-1) + S_{01} = \sum_{i=1}^{4} \frac{1}{4}(i-1) + 1 = \frac{1}{4}[0+1+2+3] + 1 = 2.5$$

The entropy increment ΔS is computed as

$$\Delta S = -\frac{1}{\log 2}\sum_{i=1}^{N} x_i \log x_i = -\frac{1}{\log 2} \times 4 \times \frac{1}{4} \times \log\left(\frac{1}{4}\right) = 2.00$$

Now the normalized base entropy or relative base entropy A is given as

$$A = \frac{\sum_{i=1}^{N} x_i (i-1)}{N-1} = \frac{\sum_{i=1}^{N} \frac{1}{4}(i-1)}{3} = 0.50$$

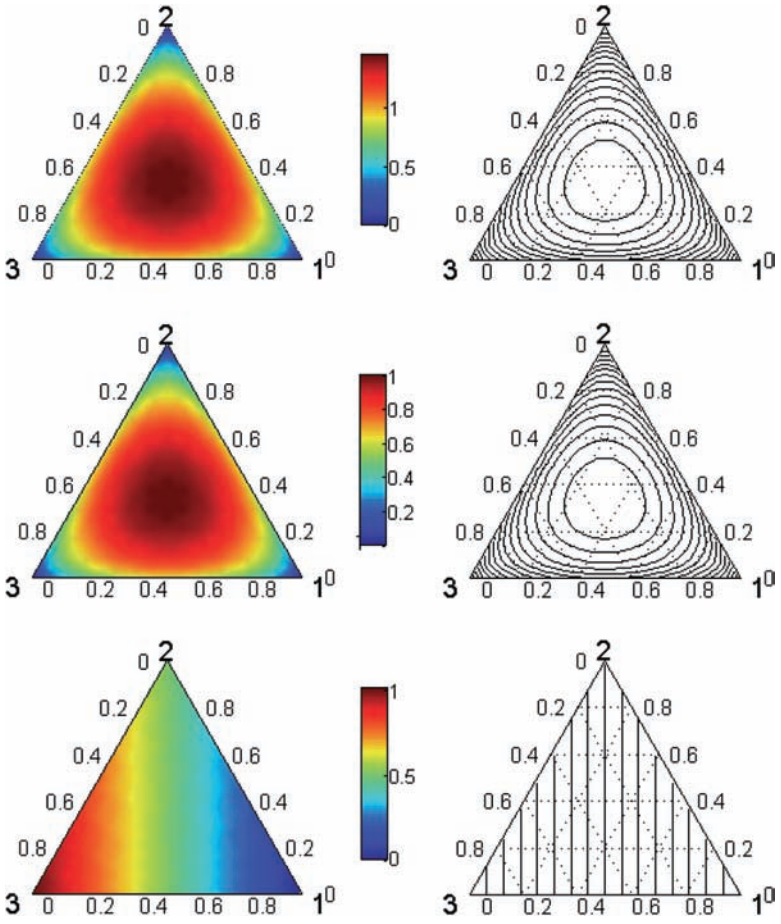

Figure 7-13 *Normalized entropy increment* B *(1st row),* B′ *(2nd row), and base entropy* A *(3rd row).*

The normalized entropy increment B is computed as

$$B = \frac{\Delta S}{\log N} = \frac{1}{\log 2} = 1.44$$

7.2.5 Grading Entropy Map

The grading entropy actually determines a projection from the standard $N - 1$ dimensional simplex (or the grain distribution set) to the two-dimensional space of the grading entropy coordinates, as illustrated in Fig. 7-14 for standard 2-simplex and 3-simplex where the grid sampled points within the standard 2- and 3-simplexes are mapped into a 2-dimensional entropy coordinate space. The grading entropy map can be defined as

$$f : \Delta_{N-1} \rightarrow [S_0 \quad \Delta S] \tag{7.73}$$

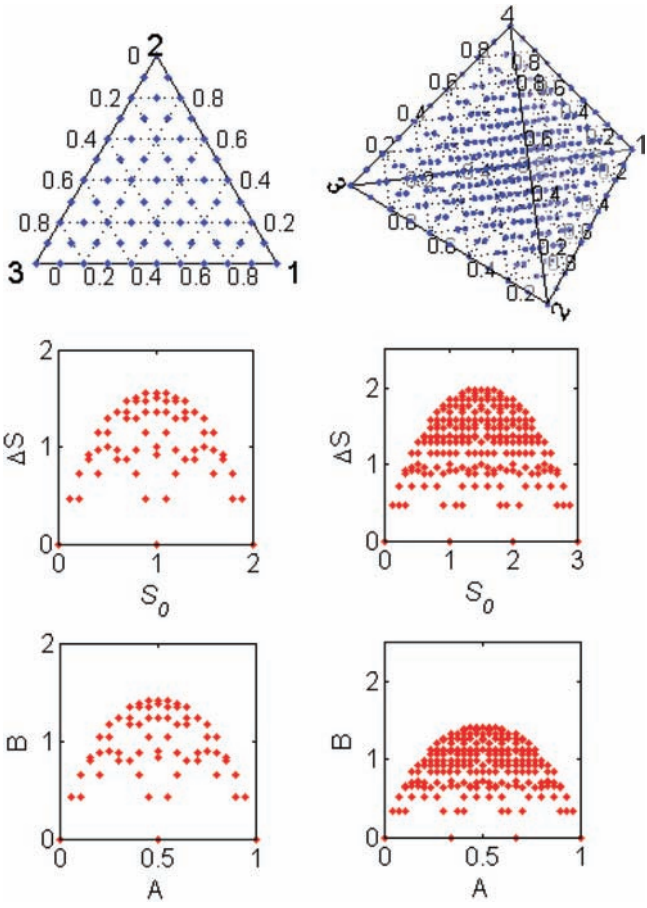

Figure 7-14 *Projection of points within 2- and 3-simplexes to grading entropy.*

and the normalized grading entropy map is defined as

$$f : \Delta_{N-1} \rightarrow [A \quad B] \tag{7.74}$$

An interesting phenomenon is observed if the grading entropy map, including normalized and nonnormalized, is plotted with increasing resolution, which means projecting more and more points within the simplex onto the two-dimensional entropy coordinate space. The resulting nonnormalized and normalized entropy diagrams for standard 2- and 3-simplexes are shown in Figs. 7-15 and 7-16, respectively. From these entropy diagrams, one can empirically conclude that under the grading entropy projection a simplex is mapped onto a closed region with an analytic maximum boundary and minimum boundary composed of several curve segments. Actually, this conclusion has a theoretical basis. If we consider the definition of base entropy S_0 (from equation [7.67a]) and entropy increment ΔS (from equation [7.60]) (or normalized base entropy A and

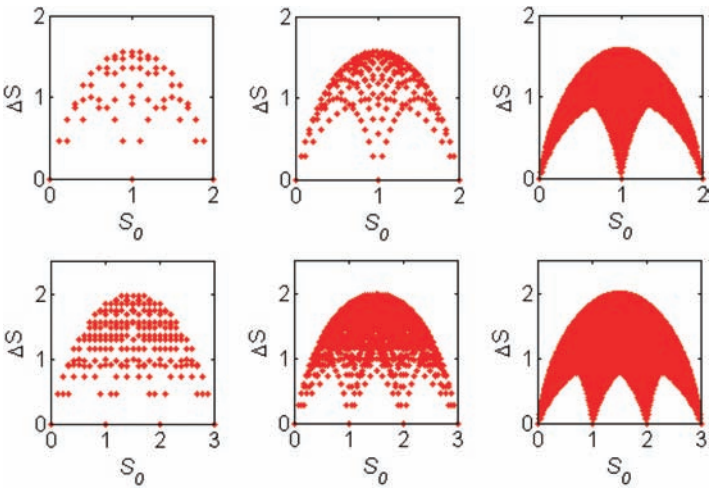

Figure 7-15 *Non-normalized grading entropy diagrams for standard 2- and 3-simplexes.*

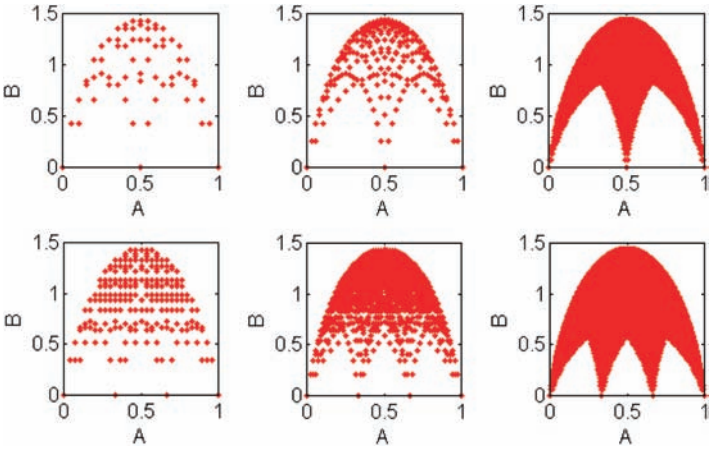

Figure 7-16 *Normalized grading entropy diagrams for standard 2- and 3-simplexes.*

entropy increment *B*), they are both analytic over the whole simplex. Because of this analytic property of the grading entropy coordinates, the entropy diagram is compact and, thus, has maximum and minimum boundaries, which are analyzed following.

Actually, not only the entropy diagram for 2-simplex and 3-simplex but also that for all other simplexes regardless of their dimension, the pattern of the diagram is the same as that shown in Fig. 7-17. A similar pattern indicates that the diagram has a maximum boundary and minimum boundary, which are formed by some curve segments. The maximum of the normalized diagram is a constant for different simplexes, which is $1/\log 2$ (approximately 1.443), as

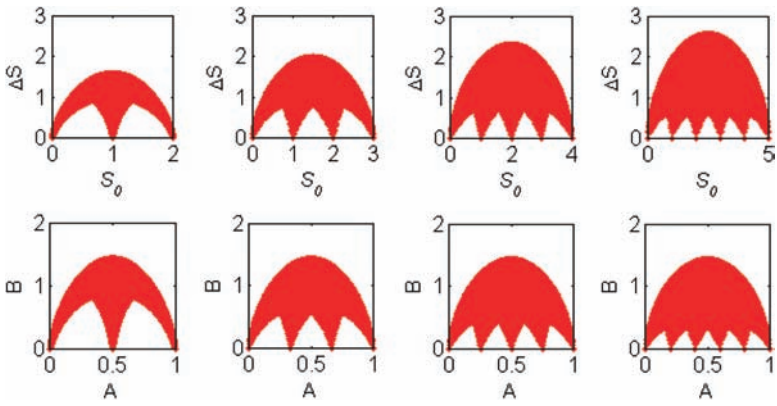

Figure 7-17 *Grading entropy diagrams for 2-, 3-, 4-, and 5-simplexes.*

derived previously, whereas in the nonnormalized entropy diagram, the maximum is not constant but varies with the total number of fractions N because the maximum entropy increment is $\log_2 N$ when grains are uniformly retained by each sieve mesh corresponding to the real cell system.

The graphs in the first row of Fig. 7-17 display an increasing trend of the normalized entropy increment ΔS as N increases from left to right. Furthermore, the minimum boundaries always span over edges of the simplex, which means that the soil mixture is composed of, at most, two fractions. This fact can be seen explicitly from the nonnormalized entropy diagram, where the S_0 axis intercepts in the diagram correspond to the eigen-entropies of the grain distribution set defined over the integrated cell system. There are in total N intercepts, and the eigen-entropies are actually the grading entropy at vertexes of the simplex, which reduce to the base entropy. As the normalization procedure just changes the value of entropy coordinates rather than the shape, the minimum boundaries in the normalized entropy diagram are also related to the edges of the simplex. The fact that minimum boundary is reached at the edges of the simplex has already been confirmed by the images of entropy increment for the case of 2-simplex in Figs. 7-12 and 7-13.

Now we discuss some properties of the entropy diagram analytically, especially for the maximum and minimum boundaries, as they are important in different applications of the grading entropy, including construction of transfer functions. They can provide valuable guidelines as to where to collect data for purposes of constructing transfer functions in a much more efficient way than that used in traditional methods.

First, the maximum boundary of the normalized entropy diagram, which is also referred to as the maximum B line, can be analyzed by maximizing the normalized entropy increment B conditioned on a specific A (Lorincz 1986). This analysis is achieved by maximizing

$$\text{maximize } B = -\frac{1}{\log N}\sum_{i=1}^{N} x_i \log_2 x_i$$

subject to equations (7.45) and (7.70). The maximization can be done using the method of Lagrange multipliers as follows:

$$L = -\frac{1}{\log_2 N}\sum_{i=1}^{N} x_i \log_2 x_i + \lambda_1\left(\sum_{i=1}^{N} x_i - 1\right) + \lambda_2\left[\sum_{i=1}^{N} x_i(i-1) - A(N-1)\right] \quad (7.75)$$

where λ_1 and λ_2 are the Lagrange multipliers corresponding to the total probability constraint and the specific A constraint, respectively.

Now differentiating the Lagrange function L with respect to the relative frequency, x_i, and equating the derivative to zero, one obtains

$$\frac{\partial L}{\partial x_i} = -\frac{1}{\log_2 N}\left(\log_2 x_i + \frac{1}{\log_2}\right) + \lambda_1 + \lambda_2(i-1) \quad (7.76)$$

Equation (7.76) can be rearranged as

$$\log_2 x_i = \log N[\lambda_1 + \lambda_2(i-1)] - \frac{1}{\log 2} \quad (7.77)$$

Then, differentiating the Lagrange function L with respect to Lagrange multipliers and equating the derivative to zero, one can have

$$\sum_{i=1}^{N} x_i - 1 = 0 \quad (7.78)$$

and

$$\sum_{i=1}^{N} x_i(i-1) - A(N-1) = 0 \quad (7.79)$$

Equations (7.77) to (7.79) constitute a system of $N + 2$ equations with $N + 2$ unknowns and can be solved.

Because our purpose is to derive an analytical formula for the maximum boundary of the normalized entropy diagram, we are interested only in the relative frequencies x_i. To that end, we consider two extreme cases where A is equal to 0 and 1, respectively. As already shown, A is equal to 0 if and only if $x_1 = 1$, $x_i = 0$ for all $i \neq 1$ and A is equal to 1 if and only if $x_{N-1} = 1$, $x_i = 0$ for all $i \neq N$. These two cases are related to two different kinds of soil mixture that are composed of a single finest fraction and a single coarsest fraction, respectively. Now one solves the system whose parameter A assumes a value falling in the open interval (0, 1). In this situation, all the relative frequencies x_i are nonzero, which means that the soil mixture is composed of N different fractions corresponding to an inner point of the standard simplex. From equation (7.77), one obtains

$$x_i = 2^{\log N[\lambda_1 + \lambda_2(i-1)] - \frac{1}{\log_2 2}} \quad (7.80)$$

For the specific case when i is equal to 1, x_1 can be expressed as

$$x_1 = 2^{\log N[\lambda_1+\lambda_2(1-1)]-\frac{1}{\log_2 2}} \tag{7.81}$$

Dividing equation (7.80) by equation (7.81), one can have

$$\frac{x_i}{x_1} = \frac{2^{\log N[\lambda_1+\lambda_2(i-1)]-\frac{1}{\log_2 2}}}{2^{\log N[\lambda_1+\lambda_2(1-1)]-\frac{1}{\log_2 2}}} = 2^{\lambda_2 \log N(i-1)} \tag{7.82}$$

Rearranging equation (7.82) as

$$x_i = 2^{\log N[\lambda_1+\lambda_2(i-1)]} x_1 \tag{7.83}$$

and letting $a = 2^{\lambda_2 \ln N}$, equation (7.83) can be rewritten as

$$x_i = a^{i-1} x_1 \tag{7.84}$$

As $a = 2^{\lambda_2 \log 2}$, it can assume positive values, and the limit of a is 0 as λ_2 tends to negative infinity as much as possible. Equation (7.84) indicates that for the normalized entropy increment B line, two terms, x_1 and a, must be determined first. Substituting equation (7.84) into the total probability constraint equation (7.45), the following is obtained:

$$\sum_{i=1}^{N} x_i = \sum_{i=1}^{N} a^{i-1} x_i = 1 \tag{7.85}$$

The right side of equation (7.85) is the sum of the first N terms of a geometric progression with factor a. Equation (7.85) can also be rewritten, if and only if $a \neq 1$, as

$$\sum_{i=1}^{N} x_i = \frac{1-a}{1-a^N} x_1 = 1 \tag{7.86}$$

Therefore,

$$x_1 = \frac{1}{\sum_{i=1}^{N} a^{i-1}} = \frac{1-a}{1-a^N} \tag{7.87}$$

It may be emphasized that the second equality is correct if and only if $a \neq 1$.

After obtaining x_1, one can further obtain x_i using the recursive expression as shown in equation (7.84). Now only the value of a remains to be determined. Recall that the third equation in the system (7.79) has not been used so far. Substituting equation (7.86) into equation (7.79), one gets

$$\sum_{i=1}^{N} x_i(i-1) = \sum_{i=1}^{N} a^{i-1}(i-1)x_1 = A(N-1) \tag{7.88}$$

Rearranging equation (7.88) as

$$\sum_{i=1}^{N} a^{i-1}(i-1) = \frac{A(N-1)}{x_i} \tag{7.89}$$

and noting that $x_1 = 1 \Big/ \sum_{i=1}^{N} a^{i-1}$ from equation (7.87) and inserting into equation (7.89), one obtains

$$\sum_{i=1}^{N} a^{i-1}(i-1) = A(N-1)\sum_{i=1}^{N} a^{i-1} \tag{7.90}$$

Equation (7.90) can be rewritten as

$$\sum_{i=1}^{N} a^{i-1}[(i-1) - A(N-1)] = 0 \tag{7.91}$$

The positive zero of the above polynomial (equation [7.91]) is just the value that we are searching for when A is not equal to either 0 or 1. Therefore, the positive root of polynomial equation (7.91) determines the formula for the maximum boundary of the normalized entropy increment B line conditioned by a specific A. The images of polynomial equation (7.91) for different N and A, including the two extreme cases, are shown in Fig. 7-18. Graphs in the first row of this figure show that when A is equal to 0, the single real root of polynomial equation (7.91) is exactly 0, which leads to $x_1 = 1$, $x_i = 0$ for all $i \neq 1$, whereas graphs in the last row indicate that there is no positive root for polynomial equation (7.91) when A is equal to 1. Therefore, in the extreme case when A assumes 1, polynomial equation (7.91) cannot be used to determine the maximum value of normalized entropy increment B. When A assumes a value falling between 0 and 1, there is only one positive root for polynomial equation (7.91), as shown in the middle two rows of Fig. 7-18. Actually this is not only an empirical conclusion but also has a theoretical basis.

According to Descartes' rule of signs, the maximum number of possible positive zeroes for a polynomial like equation (7.91) is equal to the number of times the signs of the polynomial coefficients change from positive to negative or from negative to positive when arranging the polynomial in its standard format. Examination of coefficients $i - 1 - A(N - 1)$ of polynomial equation (7.91) shows that the signs of these coefficients change only once from negative to positive as i increases from 1 to N. That means that coefficients of polynomial equation (7.91) are all negative when i is no more than $A(N - 1) + 1$ and are all positive when i is greater than $A(N - 1) + 1$. According to Descartes' rule of signs, polynomial equation (7.91) has one and only one positive root, which determines the maximum normalized entropy increment B given A between 0 and 1. From the aforementioned analysis, the procedure used to determine the maximum B line can be generalized as discussed following. Assume that the normalized base entropy A increases from 0 to 1 linearly with some increment, which can be any

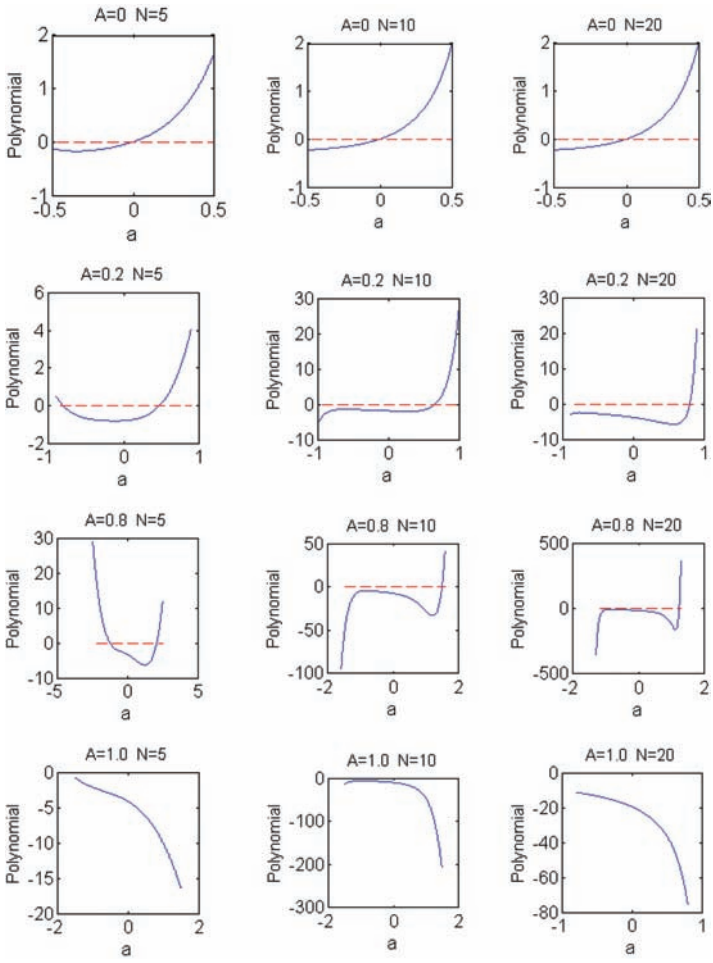

Figure 7-18 *Polynomial and its positive root.*

arbitrary positive value less than 1. Then for each A, the optimal relative frequency x_i can be computed separately for different cases. If $A = 0$, then $x_1 = 1$, and $x_i = 0$ for all $i \neq 1$. If $A = 1$, then $x_N = 1$, and $x_i = 0$ for all $i \neq N$. If $0 < A < 1$, then first, one solves for the positive zero of the polynomial given by equation (7.91). Then the relative frequency x_1 of the finest fraction is calculated by equation (7.87). Finally, all the other relative frequencies x_i, $i = 2, 3, \ldots, N$, are computed using recursive equation (7.84). Then, the optimal normalized entropy increment B is computed using its definition, i.e., equation (7.72).

The optimal normalized entropy increment B lines for 2-, 3-, 4-, and 5-simplexes, which correspond to the soil mixtures composed by 3, 4, 5, and 6 fractions, respectively, are computed, as shown in Fig. 7-19. In this figure, the image for the grain distribution corresponding to the maximum grading entropy S is also depicted as a round dot. Obviously, the grain distributions related to maximum entropy increment ΔS (or B) and maximum grading entropy S are

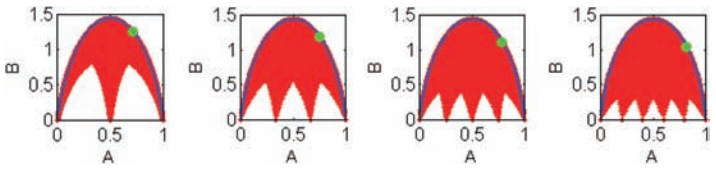

Figure 7-19 *Maximum normalized entropy increment* B *line (blue outer enveloping line) and the image of the maximum grading entropy* S *point (green spot).*

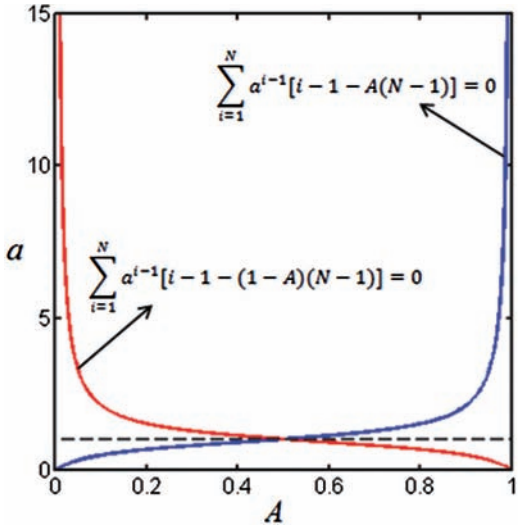

Figure 7-20 *Reciprocal relationship between positive zeroes of two polynomials indicated for* N = 7.

different. Actually, from equations (7.50) and (7.51), one can also see that the maximum grading entropy S is just a specific case of maximum entropy increment B when $a = 2$, which corresponds to different A values for different simplexes. That is why the image for the grain distribution related to the maximum grading entropy S lies on the maximum entropy increment B line.

The maximum normalized entropy increment B line is also seen to be symmetric about $A = 0.5$, as shown in Fig. 7-19. That means that the value of B for a given A is the same as that for $1 - A$. If one determines the positive zeroes of polynomial equation (7.91) for A and for $1 - A$, it is easy to find the underlying theoretical reason for observation of such a symmetry. For illustrative purposes, the graph of polynomial equation (7.91) for 6-simplex ($N = 7$) is plotted in the real Cartesian rectangular plane, as shown in Fig. 7-20. One can see from this figure that the positive zero a for polynomial equation (7.91) varies from 0 to positive infinity (infinity means no positive real zero for polynomial equation [7.91] when A is equal to 1) as A varies from 0 to 1, as shown by the left line. If we substitute A by $1 - A$ in the polynomial equation (7.91), the analogous

graph is presented as the right line in Fig. 7-19. The positive zero for the two polynomials, i.e., $\sum_{i=1}^{N} x_i(i-1) - A(N-1) = 0$ and $\sum_{i=1}^{N} x_i(i-1) - (1-A)(N-1) = 0$ is reciprocal of each other. In other words, if the positive zero of the first polynomial is a, then that for the later one will be $1/a$.

Proceeding further, assuming that given $A = A_1 \neq 0.5$, the positive zero for polynomial equation (7.91) is a_1, then the positive zero of this polynomial given $A = 1 - A_1$ is $1/a_1$, denoted as a_2. Then, the optimal grain distributions for these two cases with respect to the maximum normalized entropy increment B given normalized base entropy A are

$$\begin{matrix} x_1 & a_1 x_1 & a_1^2 x_1 & \ldots & a_1^{N-2} x_1 & a_1^{N-1} x_1 \\ x_1' & a_1 x_1' & a_1^2 x_1' & \ldots & a_1^{N-2} x_1' & a_1^{N-1} x_1' \end{matrix} \tag{7.92}$$

where since $A_1 \neq 0.5$, which means that neither a_1 nor a_2 is equal to 1, x_1 and x_1' can be computed as

$$x_1 = \frac{1 - a_1}{1 - a_1^N} \tag{7.93}$$

$$x_1' = \frac{1 - a_2}{1 - a_2^N} \tag{7.94}$$

Replacing a_2 by $1/a_1$ in equation (7.94), one can have

$$x_1' = \frac{1 - \frac{1}{a_1}}{1 - \frac{1}{a_1^N}} = \frac{(a_1 - 1)a_1^{N-1}}{a_1^N - 1} \tag{7.95}$$

At the same time, x_N is expressed as

$$x_N = a_1^{N-1} x_1 = a_1^{N-1} \frac{1 - a_1}{1 - a_1^N} = \frac{(a_1 - 1)a_1^{N-1}}{a_1^N - 1} \tag{7.96}$$

Therefore,

$$x_1' = x_N \tag{7.97}$$

Furthermore, one can also find

$$x_2' = a_2 x_1' = \frac{1}{a_1} x_N = x_{N-1} \tag{7.98}$$

Following the same method, one can have

$$\begin{aligned} x_3' &= x_{N-1} \\ \ldots &= \ldots \\ x_N' &= x_1 \end{aligned} \tag{7.99}$$

If relative frequencies x_i, corresponding to the maximum entropy increment B given the normalized base entropy A as a natural sequence series, are considered, then the previous analysis shows that the relative frequencies corresponding to that given $1 - A$ as the normalized entropy increment are a series produced by rearranging the natural one in the reverse sequence. The normalized entropy increment B is not related to the sequence of relative frequencies x_i, however, the normalized base entropy A is. Therefore, all permutations of relative frequencies x_i corresponding to maximum B conditional on A do not change the value of B. The images for all the permutations deviate from the maximum B line but still fall on the same horizontal line in the normalized entropy diagram, as shown in Fig. 7-21, except for the one in which the relative frequencies x_i are arranged in the reverse sequence, whose image point regresses back to the maximum B line again. The two image points falling on the maximum B line are symmetric about $A = 0.5$ in the normalized grading entropy diagram.

The maximum B line depends on the total number of fractions N, because the positive zero of the polynomial equation (7.91) is dependent on N. Fig. 7-22 shows the maximum B line for different numbers of fractions N varying from 2 to 100. The figure shows that the difference in the maximum B line for different

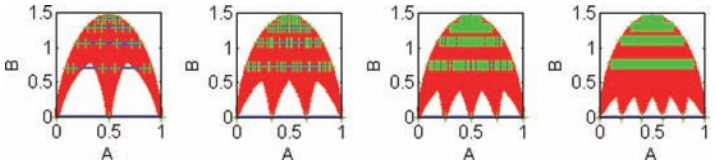

Figure 7-21 *Image points (cross) of relative frequency x_i corresponding to the maximum normalized entropy increment* B *for different specific normalized base entropies* A *(0, 0.2, 0.4, 0.6, 0.8, and 1.0 from bottom to top) and all its possible permutations.*

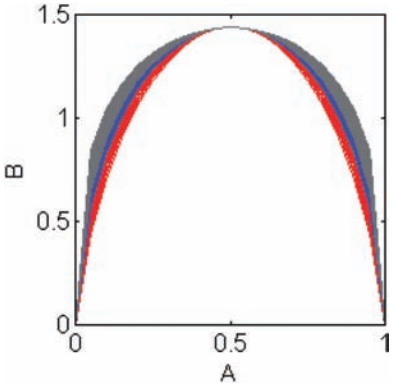

Figure 7-22 *Maximum* B *lines for* N *varying from 1 to 100 in the normalized grading entropy diagram (red, blue, and gray lines are for* N *varying from 2 to 10, 11 to 20, and 21 to 100, respectively).*

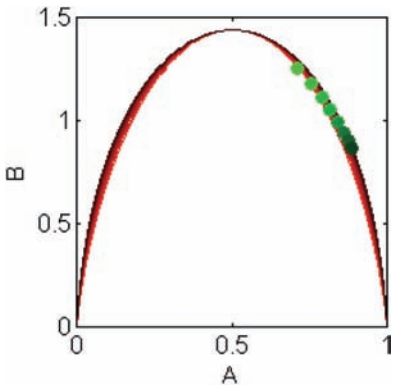

Figure 7-23 *Maximum* B *lines (red lines) for* N *varying from 1 to 10 and the corresponding images (round dots) for maximum grading entropy points (as* N *varying from 2 to 10, the color of lines and spots becomes darker).*

N values is not so much and is even negligible for small N. It follows that in practice the maximum B line can be approximated by that for small N, for example $N = 2$. In Fig. 7-23, the maximum entropy S point for different N values varying from 2 to 10 is graphed on the corresponding maximum B line. Results show that as N increases the maximum grading entropy point moves far away from the maximum normalized entropy increment B point along the right half branch of the corresponding maximum B line.

Now the minimum boundary of (normalized) grading entropy map, also referred to as the minimum B line, is analyzed. From the exploratory analysis of the entropy map, it is already known that the minima of normalized entropy increment B appear at the edges of the simplex as shown in Figs. 7-12, 7-13, and 7-17. These figures show that the global minima always appear at the vertexes of the simplex, which is mapped onto the A-axis intercepts in the normalized grading entropy map or the S_0-axis intercepts in the nonnormalized grading entropy map. Taking the $N - 1$ standard simplex as an example, which corresponds to the soil mixture composed of at most N fractions, its i-vertex is expressed as $x_i = 1$ and $x_j = 0$, for all $j \neq i$, then the normalized base entropy A and entropy increment B can be computed as

$$A(i) = \frac{1}{N-1}\sum_{k=1}^{N} x_k(k-1) = \frac{i-1}{N-1} \tag{7.100}$$

$$B(i) = -\frac{1}{\log N}\sum_{k=1}^{N} x_k \log_2 x_k = 0 \tag{7.101}$$

These results confirm the observation in the exploratory analysis that the vertexes of the simplex corresponding to the uniform soil are mapped onto the A-axis intercepts in the normalized grading entropy map. If we look at the ij-edge of this simplex, the analysis shows that all the points on the ij-edge are mapped

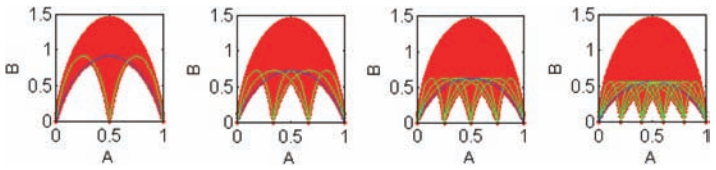

Figure 7-24 *Minimum* B *line for standard 2-, 3-, 4-, and 5-simplex from left to right, where the blue line is the minimum* B *line corresponding to the 1*N*-edge of the simplex.*

onto a closed interval in terms of the normalized base entropy A, and this interval is given by

$$[A_i, \quad A_j], \text{ i.e., } \left[\frac{i-1}{N-1}, \quad \frac{j-1}{N-1}\right] \tag{7.102}$$

For a specific case, the 1N-edge is mapped onto interval [0, 1]. Then, for any point on the ij-edge, which can be expressed as $x_i + x_j = 1$ and $x_k = 0$ for all $k \neq i$ or j, it is mapped onto the point given by

$$\left[\frac{x_i(i-1)+x_j(j-1)}{N-1}, \quad \frac{1}{\log N}(x_i \log_2 x_i + x_j \log x_j)\right] \tag{7.103}$$

on the normalized grading entropy map. Thus far, the minimum boundaries of the normalized grading entropy map can be computed. However, in practice Imre et al. (2008, 2009) state that not all the minimum B lines need to be computed and the image of the 1N-edge can be used as an acceptable approximation to the minimum B line, which for standard 2-, 3-, 4-, and 5-simplex is plotted in Fig. 7-24, where the approximate minimum B line is highlighted by a blue line.

Example 7.6 Consider a grading curve with seven fractions. Compute the grading entropy coordinates A and B. Let the eigen-entropy of the smallest fraction be $S_{01} = 10$.

Solution The relative frequencies of fractions are equal:

$$x_i = \frac{1}{7}$$

The base entropy S_0 is computed as

$$S_0 = \sum_{i=1}^{N} x_i(i-1) + S_{01} = \sum_{i=1}^{7} \frac{1}{7}(i-1) + 10 = 13.00$$

The entropy increment ΔS is computed as

$$\Delta S = -\frac{1}{\log 2}\sum_{i=1}^{N} x_i \log x_i = -\frac{1}{\log 2} \times 7 \times \frac{1}{7} \times \log\left(\frac{1}{7}\right) = 2.807 \text{ nats}$$

For the normalized base entropy r, the relative base entropy A is given as

$$A = \frac{\sum_{i=1}^{N} x_i(i-1)}{N-1} = \frac{\sum_{i=1}^{7} \frac{1}{7}(i-1)}{6} = 0.50$$

The normalized entropy increment B is calculated as

$$B = \frac{\Delta S}{\log 7} = 1.443$$

7.2.6 Inverse Image of Grading Entropy Map

There are two different kinds of points in the normalized or nonnormalized grading entropy map: regular points and critical points. Critical points are referred to as the points on the maximum entropy increment ΔS line or the normalized maximum entropy increment B line. Otherwise the points are referred to as regular points.

The inverse images of critical points are easy to obtain. Recalling the method for deriving the maximum B line, it is easy to find that the method is also suitable for finding the inverse images of critical points. For ease of understanding, the method is restated as follows. For example, we want to find the inverse image of point [A B] on the maximum B line. Then, its inverse image can be found on different paths according to the value of normalized base entropy A, as in the preceding section.

The inverse images of the maximum B line for 2- and 3-simplexes, which correspond to soil mixtures composed of three and four different fractions, respectively, are shown in Fig. 7-25. In this figure, the inverse images for the

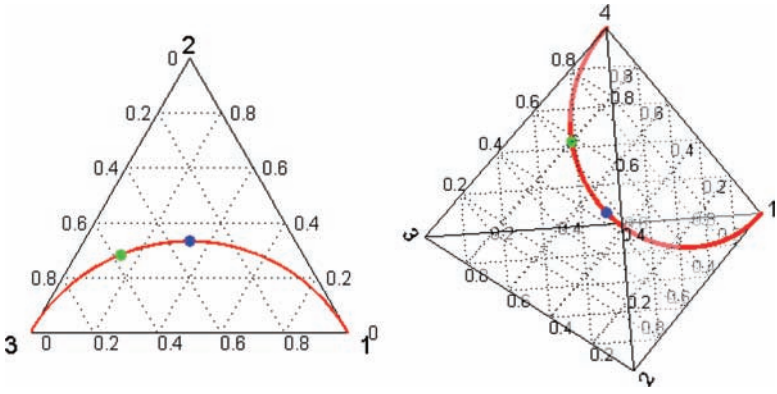

Figure 7-25 *Optimal grading curve line (inverse image of the maximum* B *line) (red line), the inverse image of maximum grading entropy* S *point (green point), and the inverse image of maximum entropy increment point (blue point) for 2- and 3-simplexes.*

maximum grading entropy *S* point and the maximum entropy increment *B* point are also depicted on the optimal grading curve line by green and blue points, respectively. Obviously, they are different points as already derived using the method of Lagrange multipliers. Fig. 7-25 also shows that the inverse images of the maximum *B* line, also known as optimal points, constitute a continuous line connecting vertex 1 and vertex *N* of the standard $N - 1$ simplex.

The inverse images of regular points can be determined theoretically from the following system of equations, which corresponds to the definition of simplex, also known as the total probability constraint equation (7.45), and the definition of normalized grading entropy coordinates given by equations (7.71) and (7.72). These equations constitute a system defining an $N - 3$ dimensional manifold. However, it is not easy to solve this system theoretically. One feasible alternative is to find its numerical solution.

Generally, the lookup table approximation method can be used to derive the approximate numerical solution for this system. One strategy is to sample the standard $N - 1$ simplex using a regular grid, as shown in the right graph of Fig. 7-26, then compute the normalized grading entropy coordinates *A* and *B* for each grid, so that a lookup table can be constructed. Next, if one wants to find the inverse image for a given [*A B*], then one just needs to scan the lookup table and locate the acceptable approximate solution. One problem involved in this method is that it becomes intractable as the number of fractions increases.

Another alternative strategy is to construct the lookup table in a random way, which means sampling the $N - 1$ simplex and all possible subsimplexes, including continuous and noncontinuous, corresponding to continuous-graded grading curve and gap-graded grading curve, respectively (continuous-graded grading curve refers to the case, for example, where there are three cells and the fraction for each cell is nonzero, whereas for the gap-graded grading curve the fraction for the second cell is zero). The result of random sampling is shown in the right graph of Fig. 7-26. Numerical experiments show that the random approximation method yields more or less the same result as that produced by the gridded approximation method for small simplexes. Furthermore, the random approximation method outperforms the former one significantly, expecially for higher

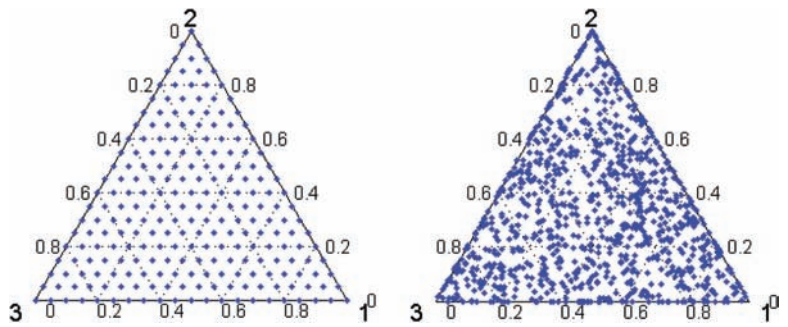

Figure 7-26 *Two different sampling strategies for the lookup table approximation method (left for grid sampling and right for random sampling).*

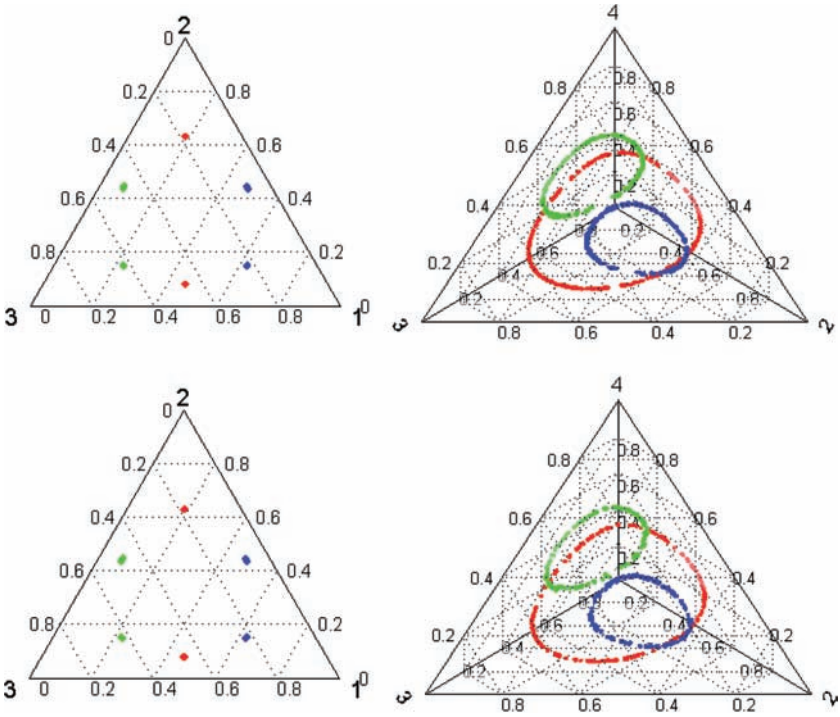

Figure 7-27 *Inverse images computed by grid lookup table approximation (upper) and random lookup table approximation for 2- and 3-simplex for different grading entropy coordinates.Note: Green:* A = *0.7,* B = *1.2; red:* A = *0.5,* B = *1.2; blue:* A = *0.3,* B = *1.2.*

dimensional simplexes. The former method cannot give an accurate solution, even for a simplex with a dimension higher than 4.

Comparison between these two different methods is shown in Fig. 7-27, where the approximation numerical solution for the inverse images of B = 1.2, A = 0.3, 0.5, and 0.7 are depicted. Results indicate that both methods yield numerical solutions for the system of grading entropy inverse image equations with an acceptable accuracy, even though the same "out of memory" problem appears quickly as the number of fractions increases. However, the inverse image of regular points is not valuable for pratical applications of grading entropy. One is always interested in the optimal B line and its inverse image and the optimal point line or optimal grading curves.

Example 7.7 Let $N = 3$, $A = 0.2$, and $B = 0.9$. Compute x_1, x_2, and x_3.

Solution As discussed earlier, it is difficult to get the theoretical solution for the inverse image of a regular point [0.2, 0.9]. Therefore, one can resort to the lookup table approximation method, as detailed earlier. Using that method, one can obtain the relationship between the regular point [0.2, 0.9] and its inverse image, as

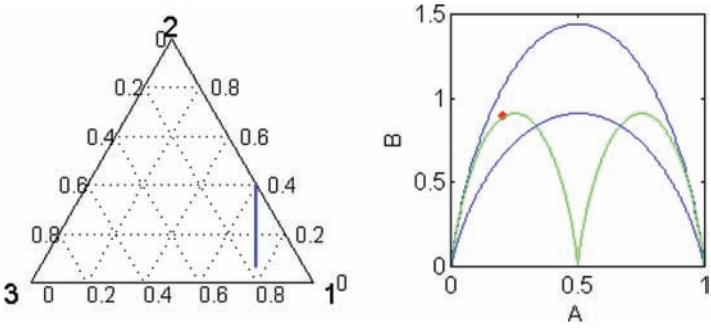

Figure 7-28 *Sampling strategy and image points of relative frequency corresponding to maximum normalized entropy increment B.*

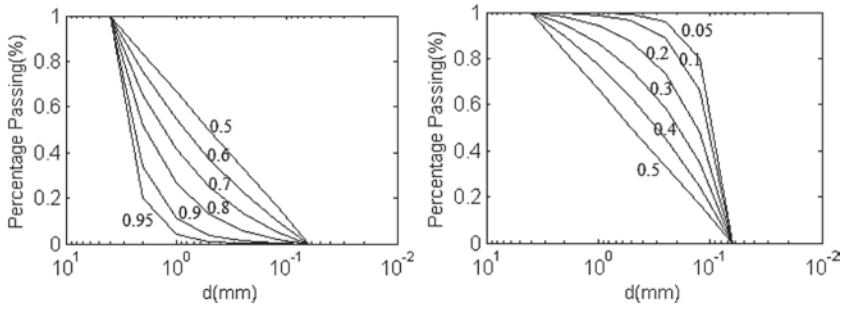

Figure 7-29 *Optimal grading curves for different normalized entropy increments* $d_0 = 2^{-4}$ *and* $N = 6$.

shown in Fig. 7-28. All the points on the line in the left of the figure are projected onto the same point in the grading entropy map, as shown in the right of the figure.

The inverse image of a grading entropy diagram can also be shown in terms of grading curve. Some interesting observations are found if the optimal grading curves for a different normalized entropy increment A are plotted. Assuming that the grading curve space of interest can be defined as $d_0 = 2^{-4}$ and $N = 6$, the optimal grading curves for different normalized base entropy A can be plotted in a semilogarithmic coordinate system, as shown in Fig. 7-29. The optimal grading curve is convex if $A > 0.5$, linear if $A = 0.5$, and concave if $A < 0.5$.

As stated, the inverse image of the maximum B line plays an important role in the application of grading entropy. The inverse images of the maximum B line are also known as the optimal grading curves. Actually, the optimal grading curve or grading distribution follows a fractal distribution (Einav 2007) whose distribution function is expressed as

$$F(d) = \frac{d^{3-n} - d_{\min}^{3-n}}{d_{\max}^{3-n} - d_{\min}^{3-n}} \tag{7.104}$$

where d is the grain diameter and n is the fractal dimension. This result can be shown if we take into account the definition of the real cell system and the inverse image of the maximum normalized entropy increment B line. The definition of a real cell system states that the diameter range of the particles retained by the ith fraction is

$$2^{i-1}d_{\min} < d^i \le 2^i d_{\min} \tag{7.105}$$

The distribution function $F(d)$ represents the relative frequencies of particles whose diameter is no more than d. Therefore, the relative frequency of the ith fraction can be expressed as

$$x_i = \text{prob}(2^{i-1}d_{\min} < d \le 2^i d_{\min}) = F(2^i d_{\min}) - F(2^{i-1}d_{\min}) \tag{7.106}$$

Using the definition of the fractal distribution function, the two terms on the right side of equation (7.106) can be written as

$$F(2^i d_{\min}) = \frac{(2^i d_{\min})^{3-n} - d_{\min}^{3-n}}{d_{\max}^{3-n} - d_{\min}^{3-n}} = \frac{[2^{i(3-n)} - 1]d_{\min}^{3-n}}{d_{\max}^{3-n} - d_{\min}^{3-n}} \tag{7.107}$$

and

$$F(2^{i-1}d_{\min}) = \frac{(2^{i-1}d_{\min})^{3-n} - d_{\min}^{3-n}}{d_{\max}^{3-n} - d_{\min}^{3-n}} = \frac{[2^{(i-1)(3-n)} - 1]d_{\min}^{3-n}}{d_{\max}^{3-n} - d_{\min}^{3-n}} \tag{7.108}$$

Therefore, the relative frequency x_i can further be expressed as

$$x_i = \frac{[d^{i(3-n)} - 1]d_{\min}^{3-n}}{d_{\max}^{3-n} - d_{\min}^{3-n}} - \frac{[2^{(i-1)(3-n)} - 1]d_{\min}^{3-n}}{d_{\max}^{3-n} - d_{\min}^{3-n}} = \frac{(2^{3-n} - 1)d_{\min}^{3-n}}{d_{\max}^{3-n} - d_{\min}^{3-n}} 2^{(3-n)(i-1)} \tag{7.109}$$

Now recalling the procedure about how to derive the maximum B line, the optimal relative frequency x_i can be computed as $x_i = a^{i-1}x_1$, where a is the positive root of polynomial equation (7.109). If

$$x_1 = \frac{(2^{3-n} - 1)d_{\min}^{3-n}}{d_{\max}^{3-n} - d_{\min}^{3-n}}, \quad a = 2^{3-n} \tag{7.110}$$

one observes that the optimal grading curves have the same form as the fractal distribution. When $A = 0.5$, a is equal to 1 regardless of the value of the number of fractions N, and the fractal dimension is equal to three. Thus, it can be stated that the optimal grading curve corresponding to the global maximum entropy increment B is fractal distributed with a fractal dimension of three.

7.2.7 Revisiting Grading Entropy Coordinates

Here the geometric and physical meaning of the normalized grading entropy coordinates is analyzed to understand the concept of grading entropy from

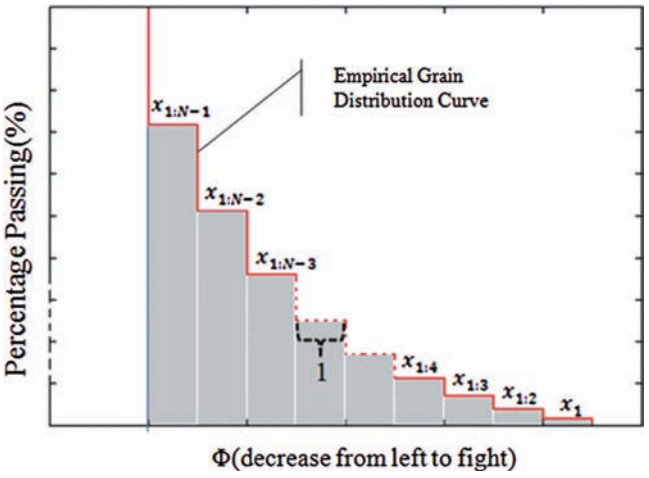

Figure 7-30 *The geometric meaning of normalized base entropy* A.

another perspective. Equations (7.70) and (7.72) for the normalized grading entropy coordinates are recalled:

$$\text{Normalized base entropy } A = \frac{1}{N-1}\sum_{i=1}^{N} x_i(i-1)$$

$$\text{Normalized entropy increment } B = -\frac{1}{\log N}\sum_{i=1}^{N} x_i \log_2 x_i$$

First, the geometric meaning of normalized base entropy A is analyzed. For this part, we begin with the statement that the normalized base entropy is a measure of the subarea of the corresponding grading curve. As stated earlier, because particle diameters always span several orders of magnitude, to effectively and conveniently describe the wide range of data, a base 2 logarithmic ϕ scale is a widely used way to represent the grain size information. For a given grain size diameter d in millimeters, the ϕ scale can be computed as

$$\phi = -\log_2 d \tag{7.111}$$

Then, using the ϕ scale as the horizontal coordinate and the percentage of particles passing though the sieve mesh with the corresponding diameter as the vertical coordinate, the empirical grain distribution can be depicted using a stairs format plot, which is widely used to plot the emperical probability distribution in statistical exploratory data analysis. The resulting grain distribution curve is like that in Fig. 7-30. The subarea of the grain curve can be computed as

$$
\begin{aligned}
S_{\text{subarea}} &= x_1 + x_{1:2} + x_{1:3} + \ldots + x_{1:N-1} \\
&= x_1 + \sum_{i=1}^{2} x_i + \sum_{i=1}^{3} x_i + \ldots + \sum_{i=1}^{N-1} x_i \\
&= 1 - \sum_{i=2}^{N} x_i + 1 - \sum_{i=3}^{N} x_i + 1 - \sum_{i=4}^{N} x_i + \ldots + \sum_{i=N}^{N} x_i \\
&= N - 1 - [x_2 + 2x_3 + 3x_4 + \ldots + (N-1)x_N] \\
&= N - 1 - [0x_1 + 1x_2 + 2x_3 + \ldots + (N-1)x_N] \\
&= N - 1 - \sum_{i=1}^{N} x_i(i-1)
\end{aligned}
\tag{7.112}
$$

Substituting the definition of normalized base entropy, one gets

$$
S_{\text{subarea}} = N - 1 - A(N-1) = (1-A)(N-1) \tag{7.113}
$$

Rearranging equation (7.113), one obtains

$$
A = 1 - \frac{S_{\text{subarea}}}{N-1} \tag{7.114}
$$

where $S_{\text{subarea}}/N-1$ is exactly the average height of the stairs in the grain distribution curve.

Sometimes the grain distribution curve can also be plotted in the same semilogarithmic coordinates as those in Fig. 7-29. In this case, the subarea of the grain distribution curve can be approximated by $(1 - A)(N - 1)$. Regardless of the kind of grain distribution curve adopted, the aforementioned analysis indicates that the normalized base entropy A is a quantitative measure of the area below the grading curve. It follows that the possible grading curves with the same A have the same subarea of the grain distribution curve and any two of them may deviate from each other in such a way that equal areas can be found below and above. For example, the grading entropy point for $A = 0.7$, $B = 1.2$ has two different original images, i.e., two different grain distribution curves. Both of them have the same normalized entropy increment: $A = 0.7$. Therefore, they also have the same subarea below the grain distribution curve, and they deviate from each other in the way that equal areas can be found below and above, as shown in Fig. 7-31.

The physical meaning of the normalized base entropy A is a measure of the stability of the grain structure (Lorincz 1986; Lorincz et al. 2008). When mapping the grading curves of different soils onto the normalized grading entropy map, we see that all grading curves with stable structure fall into the area where A is greater than or equal to 2/3 and all those with unstable structure fall into the area with A less than 2/3 (Fig. 7-32).

Now another mathematical meaning of the normalized entropy increment B is given, from which the intitutive physical meaning of B can be generalized. As already determined, the normalized entropy increment B is nothing but the application of the Shannon entropy to the real cell system. Therefore, it can be considered as a measure of uncertainty of the grain distribution and has the

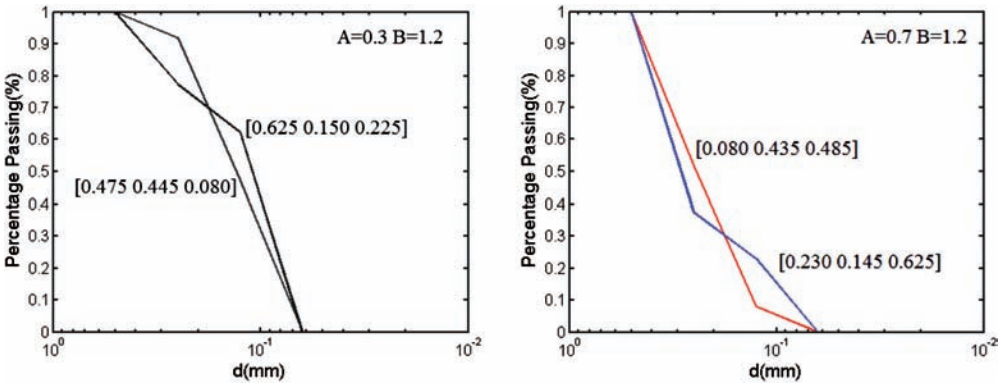

Figure 7-31 *Behavior of different grading curves with the same normalized base entropy* A.

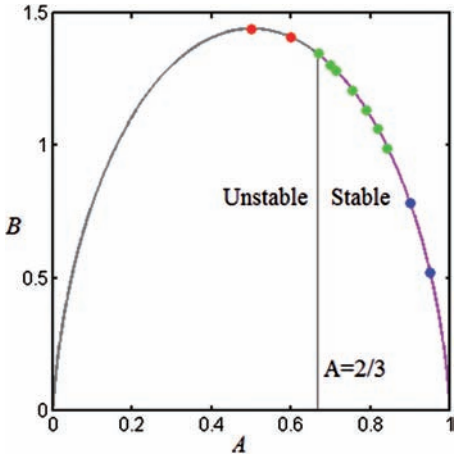

Figure 7-32 *Particle migration zones (the grain structure is stable with* A ≥ *2/3 and unstable with* A < *2/3).*

global maximum value when particles are uniformly distributed among all fractions, which corresponds to the most uniform grading curve represented by a linear line in the semilogarithmic coordinate system, as shown in Fig. 7-29.

Conversely, the normalized entropy increment B (or entropy increment ΔS) can be shown as the logarithmic geometric mean of relative frequencies x_i weighted by themselves. The generalized geometric mean of relative frequencies x_i weighted by themselves is expressed as

$$GM = \exp\left[\frac{\sum_{i=1}^{N} x_i \log_2 x_i}{\sum_{i=1}^{N} x_i}\right] = \exp\left[\sum_{i=1}^{N} x_i \log_2 x_i\right] \tag{7.115}$$

Taking the logarithm of both sides of equation (7.115), one obtains

$$\ln GM = \sum_{i=1}^{N} x_i \log_2 x_i \tag{7.116}$$

Recalling the definition of normalized entropy increment, equation (7.116) can also be rewritten as

$$B = -\frac{1}{\ln 2 \ln N} \sum_{i=1}^{N} x_i \log_2 x_i \tag{7.117}$$

Rearranging equation (7.117), one can get

$$-B \ln 2 \ln N = \sum_{i=1}^{N} x_i \log_2 x_i \tag{7.118}$$

Therefore, equation (7.116) can be written as

$$\ln GM = -B \ln 2 \ln N \text{ or } B = -\frac{\ln GM}{\ln 2 \ln N} \tag{7.119}$$

Equation (7.119) expressses the relationship between generalized weighted geometric mean GM and B and shows that the normalized entropy increment B is a kind of rescaled and logarithmic transformed geometric mean of relative frequencies x_i. Then, the maximum B line in the normalized grading entropy map can be assigned an intuitive but useful geometric explanation. Before giving this explanation, it is better to know the section of the standard $N-1$ simplex when A is a constant, which can be an arbitrary value falling between 0 and 1. For convenience, we call this section an A-section. The A-section of a standard $N-1$ simplex can be represented by equations (7.45) and (7.70):

$$A = \frac{1}{N-1} \sum_{i=1}^{N} x_i (i-1)$$

These equations define an $N-2$ dimensional hyperplane in the $N-1$ dimensional Euclidean space generated by the $N-1$ dimensional simplex, intersecting the 1N edge of the simplex at a distance A from the 1 vertex. For different A values, the A-sections are a series of parallel hyperplanes, as shown in Fig. 7-33, where the A-sections corresponding to different A for 2- and 3-dimensional simplexes are presented.

Now we give an intuitive explanation of the maximum line. First we consider the global maximum B point, which is related to $A = 0.5$. As is known, the geometric mean is greater than or equal to the arithmetic mean, and the equality is met if and only if the particles are uniformly distributed, i.e., $x_i = 1/N$. At this time, the geometric mean reaches its global minimum value, and thus the normalized entropy increment B also reaches its global maximum point. Thus, it can be concluded that the normalized entropy increment is maximized when the weighted geometric mean of relative frequencies x_1 is minimized. This situation would result in the global optimal grain distribution, which is the most uniform

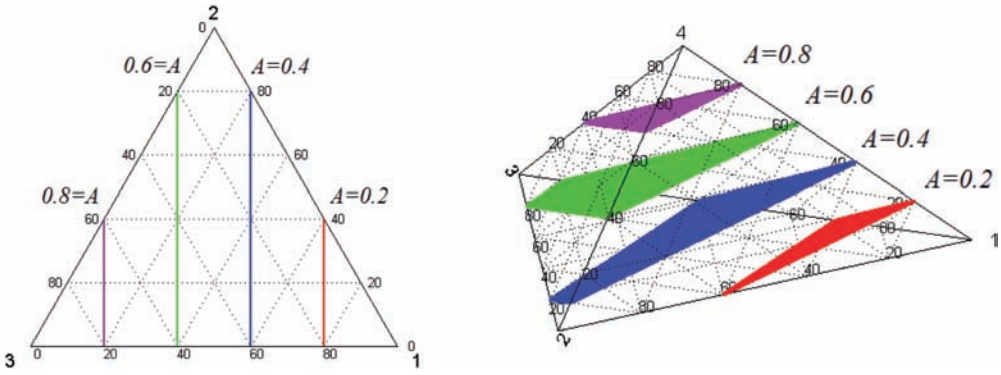

Figure 7-33 A-*sections corresponding to different* A *values for standard 2- and 3-simplexes.*

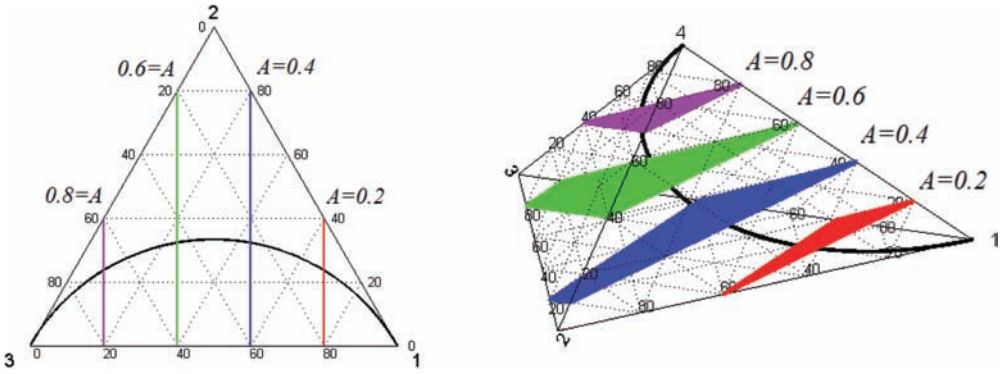

Figure 7-34 A-*sections corresponding to different* A *values for standard 2- and 3-simplexes and the optimal grading curve line (solid bold black line).*

one in the possible grading curve space. The same holds if the maximum B point is not the global maximum one but some other point on the maximum B line deviating from the peak. In such a case, the geometric meaning of this maximum B can be explained as it is met when the weighted geometric mean of relative frequencies x_i on the corresponding A-section is minimized, and it would result in an optimal grading curve, which is the most uniform in this section. Therefore, the intersection point of the A-section with the optimal grading curve line (as shown in Fig. 7-34) is related to the most uniform grain distribution among all distributions in this section.

7.2.8 Extension Property of the Entropy Diagram

The extension property of the entropy diagram is referred to as the cascade structure of the nonnormalized maximum entropy increment ΔS line in the grading entropy diagram. The grading curve space has already been defined by specifying the minimum particle diameter d_0 and the maximum number of fractions N. That

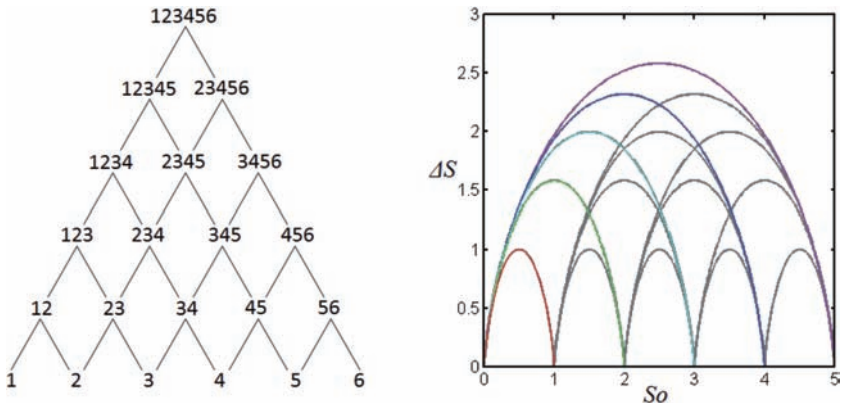

Figure 7-35 *Cascade structure of the largest simplex and its continuous subsimplex (left) and the cascade structure of the maximum entropy increment* ΔS *lines corresponding to the largest simplex and its subsimplex (right).*

means we have defined an $N - 1$ dimensional simplex. The largest simplex, together with all its continuous subsimplexes, has a lattice or cascade structure, as shown in the left graph of Fig. 7-35. Since the maximum entropy increment line is most important in the application of grading entropy, one can easily find that the maximum entropy increment lines for the largest simplex and all its continuous subsimplexes have the same cascade structure when plotting the maximum ΔS line on the nonnormalized entropy diagram, as in the right graph of Fig. 7-35. However, such a cascade structure disappears in the normalized grading entropy diagram because of the fact that the range of both normalized base entropy and entropy increment are independent of N. Such an extension property of the maximum entropy increment ΔS line in the nonnormalized grading entropy diagram plays an important role in the application of grading entropy. The method of constructing a transfer function between soil physical property and the corresponding grading curve is inspired by this property.

7.2.9 Application of Grading Entropy Theory

The so-called geometrical criterion for particle migration has always been discussed in terms of different parameters of the grain size distribution. Grading entropy coordinates can also be used for characterizing piping and suffusion phenomena, which are common in the leachate collection system of landfills (Lorincz et al. 2009). Laboratory test results show that the normalized grading entropy diagram can be divided into three different zones, i.e., the piping zone, stable zone, and stable with suffusion zone, where $A = 2/3$ is the boundary between the stable and unstable zones, as shown in Fig. 7-36. In the unstable zone, where A is less than 2/3, the coarse particles float in the matrix of the finer ones. Otherwise, in the stable zone with $A \geq 2/3$, the coarse particles form a permanent skeleton (Lorincz et al. 2009).

Grading entropy can also be used to explain the procedure of the particle breakage process (Lorincz et al. 2008). Crushing tests performed by Lorincz et al.

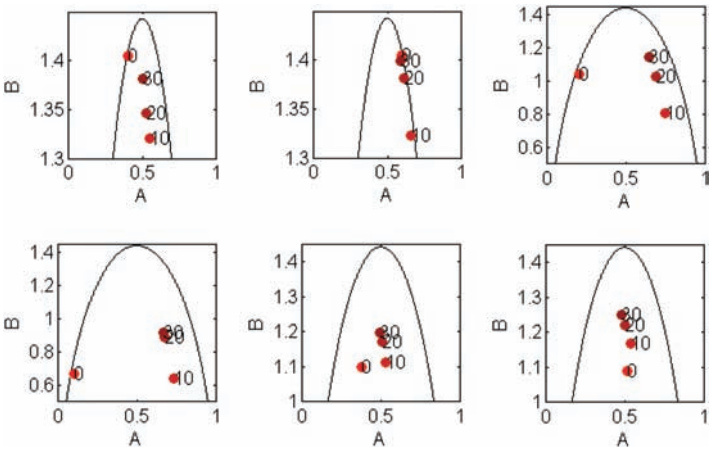

Figure 7-36 *Grading entropy paths for different crushing tests.*

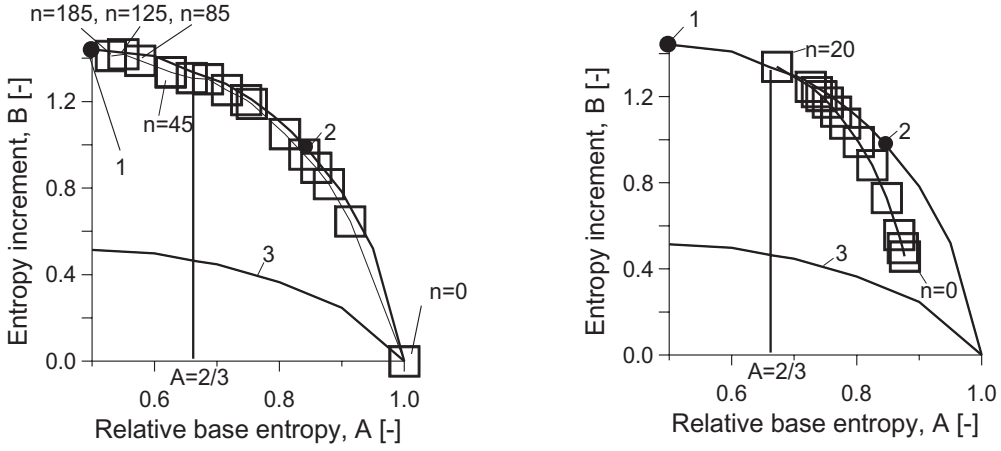

Figure 7-37 *Grading entropy variations with the number of crushing tests. Source: Adapted from Lorincz et al. 2008.*

(2005) showed that the grading entropy path always moves along the right half branch of the maximum normalized entropy increment *B* line and approaches the global maximum point. If the *A* value of the initial grading distribution is less than 0.5, after the first 10 crushings, the grading entropy point jumps abruptly from the left branch to the right branch, whether the initial grading entropy point is on the maximum entropy increment *B* line or not, and then for further crushing the grading entropy point moves along the maximum *B* line in its increasing direction but never reaches the global maximum *B* point. This procedure can be shown in Fig. 7-36 whose data are from Lorincz et al. (2008). Another well-designed crushing test, also conducted by Lorincz (1986), showed that during particle breakage the grading entropy path first moves to the right branch of the maximum *B* line, and then it moves along this line in its increasing direction until reaching the global maximum *B* point. The test results are shown in Fig. 7-37.

Another valuable application of grading entropy is to construct a transfer function between grading curves and their corresponding physical properties. Imre et al. (2009) used the extension property of the normalized maximum entropy increment line in the grading entropy diagram to construct the dry density transfer function. The procedure can be generalized in four steps. The first step is to define the large simplex, which can describe the space of possible grading curves of interest by specifying the minimum particle diameter d_0 and the total number of fractions N.

In the second step, all the continuous subsimplexes are selected and the optimal grading curves (the inverse image of the maximum normalized entropy increment B line) are specified for each subsimplex. In the third step, the soil physical property of interest is measured for each of the optimal grading curves. Finally, this physical property is interpolated in the 2-dimensional space of the nonnormalized grading entropy diagram, which means that the preliminary transfer function is constructed. According to Imre et al. (2009), the interpolated isoline is almost linear in the 2-dimensional space, as shown in Fig. 7-38. Then the physical property for any unknown continuous graded grain distribution can

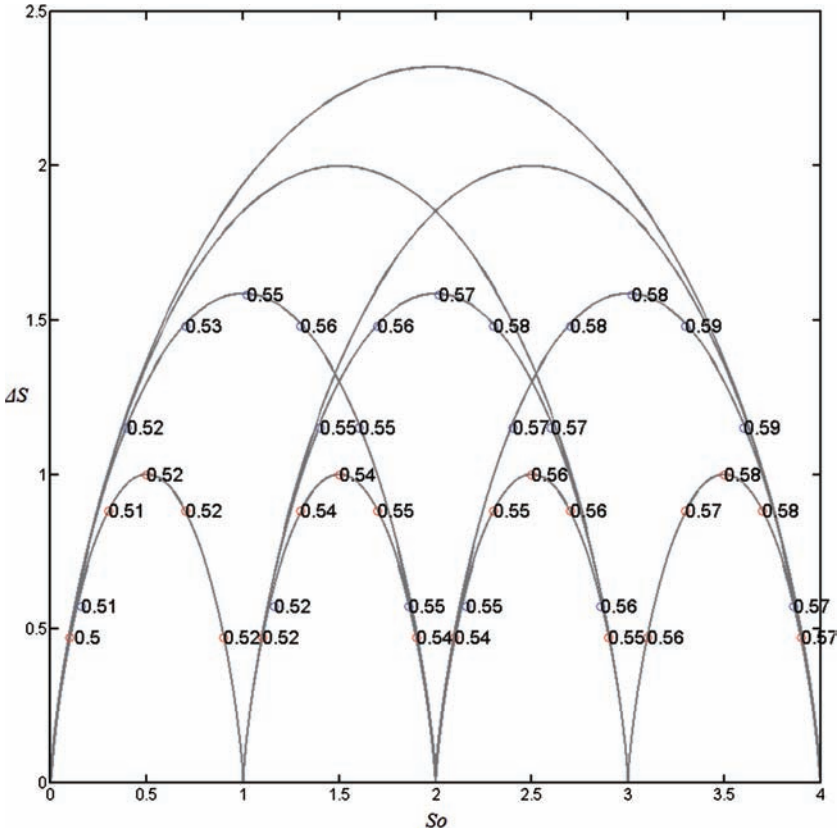

Figure 7.38 *Sampling points for transfer function construction based on grading entropy theory.*

be predicted using this preliminary transfer function. As is already known, the optimal grading curve represents a kind of most uniform distribution, so the extreme value for such properties is lost when using this method. Compared with traditional methods, the most attractive advantage of this method is that it is much more efficient, because the required number of measurements is small.

Questions

Q7.1 Collect grain size data from a sieve analysis. Plot the grain size distribution and compute the mean, standard deviation, coefficient of variation, coefficient of skewness, and coefficient of kurtosis.

Q7.2 Determine the grain size distribution for the data in Q7.1 using the method of moments and determine its goodness.

Q7.3 Determine the grain size distribution for the data in Q7.1 using entropy and determine its goodness. Then, compare this distribution with that in Q7.2.

Q7.4 Compute the eigen-entropy of the fraction between sieves of 2 mm and 4 mm, and between 4 mm and 8 mm.

Q7.5 Compute eigen-entropy values of the fractions from 2 to 10.

Q7.6 Assume that a soil system is mixed with two neighboring fractions, such that one fraction is twice the size of the other fraction. Compute the relative frequency for each fraction leading to the maximum grading entropy.

Q7.7 Assume a point [0.4, 0.6] in the Cartesian rectangular coordinate system. Project this point into the ternary coordinate system.

Q7.8 Consider a grading curve of a soil consisting of three fractions, $N = 3$. Let the smallest fraction be between the grain diameter of $d = 0.05$ mm and $d = 0.15$ mm. Compute grading entropy A and B.

Q7.9 Consider a grading curve with six fractions. Compute the grading entropy coordinates A and B. Let the eigen-entropy of the smallest fraction be $S_{01} = 10$.

Q7.10 Let $N = 3$, $A = 0.3$, and $B = 0.8$. Compute x_1, x_2, and x_3.

References

Baker, H. A. (1920). "On the investigation of the mechanical constitution of loose arenaceous sediments by the method of elutriation, with special reference to the Thanet beds of the southern side of the London basin." *Geol. Mag.*, 57, 363–370.

Blatt, H., Middleton, G., and Murray, E. (1980). *Origin of sedimentary rocks*, Prentice-Hall, Englewood Cliffs, NJ.

Einav, I. (2007). "Breakage mechanics—Part I: Theory." *J. Mech. Phys. Solids*, 55(6), 1274–1297.

Folk, R. L. (1966). "A review of grain size parameters." *Sedimentology*, 6, 3537–3548.

Folk, R. L., and Ward, W. C. (1957). "Brazos River bar—A study in the significance of grain size parameters." *J. Sediment Petrol.*, 27, 3–26.

Forrest, J., and Clark, N. R. (1989). "Characterizing grain size distributions: Evaluation of a new approach using a multivariate extension of entropy analysis." *Sedimentology*, 36, 711–722.

Friedman, G. M. (1962). "On sorting, sorting coefficients and the log-normality of grain size distribution of sand stones." *Geol. J.*, 70, 737–753.

Full, W. E., Ehrlich, R., and Kennedy, S. K. (1983). "Optimal definition of class intervals for frequency tables." *Partic. Sci. Tech.*, 1, 281–293.

Imre, E. (1995). "Characterization of dispersive and piping soils." *Proc. XI ECSMFE, Copenhagen*, 2, 49–55.

Imre, E., Lorincz, J., and Rozsa, P. (2008). "Characterization of some sand mixtures." *Proc., 12th Int. Conf. Int. Assoc. Computer Meth. Adv. Geomech.*, IACMAG, Goa, India, 2064–2075.

Imre, E., Lorincz, J., Trang, Q. P., Fityus, S., Pusztai, J., Telekes, G., and Schanz, T. (2009). "A general dry density law for sands." *KSCE J. Civil Eng.*, 13(4), 257–272.

Inman, D. L. (1952). "Measure for describing the size distribution of sediments." *J. Sediment Petrol.*, 22, 125–145.

Krstanovic, F., and Singh, V. P. (1988). *Application of entropy theory to multivariate hydrologic analysis*, Vol. l. Technical Report WRR8, Water Resources Program, Department of Civil Engineering, Louisiana State University, Baton Rouge, LA.

Krumbein, W. C., and Pettijohn, F. J. (1938). *Manual of sedimentary petrology*, D. Appleton-Century, New York.

Lorincz, J. (1986). "*Grading entropy of soils*." Ph.D. dissertation, Technical University of Budapest, Hungary.

Lorincz, J. (1990). "Relationship between grading entropy and dry bulk density of granular soils." *Periodica Polytech.*, 34(3–4), 255–263.

Lorincz, J. (1993a). "On granular filters with the help of grading entropy." *Proc., Conf. Filters Geotech. Hydraul. Eng.*, J. Brauns, M. Heibaum, and U. Shuler, eds., Balkema, Rotterdam, Netherlands, 67–69.

Lorincz, J. (1993b). "On particle migration with the help of grading entropy." *Proc., Conf. Filters Geotech. Hydraul. Eng.*, J. Brauns, M. Heibaum, and U. Shuler, eds., Balkema, Rotterdam, The Netherlands, 63–65.

Lorincz, J., Imre, E., Galos, M., Trang, Q. P., Rajkai, K., Fityus, S., and Telekes, G. (2005). "Grading entropy variation due to soil crushing." *Int. J. Geomech.*, 51(4), 311–319.

Lorincz, J., Imre, E., Karpati, L., Trang, Q. P., Galos, M., and Telekes, G. (2009). "Entropy concept to explain the article breakage." *Proc., 17th ICSMGE*, Alexandria, Egypt, 139–143.

Lorincz, J., Imre, E., Trang, Q. P., Rajkai, K., Firgi, T., and Telekes, G. (2008). "Entropy based criteria for granular filters (filtering, segregation and suffosion)." *Proc. 1st Middle European Conf. Landfill Tech.*, Budapest, Hungary, 197–207.

Mazzulo, J., and Ehrlich, R. (1980). "A vertical pattern of variation in the St. Peter sandstone–Fourier grain shape analysis." *J. Sediment Petrol.*, 50, 63–70.

Niggli, P. (1935). "Die charakterisierung der klastischen sediments nach der kornzusamensetzung." *Schweizer, Mineralog. und Petrolog. Mitt.*, 15, 31–38 (in German).

Sharp, W. E., and Fan, P. (1963). "A sorting index." *Geol. J.*, 71, 76–84.

Singh, V.P. (1998). *Entropy-based parameter estimation in hydrology*. Kluwer Academic, Dordrecht, The Netherlands.

Swan, D., Clague, J. J., and Leternauer, J. L. (1979a). "Grain size statistics I: Evaluation of the Folk and Ward graphic measures." *J. Sedimentary Petrol.*, 48, 863–878.

Swan, D., Clague, J. J., and Leternauer, J. L. (1979b). "Grain size statistics II: Evaluation of grouped moment measures." *J. Sedimentary Petrol.*, 49, 487–500.

Trask, P. D. (1932). *Origin and environment of source sediments of petroleum*. Gulf Publishing, 323 p., Houston, TX.

Udden, J. A. (1914). "Mechanical composition of clastic sediments." *Geol. Soc. Am. Bull.*, 25, 655–744.

Additional Reading

Davis, M. W., and Ehrlich, R. (1970). "Relationships between measures of sediment–size–frequency distribution and the nature of sediments." *Geolog. Soc. Am. Bull.*, 81, 3537–3548.

Friedman, G. M. (1961). "Distinction between dune, beach, and river sands from the textural characteristics." *J. Sedimentary Petrol.*, 31, 514–529.

Friedman, G. M. (1967). "Dynamic processes and statistical parameters compared for size frequency distributions of beach and river sands." *J. Sedimentary Petrol.*, 37, 327–354.

Hatch, T. (1933). "Determination of 'average particle size' from the screen analysis of non-uniform particulate substances." *J. Franklin Inst.*, 215, 27–37.

Jones, T. A. (1970). "Comparison of the descriptors of sediment–grain size distributions." *J. Sedimentary Petrol.*, 40, 1204–1215.

Kolduk, W. S. (1968). "On environment-sensitive grain-size parameters." *Sedimentology*, 10, 57–69.

Korn, G. A., and Korn, T. M. (1975). *Mathematical handbook for scientists and engineers*, 2nd ed., McGraw-Hill, New York.

Lancaster, N. (1986). "Grain-size characteristics of linear dunes in the southwestern Kalahari." *J. Sedimentary Petrol.*, 56, 395–400.

Sahu, B. K. (1964). "Transformation of weight frequency and number frequency data in size distribution studies of clastic sediments." *J. Sedimentary Petrol.*, 34, 768–773.

Sahu, B. K. (1965a). "Transformation of arithmetic and phi size-distribution moments." *J. Sedimentary Petrol.*, 35, 969–972.

Sahu, B. K. (1965b). "Transformation of weight and number frequencies for phi-normal size-distribution moments." *J. Sedimentary Petrol.*, 35, 973–975.

Scheuermann, A., and Bieberstein, A. (2007). "Determination of the soil water retention curve and the unsaturated hydraulic conductivity from the particle size distribution." *Experim. Unsat. Soil Mech.*, 421–433.

Semple, R. K., Youngman, C. E., and Zeller, R. E. (1972). "*Economic regionalization and information theory: An Ohio example*." Discussion paper 28, Department of Geography, Ohio State University, Columbus.

Sharp, W. E. (1973). "Entropy as a parity check." *Earth Res.*, 1, 27–30.

Soluhub, J. T., and Klovan, J. E. (1970). "Evaluation of grain-size parameters in lacustrine environments." *J. Sedimentary Petrol.*, 40, 81–101.

Tucker, R. W., and Vacher, H. L. (1980). "Effectiveness of discriminating beach, dune, and river sands by moments and the cumulative weight percentages." *J. Sedimentary Petrol.*, 50, 165–172.

Chapter 8

Suspended Sediment Concentration and Discharge

Sediment transport is a vast subject and has attracted a lot of attention of hydraulic engineers for more than a century. Its allure continues today. A massive compendium edited by Garcia (2008) provides perhaps the most up-to-date account of the discipline of sedimentation engineering. The suspended sediment discharge in a river can be computed from the knowledge of mean sediment concentration and mean flow velocity. Chapters 2 through 5 present derivations of entropy-based velocity distributions. Using entropy, Chiu et al. (2000) presented mathematical models of sediment concentration and Choo (2000) presented models of sediment discharge. The work of these investigators is followed in this chapter.

The total sediment discharge can be divided into suspended sediment discharge and bed-load sediment discharge, which are summed to estimate the total sediment discharge in open channels (Einstein 1950). The suspended load is composed of sediment particles that are lifted into the body of flow by turbulence, where they remain and are transported downstream. With the balance between turbulent diffusion of the grains upward and gravitational settling of the grains downward, an equilibrium distribution of suspended sediment concentration can be developed. Conversely, the bed load is the portion of the sediment carried near the bed by the physical processes of intermittent rolling, sliding, and saltation of individual grains at various random locations in the bed, so that the sediment remains in contact with the bed most of the time. Here, the focus is on suspended sediment transport.

8.1 Preliminaries

8.1.1 Definition of Sediment Discharge

Let A denote the flow cross-sectional area with depth D and width W, which can be written as

$$A = \int_0^D \int_0^W dxdy \tag{8.1}$$

where x is the transverse coordinate along which width is measured, and y is the vertical coordinate, which is measured along flow depth. The suspended sediment discharge for a channel cross section A can be expressed as

$$Q_s = \int_0^D \int_0^W C(x, y)u(x, y)dy\, dx = u_m \bar{C} A \tag{8.2a}$$

where C is sediment concentration varying in x and y, u is the velocity varying in x and y, u_m is the cross-sectional mean velocity, and $\bar{C}$ is the cross-sectional mean sediment concentration.

Assuming that C and u are uniform in x and vary only in y, not in x, i.e., $C(x, y) = C(y)$ and $u(x, y) = u(y)$, then equation (8.2a) can be written in one dimension on a unit-width basis as

$$q_s = \int_0^D C(y)u(y)dy \tag{8.2b}$$

Equation (8.2b) shows that computation of suspended sediment discharge entails two components: distribution of sediment concentration and distribution of velocity. The distribution of sediment concentration in flow can be expressed in two ways: using the theory of sediment transport or empirically, and using the entropy theory. Likewise, the velocity distribution can be expressed either using a standard velocity distribution, such as the Prandtl–von Karman universal velocity distribution or power law velocity distribution, or it can be derived using entropy. Thus, sediment discharge can be computed with the use of entropy in three ways:

1. The velocity distribution is determined by a standard formula and the concentration distribution by an entropy-based equation.
2. The velocity distribution is determined by an entropy-based equation and the concentration distribution by a standard formula.
3. The velocity distribution and the concentration distribution are both determined by entropy-based equations.

These three ways are discussed in this chapter.

8.1.2 Governing Equation for Sediment Concentration

The simplest differential equation describing the distribution of sediment concentration along a vertical axis can be expressed as

$$-\varepsilon_s \frac{dC}{dy} = w_s C \tag{8.3}$$

in which ε_s is the diffusion coefficient for sediment transfer, y is the vertical distance measured from the channel bed, C is the sediment concentration at y, and w_s is the settling velocity of sediment particles or particle fall velocity. The left side of equation (8.3) describes the upward sediment transport by diffusion, and the right side describes the downward transport by gravity.

8.1.3 Particle Fall Velocity

The particle fall velocity of a sand particle, w_s, smaller in diameter than approximately 100 μm (Stokes range) in a clear fluid can be written as

$$w_s = \frac{1}{18}\left[\frac{(s-1)gd_s^2}{\upsilon}\right] \tag{8.4}$$

where d_s is the particle size or diameter, g is the acceleration caused by gravity, $s = \rho_s/\rho$ is the specific gravity of sediment, ρ is the fluid density, ρ_s is the sediment density, and υ is the kinematic viscosity.

For suspended sediment particles of diameter in the range 100–1,000 μm, Zanke (1978) proposed an expression for w_s as

$$w_s = \frac{10\upsilon}{d_s}\left[\left(1+\frac{0.01(s-1)gd_s^3}{\upsilon^2}\right)^{0.5} - 1\right] \tag{8.5}$$

For larger particles (>1,000 μm), van Rijn (1984) computed w_s as

$$w_s = 1.1[(s-1)gd_s]^{0.5} \tag{8.6}$$

In equations (8.4)–(8.6), d_s is the representative particle diameter of suspended sediment particles, but it may be significantly smaller than d_{50}.

Cheng (1997) related the settling velocity w_s to sediment and fluid properties as

$$w_s d_s = \upsilon(\sqrt{25+1.2d^{*2}} - 5)^{1.5} \tag{8.7}$$

where

$$d^* = \left[\frac{(\rho_s-\rho)g}{\rho\upsilon^2}\right]^{1/3} d_s \tag{8.8}$$

Example 8.1 Compute the settling velocity for different sediment sizes. Take $\rho_s = 2.6 \times 10^3 \text{ kg/m}^3$, and $\upsilon = 1.03 \times 10^{-6} \text{ m}^2/\text{s}$.

Solution

For $$d_s \le 100\ \mu\text{m}, w_s = \frac{1}{18}\left[\frac{(s-1)gd_s^2}{\upsilon}\right] = \frac{1}{18}\left[\frac{1.6 \times 9.81 d_s^2}{1.03 \times 10^{-6}}\right]$$

For $$100 \le d_s \le 1000\ \mu\text{m},$$

$$w_s = \frac{10\upsilon}{d_s}\left[\left(1 + \frac{0.01(s-1)gd_s^3}{\upsilon^2}\right)^{0.5} - 1\right]$$

$$= \frac{10 \times 1.03 \times 10^{-6}}{d_s}\left[\left(1 + \frac{0.01 \times 1.6 \times 9.81 d_s^3}{(1.03 \times 10^{-6})^2}\right)^{0.5} - 1\right]$$

For $$d_s \ge = 1000\ \mu\text{m}, w_s = 1.1[(s-1)gd_s]^{0.5} = 1.1[1.6 \times 9.81 d_s]^{0.5}$$

For smaller particle sizes, Cheng's equation is used:

$$w_s = \frac{\upsilon}{d_s}(\sqrt{25 + 1.2d^{*2}} - 5)^{1.5} = \frac{1.03 \times 10^{-6}}{d_s}(\sqrt{25 + 1.2d^{*2}} - 5)^{1.5}$$

where

$$d^* = \left[\frac{(\rho_s - \rho)g}{\rho\upsilon^2}\right]^{1/3} d_s = \left[\frac{(2.6-1) \times 9.81}{(1.03 \times 10^{-6})^2}\right]^{1/3} d_s$$

Fig. 8-1 plots the settling velocity as a function of particle diameter. The equations from Cheng (1997), Stokes (1851), and Zanke (1978) are comparable, but the equation from van Rijn (1984) significantly overestimates the settling velocity.

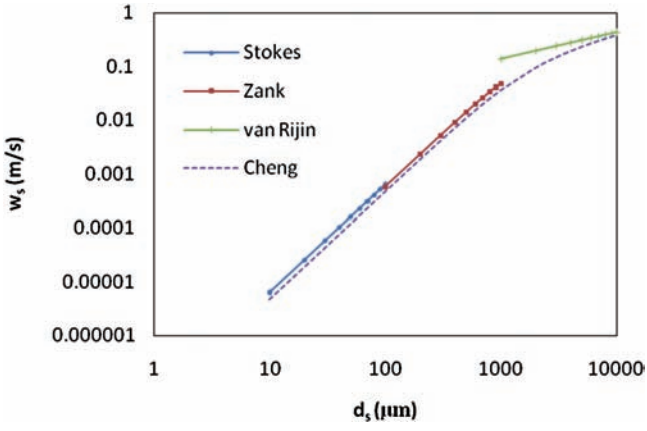

Figure 8-1 *Settling velocity as a function of a particle diameter.*

8.1.4 Diffusion Coefficient for Sediment Transport

The diffusion coefficient ε_s in equation (8.3) is often expressed as

$$\varepsilon_s = \beta\varepsilon_m \tag{8.9}$$

where β is a coefficient whose value is about unity, varying a little along the vertical between the channel bed and the water surface (Vanoni 1975), and ε_m is the diffusion coefficient for momentum transfer, which can be expressed as

$$\varepsilon_m = \frac{\tau}{\rho}\left(\frac{du}{dy}\right)^{-1} = u^{*2}\frac{\tau}{\tau_0}\left(\frac{du}{dy}\right)^{-1} \tag{8.10}$$

where ρ is the fluid density, u^* is the shear velocity $\sqrt{\tau_0/\rho}$, and τ is the shear stress given as

$$\tau = \tau_0\left(1-\frac{y}{D}\right) \tag{8.11}$$

in which τ_0 ($\rho g D S_0$) is the boundary shear at $y = 0$, g is the acceleration caused by gravity, S_0 is the bed slope, y is the vertical distance from the channel bed, and D is the flow depth. Therefore, substitution of equation (8.11) in equation (8.10) yields

$$\varepsilon_m = u^{*2}\left(1-\frac{y}{D}\right)\left(\frac{du}{dy}\right)^{-1} \tag{8.12}$$

It may be noted that for a two-dimensional velocity distribution as described in Chapter 3, the y-coordinate corresponds to the r-coordinate in the curvilinear coordinate system, and hence equation (8.11) needs to be modified as

$$\tau = \tau_0\left(1-\frac{r-r_0}{r_{\max}-r_0}\right) \tag{8.13}$$

where $r_{\max}$ is the value of r corresponding to the maximum velocity isovel, and r_0 is the value of r corresponding to the zero or minimum velocity isovel.

It is possible to introduce a scale factor that permits the coordinate transformation between y and r. Let that scale factor be h_r, which will permit us to make the product drh_r have the same unit (length) as dy in the coordinate transformation between y and r. The scale factor can also be regarded as a metric coefficient. Then, equation (8.10) can be written as

$$\varepsilon_m = \frac{\tau}{\rho}\left(\frac{du}{dy}\right)^{-1} = u^{*2}\frac{\tau}{\tau_0}\left(\frac{du}{drh_r}\right)^{-1} \tag{8.14}$$

With the substitution of equation (8.13) in equation (8.14), one gets

$$\varepsilon_m = u^{*2}\left(1-\frac{r-r_0}{r_{\max}-r_0}\right)\left(\frac{du}{drh_r}\right)^{-1} \tag{8.15}$$

Equation (8.15) shows that the diffusion coefficient for momentum transfer depends on the velocity gradient, which, in turn, depends on the velocity distribution equation used to compute the gradient.

Example 8.2 Compute and plot τ/τ_0 versus y/D. (Take y/D on the y-axis.)

Solution It is seen from equation (8.11) as $\frac{\tau}{\tau_0} = 1 - \frac{y}{D}$, showing a linear variation. The relation between τ/τ_0 and y/D is computed as shown in Table 8-1 and plotted as shown in Fig. 8-2.

Table 8-1 *Values of* τ/τ_0 *versus* y/D.

y/D	τ/τ_0	y/D	τ/τ_0
0	1	0.6	0.4
0.1	0.9	0.7	0.3
0.2	0.8	0.8	0.2
0.3	0.7	0.9	0.1
0.4	0.6	1	0
0.5	0.5		

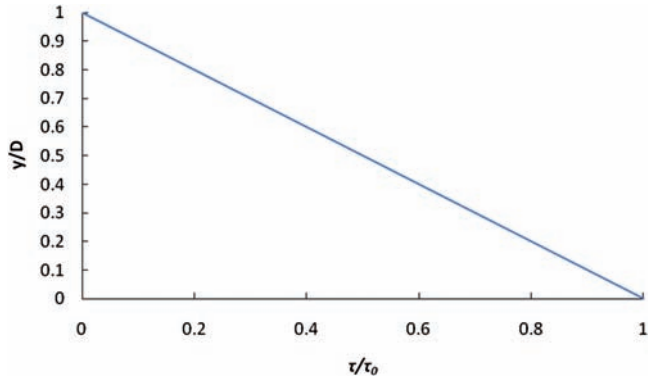

Figure 8-2 *Plot of* τ/τ_0 *versus* y/D.

8.1.5 Velocity Gradient

The velocity distribution can be expressed in many different ways. For purposes of discussion in this chapter, it is expressed in three ways: (1) power law, (2) Prandtl–von Karman universal velocity distribution, and (3) entropy based. The first two are discussed in Chapter 4, and the third in Chapters 2 and 3. For the sake of completeness, the power law velocity distribution can be expressed as

$$u = ay^b \tag{8.16}$$

where a is a proportionality factor, and b is an exponent; both can be treated as parameters. From equation (8.16), the velocity gradient du/dy can be written as

$$\frac{du}{dy} = \frac{ab}{y^{1-b}} \tag{8.17}$$

If the velocity distribution is the Prandtl–von Karman universal velocity distribution,

$$u = \frac{u^*}{k}\ln\left(\frac{y}{y_0}\right) \tag{8.18}$$

where u^* is the shear velocity, k is the von Karman universal constant, and y_0 is a parameter or the shear depth—a small value. From equation (8.18), the velocity gradient can be obtained as

$$\frac{du}{dy} = \frac{u^*}{ky} \tag{8.19}$$

The one-dimensional entropy-based velocity distribution, given by equation (2.70) (from Chapter 2), can be recast as

$$u = \frac{u^*}{k_1}\ln\left\{1 + \left[\exp\left(k_1\frac{u_D}{u^*}\right) - 1\right]\frac{y}{D}\right\} \tag{8.20}$$

where u^* is shear velocity $\sqrt{gDS_0}$, s_0 is bed slope, and k_1 is a parameter. Equation (8.20) gives velocity as monotonically increasing from the bed to the water surface, which is always true. To account for situations where the maximum velocity may occur below the water surface, the entropy-based velocity distribution, given by equation (3.35a) (from Chapter 3) can be recast in the curvilinear coordinates as

$$u = \frac{u_{\max}}{M}\ln\left[1 + \{\exp(M) - 1\}\frac{r - r_0}{r_{\max} - r_0}\right] \tag{8.21a}$$

which can also be written as

$$u = \frac{u_{\max}}{M}\ln\left[1 + \{\exp(M) - 1\}\frac{y}{D}\right] \tag{8.21b}$$

where $u = u_{\max}$ at $r = r_{\max}$; r_0 is the minimum value of r at which $u = 0$; u is the velocity at r; M is the entropy number and equals $\lambda_2 u_{\max}$; λ_2 is the Lagrange multiplier associated with the mean velocity constraint, and r is the space with which u increases. It may noted that equation (8.20) is based on the hypothesis that the average velocity in any vertical is equal to q/A (where q = discharge per unit width and D is the flow depth):

$$\frac{Q}{A} = \frac{q}{D} = \int_0^u f(u)du \tag{8.22}$$

Therefore, the average velocity u_m (Q/A) can be written as

$$\frac{u_m}{u_{\max}} = \exp(M)[\exp(M)-1]^{-1} - \frac{1}{M} \tag{8.23}$$

The velocity gradient can be obtained from equation (8.21b) as

$$\frac{du}{dy} = \frac{u_{\max}}{DM}[\exp(M)-1]\left\{1+[\exp(M)-1]\frac{y}{D}\right\}^{-1} \tag{8.24}$$

In the r-coordinate, the velocity gradient from equation (8.21a) becomes

$$\frac{du}{dy} = \frac{du}{drh_r} = \frac{u_{\max}}{DM}[\exp(M)-1]\left\{1+[\exp(M)-1]\frac{r-r_0}{r_{\max}-r_0}\right\}^{-1} \tag{8.25}$$

where

$$h_r = \frac{dy}{dr} = \left[\frac{y}{r}\left(1-\frac{y}{D-h}\right)\right]^{-1} \tag{8.26}$$

It may also be noted that the velocity gradient on the channel bed, where $u = 0$, $y = 0$, and viscous shear exists, can be expressed as

$$\left.\frac{du}{dy}\right|_{y=0} = \frac{1}{D\exp(\lambda_1)} = \frac{\tau_0}{\mu} = \frac{u^{*2}}{\upsilon} \tag{8.27}$$

where μ and υ are the dynamic and kinematic viscosities, respectively, and λ_1 is the Lagrange multiplier from equation (8.27), which results in

$$\lambda_1 = \ln\frac{\upsilon}{u^{*2}D} \tag{8.28}$$

It may be noted that r along the y-axis (where $u_{\max}$ and $r_{\max}$ occur) with $z = 0$ can be defined as

$$r = \frac{y}{D-h}\exp\left(1-\frac{y}{D-h}\right) \tag{8.29}$$

where h is the distance from the water surface to the maximum velocity and acts as a parameter.

Example 8.3 Compute and plot y/D on the y-axis and τ/τ_0 and also u/u^* on the x-axis for different values of h/D ($-\infty$, –0.5, 0.0, and 0.2) and $M = 1$ using entropy-based equations.

Solution For each value of h/D, the value of r is computed from equation (8.29): $r = \frac{y}{D-h}\exp\left(1-\frac{y}{D-h}\right)$. To include the effect of h in equation (8.29) to fine-tune

the velocity gradient, the polynomial shear-stress equation can be used. If u_{max} occurs below the water surface, where $h \geq 0$ and $r_{max} = 1$, then the shear stress distribution consistent with equation (8.29) can be expressed in the power series form as

$$\frac{\tau}{\tau_0} = \frac{h}{D}\left(1 - \frac{y}{D-h}\right) + \left(1 - \frac{h}{D}\right)\left(1 - \frac{y}{D-h}\right)^2$$

It satisfies the condition that $\tau = \tau_0$ at $y = 0$; $\tau = 0$ at $y = D - h$ where $u = u_{max}$ and also at $y = D$. If u_{max} occurs on the water surface, where $h \leq 0$ and $r_{max} = D/(D-h)$,

$$\frac{\tau}{\tau_0} = -\frac{h}{D}\left(\frac{D-y}{D-h}\right) + \left(1 - \frac{h}{D}\right)\left(\frac{D-y}{D-h}\right)^2$$

The dimensionless velocity distribution can be obtained from equation (8.21b):

$$\frac{u}{u_{max}} = \frac{1}{M}\ln\left[1 + \{\exp(M) - 1\}\frac{r - r_0}{r_{max} - r_0}\right]$$

Then, τ/τ_0 and u/u_{max} are computed, as shown in Tables 8-2 and 8-3, respectively. Fig. 8-3 plots the velocity and shear distributions for $M = 1$. It is clear that h/D has a significant influence on u/u_{max} as well.

Table 8-2 *Values of* τ/τ_0 *versus* y/D *for various values of* h.

	Values of τ/τ_0			
y/D	***h/D* = –∞**	***h/D* = –0.5**	***h/D* = 0.0**	***h/D* = 0.2**
0	1.000	1.000	1.000	1.000
0.2	0.800	0.693	0.640	0.600
0.3	0.700	0.560	0.490	0.438
0.4	0.600	0.440	0.360	0.300
0.5	0.500	0.333	0.250	0.188
0.6	0.400	0.240	0.160	0.100
0.7	0.300	0.160	0.090	0.038
0.8	0.200	0.093	0.040	0.000
0.9	0.100	0.040	0.010	–0.013
1	0.000	0.000	0.000	0.000
1.1	–0.100	–0.027	0.010	0.038
1.2	–0.200	–0.040	0.040	0.100
1.3	–0.300	–0.040	0.090	0.188
1.4	–0.400	–0.027	0.160	0.300
1.5	–0.500	0.000	0.250	0.438
1.6	–0.600	0.040	0.360	0.600

Table 8-3 *Values of* u/u$_{max}$ *versus* y/D *for various values of* h.

	Values of u/u_{max}			
y/D	$h/D = -\infty$	$h/D = -0.5$	$h/D = 0.0$	$h/D = 0.2$
0	0.000	0.000	0.000	0.000
0.2	0.295	0.461	0.568	0.660
0.3	0.416	0.600	0.712	0.805
0.4	0.523	0.706	0.812	0.898
0.5	0.620	0.788	0.882	0.957
0.6	0.709	0.853	0.931	0.993
0.7	0.790	0.904	0.965	1.012
0.8	0.865	0.944	0.985	1.017
0.9	0.935	0.976	0.997	1.012
1	1.000	1.000	1.000	1.000
1.1	1.061	1.018	0.997	0.981
1.2	1.119	1.031	0.989	0.958
1.3	1.174	1.040	0.976	0.930
1.4	1.225	1.045	0.960	0.900
1.5	1.275	1.046	0.941	0.867
1.6	1.322	1.045	0.920	0.832

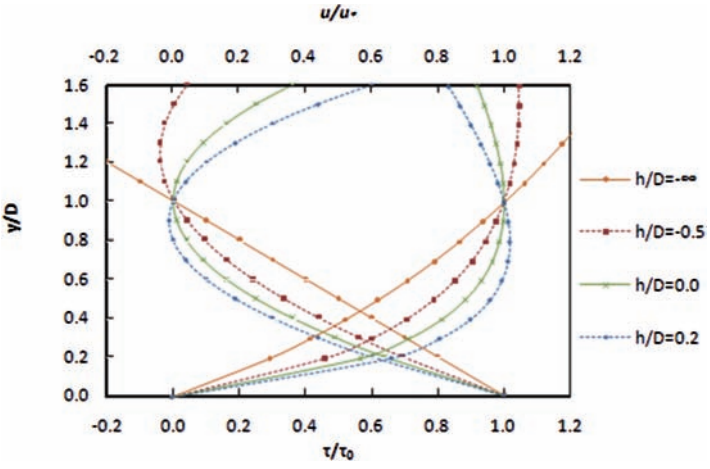

Figure 8-3 *Velocity and shear stress distributions for* M = *1.*

Example 8.4 Compute velocity gradients using the three velocity distributions and plot them. Take y/D on the y-axis and du/dy on the x-axis. Take $D = 1\,\text{m/s}$, $u_{\max} = 10\,\text{m/s}$, $u^* = 9\,\text{m/s}$, $M = 3.7$, $k = 2.26$, and $b = 2.5$.

Solution Fig. 8-4 shows du/dy versus y/D. From equation (8.17), the power law equation is

$$\frac{du}{dy} = aby^{b-1}$$

From the Prandtl–von Karman equation (8.18),

$$\frac{du}{dy} = \frac{u^*}{k}\frac{1}{y}$$

From the entropy-based equation (8.24),

$$\frac{du}{dy} = \frac{u_{\max}}{DM}[\exp(M)-1]\left\{1+[\exp(M)-1]\frac{y}{D}\right\}^{-1}$$

The velocity gradient is computed as shown in Table 8-4. Fig. 8-4 shows du/dy versus y/D.

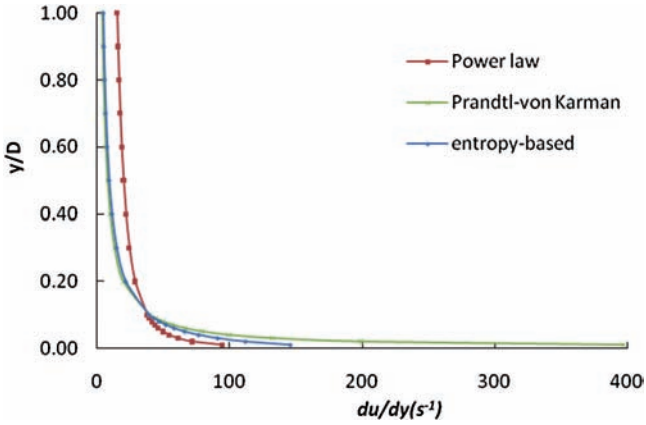

Figure 8-4 *Velocity gradient for the three distributions.*

Table 8-4 *Velocity gradients of three velocity distributions.*

	Values of *du/dy*		
y/D	Power law (s^{-1})	Prandtl–von Karman (s^{-1})	Entropy-based (s^{-1})
0.1	37.68	39.70	39.25
0.2	28.55	19.85	21.67
0.3	24.28	13.23	14.96
0.4	21.64	9.93	11.43
0.5	19.79	7.94	9.24
0.6	18.40	6.62	7.76
0.7	17.30	5.67	6.69
0.8	16.40	4.96	5.88
0.9	15.65	4.41	5.24

The power law velocity gradient is significantly different from the Prandtl–von Karman velocity gradient, as well as the entropy-based velocity gradient, which are close to each other.

Example 8.5 For a set of measured velocity data collected by Einstein and Chien (1955), given in Table 8-5, plot y/D on the y-axis and u/u^* on the x-axis for the three velocity distribution equations. Also plot on the same graph observed values. Taking $k = 0.214$, $y_0 = 3.02 \times 10^{-3}$ ft, $u^* = 0.406$ ft/s, $u_{max} = 7.11$ ft/s.

Solution The velocity distribution is computed, as shown in Table 8-5, using

Power law equation: $$\frac{u}{u^*} = \frac{a}{u^*} y^b,$$

where $u^* = 0.406$ ft/s, $a = 0.406$, and $b = 0.5$.

Table 8-5 *Comparison of observed velocity values with those computed using three velocity distribution equations.*

	Velocity u/u^*			
y/D	Observed	Power law	Prandtl–von Karman	Entropy-based
0.016	5.470	4.038	3.22	3.377
0.023	6.150	4.803	4.84	4.395
0.028	6.700	5.339	5.83	5.113
0.030	7.040	5.583	6.24	5.439
0.038	7.300	6.275	7.34	6.352
0.044	8.200	6.694	7.94	6.895
0.052	8.800	7.266	8.71	7.621
0.065	9.600	8.132	9.76	8.680
0.091	11.130	9.670	11.4	10.436
0.105	11.900	10.351	12	11.165
0.118	12.500	10.999	12.6	11.831
0.131	13.050	11.589	13.1	12.414
0.144	13.600	12.151	13.5	12.951
0.171	14.300	13.221	14.3	13.928
0.197	15.000	14.212	15	14.780
0.223	15.500	15.121	15.6	15.521
0.250	16.050	16.010	16.1	16.213
0.276	16.500	16.822	16.6	16.818
0.329	17.520	18.366	17.4	17.903

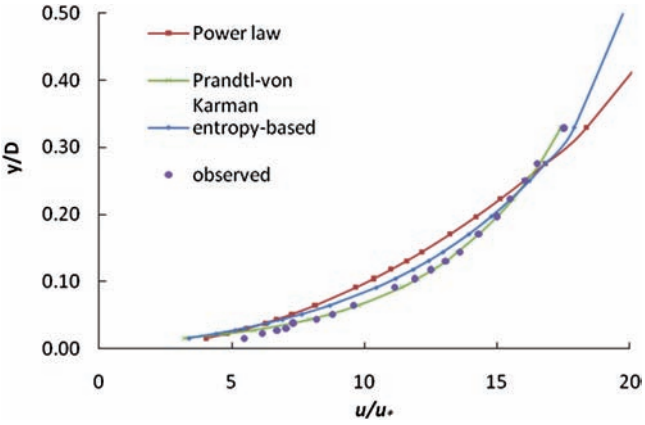

Figure 8-5 *Comparison of three velocity distributions for experimental data due to Einstein and Chien (1955).*

Prandtl–von Karman equation:
$$\frac{u}{u^*} = \frac{1}{k}\ln\frac{y}{y_0},$$

where $y_0 = 3.02 \times 10^{-3}$ ft, and $k = 0.214$.

Entropy-based equation:
$$\frac{u}{u^*} = \frac{1}{k}\ln\left[1 + \{\exp(M) - 1\}\frac{y}{D}\right],$$

where $M = 3.72$.

Fig. 8-5 shows a plot of y/D versus u/u^* for the three equations. The velocity profile computed from the power law is generally larger than the observation for the below $0.3y/D$ depth. The Prandtl–von Karman velocity profile fits the observation best in this case.

8.1.6 Diffusion Coefficient for Momentum Transfer

For the power law velocity, one combines equations (8.17) and (8.10), obtaining

$$\varepsilon_m = u^{*2}\left(1 - \frac{y}{D}\right)\frac{y^{1-b}}{ab} \tag{8.30}$$

The mean value of the diffusion coefficient for momentum transfer can now be written as

$$\overline{\varepsilon_m} = \frac{u^{*2}D^{1-b}}{ab(2-b)(3-b)} \tag{8.31}$$

Likewise, one combines equations (8.19) and (8.10), obtaining the Prandtl–von Karman universal velocity distribution:

$$\varepsilon_m = ku^* y\left(1-\frac{y}{D}\right) \tag{8.32}$$

which then yields the mean value of the diffusion coefficient for momentum transfer:

$$\overline{\varepsilon_m} = \frac{ku^* D}{6} \tag{8.33}$$

In a similar manner, coupling equations (8.24) and (8.10) for the entropy-based velocity distribution, the diffusion coefficient is obtained as

$$\varepsilon_m = \frac{Mu^{*2}D}{u_{\max}}\frac{1}{\exp(M)-1}\left\{[\exp(M)-1]\left(\frac{y}{D}\right)+1\right\}\left(1-\frac{y}{D}\right) \tag{8.34}$$

Equation (8.34) leads to the mean diffusion coefficient value:

$$\overline{\varepsilon_m} = \frac{Mu^{*2}D}{6u_{\max}}\left[\frac{3}{\exp(M)-1}+1\right] \tag{8.35}$$

Example 8.6 Compute and plot ε_m as a function of dimensionless depth y/D using three velocity distributions: power law, Prandtl–von Karman, and entropy based, using the data given by Einstein and Chien (1955) for $S-4$ series. Using $k = 0.214$, $y_0 = 3.02 \times 10^{-3}$ ft, $u^* = 0.406$ ft/s, and $u_{\max} = 7.11$ ft/s. Mean values of ε_m (ft^2/s) are $\varepsilon_m = 6.331 \times 10^{-3}$ for power law, $\varepsilon_m = 3.937 \times 10^{-3}$ for Prandtl–von Karman equation, and $\varepsilon_m = 6.245 \times 10^{-3}$ for the entropy-based equation.

Solution From equations (8.30), (8.32), and (8.34), ε_m is computed as shown in Table 8-6. Fig. 8-6 plots ε_m (m^2/s) as a function of dimensionless depth y/D. It can be seen from the figure that ε_m first increases from bottom up to about half of the depth and then starts to decrease up to the water surface. The ε_m value computed

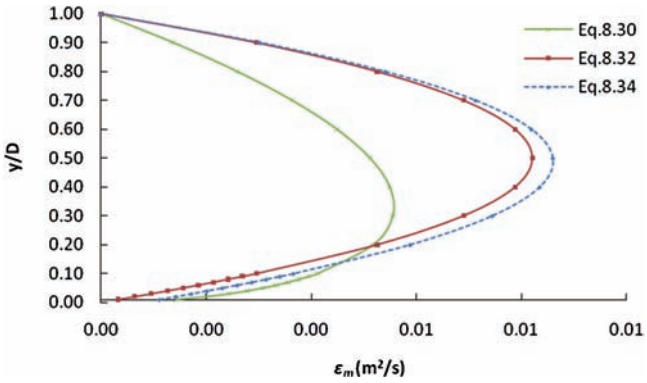

Figure 8-6 *Plot of* ε_m *(m^2/s) as a function of dimensionless depth* y/D.

Table 8-6 *Values of ε_m for various values of y/D.*

y/D	Eq. (8.34) (m^2/s)	Eq. (8.32) (m^2/s)	Eq. (8.30) (m^2/s)
0	0.0008	0.0000	0.0000
0.1	0.0037	0.0030	0.0041
0.2	0.0059	0.0053	0.0052
0.3	0.0074	0.0069	0.0056
0.4	0.0083	0.0079	0.0055
0.5	0.0086	0.0082	0.0051
0.6	0.0082	0.0079	0.0045
0.7	0.0071	0.0069	0.0036
0.8	0.0054	0.0053	0.0026
0.9	0.0030	0.0030	0.0014
1	0	0	0

from equation (8.34) increases the fastest and has the biggest peak value, and the one computed from equation (8.30) has the smallest increasing gradient and the smallest maximum value.

8.2 Sediment Concentration

8.2.1 Deterministic Equations

As shown in equation (8.9), the diffusion coefficient ε_s can be replaced by $\beta\varepsilon_m$. Using equation (8.10), the solution of equation (8.3) yields

$$\frac{C}{C_0} = \exp\left[-\frac{w_s}{\beta u^{*2}}\int_0^y \left(\frac{\tau}{\tau_0}\right)^{-1}\frac{du}{dy}dy\right] \tag{8.36}$$

where C_0 is C at $y = 0$. Depending on the mathematical description of u and τ, different models of C as a function of y can be obtained. The well-known Rouse equation can be derived from equation (8.3):

$$\frac{C}{C_a} = \left(\frac{D-y}{y}\frac{a}{D-a}\right)^{\eta} \tag{8.37}$$

where a = a small value of y; $C_a = C$ at $y = a$; D is the water depth; and

$$\eta = \frac{v_s}{\beta k u^*} \tag{8.38}$$

where v_s is the settling velocity of sediment particles. In the derivation of equation (8.37), the shear stress was expressed by equation (8.11) and the velocity by

the Prandtl–von Karman equation (8.18). Equation (8.37) does not hold at or near the channel bed and is less than adequate at the water surface. Because the sediment concentration near the bed is maximum, equation (8.37) would not satisfactorily represent the depth-averaged sediment concentration near the bed.

Solution of the diffusion equation for transport of solids in one-dimensional steady flow can be written as

$$C = C_0 \exp\left[-\frac{v_s y}{\varepsilon_s}\right] \tag{8.39}$$

where C_0 is C at $y = 0$. In deriving equation (8.39), we assume that the diffusion coefficient is constant and depth averaged.

Example 8.7 Compute and plot C/C_0 versus y/D using equation (8.36) with the power law, Prandtl–von Karman, and entropy-based velocity distributions and for a set of measured sediment concentrations collected by Einstein and Chien (1955). Take the value of $\beta = 1$, $D = 1\,\text{m/s}$, $u_{\max} = 10\,\text{m/s}$, $u^* = 9\,\text{m/s}$, $M = 3.7$, $k = 2.26$, and $b = 2.5$.

Solution For $\beta = 1$,

$$\frac{C}{C_0} = \exp\left[-\frac{w_s}{u^{*2}}\int_0^y \left(\frac{\tau}{\tau_0}\right)^{-1}\frac{du}{dy}dy\right]\frac{du}{dy}$$

is computed as in Example 8.4 for three equations.

Power law equation:
$$\frac{C}{C_0} = \exp\left[-\frac{w_s}{u^{*2}}\int_0^y \left(\frac{\tau}{\tau_0}\right)^{-1} aby^{(b-1)}dy\right]$$

Prandtl–von Karman equation:
$$\frac{C}{C_0} = \exp\left[-\frac{w_s}{u^{*2}}\int_0^y \left(\frac{\tau}{\tau_0}\right)^{-1}\frac{u^*}{k}\frac{1}{y}dy\right]$$

Entropy-based equation:

$$\frac{C}{C_0} = \exp\left[-\frac{w_s}{u^{*2}}\frac{u_{\max}}{DM}\int_0^y \left(\frac{\tau}{\tau_0}\right)^{-1}[\exp(M)-1]\left\{1+[\exp(M)-1]\frac{y}{D}\right\}^{-1}dy\right]$$

With the results from Example 8.4, the value of C/C_0 is computed as shown in Table 8-7.

Fig. 8-7 plots C/C_0 versus y/D corresponding to the power law, Prandtl–von Karman, and entropy-based velocity distributions. With β set to be 1, the dimensionless sediment concentrations computed from power law and entropy-based equations are similar, and they coincide in the figure. The sediment concentration values computed from the Prandtl–von Karman law are smaller than those from the other two methods.

Table 8-7 *Value of* C/C_0 *versus* y/D.

	Values of C/C_0		
y/D	**Power law**	**Prandtl–von Karman**	**Entropy-based**
0.1	1.54E–03	3.00E–05	1.41E–03
0.2	2.37E–06	9.01E–10	1.98E–06
0.3	3.65E–09	2.70E–14	2.79E–09
0.4	5.62E–12	8.11E–19	3.94E–12
0.5	8.66E–15	2.43E–23	5.54E–15
0.6	1.33E–17	7.30E–28	7.81E–18
0.7	2.05E–20	2.19E–32	1.10E–20
0.8	3.16E–23	6.58E–37	1.55E–23
0.9	4.87E–26	1.97E–41	2.18E–26
1	7.50E–29	5.92E–46	3.07E–29

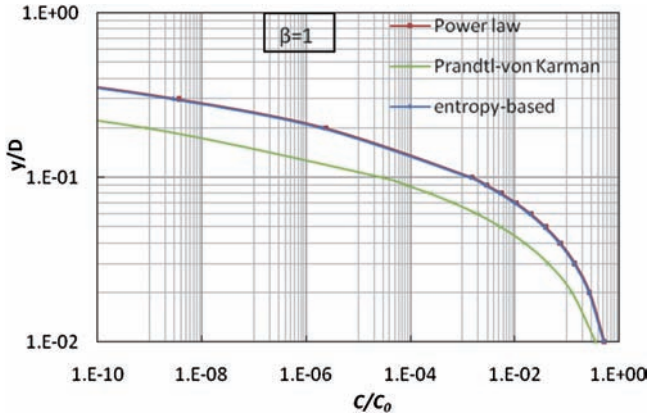

Figure 8-7 *Plot of* C/C_0 *versus* y/D *corresponding to the power law, Prandtl–von Karman, and entropy-based velocity distributions.*

Example 8.8 Compute and plot C/C_0 versus y/D using equation (8.37) with the power law, Prandtl–von Karman, and entropy-based velocity distributions and for a set of measured sediment concentrations collected by Einstein and Chien (1955). Here, compute the value of β.

Solution By curve fitting, β = 2.08 for power law, 3.29 for Prandtl–von Karman equation, and 2.31 for the entropy-based equation. Taking D = 1 m/s, $u_{\max}$ = 10 m/s, u^* = 9 m/s, M = 3.7, k = 2.26, and b = 2.5. Then, substituting in equation

$$\frac{C}{C_0} = \exp\left[-\frac{w_s}{\beta u^{*2}}\int_0^r \left(\frac{\tau}{\tau_0}\right)^{-1}\frac{du}{dy}dy\right]$$

Table 8-8 *Values of* C/C_0 *versus* y/D.

Observed C/C_0		Computed C/C_0		
y/D	Observed	Power law	Prandtl–von Karman	Entropy-based
0.136	0.065	19.003	13.980	31.256
0.141	0.070	0.012	0.012	0.018
0.095	0.078	0.051	0.049	0.066
0.086	0.089	0.069	0.066	0.087
0.072	0.104	0.107	0.103	0.130
0.044	0.126	0.251	0.245	0.283
0.022	0.147	0.505	0.500	0.536
0.017	0.173	0.594	0.589	0.622
0.010	0.200	0.725	0.721	0.746
0.007	0.234	0.806	0.803	0.821

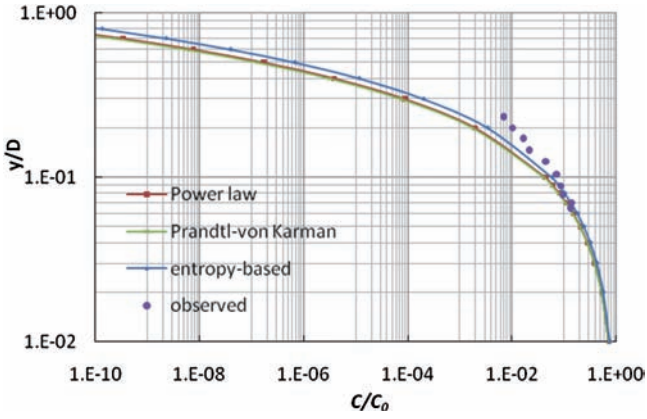

Figure 8-8 *Plot of* C/C_0 *versus* y/D *corresponding to the power law, Prandtl–von Karman, and entropy-based velocity distributions and measured values.*

values of C/C_0 are computed for various values of y/D, as shown in Table 8-8. Fig. 8-8 plots C/C_0 versus y/D corresponding to the power law, Prandtl–von Karman, and entropy-based velocity distributions and measured values.

8.2.2 Use of Entropy for Derivation of the Suspended Sediment Concentration Equation

Representing the shear stress by equation (8.13) and the velocity distribution by equation (8.21), solution of equation (8.36) yields (Chiu et al. 2000)

$$\frac{C}{C_0}=\left[\frac{1-\dfrac{y}{D}}{1+\{\exp(M)-1\}\dfrac{y}{D}}\right]^{\varsigma}=\left[\frac{1-\dfrac{r-r_0}{r_{\max}-r_0}}{1+\{\exp(M)-1\}\dfrac{r-r_0}{r_{\max}-r_0}}\right]^{\varsigma} \tag{8.40}$$

in which C_0 is C at $y = y_0$, and ζ is

$$\varsigma=\frac{w_s u_{\max}[1-\exp(-M)]}{\beta u^{*2} M}=\frac{w_s u_m[1-\exp(-M)]}{\beta u^{*2} M\phi}=\lambda G \tag{8.41}$$

$$\phi=\frac{\bar{u}}{u_{\max}}=\frac{u_m}{u_{\max}}=\frac{\exp(M)}{\exp(M)-1}-\frac{1}{M} \tag{8.42}$$

$$G=\frac{1-\exp(-M)}{M\phi} \tag{8.43}$$

$$\lambda=\frac{w_s u_m}{\beta u^{*2}} \tag{8.44}$$

where u_m is the mean velocity of flow. Equation (8.40) describes the variation of concentration in both the vertical and transverse directions.

Equation (8.40) can take on different forms along a channel vertical ($z = 0$). For wide open channels ($r = y/D$),

$$\frac{C}{C_0}=\left[\frac{1-\dfrac{y}{D}}{1+\{\exp(M)-1\}\dfrac{y}{D}}\right]^{\varsigma} \tag{8.45}$$

$$u=\frac{u_{\max}}{M}\ln\left\{1+[\exp(M)-1]\frac{y}{D}\right\} \tag{8.46}$$

If $h < 0$, $r_{\max} = 1$, and $r_0 = 0$,

$$\frac{C}{C_0}=\left[\frac{1-\dfrac{y}{D+h}\exp\left(1-\dfrac{y}{D+h}\right)}{1+[\exp(M)-1]\dfrac{y}{D+h}\exp\left[1-\dfrac{y}{D+h}\right]}\right]^{\varsigma} \tag{8.47}$$

$$u=\frac{u_{\max}}{M}\ln\left\{1+[\exp(M)-1]\frac{y}{D+h}\exp\left[1-\frac{y}{D+h}\right]\right\} \tag{8.48}$$

If $h \le 0$, $r_0 = 0$, and $u_{\max}$ occurs on the water surface but the channel is not wide, then

$$\frac{C}{C_0}=\left[\frac{1-\dfrac{y}{D}\exp\left(\dfrac{D-y}{D+h}\right)}{1+[\exp(M)-1]\dfrac{y}{D-h}\exp\left[\dfrac{D-y}{D+h}\right]}\right]^{\varsigma} \tag{8.49}$$

$$u = \frac{u_{\max}}{M} \ln\left\{1 + [\exp(M) - 1]\frac{y}{D}\exp\left[\frac{D-y}{D+h}\right]\right\} \tag{8.50}$$

Choo (2000) tested equations (8.45), (8.47), and (8.49) using flume and field data and found good agreement. There was a slight disagreement near the bed with lower than observed sediment concentration. He recommended using equation (8.40) in place of equation (8.45) or (8.47), especially when the maximum velocity occurs below the water surface.

Example 8.9 Compute and plot sediment concentration using equation (8.40) for different sediment sizes for the experimental data given by Einstein and Chien (1955). Also plot the observed values.

Solution

For $$d_s \le 100\ \mu\text{m}, w_s = \frac{1}{18}\left[\frac{(s-1)gd_s^2}{\upsilon}\right]$$

For $$100 \le d_s \le 1{,}000\ \mu\text{m}, w_s = \frac{10\upsilon}{d_s}\left[\left(1 + \frac{0.01(s-1)gd_s^3}{\upsilon^2}\right)^{0.5} - 1\right]$$

For $$d_s \ge 1{,}000\ \mu\text{m}, w_s = 1.1[(s-1)gd_s]^{0.5}$$

Then substituting

$$\varsigma = \frac{w_s u_{\max}[1 - \exp(-M)]}{\beta u^{*2} M}$$

C/C_0 is computed by

$$\frac{C}{C_0} = \left[\frac{1 - \frac{y}{D}}{1 + \{\exp(M) - 1\}\frac{y}{D}}\right]^{\varsigma}$$

Fig. 8-9 plots sediment concentration using equation (8.40) for different sediment sizes for the experimental data given by Einstein and Chien (1955) shown in Table 8-9.

Table 8-9 *Sediment concentration data given by Einstein and Chien (1955).*

y (ft)	*C* (g/l)	y (ft)	C (g/l)
0.0245	268	0.0475	87.8
0.0265	278	0.0554	43.3
0.0295	188.5	0.0654	33
0.0335	170	0.0754	20.4
0.0395	142	0.0883	13.7

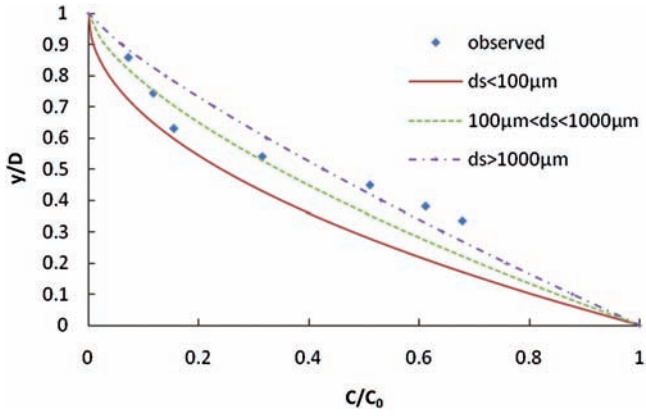

Figure 8-9 *Plot of sediment concentration using equation (8.33) for different sediment sizes for the experimental data given by Einstein and Chien (1955).*

Now the concentration corresponding to the mean velocity can be computed. Consider the case of wide open channels. Using $r = \overline{r}$, the location at which the velocity is equal to the cross-sectional mean velocity can be obtained as equation (8.21a):

$$\frac{\overline{r} - r_0}{r_{\max} - r_0} = \frac{\exp[M\phi(M)] - 1}{\exp(M) - 1} = \frac{\exp\left[\dfrac{\exp(M) - 1}{F_m(M)}\right] - 1}{\exp(M) - 1} \tag{8.51}$$

where

$$F_m(M) = \frac{[\exp(M) - 1][\exp(M) - 1]}{M\exp(M) - \exp(M) + 1} = \frac{DgRS_f}{\tau u_{\max}} \tag{8.52}$$

is a dimensionless function of M.

Substituting equation (8.51) in equation (8.40) and letting $C = C_u$ at $r = \overline{r}$, one gets

$$\frac{C_u}{C_0} = \left[\frac{1 - \dfrac{\overline{r} - r_0}{r_{\max} - r_0}}{1 + [\exp(M) - 1]\dfrac{\overline{r} - r_0}{r_{\max} - r_0}}\right]^{\zeta} = \left[\frac{\exp(M) - \exp\left[\dfrac{\exp(M) - 1}{F(M)}\right]}{[\exp(M) - 1]\exp\left[\dfrac{\exp(M) - 1}{F(M)}\right]}\right]^{\zeta} \tag{8.53}$$

where ζ is the exponent. Equation (8.53) is an analytical relation as a function of M and ζ and permits calculation of the sedimentation concentration ratio using mean velocity, channel slope, and hydraulic radius, without any concentration data.

Example 8.10 Compute and plot C_u/C_0 as a function of M for $\zeta = 2, 1, 1/2, 1/4, 1/8, 1/16, 1/32$, and $1/64$.

Solution For different values of ζ, C_u/C_0 can be computed using

$$\frac{C_u}{C_0} = \left[\frac{\exp(M) - \exp\left[\frac{\exp(M)-1}{F(M)}\right]}{[\exp(M)-1]\exp\left[\frac{\exp(M)-1}{F(M)}\right]} \right]^{\zeta}$$

as shown in Table 8-10. Fig. 8-10 plots the relation between C_u/C_0 versus M for $\zeta = 2, 1, 1/2, 1/4, 1/8, 1/16, 1/32$, and $1/64$.

Table 8-10 *Values of* C_u/C_0 *versus* M *for various values of* ζ.

	Values of C_u/C_0						
M	**ζ = 2**	**ζ = 1**	**ζ = 1/2**	**ζ = 1/4**	**ζ = 1/8**	**ζ = 1/16**	**ζ = 1/32**
0.1	0.230	0.479	0.692	0.832	0.912	0.955	0.977
0.2	0.210	0.458	0.677	0.823	0.907	0.952	0.976
0.5	0.158	0.397	0.630	0.794	0.891	0.944	0.972
1	0.091	0.302	0.550	0.741	0.861	0.928	0.963
2	0.024	0.155	0.393	0.627	0.792	0.890	0.943
3	0.005	0.069	0.263	0.513	0.716	0.846	0.920
4	0.001	0.028	0.169	0.411	0.641	0.800	0.895
5	0.000	0.011	0.105	0.324	0.569	0.755	0.869
6	0.000	0.004	0.065	0.254	0.504	0.710	0.843
7	0.000	0.002	0.039	0.198	0.446	0.667	0.817
8	0.000	0.001	0.024	0.155	0.393	0.627	0.792
9	0.000	0.000	0.015	0.121	0.347	0.589	0.768
10	0.000	0.000	0.009	0.094	0.307	0.554	0.744

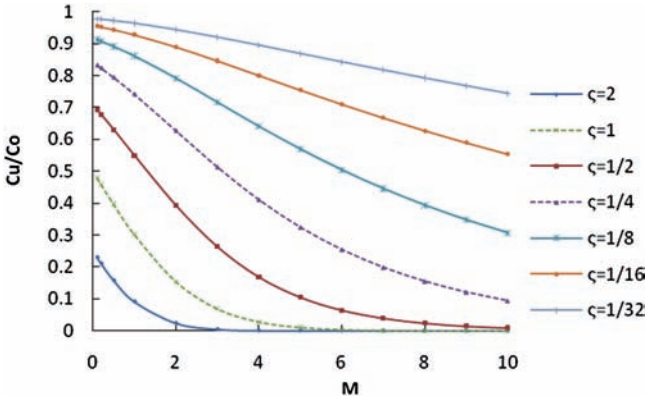

Figure 8-10 *Relation between* C_u/C_0 *versus* M *for* $\zeta = 2, 1, 1/2, 1/4, 1/8, 1/16, 1/32$, *and* $1/64$.

The sediment concentration C_0 at the bed needs to be determined, however. For a given M and ζ obtained from simple input, equation (8.53) yields C_u/C_0. From sediment concentration measured at $r = \bar{r}$ or $y = \bar{y}$ (where $u = u_m$), C_0 is obtained by dividing C_u by C_u/C_0. Furthermore, substitution of the boundary condition in equation (8.40) and $C = C_{0.2}$, $r = r_{0.2}$; $C = C_{0.5}$, $r = r_{0.5}$; and $C = C_{0.8}$, $r = r_{0.8}$ yields

$$C_0 = C_{0.2}\left[1 + \frac{\exp(M)}{4}\right]^{\zeta} \tag{8.54}$$

$$C_0 = C_{0.5}[1 + \exp(M)]^{\zeta} \tag{8.55}$$

$$C_0 = C_{0.8}[4 + \exp(M)]^{\zeta} \tag{8.56}$$

These equations can be used to describe the sediment concentration distribution.

The relationship between C and C_D (sediment concentration at the water surface) can be derived from equation (8.40) as

$$C_0 = C_D[1 + \exp(M) \times 1 \times 10^{10}] = C_D k \tag{8.57}$$

One can now examine the effect of velocity distribution on the sediment concentration. To that end, the velocity gradient is given by equation (8.25), which can be recast with $r_0 = 0$ as

$$\frac{du}{dy} = \frac{u_m[\exp(M) - 1]}{\phi M r_{\max}}\left\{h_r[1 + (\exp(M) - 1)\frac{r}{r_{\max}}\right\}^{-1} \tag{8.58}$$

where $\phi = u_m/u_{\max}$. Note that $r_{\max}$ for $h \le 0$ is unity, and is r for $y + D$ for $h > 0$. The scale factor h_r is given by equation (8.26). Therefore, equation (8.3) with the use of equation (8.58), becomes

$$\frac{C}{C_0} = \exp\left[-\zeta I\left(\frac{y}{D}, \frac{h}{D}, M\right)\right] \tag{8.59}$$

Equation (8.59) permits us to evaluate the effect of h, ζ, and M on C. Parameter h tends to increase discharge and is a measure of the effect of the location of maximum velocity. Parameter M reflects the effect of the overall local channel section characteristics. Parameter ζ is defined by equation (8.41).

Example 8.11 Compute and plot C as a function of y for $D = 0.115$ m, $d = 1.300$ mm, $u^* = 0.406$ m/s, $C_0 = 675.8$ g/l for the data of Einstein and Chien (1955). Use equations (8.37), (8.40), and (8.59).

Solution For $D = 0.171$ m, $d = 0.105$ mm, $u^* = 0.04$ m/s, $C_0 = 675.8$ g/l, C is computed as shown in Table 8-11. Fig. 8-11 plots C as a function of y.

Table 8-11 *Values of* C *as a function of* y.

Observed *C*		Computed *C*		
y (m)	Observed (g/l)	Eq. (8.37) (g/l)	Eq. (8.40) (g/l)	Eq. (8.59) (g/l)
0.007	194.000	235.872	168.229	197.848
0.008	197.500	191.538	145.690	176.456
0.009	174.500	143.398	119.218	149.781
0.010	150.000	101.696	93.881	122.438
0.012	102.400	64.723	68.467	92.902
0.014	64.250	38.696	47.691	66.889
0.017	40.500	24.930	34.936	49.947
0.020	23.650	15.416	24.796	35.891
0.023	16.080	10.074	18.256	26.541
0.027	8.780	6.220	12.858	18.662

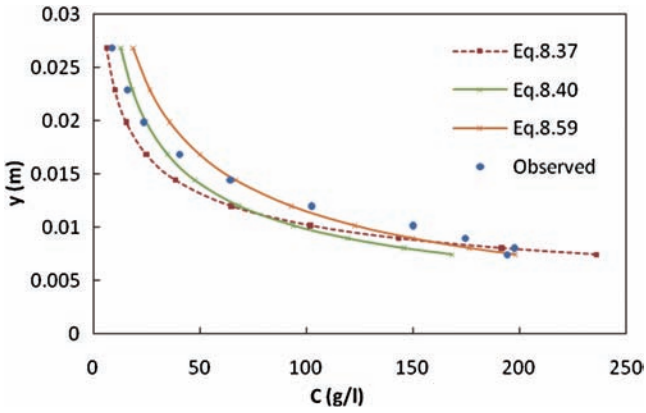

Figure 8-11 C *as a function of* y *for* D = *0.171 m,* d = *0.105 mm,* u* = *0.04 m/s,* C_0 = *675.8 g/l.*
Source: Data from Chiu et al. 2000.

Example 8.12 Compute and plot the effect of M on C/C_m.

Solution The mean sediment concentration can be computed from

$$C_m = \frac{1}{D}\int C dy$$

C can be computed from equation (8.59), in which

$$I\left(\frac{y}{D}, \frac{h}{D}, M\right) = \frac{\exp(M)}{r_{\max}}\int_0^y \left\{\left[1+(\exp(M)-1)\frac{r}{r_{\max}}\right]\frac{\tau}{\tau_0}\right\}^{-1}\frac{dr}{dy}dy$$

$$\varsigma = \frac{w_s u_{\max}[1-\exp(-M)]}{\beta u^{*2} M} = \frac{w_s u_m[1-\exp(-M)]}{\beta u^{*2} M\phi} = \lambda G$$

$$\lambda = \frac{v_s u}{\beta u^{*2}}$$

$$G = \frac{1-\exp(-M)}{M\phi}$$

For $h \geq 0$, $r_{\max} = 1$

$$\frac{\tau}{\tau_0} = \frac{h}{D}\left(1-\frac{y}{D-h}\right)+\left(1-\frac{h}{D}\right)\left(1-\frac{y}{D-h}\right)^2$$

For $h \leq 0$, $r_{\max} = \frac{D}{D-h}$

$$\frac{\tau}{\tau_0} = -\frac{h}{D}\left(\frac{D-y}{D-h}\right)+\left(1-\frac{h}{D}\right)\left(\frac{D-y}{D-h}\right)^2$$

The values of C/C_m computed at various values of y/D for different values of M are shown Table 8-12 and plotted in Figure 8-12.

Table 8-12 *Values of* C/C$_m$ *versus* y/D *for various values of* M.

Normalized Depth				
y/D	***M* = 6**	***M* = 4**	***M* = 2**	***M* = 0**
0.000	18.287	11.538	8.606	6.114
0.100	1.841	2.425	3.245	3.633
0.200	1.243	1.364	1.568	2.030
0.300	0.956	0.912	0.844	1.050
0.400	0.770	0.651	0.476	0.490
0.500	0.631	0.476	0.270	0.199
0.600	0.517	0.348	0.149	0.066
0.700	0.417	0.246	0.076	0.016
0.800	0.320	0.161	0.033	0.002
0.900	0.215	0.085	0.009	0.000
1.000	0.000	0.000	0.000	0.000

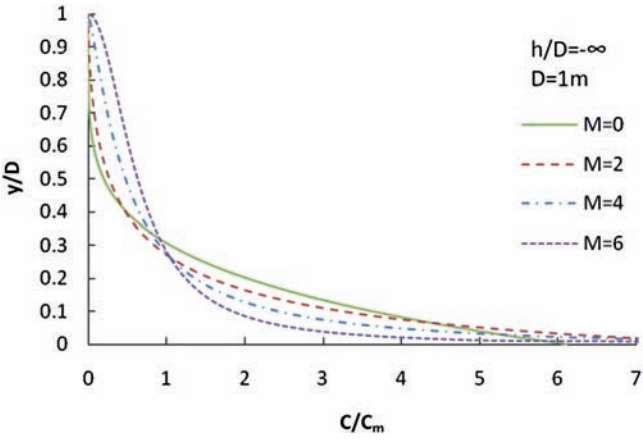

Figure 8-12 *Effect of* M *on* C/C_m.

Table 8-13 *Values of* C/C_m *as a function of* ζ.

	Values of C/C_m		
y/D	**$\zeta = 2.47$**	**$\zeta = 5.14$**	**$\zeta = 8.07$**
0.000	11.850	84.612	193.062
0.100	2.356	0.365	0.015
0.200	1.356	0.121	0.003
0.300	0.924	0.058	0.001
0.400	0.671	0.031	0.000
0.500	0.499	0.018	0.000
0.600	0.371	0.010	0.000
0.700	0.268	0.006	0.000
0.800	0.180	0.003	0.000
0.900	0.098	0.001	0.000
1.000	0.000	0.000	0.000

Example 8.13 Compute and plot the effect of ζ or particle size on sediment concentration.

Solution Using the results from Examples 8.9 and 8.10, C/C_m as a function of ζ is computed, as shown in Table 8-13. Fig. 8-13 shows the effect of ζ or particle size on sediment concentration.

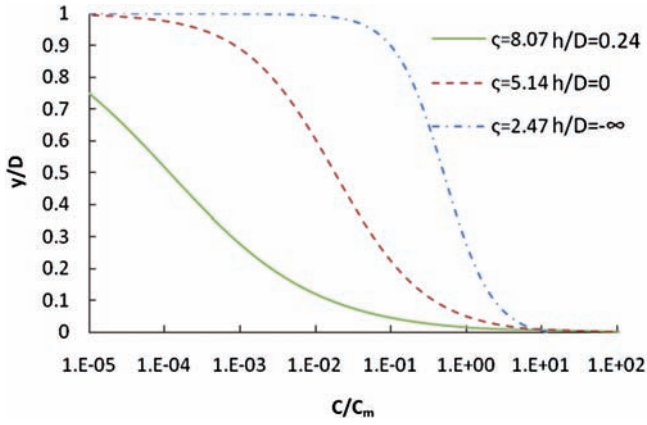

Figure 8-13 *Effect of ζ or particle size on sediment concentration.*

Example 8.14 Compute and plot the effect of ζ and h/D on sediment concentration for $M = 3$.

Solution Taking

$$r = \frac{y}{D-h}\exp\left(1-\frac{y}{D-h}\right)$$

and using results from Example 8.13, values of C/C_m are computed as shown in Table 8-14. Fig. 8-14 shows the effect of ζ and h/D on sediment concentration for $M = 3$.

Table 8-14 *Values of* C/C$_m$ *for various values of* y/D.

	Values of C/C_m							
	***h/D* = 0**				***h/D* = 0.4**			
y/D	**ζ = 0.5**	**ζ = 1**	**ζ = 2**	**ζ = 4**	**ζ = 0.5**	**ζ = 1**	**ζ = 2**	**ζ = 4**
0.000	2.421	4.908	14.047	41.556	2.615	5.925	20.680	76.814
0.100	1.561	2.041	2.429	1.243	1.508	1.970	2.287	0.939
0.200	1.327	1.475	1.269	0.339	1.272	1.402	1.157	0.241
0.300	1.185	1.175	0.806	0.137	1.132	1.110	0.726	0.095
0.400	1.078	0.972	0.551	0.064	1.027	0.915	0.493	0.044
0.500	0.987	0.815	0.388	0.032	0.940	0.765	0.345	0.021
0.600	0.903	0.683	0.272	0.016	0.860	0.640	0.242	0.010
0.700	0.820	0.562	0.185	0.007	0.780	0.527	0.164	0.005
0.800	0.728	0.444	0.115	0.003	0.693	0.416	0.102	0.002
0.900	0.609	0.310	0.056	0.001	0.580	0.291	0.050	0.000
1.000	0.002	0.000	0.000	0.000	0.000	0.000	0.000	0.000

Continued

Table 8-14 *Values of* C/C$_m$ *for various values of* y/D. *(Continued)*

Values of C/C_m								
	$h/D = -1$				$h/D = -\infty$			
y/D	$\zeta = 0.5$	$\zeta = 1$	$\zeta = 2$	$\zeta = 4$	$\zeta = 0.5$	$\zeta = 1$	$\zeta = 2$	$\zeta = 4$
0.000	2.437	4.956	14.199	41.798	1.980	3.373	7.570	19.641
0.100	1.568	2.052	2.433	1.227	1.528	2.009	2.687	2.475
0.200	1.331	1.478	1.263	0.331	1.332	1.528	1.553	0.826
0.300	1.187	1.175	0.798	0.132	1.202	1.243	1.029	0.363
0.400	1.078	0.970	0.544	0.061	1.100	1.041	0.721	0.178
0.500	0.986	0.811	0.380	0.030	1.011	0.879	0.515	0.091
0.600	0.901	0.678	0.266	0.015	0.928	0.741	0.365	0.046
0.700	0.817	0.557	0.179	0.007	0.844	0.613	0.250	0.021
0.800	0.724	0.438	0.111	0.003	0.751	0.485	0.157	0.008
0.900	0.604	0.304	0.053	0.001	0.629	0.340	0.077	0.002
1.000	0.002	0.000	0.000	0.000	0.002	0.000	0.000	0.000

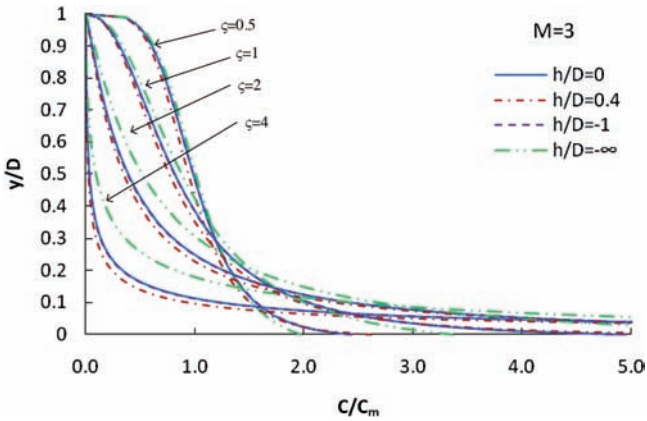

Figure 8-14 *Effect of* ζ *and* h/D *on sediment concentration for* M = *3.*

8.3 Entropy-Based Derivation of Sediment Concentration Distribution

One can also use the principle of maximum entropy (POME) to directly derive the sediment concentration distribution. To that end, entropy of the sediment concentration can be expressed as

$$H(C) = \int_{C_D}^{C_0} f(C) \ln f(C) dC \tag{8.60}$$

where C_D is the sediment concentration at the water surface $y = D$. Equation (8.60) can be maximized subject to

$$\int_{C_D}^{C_0} f(C)dC = 1 \tag{8.61}$$

$$\int_{C_D}^{C_0} Cf(C)dC = \bar{C} \tag{8.62}$$

Following the method of Lagrange multipliers,

$$f(C) = \exp[b_1 + b_2 C] \tag{8.63}$$

where b_1 and b_2 are the Lagrange multipliers. Substitution of equation (8.63) in equation (8.61) yields

$$\exp(b_1) = b_2[\exp(b_2 C_0) - \exp(b_2 C_D)]^{-1} \tag{8.64}$$

The cumulative distribution function of C, yet to be determined, can be hypothesized as

$$F(C) = \frac{D-y}{D} = 1 - \frac{y}{D} = 1 - \frac{r - r_0}{r_m - r_0} = \int_{C_D}^{C} f(C)dC \tag{8.65}$$

Substitution of equation (8.63) in equation (8.65) yields

$$C = \frac{C_0}{N} \ln\left\{\exp(N) - [\exp(N) - \exp(N/K)]\frac{r - r_0}{r_{\max} - r_0}\right\} \tag{8.66}$$

in which $N = b_2 C_0$, designated as the entropy parameter for sediment transport, similar to M in the case of velocity distribution. The ratio of sediment concentration at the bottom (C_0) to that at the water surface (C_D) can be defined as $K = (C_0/C_D)$.

Using equation (8.60), (8.62), and (8.63), we obtain the mean concentration as follows:

$$\bar{C} = \int_{C_D}^{C_0} Cf(C)dC = C_0 \Phi(N) \tag{8.67}$$

where

$$\Phi = \frac{\exp(N) - \frac{1}{K}\exp(N/K) - \frac{1}{N}[\exp(N) - \exp(N/K)]}{\exp(N) - \exp(N/K)} \tag{8.68}$$

One can calculate the mean concentration in two ways. First, equation (8.66) can be used to obtain (N, K) using the least-squares method, and equation (8.67) can be used to obtain $\bar{C}$. Second, equation (8.40), together with equation (8.67), can be used to determine $\bar{C}$.

Example 8.15 Compute and plot the mean concentration for the data of Coleman (1986), given in Table 8-15, using equation (8.67) with equation (8.66), and equation (8.67) with equation (8.40). Compare with the measured data. $D = 0.105\,\text{m}$.

Solution Using equation (8.67), first N and k are computed from equation (8.66), obtaining $N = 2.46$ and $k = 0.78$. Also one can use the results of Example 8.9 and combine equations (8.40) and (8.67) for computing the mean concentration, as shown in Table 8-15. Fig. 8-15 plots the mean concentration for the data of Coleman (1986).

Table 8-15 *Mean concentration.*

Mean concentration		
Observed	**Eq. (8.67)**	**Eq. (8.40)**
5.00E–05	4.50E–05	5.80E–05
5.30E–04	1.70E–04	3.40E–04
7.50E–04	4.30E–04	8.60E–04
1.10E–03	7.00E–04	1.40E–03
1.20E–03	7.70E–04	1.54E–03
1.50E–03	2.20E–03	2.32E–03
1.10E–03	2.70E–04	5.40E–04
1.90E–03	9.30E–04	1.86E–03
1.30E–03	3.90E–04	7.80E–04
2.40E–03	1.60E–03	3.20E–03
2.50E–03	7.60E–04	1.52E–03
2.80E–03	7.00E–04	1.40E–03
3.00E–03	1.20E–03	2.40E–03
3.10E–03	1.30E–03	2.60E–03
3.10E–03	1.60E–03	3.20E–03
3.20E–03	1.60E–03	3.20E–03
3.20E–03	1.70E–03	3.40E–03
3.20E–03	2.90E–03	2.90E–03

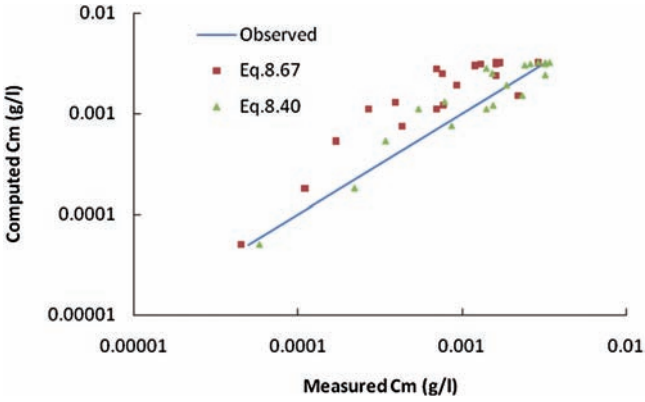

Figure 8-15 *Plot of mean sediment concentration.*

Table 8-16 *Values of concentration.*

	Concentration	
y (m)	Observed (g/l)	Equation (8.40) (g/l)
0.006	0.013	0.019
0.012	0.008	0.010
0.018	0.006	0.007
0.024	0.004	0.005
0.03	0.004	0.004
0.046	0.003	0.003
0.069	0.002	0.002
0.091	0.001	0.001
0.122	0.001	0.001
0.137	0.000	0.000
0.152	0.000	0.000
0.162	0.000	0.000

Example 8.16 Compute and plot concentration and flow velocity for the data given by Coleman (1986) for experimental run 12. $D = 0.162\,\text{m}$, $C_0 = 0.013\,\text{g/l}$, $M = 6.9$, and $\zeta = 0.7$.

Solution Substituting the given parameter values in equation (8.40), the concentration is computed as shown in Table 8-16. Fig. 8-16 plots the concentration and flow velocity. For $D = 0.162\,\text{m}$, $u_{\max} = 1.033\,\text{m/s}$, $M = 7.069$, flow velocity is computed using equation (8.21), as shown in Table 8-17. Fig. 8-17 plots the flow velocity.

Table 8-17 *Observed and computed flow velocity.*

Depth	Flow velocity	
y (m)	Observed (m/s)	Equation (8.21) (m/s)
0.006	0.598	0.574
0.012	0.669	0.679
0.018	0.731	0.741
0.024	0.796	0.785
0.03	0.83	0.819
0.046	0.912	0.884
0.069	0.964	0.947
0.091	1.004	0.989
0.122	1.052	1.034
0.137	1.058	1.052
0.152	1.045	1.068
0.162	1.033	1.078

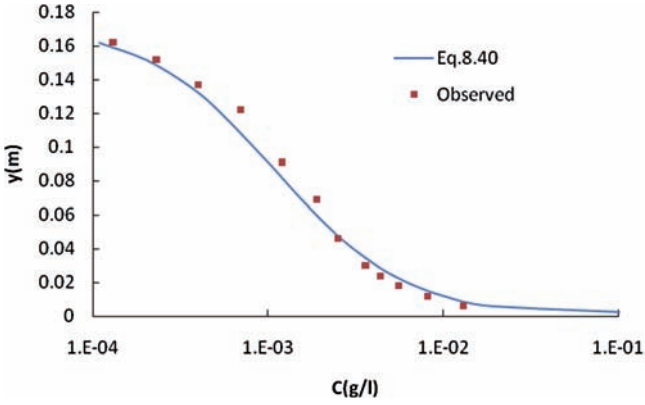

Figure 8-16 *Concentration versus flow depth.*

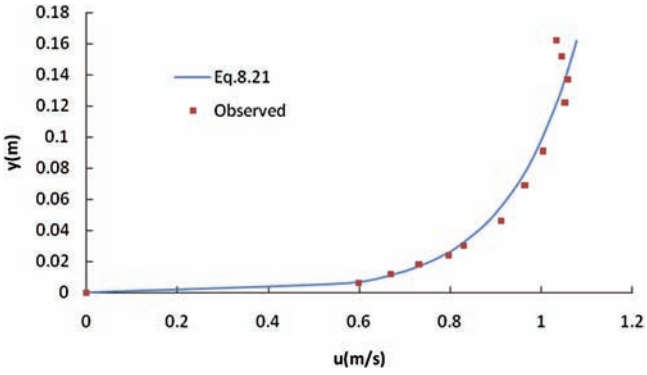

Figure 8-17 *Plot of concentration and flow velocity.*

8.4 Suspended Sediment Discharge

8.4.1 Entropy-Based Velocity Distribution and Empirical Sediment Concentration Distribution

The sediment concentration distribution given by equation (8.39) can be expressed in a slightly general form as

$$C = C_0 \exp\left[-\frac{w_s(y-a)}{\varepsilon_m}\right] \tag{8.69}$$

where ε_m is expressed by equation (8.12).

Recalling from Chapter 2, the cumulative probability distribution of time-averaged velocity u can be expressed as

$$F(u) = \frac{y}{D} \tag{8.70}$$

Differentiation of equation (8.70) yields

$$f(u) = \frac{1}{D}\frac{dy}{du} \tag{8.71}$$

or

$$\frac{du}{dy} = \frac{1}{Df(u)} \text{ or } dy = Df(u)du \tag{8.72}$$

Integrating equation (8.72), one can write

$$y = D\int_0^u f(u)du \tag{8.73}$$

Recalling from Chapter 2, the entropy-based velocity distribution can be written as

$$f(u) = \exp(\lambda_0 + \lambda_2 u) \tag{8.74}$$

where λ_0 and λ_2 are the Lagrange multipliers.

The quantity ε_m can be written as

$$\varepsilon_m = \frac{\tau}{S_f}\left(\frac{D-y}{D}\right)\frac{1}{du/dy} = u^{*2}\left(\frac{D-y}{D}\right)\frac{1}{du/dy} = u^{*2}\left(\frac{D-y}{D}\right)Df(u) \tag{8.75}$$

Therefore, equation (8.69) can be cast as

$$C = C_0 \exp\left[-\frac{w_s(y-a)}{u^{*2}(D-y)f(u)}\right] \tag{8.76}$$

If a tends to 0, equation (8.76) becomes

$$C = C_0 \exp\left[-\frac{w_s y}{u^{*2}(D-y)f(u)}\right] \tag{8.77}$$

The sediment discharge given by equation (8.2) can now be written as

$$q_s = DC_0 \int_0^{u_D} \left\{\exp\left[-\frac{w_s y}{u^{*2}(D-y)f(u)}\right]\right\} uf(u)du \tag{8.78}$$

Now consider first the exponential part in equation (8.78):

$$\exp\left[-\frac{w_s y}{u^{*2}(D-y)f(u)}\right] = G(u) = \exp\left[\frac{-w_s D\int_0^u f(u)du}{u^{*2}\left(D - D\int_0^u f(u)du\right)f(u)}\right] \tag{8.79}$$

Equation (8.74) can be written as

$$F(u) = \int_0^u \exp(\lambda_0 + \lambda_2 u)du = \frac{1}{\lambda_2}[\exp(\lambda_0 + \lambda_2 u) - \exp(\lambda_0)] \tag{8.80}$$

Inserting equation (8.74) in equation (8.79), one obtains

$$G(u) = \exp\left[-\frac{w_s}{u^{*2}}\frac{\frac{1}{\lambda_2}[\exp(\lambda_0 + \lambda_2 u) - \exp(\lambda_0)]}{\left\{1 - \frac{1}{\lambda_2}[\exp(\lambda_0 + \lambda_2 u) - \exp(\lambda_0)]\right\}\exp(\lambda_0 + \lambda_2 u)}\right] \tag{8.81}$$

Equation (8.81) can be simplified as

$$G(u) \approx 1 - \frac{w_s}{u^{*2}}\frac{[1 - \exp(-\lambda_2 u)]}{[J - \exp(\lambda_0 + \lambda_2 u)]}\Bigg], \quad J = \lambda_2 + \exp(\lambda_0) \tag{8.82}$$

Equation (8.78), with the use of equation (8.82), can be written as

$$q_s = DC_0 \int_0^{u_D} \left\{1 - \frac{w_s}{u^{*2}}\frac{[1 - \exp(-\lambda_2 u)]}{[J - \exp(\lambda_0 + \lambda_2 u)]}\right\} uf(u)du \tag{8.83}$$

Equation (8.83) can be partitioned into three components as

$$\begin{aligned} q_s = {} & DC_0 \int_0^{u_D} uf(u)du - DC_0 \int_0^{u_D} \frac{w_s}{u^{*2}}\frac{uf(u)}{[J - \exp(\lambda_0 + \lambda_2 u)]}du \\ & + DC_0 \int_0^{u_D} \frac{w_s}{u^{*2}}\frac{uf(u)\exp(-\lambda_2 u)}{[J - \exp(\lambda_0 + \lambda_2 u)]}du \end{aligned} \tag{8.84}$$

The first part I can be written as

$$I = \int_0^{u_D} uf(u)du = \overline{u} = u_m \tag{8.85}$$

where $\overline{u}$ or u_m is the mean velocity. According to equation (8.84), the DC_0 part can be taken out of I, II, and III.

The second part II can be expressed as

$$II = -\int_0^{u_D} \frac{w_s}{u^{*2}} \frac{uf(u)}{[J - \exp(\lambda_0 + \lambda_2 u)]} du \tag{8.86}$$

Equation (8.86) can be simplified as

$$II - A = \int_0^{u_D} \frac{u}{[J - \exp(\lambda_0 + \lambda_2 u)]} f(u)du = \int_0^{u_D} \frac{u\exp(\lambda_0 + \lambda_2 u)}{[J - \exp(\lambda_0 + \lambda_2 u)]} du \tag{8.87}$$

Equation (8.87) can be written as

$$II - A = \left| -\frac{u}{\lambda_2} \ln[J - \exp(\lambda_0 + \lambda_2 u)] + \frac{1}{\lambda_2} \int \ln[J - \exp(\lambda_0 + \lambda_2 u)]du \right|_0^{u_D} \tag{8.88}$$

Now consider the integral part in equation (8.88), which can be simplified by taking only the first two parts in the exponential function expansion:

$$\int \ln[J - \exp(\lambda_0 + \lambda_2 u)]du \approx -\frac{(G - \lambda_2 u)}{\lambda_2}\left[\ln\left(\frac{G - \lambda_2 u}{2.72}\right)\right], G = J - 1 - \lambda_0 \tag{8.89}$$

Substituting equation (8.89) in equation (8.88), one obtains

$$II - A = \left| -\frac{u}{\lambda_2} \ln[J - \exp(\lambda_0 + \lambda_2 u)] - \frac{1}{\lambda_2^2}(G - \lambda_2 u)\ln\left(\frac{G - \lambda_2 u}{2.72}\right) \right|_0^{u_D} \tag{8.90}$$

Equation (8.90) yields

$$\begin{aligned} II - A = & -\frac{u_D}{\lambda_2} \ln[J - \exp(\lambda_0 + \lambda_2 u_D)] \\ & -\frac{1}{\lambda_2^2}(G - \lambda_2 u_D)\ln\left(\frac{G - \lambda_2 u_D}{2.72}\right) + \frac{1}{\lambda_2^2} G \ln\left(\frac{G}{2.72}\right) \end{aligned} \tag{8.91}$$

Now consider the third part, III.

$$III = \int_0^{u_D} \frac{uf(u)\exp(-\lambda_2 u)}{J - \exp(\lambda_0 + \lambda_2 u)} du = \int_0^{u_D} \frac{u\exp(\lambda_0)}{J - \exp(\lambda_0 + \lambda_2 u)} du \tag{8.92}$$

Equation (8.92) can be simplified as follows:

$$III = \exp(\lambda_0)\left|\frac{u\ln[J-\exp(\lambda_0+\lambda_2 u)]}{\lambda_2}-\frac{1}{\lambda_2}\int \ln(J-1-\lambda_0-\lambda_2 u)\right|_0^{uD} \tag{8.93}$$

Equation (8.93) can be solved as

$$\begin{aligned} III = \exp(\lambda_0)\Bigg\{&\frac{u_D}{\lambda_2}\ln[J-\exp(\lambda_0+\lambda_2 u_D)] \\ &+\frac{1}{\lambda_2^2}(G-\lambda_2 u_D)\ln\left(\frac{G-\lambda_2 u_D}{2.72}\right)-\frac{G}{\lambda_2^2}\ln\left(\frac{G}{2.72}\right)\Bigg\} \end{aligned} \tag{8.94}$$

Thus, the sediment discharge can be written as

$$q_s = DC_0[I+II+III] \tag{8.95}$$

Conversely, using equations (8.23), (8.40), (8.67), and (8.10), Q_s can be written as

$$Q_s = u_m\bar{C}A = u_{\max}\Phi(M)C_0\Phi(N)A = u_m AC_0\Phi(N) \tag{8.96}$$

$\Phi(N)$ is a useful parameter, and knowing A and u_m, Q_s can be estimated.

8.4.2 Power Law Velocity Distribution and Entropy-Based Sediment Concentration Distribution

The sediment concentration is given by equation (8.66), with $(r - r_0)/(r_{\max} - r_0) = y/D$:

$$C = \frac{C_0}{N}\ln\left\{\exp(N)-[\exp(N)-\exp(N/K)]\frac{y}{D}\right\} \tag{8.97}$$

The power law velocity distribution is given by equation (8.16). Therefore, the sediment discharge can be expressed as

$$q_s = \frac{C_0 a}{N}\int_0^D y^b \ln\left\{\exp(N)-[\exp(N)-\exp(N/K)]\frac{y}{D}\right\}dy \tag{8.98}$$

Equation (8.98) can be solved numerically.

8.4.3 Prandtl–von Karman Velocity Distribution and Entropy-Based Sediment Concentration Distribution

The sediment concentration is given by equation (8.97). The Prandtl–von Karman velocity distribution is given by equation (8.18). Therefore, the sediment discharge can be expressed as

$$q_s = \frac{C_0 u^*}{Nk} \int_0^D \ln\left\{\exp(N) - [\exp(N) - \exp(N/K)]\frac{y}{D} + \frac{y}{y_0}\right\} dy \tag{8.99}$$

Equation (8.99) can be solved numerically.

8.4.4 Entropy-Based Velocity Distribution and Sediment Concentration Distributions

The entropy-based sediment distribution is given by equation (8.40), with three special cases prescribed by equations (8.45), (8.47), and (8.49). Corresponding to these equations, the entropy-based velocity distributions are given by equations (8.46), (8.48), and (8.50). Then the sediment concentration can be determined.

Example 8.17 Compute the suspended sediment discharge using equations (8.96), (8.98), and (8.99) for the data in Examples 8.5 and 8.15. From example 8.15, $D = 0.162\,\text{m}$, $u_{\max} = 1.033\,\text{m/s}$, $u^* = 0.095\,\text{m/s}$, $C_0 = 0.013\,\text{g/l}$, $M = 6.9$, $\zeta = 0.7$, and $N = 2.4$.

Solution From equation (8.96),

$$q_s = 1.033\Phi(6.9)0.013\Phi(2.4) = 34.88\,\text{g/s}$$

From equation (8.98),

$$q_s = \frac{0.013 \times 1.033}{2.4} \int_0^{0.162} y^{2.5} \ln\left\{\exp(2.4) - [\exp(2.4) - 1]\frac{y}{0.162}\right\} dy = 32.35\,\text{g/s}$$

From equation (8.99),

$$q_s = \frac{0.013 \times 0.095}{2.4} \int_0^{0.162} \ln\left\{\exp(2.4) - [\exp(2.4) - 1]\frac{y}{0.162} + \frac{y}{0.05y}\right\} dy = 33.97\,\text{g/s}$$

Example 8.18 Use equation $Q_s = u_m \bar{C} A$ to compute the suspended sediment discharge using different velocity and sediment concentration methods and compare each method.

Solution The mean velocity and the mean sediment concentration for each method are computed as given in Table 8-18. Using equations (8.96), (8.98), and (8.99), specific suspended sediment discharge is computed as given, along with observations, in Table 8-19. The computed suspended sediment discharge is smaller than the observed sediment discharge, and between them, the discharge computed by entropy-based velocity and empirical sediment concentration is much smaller than that computed by other methods.

Table 8-18 *Mean velocity and sediment concentration values.*

Velocity (m/s)				Sediment Concentration (g/l)		
Obs.	Entropy	Prandtl	Power	Obs.	Rouse	Entropy
4.377	4.364	4.275	4.271	31.051	10.054	28.820
5.703	5.684	5.862	5.682	54.308	15.698	46.304
5.647	5.719	5.647	5.587	70.620	20.933	56.144
4.622	4.641	4.653	4.515	97.166	26.653	65.312
5.522	5.573	5.618	5.361	156.470	43.537	138.000
4.985	5.052	4.901	4.970	14.642	7.879	12.329
4.985	5.235	4.903	4.999	29.834	15.279	29.083
4.869	5.250	5.076	4.990	37.850	14.325	28.505
4.922	5.254	5.120	4.887	66.251	28.324	50.602
4.753	5.000	4.821	4.737	95.268	38.745	76.551
4.776	4.707	4.635	4.747	19.349	16.961	16.038
5.184	5.341	5.196	5.123	77.267	53.361	65.516
4.599	4.785	4.576	3.497	136.741	100.507	115.418
5.238	5.244	5.199	4.965	145.879	101.526	120.714
4.985	4.983	5.028	4.440	249.375	132.950	185.411
4.299	4.343	4.199	3.723	265.437	150.556	202.200

Table 8-19 *Computed suspended sediment discharge (g/s).*

Obs.	Equation (8.96)	Equation (8.98)	Equation (8.99)
135.92	43.88	123.08	123.21
309.73	89.22	263.08	271.44
398.81	119.72	313.66	317.07
449.12	123.70	294.86	303.93
864.00	242.62	739.81	775.33
72.99	39.80	61.27	60.42
148.72	79.99	145.39	142.60
184.30	75.20	142.24	144.70
326.06	148.82	247.28	259.08
452.83	193.72	362.60	369.07
92.42	79.83	76.14	74.33
400.59	285.03	335.61	340.44
628.85	480.88	403.64	528.12
764.05	532.43	599.34	627.56
1,243.15	662.53	823.25	932.31
1,141.10	653.87	752.81	848.94

Questions

Q8.1 For given particle size as: 54 μm, 176 μm, and 1,879 μm, choose a proper law to compute the settling velocity.

Q8.2 For a known set of velocity data, $D = 1.49$ ft, $u_{max} = 0.409$ ft/s, $u^* = 0.04$ ft/s, and $k = 2.26$, compute the velocity gradient for the power law, Prandtl–von Karman universal law, and entropy-based velocity distribution. Plot and discuss it.

Q8.3 Compute the diffusion coefficient for momentum transfer for three equations using the data in Q8.2. Plot and discuss it. Also compute the mean value.

Q8.4 Compute the sediment concentration using the Rouse equation for $D = 1.49$ ft, $u^* = 0.04$ ft/s, and $\beta = 1$.

Q8.5 For a given set of sediment concentration data (Table 8-20), compute ζ using equation (8.41). Then compute C/C_0 using equation (8.40). Plot it and compare with observations. Take $d_s = 0.94$ mm.

Q8.6 For data used in Q8.5, compute C_u/C_0 using equation (8.53).

Q8.7 For data used in Q8.5, compute C/C_0 using equations (8.37), (8.40), and (8.59). Plot and compare each method.

Q8.8 For sediment concentration data in Q8.5, verify the hypothesis on the cumulative probability distribution in equation (8.65). Plot it and discuss.

Q8.9 For the aforementioned data, compute the N and K value in equation (8.66) using the least-squares method.

Q8.10 Compute the mean value of the sediment concentration using equations (8.40) and (8.67).

Q8.11 Compute the sediment concentration distribution using equation (8.66) with N and K computed from Q8.9. Compare the results with those of Q8.5. Discuss the results.

Table 8-20 *Sediment concentration versus dimensionless depth.*

$(h-y)/y$	Total C (g/l)	$(h-y)/y$	Total C (g/l)
14.15	328	6.66	117
12.96	295	5.53	76.5
11.5	263	4.52	45.1
9.95	230.5	3.78	28.1
8.25	167.3	2.98	14.2

References

Cheng, N.-S. (1997). "Simplified settling velocity formula for sediment particle." *J. Hydraul. Eng.*, 132(2), 149–152.

Chiu, C.-L., Jin, W., and Chen, Y.-C. (2000). "Mathematical models of distribution of sediment concentration." *J. Hydraul. Eng.*, 126(1), 16–23.

Choo, T. H. (2000). "An efficient method of the suspended sediment-discharge measurement using entropy." *Water Eng. Res.*, 1(2), 95–105.

Coleman, N. L. (1986). "Effects of suspended sediment on open channel velocity distribution." *Water Resour. Res.*, 22(10), 1377–1384.

Einstein, H. A. (1950). "The bed load function for bed load transportation in open channel flows." Technical Bulletin No. 1026, USDA Soil Conservation Service, 1–71, Washington, DC.

Einstein, H. A., and Chien, N. (1955). "Effects of heavy sediment concentration near the bed on velocity and sediment distribution." Report No. 8, M.R.D., Sediment Series, U.S. Army Corps of Engineers, Omaha, NE.

Garcia, M. H., ed. (2008). *Sedimentation engineering: Processes, measurements, modeling and practice*, ASCE Manual of Practice 110, ASCE Press, Reston, VA.

Stokes, G. G. (1851) "On the effect of the internal friction of fluids on the motion of pendulums." *Transactions of the Cambridge Philosophical Society*, 9(2), 8–106.

van Rijn, L. C. (1984). "Sediment transport, part II: Suspended load." *J. Hydraul. Eng.*, 110(11), 1613–1641.

Vanoni, V. A. (1975). *Sedimentation engineering*. ASCE Press, New York.

Zanke, U. (1978). "Berechnung der sinkgeschwindigkeiten von sedimenten." *Mitteilungen des Franzius- Instituts*, 46, 231–245 (in German).

Additional Reading

Bagnold, R. A. (1954). "Experiments on gravity-free dispersion of large solid spheres in a Newtonian fluid under shear." *Proc., Royal Society, London, Series A*, 225, 49–63.

Chang, H. H. (1988). *Fluvial processes in river engineering*, Wiley, New York.

Di Toro, D. M. (2001). *Sediment flux modeling*, Wiley, New York.

Graf, W. (1984). *Hydraulics of sediment transport*, Water Resources Publications, Littleton, CO.

Major, J. J., and Pierson, T. (1992). "Debris flow rheology: Experimental analysis of fine-grained slurries." *Water Resour. Res.*, 28(5), 841–858.

Simons, D. B., and Senturk, F. (1976). *Sediment transport technology*, Water Resources Publications, Littleton, CO.

Yang, C. T. (1996). *Sediment transport theory and practice*, McGraw-Hill, New York.

Chapter 9

Sediment Concentration in Debris Flow

A *debris flow* is a dense, poorly sorted, solid–fluid mixture. It commonly includes more than 50% sediment by volume, and the sediment particles may range in size from clay to boulders several meters in diameter (Major and Pierson 1992). In mountainous regions, debris flows are caused by prolonged heavy rainfall occurring over saturated hillslopes, earthquakes, and human activities. In debris flow, debris or rocks concentrate at the head of flow and move downhill with high concentration and strong destructive force and continue to flow downhill and through channels, increasing in volume and sediment concentration with the addition of water, sand, mud, trees, boulders, and other material. Debris flows can transport huge volumes of sediment, have a strong erosive force, and grow during the movement of gathering debris eroded from the torrent bed or banks. These flows are so powerful that they destroy whatever comes in their way, i.e, they kill people and animals; destroy roads, bridges, railway tracks, homes, and other property; and fill reservoirs.

Two fundamental factors govern debris flow and its characteristics: sediment concentration and sediment particle size (Egashira et al. 2001). Typical debris flow problems are the formation, movement, and deposition of debris; flooding zones; and damage assessment, among others. To address these problems, the equilibrium sediment concentration and its vertical distribution are needed. Debris flows, involving mixtures of debris and water, exhibit characteristics that are different from those of water flow. A physically based hydraulic model can be constructed for modeling debris flow. However, uncertainties in debris flow variables and parameters of such a model may limit its potential.

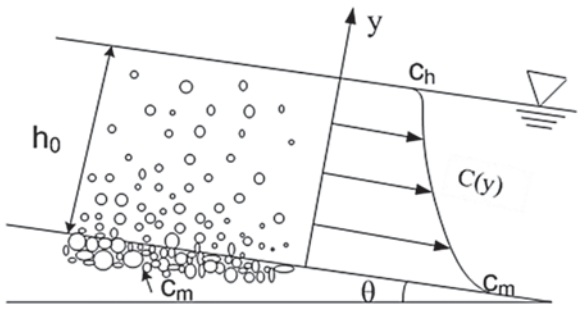

Figure 9-1 *Uniform debris flow.*

This chapter discusses the determination of sediment concentration distribution in debris flow using entropy. Lien and Tsai (2003) were probably the first to use entropy for debris flow modeling, and their work is followed here in this chapter.

9.1 Notation and Definition

Consider a steady uniform debris flow over an erodible bed, as shown in Fig. 9-1, in which the depth of flow is h_0, and the sediment concentration decreases monotonically from a maximum value of c_m at the channel bottom to an arbitrary value of c_h at the water surface. Let $c(y)$ be the sediment concentration at a vertical distance y ($0 \le y \le h_0$) from the channel bed. The sediment concentration is defined in dimensionless terms as the volume of sediment divided by the volume of the fluid–sediment mixture. Thus, it is expressed as a fraction or in percent by volume. For entropy-based formulation, it is assumed that the time-averaged sediment concentration C is a random variable.

9.2 Entropy Theory

Determination of debris flow concentration using the entropy theory entails (1) definition of the Shannon entropy, (2) specification of constraints, (3) maximization of entropy, (4) determination of the Lagrange multipliers, (5) determination of probability density function and maximum entropy, (6) sediment concentration distribution, and (7) equilibrium sediment concentration. Each of these components is discussed in the next sections.

9.2.1 Shannon Entropy

The Shannon entropy (Shannon, 1948) of concentration C, $H(C)$, can be expressed as

$$H(C) = -\int_{c_h}^{c_m} f(c) \ln f(c)\, dc \tag{9.1}$$

where c, $c_h \le c \le c_m$, is the value of random variable C, c_m is the maximum value of C or concentration at the bed, c_h is the concentration at the water surface, $f(c)$ is the probability density function (PDF) of C, and H is the entropy of $f(c)$ or C. Equation (9.1) is a measure of uncertainty of variable C. The quantity $f(c)dc$ defines the probability of sediment concentration between c and $c + dc$. The objective is to derive $f(c)$ by maximizing H, subject to specified constraints, in accordance with the principle of maximum entropy (POME) (Jaynes 1957).

9.2.2 Specification of Constraints

Since $f(c)$ is a PDF, it must satisfy

$$\int_{c_h}^{c_m} f(c)\, dc = 1 \tag{9.2}$$

which is the total probability theorem. One of the simplest constraints is the mean or equilibrium sediment concentration by volume, denoted as $\overline{c}$ or c_D. This constraint may be known or obtained from observations, and can be expressed as

$$\int_{c_h}^{c_m} cf(c)\, dc = E[c] = \overline{c} = c_D \tag{9.3}$$

For purposes of simplicity, more constraints are not used.

9.2.3 Maximization of Entropy

The entropy H of C, given by equation (9.1), can be maximized, subject to equations (9.2) and (9.3), in accordance with POME. This step is achieved by using the method of Lagrange multipliers. To that end, the Lagrangian function L is expressed as

$$L = -\int_{c_h}^{c_m} f(c) \ln f(c)\, dc - (\lambda_0 - 1)\left(\int_{c_h}^{c_m} f(c)\, dc - 1\right) - \lambda_1\left(\int_{c_h}^{c_m} cf(c)\, dc - c_D\right) \tag{9.4}$$

where λ_0 and λ_1 are the Lagrange multipliers. Differentiating equation (9.4) with respect to f, while recalling the Euler–Lagrange calculus of variation, noting f as a variable and C as a parameter and equating the derivative to zero, one obtains

$$\frac{\partial L}{\partial f} = 0 \Rightarrow -\ln f(c) - \lambda_0 - \lambda_1 c \tag{9.5}$$

Equation (9.5) results in

$$f(c) = \exp(-\lambda_0 - \lambda_1 c) = a\exp(-\lambda_1 c) = ab^{-\lambda_1}, \quad a = \exp(-\lambda_0), \quad b = \exp(c) \tag{9.6}$$

Equation (9.6) is the POME-based least biased PDF of sediment concentration C. There are two unknowns, λ_0 and λ_1, in equation (9.6) that can be determined with the use of equations (9.2) and (9.3). The Lagrange multiplier λ_1 is associated with mean concentration, and λ_0 is associated with the total probability. These multipliers have opposite signs: λ_1 is positive, and λ_0 is negative.

9.2.4 Determination of Lagrange Multipliers

Substitution of equation (9.6) in equation (9.2) yields

$$\int_{c_h}^{c_m} \exp(-\lambda_0 - \lambda_1 c)\, dc = 1 \tag{9.7}$$

Integration of equation (9.7) gives

$$\exp(-\lambda_0) = \frac{\lambda_1}{\exp(-\lambda_1 c_h) - \exp(-\lambda_1 c_m)} \tag{9.8}$$

Taking the logarithm of equation (9.8), the result is

$$\lambda_0 = -\ln\lambda_1 + \ln[\exp(-\lambda_1 c_h) - \exp(-\lambda_1 c_m)] \tag{9.9a}$$

For $c_h = 0$, equation (9.8) simplifies to

$$\lambda_0 = -\ln\lambda_1 + \ln[1 - \exp(-\lambda_1 c_m)] \tag{9.9b}$$

Differentiating equation (9.9a) with respect to λ_1, one gets

$$\frac{\partial\lambda_0}{\partial\lambda_1} = -\frac{1}{\lambda_1} - \frac{c_h \exp(-\lambda_1 c_h) - c_m \exp(-\lambda_1 c_m)}{\exp(-\lambda_1 c_h) - \exp(-\lambda_1 c_m)} \tag{9.10}$$

Furthermore, equation (9.7) can also be cast as

$$\lambda_0 = \ln \int_{c_h}^{c_m} \exp(-\lambda_1 c)\, dc \tag{9.11}$$

Differentiating equation (9.11) with respect to λ_1, multiplying both the numerator and the denominator by $\exp(-\lambda_0)$ and recalling equation (9.3), one obtains

$$\frac{\partial \lambda_0}{\partial \lambda_1} = -\frac{\int_{c_h}^{c_m} c \exp(-\lambda_0 - \lambda_1 c)\, dc}{\int_{c_h}^{c_m} \exp(-\lambda_0 - \lambda_1 c)\, dc} = -c_D \tag{9.12}$$

Equating equation (9.10) to equation (9.12), the result is the mean sediment concentration:

$$c_D = \frac{1}{\lambda_1} + \frac{c_h \exp(-\lambda_1 c_h) - c_m \exp(-\lambda_1 c_m)}{\exp(-\lambda_1 c_h) - \exp(-\lambda_1 c_m)} \tag{9.13a}$$

Equation (9.13a) contains λ_1 as the only one unknown. Because equation (9.13a) is implicit in λ_1, it can be solved numerically for the unknown λ_1. With the substitution of λ_1 so obtained in equation (9.9a), one can obtain λ_0. The mean sediment concentration is expressed in terms of the minimum sediment concentration at the water surface and the maximum concentration at the bed. Interestingly, if $c_h = 0$, equation (9.13a) reduces to

$$c_D = \frac{1}{\lambda_1} - \frac{c_m \exp(-\lambda_1 c_m)}{1 - \exp(-\lambda_1 c_m)} \tag{9.13b}$$

9.2.5 Determination of Probability Density Function and Maximum Entropy

Substitution of equation (9.8) in equation (9.6) produces the PDF of C, $f(c)$, in only one unknown λ_1 as

$$f(c) = \frac{\lambda_1 \exp(-\lambda_1 c)}{\exp(-\lambda_1 c_h) - \exp(-\lambda_1 c_m)} \tag{9.14a}$$

and the cumulative distribution function of C, $F(c)$, as

$$F(c) = \frac{\exp(-\lambda_1 c_h) - \exp(-\lambda_1 c)}{\exp(-\lambda_1 c_h) - \exp(-\lambda_1 c_m)} \tag{9.14b}$$

The maximum entropy of C is obtained by inserting equation (9.14a) in equation (9.1):

$$H(C) = -\ln \lambda_1 + \ln[\exp(-\lambda_1 c_h) - \exp(-\lambda_1 c_m)] + \lambda_1 c_D \tag{9.15}$$

which is expressed in terms of the Lagrange multiplier λ_1, mean sediment concentration c_D, lower limit of concentration, c_h, and upper limit of concentration c_m.

Example 9.1 Compute and plot $f(c)$ as a function of λ_1.

Solution Assume that $c_h = 0$ and $c = 0.7$. Then, for different values of λ_1 (0.1, 1.0, 5.0, and 10.0), $f(c)$ is computed using equation (9.14a), as given in Table 9-1 and shown in Fig. 9-2. It is seen that when $\lambda_1 = 0.1$, $f(c)$ tends to be uniform with $f(c = 0) = 1.48$. As λ_1 increases, $f(c)$ tends to be more exponential. When $\lambda_1 = 10$, $f(c)$ approaches 0 quickly. Fig. 9-2 plots the PDF of C.

Table 9-1 *Values of* f(c) *for different values of* λ_1.

c	$\lambda_1 = 0.1$	$\lambda_1 = 1$	$\lambda_1 = 5$	$\lambda_1 = 10$
0	1.479	1.986	5.156	10.009
0.1	1.464	1.797	3.127	3.682
0.2	1.450	1.626	1.897	1.355
0.3	1.435	1.472	1.150	0.498
0.4	1.421	1.332	0.698	0.183
0.5	1.407	1.205	0.423	0.067
0.6	1.393	1.090	0.257	0.025
0.7	1.379	0.986	0.156	0.009
0.8	1.365	0.893	0.094	0.003
0.9	1.352	0.808	0.057	0.001
1	1.338	0.731	0.035	0.000

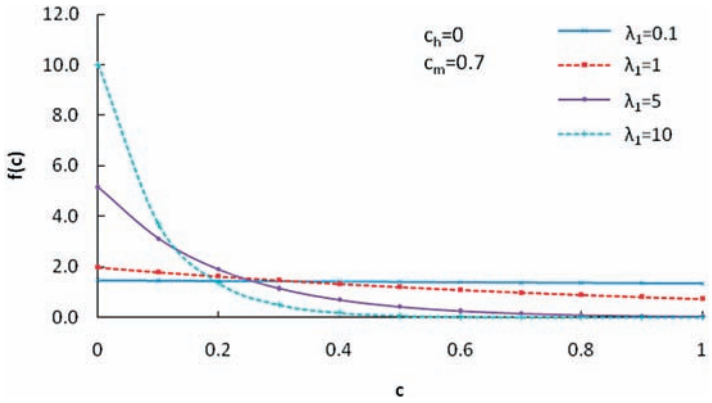

Figure 9-2 *Plot of* f(c) *as a function of* λ_1.

Table 9-2 *Values of* F(c) *for different values of* λ_1.

c	$\lambda_1 = 0.1$	$\lambda_1 = 1$	$\lambda_1 = 5$	$\lambda_1 = 10$
0	0.000	0.000	0.000	0.000
0.1	0.147	0.189	0.406	0.633
0.2	0.293	0.360	0.652	0.865
0.3	0.437	0.515	0.801	0.951
0.4	0.580	0.655	0.892	0.983
0.5	0.721	0.782	0.946	0.994
0.6	0.861	0.896	0.980	0.998
0.7	1.000	1.000	1.000	1.000

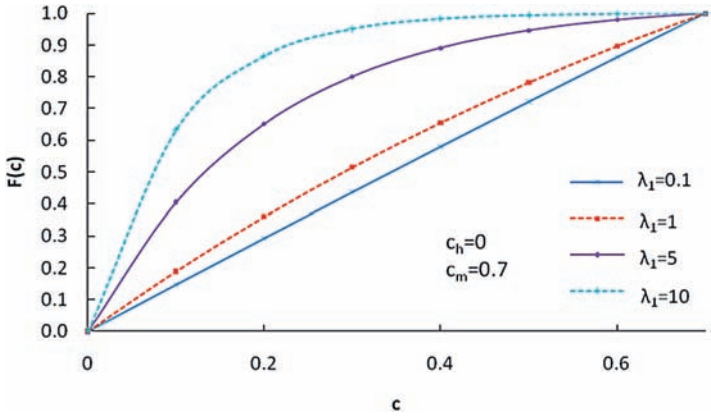

Figure 9-3 *Plot of* F(c) *as a function of* λ_1.

Example 9.2 Compute and plot $F(c)$ as a function of λ_1.

Solution Assume that $c_h = 0$ and $c_m = 0.7$. Then, for different values of λ_1 (0.1, 1.0, 5.0, and 10.0), $F(c)$ is computed using equation (9.14b), as shown in Table 9-2 and Fig. 9-3. For $\lambda_1 = 0.1$, $F(c)$ becomes linear.

Example 9.3 Compute and plot λ_0 as a function of λ_1 for various values of c_h and c_m.

Solution Assume that $c_h = 0.3$, for $c_m = 0.5$, 0.7, and 1, λ_0 is computed using equation (9.9a) for various values of λ_1 from 0 to 10, as shown in Table 9-3 and Fig. 9-4.

Assume that $c_m = 0.7$, for $c_h = 0$, 0.1, 0.3, and 0.5, compute λ_0 using equation (9.9a) for λ_1 increasing from 0 to 10, as shown in Table 9-4 and Fig. 9-5.

Table 9-3 *Values of λ_0 for different values of* c_m.

λ_1	$c_m = 0.5$	$c_m = 0.7$	$c_m = 1$
0	–1.65	–1	–0.43
1	–2.008	–1.410	–0.986
2	–2.403	–1.890	–1.576
3	–2.794	–2.357	–2.129
4	–3.183	–2.812	–2.649
5	–3.568	–3.255	–3.140
6	–3.950	–3.687	–3.607
7	–4.329	–4.109	–4.053
8	–4.705	–4.521	–4.483
9	–5.078	–4.925	–4.899
10	–5.448	–5.321	–5.303

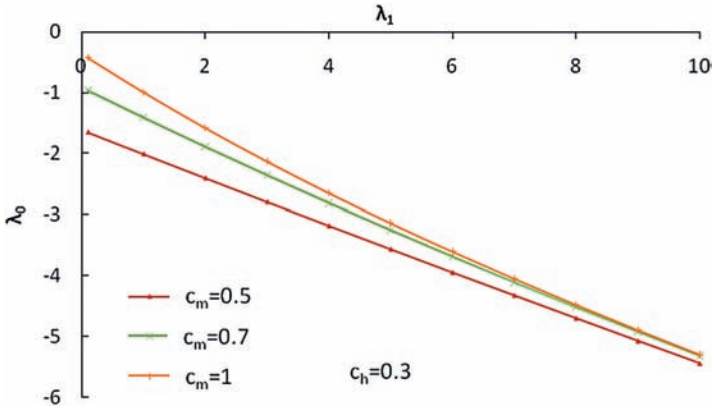

Figure 9-4 *Plot of λ_0 as a function of λ_1 for various values of* c_m *and* $c_h = 0.3$.

Table 9-4 *Values of λ_0 for different values of* c_h.

λ_1	$c_h = 0$	$c_h = 0.1$	$c_h = 0.3$	$c_h = 0.5$
0	–0.4	–0.55	–1	–1.67
1	–0.686	–0.896	–1.410	–2.208
2	–0.976	–1.252	–1.890	–2.803
3	–1.229	–1.579	–2.357	–3.394
4	–1.449	–1.881	–2.812	–3.983
5	–1.640	–2.161	–3.255	–4.568
6	–1.807	–2.419	–3.687	–5.150
7	–1.953	–2.661	–4.109	–5.729
8	–2.083	–2.888	–4.521	–6.305
9	–2.199	–3.102	–4.925	–6.878
10	–2.303	–3.305	–5.321	–7.448

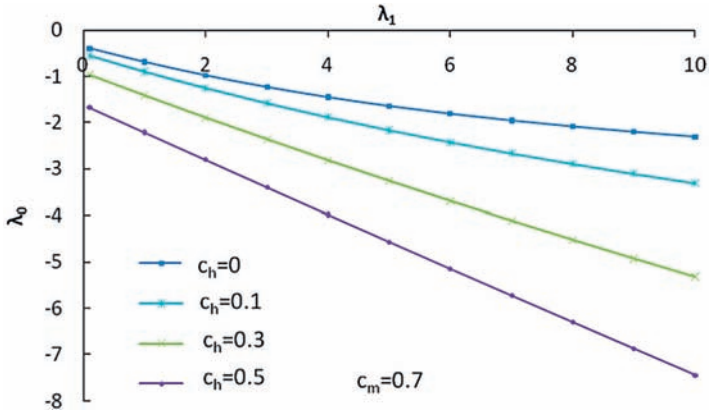

Figure 9-5 *Plot of λ_0 as a function of λ_1 for various values of* c_h *and* $c_m = 0.7$.

Example 9.4 Compute and plot c_D as a function of λ_1 for various values of c_h and c_m.

Solution Assume that $c_h = 0.3$, for $c_m = 0.5$, 0.7, and 1. c_D is computed using equation (9.13a) for various values of λ_1 from 0 to 10, as shown in Table 9-5 and Fig. 9-6.

Now assume that $c_m = 0.7$, for $c_h = 0$, 0.1, 0.3, and 0.5. Then, c_D is computed using equation (9.13a) for various values of λ_1 from 0 to 10, as shown in Table 9-6 and Fig. 9-7.

Table 9-5 *Values of* c_D *for different values of* c_m.

λ_1	$c_m = 0.5$	$c_m = 0.7$	$c_m = 1$
0	0.400	0.5	0.65
1	0.397	0.487	0.609
2	0.393	0.474	0.571
3	0.390	0.461	0.536
4	0.387	0.449	0.505
5	0.384	0.437	0.478
6	0.380	0.427	0.456
7	0.377	0.417	0.438
8	0.374	0.408	0.422
9	0.372	0.400	0.410
10	0.369	0.393	0.399

Table 9-6 *Values of* c_D *for different values of* c_h.

λ_1	$c_h = 0$	$c_h = 0.1$	$c_h = 0.3$	$c_h = 0.5$
0	0.35	0.4	0.400	0.5
1	0.309	0.370	0.397	0.487
2	0.271	0.341	0.393	0.474
3	0.236	0.315	0.390	0.461
4	0.205	0.290	0.387	0.449
5	0.178	0.269	0.384	0.437
6	0.156	0.250	0.380	0.427
7	0.138	0.234	0.377	0.417
8	0.122	0.220	0.374	0.408
9	0.110	0.208	0.372	0.400
10	0.099	0.199	0.369	0.393

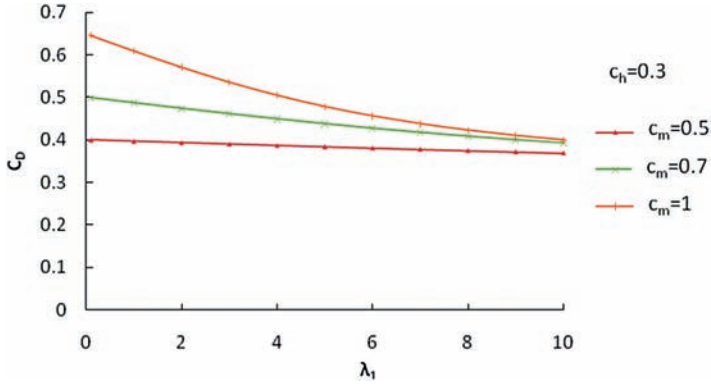

Figure 9-6 *Plot of* c_D *as a function of* λ_1 *for various values of* c_m *and* $c_h = 0.3$.

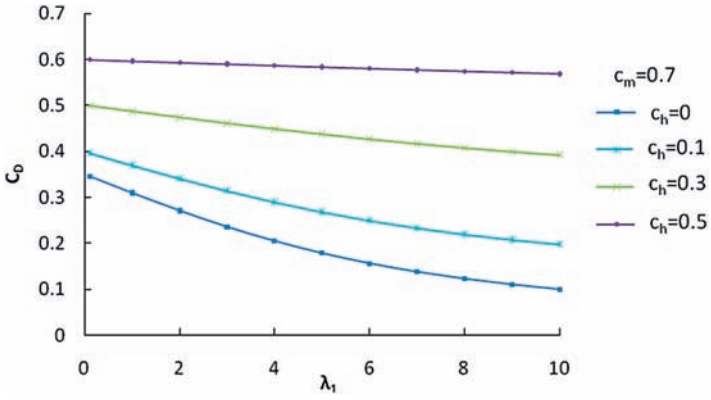

Figure 9-7 *Plot of* c_D *as a function of* λ_1 *for various values of* c_h *and* $c_m = 0.7$.

9.2.6 Sediment Concentration Distribution

It is hypothesized that the probability of sediment concentration being less than or equal to a given value c is $(h_0 - y)/h_0$. Then the cumulative distribution function of C, $F(c)$, can be written as

$$F(c) = \frac{h_0 - y}{h_0} = 1 - \frac{y}{h_0} \tag{9.16}$$

Differentiating equation (9.16) with respect to C gives the PDF of C, $f(c)$, as

$$dF(c) = f(c) = -\frac{1}{h_0}\frac{dy}{dc} \text{ or } f(c) = -\left(h_0 \frac{dc}{dy}\right)^{-1} \tag{9.17}$$

The PDF given by equation (9.17) must satisfy the constraints defined by equations (9.2) and (9.3). Therefore, substituting equation (9.14a) in equation (9.17), one gets

$$\exp(-\lambda_1 c)dc = -\frac{1}{\lambda_1 h_0}[\exp(-\lambda_1 c_h) - \exp(-\lambda_1 c_m)]dy \tag{9.18}$$

Integration of equation (9.18), with the limit, $c = c_m$ at $y = 0$, yields

$$\frac{c}{c_m} = -\frac{1}{\mu}\ln\left\{\exp(-\mu) + \frac{y}{h_0}\left[\exp\left(-\mu\left(\frac{c_h}{c_m}\right)\right) - \exp(-\mu)\right]\right\} \tag{9.19}$$

where $\mu = \lambda_1 c_m$ is a dimensionless entropy parameter. Equation (9.19) expresses the sediment concentration distribution as a function of longitudinal distance y. For $\mu = -50$ to $+50$ (at an interval of 10), c/c_m is plotted as a function of y/h_0, as shown in Figs. 9-8a and 9-8b. As μ tends to zero, c/c_m decreases linearly with y/h_0. When μ approaches ± 50, c/c_m becomes independent of y/h_0. This

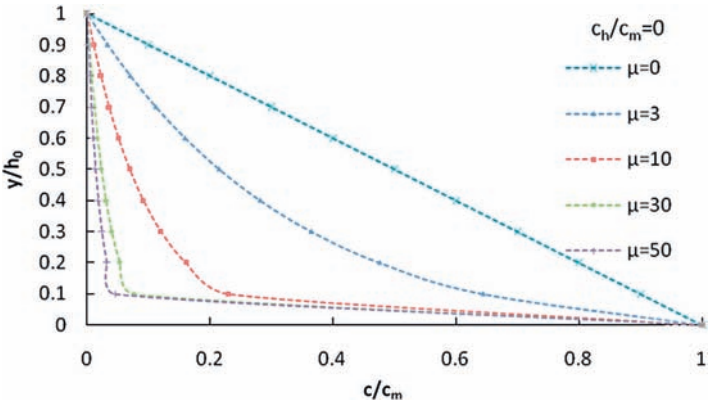

Figure 9-8a *Plot of* y/h_0 *versus* c/c_m *for various values of positive* μ.

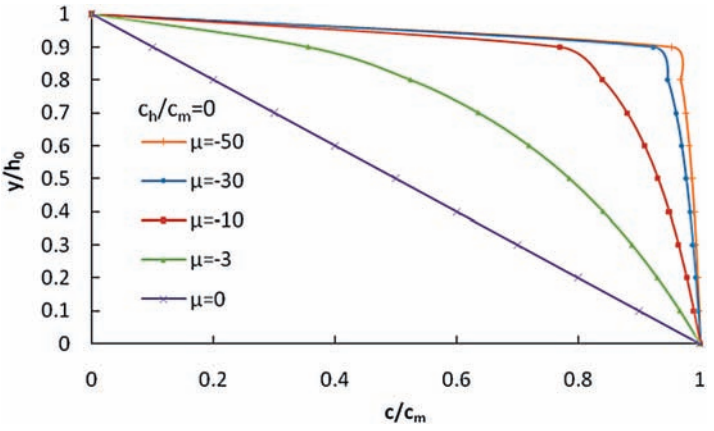

Figure 9-8b *Plot of* y/h_0 *versus* c/c_m *for various values of minus* μ.

independence suggests that parameter μ can be regarded as a measure of the uniformity of sediment concentration distribution. Equation (9.19) does not apply at the forefront of debris flow, where, because of large boulders and flow disturbance, the concentration is unsteady.

Now the dimensionless equilibrium sediment concentration can be derived. Inserting equation (9.14a) in equation (9.3) and integrating with the condition that $C = c_m$ at $y = 0$ and $C = c_h$ at $h = h_0$.

$$\frac{c_D}{c_m} = \frac{1}{\lambda_1 c_m} + \frac{\frac{c_h}{c_m} - \exp(\lambda_1 c_h - \lambda_1 c_m)}{1 - \exp(\lambda_1 c_h - \lambda_1 c_m)} = \frac{1}{\mu} + \frac{\frac{c_h}{c_m} - \exp\left[\mu\left(\frac{c_h}{c_m} - 1\right)\right]}{1 - \exp\left[\mu\left(\frac{c_h}{c_m} - 1\right)\right]} \tag{9.20}$$

Table 9-7 *Values of* c_D/c_m *for various values of* c_h/c_m.

μ	$c_h/c_m = 0$	$c_h/c_m = 0.1$	$c_h/c_m = 0.2$	$c_h/c_m = 0.3$	$c_h/c_m = 0.4$	$c_h/c_m = 0.5$
0	0.492	0.543	0.595	0.646	0.697	0.748
1	0.418	0.483	0.547	0.609	0.670	0.729
2	0.343	0.422	0.498	0.571	0.641	0.709
3	0.281	0.368	0.454	0.536	0.615	0.690
4	0.231	0.325	0.416	0.505	0.590	0.672
5	0.193	0.290	0.385	0.478	0.569	0.655
10	0.100	0.200	0.300	0.399	0.499	0.597
20	0.050	0.150	0.250	0.350	0.450	0.550
30	0.033	0.133	0.233	0.333	0.433	0.533
40	0.025	0.125	0.225	0.325	0.425	0.525
50	0.020	0.120	0.220	0.320	0.420	0.520

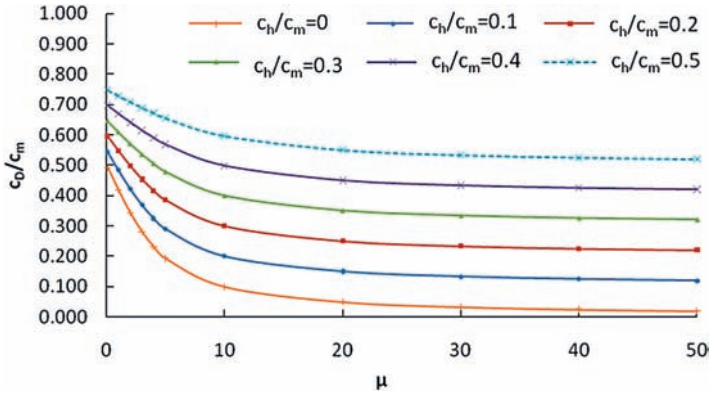

Figure 9-9 *Plot of* c_D/c_m *as a function of* μ *for various values of* c_h *and* c_m.

Example 9.5 Compute and plot c_D/c_m as a function of μ for various values of c_h and c_m.

Solution For $c_h/c_m = 0$, 0.1, 0.2, 0.3, 0.4, and 0.5, c_D/c_m is computed using equation (9.20), as shown in Table 9-7 and Fig. 9-9.

9.2.7 Equilibrium Sediment Concentration

Debris flow is caused in three ways: (1) The gully bed material is mobilized or the sediment particles from the gully bed are entrained by water runoff; (2) a natural dam formed by a landslide fails; and (3) a landside block is liquefied.

Takahashi (1978) theoretically derived a relation for computing the equilibrium sediment concentration of debris flow occurring in the first way, which can be expressed as

$$c_D = \frac{\rho \tan\theta}{(\rho_s - \rho)(\tan\phi - \tan\theta)} \tag{9.21}$$

in which θ is the angle of inclination of the channel bed from the horizontal; ϕ is the angle of internal friction; ρ_s is the density of sediment; and ρ is the density of water. Although equation (9.21) is widely used for calculating the equilibrium sediment concentration c_D at the forefront part of debris flow, in a steady uniform state it yields unrealistic results in some cases.

Example 9.6 Consider an example (Lien and Tsai 2003) where $\tan\phi = 0.756$, $\tan\theta = 0.466$ ($\theta = 25$ degrees), $\rho_s = 2.6\,\text{g/cm}^3$, and $\rho = 1\,\text{g/cm}^3$. Compute c_D.

Solution For these values, c_D obtained from equation (9.21) is $c_D \approx 1.0$. This value implies that c_D is greater than unity, which obviously is unrealistic, for flow cannot occur when the sediment concentration is that high.

Example 9.7 Compute and plot c_D/c_m as a function of $\tan\theta$ (%) ($\theta = 0.06$).

Solution Take $c_m = 0.756$, $\rho_s = 2.6\,\text{g/cm}^3$. Then, c_D/c_m is computed using equation (9.21), as shown in Table 9-8, and Fig. 9-10a.

From experimental flumes, Ou and Mizuyama (1994) developed an empirical relation for global sediment concentration using the channel bed slope as the principal factor:

$$c_{DT} = \frac{4.3(\tan\theta)^{1.5}}{1 + 4.3C_m(\tan\theta)^{1.5}} \tag{9.22}$$

Table 9-8 *Values of* C_{DT} *as a function of tan* θ *(%) (*$\theta = 0$–60*) for various values of* c_m.

$\tan\theta$	$c_m = 0.5$	$c_m = 0.6$	$c_m = 0.7$	$c_m = 0.8$	$c_m = 0.9$
0	0.000	0.000	0.000	0.000	0.000
10	0.127	0.126	0.124	0.123	0.121
20	0.323	0.312	0.303	0.294	0.286
30	0.522	0.496	0.473	0.451	0.432
40	0.705	0.658	0.618	0.582	0.550
50	0.864	0.795	0.736	0.686	0.642
60	1.000	0.909	0.833	0.769	0.714

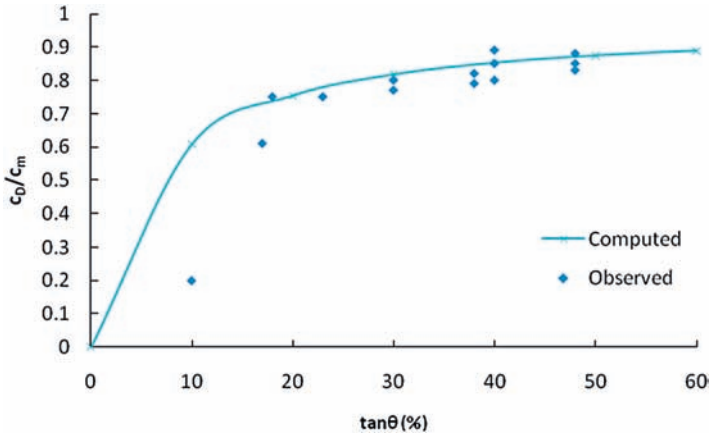

Figure 9-10a *Plot of* c_D/c_m *as a function of tan* θ *(%) (0–60).*

where c_{DT} is the average global sediment concentration of debris flow. This equation has been found to yield reasonable values of concentration, even at higher channel-bed slopes.

Example 9.8 Compute and plot c_{DT} as a function of tan θ (%) (θ = 0–60) for various values of c_m.

Solution For $c_m = 0.5$, 0.6, 0.7, 0.8, and 0.9, c_{DT} is computed using equation (9.22), as shown in Table 9-8, and Fig. 9-10b plots C_{DT} as a function of tan θ (%) (θ = 0–60) for various values of c_m.

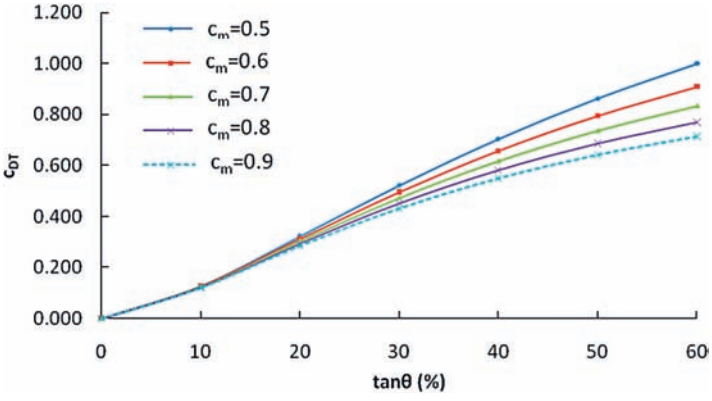

Figure 9-10b *Plot of* C_{DT} *as a function of tan* θ *(%) (*θ *= 0–60).*

Using the concept developed by Bagnold (1954) and experimental data of Takahashi (1978) and Ou and Mizuyama (1994), Lien and Tsai (2000) derived an equilibrium sediment concentration equation for simulating the forefront part as well as the global average of debris flow. This equation was further modified by Lien and Tsai (2003) as follows.

At the dynamic equilibrium condition, the sediment concentration in flow tends to attain saturation because of the balance in particle exchange between flow and channel bed. Under this condition, the effective shear stress in debris flow that acts on sediment particles resting on the channel bed is balanced by the critical shear stress of the particles. This phenomenon means that sediment particles are in incipient motion. One can then express

$$T - F\tan\alpha = \tau_c \tag{9.23}$$

where

$$T = [(\rho_s - \rho)c_D + c]gh_0 \sin\theta \tag{9.24}$$

$$F = (\rho_s - \rho)gc_D h_0 \cos\theta \tag{9.25}$$

in which $\tan\alpha$ is the dynamic friction coefficient varying from 0.32 to 0.75; T is the particle shear stress; F is the normal stress; and τ_c is the critical stress for the incipient motion of grains in the channel bed.

Example 9.9 Compute and plot F, T, and τ_c as a function of θ.

Solution The average sediment concentration c_D is computed by equation (9.21), and substituting in equations (9.24) and (9.25), F and T can be computed. Then, τ_c can be computed by equation (9.23), as shown in Table 9-9 and Fig. 9-11, which plots F, T, and τ_c as a function of θ. Let $h_0 = 1\,\text{m}$, $\rho_s = 2.6\,\text{g/cm}^3$.

Table 9-9 *Values of* F, T, *and* τ_c *as a function of* θ.

θ	T	F	τ_c
0	0.000	0.000	0.000
10	1.991	1.632	0.963
20	4.671	3.616	2.393
30	8.158	5.635	4.608
40	11.938	6.712	7.709
50	15.126	6.387	11.103
60	17.578	5.244	14.275

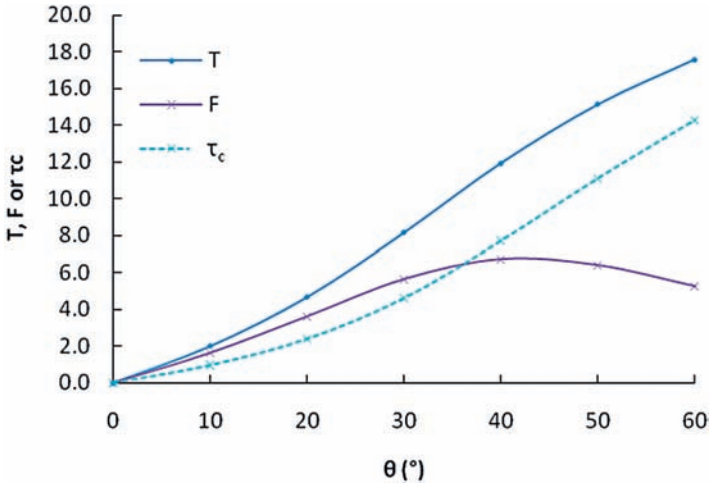

Figure 9-11 *Plot of* F, T, *and* τ_c *as a function of* θ.

For the incipient motion of uniformly sized bed material, Shields (1936) expressed the internal friction as

$$\theta = \frac{\tau_c}{(\rho_s - \rho) g d_s} \tag{9.26}$$

where θ is called the Shields parameter, representing the angle of inclination of the channel bed from the horizontal; τ_c is the shear stress; and d_s is the particle diameter. If the flow is fully developed, θ yielded by equation (9.26) ranges from 0.04 to 0.06. Inserting equations (9.24)–(9.26) in equation (9.23), one obtains

$$\frac{c_D}{c_m} = \frac{1}{2}[(1 + \chi + \beta) \pm \sqrt{(1 + \chi + \beta)^2 - 4\alpha}] \tag{9.27}$$

where

$$\chi = \frac{\rho \tan\theta}{c_m(\rho_s - \rho)(\tan\alpha - \tan\theta)} \tag{9.28}$$

and

$$\beta = \frac{\eta}{c_m \cos\theta(\tan\alpha - \tan\theta)} \tag{9.29}$$

where η is a parameter obtained experimentally, and $\tan\alpha$ is the dynamic friction coefficient shown in equation (9.23). If $\tan\theta = \tan\alpha$, the equilibrium concentration is then given by

$$\frac{c_D}{c_m} = \frac{1}{1 + \eta[(\rho_s - \rho)/\rho](1/\sin\theta)} \tag{9.30}$$

Table 9-10 c_D/c_m, χ *and* β *for different values of* $\tan\theta$ *(%).*

$\tan\theta$	χ	β	c_D/c_m
0	0.000	0.084	0.000
10	0.156	0.100	0.140
20	0.385	0.125	0.324
30	0.752	0.167	0.548
40	1.438	0.248	0.738
50	3.180	0.455	0.837
60	16.534	2.057	0.884

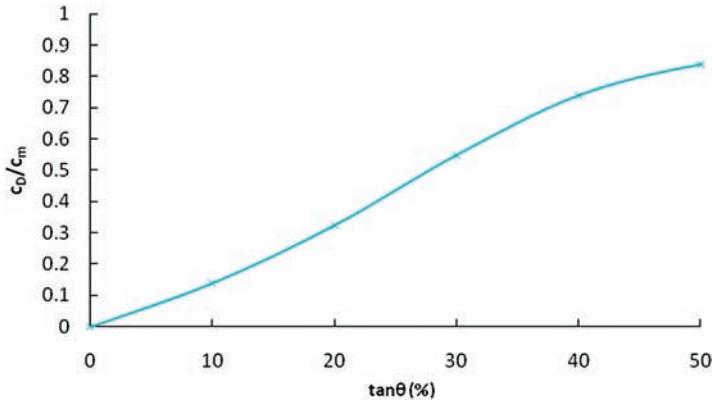

Figure 9-12a *Plot of* c_D/c_m *versus* $\tan\theta$ *(%) using equation (9.27).*

Example 9.10 Take $\eta = 0.04$. Compute and plot c_D/c_m versus $\tan\theta$ (%) using equation (9.27).

Solution c_D/c_m is computed using equation (9.27), and χ and β are computed using equations (9.28) and (9.29) for different values of $\tan\theta$ (%), as shown in Table 9-10 and Fig. 9-12a.

Example 9.11 Take $\eta = 0.04$. Compute and plot c_D/c_m versus $\tan\theta$ (%) using equation (9.30).

Solution c_D/c_m is computed using equation (9.30) for different values of $\tan\theta$ (%), as shown in Table 9-11 and Fig. 9-12b.

Table 9-11 *Values of* C_D/c_m *for various values of tan* θ *(%).*

tan θ	c_D/c_m
0	0.000
10	0.609
20	0.754
30	0.818
40	0.853
50	0.875
60	0.889

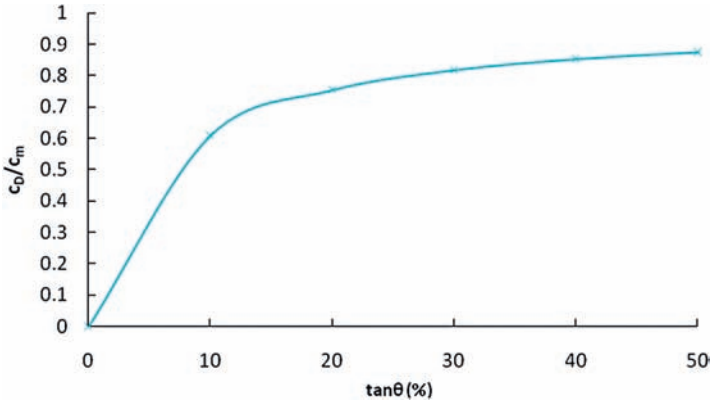

Figure 9-12b *Plot of* c_D/c_m *versus tan* θ *(%) using equation (9.30).*

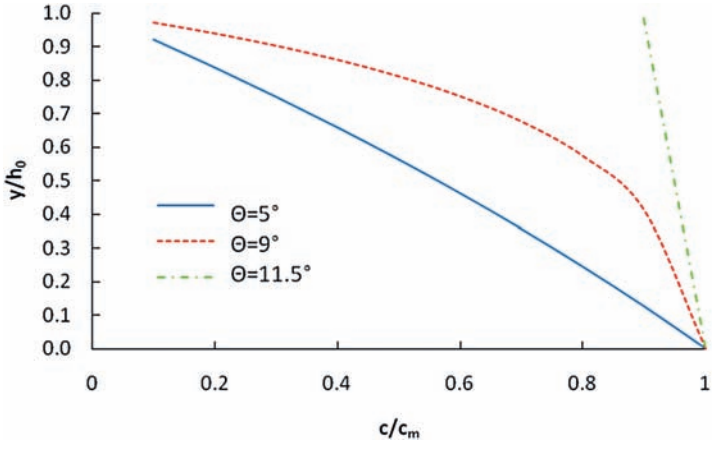

Figure 9-13 *Plot of* c/c_m *as a function of* y/h_0.

Example 9.12 Compute and plot c/c_m as a function of y/h_0.

Solution Combining equation (9.30) with equation (9.19), and taking $\eta = 0.04$, c/c_m is computed as a function of y/h_0, as shown in Table 9-12 and Fig. 9-13.

Table 9-12 *Plots of* y/h_0 *as a function of* c/c_m.

y/h_0	5°	9°	11.5°
0.1	0.920	0.971	0.999
0.2	0.836	0.938	0.999
0.3	0.749	0.902	0.998
0.4	0.658	0.860	0.997
0.5	0.562	0.810	0.995
0.6	0.461	0.751	0.994
0.7	0.356	0.675	0.992
0.8	0.244	0.573	0.989
0.9	0.126	0.411	0.985
1	0.000	0.000	0.000

Questions

Q9.1 Let μ be 0.5, –5, 1, and 5, and let y/h_0 be 0.5. Compute c/c_m. Now take $y/h_0 = 0.2$, 0.4, and 0.6 and $E = -5$ and +5 and compute c/c_m. What do these values of c/c_m say about its sensitivity to y/h_0 and μ?

Q9.2 Let $F(c)$ be hypothesized as $F(c) = 1 - \frac{y}{h_0}$. Plot and explain this hypothesis. How realistic is this hypothesis?

Q9.3 Let $\tan\phi = 0.8$, $\tan\theta = 0.5$, $\rho_s = 2.65\,\text{g/cm}^3$, and $\rho = 1\,\text{g/cm}^3$. Compute the equilibrium concentration of debris flow c_{DT}.

Q9.4 Let $\tan\theta = 0.5$ and $c_m = 0.5$. Compute the average global concentration of debris flow c_{DT}. Take $h_0 = 1\,\text{m}$.

Q9.5 Consider the dynamic friction coefficient $\tan\alpha = 0.5$, $h_0 = 2\,\text{m}$, the Shields parameter $\theta = 0.05$, $c_D = 0.5$. Compute the normal stress F, the grain shear stress T, and the critical shear stress for incipient motion of grain τ_c.

Q9.6 Compute c_D/c_m, taking $n = 0.04$, $c_m = 0.8$, $\theta = 10°$, and $\tan\alpha = 0.5$.

Q9.7 Consider $\theta = 5°$, $c_m = 0.5$, $\phi = 40°$. Compute the value of c_D. Take $c_h/c_m = 0.1$. Compute the value of μ. Compute the value of c_{DT}. Use c_D/c_m and compute μ. Also, compute c_D/c_m using equation (9.30) and then compute μ.

Q9.8 Consider $\phi = 40°$, $\theta = 10°$, $c_m = 0.6$, and compute the value of c_D. Take $c_h/c_m = 0.1$. Compute the value of μ. Compute the value of c_{DT}. Use c_D/c_m and compute μ. Also, compute c_D/c_m using equation (9.30) and then compute μ.

Q9.9 Consider $\phi = 40°$, $\theta = 12°$, $c_m = 0.6$, and compute the value of c_D. Take $c_h/c_m = 0.1$. Compute the value of μ. Compute the value of c_{DT}. Use c_D/c_m and compute μ. Also, compute c_D/c_m using equation (9.30) and then compute μ.

Q9.10 Consider $\rho_s = 2.45\,g/cm^3$, $c_m = 0.5$, $\tan\phi = 0.75$, and compute the value of c_D. Take $c_h/c_m = 0.1$. Compute the value of μ. Compute the value of c_{DT}. Use c_D/c_m and compute μ. Also, compute c_D/c_m using equation (9.30) and then compute μ.

References

Bagnold, R. A. (1954). "Experiments on gravity-free dispersion of large solid spheres in a Newtonian fluid under shear." *Proc., Royal Society of London, Series A*, 225, 49–63.

Egashira, S., Itoh, T., and Takeuchi, H. (2001). "Transition mechanism of debris flow over rigid bed to over erodible bed." *Phys. Chem. Earth*, 26(2), 169–174.

Jaynes, E. T. (1957). "Information theory and statistical mechanics I." *Phys. Rev.*, 106, 620–630.

Lien, H.-P., and Tsai, F.-W. (2000). "Debris flow control by using slit dams." *Int. J. Sediment Res.*, 15(4), 391–409.

Lien, H.-P., and Tsai, F.-W. (2003). "Sediment concentration distribution of debris flow." *J. Hydraul. Eng.*, 129(12), 995–1000.

Major, J. J., and Pierson, T. (1992)." Debris flow rheology: Experimental analysis of fine-grained slurries." *Water Resour. Res.*, 28(5), 841–857.

Ou, G., and Mizuyama, T. (1994). "Predicting the average sediment concentration of debris flow." *J. Jpn. Erosion Control Eng. Soc.*, 47(4), 9–13 (in Japanese).

Shannon, C. E. (1948). "The mathematical theory of communications, I and II." *Bell Syst. Tech. J.*, 27, 379–423.

Shields, A. (1936). "Anwendung der ahnlichkeitsmechanik und der turbulenz-forschung auf die geschiebebewegung." *Mitt. Der Preuss. Versuchanstait der Wasserbau und Schiffbau*, Berlin, 26, 98–109 (in German).

Takahashi, T. (1978). "Mechanical characteristics of debris flow." *J. Hydraul. Div.*, 104(8), 1153–1169.

Additional Reading

Chen, C.-L. (1988). "General solutions for viscoplastic debris flow." *J. Hydraul. Eng.*, 114(3), 259–282.

Egashira, S., Miyamoto, K., and Itoh, T. (1997). "Constitutive equations of debris flow and their applicability." *Debris-flow hazards mitigation: Mechanics, prediction, and assessment*, ASCE, New York, 340–349.

Jin, M., and Fread, D. L. (1999). "Modeling of mud/debris unsteady flows." *J. Hydraul. Eng.*, 125(8), 827–834.

Tsubaki, T., Hashimoto, H., and Suetsugi, T. (1982). "Grain stresses and flow properties of debris flow." *Proc., Jpn. Soc. Civil Eng.*, 317, 79–91 (in Japanese).

Wan, Z., and Wang, Z. (1994). "Hyperconcentrated flow." *Monograph Series of IAHR*, Balkema, Rotterdam, The Netherlands.

Part 3

Hydraulic Geometry

This page intentionally left blank

Chapter 10

Downstream Hydraulic Geometry

The term "hydraulic geometry" connotes the relationships between the mean stream channel form and discharge, both at a station and downstream along a stream network in a hydrologically homogeneous basin. The channel form includes the mean cross-sectional geometry (width and depth), and the hydraulic variables, including the mean slope, mean friction, and mean velocity for a given influx of water and sediment to the channel and the specified channel boundary conditions.

Hydraulic geometry relations are of two types: downstream hydraulic geometry relations and at-a-station hydraulic geometry relations. The concept of downstream hydraulic geometry involves spatial variation in channel form and process observed at *bankfull* stage or at a constant frequency of flow; this frequency may be taken as a two-year recurrence interval. The at-a-site hydraulic geometry entails mean values over a certain period of time, such as a week, a month, a season, or a year. In this case also, measurements should be made at the bankfull stage. Each type has been the subject of much interest and discussion in hydraulic and hydrologic literature. They are of great practical value in prediction of alluvial channel behavior, such as scour and fill, and channel deformation; layout of river training works; design of stable canals and intakes, river flow control works, irrigation schemes, and river improvement works; channel management; river restoration; modeling aquatic biota production systems; flow and sediment routing; flood estimation; and drainage net configurations. These relations can also be used to discriminate among different types of river

sections (Richards 1976) as well as in planning for resource and impact assessment (Allen et al. 1994). This chapter discusses the derivation of downstream hydraulic geometry relations using entropy in conjunction with minimum energy dissipation rate.

10.1 Hydraulic Geometry Relations

Leopold and Maddock (1953) expressed the hydraulic geometry relationships for a channel in the form of power functions of discharge as

$$B = aQ^b, \quad d = cQ^f, \quad V = kQ^m \tag{10.1a}$$

where B is the channel width; d is the flow depth; V is the flow velocity; Q is the flow discharge; and a, b, c, f, k, and m are parameters. Also added to equation (10.1a) are

$$n = NQ^p, \quad S = sQ^y \tag{10.1b}$$

where n is Manning's roughness factor, S is slope, and N, p, s, and y are parameters. Exponents b, f, m, p, and y represent, respectively, the rate of change of the hydraulic variables B, d, V, n, and S as Q changes; and coefficients a, c, k, N, and s are scale factors that define the values of B, d, V, n, and S when $Q = 1$.

The hydraulic variables, width, depth, and velocity, satisfy the continuity equation:

$$Q = BdV \tag{10.2a}$$

Therefore, the coefficients and exponents in equation (10.1a) satisfy

$$ack = 1, \quad b + f + m = 1 \tag{10.2b}$$

Using measurements, exponents b, f, m, p, and y, and a, c, k, N, and s are determined either graphically or by using regression analysis.

Example 10.1 Flow characteristics of Shaver Creek, in central Pennsylvania, corresponding to mean annual flood (2.3-year recurrence interval) measured by Brush (1961) are given in Table 10-1. Plot on a log-log paper flow width, depth, velocity, and slope as a function of discharge and fit straight lines. How good is the fit of these lines? Compute parameters (exponent and proportionality coefficient) of the relations between discharge and flow characteristics. Check if the sum of exponents equals 1.

Table 10-1 *Measurements of flow characteristics of Shaver Creek, Pennsylvania.*

Station no.	Mean annual flood, $Q_{2.3}$ (ft^3/s)	Bankfull width, B (ft)	Bankfull depth, d (ft)	Bankfull velocity, V (ft/s)	Slope, S (ft/ft)	Drainage area, A_d (mi^2)	Length of stream, L (mi)
1	115	16	1.4	5.1	0.021	1.83	1.8
2	171	16	1.44	7.4	0.029	3.01	2.9
3	246	19	2.19	6.3	0.032	4.71	3.5
4	300	19	2.42	6.6	0.021	6.11	4.8
5	420	22	2.54	7.5	0.0055	9.14	6.7
6	520	26	2.05	9.7	0.0042	11.92	8
7	720	35	2.55	8.1	0.0019	17.54	9.3
8	960	40	2.59	9.2	19	25.41	10.1
9	1,260	38	2.56	12.9	0.0022	35.7	11
10	1,600	43	3.2	11.6	0.002	47.6	12.1
11	1,680	50	4.07	8.3	0.0012	49.38	13.1
12	1,840	55	4.27	7.8	0.001	55.01	14.6

Source: Data from Brush (1961).

Solution The width, depth, and velocity were plotted against discharge on a log-log paper and straight lines were fitted, as shown in Fig. 10-1. The values of slopes (exponents) and intercepts (proportionality coefficients) were then determined as shown following:

a	1.4926
b	0.4658
c	0.3116
f	0.3258
k	2.2356
m	0.2029

It is noted that $ack = 1.4926 \times 0.3116 \times 2.2356 = 1.040$, and $b + f + m = 0.4658 + 0.3258 + 0.2029 = 0.995$. It is found that width is strongly related to discharge, depth is less strongly related, and velocity is even less strongly related.

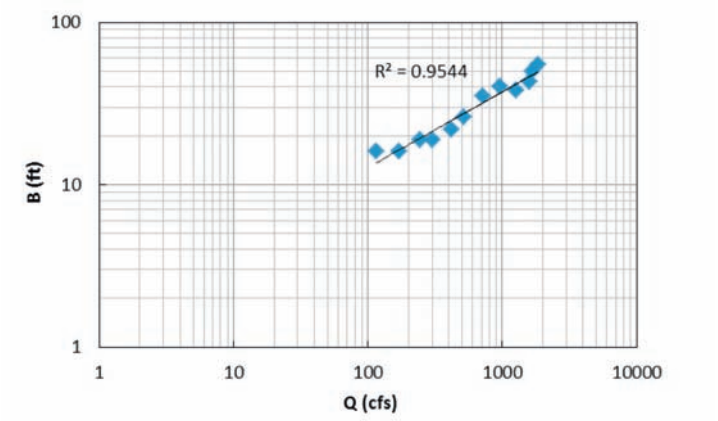

(a)

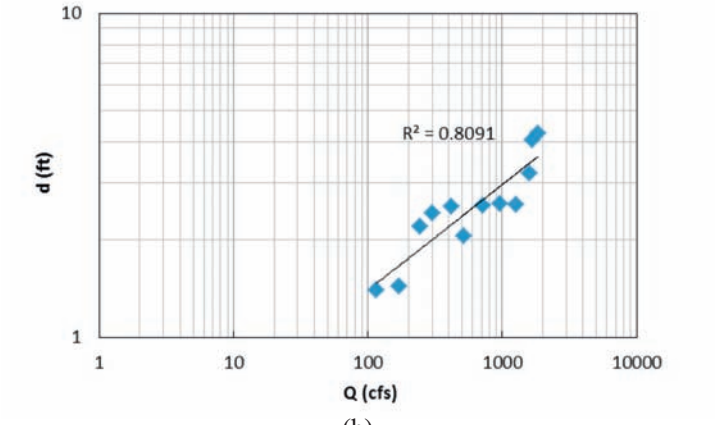

(b)

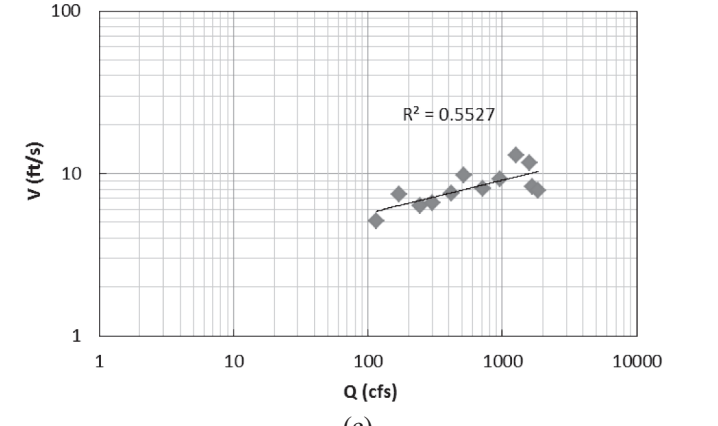

(c)

Figure 10-1 *Relation of width, depth, and velocity to discharge for Shaver Creek, Pennsylvania.*

10.2 Preliminaries

10.2.1 Type of Analyses

Richards (1982) has noted that the downstream hydraulic geometry involving channel process and form embodies two types of analyses, both of which are expressed as power functions of the form (Rhoads 1991) given by equations (10.1a) and (10.1b). The first type of analysis is typified by the works of Leopold and Maddock (1953) and Wolman (1955), who formalized a set of relations, such as equations (10.1a) and (10.1b), to relate the downstream changes in flow properties (width, mean depth, mean velocity, slope, and friction) to the mean discharge. This type of analysis describes the regulation of flow adjustment by channel form in response to the increase in discharge downstream and has been applied at particular cross sections as well as in the downstream direction.

The second type of analysis is a modification of the original hydraulic geometry concept and entails variation of channel geometry for a particular reference discharge downstream with a given frequency. Implied in this analysis is an assumption of an appropriate discharge that is the dominant flow controlling channel dimensions (Knighton 1987; Rhoads 1991). For example, for perennial rivers in humid regions, the mean discharge or a discharge that approximates bankfull flow (Q_b), such as Q_2 and $Q_{2.33,}$ with a return period of 2 and 2.33 years, respectively, is often used in equations (10.1a) and (10.1b). This concept is similar to that embodied in the regime theory (Blench 1952, 1969). It should, however, be noted that the coefficients and exponents are not constrained by the continuity equation when the selected discharge substantially differs from the bankfull flow. Conversely, Stall and Yang (1970) related hydraulic geometry to flow frequency and drainage area.

10.2.2 Mean Values of Hydraulic Variables

The mean values of the hydraulic variables of equations (10.1a) and (10.1b) are known to follow, according to Langbein (1964) and Yang et al. (1981), among others, necessary hydraulic laws and the principle of the minimum energy dissipation rate (or stream power). As a consequence, these mean values are functionally related and correspond to the equilibrium state of the channel. This state is regarded as the one corresponding to the maximum sediment-transporting capacity. The implication is that an alluvial channel adjusts its width, depth, slope, velocity, and friction to achieve a stable condition in which it is capable of transporting a certain amount of water and sediment. In other words, the average river system tends to develop in such a way as to produce an approximate equilibrium between the channel and the water and sediment it must transport (Leopold and Maddock 1953). Knighton (1977) observed that at cross sections undergoing a systematic change, the potential for adjustment toward some form of quasiequilibrium in the short term is related to the flow regime and channel boundary conditions and that the approach to quasiequilibrium or establishment

of a new equilibrium position is relatively rapid. Parker (1979) has stated that the scale factors, a, c, and k, vary from locality to locality but the exponents, b, f, and m, exhibit a remarkable degree of consistency and seem independent of location and only weakly dependent on channel type.

10.2.3 Calibration of Power Relations

The empirical hydraulic geometry relations expressed by equations (10.1a) and (10.1b) have been calibrated for a range of environments, using both field observations and laboratory simulations. Dury (1976) confirmed the validity of power function relations using extended sets of data at the 1.58-year mean annual discharge. Chong (1970) stated, without a firm basis, that hydraulic geometry relations of equations (10.1a) and (10.1b) were similar over varying environments. Parker (1978) analyzed the cause of this systematic behavior for gravel-bed rivers. It seems that the regional generalizations proposed in the literature are acceptable for rivers that have achieved "graded-time" equilibrium. Analyzing a subalpine stream in a relatively homogeneous environment, Phillips and Harlin (1984) found that hydraulic exponents were not stable over space. Knighton (1974) emphasized variations in exponents as opposed to mean values. Rhodes (1978) noted that the exponent values for high-flow conditions can be vastly different from those for low-flow conditions.

Using data from 318 alluvial channels in the midwestern United States and 50 piedmont sites, Kolberg and Howard (1995) showed that the width-discharge exponents ranged from 0.35 to 0.46 for groups of streams with width to depth (aspect) ratios less than 45. For groups of streams with width to depth ratios greater than 45, the width-discharge exponent decreased to a value below 0.15, suggesting a systematic variation in the exponents and a diminished influence of channel shape.

Klein (1981) found that the value $b = 0.5$ was a good average. The low b values normally occur for small basins under lower flows and for very large basins under very high flows. Thus, the $b = 0.5$ value, being a good average, tends to smooth out deviations from the average. The value of b ranged from 0.2 to 0.810.

This discussion shows that the exponents and coefficients of hydraulic geometry relations of equations (10.1a) and (10.1b) vary from location to location on the same river and from river to river, as well as from high-flow range to low-flow range. This phenomenon occurs, because the influx of water and sediment and the constraints (boundary conditions) that the river channel is subjected to vary from location to location, as well as from river to river. This means that for a fixed influx of water and sediment, a channel exhibits a family of hydraulic geometry relations in response to the constraints imposed on the channel. It is these constraints that force the channel to adjust its allowable hydraulic variables. For example, if a river is leveed on both sides, then it cannot adjust its width and is, therefore, left to adjust other variables, such as depth, friction, slope, and velocity. Likewise, if a canal is lined, then it cannot adjust its friction. This aspect does not seem to have been fully explored in the literature.

Example 10.2 Compare the exponents determined in Example 10.1 with those reported in the previously discussed literature. What can then be said about the Shaver Creek flow characteristics?

Solution The exponents determined in Example 10.1 compare well with the values reported in the literature. In the case of Shaver Creek, width seems to have a greater control than depth, and depth has a greater control than velocity. This situation suggests that this creek should be shallow.

Example 10.3 The values of hydraulic geometry exponents for a number of streams in Illinois, computed by Stall and Fok (1968), are given in Table 10-2. Compute mean, standard deviation, and coefficient of variation of these exponents. What do the variations in the exponent values mean hydraulically?

Table 10-2 *Values of hydraulic geometry exponents (after Stall and Fok 1968).*

	Exponents				Coefficients			
Stream station	***b***	***f***	***m***	***b + f***	***a***	***c***	***k***	***Ac***
Rock	0.62	0.26	0.12	0.88	1.92	0.49	1.07	0.93
Galena	0.71	0.22	0.07	0.93	2.1	0.54	0.88	1.13
Fox	0.57	0.29	0.14	0.86	2.33	0.41	1.05	0.96
Des Plaines	0.67	0.24	0.09	0.91	1.71	0.58	1.02	0.98
Kankabee	0.47	0.35	0.18	0.82	4.56	0.42	0.52	1.92
Vermilion (Illinois River basin)	0.48	0.35	0.17	0.83	5.38	0.3	0.62	1.61
Mackinaw	0.56	0.35	0.09	0.91	2.65	0.34	1.11	0.9
Henderson Creek	0.3	0.69	0.01	0.99	8.16	0.08	1.51	0.66
Spoon	0.45	0.47	0.08	0.92	3.76	0.19	1.39	0.72
La Moine	0.49	0.39	0.12	0.88	3.24	0.42	0.74	1.36
Sny	0.41	0.35	0.24	0.76	7.7	0.26	0.49	2.02
Sangamon	0.5	0.25	0.25	0.75	3.94	0.79	0.32	3.12
Kaskaskia	0.5	0.37	0.13	0.87	3.17	0.49	0.64	1.55
Vermilion (Wabash River basin)	0.33	0.37	0.3	0.7	8.84	0.38	0.3	3.36
Embarras	0.5	0.28	0.22	0.78	3.06	0.86	0.38	2.64
Little Wabash	0.36	0.33	0.31	0.69	9.13	0.69	0.16	6.32
Big Muddy	0.4	0.44	0.16	0.84	8.16	0.32	0.38	2.62
Big Bay Creek	0.38	0.49	0.13	0.87	6.23	0.31	0.52	1.93

Solution The values of mean, standard deviation, and coefficient of variation of hydraulic geometry exponents are computed as shown in Table 10-3. The coefficient of variation of the m exponent is the highest and that of the exponent is the lowest, suggesting that width is less variable than depth and that velocity is most variable among the three hydraulic variables.

Table 10-3 *Computed mean, standard deviation, and coefficient of variation of hydraulic geometry exponents for Example 10.3.*

	Exponents				Coefficients			
StatisticHEADING?	b	f	m	$b+f$	a	c	k	Ac
Mean	0.483	0.361	0.156	0.844	4.780	0.437	0.728	1.929
Standard deviation	0.113	0.112	0.081	0.081	2.593	0.201	0.391	1.370
Coefficient of variation	0.233	0.311	0.521	0.096	0.542	0.460	0.538	0.710

Example 10.4 The values of hydraulic geometry exponents for a number of rivers in the United States, computed by Stall and Yang (1970), are given in Table 10-4. Compute mean, standard deviation, and coefficient of variation of these exponents. What do the variations in the exponent values mean hydraulically? Compare the exponent values with those reported by Leopold and Maddock (1953) for Midwestern rivers as $b = 0.5$, $f = 0.4$, $m = 0.10$, and $b + f = 0.90$; and theoretical values by Leopold and Langbein (1962) as $b = 0.55$, $f = 0.36$, $m = 0.09$, and $b + f = 0.91$.

Table 10-4 *Values of hydraulic geometry exponents.*

	Exponents			
Stream/station	Width b	Depth f	Velocity m	Area $b+f$
Merrimack	0.55	0.36	0.09	0.91
Susquehanna	0.56	0.3	0.13	0.87
Roanoke	0.52	0.36	0.12	0.88
Big Sandy	0.46	0.34	0.2	0.8
White	0.45	0.46	0.1	0.9
Sangamon	0.9	0.3	0.21	0.79
Neches	0.48	0.47	0.04	0.95
Colorado	0.59	0.25	0.16	0.84
Tuolume	0.54	0.41	0.06	0.95
Skagit	0.46	0.32	0.22	0.78
Naqke	0.54	0.3	0.16	0.84
Rogue	0.49	0.35	0.15	0.84

Source: Data from Stall and Yang 1970.

Table 10-5 *Computed values of mean, standard deviation, and coefficient of variation of the exponents b, f, and m for Example 10.4.*

	Exponents			
	Width b	**Depth** f	**Velocity** m	**Area** $b+f$
Mean	0.545	0.352	0.137	0.863
Standard deviation	0.120	0.067	0.058	0.058
Coefficient of variation	0.221	0.189	0.422	0.067

Solution The values of mean, standard deviation, and coefficient of variation of the exponents b, f, and m are computed as shown Table 10-5. Clearly, the velocity exponent has the greatest variability and the depth exponent, the least variability. The b exponent is closer to the average value reported in the literature, and the velocity exponent is further from the average value. What is interesting is that different rivers seem to exhibit hydraulic similarity when viewed in terms of their geometry.

10.2.4 Theories of Hydraulic Geometry

A multitude of approaches have been used for deriving functional relationships among hydraulic variables for hydraulic geometry or equations (10.1a) and (10.1b) (Singh 2003). These approaches are based on the following theories: (1) empirical theory (e.g., regression theory [Leopold and Maddock 1953] and regime theory [Blench 1952]); (2) tractive force theory (Lane 1955) and its variants—threshold channel theory (Li 1974) and stability theory (Stebbings 1963); (3) hydrodynamic theory (Smith 1974); (4) thermodynamic entropy theory (Yalin and Da Silva 1997, 1999); (5) minimum extremal theories (e.g., minimum channel mobility theory [Dou 1964], minimum energy dissipation rate theory or its simplified versions of minimum unit stream power theory [Yang and Song 1986] and minimum stream power theory [Chang 1980, 1988; Yang et al. 1981], minimum energy dissipation theory [Rodriguez-Iturbe et al. 1992], minimum energy degradation theory [Brebner and Wilson 1967], minimum entropy production theory [Leopold and Langbein 1962], principle of least action [Huang and Nanson 2000], and minimum variance theory [Langbein 1964]); and (6) maximum extremal theories (maximum friction theory [Davies and Sutherland 1983], maximum sediment discharge theory [White et al. 1982], maximum sediment discharge and Froude number theory [Ramette 1980], and maximum entropy theory [Deng and Zhang 1994]). Most of these hypotheses have been used for deriving downstream hydraulic geometry relations, but empirical, the minimum variance, and tractive force theories have also been applied to at-a-station hydraulic geometry. Each hypothesis leads to unique relations between channel form parameters and discharge, and the relations corresponding to one hypothesis are not necessarily identical (in terms of exponents and proportionality constants) to those corresponding to another hypothesis.

10.3 Derivation of Hydraulic Geometry Relations

Langbein (1964), Yang et al. (1981), and Singh et al. (2003a, 2003b), among others, emphasized that equations (10.1a) and (10.1b) correspond to the case when the channel is in equilibrium state. Langbein (1964) hypothesized that when a channel adjusts its hydraulic variables corresponding to this state, the adjustment is shared equally among the hydraulic variables. Using the principle of maximum entropy and minimum stream power, Deng and Zhang (1994) derived morphological equations, assuming that for a given discharge the flow depth and width were independent variables among five hydraulic variables. However, in practice the channel is seldom in an equilibrium state, which means that the adjustment among hydraulic variables is unequal. The exact proportion in which the adjustment are shared among variables is not clear. Nevertheless, two points seem logical. First, there is a family of hydraulic geometry relations, depending on the adjustment of hydraulic variables. Second, the adjustment can explain the variability in the parameters (scale and exponents) of these relations. These two points are pursued in the next sections.

10.3.1 Defining Stream Power

Yang (1972) defined the unit stream power (USP) as the time rate of potential energy expenditure per unit weight of water in an alluvial channel. Simply put, the unit stream power is the velocity–slope product that has the dimensions of power per unit weight of water. Thus, USP, denoted as P_w, is expressed as

$$P_w = VS \tag{10.3}$$

where V is the average flow velocity, and S is the energy slope. Stream power (SP) is the rate of energy dissipation caused by flow of water:

$$SP = Q\gamma S \tag{10.4}$$

where γ is the weight density of water, and Q is the discharge of water. It should be noted that SP can be obtained by integrating USP over a given cross section.

If a channel is assumed to be rectangular with h as the depth of flow and B as the width of flow, then the flow cross-sectional area is $A = Bh$, the wetted perimeter is $P = B + 2h$, and the hydraulic radius is $R = A/P = (Bh)/(B + 2h)$. If the channel is wide rectangular, then $R \cong h$ = depth of flow. The flow discharge in equation (10.4) can be obtained from either Manning's or Chezy's or the Darcy–Weisbach equation. For wide rectangular channels, these equations can be written, respectively, as

$$Q = \frac{1}{n} AR^{2/3} S^{1/2} = \frac{1}{n} Bh^{5/3} S^{1/2} \tag{10.5}$$

$$Q = CA\sqrt{RS} = CBh^{3/2}\sqrt{S} \tag{10.6}$$

$$Q = 2\sqrt{\frac{2g}{f}}A\sqrt{RS} = 2\sqrt{\frac{2g}{f}}Bh^{3/2}\sqrt{S} \tag{10.7}$$

where n is Manning's roughness coefficient, C is Chezy's roughness coefficient, f is the Darcy–Weisbach friction factor, and g is acceleration caused by gravity. Equating equation (10.5) to equation (10.6), and equation (10.6) to equation (10.7), one obtains

$$C = \frac{1}{n}h^{1/6}; \quad C = 2\sqrt{2g/f} \tag{10.8}$$

Equations (10.5) to (10.7) can be expressed in a general from as

$$Q = \alpha Bh^{\beta}\sqrt{S} \tag{10.9}$$

in which α is a roughness measure, and β is an exponent. For Manning's equation, $\alpha = 1/n$, and $\beta = 5/3$; for Chezy's equation, $\alpha = C$, and $\beta = 3/2$; and for Darcy–Weisbach equation, $\alpha = 2(2g/f)^{0.5}$, and $\beta = 3/2$.

The energy slope S can be expressed from equation (10.9) as

$$S = \frac{Q^2}{\alpha^2 B^2 h^{2\beta}} \tag{10.10}$$

Thus, using equations (10.4) and (10.10), the stream power of a channel is expressed as

$$SP = \frac{\gamma Q^3}{\alpha^2 B^2 h^{2\beta}} \tag{10.11}$$

In equation (10.11), there are five variables: Q, S, B, α, and h; of these variables, Q, α, h, and B are on the right side of the equation, and Q and S through SP are on the left side. Three of these variables, α, B, and h, are controlling variables or constraints for a given discharge. It may be noted that the slope term S is not an independent variable here, because it is imbedded in the stream power and, hence, it is not considered as a controlling variable. Furthermore, from a practical point of view, a natural river can easily adjust its width, depth, velocity, and roughness because of changing discharge, but the longitudinal slope takes a very long time, years, if not centuries, to adjust (Yang 1996). Therefore, the longitudinal profile or slope is generally treated as constant over a short period of time. Because of this time scale difference, S is not considered as a variable when compared with velocity, depth, width, and roughness.

10.3.2 Hypothesis

A channel responds to the influx of water and sediment coming from its watershed by the adjustment of SP. Indeed Yang (1972) found USP to be the dominating factor in the determination of total sediment concentration. Yang (1986, 1996)

also related sediment load and channel geometry adjustment to SP. The spatial rate of adjustment of SP along a river, denoted by R_S, can be expressed as

$$R_S = \frac{d(SP)}{dx} = \frac{d(Q\gamma S)}{dx} \tag{10.12}$$

where x is the space coordinate along the direction of flow.

It is hypothesized that for a given influx of discharge from the watershed the channel adjusts or minimizes its stream power by adjusting the three controlling variables: depth, width, and friction. This hypothesis is similar to the one proposed by Langbein (1964) in his theory of minimum variance. Therefore, substitution of equation (10.6) in equation (10.12) yields

$$R_S = \frac{d(Q\gamma S)}{dx} = \gamma \frac{d}{dx}\left(\frac{Q^3}{\alpha^2 B^2 h^{2\beta}}\right) = \gamma Q^3 \frac{d}{dx}\left(\frac{1}{\alpha^2 B^2 h^{2\beta}}\right) \tag{10.13}$$

Equation (10.13) yields

$$R_S = -\frac{2Q^3}{\alpha^3 B^2 h^{2\beta}}\frac{d\alpha}{dx} - \frac{2\gamma Q^3}{\alpha^2 B^3 h^{2\beta}}\frac{dB}{dx} - \frac{2\gamma\beta Q^3}{\alpha^2 B^2 h^{2\beta+1}}\frac{dh}{dx} \tag{10.14}$$

The right side of equation (10.14) has three parts, designated as R_1, R_2, and R_3:

$$R_1 = -\frac{2\gamma Q^3}{\alpha^3 B^2 h^{2\beta}}\frac{d\alpha}{dx} \tag{10.15}$$

$$R_2 = -\frac{2\gamma Q^3}{\alpha^2 B^3 h^{2\beta}}\frac{dB}{dx} \tag{10.16}$$

$$R_3 = -\frac{2\beta\gamma Q^3}{\alpha^2 B^2 h^{2\beta+1}}\frac{dh}{dx} \tag{10.17}$$

Equation (10.15) can be interpreted as the spatial rate of adjustment of friction, equation (10.16) as the spatial rate of adjustment of width, and equation (10.17) as the spatial rate of adjustment of flow depth.

10.3.3 Definition of Probability

Dividing equations (10.15) to (10.17) by the total spatial rate of adjustment of SP, one gets

$$P_\alpha = \frac{R_1}{R_S} = \frac{2\gamma Q^3}{\alpha^3 B^2 h^{2\beta}}\frac{[d\alpha/dx]}{[d(SP)/dx]} \tag{10.18}$$

$$P_B = \frac{R_2}{R_S} = \frac{2\gamma Q^3}{\alpha^2 B^3 h^{2\beta}}\frac{[dB/dx]}{[d(SP)/dx]} \tag{10.19}$$

$$P_h = \frac{R_3}{R_S} = \frac{2\beta\gamma Q^3}{\alpha^2 B^2 h^{2\beta+1}} \frac{[dh/dx]}{[d(SP)/dx]} \tag{10.20}$$

Equation (10.18) can be interpreted as the proportion of the adjustment of stream power by friction, equation (10.19) as the proportion of the adjustment of stream power by channel width, and equation (10.20) as the proportion of the adjustment of stream power by flow depth. These proportions can be considered equivalent to probabilities.

10.3.4 Principle of Maximum Entropy

According to the principle of maximum entropy (Jaynes 1957), any system in equilibrium state under steady constraints tends to maximize its entropy. When a river reaches a dynamic (or quasidynamic) equilibrium, the entropy should attain its maximum value. The principle of maximum entropy (POME) states that the entropy of a system is maximum when all probabilities are equal, i.e., the probability distribution is uniform. Applying this principle to a river in its dynamic equilibrium, the following must, therefore, be true:

$$P_\alpha = P_B = P_h \tag{10.21}$$

Equation (10.21) holds, of course, under the stipulation that there are no constraints imposed on the channel and can be interpreted to mean that the self-adjustment of SP (γQS) is equally shared among α, B, and h. This interpretation is supported by Williams (1967, 1978), who found from an analysis of data from 165 gauging stations that a channel adjusted all its hydraulic parameters (B, h, S, and V) in response to changes in the influx of water and sediment and that self-adjustments were realized in an evenly distributed manner among factors. Equation (10.21) is similar to the concept embodied in the minimum variance theory (Langbein 1964).

10.3.5 Different Scenarios

Equation (10.21) involves probabilities of three variables, meaning that any two of the three cases of adjustment in hydraulic variables may coexist, as well as the probability that all three cases may coexist. These configurations of adjustment indeed occur in nature (Wolman 1955). Thus the equality among three probabilities raises four possibilities and, hence, leads to four sets of equations (Singh et al. 2003a): (1) $P_\alpha = P_B$, (2) $P_B = P_h$, (3) $P_\alpha = P_h$, and (4) $P_\alpha = P_B = P_h$. It should be noted that all four possibilities can occur in the same river in different reaches, or in the same reach at different times, or in different rivers at the same time, or at different times. In order to enumerate the consequences of these possibilities, one can use the general discharge equation (10.9), or Manning's equation (10.5), or Chezy's equation (10.6), or the Darcy–Weisbach equation (10.7). It is, however, more informative to use a specific discharge–resistance relation than the general discharge–resistance relation. Survey of literature shows that

Manning's equation is more commonly used in hydraulic and river engineering in general and more specifically in investigations on hydraulic geometry (for example, Leopold and Wolman 1957; Wolman and Brush 1961; Stall and Fok 1968; Bray 1982). Furthermore, the data that could be found on alluvial rivers and canals contain Manning's n a lot more than Chezy's C or Darcy–Weisbach's f. For these reasons, Manning's equation is used in this chapter. Consequently, possibility P_α is replaced by P_n. Expressing then equations (10.18) to (10.20) for Manning's equation, one gets

$$P_n = \frac{R_1}{R_S} = \frac{2n\gamma Q^3}{B^2 h^{10/3}} \frac{[dn/dx]}{[d(SP)/dx]} \tag{10.22}$$

$$P_B = \frac{R_2}{R_S} = -\frac{2n^2\gamma Q^3}{B^3 h^{10/3}} \frac{[dB/dx]}{[d(SP)/dx]} \tag{10.23}$$

$$P_h = \frac{R_3}{R_S} = -\frac{10\gamma n^2 Q^3}{3B^2 h^{13/3}} \frac{[dh/dx]}{[d(SP)/dx]} \tag{10.24}$$

10.3.6 Primary Morphological Equations for Different Scenarios

The four possibilities for spatial stream power adjustment lead to primary morphological equations, which are needed for deriving downstream hydraulic geometry relations. The morphological equations are, therefore, derived first.

10.3.6.1 Possibility I: $P_B = P_n$

Equating equation (10.22) for P_n to equation (10.23) for P_B, one gets

$$\frac{dn}{dx} = -\frac{n}{B}\frac{dB}{dx} \tag{10.25}$$

Equation (10.25) hypothesizes that the spatial change in stream power is accomplished by an equal spatial adjustment between flow width B and resistance expressed by Manning's n. This possibility occurs in wide rectangular channels where the flow depth is not a controlling variable but the roughness and the flow width are. The downstream ends of the Brahmaputra River before joining the Bay of Bengal in India and Bangladesh and of the Mississippi River before joining the Gulf of Mexico in the United States are examples. The hypothesis can be considered a limiting case and presumably holds under the equilibrium condition. However, such a condition is not always achieved, and, therefore, the spatial change in stream power is accomplished by an unequal adjustment between B and n. To that end, equation (10.25) is modified as

$$\frac{dn}{dx} = -\frac{wn}{B}\frac{dB}{dx} \tag{10.26}$$

where w is a weighting factor, $0 \leq w$, which accounts for the proportion in which the adjustment in stream power is shared between B and n. For the special case where the adjustment is shared equally between B and n, $w = 1$.

Integration of equation (10.26) yields

$$nB^w = C_1 \text{ or } B = C_1^* n^{-1/w} \tag{10.27}$$

where C_1 and C_1^* are constants of integration. For the limiting case ($w = 1$), equation (10.27) becomes

$$nB = C_1 \text{ or } B = C_1^* n^{-1} \tag{10.28}$$

Parameter C_1 or C_1^* can be labeled as a primary morphological coefficient and equation (10.27) or (10.28) as a primary morphological equation.

10.3.6.2 Possibility II: $P_B = P_h$

Here P_B is given by equation (10.23) and P_h by equation (10.24). This case hypothesizes that the spatial variation in stream power is accomplished by an equal spatial adjustment between flow depth and flow width. This possibility occurs in channels where the roughness is fixed, say, by lining, and the controlling variables are flow depth and width. Examples of such cases are the channels used for recreation, and trapezoidal channels that have attained a kind of equilibrium condition. The hypothesis can be considered as a limiting case and will hold under the equilibrium condition. Such a condition is, however, seldom achieved, and, therefore, the spatial change in stream power is accomplished by an unequal adjustment between h and B. Using r as a weighting factor, $0 \leq r$, which accounts for the proportion in which the adjustment of stream power is shared between h and B, one obtains

$$\frac{B}{h^{5/(3r)}} = C_2 \text{ or } h = C_2^* B^{(3r)/5} \tag{10.29}$$

where C_2 and C_2^* are constants of integration. For the limiting case ($r = 1$), where the adjustment is equally shared, equation (10.29) reduces to

$$\frac{B}{h^{5/3}} = C_2 \quad or \quad h = C_2^* B^{3/5} \tag{10.30}$$

Parameter C_2 or C_2^* can be designated as a primary morphological coefficient, and equation (10.29) or (10.30) as a primary morphological equation. It is interesting to note that equation (10.29) resembles the basic form of the regime equation expressed as

$$\frac{B^\phi}{h} = \varphi \tag{10.31}$$

where $\phi = 3/5$ and $\varphi = 1/C_2^*$.

Table 10-6 Computed values of C_2, from Example 10.5.

B (ft)	$h^{5/3}$ (ft)	$C_2 = B/h^{5/3}$
16	1.752	9.132
16	1.836	8.713
19	3.693	5.145
19	4.362	4.356
22	4.728	4.653
26	3.308	7.859
35	4.760	7.354
40	4.885	8.189
38	4.791	7.932
43	6.949	6.188
50	10.375	4.819
55	11.239	4.894

Example 10.5 Using the data from Table 10-1, check whether equation (10.30) is valid. Compute the values of C_2 and determine its spread.

Solution The values of C_2 are computed as shown in Table 10-6. C_2 has a mean of 6.603 and standard deviation of 1.772, and its range is remarkably narrow.

10.3.6.3 Possibility III: $P_n = P_h$

Here P_n is given by equation (10.22) and P_h by equation (10.24). This case hypothesizes that the spatial variation in stream power is accomplished by an equal spatial adjustment between flow depth and resistance. Examples of such a possibility are a laboratory flume with fixed walls, canals, leveed rivers, and so on. This hypothesis can be considered as a limiting case and holds under the equilibrium condition. Such a condition is not always attained, and, therefore, the spatial change in stream power is accomplished by an unequal adjustment between h and n. Using J as a weighting factor, $0 \leq J$, which accounts for the proportion in which the adjustment of stream power is shared between n and h, one gets

$$n = C_3 h^{-(5J)/3} \text{ or } h = C_3^* n^{-3/(5J)} \tag{10.32}$$

where C_3 and C_3^* are constants of integration. For the limiting case ($J = 1$), where the adjustment is equally shared, $J = 1$, equation (10.32) reduces to

$$nh^{5/3} = C_3 \text{ or } h = C_3^* n^{-3/5} \tag{10.33}$$

Parameter C_3 or C_3^* can be considered as a primary morphological coefficient and equation (10.32) or (10.33) as a primary morphological equation.

10.3.6.4 Possibility IV: $P_n = P_B = P_h$

Equation (10.27) relates n and B, equation (10.29) relates B and h, and equation (10.32) relates n and h. The first two equations can be used to eliminate n and h in equation (10.5) and express B as a function of Q. Similarly, equations (10.29) and (10.32) can be used to eliminate B and n in equation (10.5) and express h as a function of Q. Likewise, all three equations can be used to express V as a function of Q. Thus, three primary morphological equations (10.27) or (10.28), (10.29) or (10.30), and (10.32) or (10.33); and their three corresponding primary morphological coefficients, C_1, C_2, and C_3 (or C_1^*, C_2^*, and C_3^*), are obtained. Equation (10.27) can also be obtained by combining equations (10.29) and (10.32), or equation (10.28) can be obtained by combining equations (10.30) and (10.33).

10.4 Downstream Hydraulic Geometry Equations for a Given Discharge

If discharge Q and slope S of a river are known, then substitution of primary morphological equations (10.27), (10.29), and (10.32) in equation (10.5) leads to equations for the hydraulic geometry of a river.

10.4.1 Possibility I: Hydraulic Geometry Relations for Width, Roughness, and Velocity

This possibility ($P_B = P_n$: $nB^w = C_1$) leads to hydraulic geometry relations for B, V, and n. To derive these relations, three steps are involved:

1. Substitution of equation (10.27) in equation (10.5) leads to the expressions for B, V, and n in terms of Q and S:

$$B = C_B Q^{1/(1+w)} S^{-1/[2(1+w)]},\ C_B = (C_1 h^{-5/3})^{1/(1+w)} \tag{10.34}$$

$$V = C_V Q^{2w/[5(1+w)]} S^{5/[6(1+w)]},\ C_V = [C_n (C_B)^{2/3}]^{-3/5} \tag{10.35}$$

$$n = C_n Q^{-w/(1+w)} S^{w/[2(1+w)]},\ C_n = (C_1)^{1/(1+w)} h^{5w/[3(1+w)]} \tag{10.36}$$

Equations (10.34) to (10.36) contain S, which can be eliminated with the use of a sediment transport relation.

2. S can be expressed in terms of discharge, using a sediment transport relation. To that end, from the Engelund and Hansen sediment transport equation (Engelund and Hansen 1967), the channel slope S can be expressed (Knighton 1998) as

$$S = C_s Q^z \tag{10.37}$$

where C_s is a coefficient, $z = -2/5$ for gravel-bed rivers and $z = -1/6$ for sandy rivers. Such a relation is useful if S is unknown. This step leads to one set of

hydraulic geometry relations for gravel-bed rivers and another set for sandy or alluvial rivers.

3. Substitution of equation (10.37) in equation (10.34) leads to an expression for B in terms of Q alone (Knighton 1998):

$$B = C_{BS} Q^{\frac{(1-z/2)}{1+w}}, C_{BS} = \frac{C_B}{C_S^{1/2(1+w)}} \tag{10.38}$$

Substitution of $z = -2/5$ and $z = -1/6$ into equation (10.34) yields

$$B = C_{BS} Q^{-} Q^{\frac{6}{5(1+w)}} \text{ for gravel-bed rivers} \tag{10.39}$$

$$B = C_{BS} Q^{\frac{13}{12(1+w)}} \text{ for sandy rivers} \tag{10.40}$$

Likewise, with use of equation (10.37), equation (10.35) can be simplified for V as

$$V = C_{VS} Q^{\frac{5w-1}{3(1+w)}} (C_{VS} = C_V C_S^{5/[6(1+w)]}) \text{ for gravel-bed rivers} \tag{10.41}$$

$$V = C_{VS} Q^{\frac{60w-5}{36(1+w)}} \text{ for sandy rivers} \tag{10.42}$$

Similarly, inserting equation (10.39) in equation (10.38), one gets an expression for n as

$$n = C_{nS} Q^{\frac{-6w}{5(1+w)}} (C_{nS} = C_n C_S^{w/[2(1+w)]}) \text{ for gravel-bed rivers} \tag{10.43}$$

$$n = C_{nS} Q^{\frac{-13w}{12(1+w)}} \text{ for sandy rivers} \tag{10.44}$$

For the special case, $w = 1$, equations (10.38) to (10.39) reduce, respectively, to

$$B = C_B \frac{Q^{0.5}}{S^{1/4}}, C_B = (C_1)^{0.5} h^{-5/6} \tag{10.45}$$

$$B = C_{BS} Q^{\frac{3}{5}} \left(C_{BS} = \frac{C_B}{C_S^{1/2(1+w)}} \right) \text{ for gravel-bed rivers} \tag{10.46}$$

$$B = C_{BS} Q^{\frac{13}{24}} \text{ for sandy rivers} \tag{10.47}$$

$$V = C_V Q^{1/5} S^{5/12}, C_V = \left(C_n^{3/5} C_B^{2/5} \right)^{-1} \tag{10.48}$$

$$V = C_{VS} Q^{\frac{2}{3}} (C_{VS} = C_V C_S^{5/12}) \text{ for gravel-bed rivers} \tag{10.49}$$

$$V = C_{VS} Q^{\frac{55}{72}} \text{ for sandy rivers} \tag{10.50}$$

$$n = C_n \frac{S^{1/4}}{Q^{1/2}}, C_n = (C_1)^{1/2} h^{5/6} \tag{10.51}$$

$$n = C_{nS} Q^{\frac{-3}{5}} \ (C_{nS} = C_n C_S^{1/4}) \text{ for gravel-bed rivers} \tag{10.52}$$

$$n = C_{nS} Q^{\frac{-13}{24}} \text{ for sandy rivers} \tag{10.53}$$

In this possibility, the change in stream power is accomplished by the adjustment between channel width and roughness. For the three variables, the values of exponents, b, p, and m, are given in Tables 10-7, 10-8a, and 10-8b. Equations (10.39) and (10.40) show that the channel width varies with discharge raised to the power [$b = 6/\{5(1 + w)\}$ for gravel-bed rivers and $b = 13/\{12(1 + w)\}$ for sandy rivers] from some positive value greater than zero to a value of 1, and the scale factor C_B varies with flow depth. Thus, one can infer that the b exponent has a range of 0 to 1. The precise value of b depends on the value of w, meaning the proportion in which the spatial change of stream power is accomplished by the adjustment between B, n, and V. When w = 1, the channel width varies with the discharge raised to the power of 0.5, as shown by equation (10.45) for gravel-bed rivers and 0.6 for sandy rivers, as shown by equation (10.46). This exponent value of 0.5 is about the average value reported in the literature (Klein 1981). However, one should note that in equation (10.34), slope also appears with an exponent of $-1/[2(1 + w)]$. If the channel slope is constant, then the slope

Table 10-7 *Values of exponents* ***b***, ***f***, ***m***, *and* ***p*** *for three limiting cases, with slope explicitly appearing in hydraulic geometry relations.*

Possibility		I	II	III	I + II + III
b for ***B***	W.F. = 0	1 (***w*** = 0)	1 (***r*** = 0)		1 (***w*** = ***r*** = 0)
	W.F. = 1	0.5 (***w*** = 1)	0.5 (***r*** = 1)		1/3 (***w*** = ***r*** = 1)
	W.F. = ∞	0 (***w*** = ∞)	0 (***r*** = ∞)		0 (***w*** = ***r*** = ∞)
f for ***h***	W.F. = 0		0 (***r*** = 0)	3/5 (***J*** = 0)	0 (***J*** = ***r*** = 0)
	W.F. = 1		3/10 (***r*** = 1)	3/10 (***J*** = 1)	1/5 (***J*** = ***r*** = 1)
	W.F. = ∞		3/5 (***r*** = ∞)	0 (***J*** = ∞)	0 (***J*** = ***r*** = ∞)
m for ***V***	W.F. = 0	0 (***w*** = 0)	0 (***r*** = 0)	2/5 (***J*** = 0)	0 (***w*** = ***J*** = ***r*** = 0)
	W.F. = 1	1/5 (***w*** = 1)	1/5 (***r*** = 1)	7/10 (***J*** = 1)	7/15 (***w*** = ***J*** = ***r*** = 1)
	W.F. = ∞	2/5 (***w*** = ∞)	2/5 (***r*** = ∞)	1 (***J*** = ∞)	1 (***w*** = ***J*** = ***r*** = ∞)
p for ***n***	W.F. = 0	0 (***w*** = 0)		–1 (***J*** = 0)	0 (***J*** = ***w*** = 0)
	W.F. = 1	–0.5 (***w*** = 1)		–0.5 (***J*** = 1)	–1/3 (***J*** = ***w***= 1)
	W.F. = ∞	–1 (***w*** = ∞)		0 (***J*** = ∞)	–1 (***J*** = ***w*** = ∞)
Equation No.		(10.34) to (10.36)	(10.54) to (10.56)	(10.72) to (10.74)	(10.90) to (10.93)

Note: W.F. denotes the weighting factor. The weighting factors are zero, unity, and infinity for different possibilities. Usually these factors have values between the limiting values.

Table 10-8a *Values of exponents* $\boldsymbol{b}$, $\boldsymbol{f}$, $\boldsymbol{m}$, *and* $\boldsymbol{p}$ *for three limiting cases, with slope expressed as a function of discharge with the power of –1/6.*

Possibility		I	II	III	I + II + III
b for B	W.F. = 0	13/12 ($w = 0$)	13/12 ($r = 0$)		13/12 ($w = r = 0$)
	W.F. = 1	13/24 ($w = 1$)	13/24 ($r = 1$)		13/36 ($w = r = 1$)
	W.F. = ∞	0 ($w = \infty$)	0 ($r = \infty$)		0 ($w = r = \infty$)
f for h	W.F. = 0		0 ($r = 0$)	13/20 ($J = 0$)	0 ($J = r = 0$)
	W.F. = 1		13/40 ($r = 1$)	13/40 ($J = 1$)	13/60 ($J = r = 1$)
	W.F. = ∞		13/20 ($r = \infty$)	0 ($J = \infty$)	0 ($J = r = \infty$)
m for V	W.F. = 0	–5/36 ($w = 0$)	–1/12 ($r = 0$)	7/20 ($J = 0$)	–1/12 ($J = r = 0$)
	W.F. = 1	55/72 ($w = 1$)	2/15 ($r = 1$)	27/40 ($J = 1$)	19/45 ($J = r = 1$)
	W.F. = ∞	5/3 ($w = \infty$)	7/20 ($r = \infty$)	1 ($J = \infty$)	1 ($w = J = r = \infty$)
p for n	W.F. = 0	0 ($w = 0$)		–13/12 ($J = 0$)	0 ($J = w = 0$)
	W.F. = 1	–13/24 ($w = 1$)		–13/24 ($J = 1$)	–13/36 ($J = w = 1$)
	W.F. = ∞	–13/12 ($w = \infty$)		0 ($J = \infty$)	–13/12($J = w = \infty$)
Equation No.		(10.38), (10.41), and (10.43)	(10.57), (10.59), and (10.61)	(10.75), (10.77), and (10.79)	(10.94), (10.96), (10.98), and (10.100)

Note: W.F. denotes the weighting factor. The weighting factors are zero, unity, and infinity for different possibilities. Usually these factors have values between the limiting values.

component of the equation merges with coefficient C_B. This phenomenon shows that the scale factor C_B varies from one location to another and also with time through flow depth. Otherwise, slope can be expressed as a function of discharge raised to the power of $z = -2/5$ and $-1/6$ for gravel-bed rivers and for sandy rivers, respectively. Then in this case, under the special condition with weighting factor $w = 1$, the width varies with discharge raised to the power of 0.6 and 0.5, for sandy rivers and for gravel-bed rivers, respectively, which exponent values also fall within the range reported in the literature.

The average flow velocity varies with the discharge raised to the power from zero to 2/5, as shown in Table 10-7, and the scale factor C_V varies with flow depth. The precise value of exponent m depends on the value of the weighting factor w. For the limiting case $w = \infty$, $m = 2/5$, and for the special case $w = 1$, m is 1/5 as shown by equation (10.48), which is in the range of the values reported in the literature. In this case, slope also appears in equations (10.35) and (10.48), in which case the power of slope varies from 0 to 5/6. If the slope is expressed as a function of discharge with the power of –1/6, then the exponent m varies from –5/36 (–0.14) to 5/3. Most of the values reported in the literature lie within the derived range.

Manning's n varies with discharge raised to the power varying from –1 to 0, as shown in Table 10-7, and the scale factor C_n varies with flow depth. The exponent p in this case depends on the value of w. The exponent value of –0.5 is for

Table 10-8b *Values of exponents* ***b***, ***f***, ***m***, *and* ***p*** *for three limiting cases, with slope expressed as a function of discharge with the power of –2/5.*

Possibility		I	II	III	I + II + III
b for ***B***	W.F. = 0	6/5 ($w = 0$)	6/5 ($r = 0$)		6/5 ($w = r = 0$)
	W.F. = 1	3/5 ($w = 1$)	3/5 ($r = 1$)		2/5 ($w = r = 1$)
	W.F. = ∞	0 ($w = \infty$)	0 ($r = \infty$)		0 ($w = r = \infty$)
f for ***h***	W.F. = 0		0 ($r = 0$)	18/25 ($J = 0$)	0 ($J = r = 0$)
	W.F. = 1		9/25 ($r = 1$)	9/25 ($J = 1$)	6/25 ($J = r = 1$)
	W.F. = ∞		18/25 ($r = \infty$)	0 ($J = \infty$)	0 ($J = r = \infty$)
m for ***V***	W.F. = 0	–1/3 ($w = 0$)	–1/5 ($r = 0$)	7/25 ($J = 0$)	–1/5 ($J = r = 0$)
	W.F. = 1	2/3 ($w = 1$)	1/25 ($r = 1$)	16/25 ($J = 1$)	9/25 ($J = r = 1$)
	W.F. = ∞	5/3 ($w = \infty$)	7/25 ($r = \infty$)	1 ($J = \infty$)	1 ($w = J = r = \infty$)
p for ***n***	W.F. = 0	0 ($w = 0$)		–6/5 ($J = 0$)	0 ($J = w = 0$)
	W.F. = 1	–3/5 ($w = 1$)		–3/5 ($J = 1$)	–2/5 ($J = w = 1$)
	W.F. = ∞	–6/5 ($w = \infty$)		0 ($J = \infty$)	–6/5($J = w = \infty$)
Equation No.		(10.38), (10.41), and (10.43)	(10.57), (10.59), and (10.61)	(10.75), (10.77), and (10.79)	(10.94), (10.96), (10.98), and (10.100)

Note: W.F. denotes the weighting factor. The weighting factors are zero, unity, and infinity for different possibilities. Usually the values of these factors have values between the limiting values.

the special case $w = 1$. This range of exponent values encompasses the values reported in the literature. Again, if S appearing in equation (10.43) is expressed as a function of Q with the exponent of –1/6, then the exponent of Q for n varies from –13/12 to 0.0. In this case, the reported range of exponent values is –0.54 to 0.03 (Knighton 1975).

It is clear that the exponent values of b, m, and p do not possess fixed values; rather they vary over certain ranges dictated by the way the adjustment of stream power is distributed among variables. Depending on the value of w, the derived exponent values encompass the whole ranges of values reported in the literature. Furthermore, the scale parameters are variant, depending on the channel hydraulics. Indeed this observation should help with regionalization of scale parameters.

Four sets of hydraulic geometry expressions are obtained. In the first set are expressions corresponding to possibility I, wherein the channel adjusts its width, roughness, and velocity to accommodate changes in discharge and sediment load. To facilitate discussion, the values of exponents b, f, m, and p for three cases (one special and two limiting cases) when the weighting factors are zero, unity, and infinity, are tabulated for all three possibilities and their combination in Tables 10-7, 10-8a, and 10-8b. It should be pointed out that the limiting case of infinity is only a theoretically generalized case for the factors r, w, and J,

respectively, for the lack of knowledge of the values of their upper limits, which should be far less than infinity.

10.4.2 Possibility II: Hydraulic Geometry Relations for Width, Depth, and Velocity

This possibility ($P_B = P_h$: $B = C_2 h^{5/3r}$) leads to the hydraulic geometry relations for B, h, and V in terms of Q. The derivation of these relations follows the same three steps as discussed in possibility I. Substitution of equation (10.29) in equation (10.5) leads to the expressions for B, h, and V in terms of Q and S:

$$B = C_B Q^{1/(1+r)} S^{-1/[2(1+r)]},\ C_B = [n(C_2)^r]^{1/[1+r]} \tag{10.54}$$

$$h = C_h Q^{3r/(5+5r)} S^{-3r/[2(5+5r)]},\ C_h = [n(C_2)]^{3r/[5+5r]} \tag{10.55}$$

$$V = C_V Q^{2r/[5(1+r)} S^{[3(1+r)+2]/[10(1+r)]},\ C_V = n^{-3/5}(C_B)^{-2/5} \tag{10.56}$$

Substitution of equation (10.37) with $z = -2/5$ and $z = -1/6$ into equations (10.54) to (10.56) yields

$$B = C_{BS} Q^{\frac{6}{5(1+r)}} \left(C_{BS} = \frac{C_B}{C_S^{1/2(1+r)}} \right) \text{for gravel-bed rivers} \tag{10.57}$$

$$B = C_{BS} Q^{\frac{13}{12(1+r)}} \text{ for sandy rivers} \tag{10.58}$$

$$h = C_{hS} Q^{\frac{18r}{25(1+r)}} (C_{hS} = C_h C_S^{-3r/[2(5+5r)]}) \text{ for gravel-bed rivers} \tag{10.59}$$

$$h = C_{hS} Q^{\frac{13r}{20(1+r)}} \text{ for sandy rivers} \tag{10.60}$$

$$V = C_{VS} Q^{\frac{7r-5}{25(1+r)}} (C_{VS} = C_V C_S^{[3(1+r)+2]/[10(1+r)]}) \text{ for gravel-bed rivers} \tag{10.61}$$

$$V = C_{VS} Q^{\frac{21r-5}{60(1+r)}} \text{ for sandy rivers} \tag{10.62}$$

For the special case $r = 1$, equations (10.54) to (10.62) reduce, respectively, to

$$B = C_B \frac{Q^{1/2}}{S^{1/4}},\ C_B = (nC_2)^{1/2} \tag{10.63}$$

$$B = C_{BS} Q^{\frac{3}{5}} \left(C_{BS} = \frac{C_B}{C_S^{1/4}} \right) \text{for gravel-bed rivers} \tag{10.64}$$

$$B = C_{BS} Q^{\frac{13}{24}} \text{ for sandy rivers} \tag{10.65}$$

$$h = C_h \frac{Q^{3/10}}{S^{3/20}},\ C_h = (C_2)^{-3/10} n^{3/10} \tag{10.66}$$

$$h = C_{hS} Q^{\frac{9}{25}} (C_{hS} = C_h C_S^{-3/20}) \text{ for gravel-bed rivers} \tag{10.67}$$

$$h = C_{hS} Q^{\frac{13}{40}} \text{ for sandy rivers} \tag{10.68}$$

$$V = C_V Q^{1/5} S^{2/5}, C_V = [(C_n)^{3/5} (C_B)^{2/5}]^{-1} \tag{10.69}$$

$$V = C_{VS} Q^{\frac{1}{25}} (C_{VS} = C_V C_S^{2/5}) \text{ for gravel-bed rivers} \tag{10.70}$$

$$V = C_{VS} Q^{\frac{2}{15}} \text{ for sandy rivers} \tag{10.71}$$

This is the most investigated possibility. In this case, exponent b of discharge is found to vary from 0 to 1, as shown in Table 10-7, and scale factor C_B varies with flow resistance. The precise value of b depends on the weighting factor r, which specifies the proportion for adjustment of stream power among B, h, and V. For the special case $r = 1$, where the adjustment is equally proportioned, $b = 0.5$. The width–discharge relation is found to depend on the slope of the channel, S. If S is expressed as a function of discharge with an exponent of $-1/6$, then the range of b becomes 0 to 13/12. These values of b encompass the entire range of values reported in the literature.

The value of exponent f varies from 0 to 3/5 (when r ranges from 0 to ∞), shown in Table 10-7; the scale factor C_h is dependent on the flow resistance. The precise value depends on the value of r. For the special case $r = 1$, the value of f is 3/10. If the slope is expressed in terms of discharge with the power of $-1/6$, then the value of f ranges from 0 to 13/20 (when r ranges from 0 to ∞). These derived exponent values encompass the reported range.

The value of exponent m varies from 0 to 2/5, as shown in Table 10-7; the scale factor C_V is dependent on the flow depth. The exact value of m depends on the value of r. For the special case $r = 1$, the value of m is 1/5. If the slope is expressed in terms of discharge with the power of $-1/6$, then the m exponent varies from $-1/12$ to 7/20 (when r ranges from 0 to ∞). Thus, the derived exponent values are seen to envelop the reported range.

For the downstream geometry of 72 streams from a variety of exponents, Park (1977) reported the range of b as 0.03 to 0.89 with modal class as 0.4 to 0.5; the range of f as 0.09 to 0.70 with modal class as 0.3 to 0.4; and the range of m as -0.51 to 0.75 with modal class as 0.1 to 0.2. Thus, the derived exponents are in the reported ranges. This discussion illustrates that the values of exponents b, f, and m do not possess fixed values; rather they vary over certain ranges dictated by the way the adjustment of stream power is distributed among variables. Furthermore, the scale parameters are variant, depending on the channel hydraulics. This observation should be helpful with regionalization of scale factors.

10.4.3 Possibility III: Hydraulic Geometry Relations for Depth, Roughness, and Velocity

Under this possibility ($P_n = P_h$: $C_3 = nh^{5/3}$), the hydraulic geometry relations result for h, B, and n in terms of Q. Following the same three steps as under possibility I, these relations are derived for gravel-bed and alluvial rivers. Substitution of

equation (10.32) in equation (10.5) and a little algebraic manipulation yield the following:

$$h = C_h Q^{3/[5+5J]} S^{-3/[2(5+5J)]},\ C_h = (C_B)^{3/[5+5J]} B^{-3/[5+5J]} \tag{10.72}$$

$$V = C_V Q^{(2+5J)/[5(1+J)]} S^{3/[10(1+J)]},\ C_V = (C_n)^{-3/5} B^{-2/5} \tag{10.73}$$

$$n = C_n Q^{-1/[1+J]} S^{1/[2(1+J)]},\ C_n = (C_3)^{1/[1+J]} B^{1/[1+J]} \tag{10.74}$$

Substitution of equation (10.37) with $z = -2/5$ and $z = -1/6$ into equations (10.72) to (10.74) yields

$$h = C_{hS} Q^{\frac{18}{25(1+J)}}\ (C_{hS} = C_h C_S^{-3/[2(5+5J)]}) \text{ for gravel-bed rivers} \tag{10.75}$$

$$h = C_{hS} Q^{\frac{13}{20(1+J)}} \text{ for sandy rivers} \tag{10.76}$$

$$V = C_{VS} Q^{\frac{7+25J}{25(1+J)}}\ (C_{VS} = C_V C_S^{3/[10(1+J)]}) \text{ for gravel-bed rivers} \tag{10.77}$$

$$V = C_{VS} Q^{\frac{20J+7}{20(1+J)}} \text{ for sandy rivers} \tag{10.78}$$

$$n = C_{nS} Q^{\frac{-6}{5(1+J)}}\ (C_{nS} = C_n C_S^{1/[2(1+J)]}) \text{ for gravel-bed rivers} \tag{10.79}$$

$$n = C_{nS} Q^{\frac{-13}{12(1+J)}} \text{ for sandy rivers} \tag{10.80}$$

For the special case $J = 1$, equations (10.72) to (10.80) reduce to

$$h = C_h \frac{Q^{3/10}}{S^{3/20}},\ C_h = B^{-3/10} (C_3)^{3/10} \tag{10.81}$$

$$h = C_{hS} Q^{\frac{9}{25}}\ (C_{hS} = C_h C_S^{-3/20}) \text{ for gravel-bed rivers} \tag{10.82}$$

$$h = C_{hS} Q^{\frac{13}{40}} \text{ for sandy rivers} \tag{10.83}$$

$$V = C_V Q^{7/10} S^{3/20},\ C_V = (C_n)^{-3/5} B^{2/5} \tag{10.84}$$

$$V = C_{VS} Q^{\frac{16}{25}}\ (C_{VS} = C_V C_S^{3/20}) \text{ for gravel-bed rivers} \tag{10.85}$$

$$V = C_{VS} Q^{\frac{27}{40}} \text{ for sandy rivers} \tag{10.86}$$

$$n = C_n \frac{S^{0.25}}{Q^{0.5}},\ C_n = B^{0.5} (C_3)^{0.5} \tag{10.87}$$

$$n = C_{nS} Q^{\frac{-3}{5}}\ (C_{nS} = C_n C_S^{1/4}) \text{ for gravel-bed rivers} \tag{10.88}$$

$$n = C_{nS} Q^{\frac{-13}{24}} \text{ for sandy rivers} \tag{10.89}$$

The value of exponent f varies from 0 to 3/5 (when J ranges from ∞ to 0), as exhibited in Table 10-7, and scale factor C_h depends on the channel width. The exact value depends on the value of weighting factor J. For the special case $J = 1$, the value of f becomes 3/10, as shown by equation (10.81). Equations (10.72) and (10.83) contain a slope term. When the slope is expressed in terms of discharge with the power of –1/6, then the f exponent varies from 0 to 13/20 (when J ranges from 0 to ∞), as seen in Table 10-8a. The exponent values, thus, derived cover the whole range reported in the literature.

The value of exponent m varies from 2/5 to 1, as exhibited in Table 10-1, and the scale factor C_V depends on the channel width. This exact value depends on the value of the weighting factor J. For the special case $J = 1$, the exponent m assumes the value of 7/10, as shown by equation (10.84). Equations (10.77) and (10.84) contain a slope term. When this slope term is expressed in terms of discharge with the power of –1/6, the m exponent varies from 7/20 to 1, as exhibited in Table 10-8a. These exponent values encompass the range reported in the literature.

The value of exponent p varies from 0 to –1 (as J ranges from 0 to ∞), as shown in Table 10-7, and the scale factor depends on the channel width. The precise value depends on the value of J. For the special case $J = 1$, the p exponent becomes –0.5, as shown by equation (10.87). Equations (10.74) and (10.87) contain a slope term, which, when expressed in terms of discharge with the power of –1/6, results in the value of p ranging from –13/12 to 0 (as J ranges from 0 to ∞), as shown in Table 10-8a. The exponent values thus derived encompass the reported range.

This discussion shows that exponents f, m, and p do not possess fixed values; rather, they vary over certain ranges, depending on the way the adjustment of stream power is distributed among variables. Furthermore, the scale parameters are variant, depending on channel hydraulics, and this observation should help with regionalization of scale parameters.

10.4.4 Possibility IV: Hydraulic Geometry Relations for Depth, Width, Roughness, and Velocity

The objective is to derive hydraulic geometry relations for B, h, V, and n in terms of Q under this possibility. Following the same three steps as under possibility I, these relations are derived for gravel-bed and alluvial rivers. Substitution of equations (10.27), (10.29), and (10.32) in equation (10.5) results in

$$B = C_B Q^{1/[1+w+r]} S^{-1/[2(1+w+r)]},\ C_B = [C_1 (C_2)^r]^{1/[1+w+r]} \tag{10.90}$$

$$h = C_h Q^{3r/[5+5Jr+5r]} S^{-3r/[2(5+5Jr+5r)]},\ C_h = [C_3 (C_2)^{-1}]^{3r/[5+5Jr+5r]} \tag{10.91}$$

$$V = C_V Q^{\frac{3}{5}\left[\frac{2}{5}+\frac{wJ}{wJ+J+w}-\frac{2}{3(1+w+r)}\right]} S^{\frac{3}{5}\left[\frac{1}{2}-\frac{wJ}{2(wJ+J+w)}+\frac{1}{3(1+w+r)}\right]},\ C_V = [C_n (C_B)^{2/3}]^{-3/5} \tag{10.92}$$

$$n = C_n Q^{-wJ/[wJ+J+w]} S^{wJ/[2(wJ+J+w)]},\ C_n = [(C_1)^{1/w} (C_3)^{1/J}]^{wJ/[wJ+J+w]} \tag{10.93}$$

Substitution of equation (10.37) with $z = -2/5$ and $z = -1/6$ into equations (10.90) to (10.91) yields

$$B = C_{BS} Q^{\frac{6}{5(1+w+r)}} \left(C_{BS} = \frac{C_B}{C_S^{1/2(1+w+r)}} \right) \text{for gravel-bed rivers} \tag{10.94}$$

$$B = C_{BS} Q^{\frac{13}{12(1+w+r)}} \text{ for sandy rivers} \tag{10.95}$$

$$h = C_{hS} Q^{\frac{18r}{25(1+Jr+r)}} \left(C_{hS} = C_h C_S^{-3r/[2(5+5Jr+5r)]}\right) \text{for gravel-bed rivers} \tag{10.96}$$

$$h = C_{hS} Q^{\frac{13r}{20(1+Jr+r)}} \text{ for sandy rivers} \tag{10.97}$$

$$V = C_{VS} Q^{\frac{3}{25}\left(\frac{7}{3}+\frac{6wJ}{wJ+J+w}-\frac{4}{1+w+r}\right)} \left(C_{VS} = C_V (C_S)^{\frac{3}{5}\left[\frac{1}{2}-\frac{wJ}{2(wJ+J+w)}+\frac{1}{3(1+w+r)}\right]} \right) \text{for gravel-bed rivers} \tag{10.98}$$

$$V = C_{VS} Q^{\frac{1}{5}\left(\frac{7}{4}+\frac{13wJ}{4(wJ+J+w)}-\frac{13}{6(1+w+r)}\right)} \text{ for sandy rivers} \tag{10.99}$$

$$n = C_{nS} Q^{\frac{-6wJ}{5(wJ+J+w)}} \left(C_{nS} = C_n C_S^{wJ/[2(wJ+J+w)]}\right) \text{for gravel-bed rivers} \tag{10.100}$$

$$n = C_{nS} Q^{\frac{-13wJ}{12(wJ+J+w)}} \text{ for sandy rivers} \tag{10.101}$$

For the special case $w = J = r = 1$, equations (10.90) to (10.101) reduce to

$$B = C_B \frac{Q^{1/3}}{S^{1/6}}, C_B = (C_1 C_2)^{1/3} \tag{10.102}$$

$$B = C_{BS} Q^{\frac{2}{5}} \left(C_{BS} = \frac{C_B}{C_S^{1/6}} \right) \text{for gravel-bed rivers} \tag{10.103}$$

$$B = C_{BS} Q^{\frac{13}{36}} \text{ for sandy rivers} \tag{10.104}$$

$$h = C_h \frac{Q^{1/5}}{S^{1/10}}, C_h = [(C_2)^{-0.2} (C_3)^{0.2}] \tag{10.105}$$

$$h = C_{hS} Q^{\frac{6}{25}} \left(C_{hS} = C_h C_S^{-1/10}\right) \text{for gravel-bed rivers} \tag{10.106}$$

$$h = C_{hS} Q^{\frac{13}{60}} \text{ for sandy rivers} \tag{10.107}$$

$$V = C_V Q^{7/15} S^{4/15}, C_V = [(C_n)^{3/5} (C_B)^{2/5}]^{-1} \tag{10.108}$$

$$V = C_{VS} Q^{\frac{9}{25}} \left(C_{VS} = C_V C_S^{4/151}\right) \text{for gravel-bed rivers} \tag{10.109}$$

$$V = C_{VS} Q^{\frac{19}{45}} \text{ for sandy rivers} \tag{10.110}$$

$$n = C_n \frac{S^{1/6}}{Q^{1/3}}, C_n = [C_1 C_3]^{1/3} \tag{10.111}$$

$$n = C_{nS} Q^{\frac{-2}{5}} \ (C_{nS} = C_n C_S^{1/6}) \text{ for gravel-bed rivers} \tag{10.112}$$

$$n = C_{nS} Q^{\frac{-13}{36}} \text{ for sandy rivers} \tag{10.113}$$

The coefficients C_B, C_h, C_V, and C_n in equations (10.107) to (10.113) are defined in terms of morphological coefficients C_1, C_2, and C_3 as

$$C_B = [C_1 C_2]^{1/3} \tag{10.114}$$

$$C_h = (C_2)^{-0.2} (C_3)^{0.2} \tag{10.115}$$

$$C_V = [(C_1)^{1/3} (C_2)^{2/5} (C_3)^{1/5} \tag{10.116}$$

$$C_n = (C_1)^{1/3} (C_3)^{1/3} \tag{10.117}$$

Here C_B, C_h, C_V, and C_n are the coefficients associated with flow width, depth, velocity, and Manning's n, respectively, and depend on C_1, C_2, and/or C_3, given, respectively, by equations (10.27), (10.29), and (10.32). Because the discharge $Q = BhV$, equations (10.90) to (10.101) or (10.102) to (10.113) show that the sum of exponents of Q equals 1. Similarly, the sum of exponents of S from these equations equals 0.

The value of exponent b varies from 0 to 1, as exhibited in Table 10-7. The exact value depends on the values of the weighting factors. For the special case $w = r = 1$, the value of b becomes 1/3, as shown by equation (10.102). Equations (10.90) and (10.102) contain a slope term; when this slope is expressed in terms of discharge with a power of –1/6, then the exponent varies from 0 to 13/12, as shown in Table 10-8a. These values encompass the range reported in the literature.

The value of exponent f varies from 0 to 1/5, as shown in Table 10-7. For the special case $J = r = 1$, the value of f becomes 1/5, as shown by equation (10.105). Equations (10.91) and (10.105) contain a slope term. When slope is expressed in terms of Q with a power of –1/6, the exponent f varies from 0 to 13/60, as shown in Table 10-8a. These exponent values cover the reported range.

The value of exponent m varies from 0 to 1, as seen in Table 10-7. For the limiting case, $w = J = r = 1$, the m exponent value becomes 7/15, as shown by equation (10.108). Equations (10.92) and (10.108) contain a slope term. When the slope is expressed in terms of discharge with the power of –1/6, the value of the m exponent varies from –1/12 to 1, as shown in Table 10-8a. These exponent values cover the range reported in the literature.

The value of exponent p varies from –1 to 0, as shown in Table 10-7. For the special case, $J = w = 1$, the value of p becomes –1/3, as shown by equation (10.111). Equations (10.93) and (10.111) contain a slope term, which, when expressed in terms of Q with the power of –1/6, leads to the value of p ranging from –13/12 to 0, as seen in Table 10-8a.

This discussion shows that the values of the b, f, m, and p exponents are not fixed; rather, they vary over certain ranges, as exhibited by equations (10.103) to

(10.113). The variation is indeed continuous and is dictated by the way the adjustment of stream power is distributed among variables. Under this possibility, the adjustment occurs simultaneously in river width, depth, velocity, and roughness. The fourth possibility is most general and leads to hydraulic geometry expressions where the channel adjusts its width, depth, velocity, and roughness to accommodate changes in discharge.

Example 10.6 Based on the exponent values given in Tables 10-2 and 10-4, what interpretations can be made regarding different possibilities that the rivers under consideration may be satisfying?

Solution In Table 10-2, the value of exponent b ranges from 0.30 to 0.71. A high value of the exponent implies that a large change in discharge leads to a relatively small change in width. This change happens in large basins under high flows or in small basins under low flows. That is, width does not exercise as much control. In this case, the depth and velocity exercise a greater control. An example of such a case is a very wide river. In a similar fashion, the influence of exponents f and m can be evaluated. The value of the f exponent ranges from 0.22 to 0.69, and the value of the m exponent varies from 0.01 to 0.31. A higher value of the f exponent implies that a large change in discharge results in a relatively small change in depth. This change happens in very wide rivers. If the m exponent is very low, say 0.01, then a small change in discharge leads to a large change in velocity, as, for example, is the case in steeply sloping channels. In Table 10-4, the value of b varies from 0.45 to 0.9, the value of f from 0.25 to 0.47, and the value of m from 0.06 to 0.22. Similar conclusions can be drawn in this case as well.

Questions

Q10.1 Flow characteristics of Standing Stone Creek, in central Pennsylvania, corresponding to mean annual flood (2.3-year recurrence interval) measured by Brush (1961) are given in Table 10-9. Plot on a log–log paper flow width, depth, velocity, and slope as a function of discharge and fit straight lines. How good is the fit of these lines? Compute parameters (exponent and proportionality coefficient) of the relations between discharge and flow characteristics. Check if the sum of exponents equals 1.

Q10.2 Compare the exponents determined in Q10.1 with those reported in the literature, as given in Table 10-10. What can then be said about the Standing Stone Creek flow characteristics?

Q10.3 Determine if the morphological equation (10.3) relating width and depth of flow is valid. Compute the spread of the associated coefficient.

Table 10-9 *Measurements of flow characteristics of Standing Stone Creek, Pennsylvania.*

Station no.	Mean annual flood, $Q_{2.3}$ (ft^3/s)	Bankfull width, B (ft)	Bankfull depth, d (ft)	Bankfull velocity, V (ft/s)	Slope, S (ft/ft)	Drainage area, A_d (mi^2)	Length of stream, L (mi)
1	64	8	1.3	6.2	0.034	0.88	1
2	290	15	1.58	12.15	0.015	5.78	2.9
3	490	23	2.17	9.82	0.017	10.73	4.5
4	820	35	2.29	10.2	0.011	20.69	6.8
5	1,260	47	2.66	10.1	0.0038	34.27	10
6	2,150	8	2.47	15.1	0.0015	66.01	13.9
7	2,800	68	2.92	21.4	0.0024	92.63	17.7
8	3,000	75	5.19	7.7	0.012	99.88	20.1
9	3,300	100	3.7	8.9	0.001	109.72	24.7
10	3,800	100	3.18	12	0.001	133.3	28

Source: Data from Brush 1961.

Table 10-10 *Theoretically derived values of hydraulic geometry exponents as reported in the literature.*

Source	Exponents					Remarks
	b	F	m	p	y	
Langbein (1964)	0.23	0.42	0.35	–0.07	—	Theory of minimum variance
Li (1974)	0.24	0.46	0.30	0.0		Tractive force theory

Q10.4 Collect the values of hydraulic geometry exponents given in the chapter as well as from the literature. Then, plot a histogram of each exponent and compute the mean, standard deviation coefficient of variation, and coefficient of skewness of each exponent.

Q10.5 Compare the mean values of hydraulic geometry exponents computed in Q10.4 with what is normally used in the literature, as given in Table 10-10. What does the spread in each exponent value mean hydraulically? Comment on the hydraulic significance of the coefficient of skewness of each exponent value.

Q10.6 Different possibilities for hydraulic geometry adjustments have been discussed in the chapter. List these possibilities and the environments under which they occur. What is the most common possibility and why?

Q10.7 Hydraulic geometry adjustments respond to geological and climatic characteristics. The size of a river is also determined by these characteristics. Which possibility is more likely for which geological and climatic regime and why?

Q10.8 Human-made changes also affect river or channel hydraulic geometry. Assume that a river is leveed for a certain portion, as is the case for many rivers in the United States. Which possibility is more likely for such a river and why?

Q10.9 In the Indian subcontinent, there are large irrigation canal systems. What possibility is more likely for such canals and why?

Q10.10 Assume that some of the canals in Q10.9 are lined. What possibility is then more likely for such canals and why?

References

Allen, P. M., Arnold, J. G., and Byars, B. W. (1994). "Downstream channel geometry for use of in planning-level models." *Water Res. Bull.*, 30(4), 663–671.

Blench, T. (1952). "Regime theory for self-formed sediment-bearing channels." *Transactions, ASCE*, 117(1), 383–400.

Blench, T. (1969). "Coordination in mobile-bed hydraulics." *J. Hydraul. Div.*, 95(6), 1871–1998.

Bray, R. D. (1982). "Regime equations for gravel-bed rivers." *Gravel-bed rivers*, R. D. Hey, J. C. Bathurst, and C. Thorne, eds., Wiley, New York, 517–544.

Brebner, A., and Wilson, K. C. (1967). "Derivation of the regime equations from relationships for pressurized flow by use of the principle of energy-degradation rate." *Proc., Inst. Civil Eng.*, 36, 47–62.

Brush, L. M. (1961). "*Drainage basins, channels, and flow characteristics of selected streams in Central Pennsylvania*." U.S. Geological Survey Professional Paper 282–F, U.S. Government Printing Office, Washington, DC.

Chang, H. H. (1980). "Geometry of gravel streams." *J. Hydraul. Div.*, 106(9), 1443–1456.

Chang, H. H. (1988). *Fluvial processes in river engineering*, Wiley, New York.

Chong, S. E. (1970). "The width, depth and velocity of Sungei Kimla, Perak." *Geographica*, 6, 72–63.

Davies, T. R. H., and Sutherland, A. J. (1983). "Extremal hypotheses for river behavior." *Water Resour. Res.*, 19(1), 141–148.

Deng, Z., and Zhang, K. (1994). "Morphologic equations based on the principle of maximum entropy." *Int. J. Sediment Res.*, 9(1), 31–46.

Dou, G. R. (1964). "Hydraulic geometry of plain alluvial rivers and tidal river mouth." *J. Hydraul. Eng.*, 2, 1–13 (in Chinese).

Dury, G. H. (1976). "Discharge prediction, present and former, from channel dimensions." *J. Hydrol.*, 30, 219–245.

Engelund, F., and Hansen, E. (1967). *A monograph on sediment transport in alluvial streams*, Teknisk Forlag, Copenhagen, Denmark.

Huang, H. W., and Nanson, G. C. (2000). "Hydraulic geometry and maximum flow efficiency as products of the principle of least action." *Earth Surf. Proc. Land.*, 25, 1–16.

Jaynes, E. T. (1957). "Information theory and statistical mechanics, I." *Phys. Rev.*, 106, 620–630.

Klein, M. (1981). "Drainage area and the variation of channel geometry downstream." *Earth Surf. Proc. Land.*, 6, 589–593.

Knighton, A. D. (1974). "Variation in width–discharge relation and some implications for hydraulic geometry." *Geolog. Soc. Am. Bull.*, 85, 1069–1076.

Knighton, A. D. (1975). "Variations in at-a-station hydraulic geometry." *Am. J. Sci.*, 275, 186–218.

Knighton, A. D. (1977). "Alternative derivation of the minimum variance hypothesis." *Ecolog. Soc. Am. Bull.*, 83, 3813–3822.

Knighton, A. D. (1987). "River channel adjustment—The downstream dimension." *River channels: Environment and process*, K. S. Richards, ed., Basil Blackwell, Oxford, UK, 95–128.

Knighton, A. D. (1998). *Fluvial forms and processes—A new perspective*, Arnold Publishers, London.

Kolberg, F. J., and Howard, A. D. (1995). "Active channel geometry and discharge relations of U. S. piedmont and midwestern streams: The variable exponent model revisited." *Water Resour. Res.*, 31(9), 2353–2365.

Lane, E. W. (1955). "Design of stable channels." *Trans., ASCE*, 120(1), 1234–1260.

Langbein, W. B. (1964). "Geometry of river channels." *J. Hydraul. Div.*, 90(2), 301–312.

Leopold, L. B., and Langbein, W. B. (1962). "*The concept of entropy in landscape evolution*." U.S. Geological Survey Professional Paper 500-A, U.S. Government Printing Office, Washington, DC.

Leopold, L. B., and Maddock, T. J. (1953). "*Hydraulic geometry of stream channels and some physiographic implications*." U.S. Geological Survey Professional Paper 252, U.S. Government Printing Office, Washington, DC.

Leopold, L. B., and Wolman, L. B. (1957). "*River channel patterns: Braided, meandering and straight*." U.S. Geological Survey Professional Paper 282-B, U.S. Government Printing Office, Washington, DC.

Li, R. M. (1974). "*Mathematical modeling of response from small watershed*." Ph.D. dissertation, Colorado State University, Fort Collins, CO.

Park, C. C. (1977). "World-wide variations in hydraulic geometry exponents of stream channels: An analysis and some observations." *J. Hydrol.*, 33, 133–146.

Parker, G. (1978). "Self-formed rivers with equilibrium banks and mobile bed: Part II. The gravel river." *J. Fluid Mech.*, 89(1), 127–148.

Parker, G. (1979). "Hydraulic geometry of active gravel rivers." *J. Hydraul. Div.*, 105(9), 1185–1201.

Phillips, P. J., and Harlin, J. M. (1984). "Spatial dependency of hydraulic geometry exponents in a subalpine stream." *J. Hydrol.*, 71, 277–283.

Ramette, M. (1980). "A theoretical approach on fluvial processes." *Proc., Int. Symp. River Sedimentation*, Beijing, China, C16-1 to C16-17.

Rhoads, B. L. (1991). "A continuously varying parameter model of downstream hydraulic geometry." *Water Resour. Res.*, 27(8), 1865–1872.

Rhodes, D. D. (1978). "World wide variations in hydraulic geometry exponents of stream channels: An analysis and some observations—Comments." *J. Hydrol.*, 33, 133–146.

Richards, K. S. (1976). "Complex width–discharge relations in natural river sections." *Geolog. Soc. Am. Bull.*, 87, 199–206.

Richards, K. S. (1982). *Rivers: Form and process in alluvial channels*, Methuen, London.

Rodriguez-Iturbe, I., Rinaldo, A., Rigon, R., Bras, R. L., Marani, A., and Ijjasz-Vasquez, E. J. (1992). "Energy dissipation, runoff production and the three dimensional structure of river basins." *Water Resour. Res.*, 28(4), 1095–1103.

Singh, V. P. (2003). "On the theories of hydraulic geometry." *Int. J. Sediment Res.*, 18(3), 196–218.

Singh, V. P., Yang, C. T., and Deng, Z. Q. (2003a). "Downstream hydraulic geometry relations: 1. Theoretical development." *Water Resour. Res.*, 39(12), SWC2-1 to SWC2-15.

Singh, V. P., Yang, C. T., and Deng, Z. Q. (2003b). "Downstream hydraulic geometry relations: 2. Calibration and testing." *Water Resour. Res.*, 39(12), SWC3-1–SWC3-10.

Smith, T. R. (1974). "A derivation of the hydraulic geometry of steady-state channels from conservation principles and sediment transport laws." *J. Geol.*, 82, 98–104.

Stall, J. B. and Fok, Y. S. (1968). *Hydraulic geometry of Illinois streams.* University of Illinois Water Resources Research Center, Report No. 15, Urbana-Champaign, IL.

Stall, J. B., and Yang, C. T. (1970). "*Hydraulic geometry of 12 selected stream systems of the United States*." University of Illinois Water Resources Research Center, Research Report No. 32, Urbana-Champaign, IL.

Stebbings, J. (1963). "The shape of self-formed model alluvial channels." *Proc., Inst. Civil Eng., London*, 25, 485–510.

White, W. R., Bettess, R., and Paris, E. (1982). "Analytical approach to river regime." *J. Hydraul. Div.*, 108(10), 1179–1193.

Williams, G. P. (1967). "*Flume experiments on the transport of a coarse sand*." U.S. Geological Survey Professional Paper 562-B, U.S. Government Printing Office, Washington, DC.

Williams, G. P. (1978). "*Hydraulic geometry of river cross-sections—Theory of minimum variance*." U.S. Geological Survey Professional Paper 1029, U.S. Government Printing Office, Washington, DC.

Wolman, M. G. (1955). "*The natural channel of Brandywine Creek, Pennsylvania*." U. S. Geological Survey Professional Paper 271, U.S. Government Printing Office, Washington, DC.

Wolman, M. G., and Brush, L. M. (1961). "*Factors controlling the size and shape of stream channels in coarse noncohesive sands*." U.S. Geological Survey Professional Paper 282-G, U.S. Government Printing Office, Washington, DC, 183–210.
Yalin, M. S., and Da Silva, A. M. F. (1997). "On the computation of equilibrium channels in cohesionless alluvium." *J. Hydrosci. Hydraul. Eng.*, 15(2), 1–13.
Yalin, M. S., and Da Silva, A. M. F. (1999). "Regime channels in cohesionless alluvium." *J. Hydraul. Res.*, 37(6), 725–742.
Yang, C. T. (1972). "Unit stream power and sediment transport." *J. Hydr. Div.*, 98(10), 1805–1826.
Yang, C. T. (1986). "Dynamic adjustment of rivers." *Proc., 3rd Int. Symp. River Sedimentation*, Jackson, MS, 118–132.
Yang, C. T. (1996). *Sediment transport theory and practice*, McGraw-Hill, New York.
Yang, C. T., and Song, C. C. S. (1986). "Theory of minimum energy and energy dissipation rate." *Encyclopedia of fluid mechanics*, Gulf Publishing, NJ, 353–399.
Yang, C. T., Song, C. C., and Woldenberg, M. T. (1981). "Hydraulic geometry and minimum rate of energy dissipation." *Water Resour. Res.*, 17, 877–896.

Additional Reading

Cheema, M. N., Mariño, M. A., and De Vries, J. J. (1997). "Stable width of an alluvial channel." *J. Irrig. Drain. Eng.*, 123(1), 55–61.
Howard, A. D. (1980). "Thresholds in river regimes." *Thresholds in geomorphology*, D. R. Coates and J. D. Vitek, eds., Allen and Unwin, Winchester, MA, 227–258.
Osterkamp, W. R., and Hedman, E. R. (1982). "*Perennial-streamflow characteristics related to channel geometry and sediment in Missouri River basins*." U.S. Geological Survey Professional Paper 1242, U.S. Government Printing Office, Washington, DC.
Singh, V. P. (2000). "Hierarchy of hydraulic geometry relations." *Proc., 8th Int. Symp. Stochastic Hydraulics*, Beijing, China, Z.-Y. Wang and S.-X. Hu, eds. A. A. Balkema, Rotterdam, The Netherlands.
Stall, J. B., and Fok, Y. S. (1968). "*Hydraulic geometry of Illinois streams*." University of Illinois Water Resources Research Center, Research Report No. 15, Urbana, IL.
Thornes, J. B. (1970). "The hydraulic geometry of stream channels in the Xingu–Araguaia headwaters." *Geograph. J.*, 136, 376–382.
Yang, C. T. (2002). *Sediment transport theory and practice*, McGraw-Hill, New York.
Yang, C. T., and Song, C. C. S. (1981). "Discussion of 'A contribution to regime theory relating principally to channel geometry,' by D. I. H. Barr, M. K. Allan, and A. Nishat," *Proc., Inst. Civil Eng., Part 2*, 71, 961–965.

This page intentionally left blank

Chapter 11

At-a-Station Hydraulic Geometry

The previous chapter discusses downstream hydraulic geometry relations between the mean stream channel form and discharge along a stream network in a hydrologically homogeneous basin. This chapter extends the discussion to at-a-station hydraulic geometry relations.

11.1 Hydraulic Geometry Relations

Leopold and Maddock (1953) defined at-a-station hydraulic geometry as the relations of the mean stream channel form and hydraulic variables with discharge at a station on a stream. The channel form includes the mean cross-sectional geometry (e.g., the width, depth, and wetted parameter), and the hydraulic variables include the mean slope, mean friction, mean velocity, and suspended sediment load for varying influxes of water and sediment to the channel and the specified channel boundary conditions.

Hydraulic geometry relations are of great practical value in prediction of alluvial channel behavior, such as scour and fill, and channel deformation; layout of river training works; design of stable channels, canals, and intakes, river flow control works, irrigation schemes, and river improvement works; channel management; river restoration; modeling aquatic biota production systems; flow and sediment routing; flood estimation; and drainage net configurations. The

exponents of these relations can also be used to discriminate between different types of river sections (Richards 1976) and rivers in different types of landscapes, as well as in planning for resource and impact assessment (Allen et al. 1994). The at-a-station hydraulic geometry can be used to differentiate between the channel forms corresponding to the natural state and restored forms of a river. For example, one can determine the state of a restored river after a certain period of time, say 5, 10, or 15 years. In a similar vein, one can determine the effect of climate change on channel form by relating climate-related changes in runoff and land use to transport, turnover, retention, and sedimentation of nutrients and fine-grained material from land to sea. At-a-station hydraulic geometry relations have, therefore, been a subject of much interest and discussion in hydraulic and hydrologic literature.

Leopold and Maddock (1953) expressed the hydraulic geometry relationships in the form of power functions of discharge as

$$B = aQ^b, \ldots\ldots\ldots d = cQ^f, \ldots\ldots\ldots V = kQ^m \tag{11.1}$$

where B is the channel width; d is the flow depth; V is the flow velocity; Q is the flow discharge; and a, b, c, f, k, and m are parameters. Also added to equation (11.1) are

$$n = NQ^p, \ldots\ldots\ldots S = sQ^y \tag{11.2}$$

where n is Manning's roughness factor; S is the bed slope; and N, p, s, and y are parameters. Exponents b, f, m, p, and y represent, respectively, the rate of change (in the logarithmic domain) of the hydraulic variables B, d, V, n, and S as Q changes; and coefficients a, c, k, N, and s are scale factors that define the values of B, d, V, n, and S when $Q = 1$. The at-a-station hydraulic geometry entails mean values over a certain period of time.

Example 11.1 Flow characteristics of Brandywine Creek, at Cornog, Pennsylvania, measured by Wolman (1955), are given in Table 11-1. Plot on a log-log paper flow width, depth, velocity, friction factor, and slope as a function of discharge and fit straight lines. How well do these lines fit? Compute parameters (exponent and proportionality coefficients) of the relations between discharge and flow characteristics. Check if the sum of exponents equals 1.

Solution The relations given by equations (11.1) and (11.2) are plotted on log-log paper as shown in Fig. 11-1. The best fitted lines are determined and their exponents and intercepts are found, as shown in Table 11-2. Note that $ack = 30.592 \times 0.2048 \times 0.1599 = 1.002 \approx 1.00$ and $b + f + m = 0.0851 + 0.3718 + 0.5424 = 0.999 \approx 1.00$. It is seen that depth and velocity are most strongly related to discharge, width, and roughness are weakly related, and slope is poorly related to discharge.

Table 11-1 *Measurements of flow characteristics of Brandywine Creek at Cornong, Pennsylvania.*

Date	Discharge Q (ft^3/s)	Width, B (ft)	Mean depth, d (ft)	Mean velocity, V (ft/s)	Cross-sectional area (ft^2)	Slope of water surface, S (ft/ft)	Manning's roughness, n
8/1/1951	10.3	23.5	0.82	0.53	19.3	0.0033	0.14
8/6/1951	8.6	41	0.41	0.5	17	0.0033	0.094
8/11/1951	12.9	41	0.48	0.64	19.6	0.0033	0.082
9/7/1951	14.7	41.5	0.52	0.69	21.4	0.0333	0.8
9/10/1951	5.7	39.5	0.34	0.44	13.6	0.0033	0.094
4/27/1952	304	49.6	1.56	3.92	77.6	0.0034	0.034
4/28/1952	830	55.8	2.44	6.1	136	0.0037	0.027
5/27/1952	73.4	44	0.9	1.86	39.5	35	0.044
7/8/1952	19.4	43	0.57	0.79	24.4	0.0034	0.075
7/9/1952	322.4	47.7	2.09	3.22	100	0.0033	0.043
7/11/1952	35	42.7	0.79	1.04	35.09	0.0034	0.071

Note: Drainage area = 25.7 mi.^{2}, and length of reach = 645 ft.
Source: Data from Wolman 1955.

Table 11-2 *Exponents and intercepts of best-fitted lines from Example 11.1.*

a	30.592	***c***	0.2048	***k***	0.1599	***N***	0.2934	***s***	0.0053
b	0.0851	***f***	0.3718	***m***	0.5424	***P***	–0.356	***y***	–0.065

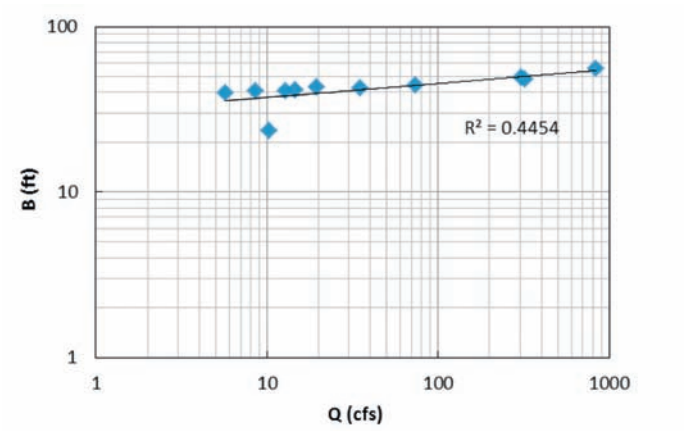

(a)

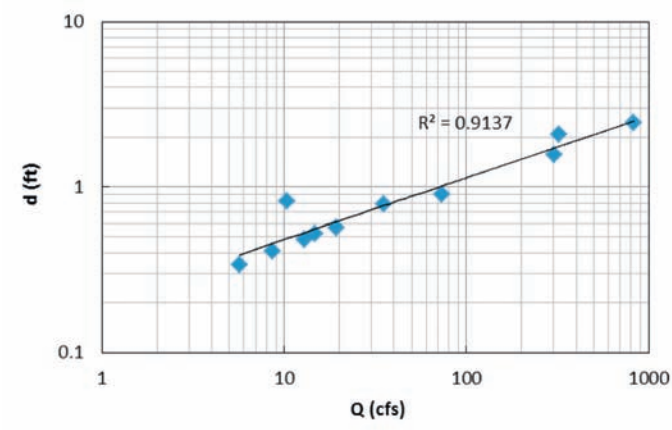

(b)

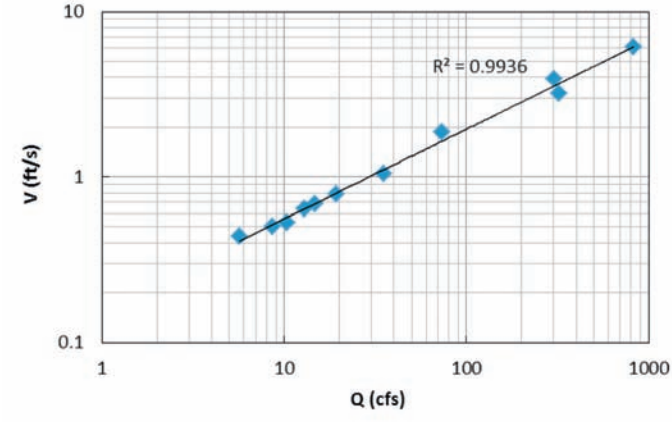

(c)

Figure 11-1 *Relations of width, depth, velocity, roughness, and slope to discharge for Brandywine Creek at Cornong, Pennsylvania.*

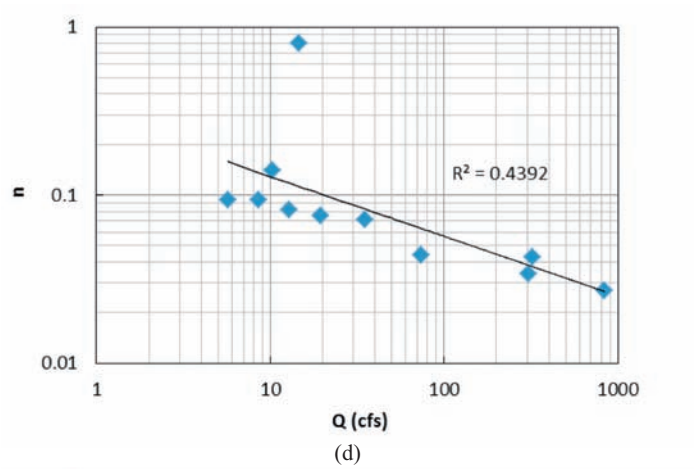

(d)

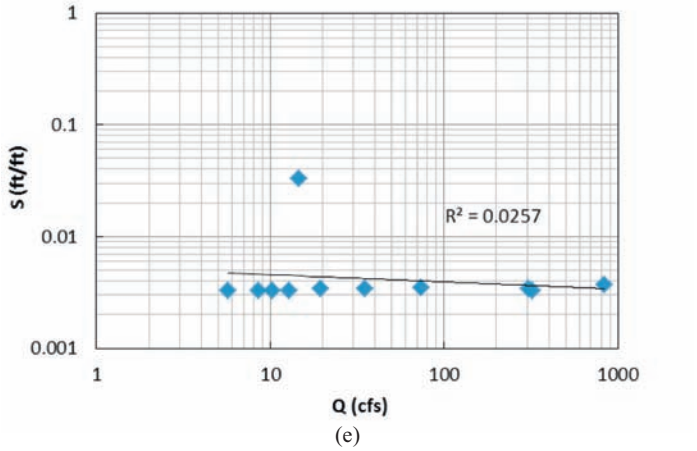

(e)

***Figure 11-1**, Continued*

Example 11.2 Flow characteristics of Brandywine Creek at Lenape, Pennsylvania, measured by Wolman (1955), are given in Table 11-3. Plot on a log-log paper flow width, depth, velocity, friction factor, and slope as a function of discharge and fit straight lines. How well do these lines fit? Compute parameters (exponent and proportionality coefficients) of the relations between discharge and flow characteristics. Check if the sum of exponents equals 1. Compare these coefficients and exponents with those computed in Example 11.1 and comment on the differences.

Solution Width, depth, velocity, roughness, and slope are plotted against discharge on a log-log paper and straight lines are fitted, as shown in Fig. 11-2. The values of slope (exponents) and intercepts (coefficients of proportionality) are determined as given in Table 11-4. Note that $ack = 61.195 \times 0.1299 \times 0.1225 = 0.974$ and $b + f + m = 0.0847 + 0.4659 + 0.4528 = 1.003$ which is close to 1.00.

Table 11-3 *Measurements of flow characteristics of Brandywine Creek at Lenape, Pennsylvania.*

Date	Discharge Q (ft^3/s)	Width, B (ft)	Mean depth, d (ft)	Mean velocity, V (ft/s)	Cross-sectional area (ft^2)	Slope of water surface, S (ft/ft)	Manning's roughness, n
7/21/1951	218.4	98	1.47	1.51	144.4	0.0075	0.034
7/31/1951	124.9	93	1.34	0.94	124.5	—	—
8/7/1951	128.7	93	1.28	1.08	119	0.0078	0.045
8/13/1951	191.5	97	1.47	1.35	142.6	0.0074	0.039
8/20/1951	646.7	101	2.78	2.3	281	0.0076	0.035
8/27/1951	115.8	92	1.17	1.08	107.6	0.0074	0.042
9/8/1951	107.2	91	1.14	1.04	103.7	0.0076	0.043
9/15/1951	385.7	100	1.9	2	190.1	76	0.031
4/27/1952	1,410	109	4.17	3.1	455	0.0032	—
4/28/1952	2,420	121	4.42	4.52	535	—	—
5/26/1952	2,190	125	4.52	3.87	565	0.0028	—
7/10/1952	1,310	113	4.14	2.8	468.2	—	—
8/8/1952	864.3	103.4	3.02	2.75	312.9	—	—

Note: Drainage area = 259 mi.^{2}, and length of reach = 758 ft.
Source: Data from Wolman 1955.

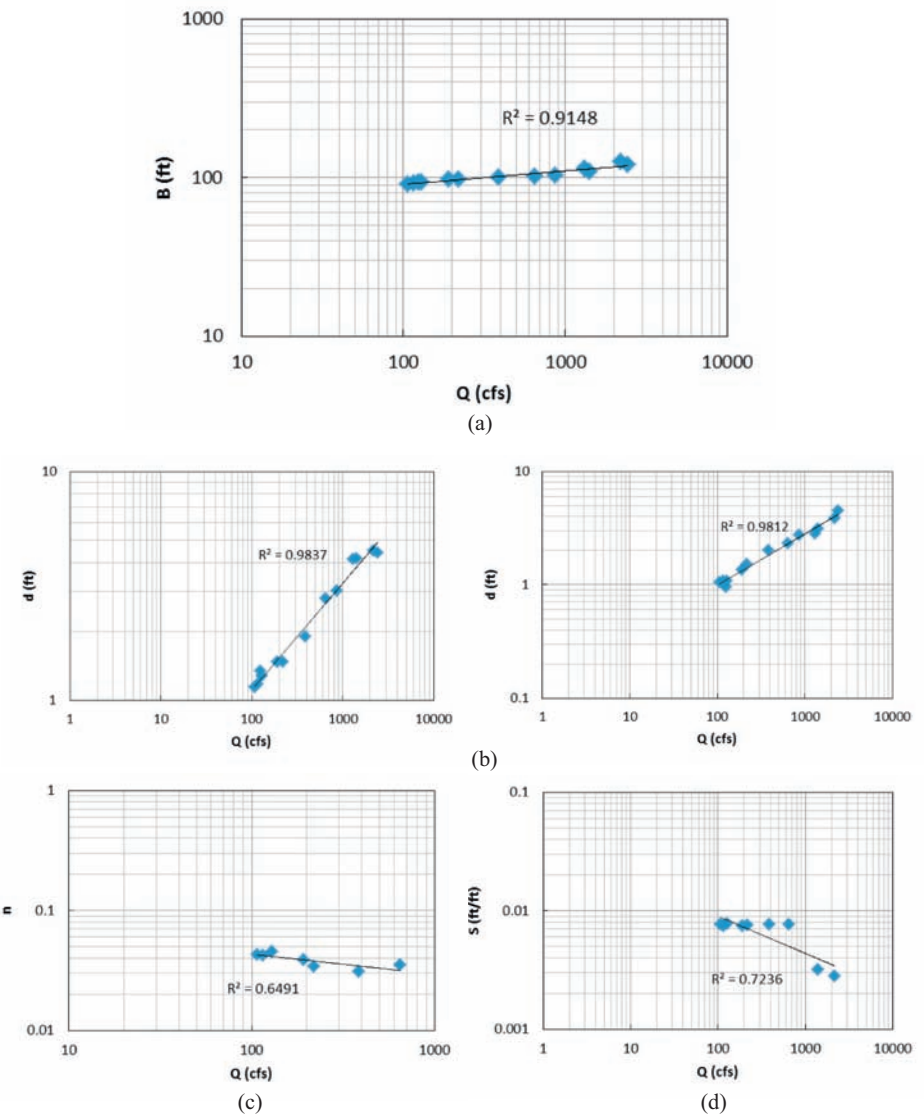

Figure 11-2 *Relations of width, depth, velocity, roughness, and slope to discharge for Brandywine Creek at Lenape, Pennsylvania.*

Table 11-4 *Exponents and coefficients for Example 11.2.*

a	61.195	***c***	0.1299	***k***	0.1225	***N***	0.0927	***s***	0.0381
b	0.0847	***f***	0.4659	***m***	0.4528	***P***	–0.167	***y***	–0.314

11.2 Preliminaries

The mean values of the hydraulic variables of equations (11.1) and (11.2) are known to follow necessary hydraulic laws and the principle of the minimum energy dissipation rate or stream power (Langbein 1964; Yang et al. 1981). These mean values correspond to the equilibrium state of the channel at a station. The implication is that an alluvial channel adjusts its width, depth, slope, velocity, and friction to achieve a stable condition, which is regarded as the one corresponding to the maximum sediment transporting capacity. The average river system tends to develop in a manner that produces an approximate equilibrium between the channel and the water and sediment it must transport (Leopold and Maddock 1953). Cheema et al. (1997) determined stable width of an alluvial channel using the hypothesis that an alluvial channel attains a stable width when the rate of change of unit stream power with respect to its width is at a minimum. This means that an alluvial channel with stable cross section has the ability to vary its width at a minimum consumption of energy per unit width per unit time. Knighton (1977) observed that at cross sections undergoing a systematic change, the potential for adjustment toward some form of quasiequilibrium in the short term is related to the flow regime and channel boundary conditions and that the approach to quasiequilibrium or establishment of a new equilibrium position is relatively rapid.

11.2.1 Discontinuities

Richards (1973) showed that there may be discontinuities in hydraulic geometry relations at the bankfull stage and there may be nonlinear response by the dependent variables to a change in discharge below the bankfull stage. The power function model of equations (11.1) and (11.2) is not a general model. The rates of change of both depth and velocity are related to the rate of change of roughness, which itself is a function of channel geometry. Richards (1973) suggested that a log-quadratic function may be more appropriate than a log-linear function, in particular, for depth–discharge and velocity–discharge relations. However, the power function model is now widely accepted in the literature.

11.2.2 Change in Behavior

The at-a-station stream behavior can change significantly over a short period of time as a result of irregular or more gradual adjustment of channel form to flow conditions. Boundary geology, geomorphology, and discharge have dominant influences among all independent variables. Braided reaches have steeper slopes than do undivided reaches, and slopes are steeper in meandering than in straight reaches.

The exponents and coefficients of at-a-station hydraulic geometry relations of equations (11.1 and 11.2) vary with time as well as from high flow range to low flow range. The variations occur because the influx of water and sediment

and the boundary conditions (called constraints) that the river is subjected to vary with time. This statement means that for varying influx of water and sediment, a channel at a given station may exhibit a range of exponents and scale factors in hydraulic geometry relations in response to the constraints imposed on the channel. It is these constraints that force the channel to adjust its allowable hydraulic variables. For example, if a river section has a pavement at the bottom, then it cannot adjust its depth and is, therefore, left to adjust other variables, such as width. Likewise, if the section is lined, then it cannot adjust its width and friction.

11.2.3 Interaction among Hydraulic Variables

Using variations in at-a-station hydraulic geometry, Knighton (1974) explained interactions of measurable hydraulic variables with changes in discharge and modification in channel form at systematically selected stations in a single river system. The rate of width adjustment is influenced by the cohesiveness of the bank material, and through its effect on the energy loss, it, in turn, influences the rate of change of the mean velocity. Resistance decreases rapidly with increasing discharge where the grain roughness is the dominant element but is less dominant where channel curvature and form roughness exert additional effects that persist for greater increases of depth. The rate of velocity increase varies accordingly. The degree of intersectional variation in hydraulic relations casts doubts on the validity of defining a mean value. The variation is systematically related to channel pattern; straight reaches are distinguishable from meander and braided reaches in terms of the rates of change of width, velocity, resistance, and slope. Pools and riffles may add a further distinction.

11.2.4 Variations in Geometry Relations

Investigating the variation in the width–discharge relation, Knighton (1974) found that in channels with cohesive banks and no marked downstream variation in bank erodibility, the at-a-station rate of change of channel width was principally controlled by bank material and composition, particularly the silt–clay content. The deposition of noncohesive sediment in the form of point bars and central islands permit the stream to increase its rate of change of width at a cross section. This situation means that meandering and braided reaches can be distinguished from straight reaches on the basis of the b-exponent value. This adjustment would reduce the velocity range. The way in which width changes with discharge affects how a stream spends its energy. In an area of homogeneous surficial material, streams may be expected to have at-a-station hydraulic geometries with relatively uniform width–discharge relations. Knighton (1974) found an average value of $b = 0.03$ for straight channel sections, and average $b = 0.24$ for meandering or braided sections. Wolman (1955) examined temporal variations in hydraulic geometry at individual stations. Myrick and Leopold (1963) investigated the hydraulic geometry of a small estuary.

11.2.5 Channel Types

Richards (1976) used hydraulic geometry exponents to discriminate between channel types of river sections, using data from pool and riffle sections. He used several width–discharge curves to cover a wide range of discharges up to the bankfull stage. He concluded that the chances of a natural river section exhibiting constant values of the parameters over a full range of within-bank flows were extremely limited. Merigliano (1997) focused on the scour and fill dynamics at cross sections and how this is related to the exponent ratio m/f.

Schumm (1960) noted that changes in width and depth with increasing discharge may occur either by erosion of banks and bed or by progressing the filling of a stable channel. When banks are more readily eroded than the bed, $b > f$, and when the reverse is true, $f > b$. For stable channels under normal conditions, $f > b$ indicates a tendency for the cross section to become proportionally deeper and narrower with respect to increasing discharge (lower B/d). If $b > f$, the width-to-depth ratio increases with discharge and the tendency is toward a wider shallow channel. For stable channels, rectangular and parabolic channels will have decreased width-to-depth ratios. The rate of decrease is greater for rectangular channels than for other shapes. Straight and meandering channels seem to be similar in their response to increasing discharge. Braided channels appear distinctly different from these two. Average values of at-a-station relationships should not be used as a basis for comparing different stream systems.

The objective of this section is to apply the theory of minimum energy dissipation rate and the principle of maximum entropy to derive at-a-station hydraulic geometry relations. Inherent in the derivation is an explanation for self-adjustment of channel morphology. It is shown that by combining the hypotheses based on the principles of maximum entropy and minimum energy dissipation rate, a family of hydraulic geometry relations is obtained. This family may encompass many of the hydraulic geometry relations derived using different hypotheses. Singh and Zhang (2008a, b) derived at-a-station hydraulic geometry using the theory of minimum energy dissipation rate and the principal of maximum entropy.

11.2.6 Theories of Hydraulic Geometry

As discussed in Chapter 10, there are many theories for deriving functional relationships among hydraulic variables for hydraulic geometry or equations (11.1) and (11.2). Most of these theories have been used for deriving downstream hydraulic geometry relations, but empirical, minimum variance, and tractive force theories have also been applied to at-a-station hydraulic geometry, and other theories can also be extended to at-a-station hydraulic geometry relations. Each hypothesis leads to unique relations between channel form parameters and discharge, and the relations corresponding to one hypothesis are not necessarily identical (in terms of exponents and proportionality constants) to those corresponding to another hypothesis.

Langbein (1964) proposed the minimum variance hypothesis to define the hydraulic geometry of a river channel at a given cross section in response to

changing discharge. Knighton (1977) provided an alternative derivation of the hypothesis. Assuming the slope to be invariant, the channel formed in stable materials attains a cross section with width varying as the 0.55 power of the mean depth ($b = 0.55f$) (Nizery and Braudeau 1955), the velocity increases as the 0.35 power, depth as the 0.42 power, and width as the 0.23 power of the discharge. If the velocity and depth increase in this manner, the resistance factor (Darcy–Weisbach's) decreases as the 0.28 power of the discharge at constant slope, whereas the Manning resistance factor would decrease as the 0.07 power of the discharge, suggesting that the assumption of a constant resistance factor would not be unduly restrictive. Applying the minimum variance hypothesis to defining the regime characteristics of the lower Namoi–Gwydir drainage basin in Australia, Riley (1978) found the power of width as 0.48, the power of 0.30 for depth, and the power of 0.22 for velocity. Williams (1978) tested the minimum variance hypothesis on 165 observed cross sections on natural rivers in the United States. For flow conditions ranging from 2.83×10^{-4} to 1,980 m^3/s, widths from 0.31 to 579 m, mean depths from 0.031 to 10.7 m, and the median bed-material sizes (d_{50}) from 0.06 to 100 mm, he found $0.00 \leq b \leq 0.82$ [width (m)], $0.10 \leq f \leq 0.78$ [depth (m)], and $0.03 \leq m \leq 0.81$ [velocity (m/s)]. The hypothesis was found to predict the average exponents reasonably accurately.

Using the threshold channel cross-sectional shape and assuming incipient motion conditions on noncohesive channel boundary for channel forming discharge in the tractive force theory, Li (1975) derived the power of 0.24 for the width, 0.46 for depth, and 0.30 for velocity and compared them with Judd and Peterson's (1969) $b = 0.18$, $f = 0.51$, and $m = 0.31$ based on field observations.

11.2.7 Triaxial b-m-f Diagram

Park (1977) analyzed exponent data, collected from literature, of hydraulic geometry for 139 at-a-station sites from Brazil, Germany, Great Britain, Malaysia, Norway, Puerto Rico, and the United States. By plotting the three exponents in a triaxial diagram, he examined variations within and between major climatic areas. Plotting histograms of frequencies of three exponents (b, m, and f,) separately, he found that the width exponent data had a strongly negatively skewed distribution, ranging in value from 0 to 0.59, but most observations were in the range of 0.00 to 0.10, different from the theoretical value of 0.23. The depth exponent showed a similar range of values with a modal class of 0.3 to 0.4, close to the theoretical value of 0.42 (Leopold and Langbein 1962). The velocity exponent ranged from 0.07 to 0.71 and was less normally distributed, with a modal class of 0.40 to 0.5; the theoretical value of 0.35 was outside this range. The general tendency for the at-a-station exponent was for the velocity to increase more rapidly relative to discharge than did the mean depth, whereas width varied little. Park (1977) examined simultaneous variations of exponents and found the three exponents to be interrelated. There was significant scatter caused by bank material composition, sediment properties, channel symmetry associated with planform variations, and flow regime and flow variability. He examined the exponents from natural, proglacial, semiarid, humid temperate, tropical streams,

flumes, and estuaries. The pattern of variation was quite different from one group to another. Thus, grouping by climate environments offered few clues, suggesting that local controls were more important. These controls include bank material, composition, the difference between meandering and braided reaches and between pool and riffle sections, flow magnitude at low flow conditions, suspended sediment load, channel stability and lateral migration, channel stabilization, modification measures, and temporal fluctuations around some quasi-equilibrium state. It is not surprising that there is a wide range of combinations of the three exponents because of factors controlling variations in streams, along streams, and between streams, casting doubt on the use of mean values of exponents to characterize the hydraulic geometry of particular areas.

In discussing Park's (1977) findings, Rhodes (1978) divided the triaxial diagram into 10 areas by plotting 5 lines representing:

1. constant values of the width/depth ratios ($b = f$),
2. competence ($m = f$),
3. Froude number ($m = f/2$),
4. velocity–cross-sectional area ratio ($m = b + f$), and
5. slope/roughness ratio ($m = 2f/3$).

He showed that those channels represented by points within one area respond similarly to changes in discharge regardless of the specific values of the exponents. In this way, the *b-m-f* diagram can help interpret hydraulic geometry. For 587 sets of exponent data, he found $b = 0.00$ to 0.84, $f = 0.01$ to 0.84, and $m = 0.03$ to 0.99. Rivers may perform their primary functions in a large variety of ways. The mean values of b and m deviate much more from the theoretical values than does f. Emphasis should be on how streams are different in terms of their hydraulic geometry. The data set analyzed is biased toward straight reaches.

Rhodes (1977) reported that the *b- f-m* diagram may be used for representation and interpretation of at-a-station hydraulic geometry. It allows an empirical classification of channel cross sections. Lewis (1966) showed that hydraulic geometry relations obtained for intermediate to high discharges did not describe the relationship of width, depth, and velocity to discharges less than $1\,ft^3/s$, because low discharges are incapable of modifying channel cross sections.

11.3 Derivation of At-a-Station Hydraulic Geometry Relations

Langbein (1964) and Yang et al. (1981), among others, emphasized that equations (11.1 and 11.2) correspond to the case when the channel is in equilibrium state. Langbein hypothesized that when a channel adjusts its hydraulic variables corresponding to this state, the adjustment is shared equally among the hydraulic variables. For varying discharge, morphological relations involve five hydraulic variables: width, depth, velocity, friction, and slope. In practice, a channel cross section is seldom in an equilibrium state; this phenomenon means that the

adjustment among hydraulic variables is unequal. The exact proportion in which the adjustment is shared among variables is not clear. Therefore, it can be hypothesized that hydraulic geometry relations depend on the adjustment of hydraulic variables, and the adjustment can explain the variability in the parameters (scale and exponents) of these relations or the variation in at-a-station hydraulic geometry. This hypothesis is pursued in the next sections.

Yang (1972) defined the unit stream power (USP) as the time rate of potential energy expenditure per unit weight of water in an alluvial channel or simply the velocity–slope product (VS) that has the dimensions of power per unit weight of water. Thus, stream power (SP) is obtained by integrating USP over a given cross section and is the rate of energy dissipation caused by water:

$$SP = VAS\gamma = Q\gamma S \tag{11.3}$$

where V is the average flow velocity, S is the energy slope, γ is the weight density of water, and Q is the discharge of water. A channel responds to the influx of water and sediment coming from its watershed by the adjustment of SP. Indeed, Yang (1972) found USP to be the dominating factor in the determination of the total sediment concentration. Yang (1976, 1986, 1996) also related sediment load and the channel geometry adjustment to SP. Thus, the temporal rate of adjustment of SP in a river cross section, R_S, can be expressed (Singh and Zhang 2008a) as

$$R_S = \frac{d(SP)}{dt} = \frac{d(Q\gamma S)}{dt} \tag{11.4}$$

where t is time.

If a channel is assumed to be rectangular, with h as the depth of flow and B as the width of flow, then the flow cross-sectional area $A = Bh$, the wetted perimeter $P = B + 2h$, and the hydraulic radius $R = A/P = Bh/(B + 2h)$. If the channel is wide rectangular, then $R \cong h$ = depth of flow. The flow discharge in equation (11.3) can be obtained from Manning's equation (11.5a), or Chezy's equation (11.5b), or Darcy–Weisbach's equation (11.5c). For wide rectangular channels, these equations can be written, respectively, as

$$Q = \frac{1}{n} AR^{2/3} S^{1/2} = \frac{1}{n} Bh^{5/3} S^{1/2} \tag{11.5a}$$

$$Q = C A\sqrt{RS} = C B h^{3/2}\sqrt{S} \tag{11.5b}$$

$$Q = 2\sqrt{\frac{2g}{f_y}} A\sqrt{RS} = 2\sqrt{\frac{2g}{f_y}} Bh^{3/2}\sqrt{S} = f_{Dw} Bh^{3/2}\sqrt{S};\ f_{Dw} = 2\sqrt{\frac{2g}{f_y}} \tag{11.5c}$$

where n is Manning's roughness coefficient, C is Chezy's roughness coefficient, f_y is the Darcy–Weisbach friction factor, and g is acceleration caused by gravity. From equations (11.5a) to (11.5c), we see that

$$C = \frac{1}{n} h^{1/6};\quad C = 2\sqrt{2g/f_y} \tag{11.6}$$

Equations (11.5a) to (11.5c) can be expressed in a general kinematic form as

$$Q = \alpha B h^{\beta} \sqrt{S} \tag{11.7}$$

in which α is a roughness measure, and β is an exponent. For Manning's equation, $\alpha = 1/n$, and $\beta = 5/3$; for Chezy's equation, $\alpha = C$, and $\beta = 3/2$; and for Darcy–Weisbach's equation, $\alpha = 2(2g/f_y)^{0.5}$ or $\alpha = f_{DW}$, and $\beta = 3/2$.

Using equations (11.3) and (11.7), the stream power of a channel is expressed as

$$\mathrm{SP} = \gamma \alpha B h^{\beta} S^{3/2} \tag{11.8}$$

On the right side of equation (11.8), there are four variables: α, B, h, and S. When discharge changes, a river cross section can adjust its width, depth, velocity, roughness, and slope, or a combination thereof. Thus, it is hypothesized that for time-varying influxes of discharge, the channel cross section adjusts or minimizes its stream power by adjusting these four variables. This hypothesis is similar to the one proposed by Langbein (1964) in his theory of minimum variance and is analogous to the one used by Singh et al. (2003a, b) for downstream hydraulic geometry (Singh and Zhang 2008a, b). Therefore, substitution of equation (11.8) in equation (11.4) yields

$$\frac{d(\mathrm{SP})}{dt} = R_S = \gamma\alpha h^{\beta} S^{3/2} \frac{dB}{dt} + \gamma\alpha B S^{3/2} \beta h^{\beta-1} \frac{dh}{dt} + \gamma B h^{\beta} S^{3/2} \frac{d\alpha}{dt} + \frac{3}{2} \gamma\alpha B h^{\beta} S^{1/2} \frac{dS}{dt} \tag{11.9}$$

Equation (11.9) expresses the change in stream power in time. It is constituted by four parts, designated as R_1, R_2, R_3, and R_4, and can be recast as

$$\frac{d(\mathrm{SP})}{dt} = R_S = R_1 + R_2 + R_3 + R_4 \tag{11.10}$$

where R_i, $i = 1, 2, 3$, and 4, is defined as

$$R_1 = \gamma\alpha h^{\beta} S^{3/2} \frac{dB}{dt}; R_2 = \gamma\alpha B S^{3/2} \beta h^{\beta-1} \frac{dh}{dt}; R_3 = \gamma B h^{\beta} S^{3/2} \frac{d\alpha}{dt}; R_4 = \frac{3}{2} \gamma\alpha B h^{\beta} S^{1/2} \frac{dS}{dt}$$

R_1 expresses the temporal adjustment of width; R_2, the temporal adjustment of depth; R_3, the temporal adjustment of friction; and R_4, the temporal adjustment of slope. Dividing by the total rate of adjustment SP, R_S, one gets

$$P_B = \frac{R_1}{R_S} = \frac{\gamma\alpha h^{\beta} S^{3/2} (dB/dt)}{d(SP)/dt} \tag{11.11}$$

$$P_h = \frac{R_2}{R_S} = \frac{\gamma\alpha B S^{3/2} \beta h^{\beta-1} (dh/dt)}{d(SP)/dt} \tag{11.12}$$

$$P_\alpha = \frac{R_3}{R_S} = \frac{\gamma B h^{\beta} S^{3/2} (d\alpha/dt)}{d(SP)/dt} \tag{11.13}$$

$$P_S = \frac{R_4}{R_S} = \frac{3}{2}\frac{\gamma\alpha h^{\beta} S^{1/2}(dS/dt)}{d(SP)/dt} \tag{11.14}$$

In equations (11.11) to (11.14), respectively, P_B can be interpreted as the proportion of the temporal change of SP caused by the temporal rate of adjustment of width; P_h, the proportion of the temporal change of SP caused by the temporal rate of adjustment of depth; P_α, the proportion of the temporal change of SP caused by the temporal rate of adjustment of friction; and P_S, the proportion of the temporal change of SP caused by the temporal rate of adjustment of slope. Singh et al. (2003a, b) used the same concept for downstream hydraulic geometry.

According to the principle of maximum entropy (Jaynes 1957), any system in equilibrium state under steady constraints tends to maximize its entropy. When a river cross section reaches a dynamic (or quasidynamic) equilibrium, the entropy should attain its maximum value. The principle of maximum entropy (POME) states that the entropy of a system is maximum when all probabilities are equal, i.e., the probability distribution is uniform. Applying this principle to a river cross section in dynamic equilibrium, equation (11.10), therefore, suggests

$$P_B = P_h = P_\alpha = P_S \tag{11.15}$$

Equation (11.15) holds, of course, under the stipulation that there are no constraints imposed on the channel section and can be interpreted to mean that the self-adjustment of SP is equally shared among B, h, α, and S. This interpretation is supported by Williams (1967, 1978) who found from an analysis of data from 165 gauging stations in the United States that a channel cross section adjusted all its hydraulic parameters (B, h, S, and V) in response to changes in the influx of water and sediment and that self-adjustments were realized in an evenly distributed manner among factors. Equation (11.15) is similar to the concept embodied in the minimum variance theory (Langbein 1964).

Equation (11.15) involves probabilities of four variables, meaning that any adjustment in hydraulic variables in combinations of two, three, or four may occur. These combinations give rise to different configurations of adjustment, which indeed occur in nature (Wolman 1955). Thus the equality among four probabilities yields 11 possibilities and hence leads to 11 sets of equations: (1) $P_B = P_h$, (2) $P_B = P_\alpha$, (3) $P_B = P_S$, (4) $P_h = P_\alpha$, (5) $P_h = P_S$, (6) $P_\alpha = P_S$, (7) $P_B = P_h = P_\alpha$, (8) $P_B = P_\alpha = P_S$, (9) $P_B = P_h = P_S$, (10) $P_h = P_\alpha = P_S$, and (11) $P_B = P_h = P_\alpha = P_S$.

It should be noted that all 11 possibilities can occur in the same river cross section at different times, or in different river cross sections at the same time or at different times. These different possibilities reflect the dynamic and morphological responses of channels to changing discharge and sediment influx. Considering velocity, depth, shear, resistance, and stream power as independent variables for investigating the minimum variance theory, Williams (1978) explored 11 cases that are similar in spirit to the above 11 possibilities. For grouping channels based on such response, Rhodes (1977) partitioned the *b-m-f* diagram

into 10 areas based on 5 lines representing constant values of (1) width/depth ratio ($b = f$), (2) competence ($m = f$), (3) Froude number ($m = f/2$), (4) velocity/cross-sectional area ratio ($m = b + f$), and (5) slope/roughness ratio ($m = 2f/3$). The channels represented by the points in the same area respond similarly to changes in discharge regardless of the specific values of the exponents. Discounting possibility 11 (the most general one), the 10 possibilities interestingly have some relationship to the 10 areas of Rhodes (1977). In the case of downstream hydraulic geometry, Singh et al. (2003a, b) considered bed slope as constant, and of course the discharge was constant. As a result, they investigated only four possibilities.

Field observations by Leopold and Maddock (1953), Wolman (1955), and others show that the variation in slope S is small as compared with velocity, depth, width, and roughness. Therefore, slope may be assumed as constant. Under this assumption, equation (11.15) reduces to

$$P_B = P_h = P_\alpha \tag{11.16}$$

Equation (11.16) suggests that adjustment in hydraulic variables occurs in four possible configurations: (1) $P_B = P_h$, (2) $P_B = P_\alpha$, (3) $P_h = P_\alpha$, and (4) $P_B = P_h = P_\alpha$. This situation constitutes a special case of the general case presented earlier. In other words, configurations 1 and 2 are the same as possibilities 1 and 2, configuration 3 is the same as possibility 4, and configuration 4 is the same as possibility 7 of the general case. These possibilities can also be visualized from physical reasoning. Width and depth are related to the energy expenditure within a channel and are related to boundary sediment and sediment discharge (Colby 1961; Maddock 1969). The width–depth ratio is closely related to sediment transport (Schumm 1968) and to boundary sediments (Schumm 1960), especially for noncohesive bed sediments (Riley 1975). This ratio is also used as a measure of channel shape. Hydraulic radius or flow depth for wide rectangular channels is a measure of hydraulic efficiency. Channel slope is controlled by bed material strength and flow impinging force. Breaks in channel slope along a cross section reflect channel boundary roughness, channel size, and geometric shape. Channel roughness is a function of bed form and grain size constituting the bed and determines the energy loss. Different possibilities reflect the variations in these channel characteristics in response to the boundary conditions and the influx of flow and sediment discharge. Riley (1975) divided 19 variables into four groups, which can be related to four possibilities in the special case as already enumerated.

To enumerate the consequences of these possibilities, one can either use the general discharge equation (11.7) or Manning's equation (11.5a), or Chezy's equation (11.5b), or Darcy–Weisbach's equation (11.5c). Survey of the literature shows that Manning's equation is used more commonly in hydraulic and river engineering in general and more specifically in investigations on hydraulic geometry (e.g., Leopold and Wolman 1957; Wolman and Brush 1961; Stall and Fok 1968, 1970; Bray 1979). However, one may use a general discharge–resistance relation and then specialize using specific discharge–resistance equations.

11.3.1 Morphological Equations

Morphological equations, reflecting the adjustment of hydraulic variables for accommodating the temporal adjustment of stream power, arise when only two hydraulic variables are considered at a time. This method leads to seven possibilities and the corresponding number of primary morphological equations, which are derived following. In general, it may be noted that the shape and longitudinal profile of a river in quasiequilibrium are determined by the discharge and sediment concentration and the characteristics of the bank material. The initial size, shape, and resistance of the material provided by the river depends on the sediment concentration (Wolman 1955). A river exhibits such local variations as being alternately wide and narrow, straight and meandering, deep and shallow. River cross sections tend to be approximately semielliptical, trapezoidal, or triangular, and increasing discharge results in increased velocity, depth, and width. It is interesting to note that Williams (1978) grouped 165 at-a-station cross sections into five classes, depending on the bank firmness. In all five cases, the slope was considered constant. It may be emphasized that the form of equations is similar if the adjustment of stream power is considered in the spatial domain.

11.3.1.1 Possibility I: $P_B = P_h$

Here P_B is given by equation (11.11) and P_h by equation (11.12). Equating these two equations, one obtains

$$\frac{dh}{dt} = \frac{1}{\beta}\frac{h}{B}\frac{dB}{dt} \tag{11.17a}$$

Equation (11.17a) hypothesizes that the temporal change in stream power is accomplished by an equal temporal adjustment between flow depth h and flow width B. This possibility occurs when the cross section has a fixed roughness and flow is controlled by width and depth. An example is stable irrigation canals where increased discharge leads to increased depth and increased width. In such canals, banks and beds are relatively stable and, hence, the changes in roughness and slope are not pronounced. Another case is Blue Creek, which is a stream flowing exclusively from the Sand Hills of Nebraska with a bed of 0.4- to 0.7-mm sand; it is almost devoid of finer sizes but with a mixture of fine material in the bank with the help of vegetation. It has cohesive banks with particles with a median diameter of 0.1 mm (Wolman and Brush 1961), and, hence, has stable banks. With changing discharge, both flow depth and width vary. This hypothesis can be considered as a limiting case and holds under the equilibrium condition. Such a condition, however, is seldom achieved, and, therefore, temporal change in stream power is accomplished by an unequal adjustment between B and h. To account for the proportion in which the adjustment of stream power is shared between h and B, equation (17a) is modified by introducing a weighting factor, r, $r \geq 0$:

$$\frac{dh}{dt} = \frac{r}{\beta}\frac{h}{B}\frac{d\mathrm{B}}{dt} \tag{11.17b}$$

Integration of equation (11.17b) yields

$$\frac{B}{h^{\beta/r}} = C_{Bh} \text{ or } h = C^*_{Bh} B^{r/\beta} \tag{11.18a}$$

where C_{Bh} or C^*_{Bh} is a constant of integration. For the limiting case, $r = 1$, equation (11.18a) reduces to

$$B = C_{Bh} h^{\beta} \text{ or } h = C^*_{Bh} B^{1/\beta} \tag{11.18b}$$

Parameter C_{Bh} or C^*_{Bh} can be designated as a primary morphological coefficient, and equation (11.18a) or (11.18b) can be designated as a primary morphological equation.

11.3.1.2 Possibility II: $P_B = P_\alpha$

Here P_B is given by equation (11.11) and P_α by equation (11.13). Equating these two equations, one obtains

$$\alpha \frac{dB}{dt} = B \frac{d\alpha}{dt} \tag{11.19a}$$

Equation (11.19a) hypothesizes that the temporal change in stream power is equally shared by temporal adjustments between flow width B and friction represented by α. This possibility occurs when the cross section has variable roughness and flow is controlled by width and roughness. An example is a river with coarse bank material (say, 2 mm in diameter) in which higher discharge leads to bank erosion and, therefore, higher width but the depth remains practically constant and the roughness also increases. Wolman and Brush (1961) discussed the case of the Platte River in Nebraska, where the braided channel is made up of shifting and stable islands. At some cross sections, banks are covered with coarse grass and contain fine material, and the river is a mile wide and an inch deep. With increasing discharge, the width increases and so does roughness, but the depth remains almost constant. The hypothesis in this case can be considered as a limiting case and holds under the equilibrium condition. Such a condition, however, is seldom achieved, and, therefore, temporal change in stream power is accomplished by an unequal adjustment between B and α. To account for the proportion in which the adjustment of stream power is shared between B and α, equation (11.19a) is modified by introducing a weighting factor, w, $w \geq 0$:

$$\frac{d\alpha}{dt} = w \frac{\alpha}{B} \frac{dB}{dt} \tag{11.19b}$$

Integration of equation (11.19b) gives

$$\alpha = c_{\alpha B} B^{w} \text{ or } B = c^*_{\alpha B} \alpha^{1/w} \tag{11.20a}$$

where $C_{\alpha B}$ or $C^*_{\alpha B}$ is a constant of integration. For the limiting case, $w = 1$,

$$\alpha = c_{\alpha B} B \text{ or } B = c^*_{\alpha B} \alpha \tag{11.20b}$$

where $C_{\alpha B}$ or $C^*_{\alpha B}$ can be designated as a morphological constant and equation (11.20a) or (11.20b) as a morphological equation.

11.3.1.3 Possibility III: $P_B = P_S$

Here P_B is given by equation (11.11) and P_S by equation (11.14). Equating these two equations, one obtains

$$S\frac{dB}{dt} = \frac{3}{2} B \frac{dS}{dt} \tag{11.21a}$$

Equation (11.21a) hypothesizes that the temporal change in stream power is equally shared by temporal adjustments between flow width B and friction slope by S. This possibility occurs when the cross section has constant roughness and flow is controlled by width and slope. An example is a river cross section transiting from straight to meandering where width varies and the slope changes. This is a highly local possibility. This hypothesis can be considered as a limiting case and holds under the equilibrium condition. Such a condition, however, is seldom achieved, and, therefore, temporal change in stream power is accomplished by an unequal adjustment between B and S. To account for the proportion in which the adjustment of stream power is shared between B and S, equation (11.21a) is modified by introducing a weighting factor, I, $\underline{I} \geq 0$:

$$\frac{1}{S}\frac{dS}{dt} = \frac{2I}{3}\frac{dB}{B} \tag{11.21b}$$

Integration of equation (11.21b) gives

$$S = c_{SB} B^{2I/3} \text{ or } B = C^*_{SB} S^{3/2I} \tag{11.22a}$$

where C_{SB} or C^*_{SB} is a constant of integration. For the limiting case, $I = 1$,

$$S = C_{SB} B^{2/3} \tag{11.22b}$$

$C_{\alpha B}$ or $C^*_{\alpha B}$ can be designated as a morphological constant, and equation (11.22a) or (11.22b) as a morphological equation.

11.3.1.4 Possibility IV: $P_h = P_\alpha$

Here P_h is given by equation (11.12) and P_α by equation (11.13). Equating these two equations, one obtains

$$\frac{1}{\alpha}\frac{d\alpha}{dt} = \frac{\beta}{h}\frac{dh}{dt} \tag{11.23a}$$

Equation (11.23a) hypothesizes that the temporal change in stream power is equally shared by temporal adjustments between flow depth h and friction

represented by α. This possibility occurs when the cross section has fixed width and variable roughness and flow is controlled by depth and friction. An example is wide flat channels with steep banks of fine material (Wolman 1955). Another example is stable, approximately rectangular irrigation canals. In such canals, depth varies with discharge and so does roughness, but width remains essentially unchanged. This hypothesis can be considered as a limiting case and holds under the equilibrium condition. Such a condition, however, is seldom achieved, and, therefore, temporal change in stream power is accomplished by an unequal adjustment between h and α. To account for the proportion in which the adjustment of stream power is shared between h and α, equation (11.23a) is modified by introducing a weighting factor, J, $J \geq 0$:

$$\frac{1}{\alpha}\frac{d\alpha}{dt} = \frac{J\beta}{h}\frac{dh}{dt} \tag{11.23b}$$

Integration of equation (11.23b) gives

$$\alpha = C_{\alpha h} h^{J\beta} \text{ or } h = C^*_{\alpha h}\alpha^{1/J\beta} \tag{11.24a}$$

where $C_{\alpha h}$ or $C^*_{\alpha h}$ is a constant of integration. For the limiting case, $J = 1$,

$$\alpha = C_{\alpha h} h^{J\beta} \text{ or } h = C^*_{\alpha h}\alpha^{1/J\beta} \tag{11.24b}$$

$C_{\alpha h}$ or $C^*_{\alpha h}$ can be designated as a morphological constant, and equation (11.24a) or (11.24b) can be designated as a morphological equation.

11.3.1.5 Possibility V: $P_h = P_S$

Here P_h is given by equation (11.12) and P_S by equation (11.14). Equating these two equations, one obtains

$$\frac{1}{S}\frac{dS}{dt} = \frac{2}{3}\frac{\beta}{h}\frac{dh}{dt} \tag{11.25a}$$

Equation (11.25a) hypothesizes that the temporal change in stream power is equally shared by temporal adjustments between flow depth h and friction slope S. This possibility occurs when the cross section has fixed width and fixed roughness and flow is controlled by depth and slope. This situation can occur locally at certain cross sections where the channel is stable, but because of a certain bed form, such as a pool or riffle, the depth changes and so does the slope. This hypothesis can be considered as a limiting case and holds under the equilibrium condition. Such a condition, however, is seldom achieved, and, therefore, temporal change in stream power is accomplished by an unequal adjustment between h and S. To account for the proportion in which the adjustment of stream power is shared between h and S, equation (11.25a) is modified by introducing a weighting factor, K, $K \geq 0$:

$$\frac{1}{S}\frac{dS}{dt} = \frac{2}{3}\frac{\beta K}{h}\frac{dh}{dt} \tag{11.25b}$$

Integration of equation (11.25b) gives

$$S = C_{Sh} h^{2\beta K/3} \text{ or } h = C^*_{Sh} s^{3/(2\beta K)} \tag{11.26a}$$

where C_{Sh} or C^*_{Sh} is a constant of integration. For the limiting case, $K = 1$,

$$S = C_{Sh} h^{2/(3\beta)} \text{ or } h = C^*_{SH} S^{3\beta/2} \tag{11.26b}$$

C_{Sh} or C^*_{Sh} can be designated as a morphological constant, and equation (11.26a) or (11.26b) can be designated as a morphological equation.

11.3.1.6 Possibility VI: $P_S = P_\alpha$

Here P_S is given by equation (11.14) and P_α by equation (11.13). Equating these two equations, one obtains

$$S\frac{d\alpha}{dt} = \frac{3}{2}\alpha\frac{dS}{dt} \tag{11.27}$$

Equation (11.27) hypothesizes that the temporal change in stream power is equally shared by temporal adjustments between friction (or bed) slope S and slope friction represented by α. This possibility occurs when the cross section has fixed width and variable roughness and flow is controlled by friction slope and friction. In a channel cross section with heterogeneous bank and bed sediment, a channel adjusts its roughness and slope because of changing discharge. This hypothesis can be considered as a limiting case and holds under the equilibrium condition. Such a condition, however, is seldom achieved, and, therefore, temporal change in stream power is accomplished by an unequal adjustment between S and α. To account for the proportion in which the adjustment of stream power is shared between S and α, equation (11.27) is modified by introducing a weighting factor, F, $F \geq 0$:

$$\frac{1}{S}\frac{dS}{dt} = \frac{2}{3}\frac{F}{\alpha}\frac{d\alpha}{dt} \tag{11.28}$$

Integration of equation (11.28) gives

$$S = C_{S\alpha}\alpha^{2F/3} \text{ or } \alpha = C^*_{S\alpha} S^{3/2F} \tag{11.29a}$$

where $C_{S\alpha}$ or $C^*_{S\alpha}$ is a constant of integration. For the limiting case, $F = 1$,

$$S = C_{S\alpha}\alpha^{2/3} \text{ or } \alpha = C^*_{S\alpha} S^{3/2} \tag{11.29b}$$

$C_{S\alpha}$ or $C^*_{S\alpha}$ can be designated as a morphological constant, and equation (11.29a) or (11.29b) can be designated as a morphological equation.

11.3.1.7 Possibilities VII–XI: $P_B = P_h = P_\alpha$, $P_B = P_\alpha = P_S$, $P_B = P_h = P_S$, $P_h = P_\alpha = P_S$, and $P_B = P_h = P_\alpha = P_S$

Morphological equations (11.18a or 11.18b), (11.20a or 11.20b), (11.22a or 11.22b), (11.24a or 11.24b), (11.26a or 11.26b), and (11.29a or 11.29b) are the primary equations and correspond to possibilities I to VI. Possibilities VII to XI are obtained by combining possibilities I to VI, and therefore, possibilities VII to XI do not lead to primary morphological equations. However, by combining the six primary equations in accordance with combined possibilities, different hydraulic geometry relations are obtained. For example, equation (18a) relates h and B, equation (20a) relates α and B. These first two equations can be used to eliminate α and h in possibility VII and express B as a function of Q. This result corresponds to possibility VII. In a similar manner, other equations can be used to express h as a function of Q, V as a function of Q, S as a function of Q, and α as a function of Q.

11.3.2 Derivations of Relations

Substitution of morphological equations (11.18a), (11.20a), (11.22a), (11.24a), (11.26a), and (11.29a) in equation (11.5) leads to equations for at-a-station hydraulic geometry. Eleven sets of hydraulic geometry expressions were derived. In the first set are expressions corresponding to possibility I, wherein the channel adjusts its width, depth, and velocity to accommodate changes in discharge (and sediment load). Possibility II corresponds to the case where the channel adjusts its width, velocity, and friction to accommodate changes in discharge. In possibility III the channel adjusts its width, slope, and velocity for accommodating changes in discharge. Possibility IV leads to hydraulic geometry expressions where the channel adjusts its depth, velocity, and roughness to accommodate changes in discharge. Possibility V results in hydraulic geometry equations where the depth, velocity, and slope are adjusted to accommodate changes in discharge. In possibility VI are hydraulic geometry expressions wherein the channel adjusts its velocity, friction, and slope to accommodate changes in discharge.

The remaining possibilities, VII to XI, result from combinations of the aforementioned six possibilities. Possibility VII corresponds to the case where the channel adjusts its width, depth, velocity, and friction to accommodate changes in discharge. In possibility VIII the channel adjusts its width, friction, slope, and velocity for accommodating changes in discharge. Possibility IX leads to hydraulic geometry expressions where the channel adjusts its width, depth, velocity, and slope to accommodate changes in discharge. Possibility X leads to hydraulic geometry equations that express the adjustment of depth, friction, velocity, and slope in response to the variation in discharge. Possibility XI results in hydraulic geometry equations showing the adjustment of width, depth, friction, slope, and velocity in response to changes in discharge.

A short discussion of each set of hydraulic geometry relations is in order. To facilitate discussion, the values of exponents b, f, m, p, and y for three cases (one special and two limiting cases) when the weighting factors are zero, unity, and infinity, are tabulated for all 11 possibilities in Table 11-5. It should be pointed

Table 11-5 *Theoretically derived values of hydraulic geometry exponents* b, f, m, p, *and* y *for different configurations under the condition that weighting factors equal 0, 1, and ∞.*

Possibility	Exponent *b*			Exponent *f*			Exponent *m*			Exponent *p*			Exponent *y*		
I: RE	$r=0$	$r=1$	$r\to\infty$	$r=0$	$r=1$	$r\to\infty$	$r=0$	$r=1$	$r\to\infty$	$r=0$	$r=1$	$r\to\infty$	$r=0$	$r=1$	$r\to\infty$
ME	1	1/2	0	0	3/10	3/5	0	1/5	2/5	—	—	—	—	—	—
CE/DWE	1	1/2	0	0	1/3	2/3	0	1/6	1/3	—	—	—	—	—	—
II: RE	$w=0$	$w=1$	$w\to\infty$	$w=0$	$w=1$	$w\to\infty$	$w=0$	$w=1$	$w\to\infty$	$w=0$	$w=1$	$w\to\infty$	$w=0$	$w=1$	$w\to\infty$
ME	1	1/2	0	—	—	—	0	1/2	1	0	–1/2	–1	—	—	—
CE/DWE	1	1/2	0	—	—	—	0	1/2	1	0	1/2	1	—	—	—
III: RE	$I=0$	$I=1$	$I\to\infty$	$I=0$	$I=1$	$I\to\infty$	$I=0$	$I=1$	$I\to\infty$	$I=0$	$I=1$	$I\to\infty$	$I=0$	$I=1$	$I\to\infty$
ME	1	3/4	0	—	—	—	0	1/4	1	—	—	—	0	1/2	2
CE/DWE	1	3/4	0	—	—	—	0	1/4	1	—	—	—	0	1/2	2
IV: RE	$J=0$	$J=1$	$J\to\infty$	$J=0$	$J=1$	$J\to\infty$	$J=0$	$J=1$	$J\to\infty$	$J=0$	$J=1$	$J\to\infty$	$J=0$	$J=1$	$J\to\infty$
ME	—	—	—	3/5	3/10	0	–2/5	3/10	1	0	–1/2	–1	—	—	—
CE/DWE	—	—	—	2/3	1/3	0	1/3	1/6	0	0	1/2	1	—	—	—
V: RE	$K=0$	$K=1$	$K\to\infty$	$K=0$	$K=1$	$K\to\infty$	$K=0$	$K=1$	$K\to\infty$	$K=0$	$K=1$	$K\to\infty$	$K=0$	$K=1$	$K\to\infty$
ME	—	—	—	9/15	9/20	0	2/5	11/20	1	—	—	—	0	1/2	2
CE/DWE	—	—	—	2/3	1/2	0	1/3	1/2	1	—	—	—	0	1/2	2
VI: RE	$F=0$	$F=1$	$F\to\infty$	$F=0$	$F=1$	$F\to\infty$	$F=0$	$F=1$	$F\to\infty$	$F=0$	$F=1$	$F\to\infty$	$F=0$	$F=1$	$F\to\infty$
ME	—	—	—	—	—	—	1	5/4	2	–1	–3/4	0	0	1/2	2
CE/DWE	—	—	—	—	—	—	1	5/4	2	1	3/4	0	0	1/2	2
VII: RE	$r=w=J=0$	$r=w=J=1$	$r=w=J\to\infty$	$r=w=J=0$	$r=w=J=1$	$r=w=J\to\infty$	$r=w=J=0$	$r=w=J=1$	$r=w=J\to\infty$	$r=w=J=0$	$r=w=J=1$	$r=w=J\to\infty$	$r=w=J=0$	$r=w=J=1$	$r=w=J\to\infty$
ME	1	1/3	0	0	1/5	0	–3/5	7/15	1	0/0	–1/3	–1	—	—	—

Continued

Table 11-5 *Theoretically derived values of hydraulic geometry exponents* b, f, m, p, *and* y *for different configurations under the condition that weighting factors equal 0, 1, and ∞. (Continued)*

Possibility	Exponent *b*			Exponent *f*			Exponent *m*			Exponent *p*			Exponent *y*		
CE/DWE	1	1/3	0	0	2/9	0	–2/3	4/9	1	0/0	1/3	1	—	—	—
VIII: RE	$w = I = F = 0$	$w = I = F = 1$	$w = I = F \to \infty$	$w = I = F = 0$	$w = I = F = 1$	$w = I = F \to \infty$	$w = I = F = 0$	$w = I = F = 1$	$w = I = F = \infty$	$w = I = F = 0$	$w = I = F = 1$	$w = I = F \to \infty$	$w = I = F = 0$	$w = I = F = 1$	$w = I = F \to \infty$
ME	1	3/7	0	—	—	—	0	34/63	1	0	–3/7	0	0/0	2/7	2
CE/DWE	1	3/7	0	—	—	—	0	34/63	1	0	3/7	0	0/0	2/7	2
IX: RE	$r = I = K = 0$	$r = I = K = 1$	$r = I = K \to \infty$	$r = I = K = 0$	$r = I = K = 1$	$r = I = K \to \infty$	$r = I = K = 0$	$r = I = K = 1$	$r = I = K \to \infty$	$r = I = K = 0$	$r = I = K = 1$	$r = I = K \to \infty$	$r = I = K = 0$	$r = I = K = 1$	$r = I = K \to \infty$
ME	1	3/7	0	0	9/35	0	0	17/70	1	—	—	—	0/0	2/7	2
CE/DWE	1	3/7	0	0	2/7	0	0	5/18	1	—	—	—	0/0	2/7	2
X: RE	$J = K = F = 0$	$J = K = F = 1$	$J = K = F \to \infty$	$J = K = F = 0$	$J = K = F = 1$	$J = K = F \to \infty$	$J = K = F = 0$	$J = K = F = 1$	$J = K = F \to \infty$	$J = K = F = 0$	$J = K = F = 1$	$J = K = F \to \infty$	$J = K = F = 0$	$J = K = F = 1$	$J = K = F \to \infty$
ME	—	—	—	1/3	1/7	0	2/5 0/0	26/35	∞/∞	0	–3/7	0	0/0	2/7	2
CE/DWE	—	—	—	2/3	2/7	0	1/3	5/7	∞/∞	0	3/7	0	0/0	2/7	2
XI: RE	$r = w = I = J = K = F = 0$	$r = w = I = J = K = F = 1$	$r = w = I = J = K = F \to \infty$	$r = w = I = J = K = F = 0$	$r = w = I = J = K = F = 1$	$r = w = I = J = K = F \to \infty$	$r = w = I = J = K = F = 0$	$r = w = I = J = K = F = 1$	$r = w = I = J = K = F \to \infty$	$r = w = I = J = K = F = 0$	$r = w = I = J = K = F = 1$	$r = w = I = J = K = F \to \infty$	$r = w = I = J = K = F = 0$	$r = w = I = J = K = F = 1$	$r = w = I = J = K = F \to \infty$
ME	1	3/10	0	0	9/50	0	0	13/25	1	0/0	3/10	0	0/0	1/5	2
CE/DWE	1	3/10	0	0	1/5	0	0	2/5	1	0/0	3/10	2	0/0	1/5	2

Note: RE Resistance equation, ME = Manning's equation, CE = Chezy's equation, and DWE = Darcy–Weisbach equation.

out that the limiting case of infinity is only a theoretically generalized case for the factors r, w, I, J, K, and F for the lack of knowledge of the values of their upper limits, which should be far less than infinity. Table 11-6 gives ranges of values, as well as mean values of the exponents reported in the literature. Table 11-7 gives the exponent values derived using other theories. In the discussion that follows, only Manning's equation will be considered for economy of space.

11.3.2.1 Possibility I: $P_B = P_h$, $B = C_{Bh}h^{\beta/r}$ or $h = C^*_{Bh}B^{r/\beta}$

The general morphological equation for this possibility is given by equation (11.18a) or the special form by equation (11.18b). Substitution of equation (11.18a) in equation (11.7) yields equations for B, h, and V:

$$B = \left(\frac{C_{Bh}^r}{\alpha S^{1/2}}\right)^{1/(1+r)} Q^{1/(1+r)} = C_B Q^{1/(1+r)}, \quad C_B = \left(\frac{C_{Bh}^r}{\alpha S^{1/2}}\right)^{1/(1+r)} \tag{11.30}$$

$$h = \left(\frac{1}{\alpha C_{Bh} S^{1/2}}\right)^{r/[(1+r)\beta]} Q^{r/[(1+r)\beta]} = C_h Q^{r/[(1+r)\beta]}, \quad C_h = \left(\frac{1}{\alpha C_{Bh} S^{1/2}}\right)^{r/[(1+r)\beta]} \tag{11.31}$$

$$h = \alpha^{(\beta+r)/[(1+r)\beta]}(C_{Bh})^{-(\beta r-r)/[(1+r)\beta]} Q^{r(\beta-1)/[(1+r)\beta]} S^{(\beta+r)/[2\beta(1+r)]} = C_V Q^{r(\beta-1)/[(1+r)\beta]}, \tag{11.32}$$
$$C_V = \alpha^{r(\beta-1)/[\beta(1+r)]}(C_{Bh})^{-(\beta r-r)/[(1+r)\beta]} S^{(r+\beta)/[2(1+r)\beta]}$$

If Manning's equation (11.5a) is used in place of equation (11.7, then with $\alpha = 1/n$ and $\beta = 5/3$, equations (11.30) to (11.32) reduce to

$$B = C_B Q^{1/(1+r)}, C_B = \left(\frac{n C_{Bh}{}^r}{S^{0.5}}\right)^{1/(1+r)} \tag{11.33}$$

$$h = C_h Q^{\frac{3r}{(1+r)5}}, C_h = \left(\frac{n}{C_{Bh} S^{1/2}}\right)^{\frac{3r}{(1+r)5}} \tag{11.34}$$

$$V = C_V Q^{\frac{2r}{5(1+r)}}, C_V = \left(\frac{1}{n}\right)^{\frac{5+3r}{5(1+r)}} \left(\frac{1}{C_{Bh}}\right)^{\frac{2r}{(1+r)5}} S^{\frac{5+3r}{10(1+r)}} \tag{11.35}$$

For the special case $r = 1$, equations (11.33) to (11.35) become

$$B = C_B Q^{0.5}, C_B = \left(\frac{n C_{Bh}}{S^{0.5}}\right)^{0.5} \tag{11.36}$$

$$h = C_h Q^{3/10}, C_h = \left(\frac{n}{C_{Bh} S^{0.5}}\right)^{3/10} \tag{11.37}$$

$$V = C_V Q^{2/10}, C_V = \left(\frac{1}{n}\right)^{4/5} \left(\frac{1}{C_{Bh}}\right)^{1/5} S^{2/5} \tag{11.38}$$

Table 11-6 *Range of at-a-station hydraulic geometry exponent values reported by different investigators.*

Source	No. datasets used	Exponents					Remarks
		b	*f*	*m*	*p*	*y*	
Park (1977)	139	0.00–0.59 (0.0–0.1)	0.06–0.73 (0.3–0.4)	0.07–0.71 (0.4–0.5)			Data from U.S., U.K., Brazil, and other countries
Rhodes (1978)	587	0.00–0.84	0.01–0.84	0.03–0.99			Worldwide
Myrick and Leopold (1963)	6	0.04–0.14 (0.09)	0.08–0.18 (0.13)	0.78 (0.78)			Tidal channel to Potomac River
Leopold and Miller (1956)	10	0.09–0.34 (0.26)	0.23–0.61 (0.33)	0.24–0.45 (0.32)			Ephemeral channels
Wolman (1955)	7	0.00–0.08 (0.04)	0.32–0.46 (0.41)	0.46–0.69 (0.55)	–0.40 to –0.10 (–0.20)	–0.03–0.15 (0.05)	Brandywine Creek, Pennsylvania
Wolman (1955)	2	0.16–0.22 (0.19)	0.30–0.45 (0.38)	0.42–0.48 (0.45)			Brandywine Creek, Pennsylvania
Leopold and Maddock (1953)	20	0.06–0.59 (0.26)	0.06–0.63 (0.40)	0.07–0.55 (0.34)			Great Plains and Southwest
Stall and Fok (1968)	18	0.13–0.49 (0.29)	0.28–0.52 (0.45)	0.15–0.40 (0.26)			Sangamon River basin and Midwest

Stall and Yang (1970)	37	0.00–0.40 (0.12)	0.31–0.71 (0.47)	0.07–0.92 (0.41)	Roanoke River basin
Riley (1978)	8	0.41–0.50 (0.42)	0.30–0.70 (0.41)	0.12–0.22 (0.16)	Gwydir River, Australia
Riley (1978)	9	0.15–0.49 (0.35)	0.36–0.67 (0.48)	0.08–0.39 (0.17)	Namoi River, Australia
Riley (1978)	5	0.19–0.40 (0.35)	0.49–0.56 (0.52)	0.08–0.25 (0.13)	Barwon River, Australia
Virmani (1973)	11	0.08–0.19 (0.13)	0.38–0.54 (0.43)	0.37–0.52 (0.43)	Bear River basin, Rocky Mountain region
Virmani (1973)	8	0.08–0.18 (0.14)	0.32–0.57 (0.40)	0.30–0.59 (0.46)	Peace River basin, Canada
Virmani (1973)	15	0.08–0.38 (0.16)	0.29–0.66 (0.45)	0.32–0.58 (0.39)	Athabasca River basin, Canada
Williams (1978)	165	0.00–0.82	0.10–0.78	0.03–0.82	Contiguous U.S.

Note: The values within parentheses are mean values; the range of values within parentheses is the modal class.

Table 11-7 *Theoretically derived values of hydraulic geometry exponents as reported in the literature.*

Source	Exponents					Remarks
	b	*F*	*m*	*p*	*y*	
Langbein (1964)	0.23	0.42	0.35	–0.07	—	Theory of minimum variance
Li (1975)	0.24	0.46	0.30		0.0	Tractive force theory

If Chezy's equation (11.5b) is used, then $\alpha = C$ and $\beta = 3/2$ and equations (11.30) to (11.32) become

$$B = C_B Q^{1/(1+r)}, C_B = \left(\frac{C_{Bh}{}^r}{CS^{0.5}} \right)^{1/(1+r)} \tag{11.39}$$

$$h = C_h Q^{2r/[3(1+r)]}, C_h = \left(\frac{1}{C_{Bh} CS^{0.5}} \right)^{2r/[3(1+r)]} \tag{11.40}$$

$$V = C_V Q^{r/[3(1+r)]}, C_V = C^{(3+2r)/[3(1+r)]} (C_{Bh})^{-r/[3(1+r)]} S^{(3+2r)/[6(1+r)]} \tag{11.41}$$

For the special case $r = 1$, equations (11.39) to (11.41) become

$$B = C_B Q^{0.5}, \quad C_B = \left(\frac{C_{Bh}}{CS^{0.5}} \right)^{1/2} \tag{11.42}$$

$$h = C_h Q^{1/3}, \quad C_h = (C_{Bh} CS^{0.5})^{-1/3} \tag{11.43}$$

$$V = C_V Q^{1/6}, \quad C_V = C^{5/6} (C_{Bh})^{-1/6} S^{5/12} \tag{11.44}$$

If the Darcy–Weisbach relation (11.5c) is used, then with $\alpha = f_y$ and $\beta = 3/2$, the exponents of discharge for B, h, and V remain the same as in the case of Chezy's equation and Chezy's coefficient C is replaced by f_y. Therefore, the hydraulic geometry relations are not repeated.

11.3.2.2 Possibility I: Hydraulic Geometry Relations for Width, Depth, and Velocity

This possibility is perhaps the most investigated and frequently occurring possibility. Equations (11.33) to (11.35) show that the channel width varies with discharge raised to the power $b = 1/(1 + r)$, the depth varies with discharge raised to the power $f = 3r/[5(1 + r)]$, and velocity varies with discharge raised to the power $m = 2r/[5(1 + r)]$. The values of exponents b, f, and m depend on the weighting factor r, which specifies the proportion for adjustment of stream power between B, h, and V, as shown in Fig. 11-3. When the weighting factor r tends to 0, b, f, and m, respectively, take on 1, 0, and 0, and when r tends to ∞, b,

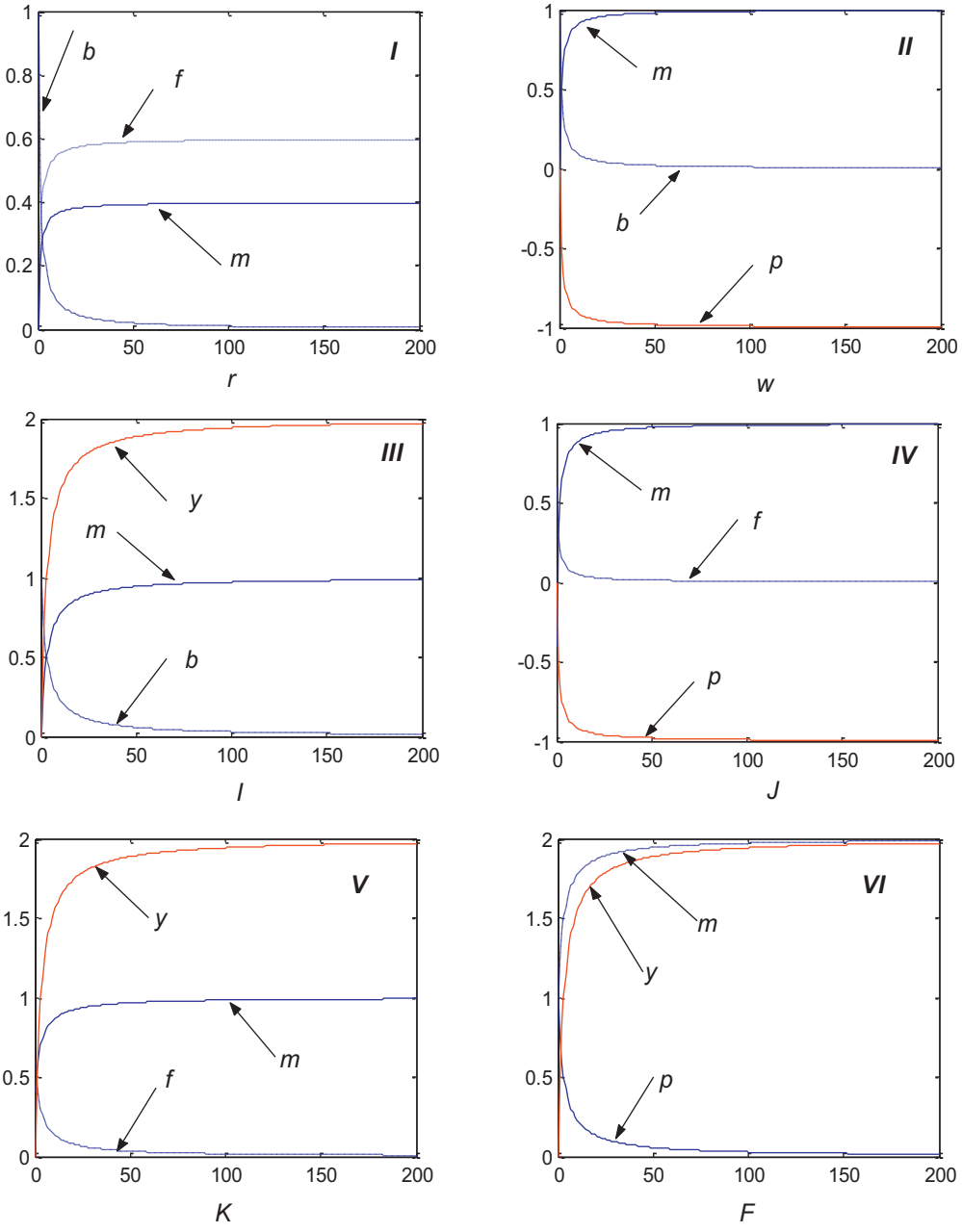

Figure 11-3 *Variation of exponents with weighting factors for different possibilities.*

Continued

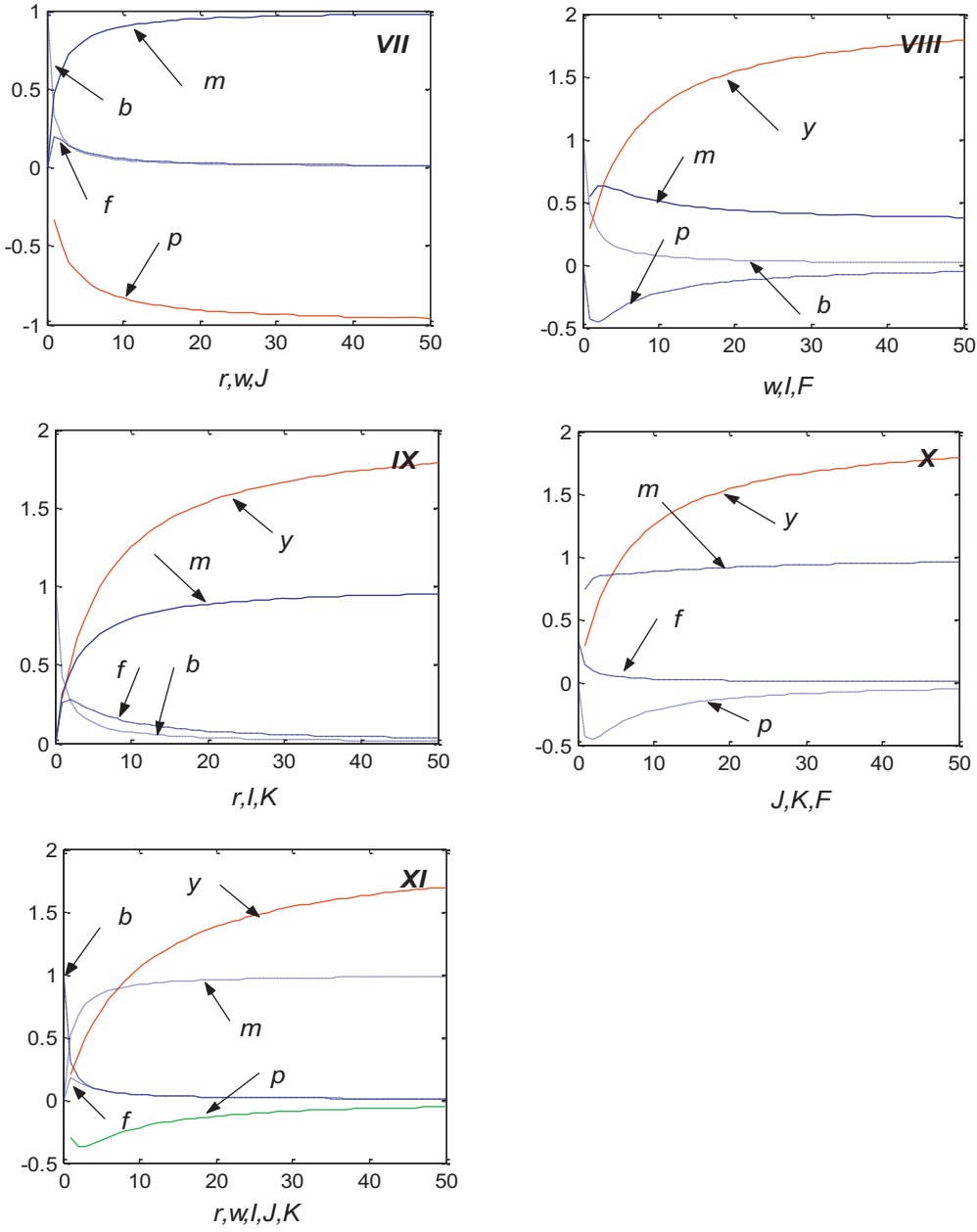

Figure 11-3, *Continued*

f, and m take on, respectively, 0, 3/5, and 2/5 (see equations (11.33)–(11.35)). For the special case $r = 1$, where the adjustment is equally proportioned, $b = 0.5$, $f = 3/10$, and $m = 1/5$. Scale factors, C_B, C_h, and C_V vary with flow resistance and slope. Thus, the derived equations show that the values of exponents, b, f, and

m do not possess fixed values; rather they vary over certain ranges dictated by the way the adjustment of stream power is distributed among variables.

For the at-a-station hydraulic geometry of 139 streams from a variety of environments, Park (1977) reported the range of b as 0.0 to 0.59 with modal class as 0.0 to 0.1; the range of f as 0.06 to 0.73 with modal class as 0.3 to 0.4; and the range of m as 0.07 to 0.71 with modal class as 0.4 to 0.5. Thus, the derived exponents are in the reported ranges.

11.4 Possibilities II to XI

11.4.1 Possibility II

Possibility II: $P_B = P_\alpha$, $\alpha = C_{\alpha B}B^w$

Inserting equation (11.20a) in equation (11.7) and a little algebraic manipulation lead to

$$B = (C_{\alpha B}S^{0.5}h^{\beta})^{-1/(1+w)}Q^{1/(1+w)} = C_BQ^{1/(1+w)},\ C_B = (C_{\alpha B}S^{0.5}h^{\beta})^{-1/(1+w)} \tag{11.45}$$

$$\begin{aligned}&\alpha = (C_{\alpha B})^{1/(1+w)}h^{-\beta w/(1+w)}Q^{w/(1+w)}S^{-w/[2(1+w)]} = C_\alpha Q^{w/(1+w)},\\ &C_\alpha = (C_{\alpha B})^{1/(1+w)}h^{-\beta h/(1+w)}S^{-w/[2(1+w)]}\end{aligned} \tag{11.46}$$

$$V = C_\alpha S^{0.5}h^{\beta-1}Q^{w/(1+w)} = C_VQ^{w/(1+w)},\ C_V = (C_{\alpha B})^{1/(1+w)}h^{[\beta-(1+w)]/(1+w)}S^{1/[2(1+w)]} \tag{11.47}$$

For Manning's equation ($\alpha = 1/n$, $\beta = 5/3$), equations (11.45) to (11.47) reduce to

$$\begin{aligned}&B = (C_{\alpha B}S^{0.5}h^{\beta})^{-1/(1+w)}Q^{1/(1+w)} = C_BQ^{1/(1+w)},\ C_B = (C_{\alpha B}S^{0.5}h^{\beta})^{-1/(1+w)}\\ &B = \left(\frac{1}{C_{\alpha B}S^{1/2}h^{5/3}}\right)^{\frac{1}{1+w}}Q^{\frac{1}{1+w}} = C_BQ^{\frac{1}{1+w}},\ C_B = \left(\frac{1}{C_{\alpha B}S^{1/2}h^{5/3}}\right)^{\frac{1}{1+w}}\end{aligned} \tag{11.48}$$

$$\begin{aligned}&n = (C_{\alpha B})^{1/(1+w)}h^{5w/[3(1+w)]}S^{w/[2(1+w)]}Q^{-w/(1+w)} = C_\alpha Q^{1/(1+w)},\\ &C_\alpha = (C_{\alpha B})^{1/(1+w)}h^{5w/[3(1+w)]}S^{w/[2(1+w)]}\end{aligned} \tag{11.49}$$

$$V = C_\alpha S^{0.5}h^{2/3}Q^{w/(1+w)} = C_VQ^{w/(1+w)},\ C_V = (C_{\alpha B})^{-1/(1+w)}h^{[2(1+w)-5]/[3(1+w)]}S^{1/[2(1+w)]} \tag{11.50}$$

For special case $w = 1$, equations (11.48) to (11.50) become

$$B = (C_{\alpha B}S^{0.5}h^{5/3})^{-1/2}Q^{1/2} = C_BQ^{1/2},\ C_B = (C_{\alpha B}S^{0.5}h^{5/3})^{-1/2} \tag{11.51}$$

$$n = (C_{\alpha B})^{-1/2}h^{5/6}S^{1/4}Q^{-1/2} = C_\alpha Q^{-1/2},\ C_\alpha = (C_{\alpha B})^{-1/2}h^{5/6}S^{1/4} \tag{11.52}$$

$$V = C_\alpha S^{0.5}h^{2/3}Q^{1/2} = C_VQ^{1/2},\ C_V = (C_{\alpha B})^{1/2}h^{-1/6}S^{1/4} \tag{11.53}$$

For Chezy's equation (11.5b) with $\alpha = C$, $\beta = 3/2$), equations (11.45) to (11.47) become

$$B = (C_{\alpha B} S^{0.5} h^{3/2})^{-1/(1+w)} Q^{1/(1+w)} = C_B Q^{1/(1+w)}, C_B = (C_{\alpha B} S^{0.5} h^{3/2})^{-1/(1+w)} \quad (11.54)$$

$$\begin{aligned} C &= (C_{\alpha B})^{1/(1+w)} h^{-5w/[3(1+w)]} S^{-w/[2(1+w)]} Q^{w/(1+w)} = C_\alpha Q^{w/(1+w)}, \\ C_\alpha &= (C_{\alpha B})^{1/(1+w)} h^{-5w/[3(1+w)]} S^{-w/[2(1+w)]} \end{aligned} \quad (11.55)$$

$$V = C_\alpha S^{0.5} h^{1/2} Q^{w/(1+w)} = C_V Q^{w/(1+w)}, C_V = (C_{\alpha B})^{1/(1+w)} h^{[3(1+w)-10w]/[6(1+w)]} S^{1/[2(1+w)]} \quad (11.56)$$

For the special case, $w = 1$, equations (11.54) to (11.56) become

$$B = (C_{\alpha B} S^{0.5} h^{3/2})^{-1/2} Q^{1/2} = C_B Q^{1/2}, C_B = (C_{\alpha B} S^{0.5} h^{3/2})^{-1/2} \quad (11.57)$$

$$C = (C_{\alpha B})^{1/2} h^{-5/6} S^{-1/4} Q^{1/2} = C_\alpha Q^{1/2}, C_\alpha = (C_{\alpha B})^{1/2} h^{-5/6} S^{1/4} \quad (11.58)$$

$$V = C_\alpha S^{0.5} h^{1/2} Q^{1/2} = C_V Q^{1/2}, C_V = (C_{\alpha B})^{1/2} h^{-1/3} S^{1/4} \quad (11.59)$$

Possibility II: Hydraulic Geometry Relations for Width, Roughness, and Velocity

In this possibility, the change in stream power is accomplished by the adjustment between channel width and roughness. Equations (11.48) to (11.50) show that the channel width varies with discharge raised to the power $b = 1/(1 + w)$, the velocity varies with discharge raised to the power $m = w/(1 + w)$, and Manning's n varies with discharge raised to the power $p = -w/(1 + w)$. The precise values of b, m, and p depend on the value of the weighting factor w, as shown in Fig. 11-3, meaning the proportion in which the spatial change of stream power is accomplished by the adjustments among B, n, and V. When the weighting factor varies from a value of zero to a value tending to ∞, b varies from 1 to 0, m varies from 0 to 1, and p varies from 0 to –1. When $w = 1$, $b = 0.5$, $m = 0.5$, and $p = -0.5$. The value of $b = 0.5$ is significantly higher than the average value reported in the literature (Table 11-6). Scale factors C_B, C_α, and C_V vary with flow depth and slope. The exponent values of b, m, and p do not possess fixed values; rather they vary over certain ranges, depending on the way the adjustment of stream power is distributed among variables. Most of the exponent values reported in the literature lie within the derived range. For example, the range of exponent p reported by Knighton (1974) is –0.54 to 0.03.

11.4.2 Possibility III

Possibility III: $P_B = P_S$, $S = C_{SB} B^{2I/3}$ or $B = C^*_{SB} S^{3/2I}$

Inserting equation (11.22a) in equation (11.7) and a little algebraic manipulation lead to

$$B = \alpha^{-3/(3+I)}(C_{SB})^{-3/[2(3+I)]}h^{-3\beta/(3+I)}Q^{3/(3+1)},\ C_B = \alpha^{-3/(3+I)}(C_{SB})^{-3/[2(3+I)]}h^{-3\beta/(3+I)} \tag{11.60}$$

$$\begin{aligned} S &= \alpha^{-2I/(3+I)}(C_{SB})^{3/(3+I)}h^{-3I\beta/(3+I)}Q^{2I/(3+1)} = C_S Q^{2I/(3+I)}, \\ C_S &= \alpha^{-2I/(3+I)}(C_{SB})^{3/(3+I)}h^{-2I\beta/(3+I)} \end{aligned} \tag{11.61}$$

$$\begin{aligned} V &= \alpha^{3/(3+I)}(C_{SB})^{3/[2(3+I)]}h^{[(\beta-1)(3+I)-I\beta]/(3+I)}Q^{I/(I+w)} = C_V Q^{I/(I+w)}, \\ C_V &= \alpha^{3/(3+I)}(C_{SB})^{3/([2(I+w)}h^{[(I+w)(3+I)-I\beta]/[I+w]} \end{aligned} \tag{11.62}$$

For Manning's equation, $\alpha = 1/n$ and $\beta = 5/3$. Equations (11.60) to (11.62) become

$$\begin{aligned} B &= n^{3/(3+I)}(C_{SB})^{-3/[2(3+I)]}h^{-5/(3+I)}Q^{3/(3+1)} = C_B Q^{3/(3+I)}, \\ C_B &= n^{3/(3+I)}(C_{SB})^{-3/[2(3+I)]}h^{-5/(3+I)} \end{aligned} \tag{11.63}$$

$$\begin{aligned} S &= n^{2I/(3+I)}(C_{SB})^{3/(3+I)}h^{-10I/[3(3+I)]}Q^{2I/(3+1)} = C_S Q^{2I/(3+I)}, \\ C_S &= n^{2I/(3+I)}(C_{SB})^{3/(3+I)}h^{-10I/[3(3+I)]} \end{aligned} \tag{11.64}$$

$$\begin{aligned} V &= n^{-3/(3+I)}(C_{SB})^{3/[2(3+I)]}h^{[6(3+I)-15I]/[3(3+I)]}Q^{I/(I+3)} = C_V Q^{I/(I+3)}, \\ C_V &= n^{-3/(3+I)}(C_{SB})^{3/([2(I+w)}h^{[6(3+I)-15I]/[I+3]} \end{aligned} \tag{11.65}$$

For the special case $I = 1$, equations (11.63) to (11.65) become

$$B = \left(\frac{nQ}{h^{5/3}C_{SB}^{1/2}}\right)^{3/4} = C_B Q^{3/4},\ C_B = \left(\frac{n}{h^{5/3}C_{SB}^{1/2}}\right)^{3/4} \tag{11.66}$$

$$S = n^{1/2}(C_{SB})^{3/4}h^{-5/6}Q^{1/2} = C_S Q^{1/2},\ C_S = n^{1I2}(C_{SB})^{3/4}h^{-5/6} \tag{11.67}$$

$$V = n^{-3/4}(C_{SB})^{3/8}h^{1/4}Q^{1/4} = C_V Q^{1/4},\ C_V = n^{-3/4}(C_{SB})^{-3/8}h^{1/4} \tag{11.68}$$

For Chezy's relation, $\alpha = C$ and $\beta = 3/2$, equations (11.60) to (11.62) become

$$\begin{aligned} B &= C^{-3/(3+I)}(C_{SB})^{-3/[2(3+I)]}h^{-9/[2(3+I)]}Q^{3/(3+I)} = C_B Q^{3/(3+I)}, \\ C_B &= C^{-3/(3+I)}(C_{SB})^{-3/[2(3+I)]}h^{-9/[2(3+I)]} \end{aligned} \tag{11.69}$$

$$S = C^{-\frac{2I}{3+I}}(C_{SB})^{\frac{3}{3+I}}h^{-\frac{3}{3+I}}Q^{\frac{2I}{3+I}} = C_S Q^{\frac{2I}{3+I}},\ C_s = C^{-\frac{2I}{3+I}}(C_{SB})^{\frac{3}{3+I}}h^{-\frac{3}{3+I}} \tag{11.70}$$

$$V = C^{\frac{3}{3+I}}C_{SB}^{\frac{3}{2(3+I)}}h^{\frac{3-2I}{2(3+I)}}Q^{\frac{I}{I+3}} = C_V Q^{\frac{I}{I+3}},\ C_V = C^{\frac{3}{3+I}}C_{SB}^{\frac{3}{2(3+I)}}h^{\frac{3-2I}{2(3+I)}} \tag{11.71}$$

For the special case $I = 1$, equations (11.69) to (11.71) become

$$B = \left(\frac{Q}{Ch^{3/2}C_{SB}{}^{1/2}}\right)^{3/4} = C_B Q^{3/4},\ C_B = (Ch^{3/2}C_{SB}{}^{1/2})^{-3/4} \tag{11.72}$$

$$S = C^{-1/2}(C_{SB})^{3/4}h^{-3/4}Q^{1/2}, C_S = C^{-1/2}(C_{SB})^{-3/4}h^{-3/4} \tag{11.73}$$

$$V = C^{\frac{3}{4}}C_{SB}^{\frac{3}{8}}h^{\frac{1}{8}}Q^{\frac{1}{4}} = C_V Q^{\frac{1}{4}}, C_V = C^{\frac{3}{4}}C_{SB}^{\frac{3}{8}}h^{\frac{1}{8}} \tag{11.74}$$

Possibility III: Hydraulic Geometry Relations for Width, Velocity, and Slope

For weighting factor $I = 0$, $b = 1$, $m = 0$, and $y = 0$; and when the weighting factor tends to ∞, $b = 1$, $m = 1$, and $y = 1$, as shown by equations (11.63) to (11.65). These equations show that the channel width varies with discharge raised to the power $b = 3/(3 + I)$, the velocity varies with discharge raised to the power $m = I/(3 + I)$, and slope varies with discharge raised to the power $p = 2I/(3 + I)$. The exact exponent values depend on the value of the weighting factor I, as shown in Fig. 11-3. For the special case, $I = 1$, the value of b becomes 3/4, as shown by equation (11.66), the m exponent assumes a value of 1/4, as shown by equation (11.68), and the y exponent becomes 0.5, as shown by equation (11.67) (see Table 11-5); for this special case, the value of m is lower than the average value reported in the literature, whereas the value of y is higher than that reported by Wolman (1955). The exponent values thus derived cover the whole range reported in the literature. Scale factors C_B, C_V, and C_S depend on the channel roughness and flow depth. This discussion shows that exponents b, m, and y do not possess fixed values; rather, they vary over certain ranges, depending on the way the adjustment of stream power is shared among variables.

11.4.3 Possibility IV

Possibility IV: $P_h = P_\omega$, $\alpha = C_{\alpha h}h^{J\beta}$ or $h = C_{\alpha h}^{*}\alpha^{1/J\beta}$

Inserting equation (11.24a) in equation (11.7) and a little algebraic manipulation lead to

$$h = \left(\frac{1}{C_{\alpha h}BS^{1/2}}\right)^{\frac{1}{(J+1)\beta}} Q^{\frac{1}{(J+1)\beta}} = C_h Q^{\frac{1}{\beta(J+1)}}, C_h = \left(\frac{1}{C_{\alpha h}BS^{1/2}}\right)^{\frac{1}{(J+1)\beta}} \tag{11.75}$$

$$\alpha = (C_{\alpha h})^{\frac{1}{1+J}}\left(\frac{1}{BS^{1/2}}\right)^{\frac{J}{1+J}} Q^{\frac{J}{1+J}} = C_\alpha Q^{\frac{J}{1+J}}, C_\alpha = (C_{\alpha h})^{\frac{1}{J+1}}\left(\frac{1}{BS^{1/2}}\right)^{\frac{J}{1+J}} \tag{11.76}$$

$$V = (C_{\alpha h})^{\frac{1}{(J+1)\beta}}\left(\frac{1}{B}\right)^{\frac{J\beta+\beta-1}{(J+1)\beta}} S^{\frac{1}{2\beta(1+J)}} Q^{\frac{J\beta+\beta-1}{(J+1)\beta}} = C_V Q^{\frac{J\beta+\beta-1}{(J+1)\beta}}, C_V = (C_{\alpha h})^{\frac{1}{(J+1)\beta}}\left(\frac{1}{B}\right)^{\frac{J\beta+\beta-1}{(J+1)\beta}} S^{\frac{1}{2\beta(1+J)}} \tag{11.77}$$

For Manning's equation, $\alpha = 1/n$ and $\beta = 5/3$, equations (11.75) to (11.77) reduce to

$$h = \left(\frac{1}{C_{\alpha h}BS^{1/2}}\right)^{\frac{3}{5(J+1)}} Q^{\frac{3}{5(J+1)}} = C_h Q^{\frac{3}{5(J+1)}}, C_h = \left(\frac{1}{C_{\alpha h}BS^{1/2}}\right)^{\frac{3}{5(J+1)}} \tag{11.78}$$

$$n = (C_{\alpha h})^{-\frac{1}{1+J}} \left(BS^{1/2}\right)^{\frac{J}{1+J}} Q^{-\frac{J}{1+J}} = C_\alpha Q^{-\frac{J}{1+J}}, C_\alpha = (C_{\alpha h})^{-\frac{1}{J+1}} \left(BS^{1/2}\right)^{\frac{J}{1+J}} \tag{11.79}$$

$$V = (C_{\alpha h})^{\frac{3}{(J+1)5}} \left(\frac{1}{B}\right)^{\frac{5J-2}{5(J+1)}} S^{\frac{3}{10(1+J)}} Q^{\frac{5J-2}{5(J+1)}} = C_V Q^{\frac{5J-2}{5(J+1)}}, C_V = (C_{\alpha h})^{\frac{3}{5(J+1)}} \left(\frac{1}{B}\right)^{\frac{5J-2}{5(J+1)}} S^{\frac{3}{10(1+J)}} \tag{11.80}$$

For the special case $J = 1$, equations (11.78) to (11.80) reduce to

$$h = \left(\frac{1}{C_{\alpha h} BS^{1/2}}\right)^{3/10} Q^{3/10} = C_h Q^{3/10}, C_h = \left(\frac{1}{C_{\alpha h} BS^{1/2}}\right)^{3/10} \tag{11.81}$$

$$n = (C_{\alpha h})^{-\frac{1}{2}} \left(BS^{1/2}\right)^{\frac{1}{2}} Q^{-\frac{1}{2}} = C_\alpha Q^{-\frac{1}{2}}, C_\alpha = (C_{\alpha h})^{-\frac{1}{2}} \left(BS^{1/2}\right)^{\frac{1}{2}} \tag{11.82}$$

$$V = (C_{\alpha h})^{\frac{3}{10}} \left(\frac{1}{B}\right)^{\frac{3}{10}} S^{\frac{3}{20}} Q^{\frac{3}{10}} = C_V Q^{\frac{3}{10}}, C_V = (C_{\alpha h})^{\frac{3}{10}} \left(\frac{1}{B}\right)^{\frac{3}{10}} S^{\frac{3}{20}} \tag{11.83}$$

For Chezy's equation, $\alpha = C$ and $\beta = 3/2$, equations (11.75) to (11.77) reduce to

$$h = \left(\frac{1}{C_{\alpha h} BS^{1/2}}\right)^{\frac{2}{3(J+1)}} Q^{\frac{2}{3(J+1)}} = C_h Q^{\frac{2}{3(J+1)}}, C_h = \left(\frac{1}{C_{\alpha h} BS^{1/2}}\right)^{\frac{2}{3(J+1)}} \tag{11.84}$$

$$C = (C_{\alpha h})^{\frac{1}{1+J}} \left(\frac{1}{BS^{1/2}}\right)^{\frac{J}{1+J}} Q^{\frac{J}{1+J}} = C_\alpha Q^{\frac{J}{1+J}}, C_\alpha = (C_{\alpha h})^{\frac{1}{J+1}} \left(\frac{1}{BS^{1/2}}\right)^{\frac{J}{1+J}} \tag{11.85}$$

$$V = C_V Q^{\frac{1}{3(J+1)}}, C_V = CC_h^{1/2} S^{1/2} \tag{11.86}$$

For the special case $J = 1$, equations (11.84) to (11.86) become

$$h = \left(\frac{1}{C_{\alpha h} BS^{1/2}}\right)^{1/3} Q^{1/3} = C_h Q^{1/3}, C_h = \left(\frac{1}{C_{\alpha h} BS^{1/2}}\right)^{1/3} \tag{11.87}$$

$$C = (C_{\alpha h})^{1/2} \left(\frac{1}{BS^{1/2}}\right)^{1/2} Q^{1/2} = C_\alpha Q^{1/2}, C_\alpha = (C_{\alpha h})^{1/2} \left(\frac{1}{BS^{1/2}}\right)^{1/2} \tag{11.88}$$

$$V = (C_{\alpha h})^{\frac{1}{3}} \left(\frac{1}{B}\right)^{\frac{2}{3}} S^{\frac{1}{6}} Q^{\frac{2}{3}} = C_V Q^{\frac{2}{3}}, C_V = (C_{\alpha h})^{\frac{1}{3}} \left(\frac{1}{B}\right)^{\frac{2}{3}} S^{\frac{1}{6}} \tag{11.89}$$

Possibility IV: Hydraulic Geometry Relations for Depth, Velocity and Roughness

Equations (11.78) to (11.80) show that the flow depth varies with discharge raised to the power $f = 3/[5(1 + J)]$, the velocity varies with discharge raised to the power

$m = (5J - 2)/[5(1 + J)]$ and Manning's n varies with discharge raised to the power $p = J/(1 + J)$. The precise values of f, m, and p depend on the weighting factor J, which specifies the proportion for adjustment of stream power among h, n, and V, as shown in Fig. 11-3. In limiting cases, exponent f varies from 1 to 0, m from –2/5, and p from –1 to 0 when the weighting factor varies from $J = 0$ to $J = \infty$, as shown in Table 11-5. These derived exponent values encompass the range reported by Wolman (1955), as shown in Table 11-6. For the special case $J = 1$, where the adjustment is equally proportioned, $f = 0.3$ as seen in equation (11.81), $m = 3/10$ as shown by equation (11.83), and p is –1/2, as exhibited by equation (11.82); the f value is close to what Langbein (1964) found using the principle of minimum variance; and the m value is the same as derived by Li (1975) using the tractive force theory. Scale factors C_h, C_V, and C_α vary with flow resistance and slope. This discussion illustrates that the values of exponents f, m, and p do not possess fixed values; rather, they vary over certain ranges dictated by the way the adjustment of stream power is distributed among variables.

11.4.4 Possibility V

Possibility V: $P_h = P_S$, $S = C_{Sh}h^{2\beta K/3}$ or $h = C_{Sh}^{*}S^{3/(2\beta K)}$

Inserting equation (11.26a) in equation (11.7) and a little algebraic manipulation lead to

$$h = \left(\frac{1}{\alpha B}\right)^{\frac{3}{\beta(3+K)}}\left(\frac{1}{C_{Sh}}\right)^{\frac{3}{2\beta(3+K)}} Q^{\frac{3}{\beta(3+K)}} = C_h Q^{\frac{3}{\beta(3+K)}},\ C_h = \left(\frac{1}{\alpha B}\right)^{\frac{3}{\beta(3+K)}}\left(\frac{1}{C_{Sh}}\right)^{\frac{3}{2\beta(3+K)}} \tag{11.90}$$

$$S = \left(\frac{1}{\alpha B}\right)^{\frac{2K}{3+K}} (C_{Sh})^{\frac{3}{3+K}} Q^{\frac{2K}{3+K}} = C_S Q^{\frac{2K}{3+K}},\ C_S = \left(\frac{1}{\alpha B}\right)^{\frac{2K}{3+K}} (C_{Sh})^{\frac{3}{3+K}} \tag{11.91}$$

$$V = \alpha C_h^{\beta-1} C_S^{\frac{1}{2}} Q^{\frac{3(\beta-1)+K\beta}{\beta(3+K)}} = C_V Q^{\frac{3(\beta-1)+K\beta}{\beta(3+K)}},\ C_V = \alpha C_h^{\beta-1} C_S^{\frac{1}{2}} \tag{11.92}$$

For Manning's equation, $\alpha = 1/n$ and $\beta = 5/3$, equations (11.90) to (11.92) reduce to

$$h = \left(\frac{n}{B}\right)^{\frac{9}{5(3+K)}}\left(\frac{1}{C_{Sh}}\right)^{\frac{9}{10(3+K)}} Q^{\frac{9}{5(3+K)}} = C_h Q^{\frac{9}{5(3+K)}},\ C_h = \left(\frac{1}{\alpha B}\right)^{\frac{9}{5(3+K)}}\left(\frac{1}{C_{Sh}}\right)^{\frac{9}{10(3+K)}} \tag{11.93}$$

$$S = \left(\frac{n}{B}\right)^{\frac{2K}{3+K}} (C_{Sh})^{\frac{3}{3+K}} Q^{\frac{2K}{3+K}} = C_S Q^{\frac{2K}{3+K}},\ C_S = \left(\frac{n}{B}\right)^{\frac{2K}{3+K}} (C_{Sh})^{\frac{3}{3+K}} \tag{11.94}$$

$$V = \alpha C_h^{\frac{2}{3}} C_S^{\frac{1}{2}} Q^{\frac{6+5K}{5(3+K)}} = C_V Q^{\frac{6+5K}{5(3+K)}},\ C_V = \alpha C_h^{\frac{2}{3}} C_S^{\frac{1}{2}} \tag{11.95}$$

For the special case $K = 1$, equations (11.93) to (11.95) become

$$h = \left(\frac{n}{B}\right)^{\frac{9}{20}} \left(\frac{1}{C_{Sh}}\right)^{\frac{9}{40}} Q^{\frac{9}{20}} = C_h Q^{\frac{9}{20}}, C_h = \left(\frac{1}{\alpha B}\right)^{\frac{9}{20}} \left(\frac{1}{C_{Sh}}\right)^{\frac{9}{40}} \tag{11.96}$$

$$S = \left(\frac{n}{B}\right)^{1/2} (C_{Sh})^{3/4} Q^{1/2} = C_S Q^{1/2}, C_S = \left(\frac{n}{B}\right)^{1/2} (C_{Sh})^{3/4} \tag{11.97}$$

$$V = \alpha C_h^{\frac{2}{3}} C_S^{\frac{1}{2}} Q^{\frac{11}{20}} = C_V Q^{\frac{11}{20}}, C_V = \alpha C_h^{\frac{2}{3}} C_S^{\frac{1}{2}} \tag{11.98}$$

For Chezy's equation, $\alpha = C$ and $\beta = 3/2$, equations (11.90) to (11.92) become

$$h = \left(\frac{1}{CB}\right)^{\frac{2}{3(3+K)}} \left(\frac{1}{C_{Sh}}\right)^{\frac{1}{3+K}} Q^{\frac{2}{3+K}} = C_h Q^{\frac{2}{3+K}}, C_h = \left(\frac{1}{CB}\right)^{\frac{2}{3(3+K)}} \left(\frac{1}{C_{Sh}}\right)^{\frac{1}{3+K}} \tag{11.99}$$

$$S = \left(\frac{1}{CB}\right)^{\frac{2K}{3+K}} (C_{Sh})^{\frac{3}{3+K}} Q^{\frac{2K}{3+K}} = C_S Q^{\frac{2K}{3+K}}, C_S = \left(\frac{1}{CB}\right)^{\frac{2K}{3+K}} (C_{Sh})^{\frac{3}{3+K}} \tag{11.100}$$

$$V = C C_h^{\frac{1}{2}} C_s^{\frac{1}{2}} Q^{\frac{K+1}{3+K}} = C_V Q^{\frac{K+1}{(3+K)}}, C_V = C C_h^{\frac{1}{2}} C_s^{\frac{1}{2}} \tag{11.101}$$

For the special case $K = 1$, equations (11.99) to (11.101) reduce to

$$h = \left(\frac{1}{CB}\right)^{1/6} \left(\frac{1}{C_{Sh}}\right)^{1/4} Q^{1/2} = C_h Q^{1/2}, C_h = \left(\frac{1}{CB}\right)^{1/6} \left(\frac{1}{C_{Sh}}\right)^{1/4} \tag{11.102}$$

$$S = \left(\frac{1}{CB}\right)^{1/2} (C_{Sh})^{3/4} Q^{1/2} = C_S Q^{1/2}, C_S = \left(\frac{1}{CB}\right)^{1/2} (C_{Sh})^{3/4} \tag{11.103}$$

$$V = C C_h^{\frac{1}{2}} C_s^{\frac{1}{2}} Q^{\frac{1}{2}} = C_V Q^{\frac{1}{2}}, C_V = C C_h^{\frac{1}{2}} C_s^{\frac{1}{2}} \tag{11.104}$$

Possibility V: Hydraulic Geometry Relations for Depth, Velocity, and Slope

Equations (11.93) to (11.95) show that the flow depth varies with discharge raised to the power $f = 9/[5(3 + K)]$, the velocity varies with discharge raised to the power $m = (6 + 5K)/[5(3 + K)]$, and slope varies with discharge raised to the power $y = 2K/(3 + K)$. The precise values of f, m, and y depend on the weighting factor K, which specifies the proportion for adjustment of stream power among h, S, and V, as shown in Fig. 11-3. In limiting cases, exponent f varies from 9/15 to 0, m varies from 2/5 to 1, and y varies from 0 to 2, when the weighting factor varies from $K = 0$ to $K = \infty$ (Table 11-5). The m value of 0.4 (for $K = 0$) is the same

as that reported in the literature (Singh 2003; Singh and Zhang, 2008a, b). The derived exponent values are seen to envelop the reported range, as seen in Table 11-6. The precise exponent values depend on the value of K, which specifies the proportion for adjustment of stream power among h, S, and V. For the special case $K = 1$, where the adjustment is equally proportioned, $f = 9/20$, as seen in equation (11.99), m is 11/20 as seen in equation (11.101), and y is 1/5, as exhibited by equation (11.100); the f value is about as large as that derived by Langbein (1964) using the theory of minimum variance. Scale factors C_h, C_V, and C_S vary with width and resistance. Thus it is seen that the values of exponents f, m, and y do not possess fixed values; rather they vary over certain ranges, dictated by the way the adjustment of stream power is distributed among variables.

11.4.5 Possibility VI

Possibility VI: $P_S = P_\alpha$, $S = C_{S\alpha}\alpha^{2F/3}$ or $\alpha = C^*_{S\alpha}S^{3/(2F)}$

Inserting equation (11.29a) in equation (11.7) and a little algebraic manipulation lead to

$$\alpha = \left(\frac{1}{C_{S\alpha}}\right)^{\frac{3}{2(3+F)}}\left(\frac{1}{B}\right)^{\frac{3}{3+F}}\left(\frac{1}{h}\right)^{\frac{3\beta}{3+F}}Q^{\frac{3}{3+F}} = C_\alpha Q^{\frac{3}{3+F}}, C_\alpha = \left(\frac{1}{C_{S\alpha}}\right)^{\frac{3}{2(3+F)}}\left(\frac{1}{B}\right)^{\frac{3}{3+F}}\left(\frac{1}{h}\right)^{\frac{3\beta}{3+F}} \tag{11.105}$$

$$S = (C_{S\alpha})^{\frac{3}{F+3}}B^{-\frac{2F}{F+3}}h^{-\frac{2\beta F}{F+3}}Q^{\frac{2F}{3+F}} = C_S Q^{\frac{2F}{3+F}}, C_S = (C_{S\alpha})^{\frac{3}{F+3}}B^{-\frac{2F}{F+3}}h^{-\frac{2\beta F}{F+3}} \tag{11.106}$$

$$V = h^{\beta-1}C_\alpha C_S Q^{\frac{3+2F}{3+F}} = C_V Q^{\frac{3+2F}{3+F}}, C_V = h^{\beta-1}C_\alpha C_S \tag{11.107}$$

For Manning's equations, $\alpha = 1/n$ and $\beta = 5/3$, equations (11.105) to (11.107) reduce to

$$n = C_{S\alpha}^{\frac{3}{2(3+F)}}B^{\frac{3}{3+F}}h^{\frac{5}{3+F}}Q^{-\frac{3}{3+F}} = C_\alpha Q^{-\frac{3}{3+F}}, C_\alpha = C_{S\alpha}^{\frac{3}{2(3+F)}}B^{\frac{3}{3+F}}h^{\frac{5}{3+F}} \tag{11.108}$$

$$S = (C_{S\alpha})^{\frac{3}{F+3}}B^{-\frac{2F}{F+3}}h^{-\frac{2\beta F}{F+3}}Q^{\frac{2F}{3+F}} = C_S Q^{\frac{2F}{3+F}}, C_S = (C_{S\alpha})^{\frac{3}{F+3}}B^{-\frac{2F}{F+3}}h^{-\frac{10F}{3(F+3)}} \tag{11.109}$$

$$V = C_V Q^{\frac{3+2F}{3+F}}, C_V = h^{3/2}C_\alpha C_S \tag{11.110}$$

For the special case $F = 1$, equations (11.108) to (11.110) reduce to

$$n = C_{S\alpha}^{3/8}B^{3/4}h^{5/4}Q^{-3/4} = C_\alpha Q^{-3/4}, C_\alpha = C_{S\alpha}^{3/8}B^{3/4}h^{5/4} \tag{11.111}$$

$$S = (C_{S\alpha})^{3/4}B^{-1/2}h^{-5/2}Q^{1/2} = C_S Q^{1/2}, C_S = (C_{S\alpha})^{3/4}B^{-1/2}h^{-5/6} \tag{11.112}$$

$$V = C_V Q^{5/4}, C_V = h^{2/3}C_\alpha C_S \tag{11.113}$$

For Chezy's equation, $\alpha = C$ and $\beta = 3/2$, equations (11.111) to (11.113) reduce to

$$C = C_{S\alpha}^{-\frac{3}{2(3+F)}} B^{-\frac{3}{3+F}} h^{-\frac{9}{2(3+F)}} Q^{\frac{3}{3F}} = C_\alpha Q^{\frac{3}{3+F}}, C_\alpha = C_{S\alpha}^{-\frac{3}{2(3+F)}} B^{-\frac{3}{3+F}} h^{-\frac{9}{2(3+F)}} \quad (11.114)$$

$$S = (C_{S\alpha})^{\frac{3}{F+3}} B^{-\frac{2F}{F+3}} h^{-\frac{3F}{F+3}} Q^{\frac{2F}{3+F}} = C_S Q^{\frac{2F}{3+F}}, C_S = (C_{S\alpha})^{\frac{3}{F+3}} B^{-\frac{2F}{F+3}} h^{-\frac{3F}{F+3}} \quad (11.115)$$

$$V = C_V Q^{\frac{3+2F}{3+F}}, C_V = h^{1/2} C_\alpha C_S \quad (11.116)$$

For the special case, $F = 1$, equations (11.114) to (11.116) reduce to

$$C = C_{S\alpha}^{-3/8} B^{-3/4} h^{-9/8} Q^{3/4} = C_\alpha Q^{3/4}, C_\alpha = C_{S\alpha}^{-3/8} B^{-3/4} h^{-9/8} \quad (11.117)$$

$$S = (C_{S\alpha})^{3/4} B^{-1/2} h^{-3/4} Q^{1/2} = C_S Q^{1/2}, C_S = (C_{S\alpha})^{3/4} B^{-1/2} h^{-3/4} \quad (11.118)$$

$$V = C_V Q^{5/4}, C_V = h^{1/2} C_\alpha C_S \quad (11.119)$$

Possibility VI: Hydraulic Geometry Relations for Velocity, Roughness, and Slope

Equations (11.108) to (11.110) show that slope varies with discharge raised to the power $y = 2F/(3 + F)$, the velocity varies with discharge raised to the power $m = [3 + 2F]/(3 + F)$], and Manning's n varies with discharge raised to the power $p = 3/(3 + F)$. In limiting cases, when the weighting factor $F = 0$, exponents $m = 2$, $p = -1$, and $y = 0$; and when F tends to ∞, $m = 1$, $p = 0$, and $y = 2$. These derived exponent values encompass the reported range (Table 11-6). The precise values of m, p, and y depend on the weighting factor F, which specifies the proportion for adjustment of stream power among V, n, and S, as shown in Fig. 11-3. For the special case $F = 1$, where the adjustment is equally proportioned, $m = 5/4$, as seen in equation (11.116), the value of f is $-3/4$ as shown by equation (11.114), and F is $1/2$, as exhibited by equation (11.115). Scale factors C_V, C_n, and C_p vary with the flow depth and width. This discussion illustrates that the values of exponents m, p, and y do not possess fixed values; rather they vary over certain ranges, depending on the way the adjustment of stream power is distributed among variables.

11.4.6 Possibility VII

Possibility VII: $P_B = P_h = P_\omega$, $B = C_{Bh} h^{\beta/r}$, $\alpha = C_{\alpha B} B^w$, or $\alpha = C_{\alpha h} h^{I\beta}$

Substitution of equations (11.18a), (11.20a), and (11.24a) in equation (11.7) leads to

$$B = C_{\alpha B}^{-\frac{1}{1+w+\gamma}} C_{Bh}^{\frac{\gamma}{1+w+r}} S^{-\frac{1}{2(1+w+r)}} Q^{\frac{1}{1+w+\gamma}} = C_B Q^{\frac{1}{1+w+r}}, C_B = C_{\alpha B}^{-\frac{1}{1+w+r}} C_{Bh}^{\frac{\gamma}{1+w+r}} S^{-\frac{1}{2(1+w+r)}} \quad (11.120)$$

$$h = (C_{Bh}C_{\alpha h})^{-\frac{r}{\beta(1+r+rJ)}} S^{-\frac{1}{2\beta(1+r+rJ)}} Q^{\frac{r}{\beta(1+r+rJ)}} = C_h Q^{\frac{r}{\beta(1+r+rJ)}},$$
$$C_h = (C_{Bh}C_{\alpha h})^{-\frac{r}{\beta(1+r+rJ)}} S^{-\frac{1}{2\beta(1+r+rJ)}} \tag{11.121}$$

$$V = \frac{1}{C_B C_h} Q^{1-\frac{1}{1+w+r}-\frac{\gamma}{\beta(1+r+rJ)}} = C_V Q^{1-\frac{1}{1+w+r}-\frac{\gamma}{\beta(1+r+rJ)}}, C_V = \frac{1}{C_B C_h} \tag{11.122}$$

$$\alpha = C_{\alpha B}^{\frac{J}{J+w+Jw}} C_{\alpha h}^{\frac{w}{J+w+Jw}} S^{-\frac{wJ}{2(J+w+Jw)}} Q^{\frac{Jw}{J+w+Jw}} = C_\alpha Q^{\frac{Jw}{J+w+Jw}},$$
$$C_\alpha = C_{\alpha B}^{\frac{J}{J+w+Jw}} C_{\alpha h}^{\frac{w}{J+w+Jw}} S^{-\frac{wJ}{2(J+w+Jw)}} \tag{11.123}$$

For Manning's equation, $\alpha = 1/n$ and $\beta = 5/3$, equations (11.120) to (11.123) reduce to

$$B = C_{\alpha B}^{-\frac{1}{1+w+\gamma}} C_{Bh}^{\frac{r}{1+w+r}} S^{-\frac{1}{2(1+w+r)}} Q^{\frac{1}{1+w+r}} = C_B Q^{\frac{1}{1+w+r}},$$
$$C_B = C_{\alpha B}^{-\frac{1}{1+w+r}} C_{Bh}^{\frac{r}{1+w+r}} S^{-\frac{1}{2(1+w+r)}} \tag{11.124}$$

$$h = (C_{Bh}C_{\alpha h})^{-\frac{3r}{5(1+r+rJ)}} S^{-\frac{3}{10(1+r+rJ)}} Q^{\frac{3r}{5(1+r+rJ)}} = C_h Q^{\frac{3r}{5(1+r+rJ)}},$$
$$C_h = (C_{Bh}C_{\alpha h})^{-\frac{3r}{5(1+r+rJ)}} S^{-\frac{3}{10(1+r+rJ)}} \tag{11.125}$$

$$V = \frac{1}{C_B C_h} Q^{1-\frac{1}{1+w+r}-\frac{3}{5(1+r+rJ)}} = C_V Q^{1-\frac{1}{1+w+r}-\frac{3}{5(1+r+rJ)}}, C_V = \frac{1}{C_B C_h} \tag{11.126}$$

$$n = C_{\alpha B}^{-\frac{J}{J+w+Jw}} C_{\alpha h}^{-\frac{w}{J+w+Jw}} S^{\frac{wJ}{2(J+w+Jw)}} Q^{-\frac{Jw}{J+w+Jw}} = C_\alpha Q^{-\frac{Jw}{J+w+Jw}},$$
$$C_\alpha = C_{\alpha B}^{-\frac{J}{J+w+Jw}} C_{\alpha h}^{-\frac{w}{J+w+Jw}} S^{\frac{wJ}{2(J+w+Jw)}} \tag{11.127}$$

For the special case $J = r = w = 1$, equations (11.124) to (11.127) become

$$B = C_{\alpha B}^{-1/3} C^{1/3} S^{-1/6} Q^{1/3} = C_B Q^{1/3}, C_B = C_{\alpha B}^{-1/3} C_{Bh}^{1/3} S^{-1/6} \tag{11.128}$$

$$h = (C_{Bh}C_{\alpha h})^{-1/5} S^{-1/10} Q^{1/5} = C_h Q^{1/5}, C_h = (C_{Bh}C_{\alpha h})^{-1/5} S^{-1/10} \tag{11.129}$$

$$V = \frac{1}{C_B C_h} Q^{7/15} = C_V Q^{7/15}, C_V = \frac{1}{C_B C_h} \tag{11.130}$$

$$n = C_{\alpha\beta}^{-1/3} C_{\alpha h}^{-1/3} S^{1/6} Q^{-1/3} = C_\alpha Q^{-1/3}, C_\alpha = C_{\alpha\beta}^{-1/3} C_{\alpha h}^{-1/3} S^{1/6} \tag{11.131}$$

For Chezy's equation, $\alpha = C$ and $\beta = 3/2$, equations (11.120) to (11.123) reduce to

$$\begin{aligned} B &= C_{\alpha B}^{-\frac{1}{1+w+\gamma}} C_{Bh}^{\frac{\gamma}{1+w+r}} S^{-\frac{1}{2(1+w+r)}} Q^{\frac{1}{1+w+\gamma}} = C_B Q^{\frac{1}{1+w+r}}, \\ C_B &= C_{\alpha B}^{-\frac{1}{1+w+r}} C_{Bh}^{\frac{\gamma}{1+w+r}} S^{-\frac{1}{2(1+w+r)}} \end{aligned} \tag{11.132}$$

$$\begin{aligned} h &= (C_{Bh} C_{\alpha h})^{-\frac{2r}{3(1+r+rJ)}} S^{-\frac{1}{3(1+r+rJ)}} Q^{\frac{2r}{3(1+r+rJ)}} = C_h Q^{\frac{2r}{3(1+r+rJ)}}, \\ C_h &= (C_{Bh} C_{\alpha h})^{-\frac{2r}{3(1+r+rJ)}} S^{-\frac{1}{3(1+r+rJ)}} \end{aligned} \tag{11.133}$$

$$V = \frac{1}{C_B C_h} Q^{1-\frac{1}{1+w+r}-\frac{2}{3(1+r+rJ)}} = C_V Q^{1-\frac{1}{1+w+r}-\frac{2}{3(1+r+rJ)}}, C_V = \frac{1}{C_B C_h} \tag{11.134}$$

$$\begin{aligned} C &= C_{\alpha B}^{\frac{J}{J+w+Jw}} C_{\alpha h}^{\frac{w}{J+w+Jw}} S^{-\frac{wJ}{2(J+w+Jw)}} Q^{\frac{Jw}{J+w+Jw}} = C_\alpha Q^{\frac{Jw}{J+w+Jw}}, \\ C_\alpha &= C_{\alpha B}^{\frac{J}{J+w+Jw}} C_{\alpha h}^{\frac{w}{J+w+Jw}} S^{-\frac{wJ}{2(J+w+Jw)}} \end{aligned} \tag{11.135}$$

For the special case $r = w = J = 1$, equations (11.132) to (11.135) reduce to

$$B = C_{\alpha B}^{-1/3} C_{Bh}^{1/3} S^{-1/6} Q^{1/3} = C_B Q^{1/3}, C_B = C_{\alpha B}^{-1/3} C_{Bh}^{1/3} S^{-1/6} \tag{11.136}$$

$$h = (C_{Bh} C_{\alpha h})^{-2/9} S^{-1/9} Q^{2/9} = C_h Q^{2/9}, C_h = (C_{Bh} C_{\alpha h})^{-2/9} S^{-1/9} \tag{11.137}$$

$$V = \frac{1}{C_B C_h} Q^{4/9} = C_V Q^{4/9}, C_V = \frac{1}{C_B C_h} \tag{11.138}$$

$$C = C_{\alpha\beta}^{1/3} C_{\alpha h}^{1/3} S^{-1/6} Q^{1/3} = C_\alpha Q^{1/3}, C_\alpha = C_{\alpha\beta}^{1/3} C_{\alpha h}^{1/3} S^{-1/6} \tag{11.139}$$

Possibility VII: Hydraulic Geometry Relations for Width, Depth, Velocity, and Roughness

Equations (11.124) to (11.126) show that the flow width varies with discharge raised to the power $b = 1/(1 + w + r)$, depth varies with discharge raised to the power $f = 3r/[5(1 + r + rJ)]$, velocity varies with discharge raised to the power $m = 1 - [1/(1 + w + r)] - \{3/[5(1 + r + rJ)]\}$, and Manning's n varies with discharge raised to the power $p = Jw/(J + w + Jw)$. The precise values of b, f, m, and p depend on the weighting factors r, w, and J, which specify the proportion for adjustment of stream power among B, h, V, and n, as shown in Fig. 11-3. The value of exponent b varies from 0 to 1, exponent f varies from 0 to 1/5 to 0, m varies from –3/5 to 1, and p varies from –1 to 0, as exhibited in Table 11-5, as the weighting factors w, r, and J vary from 0 to ∞. For the special case $w = r = J = 1$, the value of b

becomes 1/3, as shown in equation (11.122), f becomes 1/5, as shown in equation (11.123), the m exponent value becomes 7/15, as shown in equation (11.123), and the value of p becomes –1/3, as shown in equation (11.125). The derived exponent values encompass the range reported in the literature (Singh 2003; Singh and Zhang, 2008a, b; Table 11-6). The discussion shows that the values of the b, f, m, and p exponents are not fixed; rather, they vary over certain ranges, as exhibited in equations (11.122) to (11.125). The variation is indeed continuous and is dictated by the way the adjustment of stream power is distributed among variables. Under this possibility, the adjustment occurs simultaneously in river width, depth, velocity, and roughness.

11.4.7 Possibility VIII

Possibility VIII: $P_B = P_\alpha = P_S$, $\alpha = C_{\alpha B}B^w$, $S = C_{S\alpha}\alpha^{2F/3}$, or $S = C_{SB}B^{2I/3}$

Substitution of equations (11.20a), (11.22a), and (11.29a) in equation (11.7) lead to

$$\begin{aligned} B &= (C_{\alpha B}C_{SB}^{1/2})^{-\frac{3}{3w+3+I}} h^{-\frac{3\beta}{3w+3+I}} Q^{\frac{3}{3w+3+I}} = C_B Q^{\frac{3}{3w+3+I}}, \\ C_B &= (C_{\alpha B}C_{SB}^{1/2})^{-\frac{3}{3w+3+I}} h^{-\frac{3\beta}{3w+3+I}} \end{aligned} \tag{11.140}$$

$$\begin{aligned} \alpha &= C_{\alpha B}^{\frac{3}{3+3w+Fw}} C_{S\alpha}^{-\frac{3w}{2(3+3w+Fw)}} h^{-\frac{3w\beta}{3w+3+Fw}} Q^{\frac{3w}{3w+3+Fw}} = C_\alpha Q^{\frac{3w}{3w+3+Fw}}, \\ C_\alpha &= C_{\alpha B}^{\frac{3}{3+3w+Fw}} C_{S\alpha}^{-\frac{3w}{2(3+3w+Fw)}} h^{-\frac{3w\beta}{3w+3+Fw}} \end{aligned} \tag{11.141}$$

$$\begin{aligned} S &= C_{S\alpha}^{-\frac{3I}{3I+3F+FI}} C_{SB}^{\frac{3F}{3I+3F+FI}} h^{-\frac{2\beta FI}{3I+3F+3FI}} Q^{\frac{2FI}{3I+3F+FI}} = C_s Q^{\frac{2FI}{3I+3F+FI}}, \\ C_S &= C_{S\alpha}^{-\frac{3I}{3I+3F+FI}} C_{SB}^{\frac{3F}{3I+3F+FI}} h^{-\frac{2\beta FI}{3I+3F+3FI}} \end{aligned} \tag{11.142}$$

$$\begin{aligned} V &= C_\alpha C_S^{1/2} h^{\beta-1} Q^{\frac{3w}{3+3w+Fw}+\frac{FI}{3I+3F+3FI}} = C_V Q^{\frac{3w}{3+3w+Fw}+\frac{FI}{3I+3F+3FI}}, \\ C_V &= C_\alpha C_S^{1/2} h^{\beta-1} \end{aligned} \tag{11.143}$$

For Manning's equation, $\alpha = 1/n$ and $\beta = 5/3$, equations (11.140) to (11.143) reduce to

$$\begin{aligned} B &= (C_{\alpha B}C_{SB}^{1/2})^{-\frac{3}{3w+3+I}} h^{-\frac{5}{3w+3+I}} Q^{\frac{3}{3w+3+I}} = C_B Q^{\frac{3}{3w+3+I}}, \\ C_B &= (C_{\alpha B}C_{SB}^{1/2})^{-\frac{3}{3w+3+I}} h^{-\frac{5}{3w+3+I}} \end{aligned} \tag{11.144}$$

$$\begin{aligned} n &= C_{\alpha B}^{-\frac{3}{3+3w+Fw}} C_{S\alpha}^{\frac{3w}{2(3+3w+Fw)}} h^{\frac{5w}{3w+3+Fw}} Q^{-\frac{3w}{3w+3+Fw}} = C_\alpha Q^{-\frac{3w}{3w+3+Fw}}, \\ C_\alpha &= C_{\alpha B}^{-\frac{3}{3+3w+Fw}} C_{S\alpha}^{\frac{3w}{2(3+3w+Fw)}} h^{\frac{5w}{3w+3+Fw}} \end{aligned} \tag{11.145}$$

$$S = C_{S\alpha}^{-\frac{3I}{3I+3F+FI}} C_{SB}^{\frac{3F}{3I+3F+FI}} h^{-\frac{10FI}{3(3I+3F+3FI)}} Q^{\frac{2FI}{3I+3F+FI}} = C_s Q^{\frac{2FI}{3I+3F+FI}},$$
$$C_S = C_{S\alpha}^{-\frac{3I}{3I+3F+FI}} C_{SB}^{\frac{3F}{3I+3F+FI}} h^{-\frac{10FI}{3(3I+3F+3FI)}} \tag{11.146}$$

$$V = C_\alpha C_S^{1/2} h^{2/3} Q^{\frac{3w}{3+3w+Fw}+\frac{FI}{3I+3F+3FI}} = C_V Q^{\frac{3w}{3+3w+Fw}+\frac{FI}{3I+3F+3FI}},$$
$$C_V = C_\alpha C_S^{1/2} h^{2/3} \tag{11.147}$$

For the special case $I = w = F = 1$, equations (11.144)-(11.147) become

$$B = (C_{\alpha B} C_{SB}^{1/2})^{-\frac{3}{7}} h^{-\frac{5}{7}} Q^{\frac{3}{7}} = C_B Q^{\frac{3}{7}}, C_B = (C_{\alpha B} C_{SB}^{1/2})^{-\frac{3}{7}} h^{-\frac{5}{7}} \tag{11.148}$$

$$n = C_{\alpha B}^{\frac{3}{7}} C_{S\alpha}^{-\frac{3}{14}} h^{-\frac{5}{7}} Q^{-\frac{3}{7}} = C_\alpha Q^{-\frac{3}{7}}, C_\alpha = C_{\alpha B}^{\frac{3}{7}} C_{S\alpha}^{-\frac{3}{14}} h^{-\frac{5}{7}} \tag{11.149}$$

$$S = C_{S\alpha}^{-3/7} C_{SB}^{3/7} h^{-10/27} Q^{2/7} = C_s Q^{2/7}, C_S = C_{S\alpha}^{-3/7} C_{SB}^{3/7} h^{-10/27} \tag{11.150}$$

$$V = C_\alpha C_S^{1/2} h^{2/3} Q^{\frac{34}{63}} = C_V Q^{\frac{34}{63}}, C_V = C_\alpha C_S^{1/2} h^{2/3} \tag{11.151}$$

For Chezy's equations, $\alpha = C$ and $\beta = 3/2$, equations (11.140) to (11.143) reduce to

$$B = (C_{\alpha B} C_{SB}^{1/2})^{-\frac{3}{3w+3+I}} h^{-\frac{9}{2(3w+3+I)}} Q^{\frac{3}{3w+3+I}} = C_B Q^{\frac{3}{3w+3+I}},$$
$$C_B = (C_{\alpha B} C_{SB}^{1/2})^{-\frac{3}{3w+3+I}} h^{-\frac{9}{2(3w+3+I)}} \tag{11.152}$$

$$C = C_{\alpha B}^{\frac{3}{3+3w+Fw}} C_{S\alpha}^{-\frac{3w}{2(3+3w+Fw)}} h^{-\frac{9w}{2(3w+3+Fw)}} Q^{\frac{3w}{3w+3+Fw}} = C_\alpha Q^{\frac{3w}{3w+3+Fw}},$$
$$C_\alpha = C_{\alpha B}^{\frac{3}{3+3w+Fw}} C_{S\alpha}^{-\frac{3w}{2(3+3w+Fw)}} h^{-\frac{9w}{2(3w+3+Fw)}} \tag{11.153}$$

$$S = C_{S\alpha}^{-\frac{3I}{3I+3F+FI}} C_{SB}^{\frac{3F}{3I+3F+FI}} h^{-\frac{10FI}{3(3I+3F+3FI)}} Q^{\frac{2FI}{3I+3F+FI}} = C_s Q^{\frac{2FI}{3I+3F+FI}},$$
$$C_S = C_{S\alpha}^{-\frac{3I}{3I+3F+FI}} C_{SB}^{\frac{3F}{3I+3F+FI}} h^{-\frac{10FI}{3(3I+3F+3FI)}} \tag{11.154}$$

$$V = C_\alpha C_S^{1/2} h^{1/2} Q^{\frac{3w}{3+3w+Fw}+\frac{FI}{3I+3F+3FI}} = C_V Q^{\frac{3w}{3+3w+Fw}+\frac{FI}{3I+3F+3FI}},$$
$$C_V = C_\alpha C_S^{1/2} h^{1/2} \tag{11.155}$$

For the special case $I = F = w = 1$, equations (11.152) to (11.155) become

$$B = (C_{\alpha B} C_{SB}^{1/2})^{-\frac{3}{7}} h^{-\frac{9}{14}} Q^{\frac{3}{7}} = C_B Q^{\frac{3}{7}}, C_B = (C_{\alpha B} C_{SB}^{1/2})^{-\frac{3}{7}} h^{-\frac{9}{14}} \tag{11.156}$$

$$C = C_{\alpha B}^{\frac{3}{7}} C_{S\alpha}^{-\frac{3}{14}} h^{-\frac{9}{14}} Q^{\frac{3}{7}} = C_\alpha Q^{\frac{3}{7}}, C_\alpha = C_{\alpha B}^{\frac{3}{7}} C_{S\alpha}^{-\frac{3}{14}} h^{-\frac{9}{14}} \tag{11.157}$$

$$S = C_{S\alpha}^{-3/7} C_{SB}^{3/7} h^{-10/27} Q^{2/7} = C_S Q^{2/7}, C_S = C_{S\alpha}^{-3/7} C_{SB}^{3/7} h^{-10/27} \tag{11.158}$$

$$V = C_\alpha C_S^{1/2} h^{1/2} Q^{34/63} = C_V Q^{34/63}, C_V = C_\alpha C_S^{1/2} h^{1/2} \tag{11.159}$$

Possibility VIII: Hydraulic Geometry Relations for Width, Velocity, Roughness, and Slope

Equations (11.144) to (11.147) show that the width varies with discharge raised to the power $b = 3/[3(I + 3w + 3)]$, velocity varies with discharge raised to the power $m = [3w/(3 + 3w + Fw)] - \{FI/[(3I + 3F + 3FI)]\}$, Manning's n varies with discharge raised to the power $p = -3w/(3 + 3w + Fw)$, and slope varies with discharge raised to the power $y = (2FI)/(3I + 3F + FI)$. The precise values of b, m, p, and y depend on the weighting factors w, I, and F, which specify the proportion for adjustment of stream power among B, V, n, and S, as shown in Fig. 11-3. In limiting cases, exponent b varies from 0 to 1, m varies from 0 to 1, p varies from 0 to –3/7 to 0, and y varies from 0 to 2 C_V, when $w = F = I = 0$ to $w = F = I = \infty$. For the special case $w = F = I = 1$, where the adjustment is equally proportioned, $b = 3/7$, as seen in equation (11.142), the value of m is 17/32, as shown in equation (11.145), the value of p is –3/7, and $y = 2/7$, as exhibited in equation (11.143). These derived exponent values encompass the reported range, as shown in Table 11-6. The precise values of b, m, p, and y depend on the weighting factors w, F, and I, which specify the proportion for adjustment of stream power among B, n, S, and V. Scale factors C_B, C_n, C_V, and C_p vary with flow resistance and depth. This discussion shows that the values of exponents, b, m, p, and y do not possess fixed values; rather they vary over certain ranges dictated by the way the adjustment of stream power is distributed among variables.

11.4.8 Possibility IX

Possibility IX: $P_B = P_h = P_S$, $B = C_{Bh} h^{\beta/r}$, $S = C_{Sh} h^{2\beta K/3}$, or $S = C_{SB} B^{2I/3}$

Substitution of equations (11.18a), (11.22a), and (11.26a) in equation (11.7) lead to

$$h = (\alpha C_{Bh} C_{Sh}^{1/2})^{-\frac{3r}{3\beta+3\beta r+\beta rK}} Q^{\frac{3r}{3\beta+3\beta r+\beta rK}}, C_h = (\alpha C_{Bh} C_{Sh}^{1/2})^{-\frac{3r}{3\beta+3\beta r+\beta rK}} \tag{11.160}$$

$$B = \left(\frac{C_{Bh}^r}{\alpha C_{SB}^{1/2}}\right)^{\frac{3}{3+3r+I}} Q^{\frac{3}{3+3\gamma+I}} = C_B Q^{\frac{3}{3+3r+I}}, C_B = \left(\frac{C_{Bh}^r}{\alpha C_{SB}^{1/2}}\right)^{\frac{3}{3+3r+I}} \tag{11.161}$$

$$S = \left(\frac{C_{SB}^{3/2I} C_{Sh}^{3/2K}}{\alpha}\right)^{\frac{2IK}{3I+3K+IK}} Q^{\frac{2IK}{3I+3K+IK}} = C_S Q^{\frac{2IK}{3I+3K+IK}}, C_S = \left(\frac{C_{SB}^{3/2I} C_{Sh}^{3/2K}}{\alpha}\right)^{\frac{2IK}{3I+3K+IK}} \tag{11.162}$$

$$V = \frac{1}{C_h C_B} Q^{1-\frac{3}{3+3rI}-\frac{3r}{3\beta+3\beta r+\beta rK}} = C_V Q^{1-\frac{3}{3+3rI}-\frac{3r}{3\beta+3\beta r+\beta rK}}, C_V = \frac{1}{C_h C_B} \tag{11.163}$$

For Manning's equation, $\alpha = 1/n$ and $\beta = 5/3$, equations (11.159) to (11.163) reduce to

$$h = \left(\frac{1}{n} C_{Bh} C_{Sh}^{1/2}\right)^{-\frac{9r}{15+15r+5rK}} Q^{\frac{9r}{15+15r+5rK}}, C_h = \left(\frac{1}{n} C_{Bh} C_{Sh}^{1/2}\right)^{-\frac{9r}{15+15r+5rK}} \tag{11.164}$$

$$B = \left(\frac{nC_{Bh}^r}{C_{SB}^{1/2}}\right)^{\frac{3}{3+3r+I}} Q^{\frac{3}{3+3r+I}} = C_B Q^{\frac{3}{3+3r+I}}, C_B = \left(\frac{nC_{Bh}^r}{C_{SB}^{1/2}}\right)^{\frac{3}{3+3r+I}} \tag{11.165}$$

$$S = \left(nC_{SB}^{\frac{3}{2I}} C_{Sh}^{\frac{3}{2K}}\right)^{\frac{2IK}{3I+3K+IK}} Q^{\frac{2IK}{3I+3K+IK}} = C_S Q^{\frac{2IK}{3I+3K+IK}}, C_S = \left(nC_{SB}^{\frac{3}{2I}} C_{Sh}^{\frac{3}{2K}}\right)^{\frac{2IK}{3I+3K+IK}} \tag{11.166}$$

$$V = \frac{1}{C_h C_B} Q^{1-\frac{3}{3+3rI}-\frac{9r}{15+15r+5rK}} = C_V Q^{1-\frac{3}{3+3rI}-\frac{9r}{15+15r+5rK}}, C_V = \frac{1}{C_h C_B} \tag{11.167}$$

For the special case $r = k = I = 1$, equations (11.163) to (11.167) become

$$h = \left(\frac{1}{n} C_{Bh} C_{Sh}^{1/2}\right)^{-9/35} Q^{9/35} = C_h Q^{9/35}, C_h = \left(\frac{1}{n} C_{Bh} C_{Sh}^{1/2}\right)^{-9/35} \tag{11.168}$$

$$B = \left(\frac{nC_{Bh}^r}{C_{SB}^{1/2}}\right)^{\frac{3}{7}} Q^{\frac{3}{7}} = C_B Q^{\frac{3}{7}}, C_B = \left(\frac{nC_{Bh}^r}{C_{SB}^{1/2}}\right)^{\frac{3}{7}} \tag{11.169}$$

$$S = (nC_{SB}^{\frac{3}{2}} C_{Sh}^{\frac{3}{2}})^{\frac{2}{7}} Q^{\frac{2}{7}} = C_S Q^{\frac{2}{7}}, C_S = (nC_{SB}^{\frac{3}{2}} C_{Sh}^{\frac{3}{2}})^{\frac{2}{7}} \tag{11.170}$$

$$V = \frac{1}{C_h C_B} Q^{11/35} = C_V Q^{11/35}, C_V = \frac{1}{C_h C_B} \tag{11.171}$$

For Chezy's equation, $\alpha = C$ and $\beta = 3/2$, equations (11.160) to (11.163) reduce to

$$h = (CC_{Bh} C_{Sh}^{1/2})^{-\frac{6r}{9+9r+3rK}} Q^{\frac{6r}{9+9r+3rK}}, C_h = (\alpha C_{Bh} C_{Sh}^{1/2})^{-\frac{6r}{3+9r+3rK}} \tag{11.172}$$

$$B = \left(\frac{C_{Bh}^r}{CC_{SB}^{1/2}}\right)^{\frac{3}{3+3r+I}} Q^{\frac{3}{3+3r+I}} = C_B Q^{\frac{3}{3+3r+I}}, C_B = \left(\frac{C_{Bh}^r}{CC_{SB}^{1/2}}\right)^{\frac{3}{3+3r+I}} \tag{11.173}$$

$$\begin{aligned} S &= \left(\frac{C_{SB}^{3/2I} C_{Sh}^{3/2K}}{C}\right)^{\frac{2IK}{3I+3K+IK}} Q^{\frac{2IK}{3I+3K+IK}} = C_S Q^{\frac{2IK}{3I+3K+IK}}, \\ C_S &= \left(\frac{C_{SB}^{3/2I} C_{Sh}^{3/2K}}{C}\right)^{\frac{2IK}{3I+3K+IK}} \end{aligned} \tag{11.174}$$

$$V = \frac{1}{C_h C_B} Q^{1-\frac{3}{3+3rI}-\frac{6r}{9+9r+3rK}} = C_V Q^{1-\frac{3}{3+3rI}-\frac{6r}{9+9r+9rK}}, C_V = \frac{1}{C_h C_B} \tag{11.175}$$

For the special case $I = r = K = 1$, equations (11.172) to (11.175) reduce to

$$h = (CC_{Bh}C_{Sh}^{1/2})^{-2/7} Q^{2/7} = C_h Q^{2/7}, C_h = (CC_{Bh}C_{Sh}^{1/2})^{-2/7} \tag{11.176}$$

$$B = \left(\frac{C_{Bh}}{CC_{SB}^{1/2}}\right)^{3/7} Q^{3/7} = C_B Q^{3/7}, C_B = \left(\frac{C_{Bh}}{CC_{SB}^{1/2}}\right)^{3/7} \tag{11.177}$$

$$S = \left(\frac{C_{SB}^{3/2}C_{Sh}^{3/2}}{\alpha}\right)^{2/7} Q^{2/7} = C_S Q^{2/7}, C_S = \left(\frac{C_{SB}^{3/2}C_{Sh}^{3/2}}{\alpha}\right)^{2/7} \tag{11.178}$$

$$V = \frac{1}{C_h C_B} Q^{2/7} = C_V Q^{2/7}, C_V = \frac{1}{C_h C_B} \tag{11.179}$$

Possibility IX: Hydraulic Geometry Relations for Width, Depth, Velocity, and Slope

Equations (11.164) to (11.167) show that the width varies with discharge raised to the power $b = 3/(I + 3r + 3)$, depth varies with discharge raised to the power $f = 9r/(15 + 15r + 5rK)$, velocity varies with discharge raised to the power $m = 1 - [3/(3 + 3rI)] - [9r/(15 + 15r + 5rk)]$, and slope varies with discharge raised to the power $y = (2IK)/(3I + 3K + KI)$. The precise values of b, f, m, and y depend on the weighting factors r, I, and K, which specify the proportion for adjustment of stream power among B, h, V, and S, as shown in Fig. 11-3. The value of exponent b varies from 0 to 1, exponent f varies from 0 to 9/35 to 0, exponent m varies from 0 to 1, and exponent y varies from 0 to 2, as shown in Table 11-5. These values encompass the range reported in the literature, as shown in Table 11.3. For the special case $r = I = K = 1$, $b = 3/7$, as shown in equation (11.169), $f = 9/35$, as shown in equation (11.168), $m = 11/35$, as shown in equation (11.171), and $y = 2/7$, as shown in equation (11.170). This discussion shows that the values of the b, f, m, and y exponents are not fixed; rather they vary over certain ranges, as exhibited by equations (11.166) to (11.167). The variation is indeed continuous and is dictated by the way the adjustment of stream power is distributed among variables. Under this possibility, the adjustment occurs simultaneously in river width, depth, velocity, and slope.

11.4.9 Possibility X

Possibility X: $P_h = P_\alpha = P_S$, $\alpha = C_{\alpha h} h^{J\beta}$, $S = C_{S\alpha}\alpha^{2F/3}$, or $S = C_{Sh} h^{2\beta K/3}$

Substitution of equations (11.24a), (11.26a), and (11.29a) in equation (11.7) lead to

$$h = \left(\frac{1}{C_{\alpha h} C_{Sh}^{1/2}}\right)^{\frac{3}{\beta(3+3J+K)}} \left(\frac{1}{B}\right)^{\frac{3}{\beta(3+3J+K)}} Q^{\frac{3}{\beta(3+3J+K)}} = C_h Q^{\frac{3}{\beta(3+3J+K)}},$$
$$C_h = \left(\frac{1}{C_{\alpha h} C_{Sh}^{1/2}}\right)^{\frac{3}{\beta(3+3J+K)}} \left(\frac{1}{B}\right)^{\frac{3}{\beta(3+3J+K)}} \tag{11.180}$$

$$\alpha = \left(\frac{C_{\alpha h}}{C_{S\alpha}^{1/2}}\right)^{\frac{3J}{3J+FJ+3}} B^{-\frac{3J}{3J+FJ+3}} Q^{\frac{3J}{3J+FJ+3}} = C_\alpha Q^{\frac{3J}{3J+FJ+3}},$$
$$C_\alpha = \left(\frac{C_{\alpha h}}{C_{S\alpha}^{1/2}}\right)^{\frac{3J}{3J+FJ+3}} B^{-\frac{3J}{3J+FJ+3}} \tag{11.181}$$

$$S = (C_{S\alpha})^{\frac{3K}{FK+3K+3F}} (C_{Sh})^{\frac{3F}{FK+3K+3F}} \left(\frac{1}{B}\right)^{\frac{2FK}{FK+3K+3F}} Q^{\frac{2FK}{FK+3K+3K}} = C_{Sh} Q^{\frac{2FK}{Fk+3K+3K}}$$
$$C_{Sh} = (C_{S\alpha})^{\frac{3K}{FK+3K+3F}} (C_{Sh})^{\frac{3F}{FK+3K+3F}} \left(\frac{1}{B}\right)^{\frac{2FK}{FK+3K+3F}} \tag{11.182}$$

$$V = (C_{\alpha h} C_{Sh}^{1/2}) C_h^{J\beta+\beta+\beta K/3} Q^{\frac{3J\beta+3\beta+\beta K-3}{\beta(3+3J+K)}}, C_V = (C_{\alpha h} C_{Sh}^{1/2}) C_h^{J\beta+\beta+\beta K/3} \tag{11.183}$$

For Manning's equation, $\alpha = 1/n$ and $\beta = 5/3$, equations (11.180) to (11.183) reduce to

$$h = \left(\frac{1}{C_{\alpha h} C_{Sh}^{1/2}}\right)^{\frac{9}{5(3+3J+K)}} \left(\frac{1}{B}\right)^{\frac{9}{5(3+3J+K)}} \cdot Q^{\frac{9}{9(3+3J+K)}} = C_h Q^{\frac{9}{9(3+3J+K)}},$$
$$C_h = (C_{\alpha h} C_{Sh}^{1/2})^{-9/[5(3+3J+K)]} B^{-9/[5(3+3J+K)]} \tag{11.184}$$

$$n = \left(\frac{C_{\alpha h}}{C_{S\alpha}^{1/2}}\right)^{-\frac{3J}{3J+FJ+3}} B^{-\frac{3J}{3J+FJ+3}} Q^{-\frac{3J}{3J+FJ+3}} = C_\alpha Q^{-\frac{3J}{3J+FJ+3}},$$
$$C_\alpha = \left(\frac{C_{\alpha h}}{C_{S\alpha}^{1/2}}\right)^{-\frac{3J}{3J+FJ+3}} B^{-\frac{3J}{3J+FJ+3}} \tag{11.185}$$

$$S = (C_{S\alpha})^{\frac{3K}{FK+3K+3F}} (C_{Sh})^{\frac{3F}{FK+3K+3F}} \left(\frac{1}{B}\right)^{\frac{2FK}{FK+3K+3F}} Q^{\frac{2FK}{FK+3K+3K}} = C_{Sh} Q^{\frac{2FK}{Fk+3K+3K}}$$
$$C_{Sh} = (C_{S\alpha})^{\frac{3K}{FK+3K+3F}} (C_{Sh})^{\frac{3F}{FK+3K+3F}} \left(\frac{1}{B}\right)^{\frac{2FK}{FK+3K+3F}} \tag{11.186}$$

$$V = C_V Q^{\frac{3J}{3J+FJ+3} + \frac{6}{5(3+3J+K)} + \frac{FK}{FK+3K+3F}}, C_V = (C_{\alpha h} C_{Sh}^{1/2}) C_h^{\frac{15J+15+5K}{9}} \tag{11.187}$$

For the special case $J = K = F = 1$, equations (11.184) to (11.187) become

$$h = \left(C_{\alpha h} C_{Sh}^{1/2}\right)^{9/35} B^{-9/35} Q^{9/35} = C_h Q^{9/35}, C_h = \left(C_{\alpha h} C_{Sh}^{1/2}\right)^{9/35} B^{-9/35} \tag{11.188}$$

$$n = \left(\frac{C_{\alpha h}}{C_{S\alpha}^{1/2}}\right)^{-3/7} B^{3/7} Q^{-3/7} = C_\alpha Q^{-3/7}, C_\alpha = \left(\frac{C_{\alpha h}}{C_{S\alpha}^{1/2}}\right)^{-3/7} B^{3/7} \tag{11.189}$$

$$S = \left(C_{S\alpha} C_{Sh}\right)^{3/7} B^{-2/7} Q^{2/7} = C_{Sh} Q^{2/7}, \quad C_{Sh} = \left(C_{S\alpha} C_{Sh}\right)^{3/7} B^{-2/7} \tag{11.190}$$

$$V = C_V Q^{26/35} \tag{11.191}$$

For Chezy's equation, $\alpha = C$ and $\beta = 3/2$, equations (11.180) to (11.183) reduce to

$$\begin{aligned} h &= \left(C_{\alpha h} C_{Sh}^{-1/2}\right)^{-\frac{2}{3+3J+K}} B^{-\frac{2}{3+3J+K}} Q^{\frac{2}{3+3J+K}} = C_h Q^{\frac{2}{3+3J+K}}, \\ C_h &= \left(C_{\alpha h} C_{Sh}^{-1/2}\right)^{-\frac{2}{3+3J+K}} B^{-\frac{2}{3+3J+K}} \end{aligned} \tag{11.192}$$

$$\begin{aligned} C &= \left(C_{\alpha h} C_{S\alpha}^{-1/2}\right)^{\frac{3J}{3+3J+FJ}} B^{-\frac{3J}{3+3J+FJ}} Q^{\frac{3J}{3+3J+FJ}} = C_\alpha Q^{\frac{3J}{3+3J+FJ}}, \\ C_\alpha &= \left(C_{\alpha h} C_{S\alpha}^{-1/2}\right)^{\frac{3J}{3+3J+FJ}} B^{-\frac{3J}{3+3J+FJ}} \end{aligned} \tag{11.193}$$

$$\begin{aligned} S &= \left(C_{S\alpha}\right)^{\frac{3K}{FK+3K+3F}} \left(C_{Sh}\right)^{\frac{3F}{FK+3K+3F}} \left(\frac{1}{B}\right)^{\frac{2FK}{FK+3K+3F}} Q^{\frac{2FK}{FK+3K+3K}} = C_{Sh} Q^{\frac{2FK}{Fk+3K+3K}} \\ C_{Sh} &= \left(C_{S\alpha}\right)^{\frac{3K}{FK+3K+3F}} \left(C_{Sh}\right)^{\frac{3F}{FK+3K+3F}} \left(\frac{1}{B}\right)^{\frac{2FK}{FK+3K+3F}} \end{aligned} \tag{11.194}$$

$$V = \left(C_{\alpha h} C_{Sh}^{1/2}\right) C_h^{(3J+1+K)/2} Q^{\frac{3J+K+1}{3+3J+K}}, C_V = \left(C_{\alpha h} C_{Sh}^{1/2}\right) C_h^{\frac{3J+1+K}{2}} \tag{11.195}$$

For the special case $J = K = F = 1$, equations (11.192) to (11.195) become

$$h = \left(C_{\alpha h} C_{Sh}^{-1/2}\right)^{-2/7} B^{-2/7} Q^{2/7} = C_h Q^{2/7}, C_h = \left(C_{\alpha h} C_{Sh}^{-1/2}\right)^{-2/7} B^{-2/7} \tag{11.196}$$

$$C = \left(C_{\alpha h} C_{S\alpha}^{-1/2}\right)^{3/7} B^{-3/7} Q^{3/7} = C_\alpha Q^{3/7}, C_\alpha = \left(C_{\alpha h} C_{S\alpha}^{-1/2}\right)^{3/7} B^{-3/7} \tag{11.197}$$

$$S = \left(C_{S\alpha} C_{Sh}\right)^{3/7} B^{-2/7} Q^{2/7} = C_{Sh} Q^{2/7}, C_{Sh} = \left(C_{S\alpha} C_{Sh}\right)^{3/7} B^{-2/7} \tag{11.198}$$

$$V = C_V Q^{5/7} \tag{11.199}$$

Possibility X: Hydraulic Geometry Relations for Depth, Roughness, Slope, and Velocity

Equations (11.184) to (11.187) show that the flow depth varies with discharge raised to the power $f = 9/[9(3 + 3J + K)]$, velocity varies with discharge raised to

the power $m = [3J/(3J + FJ + 3)] + [6/\{5(3 + 3J + K)\}] + [FK/(FK + 3K + 3F)]$, Manning's n varies with discharge raised to the power $p = 3J/(3J + FJ + 3)$, and slope varies with discharge raised to the power $y = (2FK)/(3F + 3K + KF)$. The precise values of f, m, p, and y depend on the weighting factors J, K, and F, which specify the proportion for adjustment of stream power among h, V, n, and S, as shown in Fig. 11-3. The value of exponent f varies from 0 to 1, m varies from 2/5 to an undefined value, p varies from 0 to 2, and y varies from 0/0 to 2, as exhibited in Table 11-5. These values encompass the range reported in the literature, as shown in Table 11-6. The exact exponent values depend on the values of the weighting factors. For the special case $J = K = F = 1$, $f = 9/35$, as shown in equation (11.188), $m = 26/35$, as shown in equation (11.191), $p = -3/7$, as shown in equation (11.189), and $y = 2/7$ from equation (11.190). Thus, it is seen that the values of the f, m, p, and y exponents are not fixed; rather they vary over certain ranges, as exhibited in equations (11.184) to (11.187). The variation is indeed continuous and is dictated by the way the adjustment of stream power is distributed among variables. Under this possibility, the adjustment occurs simultaneously in river depth, velocity, slope, and roughness.

11.4.10 Possibility XI

Possibility XI: $P_B = P_h = P_\alpha = P_S$, $B = C_{Bh}h^{\beta/r}$, $\alpha = C_{\alpha B}B^{w}$, $S = C_{SB}B^{2I/3}$, $S = C_{Sh}h^{2\beta K/3}$, $\alpha = C_{\alpha h}h^{J\beta}$, or $S = C_{S\alpha}\alpha^{2F/3}$

Substitution of equations (11.18a), (11.20a), (11.22a), (11.24a), (11.26a), and (11.29a) in equation (11.7) lead to

$$B = \left(\frac{C_{Bh}^{r}}{C_{\alpha B}C_{SB}^{1/2}}\right)^{\frac{3}{3+3W+3r+I}} Q^{\frac{3}{3+3W+3r+I}} = C_B Q^{\frac{3}{3+3W+3r+I}},\ C_B = \left(\frac{C_{Bh}^{r}}{C_{\alpha B}C_{SB}^{1/2}}\right)^{\frac{3}{3+3W+3r+I}} \tag{11.200}$$

$$\begin{aligned} h &= (C_{Bh}C_{\alpha h}C_{Sh}^{1/2})^{-\frac{3r}{3\beta+3\beta r+3\beta rJ+\beta rK}} Q^{\frac{3r}{3\beta+3\beta r+3\beta rJ+\beta rK}} = C_h Q^{\frac{3r}{3\beta+3\beta r+3\beta rJ+\beta rK}} \\ C_h &= (C_{Bh}C_{\alpha h}C_{Sh}^{1/2})^{-\frac{3r}{3\beta+3\beta r+3\beta rJ+\beta rK}} \end{aligned} \tag{11.201}$$

$$\begin{aligned} \alpha &= (C_{\alpha B}^{1/w}C_{\alpha h}^{1/J}C_{S\alpha}^{-1/2})^{\frac{3wJ}{3w+3J+3wJ+FJw}} Q^{\frac{3wJ}{3w+3J+3wJ+FJw}} = C_\alpha Q^{\frac{3wJ}{3w+3J+3wJ+FJw}} \\ C_\alpha &= (C_{\alpha B}^{1/w}C_{\alpha h}^{1/J}C_{S\alpha}^{-1/2})^{\frac{3wJ}{3w+3J+3wJ+FJw}} \end{aligned} \tag{11.202}$$

$$\begin{aligned} S &= (C_{SB}^{3/2I}C_{Sh}^{3/2K}C_{S\alpha}^{3/2F})^{\frac{2FIK}{3IK+3FK+3FI+FIK}} Q^{\frac{2FIK}{3IK+3FK+3FI+FIK}} = C_S Q^{\frac{2FIK}{3IK+3FK+3FI+FIK}} \\ C_S &= (C_{SB}^{3/2I}C_{Sh}^{3/2K}C_{S\alpha}^{3/2F})^{\frac{2FIK}{3IK+3FK+3FI+FIK}} \end{aligned} \tag{11.203}$$

$$V = \frac{1}{C_B C_h} Q^{1-\frac{3}{3+3W+3r+I}-\frac{3r}{3\beta+3\beta r+3\beta rJ+\beta rK}} \tag{11.204}$$

For Manning's equation, $\alpha = 1/n$ and $\beta = 5/3$, equations (11.200) to (11.204) reduce to

$$B = \left(\frac{C_{Bh}^{r}}{C_{\alpha B}C_{SB}^{1/2}}\right)^{\frac{3}{3+3w+3r+I}} Q^{\frac{3}{3+3w+3r+I}} = C_B Q^{\frac{3}{3+3w+3r+I}}, C_B = \left(\frac{C_{Bh}^{r}}{C_{\alpha B}C_{SB}^{1/2}}\right)^{\frac{3}{3+3w+3r+I}} \tag{11.205}$$

$$\begin{aligned} h &= (C_{Bh}C_{\alpha h}C_{Sh}^{1/2})^{-\frac{9r}{15+15r+15rJ+5rK}} Q^{\frac{9r}{15+15r+15\gamma J+5rK}} = C_h Q^{\frac{9r}{15+15r+15rJ+5rK}}, \\ C_h &= (C_{Bh}C_{\alpha h}C_{Sh}^{1/2})^{-\frac{9r}{15+15r+15rJ+15rK}} \end{aligned} \tag{11.206}$$

$$\begin{aligned} n &= (C_{\alpha B}^{1/w}C_{\alpha h}^{1/J}C_{S\alpha}^{-1/2})^{-\frac{3wJ}{3w+3J+3wJ+FJw}} Q^{-\frac{3wJ}{3w+3J+3wJ+FJw}} = C_\alpha Q^{-\frac{3wJ}{3w+3J+3wJ+FJw}} \\ C_\alpha &= (C_{\alpha B}^{1/w}C_{\alpha h}^{1/J}C_{S\alpha}^{-1/2})^{-\frac{3wJ}{3w+3J+3wJ+FJw}} \end{aligned} \tag{11.207}$$

$$\begin{aligned} S &= (C_{SB}^{3/2I}C_{Sh}^{3/2K}C_{S\alpha}^{3/2F})^{\frac{2FIK}{3IK+3FK+3FI+FIK}} Q^{\frac{2FIK}{3IK+3FK+3FI+FIK}} = C_S Q^{\frac{2FIK}{3IK+3FK+3FI+FIK}} \\ C_S &= (C_{SB}^{3/2I}C_{Sh}^{3/2K}C_{S\alpha}^{3/2F})^{\frac{2FIK}{3IK+3FK+3FI+FIK}} \end{aligned} \tag{11.208}$$

$$V = \frac{1}{C_B C_h} Q^{1-\frac{3}{3+3w+3r+I}-\frac{9r}{15+15r+15rJ+5rK}} \tag{11.209}$$

For the special case $r = J = I = K = F = w = 1$, equations (11.205) to (11.209) become

$$B = \left(\frac{C_{Bh}^{r}}{C_{\alpha B}C_{SB}^{1/2}}\right)^{\frac{3}{10}} Q^{\frac{3}{10}} = C_B Q^{\frac{3}{10}}, C_B = \left(\frac{C_{Bh}^{r}}{C_{\alpha B}C_{SB}^{1/2}}\right)^{\frac{3}{10}} \tag{11.210}$$

$$h = (C_{Bh}C_{\alpha h}C_{Sh}^{1/2})^{-9/50} Q^{9/50} = C_h Q^{9/50}, \quad C_h = (C_{Bh}C_{\alpha h}C_{Sh}^{1/2})^{-9/50} \tag{11.211}$$

$$n = (C_{\alpha B}C_{\alpha h}C_{S\alpha}^{-1/2})^{-3/10} Q^{-3/10} = C_\alpha Q^{-3/10}, \quad C_\alpha = (C_{\alpha B}C_{\alpha h}C_{S\alpha}^{-1/2})^{-3/10} \tag{11.212}$$

$$S = (C_{SB}^{3/2}C_{Sh}^{3/2}C_{S\alpha}^{3/2})^{1/5} Q^{1/5} = C_S Q^{1/5}, \quad C_S = (C_{SB}^{3/2}C_{Sh}^{3/2}C_{S\alpha}^{3/2})^{1/5} \tag{11.213}$$

$$V = \frac{1}{C_B C_h} Q^{13/25} \tag{11.214}$$

For Chezy's equation, $\alpha = C$ and $\beta = 3/2$, equations (11.200) to (11.204) reduce to

$$B = \left(\frac{C_{Bh}^{r}}{C_{\alpha B}C_{SB}^{1/2}}\right)^{\frac{3}{3+3W+3r+I}} Q^{\frac{3}{3+3W+3r+I}} = C_B Q^{\frac{3}{3+3W+3r+I}}, C_B = \left(\frac{C_{Bh}^{r}}{C_{\alpha B}C_{SB}^{1/2}}\right)^{\frac{3}{3+3W+3r+I}} \tag{11.215}$$

$$\begin{aligned} h &= (C_{Bh}C_{\alpha h}C_{Sh}^{1/2})^{-\frac{6r}{9+9r+9rJ+3rK}} Q^{\frac{6r}{9+9r+9\gamma J+3\gamma K}} = C_h Q^{\frac{6r}{9+9r+9rJ+3rK}}, \\ C_h &= (C_{Bh}C_{\alpha h}C_{Sh}^{1/2})^{-\frac{6r}{9+9r+9rJ+3rK}} \end{aligned} \tag{11.216}$$

$$C = (C_{\alpha B}^{1/w} C_{\alpha h}^{1/J} C_{S\alpha}^{-1/2})^{\frac{3wJ}{3w+3J+3wJ+FJw}} Q^{\frac{3wJ}{3w+3J+3wJ+FJw}} = C_\alpha Q^{\frac{3wJ}{3w+3J+3wJ+FJw}}$$
$$C_\alpha = (C_{\alpha B}^{1/w} C_{\alpha h}^{1/J} C_{S\alpha}^{-1/2})^{\frac{3wJ}{3w+3J+3wJ+FJw}} \tag{11.217}$$

$$S = (C_{SB}^{3/2I} C_{Sh}^{3/2K} C_{S\alpha}^{3/2F})^{\frac{2FIK}{3IK+3FK+3FI+FIK}} Q^{\frac{2FIK}{3IK+3FK+3FI+FIK}} = C_S Q^{\frac{2FIK}{3IK+3FK+3FI+FIK}}$$
$$C_S = (C_{SB}^{3/2I} C_{Sh}^{3/2K} C_{S\alpha}^{3/2F})^{\frac{2FIK}{3IK+3FK+3FI+FIK}} \tag{11.218}$$

$$V = \frac{1}{C_B C_h} Q^{1-\frac{3}{3+3W+3r+I}-\frac{9r}{9+9r+9rJ+3rK}} \tag{11.219}$$

For the special case $I = J = K = F = w = 1$, equations (11.215) to (11.219) become

$$B = \left(\frac{C_{Bh}^r}{C_{\alpha B} C_{SB}^{1/2}}\right)^{\frac{3}{10}} Q^{\frac{3}{10}} = C_B Q^{\frac{3}{10}}, C_B = \left(\frac{C_{Bh}^r}{C_{\alpha B} C_{SB}^{1/2}}\right)^{\frac{3}{10}} \tag{11.220}$$

$$h = (C_{Bh} C_{\alpha h} C_{Sh}^{1/2})^{-1/5} Q^{1/5} = C_h Q^{1/5}, C_h = (C_{Bh} C_{\alpha h} C_{Sh}^{1/2})^{-1/5} \tag{11.221}$$

$$C = (C_{\alpha B} C_{\alpha h} C_{S\alpha}^{-1/2})^{3/10} Q^{3/10} = C_\alpha Q^{3/10}, \quad C_\alpha = (C_{\alpha B} C_{\alpha h} C_{S\alpha}^{-1/2})^{3/10} \tag{11.222}$$

$$S = (C_{SB}^{3/2} C_{Sh}^{3/2} C_{S\alpha}^{3/2})^{1/5} Q^{1/5} = C_S Q^{1/5}, \quad C_S = (C_{SB}^{3/2} C_{Sh}^{3/2} C_{S\alpha}^{3/2})^{1/5} \tag{11.223}$$

$$V = \frac{1}{C_B C_h} Q^{\frac{19}{70}} \tag{11.224}$$

Possibility XI: Hydraulic Geometry Relations for Width, Depth, Roughness, Slope, and Velocity

Equations (11.205) to (11.209) show that the flow width varies with discharge raised to the power $b = 3/(3 + 3w + 3r + I)$, depth varies with discharge raised to the power $f = 9r/(15 + 15r + 15rJ + 5rK)$, velocity varies with discharge raised to the power $m = 1 - [3/(3 + 3w + 3r + I)] + [9r/(15 + 15r + 15rJ + 5rK)]$, Manning's n varies with discharge raised to the power $p = -3wJ/(3w + 3J + 3wJ + FJw)$, and slope varies with discharge raised to the power $y = (2FIK)/(3IK + 3FK + 3FI + FJw)$. The precise values of b, f, m, p, and y depend on the weighting factors r, w, I, J, K, and F, which specify the proportion for adjustment of stream power among b, h, V, n, and S, as shown in Fig. 11-3. The value of exponent b varies from 0 to 1, exponent f varies from 0 to 9/50 to 0, m varies from 0 to 1, p varies from an undefined value to 2, and y varies from an undefined value to 2, as shown in Table 11-5. These values encompass the range reported in the literature (Singh, 2003; Singh and Zhang, 2008a, b), as shown in Table 11-6. The exact exponent values depend on the values of the weighting factors. For the special case $r = w = I = J = K = F = 1$, $b = 3/10$, as shown in equation (11.210), $f = 9/50$, as shown in equation (11.211), $m = 13/25$, as shown in equation (11.214),

$p = -3/10$, as shown in equation (11.212), and $y = 1/5$, as shown in equation (11.213), as shown in Table 11-1. This discussion shows that the values of the b, f, m, p, and y exponents are not fixed; rather they vary over certain ranges, as exhibited by equations (11.205) to (11.209). The variation is indeed continuous and depends on the way the adjustment of stream power is distributed among variables. Under this possibility, the adjustment occurs simultaneously in river width, depth, velocity, slope, and roughness.

Questions

Q11.1 Flow characteristics of Brandywine Creek, at Embreeville, Pennsylvania, measured by Wolman (1955), are given in Table 11-8. Plot on a log-log paper flow width, depth, velocity, friction factor, and slope as a function of discharge and fit straight lines. How well do these lines fit? Compute parameters (exponent and proportionality coefficients) of the relations between discharge and flow characteristics. Check if the sum of exponents equals 1.

Table 11-8 *Measurements of flow characteristics of Brandywine Creek at Embreeville, Pennsylvania.*

Date	Discharge Q (ft^3/s)	Width, B (ft)	Mean depth, d (ft)	Mean velocity, V (ft/s)	Cross-sectional area (ft^2)	Slope of water surface, S (ft/ft)	Manning's roughness, n
7/30/1951	73.8	76.5	1.15	0.84	88	0.00043	0.04
8/3/1951	57	76	1.11	0.69	84	0.00036	0.044
8/14/1951	81.6	77.5	1.21	0.87	93.5	0.00042	0.038
9/7/1951	79.7	78	1.18	0.86	92.1	0.00035	0.036
9/10/1951	51.9	78	1.05	0.63	82.2	0.00031	0.043
9/15/1951	160.5	79	1.49	1.36	118.4	0.00043	0.03
4/28/1952	2,340	88	5.26	5.05	463.1	0.00069	0.024
5/26/1952	1,075	84	3.64	3.98	305.7	0.0006	0.028
6/6/1952	319.2	81	1.98	2	160.4	59	0.028
8/7/1952	259.8	81	1.87	1.71	151.9	0.0006	0.032
9/19/1952	540	81	2.31	2.91	186.8	0.00061	0.022
12/16/52	191.7	80	1.62	1.47	130	0.0007	0.037

Note: Drainage area = 117 mi.^{2}, and length of reach = 850 ft.
Source: Data from Wolman 1955.

Table 11-9 *Measurements of flow characteristics of Brandywine Creek at Wawaset, Pennsylvania.*

Date	Discharge Q (ft^3/s)	Width, B (ft)	Mean depth, d (ft)	Mean velocity, V (ft/s)	Cross-sectional area (ft^2)	Slope of water surface, S (ft/ft)	Manning's roughness, n
7/24/1951	98.5	60	1.23	1.34	73.6	0.00098	0.042
7/30/1951	80.2	61	1.1	1.2	67	0.00097	0.041
8/3/1951	68.2	60	1.1	1.04	66	0.0009	0.046
8/20/1951	312	64	2.05	2.38	131.1	0.0012	0.038
8/27/1951	66.4	60.5	1.08	1.02	65.1	0.00085	0.045
4/27/1952	1,117	67	3.42	4.8	229	—	—
4/28/1952	2,400	75.5	4.93	6.46	372	0.00062	0.017
5/26/1952	1,750	69	4.02	6.33	277	—	—
7/10/1952	1,036	71.6	3.12	4.64	223	—	—
8/7/1952	293.9	64.5	2.02	2.26	130	—	—
9/19/1952	623	67.5	2.84	3.24	192.4	—	—

Note: Drainage area = 134 mi.^{2}, and length of reach = 403 ft.
Source: Data from Wolman, 1955.

Q11.2 Flow characteristics of Brandywine Creek at Wawaset, Pennsylvania, measured by Wolman (1955), are given in Table 11-9. Plot on a log-log paper flow width, depth, velocity, friction factor, and slope as a function of discharge and fit straight lines. How well do these lines fit? Compute parameters (exponent and proportionality coefficients) of the relations between discharge and flow characteristics. Check if the sum of exponents equals 1. Compare these coefficients and exponents with those computed in Q 11.1 and comment on the differences.

Q11.3 Compare the exponents determined in Q11.1 with those reported in the literature cited. What can then be said about the Brandywine Creek flow characteristics?

Q11.4 Compare the exponents determined in Q11.2 with those reported in the literature cited. What can then be said about the Brandywine Creek flow characteristics?

Q11.5 Determine the morphological equations relating width and depth of flow, width and Manning's n, and flow depth and Manning's n and check if the derived equations are valid. Compute the spread of the associated coefficients.

Q11.6 Collect the values of hydraulic geometry exponents given in the chapter as well as from the literature. Then, plot a histogram of each exponent and compute the mean, standard deviation, coefficient of variation, and coefficient of skewness of each exponent.

Q11.7 Compare the mean values of hydraulic geometry exponents computed in Q11.1 and Q11.2 with what is normally used in the literature, as given in Table 11-5. What does the spread in each exponent value mean hydraulically? Comment on the hydraulic significance of the coefficient of skewness of each exponent value.

Q11.8 Different possibilities for hydraulic geometry adjustments have been discussed in the chapter. List these possibilities and the environments under which they occur. What is the most common possibility and why?

Q11.9 Hydraulic geometry adjustments respond to geological and climatic characteristics. The size of a river is also determined by these characteristics. Which possibility is more likely for which geological and climatic regime and why?

Q11.10 Human-made changes also affect river or channel hydraulic geometry. Assume that a river is leveed for a certain portion, as is the case for many rivers in the United States. Which possibility is more likely for such a river and why?

Q11.11 On the Indian subcontinent, there are large irrigation canal systems. What possibility is more likely for such canals and why?

Q11.12 Assume that some of the canals in Q10.9 are lined. What possibility is then more likely for such canals and why?

References

Allen, P. M., Arnold, J. G., and Byars, B. W. (1994). "Downstream channel geometry for use of in planning-level models." *Water Resour. Bull.*, 30(4), 663–671.

Bray, D. I. (1979). "Estimating average velocity in gravel-bed rivers." *J. Hydraul. Div.*, 105(9), 1103–1122.

Cheema, M. N., Mariño, M. A., and De Vries, J. J. (1997). "Stable width of an alluvial channel." *J. Irrig. Drain. Eng.*, 123(1), 55–61.

Colby, B. R. (1961). "*The effect of depth of flow on discharge of bed material*." U.S. Geological Survey Water Supply Paper 1498-D, U.S. Geological Survey, Washington, DC.

Judd, H. E. and Peterson, D. F. (1969). "*Hydraulics of large bed element channels*." PRWG 17-6, Utah State University, Utah Water Research Laboratory, Logan, UT.

Jaynes, E. T. (1957). "Information theory and statistical mechanics, I." *Phys. Rev.*, 106, 620–630.

Knighton, A. D. (1974). "Variation in width-discharge relation and some implications for hydraulic geometry." *Geolog. Soc. Am. Bull.*, 85, 1069–1076.
Knighton, A. D. (1977). "Alternative derivation of the minimum variance hypothesis." *Geolog. Soc. Am. Bull.*, 83, 3813–3822.
Langbein, W. B. (1964). "Geometry of river channels." *J. Hydraul. Div.*, 90(2), 301–312.
Leopold, L. H., and Langbein, W. B. (1962). "The concept of entropy in landscape evolution." U.S. Geological Survey Professional Paper 500-A, U.S. Geological Survey, Washington, DC.
Leopold, L. B., and Maddock, T. J. (1953). "*Hydraulic geometry of stream channels and some physiographic implications*." U.S. Geological Survey Professional Paper 252, U.S. Geological Survey, Washington, DC.
Leopold, L. B., and Miller, J. P. (1956). "*Ephemeral streams—Hydraulic factors and their relation to the drainage net*." U.S. Geological Survey Professional Paper 282-A, U.S. Geological Survey, Washington, DC.
Leopold, L. B., and Wolman, L. B. (1957). "*River channel patterns: Braided, meandering and straight*." U.S. Geological Survey Professional Paper 282-B, U.S. Geological Survey, Washington, DC.
Lewis, L. (1966). "The relations of hydrology and geomorphology in a humid tropical stream basin, the Rio Grande de Manati, Puerto Rico." *Diss. Abstr.*, 26, 7255.
Li, R. M. (1975). "*Mathematical modeling of response from small watershed*." Ph.D. dissertation, Colorado State University, Fort Collins, CO.
Maddock, T. (1969). "*The behavior of straight open channels with movable beds*." U.S. Geological Survey Professional Paper 622-A, U.S. Geological Survey, Washington, DC.
Merigliano, M. F. (1997). "Hydraulic geometry and stream channel behavior: An uncertain link." *J. Am. Water Resour. Assoc.*, 33(6), 1327–1336.
Myrick, R. M., and Leopold, L. B. (1963). "*Hydraulic geometry of a small tidal estuary*." U.S. Geological Survey Professional Paper 422-B, U.S. Geological Survey, Washington, DC.
Nizery, A., and Braudeau, G. (1955). "Discussion of 'design of stable channels,' by E. W. Lane." *Trans. ASCE*, 120(1), 1266–1269.
Park, C. C. (1977). "World-wide variations in hydraulic geometry exponents of stream channels: An analysis and some observations." *J. Hydrol.*, 33, 133–146.
Rhodes, D. D. (1977). "The b-f-m diagram: Graphical representation and interpretation of at-a-station hydraulic geometry." *Am. J. Sci.*, 277, 73–96.
Rhodes, D. D. (1978). "World wide variations in hydraulic geometry exponents of stream channels: An analysis and some observations—Comments." *J. Hydrol.*, 33, 133–146.
Richards, K. S. (1973). "Hydraulic geometry and channel roughness—A nonlinear system." *Am. J. Sci.*, 273, 877–896.
Richards, K. S. (1976). "Complex width-discharge relations in natural river sections." *Geolog. Soc. Am. Bull.*, 87, 199–206.

Riley, S. J. (1975). "The channel shape-grain size relation in eastern Australia and some paleohydrologic implications." *Sedimentatary Geolog.*, 14, 253–258.

Riley, S. J. (1978). "The role of minimum variance theory in defining the regime characteristics of the lower Namoi-Gwydir basin." *Water Resour. Bull.*, 14, 1–11.

Schumm, S. A. (1960). "*The shape of alluvial channels in relation to sediment type*." U.S. Geological Survey Professional Paper 352B, U.S. Geological Survey, Washington, DC.

Schumm, S. A. (1968). "*River adjustment to altered hydrologic regime—Murrumbidgee River and Paleo channels, Australia*." U.S. Geological Survey Professional Paper 598, U.S. Geological Survey, Washington, DC.

Singh, V. P. (2003). "On the theories of hydraulic geometry." *Int. J. Sed. Res.*, 18(3), 196–218.

Singh, V. P., Yang, C. T., and Deng, Z. Q. (2003a). "Downstream hydraulic geometry relations: 1. Theoretical development." *Water Resour. Res.*, 39(12), SWC2-1–SWC2-15.

Singh, V. P., Yang, C. T., and Deng, Z. Q. (2003b). "Downstream hydraulic geometry relations: 1. Calibration and testing." *Water Resour. Res.*, 39(12), SWC3-1–SWC3-10.

Singh, V. P., and Zhang, L. (2008a). "At-a-station hydraulic geometry: I. Theoretical development." *Hydrolog. Proc.*, 22, 189–215.

Singh, V. P., and Zhang, L. (2008b). "At-a-station hydraulic geometry: II. Calibration and testing." *Hydrolog. Proc.*, 22, 216–228.

Stall, J. B., and Fok, Y.-S. (1968). "*Hydraulic geometry of Illinois streams*." University of Illinois Water Resources Center, Research Report No. 15, Urbana, IL.

Stall, J. B., and Yang, C. T. (1970). "*Hydraulic geometry of 12 selected stream systems of the United States*." University of Illinois Water Resources Research Center, Research Report No. 32, Urbana, IL.

Virmani, J. K. (1973). "*The relationship between channel forming flows and the cross-section shape, slope, and bed materials in large bed element streams*." Ph.D. dissertation, Utah State University, Logan, UT.

Williams, G. P. (1967). "*Flume experiments on the transport of a coarse sand*." U.S. Geological Survey Professional Paper 562-B, U.S. Geological Survey, Washington, DC.

Williams, G. P. (1978). "*Hydraulic geometry of river cross-sections—Theory of minimum variance*." U.S. Geological Survey Professional Paper 1029, U.S. Geological Survey, Washington, DC.

Wolman, M. G. (1955). "*The natural channel of Brandywine Creek, Pennsylvania*." U.S. Geological Survey Professional Paper 271, U.S. Geological Survey, Washington, DC.

Wolman, M. G., and Brush, L. M. (1961). "*Factors controlling the size and shape of stream channels in coarse noncohesive sands*." U.S. Geological Survey Professional Paper 282-G, U.S. Geological Survey, Washington, DC.

Yang, C. T. (1972). "Unit stream power and sediment transport." *J. Hydraul. Div.*, 98(10), 1805–1826.

Yang, C. T. (1976). "Minimum unit stream power and fluvial hydraulics." *J. Hydraul. Div.*, 102(7), 919–934.
Yang, C. T. (1986). "Dynamic adjustment of rivers." *Proc., 3rd Int. Symp. River Sedimentation*, Jackson, MS, 118–132.
Yang, C. T. (1996). *Sediment transport theory and practice*, McGraw-Hill, New York.
Yang, C. T., Song, C. C., and Woldenberg, M. T. (1981). "Hydraulic geometry and minimum rate of energy dissipation." *Water Resour. Res.*, 17, 877–896.

Additional Reading

Blench, T. (1952). "Regime theory for self-formed sediment-bearing channels." *Trans. ASCE*, 117(1), 383–400.
Brebner, A. and Wilson, K. C. (1967). "Derivation of the regime equations from relationships for pressurized flow by use of the principle of energy-degradation rate." *Proc., Inst. Civil Eng.*, 36, 47–62.
Chang, H. H. (1980). "Geometry of gravel streams." *J. Hydraul. Div.*, 106(9), 1443–1456.
Chang, H. H. (1988). *Fluvial processes in river engineering*, Wiley, New York.
Davies, T. R. H., and Sutherland, A. J. (1983). "Extremal hypotheses for river behavior." *Water Resour. Res.*, 19(1), 141–148.
Deng, Z., and Zhang, K. (1994). "Morphologic equations based on the principle of maximum entropy." *Int. J. Sed. Res.*, 9(1), 31–46.
Dou, G. R. (1964). "Hydraulic geometry of plain alluvial rivers and tidal river mouth." *J. Hydraul. Eng.*, (2), 1–13 (in Chinese).
Huang, H. Q., and Nanson, G. C. (2000). "Hydraulic geometry and maximum flow efficiency as products of the principle of least action." *Earth Surf. Proc. Land.*, 25, 1–16.
Lane, E. W. (1955). "Design of stable channels." *Trans. ASCE*, 120(1), 1234–1260.
Ramette, M. (1980). "A theoretical approach on fluvial processes." *Proc. Int. Symp. River Sed.*, Theme No. 3, Beijing, China, C16-1–C16-22.
Rodriguez-Iturbe, I., Rinaldo, A., Rigon, R., Bras, R. L., Marani, A., and Ijjasz-Vasquez, E. J. (1992). "Energy dissipation, runoff production and the three-dimensional structure of river basins." *Water Resour. Res.*, 28(4), 1095–1103.
Smith, T. R. (1974). "A derivation of the hydraulic geometry of steady-state channels from conservation principles and sediment transport laws." *J. Geolog.*, 82, 98–104.
Stebbings, J. (1963). "The shape of self-formed model alluvial channels." *Proc., Inst. Civil Eng.*, London, 25, 485–510.
White, W. R., Bettess, R., and Paris, E. (1982). "Analytical approach to river regime." *J. Hydraul. Div.*, 108(10), 1179–1193.
Yalin, M. S., and Da Silva, A. M. F. (1997). "On the computation of equilibrium channels in cohesionless alluvium." *J. Hydrosci. Hydraul. Eng.*, 15(2), 1–13.

Yalin, M. S., and Da Silva, A. M. F. (1999). "Regime channels in cohesionless alluvium." *J. Hydraul. Res.*, 37(6), 725–742.

Yang, C. T., and Song, C. C. S. (1986). "Theory of minimum energy and energy dissipation rate." *Encyclopedia of Fluid Mechanics*, Gulf Publishing, Houston, TX, 332–399.

Part 4

Channel Design

This page intentionally left blank

Chapter 12

Longitudinal River Profile

The longitudinal profile of a river is linked with the distribution of energy gradient along the river. The distribution of energy gradient is needed for design of river training works, analysis of channel changes, modeling of regime rivers, investigations of morphology and landscapes of rivers, sediment transport, navigation, and flood control. The energy gradient depends on a number of factors, including sediment size, water discharge, sediment load, geological conditions, human intervention, and climatic conditions. Some of these factors are interactive. For example, the flow and sediment load that a river carries depend on the conditions in its basin, which, in turn, depend on human activities and geology. Likewise, climate determines land use, which then influences sediment load and flow to the river and its formation. These factors have inherent uncertainties, and so do their interactions. Thus, it would be logical to state that there is inherent randomness in the energy gradient distribution. This randomness permits us to derive longitudinal river profiles using entropy, and this phenomenon constitutes the subject matter of this chapter.

12.1 Longitudinal Profiles

Field observations of longitudinal profiles of rivers suggest that the profiles are concave, convex, or straight, as shown in Fig. 12-1. Concave profiles are most

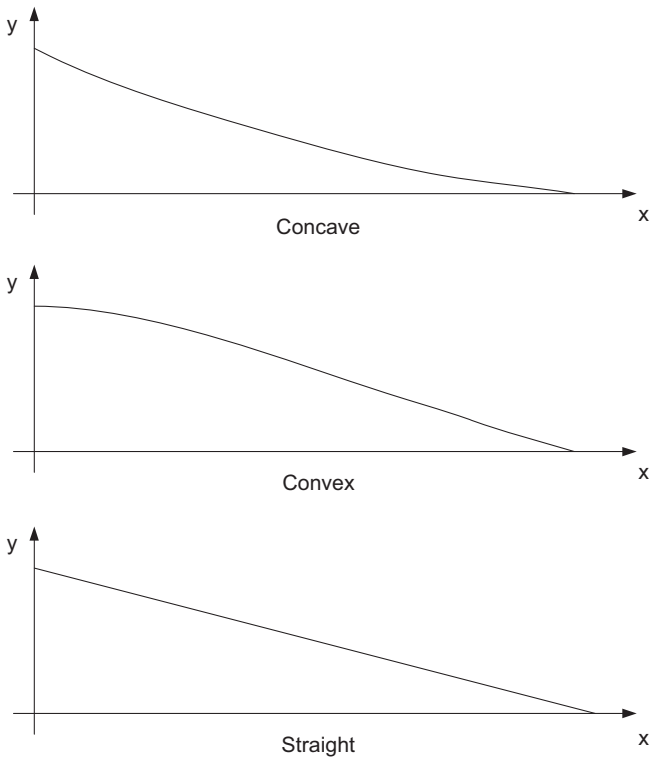

Figure 12-1 *Longitudinal river profiles: Concave, convex, and straight. Note:* x *is the longitudinal distance, and* y *is the elevation with respect to a datum.*

common in nature, whereas convex profiles are found in arid areas or over certain river reaches. Straight profiles are observed for reaches with uniform flow, sediment, and boundary conditions. Such profiles are found in the downstream reaches of large rivers, such as the Yangtze, the Mississippi, the Ganges-Brahmaputra, and the Nile.

12.2 Energy Gradient

Consider an alluvial reach of length L with a total elevation of Y over the reach length. Let the longitudinal distance measured from the upstream end of the reach be denoted as x and the elevation above the downstream end be denoted as y. The energy gradient may be denoted by S with its specific value s defined as $s = dy/dx$. For most rivers, the discharge increases and the sediment concentration and sediment particle size decrease along the longitudinal distance in the direction of flow. Therefore, the energy gradient also decreases downstream, and s is the highest at the upstream end and the lowest at the downstream end. It is assumed that the channel bed slope for a gradually varied flow can be

approximated by the energy gradient. Cao and Chang (1988) used entropy theory for deriving the energy gradient distribution.

12.3 Derivation of Longitudinal Profiles

It may be useful to nondimensionalize variables to be used here. When we define the normalizing quantities L as the river reach length and Y_0 as elevation at the upstream end, the dimensionless distance can be expressed as $x^* = x/L$, and the dimensionless elevation as $y^* = y/Y_0$. In dimensionless terms, slope $s = dy/dx$ can be defined as $s^* = dy^*/dx^*$.

12.3.1 Shannon Entropy

It is assumed that the temporally averaged energy gradient S is a random variable. Taking S as a continuous variable, its Shannon entropy H (Shannon 1948) can be expressed as

$$H(s) = -\int_{s_d}^{s_u} f(s) \ln f(s) ds \tag{12.1}$$

where s is the value of random variable S, $f(s)$ is the probability density function (PDF) of S, H is the entropy of $f(s)$ or S, s_u is the value of slope at the upstream end, and s_d is the value of slope at the downstream end. Equation (12.1) is a measure of uncertainty of $f(s)$ of variable S. The objective is to derive $f(s)$ by maximizing H, subject to specified constraints on S, in accordance with the principle of maximum entropy (POME) (Jaynes 1957). Maximization of H makes $f(s)$ as uniform as possible, simultaneously satisfying the constraints as a river profile tends toward the state of dynamic equilibrium corresponding to its entropy being maximum.

12.3.2 Specification of Constraints

For purposes of simplicity, two constraints are specified. The first constraint is the total probability theorem that $f(s)$ must satisfy and can be formulated as

$$\int_{s_d}^{s_u} f(s) ds = 1 \tag{12.2}$$

The second constraint can be expressed as the mean energy gradient or mean value of S as

$$\int_{s_d}^{s_u} s f(s) ds = E[S] = \bar{s} = s_m \tag{12.3}$$

where E is the expectation operator, and $\bar{s}$ or s_m is the mean energy gradient.

12.3.3 Maximization of Entropy

To obtain the least biased $f(s)$ that satisfies equations (12.2) and (12.3), equation (12.1) is maximized following POME. This step is achieved by using the method of Lagrange multipliers. To that end, the Lagrangian function L is expressed as

$$L = -\int_{s_d}^{s_u} f(s)\ln f(s)ds - (\lambda_0 - 1)\left(\int_{s_d}^{s_u} f(s)ds - 1\right) - \lambda_1\left(\int_{s_d}^{s_u} sf(s)ds - s_m\right) \tag{12.4}$$

where λ_0 and λ_1 are the Lagrange multipliers. Differentiating equation (12.4) with respect to f, while recalling the Euler–Lagrange equation of calculus of variation, noting f as variable and s as parameter, and equating the derivative to zero, one obtains

$$\frac{\partial L}{\partial f} = 0 \Rightarrow -\ln f(s) - \lambda_0 - \lambda_1 s \tag{12.5}$$

12.3.4 Probability Distribution of Energy Gradient

Equation (12.5) yields

$$f(s) = \exp(-\lambda_0 - \lambda_1 s) \tag{12.6}$$

Equation (12.6) is the POME-based PDF of longitudinal slope S. The Lagrange multipliers λ_0 and λ_1 can be determined using equations (12.2) and (12.3).

12.3.5 Determination of Lagrange Multipliers

Substitution of equation (12.6) in equation (12.2) yields

$$\exp(\lambda_0) = \frac{1}{\lambda_1}[\exp(-\lambda_1 s_d) - \exp(-\lambda_1 s_u)] \tag{12.7}$$

which defines the partition function. Taking the logarithm of equation (12.7), the result is

$$\lambda_0 = -\ln\lambda_1 + \ln[\exp(-\lambda_1 s_d) - \exp(-\lambda_1 s_u)] \tag{12.8}$$

which defines a relation between λ_0 and λ_1. Differentiating equation (12.8) with respect to λ_1, one obtains

$$\frac{\partial\lambda_0}{\partial\lambda_1} = -\frac{1}{\lambda_1} - \frac{s_d\exp(-\lambda_1 s_d) - s_u\exp(-\lambda_1 s_u)}{\exp(-\lambda_1 s_d) - \exp(-\lambda_1 s_u)} \tag{12.9}$$

Conversely, substitution of equation (12.6) in equation (12.2) also yields

$$\lambda_0 = \ln\int_{s_d}^{s_u}\exp(-\lambda_1 s)ds \tag{12.10}$$

Differentiating equation (12.10) with respect to λ_1 yields

$$\frac{\partial \lambda_0}{\partial \lambda_1} = -\frac{\int_{s_d}^{s_u} s\exp(-\lambda_1 s)ds}{\int_{s_d}^{s_u} \exp(-\lambda_1 s)ds} \tag{12.11}$$

When multiplying and dividing equation (12.11) by $\exp(-\lambda_0)$, one can express the result as

$$\frac{\partial \lambda_0}{\partial \lambda_1} = -\frac{\int_{s_d}^{s_u} s\exp(-\lambda_0 - \lambda_1 s)ds}{\int_{s_d}^{s_u} \exp(-\lambda_0 - \lambda_1 s)ds} = -s_m \tag{12.12}$$

Equating equation (12.9) to equation (12.12), the result is

$$s_m = \frac{1}{\lambda_1} + \frac{s_d \exp(-\lambda_1 s_d) - s_u \exp(-\lambda_1 s_u)}{\exp(-\lambda_1 s_d) - \exp(-\lambda_1 s_u)} \tag{12.13}$$

Equation (12.13) expresses the relation between the mean slope and the upstream and downstream slopes. It is an implicit expression for λ_1 in terms of s_m and can be solved numerically for any unknown λ_1.

Example 12.1 For $s_d = 0.001$, $s_u = 0.088$, and $s_m = 0.045$, compute λ_1 = using equation (12.13). Plot λ_1 as a function of s_m. To what kind of curve does this function correspond?

Solution We are given that $s_d = 0.001$, $s_u = 0.088$, and $s_m = 0.045$. Substituting these values in equation (12.13) and solving it numerically, one obtains $\lambda_1 = -0.793$. Table 12-1 shows values of λ_1 for different values of s_m. Fig. 12-2 plots λ_1 as a

Table 12-1 *Values of λ_1 for different values of* s_m.

λ_1	s_m	λ_1	s_m
–300	0.085	0.5	0.044
–100	0.078	1	0.044
–10	0.051	5	0.041
–5	0.048	10	0.038
–1	0.045	50	0.020
–0.5	0.045	100	0.011
–0.1	0.045	500	0.003
0.1	0.044	1,000	0.002

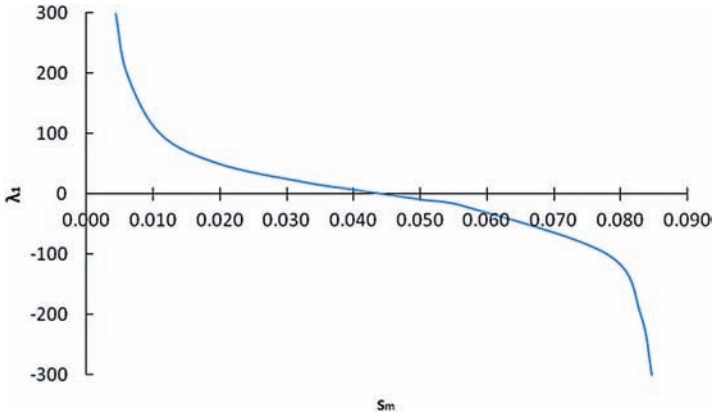

Figure 12-2 *Plot of λ_1 as a function of* s_m.

function of s_m. It is seen that λ_1 becomes zero at about $s_m = 0.043$, and, hence, the curve changes from concave to convex.

In natural channels, rivers, or streams, bed slopes are quite small, usually less than 1%. Of course, in upper reaches, depending on the geology, slopes can be quite high, especially in mountainous streams. It is interesting to observe that as mean slope increases beyond about 0.043, the value of λ_1 goes from positive to negative.

12.3.6 Maximum Entropy and Probability Distribution

Substitution of equation (12.7) in equation (12.6) leads to the PDF of S as

$$f(s) = \frac{\lambda_1 \exp(-\lambda_1 s)}{\exp(-\lambda_1 s_d) - \exp(-\lambda_1 s_u)} \tag{12.14a}$$

Equation (12.14a) has only one unknown Lagrange multiplier, λ_1, which can be obtained by numerically solving equation (12.13). The CDF of S can be written as

$$F(s) = \frac{\exp(-\lambda_1 s_d) - \exp(-\lambda_1 s)}{\exp(-\lambda_1 s_d) - \exp(-\lambda_1 s_u)} \tag{12.14b}$$

Substituting equation (12.14a) in equation (12.1), one gets the maximum entropy as

$$H(s) = \lambda_1 s_m - \ln \lambda_1 + \ln[\exp(-\lambda_1 s_d) - \exp(-\lambda_1 s_u)] \tag{12.15}$$

Table 12-2 *Values of* f(s) *for various values of* s.

s	*f*(*s*)	*S*	*f*(*s*)
0	11.9	0.05	11.442
0.01	11.811	0.06	11.352
0.02	11.717	0.07	11.262
0.03	11.625	0.08	11.173
0.04	11.533	0.088	11.102

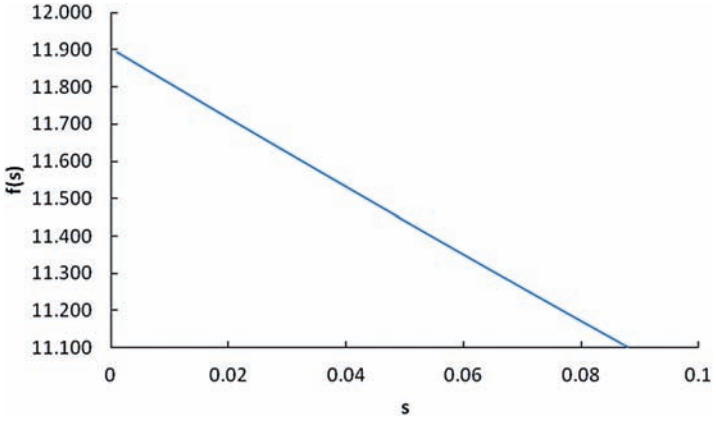

Figure 12-3 *Plot of* f(s) *versus* s.

Example 12.2 For $s_d = 0.001$, $s_u = 0.088$, and $s_m = 0.045$, compute the PDF of S using equation (12.14a) and plot it.

Solution $\lambda_1 = -0.793$, as computed in Example 12.1. Note that the value of $f(s)$ at $s = 0$ is

$$f(s)\big|_{s=0} = \frac{\lambda_1}{\exp(-\lambda_1 s_d) - \exp(-\lambda_1 s_u)} = 11.9$$

Using equation (12.14a), we see that the PDF of S, $f(s)$, is computed and tabulated in Table 12-2 and is shown in Fig. 12-3. It is a negative exponential function.

Example 12.3 For $s_d = 0.001$, $s_u = 0.088$, and $s_m = 0.045$, compute the CDF of S using equation (12.14b) and plot it.

Solution For $\lambda_1 = -0.793$, $F(s)$ is computed as a function of s, as shown in Table 12-3, and Fig. 12-4 plots $F(s)$ versus s.

Table 12-3 *Values of* F(s) *for various values of* s.

s	*F*(*s*)	*s*	*F*(*s*)
0	0	0.05	0.572
0.01	0.107	0.06	0.686
0.02	0.224	0.07	0.799
0.03	0.341	0.08	0.911
0.04	0.457	0.088	1.000

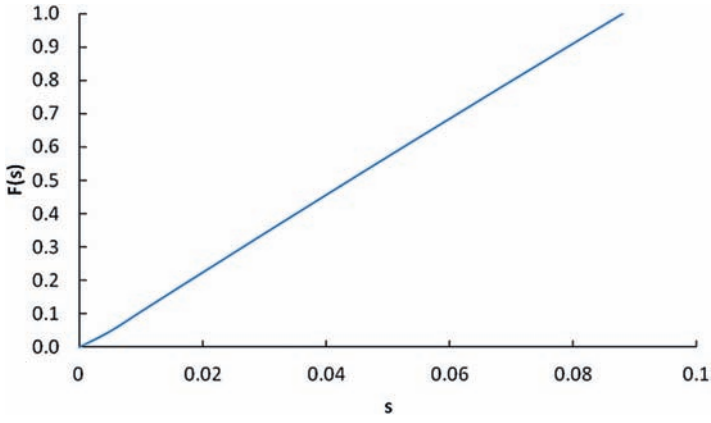

Figure 12-4 *Plot of* F(s) *versus* s.

Table 12-4 *Probability values for given s values.*

s	$F(s) = P(D \leq s)$
0.02	0.224
0.03	0.341
0.04	0.457
0.05	0.572
0.06	0.686
0.07	0.799
0.08	0.911

Example 12.4 Compute the probability of *S* less than or equal to 0.02, 0.03, 0.04, 0.05, 0.06, 0.07, and 0.08. Use equation (12.14b).

Solution For $\lambda_1 = -0.793$, as computed in Example 12.1, the values of probability are computed for given *s* values, as tabulated in Table 12-4.

Example 12.5 Compute entropy of S using equation (12.15) for s_d = 0.001, s_u = 0.088, and s_m = 0.045. First, compute the value of λ_1, noting that s_m and λ_1 are related by equation (12.13).

Solution

$$\begin{aligned} H(s) &= \lambda_1 s_m - \ln\lambda_1 - \ln[\exp(-\lambda_1 s_d) - \exp(-\lambda_1 s_u)] \\ &= (-0.793 \times 0.045) - \ln 0.793 - \ln[(\exp(0.793 \times 0.001) - \exp(0.793 \times 0.088)] \\ &= 2.835 \text{ Napier} \end{aligned}$$

Example 12.6 Compute and plot $H(S)$ as a function of s_m. Note that s_m and λ_1 are related by equation (12.13).

Solution $H(S)$ is computed as a function of s_m using equation (12.15), as shown in Table 12-5, and then $H(S)$ is plotted as shown in Fig. 12-5, which shows that H decreases with increasing s_m.

Table 12-5 *Values of* H(S) *for given values of* s_m.

s_m	$H(s)$	s_m	$H(s)$
0.0458	0.874	0.0451	2.352
0.0457	0.986	0.0450	2.816
0.0456	1.103	0.0449	3.410
0.0455	1.357	0.0448	4.239
0.0454	1.642	0.0447	4.823
0.0453	1.969	0.0446	7.038
0.0452	2.152		

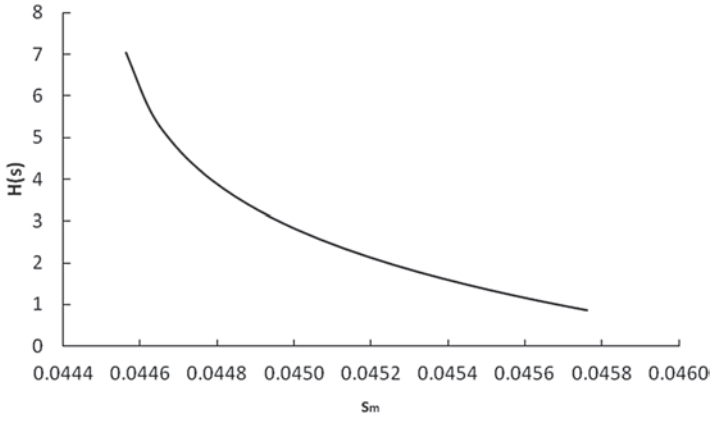

Figure 12-5 *Plot of* H(S) *as a function of* s_m.

Table 12-6 *Values of* H(S) *as a function of* λ_1 *and the corresponding* s_m.

λ_1	s_m	H	λ_1	s_m	H
–2	0.046	0.874	–1	0.045	2.352
–1.8	0.046	1.103	–0.8	0.045	2.816
–1.6	0.046	1.357	–0.6	0.045	3.410
–1.4	0.045	1.642	–0.4	0.045	4.239
–1.2	0.045	1.969	–0.2	0.045	5.643

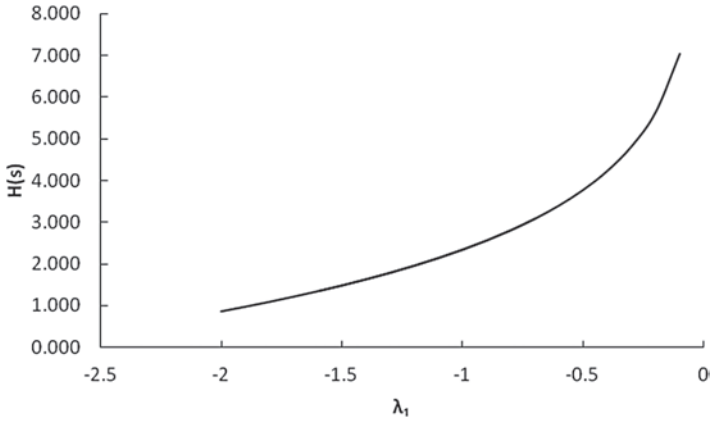

Figure 12-6 *Plot of* H(S) *as a function of* λ_1.

Example 12.7 Compute and plot $H(S)$ as a function of λ_1. Note that λ_1 and s_m are related by equation (12.13).

Solution Values of $H(S)$ are computed as a function of λ_1, as shown in Table 12-6, and Fig. 12-6 plots $H(s)$. It is seen that H increases with increasing λ_1.

12.3.7 Distribution of Energy Gradient

The energy gradient decreases from one point to another in the downstream direction, i.e., $s_d \le s \le s_u$, $s(x)$ is a decreasing function of the longitudinal distance, $0 \le x \le L$. It is assumed that the probability of any value of x being sampled is the same as that of another value. Thus, the probability of an energy gradient being equal to or less than a given value can be expressed as

$$F(s) = 1 - \frac{x(s)}{L} \tag{12.16}$$

where $F(s)$ is the cumulative distribution function. Differentiating equation (12.16) yields the PDF of S as

$$f(s)ds = -\frac{1}{L}dx \text{ or } f(s) = -\frac{1}{L}\frac{dx}{ds} = \left(L\frac{ds}{dx}\right)^{-1} \tag{12.17}$$

The PDF of S given by equation (12.17) must satisfy the constraints defined by equations (12.2) and (12.3).

Equating equation (12.17) to equation (12.14a), one gets

$$\frac{\lambda_1 \exp(-\lambda_1 s)}{\exp(-\lambda_1 s_d) - \exp(-\lambda_1 s_u)}ds = -\frac{1}{L}dx \tag{12.18}$$

Integration of equation (12.18) with the condition $s = s_u$ at $x = 0$, leads to

$$s = \frac{1}{\lambda_1}\ln\left\{\frac{\exp(\lambda_1 s_u)}{1+\frac{x}{L}[\exp[-\lambda_1(s_d - s_u)]-1]}\right\} \tag{12.19a}$$

Equation (12.19a) defines the longitudinal slope or energy distribution for concave profiles. For convex profiles, the boundary condition changes in that $s_d > s_u$. However, equation (12.19a) remains the same except for a change of limits as

$$s = \frac{1}{\lambda_1}\ln\left\{\frac{\exp(\lambda_1 s_d)}{1+\left(\frac{x}{L}-1\right)[1-\exp[-\lambda_1(s_u - s_d)]]}\right\} \tag{12.19b}$$

Example 12.8 For $s_d = 0.001$, $s_u = 0.088$, $s_m = 0.045$, and λ_1 computed from equation (12.13), compute s as a function of x/L and plot the slope relation.

Solution For $\lambda_1 = -0.793$, values of s are computed as a function of x/L, as given in Table 12-7, and Fig. 12-7 plots s as a function of x/L. The profile looks like a concave profile.

Table 12-7 *Values of* s *corresponding to* x/L.

x/L	s	x/L	s
0	0.088	0.2	0.071
0.01	0.087	0.3	0.063
0.05	0.084	0.5	0.045
0.1	0.080	1	0.001

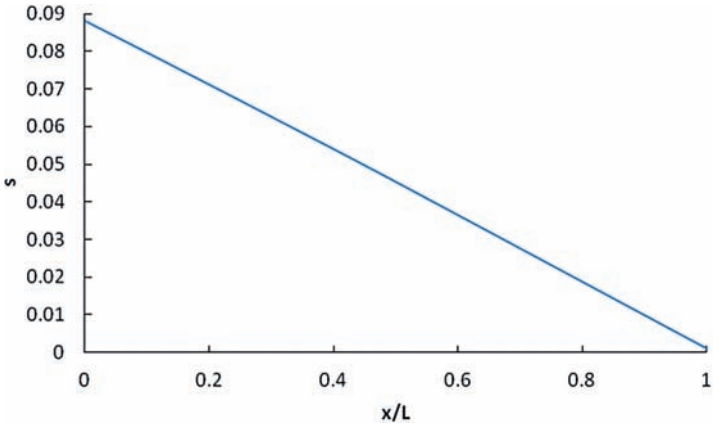

Figure 12-7 *Plot of* s *versus* x/L.

Table 12-8 *Values of* s *corresponding to* x/L *in Example 12.9.*

x/L	s	x/L	s
0	0.0003	0.2	0.0009
0.01	0.0003	0.3	0.0012
0.05	0.0004	0.5	0.0017
0.1	0.0006	1	0.0032

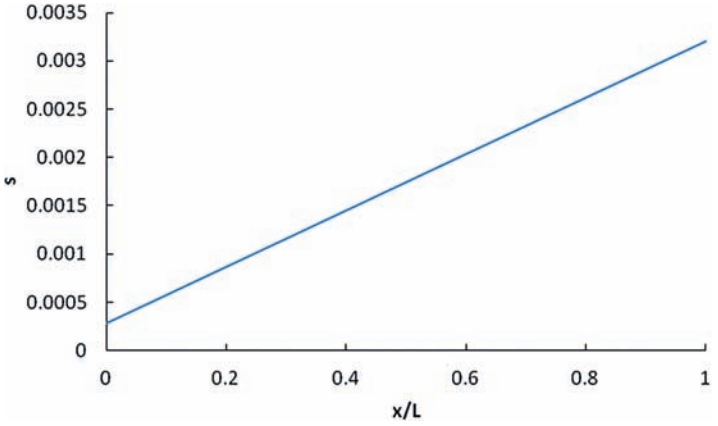

Figure 12-8 *Plot of* s *versus* x/L.

Example 12.9 For $s_d = 0.0032$, $s_u = 0.00028$, $s_m = 0.0017$, and λ_1 computed from equation (12.13), compute s as a function of x/L and plot the slope relation.

Solution The value of λ_1 is computed from equation (12.13) and is found as $\lambda_1 = -0.01$. Then, s is computed as a function of x/L, as shown in Table 12-8. Fig. 12-8 plots the slope relation.

Equations (12.19a) and (12.19b) express the longitudinal distribution of the energy gradient. Note that $s = dy/dx$. Therefore, equation (12.19a) can be written as

$$\frac{dy}{dx} = \frac{1}{\lambda_1} \ln \left\{ \frac{\exp(-\lambda_1 s_u)}{1 + \frac{x}{L}[\exp[-\lambda_1 (s_d - s_u)] - 1]} \right\} \tag{12.20}$$

Integrating equation (12.20) with the condition $y = Y_0$ at $x = 0$, one gets

$$y = Y_0 - s_u x + \frac{x}{\lambda_1} - \frac{1}{\lambda_1} \ln \left\{ 1 + \frac{x}{L}[\exp(-\lambda_1 (s_d - s_u)) - 1] \right\} \{x + L[\exp(-\lambda_1 (s_d - s_u)) - 1]^{-1}\} \tag{12.21}$$

Taking the limit of equation (12.18) where s_d approaches s_u, one gets

$$\lim_{s_d \to s_u} s = s_m \tag{12.22}$$

This result means that $s_m = s_u = s_d$. The implication is that the energy gradient of the river reach tends to attain the mean value s_m. Then, the longitudinal profile is straight and can be obtained by the integration of equation (12.22) with the integration constant Y_0 as

$$y = Y_0 - s_m x \tag{12.23}$$

Example 12.10 For $s_d = 0.001$, $s_u = 0.088$, $s_m = 0.045$, $L = 70$ km, and λ_1 computed from equation (12.13), compute y as a function of x and plot the relation.

Solution The value of λ_1 is computed using equation (12.23) and is found to be –0.793, and values of y versus x are computed as shown in Table 12-9. Fig. 12-9 plots the elevation versus distance, where the profile looks like a concave profile.

Table 12-9 *Values of elevation* y *at different distances* x.

x (km)	y (m)	x (km)	y (m)
0	3.080	30	1.013
1	2.993	40	0.576
2	2.907	50	0.262
5	2.656	60	0.070
10	2.264	70	0.000
20	1.576		

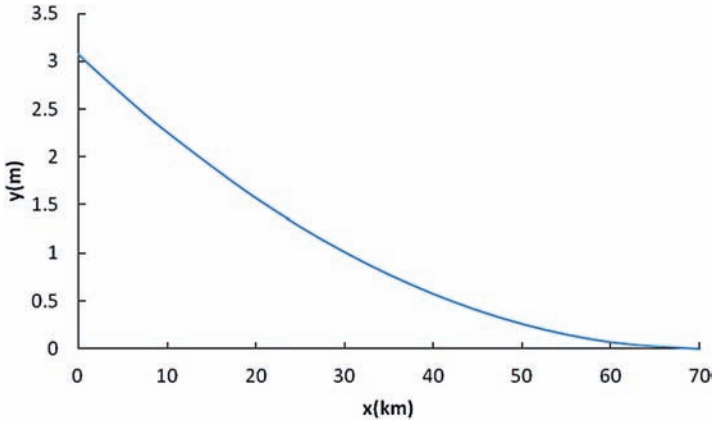

Figure 12-9 *Dimensionless concave longitudinal profile.*

Table 12-10 *Values of* y *at different distances* x.

x (km)	y (m)	x (km)	y (m)
0	0.068	120	0.021
5	0.067	130	0.016
10	0.065	140	0.011
50	0.052	150	0.006
100	0.031	160	0.000
110	0.026		

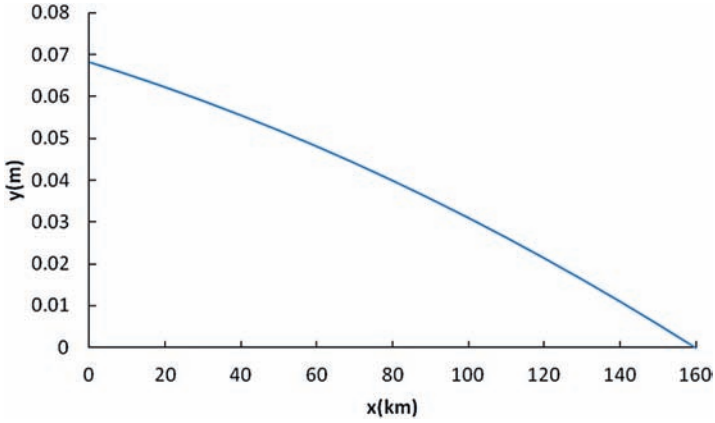

Figure 12-10 *Dimensionless convex longitudinal profile.*

Example 12.11 For $s_d = 0.0032$, $s_u = 0.00028$, $s_m = 0.0017$, $L = 160$ km, and λ_1 computed from equation (12.13), compute y as a function of x/L and plot the relation.

Solution The value of λ_1 is computed using equation (12.13) and is found to be –0.01. Then, values of y versus x are computed as shown in Table 12-10. Fig. 12-10 plots the elevation versus distance. The profile looks like a convex profile.

Table 12-11 *Values of* y *at different distances* x.

x (km)	y (m)	x (km)	y (m)
0	0.9773	100	0.9123
10	0.9708	150	0.8798
20	0.9643	200	0.8473
50	0.9448	250	0.8148

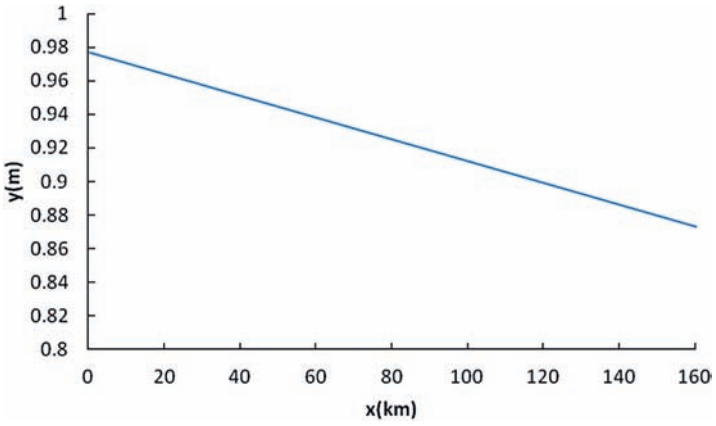

Figure 12-11 *Dimensionless uniform longitudinal profile.*

Example 12.12 Consider a river reach 250 km long, $s_m = 0.00065$, and $Y_0 = 0.9773$. Compute y as a function of x/L and plot the relation.

Solution Using equation (12.23), elevation y is computed for different distances, as given in Table 12-11. Fig. 12-11 plots the elevation versus distance. The profile looks like a straight profile.

12.4 Longitudinal Channel Profile from Fall Entropy

Using entropy-based geomorphological analysis, Fiorentino et al. (1993) derived the longitudinal bed profile of a channel as a function of fall in elevation as

$$Y = -\alpha \ln \beta + \alpha H \tag{12.24}$$

where Y is the fall in elevation from the source to the outlet of the main channel of the drainage basin whose entropy is H, and α is a parameter. Treating $\alpha \ln \beta$ and α as regression constants, Fiorentino et al. (1993) obtained the best fit line for the plot of elevation drop against entropy for each link of the main stream and found that equation (12.24) explained more than 90% of the variance in the fall in elevation for all basins considered.

Questions

Q12.1 Consider a river reach 68 km long where the upstream slope is 0.088 and the downstream slope is 0.001. Take the mean slope as 0.050. Compute the values of the Lagrange multipliers λ_0 and λ_1. Then compute the longitudinal profile of the reach. What does the profile look like? Compute the slope entropy.

Q12.2 Consider a 10-km-long river reach where the upstream slope is 0.02, the downstream slope is 0.08, and the mean slope is 0.040. Compute the values of the Lagrange multipliers λ_0 and λ_1. Then compute the slope profile and the longitudinal profile of the reach. What does the profile look like? Compute the slope entropy.

Q12.3 Consider a 10-km-long river reach where the upstream slope is 0.08, the downstream slope is 0.02, and the mean slope is 0.050. Compute the values of the Lagrange multipliers λ_0 and λ_1. Then compute the slope profile and the longitudinal profile of the reach. What does the profile look like? Compute the slope entropy.

Q12.4 Consider a 160-km-long reach of the Zijiang River, China, where the upstream slope is 0.000212, the downstream slope is 0.000315, and the mean slope is 0.0002635. Compute the values of the Lagrange multipliers λ_0 and λ_1. Then compute the slope profile and the longitudinal profile of the reach. What does the profile look like? Compute the slope entropy.

Q12.5 What factors determine the bed slope of a river reach?

Q12.6 Why and under what conditions is a river section bed concave, flat, or convex?

Q12.7 Does the river bed slope change with the river size, and if yes, then why?

Q12.8 Can a river have different slope profiles in different reaches? If the answer is yes, then why?

References

Cao, S. Y., and Chang, H. H. (1988). "Entropy as a probability concept in energy gradient distribution." *Hydraulic Engineering*, S. R. Abt and J. Gessler, eds., ASCE, New York, 1013–1018.

Fiorentino, M., Claps, P., and Singh, V. P. (1993). "An entropy-based morphological analysis of river basin networks." *Water Resour. Res.*, 29(4), 1215–1224.

Jaynes, E. T. (1957). "Information theory and statistical mechanics I." *Phys. Rev.*, 106, 620–630.

Shannon, C. E. (1948). "The mathematical theory of communication, I and II." *Bell Syst. Tech. J.*, 27, 379–423.

Additional Reading

Chang, H. H. (1984a). "Modeling of river changes." *J. Hydraul. Eng.*, 110(2), 157–172.

Chang, H. H. (1984b). "Analysis of river meanders." *J. Hydraul. Eng.*, 110(1), 503–519.

Davies, D. K., Vessel, R. V., Miles, R. C., Foley, M. G., and Bonis, S. B. (1978). "Fluvial transport and downstream sediment modifications in an active volcanic region." In *Fluvial sedimentology*, A. D. Miall, ed., Memoir No. 5, Canadian Society of Petroleum Geologists, Ottawa, 61–84.

Davy, B. W., and Davies, T. R. H. (1979). "Entropy concepts in fluvial geomorphology: A reevaluation." *Water Resour. Res.*, 15(1), 103–106.

Leopold, L. B., and Langbein, W. B. (1962). "The concept of entropy in landscape evolution." U.S. Geological Survey Professional Paper 500-A, U.S. Government Printing Office, Washington, DC.

Shulits, S. (1941). "Rational equation of river bed profile." *Trans. Am. Geophys. Union*, 36, 655–663.

Yang, C. T. (1971). "Potential energy and stream morphology." *Water Resour. Res.*, 7(2), 311–322.

Zhu, Z. (1984). "Bed load calculation of rivers with low sediment concentration." *J. Sediment Res.*, 1, 56–62 (in Chinese).

This page intentionally left blank

Chapter 13

Design of Alluvial Channels

The design of an alluvial channel involves determining the cross-sectional shape of the channel that is stable. In nature, cross-sectional shapes take on different forms that are irregular and complicated. These shapes are often approximated as rectangular, triangular, trapezoidal, or parabolic. Chow (1959) pointed out that natural channel sections are in general very irregular, varying from an approximate parabola to an approximate trapezoid. King (1939) also found that a parabolic section approximates the form assumed by many natural streams and old canals. Henderson (1966) divided cross-sectional shapes of stable alluvial channels in two types, as shown in Fig. 13-1. A type 1 channel is characterized by two curved banks with a constant depth and a finite width section in between at the bottom, whereas a type 2 channel consists of two curves that meet at the bed and extend to the point of the highest flow depth. Thus, if the finite width at the bottom in type 1 is reduced to a point, it reduces to type 2.

In the simplest case of channel design, it is assumed that the channel is unlined and carries only water and when the channel is flowing bankfull, the sediment particles along the perimeter of this channel are in a state of impending motion. This means that the channel is a threshold channel. Therefore, the knowledge of the threshold is needed for designing a stable channel with threshold banks and mobile bed and is important for design of irrigation canals and channelization works and for determining the channel response to flow regulation.

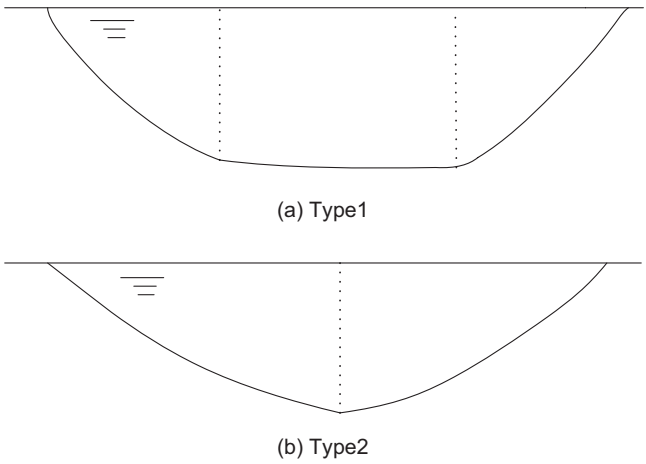

Figure 13-1 *Stable channel types.*

There are a number of approaches to design of stable channels. One of the commonly used approaches is the tractive force approach introduced by Glover and Florey (1951). This approach results in a cosine profile, which is widely cited in the sediment transport literature (Simons and Senturk 1976). Although the cosine profile for the shape of a threshold bank has been supported by a number of investigations (Parker 1978; Ikeda et al. 1988; Pizzuto 1990), it is not accepted universally. For example, Mironenko et al. (1984) suggested a parabolic shape, whereas Ikeda (1981), Diplas (1990), and others simulated the shape using an exponential function.

This chapter discusses the application of entropy theory to the design of stable channels of type 2. The application of entropy to channel design has been presented by Cao and Knight (1995a, 1995b, 1997), and Cao and Chang (1988), and this chapter draws from their works.

13.1 Channel Cross Section

The shape of a channel is assumed to be curved, as shown in Fig. 13-1b. Thus, the distribution of transverse slopes needs to be determined. This determination then leads to the cross-sectional bank profile. It is assumed that the dimensions and shape depend on the discharge and boundary sediment size or angle of repose of particles. Furthermore, the two bank profile curves on the sides of the centerline meet at the centerline at the bottom, and the shape curve must satisfy the continuity at the meeting point. The shape on either side of the centerline is the same. The elevation from the horizontal datum to the bank is denoted as y, varying from 0 to D at the water surface ($0 \leq y \leq$ D).

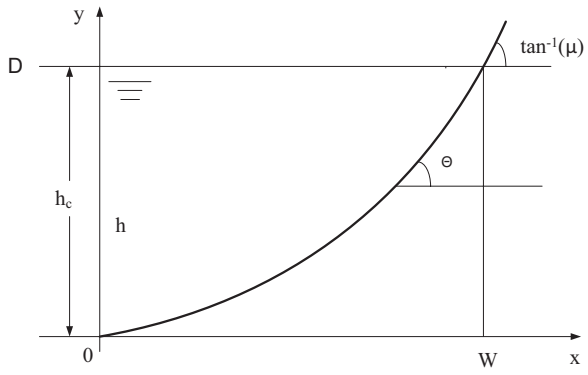

Figure 13-2 *Half channel width and notations.*

13.2 Notation

Let x be the lateral distance from the centerline, varying from 0 to W, where W is the half channel width from the centerline. Then, the total width would be $2W$ or B. The flow depth is denoted by h, varying from 0 to h_c, which equals D, where D is the bankfull flow depth at the centerline. The transverse slope is denoted by $s = \tan\theta = dy/dx$, varying from 0 to s_0, where s_0 is the submerged coefficient of friction, y is the elevation of the bank at x, s_0 is the maximum slope equal to the angle of repose μ, the angle of internal friction for sediment, or the static coefficient of Coulomb friction, as shown in Fig. 13-2. It is assumed that the transverse slope increases monotonically from the centerline to the water surface. Furthermore, the transverse slope is found to vary from one cross section to another. In other words, it has spatial variability. Therefore, it is not unduly restrictive to assume that the transverse slope is a random variable denoted by S whose specific value is denoted by s.

13.3 Shannon Entropy

The Shannon entropy (Shannon 1948) of the transverse slope S can be expressed as

$$H(S) = -\int_0^{s_0} f(s)\ln f(s)\,ds \tag{13.1}$$

where s is the value of random variable S, $f(s)$ is the probability density function (PDF) of S, and H is the entropy of $f(s)$ or S. Equation (13.1) is a measure of uncertainty of $f(s)$ of variable S. The objective is to derive $f(s)$ by maximizing H,

subject to specified constraints, in accordance with the principle of maximum entropy (POME) (Jaynes 1957).

Two cases are considered. In the first case, no constraints other than the total probability on the transverse are imposed. In the second case, an average slope constraint is imposed. It may be noted that the first case is a limiting case of the more general second case.

13.4 Entropy Method, Case 1: No Constraint

13.4.1 Specification of Constraints

For purposes of simplicity, the constraint that $f(s)$ must satisfy is formulated as

$$\int_0^{s_0} f(s)\,ds = 1 \tag{13.2}$$

which is the total probability theorem. In a sense, this is really not a constraint, because all probability distributions must satisfy equation (13.2).

13.4.2 Probability Density Function and Maximum Entropy

The least biased probability distribution function $f(s)$ is obtained by maximizing the entropy given by equation (13.1), subject to equation (13.2). This step is done by using the method of Lagrange multipliers where the Lagrangian function L can be expressed as

$$L = -\int_0^{s_0} f(s)\ln f(s)\,ds - (\lambda_0 - 1)\left(\int_0^{s_0} f(s)\,ds - 1\right) \tag{13.3}$$

where λ_0 is the Lagrange multiplier. Differentiating equation (13.3) with respect to f, while recalling the Euler–Lagrange calculus of variation, noting that f is variable and s is parameter, and equating the derivative to zero, one obtains

$$\frac{\partial L}{\partial f} = 0 \Rightarrow -\ln f(s) - \lambda_0 = 0 \tag{13.4}$$

Equation (13.4) yields

$$f(s) = \exp(-\lambda_0) \tag{13.5}$$

Equation (13.5) is a uniform PDF of transverse slope S. The cumulative distribution function (CDF) of S is obtained by integrating equation (13.5) as

$$F(s) = \exp(-\lambda_0)s \tag{13.6}$$

The maximum entropy of S is obtained by inserting equation (13.5) in equation (13.1):

$$H(S) = \lambda_0 \tag{13.7}$$

which is expressed in terms of the Lagrange multiplier λ_0 and is constant.

13.4.3 Determination of Lagrange Multipliers

Substitution of equation (13.5) in equation (13.1) yields

$$\exp(-\lambda_0) = \frac{1}{s_0} \tag{13.8}$$

Therefore,

$$\lambda_0 = \ln s_0 \tag{13.9}$$

Substitution of equation (13.8) in equation (13.5) leads to the PDF of S as

$$f(s) = \frac{1}{s_0} \tag{13.10}$$

Likewise, substitution of equation (13.8) in equation (13.6) yields the CDF of S:

$$F(s) = \frac{s}{s_0} \tag{13.11}$$

Similarly, substitution of equation (13.8) in equation (13.7) yields

$$H(S) = \ln s_0 \tag{13.12}$$

13.4.4 Distribution of Transverse Slope

At any lateral distance from the centerline less than x, the transverse slope at that distance is less than s. It can then be reasoned that all values of x between 0 and W along the x-axis are equally likely to be sampled or have the same probability of occurrence. Then the probability of transverse slope that is equal to or less than s is x/W. The CDF of S can then be expressed in a simple form as

$$F(s) = \frac{x}{W} \tag{13.13}$$

Differentiating equation (13.13) yields the PDF of S as

$$f(s)ds = \frac{1}{W}dx \text{ or } f(s) = \frac{1}{W}\frac{dx}{ds} = \left(W\frac{ds}{dx}\right)^{-1} \tag{13.14}$$

The PDF given by equation (13.5) must satisfy the constraint defined by equation (13.2). Inserting equation (13.5) in equation (13.14), one gets

$$\frac{1}{s_0} = \frac{1}{W}\frac{dx}{ds} \tag{13.15}$$

Integration of equation (13.15) yields

$$s = \frac{s_0}{W}x \tag{13.16}$$

Equation (13.16) expresses the distribution of transverse slope as a function of transverse distance and satisfies the condition that $s = 0$ at $x = 0$ and $s = s_0$ at $x = W$.

13.4.5 Cross-Sectional Shape

Recalling the definition of slope, $s = dy/dx$, and equating it to equation (13.16), one gets

$$\frac{dy}{dx} = \frac{s_0}{W}x \tag{13.17}$$

Integrating equation (13.17) with the condition that $s = 0$ at $x = 0$, the bank profile becomes

$$y = \frac{s_0}{2W}x^2 \tag{13.18}$$

Equation (13.18) gives the elevation of the right bank or water margin as a function of transverse distance x from the centerline up to $x = W$. This is the shape function $y = y(x)$. At $x = W$, $y = D$, which is also the flow depth at the centerline h_c and is given by equation (13.18) as

$$D = h_c = \frac{s_0 W}{2} \tag{13.19}$$

Subtracting equation (13.18) from equation (13.19), one gets the lateral distribution of local water flow depth as

$$h = D - y = \frac{s_0}{2}\left(W - \frac{x^2}{W}\right) \tag{13.20}$$

The aspect ratio $B/D = 2W/D$ then becomes

$$\frac{B}{D} = \frac{4}{s_0} \tag{13.21}$$

Equation (13.19) specifies the depth at the centerline, and equation (13.20) specifies the boundary elevation from the bed. Taking the difference of these two equations results in the lateral distribution of flow depth $h(x)$ as a function of lateral distance as

$$h(x) = \frac{s_0 W}{2}\left[1 - \left(\frac{x}{W}\right)^2\right] \tag{13.22}$$

Noting that $hdx = dA$, the cross-sectional area A can be obtained by integrating equation (13.22) as

$$A = \frac{2}{3} s_0 W^2 \tag{13.23a}$$

For $s_0 = 0.5$, the aspect ratio given by equation (13.23a) can be written as

$$\frac{B}{h_c} = \frac{4}{s_0} = 8, \quad B = 2W \tag{13.23b}$$

where B = water surface width. Then, the cross-sectional area can be defined as

$$A = \frac{W^2}{3} = \frac{8}{3}\left(\frac{h_2^2}{s_0}\right) = \frac{16}{3} h_c^2 \tag{13.24}$$

Now the wetted perimeter P_w is computed as follows: Consider an arc element of wetted perimeter $dPw = (dx^2 + dy^2)^{1/2}$. From equation (13.17), $dy = x^2 s_0/(2W)$. Therefore, $dy = x s_0/W$, and

$$dP_w = \left[dx^2\left(\frac{x s_0}{W} dx\right)^2\right]^{1/2} = \left[1 + \frac{x^2 s_0^2}{W^2}\right] dx = \left(\frac{s_0}{W}\right)\left[\frac{W^2}{{s_0}^2} + x^2\right] dx \tag{13.25a}$$

Integrating equation (13.25a) leads to

$$\begin{aligned} P_w &= \frac{W}{s_0}\{s_0\sqrt{1+s_0^2} + \ln[s_0 + \sqrt{1+s_0^2}]\} \\ &= \frac{2h_c}{s_0^2}\{s_0\sqrt{1+s_0^2} + \ln[s_0 + \sqrt{1+s_0^2}]\} \end{aligned} \tag{13.25b}$$

The hydraulic radius R can now be expressed as

$$R = \frac{2 s_0 L^2}{3 P_w} = \frac{8 h_c^2}{3 s_0 P_w} \tag{13.25c}$$

13.5 Entropy Method, Case 2: One Constraint

13.5.1 Specification of Constraints

In this case, two constraints are defined. The first constraint is given by equation (13.2), and the second constraint is expressed by the mean value of S as

$$\int_0^{s_0} sf(s)ds = E[S] = \overline{s} = s_m \tag{13.26}$$

where $\overline{s} = s_m$ is the mean transverse slope of the entire cross section, and E is the expectation operator.

13.5.2 Probability Density Function and Maximum Entropy

To obtain the least-biased $f(s)$ that satisfies equations (13.2) and (13.26), equation (13.1) is maximized according to POME. This maximization is achieved by using the method of Lagrange multipliers. To that end, the Lagrangian function L is expressed as

$$L = -\int_0^{s_0} f(s)\ln f(s)ds - (\lambda_0 - 1)\left(\int_0^{s_0} f(s)ds - 1\right) - \lambda_1\left(\int_0^{s_0} sf(s)ds - s_m\right) \tag{13.27}$$

where λ_0 and λ_1 are the Lagrange multipliers. Differentiating equation (13.27) with respect to f, while recalling the Euler–Lagrange calculus of variation, noting that f is variable and s is parameter, and equating the derivative to zero, one obtains

$$\frac{\partial L}{\partial f} = 0 \Rightarrow -\ln f(s) - \lambda_0 - \lambda_1 s = 0 \tag{13.28}$$

Equation (13.28) yields

$$f(s) = \exp(-\lambda_0 - \lambda_1 s) \tag{13.29}$$

Equation (13.29) is the POME-based PDF of transverse slope S. It may be noted that $f(s) = \exp(-\lambda_0)$ at $s = 0$. The CDF of S is obtained by integrating equation (13.29):

$$F(s) = \frac{1}{\lambda_1}[\exp(-\lambda_0) - \exp(-\lambda_0 - \lambda_1 s)] \tag{13.30}$$

The maximum entropy of S is obtained by inserting equation (13.29) in equation (13.1):

$$H(s) = \lambda_0 + \lambda_1 s_m \tag{13.31}$$

which is expressed in terms of the Lagrange multipliers λ_0 and λ_1 and mean transverse slope s_m.

13.5.3 Determination of Lagrange Multipliers

Substitution of equation (13.29) in equation (13.2) yields

$$\exp(-\lambda_0) = \frac{\lambda_1}{1-\exp(-\lambda_1 s_0)} \tag{13.32}$$

Therefore,

$$\lambda_0 = -\ln\lambda_1 + \ln[1-\exp(-\lambda_1 s_0)] \tag{13.33}$$

Differentiating equation (13.33) with respect to λ_1, one gets

$$\frac{\partial\lambda_0}{\partial\lambda_1} = -\frac{1}{\lambda_1} + \frac{s_0\exp(-\lambda_1 s_0)}{1-\exp(-\lambda_1 s_0)} \tag{13.34}$$

Furthermore, substitution of equation (13.29) in equation (13.2) also yields

$$\lambda_0 = \ln\int_0^{s_0}\exp(-\lambda_1 s)\,ds \tag{13.35}$$

Differentiating equation (13.35) with respect to λ_1 yields

$$\frac{\partial\lambda_0}{\partial\lambda_1} = -\frac{\int_0^{s_0} s\exp(-\lambda_0-\lambda_1 s)\,ds}{\int_0^{s_0}\exp(-\lambda_0-\lambda_1 s)\,ds} = -s_m \tag{13.36}$$

Equating equation (13.34) to equation (13.36), the result is

$$s_m = \frac{1}{\lambda_1} - \frac{s_0\exp(-\lambda_1 s_0)}{1-\exp(-\lambda_1 s_0)} \tag{13.37}$$

Thus, equation (13.37) is implicit in λ_1 and can be solved numerically for unknown λ_1.

Substitution of equation (13.32) in equation (13.29) leads to the PDF of S as

$$f(s) = \frac{\lambda_1\exp(-\lambda_1 s)}{1-\exp(-\lambda_1 s_0)} \tag{13.38}$$

At $s=0, f(s)=\lambda_1/[1-\exp(-\lambda_1 s_0)]$. Equation (13.38) has only one unknown Lagrange multiplier λ_1. Likewise, the CDF becomes

$$F(s) = \frac{1-\exp(-\lambda_1 s)}{1-\exp(-\lambda_1 s_0)} \tag{13.39}$$

Fig. 13-3 shows a plot of $f(s)$ as well as $F(s)$ with $s_0 = 0.5$ for different values of λ_1. As λ_1 increases to –0.1, the PDF tends to become uniform.

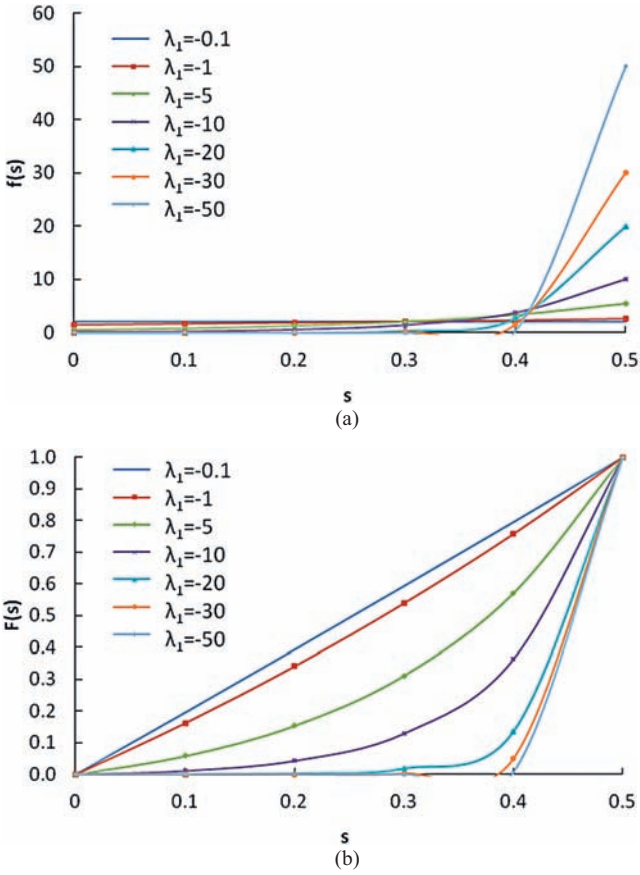

Figure 13-3 *Probability density function (a) and cumulative probability distribution function (b) of* s *for* s_0*=0.5.*

Table 13-1 *Computation of probability of S being less than or equal to 0.2, 0.3, and 0.4, Example 13.1.*

s	$F(s) = P(S \leq s)$	$P(S \geq s) = 1 - F(s)$
0.2	0.043	0.957
0.3	0.129	0.871
0.4	0.364	0.636

Example 13.1 Consider $s_0 = 0.5$ and $\lambda_1 = -10$. Compute the probability of S less than or equal to 0.2, 0.3, and 0.4.

Solution Using equation (13.39) with $s_0 = 0.5$ and $\lambda_1 = -10$, the probability of S being less than or equal to 0.2, 0.3, and 0.4 is shown in Table 13-1.

13.5.4 Distribution of Transverse Slope

Inserting equation (13.29) in equation (13.14), one gets

$$\frac{\lambda_1 \exp(-\lambda_1 s)}{1-\exp(-\lambda_1 s_0)} = \frac{1}{W}\frac{dx}{ds} \tag{13.40}$$

Integration of equation (13.40) yields

$$-\frac{\exp(-\lambda_1 s)}{1-\exp(-\lambda_1 s_0)} = \frac{1}{W}x + \text{cons} \tag{13.41}$$

where cons is the constant of integration. Using the boundary condition, $s = 0$ at $x = 0$, one obtains

$$\text{cons} = -\frac{1}{1-\exp(-\lambda_1 s_0)} \tag{13.42}$$

Substitution of equation (13.42) in equation (13.41) gives

$$-[1-\exp(-\lambda_1 s_0)]^{-1}\exp(-\lambda_1 s) = \frac{x}{W} - [1-\exp(-\lambda_1 s_0)]^{-1} \tag{13.43}$$

Equation (13.43) can be simplified as

$$s = -\frac{1}{\lambda_1}\ln\left\{1 - \frac{x}{W}[1-\exp(-\lambda_1 s_0)]\right\} \tag{13.44}$$

Equation (13.44) can also be written as

$$s = \frac{1}{\lambda_1}\ln\left\{\frac{\exp(\lambda_1 s_0)}{\exp(\lambda_1 s_0) - \frac{x}{W}[\exp(\lambda_1 s_0)-1]}\right\} \tag{13.45}$$

Equation (13.45) expresses the distribution of transverse slope as a function of transverse distance and satisfies the condition that $s = 0$ at $x = 0$ and $s = s_0$ at $x = W$. The Lagrange multiplier λ_1 is obtained from the solution of equation (13.37) for the specified mean slope, which should be related to hydraulic and geometric parameters.

Example 13.2 For $\lambda_1 = -10$ and $s_0 = 0.5$, $W = 1$ m, compute the value of s at $x = 0.1$, 0.3, 0.5, and 1.

Solution Using equation (13.45), one obtains the following:

x	0.1	0.3	0.4	0.5	1
s	0.276	0.381	0.409	0.431	0.5

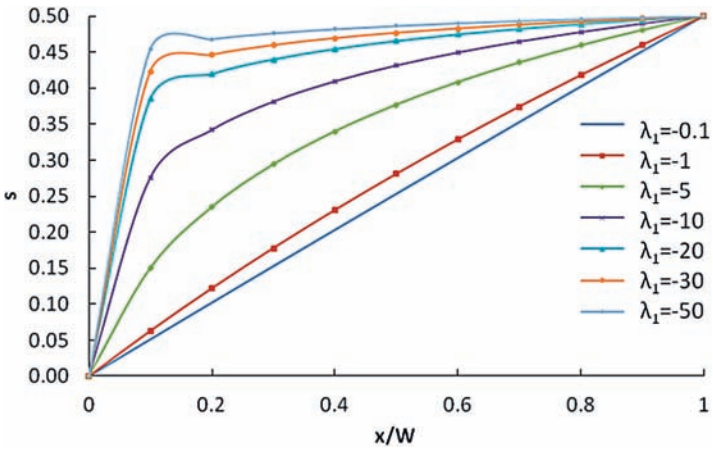

Figure 13-4 *Lateral slope as a function of dimensionless distance for various values of* λ_1 *and* $s_0 = 0.5$.

13.5.5 Characteristics of Slope Distribution

The transverse slope s is plotted as a function of dimensionless distance x/W for various values of λ_1 ($\lambda_1 = -0.1, -1, -5, -10, -20, -30$, and -50) (Fig. 13-4). It is seen that when $\lambda_1 = 0$, s becomes infinite and the bank becomes vertical. Conversely, if λ_1 is infinite (negative), s becomes zero, meaning that the bank becomes horizontal.

13.5.6 Cross-Sectional Shape

Recalling the definition of slope, $s = dy/dx$, and equating it to equation (13.45), one gets

$$\frac{dy}{dx} = \frac{1}{\lambda_1}\ln\left\{\frac{1}{1-\frac{x}{W}[1-\exp(-\lambda_1 s_0)]}\right\} = -\frac{1}{\lambda_1}\ln\left\{1-\frac{x}{W}[1-\exp(-\lambda_1 s_0)]\right\} \quad (13.46)$$

Integrating equation (13.46) with the condition that $s = 0$ at $x = 0$, the bank profile becomes

$$y = \frac{W}{\alpha\lambda_1}\left(1-\frac{x}{W}\alpha\right)\left[\ln\left(1-\frac{x}{W}\alpha\right)-1\right] \quad (13.47)$$

where $\alpha = 1 - \exp(-\lambda_1 s_0)$. Equation (13.47) gives the elevation of the right bank or water margin as a function of transverse distance x from the centerline up to $x = W$. This is the shape function $y = y(x)$. At $x = W$, $y = D$, which is also the flow depth at the centerline h_c, and is given by equation (13.47) as

$$D = \frac{W}{\alpha\lambda_1}(1-\alpha)[\ln(1-\alpha)-1] \tag{13.48}$$

Subtracting equation (13.47) from equation (13.48), one gets the lateral distribution of local water flow depth as

$$h = \frac{W}{\alpha\lambda_1}\left\{(1-\alpha)[\ln(1-\alpha)-1]-(1-\frac{x}{W}\alpha)\left[\ln\left(1-\frac{x}{W}\alpha\right)-1\right]\right\} \tag{13.49}$$

Example 13.3 Plot α as a function of λ_1 for $s_0 = 0.5$.

Solution Here $\alpha = 1 - \exp(-\lambda_1 s_0)$. The values of α for various values of λ_1 for $s_0 = 0.5$ are given in Table 13-2. Fig. 13-5 plots α as a function of λ_1.

Table 13-2 *Computation of a as a function of λ_1 for s_0=0.5, Example 13.3.*

λ_1	α
0	0
–1	–0.649
–2	–1.718
–3	–3.482
–5	–11.182
–7	–32.115

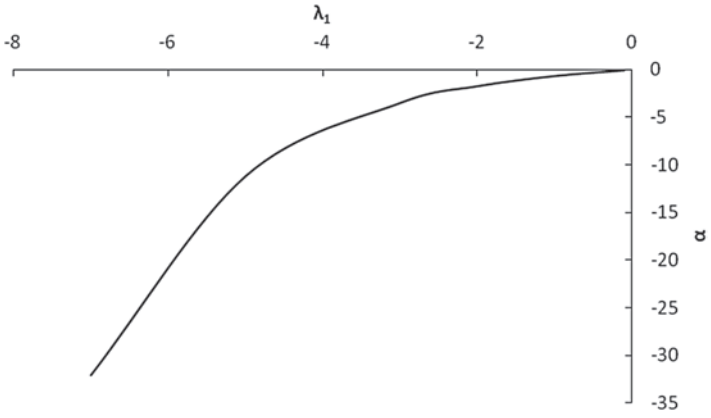

Figure 13-5 *Plot of α as a function of λ_1 for $s_0 = 0.5$.*

Example 13.4 Select a value of α from the plot in Fig. 13-5 for Example 13.3. Take $s_0 = 0.5$, and get a value of λ_1 accordingly. Then compute the value of D for $W = 1, 2, 3, 4$, and 5 m.

Solution For $\alpha = -20$, $\lambda_1 = [1/s_0]\ln[1/(1-\alpha)] = -0.6089$. Using equation (13.48), the values of D for various values of W are computed as tabulated in Table 13-3.

Table 13-3 *Computation of values of* D *for various values of* W*, Example 13.4.*

W (m)	D (m)
1	0.353
2	0.705
3	1.058
4	1.410

Example 13.5 For various values of W and x, compute values of y for $s_0 = 0.5$. Select the value of α.

Solution As in Example 13.4, $\alpha = -20$, $\lambda_1 = -6.089$. Using equation (13.47), the values of y are computed and tabulated in Table 13-4.

Table 13-4 *Values of* y *(in meters) for different values of* x *and* W.

x (m)	$W = 1$ m	x (m)	$W = 2$ m	x (m)	$W = 3$ m	x (m)	$W = 4$ m	x (m)	$W = 5$ m
0.1	0.002	0.2	0.005	0.3	0.007	0.4	0.010	0.5	0.012
0.2	0.025	0.4	0.050	0.6	0.075	0.8	0.100	1.0	0.125
0.3	0.054	0.6	0.109	0.9	0.163	1.2	0.217	1.5	0.272
0.5	0.126	1.0	0.253	1.5	0.379	2.0	0.505	2.5	0.631
1	0.353	2.0	0.705	3.0	1.058	4.0	1.410	5.0	1.763

Example 13.6 Compute h for selected values of W and α from Examples 13.4 and 13.5.

Solution Using equation (13.49) for $s_0 = 0.5$, values of h are computed for selected values of W and α, as tabulated in Table 13-5.

Table 13-5 *Values of* h *(in meters) for different values of* x *and* W.

x (m)	$W = 1$ m	x (m)	$W = 2$ m	x (m)	$W = 3$ m	x (m)	$W = 4$ m	x (m)	$W = 5$ m
0.1	0.350	0.2	0.700	0.3	1.050	0.4	1.401	0.5	1.751
0.2	0.328	0.4	0.655	0.6	0.983	0.8	1.310	1.0	1.638
0.3	0.298	0.6	0.596	0.9	0.895	1.2	1.193	1.5	1.491
0.5	0.226	1.0	0.453	1.5	0.679	2.0	0.905	2.5	1.131
1	0.000	2.0	0.000	3.0	0.000	4.0	0.000	5.0	0.000

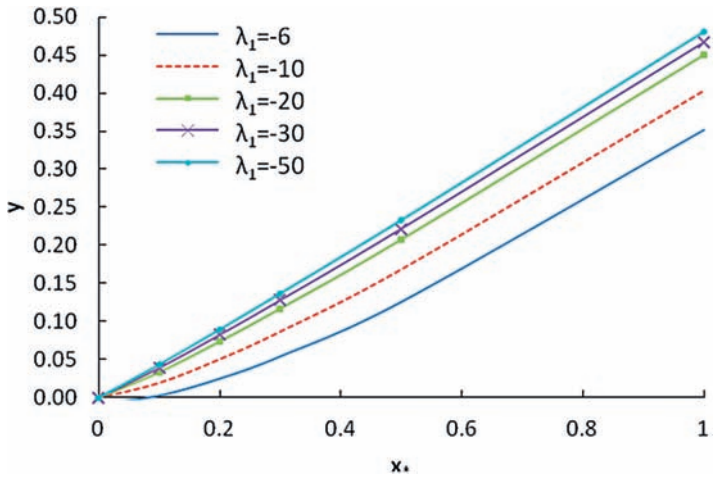

Figure 13-6 *Elevation of a bank profile as a function of dimensionless distance for different values of* λ_1 *and* $s_0 = 0.5$.

Now the effect of λ_1 on the bank profile of a threshold channel can be numerically evaluated. For λ_1 between 1 and 50 and $s_m = 0.5$, this effect is shown in Fig. 13-6. This figure shows that the bank profile is a curve with two boundary conditions where $y = 0$ at $x = 0$, and $dy/dx = s_0$ at $x = W$. The shape approaches a trapezoidal shape as λ_1 becomes large. The curvature of the bank profile increases, but the slope of the bank profile decreases with decreasing λ_1. Furthermore, the larger value of λ_1 decreases the aspect ratio (width/depth).

13.5.7 Lagrange Multiplier λ_1 and Its Effect

The physical meaning of the Lagrange multiplier λ_1 is now explored. Consider two extreme cases: when $\lim_{\lambda_1 \to 0} s = \frac{x}{W} s_0$ tends to 0 and when λ_1 tends to infinity. The first extreme case corresponds to case 1, which was dealt with earlier. To that end, L'Hospital's rule of limit theory is applied to equation (13.44). First, equation (13.44) is rewritten as

$$s = s_0 - \frac{1}{\lambda_1} \ln\left[\left(1 - \frac{x}{W}\right)\exp(\lambda_1 s_0) + \frac{x}{W}\right] \tag{13.50}$$

Taking the limit when $\lambda_1 \to 0$,

$$\lim_{\lambda_1 \to 0} s = s_0 - \lim_{\lambda_1 \to 0} \frac{\frac{d}{d\lambda_1} \ln\left[\left(1 - \frac{x}{W}\right)\exp(\lambda_1 s_0) + \frac{x}{W}\right]}{\frac{d}{d\lambda_1}(\lambda_1)} \tag{13.51}$$

Equation (13.51) can be written as

$$\lim_{\lambda_1 \to 0} s = s_0 - \lim_{\lambda_1 \to 0} \frac{s_0\left(1 - \frac{x}{W}\right)\exp(\lambda_1 s_0)}{\left(1 - \frac{x}{W}\right)\exp(\lambda_1 s_0) + \frac{x}{W}} \tag{13.52}$$

Equation (13.52) becomes

$$\lim_{\lambda_1 \to 0} s = \frac{x}{W} s_0 \tag{13.53}$$

Likewise, equation (13.50) with $\lambda_1 \to \infty$ yields

$$\lim_{\lambda_1 \to \infty} s = \mu \to 0 \tag{13.54}$$

Equation (13.54) shows that the transverse slope approaches a horizontal line $s = \mu$ as λ_1 increases to a large value, as seen from Fig. 13-4.

The boundary elevation above the bed at the center of these two cases is obtained by expressing $s = dy/dx$ and integrating equations (13.53) and (13.54), respectively, as

$$\lim_{\lambda_1 \to 0} y = \frac{x^2}{2W} s_0 \tag{13.55}$$

which is the same as equation (13.19).

$$\lim_{\lambda_1 \to \infty} y = \mu x \tag{13.56}$$

Equation (13.55) expresses a simple parabolic bank profile as λ_1 approaches zero. Equation (13.56) results in a trapezoidal bank profile as λ_1 approaches a large value.

The centerline channel depth $h_c = D$ is obtained by inserting $x = W$ in equations (13.55) and (13.56) as

$$\lim_{\lambda_1 \to 0} h_c = \frac{W}{2} s_0 \tag{13.57}$$

which is the same as in equation (13.20).

$$\lim_{\lambda_1 \to \infty} h_c = \mu W \tag{13.58}$$

The aspect ratios can now be given as

$$\lim_{\lambda_1 \to 0}\left(\frac{2W}{D}\right) = \frac{4}{s_0} \tag{13.59}$$

which is the same as in equation (13.21).

$$\lim_{\lambda_1 \to \infty} \left(\frac{2W}{D} \right) = \frac{2}{\mu} \tag{13.60}$$

Equations (13.59) and (13.60) show that the aspect ratio increases twofold as λ_1 decreases from a large value to zero.

Let

$$\lambda_1 = \beta \tau^* \tag{13.61}$$

where β is an empirical coefficient and τ^* is the dimensionless effective Shields parameter defined as

$$\tau^* = \frac{\tau - \tau_c}{\tau_c} \tag{13.62}$$

where τ is the actual Shields parameter (shear stress) and τ_c is the critical Shields parameter. Thus, the use of equation (13.61) requires computation of τ and τ_c.

Although the physical basis of equation (13.61) is not yet developed, Chang (1988) notes that a flat-bed upper regime flow is caused when τ^* is larger than 25. A trapezoidal channel is formed when $\lambda_1 < -50$, which would correspond to $\beta = -2$ for an upper-regime flat-bed flow. If $\tau = \tau_c$, $\tau^* = 0$; this equivalence corresponds to the channel being at threshold. In this case, equation (13.61) yields $\lambda_1 = 0$. If equations (13.61) and (13.62) are correct, then equation (13.55) leads to the shape of a threshold channel and equation (13.56) gives the shape of a flat bed in the upper-regime flow condition, i.e., $\lambda_1 < -50$.

13.6 Comparison with Two Bank Profiles

In the hydraulics literature, bank profiles of straight threshold channels have been expressed using a variety of equations (Henderson 1966; Diplas and Vigilar 1992). The bank profiles of threshold channels given by Diplas and Vigilar (1992) and the U.S. Bureau of Reclamation (USBR) (Henderson 1966) are approximated by the entropy method for the case of λ_1 tending to zero. It may be interesting to compare the cross-sectional area A, the depth at the centerline h_c (or D), and the aspect ratio $2W/h_c$ of these two approaches with those given by the entropy method. Following the same procedure as for case 1, the lateral distribution of flow depth $h(x)$ as a function of the lateral distance, cross-sectional area A, aspect ratio, wetted perimeter, and hydraulic radius can be derived.

It may be noted that the entropy method yields a parabolic form of the bank profile, given by equation (13.55). The simple parabolic form seems to play a very important role in science. Examples where such a form has been used include Einstein's most celebrated equation of the special theory of relativity ($E = mc^2$, where E = energy, m = mass, and c = speed of light); the kinetic energy equation (KE = $mv^2/2$, where KE = kinetic energy, m = mass, and v = velocity);

the acceleration of uniform circular motion ($a_c = v^2/r$, where a_c = acceleration, v = velocity, and r = radius); and equation of distance traveled in a straight line motion ($l = at^2/2$, where l = distance, t = time, and a = acceleration), among others.

According to Diplas and Vigilar (1992) (the D–V approach), the dimensionless cross-sectional area A^* can be expressed as

$$A^* = 0.69B^* \tag{13.63}$$

where $A^* = A/h_c^2$ and

$$B^* = \frac{B}{h_c} = -16.1814s_0^3 + 44.3206s_0^2 - 43.5548s_0 + 21.1496 \tag{13.64}$$

Therefore,

$$A = 0.69h_c \tag{13.65}$$

From the aspect ratio given by equation (13.64), $B/h_c = 8.42$ for $s_0 = 0.5$, one obtains

$$h_c = D = \frac{B}{8.42} = 0.24s_0B \tag{13.66}$$

Following the USBR approach, h_c can be obtained as

$$\frac{h}{h_c} = \cos\left(\frac{x\tan\phi}{h_c}\right) \tag{13.67}$$

where ϕ = the friction angle of the boundary material, which is taken as equal to s_0. When $x = W$ and $h = 0$, equation (13.62) yields $(x\ \tan\phi)/h_c = 0$, resulting in

$$h_c = \frac{2Ws_0}{\pi} = B\frac{s_0}{\pi} \tag{13.68}$$

The aspect ratio, B/h_c, can be obtained for s_0 as

$$\frac{B}{h_c} = \frac{\pi}{s_0} = 6.28 \tag{13.69}$$

$$A = \frac{2h_c^2}{s_0} = \frac{2h_cB}{\pi} \tag{13.70}$$

where h = local depth, h_c = centerline depth, and x = lateral distance from the channel center.

Cao and Knight (1997) compared the entropy method (designated here as the C–K method) with the Diplas and Vigilar (D–V) and the USBR method, as shown in Table 13-6. For $s_0 = 0.5$, the entropy method is closer to the D–V method than to the USBR method. The entropy method yields results between the maximum values caused by the D–V method and the minimum values caused by the USBR method.

Table 13-6 *Comparison of the entropy method with the D–V and USBR methods.*

Channel geometry parameter	D–V method	Entropy method (C–K)	USBR method
h_c	0.24 s_0B, $s_0 = 0.5$	0.25 s_0B	0.32 s_0B
A	0.69 Bh_c	0.67 Bh_c	0.64 Bh_c
B/h_c	Equation (13.66)	$4/s_0$	π/s_0
B/h_c, $s_0 = 0.5$	8.42	8.0	6.28

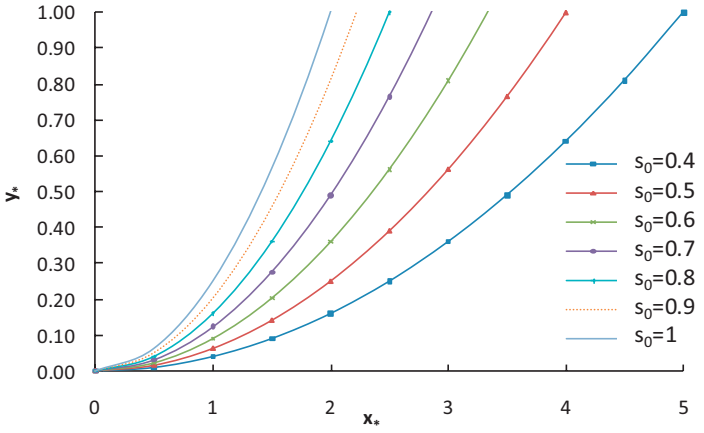

Figure 13-7 *Bank profiles of threshold channels for different values of* s_0.

It may now be worthwhile to investigate the relationships among the shape of the bank profile, hydraulic parameters, and boundary material diameter or submerged static friction factor s_0. To that end, it is convenient to use dimensionless quantities. The dimensionless profile can be expressed from equations (13.55) and (13.59) as

$$y^* = \left(\frac{s_0^2}{4}\right) x^{*2} \tag{13.71}$$

where $y^* = y/h_c$ and $x^* = x/h_c$. Fig. 13-7 shows dimensionless elevation versus dimensionless lateral distance for several values of s_0. Likewise, the dimensionless channel width B^* versus s_0 and the dimensionless cross-sectional area A^* versus s_0 are shown for three methods in Figs. 13-8 and 13-9, respectively. Here $B^* = B/h_c$, $A^* = A/h_c^2$, and h_c = geometry depth at the channel center. The dimensionless width and dimensionless area decrease with increasing s_0 for all three methods. The D–V method yields the highest values, the USBR method the smallest values, and the entropy method in between for $s_0 > 0.44$. However, for $s_0 < 0.44$, this statement is not true. For smaller values of s_0, the entropy method is closer to the D–V method, but for higher values, it is closer to the USBR method.

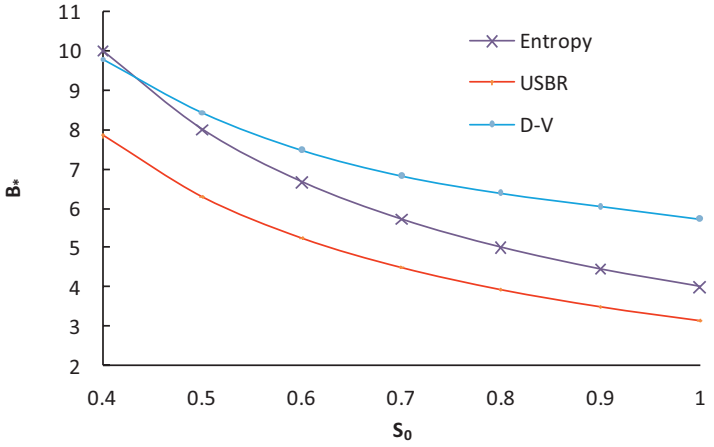

Figure 13-8 *Dimensionless channel width as a function of submerged static friction coefficient for the entropy, D–V, and USBR approaches.*

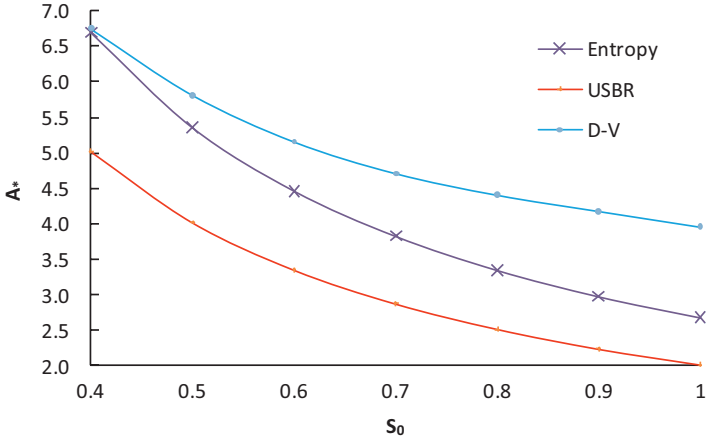

Figure 13-9 *Dimensionless cross-sectional area as a function of submerged static friction coefficient for the entropy, D–V, and USBR approaches.*

13.7 Evaluation of Entropy-Based Bank Profiles of Threshold Channels

A threshold channel means that at every point along the boundary the actual shear stress equals the critical shear stress. To evaluate the entropy-based equations, the following parameters are defined on the side slopes and on the level: dimensionless critical shear stress, dimensionless stress depth, dimensionless local depth, dimensionless actual shear stress, dimensionless actual stress depth, and shear stress distribution.

13.7.1 Dimensionless Critical Shear Stress

This parameter is the same as the critical Shields parameter and can be defined for the side slopes as

$$\tau_{cs}^{*} = \frac{\tau_{cs}}{(\rho_s - \rho)gd} = \frac{h_{cs}S_0}{\rho^{*}d} \tag{13.72}$$

and on the level as

$$\tau_{co}^{*} = \frac{\tau_{co}}{(\rho_s - \rho)gd} = \frac{h_{co}S_0}{\rho^{*}d} \tag{13.73}$$

where $\tau_{cs} = \rho g h_{cs} S_0$ = the critical shear stress on the slopes; $\tau_{c0} = \rho g h_{co} S_0$ = the critical shear stress on the level; h_{cs} = the critical shear stress depth on the slope; h_{co} = the critical stress depth on the level; $\rho^{*} = (\rho_s - \rho)/\rho_s$; ρ = the density of water; ρ_s = the density of sediment; S_0 = the streamwise slope; and d = diameter of sediment particles.

13.7.2 Dimensionless Shear Stress Depth

The dimensional shear stress depth is defined on the slope as

$$h_{cs}^{*} = \frac{h_{cs}}{h_c},\ h_c = D \tag{13.74}$$

and on the level as

$$h_{co}^{*} = \frac{h_{co}}{h_c},\ h_c = D \tag{13.75}$$

where h_{cs}^{*} and h_{co}^{*} are the dimensionless depths related to critical stress on the side slopes and the critical stress on the level, respectively.

13.7.3 Dimensionless Local Depth

The dimensionless local depth is defined as

$$h^{*} = \frac{h}{h_c} \tag{13.76}$$

and the dimensionless depth at the centerline as

$$h_c^{*} = \frac{h_c}{h_c} = 1 \tag{13.77}$$

where h is the local depth and h_c is the depth at the center of the threshold channel. Thus, h^{*} and h_c^{*} are the dimensionless depths related to the local geometry and the geometry centerline, respectively.

13.7.4 Dimensionless Actual Shear Stress

The dimensionless actual shear stress is defined on the slope as

$$\tau_{as}^{*} = \frac{\tau_{as}}{(\rho_s - \rho)gd} = \frac{h_{as}S_0}{\rho^{*}d} \tag{13.78}$$

and the dimensionless actual shear stress is defined on the level as

$$\tau_{ao}^{*} = \frac{\tau_{ao}}{(\rho_s - \rho)gd} = \frac{h_{ao}S_0}{\rho^{*}d} \tag{13.79}$$

where $\tau_{as} = \rho g h_{as} S_0$ = the actual shear stress on the slope, and $\tau_{ao} = \rho g h_{ao} S_0$ = the actual shear stress on the level.

13.7.5 Dimensionless Actual Stress Depth

The actual shear stress depth is defined on the slope as

$$h_{as}^{*} = \frac{h_{as}}{h_c},\ h_c = D \tag{13.80}$$

and the actual shear stress depth is defined on the level as

$$h_{ao}^{*} = \frac{h_{ao}}{h_c},\ h_c = D \tag{13.81}$$

where h_{as} = the actual stress depth on the slope and h_{ao} = the actual stress depth on the level.

13.7.6 Shear Stress Distribution

Ikeda (1982) derived a dimensionless shear stress distribution on a slope as

$$K = \frac{-\psi \tan^2\phi\cos\theta + (\tan^2\phi\cos^2\theta + \psi^2\tan^2\phi\sin^2\theta - \sin^2\theta)^{0.5}}{(1 - \psi\tan\phi)\tan\phi} \tag{13.82}$$

where $K = \tau_{cs}^{*}/\tau_{co}^{*} = \tau_{cs}/\tau_{co} = h_{cs}/h_{co}$; ϕ = the angle of repose of sand; θ = the lateral inclination of the side (bank) slope; and ψ = the ratio of lift force to drag force acting on a boundary particle. Ikeda (1982) considered the effects of viscous sublayer turbulence, drag and lift forces, static friction, and submerged weight of the particle. He balanced the forces acting on a side slope particle at the threshold of motion lying on a plane that is tangential to the bank at an angle θ with respect to the horizontal. It can be noted that $\tan\phi = s_0$ = submerged coefficient of friction. Equation (13.82) can be recast as

$$K = \frac{\cos\theta[-\psi s_0 + (s_0^2 + \psi^2 s_0^2\tan^2\theta - \tan^2\theta)^{0.5}}{(1 - \psi s_0)s_0} \tag{13.83}$$

The value of ψ, the lift force to drag force ratio, needs to be specified. Experimental investigations of Einstein and El-Sammi (1949), Chepil (1958), Coleman (1967), Christensen (1972), Davies and Samad (1978), and others showed that ψ varied from –0.4 to 0.9. Ikeda (1982) suggested a value of ψ as 0.4, whereas Diplas and Vigilar (1992) suggested a value of ψ as 0.85. Christensen (1972) showed that ψ decreases as the particle sizes increases. For the range of particles encountered in river engineering ($0.4 < s_0 < 1.0$), a relationship between ψ and s_0 was expressed by Cao and Knight (1997) as

$$\psi = 1.15 - 0.75 s_0 \tag{13.84}$$

where $\psi = 0.85$ for $s_0 = 0.4$ (Diplas and Vigilar's [1992] recommendation), and $\psi = 0.4$ for $s_0 = 1$ (Ikeda's [1982] recommendation).

13.8 Local Boundary Stress by Different Methods

Lundgren and Jonsson (1964) compared five methods for calculating the local boundary shear stress in a channel and showed that the area method provided a satisfactory approximation to the true shear stress distribution. Accordingly, the actual stress acting on a slope τ_a can be expressed as

$$\tau_a = \gamma S_0 h_a = \gamma S_0 h_n \left(1 - \frac{j}{2}\right) \tag{13.85}$$

where $h_a = h_n(1–j/2)$ = actual stress depth on the boundary; $j = Ch_n$; and C = curvature of the boundary calculated as

$$C = \frac{\dfrac{d \tan\theta}{dx}}{(1 + \tan^2\theta)} \tag{13.86}$$

and h_n = the depth measured along the normal given as

$$h_n = h(1 + \tan^2\theta)^{0.5} \tag{13.87}$$

13.9 Channel Shape

Using $\tau_0 = \gamma h_c S_0$, equation (13.85) can be normalized as

$$h_a^* = \tau_a^* = \frac{\tau_a}{\tau_0} = \frac{h_a}{h_0} = h_n \left(1 - \frac{j}{2}\right) \frac{1}{h_c} = h^*(1 + \tan^2\theta)\left(1 - \frac{j}{2}\right) \tag{13.88}$$

where $h_a^* = h_a / h_c$ where h and h_c are geometry depths of bank and channel center, respectively.

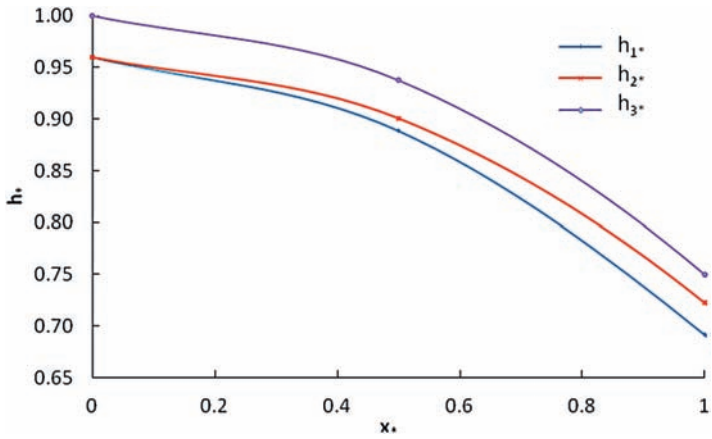

Figure 13-10 *Dimensionless depth as a function of dimensionless lateral distance. Note:* h_1^* *= the dimensionless critical stress depth,* h_2^* *= the dimensionless actual stress depth, and* h_3^* *= the dimensionless geometry depth.*

Now the entropy-based shape equation (13.22) can be normalized as

$$h^* = 1 - \left(\frac{s_0 x^*}{2}\right)^2 \tag{13.89}$$

where $x^* = x/h_c$. Equation (13.88) can be expressed with $\tan\theta = s_0 x/W$ (equation [13.53]) and $W = 2h_c/s_0$ (equation [13.57]) as

$$h_a^* = h^*\left[1 + \left(s_0^2 \frac{x^*}{2}\right)^2\right]^{0.5}\left\{\frac{1 - 0.25 s_0^2 h^*[1 + (s_0^2 x^*/2)^2]}{[1 + (s_0^2 x^*/2)^2]^{1.5}}\right\} \tag{13.90}$$

The dimensionless channel geometry can be calculated using equation (13.71). The dimensionless critical shear stress distribution can be determined using equations (13.50) and (13.73), (13.74) and (13.77), and (13.84), and the actual stress depth distribution using equation (13.68). It can be assumed that the critical shear stress at the centerline of the channel is the same as the actual stress at the same point. Fig. 13-10 shows the dimensionless shear stress versus dimensionless lateral distance. This figure shows that in the center of the channel the geometry depth is higher than the shear stress depth, but for part of the bank the reverse holds. The actual stress depth coincides with the critical stress depth reasonably well.

13.10 Design of Threshold Channels

The variables to be considered when designing a threshold alluvial channel include discharge Q, channel bed material characteristic d or s_0, streamwise slope S_0, depth at the channel center h_c, and top width of the channel B. In general, the

first two variables (Q and d or s_0) are known, and the latter three (S_0, h_c, and B) as well as the bank shape $y(x)$ have to be determined.

The wetted perimeter P can be obtained by doing arc integration of an element:

$$dP = (dy^2 + dx^2)^{1/2} \tag{13.91}$$

where $y = s_0x^2/(2W)$. Hence,

$$dP = \left(\frac{s_0}{W}\right)\left[x^2 + \left(\frac{W}{s_0}\right)^2\right]^{1/2} \tag{13.92}$$

Integration of equation (13.92) yields the wetted perimeter of a threshold channel as

$$P = \frac{W}{s_0}\{s_0\sqrt{1+s_0^2} + \ln[s_0 + \sqrt{1+s_0^2}]\} \tag{13.93}$$

The hydraulic radius is obtained from the division of equation (13.24) by equation (13.93):

$$R = \frac{A}{P} = 2s_0W^2/(3P) \tag{13.94}$$

If Q and d or s_0 are specified, a threshold channel can be designed using a trial and error method as follows:

1. Assume a depth at the center of the channel, h_c.
2. For the given sediment particle diameter, obtain a threshold Shields parameter.
3. Calculate the streamwise slope S_0 using

$$\tau = \frac{\gamma h_c S_0}{d(\gamma_s - \gamma)} \tag{13.95}$$

4. Calculate the Darcy–Weisbach friction factor f_l using an appropriate sediment resistance relation, such as the White–Paris–Bettes (W–P–B) equation (White et al. 1980).
5. Compute the average cross-sectional velocity:

$$h_f = f_l\frac{l}{d}\frac{v^2}{2g} = S_0 l \tag{13.96}$$

6. Compute the half width, W using equation (13.22).
7. Calculate the cross-sectional area using equation (13.24).
8. Calculate discharge Q_c by multiplying the mean velocity from step 5 by the cross-sectional area from step 6. If the computed discharge equals the given discharge, then center depth and semiwidth are reasonable, otherwise repeat steps.
9. Determine the channel shape or depth distribution using equation (13.56) or equation (13.23).

Example 13.7 According to Cao and Knight (1997), consider the boundary sediment diameter d_{50} = 0.8 mm, s_0 = 0.5, and Q = 0.05, 0.1, 0.15, 0.2, 0.3, 0.4, and 0.5 m^3/s. Assume that the depth at the center of the channel, h_c = 0.156 m. Compute s_0, B, and h_c, and compare them with those based on the D–V and USBR methods.

Solution Given particle size, shear stress can be found from the Shields diagram shown in Fig. 13-11, which is τ = 0.09. Then, using equation (13.94), s_0 is computed and one obtains 4.615×10^{-4}. Then the friction factor f_l is computed and one obtains 5.11×10^{-5}. Substituting in the Darcy–Weisbach equation, the average cross-sectional velocity is obtained as 0.376 m/s. Then, by using equations (13.22) and (13.24), B and A are computed as B = 1.248 m and A = 0.13 m^2. Thus, Q is computed as $Q = vA$ = 0.049 m^3/s. It is then seen that the assumption of depth 0.156 m is appropriate. Calculated values are shown in Table 13-7. Fig. 13-12 shows the boundary elevation y (between 0 and 0.5 m) versus the lateral distance x (between 0 and 2 m) for various values of discharge Q. Table 13-8 gives parameters of threshold channels. Fig. 13-13 shows design bank profiles by the D–V, entropy, and USBR approaches for Q = 0.05 m^3/s.

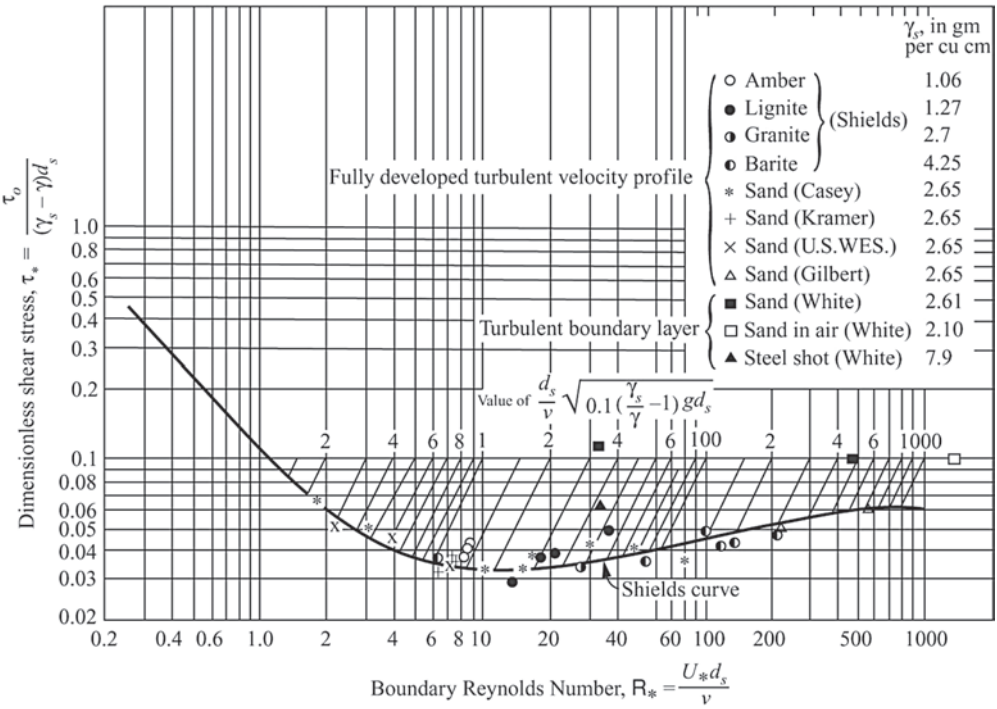

Figure 13-11 *Shields diagram.*
Source: Figure 2.43 from Vanoni (2006). Reproduced with permission.

Table 13-7 *Values of Q,* s_0, B, *and* h_c.

Q (m^3/s)	s_0 (10^{-4})	B (m)	h_c (m)
0.05	4.615	1.248	0.156
0.1	3.333	1.728	0.216
0.15	2.657	2.168	0.271
0.2	2.286	2.52	0.315
0.3	1.865	3.088	0.386
0.4	1.614	3.568	0.446
0.5	1.446	3.984	0.498

Table 13-8 *Parameters of threshold channels.*

Q (m^3/s)	Investigator	s_0 (10^{-})	B (m)	h_c (m)
0.05	Diplas & Vigilar	3.69	1.322	0.157
	Cao & Knight	4.66	1.249	0.156
	USBR	5.43	1.055	0.168
0.1	Diplas & Vigilar	2.67	1.87	0.217
	Cao & Knight	3.37	1.728	0.216
	USBR	3.95	1.452	0.230
0.15	Diplas & Vigilar	2.21	2.211	0.262
	Cao & Knight	2.75	2.091	0.261
	USBR	3.28	1.749	0.278
0.2	Diplas & Vigilar	1.93	2.53	0.300
	Cao & Knight	2.43	2.393	0.299
	USBR	2.87	1.996	0.317

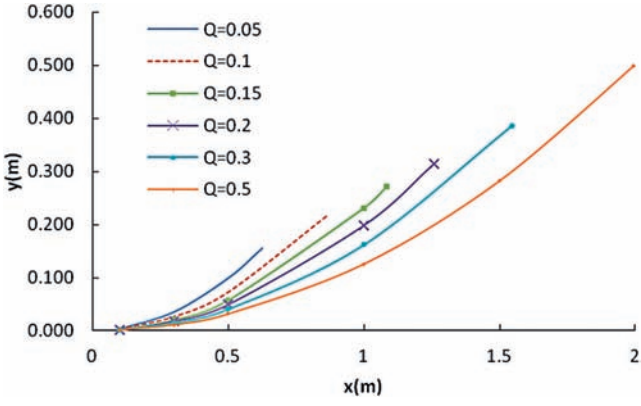

Figure 13-12 *Boundary elevation (between 0 and 0.5 m) versus lateral distance (between 0 and 2 m) for various values of discharge* Q.

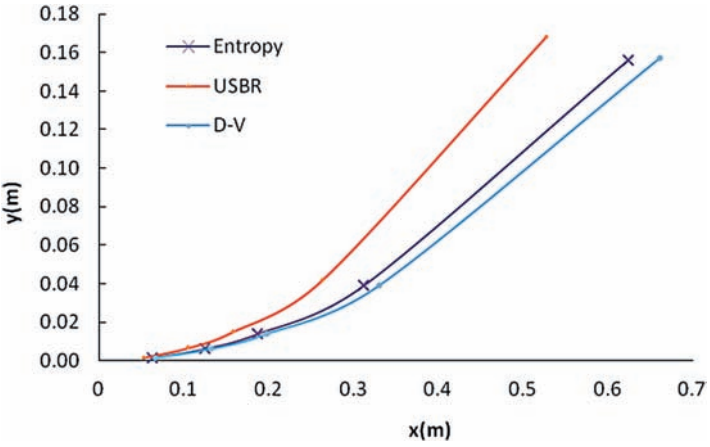

Figure 13-13 *Design bank profiles by the D–V, entropy, and USBR approaches for* $Q = 0.05\,m^3/s$.

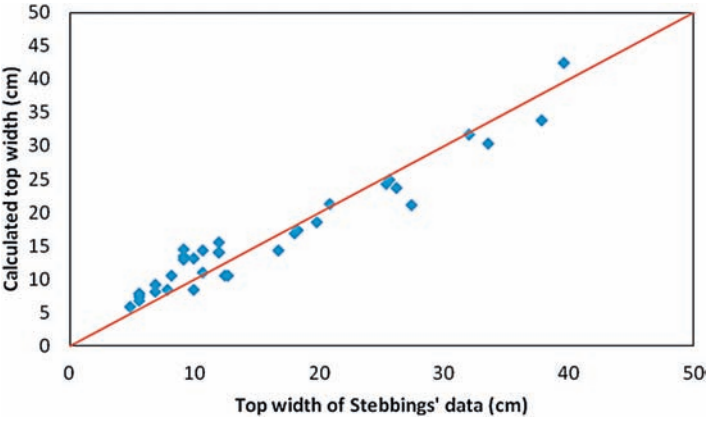

Figure 13-14 *Comparison of computed top width and observed top width for Stebbings's data for* $s_0 = 0.51$.

13.11 Evaluation Using Laboratory Data

Stebbings (1963) conducted small-scale experiments, which can be used to evaluate the top width and cross-sectional area obtained from the entropy method. The channel boundary material had a diameter of d_{50} = 0.88 mm and s_0 = 0.51. The aspect ratio was B/h_c, and the channel width B and cross-sectional area are obtained from equations (13.22) and (13.24). The average aspect ratio for 34 experiments was 7.31, and it was 7.8 for the entropy method, 8.3 for the D–V method, and 6.16 for the USBR method. Figs. 13-14 and 13-15 show predicted and observed B and A for Stebbings's data.

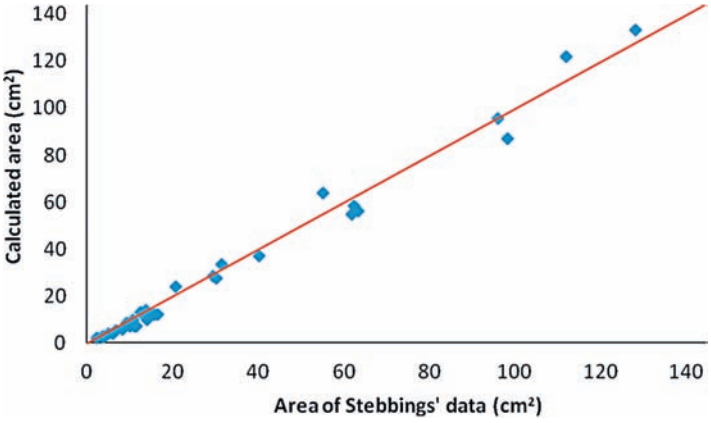

Figure 13-15 *Comparison of computed cross-sectional area with observed cross-sectional area for Stebbings's data for* $s_0 = 0.51$.

13.12 Determination of Friction Factor

White et al. (1980) developed a method for determining frictional resistance of alluvial channels and tested it on a wide range of field and experimental flume (0.04- to 68-mm sand sizes) data. In natural channels, characteristics related to the composition of bed and banks, irregularities, shape, and sediment transport vary significantly. The White et al. method involves the following steps:

1. Compute the shear velocity v^* (m/s) as

$$v^* = \sqrt{gdS_f} \tag{13.97}$$

where g is the acceleration caused by gravity (m/s^2), d is the mean depth f flow (m), and S_f is the friction slope ($v^{*2}/(gd)$).

2. Compute the dimensionless grain size D_{gr} as

$$D_{gr} = D_s\left[g\frac{s_g - 1}{\upsilon^2}\right]^{1/3} \tag{13.98}$$

where D_s is the sediment diameter (m), s_g is the specific gravity of sediment ρ_s/ρ, ρ is the fluid density (kg/liter), ρ_s is the sediment density (kg/liter), and υ is the kinematic viscosity (m^2/s).

3. For $D_s = D_{35}$ (bed material), calculate parameter n and a as

$$\text{If } D_{gr} \geq 60, \text{ then } \quad n = 0 \text{ and } a = 0.17 \tag{13.99}$$

$$\text{If } 1 \leq D_{gr} \leq 60, \text{ then } \quad n = 1.0 - 0.56\log_{10} D_{gr} \tag{13.100}$$

$$a = \frac{0.23}{\sqrt{D_{gr}}} + 0.14 \tag{13.101}$$

4. Compute the sediment mobility F_{fg} for fine grains as

$$F_{fg} = \frac{v^*}{[sD_s(s_g - 1)]^{0.5}} \tag{13.102}$$

5. Compute the sediment mobility in general F_{gr} as

$$\frac{F_{gr} - a}{F_{fg} - a} = 1.0 - 0.76[1.0 - \frac{1}{\exp[(\log_{10} D_{gr})^{1.7}]}] \tag{13.103}$$

6. Compute the mean velocity u_m (m/s) as

$$F_{gr} = \frac{v^{*2}}{[gD_s(s_g - 1)]^{0.5}}[\frac{u_m}{\sqrt{32}\log_{10}(10d/D)}]^{1-n} \tag{13.104}$$

7. Compute the friction factor as

$$\lambda = 8\left(\frac{v^*}{u_m}\right)^2 \tag{13.105}$$

13.13 Type I Channels

The cross section of a type I stable channel is shown in Fig. 13-16. The cross section consists of three parts: the central zone, the right bank, and the left bank. It is assumed, for purposes of simplicity, that the left and right banks are symmetric and hence that only one bank needs to be modeled. The previous discussion shows that the entropy-based bank profile is threshold, i.e, for a given discharge every point on the bank profile corresponds to a state wherein sediment is at a threshold. Field and experimental data show that river cross sections, unlined irregular canals, and irrigation furrows tend to become parabolic, supporting the entropy-based construct (Ikeda 1981; Mironenko et al. 1984).

The bank profile equations for type II channels are derived in the preceding section. The equations for type I bank profile are similar; therefore, they are given without derivation, in terms of notation given in Fig. 13-16.

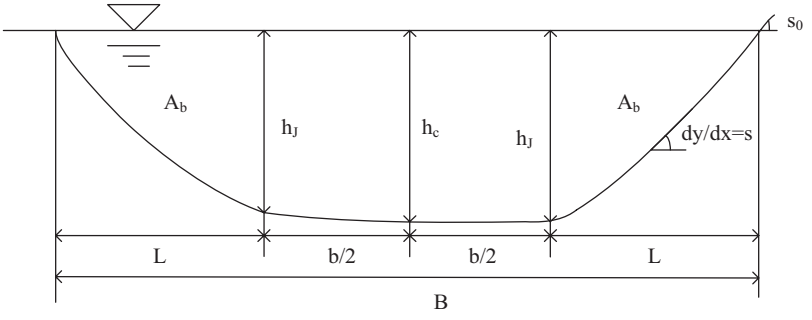

Figure 13-16 *Cross section of a stable channel of type 1.*

13.13.1 Bank Profile Equations

The cross-sectional transverse slope s_1 of the right bank ($x > b/2$) can be expressed as

$$\frac{dy}{dx} = s_1 = \frac{s_0}{L}\left(x - \frac{b}{2}\right) \tag{13.106}$$

Integration of equation (13.106) with the condition that $y = 0$ at the center ($x = 0$), making the boundary elevation of the bank region above the bed at the center, yields

$$y_b = \frac{s_0}{2L}\left(x - \frac{b}{2}\right)^2 \tag{13.107}$$

The depth at the channel center, h_c, can be expressed as

$$h_c = \frac{s_0 L}{2} \tag{13.108}$$

The lateral distribution of depth $h(x)$ in the bank region can be written as

$$h_b(x) = \frac{s_0 L}{2}\left[1 - \left(\frac{x - 0.5b}{L}\right)^2\right] \tag{13.109}$$

The cross-sectional area of the bank region, A_b, can be written as

$$A_b = \frac{2}{3} s_0 L^2 \tag{13.110}$$

The wetted perimeter of the banks can be written as

$$P_b = \frac{L}{s_0}\{s_0\sqrt{1 + s_0^2} + \ln[s_0 + \sqrt{1 + s_0^2}]\} \tag{13.111}$$

The hydraulic radius of the bank regions is

$$R_b = \frac{2 s_0 L^2}{3 P_b} \tag{13.112}$$

13.13.2 Cross-Sectional Geometry

The bank profile equations can be normalized by the depth of channel at the centerline h_c given by equation (13.108):

$$y_b^* = \frac{1}{4}\left[s_0\left(x - \frac{b}{2}\right)^*\right]^2 \tag{13.113}$$

$$h_b^* = 1 - \frac{1}{4}\left[s_0\left(x - \frac{b}{2}\right)^*\right]^2 \tag{13.114}$$

where $y_b^* = y_b/h_c$; $h_b^* = h_b(x)/h_c$; and $[x - (b/2)]^* = [x - (b/2)]/h_c$. Likewise,

$$(B-b)^* = \frac{4}{s_0} \tag{13.115}$$

$$A_b^* = \frac{8}{3s_0} \tag{13.116}$$

$$P_b^* = \frac{2}{s_0^2}\{s_0(1+s_0^2)^{1/2} + \ln[s_0 + (1+s_0^2)^{1/2}]\} \tag{13.117}$$

and

$$R_b^* = \frac{4s_0}{3\{s_0(1+s_0^2)^{1/2} + \ln[s_0 + (1+s_0^2)^{1/2}]\}} \tag{13.118}$$

where $(B-b)^*$, A_b^*, P_b^*, and R_b^* are dimensionless width, area, wetted perimeter, and hydraulic radius of the bank regions, respectively.

For a stable cross-section, $dy/dx = 0$ in the bed region, i.e., the depth should be constant and equal to that at the junction points:

$$\frac{h_c}{h_J} = 1 \tag{13.119}$$

The lateral profile of a straight channel in dynamic equilibrium can be obtained by equations (13.114) and (13.119), which can be expressed in dimensionless form by the following parameters:

$$B^* = b^* + \frac{4}{s_0} \tag{13.120}$$

$$P^* = \left(1 + \frac{P_b^*}{b^*}\right) b^* \tag{13.121}$$

$$A^* = \left[1 + \frac{8}{3s_0 a^*}\right] a^* = \left[1 + \frac{8}{3s_0 b^*}\right] b^* \tag{13.122}$$

$$R^* = \frac{1 + \dfrac{8}{3s_0 b^*}}{1 + \dfrac{P_b^*}{b^*}} \tag{13.123}$$

where $b^* = b/h_c$ = the dimensionless channel center bed width; $B^* = B/h_c$ = the dimensionless total width; $P^* = P/h_c$ = the dimensionless wetted perimeter; $A^* = A/h_c^2$ = the dimensionless cross-sectional area; $R^* = R/h_c$ = the dimensionless hydraulic radius; $a^* = h_c^* b^* = b^*$ the dimensionless center bed area; $h_c^* = h_c/h_c = 1$ = the dimensionless channel center bed depth; and $P_b^* = P_b/h_c$ = the dimensionless wetted perimeter of the bank zones.

13.13.3 Center Bed Width

As the equations for the geometry of stable channels depend on h_c or h_J, it must be computed first. The center bed width can be expressed as (Cao and Knight 1997):

$$h_c = \frac{\rho^* d \tau_c^*}{S_0(1-\beta)} \tag{13.124}$$

where τ_c^* is the critical Shields parameter for uniform boundary material; $\rho^* = [(\rho_s - \rho)/\rho]$; and ρ_s and ρ are the densities of sediment and water, respectively. For gravel-bed rivers, the critical value of the Shields shear stress is taken as 0.06, but it is found to be too high. The average value of 0.034 seems more appropriate.

$$\frac{h_c}{h_{cJ}} = \frac{1}{1-\beta} \tag{13.125}$$

where $h_{cJ} = \tau_{cJ}/(\rho g s)$ = the shear depth at junction points. When $\beta = 0.15$, then $h_c/h_{cJ} = 1.176$ (Shiono and Knight 1991).

Parker (1978, 1979) presented a relation between the average center bed Shields parameter τ_b^* and the critical Shields parameter τ_c^* for self-formed gravel channel as

$$\tau_b^* = c\tau_c^* \tag{13.126}$$

where c is approximately equal to 1.2.

13.13.4 Design Steps

Equation (13.124) gives the centerline depth of a stable channel. The bank shape is determined using equations (13.113) to (13.118). The width of the center bed region is yet to be determined. The variables involved include discharge Q, bed material characteristics of the channel boundary D_s or s_0, streamwise water surface slope S_0, depth at the channel center h_c, surface width of the channel B, and width of the center region b. The first three variables Q, D_s, and S_0 are known or given; the other three variables h_c, B, and b are to be determined. If the streamwise slope is given as input, the steps for a stable channel design are as follows:

1. Compute the depth of the center bed region, h_c, using equation (13.124).
2. Compute the dimensionless width, area, wetted perimeter, and hydraulic radius of the bank region using equations (13.115) to (13.118).
3. Assume a value of channel width b.
4. Compute the dimensionless width, wetted perimeter, area, and hydraulic radius of the full cross section using equations (13.120) to (13.123).
5. Compute the dimensions of hydraulic geometric parameters.
6. Compute the average cross-sectional velocity using an appropriate resistance, such as the W–P–B formula.

7. Compute discharge by multiplying the velocity obtained in step 6 with the area obtained in step 5. Compare the calculated discharge with the given discharge, and if both discharge values agree, then the channel geometry parameters are obtained correctly. If not, then adjust the value of b in step 5 and repeat steps 4 to 6.
8. Determine the channel profile, once b and y are obtained.

In some cases, streamwise slope is unknown, but sediment concentration is specified. First, an initial value of the slope is assumed. Then the sediment concentration is calculated using an appropriate sediment transport relation. If the calculated concentration matches the specified concentration, then the streamwise slope is correct. If not, the slope is adjusted and steps are repeated.

Example 13.8 Consider a channel with well-graded sediment (diameter d = 1.3 mm and d_{90} = 1.79 mm), s_0 = 0.6, the longitudinal water surface slope S_0 = 0.002146 (1/466), and discharge $Q = 0.00826\,\text{m}^3/\text{s}$. Parameters of the centerline depth are given as $\tau_c^* = 0.034$ and $\beta = 0.15$. Design the channel. Ikeda (1981) reported $B = 0.6480\,\text{m}$ and $h_{cr} = 0.0359\,\text{m}$.

Solution With given d, S_0, and τ_c^*, from equation (13.124), $h_c = 0.039\,\text{m}$.

$$(B-b)^* = \frac{4}{s_0} = 6.667$$

$$A_b^* = \frac{8}{3s_0} = 4.444$$

Assume the channel width b as 0.5 m.

$$b^* = \frac{b}{h_c} = 12.82$$

$$B^* = b^* + \frac{4}{s_0} = 19.488$$

$$A^* = \frac{1}{b^*}\left[1 + \frac{8}{3s_0 b^*}\right] = 0.105$$

Compute the shear velocity as

$$v^* = \sqrt{gdS_f} = 0.029\ \text{m/s}$$

Compute the dimensionless grain size as

$$D_{gr} = D_s\left[g\frac{s_g - 1}{\upsilon^2}\right]^{1/3} = 5.19 < 60$$

Thus,

$$n = 1.0 - 0.56\log_{10} D_{gr} = 0.599$$

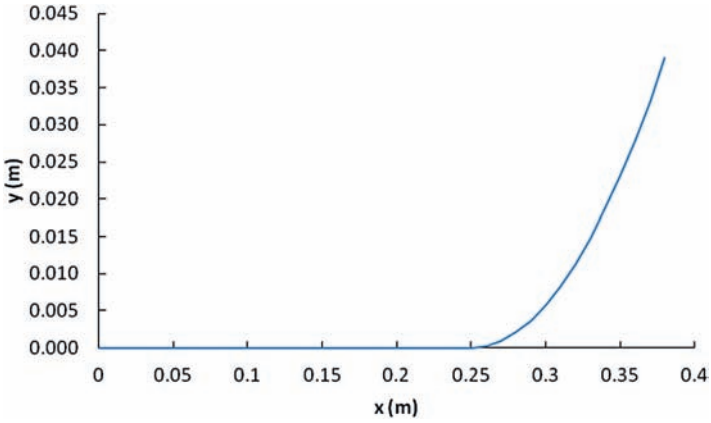

Figure 13-17 *Right channel bank.*

$$a = \frac{0.23}{\sqrt{D_{gr}}} + 0.14 = 0.241$$

Compute the sediment mobility as

$$F_{fg} = \frac{v^*}{[sD_s(s_g - 1)]^{0.5}} = 0.821$$

Computing the sediment mobility from equation (13.103), one obtains $F_{gr} = 0.629$. Then the mean velocity can be obtained from equation (13.104), $v = 1.954\,\text{m/s}$. Thus, $Q = vA = 0.008\,\text{m}^3/\text{s}$, comparable to $Q = 0.00826\,\text{m}^3/\text{s}$. $b = 0.5\,\text{m}$ and $B = 0.76\,\text{m}$, as shown in Fig. 13-17 for the right side of the channel bank.

13.13.5 Effect of Gradation of Boundary Material

In natural rivers, boundary bed materials are usually heterogeneous. Using laboratory data collected by Ikeda (1981) and Ikeda et al. (1988) for the evaluation of the effect of gradation on the channel width and depth, Cao and Knight (1987) developed a procedure for design of stable channels. Flow is characterized as hydraulically smooth if the particle Reynolds number $\text{Re}^* = v^* d_{50}/\upsilon < 5.5$ and rough for $\text{Re}^* > 51$ (Ikeda 1981). As $\xi = d_{90}/d_{50}$ increases, the stable width is more sensitive to the nonuniform distribution of sand diameter. Thus, the first step is to compute the nonuniform sediment threshold condition. For $d_i > d_{50}$, Hayashi et al. (1980) used

$$\tau_{ci}^* = \tau_c^* \frac{\log 8}{\log\left(\frac{8d_i}{d_{50}}\right)} \tag{13.127}$$

where d_{50} is the median size of the boundary material mixture; d_i is a size larger than d_{50}; τ_c^* and τ_{ci}^* are the critical Shields parameters of uniform size d_i or of the

same size in the mixture. If the boundary material is uniform, then $d_i = d_{50}$ and $\tau_{ci}^* = \tau_c^*$. This situation means that banks are stable, but the center region may not be stable.

The depth at the junction points can be obtained by inserting equation (13.127) into equation (13.124):

$$h_c = \frac{\tau_c^* \rho^* \xi d_{50} [\log 8 / \log(8\xi)]^2}{S_0(1-\beta)} \tag{13.128}$$

where $\xi = d_{90}/d_{50}$ = the boundary gradation. Equation (13.128) indicates four parameters ξ, S_0, d_{50}, and β, upon which h_c depends.

Egiazaroff (1965) proposed another condition for nonuniform material:

$$\tau_{ci}^* = \frac{0.1}{\left[\log\left(\frac{19 d_i}{d_{50}}\right)\right]^2} \tag{13.129}$$

For uniform $d_i = d_{50}$, equation (13.129) reduces to a constant value $\tau_{ci}^* = 0.0612$. Taking the critical value of the threshold Shields stress τ_c^* as 0.035 for hydraulically rough channels, equation (13.129) becomes

$$\tau_{ci}^* = \frac{0.0556}{\left[\log\left(\frac{19 d_i}{d_{50}}\right)\right]^2} \tag{13.130}$$

Inserting equation (13.130) in equation (13.124), one gets

$$h_c = \frac{[90.0556 \rho^* \xi d_{50}] / [\log(19\xi)]^2}{S_0(1-\beta)} \tag{13.131}$$

Equation (13.131) shows that the depth increases and width decreases with increasing gradation. For size gradation equal to 5, depths may be twice the depths for uniform bed material. With h_c obtained using equation (13.131) or (13.128), the design procedure is the same as before.

Questions

Q13.1 Consider a one-constraint case. Let $s_0 = 0.3$ and $\lambda_1 = -8$. Compute the probability of S less than or equal to 0.1, 0.15, 0.2, and 0.25.

Q13.2 For $\lambda_1 = -8$, $s_0 = 0.3$, and $W = 1$ m, compute the value of s at $x = 0.1$, 0.2, 0.4, 0.6, 0.8, and 1.

Q13.3 Plot α as a function of λ_1 for $s_0 = 0.2$, 0.3, 0.4, and 0.5. What can be concluded from this plot?

Q13.4 First select a value of α. Then taking $s_0 = 0.3$, obtain a value of λ_1. Then compute the value of D for $W = 1, 2, 3, 4$, and 5 m.

Q13.5 For various values of W and x, compute values of y for $s_0 = 0.3$. Select the value of α.

Q13.6 Compute h for selected values of W and α.

Q13.7 Consider a channel 4 m wide with the submerged coefficient s_0 as 0.3. Assume that there are no constraints that the probability density function of bank slope has to satisfy other than the total probability law. Compute the angle of internal friction for sediment, depth at the channel center, aspect ratio, cross-sectional area, wetted perimeter, and hydraulic radius.

Q13.8 If the sediment diameter is 0.4 mm and the streamwise slope is 3.5×10^{-4}, compute the threshold Shields parameter for the given boundary sediment diameter.

Q13.9 Using the USBR and Diplas and Vigilar methods, compute the channel parameters of Q13.1 and compare them with the values obtained using the entropy method.

Q13.10 Consider the channel of Q13.7. The PDF of S must now satisfy the mean slope constraint of value 0.25. Compute the channel parameters. Compare these parameter values with those obtained in Q13.7 and Q13.9. Comment on the comparative values.

Q13.11 Consider a channel with a flow depth of 1 m, bed slope of 0.002, $D_{35} =$ 0.08 mm, $\upsilon = 1.57 \times 10^{-5}\,\mathrm{m^2/s}$, and $s_g = 2.65$. Compute the friction factor using the W–P–B method.

References

Cao, S., and Chang, H. H. (1988). "Entropy as a probability concept in energy gradient distribution." *Proc., Natl Conf. Hydraul. Eng.*, Colorado Springs, CO, ASCE, New York.

Cao, S., and Knight, D. W. (1995a). "Design of threshold channels." *Hydra 2000, Proc., 26th IAHR Congr.*, London, IAHR, Delft, The Netherlands.

Cao, S., and Knight, D. W. (1995b). "New concept of hydraulic geometry of threshold channels." *Proc., 2nd Symp. Basic Theory Sedimentation*, Beijing, China.

Cao, S., and Knight, D. W. (1997). "Entropy-based approach of threshold alluvial channels." *J. Hydraul. Res.*, 35(4), 505–524.

Chang, H. (1988). *Fluvial processes in river engineering*, Wiley, New York.

Chepil, W. S. (1958). "The use of evenly spaced hemispheres to evaluate aerodynamic forces on a soil surface." *Trans. Am. Geophys. Union*, 39(3), 397–404.

Chow, V. T. (1959). *Open channel hydraulics*, McGraw-Hill, New York.

Christensen, B. A. (1972). "Incipient motion on cohesionless channel banks." In *Sedimentation Symposium in Honor of Professor H. A. Einstein*, H. W. Shen, ed., Water Resources Publications, Fort Collins, CO, 4-1, 4-22.

Coleman, N. L. (1967). "A theoretical and numerical study of drag and lift forces acting on a sphere resisting on a hypothetical stream bed." *Proc., 12th IAHR Cong.*, Vol. 3, IAHR, Delft, The Netherlands.

Davies, T. R. H., and Samad, M. F. A. (1978). "Fluid dynamic lift on a bed particle." *J. Hydraul. Div.*, 104(8), 1171–1182.

Diplas, P. (1990). "Characteristics of self-formed straight channels." *J. Hydraul. Eng.*, 116(5), 707–728.

Diplas, P., and Vigilar, G. (1992). "Hydraulic geometry of threshold channels." *J. Hydraul. Eng.*, 118(4), 597–614.

Egiazaroff, I. V. (1965). "Calculation of non-uniform sediment concentrations." *J. Hydraul. Div.*, 91(4), 225–247.

Einstein, H. A., and El-Sammi, E. A. (1949). "Hydrodynamic forces on a rough wall." *Rev. Mod. Phys.*, 21(3), 520–524.

Glover, R. E., and Florey, Q. L. (1951). "*Stable channel profiles*." U.S. Bureau of Reclamation, Washington, DC.

Hayashi, T., Ozaki, S. and Ichibashi, T. (1980). "Study on bed load transport of sediment mixture." *Proc., 24th Jpn. Conf. Hydraul. Tokyo*.

Henderson, F. M. (1966). *Open channel flow*, Macmillan, New York.

Ikeda, S. (1981). "Self-formed straight channels in sandy beds." *J. Hydraul. Div.*, 107(4), 389–406.

Ikeda, S. (1982). "Incipient motion of sand particles on side slopes." *J. Hydraul. Div.*, 108(1), 95–114.

Ikeda, S., Parker, G., and Kimura, Y. (1988). "Stable width and depth of straight gravel rivers with heterogeneous bed materials." *Water Resour. Res.*, 24(5), 713–722.

Jaynes, E. T. (1957). "Information theory and statistical mechanics I." *Phys. Rev.*, 106, 620–630.

King, H. W. (1939). *Handbook of hydraulics*, McGraw-Hill, New York.

Lundgren, H., and Jonsson, I. G. (1964). "Shear and velocity distribution in shallow channels." *J. Hydraul. Div.*, 90(1), 1–21.

Mironenko, A. P., Willardson, L. S., and Jenab, S. A. (1984). "Parabolic canal design and analysis." *J. Irrig. Drain. Eng.*, 110(2), 241–246.

Parker, G. (1978). "Self-formed straight rivers with equilibrium banks and mobile bed. Part 2: The gravel river." *J. Fluid Mech.*, 89(1), 127–146.

Parker, G. (1979). "Hydraulic geometry of active gravel rivers." *J. Hydraul. Eng.*, 105(9), 1185–1200.

Pizzuto, J. E. (1990). "Numerical simulation of gravel river widening." *Water Resour. Res.*, 26(9), 1971–1980.

Shannon, C. E. (1948). "A mathematical theory of communication." *Bell Syst. Tech. J.*, 27, 623–656.

Shiono, K. and Knight, D.W. (1991). "Turbulent open channel flows with variable depth across the channel." *J. Fluid Mech.*, 222, 617–646.

Simons, D. B., and Senturk, F. (1976). *Sediment transport technology*, Water Resources Publications, Highlands Ranch, CO.
Stebbings, J. (1963). "The shape of self-formed model alluvial channels." *Proc., Inst. Civil Eng.*, London, 25(4), 485–510.
Vanoni, V.A. (2006). *Sedimentation engineering,* Manual of Practice No. 54. ASCE, Reston, VA.
White, W. R., Paris, E., and Bettes, R. (1980). "The frictional characteristics of alluvial stream: A new approach." *Proc. Inst. of Civil Eng.*, 42(2), 737–750.

Additional Reading

Ackers, P. (1972). "River regime: Research and application." *J. Inst. Water Eng.*, 26(5), 257–281.
Ackers, P. (1992a). "Hydraulic design of two-stage channels." *Proc., Inst. Civil Eng., Waterways, Maritime and Energy*, 96, 247–257.
Ackers, P. (1992b). "Gerald Lacey memorial lecture on canal and river regime in theory and practice: 1929–92." *Proc., Inst. Civil Eng.—Waterways, Maritime and Energy*, 96(3), 167–178.
Blench, T. (1957). *Regime behavior of canals and rivers*, Butterworth, London.
Cao, S. (1996). *Fluvial hydraulic geometry*, Chengdu University of Science and Technology Press, Chengdu, China.
Cao, S. (1995). "Regime theory and geometric model for stable alluvial channels." Ph.D. dissertation, University of Birmingham, Birmingham, UK.
Chang, H. H. (1980). "Stable alluvial canal design." *J. Hydraul. Div.*, 106(5), 873–891.
Hey, R. D., and Thorne, C. R. (1986). "Stable channels with mobile gravel beds." *J. Hydraul. Eng.*, 112(8), 671–689.
Inglis, C. C., and Allen, F. H. (1957). "The regime of the Thames estuary as affected by currents, salinities and river flows." *Proc., Inst. Civil Eng.*, 7, 827–878.
Kennedy, R. G. (1895). "The prevention of silting in irrigation canals." *Proc., Inst. Civil Eng.*, 119, 281–290.
Lacey, G. (1929). "Stable channels in alluvium." *Proc., Inst. Civil Eng.*, 229, 258–384.
Lane, E. W. (1955). "Design of stable channels." *Trans. ASCE*, 120(1), 1234–1260.
Millar, R. G., and Quick, M. C. (1993). "*Effect of bank stability on geometry of gravel rivers*." *J. Hydraul. Eng.*, 119(12), 1343–1363.
Varma, C. V. J., Saxena, K. R., and Rao, M. K. (1989). "*River behavior management and training*." Vol. 1, Central Board of Irrigation and Power, New Delhi.

This page intentionally left blank

Part 5

Water Flow and Level Monitoring

This page intentionally left blank

Chapter 14

Water-Level Monitoring Networks

Data are required for the efficient planning, design, operation, and management of virtually all water resource systems, including water supply reservoirs, recreation and fisheries facilities, flood control structures, and hydroelectric plants, to name but a few. The purpose of data collection is to collect information because decision making in water resources project design and evaluation is closely linked to the amount of information available. If enough accurate and relevant information is available, the likelihood of an underdesign or overdesign is reduced. Thus, economic losses can be minimized, resulting in an overall increase in the benefit-cost ratio. However, it is not always easy to quantitatively define the optimum level of information needed for planning, design, and development of a specific project in a watershed. This situation is largely caused by the difficulty in developing cost and benefit functions of hydraulic and hydrologic information. This difficulty then leads to the difficulty of achieving an optimum balance between the economic risk caused by inadequate information and the cost of a network capable of providing the required information.

Data are measured by monitoring networks. There is a significant body of literature on environmental monitoring networks, including hydrometric, hydrologic, and water quality. Many studies have applied the entropy theory to assess and optimize data collection networks (e.g., water quality, rainfall, streamflow, hydrometric, temperature, wind, elevation data, and landscape). Alfonso (2010) and Alfonso et al. (2010a, b) dealt with water-level monitoring, which has received

much less attention, and their work is discussed in this chapter. The objective of this chapter, therefore, is to present entropy-based methods for designing water-level monitoring networks. The methods can be easily applied to evaluating and designing other types of networks.

14.1 Design Considerations

A methodology for data collection network design must take into account the information of each monitoring station or potential monitoring station in the network. A station with higher information content would generally be given a higher priority over other stations that have lower information contents. The information content of a station must, however, be balanced with site-specific uses and users of the data collected at the station. For example, a station that is used by one user might be given a lower priority than a station that has diverse uses. Burn and Goulter (1991) developed a data collection network design framework that considers such issues.

In general, a framework for network design or evaluation considers a range of factors, including (1) objectives of sampling, (2) variables to be sampled, (3) locations of measurement stations, (4) frequency of sampling, (5) duration of sampling, (6) uses and users of data, and (7) socioeconomic considerations. Effective monitoring is also related to these factors. Evaluation of a network has two modes: number of gauges and their location (space evaluation), and time interval for measurement (time evaluation). The information in one mode may be supplemented by the other with appropriate transfer mechanisms and by cross-correlation structure (space–time tradeoff). Space–time evaluation of networks should not be considered as fixed but should periodically be subject to revision and should, therefore, be evolutionary. Uslu and Tanriover (1979) analyzed the entropy concept for the delineation of optimum sampling intervals in data collection systems, both in space and time.

All designs, whether of the network or the monitoring program, must be cost effective in gathering data and cost efficient in obtaining information from data. These two requirements call for evaluating the performance of a network. Such an evaluation must consider benefits of monitoring with respect to the objectives of monitoring and the cost, both marginal and average, of obtaining those benefits. Sometimes it is the budget that controls the design of a network and monitoring program. Then, the problem reduces to one of obtaining the greatest benefit (most information) for the available budget.

Even though there are many considerations for the network evaluation and design, here we only focus on the fundamental theme, i.e., selecting an optimum number of stations and their optimum locations. Other considerations, such as the cost of placing new stations and their operational cost, are not included. Nevertheless, they can be easily incorporated into the objective by introducing an additional penalty function. The crucial point is to find a suitable way to measure the economic cost in terms of information units.

Frequently occurring questions when doing network design are the following: How much information is retained when considering two or more gauging stations simultaneously? How much of the uncertainty or information related to one gauge is still left if the information about another gauge is already known? How much information about gauge 1 can be inferred from the information of gauge 2? Which gauge is more important? How many gauges should there be? Where should gauges be located? These questions can be addressed using entropy.

14.2 Information-Related Approaches

Many approaches have been used in network evaluation and analysis. These include entropy; information variance; correlation function; transfer function variance; simulation; economic-worth of data approach; decision theory and Bayesian analysis; and linear estimation techniques, such as Thiessen polygons and spline surface fitting; kriging; and square grid technique, among others. The first four approaches are directly related to the concept of information espoused in this book. This chapter discusses only the first three approaches, with particular emphasis on the entropy-based approaches.

14.2.1 Shannon Entropy

Because entropy is a measure of information or uncertainty associated with a random variable or its probability distribution, it can be used for measuring the information content of observations of the random variable at a monitoring station. A series of observations about an uncertain event contains more information about the event than do observations about a less uncertain event. The Shannon entropy (Shannon 1948) $H(X)$ of a discrete random variable X: $\{x_1, x_2, \ldots, x_n\}$ that has probability distribution P: $\{p_1, p_2, \ldots, p_n\}$ where x_i is the ith value of X that has probability p_i, $i = 1, 2, \ldots, n$, is defined as

$$H(X) = -\sum_{i=1}^{n} p(x_i) \log p(x_i) \tag{14.1}$$

Information reduces uncertainty, i.e., information I is a reduction in uncertainty and can be defined as

$$I = H_I - H_O \tag{14.2}$$

where H_I is the entropy (or uncertainty) of input (or message sent through a channel), and H_O is that of the output (or message received). Equation (14.2) defines a reduction in uncertainty. In an input–output channel, if there were no noise, the output (the message received by the receiver or receptor) would be certain as soon as the input (message sent by the emitter) is known. This

phenomenon means that the uncertainty in output H_O would be 0 and I would be equal to H_I.

14.2.2 Continuous Time Series Discretization

The Shannon entropy for a discrete random variable is defined by equation (14.1). In network evaluation and design, continuous data are often involved. Before entropy-based analysis, therefore, the continuous time series data need to be discretized. Several methods are available for continuous data discretization, such as the histogram-based density estimator (Scott 1979; Freedman and Diaconis 1981; Birgé and Rozenholc 2002; Shimazaki and Shinomoto 2007), and mathematical floor function (Alfonso et al. 2010a, b; Alfonso and Price, 2012). Some approaches directly estimate continuous analogs of entropy terms without discretization, like the work by Paninski (2003). However, these methods are inflexible for computation of multivariate entropy terms, such as joint entropy and total correlation, which are described in the next sections.

By minimizing the integrated mean square error (IMSE), Scott (1979) proposed an asymptotic optimal choice for bin width h_{opt} as

$$h_{\text{opt}} = \left(\frac{6}{\int [f'(x)]^2 dx} \right)^{\frac{1}{3}} n^{\frac{1}{3}} \tag{14.3}$$

where $f(x)$ is the true underlying density, $[f'(x)]^2$ is the squared derivative of the assumed density, and n is the random sample size. In practice, the true density is unknown. Tukey (1977) suggested using the Gaussian density as a reference standard. Substituting the standardized Gaussian density function $f(x) = (1/2\pi)\exp(-x^2/2)$ in equation (14.3), one can have

$$h_{\text{opt}} = 2\left(\frac{1}{3}\right)^{1/3} \pi^{1/6} \sigma n^{-1/3} \tag{14.4}$$

Replacing the underlying true standard deviation σ by the sampling standard deviation s, Scott's data-based choice for the optimal bin width is expressed as

$$h^*_{\text{opt}} = 3.49 s n^{-1/3} \tag{14.5}$$

Scott (1979) used this equation to estimate the probability density for several heavy-tailed non-Gaussian distributions and concluded that it produced satisfactory results.

A continuous time series can be discretized (or labeled) by histogram partition as follows. First, determine the number of bins, assumed as m, according to the optimal bin width h^*_{opt} and the data range. Then, compute the empirical quantiles $q(i/m)$, where $i = 0, 1, 2, \ldots, m$. These empirical quantiles are the thresholds to label the continuous time series data. Finally, all data falling in the interval

$[q((k-1)/m), q(k/m)]$, where $k = 1, 2, \ldots, m$, are labeled as k. After discretization, a continuous random sample becomes a discrete (or categorical) one. This method has been widely used by Caselton and Husain (1980), Chapman (1986), Markus et al. (2003), and Mishra and Coulibaly (2010), among others.

Example 14.1 For a streamflow network as shown in Fig. 14-1, the observations for the station (08082500) are given in Table 14-33 in Appendix 14.1. Using the histogram method, first discretize the continuous streamflow time series and then compute its marginal entropy.

Solution The length of the streamflow time series (number of observations) is 240. The standard deviation of streamflow observations is 13.47. Substituting them into equation (14.5) yields

$$h^*_{\text{opt}} = 3.49 \times 13.47 \times 240^{-\frac{1}{3}} = 7.56$$

The range of the observations is approximately from 0 to 99.25. The time series can be partitioned into 14 equally sized intervals. Each interval has a size of 7.10. All observations falling in the first interval (0 ~ 7.10) are labeled as 1. Similarly, all observations falling in the second interval (7.11 ~ 14.20) are labeled as 2, and so on. After discretization, the one-dimensional contingency table can be

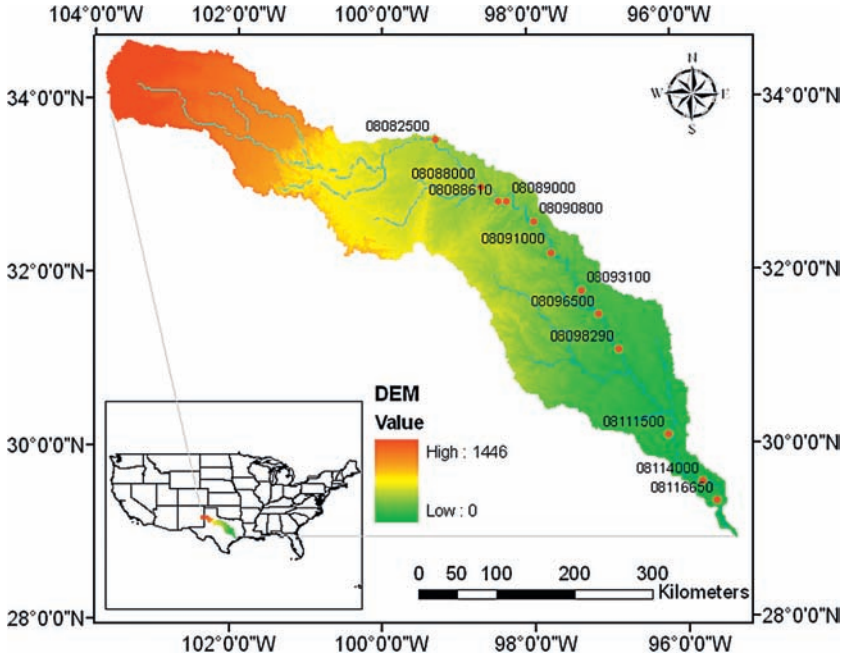

Figure 14-1 *Location map of the Brazos River basin and streamflow gauges on the mainstream.*

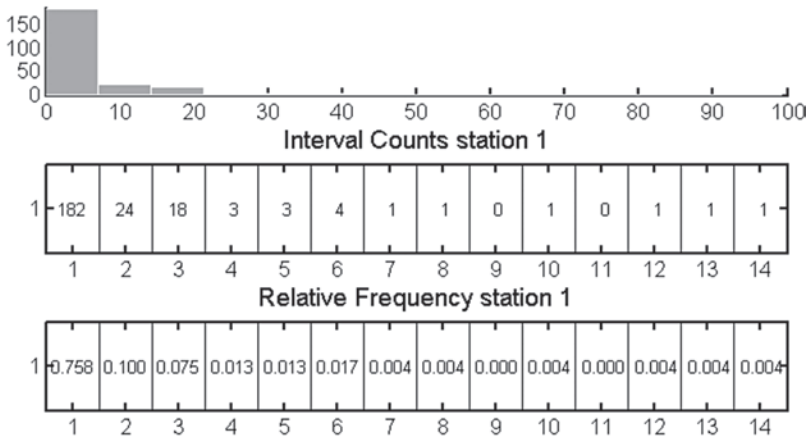

Figure 14-2 *Contingency table for station 1 (08082500). Note: Numbers in the first table are the number of values in different intervals. Likewise, the values in the second table are those of relative frequencies of different intervals.*

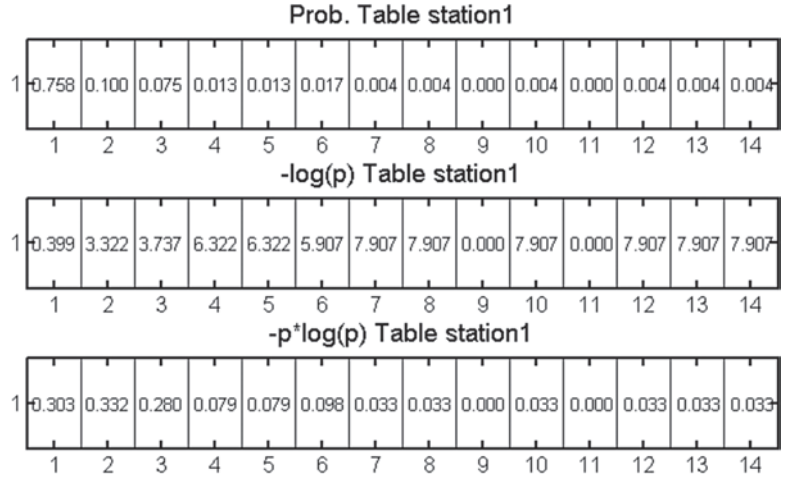

Figure 14-3 *Computation of each term appearing in the definition equation of entropy.*

constructed, as shown in Fig. 14-2. Then from the results in Fig. 14-2 and according to the definition of entropy, each term in the entropy definition equation can be computed and presented in Fig. 14-3. Summation of all quantities in the last table yields the final marginal entropy of streamflow for the first station:

$$H(\text{station 1}) = -\sum_{i=1}^{14} p_i \log_2 p_i = 0.303 + 0.332 + \ldots + 0.033 = 1.369 \text{ bits}$$

Besides the histogram partition method, mathematical floor function also can be exploited for data discretization. The application of the mathematical floor

function requires that a continuous value x be converted to its nearest lowest integer multiple of a constant a, i.e.,

$$x_q = a\left\lfloor \frac{2x + a}{2a} \right\rfloor \tag{14.6}$$

where $\lfloor \cdot \rfloor$ represents the conventional mathematical floor function. Selecting a suitable constant a is crucial for the discretization and, in turn, for the computation of entropy terms. It should be neither too large nor too small. A too-large value of a would make stations with relatively small values of the variable of interest insignificant in terms of information content, whereas a too-small value of a would make every station have similar information content. Considering that the entropy theory-based network evaluation and design is essentially ranking the importance of different candidate stations, rules of thumb can be used to guide the selection of parameter a: (1) it should guarantee that all candidate stations have significant and distinguishable information contents; (2) the spatial and temporal variability of time series of stations should be preserved as much as possible before and after discretization; and (3) the selected stations should be stable as much as possible, when a fluctuates within a narrow interval centered at its optimal value.

One point worth noting is that after applying the mathematical floor function, the marginal entropy (equation [14.1]) is no longer a measure of uncertainty (or information) of the continuous random variable X, but it is rather the uncertainty of X rounded to its nearest lowest integer multiple of a constant (Papoulis and Pillai 2001). In the context of hydrometric network evaluation and design, we do not need to exactly quantify the information (or uncertainty) retained by stations. Reasonable approximation is sufficient as long as the relative relationship among stations can be reproduced in terms of information content. For example, the information "station 1 contains more uncertainty (or information) than station 2" should be efficiently presented after discretization.

Example 14.2 For the same streamflow-monitoring network as in Example 14.1, select a suitable value for parameter a, discretize the streamflow time series for all stations, and then compute their marginal entropies.

Solution If we take any station, say station 8, as an example, we can adopt a value of $150\,m^3/s$ for a and discretize the continuous streamflow time series. The results are presented in the Fig. 14-4. The value of a is selected in the context of the streamflow-monitoring network evaluation according to the three rules of thumb given in this section. For more detail. one can refer to Li et al. (2012).

In the same way, the streamflow time series for other stations can also be discretized. After discretization, the marginal entropy can be computed. Following the same method as in Example 14.1, the marginal entropy for each station can be computed by constructing a one-dimensional contingency table and then applying the Shannon discrete entropy defined by equation (14.1). For economy

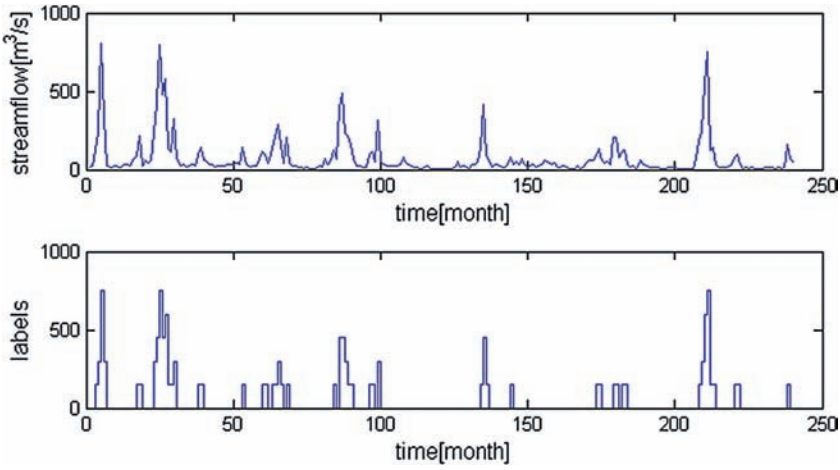

Figure 14-4 *Streamflow time series before and after discretization.*

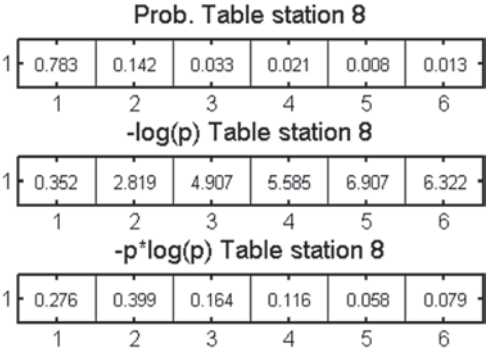

Figure 14-5 *Computation of each term in the definition equation of entropy.*

Table 14-1 *Contingency table for station 8 using the mathematical floor function for discretization.*

Label	1	151	301	451	601	751
Counts	188	34	8	5	2	3
Frequency	0.783	0.142	0.033	0.021	0.008	0.013

of space, only the results for station 8 are presented in this section. The one-dimensional contingency table for station 8 can be constructed as in Table 14-1.

Then from Table 14-1, each term in the definition of entropy can be computed, as presented in Fig. 14-5.

Summation of all quantities in the last table yields the final marginal entropy of streamflow for station 8:

$$H(\text{station 8}) = -\sum_{i=1}^{6} p_i \log_2 p_i = 0.276 + 0.399 + \ldots + 0.079 = 1.091 \text{ bits}$$

Table 14-2 *Marginal entropy for each of the 12 stations.*

Station ID	1	2	3	4	5	6	7	8	9	10	11	12
Entropy H	0.097	0.337	0.352	0.407	0.573	0.638	0.743	1.092	1.334	2.385	2.447	2.469

The results for other stations are tabulated in Table 14-2.

Comparing the marginal entropy for station 1 computed in Example 14.1, the result is much smaller here. In this example, all the stations are considered simultaneously, and this is always the case in hydrometric network evaluation and design. In this case, it should be guaranteed that all candidate stations have significant and distinguishable information contents after discretization. In this sense, the computed marginal entropies seem reasonable.

14.2.3 Types of Entropy

The measures of information are marginal entropy, conditional entropy, joint entropy, and transinformation. The information observed at different sites (monitoring stations) can be inferred, to some extent, from the observations at other sites. The information transferred among information emitters (predictor stations) and the information receivers (predicted stations) can be measured by transinformation, which is also known as mutual information. Mutual information is used for measuring the inferred information or equivalently for information transmission. Entropy and mutual information have advantages over other measures of information because they provide a quantitative measure of the information at a station, the information transferred and the information lost during transmission, and a description of the relationship among stations based on their information transmission characteristics.

Let the data being collected at a station correspond to a random variable X. Then, the marginal entropy, $H(X)$, given by equation (14.1), can be defined as the potential information of the variable; this is also the information of that monitoring station. For two monitoring stations, X and Y, the joint entropy $H(X,Y)$is the total information content contained in both X and Y, i.e., it is the sum of marginal entropy of one of the stations and the uncertainty that remains in the other station when a certain amount of information that it can convey is already present in the first station. Mathematically, joint entropy can be defined as

$$H(X, Y) = -\sum_{i=1}^{n}\sum_{j=1}^{m} p(x_i, y_j)\log p(x_i, y_j) \tag{14.7}$$

Joint entropy is symmetric with respective its arguments.

There exists an inequality relationship between joint entropy $H(X,Y)$ and marginal entropies $H(X)$ and $H(Y)$ that can be expressed as

$$H(X, Y) \le H(X) + H(Y) \tag{14.8}$$

This inequality gives the upper boundary of joint entropy $H(X,Y)$, which is reached when the two random variables X and Y are statistically independent. In other words, the joint entropy of two dependent random variables deviates from the sum of their marginal entropies. Furthermore, the greater the magnitude of the dependence, the larger the inequality.

There is a natural extension from the bivariate joint entropy given by equation (14.7) to the multivariate joint entropy for any number of variables or stations. The multidimensional joint entropy for N gauges represents the common uncertainty of their measured data sets. Multivariate entropy helps quantify the amount of information retained by more than two stations simultaneously. The multivariate joint entropy can be defined as

$$H(X_1, X_2, \ldots, X_N) = -\sum_{1_i}^{n_1}\sum_{2_i}^{n_2}\ldots\sum_{N_i}^{n_3} p(x_{1i}, x_{2i}, \ldots, x_{Ni}) \log p(x_{1i}, x_{2i}, \ldots, x_{Ni}) \tag{14.9}$$

where x_{ji}, $j = 1, 2, \ldots, N$; $i = 1, 2, \ldots, n_j$, represents the ith value of variable X_j or station X_j; there are N stations, each with different n_j values. Similar to bivariate entropy, multivariate joint entropy is also symmetric with respect to its arguments. Of course, the inequality relationship between multivariate joint entropy and the marginal entropies also holds, which for the multivariate case is just an analogy of inequality (14.8). Therefore, the multivariate joint entropy is maximized when all the random variables are independent.

Example 14.3 For the water-level monitoring network shown in Fig. 14-6 (from Alfonso 2010a, b), observations are given in Table 14-34 in Appendix 14.1. Selecting the first two monitors as illustrations, compute their marginal entropies and joint entropy and verify that the joint entropy is symmetric and that the inequality as in equation (14.8) holds.

Solution The given water-level data are quantized, which means that they have been transformed from continuous type to discrete. Therefore, a contingency table can be constructed by treating the same discrete values as a single event. For example, at gauge 1, all the 100 values are considered as the same event. Taking gauge 1 as an example, the contingency table is constructed as shown in Table 14-3.

Table 14-3 *Contingency table for gauge 1.*

Water level	75	80	85	90	95	100	105
Counts	18	59	33	18	17	23	32
Probability	0.090	0.295	0.165	0.090	0.085	0.115	0.160

Figure 14-6 *Water-level monitoring network in The Netherlands.*

Then, the marginal entropy for gauge 1 can be computed as

$$H(X_1) = -\sum_{i=1}^{n} p(x_i) \log p(x_i) = -0.09 \log_2 0.09 - 0.295 \log_2 0.295$$
$$- \ldots - 0.160 \log_2 0.160 = 2.6579 \text{ bits}$$

Likewise, the entropy of gauge 2 is computed, as follows: for gauge 1, $H(X)$ is 2.6579; for gauge 2, it is 3.0235.

To compute the joint entropy, a two-dimensional contingency table is constructed, as shown in Table 14-4. Taking $X_1 = 75$ and $X_2 = 80$ as an example, the joint probability $p(X_1 = 75, X_2 = 80)$ is computed as

$$p(X_1 = 75, X_2 = 80) = \frac{17}{200} = 0.085$$

Table 14-4 *Two-dimensional contingency table for gauges 1 and 2.*

	Gauge 2									
Gauge 1	**80**	**85**	**90**	**95**	**100**	**105**	**110**	**115**	**120**	**Sum**
75	17	1	0	0	0	0	0	0	0	18
80	31	27	1	0	0	0	0	0	0	59
85	0	2	22	8	1	0	0	0	0	33
90	0	0	0	8	8	1	1	0	0	18
95	0	0	0	0	4	10	2	1	0	17
100	0	0	0	0	0	0	14	8	1	23
105	0	0	0	0	0	0	0	9	23	32
Sum	48	30	23	16	13	11	17	18	24	200

Table 14-5 *Contingency table for gauges 1 and 2 for computation of joint probability.*

	Gauge 2									
Gauge 1	**80**	**85**	**90**	**95**	**100**	**105**	**110**	**115**	**120**	**Sum**
75	0.085	0.005	0	0	0	0	0	0	0	0.090
80	0.155	0.135	0.005	0	0	0	0	0	0	0.295
85	0	0.010	0.110	0.040	0.005	0	0	0	0	0.165
90	0	0	0	0.040	0.040	0.005	0.005	0	0	0.090
95	0	0	0	0	0.020	0.050	0.010	0.005	0.00	0.085
100	0	0	0	0	0	0	0.070	0.040	0.005	0.115
105	0	0	0	0	0	0	0	0.045	0.1145	0.160
Sum	0.240	0.150	0.115	0.080	0.065	0.055	0.085	0.090	0.120	1.0

Similarly, the joint probability mass table can be constructed as shown in Table 14-5.

Then the joint entropy of gauges 1 and 2 can be computed as

$$\begin{aligned} H(X_1, X_2) &= -\sum_{i=1}^{7}\sum_{j=1}^{9} p(x_i, y_j)\log\left(p(x_i, y_j)\right) \\ &= -0.085\log_2 0.085 - 0.005\log_2 0.005 - \ldots - 0.160\log_2 \\ &= 0.160 \text{ bits} \end{aligned}$$

Since the probability mass table for $P(X_2, X_1)$ is just the transpose of that for $P(X_1, X_2)$, the value for $H(X_2, X_1)$ is definitely equal to $H(X_1, X_2)$. In other words, the joint entropy is symmetric with respective to its arguments.

The inequality expressed by equation (14.8) can be easily verified as follows:

$$H(X_1) + H(X_2) = 2.6579 + 3.0235 = 5.6814 \geq 3.7606 = H(X_1, X_2)$$

The conditional entropy $H(X|Y)$ is a measure of the information content of X, which is not contained in Y, or entropy of X given the knowledge of Y or the amount of information that still remains in X even if Y is known. It can be mathematically expressed as

$$H(X|Y) = -\sum_{i=1}^{n}\sum_{j=1}^{m} p(x_i, y_j)\log p(x_i|y_j) \tag{14.10a}$$

where $p(x_i|y_j)$ represents the conditional probability mass function of random variable X given random variable Y. Unlike joint entropy, conditional entropy is not symmetric, i.e., in general, $H(X|Y)$ is not equal to $H(Y|X)$.

Recalling that the conditional entropy $H(X|Y)$ is the amount of uncertainty still left in X after knowing Y and the joint entropy $H(X|Y)$ is the amount of uncertainty or information retained by X and Y simultaneously, one can intuitively generalize that the joint uncertainty quantified by $H(X,Y)$ is reduced by the knowledge of X, and the magnitude of this reduction is the conditional entropy $H(Y|X)$. This statement can be expressed mathematically as

$$H(Y|X) = H(X, Y) - H(X) \tag{14.10b}$$

The conditional entropy can also be interpreted as the amount of lost information. The conditional entropy $H(Y|X)$, as the information error or noise, is the amount of information about Y that cannot be inferred from the knowledge of X or the amount of information retained by Y that has not been transferred out when using Y to evaluate or estimate X. $H(Y|X)$ represents the amount of information received as noise, that is, the part that was never sent by X but was received by Y. Clearly, both of these quantities must be positive. It may be noted that conditional entropy $H(X|Y)$ represents the amount of information loss during transmission, meaning the part of X that never reaches Y.

Equation (14.10a) can be extended to any number of variables or gauges. In multivariate cases, the amount of uncertainty left in the gauge with the most information or entropy when the records of all other gauges are known is expressed by the multivariate conditional entropy of the central gauge conditioned on all other records. Similarly, the uncertainty left in the group of gauges (1_1, …, N_N) when any new gauge is added (i.e., the expansion of the existing gauge network) can be defined as

$$H[(X_1, X_2, \ldots, X_N)|X_{N+1}] = -\sum_{1_1}^{M_1}\cdots\sum_{N_{n+1}}^{M_{N+1}} p(x_1, x_2, \ldots, x_{N+1})\log[p(x_1, x_{2.}, \ldots, x_N|x_{N+1})] \tag{14.11a}$$

or

$$H[(X_1, X_2, \ldots, X_N)|X_{N+1}] = H(X_1, X_2, \ldots, X_n, X_{N+1}) - H(X_{N+1}) \tag{14.11b}$$

where M_i, $i = 1, 2, N + 1$, is the number of points or values of X_i.

Example 14.4 Using the same data set as in Example 14.3, denoting respectively, the water levels at gauges 1 and 2 by X_1 and X_2, compute the conditional entropy $H(X_2 \mid X_1)$ and $H(X_1 \mid X_2)$. Discuss the results.

Solution To compute the conditional entropy using equation (14.10a), the conditional probability distribution needs to be computed first. The joint probability distribution for X_1 and X_2 has been obtained in Example 14.3; for ease of understanding, it is tabulated again as Table 14-6.

The conditional probability $p(x_{2i} \mid x_{1j})$ can be computed from the above two-dimensional contingency table. Taking $X_1 = 75$ and $X_2 = 80$ as an example, the conditional probability

$$p(X_2 = 80 \mid X_1 = 75)$$

is computed as

$$p(X_2 = 80 \mid X_1 = 75) = \frac{p(X_2 = 80, X_1 = 75)}{p(X_1 = 75)} = \frac{0.085}{0.090} = 0.944$$

Similarly, we can obtain the conditional probability distribution $p(x_{2i} \mid x_{1j})$ as shown in Table 14-7.

According to the definition of conditional entropy, we can compute the conditional entropy of X_2 given X_1 from the previous table as

$$\begin{aligned} H(X_2|X_1) &= -\sum_{i=1}^{n}\sum_{j=1}^{m} p(x_{1i}, x_{2j}) \log p(x_{2i}|x_{1j}) \\ &= -0.085 \log_2 0.9444 - 0.005 \log_2 0.0556 - \ldots - 0.045 \log_2 0.0435 \\ &= 1.1027 \text{ bits} \end{aligned}$$

Table 14-6 *Joint probability distribution of gauges 1 and 2.*

	Gauge 2									
Gauge 1	**80**	**85**	**90**	**95**	**100**	**105**	**110**	**115**	**120**	**Sum**
75	0.085	0.005	0	0	0	0	0	0	0	0.090
80	0.155	0.135	0.005	0	0	0	0	0	0	0.295
85	0	0.010	0.110	0.040	0.005	0	0	0	0	0.165
90	0	0	0	0.040	0.040	0.005	0.005	0	0	0.090
95	0	0	0	0	0.020	0.050	0.010	0.005	0.005	0.085
100	0	0	0	0	0	0	0.070	0.040	0.040	0.115
105	0	0	0	0	0	0	0	0.045	0.045	0.160
Sum	0.240	0.150	0.115	0.080	0.065	0.055	0.085	0.090	0.120	1.0

Table 14-7 *Conditional probability distribution.*

	Gauge 2									
Gauge 1	**80**	**85**	**90**	**95**	**100**	**105**	**110**	**115**	**120**	**Sum**
75	0.9444	0.0556	0	0	0	0	0	0	0	1.0
80	0.5254	0.4576	0.0170	0	0	0	0	0	0	1.0
85	0	0.0606	0.6667	0.2424	0.0303	0	0	0	0	1.0
90	0	0	0	0.4444	0.4444	0.0556	0.0556	0	0	1.0
95	0	0	0	0	0.2353	0.5882	0.1176	0.0589	0	1.0
100	0	0	0	0	0	0	0.6087	0.3478	0.0435	1.0
105	0	0	0	0	0	0	0	0.2813	0.7187	1.0

Following the same procedure, the conditional entropy of X_1 given X_2 can be computed, i.e., $H(X_1 \mid X_2) = 0.7371$ bits. This result also shows that $H(X_1 \mid X_2) \neq H(X_2 \mid X_1)$, indicating the asymmetric property of conditional entropy. In addition, in Example 14.3, $H(X_1) = 2.6579$ bits and $H(X_1, X_2) = 3.7606$ bits have already been obtained. Thus, one can easily verify that equation (14.10b) holds, i.e., $H(X_1, X_2) - H(X_1) = 3.7606 - 2.6579 = 1.1027 = H(X_2 \mid X_1)$.

The mutual entropy (information) between X and Y, also called transinformation, $T(X, Y)$, is interpreted as the reduction in the original uncertainty of X caused by the knowledge of Y. It can also be defined as the information content of X that is contained in Y. In other words, it is the difference between the joint entropy and the sum of entropies of two stations. This information is repeated or common information in both X and Y and defines the amount of uncertainty that can be reduced in one of the stations when the other station is known.

The information transmitted from station X to station Y is represented by the mutual information $T(X, Y)$ and is given (Lathi 1969) as

$$T(X,Y) = \sum_i \sum_j p(x_i, y_j) \log \frac{p(x_i \mid y_j)}{p(x_i)} \tag{14.12a}$$

or

$$T(X, Y) = \sum_i \sum_j p(x_i, y_j) \log \frac{p(x_i, y_j)}{p(x_i)p(y_j)} \tag{14.12b}$$

Conceptually, transinformation $T(X, Y)$ is the amount of common (overlapped) information between X and Y. The sum of information retained by X and Y is computed as $H(X) + H(Y)$. However, some of this information overlaps because of the dependence between X and Y. The total information retained by X and Y simultaneously is the joint entropy $H(X, Y)$. Therefore, the overlapped information is just the difference between the sum of marginal entropies $H(X)$ and $H(Y)$ and the joint entropy $H(X, Y)$. In this sense, transinformation is also a

measure of dependence between two random variables. The relationships among marginal entropy, joint entropy, and conditional entropy are

$$T(X,Y) = H(X) + H(Y) - H(X,Y) \tag{14.13a}$$

$$T(X,Y) = H(X) - H(X \mid Y) \tag{14.13b}$$

$$T(X,Y) = H(Y) - H(Y \mid X) \tag{14.13c}$$

$T(X, Y)$ is symmetric, i.e., $T(X, Y) = T(Y, X)$, and is nonnegative. A zero value occurs when two stations are statistically independent so that no information is mutually transferred, that is, $T(X, Y) = 0$ if and only if X and Y are independent. When two stations are functionally dependent, the information at one site, say X, can be fully transmitted to another site Y with no loss of information at all. Subsequently, $T(X, Y) = H(X)$. Otherwise, $0 \le T(X, Y) \le H(X)$. Larger values of T correspond to greater amounts of information transferred. Thus, T is an indicator of the capability of the information transmission and the degree of dependency of two stations. That is the reason that transinformation has been widely used in hydrometric network design. Furthermore, transinformation is superior to using the correlation coefficient. The attractiveness of transinformation is that it captures not only linear relationship but also nonlinear relationship, whereas the correlation coefficient can only apply to the linear relationship, or more generally, it measures the dependence in multivariate spherical and elliptical distributed random variables, such as those that follow a multivariate Gaussian distribution.

Example 14.5 For the same water-level monitoring network as in Example 14.3, observations are given in Table 14-33 in Appendix 14.1. Choosing the first five monitoring gauges, compute the transinformation between different gauges.

Solution There are several ways to compute the transinformation. One is to use its definition equation, as shown in equations (14.12a) and (14.12b). Another one is to use the shortcut formulas, as shown in equations (14.13a), (14.13b), and (14.13c). First we use the definition equation (14.12b) to calculate the transinformation, taking gauge 1 and gauge 2 as an example. First, the marginal distributions of gauge 1 and gauge 2 need to be calculated. Then their joint distribution is calculated. Finally, using the definition equation, the transinformation can be computed. Example 14.3 illustrates how to compute the marginal probability mass table, following which the marginal distribution for gauge 1 is computed and shown in Table 14-8. Similarly, the marginal distribution for gauge 2 is given in Table 14-9.

Table 14-8 *Marginal probability distribution of gauge 1.*

Water level	75	80	85	90	95	100	105
Counts	18	59	33	18	17	23	32
Probability	0.090	0.295	0.165	0.090	0.085	0.115	0.160

Table 14-9 *Marginal probability distribution of gauge 2.*

Water level	80	85	90	95	100	105	110	115	120
Counts	48	30	23	16	13	11	17	18	24
Probability	0.240	0.150	0.115	0.080	0.065	0.055	0.085	0.090	0.120

Table 14-10 *Contingency table for gauges 1 and 2.*

	Gauge 2									
Gauge 1	**80**	**85**	**90**	**95**	**100**	**105**	**110**	**115**	**120**	**Sum**
75	0.085	0.005	0	0	0	0	0	0	0	0.090
80	0.155	0.135	0.005	0	0	0	0	0	0	0.295
85	0	0.010	0.110	0.040	0.005	0	0	0	0	0.165
90	0	0	0	0.040	0.040	0.005	0.005	0	0	0.090
95	0	0	0	0	0.020	0.050	0.010	0.005	0.005	0.085
100	0	0	0	0	0	0	0.070	0.040	0.040	0.115
105	0	0	0	0	0	0	0	0.045	0.045	0.160
Sum	0.240	0.150	0.115	0.080	0.065	0.055	0.085	0.090	0.120	1.0

Example 14.3 also illustrates how to construct a two-dimensional contingency table. For convenience, final results are directly tabulated in Table 14-10.

Then, from the definition given by equation (14.12b), transinformation can be computed as

$$
\begin{aligned}
T(X_{\text{gauge 1}}, Y_{\text{gauge 2}}) &= \sum_i \sum_j p(x_i, y_j) \log \frac{p(x_i, y_j)}{p(x_i)p(y_j)} \\
&= 0.085 \times \log\left(\frac{0.085}{0.240 \times 0.090}\right) + 0.005 \times \log\left(\frac{0.005}{0.150 \times 0.090}\right) \\
&\quad + 0.155 \times \log\left(\frac{0.155}{0.240 \times 0.295}\right) + 0.135 \times \log\left(\frac{0.135}{0.150 \times 0.295}\right) \\
&\quad + 0.005 \times \log\left(\frac{0.005}{0.115 \times 0.295}\right) + \cdots\cdots \\
&\quad + 0.045 \times \log\left(\frac{0.045}{0.090 \times 0.160}\right) + 0.045 \times \log\left(\frac{0.045}{0.120 \times 0.160}\right) \\
&= 1.9208 \text{ bits}
\end{aligned}
$$

In the same way, the transinformation values for other paired gauges can be computed and the results are tabulated in Table 14-11.

Table 14-11 *Transinformation values.*

	Gauge 1	Gauge 2	Gauge 3	Gauge 4	Gauge 5
Gauge 1	2.6579	1.9208	2.6579	0.0234	1.8371
Gauge 2	1.9208	3.0235	1.9208	0.0336	2.1469
Gauge 3	2.6579	1.9208	2.6579	0.0234	1.8371
Gauge 4	0.0234	0.0336	0.0234	0.1687	0.0764
Gauge 5	1.8371	2.1469	1.8371	0.0764	3.5642

Conversely, the shortcut formulas (equations (14.13a), (14.13b), and (14.13c)) can also be exploited for the computation of transinformation. For example,

$$\begin{aligned} T\left(X_{\text{gauge 1}}, Y_{\text{gauge 2}}\right) &= H\left(X_{\text{gauge 1}}\right) + H\left(Y_{\text{gauge 2}}\right) - H\left(X_{\text{gauge 1}}, Y_{\text{gauge 2}}\right) \\ &= 2.6579 + 3.0235 - 3.7606 \\ &= 1.9208 \text{ bits} \end{aligned}$$

$$\begin{aligned} T\left(X_{\text{gauge 1}}, Y_{\text{gauge 2}}\right) &= H\left(X_{\text{gauge 1}}\right) - H\left(X_{\text{gauge 1}} \mid Y_{\text{gauge 2}}\right) \\ &= 2.6579 - 0.7371 \\ &= 1.9208 \text{ bits} \end{aligned}$$

$$\begin{aligned} T\left(X_{\text{gauge 1}}, Y_{\text{gauge 2}}\right) &= H\left(Y_{\text{gauge 2}}\right) - H\left(Y_{\text{gauge 2}} \mid X_{\text{gauge 1}}\right) \\ &= 3.0235 - 1.1027 \\ &= 1.9208 \text{ bits} \end{aligned}$$

Clearly, no matter which method is used, the final result for transinformation is the same.

14.2.4 Interaction Information

Interaction information (or co-information) was defined by McGill (1954). For three variables X, Y, and Z, it can be expressed as

$$\begin{aligned} I(X, Y, Z) &= H(X) + H(Y) + H(Z) - [H(X, Y) + H(Y, Z) + H(X, Z)]H(X, Y, Z) \\ &= I(X, Y; Z) - I(X, Y) - I(Y, Z) \end{aligned} \tag{14.14}$$

Interaction information has been interpreted differently in the literature. To illustrate these interpretations, consider three variables X, Y, and Z. Jakulin and Bratko (2003) interpret it as a measure of the amount of information common to X, Y, and Z (all variables) but that is not present in any of these three variables. The interaction information can be positive or negative, because the dependency

among variables (say X and Y) can increase or decrease with the knowledge of a new variable (say Z). Jakulin and Bratko (2004) interpret a positive interaction information value as a synergy among X, Y, and Z, whereas a negative value is a redundancy among these variables.

Interaction information is interpreted by Srinivasa (2005) as a gain or loss in the information transmitted between a set of variables (say X and Y) caused by the knowledge of a new variable (say Z). The interpretation by Fass (2006) is as the name interaction information suggests. It reflects the influence of one variable (say, X) on the amount of information shared among the remainder of the variables (say, Y and Z). He goes on to state that with the knowledge of the third variable (say, Z) a positive interaction information strengthens the correlation between the two variables (say, X and Y). Conversely, a negative value of correlation diminishes the correlation between X and Y.

The bivariate transinformation can be extended to the multivariate case for measuring different relationship characteristics among several dependent random variables, such as interaction information and total correlation. Interaction information can be generalized as

$$I(X_1, X_2, \ldots, X_N) = \sum_{S_1} H(X_i) - \sum_{S_2} H(X_i, X_j) + \cdots + (-1)^{N-1} \sum_{S_N} H(X_1, X_2, \cdots, X_N) \tag{14.15}$$

where S_i denotes all possible combinations consisting of i different random variables or stations and the sum notation means the sum over all possible combinations, respectively. The interaction information reduces to transinformation when $N = 2$. However, unlike transinformation, which is always positive, multivariate interaction information can assume all real values. From the definition, it is clear that it is burdensome to compute interaction information, for it entails computation of many marginal entropy and joint entropy terms, especially when the number of random variables N is large. In practice, especially in hydrometric network design, the amount of common information shared by several random variables quantified by the interaction information is not attractive because of its intractable computation and its sensitivity to the new added station. Conversely, to evaluate the redundancy of a hydrometric network, the interest is usually in the amount of repeated information among all existing or selected stations. The concept of total correlation provides a direct and effective way of assessing such kinds of repeated information, which is discussed in the subsequent section.

14.2.5 Total Correlation

McGill (1954) and Watanabe (1960), among others, have used total correlation defined as

$$C(X_1, X_2, \ldots, X_N) = \sum_{i=1}^{N} H(X_i) - H(X_1, X_2, \ldots, X_N) \tag{14.16}$$

Equation (14.16) evaluates the total amount of duplication information among the N gauges and provides an alternative way of examining multivariate dependency. Total correlation is symmetric with respect to its arguments. The total correlation is always nonnegative because the sum of marginal entropies of N variables is no less than their joint entropy. If the N variables are independent, then C is 0. Otherwise, it is greater than 0. A large value of C may imply either a strong dependency among a few variables or a relatively small dependency among all of them. If $N = 2$, equation (14.16) reduces to the conventional transinformation T.

Equation (14.16) involves two components: marginal entropies and joint entropy. The total correlation can be computed without resorting to the computation of multivariate entropy or multivariate probabilities. This step can be accomplished by recalling the grouping property of total correlation and accordingly a systematic grouping of bivariate entropies. For trivariate total correlation $C(X_1, X_2, X_3)$, the grouping property can be expressed as (Kraskov et al. 2003)

$$C(X_1, X_2, X_3) = C(X_1, X_2) + C(X_{1:2}, X_3) \tag{14.17}$$

where $X_{1:2}$ represents the merged variable of X_1 and X_2, which is detailed in the next section. Sequentially using the grouping property, the multivariate total correlation can be computed recursively as

$$\begin{aligned} C(X_1, X_2, X_3, \cdots, X_N) &= C(X_1, X_2, X_{3\to N}) \\ &= C(X_1, X_2) + C(X_{1:2}, X_{3\to N}) \\ &= C(X_1, X_2) + C(X_{1:2}, X_3, X_{4\to N}) \\ &= C(X_1, X_2) + C(X_{1:2}, X_3) + C(X_{1:3}, X_{4\to N}) \\ &\quad \cdots\cdots \\ &= C(X_1, X_2) + C(X_{1:2}, X_3) + C(X_{1:3}, X_4) + \cdots C(X_{1:N-1}, X_N) \\ &= \sum_{i=1}^{N-1} C(X_{1:i}, X_{i+1}) \end{aligned} \tag{14.18}$$

In equation (14.18), notation $X_{1:i}$ represents the merged variable of X_1, X_2, …, X_i. It can be seen that the total correlation is finally factorized as a summation of bivariate total correlation, which is just the conventional transinformation. In other words, the grouping property can reduce the dimension of multivariate total correlation, and thus, the estimation of multivariate probability distribution and multivariate joint entropy can be avoided.

Although the total correlation concept has been widely used in medicine, neurology, psychology, clustering, significant feature selection, and genetics (Jakulin and Bratko, 2004; Fass, 2006), there appears to have been limited application of total correlation in hydrology and water resources. Krstanovic and Singh (1992a, b) used it for evaluating multivariate ($N > 2$) dependence, where it has been assumed that the random variables follow normal or lognormal distribution, which is not always the case for hydraulic variables. Furthermore, in

network evaluation and design, most of the entropy theory-based analyses have been restricted up to the bivariate level. A major reason is the difficulty of estimating multivariate probability distributions and the limited availability of data. However, often there is a need to evaluate the total amount of information or uncertainty duplicated by several stations under consideration.

14.2.6 Discrete Variable Merging

Multivariate joint entropy and total correlation can be computed at any dimension with the aid of categorical variable merging. The basic idea for variable merging lies in creating a new variable X, such that the information retained by it is equal to that retained by the original variables, say X_1, X_2, …, X_n. As an example, consider merging two categorical variables: $X_1 = [1, 2, 1, 2, 1, 3, 3]^T$ and $X_2 = [1, 2, 2, 2, 1, 3, 2]^T$. Then the new variable X can be obtained by pairwise welding the corresponding digits together (Alfonso et al. 2010a, b), i.e., $X = [11, 22, 12, 22, 11, 33, 32]^T$. It can be verified that the information amount keeps invariant before and after merging, i.e., the information content of X_1 and X_2 together is the same as that of X. The direct welding approach, however, has a serious defect that may cause it to "run out of memory" as the number of variables to be merged increases, especially when the sample size is large. An efficient alternative to the direct welding approach, which avoids this problem, is generalized in the following steps.

1. Create a new sample X from X_1 and X_2 by the direct welding approach.
2. Pick out the unique values in X and rank them in ascending order, resulting in another ranked sample X_r, whose length is l.
3. Access the location index of each element of X in the ranked sample X_r.
4. Assign a new label to each element of X as the number obtained by subtracting its location index from l then adding 1.

After applying the variable merging procedure, each element in the new merged sample is relabeled by an integer ranging from 1 to l. Remember that the merging approach is only suitable for categorical variables rather than the continuous type. That is why the histogram method or the mathematical floor function is used to discretize the continuous hydrologic time series data. In Example 14.6, we illustrate the step-by-step procedure for discrete variable merging using the aforementioned algorithm.

Example 14.6 Considering the two records of monthly precipitation presented in Table 14-12, create a merged series such that entropy of the merged series is equal to the joint entropy of the original two series.

Solution For ease of understanding the step-by-step procedure of discrete variable merging, we start with the original continuous time series by discretizing them using the histogram-based method. By dividing the observations into five equal-sized intervals, discretization of the continuous precipitation sequence can be explicitly illustrated by Fig. 14-7. Using the way illustrated in Fig. 14-7, the

Table 14-12 *Monthly precipitation (in inches) of two stations in Texas.*

Year	1	2	3	4	5	6	7	8	9	10	11	12
Station 1												
2006	0.17	0.09	0.81	0.25	0.91	0.47	0.5	0.31	5.17	0.67	0.02	1.02
2007	3.8	0.05	2.95	0.92	5.33	4.55	3.19	1.11	2.53	0.34	0.3	0.21
2008	0.45	0.05	0.56	0.15	1.63	0.09	0.09	4.77	0.99	0.61	0.07	0.2
2009	0.07	0.05	0.96	0.1	1.76	0.23	0.02	0.47	2.79	2.84	1.34	0.94
2010	2.23	1.83	0.74	0.01	2.39	1.92	0.83	0.22	3.54	0.03	0.38	0.15
Station 2												
2006	0.08	0.26	0.2	0.02	4.51	0.09	2.22	0.01	2.52	0.68	0.01	1.64
2007	2.98	0.32	2.58	0.73	4.38	1.77	11.11	0.18	4.02	0.24	0.7	0.77
2008	0.24	0.05	0.55	3.19	3.43	0.31	3.97	10.35	3.32	1.02	0	0.35
2009	0.04	0.07	0.09	0.34	1.74	0	0.42	0.68	1.8	0.26	0.52	0.71
2010	4.98	3.63	0.65	2.74	0.41	0.01	3.08	0.26	5.62	0.06	0.01	0.08

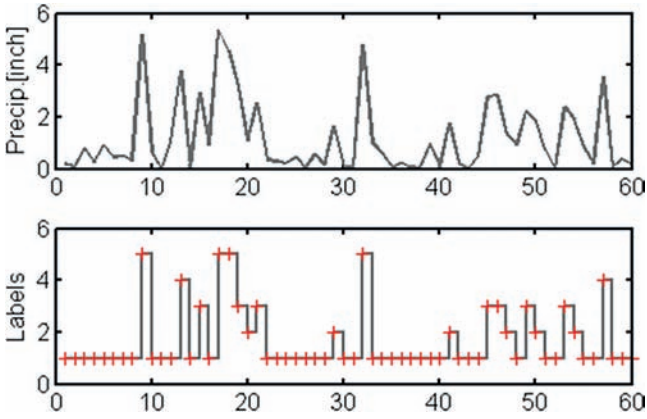

Figure 14-7 *Illustration for continuous data discretization of the precipitation time series of station 1.*

continuous precipitation time series for the two stations can be discretized and labeled, as tabulated in Table 14-13.

The first step of variable merging is to put all the corresponding digits of the two discretized series together. The merged series thus obtained is shown in Table 14-14. Then, pick out the unique values in the merged series and sort them in ascending order. Thus, one has Table 14-15.

The next step is to access the location index of each element of the direct merged series in the sorted unique value sequence and assign the location index as the new label for the corresponding element in the direct merged series. For

Table 14-13 *Discretized precipitation sequence.*

Year	1	2	3	4	5	6	7	8	9	10	11	12
Station 1												
2006	1	1	1	1	1	1	1	1	5	1	1	1
2007	4	1	3	1	5	5	3	2	3	1	1	1
2008	1	1	1	1	2	1	1	5	1	1	1	1
2009	1	1	1	1	2	1	1	1	3	3	2	1
2010	3	2	1	1	3	2	1	1	4	1	1	1
1: 0 ~ 1.064; **2**: 1.065 ~ 2.128; **3**: 2.129 ~ 3.192; **4**: 3.193 ~ 4.256; **5**: 4.257 ~ 5.320												
Station 2												
2006	1	1	1	1	3	1	1	1	2	1	1	1
2007	2	1	2	1	2	1	5	1	2	1	1	1
2008	1	1	1	2	2	1	2	5	2	1	1	1
2009	1	1	1	1	1	1	1	1	1	1	1	1
2010	3	2	1	2	1	1	2	1	3	1	1	1
1: 0 ~ 2.222; **2**: 2.223 ~ 4.444; **3**: 4.445 ~ 6.666; **4**: 6.667 ~ 8.888; **5**: 8.889 ~ 11.110												

Table 14-14 *Directly welded sequence.*

Station 1 + station 2												
Month	**1**	**2**	**3**	**4**	**5**	**6**	**7**	**8**	**9**	**10**	**11**	**12**
2006	11	11	11	11	13	11	11	11	52	11	11	11
2007	42	11	32	11	52	51	35	21	32	11	11	11
2008	11	11	11	12	22	11	12	55	12	11	11	11
2009	11	11	11	11	21	11	11	11	31	31	21	11
2010	33	22	11	12	31	21	12	11	43	11	11	11

Table 14-15 *Sorted unique value sequence.*

1	2	3	4	5	6	7	8	9	10	11	12	13	14
11	12	13	21	22	31	32	33	35	42	43	51	52	55

Table 14-16 *Final merged sequence.*

Station 1 + station 2												
Month	**1**	**2**	**3**	**4**	**5**	**6**	**7**	**8**	**9**	**10**	**11**	**12**
2006	1	1	1	1	3	1	1	1	13	1	1	1
2007	10	1	7	1	13	12	9	4	7	1	1	1
2008	1	1	1	2	5	1	2	14	2	1	1	1
2009	1	1	1	1	4	1	1	1	6	6	4	1
2010	8	5	1	2	6	4	2	1	11	1	1	1

Table 14-17 *Contingency table for the merged sequence.*

Counts							
Label	**1**	**2**	**3**	**4**	**5**	**6**	**7**
	35	5	1	4	2	3	2
Label	**8**	**9**	**10**	**11**	**12**	**13**	**14**
	1	1	1	1	1	2	1
Frequency							
Label	**1**	**2**	**3**	**4**	**5**	**6**	**7**
	0.5833	0.0833	0.0167	0.0667	0.0333	0.0500	0.0333
Label	**8**	**9**	**10**	**11**	**12**	**13**	**14**
	0.0167	0.0167	0.0167	0.0167	0.0167	0.0333	0.0167

example, the first element of the direct merged sample is 21, in the sorted unique value sequence the location index of 21 is 6, then 6 is the new label for the first element of the direct merged sample. In this manner, the new merged series is shown in Table 14-16.

Then the marginal contingency table for the merged series can be summarized as shown in Table 14-17. From Table 14-17, the marginal entropy of the merged series can be computed as

$$\begin{aligned} H(X_{1:2}) = &-0.5833\log_2 0.5833 - 0.0833\log_2 0.0833 - 0.0167\log_2 0.0167 \\ &- \ldots - 0.0167\log_2 0.0167 - 0.0167\log_2 0.0167 \\ &- 0.0333\log_2 0.0333 - 0.0167\log_2 0.0167 \\ = &\ 2.4087 \text{ bits} \end{aligned}$$

Conversely, from Table 14-13, one can also summarize the joint contingency table for station 1 and station 2. The results are presented in Table 14-18.

Table 14-18 *Joint contingency table for the two stations.*

Counts Table						
	Station 2					
Station 1	**0~2.222**	**2.223~4.444**	**4.445~6.666**	**6.665~8.888**	**8.889~11.110**	**Sum**
0~1.064	35	5	1	0	0	41
1.065~2.128	4	2	0	0	0	6
2.129~3.192	3	2	1	0	1	7
3.193~4.256	0	1	1	0	0	2
4.257~5.320	1	2	0	0	1	4
Sum	43	12	3	0	2	120
Frequency Table						
	Station 2					
Station 1	**0~2.222**	**2.223~4.444**	**4.445~6.666**	**6.665~8.888**	**8.889~11.110**	**Sum**
0~1.064	0.583	0.083	0.017	0.000	0.000	0.683
1.065~2.128	0.067	0.033	0.000	0.000	0.000	0.100
2.129~3.192	0.050	0.033	0.017	0.000	0.017	0.117
3.193~4.256	0.000	0.017	0.017	0.000	0.000	0.033
4.257~5.320	0.017	0.033	0.000	0.000	0.017	0.067
Sum	0.717	0.200	0.050	0.000	0.033	1.0

Then the joint entropy between the two stations can be computed directly from Table 14-17 as

$$\begin{aligned} H(X_1, X_2) &= -0.583\log_2 0.583 - 0.083\log_2 0.083 - 0.017\log_2 0.017 \\ &\quad - \ldots - 0.017\log_2 0.017 \\ &= 2.4087 \text{ bits} \end{aligned}$$

Obviously, one can see that the information content retained by the two stations remains invariant before and after variable merging.

The variable merging approach satisfies the laws of association and commutation in terms of information content. Taking the merging of three variables as an example, according to the law of association and commutation, the following equalities are satisfied:

$$\begin{aligned} H(<X_1, X_2, X_3>) &= H(<<X_1, X_2>, X_3>) \\ &= H(<X_1, <X_2, X_3>>) \\ &= H(<X_1, X_3>, X_2) \end{aligned} \tag{14.19}$$

where angle brackets denote the merging operation for the convenience of indicating the merging sequence.

Example 14.7 Assuming that $X_1 = [1, 2, 1, 2, 1, 3, 3]^T$, $X_2 = [1, 2, 2, 2, 1, 3, 2]^T$, and $X_3 = [1, 1, 2, 2, 1, 3, 3]^T$, verify that the variable merging approach satisfies the law of association and commutation.

Solution To verify the law of association and commuatation, equation (14.19) just needs to be verified. Using the variable merging procedure, as demonstrated in Example 14.6, first we merge X_1 and X_2 as follows:

X_1	1	2	1	2	1	3	3
				$<\cdot>$			
X_2	1	2	2	2	1	3	2
				=			
X_{12}	5	3	4	3	5	1	2

Then we merge the new variable X_{12} with the third variable, as shown in the following:

X_{12}	5	3	4	3	5	1	2
				$<\cdot>$			
X_3	1	1	2	2	1	3	3
				=			
X_{123}	1	4	2	3	1	6	5

In the same way, one can obtain

$$X_{231} = [1, \quad 2, \quad 4, \quad 3, \quad 1, \quad 6, \quad 5]^T$$

$$X_{132} = [1, \quad 3, \quad 2, \quad 4, \quad 1, \quad 5, \quad 6]^T$$

Using the definition of marginal entropy, it is easy to get

$$H(X_{123}) = H\left([1, \quad 4, \quad 2, \quad 3, \quad 1, \quad 6, \quad 5]^T\right) = 2.522 \text{ bits}$$

$$H(X_{231}) = H\left([1, \quad 2, \quad 4, \quad 3, \quad 1, \quad 6, \quad 5]^T\right) = 2.522 \text{ bits}$$

$$H(X_{132}) = H\left([1, \quad 3, \quad 2, \quad 4, \quad 1, \quad 5, \quad 6]^T\right) = 2.522 \text{ bits}$$

In terms of variable merging, the multivariate joint entropy, $H(X_1, X_2, \ldots, X_n)$, can be computed by sequentially applying algorithm 1, i.e.,

$$\begin{aligned} H(X_1, X_2, \ldots, X_n) &= H(<X_1, X_2>, X_3, \ldots, X_n) \\ &= H(<<X_1, X_2>, X_3>, \ldots, X_n) \\ &= H(<\ldots<<X_1, X_2>, X_3>, \ldots X_{n-1}>, X_n) \\ &\quad \ldots\ldots \\ &= H(<\ldots<\ldots<<X_1, X_2>, X_3>, \ldots, X_{n-1}>, X_n>) \end{aligned} \tag{14.20}$$

Therefore, the estimation of multivariate probability distribution can be successfully bypassed. The total correlation can also be computed by the aid of its grouping property (equation [14.18]) and the variable merging method.

Example 14.8 For the five water-level monitoring stations considered in Example 14.3, compute the total correlation.

Solution Here $N = 5$. Using equation (14.18), the total correlation can be decomposed as

$$C(X_1, X_2, X_3, X_4, X_5) = C(X_1, X_2) + C(X_{1:2}, X_3) + C(X_{1:3}, X_4) + C(X_{1:4}, X_5)$$

From Example 14.5, we have

$$C(X_1, X_2) = T(X_1, X_2) = 1.9208 \text{ bits}$$

To compute $C(X_{1:2}, X_3)$, first a new variable $X_{1:2}$ needs to be created such that $H(X_{1:2}) = H(X_1, X_2)$. For illustrative purposes, only the first 10 records of gauge 1 (X_1) and gauge 2 (X_2) are considered, i.e., $[X_1^p, X_2^p]$, as an example. Part of the original record is repeated in Table 14-19. A series of new records can be created by merging X_1 and X_2 together, as shown in Table 14-20.

It is easy to verify that $H(X_{1:2}^p) = H(X_1^p, X_2^p)$ as follows. First, the marginal entropy of the new variable $X_{1:2}^p$ is computed. Its contingency table is shown as Table 14-21. Therefore,

$$H(X_{1:2}^p) = -\sum_{i=1}^{10} p_i \log_2(p_i) = -\log_2(0.1) = 3.3219$$

Table 14-19 *The first 10 records of gauges 1 and 2.*

X_1^p	75	80	80	85	85	90	90	95	95	100
X_2^p	85	85	90	95	100	105	110	110	115	115

Note: The superscript denotes that the data are only a portion of the original data set.

Table 14-20 *Creation of a new record.*

$X_{1:2}^p$	7585	8085	8090	8595	85100	90105	90110	95110	95115	100115

Table 14-21 *Contingency table.*

Events	7585	8085	8090	8595	85100	90105	90110	95110	95115	100115
Counts	1	1	1	1	1	1	1	1	1	1
Probability	0.1	0.1	0.1	0.1	0.1	0.1	0.1	0.1	0.1	0.1

Table 14-22 *Two-dimensional contingency table.*

	X_2^p							
X_1^p	**85**	**90**	**95**	**100**	**105**	**110**	**115**	**Sum**
75	1	0	0	0	0	0	0	1
80	1	1	0	0	0	0	0	2
85	0	0	1	1	0	0	0	2
90	0	0	0	0	1	1	0	2
95	0	0	0	0	0	1	1	2
100	0	0	0	0	0	0	1	1
Sum	2	1	1	1	1	2	2	10

Table 14-23 *Joint probability distribution.*

	X_2^p							
X_1^p	**85**	**90**	**95**	**100**	**105**	**110**	**115**	**Sum**
75	0.1	0	0	0	0	0	0	0.1
80	0.1	0.1	0	0	0	0	0	0.2
85	0	0	0.1	0.1	0	0	0	0.2
90	0	0	0	0	0.1	0.1	0	0.2
95	0	0	0	0	0	0.1	0.1	0.2
100	0	0	0	0	0	0	0.1	0.1
Sum	0.2	0.1	0.1	0.1	0.1	0.2	0.2	1.0

The two-dimensional contingency table for $[X_1^p, X_2^p]$ can be calculated as shown in Table 14-22. The joint probability distribution is given as Table 14-23. Then the joint entropy of $[X_1^p, X_2^p]$ is calculated in bits as

$$\begin{aligned} H(X_1^p, X_2^p) &= -\sum_{i=1}^{10}\sum_{j=1}^{10} p_{ij}\log_2\left(p_{ij}\right) \\ &= -0.1\log_2(0.1) - 0.1\log_2 0.1 - \ldots.. \\ &= 3.3219 \text{ bits} \end{aligned}$$

This result verifies that the merging of variables is justified.

By following this procedure, we see that the new variable can be sequentially created. Then, using the definition of bivariate transinformation, the components of the total correlation are

$$C\left(X_{1:2}, X_3\right) = 2.6579$$

$$C\left(X_{1:3}, X_4\right) = 0.1161$$

$$C\left(X_{1:4}, X_5\right) = 2.5574$$

Therefore, the final result for the total correlation is

$$\begin{aligned} C(X_1, X_2, X_3, X_4, X_5) &= C(X_1, X_2) + C(X_{1:2}, X_3) + C(X_{1:3}, X_4) + C(X_{1:4}, X_5) \\ &= 1.9208 + 2.6579 + 0.1161 + 2.5574 \\ &= 7.2522 \text{ bits} \end{aligned}$$

Example 14.9 For the five water-level monitoring stations considered in Example 14.3, compute the joint entropy.

Solution By sequentially applying the variable merging method, we can construct the merged variable $X_{1:5}$. Then the joint entropy of the five monitoring gauges can be computed from the definition of marginal entropy. For economy of space, only the final result is given

$$H(X_1, X_2, X_3, X_4, X_5) = H(X_{1:5}) = 4.8200 \text{ bits}$$

Conversely, the total correlation can also be computed by the shortcut formula as given in equation (14.16). First the marginal entropy for each of the five gauges can be computed, as listed in the following.

Gauge 1	Gauge 2	Gauge 3	Gauge 4	Gauge 5
2.6579	3.0235	2.6579	0.1687	3.5642

From Example 14.8, the total correlation has already been computed.

$$C(X_1, X_2, X_3, X_4, X_5) = 7.2522 \text{ bits}$$

Then, by applying equation (14.16), we see that the joint entropy is

$$\begin{aligned} H(X_1, X_2, \ldots, X_5) &= \sum_{i=1}^{5} H(X_i) - C(X_1, X_2, \ldots, X_5) \\ &= 2.6579 + 3.0235 + 2.6579 + 0.1687 + 3.5642 - 7.2522 \\ &= 4.8200 \text{ bits} \end{aligned}$$

Clearly, no matter which method is used, the final results for multivariate joint entropy are the same.

Example 14.10 For the five water-level monitoring stations considered in Example 14.3, compute the interaction of the first three monitoring gauges.

Solution According to equation (14.14), to compute the interaction of the marginal entropies, the joint entropy for each pair of gauges and the trivariate joint entropy of the three monitoring gauges need to be computed. From Example 14.9 we have

$$H(\text{gauge 1}) = 2.6579 \text{ bits}$$

$$H(\text{gauge 2}) = 3.0235 \text{ bits}$$

$$H(\text{gauge 3}) = 2.6579 \text{ bits}$$

By using Example 14.3, we can compute the joint entropy for each pair of gauges, and the results are

$$H(\text{gauge 1, gauge 2}) = 3.7606 \text{ bits}$$

$$H(\text{gauge 2, gauge 3}) = 3.7606 \text{ bits}$$

$$H(\text{gauge 1, gauge 3}) = 2.6579 \text{ bits}$$

By using Example 14.9, we can compute the trivariate joint entropy, and the result is

$$H(\text{gauge 1, gauge 2, gauge 3}) = 3.7606 \text{ bits}$$

By applying equation (14.14), we see that the interaction is computed as

$$\begin{aligned} I(\text{gauge 1; gauge 2; gauge 3}) &= H(\text{gauge 1}) + H(\text{gauge 2}) + H(\text{gauge 3}) \\ &\quad - H(\text{gauge 1, gauge 2}) - H(\text{gauge 2, gauge 3}) \\ &\quad - H(\text{gauge 1, gauge 3}) + H(\text{gauge 1, gauge 2, gauge 3}) \\ &= 2.6579 + 3.0235 + 2.6579 - 3.7606 \\ &\quad - 3.7606 - 2.6579 + 3.7606 \\ &= 1.9208 \text{ bits} \end{aligned}$$

With the aid of variable merging, one can define the multivariate transinformation between single and grouped variables, and between two grouped variables. The first type of multivariate transinformation, denoted as $T(X_{1:n}; X)$, measures the information amount of a single variable that can be inferred from that of variables in the group, and vice versa. Transinformation between grouped variables, $T(X_{1:n}; X'_{1:m})$, measures the common information shared by the two grouped variables. The aforementioned two types of multivariate transinformation can be easily computed by first merging variables in the group and then applying the definition of bivariate transinformation.

An intuitive explanation about the probabilistic rationality for discrete variable merging is given in this section through a simple random experiment. Assume that there are two nontransparent boxes, each of which contains three balls of different colors (red, green, and blue). All attributes of the balls are the same except for their colors, which means that they are equally likely to be drawn from the box. One can think of the following random experiment in which one sequentially draws three balls with replacement from the first box. The resulting random sample is denoted as X = {Red, Blue, Blue}. Then repeat the procedure again to obtain another random sample from the second box, denoted as

Table 14-24 *Two-dimensional (A) and one-dimensional (B) contingency tables (counts) for the two different representations of the same random experiment.*

		Y		
A: Two-dimensional				
X		***Red***	***Green***	***Blue***
	Red	0	1	0
	Green	0	0	0
	Blue	1	1	0
B: One-dimensional				
		Red–Green	***Blue–Red***	***Blue–Green***
XY		1	1	1

Y = {Green, Red, Green}. We are interested in the uncertainty of this random experiment.

Results of this experiment can be described in two different ways. First, they can be described in an analogous way as that in which the random experiment is carried out, i.e., the joint outcomes of two individual samples. The joint outcomes can be fully represented by a two-dimensional contingency table (Table 14-24A). Then the uncertainty measured by the joint entropy of the two random trials can be computed through equation (14.7) from the contingency table.

Second the experiment can also be represented by a single welding sample as XY = {Red–Green, Blue–Red, Blue–Green}. This method is like carrying out the random sampling in the following manner: First draw a ball from the first box and then draw another ball from the second box, resulting in a random event denoted as Red–Green; then repeat the same procedure, resulting in another event denoted as Blue–Red; finally the third trial can be done, leading to an event of Blue–Green. Similarly, the welding sample is fully described by a one-dimensional contingency table (Table 14-24B). The uncertainty of the welding sample can be computed from equation (14.1).

Obviously, the two-dimensional and one-dimensional contingency tables are different representations of the same random experiment, whose uncertainty is invariant no matter which way is used to describe the experimental outcomes. This conclusion can also be verified by numerical results of joint entropy and marginal entropy corresponding to the different representations. One requirement of the variable merging approach is that the two samples must have the same length, which is a small limitation.

14.2.7 Directional Information Transfer Index

Although transinformation indicates the dependence of two variables, it is not a good index of dependence because its upper bound varies from site to site (it

varies from 0 to marginal entropy H). Therefore, the original definition of T can be normalized by dividing by the marginal entropy. Yang and Burn (1994) normalized T as

$$\frac{T}{H} = DIT = \frac{(H - H_{\text{Lost}})}{H} = 1 - \frac{H_{\text{Lost}}}{H} \tag{14.21}$$

where H_{Lost} is the amount of information lost. The ratio of T by H is called the directional information transfer (DIT) index. Mogheir and Singh (2002) called it the information transfer index (ITI). The physical meaning of DIT is the fraction of information transferred from one site to another. DIT varies from zero to unity when T varies from zero to H. The zero value of DIT corresponds to the case where sites are independent and therefore no information is transmitted. A value of unity for DIT corresponds to the case where sites are fully dependent and no information is lost. Any other value of DIT between zero and one corresponds to a case between fully dependent and fully independent.

DIT is not symmetrical, as $\text{DIT}_{XY} = T/H(X)$ is not in general equal to $\text{DIT}_{YX} = T/H(Y)$. DIT_{XY} describes the fractional information inferred by station Y about station X, whereas DIT_{YX} describes the fractional information inferred by station X about station Y. Between two stations, the station with the higher DIT should be given higher priority because of its higher capability of inferring (predicting) the information at other sites.

DIT can be applied to the regionalization of the network. If both DIT_{XY} and DIT_{YX} are high, the two related stations can be arranged in the same group, because they are strongly dependent and information can be mutually transferred between them. If neither of the DIT values is high, they should be kept in separate groups. If DIT_{XY} is high, station Y, whose information can be predicted by X, can join station X if station Y does not belong to another group; otherwise, it stays in its own group. The predictor station X cannot join station Y's group, because if it were discontinued, the information at that site would be lost.

DIT can be both a measure of information transmission capability and an indicator of the dependency of a station. This phenomenon is an indicator of the information connection. In the station selection process, a predicted station should be removed first, because it recovers information efficiently but does not predict it efficiently. When all remaining stations in the group have strong mutual connections with each other (i.e., both DIT_{XY} and DIT_{YX} are high), they can be further selected based on a criterion, designated as SDIT_i, defined as

$$\text{SDIT}_i = \sum_{j=1, j\neq i}^{m} \text{DIT}_{ij} \tag{14.22}$$

where DIT_{ij} is the information inferred by station i about station j, and m = the number of stations in the group. The station in each group with the highest value of SDIT, in comparison with members in the group, should be retained in the network.

To be able to use transinformation and DIT, the probability density function of the variable being sampled must be determined. To that end, a nonparametric estimation method can be used. Nonparametric estimation does not describe a probability density function by a formula and parameters but rather by a set of point values everywhere in the domain. If the values of the density function are known everywhere, then the function is known numerically. This method of describing the density function is known as the nonparametric method, using a kernel estimator (Parzen 1962). For a multidimensional case where $X = X(x_1, x_2, \ldots, x_N)$, Cacoullos (1966) presents the kernel estimator in which components of X:$\{X_1, X_2, \ldots, X_p\}$could be mutually dependent or independent, but observations of each component are still assumed to be independent and identically distributed.

According to Adamowski (1989), the choice of a kernel is not crucial for the estimation. However, the selection of parameter h in the estimation method is crucial, because it affects both the bias and the mean square error of the estimator. Some common forms of kernels are presented by Parzen (1962) and Wertz (1979). In practice, hydrologic variables are nonnegative. Therefore, the original variables are logarithmically transformed and a Gaussian kernel is chosen to form the estimator.

Example 14.11 Compute the DIT using data from five stations considered in Example 14.3.

Solution The marginal information and transinformation are computed in Examples 14.9 and 14.5, respectively. The marginal entropies, $H(X)$, are

	Gauge 1	Gauge 2	Gauge 3	Gage 4	Gage 5
$H(X)$	2.6579	3.0235	2.6579	0.1687	3.5642

The bivariate transinformation values are given in Table 14-25. For example,

$$DIT_{\text{gauge 1}\rightarrow\text{gauge 2}} = \frac{T(\text{gauge 1, gauge 2})}{H(\text{gauge 2})} = \frac{1.9208}{3.0235} = 0.6353$$

Table 14-25 *Bivariate transinformation.*

	Gauge 1	Gauge 2	Gauge 3	Gauge 4	Gauge 5
Gauge 1	2.6579	1.9208	2.6579	0.0234	1.8371
Gauge 2	1.9208	3.0235	1.9208	0.0336	2.1469
Gauge 3	2.6579	1.9208	2.6579	0.0234	1.8371
Gauge 4	0.0234	0.0336	0.0234	0.1687	0.0764
Gauge 5	1.8371	2.1469	1.8371	0.0764	3.5642

Table 14-26 *DIT values.*

	Gauge 1	Gauge 2	Gauge 3	Gauge 4	Gauge 5
Gauge 1	1.0000	0.6353	1.0000	0.1387	0.5154
Gauge 2	0.7227	1.0000	0.7227	0.1992	0.6024
Gauge 3	1.0000	0.6353	1.0000	0.1387	0.5154
Gauge 4	0.0088	0.0111	0.0088	1.0000	0.0214
Gauge 5	0.6912	0.7101	0.6912	0.4529	1.0000

$$DIT_{\text{gauge 2}\rightarrow\text{gauge 1}} = \frac{T(\text{gauge 1, gauge 2})}{H(\text{gauge 1})} = \frac{1.9208}{2.6579} = 0.7227$$

Similarly, the DIT matrix is constituted as Table 14-26.

14.3 Method of Application

Consider the problem of locating water-level gauges in a canal network. Data on time series of water level and discharge are needed. These data can be generated at a dense set of points using a hydrodynamic model, where each point is a potential monitoring site. The objective then is to determine the set of points that collectively yield the highest information content or prediction skill while they are most independent of one another.

14.3.1 The WMP Approach

Water-level monitoring in polders (WMP) design method is an adapted version of the method proposed by Krstanovic and Singh (1992a, b). According to Alfonso et al. (2010), this approach can be accomplished as follows:

1. Using a hydrodynamic model, generate a water-level time series for each calculation point, s_i, $i = 1, 2, \ldots, N$, where N = number of calculation points.
2. Using the mathematical floor function as given in equation (14.6), convert the continuous water level, say X, to a quantized value x_q, which is rounded to the nearest multiple of a.
3. Compute the marginal entropy $H(_{Xi})$ at each point s_i, using equation (14.1).
4. For each point s_i, compute transinformation using equation (14.12a) or (14.12b) with respect to each of the remaining points. In this manner, construct a symmetric transinformation matrix like this:

$$T = \begin{bmatrix} T(X_1, X_1) & T(X_1, X_2) & \cdots & T(X_1, X_N) \\ T(X_2, X_1) & T(X_2, X_2) & \cdots & T(X_2, X_N) \\ \vdots & \vdots & \cdots & \vdots \\ \vdots & \vdots & \cdots & \vdots \\ \vdots & \vdots & \cdots & \vdots \\ T(X_N, X_1) & T(X_N, X_2) & \cdots & T(X_N, X_N) \end{bmatrix}$$

5. Identify the central station that has the largest value of $H(X_i)$ or information, i.e., $\max[H(X_i)]$, and designate it as s_1.
6. Obtain the transinformation vector V_1 corresponding to point s_1.
7. Select a small value of transinformation threshold ε such that when two sites have a transinformation value less than or equal to this value, the sites can be considered independent.
8. Inspect the elements of V_1 and, using the selected value of ε, determine the set of points that are independent of s_1, i.e., $T(X_1, X_i) < \varepsilon$.
9. Within the set of independent points or sites, determine the point with the highest information content $V_2 = \max[H(X_i \varepsilon S_{\text{ind } 1})]$.
10. Obtain the transinformation vector V_2 of point s_2.
11. Sum the two vectors V_1 and V_2 as $V_3 = V_1 + V_2$.
12. Rename V_3 as V_1 and repeat steps 8 onward until a maximum number of points is determined or until the remaining points do not contribute a significant amount of information.

Matrix T can be replaced by DIT_{XY} and DIT_{YX} when the DIT-based criteria are adopted. The main point in this method is that each new selected point leads to the maximum reduction in uncertainty.

Example 14.12 Consider a network of water-level monitoring stations as shown in Fig. 14-6. Evaluate this water-level monitoring network using WMP.

Solution *Step 1: Continuous data quantization:* Water-level data in Table 14-34 in Appendix 14.1 are quantized data. Therefore, they can be directly used for further calculation.

Step 2: Marginal entropy computation: As in Example 14.9, the marginal entropy is computed and is as follows:

	Gauge 1	Gauge 2	Gauge 3	Gauge 4	Gauge 5
$H(x)$	2.6579	3.0235	2.6579	0.1687	3.5642

Step 3: Transinformation matrix calculation: Following the procedure in Example 14.5, the transinformation matrix between gauges can be obtained, as shown in Table 14-27.

Step 4: Central station identification: From the results obtained in step 1, it can be seen that gauge 5 has the highest marginal entropy among others. So gauge 5 is identified as the central station, i.e., s_1 = gauge 5.

Table 14-27 *Bivariate transinformation.*

	Gauge 1	Gauge 2	Gauge 3	Gauge 4	Gauge 5
Gauge 1	2.6579	1.9208	2.6579	0.0234	1.8371
Gauge 2	1.9208	3.0235	1.9208	0.0336	2.1469
Gauge 3	2.6579	1.9208	2.6579	0.0234	1.8371
Gauge 4	0.0234	0.0336	0.0234	0.1687	0.0764
Gauge 5	1.8371	2.1469	1.8371	0.0764	3.5642

Step 5: Obtain the transinformation vector of gauge 5: The transinformation vector corresponding to gauge 5 is V_1 = [1.8371 2.1469 1.8371 0.0764 3.5642].

Step 6: Determination of independent gauges: Determine the independent gauges remaining in the candidate set.

	Gauge 1	Gauge 2	Gauge 3	Gauge 4	Gauge 5
Gauge 5	1.8371	2.1469	1.8371	0.0764	3.5642

Assume that ε = 3.0. Then, gauges 1, 2, 3, and 4 as shown in this table are independent of gauge 5.

Step 7: Select the next independent gauge with the highest information. Among these independent gauges, gauge 2 has the highest marginal entropy, 2.1469 bits. Therefore, s_2 = gauge 2.

Step 8: Obtain transinformation vectors in the selected sets and add them together. The transinformation vector associated with gauge 2 is V_2 = [1.9208 3.0235 1.9208 0.0336 2.1469]. Then, add the transinformation vectors together:

	Gauge 1	Gauge 2*	Gauge 3	Gauge 4	Gauge 5*
Gauge 5	1.8371	2.1469	1.8371	0.0764	3.5642
			+		
	Gauge 1	**Gauge 2***	**Gauge 3**	**Gauge 4**	**Gauge 5***
Gauge 2	1.9208	3.0235	1.9802	0.0336	2.1469
			=		
	Gauge 1	**Gauge 2***	**Gauge 3**	**Gauge 4**	**Gauge 5***
Gauge 2 + 5	3.7579	5.1704	3.8173	0.1100	5.7111
Note: * denotes already selected gauges.					

So V_3 = [3.7579 5.1704 3.8173 0.1100 5.7111]

Step 9: Determine independent gauges remaining in the candidate set. At this time, only gauges 1, 3, and 4 remain in the candidate set. Since ε = 3.0, only gauge 4 is found independent, as shown in the previous table. Therefore, gauge 4 is added to the selected set. Because only one gauge satisfies the independence

requirement, it is not necessary to determine which one in the independent set retains the most information.

Step 10: Obtain transinformation vectors in the selected sets and add them together:

	Gauge 1	Gauge 2*	Gauge 3	Gauge 4	Gauge 5*
Gauge 2 + 5	3.7579	5.1704	3.8173	0.1100	5.7111
		+			
	Gauge 1	**Gauge 2***	**Gauge 3**	**Gauge 4***	**Gauge 5***
Gauge 4	0.0234	0.0336	0.0234	0.1687	0.0764
		=			
	Gauge 1	**Gauge 2***	**Gauge 3**	**Gauge 4***	**Gauge 5***
Gauge 2 + 5 + 4	3.7813	5.2040	3.8407	0.2787	5.7875

Note: * denotes already selected gauges.

Step 11: Determine the independent gauges remaining in the candidate set.

At this time, only gauge 1 and gauge 2 are left in the candidate set. As $\varepsilon = 3.0$, there is no gauge in the candidate set satisfying the independence requirement. Thus, gauges 5, 2, and 4 are selected sequentially for monitoring the water level.

14.3.2 MIMR-Based Approach

The idea of maximum information minimum redundancy (MIMR) criterion for hydrometric network evaluation and design lies in selecting (or ranking) stations from a candidate set, through which the selected stations can maximize the overall information amount, maximize the prediction ability, and minimize the redundant information.

Let there be N potential candidate hydrometric stations of interest, X_1, X_2, X_3, …, X_N. It is assumed that for each candidate station there are several years of records about the hydrometric variable, such as water level, sediment concentration, and scour. Let S denote the set of hydrometric stations already selected for the network, and its elements are denoted by $X_{S_1}, X_{S_2}, X_{S_3}, \cdots, X_{S_k}$, where S_i can be 1, 2, …, N, or only some of them. Similarly, let F denote the set of candidate stations to be selected, and similarly its elements are denoted by $X_{F_1}, X_{F_2}, X_{F_3}, \cdots, X_{F_m}$, where F_i can be 1, 2, …, N, or only some of them. The summation of k and m is equal to N, the total number of potential candidate stations. The amount of effective information retained by S can be modeled in terms of joint entropy and transinformation as

$$H(X_{S_1}, X_{S_2}, \cdots, X_{S_k}) + \sum_{i=1}^{m} T(X_{S_1:S_k}; X_{F_i}) \tag{14.23a}$$

where $X_{S_{1:S_k}}$ denotes the merged time series of $X_{S_1}, X_{S_2}, X_{S_3}, \cdots, X_{S_k}$ such that its marginal entropy is the same as the multivariate joint entropy of $X_{S_1}, X_{S_2}, X_{S_3}, \cdots, X_{S_k}$. In other words, the merged variable $X_{S_{1:S_k}}$ contains the same amount of information as that retained by all of its individual members $X_{S_1}, X_{S_2}, X_{S_3}, \cdots, X_{S_k}$.

The effective information contains two parts. The first part is the joint entropy of the selected stations, measuring the total but not duplicated amount of information that can be obtained from the selected stations. The second part is the summation of transinformation from the group of already selected stations to each station still remaining in the candidate set. When doing network design, one should keep in mind that the major function of a hydrometric network is to monitor the hydrometric variables of interest and to do the prediction. Therefore, the predictive ability of the network should not be neglected in the design. $T(X_{S_{1:S_k}}, X_{F_i})$ is a quantitative measure of the amount of information about the unselected station X_{F_i}, which can be inferred from the selected stations. In other words, it is a measure of the predictive ability of the selected stations.

Husain (1987) and Al-Zahrani and Husain (1998) considered the predictive ability of an optimal network. However, the effective information equation (14.23a) differs from the one they used in two respects. The first respect is that the predictive ability of equation (14.23a) is measured while considering the selected stations as a whole group containing the same amount of information as that of all its elements rather than treating them separately. This predictive ability measure can successfully filter the duplicated information (redundancy) of the selected stations. Second, the multivariate joint entropy is used to quantify the total information rather than using the summation of marginal entropies in which the duplicated information is summed again and again.

Besides equation (14.23a), the effective information can also be expressed as

$$H(X_{S_1}, X_{S_2}, \cdots, X_{S_k}) + T(X_{S_{1:S_k}}; X_{F_{1:F_m}}) \tag{14.23b}$$

It also contains two components: the total effective information part and the predictive ability part. In this equation, the unselected stations are also treated as a whole group. Transinformation $T(X_{S_{1:S_k}}, X_{F_{1:F_m}})$ is the amount of information about the unselected group that can be inferred from the selected group.

Another key point worthy of consideration in network design is the redundant information among selected stations. Such redundancy means that the selected stations are not fully and effectively used since a lot of hydraulic information collected from the network overlaps. In other words, some of the stations are not necessary and therefore the network is not an economically effective one. Even worse, the redundancy may deteriorate the predictive ability of the network even though the same amount of information can be obtained from a redundant network as that obtained from a less redundant one, considering that no redundancy is impossible in real practice.

The total correlation of the selected stations can measure the redundancy among them, i.e., $C(X_{S_1}, X_{S_2}, \cdots, X_{S_k})$. The total correlation of already selected

stations measures the common information shared by any combination of these stations. Interaction information is sensitive to the newly added stations; in other words, it may change abruptly from positive to negative when a new station is added to the network. To understand this phenomenon, there may be a large amount of duplicated information between two stations; however, when adding a new station, these three stations may have no simultaneous common information. In this sense, the total correlation is a more reliable measure of redundancy than interaction information.

14.3.2.1 Optimization

An informative hydrometric network should provide as much information as possible and at the same time constrain the redundant information as much as possible. This kind of maximum information and minimum redundancy network can be determined as

$$\begin{cases} \max : H(X_{S_1}, X_{S_2}, \cdots X_{S_k}) + \sum_{i=1}^{m} T(X_{S_1:S_k}; X_{F_i}) \\ \min : C(X_{S_1}, X_{S_2}, \cdots, X_{S_k}) \end{cases} \tag{14.24a}$$

or

$$\begin{cases} \max : H(X_{S_1}, X_{S_2}, \cdots X_{S_k}) + \sum_{i=1}^{m} T(X_{S_1:S_k}; X_{F_i:Fm}) \\ \min : C(X_{S_1}, X_{S_2}, \cdots, X_{S_k}) \end{cases} \tag{14.24b}$$

This set of maxims constitutes a multiobjective optimization problem, but it can be reduced to a single objective optimization problem by recalling that both the effective information part and the redundancy part have the same unit. The two objectives can be unified as

$$\max : \lambda_1 [H(X_{S_1}, X_{S_2}, \cdots, X_{S_k}) + \sum_{i=1}^{m} T(X_{S_1:S_k}; X_{F_i})] - \lambda_2 C(X_{S_1}, X_{S_2}, \cdots, X_{S_k}) \tag{14.25a}$$

or

$$\max : \lambda_1 [H(X_{S_1}, X_{S_2}, \cdots, X_{S_k}) + T(X_{S_1:S_k}; X_{F_1:F_m})] - \lambda_2 C(X_{S_1}, X_{S_2}, \cdots, X_{S_k}) \tag{14.25b}$$

where λ_1 and λ_2, whose summation is 1, are the information weight and redundancy weight, respectively, since sometimes the decision maker needs a trade-off between the informativeness and redundancy of the hydrometric network. One can unify the information and redundancy objectives using a different strategy, such as

$$\max : \frac{H(X_{S_1}, X_{S_2}, \cdots, X_{S_k}) + \sum_{i=11}^{m} T(X_{S_1:S_k}; X_{F_i})}{\lambda C(X_{S_1}, X_{S_2}, \cdots, X_{S_k})} \tag{14.26a}$$

or

$$\max : \frac{H(X_{S_1}, X_{S_2}, \cdots, X_{S_k}) + T(X_{S_1:S_k}; X_{F_1:F_m})}{\lambda C(X_{S_1}, X_{S_2}, \cdots, X_{S_k})} \tag{14.26b}$$

where λ is the coefficient that makes trade-off between informativeness and redundancy of the network. Either of the two methods unifying informativeness and redundancy objectives can be adopted in the hydrometric network design.

14.3.2.2 Selection Procedure

Using the MIMR criterion, the selection procedure for a hydrometric network design entails the following steps:

1. Collect data of hydrometric variable of interest (such as precipitation or streamflow) at each candidate station.
2. Discretize the continuous time series data by the mathematical floor function or by a histogram-based partition.
3. Initialize the optimal set S as an empty set and the candidate set F as the one containing all candidate stations.
4. Identify the central station as the one with maximum marginal entropy among all candidates.
5. Update sets S and F.
6. Select the next optimal station from F by the MIMR criterion. In this step, all stations in the F set are scanned to search the one satisfying equation (14.25a) or equation (14.25b).
7. Repeat steps 5 and 6 iteratively until the expected number of stations have been selected.

A pseudo code for this procedure is given in Table 14-28. Convergence of the selection can be determined by the ratio of joint entropy of the selected stations to that of all the candidates. If the ratio is over a threshold, like 0.90, the selection procedure stops. If no threshold is provided, then all candidate stations are ranked in descending order of priority.

Other than the forward selection procedure, the optimal stations can also be determined in an opposite direction. For backward selection, the criterion should be changed to minimum information reduction and maximum redundancy reduction, which is also based on the principle of MIMR. The reduced information and redundancy can be quantified by the difference between the joint entropies and total correlations of stations before and after one is deleted, respectively. At the same time, we should guarantee that the information of the station to be deleted can be inferred from the remaining stations as much as possible.

Table 14-28 *Pseudo code for the MIMR-based greedy selection algorithm.*

1.	$\boldsymbol{F} \leftarrow$ candidate set, including all candidate stations $\boldsymbol{S} \leftarrow$ empty set	Initialize candidate set $\boldsymbol{F}$ and empty set $\boldsymbol{S}$.
2.	Discretize the continuous time series.	
3.	$\boldsymbol{t}$Info $\leftarrow \boldsymbol{H}(\boldsymbol{F}) \leftarrow$ Equation (14.9)	Compute the total information of all the potential stations.
4.	For $\boldsymbol{i} = 1{:}\boldsymbol{N}$ $\boldsymbol{H}(\boldsymbol{X_i}) \leftarrow$ Equation (14.1) End	Compute the marginal entropy of each potential station.
5.	$X_i \leftarrow \arg\max_{X_i}[H(X_i)]$	Select the first central station.
6.	$\boldsymbol{F} \leftarrow \boldsymbol{F} - \boldsymbol{X_i}$ $\boldsymbol{S} \leftarrow \boldsymbol{S} + \boldsymbol{X_i}$	Update $\boldsymbol{F}$ and $\boldsymbol{S}$ for the first time.
7.	For $\boldsymbol{i} = 2{:}\boldsymbol{N}$ $\boldsymbol{m} \leftarrow$ size ($\boldsymbol{F}$) $\boldsymbol{n} \leftarrow$ size ($\boldsymbol{S}$) For $\boldsymbol{k} = 1{:}\boldsymbol{m}$ $\mathrm{MIMR}_{S+X_{Fk}} \leftarrow$ Equation (14.25) End $X_{Fk} = \arg\max_{X_{Fk}}\left(\mathrm{MIMR}_{S+X_{Fk}}\right)$ $F \leftarrow F - X_{Fk}$ $S \leftarrow S + X_{Fk}$ End	Sequentially select stations from the updated candidate set according to the MIMR criterion. Update the candidate set and already selected set successively.
8.	For $\boldsymbol{i} = 1 : \boldsymbol{N}$ $p\mathrm{Info} \leftarrow H\left(X_{S_1}, X_{S_2}, \ldots, X_{S_i}\right)$ $pct \leftarrow \dfrac{p\mathrm{Info}}{t\mathrm{Info}}$ If $\lvert \boldsymbol{pct} - \mathbf{threshold} \rvert < \boldsymbol{eps}$ $S_{\mathrm{final}} \leftarrow \{X_{S_1}, X_{S_2}, \ldots, X_{S_i}\}$ return End End	Determine the final optimal station set $\boldsymbol{S_{final}}$ according to the information fraction of the selected set to the total information.

Example 14.13 Consider a network of water-level monitoring stations as shown in Fig. 14-6. Rank the gauges using the MIMR criterion. Show each step as above with computations and results.

Solution *Step 1: Continuous data quantization*: As in Example 14.3, water-level records in Table 14-34 in Appendix 14.1 are quantized data. They can be directly used for further calculation.

Step 2: Candidate and selected set initialization: At the initial stage, the candidate set and selected set obviously are

$$F = \{\text{gauge 1, gauge 2, gauge 3, gauge 4, gauge 5}\}$$

$$S = \{\}, \text{ i.e., empty set.}$$

Step 3: Central gauge identification: The central gauge is identified as the one with maximum marginal entropy. Following Example 14.9, the marginal entropy for each candidate gauge is computed as follows:

	Gauge 1	Gauge 2	Gauge 3	Gauge 4	Gauge 5
$H(x)$	2.6579	3.0235	2.6579	0.1687	3.5642

Gauge 5 has the highest marginal entropy among stations, so gauge 5 is identified as the central gauge, i.e., s_1 = gauge 5. Then the candidate and selected sets can be updated as

$$F = \{\text{gauge 1, gauge 2, gauge 3, gauge 4}\}$$

$$S = \{\text{gauge 5}\}$$

Step 4: Second gauge selection: According to MIMR, equation (14.25a) is chosen as the objective function. One can also use others, say equation (14.25b), equation (14.26a), or equation (14.26b). For simplicity, equal weights are used for information and redundancy, i.e., $\lambda_1 = \lambda_2 = 0.5$.

Compute joint entropy of set S with each gauge in F: Taking the joint entropy of gauge 5 and gauge 1 as an example, calculate the joint contingency table as shown in Table 14-29. The joint probability is shown in Table 14-30. By using equation (14.7), we see that the joint entropy is

$$H(\text{gauge 5, gauge 1}) = 4.3851 \text{ bits}$$

Similarly,

$$H(\text{gauge 5, gauge 2}) = 4.4408 \text{ bits}$$

Table 14-29 *Joint contingency table.*

Gauge 1	Gauge 5													
	35	**40**	**45**	**50**	**55**	**60**	**65**	**70**	**75**	**80**	**85**	**90**	**95**	**100**
75	2	15	0	1	0	0	0	0	0	0	0	0	0	0
80	0	18	10	9	8	7	7	0	0	0	0	0	0	0
85	0	0	0	0	0	2	2	9	10	10	0	0	0	0
90	0	0	0	0	0	0	2	0	0	0	12	4	0	0
95	0	0	0	0	0	0	0	2	0	0	0	9	6	0
100	0	0	0	0	0	0	0	0	1	2	1	0	11	8
105	0	0	0	0	0	0	0	0	0	0	1	2	3	26

Table 14-30 *Joint probability values.*

Gauge 1	Gauge 5													
	35	**40**	**45**	**50**	**55**	**60**	**65**	**70**	**75**	**80**	**85**	**90**	**95**	**100**
75	0.01	0.075	0	0.005	0	0	0	0	0	0	0	0	0	0
80	0	0.090	0.050	0.045	0.040	0.035	0.035	0	0	0	0	0	0	0
85	0	0	0	0	0	0.01	0.01	0.045	0.05	0.05	0	0	0	0
90	0	0	0	0	0	0	0.01	0	0	0	0.06	0.020	0	0
95	0	0	0	0	0	0	0	0.01	0	0	0	0.045	0.030	0
100	0	0	0	0	0	0	0	0	0.05	0.01	0.005	0	0.055	0.040
105	0	0	0	0	0	0	0	0	0	0	0.005	0.010	0.015	0.130

$$H(\text{gauge 5, gauge 3}) = 4.3851 \text{ bits}$$

$$H(\text{gauge 5, gauge 4}) = 3.6564 \text{ bits}$$

Compute transinformation between gauges in S and each gauge in F and the other gauges in F. Here variables need to be merged such that information contained in the merged variable is the same as that retained by the original variables. For merging variables, one can follow the procedure discussed in Example 14.6. Assuming that gauge 1 is selected in this step, then the predictive ability of S is evaluated.

$$T(\text{gauge 5} + \text{gauge 1, gauge 2}) = 2.6080 \text{ bits}$$

$$T(\text{gauge 5} + \text{gauge 1, gauge 3}) = 2.6579 \text{ bits}$$

$$T(\text{gauge 5} + \text{gauge 1, gauge 4}) = 0.1243 \text{ bits}$$

Assume that gauge 2 is selected in this step. Then evaluate the predictive ability of the S set.

$$T(\text{gauge } 5 + \text{gauge } 2, \text{gauge } 1) = 2.2982 \text{ bits}$$

$$T(\text{gauge } 5 + \text{gauge } 2, \text{gauge } 3) = 2.2982 \text{ bits}$$

$$T(\text{gauge } 5 + \text{gauge } 2, \text{gauge } 4) = 0.1385 \text{ bits}$$

Assume that gauge 3 is selected in this step. Then evaluate the predictive ability of the S set.

$$T(\text{gauge } 5 + \text{gauge } 3, \text{gauge } 1) = 2.6579 \text{ bits}$$

$$T(\text{gauge } 5 + \text{gauge } 3, \text{gauge } 2) = 2.6080 \text{ bits}$$

$$T(\text{gauge } 5 + \text{gauge } 3, \text{gauge } 4) = 0.1243 \text{ bits}$$

Assume that gauge 4 is selected in this step. Then evaluate the predictive ability of the S set.

$$T(\text{gauge } 5 + \text{gauge } 4, \text{gauge } 1) = 1.8849 \text{ bits}$$

$$T(\text{gauge } 5 + \text{gauge } 4, \text{gauge } 2) = 2.2089 \text{ bits}$$

$$T(\text{gauge } 5 + \text{gauge } 4, \text{gauge } 3) = 1.8849 \text{ bits}$$

Compute the total correlation of all in the S set and each gauge in the F set. As only one gauge is in set S, the total correlation is reduced to transinformation (bits). Therefore,

$$C(\text{gauge } 5, \text{gauge } 1) = 1.8371$$

$$C(\text{gauge } 5, \text{gauge } 2) = 2.1469$$

$$C(\text{gauge } 5, \text{gauge } 3) = 1.8371$$

$$C(\text{gauge } 5, \text{gauge } 4) = 0.0764$$

Compute the final score for each gauge in F. From equation (14.25a), we have

$$\begin{aligned}\text{Gauge } 1 = {} & H(\text{gauge } 5, \text{gauge } 1) + T(\text{gauge } 5 + \text{gauge } 1, \text{gauge } 2) \\ & + T(\text{gauge } 5 + \text{gauge } 1, \text{gauge } 3) + T(\text{gauge } 5 + \text{gauge } 1, \text{gauge } 4) \\ & - C(\text{gauge } 5, \text{gauge } 1) \\ = {} & 4.3851 + 2.6080 + 2.6579 + 0.1243 - 1.8371 \\ = {} & 7.9382 \text{ bits}\end{aligned}$$

$$\begin{aligned}\text{Gauge 2} &= H(\text{gauge 5, gauge 2}) + T(\text{gauge 5} + \text{gauge 2, gauge 1}) \\ &\quad + T(\text{gauge 5} + \text{gauge 2, gauge 3}) + T(\text{gauge 5} + \text{gauge 2, gauge 4}) \\ &\quad - C(\text{gauge 5, gauge 2}) \\ &= 4.4408 + 2.2982 + 2.2982 + 0.1385 - 2.1469 \\ &= 7.0288 \text{ bits}\end{aligned}$$

$$\begin{aligned}\text{Gauge 3} &= H(\text{gauge 5, gauge 3}) + T(\text{gauge 5} + \text{gauge 3, gauge 1}) \\ &\quad + T(\text{gauge 5} + \text{gauge 3, gauge 2}) + T(\text{gauge 5} + \text{gauge 3, gauge 4}) \\ &\quad - C(\text{gauge 5, gauge 3}) \\ &= 4.3851 + 2.6579 + 2.6080 + 0.1243 - 1.8371 \\ &= 7.9382 \text{ bits}\end{aligned}$$

$$\begin{aligned}\text{Gauge 4} &= H(\text{gauge 5, gauge 4}) + T(\text{gauge 5} + \text{gauge 4, gauge 1}) \\ &\quad + T(\text{gauge 5} + \text{gauge 4, gauge 2}) + T(\text{gauge 5} + \text{gauge 4, gauge 3}) \\ &\quad - C(\text{gauge 5, gauge 4}) \\ &= 3.6564 + 1.8849 + 2.2089 + 1.8849 - 0.0764 \\ &= 9.5587 \text{ bits}\end{aligned}$$

Obviously, gauge 4 has the highest score. Therefore, it is selected into set S. Then, set F and set S can be updated as

$$F = \{\text{gauge 1, gauge 2, gauge 3}\}$$

$$S = \{\text{gauge 5, gauge 4}\}$$

Step 5: *Third gauge selection.* Following the same procedure as in step 4, one can select the third gauge using the MIMR criterion.

Compute the joint entropy of set S with each gauge in F. Multivariate joint entropy can be computed using the shortcut formula between marginal entropies and total correlation. For the computation procedure, one can refer to Example 14.9. Using the same method as in Example 14.9, the joint entropies are

$$H(\text{gauge 5, gauge 4, gauge 1}) = 4.4294 \text{ bits}$$

$$H(\text{gauge 5, gauge 4, gauge 2}) = 4.4710 \text{ bits}$$

$$H(\text{gauge 5, gauge 4, gauge 3}) = 4.4294 \text{ bits}$$

Compute transinformation between (gauges in S and each gauge in F) and (the other gauges in F):

Assume that gauge 1 is selected in this step. Then evaluate the predictive ability of the S set.

$$T(\text{gauge 5} + \text{gauge 4} + \text{gauge 1}, \text{gauge 2}) = 2.6329 \text{ bits}$$

$$T(\text{gauge 5} + \text{gauge 4} + \text{gauge 1}, \text{gauge 3}) = 2.6579 \text{ bits}$$

Assume that gauge 2 is selected in this step. Then evaluate the predictive ability of the S set.

$$T(\text{gauge 5} + \text{gauge 4} + \text{gauge 2}, \text{gauge 1}) = 2.3089 \text{ bits}$$

$$T(\text{gauge 5} + \text{gauge 4} + \text{gauge 2}, \text{gauge 3}) = 2.3089 \text{ bits}$$

Assume that gauge 3 is selected in this step. Then evaluate the predictive ability of the S set.

$$T(\text{gauge 5} + \text{gauge 4} + \text{gauge 3}, \text{gauge 1}) = 2.6579 \text{ bits}$$

$$T(\text{gauge 5} + \text{gauge 4} + \text{gauge 3}, \text{gauge 2}) = 2.6329 \text{ bits}$$

Compute the total correlation of all in S and each gauge in F. Assume that gauge 1 is selected in this step. Then,

$$C(\text{gauge 5}, \text{gauge 4}, \text{gauge 1}) = 1.9613 \text{ bits}$$

Assume that gauge 2 is selected in this step. Then,

$$C(\text{gauge 5}, \text{gauge 4}, \text{gauge 2}) = 2.2854 \text{ bits}$$

Assume that gauge 3 is selected in this step. Then,

$$C(\text{gauge 5}, \text{gauge 4}, \text{gauge 3}) = 1.9613 \text{ bits}$$

Now compute the final score for each gauge in F:

$$\begin{aligned}\text{Gauge 1} = {} & H(\text{gauge 5}, \text{gauge 4}, \text{gauge 1}) \\ & + T(\text{gauge 5} + \text{gauge 4} + \text{gauge 1}, \text{gauge 2}) \\ & + T(\text{gauge 5} + \text{gauge 4} + \text{gauge 1}, \text{gauge 3}) \\ & - C(\text{gauge 5}, \text{gauge 4}, \text{gauge 1}) \\ = {} & 4.4294 + 2.6329 + 2.6579 - 1.9613 \\ = {} & 7.7589 \text{ bits}\end{aligned}$$

$$\begin{aligned}\text{Gauge 2} = {} & H(\text{gauge 5}, \text{gauge 4}, \text{gauge 2}) \\ & + T(\text{gauge 5} + \text{gauge 4} + \text{gauge 2}, \text{gauge 1}) \\ & + T(\text{gauge 5} + \text{gauge 4} + \text{gauge 2}, \text{gauge 3}) \\ & - C(\text{gauge 5}, \text{gauge 4}, \text{gauge 2}) \\ = {} & 4.4710 + 2.3089 + 2.3089 - 2.2854 \\ = {} & 6.8034 \text{ bits}\end{aligned}$$

$$\begin{aligned}\text{Gauge 3} &= H(\text{gauge 5, gauge 4, gauge 3}) \\ &\quad + T(\text{gauge 5} + \text{gauge 4} + \text{gauge 3, gauge 1}) \\ &\quad + T(\text{gauge 5} + \text{gauge 4} + \text{gauge 3, gauge 2}) \\ &\quad - C(\text{gauge 5, gauge 4, gauge 3}) \\ &= 4.4294 + 2.6579 + 2.6329 - 1.9613 \\ &= 7.7589 \text{ bits}\end{aligned}$$

Gauge 1 and gauge 3 have the same scores. We can make the final selection between them by their marginal entropies. Here gauge 1 and gauge 3 also have the same marginal entropy. In this case, we can arbitrarily select one, say gauge 1, and add to set S. Then set F and S can be updated as

$$F = \{\text{gauge 2, gauge 3}\}$$

$$S = \{\text{gauge 5, gauge 4, gauge 1}\}$$

Step 6: Select the fourth gauge. Compute the joint entropy of set S with each gauge in F:

$$H(\text{gauge 5, gauge 4, gauge 1, gauge 2}) = 4.8200 \text{ bits}$$

$$H(\text{gauge 5, gauge 4, gauge 1, gauge 3}) = 4.4294 \text{ bits}$$

Compute transinformation between (gauges in S and each gauge in F) and (the other gauges in F). Assume that gauge 2 is selected in this step. Then evaluate the predictive ability of the S set.

$$T(\text{gauge 5} + \text{gauge 4} + \text{gauge 1} + \text{gauge 2, gauge 3}) = 2.6579 \text{ bits}$$

Assume that gauge 3 is selected in this step. Then evaluate the predictive ability of the S set.

$$T(\text{gauge 5} + \text{gauge 4} + \text{gauge 1} + \text{gauge 3, gauge 2}) = 2.6329 \text{ bits}$$

Compute the total correlation of all gauges in S and each gauge in F. Assume that gauge 2 is selected in this step. Then,

$$C(\text{gauge 5, gauge 4, gauge 1, gauge 2}) = 4.5942 \text{ bits}$$

Assume that gauge 3 is selected in this step. Then,

$$C(\text{gauge 5, gauge 4, gauge 1, gauge 3}) = 4.6193 \text{ bits}$$

Now compute the final score for each gauge in F.

$$\begin{aligned}\text{Gauge 2} &= H(\text{gauge 5, gauge 4, gauge 1, gauge 2}) \\ &\quad + T(\text{gauge 5} + \text{gauge 4} + \text{gauge 1} + \text{gauge 2, gauge 3}) \\ &\quad - C(\text{gauge 5, gauge 4, gauge 1, gauge 2}) \\ &= 4.8200 + 2.6579 - 4.5942 \\ &= 2.8837 \text{ bits}\end{aligned}$$

$$\begin{aligned}\text{Gauge 3} &= H(\text{gauge 5, gauge 4, gauge 1, gauge 3}) \\ &\quad + T(\text{gauge 5} + \text{gauge 4} + \text{gauge 1} + \text{gauge 3, gauge 2}) \\ &\quad - C(\text{gauge 5, gauge 4, gauge 1, gauge 3}) \\ &= 4.4294 + 2.6329 - 4.6193 \\ &= 2.4443 \text{ bits}\end{aligned}$$

Gauge 2 has a larger final score. Therefore, gauge 2 is selected in this step since there are only five gauges, among which four gauges have been ranked. The final ranking for these five gauges is

{gauge 5, gauge 4, gauge 1, gauge 2, gauge 3}

The results are different from those obtained in Example 14.12, where the top three monitoring gauges are {gauge 5, gauge 2, gauge 4}.

14.4 Informational Correlation Coefficient

A measure of information is cross-correlation among records from nearby sites. Cross-correlation helps with the space–time trade-off and regional data collection. The correlation coefficient r_{xy} is calculated for each pair of stations as

$$r_{xy} = \frac{\text{Cov}_{xy}}{S_x S_y} \tag{14.27}$$

where Cov_{xy} is the covariance between random variables X and Y; S_x and S_y are the standard deviation of variables X and Y, respectively. Cov_{xy} can be obtained as

$$\text{Cov}_{xy} = \frac{\sum_{i=1}^{n}(x_i - \bar{x})(y_i - \bar{y})}{n-1} \tag{14.28}$$

where $\bar{x}$ and $\bar{y}$ are the means of variable X and Y, respectively.

Example 14.14 Compute correlation coefficients between the water-level monitoring stations shown in Fig. 14-2. Determine the amount of explained variance between them. You may want to prepare a matrix of correlation coefficients.

Solution The water-level values are first normalized so that the variance becomes unity. The correlation coefficient between gauge 1 and gauge 2 is computed as

$$\text{Cov}_{xy} = \frac{\sum_{i=1}^{n}(x_i - \bar{x})(y_i - \bar{y})}{n-1} = \frac{\sum_{i=1}^{n}(x_i - 1.95)(y_i - 1.98)}{400-1} = 0.976$$

Table 14-31 *Values of the coefficients of correlation.*

	Gauge 1	Gauge 2	Gauge 3	Gauge 4	Gauge 5
Gauge 1	1.000	0.976	1.000	0.124	0.911
Gauge 2	0.976	1.000	0.976	0.059	0.902
Gauge 3	1.000	0.976	1.000	0.124	0.911
Gauge 4	0.124	0.059	0.124	1.000	0.124
Gauge 5	0.911	0.902	0.911	0.124	1.000

Similarly, coefficients of correlation between different pairs of stations are evaluated and the correlation matrix is then prepared, as shown in Table 14-31.

Transferability of information between hydrologic variables depends on the degree and the structure of dependence or interdependence of variables. The most likely measure of association between variables is the correlation coefficient. Its use is valid under the assumption of normality of variables and linearity of relationship between them. If variables are nonlinearly related, then either the variables have to be transformed to linearize the regression function or nonlinear regression has to be developed. For both linear and nonlinear types of interdependence, the correlation coefficient measures the amount of information that is actually transferred by the assumed regression relationship. If the correlation coefficient is zero, it does not necessarily mean the absence of association between variables, but it may also be caused by the inappropriate choice of the regression relation. The informational correlation coefficient and transinformation represent the extent of transferable information without assuming any particular type of interdependence. They also provide a means of judging the amount of information actually transferred by regression. The informational correlation coefficient R_0 can be expressed as

$$R_0 = \sqrt{1 - \exp(-2T_0)} \tag{14.29a}$$

When the marginal and joint probability distributions of stations X and Y are approximated by their relative frequency distributions or when no particular probability distribution is assumed for the stations, then T_0 represents the upper limit of transferable information between stations. The informational correlation coefficient R_0 (Linfoot 1957) is a dimensionless measure of stochastic interdependence that varies between 0 and 1 and is a function of mutual information T_0 between stations. It does not assume normality or any type of functional relationship between stations and, therefore, has advantages over ordinary correlation coefficients. It reduces to the classical correlation coefficient when the normality and linearity assumptions are satisfied. Although R_0 and T_0 do not provide any functional relationship between stations to transfer information, they serve as criteria for checking the validity of assumed types of dependence and probability distributions of the stations. Because T_0 represents the upper limit of transferable

information, it can be used as a criterion for defining the amount of actually transferred information under the assumptions made. If T_1 represents the transinformation for any assumed type of relation between stations, then the ratio

$$t_1 = \frac{T_0 - T_1}{T_0} = 1 - \frac{T_1}{T_0} \tag{14.29b}$$

measures the amount of nontransferred information, and $1 - t_1$ measures the amount of transferred information. Likewise, R_0, and t_1 can be used as criteria to judge the validity of assumptions made about the dependence between stations. Entropy or transinformation does not provide any means of transferring information but rather provides a means for measuring transferable information. Thus, it can help improve the transfer of information by regression analysis.

If the actual amount of information transferred by regression analysis is far below the transferable information defined by entropy measures, then one can attempt to improve the regression analysis. This step can be accomplished by (1) selecting marginal and joint distributions that better fit the data, (2) searching for better relationships between stations, (3) analyzing the effect of autocorrelation of each station upon interdependence and regression, and (4) analyzing the effect of lag cross-correlation upon interdependence and information transfer.

The coefficient of nontransferred information, defined by equation (14.29b) as a measure of the nontransferred information as a percentage of the total transferable information (Harmancioglu and Yevjevich 1985, 1987), is used. Here T_0 is the total transferable information (not necessarily achieved by the hydrometric network), and T_1 is the measured transinformation between X_1 and X_2. To illustrate, assume that X_1 is associated with the water-level record of the gauge that has the highest marginal entropy or information in the region, and $X_2 = X_i$ (i = 2, …, n) associated with water-level records of any other gauge. Then,

$$T_1 = T(X_1, X_i) = H(X_1) - H(X_1 \mid X_i), \quad i = 2, 3, \ldots, n \tag{14.30}$$

The value of T_0 can be expressed as

$$T_0 = H(X_1) \tag{14.31}$$

Thus, the coefficient of nontransferred information is

$$t_1 = \frac{H\left(X_1 | X_i\right)}{H(X_1)}, \quad 0 \le t_1 \le 1 \tag{14.32}$$

Similarly, $1 - t_1$ defines the coefficient of transferred information, or transferred information as the fraction of the total transferable information:

$$1 - t_1 = \frac{T_1}{T_0} \tag{14.33}$$

By computing the coefficient of transferred information for all gauges, the isoinformation contours can be constructed. These contours are the lines of equal

transfer of information in the region (Singh and Krstanovic 1986). The isoinformation contour of the bivariate water-level record is the line of equal common information between any gauge in the watershed and the other existing gauges located in the watershed. In the selection process, the first chosen gauge has the highest information content, and this gauge can be designated as the central gauge. Thus, it is convenient to choose that gauge as the reference point in the construction of all isoinformation contours when choosing gauges in order of descending importance. It is true that an isoinformation contour can be constructed between any two gauges, but it does not benefit the gauge selection process.

Example 14.15 Compute informational correlation coefficients between water-level monitoring stations shown in Fig. 14-2. Determine the amount of explained variance between them. Prepare a matrix of correlation coefficients.

Solution From computations in Example 14.3 and Example 14.5 for gauges 1 and 2, $T_0 = H(X_2) = 3.0235$ bits, $T_1 = T(X_1, X_2) = 1.9208$ bits. The transferable information between gauge 1 and gauge 2 is

$$1 - t_1 = \frac{T_1}{T_0} = 1 - \frac{1.9208}{3.0235} = 0.3647$$

Likewise, the transferable information between other pairs of gauges can be computed in the same way. Then the matrix of transferable information can be constructed as shown in Table 14-32.

Table 14-32 *Transferable information.*

	Gauge 1	Gauge 2	Gauge 3	Gauge 4	Gauge 5
Gauge 1	0.0000	0.3647	0.0000	0.8613	0.4846
Gauge 2	0.2773	0.0000	0.2773	0.8008	0.3976
Gauge 3	0.0000	0.3647	0.0000	0.8613	0.4846
Gauge 4	0.9912	0.9889	0.9912	0.0000	0.9786
Gauge 5	0.3088	0.2899	0.3088	0.5471	0.0000

Questions

Q14.1 Obtain continuous observations from a streamflow gauging station for a river. First discretize the continuous streamflow time series and then compute its marginal entropy.

Q14.2 For the same streamflow data as in Q14.1, select a suitable value for parameter *a*, discretize the streamflow time series, and then compute

its marginal entropy. Compare this value of marginal entropy with that obtained in Q14.1.

Q14.3 Select two water monitors from Fig. 14-6. Using the observations from these monitors given in Table 14-1, compute their marginal entropies and joint entropy and verify that joint entropy is symmetric and that the inequality holds.

Q14.4 Using the same data set as in Q14.3, denoting, respectively, the water levels in gauges 1 and 2 by X_1 and X_2, compute the conditional entropy $H(X_2 \mid X_1)$ and $H(X_1 \mid X_2)$. Discuss the results.

Q14.5 For the same water-level monitoring network as in Q14.3, choose five monitoring gauges and compute the transinformation between different gauges.

Q14.6 Choose monthly streamflow observations from two nearby streamflow gauging stations. Then create a merged series such that the entropy of the merged series is equal to the joint entropy of the original two series.

Q14.7 Consider merging two categorical variables: $X_1 = [1, 3, 1, 3, 1, 4, 4]^T$ and $X_2 = [1, 3, 3, 2, 1, 4, 3]^T$. Then obtain a new variable X by pairwise welding the corresponding digits together. Verify that the information amount keeps invariant before and after merging, i.e., that the information content of X_1 and X_2 together is the same as that of X.

Q14.8 Select five streamflow gauging stations in a river basin and obtain their streamflow records. Then, compute the total correlation of these gauging stations.

Q14.9 For the five gauging stations considered in Q14.8, compute the joint entropy.

Q14.10 For the five gauging stations considered in Q14.8, compute the interaction of the first three gauges.

Q14.11 Compute DIT using data of the five gauging stations considered in Q14.8.

Q14.12 Take water-level data for several monitoring stations in a canal network. Compute marginal entropy of water level at each monitoring station and plot it as a function of distance between monitoring stations. What do you conclude from this plot? Discuss it.

Q14.13 For the water-level data in Q14.12, compute transinformation of water levels. Are all monitoring stations needed? What is the redundant information? What can be said about increasing or decreasing the number of monitoring stations?

Q14.14 Consider a drainage basin that has a number of water-level measuring stations. Obtain daily water-level values for each monitoring station. Using daily water-level values, determine marginal entropy at each

station and also compute transinformation among stations. Comment on the adequacy of the water-level monitoring network.

Q14.15 Consider the same basin and the water-level monitoring network as in Q14.14. Now obtain hourly water-level values and compute marginal entropy, as well as transinformation. Comment on the adequacy of the water-level network. How does the adequacy change with reduced time interval? Which stations are necessary, and which are not?

Q14.16 Can entropy be used for designing a monitoring network? If yes, then how? Can entropy be used for evaluating the adequacy of an existing network? If yes, how?

Appendix 14.1

Table 14-33 *Monthly streamflow (m^3/s) of USGS stations.*

	Station 08082500											
	1	**2**	**3**	**4**	**5**	**6**	**7**	**8**	**9**	**10**	**11**	**12**
1990	2.45	1.19	8.43	37.32	15.53	99.25	4.90	9.21	3.55	1.95	2.51	1.79
1991	3.62	2.20	1.14	0.81	15.83	90.67	2.57	12.63	21.98	7.10	6.35	17.06
1992	12.29	35.28	14.15	10.05	32.33	84.89	11.50	5.53	4.09	0.71	2.99	3.15
1993	2.65	9.08	8.18	2.72	4.40	9.00	0.64	0.45	2.02	0.71	0.48	1.01
1994	0.67	1.20	1.15	0.54	20.61	2.47	0.27	0.70	4.96	2.42	2.75	1.09
1995	1.03	0.60	1.17	0.45	17.53	22.34	2.45	28.83	5.67	2.24	2.84	0.90
1996	1.04	0.57	0.88	0.62	0.10	2.62	0.96	6.59	41.91	2.01	1.90	1.91
1997	0.57	8.24	2.95	14.78	21.05	18.30	9.33	5.22	2.28	0.92	0.56	2.24
1998	1.41	3.48	6.38	1.43	1.57	0.93	1.76	0.07	0.06	0.07	0.24	0.09
1999	1.12	0.93	4.04	1.82	15.87	54.25	6.88	1.76	1.64	0.49	0.08	0.16
2000	0.23	0.12	27.18	4.83	4.97	9.56	4.36	0.01	0.00	6.42	9.70	1.79
2001	1.59	6.59	19.81	4.05	3.99	3.73	0.11	0.71	1.29	0.08	4.17	1.29
2002	0.32	0.32	0.60	8.49	2.36	6.61	17.95	2.69	0.44	3.96	3.92	3.07
2003	1.71	0.97	0.97	0.49	0.42	20.18	2.48	0.02	1.86	0.11	0.20	0.10
2004	0.27	0.68	8.24	6.89	0.98	14.81	41.12	14.61	2.65	12.70	46.41	12.88
2005	7.37	6.95	5.39	2.59	1.85	4.34	2.53	67.64	4.19	3.82	1.50	1.21
2006	1.05	0.97	1.47	2.02	17.56	1.44	0.49	0.10	4.15	38.34	6.37	3.18
2007	3.17	2.40	5.65	7.64	17.09	20.99	7.84	18.81	4.79	1.77	1.15	1.88
2008	1.29	1.29	1.19	3.89	3.69	4.49	1.13	2.04	9.75	10.21	3.73	1.72
2009	1.11	0.86	0.63	0.84	1.37	4.46	4.68	2.53	1.51	0.96	0.56	0.59

Station 08088000												
	1	2	3	4	5	6	7	8	9	10	11	12
1990	3.38	3.87	39.87	153.90	190.88	121.56	7.82	17.73	36.27	8.91	6.06	3.59
1991	11.73	7.12	3.95	2.72	33.33	160.27	13.98	29.17	35.00	33.02	17.33	170.58
1992	47.35	254.48	117.32	32.90	44.83	225.83	42.98	18.78	11.73	2.97	10.28	15.10
1993	10.75	19.97	23.48	11.58	10.91	18.95	1.77	0.53	3.09	12.62	2.43	3.08
1994	2.32	3.37	2.36	1.41	62.41	6.23	3.78	0.49	5.15	23.50	8.06	3.58
1995	2.34	1.93	3.39	2.01	13.76	38.06	5.97	44.85	15.52	4.92	3.81	1.82
1996	2.29	1.61	1.47	2.54	0.57	2.62	1.10	10.72	68.36	6.21	15.14	12.88
1997	2.87	64.31	28.11	25.68	47.03	90.50	18.51	7.17	1.90	1.44	1.04	3.30
1998	3.05	4.69	40.32	3.58	2.53	1.83	1.79	0.00	0.00	0.11	0.33	0.71
1999	0.81	2.46	14.89	6.90	11.01	50.06	6.18	1.23	0.42	0.57	0.21	0.19
2000	0.17	0.09	23.99	9.56	6.78	9.67	7.71	0.02	0.00	2.24	16.55	4.24
2001	3.58	30.47	48.65	7.00	8.20	3.71	4.16	0.99	9.47	4.74	4.71	1.77
2002	0.49	0.73	1.52	21.63	13.97	15.93	29.17	7.46	1.83	4.89	8.48	4.76
2003	2.52	1.73	1.48	0.67	0.77	37.49	7.56	0.07	2.94	0.13	0.14	0.04
2004	0.14	1.43	9.17	10.78	3.50	23.50	51.59	62.27	11.00	19.40	115.02	23.40
2005	14.36	11.71	10.45	5.86	4.97	10.08	3.42	193.91	19.55	8.00	3.84	2.99
2006	2.41	1.88	3.11	4.20	32.88	2.72	0.47	0.03	6.18	35.96	10.34	3.53
2007	3.08	2.43	7.66	9.28	71.47	146.62	72.97	84.98	16.93	4.90	2.79	4.07
2008	3.13	2.82	13.47	13.73	12.03	13.46	1.18	2.29	16.21	11.07	4.83	2.36
2009	1.74	1.42	1.17	0.86	4.13	10.66	7.74	5.24	3.13	2.25	0.71	0.68

Continued

Table 14-33 *Monthly streamflow (m^3/s) of USGS stations. (Continued)*

	Station 08088610											
	1	**2**	**3**	**4**	**5**	**6**	**7**	**8**	**9**	**10**	**11**	**12**
1990	3.26	2.98	48.87	225.18	240.78	109.98	7.12	16.47	40.12	14.86	8.56	8.81
1991	11.59	7.93	15.92	9.61	34.60	205.27	19.88	31.88	42.67	51.51	18.58	203.09
1992	62.21	245.20	140.11	34.97	31.26	227.21	34.01	23.70	13.20	4.01	8.51	7.31
1993	6.48	6.76	25.58	16.54	14.52	22.09	15.63	9.56	8.13	5.60	3.09	2.23
1994	2.65	1.66	2.24	3.57	70.65	9.52	11.05	12.03	8.69	5.08	14.66	13.72
1995	7.44	6.64	4.73	11.94	12.63	17.95	14.87	34.77	11.04	6.11	6.22	5.84
1996	6.91	4.16	5.50	2.54	1.78	1.98	1.15	1.50	49.58	13.69	12.38	18.82
1997	6.92	81.61	36.95	27.55	45.87	55.08	20.87	15.78	9.97	7.18	2.42	4.79
1998	3.59	3.26	14.49	9.54	13.04	12.90	8.18	5.57	4.34	1.25	1.87	2.42
1999	1.42	0.79	1.29	2.41	2.01	9.77	14.19	16.14	5.00	2.66	0.95	0.79
2000	0.84	0.87	1.67	2.79	4.94	3.32	3.46	7.66	4.82	1.30	1.27	3.23
2001	1.82	18.29	51.00	7.31	7.76	3.87	5.11	7.03	2.15	1.03	0.77	1.24
2002	3.32	5.24	3.57	4.59	5.07	3.16	15.51	10.28	8.49	6.68	4.50	5.09
2003	3.79	4.86	4.65	4.38	5.14	5.26	9.02	6.18	3.22	3.89	4.40	3.25
2004	2.19	1.62	2.27	5.74	4.98	3.09	9.91	26.65	10.54	6.41	85.60	19.79
2005	14.36	14.06	12.78	10.80	7.64	8.38	5.73	119.70	20.91	9.84	6.33	4.56
2006	2.70	2.19	4.72	6.00	16.15	6.29	9.32	6.53	2.35	1.96	4.26	2.48
2007	2.16	2.12	14.88	19.38	55.02	174.54	109.56	52.36	13.95	1.29	1.46	1.71
2008	1.57	1.76	15.90	14.20	11.76	8.22	6.10	4.28	3.70	7.44	4.22	1.63
2009	1.68	3.49	3.23	3.62	3.43	3.23	4.61	6.73	3.13	2.58	2.96	1.55

Station 08089000												
	1	2	3	4	5	6	7	8	9	10	11	12
1990	2.96	4.27	51.88	237.44	239.84	118.79	7.46	16.14	38.74	14.69	9.32	9.14
1991	14.16	10.32	18.07	10.17	34.52	208.38	25.69	31.35	42.90	52.05	19.22	220.87
1992	63.83	256.66	149.51	37.35	36.39	229.71	41.63	21.14	14.13	4.36	8.98	8.02
1993	7.02	10.42	27.11	17.30	14.66	23.31	16.04	8.94	8.66	8.25	4.04	2.80
1994	2.89	2.30	2.73	2.82	53.89	10.41	10.27	10.61	7.85	5.84	20.03	21.38
1995	9.11	9.17	5.57	19.64	19.35	24.55	18.63	45.96	15.00	6.73	7.18	7.05
1996	8.38	5.43	8.51	3.80	2.52	2.98	1.41	7.00	81.30	26.68	22.01	28.40
1997	8.90	106.13	39.13	37.97	58.84	86.22	26.68	19.80	14.89	8.38	3.10	4.33
1998	5.34	4.97	29.59	12.95	17.39	15.16	10.84	7.01	5.01	1.45	2.41	2.79
1999	1.11	1.15	4.79	2.18	2.28	11.85	15.40	18.40	4.10	3.10	1.15	1.13
2000	1.43	1.40	2.13	3.02	4.72	4.06	4.42	6.90	5.07	1.48	2.02	3.92
2001	2.83	39.90	86.14	13.60	10.59	3.68	6.50	9.92	2.39	1.18	0.96	1.20
2002	4.24	6.98	10.19	6.84	6.69	2.90	19.67	10.69	9.74	8.04	5.20	6.48
2003	4.50	5.94	6.22	5.35	6.50	7.90	9.37	6.24	3.56	3.24	5.10	3.33
2004	2.28	3.75	3.83	6.86	5.73	5.09	12.50	32.99	10.36	6.57	109.33	22.02
2005	17.13	19.13	18.86	14.26	8.21	7.91	4.87	129.80	28.19	11.77	5.75	4.72
2006	3.60	4.34	5.51	7.39	19.26	5.78	9.76	7.71	2.78	1.91	5.25	2.62
2007	2.33	2.61	26.86	28.10	67.93	222.85	145.77	64.05	17.84	1.88	1.78	1.63
2008	1.54	1.55	29.28	22.40	15.43	8.98	6.52	4.78	3.51	8.64	4.88	1.52
2009	1.61	3.98	2.80	3.22	3.17	3.22	4.59	6.86	3.47	4.17	3.57	1.81

Continued

Table 14-33 *Monthly streamflow (m^3/s) of USGS stations. (Continued)*

	Station 08090800											
	1	**2**	**3**	**4**	**5**	**6**	**7**	**8**	**9**	**10**	**11**	**12**
1990	6.72	5.45	56.89	377.18	342.35	127.11	8.21	16.51	36.13	17.02	9.87	7.98
1991	12.65	10.09	12.15	6.43	29.87	186.07	30.38	33.84	33.33	85.86	34.89	346.60
1992	80.28	269.86	169.05	32.99	41.23	241.17	40.61	22.54	18.32	6.56	9.76	11.66
1993	9.25	20.41	30.95	17.81	16.25	22.38	16.26	9.51	9.54	43.55	4.30	5.11
1994	3.86	3.57	3.19	2.74	84.27	13.45	11.30	7.83	10.59	14.87	34.46	16.96
1995	9.23	7.05	8.33	19.05	40.07	26.32	17.53	83.19	27.02	7.36	7.71	6.88
1996	7.55	4.99	5.67	3.58	1.71	5.59	1.71	18.66	104.21	29.87	50.74	42.33
1997	9.55	229.22	90.02	73.43	88.29	90.64	37.66	19.80	12.00	8.33	3.48	4.97
1998	6.34	7.16	63.12	10.32	14.77	9.65	7.70	5.75	4.13	2.55	3.39	2.83
1999	1.40	0.82	14.31	5.07	5.67	14.76	11.90	16.08	4.39	2.44	1.02	1.01
2000	0.93	0.75	1.86	2.66	5.30	17.30	3.47	4.58	4.52	1.56	4.78	3.86
2001	7.91	82.85	117.60	22.83	12.73	3.83	4.46	7.92	2.98	0.78	1.18	1.61
2002	4.23	6.12	22.31	10.87	9.85	3.23	17.86	10.17	9.34	13.31	5.36	7.99
2003	4.54	5.67	5.98	4.77	4.29	7.16	8.23	6.14	5.11	3.35	5.77	3.92
2004	2.95	6.94	6.65	6.28	7.22	19.16	21.84	26.91	9.36	5.62	95.14	23.78
2005	16.68	15.39	18.24	12.03	8.13	5.66	3.40	113.10	24.24	9.12	5.13	5.32
2006	2.64	3.05	6.83	7.38	21.91	7.25	7.74	5.62	2.53	1.52	4.67	3.21
2007	3.04	2.16	37.52	71.87	95.54	309.79	224.13	70.14	22.56	2.46	2.21	2.25
2008	2.02	2.00	49.70	45.84	17.11	9.21	6.19	7.64	4.13	8.08	5.99	1.77
2009	1.61	3.72	3.78	3.72	4.30	3.44	5.82	9.28	8.81	28.19	7.13	2.65

Station 08091000												
	1	2	3	4	5	6	7	8	9	10	11	12
1990	4.83	9.87	72.32	406.63	394.17	136.29	6.50	19.54	34.07	15.12	10.21	8.02
1991	18.32	12.12	10.99	13.64	35.14	222.03	19.22	33.58	37.86	129.24	52.92	423.62
1992	87.75	319.70	189.27	27.10	33.98	229.68	35.65	22.17	19.59	2.70	11.23	17.04
1993	11.67	32.22	36.98	21.49	17.26	21.59	7.77	2.76	6.17	50.77	3.65	6.60
1994	5.17	3.38	4.21	3.00	91.92	17.35	10.05	3.56	16.34	21.54	45.39	32.34
1995	15.59	6.34	18.85	24.23	21.14	28.52	9.61	96.39	29.53	5.13	6.73	7.22
1996	9.27	5.97	3.51	3.03	0.44	0.50	0.62	15.81	108.40	31.18	61.16	56.97
1997	14.40	278.21	137.36	115.65	104.97	84.78	43.15	19.98	13.16	8.83	3.03	9.52
1998	16.08	23.29	106.98	14.57	20.55	10.51	6.47	1.51	0.45	0.87	2.53	5.61
1999	1.48	1.21	10.13	3.33	2.20	16.97	6.97	14.29	0.73	0.86	0.61	0.93
2000	0.91	0.82	0.98	0.61	0.52	33.87	1.26	0.35	0.50	1.37	1.83	2.21
2001	11.13	122.78	154.67	47.86	22.74	3.28	1.65	1.21	1.20	0.81	0.36	0.72
2002	0.77	1.56	30.92	27.28	24.57	1.90	14.63	2.48	4.04	10.13	2.45	5.33
2003	2.73	9.17	9.86	3.29	1.77	5.01	2.02	1.66	4.58	4.53	4.46	1.80
2004	0.93	10.00	10.00	7.63	10.95	54.48	26.04	23.27	7.19	4.32	94.21	29.79
2005	21.99	20.91	28.68	13.56	4.43	2.64	1.82	89.17	22.66	5.56	3.65	2.89
2006	2.19	2.44	17.03	5.08	24.77	2.59	3.65	1.95	1.68	0.66	1.80	0.71
2007	1.35	1.12	32.37	100.16	112.87	363.59	279.83	68.75	22.91	1.48	1.45	2.04
2008	1.55	1.48	45.82	51.48	17.83	7.03	2.67	2.85	2.30	2.29	1.98	0.81
2009	0.73	0.66	1.09	2.45	3.58	2.64	1.66	4.99	2.07	28.37	10.37	3.04

Continued

Table 14-33 *Monthly streamflow (m^3/s) of USGS stations. (Continued)*

	Station 08093100											
	1	**2**	**3**	**4**	**5**	**6**	**7**	**8**	**9**	**10**	**11**	**12**
1990	10.55	10.76	75.86	206.29	652.14	298.46	16.59	19.09	11.64	24.62	11.60	10.88
1991	15.87	17.11	10.09	43.49	49.02	204.31	18.10	39.64	26.23	63.63	188.84	202.41
1992	509.99	316.86	387.94	83.17	68.50	289.68	73.06	22.56	28.32	11.86	15.81	11.78
1993	14.28	28.12	85.63	33.36	32.25	21.82	25.17	22.71	25.36	17.98	16.00	34.52
1994	25.84	10.73	14.05	11.73	47.09	34.09	25.36	20.09	18.19	12.79	41.00	44.83
1995	36.78	15.11	54.82	66.37	127.91	92.94	29.25	148.72	26.83	16.31	18.35	13.86
1996	19.31	11.80	11.20	4.34	3.01	7.48	20.98	8.43	32.31	24.30	52.73	68.19
1997	26.32	198.47	268.19	129.29	144.67	91.75	56.92	23.75	24.78	14.21	12.65	19.77
1998	16.69	18.25	181.43	24.88	18.80	26.66	26.91	22.72	19.53	6.48	6.19	10.74
1999	12.28	9.88	7.40	4.22	1.23	2.70	9.72	14.35	0.81	0.74	0.76	0.83
2000	0.75	0.65	1.11	0.73	6.82	5.29	12.01	21.79	15.53	2.41	9.32	11.47
2001	4.14	65.02	249.44	39.22	28.63	9.87	28.32	25.06	6.73	8.67	11.26	8.57
2002	8.80	12.31	5.58	39.45	26.84	10.62	26.88	34.40	16.79	22.09	25.24	17.81
2003	5.85	11.86	5.84	8.94	11.69	11.91	13.56	8.48	5.08	4.08	10.33	5.34
2004	3.53	4.26	6.82	15.63	19.84	78.78	51.11	38.06	64.42	11.73	76.17	122.05
2005	29.79	63.43	56.35	15.87	3.72	16.33	6.23	59.13	31.71	17.28	12.33	16.69
2006	7.75	8.49	3.90	7.19	6.47	10.72	17.15	13.90	8.44	6.44	5.46	3.77
2007	2.20	2.85	13.26	107.72	133.20	346.88	550.48	94.52	97.89	24.55	11.38	8.70
2008	9.57	9.36	12.38	55.36	56.80	28.43	8.47	16.80	8.62	9.27	7.27	8.10
2009	4.97	1.52	6.32	3.98	2.60	4.33	23.55	12.80	9.43	14.24	27.35	42.42

Station 08096500												
	1	2	3	4	5	6	7	8	9	10	11	12
1990	10.29	27.08	120.94	236.62	807.03	331.87	20.30	16.97	14.60	26.83	11.63	10.86
1991	28.11	30.92	19.05	66.01	85.77	216.62	26.65	63.34	37.55	61.62	243.04	426.73
1992	796.83	477.42	573.70	132.72	114.09	321.11	68.36	23.18	28.43	11.99	22.29	34.32
1993	25.96	94.89	145.21	60.97	46.58	31.32	29.00	16.81	18.67	26.75	19.44	33.16
1994	31.26	35.42	37.49	29.22	137.73	56.32	23.15	12.41	21.86	22.02	69.09	112.98
1995	94.55	39.70	134.87	209.94	282.04	158.21	42.02	206.71	42.93	23.93	21.65	12.97
1996	14.72	8.89	10.64	6.92	3.28	7.46	20.03	10.02	66.01	29.73	62.58	124.20
1997	69.43	393.60	482.24	229.34	212.35	161.83	69.09	24.42	22.02	18.00	17.55	91.49
1998	110.38	52.44	309.50	52.90	28.57	26.48	25.99	19.30	18.71	19.19	32.90	73.74
1999	40.63	25.41	13.92	15.52	4.93	4.01	12.05	20.59	0.94	1.09	1.22	2.25
2000	5.55	1.03	2.02	4.66	11.76	45.96	12.08	20.29	14.94	3.34	33.16	31.77
2001	51.62	141.10	417.67	82.09	62.18	12.97	33.84	33.13	11.12	12.45	32.31	81.44
2002	27.43	50.69	27.84	67.88	28.60	14.94	24.52	30.64	16.32	23.56	33.53	63.09
2003	37.92	32.03	44.57	12.95	16.33	19.14	12.56	8.23	7.08	8.12	18.66	6.31
2004	17.08	39.73	54.85	56.46	87.53	136.32	56.18	45.11	49.84	29.90	208.10	204.14
2005	72.77	113.27	121.05	34.35	10.35	20.91	9.02	58.79	33.22	19.07	13.83	15.66
2006	10.97	9.57	7.29	6.17	8.12	9.96	16.57	12.92	6.76	7.06	4.94	4.94
2007	5.44	3.86	65.98	188.62	243.64	548.21	750.40	118.65	138.36	32.48	11.71	11.90
2008	11.12	10.96	30.38	80.36	91.27	27.81	7.68	17.80	8.57	9.87	7.19	8.27
2009	3.95	1.96	15.34	15.56	11.84	4.45	17.88	6.42	14.49	157.84	71.30	52.95

Continued

Table 14-33 *Monthly streamflow (m^3/s) of USGS stations. (Continued)*

	Station 08098290											
	1	**2**	**3**	**4**	**5**	**6**	**7**	**8**	**9**	**10**	**11**	**12**
1990	12.26	35.31	183.29	226.56	853.47	343.20	30.53	21.96	19.50	39.90	23.77	14.17
1991	94.32	68.92	23.59	89.62	128.70	221.18	25.78	72.07	51.68	64.73	286.57	476.57
1992	904.16	617.87	643.64	168.15	157.55	377.75	87.95	30.58	36.22	16.66	31.94	57.74
1993	40.52	128.28	214.64	104.12	77.73	40.18	30.33	22.14	27.84	36.59	29.05	38.77
1994	31.01	58.13	37.43	18.82	185.33	57.99	22.83	19.69	22.98	17.72	61.96	124.31
1995	97.04	37.66	151.30	216.00	311.20	170.61	36.78	243.52	43.13	24.08	22.95	16.89
1996	21.31	16.18	17.60	13.39	6.40	10.79	19.61	14.88	79.94	35.20	70.45	147.33
1997	82.49	439.19	537.17	316.86	261.08	200.85	85.21	27.28	25.32	21.79	21.76	138.10
1998	205.50	72.58	320.83	59.32	31.35	33.05	27.62	22.09	21.61	60.97	60.60	108.45
1999	58.64	43.58	21.13	26.74	8.61	6.13	12.50	21.17	3.28	3.68	3.04	5.43
2000	8.73	3.15	5.79	10.90	17.12	70.40	12.10	17.07	15.16	4.89	58.33	63.57
2001	87.36	145.94	476.85	85.29	67.65	16.52	29.22	46.47	22.53	24.63	58.64	168.85
2002	39.64	71.64	38.60	86.28	32.73	23.47	29.39	34.97	20.46	30.70	37.10	93.11
2003	53.60	90.33	63.54	16.29	16.94	24.50	12.53	8.91	9.47	30.89	21.31	8.36
2004	21.23	60.71	73.51	78.21	126.66	243.50	102.48	58.96	61.90	49.04	321.96	245.59
2005	86.73	156.08	160.33	47.09	15.68	27.51	11.22	109.25	38.88	20.62	16.92	21.05
2006	16.71	14.38	18.08	13.00	27.67	11.03	18.13	14.23	8.79	9.27	5.78	7.43
2007	56.44	5.57	96.36	237.63	402.66	625.23	837.61	140.31	150.53	40.89	15.11	17.67
2008	14.19	15.24	50.15	91.69	123.15	29.53	9.33	26.97	10.81	10.91	8.83	9.51
2009	5.42	4.03	21.50	28.23	23.82	3.42	16.21	6.69	25.25	270.06	106.58	74.84

Station 08111500												
	1	2	3	4	5	6	7	8	9	10	11	12
1990	30.98	64.87	264.68	307.24	1169.48	576.53	97.32	48.14	44.68	47.35	53.18	31.38
1991	605.70	306.67	129.69	338.67	353.96	318.28	58.93	81.61	93.16	57.43	321.96	984.86
1992	1585.46	1550.34	1428.58	647.61	655.82	909.82	442.03	233.61	94.97	47.60	69.04	185.53
1993	239.76	270.14	575.68	432.11	483.08	394.45	176.24	52.02	41.51	62.78	54.09	58.33
1994	62.67	126.55	133.03	54.31	286.85	187.03	50.94	37.41	42.33	496.39	135.50	398.70
1995	385.39	132.55	355.09	411.73	415.12	331.59	84.89	325.93	74.56	46.69	42.50	70.68
1996	35.06	24.00	22.72	26.67	27.00	54.34	30.75	21.87	155.83	63.06	82.43	237.32
1997	185.59	690.08	1062.73	764.27	593.24	499.79	283.17	82.26	47.63	53.60	58.47	257.80
1998	616.46	357.36	572.57	250.24	65.95	47.40	35.25	29.19	108.37	518.20	610.23	440.61
1999	192.33	284.02	109.84	101.23	92.91	55.19	46.58	32.54	14.63	10.07	10.69	12.12
2000	21.74	13.70	42.42	41.34	84.44	97.18	23.13	20.23	22.30	23.12	331.31	202.38
2001	404.08	307.80	888.58	291.38	219.71	159.57	72.12	46.41	247.46	89.03	167.04	502.06
2002	147.28	178.96	88.35	186.86	48.25	51.42	178.54	101.29	42.67	147.11	442.59	495.54
2003	267.08	518.20	423.05	121.17	53.80	81.41	36.98	19.19	52.90	188.53	78.35	35.79
2004	104.12	311.20	214.13	183.35	623.25	797.40	535.47	140.14	124.99	111.71	743.60	760.02
2005	346.03	532.36	605.98	157.41	65.02	64.17	32.62	219.57	72.80	38.74	32.56	34.69
2006	31.49	42.70	34.49	59.38	98.54	30.47	29.85	17.47	17.55	141.64	26.60	37.41
2007	530.94	64.53	441.46	549.35	809.58	1105.20	1646.06	592.39	455.05	229.31	58.47	65.86
2008	38.34	93.33	138.33	104.49	272.41	53.94	25.40	58.98	33.16	22.84	27.93	19.76
2009	14.97	13.97	31.63	109.47	168.77	18.26	33.90	24.33	82.66	476.57	410.59	229.85

Continued

Table 14-33 *Monthly streamflow (m^3/s) of USGS stations. (Continued)*

	Station 08114000											
	1	**2**	**3**	**4**	**5**	**6**	**7**	**8**	**9**	**10**	**11**	**12**
1990	38.60	78.52	263.06	294.21	1117.66	558.69	94.55	43.58	43.49	44.17	55.36	32.99
1991	643.92	355.94	146.68	428.43	394.74	349.15	70.68	80.84	99.87	56.63	316.02	788.06
1992	1713.17	1540.72	1530.52	736.24	652.99	927.66	447.12	255.22	102.31	42.96	76.09	209.94
1993	276.80	298.74	574.26	473.74	560.11	507.44	207.99	45.22	36.16	67.93	64.85	64.99
1994	69.60	144.87	150.62	53.69	312.90	207.68	47.01	33.24	48.11	584.74	163.93	416.26
1995	461.56	162.99	401.82	442.31	434.38	372.08	90.95	334.14	77.62	53.77	49.44	84.47
1996	51.59	34.60	25.67	22.64	23.18	52.27	35.34	24.03	185.50	84.44	88.80	231.15
1997	196.66	609.09	1116.81	777.58	595.50	504.61	302.14	91.38	60.23	89.20	65.89	289.68
1998	624.95	379.45	593.24	271.02	78.47	46.13	32.22	27.07	134.82	618.44	723.78	449.67
1999	195.27	287.13	122.10	114.06	106.24	77.96	58.33	37.52	18.54	11.88	14.12	14.72
2000	21.95	14.94	41.20	43.55	90.95	91.60	23.34	22.74	16.92	21.14	345.75	188.70
2001	415.12	300.72	895.94	341.78	225.63	175.73	66.15	36.42	274.47	119.58	155.60	501.77
2002	168.34	176.47	81.55	211.16	41.40	45.34	171.57	116.16	55.25	203.17	558.69	521.60
2003	305.82	487.90	470.34	129.49	53.32	74.84	34.69	18.22	54.20	176.05	85.09	36.61
2004	105.51	321.40	209.29	165.14	654.40	751.81	622.40	138.81	138.64	100.89	743.60	795.42
2005	339.24	562.09	641.09	182.59	77.84	71.27	39.45	210.14	86.42	41.09	36.19	37.21
2006	31.54	40.46	31.83	61.56	94.35	30.21	32.20	20.01	18.00	153.65	32.93	24.05
2007	583.61	80.65	457.88	609.38	843.84	1218.47	1727.61	662.05	473.17	249.95	112.87	94.75
2008	64.70	123.23	162.76	112.67	276.54	60.91	22.03	55.67	39.22	21.10	36.25	19.26
2009	13.64	13.03	28.28	141.30	178.99	12.98	31.12	24.54	83.22	408.33	469.49	264.42

Station 08116650												
	1	2	3	4	5	6	7	8	9	10	11	12
1990	36.16	80.45	245.14	274.93	1114.83	596.07	94.24	30.58	37.32	42.11	50.04	29.68
1991	684.98	368.40	144.76	479.69	369.25	349.15	69.26	62.16	84.84	53.12	324.23	661.48
1992	1998.03	1714.02	1703.82	839.03	740.77	1071.51	440.61	245.48	106.73	49.55	88.21	202.80
1993	279.06	284.58	598.33	508.00	585.59	542.55	188.56	37.60	33.98	77.81	104.18	75.10
1994	70.74	147.28	174.29	52.36	342.07	213.68	36.42	31.38	53.92	634.58	184.77	468.93
1995	545.38	197.51	468.93	521.03	473.17	379.73	97.24	321.96	75.78	60.00	56.35	118.17
1996	48.68	31.94	22.00	14.46	11.63	35.31	22.54	22.45	190.69	89.85	86.39	226.62
1997	219.77	638.54	1226.68	863.66	633.73	499.51	286.57	85.83	90.78	113.69	59.58	292.80
1998	685.55	406.35	667.71	265.81	77.81	41.54	23.79	23.78	207.05	643.64	803.91	470.91
1999	201.67	289.96	127.48	103.33	91.72	70.42	47.77	28.88	12.71	9.70	12.07	14.28
2000	18.82	12.34	30.58	40.61	79.85	84.27	12.74	11.34	9.81	16.53	357.36	170.84
2001	416.54	273.40	878.67	328.76	198.98	179.02	56.49	39.33	317.71	137.96	150.96	506.30
2002	177.18	170.69	86.82	210.48	47.94	43.15	160.73	140.14	63.29	222.91	552.46	496.39
2003	306.67	439.48	477.14	136.01	59.35	73.03	43.95	17.84	79.34	185.05	122.61	52.61
2004	130.91	362.17	226.22	174.01	690.93	765.12	674.51	165.68	170.47	132.13	720.10	816.09
2005	330.46	555.01	635.15	175.22	81.55	57.45	31.01	173.70	85.23	41.34	34.21	38.99
2006	33.22	40.75	33.30	69.74	104.32	41.20	58.59	23.21	20.51	219.77	51.42	26.58
2007	587.86	98.63	430.98	613.34	759.74	1191.85	1697.03	686.68	451.09	265.05	135.41	103.19
2008	97.98	139.69	174.06	117.94	288.83	65.50	19.26	53.43	47.54	18.69	40.75	22.75
2009	15.36	14.47	31.12	175.37	204.11	6.58	15.16	11.98	73.43	379.45	481.10	283.45

Table 14-34 *Water level data at 17 points in a canal network in The Netherlands.*

Time	Water level (cm) at point																
(min)	1	2	3	4	5	6	7	8	9	10	11	12	13	14	15	16	17
0	75	85	75	165	50	15	50	50	45	40	60	75	40	40	40	350	300
30	80	85	80	165	50	15	50	50	45	40	60	75	45	45	45	355	300
60	80	90	80	165	55	20	55	55	50	45	65	80	50	45	50	355	305
90	85	95	85	165	60	25	60	60	50	50	70	85	55	50	50	360	305
120	85	100	85	165	60	30	60	60	55	55	75	85	60	55	55	360	310
150	90	105	90	170	65	35	65	60	60	55	80	90	65	55	60	360	315
180	90	110	90	170	65	40	65	65	60	60	80	90	65	60	60	365	315
210	95	110	95	170	70	40	70	65	65	65	85	90	70	65	65	365	320
240	95	115	95	170	70	45	70	70	70	65	85	90	70	65	65	365	320
270	100	115	100	170	75	45	75	75	70	70	85	90	75	70	70	365	325
300	100	115	100	170	80	50	80	75	75	75	90	90	75	75	75	365	325
330	100	115	100	170	80	50	80	80	80	75	90	90	80	80	80	365	330
360	100	120	100	170	85	55	85	85	80	80	90	90	80	80	80	365	330
390	105	120	105	170	85	55	85	85	85	85	95	95	85	85	85	365	335
420	105	120	105	170	90	60	90	90	85	85	95	95	85	85	85	365	335
450	105	120	105	170	90	60	90	90	90	90	95	95	90	90	90	365	335
480	105	120	105	170	95	60	95	95	90	90	95	95	90	90	90	365	340
510	105	120	105	170	95	60	95	95	95	90	100	95	90	90	95	365	340
540	105	120	105	170	95	65	95	95	95	95	100	100	95	95	95	365	340
570	105	120	105	170	100	65	100	95	95	95	100	100	95	95	95	365	340
600	105	120	105	170	100	65	100	100	95	95	100	100	95	95	95	365	340
630	105	120	105	170	100	65	100	100	95	95	100	100	95	95	95	365	345
660	105	120	105	170	100	65	100	100	100	95	100	100	95	100	100	360	345
690	105	120	105	170	100	65	100	100	100	95	100	100	95	100	100	360	345
720	105	120	105	170	100	65	100	100	100	100	100	100	95	100	100	360	345
750	105	120	105	170	100	65	100	100	100	100	105	100	100	100	100	360	345
780	105	120	105	170	100	65	100	100	100	100	105	100	100	100	100	360	345
810	105	120	105	170	100	65	100	100	100	100	105	100	100	100	100	360	345
840	105	120	105	170	100	65	100	100	100	100	105	100	100	100	100	360	345
870	105	120	105	170	100	65	100	100	100	100	105	100	100	100	100	355	345
900	105	120	105	170	100	70	100	100	100	100	105	100	100	100	100	355	345
930	105	120	105	170	100	70	100	100	100	100	105	100	100	100	100	355	345
960	105	120	105	170	100	70	100	100	100	100	105	100	100	100	100	355	345

Table 14-34 *Water level data at 17 points in a canal network in The Netherlands. (Continued)*

Time (min)	Water level (cm) at point																
	1	2	3	4	5	6	7	8	9	10	11	12	13	14	15	16	17
990	105	120	105	170	100	70	100	100	100	100	105	100	100	100	100	355	345
1020	105	120	105	170	100	70	100	100	100	100	105	100	100	100	100	355	345
1050	105	120	105	170	100	70	100	100	100	100	105	100	100	100	100	355	345
1080	105	115	105	170	100	70	100	100	100	100	105	100	100	100	100	355	345
1110	105	115	105	170	100	70	100	100	100	100	105	100	100	100	100	355	345
1140	105	115	105	170	100	70	100	100	100	100	105	100	100	100	100	355	345
1170	105	115	105	170	100	65	100	100	100	100	105	100	100	100	100	355	345
1200	105	115	105	170	100	65	100	100	100	100	105	100	100	100	100	355	345
1230	105	115	105	170	100	65	100	100	100	100	105	100	100	100	100	355	340
1260	105	115	105	170	100	65	100	100	100	100	105	100	95	100	100	355	340
1290	105	115	105	170	100	65	100	100	100	95	105	100	95	100	100	355	340
1320	105	115	105	170	100	65	100	100	100	95	100	100	95	100	100	355	340
1350	100	115	100	170	100	65	100	100	100	95	100	100	95	100	100	355	340
1380	100	115	100	170	100	65	100	100	100	95	100	100	95	95	100	350	340
1410	100	115	100	170	100	65	100	100	95	95	100	100	95	95	95	350	340
1440	100	115	100	170	100	65	100	100	95	95	100	100	95	95	95	350	340
1470	100	115	100	170	100	65	100	100	95	95	100	100	95	95	95	350	340
1500	100	110	100	170	100	65	100	100	95	95	100	100	95	95	95	350	340
1530	100	110	100	170	100	65	100	100	95	95	100	100	95	95	95	350	340
1560	100	110	100	170	100	65	100	95	95	95	100	100	95	95	95	350	340
1590	100	110	100	170	95	65	95	95	95	95	100	100	95	95	95	350	340
1620	100	110	100	170	95	65	95	95	95	95	100	100	95	95	95	350	340
1650	100	110	100	170	95	65	95	95	95	95	100	100	95	95	95	350	340
1680	100	110	100	170	95	65	95	95	95	95	100	95	95	95	95	350	335
1710	100	110	100	170	95	65	95	95	95	95	100	95	95	95	95	350	335
1740	100	110	100	170	95	65	95	95	95	95	100	95	95	95	95	350	335
1770	100	110	100	170	95	65	95	95	95	95	100	95	95	95	95	350	335
1800	100	110	100	170	95	65	95	95	95	95	100	95	95	95	95	350	335
1830	100	110	100	170	95	65	95	95	95	95	100	95	95	95	95	350	335
1860	100	110	100	170	95	65	95	95	95	90	100	95	95	95	95	350	335
1890	100	110	100	170	95	65	95	95	95	90	100	95	90	95	95	350	335
1920	95	110	95	170	95	65	95	95	95	90	100	95	90	90	95	350	335
1950	95	105	95	170	95	65	95	95	90	90	100	95	90	90	90	350	335
1980	95	105	95	170	95	65	95	95	90	90	100	95	90	90	90	350	330

Continued

Table 14-34 *Water level data at 17 points in a canal network in The Netherlands. (Continued)*

Time	Water level (cm) at point																
(min)	1	2	3	4	5	6	7	8	9	10	11	12	13	14	15	16	17
2010	95	105	95	170	95	60	95	95	90	90	100	95	90	90	90	350	330
2040	95	105	95	170	95	60	95	90	90	90	100	95	90	90	90	350	330
2070	95	105	95	170	95	60	90	90	90	90	100	95	90	90	90	350	330
2100	95	105	95	170	90	60	90	90	90	90	100	95	90	90	90	350	330
2130	95	105	95	170	90	60	90	90	90	90	95	95	90	90	90	350	330
2160	95	105	95	170	90	60	90	90	90	90	95	95	90	90	90	350	330
2190	95	105	95	170	90	60	90	90	90	90	95	95	90	90	90	350	330
2220	95	105	95	170	90	60	90	90	90	90	95	95	90	90	90	345	325
2250	95	100	95	170	90	60	90	90	90	90	95	95	90	90	90	345	325
2280	95	100	95	170	90	60	90	90	90	90	95	95	90	90	90	345	325
2310	95	100	95	170	90	60	90	90	90	85	95	90	90	90	90	345	325
2340	95	100	95	170	90	60	90	90	90	85	95	90	90	90	90	345	325
2370	90	100	90	170	90	60	90	90	85	85	95	90	85	85	85	345	325
2400	90	100	90	170	90	60	90	90	85	85	95	90	85	85	85	345	325
2430	90	100	90	170	90	60	90	90	85	85	95	90	85	85	85	345	320
2460	90	100	90	170	90	60	90	85	85	85	95	90	85	85	85	345	320
2490	90	100	90	170	85	60	85	85	85	85	95	90	85	85	85	345	320
2520	90	100	90	170	85	60	85	85	85	85	95	90	85	85	85	345	320
2550	90	100	90	170	85	60	85	85	85	85	95	90	85	85	85	345	320
2580	90	100	90	170	85	55	85	85	85	85	95	90	85	85	85	345	320
2610	90	95	90	170	85	55	85	85	85	85	95	90	85	85	85	345	315
2640	90	95	90	170	85	55	85	85	85	85	95	90	85	85	85	345	315
2670	90	95	90	170	85	55	85	85	85	80	95	90	85	85	85	345	315
2700	90	95	90	170	85	55	85	85	85	80	95	90	85	85	85	345	315
2730	90	95	90	170	85	55	85	85	80	80	90	90	85	80	80	345	315
2760	90	95	90	170	85	55	85	85	80	80	90	90	80	80	80	345	310
2790	90	95	90	170	85	55	85	85	80	80	90	90	80	80	80	345	310
2820	90	95	90	170	85	55	85	80	80	80	90	85	80	80	80	345	310
2850	85	95	85	170	80	55	80	80	80	80	90	85	80	80	80	345	310
2880	85	95	85	170	80	55	80	80	80	80	90	85	80	80	80	345	310
2910	85	95	85	170	80	55	80	80	80	80	90	85	80	80	80	345	310
2940	85	95	85	170	80	55	80	80	80	80	90	85	80	80	80	345	305
2970	85	95	85	170	80	55	80	80	80	80	90	85	80	80	80	345	305

Table 14-34 *Water level data at 17 points in a canal network in The Netherlands. (Continued)*

Time (min)	Water level (cm) at point																
	1	2	3	4	5	6	7	8	9	10	11	12	13	14	15	16	17
3000	85	95	85	170	80	55	80	80	80	75	90	85	80	80	80	345	305
3030	85	95	85	170	80	50	80	80	80	75	90	85	80	75	75	345	305
3060	85	90	85	170	80	50	80	80	75	75	90	85	80	75	75	345	305
3090	85	90	85	170	80	50	80	80	75	75	90	85	75	75	75	345	300
3120	85	90	85	170	80	50	80	75	75	75	90	85	75	75	75	345	300
3150	85	90	85	170	75	50	75	75	75	75	90	85	75	75	75	345	300
3180	85	90	85	170	75	50	75	75	75	75	90	85	75	75	75	345	300
3210	85	90	85	170	75	50	75	75	75	75	90	85	75	75	75	345	300
3240	85	90	85	170	75	50	75	75	75	75	85	85	75	75	75	345	295
3270	85	90	85	170	75	50	75	75	75	75	85	85	75	75	75	345	295
3300	85	90	85	170	75	50	75	75	75	70	85	85	75	75	75	345	295
3330	85	90	85	170	75	50	75	75	70	70	85	85	75	70	70	345	295
3360	85	90	85	170	75	50	75	75	70	70	85	80	75	70	70	345	290
3390	85	90	85	170	75	45	75	75	70	70	85	80	70	70	70	345	290
3420	85	90	85	170	75	45	75	70	70	70	85	80	70	70	70	345	290
3450	85	90	85	170	70	45	70	70	70	70	85	80	70	70	70	345	290
3480	85	90	85	170	70	45	70	70	70	70	85	80	70	70	70	345	290
3510	85	90	85	170	70	45	70	70	70	70	85	80	70	70	70	345	290
3540	85	90	85	170	70	45	70	70	70	70	85	80	70	70	70	345	290
3570	85	90	85	170	70	45	70	70	70	65	85	80	70	65	70	345	290
3600	85	90	85	170	70	45	70	70	65	65	85	80	70	65	65	345	290
3630	85	90	85	170	70	45	70	70	65	65	85	80	70	65	65	345	290
3660	85	90	85	170	70	45	70	70	65	65	80	80	70	65	65	345	290
3690	85	90	85	170	70	45	70	65	65	65	80	80	65	65	65	345	290
3720	85	85	85	170	65	40	65	65	65	65	80	80	65	65	65	345	290
3750	85	85	85	170	65	40	65	65	65	65	80	80	65	65	65	345	290
3780	80	85	80	170	65	40	65	65	65	65	80	80	65	65	65	345	290
3810	80	85	80	170	65	40	65	65	65	60	80	80	65	65	65	345	290
3840	80	85	80	170	65	40	65	65	65	60	80	80	65	60	60	345	290
3870	80	85	80	170	65	40	65	65	60	60	80	80	65	60	60	345	290
3900	80	85	80	170	65	40	65	65	60	60	80	80	65	60	60	345	290
3930	80	85	80	170	65	40	65	65	60	60	80	80	60	60	60	345	290
3960	80	85	80	170	65	40	60	60	60	60	80	80	60	60	60	345	290
3990	80	85	80	170	60	35	60	60	60	60	80	80	60	60	60	345	290

Continued

Table 14-34 *Water level data at 17 points in a canal network in The Netherlands. (Continued)*

Time (min)	Water level (cm) at point																
	1	2	3	4	5	6	7	8	9	10	11	12	13	14	15	16	17
4020	80	85	80	170	60	35	60	60	60	55	80	75	60	60	60	345	290
4050	80	85	80	170	60	35	60	60	60	55	75	75	60	55	55	345	290
4080	80	85	80	170	60	35	60	60	55	55	75	75	60	55	55	345	290
4110	80	85	80	170	60	35	60	60	55	55	75	75	60	55	55	345	290
4140	80	85	80	170	60	35	60	60	55	55	75	75	60	55	55	345	290
4170	80	85	80	170	60	35	60	55	55	55	75	75	60	55	55	345	290
4200	80	85	80	170	55	35	55	55	55	55	75	75	55	55	55	345	290
4230	80	85	80	170	55	30	55	55	55	50	75	75	55	50	55	345	290
4260	80	85	80	170	55	30	55	55	55	50	75	75	55	50	50	345	290
4290	80	85	80	170	55	30	55	55	50	50	75	75	55	50	50	345	290
4320	80	85	80	170	55	30	55	55	50	50	75	75	55	50	50	345	290
4350	80	85	80	170	55	30	55	55	50	50	75	75	55	50	50	345	290
4380	80	85	80	170	55	30	55	50	50	50	75	75	55	50	50	345	290
4410	80	85	80	170	50	30	50	50	50	45	70	75	55	45	50	345	290
4440	80	85	80	170	50	30	50	50	50	45	70	75	50	45	45	345	290
4470	80	85	80	170	50	30	50	50	45	45	70	75	50	45	45	345	290
4500	80	85	80	170	50	25	50	50	45	45	70	75	50	45	45	345	290
4530	80	85	80	170	50	25	50	50	45	45	70	75	50	45	45	345	290
4560	80	80	80	170	50	25	50	50	45	45	70	75	50	45	45	345	290
4590	80	80	80	170	50	25	50	50	45	45	70	75	50	40	45	345	290
4620	80	80	80	170	50	25	50	45	45	40	70	75	50	40	40	345	290
4650	80	80	80	170	45	25	45	45	45	40	65	75	50	40	40	345	290
4680	80	80	80	170	45	25	45	45	40	40	65	75	45	40	40	345	290
4710	80	80	80	170	45	25	45	45	40	40	65	75	45	40	40	345	290
4740	80	80	80	170	45	20	45	45	40	40	65	75	45	40	40	345	290
4770	80	80	80	170	45	20	45	45	40	35	65	75	45	35	40	345	290
4800	80	80	80	170	45	20	45	45	40	35	65	75	45	35	35	345	290
4830	80	80	80	170	45	20	45	40	40	35	65	75	45	35	35	345	290
4860	80	80	80	170	45	20	45	40	40	35	65	75	45	35	35	340	290
4890	80	80	80	170	45	20	45	40	40	40	65	75	45	40	40	340	290
4920	80	80	80	170	45	20	45	40	40	35	65	75	45	35	35	340	290
4950	80	80	80	170	40	15	40	40	40	35	65	75	45	35	35	340	290

Table 14-34 *Water level data at 17 points in a canal network in The Netherlands. (Continued)*

Time (min)	Water level (cm) at point																
	1	2	3	4	5	6	7	8	9	10	11	12	13	14	15	16	17
4980	80	80	80	170	40	15	40	40	40	35	65	75	45	35	35	340	290
5010	80	80	80	170	40	15	40	40	40	40	65	75	45	40	40	340	290
5040	80	80	80	170	40	15	40	40	40	35	65	75	45	35	35	340	290
5070	80	80	80	170	40	15	40	40	35	35	65	75	45	35	35	340	290
5100	80	80	80	170	40	15	40	40	40	40	65	75	45	40	40	340	290
5130	80	80	80	170	40	10	40	40	40	35	65	75	45	35	35	340	290
5160	80	80	80	170	40	10	40	40	35	35	65	75	45	35	35	340	290
5190	80	80	80	170	40	10	40	40	35	35	65	75	45	35	35	340	290
5220	80	80	80	170	40	10	40	40	40	40	60	75	45	40	40	340	290
5250	80	80	80	170	40	10	40	40	40	35	60	75	45	35	35	340	290
5280	80	80	80	170	40	5	40	40	35	35	60	75	45	35	35	340	290
5310	80	80	80	170	40	5	40	40	40	35	60	75	45	40	40	340	290
5340	80	80	80	170	40	5	40	40	40	35	60	75	45	35	35	340	290
5370	80	80	80	170	40	5	40	40	35	35	60	75	40	35	35	340	290
5400	80	80	80	170	40	5	40	40	35	35	60	75	45	35	35	340	290
5430	80	80	80	170	40	0	40	40	40	40	60	75	45	40	40	340	290
5460	80	80	80	170	40	0	40	40	35	35	60	75	45	35	35	340	290
5490	75	80	75	170	40	5	40	40	35	35	60	75	45	35	35	340	290
5520	75	80	75	170	40	5	35	35	35	35	60	75	45	35	35	340	290
5550	75	80	75	170	40	5	40	40	40	40	60	75	45	40	40	340	290
5580	75	80	75	170	40	5	40	40	35	35	60	75	45	35	35	340	290
5610	75	80	75	170	40	5	35	35	35	35	60	70	40	35	35	340	290
5640	75	80	75	170	35	5	35	35	35	35	60	70	45	35	35	340	290
5670	75	80	75	170	35	10	35	35	35	35	60	70	45	35	35	340	290
5700	75	80	75	170	40	10	40	40	35	35	60	70	45	35	35	340	290
5730	75	80	75	170	40	10	40	40	40	40	60	70	45	40	40	340	290
5760	75	80	75	170	40	10	40	35	35	35	60	70	40	35	35	340	290
5790	75	80	75	170	40	10	35	35	35	35	60	70	40	35	35	340	290
5820	75	80	75	170	40	5	40	40	35	35	60	70	45	35	35	340	290
5850	75	80	75	170	40	5	40	40	40	40	60	70	45	40	40	340	290
5880	75	80	75	170	40	5	40	40	35	35	60	70	40	35	35	340	290
5910	75	80	75	170	40	0	40	40	35	35	60	70	40	35	35	340	290
5940	75	80	75	170	40	0	40	40	35	35	60	70	40	35	35	340	290
5970	75	80	75	170	40	5	40	35	35	35	60	70	45	35	35	340	290

References

Adamowski, K. (1989). "A Monte Carlo comparison of parametric and nonparametric estimation of flood frequencies." *J. Hydrol.*, 108, 295–309.

Al-Zahrani, M., and Husain, T. (1998). "An algorithm for designing a precipitation network in the south-western region of Saudi Arabia." *J. Hydrol.*, 295(3–4), 205–216.

Alfonso, L. (2010a, 2010b). "*Optimisation of monitoring networks for water distribution systems*." Ph.D. dissertation, Delft University of Technology, Delft, The Netherlands.

Alfonso, L., Lobbrecht, A., and Price, R. (2010a). "Information theory-based approach for location of monitoring water level gauges." *Water Resour. Res.*, 46, W03528, doi:10.1029/2009WR008101.

Alfonso, L., Lobbrecht, A., and Price, R. (2010b). "Optimization of water level monitoring netowrok in polder systems using information theory." *Water Resour. Res.*, 46, W12553, doi:10.1029/2009WR008953.

Alfonso, L., and Price, R. (2010). "Coupling hydrodynamic models and value of information for designing stage monitoring networks." *Water Resour. Res.*, 48, W08530, doi:10.1029/2012WR012040.

Birgé, L., and Rozenholc, Y. (2002). "*How many bins should be put in a regular histogram*." Pre-publication no 721, Laboratoire de Probabilities et Modeles Aleatoires, CNRS-UMR 7599, Universite Paris VI & VII.

Burn, D. H., and Goulter, I. C. (1991). "An approach to the rationalization of streamflow data collection networks." *J. Hydrol.*, 122, 71–91.

Cacoullos, T. (1966). "Estimation of a multivariate density." *Inst. Stat., Math. Ann.*, 18, 179–189.

Caselton, W. F., and Husain, T. (1980). "Hydrologic networks: Information transition." *J. Water Resour. Plann. Manage.*, 106(2), 503–520.

Chapman, T. G. (1986). "Entropy as a measure of hydrologic data uncertainty and model performance." *J. Hydrol.*, 85, 111–126.

Fass, D. M. (2006). "*Human sensitivity to mutual information*." Ph.D. dissertation, Rutgers, New Brunswick, NJ.

Freedman, D., and Diaconis, P. (1981). "On the histogram as a density estimator: L2 theory." *Z. Wahrscheinlichkeitstheor. Verw. Geb.*, 57, 453-476.

Harmancioglu, N. B., and Yevjevich, V. (1985). "Transfer of hydrologic information along rivers fed by karstified limestones." *Proc., Ankara-Antalya Symp. Karst Water Res.*, IAHS Publication 61, 151–131, Oxfordshire, UK.

Harmancioglu, N. B., and Yevjevich, V. (1987). "Transfer of hydrologic information among river points." *J. Hydrol.*, 91, 103–1114.

Husain, T. (1987). "Hydrologic network design formulation." *Can. Water Resour. J.*, 12(1), 44–63.

Jakulin, A., and Bratko, I. (2003). "*Quantifying and visualizing attribute interactions*." ArXiv preprint cs.AI/0308002.

Jakulin, A., and Bratko, I. (2004). "Testing the significance of attribute interactions." *Proc., 21st Int. Conf. Machine Learning, ACM, Banff, Canada*.

Kraskov, A., Stogbauer, H., Andrzejak, R. G., and Grassberger, P. (2003). "*Hierarchical clustering based on mutual information*." ArXiv preprint q-bio. QM/0311039.

Krstanovic, P. F., and Singh, V. P. (1992a). "Evaluation of rainfall networks using entropy: 1. Theoretical development." *Water Resour. Manag.*, 6, 279–293.

Krstanovic, P. F., and Singh, V. P. (1992b). "Evaluation of rainfall networks using entropy: 1. Application." *Water Resour. Manag.*, 6, 295–314.

Lathi, B. P. (1969). *An introduction to random signals and communication theory*, International Textbook, Scranton, PA.

Li, C., Singh, V. P. and Mishra, A. K. (2012). Entropy theory-based criterion for hydrometric network evaluation and design: maximum information minimum redundancy." *Water Resour. Res.*, 48, W05521, doi: 10.1029/2011WR011251.

Linfoot, E. H. (1957). "An informational measure of correlation." *Inform. Control*, 1, 85–89.

Markus, M., Knapp, H. V., and Tasker, G. D. (2003). "Entropy and generalized least square methods in assessment of the regional value of streamflow gages." *J. Hydrol.*, 283, 107–121.

McGill, W. J. (1954). "Multivariate information transmission." *Psychometrika*, 19, 97–116.

Mishra, A. K., and P. Coulibaly (2010). "Hydrometric network evaluation for Canadian watersheds." *J. Hydrol.*, 380, 420–437.

Mogheir, Y., and Singh, V. P. (2002). "Application of information theory to groundwater quality monitoring networks." *Water Resour. Manag.*, 16(1), 37–49.

Paninski, L. (2003). "Estimation of entropy and mutual information." *Neural Comput.*, 15, 1191–1253.

Papoulis, A., and Pillai, S. U. (2001), *Probability, Random Variables and Stochastic processes*, McGraw-Hill, New York.

Parzen, E. (1962). "On estimation of a probability density function and mode." *Ann. Math. Stat.*, 33, 1065–1076.

Scott, D. W. (1979). "On optimal and data-based histograms." *Biometrika*, 66*(3)*, 605–610.

Shannon, C. E. (1948). "A mathematical theory of communications, I and II." *Bell Syst. Techn. J.*, 27, 379–443.

Shimazaki, H., and S. Shinomoto (2007). "A method for selecting the bin size of a time histogram." *Neural Comput.*, 19*(6)*, 1503-1527.

Singh, V. P., and Krstanovic, P. F. (1986). "Design of rainfall networks using entropy." *Completion Report*, Louisiana Water Resources Research Institute, Louisiana State University, Baton Rouge, LA.

Srinivasa, S. (2005). "*A review of multivariate mutual information*." www3.nd.edu/~jnl/ee80653/Fall2005/tutorials/sunil.pdf, University of Notre dame, South Bend, IN.

Tukey, J. W. (1977). *Exploratory data analysis*. Addison-Wesley, Reading, MA.

Uslu, O., and Tanriover, A. (1979). "Measuring the information content of hydrological process." *Proc., 1st Natl Cong. Hydrol.*, Istanbul, 437–443.

Watanabe, S. (1960). "Information theoretical analysis of multivariate correlation." *IBM J. Res. Develop.*, 6, 66–82.
Wertz, W. (1979). *Statistical density estimation: A survey,* Vandenhoeck & Ruprecht, Göttingen, Germany.
Yang, Y., and Burn, D. H. (1994). "An entropy approach to data collection network design." *J. Hydrol.*, 157, 307–324.

Additional Reading

Berthouex, P. M., and Brown, L. C. (1994). *Statistics for environmental engineers*, CRC Press, Boca Raton, FL.
Bueso, M. C., Angulo, J. M., Cruz-Sanjulian, J., and Carcia-Arostegui, J. L. (1999). "Optimal spatial sampling design in a multivariate framework." *Math. Geolog.*, 31(5), 507–525.
Cressie, N. C. (1990). *Statistics for spatial data, revised edition,* Wiley, New York.
Fano, R. (1968). *Transmission of information,* MIT Press, Cambridge, MA.
Guiasu, S. (1977). *Information theory with applications,* McGraw Hill, London.
Han, T. S. (1980). "Multiple mutual informations and multiple interactions in frequency data." *Inform. Control*, 46, 26–45.
Harmancioglu, N. B. (1981). "Measuring the information content of hydrological processes by the entropy concept." *J. Civil Eng.*, Special Issue: Centennial of Ataturk's Birth, Izmir, Turkey, 13–40.
Harmancioglu, N. B. (1984). "Entropy concept as used in determination of optimum sampling intervals." *Proc., Hydrosoft '84, Int. Conf. Hydraul. Eng. Software*, Portoroz, Yugoslavia, 6–99 to 6–110.
Harmancioglu, N. B., and Alpaslan, N. (1992). "Water quality monitoring network design." *Water Resour. Bull.*, 28(1), 179–192.
Harmancioglu, N. B., Fistikoglu, O., Ozkul, S. D., Singh, V. P., and Alpaslan, M. N. (1999). *Water quality monitoring network design,* Kluwer Academic, Boston.
Husain, T. (1979). "*Shannon's information theory in hydrologic design and estimation*." Ph.D. dissertation, University of British Columbia, Vancouver, Canada.
Husain, T. (1989). "Hydrologic uncertainty measure and network design." *Water Resour. Bull.*, 25(3), 527–534.
Husain, T., and Khan, H. U. (1983). "Shannon's entropy concept in optimum air monitoring network design." *Sci. Total Environ.*, 30, 181–190.
Husain, T., and Ukayli, M. A. (1983). "Meteorological network expansion for Saudi Arabia." *J. Res. Atmos.*, 16, 281–294.
Husain, T., Ukayli, M. A., and Khan, H. U. (1986). "Meteorological network expansion using information decay concept." *J. Atmos. Ocean. Techn.*, 3(1), 27–37.
Jessop, A. (1995). *Informed assessments: An introduction to information, entropy and statistics,* Ellis Horwood, New York.

Kapur, J. N., and Kesavan, H. K. (1992). *Entropy optimisation principles with applications*, Academic Press, San Diego.

Krstanovic, P. F., and Singh, V. P. (1984). "*Application of entropy theory to multivariate hydrologic analysis*." Technical Reports WRR8 and WRR9, Department of Civil Engineering, Louisiana State University, Baton Rouge, LA.

Lee, Y., and Ellis, J. H. (1997). "On the equivalence of kriging and maximum entropy estimators." *Math. Geolog.*, 29(1), 131–152.

Lubbe, C. A. (1996). *Information theory,* Cambridge University Press: Cambridge, UK.

Ozkul, S., Harmancioglu, N., and Singh, V. P. (2000). "Entropy-based assessment of water quality monitoring networks." *J. Hydrol. Eng.*, 5(1), 90–100.

Rodriguez-Iturbe, I., and Mejia, J. M. (1974). "The design of rainfall networks in time and space." *Water Resour. Res.*, 10(4), 713–728.

Sanders, T., Ward, R. C., Loftis, J. C., Steele, T. D., Adrian, D. D., and Yevjevich, V. (1983). *Design of networks for monitoring water quality*, Water Resources Publications, Littleton, CO.

Singh, V. P. (1998). *Entropy-based parameter estimation in hydrology*, Kluwer Academic, Boston.

This page intentionally left blank

Chapter 15

Rating Curves

A rating curve, in principle, is a relation between flux (usually volumetric) and concentration related to a river or stream. A volumetric flux can be represented by flow discharge (cubic meters per second) and its corresponding flow concentration by flow depth or stage above a datum. The relation between stage and discharge is often referred to as the stage–discharge relation or stage–discharge rating curve. It is treated as a kinematic relation (Singh 1993). Likewise, concentration can also be represented by suspended sediment concentration. Then the relation between suspended sediment concentration and discharge defines a suspended sediment rating curve. Of course, the product of discharge and sediment concentration yields the sediment discharge. Similarly, if concentration is represented by pollutant concentration, then the relation between pollutant concentration and discharge corresponds to the pollutant rating cure. The pollutant discharge is obtained by multiplying the pollutant concentration with discharge. In a similar vein, the relation between infiltration capacity rate and cumulative infiltration can be viewed as infiltration rating curve. Thus, there are different types of rating curves used in hydraulics and hydrology. Since the rating curves are of similar form from an algebraic viewpoint, and fundamental to all rating curves is the estimation of flux, this chapter focuses on the stage–discharge rating curve only.

15.1 Stage–Discharge Relation

Experimental measurements of discharge and the corresponding observations of stage at a station or gauge are used to develop a stage–discharge relation or

rating curve. This relation is used for the determination of discharge for a measured stage. Rating curves are used for a variety of purposes. They are used for constructing continuous records of discharge, continuous time series of sediment discharge or sediment concentration, continuous pollutant graphs, floodplain mapping, storage variation, hydraulic design, catchment routing, damage assessment, and so on.

The first step in establishing a rating curve is to obtain data on discharge and stage. Discharge is a product of cross-sectional flow area and flow velocity, and since cross-sectional area is computed using depth and width, it is desirable to determine the discharge at a place where velocity variations are kept to a minimum. For example, at a weir as water flow increases, the flow cross-sectional area increases but the velocity changes are kept to a minimum, and the discharge increases with the flow cross-sectional area. This phenomenon means that the discharge can be easily computed by knowing the weir geometry, and the height of the water above the weir crest can be translated into discharge with the use of a mathematical relation called rating curve. Where emplacement of a weir is not an option, a stable river cross section should be selected. Such a cross section is usually associated with a high depth-to-width ratio, and erosion and deposition of sediment is relatively small.

Ideally, the station rating curve should be a smooth curve of parabolic shape, without reversals in curvature. In the absence of an abrupt change in the slope of the rating curve, the rate of increase in stage corresponding to a specified increase in discharge should be reasonably consistent throughout the stage. In the case of stage–discharge relation for a channel, the channel must be capable of regulating or stabilizing the flow past the gauge such that for a given stage or height of the water surface, the discharge past the gauge must remain unaltered. The stage–discharge relation is controlled by a section or reach of the channel below the gauge, known as the section control. It eliminates the influence of all other boundary conditions on the velocity of flow at the stage. A control includes all the channel physical features that hydraulically determine the weir height at a given point for a certain rate of flow. All conditions influencing the velocity of flow past the gauge must be included as part of the control. It is clear that control plays a fundamental role in establishing a stage–discharge relation.

A control may be complete or partial. A complete control, as the name suggests, governs the stage–discharge relation for the full range of the stage and is independent of all downstream conditions. On the other hand, a partial control governs the relation for only part of the range in the stage. It may act in concert with other controls and be an essential part of the complete control.

The section control may be natural or artificial, and it must be capable of maintaining a fairly stable relation between discharge and water stage at the selected point above it. It entails controlling elements that are situated in a short length of the river. Examples of control include a boulder-covered rifle, rocks crossing the river, an indurated bed, and an overflow dam. For artificial controls, such as dams and weirs, the stage–discharge relation may be developed in laboratory conditions but must be verified by field measurements for their use.

The channel control is composed of channel slope, resistance, and dimensions over a considerable distance. This distance varies inversely with slope and increases with increasing stage. If the distance increases farther downstream and if it includes controls of new downstream features, then the curvature of the rating curve may exhibit reversals. If a channel has a flat slope, the control at high stages may extend so far downstream that it may involve backwater effects that may not occur at lower stages. Abrupt changes in controls and submergence of controls most likely cause irregularities in the slope of the stage–discharge relation.

In order for a stage–discharge relation to be stable for a given discharge, both relations of slope to stage and slope to discharge must remain unaltered. This stability corresponds to a complete control in its effectiveness. These relations would be constant for steady-state conditions, which do not occur often. Nevertheless, the sites for the position of gauges and controls must be selected such that the variation in discharge for a given stage caused by variations in slope, velocity, or channel conditions is small during the period involved.

A permanent control ensures a permanent stage–discharge relation at all times, as long as the slope remains the same. For a permanent control, the position with respect to the datum of the gauge, its distance downstream from the gauge, and the condition of the streambed between the gauge and part of the channel controlling the stage–discharge relation must remain unchanged. However, in real life these conditions are seldom met, and a permanent control and consequent permanent stage–discharge relation do not remain unchanged. Even if the control may seem permanent, the stage–discharge relation may change.

15.2 Forms of Stage–Discharge Relations

A rating curve for a gauge in a channel dominated by friction is normally expressed in a power form (Corbett 1962) as

$$Q = a(y - y_0)^b + c \tag{15.1}$$

where Q is discharge; y is stage or height of water surface; y_0 is the height when discharge is negligible, or a constant, or a parameter; b is an exponent; and a and c are parameters. Equation (15.1) specializes into three types.

15.2.1 Type 1

In this case, $y_0 = 0$ and $c = 0$. Equation (15.1) then becomes

$$Q = ay^b \tag{15.2a}$$

or

$$\log Q = \log a + b \log y \tag{15.2b}$$

15.2.2 Type 2

In this case, $c = 0$. Equation (15.1) then becomes

$$Q = a(y - y_0)^b \tag{15.3a}$$

or

$$\log Q = \log a + b \log(y - y_0) \tag{15.3b}$$

15.2.3 Type 3

In this case, $y_0 = 0$. Equation (15.1) then becomes

$$Q = ay^b + c \tag{15.4a}$$

or

$$\log(Q - c) = \log a + b \log y \tag{15.4b}$$

It should be noted that values of parameters a, b, and c vary from one relation to another. In the hydraulics literature, equations (15.1) to (15.4) have been applied. The objective here is to derive these relations using the entropy theory.

Example 15.1 A set of observed data of stage and discharge at the Lakhwar Dam site on the Yamuna River, India, is given in Table 15-1. Plot the stage–discharge data on log-log graph paper. Then fit a curve to the data. Which type of rating curve best represents this data set? Estimate the parameters of the equation representing this curve.

Solution The stage–discharge observations are plotted on log-log graph paper, as shown in Fig. 15-1(a) and in arithmetic scale in Fig. 15-1b. From the plot in Fig. 15-1(b), it seems that rating curve type 3 better repesents the measurements. From the graph paper, parameters of the equation corresponding to this curve are $c = 3.577$, $\log a = -5958.6$, $b = 926.76$. Rating curves are fitted to the data using the least-squares method.

Type 1

$$\log a = -5752.5,\ b = 897.74$$

$$\log Q = \log a + b \log y = -5752.5 + 897.74 \log y$$

Table 15-1 *Stage–discharge data observed in 1978 at the Lakhwar dam site on the Yamuna River, India.*

Stage (m)	Discharge (m^3/s)	Stage (m)	Discharge (m^3/s)	Stage (m)	Discharge (m^3/s)
622.23	31.25	622.57	69.8	623.36	224.29
622.23	30.63	622.79	96.4	623.37	225.86
622.24	31.48	622.85	109.98	623.37	236.49
622.26	30.56	622.92	124.04	623.43	186.6
622.26	31.82	622.93	117.99	623.43	250.13
622.285	34.53	622.96	139.61	623.44	213
622.287	35.37	622.99	122.95	623.44	252.05
622.29	32.94	623	178.24	623.46	241.74
622.29	36.83	623	122.86	623.48	264.66
622.3	36.36	623.01	126.51	623.48	271.69
622.3	38.52	623.02	148.61	623.49	281.11
622.31	32.24	623.02	129.54	623.49	259.71
622.32	39.3	623.08	165.08	623.51	256.8
622.32	38.53	623.1	180.46	623.6	303.99
622.358	43.82	623.11	201.3	623.6	227.45
622.38	45.66	623.15	183.23	623.69	316.45
622.44	50.49	623.15	148.08	623.71	302.73
622.46	57.51	623.19	182.06	623.73	269.29
622.53	70.13	623.28	215.77	623.78	281.26
622.57	73.3	623.31	215.71	623.82	329.83
624.14	425.71	624	326.35	623.83	336.98
624.24	451.87	624.12	408.1	623.91	345.4
622.23	30.56				

Type 2

$$y_0 = 622.2, \log a = 5.2646, b = 0.6952$$

$$\log Q = \log a + b \log(y - y_0) = 5.2646 + 0.6952 \log(y - 622.2)$$

Type 3

$$c = 3.577, \log a = -5958.6, b = 926.76$$

$$\log(Q - 3.577) = \log a + b \log y = -5958.6 + 926.76 \log y$$

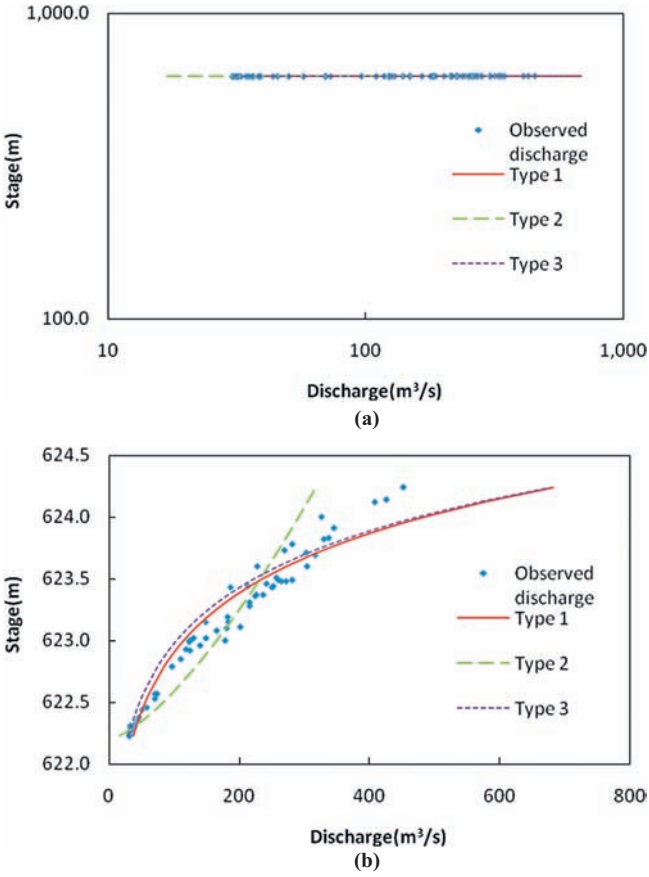

Figure 15-1 *Stage–discharge relation for Yamuna River at the Lakhwar Dam site, India.*

Example 15.2 A set of data of stage and discharge observed for the Tennessee River near Scottsboro, Alabama, is given in Table 15-2. Plot the stage–discharge data on log-log graph paper. Then fit a curve to the data. Which type of rating curve best represents this data set? Estimate the parameters of the equation representing this curve.

Solution The stage–discharge observations are plotted on log-log graph paper, as shown in Fig. 15-2. From the plot, it seems that rating curve type 2 better repesents the measurements. From the graph paper, parameters of the equation corresponding to this curve are $\log a = 5.0454$ and $b = 2.0815$. Rating curves are fitted to the observed data using the least-squares method.

Type 1

$$\log a = 8.5492, b = 1.1246$$

$$\log Q = \log a + b \log y = 8.5492 + 1.1246 \log y$$

Table 15-2 *Stage–discharge data observed for the Tennessee River near Scottsboro, Alabama.*

Stage (ft)	Discharge (ft^3/s)	Stage (ft)	Discharge (ft^3/s)	Stage (ft)	Discharge (ft^3/s)
26.28	247,000	16.85	124,000	9.44	59,300
24.36	215,000	15.64	96,500	8.52	53,200
24.19	216,000	14.91	91,000	7.38	45,200
23.3	202,000	14.73	107,000	6.46	40,100
23.22	188,000	13.96	95,800	5.09	31,400
22.5	180,000	11.26	79,200	4.54	28,800
19.39	131,000	11.29	68,200	3.98	25,000
18.74	132,000	10.76	73,200	2.04	14,800
18.61	136,000				

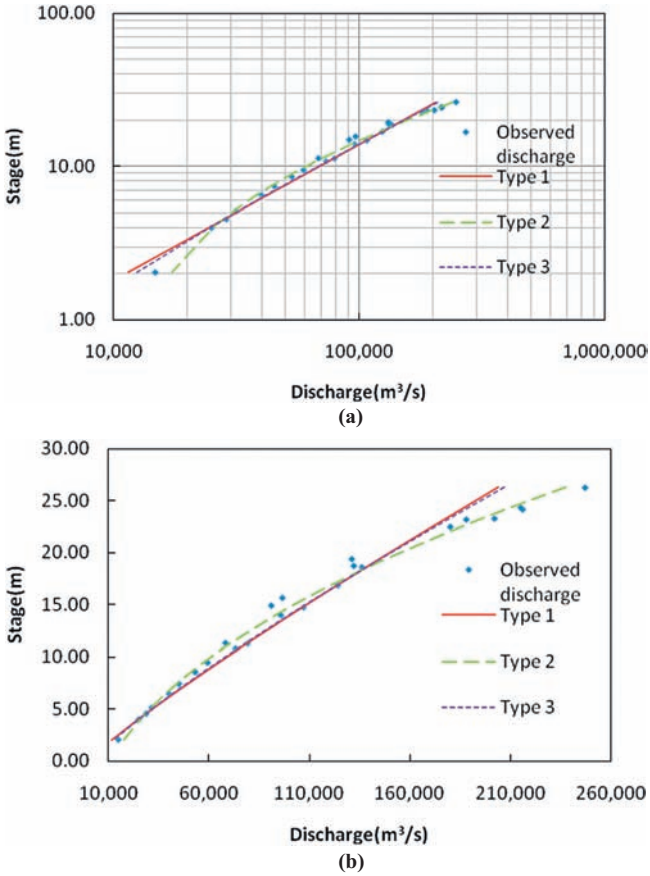

Figure 15-2 *Stage–discharge relation for the Tennessee River near Scottsboro, Alabama.*

Type 2

$$y_0 = 7.6, \log a = 5.0454, b = 2.0815$$

$$\log Q = \log a + b\log(y - y_0) = 5.0454 + 2.0815\log(y - 7.6)$$

Type 3

$$c = -2426.174, \log a = 8.3726, b = 1.1795$$

$$\log(Q + 2426.174) = \log a + b\log y = 8.3726 + 1.1795\log y$$

Type 3 seems to better represent the data.

Consider, for example, equation (15.3a) or (15.3b). Parameters a and b can be estimated using a least-squares method for given observations of stage and discharge (Singh 1993). Plotting equation (15.3b) on logarithmic paper requires an a priori estimation of y_0. To that end, one can plot stage against discharge for several values of y_0 and select the value that yields the best fit curve. Another simple way is to extend the curve to $Q = 0$ and from there get the value of y_0. Then, one plots $\log(y - y_0)$ versus $\log Q$. If the plot is a straight line, the value of y_0 obtained by extrapolation is acceptable. Otherwise, another value of y_0 in the neighborhood of the previously selected value is used, and the procedure is repeated until a straight line is obtained.

One can also compute y_0 analytically as follows. Consider a smooth curve between Q and y and select three points, designated as 1, 2, and 3, on this curve such that $Q_1/Q_2 = Q_2/Q_3$. The coordinates of these points are (Q_1, y_1), (Q_2, y_2), and (Q_3, y_3). Then, one can write from equation (15.3a)

$$\frac{(y_1 - y_0)^b}{(y_2 - y_0)^b} = \frac{(y_2 - y_0)^b}{(y_3 - y_0)^b} \tag{15.5}$$

Equation (15.5) can be written as

$$\frac{(y_1 - y_0)}{(y_2 - y_0)} = \frac{(y_2 - y_0)}{(y_3 - y_0)} \tag{15.6}$$

Solving equation (15.6), one obtains

$$y_0 = \frac{y_1 y_3 - y_2^2}{y_1 + y_3 - 2y_2} \tag{15.7}$$

Equation (15.7) is an explicit expression for y_0.

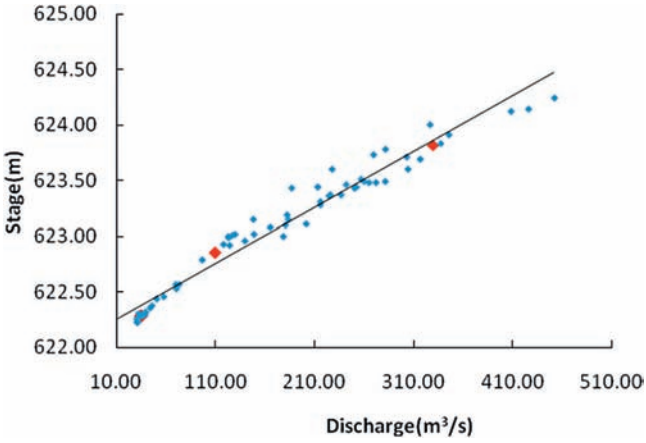

Figure 15-3 *Graphical method for determining* y_0.

Example 15.3 If equation (15.3a) represents the data in Example 15.1 well, then determine parameter y_0 using equation (15.7). Also determine this parameter graphically. How close are the two estimates?

Solution Choose three points which are highlighted in Fig. 15-3. Their coordinates are

Stage (m)	Discharge (m^3/s)
622.26	31.82
622.79	96.4
623.6	227.45

$$y_0 = \frac{y_1 y_3 - y_2^2}{y_1 + y_3 - 2y_2} = \frac{622.26 \times 623.6 - 622.79^2}{622.26 + 623.6 - 2 \times 622.79} = 621.26\,\text{m}$$

From the graph, the trend line meets the storage axis at y_0 = 622.2 m. The two values are not the same, but they are not far apart either.

15.3 Derivation of Rating Curves Using Entropy

Let the maximum stage (channel flow depth) be denoted as D. It is then assumed that all values of stage y measured from the bed to any point between 0 and D are equally likely (Singh 2010). In reality, this is not highly unlikely because at

different times different values of stages do occur. Then the cumulative probability distribution of discharge can be expressed as the ratio of the stage to the point where discharge is to be considered and the stage up to the maximum water surface. The probability of discharge being equal to or less than a given value of Q is y/D; at any stage (measured from bed) less than a given value, y, the discharge is less than a given value, say Q; thus the cumulative distribution function of discharge,

$$F(Q) = P\,(\text{discharge} \le \text{a given value of } Q),\ P = \text{probability},$$

can be expressed as

$$F(Q) = \frac{y}{D} \tag{15.8}$$

$F(Q)$ denotes the cumulative distribution function, and Q = discharge (m^3/s). The probability density function is obtained by differentiating equation (15.8) with respect to Q:

$$f(Q) = \frac{dF(Q)}{dQ} = \frac{1}{D}\frac{dy}{dQ} \text{ or } f(Q) = \left(D\frac{dQ}{dy}\right)^{-1} \tag{15.9}$$

The term $f(Q)dQ = F(Q + dQ) - F(Q)$ denotes the probability of the discharge being between Q and $Q + dQ$. Since equation (15.9) constitutes the fundamental hypothesis used here for deriving stage–discharge relations using entropy, it is useful to evaluate its validity. This hypothesis (i.e., the relation between the cumulative probability $F(Q)$ and the ratio (y/D) should be tested for a number of natural rivers.

Example 15.4 Consider the set of data on stage and discharge. Determine if the hypothesis given by equation (15.8) is valid.

Solution For the data shown in Example 15.1, the histogram of discharge values corresponding to their probabilities is plotted as shown in Fig. 15-4a. Then the cumulative probability distribution against y/D can be plotted as shown in Fig. 15-4b. This figure shows that the hypothesis is only approximately valid.

The objective here is to determine the probability density function of Q, $f(Q)$. This goal is accomplished by maximizing the Shannon entropy (Shannon 1948) of discharge, $H(Q)$:

$$H(Q) = -\int_{Q_0}^{Q_D} f(Q)\ln f(Q)dQ \tag{15.10}$$

where Q_0 and Q_D represent the lower and upper limits of discharge for integration. Equation (15.10) expresses a measure of uncertainty about $f(Q)$ or the average information content of sampled Q. Maximizing $H(Q)$ is equivalent to maximizing $f(Q)\ln f(Q)$. To determine the $f(Q)$ that is least biased toward what is not known about discharge, the principle of maximum entropy (POME)

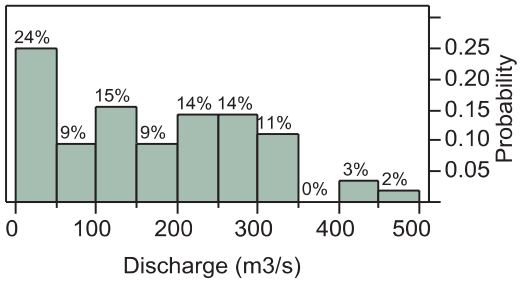

Figure 15-4a *Probability mass function of discharge.*

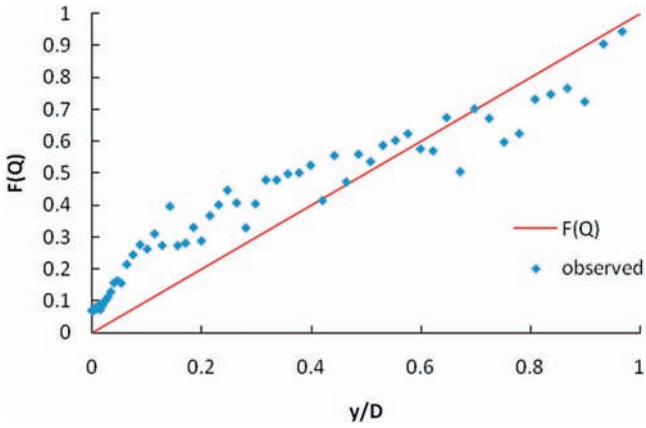

Figure 15-4b *Relation between the cumulative probability* F(Q) *and the ratio* y/D.

developed by Jaynes (1957, 1982) is invoked, which requires specification of certain information, called constraints, on discharge. According to POME, the most appropriate probability distribution is the one that has the maximum entropy or uncertainty, subject to these constraints.

For deriving the stage–discharge relation, according to Singh (1998, 2010), the constraint to be specified is the total probability law, which must always be satisfied by the probability density function of discharge, which is written as

$$C_1 = \int_{Q_0}^{Q_D} f(Q)dQ = 1 \tag{15.11}$$

and

$$C_2 = \int_{Q_0}^{Q_D} \ln Q f(Q)dQ = \overline{\ln Q} \tag{15.12}$$

Equation (15.12) is the mean of the logarithmic discharge values, $\overline{\ln Q}$. Equation (15.11) is the first constraint defining the total probability law, C_1, and equation (15.12) is the second constraint, C_2.

To obtain the least biased probability distribution of Q, $f(Q)$, the Shannon entropy, given by equation (15.10), is maximized according to POME, subject to equations (15.11) and (15.12). To that end, the method of Lagrange multipliers is used. The Lagrangian function then becomes

$$L = -\int_{Q_u}^{Q_D} f(Q)\ln f(Q)dQ - (\lambda_0 - 1)\left(\int_{Q_0}^{Q_D} f(Q)dQ - C_1\right) - \lambda_1\left(\int_{Q_0}^{Q_D} \ln Q f(Q)dQ - C_2\right) \quad (15.13)$$

where λ_0 and λ_1 are the Lagrange multipliers. Recalling the Euler–Lagrange calculus of variation and differentiating equation (15.13) with respect to f , noting that f is variable and Q is a parameter, and equating the derivative to zero, one obtains

$$\frac{\partial L}{\partial f} = 0 = -[\ln f(Q) + 1] - (\lambda_0 - 1) - \lambda_1 Q \quad (15.14)$$

Equation (15.14) leads to the entropy-based probability density function (PDF) of velocity as

$$f(Q) = \exp[-\lambda_0 - \lambda_1 \ln Q]$$

or

$$f(Q) = \exp(-\lambda_0)Q^{-\lambda_1} \quad (15.15)$$

The PDF of Q contains the Lagrange multipliers λ_0 and λ_1, which can be determined using equations (15.11) and (15.12).

Substituting equation (15.15) in equation (15.11), one gets

$$\frac{\exp(-\lambda_0)}{-\lambda_1 + 1} Q^{-\lambda_1+1}\Big|_{Q_0}^{Q} = \frac{1}{D} y\Big|_{y_0}^{y} \quad (15.16)$$

Equation (15.16) yields

$$Q = \left[Q_0^{-\lambda_1+1} + \frac{\exp(\lambda_0)(-\lambda_1 + 1)}{D}(y - y_0)\right]^{\frac{1}{-\lambda_1+1}} \quad (15.17)$$

Equation (15.17) gives a general rating curve corresponding to the constraints given by equations (15.11) and (15.12).

15.3.1 Rating Curve Type 1

If $y_0 = 0$ and $Q_0 = 0$, then equation (15.17) leads to

$$Q = \left[\frac{\exp(\lambda_0)(-\lambda_1 + 1)}{D} y\right]^{\frac{1}{-\lambda_1+1}} \quad (15.18)$$

Let

$$a = \left[\frac{\exp(\lambda_0)}{D}(-\lambda_1 + 1)\right]^{\frac{1}{-\lambda_1+1}} \tag{15.19}$$

and

$$b = \frac{1}{-\lambda_1 + 1} \tag{15.20}$$

Equation (15.18), with the use of equations (15.19) and (15.20), can then be expressed as

$$Q = ay^b \tag{15.21}$$

which is the same as equation (15.2a). It may now be interesting to evaluate the Lagrange multipliers for this simple case, first.

Substitution of equation (15.15) in equation (15.11) with Q_0 yields

$$\exp(\lambda_0) = \frac{Q_D^{-\lambda_1+1}}{-\lambda_1 + 1} \text{ or } \lambda_0 = -\ln(-\lambda_1 + 1) + (-\lambda_1 + 1)\ln(Q_D) \tag{15.22}$$

where Q_D is the discharge at $y = D$.

Differentiating equation (15.22) with respect to λ_1, one obtains

$$\frac{\partial \lambda_0}{\partial \lambda_1} = -\ln Q_D + \frac{1}{-\lambda_1 + 1} \tag{15.23}$$

One can also write from equations (15.15) and (15.11)

$$\lambda_0 = \ln \int_0^{Q_D} Q^{-\lambda_1} dQ \tag{15.24}$$

Differentiating equation (15.24) with respect to λ_1 and simplifying, one obtains

$$\frac{\partial \lambda_0}{\partial \lambda_1} = -\overline{\ln Q} \tag{15.25}$$

Equating equation (15.23) to equation (15.25) leads to an estimate of λ_1:

$$\lambda_1 = 1 - \frac{1}{\ln Q_D - \overline{\ln Q}} \tag{15.26}$$

Therefore, exponent b of the power form rating curve given by equation (15.21) becomes

$$b = \ln Q_D - \overline{\ln Q} \tag{15.27}$$

Equation (15.27) shows that exponent b of the power form rating curve can be estimated from the values of the logarithm of maximum discharge at the water surface that covers the channel fully and the average of the logarithmic values of discharge. The higher the difference between these logarithm values, the higher the exponent.

The Lagrange multiplier λ_0 can now be expressed as

$$\lambda_0 = \frac{\ln Q_D}{\ln Q_D - \overline{\ln Q}} + \ln\left(\ln Q_D - \overline{\ln Q}\right) = \frac{1}{b}\ln Q_D + \ln b \tag{15.28}$$

The PDF of Q can be expressed as

$$f(Q) = \exp(-\lambda_0) Q^{\frac{1}{b}-1} \tag{15.29}$$

and the CDF as

$$F(Q) = b\exp(-\lambda_0) Q^{\frac{1}{b}} \tag{15.30}$$

For $b > 1$, the PDF monotonically increases from 0 to 1. For $b > 1$, dF/dQ, which is equation (15.29), is always bigger than 0. Thus, $F(Q)$ is a monotonically increasing function, which is minimum at $Q = 0$ and maximum at $Q = Q_D$, as shown in Fig. 15-5.

When $Q = Q_D$, according to equation (15.30), $F(Q) = b\exp(-\lambda_0) Q_D^{\frac{1}{b}}$, by substituting λ_0 from equation (15.28):

$$F(Q) = b\exp(-\lambda_0) Q_D^{\frac{1}{b}} = b\exp\left(-\frac{1}{b}\ln Q_D - \ln b\right) Q_D^{\frac{1}{b}} = bQ_D^{-\frac{1}{b}} \frac{1}{b} Q_D^{\frac{1}{b}} = 1$$

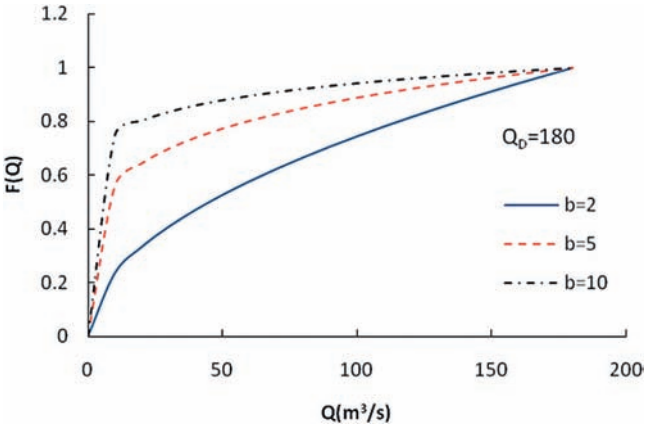

Figure 15-5 *Cumulative probability distribution of discharge.*

The entropy (in Napier) of the discharge probability distribution can be obtained by substituting equation (15.29) in equation (15.10):

$$H = \lambda_0 - \left(\frac{1}{b} - 1\right)\overline{\ln Q} \tag{15.31}$$

Equation (15.31) shows that the entropy value increases with increasing discharge, because the average of the log discharge values is higher. This result means that the rating curve has more uncertainty.

Example 15.5 Using the observed data set given in Examples 15.1 and 15.2, compute parameters a and b. Then fit the theoretical rating curve and evaluate how good the parameter values are.

Solution *Lakhwar Dam site.* For the data at the Lakhwar Dam site on the Yamuna River, India, in Example 15.1, it is seen from Table 15-1 that the rating curve does not satisfy the assumption $y_0 = 0$ and $Q_0 = 0$. To apply the type 1 rating curve with equation (15.21), let $y' = y - 622\,\text{m}$, so that it can fit the $y_0 = 0$ and $Q_0 = 0$ assumption. Now $D = 2.4\,\text{m}$.

$$\lambda_1 = 1 - \frac{1}{\ln Q_D - \overline{\ln Q}} = 1 - \frac{1}{6.44 - 4.84} = 0.214$$

$$\lambda_0 = \frac{\ln Q_D}{\ln Q_D - \overline{\ln Q}} + \ln\left(\ln Q_D - \overline{\ln Q}\right) = \frac{6.44}{6.44 - 4.84} + \ln(6.44 - 4.84) = 5.046$$

$$b = \frac{1}{-\lambda_1 + 1} = \frac{1}{-0.373 + 1} = 1.272$$

$$a = \left[\frac{\exp(\lambda_0)}{D}(-\lambda_1 + 1)\right]^{\frac{1}{-\lambda_1+1}} = \left[\frac{\exp(5.046)}{2.4}(1 - 0.214)\right]^{1.272} = 148.2$$

$$Q = ay^b = 148.2y'^{1.272}$$

Now change y' back to y, and the curve is as shown in Fig. 15-6a.
Tennessee River site. For data from the Tennessee River in Example 15.2, it is seen from Table 15-2 that it satisfies the $y_0 = 0$ and $Q_0 = 0$ assumption. Thus, equations (15.19) and (15.20) can be used directly to determine parameters a and b without any modification.

$$\lambda_1 = 1 - \frac{1}{\ln Q_D - \overline{\ln Q}} = 0.066$$

$$\lambda_0 = \frac{\ln Q_D}{\ln Q_D - \overline{\ln Q}} + \ln\left(\ln Q_D - \overline{\ln Q}\right) = 11.665$$

$$b = \frac{1}{-\lambda_1 + 1} = 1.071$$

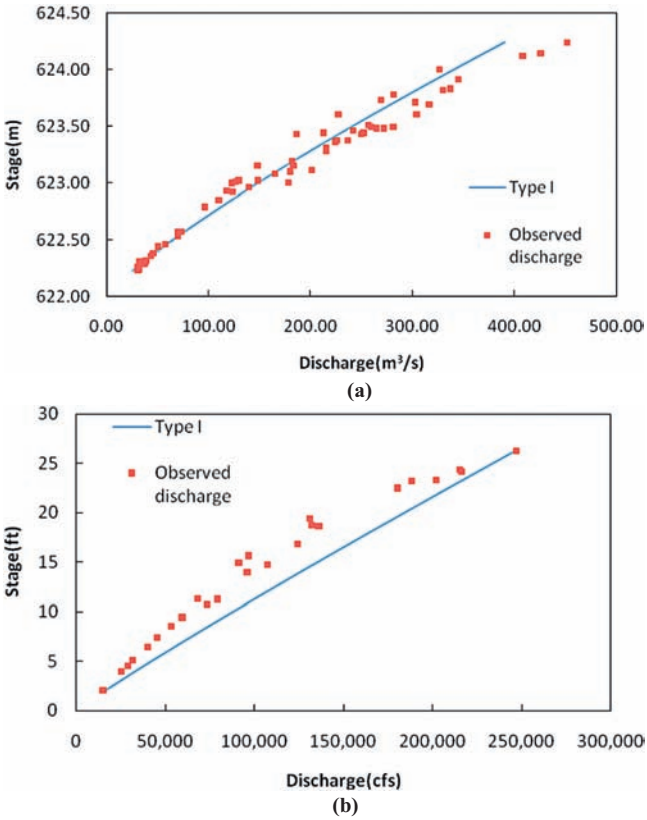

Figure 15-6 *Type 1 curve at (a) the Lakhwar Dam site and (b) the Tennessee River.*

$$a = \left[\frac{\exp(\lambda_0)}{D}(-\lambda_1 + 1)\right]^{\frac{1}{-\lambda_1+1}} = 7,459$$

$$Q = ay^b = 7,459y^{1.071}$$

The curve is plotted in Fig. 15-6b.

15.3.2 Rating Curve Type 2

In this case, $Q = 0$ at $y = y_0$. Therefore, equation (15.17) becomes

$$Q = \left[\frac{\exp(\lambda_0)(-\lambda_1 + 1)}{D}\right]^{\frac{1}{-\lambda_1+1}} (y - y_0)^{\frac{1}{-\lambda_1+1}} \tag{15.32}$$

Using equation (15.19), equation (15.32) becomes

$$Q = a(y - y_0)^b \tag{15.33}$$

Example 15.6 Using the observed data set from Examples 15.1 and 15.2, compute parameters a, b, and y_0. Then fit the theoretical rating curve and evaluate how good the parameter values are.

Solution *Lakhwar Dam site.* For the data at the Lakhwar Dam site on the Yamuna River, India, it is seen from Example 15.3 that y_0 is computed as 622.2 m. As no change has been made in Q, equations (15.26) and (15.28) are still valid. As computed in Example 15.5,

$$\lambda_1 = 0.214 \; \lambda_0 = 5.046$$

Thus,

$$b = \frac{1}{-\lambda_1 + 1} = \frac{1}{-0.373 + 1} = 1.272$$

$$a = \left[\frac{\exp(\lambda_0)}{D}(-\lambda_1 + 1)\right]^{\frac{1}{-\lambda_1+1}} = \left[\frac{\exp(5.046)}{624.4}(1 - 0.214)\right]^{1.272} = 0.126$$

$$Q = a(y - y_0)^b = 0.126(y - 622.2)^{1.272}$$

The rating curve is plotted in Fig. 15-7a.

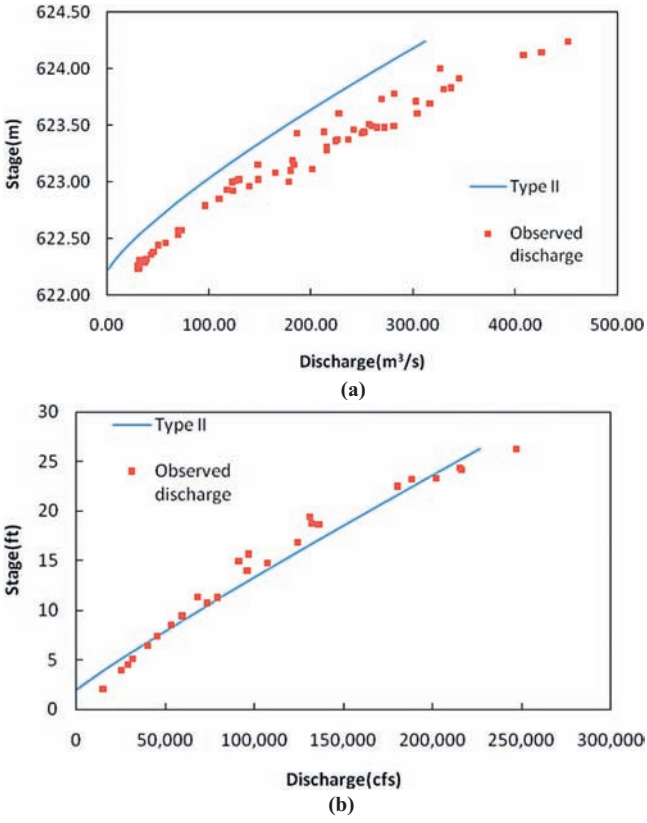

Figure 15-7 *Type 2 curve at (a) the Lakhwar Dam site and (b) the Tennessee River.*

Tennessee River site. For the data from the Tennessee River, choose $y_0 = 2$ ft, a and b are the same as the value computed in Example 15.5.

$$Q = a(y - y_0)^b = 7,459(y - 2)^{1..07}$$

The rating curve is plotted in Fig. 15-7b.

15.3.3 Rating Curve Type 3

In this case, let $q = Q - Q_0$, where Q_0 is some small value. It is assumed that $q = 0$ at $y = 0$. Then the derivation in the case of rating curve type 1 holds, and equation (15.17) becomes

$$Q = ay^b + c \tag{15.34}$$

which is the same as equation (15.4a). Here parameters a and b have the same definitions, but Q is replaced by q, as in case I, and $c = Q_0$.

Example 15.7 Using the observed data set given in Tables 15.1 and 15.2, compute parameters a, b, and c. Then fit the theoretical rating curve and evaluate how good the parameter values are.

Solution *Lakhwar Dam site.* For the data at the Lakhwar Dam site on the Yamuna River, India, it is seen from Example 15.3 and from Fig. 15-5 that $c = 40\,\text{m}^3/\text{s}$, and $q = Q - 40\,\text{m}^3/\text{s}$. Thus, the Lagrange multipliers λ_0 and λ_1 should be computed by taking q instead of Q in equations (15.26) and (15.28).

$$\lambda_1 = 1 - \frac{1}{\ln q_D - \overline{\ln q}} = -0.012$$

$$\lambda_0 = \frac{\ln q_D}{\ln q_D - \overline{\ln q}} + \ln\left(\ln q_D - \overline{\ln q}\right) = 6.132$$

$$b = \frac{1}{-\lambda_1 + 1} = 1.013$$

$$a = \left[\frac{\exp(\lambda_0)}{D}(-\lambda_1 + 1)\right]^{\frac{1}{-\lambda_1+1}} = 217.3$$

$$q = ay^b = 217.3y^{1.013}$$

$$Q = ay^b + c = 217.3y^{1.013} + 40$$

The rating curve is plotted in Fig. 15-8a.

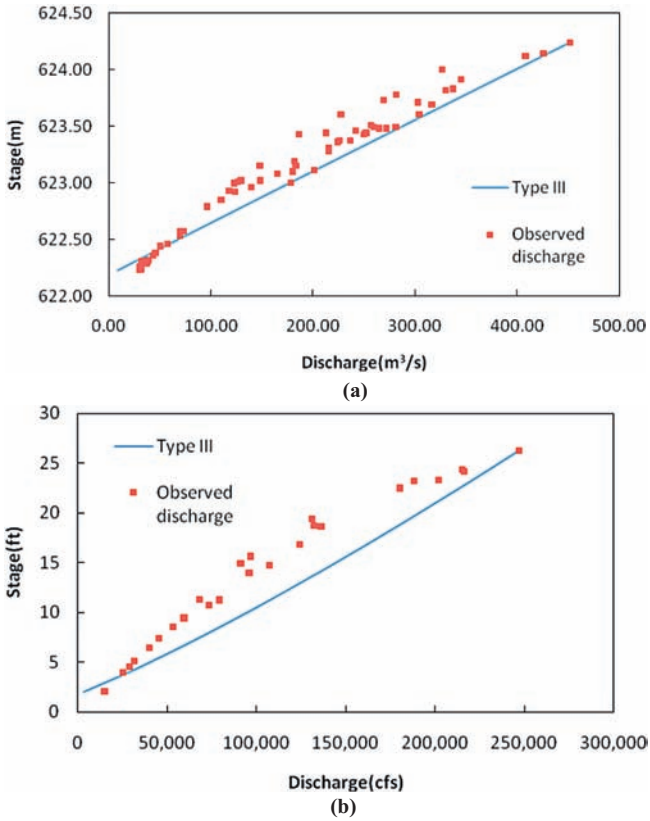

Figure 15-8 *Type 3 curve at (a) the Lakhwar Dam site and (b) the Tennessee River.*

Tennessee River site. It is seen from Fig. 15-8a that $c = -30{,}284\,\text{m}^3/\text{s}$ and $q = Q + 30{,}284\,\text{m}^3/\text{s}$.

$$\lambda_1 = 1 - \frac{1}{\ln q_D - \overline{\ln q}} = -11.106$$

$$\lambda_0 = \frac{\ln q_D}{\ln q_D - \overline{\ln q}} + \ln\left(\ln q_D - \overline{\ln q}\right) = 14.988$$

$$b = \frac{1}{-\lambda_1 + 1} = 0.0826$$

$$a = \left[\frac{\exp(\lambda_0)}{D}(-\lambda_1 + 1)\right]^{\frac{1}{-\lambda_1+1}} = 18{,}657.6$$

$$q = ay^b = 18{,}657.6y^{0.0826}$$

$$Q = ay^b + c = 18{,}657.6y^{0.0826} - 30{,}284$$

The rating curve is plotted in Fig. 15-8b.

Table 15-3 *Observed stage–discharge data.*

Stage (m)	Discharge (m^3/s)	Stage (m)	Discharge (m^3/s)	Stage (m)	Discharge (m^3/s)
0.39	78.7	1	31.9	1.81	739
0.39	79.2	1.01	150	1.87	459
0.42	87.8	1.04	144	1.98	507
0.52	33.9	1.1	60.9	2.02	597
0.54	10	1.12	138	2.06	606
0.58	7.45	1.16	160	2.16	574
0.58	20.7	1.17	168	2.18	852
0.61	62.7	1.23	132	2.2	1,200
0.71	25.6	1.24	57.1	2.44	1,440
0.72	15.9	1.29	127	2.82	1,440
0.78	77.3	1.31	360	2.99	1,440
0.8	19.7	1.4	156	3.2	2,330
0.88	166	1.44	178	3.56	3,660
0.9	124	1.54	340	4.39	5,550
0.9	17.6	1.55	434	4.51	7,780
0.93	33.6	1.74	610	5.64	13,100
0.94	18.9	1.78	229	5.64	13,100
0.98	142	1.78	246		

Example 15.8 Compute the rating curves by the least-squares method for the stage–discharge data from USGS-08080500-DMF-Brazos (2006–2009) given in Table 15-3.

Solution Using the least-squares method, parameters of rating curve types 1, 2, and 3 are computed and parameter values are found to be

Type 1: $$\log a = 4.65, b = 2.45$$

Type 2: $$y_0 = -2.5 \text{ m}, \log a = -0.20, b = 5.09$$

Type 3: $$Q_0 = 64 \text{ m}^3/\text{s}, \log a = 3.41, b = 3.59$$

The rating curves are plotted in Fig. 15-9. It is seen from Fig. 15-9 that the type 2 curve fits the observation better than other curves.

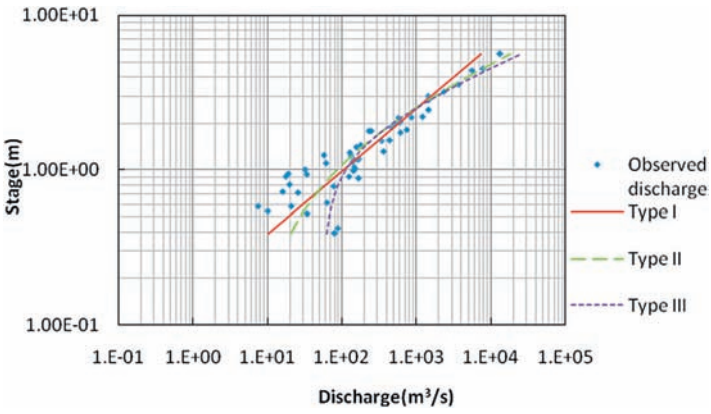

Figure 15-9 *Rating curves using the least-squares method at USGS-08080500-DMF-Brazos (2006–2009).*

Example 15.9 Use the entropy-based method to compute the type 1 rating curve for the data given in Table 15-3. Compare with the result from the least-squares method.

Solution First, we need to find out whether a modification is needed for the type 1 curve assumption. When $y_0 = 0$, Q_0 is small but not 0; thus, let $y' = y - 1.2\,\text{m}$.

$$\lambda_1 = 1 - \frac{1}{\ln Q_D - \overline{\ln Q}} = 0.681$$

$$\lambda_0 = \frac{\ln Q_D}{\ln Q_D - \overline{\ln Q}} + \ln\left(\ln Q_D - \overline{\ln Q}\right) = 4.164$$

$$b = \frac{1}{-\lambda_1 + 1} = 3.14$$

$$a = \left[\frac{\exp(\lambda_0)}{D}(-\lambda_1 + 1)\right]^{\frac{1}{-\lambda_1+1}} = 57.49$$

$$Q = ay^b = 57.49y^{3.14}$$

The rating curve is plotted in Fig. 15-10. It is seen from Fig. 15-10 that the entropy-based method fits the observation better.

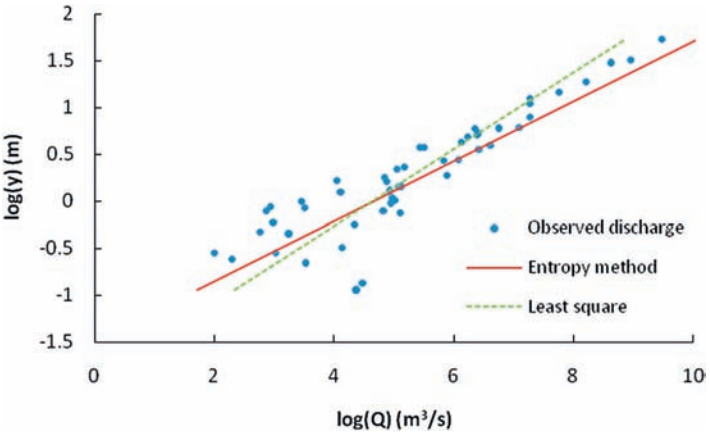

Figure 15-10 *Type 1 rating curves for different methods.*

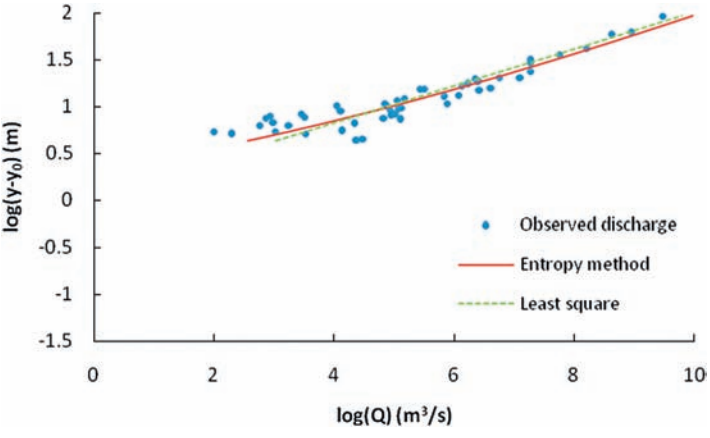

Figure 15-11 *Type 2 rating curves for different methods.*

Example 15.10 Using the entropy-based method, compute the type 2 rating curve for the data given in Table 15-3. Compare with the result from the least-squares method.

Solution Taking $y_0 = -0.7$ m, λ_0 and λ_1 are the same as those computed in Example 15.9.

$$Q = a(y - y_0)^b = 57.49(y + 0.7)^{3.14}$$

The rating curves are plotted in Fig. 15-11. It is seen from Fig. 15-8 that the results for the two methods are similar to each other.

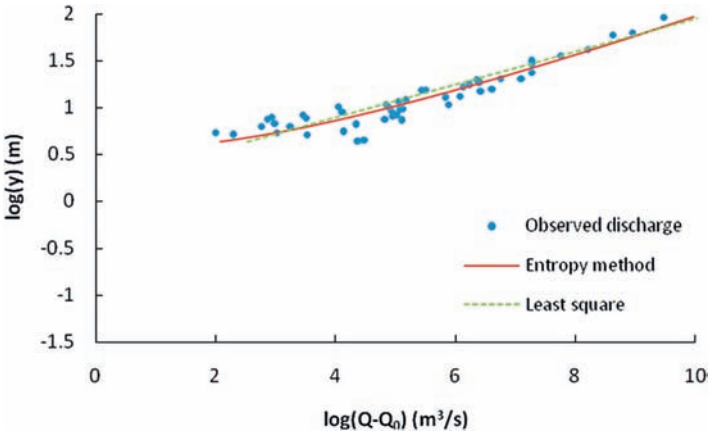

Figure 15-12 *Type 3 rating curves for different methods.*

Example 15.11 Using the entropy-based method, compute the type 3 rating curve for the data given in Table 15-3. Compare with the result from the least-squares method.

Solution Taking $Q_0 = 19.5\,\text{m}^3/\text{s}$ and using the parameters computed in Example 15.9,

$$Q = ay^b + c = 57.49y^{3.14} + 19.5$$

The type 3 rating curves are plotted in Fig. 15-12. It is seen from Figs. 15-11 and 15-12 that the type 3 curves are slightly bigger than type 2 curves at small values of discharge.

Example 15.12 Compute the rating curves by the least-squares method for the stage–discharge data from USGS-08083100-FK-Brazos (2006–2009) give in Table 15-4.

Solution For the type 1 curve, $a = 0.068$ and $b = 3.83$. For the type 2 curve, $y_0 = -1.9\,\text{m}$, $a = 0.001$, and $b = 5.08$. For the type 3 curve, $Q_0 = 0.67\,\text{m}^3/\text{s}$, $a = 0.878$, and $b = 3.1$. Rating curves are plotted in Fig. 15-13. It is seen from the figure that type 1 and type 2 curves are a better fit than the type 3 curve.

Table 15-4 *Observed stage–discharge data.*

Stage (m)	Discharge (m^3/s)	Stage (m)	Discharge (m^3/s)	Stage (m)	Discharge (m^3/s)	Stage (m)	Discharge (m^3/s)
2.14	1.02	2.5	4.17	2.84	3.21	4.18	40
2.16	1.02	2.51	2.55	2.9	9.21	4.52	33.7
2.21	1.14	2.52	1.79	2.93	13	4.76	24.3
2.26	1.11	2.52	2.25	2.97	3.33	5.14	59.5
2.26	1.85	2.54	2.66	2.97	7.43	5.16	32.2
2.27	0.93	2.55	4.14	3.06	4.84	5.17	49
2.3	1.05	2.56	3.1	3.06	7.51	6.78	125
2.37	1.02	2.57	1.44	3.16	4.87	7.87	190
2.37	1.03	2.57	1.49	3.18	2.92	8.85	327
2.38	1.12	2.58	1.86	3.21	15.4	10.46	504
2.39	1.04	2.59	2.21	3.26	7.97	11.08	692
2.39	1.47	2.61	2.56	3.27	3.93	11.66	987
2.4	1.49	2.62	3.44	3.3	2.87	11.73	876
2.42	1.44	2.63	1.51	3.31	9.62	12.39	1,090
2.42	1.85	2.63	2.57	3.47	13.4	13.06	1,230
2.42	4.29	2.64	2.62	3.54	9.17	13.44	1,280
2.43	2.92	2.68	2.68	3.56	16.7	13.56	1,350
2.45	1.88	2.68	2.93	3.6	4.15	13.77	1,210
2.46	3.11	2.69	2.29	3.7	17.5	15.5	1,970
2.47	1.01	2.69	3.94	3.73	28.1	18.32	3,380
2.47	1.48	2.74	2.54	3.85	21.1	19.07	4,030
2.48	4.54	2.79	7.92	4.02	20.4	20.48	5,110
2.49	0.87	2.84	2.33	4.04	35.1	21.55	6,960

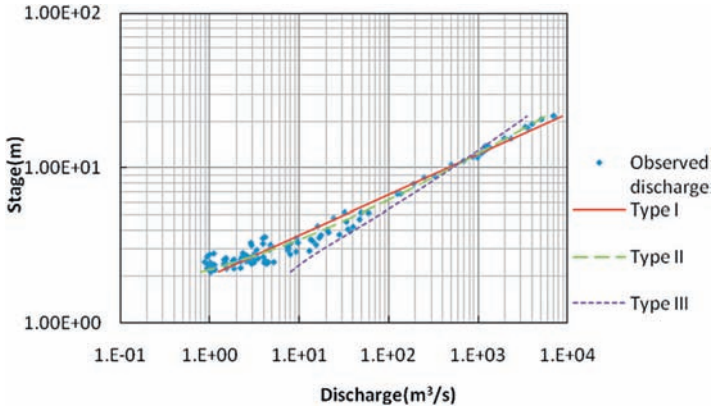

Figure 15-13 *Rating curves using the least-squares method at USGS-08083100-FK-Brazos (2006–2009).*

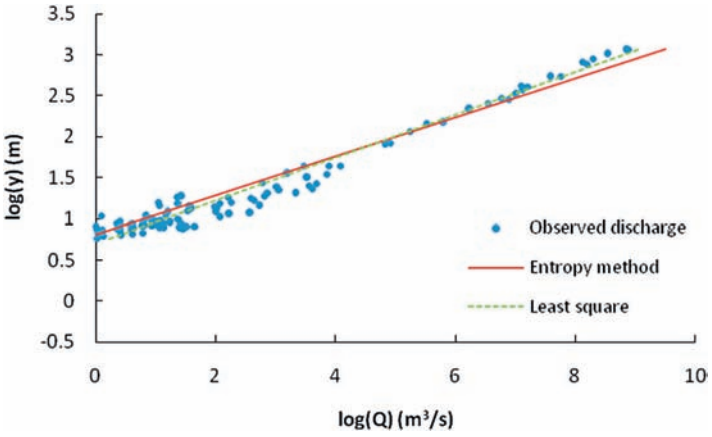

Figure 15-14 *Type 1 rating curves for different methods.*

Example 15.13 Using the entropy-based method, compute the type 1 rating curve for the data given in Table 15-4. Compare with the result from the least-squares method.

Solution First, we need to find out whether a modification is needed for the type 1 curve assumption. When $y_0 = 0$, Q_0 is small but not 0. Thus, let $y' = y - 2.05\,\text{m}$. Then,

$$\lambda_1 = 1 - \frac{1}{\ln Q_D - \overline{\ln Q}} = 0.762$$

$$\lambda_0 = \frac{\ln Q_D}{\ln Q_D - \overline{\ln Q}} + \ln\left(\ln Q_D - \overline{\ln Q}\right) = 3.544$$

$$b = \frac{1}{-\lambda_1 + 1} = \frac{1}{-0.373 + 1} = 4.21$$

$$a = \left[\frac{\exp(\lambda_0)}{D}(-\lambda_1 + 1)\right]^{\frac{1}{-\lambda_1+1}} = 0.03$$

$$Q = ay^b = 0.03y'^{4.21}$$

The type 1 rating curve is plotted in Fig. 15-14.

Example 15.14 Using the entropy-based method, compute the type 2 rating curve for the data given in Table 15-4. Compare with the result from the least-squares method.

Solution Taking $y_0 = -1.9\,\text{m}$, λ_0 and λ_1 are the same as those computed in Example 15.13.

$$Q = a(y - y_0)^b = 0.03(y + 1.9)^{4.21}$$

The type 2 rating curve is plotted in Fig. 15-15.

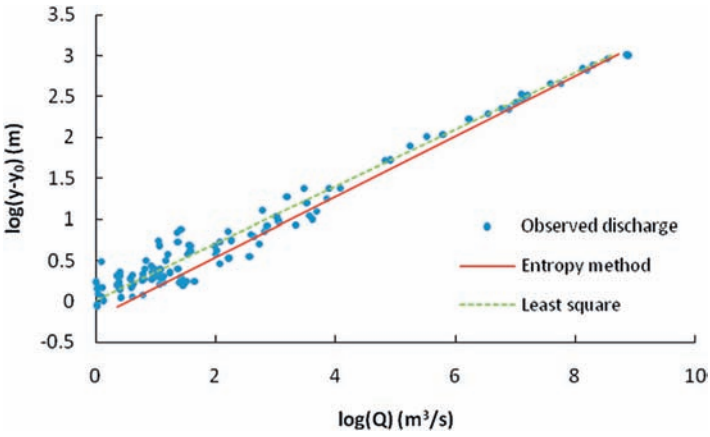

Figure 15-15 *Type 2 rating curves for different methods.*

Example 15.15 Using the entropy-based method, compute the type 3 rating curve for the data given in Table 15-4. Compare with the result from the least-squares method.

Solution Taking $Q_0 = 11.5\,\mathrm{m}^3/\mathrm{s}$ and using the parameters computed in Example 15.13, the type 3 rating curve is computed and plotted in Fig. 15-16.

$$Q = ay^b + c = 0.03y^{4.21} + 11.5$$

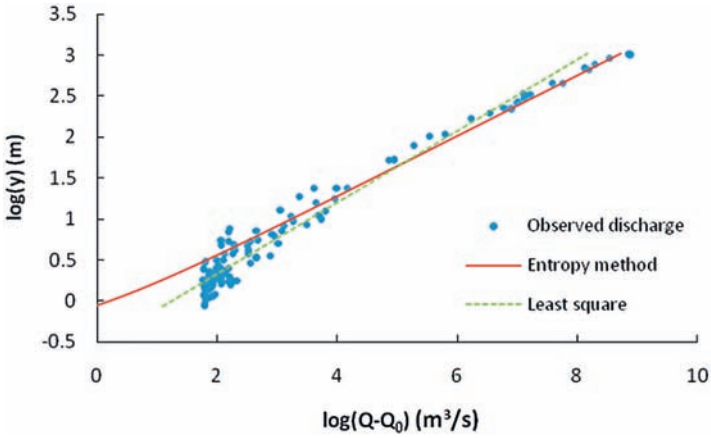

Figure 15-16 *Type 3 rating curves for different methods.*

Questions

Stage–discharge data from the USGS-08079600-DMF-Brazos station at the Brazos River in Texas are given in Table 15-5.

Q15.1 Verify the assumption on the cumulative distribution of equation (15.8) and plot it.

Q15.2 Verify if the set of data can be considered for using the type 1 rating curve. (Examine whether $y_0 = 0$ and $Q_0 = 0$.)

Q15.3 If the answer of Q15.2 is yes, compute the Lagrange multipliers λ_0 and λ_1 using equations (15.26) and (15.28).

Q15.4 Compute parameters a and b and fit the type 1 curve. Plot it and discuss the plot.

Q15.5 If $y_0 \neq 0$, find y_0 from both the plot and equation (15.7).

Q15.6 With y_0 computed from Q15.5, fit the type 2 curve. Plot it and discuss the plot.

Q15.7 If $Q_0 \neq 0$, find Q_0 from the plot.

Table 15-5 *Stage–discharge data.*

Stage (m)	Discharge (m^3/s)	Stage (m)	Discharge (m^3/s)
0.15	6.07	0.64	26.2
0.2	6.9	0.8	53
0.22	28.1	0.86	49.8
0.24	9.54	0.89	34.3
0.25	7.96	0.91	60.8
0.27	5.5	0.96	36.3
0.31	11.6	0.98	35.2
0.33	5.58	1.02	112
0.39	13.8	1.27	70.7
0.42	11.5	1.36	112
0.42	4.58	1.72	160
0.47	15.9	2.1	268
0.5	17.8	2.44	466
0.52	19.9	6.59	2,150
0.53	21.4	6.92	2,440
0.55	21.7	0.59	28.1

Q15.8 Compute the Lagrange multipliers λ_0 and λ_1 again with Q_0, and state how different they are from those computed in Q15.3.

Q15.9 Compute parameters a and b, fit the type 3 curve, and plot it. Discuss the plot to evaluate how well it fits.

Q15.10 Compare the entropy-based methods with the least-squares method.

References

Corbett, D. M. (1962). "Stream-gaging procedure: A manual describing methods and practices of the Geological Survey." *Geological Survey Water Supply Paper 888*, U.S. Department of the Interior, Washington, DC.

Jaynes, E. T. (1957). "Information theory and statistical mechanics, I." *Phys. Rev.*, 106, 620–630.

Jaynes, E. T. (1982). "On the rationale of maximum entropy methods." *Proc., IEEE*, 70, 939–952.

Shannon, C. E. (1948). "A mathematical theory of communications, I and II." *Bell Sys. Tech. J.*, 27, 379–443.

Singh, V. P. (1993). *Elementary hydrology,* Prentice Hall, Englewood Cliffs, NJ.

Singh, V. P. (1998). *Entropy-based parameter estimation in hydrology,* Kluwer Academic, Boston.

Singh, V. P. (2010). "Derivation of rating curves using entropy theories." *Trans. ASABE*, 53(6), 1811–1821.

Additional Reading

Chiu, C.-L. (1987). "Entropy and probability concepts in hydraulics." *J. Hydraul. Eng.*, 113(5), 583–600.

Clarke, R. T. (1999). "Uncertainty in the estimation of mean annual flood due to rating-curve indefinition." *J. Hydrol.*, 222, 185–190.

DeGagne, M. P. J., Douglas, G. G., Hudson, H. R., and Simonovic, S. P. (1996). "A decision support system for the analysis and use of stage–discharge rating curves." *J. Hydrol.*, 184, 225–241.

Herschy, R. W. (1995). *Streamflow measurements*, 2nd Ed., Chapman & Hall, London.

Kennedy, E. J. (1964). "Discharge rating at gaging stations." Chapter A10, Book 3: *Applications of hydraulics*, U.S. Geological Survey, Washington, DC.

Lambie, J. C. (1978). "Measurement of flow-velocity-area-methods." Chapter 1. In *Hydrometry: Principles and practices*, R. W. Herschy, ed., Wiley, Chichester, UK.

Lee, W. S., Lee, K. S., Kim, S. U., and Chung, E. S. (2010). "The development of rating curve considering variance function using pseudo-likelihood estimation method." *Water Resour. Manage.*, 24, 321–348.

Overlier, P. (2006). "Modeling stage–discharge relationships affected by hysteresis using the Jones formula and nonlinear regression." *Hydrolog. Sci.*, 51(3), 365–388.

Petersen-Overleir, A. (2004). "Accounting for heteroscedasticity in rating curve estimates." *J. Hydrol.*, 292, 173–181.

Petersen-Overleir, A., and Reiten, T. (2005). "Objective segmentation in compound rating curves." *J. Hydrol.*, 311, 188–201.

Sauer, V. B., and Meyer, R. W. (1992). "Determination of error in individual discharge measurements." *U.S. Geological Survey Open-File Report, 92–144*, U.S. Geological Survey, Washington, DC.

Schmidt, A. R., and Yen, B. C. (2002). "Stage–discharge ratings revisited. Hydraulic measurements and experimental methods." *Proc., EWRI and IAHR Joint Conf.*, Colorado Springs, CO, ASCE, Reston, VA.

Siavapragasam, C., and Mutill, N. (2005). "Discharge curve extension—A new approach." *Water Resour. Manage.*, 19, 505–520.

Singh, V. P. (2010a). "Entropy theory for derivation of infiltration equations." *Water Resour. Res.*, 46, 1–20, W03527, doi: 10-1029/2009WR008193.

Singh, V. P. (2010b). "Tsallis entropy theory for derivation of infiltration equations." *Trans. ASABE*, 53(2), 447–463.

Singh, V. P. (2010c). "Entropy theory for movement of moisture in soils." *Water Resour. Res.*, 46, 1–12, W03516, doi: 10-1029/2009WR008288.

Torsten, D., Gerd, M., and Torsten, S. (2002). "Extrapolating stage–discharge relationships by numerical modeling." *Proc., Int. Conf. Hydraul. Eng.*, Warsaw, Poland.

World Meteorological Organization. (1994). *Guide to hydrological practices*. 5th Ed., WMO-No. 168, World Meteorological Organization, Geneva.

Yoo, C., and Park, J. (2010). "A mixture-density-network based approach for finding rating curves: Facing multimodality and unbalanced data distribution." *KSCE J. Civil Eng.*, 14(2), 243–250.

This page intentionally left blank

Part 6

Water Distribution Systems

This page intentionally left blank

Chapter 16

Reliability of Water Distribution Systems

A typical urban water supply system is comprised of five subsystems: water source, bulk transmission, treatment facility, finished water storage, and water distribution system. A nonurban water distribution system may simply be composed of a network of pipes along with pumps, valves, and storage tanks. Each subsystem can be investigated separately as a system. In general, pumps, storage systems, and bulk transmission and treatment are designed with significant redundancy. That is why large municipal water distribution systems do not fail completely when there is a breakage of a pipe, or a pump, or other components. Pipes are of different sizes and carry water to demand centers. Pipes and pumps account for a large portion of the network cost, and their physical condition greatly determines the network reliability (Germanopoulos et al. 1986).

A water distribution network is represented as nodes connected by links that are made up of pipes and valves. Nodes are demand centers that are fed with water carried by links. The sources of water are denoted as nodes because water flows into them during low water demand and out of them during high demand. Both pipes and pumps are represented as links. Each pipe has a diameter, and each pump has a pumping capacity in terms of flow rate and static head. Valves are located on the links, and they control the direction and magnitude of flow in the links; therefore, they are indicated by arrows. Junctions of links without demands are not considered to be nodes. In this manner, all the components of a water distribution network are considered links (arcs) or nodes (sinks).

Thus, from the standpoint of evaluating performance, a water distribution network is comprised of sources (one or more), nodes (demand points), and links (or pipes). A node represents a group of consumer units of water assigned to the end of the nearest link. Links are pipe mains. In the design, only pipes are considered, and small service pipes connecting to households may be ignored. Traditional designs are based on relationships among the parameters of flow, diameter, and head loss within a pipe. Because the objective of the network is to supply water to meet demand at demand nodes, the water can be supplied to a demand node through one or more links. The links can receive the water directly from the source or from a node. Thus, there can be many layouts for water distribution networks, depending on the way water is supplied. Fig. 16-1 shows a

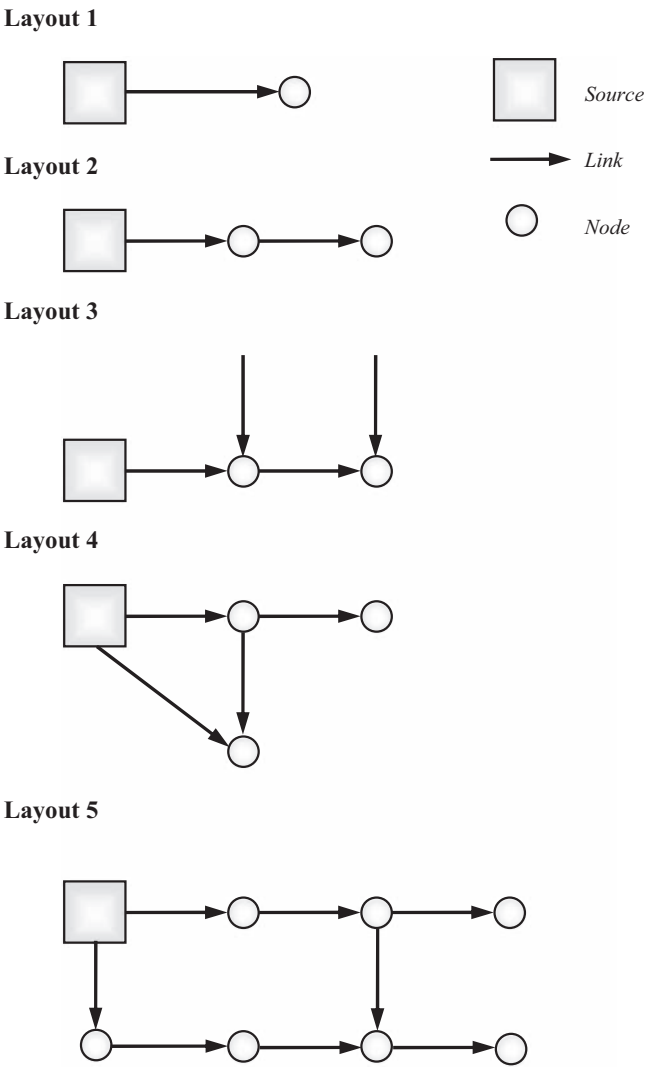

Figure 16-1a *Eight simple layouts.*

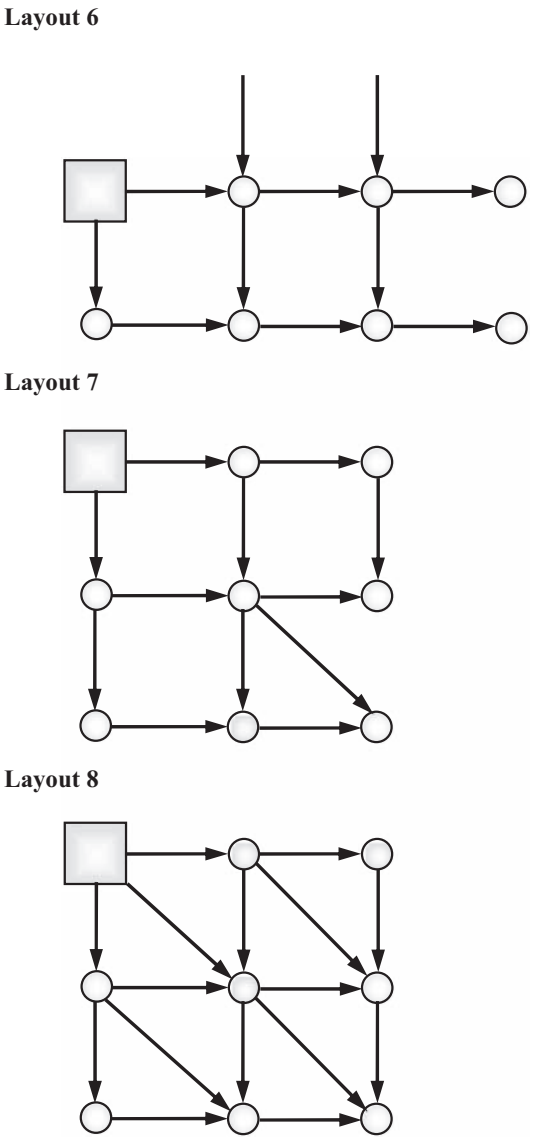

Figure 16-1a, *Continued*

sample of water distribution network layouts. These networks are designed for different demands and have different levels of reliability in terms of meeting demand at nodes in case one or more links fail, which is not unusual in real life.

Consider, for example, a single demand node, as shown in Fig. 16-2, with a demand flow of Q (m^3/h). This demand flow is satisfied in five alternative ways. It can be argued that layouts B, C, D, and E have redundant flow links or flow paths. It is intuitive to assume that in case of a link or pipe failure, the layout with more pipes feeding into the demand node is more reliable. Thus, it can be surmised that greater redundancy leads to greater reliability. Fundamentally,

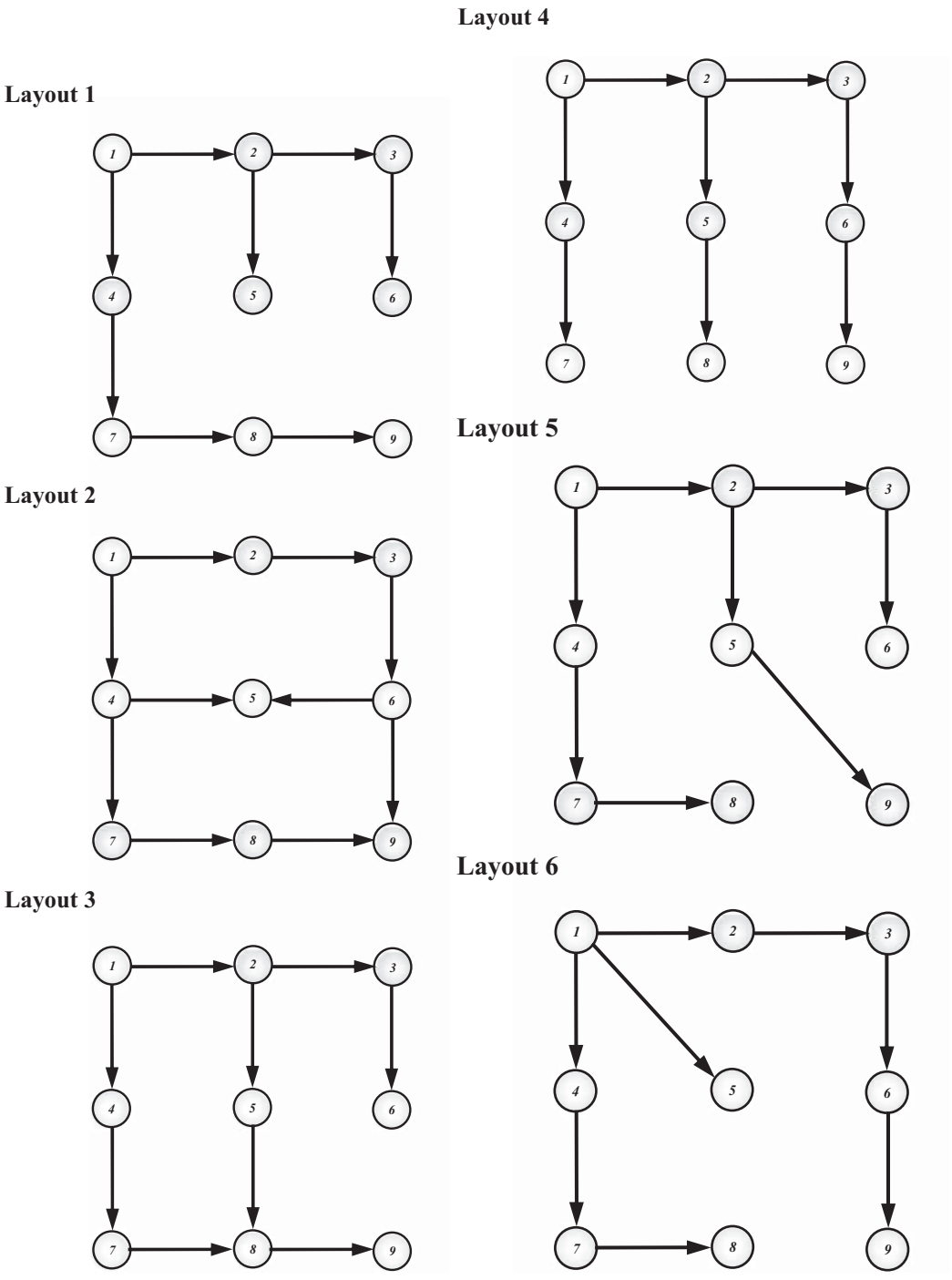

Figure 16-1b *Six alternative simple layouts.*

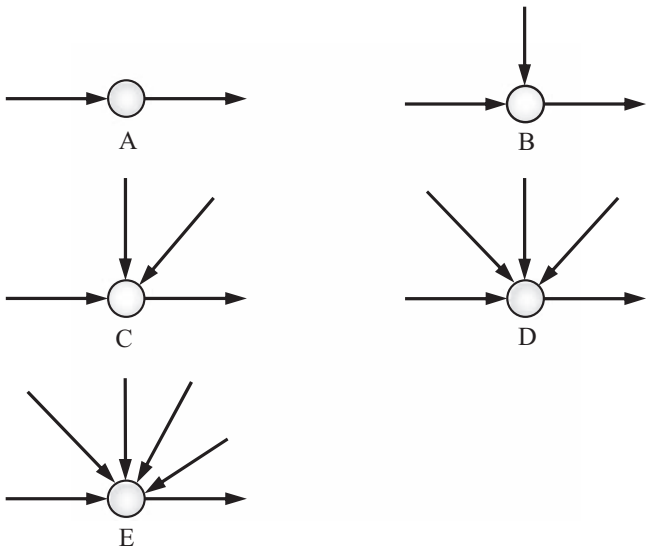

Figure 16-2 *Five single-node water distribution layouts.*

redundancy in a water distribution network means that demand points or nodes have alternative supply paths for water in the event that some links go out of service. In a redundant network, there is sufficient residual capacity to meet water flow requirements. For example, if any two links in layout D happen to go out of operation, demand can be met with supply from the other two links. Thus, redundancy is a characteristic of a water distribution system and is related to its reliability. This statement leads us to suggest that redundancy can be used as a measure of reliability. To ensure reliability, water distribution network design must incorporate some amount of redundancy.

Since the flow required for a node in the water distribution system is distributed in or carried by the links incident on the node, it is logical to interpret the redundancy at this node as a measure of disorder or diversity. These incident links are alternate paths, and clearly this disorder or diversity is related to the number of these paths or links. Now consider a case where there is only one link or flow path between the source and the node, implying a single link incident on the demand node. Then this system can be considered as a perfectly ordered system, because the geometric configuration of the system is a branched network type or a network that has no loops. This system has no redundancy, and there is a complete knowledge about the flow distribution in the system. For a given demand pattern or design demands, one can compute flow rates in all pipes by working backward from a demand node and accumulating demand flows in each pipe up to a source node. This situation means that there is no uncertainty, no disorder, and no diversity and, hence, that its entropy is zero. Conversely, if there are alternate paths or links caused by the presence of loops carrying flows to the node, there is the possibility of flow variation in the links and, hence,

diversity or disorder and redundancy. In this case, the knowledge about the flow distribution in links is less than complete, implying nonzero system entropy. In this case, the system is more reliable. Thus, it is intuitive that one would want to maximize redundancy or disorder at the node. Hence, redundancy or reliability can be quantified using entropy.

This chapter focuses on the water distribution system only and discusses network reliability, which is evaluated in terms of the rate of failure of components and their effect on the network, and the failure of the network to provide the required level of service during critical conditions. Discussion in the chapter draws heavily from the work of Awumah (1990) and Awumah et al. (1991). The need for reliability stems from uncertainties in consumer demand, fire flow requirements and their locations, pumping system failures, inefficient storage, pipe failures and their locations, valve leakages and their locations, and reduced capacity caused by sedimentation. Goulter (1988) argues that the shape or layout of a network determines the level of reliability that can be imposed on the network.

16.1 Preliminary Considerations

16.1.1 Concept of Redundancy

Redundancy means that a network, which is composed of components, remains useful if one or more of its constituent components fail. This usefulness occurs, because the service provided by the failed components is taken over by other functioning components. In other words, the system provides backup capability. This design is how redundancy increases reliability of the network. The redundancy can be provided in many ways, depending on the nature of the geometric configuration. The effect of adding redundancy can be evaluated by a measure of the reliability of the system. If a system is such that its failure can be catastrophic, then a very high level of redundancy must be built into the components or stages that are considered critical to give high system reliability.

Redundancy may be applied at different levels to a multicomponent multistage system, such as at the component level, stage level, subsystem level, or the system level itself. In the case of the component level, redundant components are added in parallel to some components at a particular stage. In the case of the stage level, some stages may be duplicated using parallel connections. In the case of the subsystem level, a group of stages forming the subsystem may be duplicated. In the case of the system level, the entire system is duplicated.

Redundancy is a characteristic of the network geometry that is related to its reliability. Thus, redundancy can be considered as a reliability measure, reflecting resilience or flexibility of the network to external factors. In other words, if a network is truly redundant, then if a component fails the network has enough residual capacity to meet all flow requirements. When a network is old and requires frequent maintenance and reconstruction, the redundancy built into the

system at the planning stage comes in handy and seems to be the only way to continue to provide uninterrupted service as repair or reconstruction proceeds. This chapter discusses reliability via redundancy using entropy.

Redundancy can be expressed in terms of entropy, which is a measure of uncertainty. Redundancy at a particular node of a water distribution network can be viewed as a measure of uncertainty of the distribution of the required flow to the node in the links incident to the node, which are actually alternative flow paths. The uncertainty depends on the number of incident links that carry the water from the source to the node. If there is only one link between the source and the node, then the uncertainty or redundancy is zero; this configuration, which has one link incident on a demand node, can be considered a perfectly certain system, that is, the configuration has no uncertainty. If there are more links carrying water to the node, the system uncertainty increases.

16.1.2 Types of Redundancy

Two types of redundancy can be distinguished. The first is active redundancy, in which all system components keep functioning permanently and mutually share the burden of keeping the system functioning, even when some of the components are not strictly needed or are underused in the nonfailed state of components. If any one component fails, others keep the system functioning, either at its normal level or at a reduced level, depending on the built-in redundancy, until the failed component can be repaired or replaced. Examples include four aircraft engines and military reserves.

The second is passive redundancy, which involves arranging the redundant components in parallel to the regular components and keeping them in reserve. The redundant components are used only when regular components go out of service because of failure. Examples are the spare tire in a car or a standby electric generator in the event of failure of electricity.

In water distribution systems, mechanical and hydraulic redundancies are recognized. Hydraulic redundancy depends on the pumping head available, the availability of elevated storage tanks and their elevation, the time of the occurrence of failure, and the availability of the network to reverse flow in some links. It is a measure of the degradation of network performance that occurs, in terms of the percentage of the demand flow that can be supplied at some minimum pressure heads. Mechanical redundancy depends on the network layout (shape and size of components) and is a measure of the ability of the network to meet demand flows when a component fails, because water is carried by pipes. This type of redundancy is the focus of this chapter.

16.1.3 Relation to Reliability

Redundancy and reliability are related but are not one and the same. Reliability directly relates to probability and is stated by the percentage of times (or probability) the system is deemed to have operated without failure. Thus, it is a measure of the frequency of failure, and, hence, explicitly measures risk. Conversely,

redundancy ensures that the system continues to operate when any of the components that make up the system fail. Thus, redundancy relates only to the ability of the system to function in the event of failure and is not a measure of the frequency of the occurrence of failure. Because increased redundancy results in increased reliability, reliability and redundancy are positively correlated.

Redundancy improves reliability by reducing the frequency of failure of the system, because it ensures that component failures do not affect the system adversely. It may be noted that the frequency of system failure is different from the frequency of individual component failure. Redundancy is a property of the network geometric configuration that, in the event of pipe failures, determines if alternate supply paths can meet demand flows. The capacity of supply paths also becomes a factor in the redundancy measure. Thus, redundancy should incorporate both the layout structure and the hydraulic parameters, such as flow, within the layout. Conversely, reliability is a property of such things as the material, corrosion, age and strength of pipes, soil environment, distribution of demands, and fire requirements.

16.1.4 Units of Measuring Redundancy

Reliability can be measured on a scale of 0 to 1; zero means very unreliable, and one means highly reliable. Usually, a time frame is invoked when speaking of reliability. As a frequency measure, it is the fraction or the percentage of a given time span for which the component functions. Redundancy, however, depends on the factors, such as life span or design life, which must be taken into account for adequately stating the system performance. For example, it can be the number of alternative units of a component in the event of system failure. If the system performance is maintained at the normal level, its redundancy can be said to be one. If the system performance is a fraction, then the redundancy can be that fraction. In water distribution networks, one way to build redundancy is by providing looped networks, in other words, by providing two independent alternative paths from the source to each demand node. Thus, there is flexibility in developing a redundancy measure. However, the measure depends on the factors that lead to adequate system performance.

Factors that may be included in a redundancy measure entail (1) the reliability of the redundant component by comparison with the regular component; (2) the efficiency or the output of the system under the two conditions, that is, under regular conditions and when the redundant component alone is in service; and (3) the type of redundancy in place. Now consider the case of a regular component and a parallel redundant component where both components are of equal capacity. If the capacity of the component is what is required by the system to operate fully, then the system can be characterized as having a redundancy of one unit with respect to this component, and this situation can be denoted as level-one redundancy. If the redundant component is half as full, then one can characterize the redundancy as half instead of unity. Likewise, if the system, under emergency, can deliver only a small fraction of the normal output, then the redundancy can be taken as this fraction.

Redundancy can also be viewed a little differently. Consider the number of times or the proportion of time the system performs satisfactorily when each of the components fails in isolation and when failures occur one at a time. In this case, redundancy can be evaluated by removing a component from the system and then assessing the system performance. This step is repeated for each component. Then, redundancy can be measured by the system output in each case as a fraction of the required output. The system can be considered redundant with respect to a particular component if the system output does not degrade below the desired level.

In the case of passive redundancy, the number of extra components in reserve or in parallel with regular components can be considered as a measure of redundancy. However, in the case of active redundancy, the measure of redundancy is not straightforward. The reason is that all components of the system are in operation simultaneously, and neither of the components is totally regular nor totally redundant. In this case, if one component fails and the system continues to operate satisfactorily, then the system is redundant, but the unit it should have is not clear—should it be one? What happens when two components fail and the system continues to operate satisfactorily? Should it then have two units? What about more components failing? If the system output is a fraction of the required output, then the unit of redundancy can be a fraction. This discussion suggests that a universal definition of redundancy is lacking and so is its unit of measurement.

16.1.5 Redundancy in Water Distribution Networks

Clearly, a water distribution system must include some amount of redundancy through looped networks or through provision of independent paths of the source to each node, and there should be an appropriate measure of redundancy. The redundancy measure can be used to compare different network layouts, select the most appropriate layout, allocate redundancy within the distribution networks, determine the cost-redundancy frontier, and help with identifying the most reliable network.

A major component of a water distribution system is pumps, and the redundancy thereof is important. For the pump system, both types of redundancy can be provided. For smaller water distribution systems, it is usual to provide passive redundancy in the pump arrangement, because this component is relatively inexpensive. However, for large distribution systems, active redundancy is the norm, because large-capacity pumps are expensive for passive redundancy. Rather, multiple smaller pumps can be provided so that when one pump goes out of service others can keep running at a satisfactory level. Pumps are usually selected to meet peak flow demand, and, hence, they have built-in redundancy with reference to average flow conditions. Storage tanks, both elevated and underground, are compartmentalized tanks, adding redundancy in the active form to the system. When a particular tank is scheduled for maintenance, the system continues to function, because other tanks or compartments remain active. This fact explains why large distribution systems do not fail completely

because of the failure of a pipe or pump or other components, because there is a large amount of redundancy built into these systems.

16.1.6 Mechanical and Hydraulic Redundancies

In water distribution systems, two types of redundancy can be identified: mechanical and hydraulic. Mechanical redundancy is the property of the layout (shape and size of components) and is a measure of the ability of the network to meet demand flows when a component fails. Conversely, hydraulic redundancy is a measure of the degradation of network performance expressed by the percentage of the demand flow that can be supplied at some minimum pressure heads. Hydraulic redundancy depends on pumping head available, the availability of elevated tanks and their elevations, time of occurrence of failure, and the ability of the network to change direction of flow in some links. Hydraulic redundancy contributes to network reliability by considering the percentage of degradation of network as the level of failure of the network. The discussion in this chapter focuses on mechanical redundancy.

16.2 Entropy-Based Redundancy Measures

In designing a water distribution network, a critically important requirement is that the flow to a demand node must be carried by multiple links instead of just one link, and these links should be connected directly to the node. Although these links may carry equal or unequal proportions of flow to the demand node, Goulter and Coals (1986) and Walters (1988) have shown that from a reliability point of view it is more advantageous to carry equal proportions of flow for two reasons. First, in the case of unequal proportions of flow, network reliability is severely affected if the link carrying the larger proportion goes out of service. Second, it is hydraulically inefficient. To illustrate, let the discharge in a pipe connecting nodes i to j, q_{ij}, be expressed by the Hazen–Williams equation:

$$q_{ij} = kC_{ij}\frac{h_{ij}^{0.54}}{L_{ij}^{0.54}}D_{ij}^{2.63} \tag{16.1}$$

where C_{ij} is the Hazen–Williams roughness coefficient, L_{ij} is the pipe length, h_{ij} is the head loss through the pipe, D_{ij} is the pipe diameter, and k is the conversion factor for units. For a given pipe network, head loss and discharge are variable but length and diameter are fixed.

It is known from equation (16.1) that for a fixed pipe size, discharge q carried by a pipe is approximately proportional to the 0.54 power of the head loss h_L in that pipe, i.e., $q \propto h_L^{0.54}$ or approximately $h_L \propto q^2$. When a larger pipe fails and the flow is to be increased in a smaller pipe, then head loss would increase

quadratically as a function of discharge. For example, doubling the flow would quadruple the head loss, and tripling the flow would increase the head loss sixfold. Conversely, increasing the flow in a larger pipe would not cause the same order of head loss.

To develop a redundancy measure for a water distribution network, Awumah and Goulter (1989), Awumah et al. (1990, 1991), and Goulter (1992) defined four axioms. Following their work here, we consider a network with N nodes. Let the number of links incident at node j be $n(j)$. A particular link incident at node j is denoted by i; thus $i = 1, 2, 3, \ldots, n(j)$. Let the flow carried by this ith link to node j be denoted by q_{ij}, flow in pipe-connecting links incident on node j, or the total flow at node j by Q_j, and the fraction of flow carried by link i by W_{ij}. Then, for a particular flow pattern, fraction W_{ij} can be denoted by

$$W_{ij} = \frac{q_{ij}}{Q_j} \tag{16.2a}$$

Clearly,

$$\sum_{i=1}^{n(j)} W_{ij} = 1 \tag{16.2b}$$

where

$$Q_j = \sum_{i=1}^{n(j)} q_{ij} \tag{16.3}$$

W_{ij} defines the relative contribution of link i to flow at node j and is, therefore, an indicator of relative flow capacity of the link incident at node j. Thus, it can be construed as a measure of the potential contribution of the link to the required demand at the node if a link failed. Further, it enables consideration of relative flow capacities of links in the redundancy measure.

Let the redundancy at node j be denoted by S_j. According to Awumah et al. (1990), four axioms (in the next four sections) can now be stated.

16.2.1 Axiom 1

The first axiom states that S_j is a symmetric function of W_{ij}, the variable of redundancy:

$$S_j = S(W_{1j}, W_{2j}, \ldots, W_{n(j)j}) \tag{16.4}$$

This measure should be a property of the geometric configuration. Consider two identical networks where one is a replica of the other, but they differ in size. If the ratios of flows in links of their configuration are the same, the redundancy is the same. Equation (16.4) states that if the values of flows were interchanged, the redundancy measure should remain the same.

16.2.2 Axiom 2

The second axiom states that if the number of links incident on node j, $n(j)$, is one, then the redundancy at node j is zero, i.e.,

$$S_j = 0 \text{ if } n(j) = 1 \tag{16.5}$$

The number of links incident on node j represents the number of paths.

16.2.3 Axiom 3

The third axiom states that for a given number of links incident at node j, redundancy should be maximum if all flows are equally proportioned, i.e.,

$$S_j \rightarrow \text{maximum if } W_{1j} = W_{2j} = W_{3j} = \ldots = W_{n(j)j} \tag{16.6}$$

This notion implies that $q_{1j} = q_{2j} = \ldots = q_{n(j)j}$.

16.2.4 Axiom 4

The fourth axiom states that for a given node the maximum value of $S_j = S(W_{1j}, W_{2j}, \ldots, W_{n(j)j})$ should monotonically increase with $n(j)$. This axiom means that for equal flows through links, the redundancy at node j should increase with the number of incident links. Indeed, the closer the components in all their physical properties, the higher the redundancy. For unequal flows, the contribution to the redundancy by the link with the larger value of W_i should be less than the contribution by the link with a smaller W_j, i.e., if $W_i \geq W_j$, then $R_i \leq R_j$, where R_i and R_j are the relative contributions to redundancy by links i and j, respectively. This idea can be explained by observing that a system with a larger link is more vulnerable to the failure of a larger link and the system is less useful if this link fails.

It is desired that S_j be a continuous concave, symmetrical, and differentiable function of instances of W_i. Furthermore, the overall network redundancy is a weighted function of the nodal redundancies.

These four axioms are satisfied by the Shannon entropy (Shannon 1948). To develop a redundancy measure using the Shannon entropy, consider a network with N nodes in which these nodes constitute subsystems. The Shannon entropy of a node j can now be expressed in terms of W_{ij} as

$$S_j = -\sum_{i=1}^{n(j)} W_{ij} \ln W_{ij} = -\sum_{i=1}^{n(j)} \frac{q_{ij}}{Q_j} \ln \frac{q_{ij}}{Q_j} \tag{16.7}$$

where S_j is an entropic measure of redundancy at node j; this situation is called local redundancy. Maximizing S_j would maximize the redundancy of node j and is equivalent to maximizing entropy at node j. The maximum value of S_j is achieved when all instances of W_{ij} or q_{ij}/Q_j are equal. This situation occurs when all instances of q_{ij} are equal.

For the entire water distribution network, redundancy is a function of redundancies (S_j) of individual nodes in the network. The network redundancy or reliability, S_N, cannot be expressed as the sum of local or nodal redundancies:

$$S_N \neq \sum_{j=1}^{N} S_j \tag{16.8}$$

Now let Q_0 be the total flow in the network that is equal to the sum of flows in all links in the network, i.e.,

$$Q_0 = \sum_{j=1}^{N} Q_j \tag{16.9}$$

where N is the number of nodes in the network. It should be emphasized that Q_0 is not the total demand in the network or the total flow supply to the network; it is usually greater than the total demand in the network. To assess the overall network redundancy, the relative importance of a link to the total flow should, if a link fails, be recognized, i.e., q_{ij}/Q_0. The importance of a link relative to the local flow is not as important, and that is the reason that the network redundancy is not a sum of nodal redundancies. Therefore, in equation (16.7), q_{ij}/Q_j should be replaced by q_{ij}/Q_0:

$$S_j^* = -\sum_{i=1}^{n(j)} \frac{q_{ij}}{Q_0} \ln \frac{q_{ij}}{Q_0} \tag{16.10a}$$

Then, the network redundancy can be expressed as

$$S_N = \sum_{j=1}^{N} S_j^* = -\sum_{j=1}^{N} \left[\sum_{i=1}^{n(j)} \frac{q_{ij}}{Q_0} \ln \frac{q_{ij}}{Q_0} \right] \tag{16.10b}$$

where S_N is the network redundancy and is a function of redundancies of individual nodes S_j^* in the network. In equation (16.10b), the summation is of the relative importance of links incident on a node, as opposed to the simple summation of the individual redundancies in the network. Equation (16.10b) can be simplified as

$$S_N = -\sum_{j=1}^{N} \left[\sum_{i=1}^{n(j)} \frac{q_{ij}}{Q_j} \frac{Q_j}{Q_0} \ln \frac{q_{ij}}{Q_j} \frac{Q_j}{Q_0} \right] \tag{16.11a}$$

or

$$S_N = -\sum_{j=1}^{N} \sum_{i=1}^{n(j)} \left(\frac{Q_j}{Q_0} \right) \left(\frac{q_{ij}}{Q_j} \right) \ln \frac{q_{ij}}{Q_j} - \sum_{j=1}^{N} \sum_{i=1}^{n(j)} \left(\frac{q_{ij}}{Q_j} \right) \left(\frac{Q_j}{Q_0} \right) \ln \frac{Q_j}{Q_0}] \tag{16.11b}$$

or

$$S_N = -\sum_{j=1}^{N} \frac{Q_j}{Q_0} \sum_{i=1}^{n(j)} \left(\frac{q_{ij}}{Q_j} \right) \ln \frac{q_{ij}}{Q_j} - \sum_{j=1}^{N} \frac{Q_j}{Q_0} \ln \frac{Q_j}{Q_0} \sum_{i=1}^{n(j)} \frac{q_{ij}}{Q_j} \tag{16.11c}$$

This set of equations shows that the term within brackets in equation (16.10b) expresses the individual contribution of node j, $\breve{S}_j$. Thus, considering the flow distribution at node j only, the contribution $\breve{S}_j$ to the network redundancy can be cast as

$$\breve{S}_j = \frac{Q_j}{Q_0} S_j - \frac{Q_j}{Q_0} \ln \frac{Q_j}{Q_0} \tag{16.12a}$$

It should be noted that $\breve{S}$ is different from S_j; $\breve{S}$ is the redundancy at a node considering the flow distribution at this node relative to the total network flow, whereas S_j is the redundancy at a node. Thus, the network redundancy can be expressed as

$$S_N = \sum_{j=1}^{N} \frac{Q_j}{Q_0} S_j - \sum_{j=1}^{N} \frac{Q_j}{Q_0} \ln \frac{Q_j}{Q_0} \tag{16.12b}$$

Equation (16.12b) yields the overall network redundancy, expressed as a weighted sum of nodal redundancies plus network entropy. The weight Q_j/Q_0 defines the ratio of flow passing through node j to the total flow or the contribution of flow at node j to the total flow. Thus, the first term in equation (16.12b) can be interpreted as nodal redundancy weighted by the relative flow or importance of the node. Thus, a node with a higher flow would be weighted more heavily than the one with a lower flow, even if they both have the same value of local redundancy. This statement recognizes the difference between nodes that have the same value of redundancy. Improvement in redundancy at an individual node can be achieved if flows in the links to the node can be equalized. This idea also has implications in repair, replacement, or maintenance of the network.

The second term on the right side in equation (16.12b) can be interpreted as the redundancy among nodes, because it is a measure of the distribution of flows to the nodes in the network. Because its form is the same as the Shannon entropy, it can be construed as the network entropy. Tanyimboh and Templeman (1993a, b) also used the Shannon entropy for computing maximum entropy flows in networks. If the flows among the nodes can be equalized, then improvement in the network redundancy can be achieved. This equalization would mean that the demand distribution among nodes would also have to be equalized. A network with nodes that have values of Q_j/Q_0 close to each other would have a better internodal measure of redundancy because it would be less vulnerable to the effect of pipe failures.

Xu and Jowitt (1992) derived equations (16.10a and 1610b) and (16.12a and 1612b) by recognizing that the use of entropy measure to operate on the proportions of flow is functionally equivalent to the entropy of the set $A \cap B$, where A and B are each a set of mutually exclusive propositions $A = (a_1, a_2, \ldots, a_{n)}$ and $B = (b_1, b_2, \ldots, b_n)$, such that $A \cap B$ is the set of mutually exclusively and collectively exhaustive (though not statistically independent) elements of the type $a_i \cap b_j$. The entropy measure of $A \cap B$ can be expressed as

$$S = -\sum_j \sum_i p(a_i b_j) \ln p(a_i b_j) \tag{16.13a}$$

or

$$S = -\sum_j \sum_i p(a_i|b_j)p(b_j)\ln p(a_i|b_j)p(b_j) \tag{16.13b}$$

or

$$S = -\sum_j p(b_j)\sum_i p(a_i|b_j)\ln p(a_i|b_j) - \sum_j p(b_j)\ln p(b_j)\sum_i p(a_i|b_j) \tag{16.13c}$$

Equation (16.13c) can be written as

$$S = -\sum_j p(b_j)S_{A|b_j} - S_B \tag{16.14}$$

where $S_{A|b_j}$ is the entropy associated with A conditioned on the occurrence of b_j; S_B is the entropy associated with B; $p(b_j)$ is the probability of b_j; and $p(a_i \mid b_j)$ is the probability of a_i conditioned on the occurrence of b_j. Equation (16.14) is equivalent to equation (16.12b).

Example 16.1 Using Xu and Jowitt (1992), consider three simple distribution network layouts, as shown in Fig. 16-3. The demand at point (node) A is one unit, and that at node B is 10 units. In configuration 2, the demand at point B is supplied via node A. Compute the redundancy of the three layouts.

Solution For layout 1,

$$S_A = -\sum_{i=1}^{n_A(j)} \frac{q_{ij}}{Q_j}\ln\frac{q_{ij}}{Q_j} = -2\times\frac{0.5}{1}\log_2\left(\frac{0.5}{1}\right) = 1 \text{ bit}$$

$$S_B = -\sum_{i=1}^{n_B(j)} \frac{q_{ij}}{Q_j}\ln\frac{q_{ij}}{Q_j} = -2\times\frac{5}{10}\log_2\left(\frac{5}{10}\right) = 1 \text{ bit}$$

For layout 2,

$$S_A = -2\times\frac{5.5}{11}\log_2\left(\frac{5.5}{11}\right) = 1 \text{ bit}$$

$$S_B = -2\times\frac{5}{10}\log_2\left(\frac{5}{10}\right) = 1 \text{ bit}$$

For layout 3,

$$S_A = -2\times\frac{0.5}{1}\log_2\left(\frac{0.5}{1}\right) = 1 \text{ bit}$$

$$S_B = -2\times\frac{5.5}{11}\log_2\left(\frac{5.5}{11}\right) = 1 \text{ bit}$$

The redundancy is the same for the three layouts.

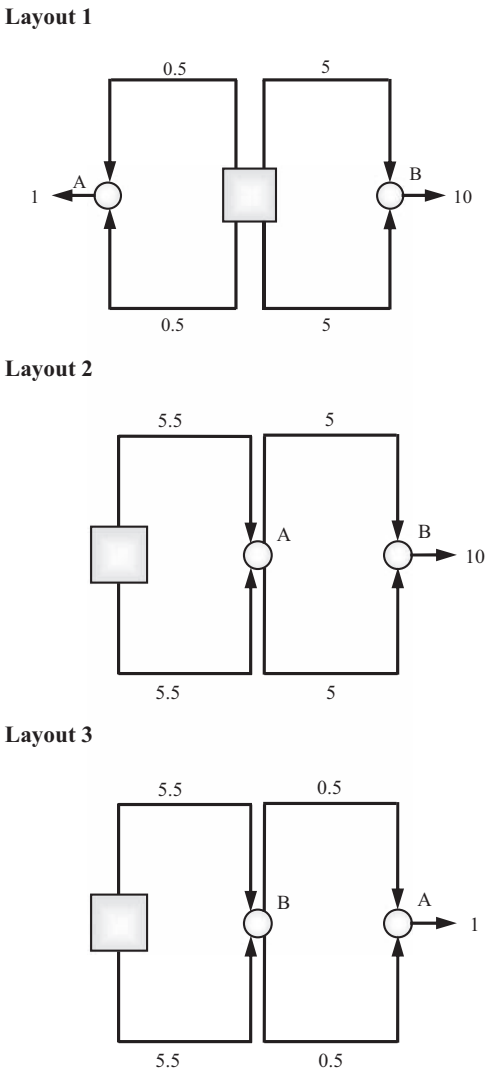

Figure 16-3 *Three simple distribution network layouts.*
Note*:* A *and* B *are demand nodes.*

Example 16.2 Consider five simple single-node layouts, as shown in Fig. 16-4. Compute the redundancy of each layout.

Solution *Case 1: A*. It has only one link, i.e., $n(j) = 1$. Therefore,

$$S_j = -\sum_{i=1}^{n(j)} \frac{q_{ij}}{Q_j} \ln \frac{q_{ij}}{Q_j} = -\frac{240}{240} \log_2 \left(\frac{240}{240} \right) = 0$$

This means that it has no redundancy.

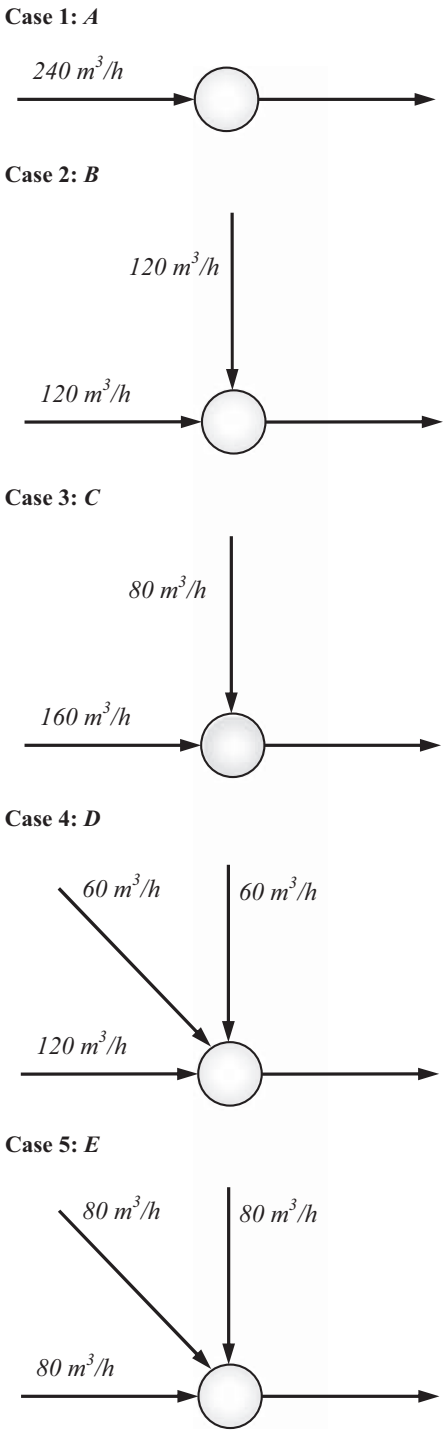

Figure 16-4 *Five simple single-node water distribution layouts.*

Case 2: B. It has two links, i.e., $n(j) = 2$, with equal flow. Therefore,

$$S_j = -\sum_{i=1}^{n(j)} \frac{q_{ij}}{Q_j} \ln \frac{q_{ij}}{Q_j}$$
$$= -\left[\frac{120}{240}\log_2\left(\frac{120}{240}\right)\right] - \left[\frac{120}{240}\log_2\left(\frac{120}{240}\right)\right] = -1\log_2\left(\frac{120}{240}\right) = 1 \text{ bit}$$

Case 3: C. It has two links i.e., $n(j) = 2$, with unequal flows. Therefore,

$$S_j = -\sum_{i=1}^{n(j)} \frac{q_{ij}}{Q_j} \ln \frac{q_{ij}}{Q_j}$$
$$= -\left[\frac{80}{240}\log_2\left(\frac{80}{240}\right)\right] - \left[\frac{160}{240}\log_2\left(\frac{160}{240}\right)\right] = 0.918 \text{ bit}$$

Case 4: D. It has three links, i.e., $n(j) = 3$, with unequal flows. Therefore,

$$S_j = -\sum_{i=1}^{n(j)} \frac{q_{ij}}{Q_j} \ln \frac{q_{ij}}{Q_j}$$
$$= -\left[\frac{120}{240}\log_2\left(\frac{120}{240}\right)\right] - \left[\frac{60}{240}\log_2\left(\frac{60}{240}\right)\right] - \left[\frac{60}{240}\log_2\left(\frac{60}{240}\right)\right] = 1.5 \text{ bit}$$

Case 5: E. It has three links, i.e., $n(j) = 3$, with equal flow. Therefore,

$$S_j = -\sum_{i=1}^{n(j)} \frac{q_{ij}}{Q_j} \ln \frac{q_{ij}}{Q_j} = -3 \times \left[\frac{80}{240}\log_2\left(\frac{80}{240}\right)\right] = 1.585 \text{ bit}$$

Since the higher the entropy, the higher the redundancy of the node, and, therefore, the more reliable the node, case 1 has only one input and one output. The entropy of the node is 0 bits, which means that if the incoming flow line fails, there shall be no outflow. Cases 2 and 3 have two incoming flows and one outflow. The flow in case 2 is equally distributed, and that in case 3 is distributed with a ratio of 2:1. The entropy is 1 bit for case 2 and 0.918 bit for case 3. The higher entropy of case 2 implies that the case with equally distributed inflow is more reliable than the case with nonequally distributed inflow. For example, if the probability of failure of pipes is half, case 2 is a better design than case 3. Cases 4 and 5 have three incoming pipes for one outflow. Both cases 4 and 5 give higher entropy values than does case 2; this fact means that a three-pipe arrangement is more suitable than a two-pipe arrangement. Furthermore, equal distribution of incoming flow, as in case 5, gives a higher entropy value than does case 4 (similar to cases 2 and 3 as discussed). Again, assuming the probability of failure to be equal for each pipe, case 5 is a more robust design capable of coping more efficiently with the failure of one inflow pipe.

Example 16.3 Consider the eight layouts shown in Fig. 16-5. The demand at the sources is 2,000 m^3/h. The demand at each node of layout 1 is specified in Table 16-1. Note that the sum of demands at nodes equals the demand at the source. Compute the redundancy of each layout and discuss which layout should be preferred.

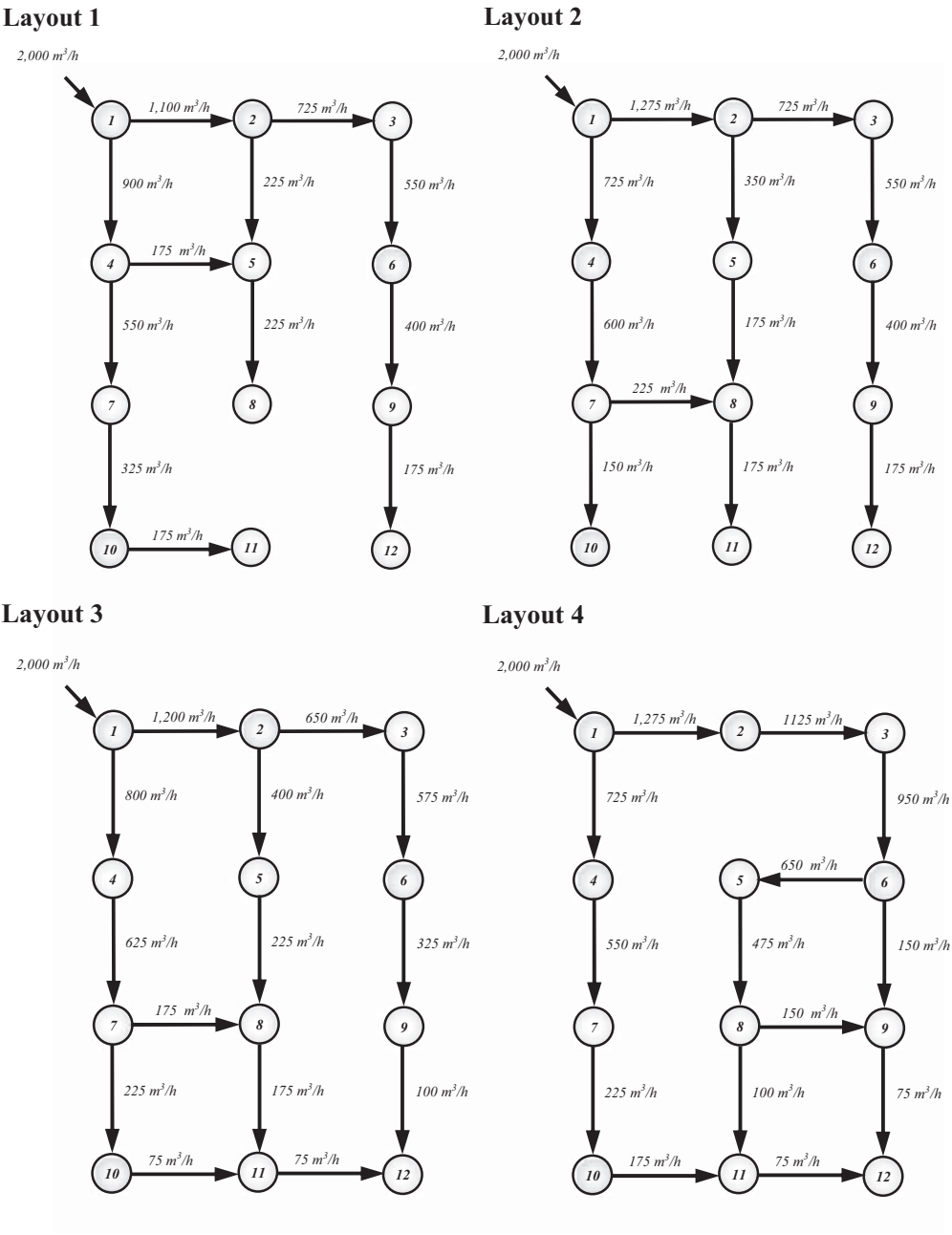

Figure 16-5 *Eight alternative water distribution network layouts.*

Layout 5

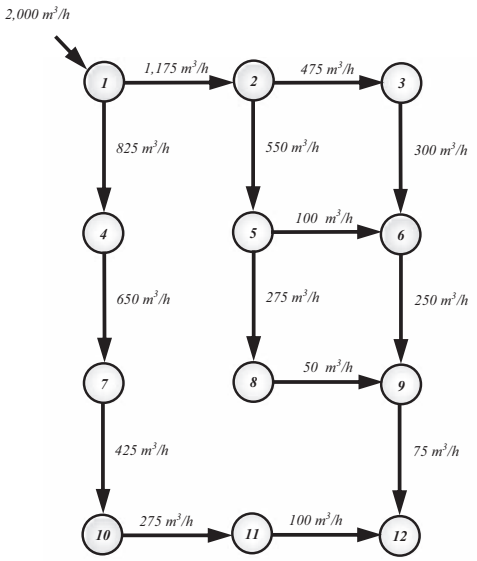

Layout 7

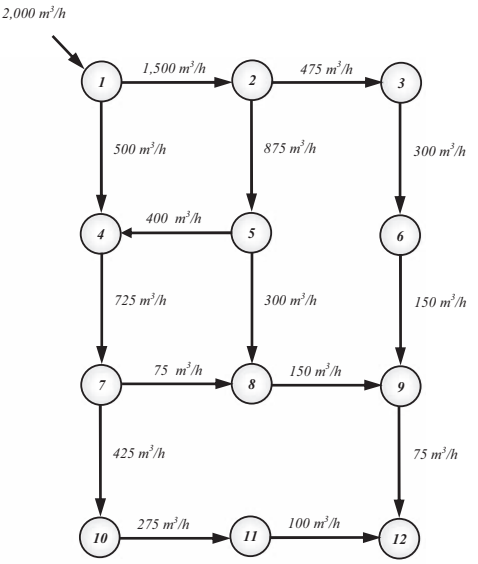

Layout 6

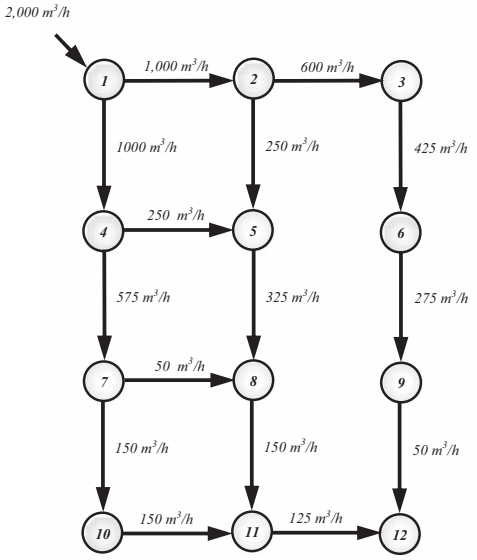

Layout 8

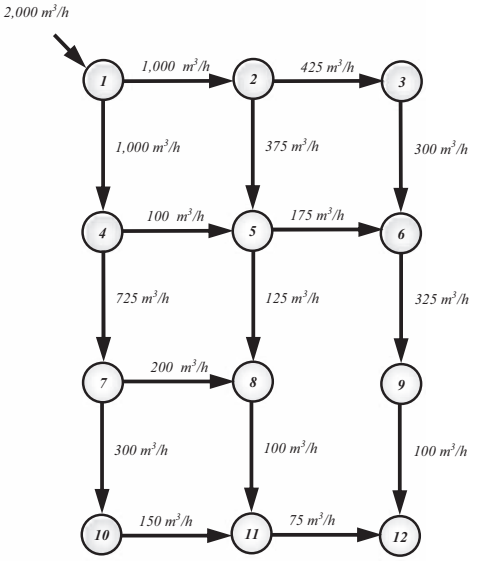

Figure 16-5, *Continued*

Table 16-1 *Demand at each node of 1ayout 1 in Example 16.3.*

Node	Demand (m^3/h)
1	2,000
2	150
3	175
4	175
5	175
6	150
7	225
8	225
9	225
10	150
11	175
12	175

Solution The network redundancy can be expressed as

$$S_N = \sum_{j=1}^{N} \frac{Q_j}{Q_0} S_j - \sum_{j=1}^{N} \frac{Q_j}{Q_0} \log \frac{Q_j}{Q_0}$$

Layout 1: In layout 1, for nodes 2, 3, 4, 6, 7, 8, 9, 10, 11, and 12, $S_j = 0$, as the number of link incidences equals one. The only node with redundancy is node 5, for which entropy is calculated as

$$\begin{aligned} S_5 &= -\frac{q_{25}}{Q_5} \log \frac{q_{25}}{Q_5} - \frac{q_{45}}{Q_1} \log \frac{q_{45}}{Q_5} \\ &= -\frac{225}{400} \log \frac{225}{400} - \frac{175}{400} \log \frac{175}{400} \\ &= 0.9887 \text{ bit} \end{aligned}$$

$$S_N = \frac{Q_5}{Q_0} S_5 - \sum_{j=1}^{N} \frac{Q_j}{Q_0} \log \frac{Q_j}{Q_0} = 3.3013 \text{ bits}$$

Therefore, the total redundancy of the network is 3.3013 bits.

Layout 2: In this layout, only for node 8, $S_j \neq 0$.

$$\begin{aligned} S_8 &= -\frac{q_{58}}{Q_8} \log \frac{q_{58}}{Q_8} - \frac{q_{78}}{Q_8} \log \frac{q_{78}}{Q_8} \\ &= -\frac{175}{400} \log \frac{175}{400} - \frac{225}{400} \log \frac{225}{400} \\ &= 0.9887 \text{ bit} \end{aligned}$$

$$S_N = \frac{Q_8}{Q_0} S_8 - \sum_{j=1}^{N} \frac{Q_j}{Q_0} \log \frac{Q_j}{Q_0} = 3.2653 \text{ bits}$$

Therefore, the total redundancy of the network is 3.2653 bits.

Layout 3: Entropy for nodes 1 to 12, except node 8, 11, and 12 is 0. Entropy values for nodes 8, 11, and 12 are calculated as

$$S_8 = -\frac{175}{400}\log\left(\frac{175}{400}\right) - \frac{225}{400}\log\left(\frac{225}{400}\right) = 0.9887 \text{ bit}$$

$$S_{11} = -\frac{175}{250}\log\left(\frac{175}{250}\right) - \frac{75}{250}\log\left(\frac{75}{250}\right) = 0.8813 \text{ bit}$$

$$S_{12} = -\frac{100}{175}\log\left(\frac{100}{175}\right) - \frac{75}{175}\log\left(\frac{75}{175}\right) = 0.9852 \text{ bit}$$

Total redundancy is

$$\begin{aligned} S_N &= \sum_{j=1}^{N} \frac{Q_j}{Q_0} S_j - \sum_{j=1}^{N} \frac{Q_j}{Q_0} \log \frac{Q_j}{Q_0} \\ &= \frac{Q_8}{Q_0} S_8 + \frac{Q_{11}}{Q_0} S_{11} + \frac{Q_{12}}{Q_0} S_{12} - \sum_{j=1}^{12} \frac{Q_j}{Q_0} \log \frac{Q_j}{Q_0} \\ &= 3.3853 \text{ bits} \end{aligned}$$

Layout 4: For this layout, entropy is zero for all nodes except nodes 9, 11, and 12 for which entropy values are calculated as

$$S_9 = -2 \times \frac{150}{300}\log\frac{150}{300} = 1 \text{ bit}$$

$$S_{11} = -\frac{100}{275}\log\frac{100}{275} - \frac{175}{275}\log\frac{175}{275} = 0.9457 \text{ bit}$$

$$S_{12} = -\frac{75}{150}\log\frac{75}{150} - \frac{75}{150}\log\frac{75}{150} = 1 \text{ bit}$$

Total redundancy is

$$\begin{aligned} S_N &= \sum_{j=1}^{N} \frac{Q_j}{Q_0} S_j - \sum_{j=1}^{N} \frac{Q_j}{Q_0} \log \frac{Q_j}{Q_0} \\ &= \frac{Q_9}{Q_0} S_9 + \frac{Q_{11}}{Q_0} S_{11} + \frac{Q_{12}}{Q_0} S_{12} - \sum_{j=1}^{12} \frac{Q_j}{Q_0} \log \frac{Q_j}{Q_0} \\ &= 3.3106 \text{ bits} \end{aligned}$$

Layout 5: For all nodes 1 to 12, except nodes 6, 9, and 12, entropy is 0. Entropy values for these three nodes are calculated as

$$S_6 = -\left[\frac{300}{400}\log\frac{300}{400} + \frac{100}{400}\log\frac{100}{400}\right] = 0.8113 \text{ bit}$$

$$S_9 = -\left[\frac{250}{300}\log\frac{250}{300} + \frac{50}{300}\log\frac{50}{300}\right] = 0.6500 \text{ bit}$$

$$S_{12} = -[\frac{100}{175}\log\frac{100}{175} + \frac{75}{175}\log\frac{75}{175}] = 0.9852 \text{ bit}$$

Total redundancy is

$$\begin{aligned} S_N &= \sum_{j=1}^{N}\frac{Q_j}{Q_0}S_j - \sum_{j=1}^{N}\frac{Q_j}{Q_0}\log\frac{Q_j}{Q_0} \\ &= \frac{Q_6}{Q_0}S_6 + \frac{Q_9}{Q_0}S_9 + \frac{Q_{12}}{Q_0}S_{12} - \sum_{j=1}^{12}\frac{Q_j}{Q_0}\log\frac{Q_j}{Q_0} \\ &= 3.3845 \text{ bits} \end{aligned}$$

Layout 6: For nodes 5, 8, 11, and 12, the entropy values are calculated as follows:

$$S_5 = -2\times\frac{250}{500}\log\frac{250}{500} = 1 \text{ bit}$$

$$S_8 = -\frac{50}{325}\log\frac{50}{325} - \frac{250}{325}\log\frac{250}{325} = 0.5665 \text{ bit}$$

$$S_{11} = -2\times\frac{150}{300}\log\frac{150}{300} = 1 \text{ bit}$$

$$S_{12} = -\frac{50}{175}\log\frac{20}{175} - \frac{125}{175}\log\frac{125}{175} = 0.8631 \text{ bit}$$

Total redundancy is

$$\begin{aligned} S_N &= \sum_{j=1}^{N}\frac{Q_j}{Q_0}S_j - \sum_{j=1}^{N}\frac{Q_j}{Q_0}\log\frac{Q_j}{Q_0} \\ &= \frac{Q_5}{Q_0}S_5 + \frac{Q_8}{Q_0}S_8 + \frac{Q_{11}}{Q_0}S_{11} + \frac{Q_{12}}{Q_0}S_{12} - \sum_{j=1}^{12}\frac{Q_j}{Q_0}\log\frac{Q_j}{Q_0} \\ &= 3.4502 \text{ bits} \end{aligned}$$

Layout 7: For this layout, entropy is 0 for all nodes except nodes 4, 8, 9, and 12, for which entropy values are

$$S_4 = -\frac{500}{900}\log\frac{500}{900} - \frac{400}{900}\log\frac{400}{900} = 0.9910 \text{ bit}$$

$$S_8 = -\frac{300}{375}\log\frac{300}{375} - \frac{75}{375}\log\frac{75}{375} = 0.7219 \text{ bit}$$

$$S_9 = -\frac{150}{300}\log\frac{150}{300} - \frac{150}{300}\log\frac{150}{300} = 1 \text{ bit}$$

$$S_{12} = -\frac{75}{175}\log\frac{75}{175} - \frac{100}{175}\log\frac{100}{175} = 0.9852 \text{ bit}$$

Total redundancy is

$$\begin{aligned} S_N &= \sum_{j=1}^{N}\frac{Q_j}{Q_0}S_j - \sum_{j=1}^{N}\frac{Q_j}{Q_0}\log\frac{Q_j}{Q_0} \\ &= \frac{Q_4}{Q_0}S_4 + \frac{Q_8}{Q_0}S_8 + \frac{Q_9}{Q_0}S_9 + \frac{Q_{12}}{Q_0}S_{12} - \sum_{j=1}^{12}\frac{Q_j}{Q_0}\log\frac{Q_j}{Q_0} \\ &= 3.4451 \text{ bits} \end{aligned}$$

Layout 8: Entropies for nodes 5, 6, 8, 11, and 12 are calculated as

$$S_5 = -\frac{100}{475}\log\frac{100}{475} - \frac{375}{475}\log\frac{375}{475} = 0.7425 \text{ bit}$$

$$S_6 = -\frac{300}{475}\log\frac{300}{475} - \frac{175}{475}\log\frac{175}{475} = 0.9495 \text{ bit}$$

$$S_8 = -\frac{200}{325}\log\frac{200}{325} - \frac{125}{325}\log\frac{125}{325} = 0.9612 \text{ bit}$$

$$S_{11} = -\frac{150}{250}\log\frac{150}{250} - \frac{100}{250}\log\frac{100}{250} = 0.9710 \text{ bit}$$

$$S_{12} = -\frac{75}{175}\log\frac{75}{175} - \frac{100}{175}\log\frac{100}{175} = 0.9852 \text{ bit}$$

Total redundancy is

$$\begin{aligned} S_N &= \sum_{j=1}^{N}\frac{Q_j}{Q_0}S_j - \sum_{j=1}^{N}\frac{Q_j}{Q_0}\log\frac{Q_j}{Q_0} \\ &= \frac{Q_5}{Q_0}S_5 + \frac{Q_6}{Q_0}S_6 + \frac{Q_{11}}{Q_0}S_{11} + \frac{Q_{12}}{Q_0}S_{12} - \sum_{j=1}^{12}\frac{Q_j}{Q_0}\log\frac{Q_j}{Q_0} \\ &= 3.5355 \text{ bits} \end{aligned}$$

Layout 8 has the highest redundancy.

16.3 Transmission of Redundancy through Network

In a water distribution network, nodes are connected to one another. Failure of one link affects not only the node upon which it is incident but also the downstream nodes, because the links upstream of the node service the downstream

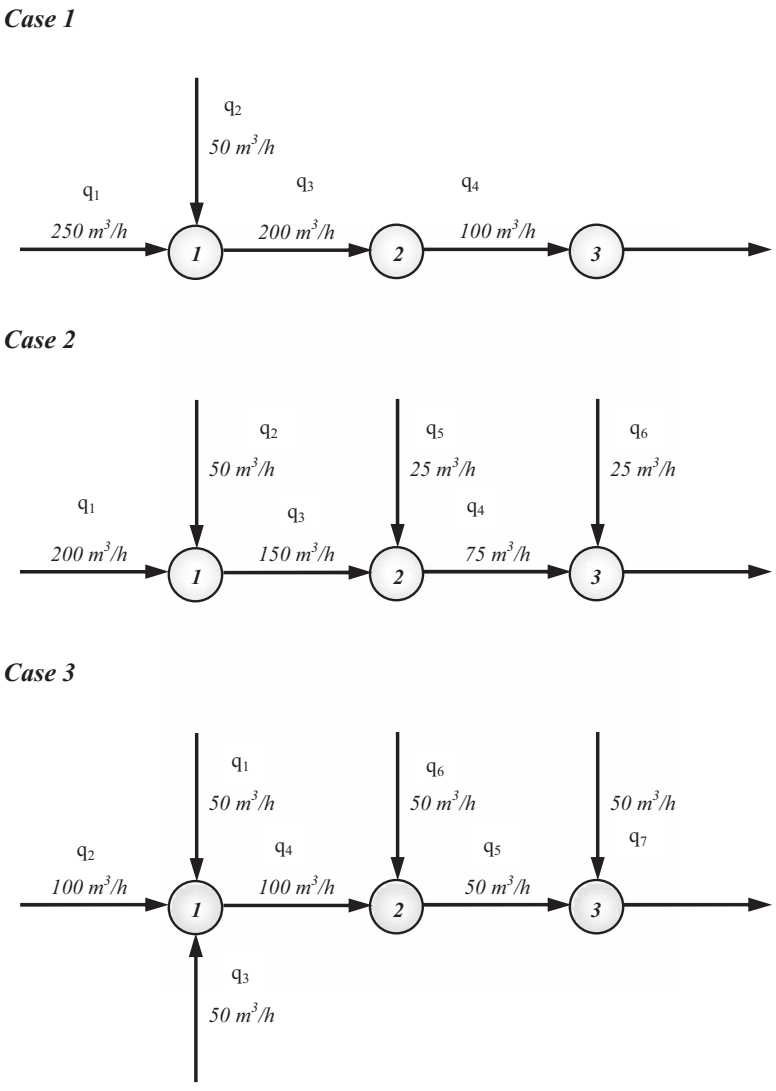

Figure 16-6 *Three simple layouts.*

nodes via redistribution of flows. Consider, for example, Fig. 16-6, which shows three simple networks in which one node receives flow from another. In the first network, node 1 has two independent paths or links and, hence, has some degree of redundancy. Node 2 receives flow from node 1 and hence has some redundancy caused by the redundancy in node 1. In other words, some redundancy may be transferred from node 1 to node 2. Likewise, node 3 has some redundancy because of the redundancy in node 2 and, hence, indirectly because of that in node 1. Intuitively, one can estimate the redundancy at node 2 by the proportion of flow coming from node 1 to the total flow coming into node 1. The implication here is that any shortfall at node 1 is transmitted downstream to node 2

and hence to node 3. Thus, redundancy from node 2 is transmitted to node 3 directly in proportion to the ratio of the total flow entering node 3 from node 2 to the total flow entering node 2. This ratio of flows defines what Awumah et al. (1991) called *transmissivity*. More precisely, transmissivity can be defined empirically as the ratio of the flow through the link to the total flow into node at the upstream end of the link. One can analyze networks 2 and 3 in a similar manner. In this sense, redundancy in one area of the network affects the redundancy in another.

To determine the propagation of redundancy in one node upstream to another node downstream, one can define the percentage of the redundancy at the upstream end that is transmitted to the downstream node and approximate it by the ratio of flow coming from that upstream node into the downstream node to the total flow entering the upstream node. Consider two nodes j and k. The transmissivity of the connection between these two nodes can be expressed as

$$t_{jk} = \frac{q_{kj}}{\sum_{l \in \breve{U}_k} q_{lj}} \tag{16.15}$$

where q_{kj} is the flow in link i incident on node j; t_{jk} is the transmissivity from node k to node j; and $\breve{U}_k$ is the set of nodes immediately upstream of node k. Note that flow is positive toward node k. The entropy measure defined by equation (16.7) can now be extended to include this consideration as

$$S'_j = S_j + \sum_{k \in \breve{U}_j} t_{jk} S'_k \tag{16.16}$$

where S'_j is the measure of the total (global) redundancy at node j.

Equation (16.16) shows that the global redundancy at node j is the sum of local redundancy at the node and the contribution from upstream supplies to the redundancy performance of that node. It should be noted that the global redundancy at each node depends on the global redundancy of all upstream nodes. Therefore, it may be necessary to apply equation (16.16) recursively with distance or with the number of nodes distant from the source. In this recursive manner, redundancy of a particular node caused by the redundancy at all upstream nodes is included in the redundancy measure of that node.

To illustrate the transmissivity concept, consider network layout 3 in Fig. 16-6. The global redundancy at node 1 (using simple notation of the figure) can be expressed as

$$\begin{aligned} S'_1 = S_1 = -\Bigg[& \frac{q_1}{q_1+q_2+q_3} \ln \frac{q_1}{q_1+q_2+q_3} + \frac{q_2}{q_1+q_2+q_3} \ln \frac{q_2}{q_1+q_2+q_3} \\ & + \frac{q_3}{q_1+q_2+q_3} \ln \frac{q_3}{q_1+q_2+q_3} \Bigg] \end{aligned} \tag{16.17}$$

For node 2,

$$S_2' = S_2 + t_{21} S_1' \tag{16.18}$$

where t_{21} is the transmissivity from node 1 to node 2 and is given by

$$t_{21} = \frac{q_4}{q_1 + q_2 + q_3} \tag{16.19}$$

Therefore,

$$S_2' = -\left[\frac{q_4}{q_4 + q_6} \ln\left(\frac{q_4}{q_4 + q_6}\right) + \frac{q_6}{q_4 + q_6} \ln\left(\frac{q_6}{q_4 + q_6}\right)\right] + \left[\frac{q_4}{q_1 + q_2 + q_3} S_1'\right] \tag{16.20}$$

Similarly, for node 3,

$$S_3' = S_3 + t_{32} S_2' \tag{16.21}$$

where t_{32} is the redundancy between nodes 2 and 3 and can be written as

$$t_{32} = \frac{q_5}{q_4 + q_6} \tag{16.22}$$

Note that transmissivities are always less than or equal to unity.

Example 16.4 Consider three simple layouts as shown in Fig. 16-6, Table 16-2, and Table 16-3. For each layout, indicate the number of loops and compute the redundancy measure derived from local redundancy and from global redundancy. Show redundancy at each node and redundancy among nodes. Discuss the results. Which layout is preferable?

Table 16-2 *Flow data for three simple layouts in Example 16.4.*

Case 1 Q	Flow (m^3/hr)	Case 2 Q	Flow (m^3/hr)	Case 3 Q	Flow (m^3/hr)
1	50	1	50	1	50
2	250	2	200	2	100
3	200	3	150	3	50
4	100	4	75	4	100
5		5	25	5	50
6		6	25	6	50
7				7	50

Table 16-3 Demand data for three nodes in Example 16.4.

Node	Flow (m^3/hr)
1	100
2	100
3	100

Solution To compute the global redundancy at a node S_j, transmissivity t_{jk} from node k to node j is taken into account. The global redundancy, S'_j, is calculated as follows:

Case 1

$$\begin{aligned} S_1 &= -\frac{q_1}{q_1+q_2}\log_2\frac{q_1}{q_1+q_2} - \frac{q_2}{q_1+q_2}\log_2\frac{q_2}{q_1+q_2} \\ &= -\frac{250}{300}\log_2\frac{250}{300} - \frac{50}{300}\log_2\frac{50}{300} \\ &= 0.65 \text{ bit} \end{aligned}$$

In this case,

Node 1: $$S'_1 = S_1$$

Node 2: $$S'_2 = S_2 + t_{21}S'_1$$

$$S_2 = -\frac{200}{200}\log_2\frac{200}{200} = 0 \text{ bit}$$

$$t_{21} = \frac{q_3}{q_1+q_2} = \frac{200}{250+50} = \frac{2}{3} = 0.67$$

$$S'_2 = 0.0 + 0.67 \times 0.65 = 0.43 \text{ bit}$$

Node 3: $$S'_3 = S_3 + t_{32}S'_2$$

$$S_3 = -\frac{100}{100}\log_2\frac{100}{100} = 0 \text{ bit}$$

$$t_{32} = \frac{q_4}{q_3} = \frac{100}{200} = 0.5$$

Therefore,

$$S'_3 = 0 + 0.5 \times 0.44 = 0.22 \text{ bit}$$

Case 2

Node 1: $S_1' = S_1$

$$S_1' = -\frac{q_1}{q_1+q_2}\log_2\frac{q_1}{q_1+q_2} - \frac{q_2}{q_1+q_2}\log_2\frac{q_2}{q_1+q_2}$$
$$= -\frac{50}{250}\log_2\frac{50}{250} - \frac{200}{250}\log_2\frac{200}{250}$$
$$= 0.72 \text{ bit}$$

Node 2: $S_2' = S_2 + t_{21}S_1$

$$S_2 = -\frac{150}{175}\log_2\frac{150}{175} - \frac{25}{175}\log_2\frac{25}{175} = 0.59 \text{ bit}$$

$$t_{21} = \frac{q_3}{q_1+q_2} = \frac{150}{250} = 0.6$$

$$S_2' = 0.59 + 0.6 \times 0.72 = 1.02 \text{ bits}$$

Node 3: $S_3' = S_3 + t_{32}S_2'$

$$S_3 = -\frac{75}{100}\log_2\frac{75}{100} - \frac{25}{100}\log_2\frac{25}{100} = 0.81 \text{ bit}$$

$$t_{32} = \frac{q_4}{q_3+q_5} = \frac{75}{150+25} = 0.43$$

Therefore,

$$S_3' = 0.81 + 0.43 \times 1.02 = 1.25 \text{ bits}$$

Case 3

Node 1: $S_1' = S_1$

$$S_1' = -\frac{q_1}{q_1+q_2+q_3}\log_2\frac{q_1}{q_1+q_2+q_3} - \frac{q_2}{q_1+q_2+q_3}\log_2\frac{q_2}{q_1+q_2+q_3}$$
$$+ \frac{q_3}{q_1+q_2+q_3}\log_2\frac{q_3}{q_1+q_2+q_3}$$
$$= -\frac{50}{200}\log_2\frac{50}{200} - \frac{100}{200}\log_2\frac{100}{200} - \frac{50}{200}\log_2\frac{50}{200} = 1.5 = S_1'$$
$$= 1.5 = S_1' \text{ bits}$$

Node 2: $$S_2' = S_2 + t_{21} S_1'$$

$$S_2 = -\frac{50}{150}\log_2\frac{50}{150} - \frac{100}{150}\log_2\frac{100}{150} = 0.92 \text{ bit}$$

$$t_{21} = \frac{q_4}{q_1 + q_2 + q_3} = \frac{100}{200} = 0.5$$

$$S_2' = 1.5 + 0.5 \times 1.5 = 1.67 \text{ bits}$$

Node 3: $$S_3' = S_3 + t_{32} S_2'$$

$$S_3 = -\frac{50}{100}\log_2\frac{50}{100} - \frac{50}{100}\log_2\frac{50}{100} = 1 \text{ bit}$$

$$t_{32} = \frac{q_5}{q_4 + q_6} = \frac{50}{150} = 0.33$$

Therefore,

$$S_3' = 1.0 + 0.33 \times 1.67 = 1.56 \text{ bits}$$

In case 1, it is evident that there is only a small amount of redundancy, and the transmissivity of the nodes only further reduces the global redundancy. Case 2 appears to be more reliable, primarily because there is an additional link connecting to nodes 2 and 3. Case 3 is the most reliable, with a global redundancy almost twice that of case 2. This large increase is caused by the addition of a link feeding into node 1 and several links that have the same flow of 50 m^3/hr.

Example 16.5 Consider the eight simple layouts in Fig. 16-5. For each layout, indicate the number of loops, and then compute the redundancy measure derived from local redundancy and from global redundancy. Show redundancy at each node and redundancy among nodes.

Solution Calculating the local redundancy and global redundancy:

$$t_{jk} = \frac{q_{kj}}{\sum_{l \in \breve{U}_k} q_{lj}}$$

$$S_j' = S_j + \sum_{k \in \breve{U}_j} t_{jk} S_k'$$

where S_j' is the measure of total (global) redundancy at node j; S_j is the entropic measure of local redundancy at node j; t_{jk} is the transmissivity from node k to node j; and $\breve{U}_j$ is the set of nodes immediately upstream of node j.

Layout 1

There is one loop for this layout. For all nodes, except nodes 5 and 8, the total redundancy is 0.

For node 5: $$S_5' = S_5 = 0.9887 \text{ bit}$$

For node 8: $$S_8' = S_8 + t_{85}S_5' = 0 + \frac{225}{400}S_5' = 0.5561 \text{ bit}$$

$$S_N = \sum_{j=1}^{N} \frac{Q_j}{Q_0} S_j' - \sum_{j=1}^{N} \frac{Q_j}{Q_0} \ln \frac{Q_j}{Q_0} = \frac{Q_5}{Q_0} S_5' + \frac{Q_8}{Q_0} S_8' - \sum_{j=1}^{12} \frac{Q_j}{Q_0} \log_2 \frac{Q_j}{Q_0}$$
$$= 3.3239 \text{ bits}$$

Layout 2

There is one loop for this layout. For all nodes, except nodes 8 and 11, the total redundancy is 0.

$$S_8' = S_8 = 0.9887 \text{ bit}$$

$$S_{11}' = S_{11} + t_{118}S_8' = 0 + \frac{175}{400}S_8' = 0.4326 \text{ bit}$$

$$S_N = \sum_{j=1}^{N} \frac{Q_j}{Q_0} S_j' - \sum_{j=1}^{N} \frac{Q_j}{Q_0} \ln \frac{Q_j}{Q_0}$$
$$= \frac{Q_8}{Q_0} S_8' + \frac{Q_{11}}{Q_0} S_{11}' - \sum_{j=1}^{12} \frac{Q_j}{Q_0} \log_2 \frac{Q_j}{Q_0} = 3.2790 \text{ bits}$$

Layout 3

There are three loops for this layout. For all nodes, except nodes 8, 11, and 12, the total redundancy is 0. The redundancy values of these three nodes are calculated as follows:

For node 8: $$S_8' = S_8 = 0.9887 \text{ bit}$$

For node 11: $$t_{118} = \frac{175}{400} = 0.4375$$

$$S_{11}' = S_{11} + t_{118}S_8 = 0.8813 + 0.4375 \times 0.9887 = 1.3139 \text{ bits}$$

For node 12: $$S_{12} = 0.9852 \text{ bits}; t_{1211} = 75 / 250 = 0.3$$

$$S_{12}' = S_{12} + t_{1211}S_{11}' = 0.9853 + 0.3 \times 1.3139 \text{ bits}$$
bits

$$S_N = \sum_{j=1}^{N} \frac{Q_j}{Q_0} S'_j - \sum_{j=1}^{N} \frac{Q_j}{Q_0} \ln \frac{Q_j}{Q_0}$$
$$= \frac{Q_8}{Q_0} S'_8 + \frac{Q_{11}}{Q_0} S'_{11} + \frac{Q_{12}}{Q_0} S'_{12} - \sum_{j=1}^{12} \frac{Q_j}{Q_0} \log_2 \frac{Q_j}{Q_0} = 3.4168 \text{ bits}$$

Layout 4

There are three loops for this layout. For all nodes, except nodes 9, 11, and 12, the total redundancy is 0. The redundancy values of these three nodes are calculated as follows:

For node 9: $S'_9 = S_9 = 1 \text{ bit}$

For node 11: $S'_{11} = S_{11} = 0.9457 \text{ bit}$

For node 12: $S_{12} = 1 \text{ bit}$

$$t_{1211} = 75/275 = 0.2727$$

$$t_{129} = 75/300 = 0.25$$

$$S'_{12} = S_{12} + t_{1211} S'_{11} + t_{129} S'_9 = 1 + 0.2727 \times 0.9457 + 0.25 \times 1 = 1.5079 \text{ bits}$$

$$S_N = \sum_{j=1}^{N} \frac{Q_j}{Q_0} S'_j - \sum_{j=1}^{N} \frac{Q_j}{Q_0} \ln \frac{Q_j}{Q_0}$$
$$= \frac{Q_9}{Q_0} S'_9 + \frac{Q_{11}}{Q_0} S'_{11} + \frac{Q_{12}}{Q_0} S'_{12} - \sum_{j=1}^{12} \frac{Q_j}{Q_0} \log_2 \frac{Q_j}{Q_0} = 3.3387 \text{ bits}$$

Layout 5

There are three loops for this layout. For all nodes, except nodes 6, 9, and 12, the total redundancy is 0. The redundancy values of these three nodes are calculated as follows:

For node 6: $S'_6 = S_6 = 0.8113 \text{ bit}$

For node 9: $S'_9 = S_9 + t_{96} S'_6 = 0.6500 + \frac{250}{400} \times 0.8113 = 1.1571 \text{ bits}$

For node 12: $S'_{12} = S_{12} + t_{129} S'_9 = 0.9852 + \frac{75}{300} \times 1.1571 = 1.2745 \text{ bits}$

$$S_N = \sum_{j=1}^{N} \frac{Q_j}{Q_0} S'_j - \sum_{j=1}^{N} \frac{Q_j}{Q_0} \ln \frac{Q_j}{Q_0}$$
$$= \frac{Q_6}{Q_0} S'_6 + \frac{Q_9}{Q_0} S'_9 + \frac{Q_{12}}{Q_0} S'_{12} - \sum_{j=1}^{12} \frac{Q_j}{Q_0} \log_2 \frac{Q_j}{Q_0} = 3.4212 \text{ bits}$$

Layout 6

There are four loops for this layout. For all nodes, except nodes 5, 8, 11, and 12, the total redundancy is 0. The redundancy values of these three nodes are calculated as follows:

For node 5: $$S_5' = S_5 = 1 \text{ bit}$$

For node 8: $$S_8' = S_8 + t_{85} \times S_5' = 0.5665 + \frac{325}{500} \times 1 = 1.2165 \text{ bits}$$

For node 11: $$S_{11}' = S_{11} + t_{118} \times S_8' = 1 + \frac{150}{375} \times 1.2165 = 1.4866 \text{ bits}$$

For node 12: $$S_{12}' = S_{12} + t_{1211} \times S_{11}' = 0.8631 + \frac{125}{300} \times 1.4866 = 1.4825 \text{ bits}$$

$$S_N = \sum_{j=1}^{N} \frac{Q_j}{Q_0} S_j' - \sum_{j=1}^{N} \frac{Q_j}{Q_0} \ln \frac{Q_j}{Q_0}$$

$$= \frac{Q_5}{Q_0} S_5' + \frac{Q_8}{Q_0} S_8' + \frac{Q_{11}}{Q_0} S_{11}' + \frac{Q_{12}}{Q_0} S_{12}' - \sum_{j=1}^{12} \frac{Q_j}{Q_0} \log_2 \frac{Q_j}{Q_0} = 3.5429 \text{ bits}$$

Layout 7

There are four loops for this layout. There are two paths to node 12, 4–7–10–11–12 and 4–7–8–9–12.

For node 4: $$S_4' = S_4 = 0.9910 \text{ bit}$$

For node 7: $$S_7' = S_7 + t_{74} \times S_4' = 0 + \frac{725}{900} \times 0.9910 = 0.7983 \text{ bit}$$

For the path 4–7–10–11–12,

For node 10: $$S_{10}' = S_{10} + t_{107} \times S_7' = 0 + \frac{425}{725} \times 0.7983 = 0.4680 \text{ bit}$$

For node 11: $$S_{11}' = S_{11} + t_{1110} S_{10}' = 0 + \frac{275}{425} \times 0.4680 = 0.3028 \text{ bit}$$

For the path 4–7–8–9–12,

For node 8: $$S_8' = S_8 + t_{87} \times S_7' = 0.7219 + \frac{75}{725} \times 0.7983 = 0.8045 \text{ bit}$$

For node 9: $$S_9' = S_9 + t_{98} S_8' = 1 + \frac{150}{375} \times 0.8045 = 1.3218 \text{ bits}$$

Then for node 12,

$$S'_{12} = S_{12} + t_{129}S'_9 + t_{1211}S'_{11}$$
$$= 0.9852 + \frac{75}{300} \times 1.3218 + \frac{100}{275} \times 0.3028 = 1.4258 \text{ bits}$$

$$S_N = \sum_{j=1}^{N} \frac{Q_j}{Q_0} S'_j - \sum_{j=1}^{N} \frac{Q_j}{Q_0} \ln \frac{Q_j}{Q_0}$$
$$= \frac{Q_4}{Q_0} S'_4 + \frac{Q_7}{Q_0} S'_7 + \frac{Q_8}{Q_0} S'_8 + \frac{Q_9}{Q_0} S'_9 + \frac{Q_{10}}{Q_0} S'_{10} + \frac{Q_{11}}{Q_0} S'_{11} + \frac{Q_{12}}{Q_0} S'_{12} - \sum_{j=1}^{12} \frac{Q_j}{Q_0} \log_2 \frac{Q_j}{Q_0}$$
$$= 3.6136 \text{ bits}$$

Layout 8

There are five loops for this layout. There are two paths to node 12, 5–6–9–12 and 5–8–11–12.

For node 5: $S'_5 = S_5 = 0.7425$ bit

For node 6: $S'_6 = S_6 + t_{65} \times S'_5 = 0.9495 + \frac{175}{475} \times 0.7425 = 1.2231$ bits

For node 9: $S'_9 = S_9 + t_{96} \times S'_6 = 0 + \frac{325}{475} \times 1.2231 = 0.8369$ bit

For the path 5–8–11–12,

For node 8: $S'_8 = S_8 + t_{85} \times S'_5 = 0.9612 + \frac{125}{475} \times 0.7425 = 1.1566$ bits

For node 11: $S'_{11} = S_{11} + t_{118}S'_8 = 0.9710 + \frac{100}{325} \times 1.1566 = 1.3269$ bits

Then for node 12,

$$S'_{12} = S_{12} + t_{129}S'_9 + t_{1211}S'_{11}$$
$$= 0.9852 + \frac{100}{325} \times 0.8369 + \frac{75}{250} \times 1.3269 = 1.6408 \text{ bits}$$

$$S_N = \sum_{j=1}^{N} \frac{Q_j}{Q_0} S'_j - \sum_{j=1}^{N} \frac{Q_j}{Q_0} \ln \frac{Q_j}{Q_0}$$
$$= \frac{Q_5}{Q_0} S'_5 + \frac{Q_6}{Q_0} S'_6 + \frac{Q_8}{Q_0} S'_8 + \frac{Q_9}{Q_0} S'_9 + \frac{Q_{11}}{Q_0} S'_{11} + \frac{Q_{12}}{Q_0} S'_{12} - \sum_{j=1}^{12} \frac{Q_j}{Q_0} \log_2 \frac{Q_j}{Q_0}$$
$$= 3.6577 \text{ bits}$$

16.4 Extension of Entropy-Based Redundancy Measures

When a link connecting to a node fails, alternative paths that supply water to the node may originate some distance away in the immediate vicinity of the failed link. The number of these alternative paths significantly affects the network redundancy and reliability. This notion shows that equation (16.7) does not entirely represent the redundancy at a node. In the redundancy measures discussed thus far, it has been implicitly assumed that the number of alternative paths from source to a demand node (point) is the same as the number of links incident on the node. This assumption is not always realistic. Consider, for example, a demand node that has three incident links but flow to these three links from a source that passes through two links some distance upstream and there are no other alternative links, as shown in Fig. 16-7. In this case, the three paths from the source to the demand node are not independent. The contribution to the redundancy at a node by one of its incident links depends, therefore, on both the percentage of flow it brings to the node and also the number of paths between the supply source and the node via that link. In Fig. 16-7a, node 5 receives water through three paths: 1–2–5, 1–3–5, and 1–3–4–5, of which the latter two paths are independent. If link 4–5 fails, node 5 may continue to receive water through the remaining two paths. In this case, the network has redundancy because of alternative paths. From the source, there are two links that bring water: 1–2, and 1–3. If one of these two links fails, the demand at node 5 can still be met uninterrupted because of the availability of alternative paths. Of course, the redundancy in the two cases of failure is not the same. Likewise, in Figure 16-7b, node 7 receives water from three different links: 3–7, 5–7, and 6–7. Thus, the network has redundancy because even if one of these links failed, node 7 would continue to operate uninterrupted. Of course, the redundancy would depend on the failure of a particular link and its contribution of flow to node 7.

Now consider the two layouts in Fig. 16-8, where the redundancy of node 6 is analyzed. Incident link 5–6 in the two layouts is not the same because in layout A it has only one path from the source to node 6: 1–3–4–5–6; whereas in layout B, there are two paths: 1–3–4–5–6 and 1–3–5–6. If incident links 3–5 and 4–5 are carrying equal ratios of flow to node 6, then layout B should have more reliability. The redundancy measure should incorporate this consideration using what Awumah (1990) called *path parameter*. Let the path parameter for node j be a_j, which is considered to be equal to the number of alternative independent paths between the source and node j. This number of paths depends on the degree of overlap between paths. To that end, one needs to know the number of links used by different paths. Thus, the total number of independent paths may be less than the total number of paths. In the case of dependent paths, the effective alternative independent number of paths from the given number of dependent paths can be derived.

Consider three simple layouts as shown in Fig. 16-9. Network A has two independent paths: S–1–j and S–2–j; network B has two dependent paths: S–1–2–j

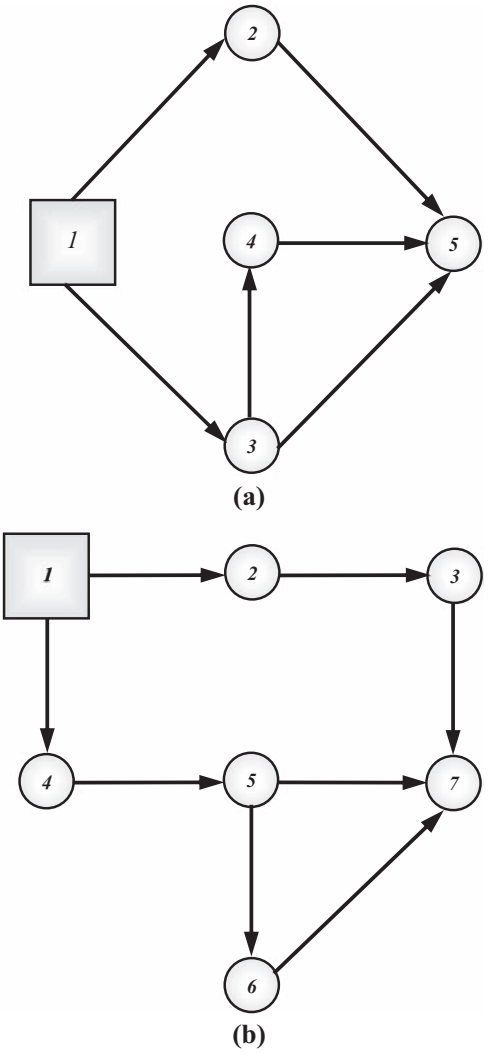

Figure 16-7 *(a) Water distribution network. (b) Water distribution network: 1 is source, 2, 3, 4, and 5 are demand nodes.*
Note: Node 5 received water from three lines, but paths are not independent.

and S–1–3–*j*; and network C has two dependent paths: S–1–2–4–*j* and S–1–3–4–*j*. Addition of link S–1 in the network effectively reduces the independence of paths from source S to node *j* because that link is shared by two paths. Similarly, addition of link 4–*j* further reduces the number of independent paths. Following Awumah (1990), let the number of paths to which a link belongs define the degree of that link. If different paths have no common links, then each link in these independent paths has one degree. If a link is common between two paths, as in network B of Fig. 16-9, then it has a degree of dependency of one unit. If the link is shared by three paths, then it has a degree of dependency of two units.

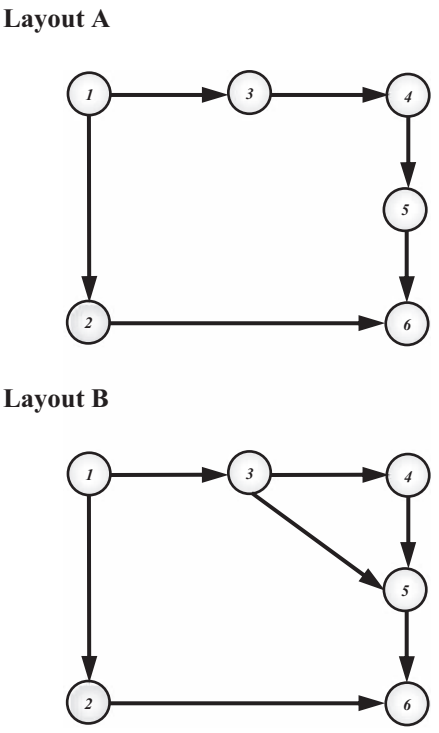

Figure 16-8 *Water distribution network: Availability of incident links.*

If the degree of link is denoted by d_l, then its degree of dependency D_l is given as

$$D_l = d_l - 1 \tag{16.23}$$

If the number of alternative dependent paths from the source to the given node is n_d, then the effective number of independent paths can be obtained by removing dependencies from the links. The required path parameter a_j, which is the adjusted number of independent paths, can be expressed for node j as

$$a_j = n_d \left[\frac{\sum_{l=1}^{M} d_l - \sum_{l=1}^{M} D_l}{\sum_{l=1}^{M} d_l} \right] \tag{16.24}$$

where M is the number of links in the n_d number of paths. Equation (16.24) can be written as

$$a_j = n_d \left[1 - \frac{\sum_{l=1}^{M} D_l}{\sum_{l=1}^{M} d_l} \right] \tag{16.25}$$

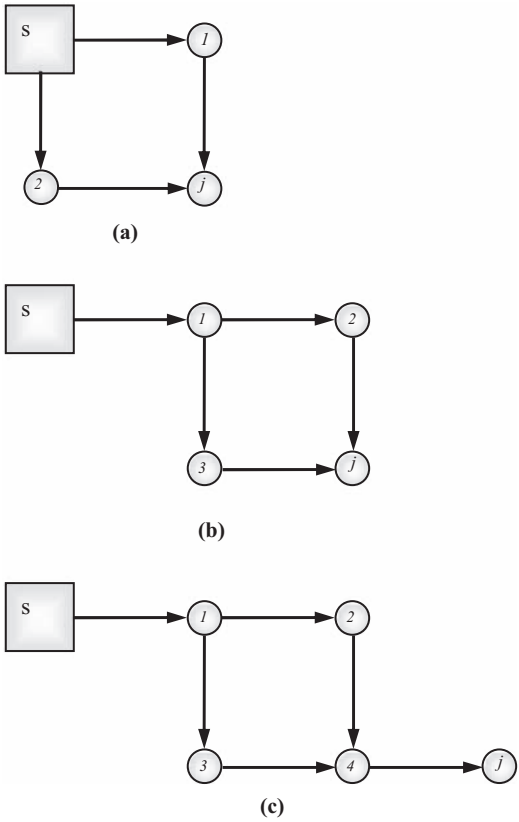

Figure 16-9 *Three alternative networks.*

The term within brackets is the factor that reduces the number of dependent paths to equivalent independent paths. For independent paths, the term $\sum_{l=1}^{M} D_l = 0$, and, hence, $a_j = n_d$. Equation (16.25) shows that the value of a_j decreases with increasing dependency, as seen from network A through C in Fig. 16-9.

To incorporate the path parameter in the entropy-based measure of dependency that is based on nodes, not on links, let a_{ij} denote the effective number of independent paths from the source through link ij from node i incident on node j, defined as

$$a_{ij} = n_{d_{ij}} \left[1 - \frac{\sum_{l=1}^{M_{ij}} D_l}{\sum_{l=1}^{M_{ij}} d_l} \right] \tag{16.26}$$

where $n_{d_{ij}}$ is the number of dependent paths from the source through link ij from node i incident on node j, and M_{ij} is the number of links in the $n_{d_{ij}}$ number of

paths. The total number of effective independent paths for node j, therefore, equals the sum of paths through node $n(j)$ incident links:

$$a_j = \sum_{l=1}^{n(j)} a_{ij} \tag{16.27}$$

Equation (16.27) permits a_j to take on noninteger values and is the total number of paths to node j, not the number of paths to a particular link. It may be noted that the lower bound for a_j would be unity in all cases and would then represent a single branch from the source to the demand point.

16.5 Modified Redundancy Measure with Path Parameter

Equation (16.7) can now be modified by including the path parameter as

$$S_j = -\sum_{i=1}^{n(j)} \frac{q_{ij}}{Q_j} \ln\left(\frac{q_{ij}}{a_{ij}Q_j}\right) \tag{16.28}$$

Note that the first term q_{ij}/Q_j does not have parameter a_{ij} because the objective is to increase the basic redundancy measure if the number of independent paths between the source and the node is greater than one. This goal is accomplished by dividing the term with the logarithm by a_{ij}. Note that $(q_{ij}/Q_j) < [q_{ij}/(a_{ij}Q_j) \leq 1]$; therefore, $\ln(q_{ij}/Q_j) > \ln[q_{ij}/(a_{ij}Q_j) \leq 1]$. This increase is significantly offset if the term outside of the logarithm is also divided by a_{ij}, which is larger than 1 for the node that has more than one independent path through incident link ij. Therefore, a_{ij} is not inserted in the term outside of the logarithm, and also the measure is qualitative at this juncture.

Equation (16.28) can be written as

$$S_j = -\sum_{i=1}^{n(j)} \left[\frac{q_{ij}}{Q_j}\right] \ln\left(\frac{q_{ij}}{Q_j}\right) + \sum_{i=1}^{n(j)} \left(\frac{q_{ij}}{Q_j}\right) \ln a_{ij} \tag{16.29}$$

The first term in equation (16.29) represents the redundancy measure for node j assuming independent paths from the source to node j, as defined by equation (16.7). The second term is a correction factor for reducing the number of alternative paths if some of the paths are dependent.

It may be interesting to note the usefulness of equation (16.29). First, in the case of nodes with one incident link but several paths through the network upstream of the single incident link, if the equivalent number of paths exceeds 1, then $a_{ij} > 0$ and the second term makes a positive contribution to the redundancy of the node. Second, for nodes with two or more incident links where each link is equal to one path from the source to the node, the second term ceases since $a_{ij} = 1$ and then equation (16.29) reduces to equation (16.7). Third, for nodes

with several incident links so that equivalent paths through some of these links are less than one, a_{ij} would be less than one, and the second term would be negative. Then the redundancy measure would be less than that given by equation (16.7). The path parameter would still be less than one since it measures total equivalent paths, not the value for a particular link.

Example 16.6 Consider the following two networks, as shown in Fig. 16-10. Compute the values of a_{ij}.

Solution

$$a_{ij} = n_{d_{ij}} \left[1 - \frac{\sum_{l=1}^{M_{ij}} D_l}{\sum_{l=1}^{M_{ij}} d_l} \right] a_j = \sum_{l=1}^{n(j)} a_{ij}$$

Layout 1

$$a_1 = a_{s1} = 1\, a_2 = a_{s2} = 1\, a_j = a_{1j} + a_{2j}$$

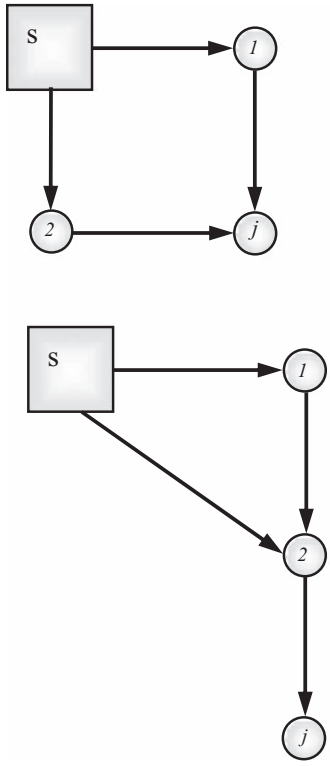

Figure 16-10 *Two simple networks.*

The number of paths through the link from node 1 to node *j*: $n_{d_{1j}} = 1$; the number of links in the $n_{d_{1j}}$ paths: $M_{d_{2j}} = 2$; the degree of links: $d_1 = d_2 = 1$. Thus $a_{1j} = 1$. Similarly, $a_{2j} = 1$. Therefore, $a_j = a_{1j} + a_{2j} = 2$.

Layout 2

$$a_1 = a_{s1} = 1.\ a_2 = a_{s2} + a_{12}$$

$$a_{s2} = 1\left(1 - \frac{0}{1}\right) = 1;\ a_{12} = 1\left(1 - \frac{0}{2}\right) = 1;\ a_2 = a_{s2} + a_{12} = 2$$

$a_j = a_{2j}.\ n_{d_{2j}} = 2,\ M_{d_{1j}} = 4,\ d_1 = d_2 = d_3 = 1,\ d_4 = 2$, therefore,

$$a_j = a_{2j} = 2\left(1 - \frac{1}{5}\right) = \frac{8}{5}$$

Example 16.7 Consider the layout as shown in Fig. 16-11. Compute the value of a_{ij}.

Solution Computation of the value of a_{ij} is done for different sub-networks as shown in Fig. 16-12.

$$a_1 = a_2 = a_3 = a_6 = 1$$

Node 4: $$a_4 = a_{14} + a_{34} = 1 + 1 = 2$$

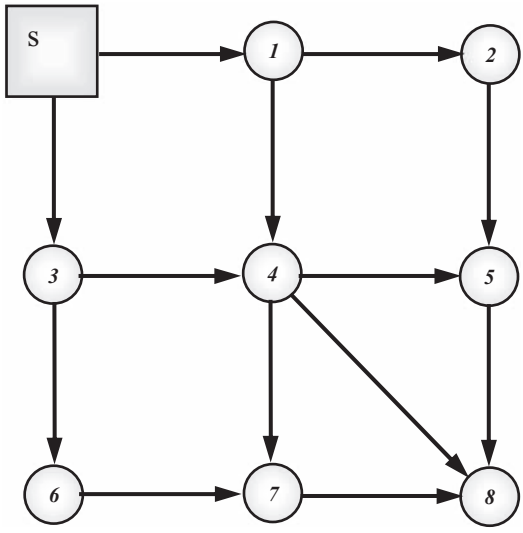

Figure 16-11 *A water distribution network layout.*

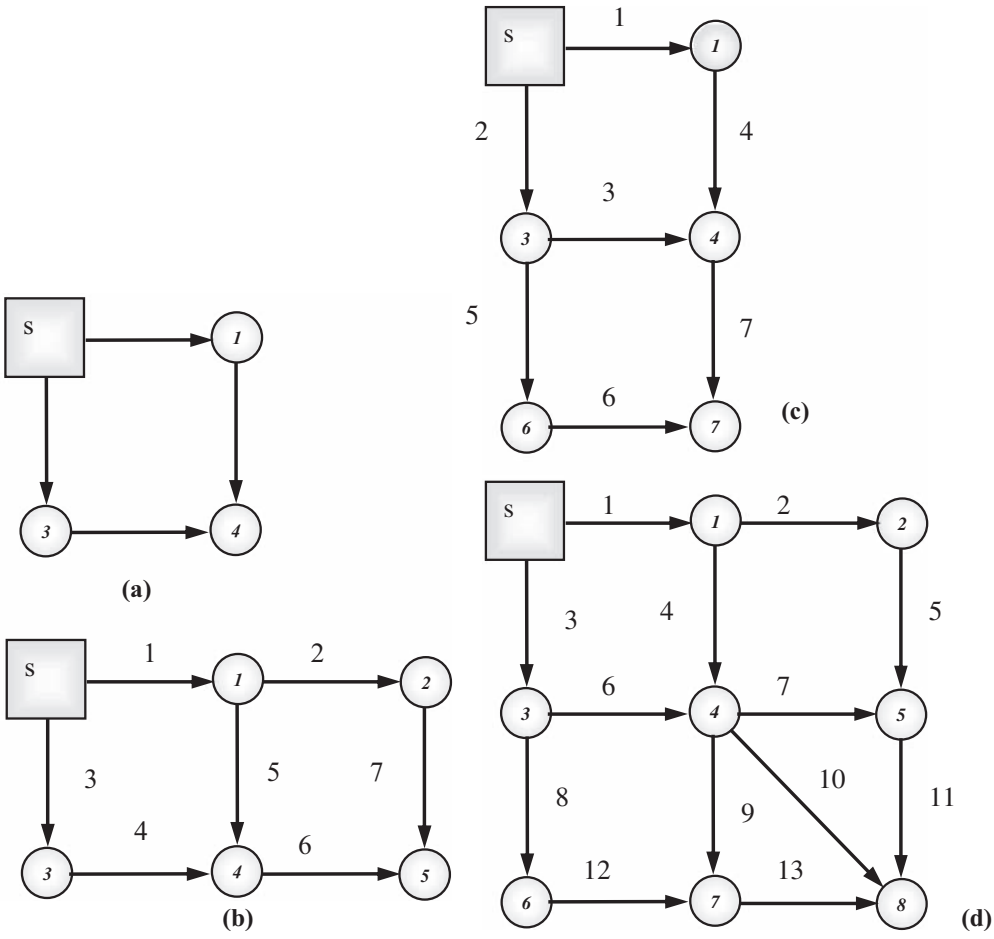

Figure 16-12 *(a) Two paths for node 4. (b) Three paths for node 5. (c) Three paths for node 7. (d) Paths for node 8.*

Node 5: There are three paths: s–1–2–5, s–1–4–5, and s–3–4–5.

$$d_2 = d_3 = d_4 = d_5 = d_7 = 1, d_1 = d_6 = 2$$

$$a_{25} = 1 - \frac{1}{4} = \frac{3}{4}; a_{45} = 2\left(1 - \frac{2}{7}\right) = \frac{10}{7}$$

$$a_5 = a_{25} + a_{45} = 2.18$$

Node 7: There are three paths to node 7: s–1–4–7, s–3–4–7, and s–3–6–7.

$$d_1 = d_3 = d_4 = d_5 = d_6 = 1; d_2 = d_7 = 2$$

$$a_{67} = 1 - \frac{1}{4} = \frac{3}{4}; a_{47} = 2\left(1 - \frac{2}{7}\right) = \frac{10}{7}; a_7 = a_{67} + a_{47} = 2.18$$

For node 8: There are eight paths to node 8: s–1–2–5–8, s–1–4–5–8, s–3–4–5–8, s–1–4–8, s–3–4–8, s–1–4–7–8, s–3–4–7–8, and s–3–6–7–8.

$$d_1 = 4, d_2 = 1, d_3 = 4, d_4 = 3, d_5 = 1, d_6 = 3, d_7 = 2,$$

$$d_8 = 1, d_9 = 2, d_{10} = 2, d_{11} = 3, d_{12} = 1, d_{13} = 3$$

$$a_8 = a_{48} + a_{58} + a_{78}$$

For a_{48}, there are two paths, s–1–4–8 and s–3–4–8, through link 10.

$$n_{d48} = 2; d_1 = 4, d_3 = 4, d_4 = 3, d_6 = 3, d_{10} = 2$$

$$a_{48} = 2\left(1 - \frac{11}{16}\right) = \frac{5}{8}$$

For a_{58}, there are three paths, s–1–2–5–8, s–1–4–5–8, and s–3–4–5–8, through link 11.

$$n_{d58} = 3; d_1 = 4, d_2 = 1, d_3 = 4, d_4 = 3, d_5 = 1, d_6 = 3, d_7 = 2, d_{11} = 3$$

Therefore,

$$a_{58} = 3\left(1 - \frac{13}{21}\right) = \frac{8}{7}$$

For a_{78}, there are three paths, s–1–4–7–8, s–3–4–7–8, and s–3–6–7–8, through link 13.

$$n_{d78} = 3; d_1 = 4, d_3 = 4, d_4 = 3, d_6 = 3, d_8 = 1, d_9 = 2, d_{12} = 1, d_{13} = 3$$

Therefore,

$$a_{78} = 3\left(1 - \frac{13}{21}\right) = \frac{8}{7}$$

$$a_8 = a_{48} + a_{58} + a_{78} = \frac{5}{8} + \frac{8}{7} + \frac{8}{7} \approx 2.91$$

16.6 Modified Redundancy Measure with Age Factor

Let u_{ij} be the age factor parameter for the pipe material in link ij. This factor reflects the degree of deterioration of the pipe with age and the consequent reduction in carrying capacity and its contribution to redundancy. If the Hazen–Williams formula for flow through pipes is used, then its friction coefficient C_{ij} (dimensionless) reflects the characteristic of the pipe material as well as its age.

Its value ranges from 100 to 150. For example, for steel and plastic pipes, it is between 140 and 150; for bricks, it is around 100. For cast iron pipes, the C values can degrade from about 130 to 75 over a period of 50 years. Awumah (1990) expressed the equation as

$$u_{ij} = 0.2 \ln C_{ij}(t) \tag{16.30}$$

where t is time after installation of pipes in years, C_{ij} is the Hazen–Williams friction factor for pipe between nodes i and j, and u_{ij} is the age factor after time t.

Awumah (1990) used $C = 150$ as the upper reference limit and scaled down all values therefrom. The reference point value for the age factor parameter is $\ln(150) = 5.0$. Dividing the parameter by 5.0 so that the age factor parameter for pipes with the Hazen–Williams friction coefficient $C_{ij} = 150$ becomes unity leads to the scale factor of 0.2. Hwang (1981) found a linear relationship between the logarithm of C and the age of pipe in years with a correlation coefficient of 0.935.

Entropy-based redundancy equation (16.7) can be modified as

$$S_j = -\sum_{i=1}^{n(j)} \left[u_{ij} \left(\frac{q_{ij}}{Q_j} \right) \ln \left(\frac{q_{ij}}{Q_j} \right) \right] \tag{16.31}$$

where u_{ij} is the age factor for link ij incident on node j.

The redundancy measure incorporating both the path parameter and the age factor can be expressed by modifying equation (16.31) as

$$S_j = -\sum_{i=1}^{n(j)} \left[u_{ij} \left(\frac{q_{ij}}{Q_j} \right) \ln \left(\frac{q_{ij}}{a_{ij} Q_j} \right) \right] \tag{16.32}$$

Equation (16.32) can be recast as

$$S_j = -\sum_{i=1}^{n(j)} \left[u_{ij} \left(\frac{q_{ij}}{Q_j} \right) \ln \left(\frac{q_{ij}}{Q_j} \right) \right] + \sum_{i=1}^{n(j)} u_{ij} \left(\frac{q_{ij}}{Q_j} \right) \ln a_{ij} \tag{16.33}$$

16.7 Modified Overall Network Redundancy

The overall network redundancy given by equation (16.7) can be modified incorporating u_{ij} and a_{ij} as

$$\hat{S} = -\sum_{j=1}^{N} \left[\sum_{i=1}^{n(j)} \frac{u_{ij} q_{ij}}{Q_0} \ln \left(\frac{q_{ij}}{a_{ij} Q_0} \right) \right] \tag{16.34}$$

The term within brackets represents the contribution from node j to the network redundancy:

$$\tilde{S}_j = -\sum_{i=1}^{n(j)} \frac{u_{ij} q_{ij}}{Q_0} \ln \frac{q_{ij}}{a_{ij} Q_0} \tag{16.35}$$

The contribution from a node can be decomposed as

$$\tilde{S}_j = -\sum_{i=1}^{n(j)} \frac{u_{ij} q_{ij}}{Q_j} \frac{Q_j}{Q_0} \ln \frac{q_{ij}}{a_{ij} Q_j} \frac{Q_j}{Q_0}$$

or

$$\tilde{S}_j = -\frac{Q_j}{Q_0} \left[\sum_{i=1}^{n(j)} \frac{u_{ij} q_{ij}}{Q_j} \ln \frac{q_{ij}}{a_{ij} Q_j} + \sum_{i=1}^{n(j)} \frac{u_{ij} q_{ij}}{Q_j} \ln \frac{Q_j}{Q_0} \right] \tag{16.36}$$

Let

$$\sum_{i=1}^{n(j)} u_{ij} = U_j \tag{16.37}$$

$$\tilde{S}_j = \frac{Q_j}{Q_0} S_j - U_j \frac{Q_j}{Q_0} \ln \frac{Q_j}{Q_0} \tag{16.38}$$

Summing equation (16.38) over the N nodes yields the overall network redundancy:

$$\tilde{S} = \sum_{j=1}^{N} \left[\frac{Q_j}{Q_0} \right] S_j - \sum_{j=1}^{N} \left[U_j \frac{Q_j}{Q_0} \right] \ln \left[\frac{Q_j}{Q_0} \right] \tag{16.39}$$

Equation (16.39) is similar to equation (16.12a), except for the second term that includes U_j—the sum of age factor parameters of the links incident on node j. The second term is similar to the expression for useful entropy. Thus, the overall network redundancy is the sum of weighted nodal useful entropies and the useful entropies among nodes. It can be shown that equation (16.33) and, hence, equation (16.39) are concave.

16.8 Flow Reversal and Dual Flow Directions

In looped networks, it often happens that when a link fails, outflow links from some nodes can become inflow links to the same nodes. For example, if a link upstream of node A fails, the flow can be provided to this node by diverting it around the other portions of the loop. The outflow link from node A could then become the inflow link to that node. The flow reversal can be a critical factor in allowing the network to satisfy the demand flow as much as possible. This reversal means that the outflow links provide additional flow paths to a node and,

hence, affect the network redundancy and reliability. Equation (16.39) can be modified to include all incident links rather than only those that supply water under normal conditions. Thus, one obtains

$$S_j' = -\sum_{i\in\overline{U}_j} u_{ij}\left[\frac{q_{ij}}{Q_j'}\ln\frac{q_{ij}}{a_{ij}Q_j'}\right] - \sum_{k\in\overline{L}_j} u_{jk}\left[\frac{q_{jk}}{Q_j'}\ln\frac{q_{kj}}{a_{jk}Q_j'}\right] \tag{16.40}$$

where Q_j' is the total of all flows leaving and entering node j by links contained in $\overline{U}_j$ and $\overline{L}_j$ expressed as

$$Q_j' = \sum_{i\in\overline{U}_j} q_{ij} + \sum_{k\in\overline{L}_j} q_{jk} \tag{16.41}$$

where $\overline{L}_j$ is the set of outflow links under normal conditions connected to node j in which the link j–k belongs to a loop containing node j, and $\overline{U}_j$ is the set of n nodes on the upstream ends under normal conditions of links incident on node j. It should be noted that only those outflow links are included that are part of the loop containing node j and do not include those that are part of pure branches.

To illustrate, consider a network as shown in Fig. 16-13. Link 6–7 cannot contribute to supply node 6 if either link 3–5 or 4–6 of the main loop fails. This problem shows that pure branches cannot contribute to supply a node should one of the supply links fail. If only the outflow links that are part of a loop containing node j are counted and outflow links from node j that are part of pure branches are not counted, then the network redundancy can be expressed as

$$\tilde{S} = \sum_{j=1}^{N}\left[\frac{Q_j}{Q_0}S_j' - \sum_{j=1}^{N}\left[U_j\frac{Q_j}{Q_0}\ln\frac{Q_j}{Q_0}\right]\right. \tag{16.42}$$

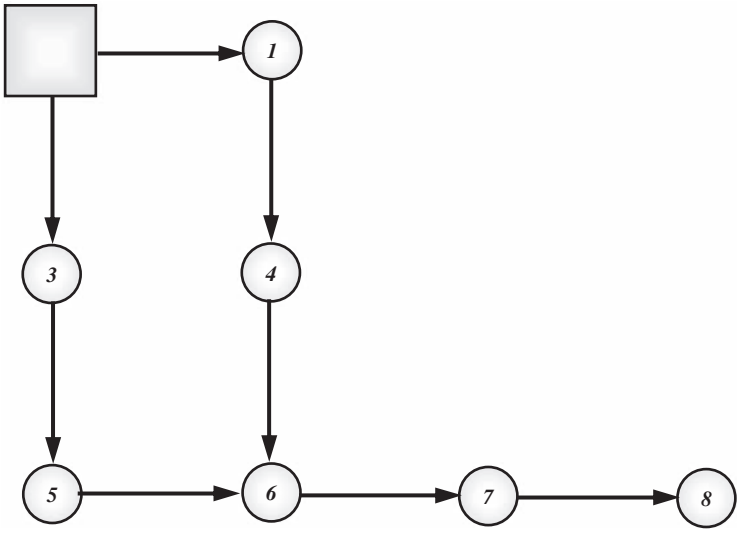

Figure 16-13 *A network layout.*

which is the same as equation (16.39), except that S_j in equation (16.32) is replaced by S'_j from equation (16.40).

16.9 Other Considerations

In the real world, there are distribution networks that have several source nodes to serve the demand nodes. The procedure for redundancy calculation, however, remains the same. Because all nodes are interconnected, each node upstream of another node is a source node to the node downstream to it. Incident links are counted as those links connected to the upstream nodes that are source nodes to the downstream node for which redundancy is determined. In case of multiple sources connected to a demand node by a single link, this node may have multiple incident links and has a nonzero redundancy measure. Equation (16.32) or (16.39) for single or multiple links can be used for measure of redundancy.

Another aspect that occurs in the real world is that flows in links are not fixed but vary with time in response to changing demands at nodes. The question arises, Which flow pattern yields the redundancy measure? Answering this question entails defining the flow pattern. One may compute the redundancy measure for peak demand pattern or average flow pattern. The method of computation, however, remains unaltered.

Pumps also contribute to the network redundancy. Because pumps are regarded as links in the network, the concepts applied to pipes also apply to pumps. The hydraulic property of pumps can be expressed as

$$h_{ij} = Aq_{ij}^2 + Bq_{ij} \tag{16.43}$$

where h_{ij} is the pressure head of pump between nodes i and j; q_{ij} is the pumping rate of the pump between nodes i and j; and A and B are constants. When considering pumps as links, the rate of pumping is related to the square of the pumping head $q_{ij} \propto h_{ij}^{0.5}$. In the case of two pumps, the redundancy is better if the two pumps are close to being of equal capacity. Likewise for multiple pumps. For inclusion in the redundancy measure, the relative pumping capacities are used in place of relative flow rates.

Valves are located on the pipes or links in the water distribution network. Therefore, their existence has the same meaning as that of pipes. Their hydraulic characteristics can also be described by the Hazen–Williams equation as for pipes, but the friction coefficient of the pipe is modified by the presence of a valve thereon as

$$q_{ij} = k(C_{ij} - CV_{ij})\frac{h_{ij}^{0.54}}{L_{ij}^{0.54}}D_{ij}^{2.63} \tag{16.44}$$

where CV_{ij} is the Hazen–Williams roughness coefficient of the valve, C_{ij} is the Hazen–Williams coefficient of the pipe on which the valve is located, L_{ij} is the

length of the pipe on which the valve is located, h_{ij} is the head loss through the pipe, D_{ij} is the diameter of the pipe, and k is the conversion factor for units. In this manner, the contribution of valves to the network redundancy is regarded through the pipes on which they are located.

Storage tanks within the distribution network are considered as demand nodes; the amount of water consumed is equal to the amount of water stored at these nodes, which is the same as the difference between inflow to the tanks and outflow from the tanks multiplied by the time of storage. Thus, redundancy of these nodes is calculated as for other demand nodes. Their presence contributes to the network redundancy measure.

16.10 Optimization for Design of Networks Incorporating Redundancy

There can be two approaches by which entropy-based redundancy measures can be considered in developing optimization models for design of water distribution networks. In one approach, the cost of the network is minimized, subject to a minimum level of redundancy (entropy) and the usual hydraulic constraints. In the other approach, the network redundancy is maximized, subject to the necessary hydraulic constraints and the cost constraint. Both approaches assume that water demands at nodes are known and can accommodate both single demand pattern and multiple demand pattern.

16.10.1 Cost Minimization

There are two types of costs involved in a water distribution network: capital cost and energy cost. The capital cost is usually the cost of installing pipes, which is a function of pipe diameter and its length. U.S. Army Corps of Engineers (1980) has developed a cost function that can be used:

$$M_{ij} = 0.39 D_{ij}^{1.51} \tag{16.45}$$

where M_{ij} is the unit cost of installing pipe between nodes i and j in \$$10^6$ per kilometer of pipe length; and D_{ij} is the diameter of pipe in meters between nodes i and j. If the total number of links is N_L and the length of pipe between nodes i and j is L_{ij} in kilometers, then the total capital cost C_P for the network in \$$10^6$ can be expressed as

$$C_P = \sum_{ij=1}^{N_L} M_{ij} L_{ij} = \sum_{ij=1}^{N_L} 0.39 L_{ij} D_{ij}^{1.51} \tag{16.46}$$

In equation (16.46), the lengths of links are fixed. Denoting

$$\alpha_{ij} = 0.39 L_{ij} \tag{16.47}$$

equation (16.46) can be written as

$$C_P = \sum_{ij=1}^{N_L} \alpha_{ij} D_{ij}^{1.51} \tag{16.48}$$

The cost of energy, C_E, that is needed to carry water depends on the rate of flow and pressure heads in the network and can be expressed as

$$C_E = \beta \left[\sum_{ij=1}^{N_L} q_{ij} h_{ij} + \sum_{j=1}^{N} \Delta_j H_j \right] \tag{16.49}$$

where β is the price of one unit of energy, q_{ij} is the flow rate in pipe between nodes i and j, h_{ij} is the loss of pressure head between nodes i and j, Δ_j is the flow demand at node j, and N is the total number of nodes in the network. From the Hazen–Williams equation, it can be shown that

$$q_{ij} h_{ij} = k \frac{C_{ij}}{L_{ij}^{0.54}} h_{ij}^{1.54} D_{ij}^{2.63} = K_{ij} h_{ij}^{1.54} D_{ij} 2.63 \tag{16.50}$$

where

$$K_{ij} = k \frac{C_{ij}}{L_{ij}^{0.54}} \tag{16.51}$$

where, as before, k is the conversion factor for units, and C_{ij} is the Hazen–Williams coefficient for link ij. Let

$$\gamma_{ij} = \frac{\beta k C_{ij}}{L_{ij}^{0.54}} \tag{16.52}$$

The demand at a node is constant and is known. Then, let

$$\eta_j = \beta \Delta_j \tag{16.53}$$

The service head can also be expressed in terms of the head loss and pressure head at the source node as

$$H_j = H_S + (Z_S - Z_j) - \sum_{(ij) \in P_{Sj}} h_{ij} \tag{16.54}$$

where H_S is the pressure head at the source node, Z_S is the height of the source node above a datum, Z_j is the height of node j above the datum, and P_{Sj} is the set of links between the source node S and demand node j. Because the first two terms in equation (16.54) are constant, one can write

$$\phi_j = H_S + Z_S - Z_j \tag{16.55}$$

Equation (16.49) can be written as

$$C_E = \sum_{ij=1}^{N_L} \gamma_{ij} h_{ij}^{1.54} D_{ij}^{2.63} + \sum_{j=1}^{N} \eta_j \left[\phi_j - \sum_{ij \in P_{Sj}} h_{ij} \right] \tag{16.56}$$

Now the objective function for minimization of the sum of all costs (equations [16.48] and [16.56]), or the network cost, can be expressed as

$$\text{Minimize } C_T = \sum_{ij=1}^{N_L} (\beta_{ij} D_{ij}^{1.51} + \gamma_{ij} h_{ij}^{1.54} D_{ij}^{2.63}) + \sum_{j=1}^{N} \eta_j \left(\phi_j - \sum_{ij \in P_{Sj}} h_{ij} \right) \tag{16.57}$$

where C_T is the total network cost.

The minimization of the total cost is done subject to the specified constraints that are now expressed. First, hydraulic constraints are defined. These constraints relate to flow rates, pressure heads, head losses, and flow continuity. The flow rate in each link should be defined in terms of head loss through that link for either single demand pattern or multiple demand pattern. For a single demand pattern,

$$q_{ij} = K_{ij} h_{ij}^{0.54} D_{ij}^{2.63} \quad \forall \text{ links}(ij) \in N_L \tag{16.58}$$

For a multiple demand pattern, equation (16.58) can be extended as

$$q_{ij} = K_{ij} h_{ijm}^{0.54} D_{ij}^{2.63} \quad \forall \text{ demands}(ijm) \in D_M; \forall \text{ links}(ij) \in N_L \tag{16.59}$$

where D_M is the set of multiple demand patterns, and h_{ijm} is the pressure head loss in the link from node i to node j for demand pattern m.

The mass should be conserved at all nodes, that is, the difference between total inflow and outflow must be equal to the demand at that node. For a single demand pattern, the flow continuity can be expressed as

$$\sum_{(i,j) \in [\overline{h_i} > \overline{h_j}]} q_{ij} - \sum_{(j,k) \in [\overline{h_j} > \overline{h_k}]} q_{jk} = \Delta_j \quad \forall \text{ nodes } j \tag{16.60}$$

where $\overline{h_i}$ is the head at node i, $[\overline{h_i} > \overline{h_j}]$ is the set of links connected to demand node j where the head at node j is less than the head at node i at the other end of the link; and $[\overline{h_j} > \overline{h_k}]$ is the set of links connected to node k where the head at node j is greater than the head at node k at the other end of the link.

For multiple demand patterns, the continuity equation can be written as

$$\sum_{(i,j) \in [\overline{h_i} > \overline{h_j}]} q_{ijm} - \sum_{(j,k) \in [\overline{h_j} > \overline{h_k}]} q_{jkm} = \Delta_{jm} \quad \forall \text{ nodes } j; \forall \text{ demands } m \in D_M \tag{16.61}$$

where q_{ijm} is the flow in link from node i to node j for demand pattern m, and q_{jkm} is the flow in link from node j to node k for demand pattern m.

Now the nodal pressure head constraint is expressed. The usual requirement is that pressure head at each node must be neither above some maximum value

nor below some minimum value. For a single demand pattern, this requirement can be expressed as

$$H_{j\max} \geq H_j \geq H_{j\min} \quad \forall \text{ nodes } j \tag{16.62}$$

where $H_{j\max}$ is the maximum pressure head allowed at node j, $H_{j\min}$ is the minimum pressure head permitted at node j, and H_j is the service pressure head at node j as expressed by equation (16.54). Likewise, for multiple demand patterns, equation (16.62) can be extended to

$$H_{j\max,m} \geq H_j \geq H_{j\min,m} \quad \forall \text{ nodes } j; \forall \text{ demands } m \in D_M \tag{16.63}$$

in which subscript m refers to the particular demand pattern.

The next constraint is about the net pressure head loss. In the links of every loop, the net pressure head loss must be zero according to hydraulic principles. For a single demand pattern, this requirement can be expressed as

$$\sum_{ij \in LP^+} h_{ij} - \sum_{jk \in LP^-} h_{jk} = 0 \; \forall \text{ LP} \in \text{Loops} \tag{16.64}$$

where Loops denotes the total number of loops in the network, LP^+ is the set of links in loop LP that have positive flow direction (clockwise), and LP^- is the set of links in loop LP that have negative flow direction (counterclockwise). In a similar vein, for multiple demand patterns, one can write

$$\sum_{ij \in LP^+} h_{ij,m} - \sum_{jk \in LP^-} h_{jk,m} = 0 \; \forall \text{ LP} \in \text{Loops}; \forall \; m \in D_M \tag{16.65}$$

The last constraint is the nodal redundancy. At each node, the redundancy must be above some minimum value. This requirement may lead to changes in the layout and component design of the network. For example, it may lead to the elimination of links between nodes if it is cheaper without compromising redundancy. For a single demand pattern, the redundancy can be expressed as

$$S_j = -\sum_{i=1}^{n(j)} u_{ij} \left[\frac{q_{ij}}{Q_j} \ln\left(\frac{q_{ij}}{a_{ij} Q_j} \right) \right] \geq S_{j\min} \; \forall \text{ nodes } j \tag{16.66}$$

where $S_{j\min}$ is the minimum entropic redundancy permitted for node j and S_j is the entropic redundancy at node j given by equation (16.32).

Likewise for multiple demand patterns, equation (16.66) can be extended to

$$S_j = -\sum_{i=1}^{n(j)} u_{ij} \left[\frac{q_{ijm}}{Q_{jm}} \ln\left(\frac{q_{ijm}}{a_{ij} Q_{jm}} \right) \right] \geq S_{j\min} \; \forall \text{ nodes } j; \forall \text{ demands } m \in D_M \tag{16.67}$$

This equation completes the formulation of optimum design based on cost minimization.

16.10.2 Entropic Redundancy Maximization

Here the objective is to maximize the overall network entropy-based network redundancy. Thus, the objective function can be expressed as

$$\text{Maximize } \tilde{S} = \sum_{j=1}^{N}\left[\frac{Q_j}{Q_0}\right]S_j - \sum_{j=1}^{N}\left[U_j\frac{Q_j}{Q_0}\right]\ln\left[\frac{Q_j}{Q_0}\right] \tag{16.68}$$

where the symbols are as defined earlier. The maximization is achieved, subject to the hydraulic and budgetary constraints. The hydraulic constraints specified in the earlier case are also valid here, so they are not repeated. The total cost given by equation (16.57) must be less than or equal to the maximum allowable cost, $C_{T\max}$.

16.10.3 Relation to Reliability

For a number of layouts, Awumah (1990) computed parameters of nodal pair reliability (NPR) and percentage of demand supplied at adequate pressure (PSPF) and compared them with redundancy measures. NPR measures the probability that the source node and each of the demand nodes are connected and has been used by Quimpo and Shamsi (1988) and Wagner et al. (1988a, b). The PSPF allows an assessment of the resilience of water distribution systems and, hence, permits a statement of hydraulic redundancy. Using the data from Awumah (1990), redundancy and NPR reliability are plotted as shown in Fig. 16-14 and that of PSPF in Fig. 16-15. There is almost a one-to-one relation, and this relation can be used in entropy-based evaluation and design of water distribution networks.

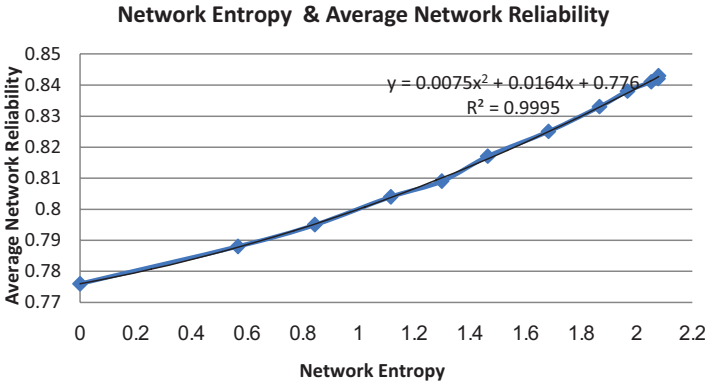

Figure 16-14 *Relation between network entropy and average network reliability.*

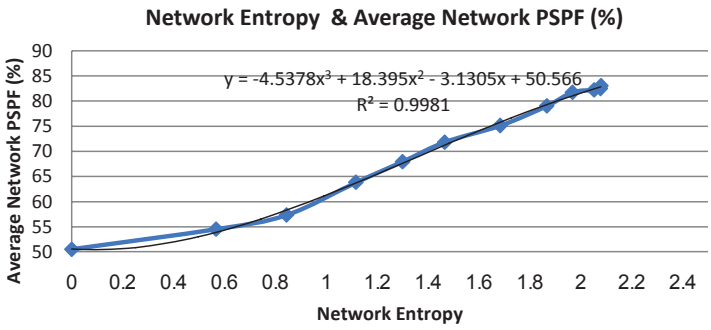

Figure 16-15 *Network entropy versus average network PSPF.*

Questions

Q16.1 Consider five simple single-node layouts as shown in Fig. 16-16. Compute the redundancy of each layout and discuss the results.

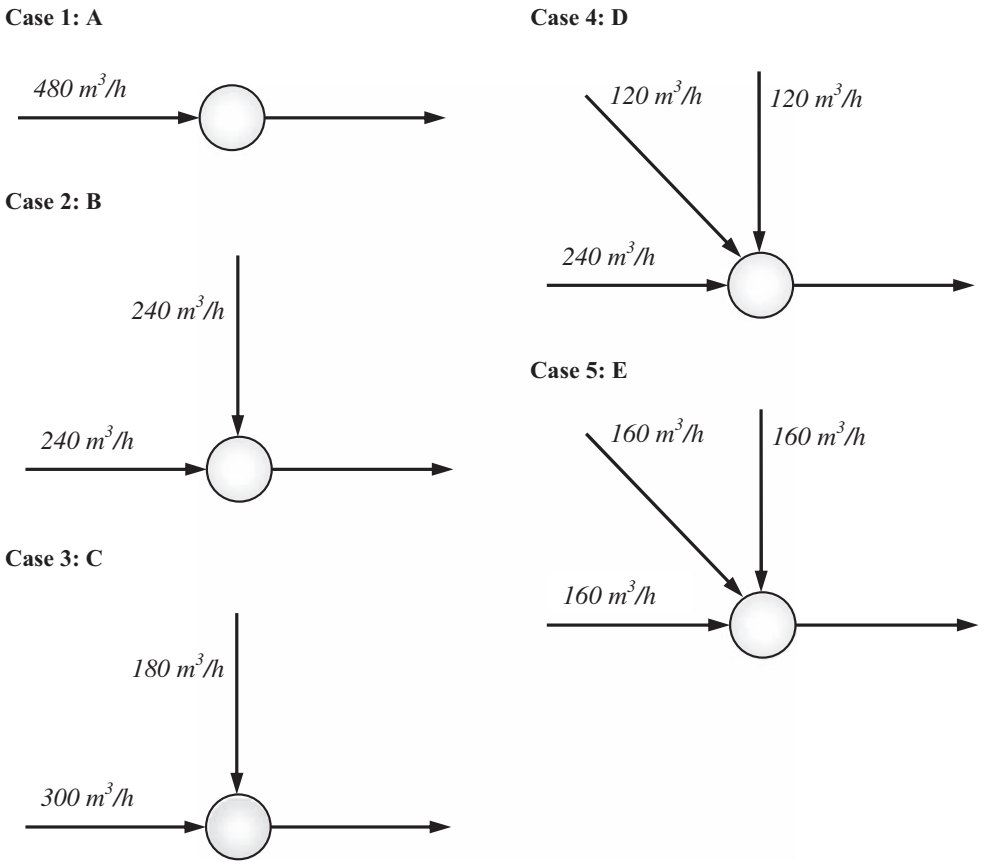

Figure 16-16 *Five simple single-node water distribution layouts.*

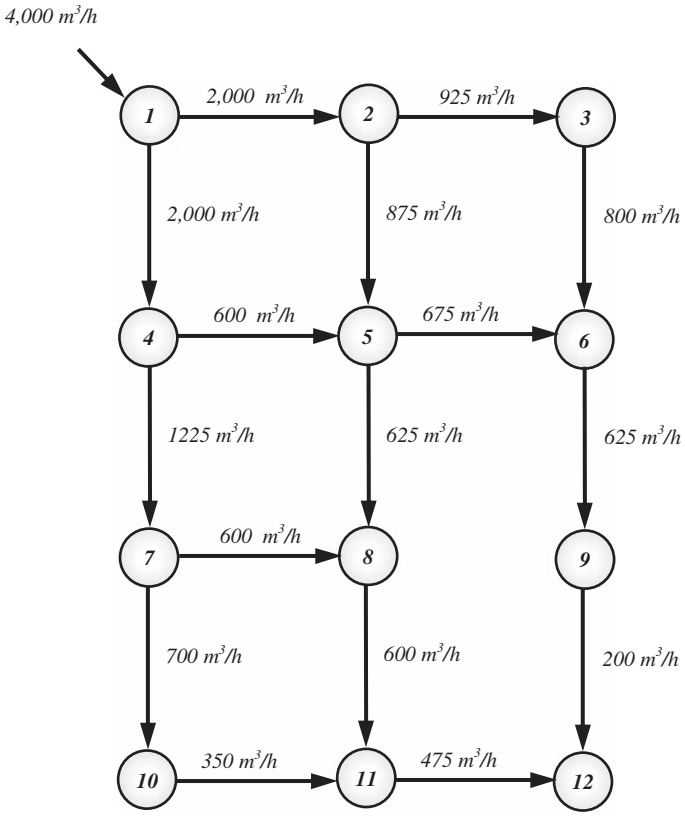

Figure 16-17 *A simple single-node water distribution layout.*

Q16.2 Consider a pipe network layout as shown in Fig. 16-17. Determine the redundancy measure at each node. Then determine the redundancy measure of the entire layout or network.

Q16.3 Using the layout in Q16.2, calculate the transmissivity at each node. Considering the transmissivity, calculate the modified or global redundancy measure at each node. Compare the redundancy values with those derived in Q16.2. Also compute the global redundancy measure for the network.

Q16.4 For the layout in Q16.2, compute the path parameter for each node. Considering the path parameter, compute the redundancy measure at each node. Then compute the global redundancy measure for the network.

Q16.5 For the layout in Q16.2, assume that pipes or links are somewhat old such that the friction factor for all links is 115. Then compute the redundancy measure at each node. Here you should also take into account the path dependency or path parameter. Then compute the global redundancy measure for the whole network.

Q16.6 For the layout in Q16.2, assume that pipes or links are somewhat old such that the friction factor C for links is as follows: $C = 115$ for links 1–2 and 2–3; $C = 120$ for links 1–4, 2–5, and 3–6; $C = 125$ for links 4–5, 5–6, 4–7, 5–8, and 6–9; $C = 130$ for links 7–10, 8–11, and 7–8; and $C = 140$ for links 10–11, 11–12, and 9–12. Compute the redundancy measure at each node. Here you should also take into account the path dependency or parameter. Then compute the global redundancy measure for the whole network.

Q16.7 Consider the eight layouts shown in Fig. 16-18. The demand at the sources is 2,500 m^3/h. The demand at each node is specified in Table 16-4. Compute the flow in each link. Note that in this example the sum of demands at nodes equals the demand at the source. Compute the redundancy of each layout and discuss which layout should be preferred.

Q16.8 Consider the eight simple layouts in Fig. 16-18. For each layout, indicate the number of loops and compute the redundancy measure derived from local redundancy and from global redundancy. Show redundancy at each node and redundancy among nodes. Discuss the results. Which layout is preferable?

Note that the sum of demands at nodes equals the demand at the source. Compute the redundancy of each layout and discuss which layout should be preferred.

Table 16-4 *Demand at each node in Q16.7.*

Node	Demand (m^3/h)
1-Source	2,500
2	250
3	275
4	225
5	250
6	200
7	250
8	200
9	250
10	200
11	200
12	200

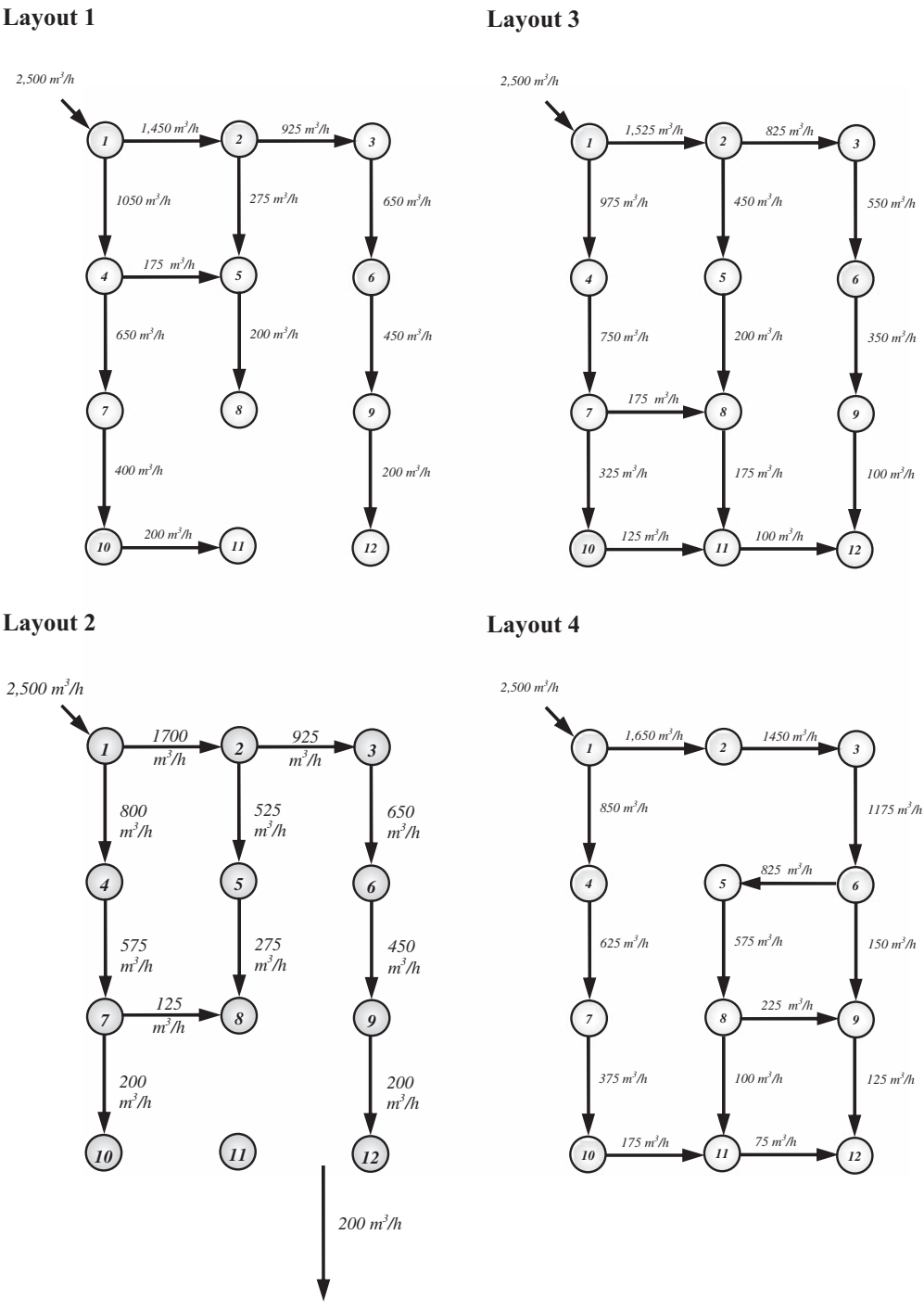

Figure 16-18 *Eight alternative water distribution network layouts.*

Layout 5

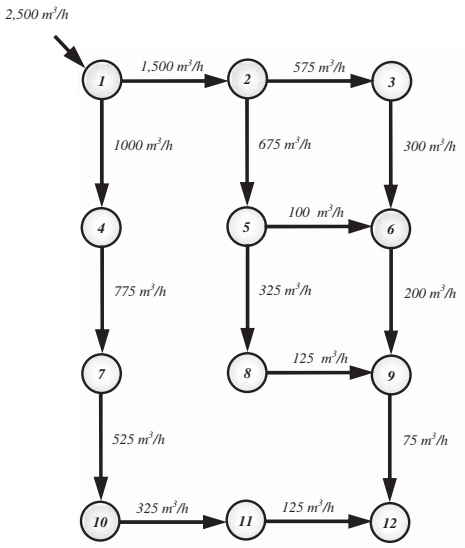

Layout 7

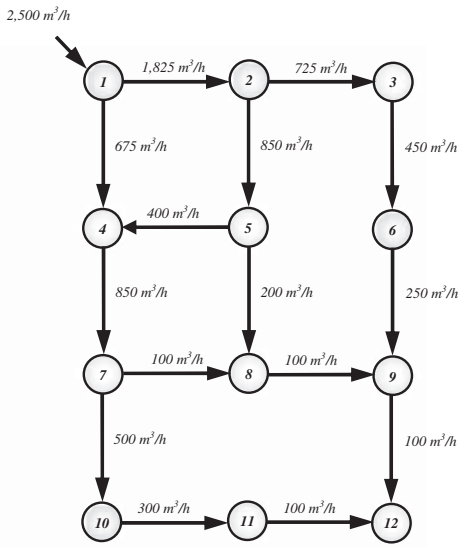

Layout 6

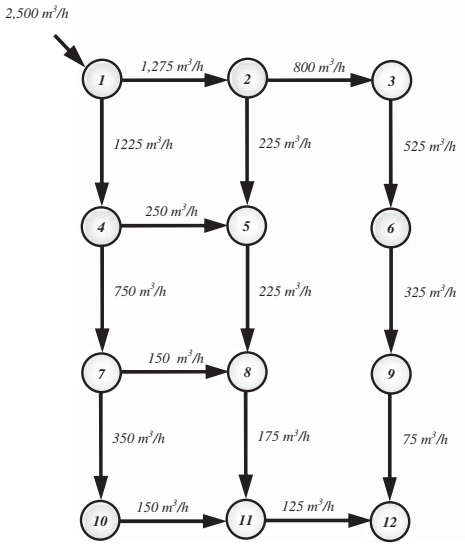

Layout 8

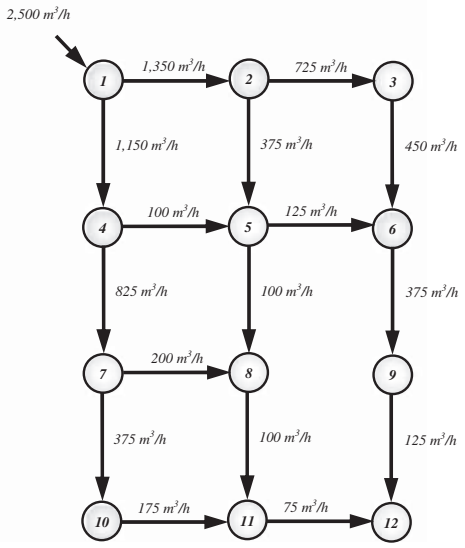

Figure 16-18, *Continued*

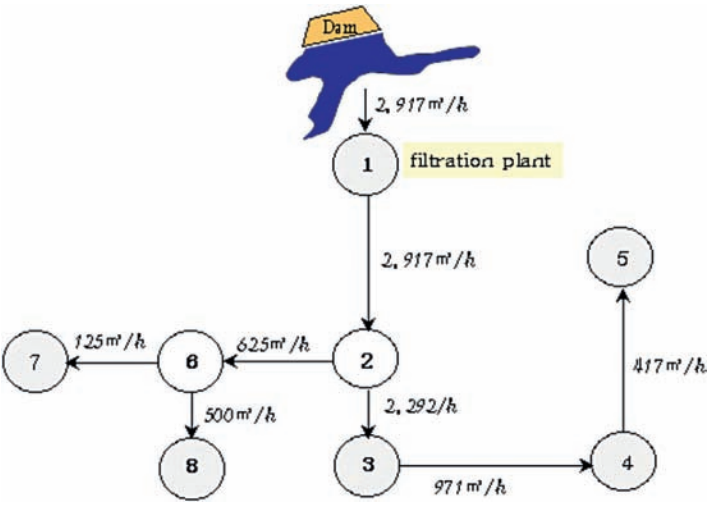

Figure 16-19 *City water distribution layout.*

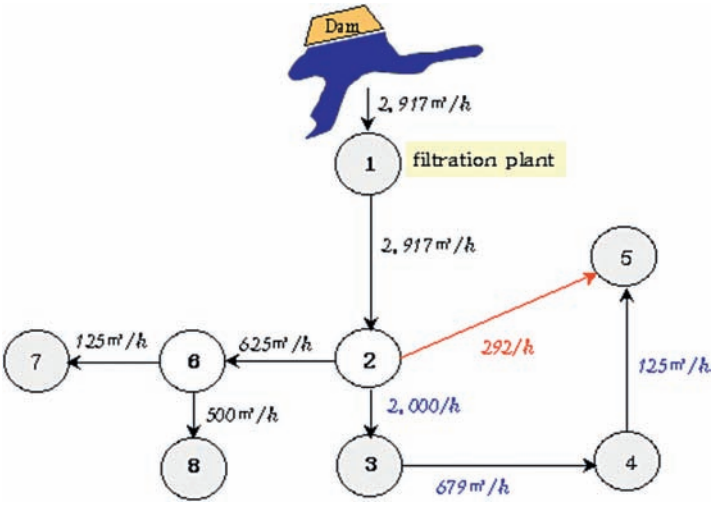

Figure 16-20 *An alternate city water distribution layout.*

Q16.9 Consider a layout shown in Fig. 16-19, in which number 1 denotes a filtration plant, numbers 3 and 4 denote the Taebaek city water reservoir, number 5 denotes the Samcheok city water reservoir, number 7 denotes the Yeongwul city water reservoir, number 8 denotes the Jeongseon city water reservoir, and other numbers denote nodes. Compute the redundancy of the entire layout, transmission of redundancy, path parameter of redundancy, and age factor of redundancy (with $C = 140$ for steel).

Q16.10 Consider a layout shown in Fig. 16-20, in which the real distance between node 2 and node 5 is 40 km. Numbers have the same meaning as in Q16.9. Compute common redundancy, transmission of redundancy, path parameter of redundancy, and age factor of redundancy.

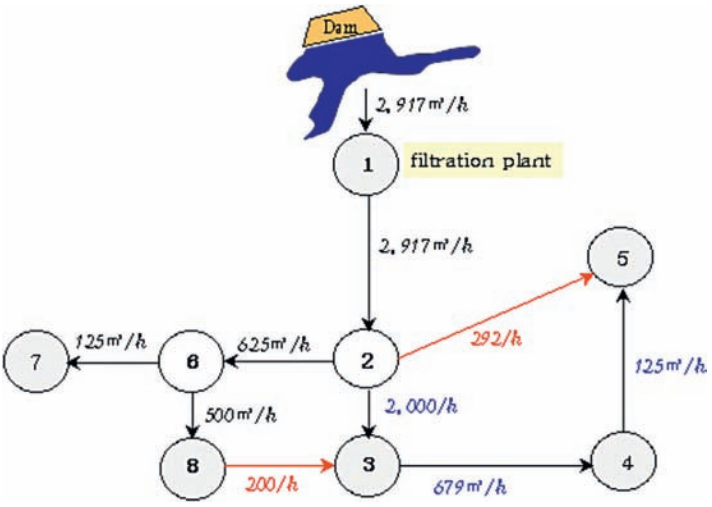

Figure 16-21 *Another alternative city water distribution layout.*

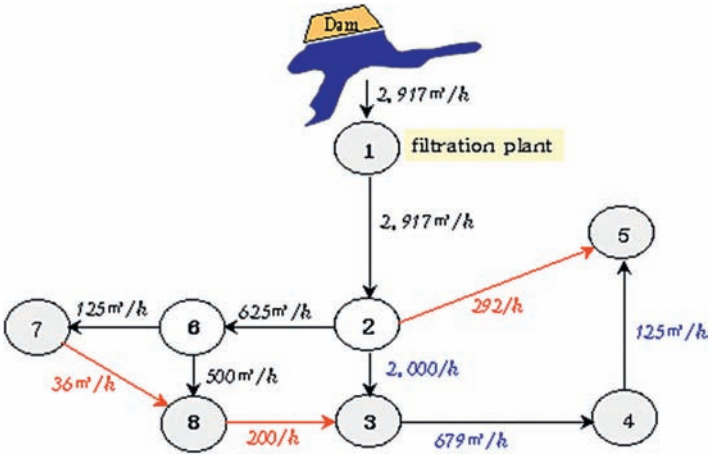

Figure 16-22 *Another alternate city water distribution layout.*

Q16.11 Consider a layout shown in Fig. 16-21, in which the distance between nodes 2 and 5 is 40 km and the distance between nodes 8 and 3 is 30 km. Numbers have the same meaning. Compute common redundancy, transmission of redundancy, path parameter of redundancy, and age factor of redundancy.

Q16.12 Consider a layout shown in Fig. 16-22, in which the distance between nodes 2 and 5 is 40 km, the distance between nodes 8 and 3 is 30 km, and the distance between nodes 7 and 8 is 40 km. Numbers have the same meaning. Compute common redundancy, transmission of redundancy, path parameter of redundancy, and age factor of redundancy.

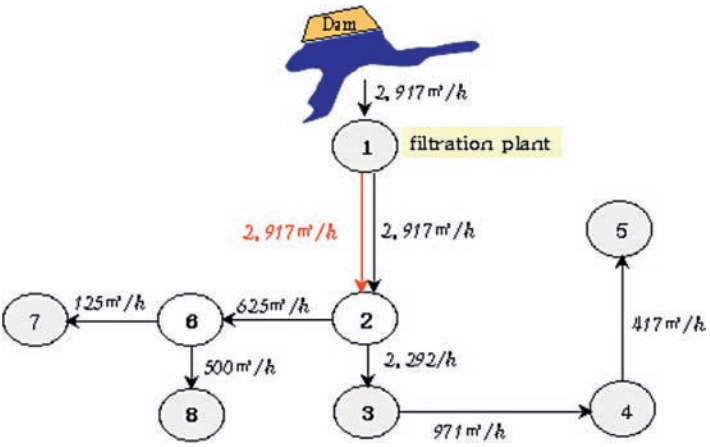

Figure 16-23 *Another alternate city water distribution layout.*

Q16.13 Consider a layout shown in Fig. 16-23, in which the distance between nodes 1 and 2 is 80 km. Numbers have the same meaning. Compute common redundancy, transmission of redundancy, path parameter of redundancy, and age factor of redundancy.

References

Awumah, K. (1990). "*Entropy based measures in water distribution network design*." Ph.D. dissertation, University of Manitoba, Winnipeg, Canada.

Awumah, K., and Goulter, I. (1989). "Redundancy and reliability of water distribution networks: An entropy based approach." *Hydraulic Engineering*, M. A. Ports, ed., ASCE, New York, 768–773.

Awumah, K., Goulter, I., and Bhatt, S. K. (1990). "Assessment of reliability in water distribution networks using entropy based measures." *Stoch. Hydrol. Hydraul.*, 4, 309–320.

Awumah, K., Goulter, I., and Bhatt, S. K. (1991). "Entropy-based redundancy measures in water-distribution networks." *J. Hydraul. Eng.*, 117(5), 595–614.

Germanopoulos, G., Jowitt, P. W., and Lumbers, J. P. (1986). "Assessing the reliability of supply and level of service for water distribution systems." *Proc., Inst. Civil Eng., Part I*, 80, 413–428.

Goulter, I. C. (1988). "Measures of inherent redundancy in water distribution network layouts." *J. Inform. Optim. Sci.*, 9(3), 363–390.

Goulter, I. C. (1992). "Assessing the reliability of water distribution networks using entropy based measures of network redundancy." In *Entropy and energy dissipation in water resources*, V. P. Singh and M. Fiorentino, eds., Kluwer Academic, Dordrecht, The Netherlands, 217–238.

Goulter, I. C., and Coals, A. V. (1986). "Quantitative approaches to reliability assessment in pipe networks." *J. Transp. Eng.*, 112(3), 287–301.
Hwang, N. H. C. (1981). *Fundamentals of hydraulic engineering systems*, Prentice Hall, Englewood Cliffs, NJ.
Quimpo, R. G., and Shamsi, U. M. (1988). "Network reliability for water distribution network management." *Proc., 5th IAHR Int. Symp. Stochastic Hydraul.*, University of Birmingham, Birmingham, UK.
Shannon, C.E. (1948). "A mathematical theory of communication." *Bell Sys. Tech. J.*, 27, 623–659.
Tanyimboh, T. T., and Templeman, A. B. (1993a). "Maximum entropy flows for single-source networks." *Eng. Optimization*, 22, 49–63.
Tanyimboh, T. T., and Templeman, A. B. (1993b). "Calculating maximum entropy flows in networks." *J. Oper. Res.*, 44, 383–396.
U.S. Army Corps of Engineers. (1980). "Methodology for areawide planning." *Engineer Manual 1110-2-502,* U.S. Army Corps of Engineers, Washington, DC.
Wagner, J. M., Shamir, U., and Marks, D. H. (1988a). "Water distribution reliability: Analytical methods." *J. Water Resour. Plann. Manage.*, 114(3), 253–275.
Wagner, J. M., Shamir, U., and Marks, D. H. (1988b). "Water distribution reliability: Simulation methods." *J. Water Resour. Plann. Manage.*, 114(3), 276–294.
Walters, G. (1988). "Optimal design of pipe networks: A review." *Proc., 1st Int. Conf. Comput. Water Resour.*, Vol. 2, Computational Mechanics, Southampton, UK, 21–32.
Xu, C.-C., and Jowitt, P. W. (1992). "Discussion of 'Entropy-based redundancy measures in water-distribution networks.'" *J. Hydraul. Eng.*, 118(7), 1064–1066.

Additional Reading

Alperovits, E., and Shamir, U. (1977). "Design of optimal water distribution systems." *Water Resour. Res.*, 13(6), 885–900.
Awumah, K., Bhatt, S. K., and Goulter, I. C. (1989). "An integer programming model for layout design of water distribution networks." *Eng. Optimization*, 5, 57–70.
Bagheri, A., Darijani, M., Asgary, A., and Morid, S. (2010). "Crisis in urban water supply systems during the reconstruction period: A system dynamics analysis of alternative policies after the 2003 earthquake in Bam-Iran." *Water Resources Manag.*, 24, 2567–2596.
Ball, M. O. (1980). "Complexity of network reliability calculations." *Networks*, 10(2), 153–165.
Bhave, P., and Sonak, V. (1992). "A critical study of the linear programming gradient method for optimal design of water supply networks." *Water Resour. Res.*, 28(6), 1577–1584.

Biem, G. K., and Hobbs, B. (1988). "Analytical simulation of water system capacity reliability, 2. A Markov chain approach and verification of the modes." *Water Resour. Res.*, 24, 1445–1459.

Cendese, A., and Mele, P. (1978). "Optimal design of water distribution networks." *J. Hydraul. Div.*, 104(2), 237–248.

Chiplunkar, A., Mehandiratta, V., and Khanna, S. L. (1986). "Looped water distribution system optimization for single loading." *J. Environ. Eng.*, 112(2), 264–279.

Christodoulou, S. E. (2011). "Water network assessment and reliability analysis by use of survival analysis." *Water Resour. Manage.*, 25, 1229–1238.

Christodoulou, S., Agathokleous, A., Charalambous, B., and Adamou, A. (2010). "Proactive risk-based integrity assessment of water distribution networks." *Water Resour. Manage.*, 24, 3715–3730.

Cisty, M. (2010). "Hybrid genetic algorithm and linear programming method for least-cost design of water distribution systems." *Water Resour. Manage.*, 24, 1–24.

Dandy, G. C., Simpson, A. R., and Murphy, L. J. (1996). "An improved genetic algorithm for pipe network optimization." *Water Resour. Res.*, 32(2), 449–458.

Deb, A. K. (1974). "Least cost design of branched pipe network system." *J. Env. Engrg. Div.*, 100(4), 821–835.

Eusuff, M. M., and Lansey, K. E. (2003). "Optimization of water distribution network design using the shuffled frog leaping algorithm." *J. Water Resour. Plann. Manage.*, 129(3), 210–225.

Fujiwara, O., and Khamg, D. B. (1990). "A two-phase decomposition method for optimal design of looped water distribution networks." *Water Resour. Res.*, 26(4), 539–549.

Giustolisi, O., Laucelli, D., and Colombo, A. F. (2009). "Deterministic versus stochastic design of water distribution networks." *J. Water Resour. Plann. Manage.*, 135(2), 117–127.

Goulter, I. C. (1987). "Current and future use of systems analysis in water distribution network design." *Civil Eng. Syst.*, 4(4), 175–184.

Goulter, I. C., and Bouchart, F. (1990). "Reliability-constrained pipe network model." *J. Hydraul. Eng.*, 116(2), 211–229.

Goulter, I. C., and Morgan, D. R. (1984). "Discussion of 'Obtaining the layout of water distribution systems networks.'" *J. Hydraul. Eng.*, 110(1), 67–68.

Goulter, I. C., and Morgan, D. R. (1985). "An integrated approach to the layout and design of water distribution networks." *Civil Eng. Sys.*, 2(2), 104–113.

Haghighi, A., Samani, H. M. V., and Samani, Z. M. V. (2011). "GA-ILP method for optimization of water distribution networks." *Water Resour. Manage.*, 25, 1791–1808.

Hobb, B., and Biem, G. K. (1988). "Analytical simulation of water supply capacity reliability, 1. Modified frequency duration analysis." *Water Resour. Res.*, 24, 1431–1444.

Jacoby, S. L. (1968). "Design of optimal hydraulic networks." *J. Hydraul. Div.*, 94(3), 641–662.

Jacoby, S. L., and Goulter, I. C. (1989). "Optimization of redundancy in water distribution networks using graph theoretic principles." *Eng. Optim.*, 15, 71–82.

Kadu, M. S., Gupta, R., and Bhave, P. R. (2008). "Optimal design of water networks using a modified genetic algorithm with reduction in search space." *J. Water Resour. Plann. Manage.*, 134(2), 147–160.

Kally, E. (1972). "Computerized planning of the least cost water distribution network." *Water Sewage Works*, 121–127.

Karmeli, D., Gadish, Y., and Meyer, S. (1968). "Design of optimal water distribution networks." *J. Pipeline Div.*, 94(1), 1–10.

Keisler, A., Ormsbee, L., and Shamir, U. (1990). "A methodology for least-cost design of invulnerable water distribution networks." *Civil Eng. Syst.*, 7(1), 20–28.

Kessler, A., and Shamir, U. (1989). "Analysis of the linear programming method for optimal design of water supply networks." *Water Resour. Res.*, 25(7), 1469–1480.

Kumar, V. (1987). "Entropic measure of manufacturing flexibility." *Int. J. Prod. Res.*, 25, 957–966.

Kuo, C. L., and Hsu, N. S. (2011). "An optimization model for crucial key pipes and mechanical reliability: A case study on a water distribution system in Taiwan." *Water Resour. Manage.*, 25, 763–775.

Kwon, H. J., and Lee, C. E. (2008). "Reliability analysis of pipe network regarding transient flow." *KSCE J. Civil Eng.*, 12(6), 409–416.

Lansey, K. E., and Mays, L. W. (1989). "Optimization model for water distribution system design." *J. Hydraul. Eng.*, 115(10), 1401–1418.

Lansey, K. E., Duan, N., Mays, L. W., and Tung, Y.-K. (1989). "Water distribution system design under uncertainties." *J. Water Resour. Plann. Manage.*, 115(5), 630–645.

Makropoulos, C. K., and Butler, D. (2010). "Distributed water infrastructure for sustainable communities." *Water Resources Manage.*, 24, 2795–2816.

Manca, A., Sechi, G. M., and Zuddas, P. (2010). "Water supply network optimization using equal flow algorithms." *Water Resources Manag.*, 24, 3665–3678.

Martin, Q. W. (1980). "Optimal design of water conveyance systems." *J. Hydraul. Div.*, 106(9), 1415–1433.

Martinez-Rodriguez, J. B., Montalvo, I., Izquierdo, J., and Perez-Garcia, R. (2011). "Reliability and tolerance comparison in water supply networks." *Water Resour. Manage.*, 25, 1437–1448.

Misra, K. B. (1970). "An algorithm for reliability evaluation of redundant networks." *IEEE Trans. Reliabil.*, R-19, 146–151.

Morgan, D. R., and Goulter, I. C. (1985). "Optimal urban water distribution design." *Water Resour. Res.*, 21(5), 642–652.

Park, H., and Liebman, J. C. (1993). "Redundancy-constrained minimum cost design of water-distribution nets." *J. Water Resour. Plann. Manage.*, 119(1), 83–98.

Prasad, T. D., and Park, N.-S. (2004). "Multiobjective genetic algorithms for design of water distribution networks." *J. Water Resour. Plann. Manage.*, 130(1), 73–82.

Quimpo, R. G., and Shamsi, U. M. (1991). "Reliability-based distribution system maintenance." *J. Water Resour. Plann. Manage.*, 117(3), 321–339.

Quindry, G. E., Liebman, J. C., and Brill, E. D. (1981). "Optimization of looped water distribution systems." *J. Environ. Eng. Div.*, 107(4), 665–679.

Reca, J., Martines, J., Gil, C., and Banos, R. (2008). "Application of several metaheuristic techniques to the optimization of real looped water distribution networks." *Water Resour. Manage.*, 1367–1379.

Rowell, W. F., and Barnes, J. W. (1982). "Obtaining the layout of water distribution systems." *J. Hydraul. Div.*, 108(1), 137–148.

Samani, H. M. V., and Mottaghi, A. (2006). "Optimization of water distribution networks using integer linear programming." *J. Hydraul. Eng.*, 132(5), 501–509.

Samani, H. M. V., and Naeeni, S. T. (1996). "Optimization of water distribution networks." *J. Hydraul. Res.*, 34(5), 623–632.

Savic, D. A., and Walters, G. A. (1997). "Genetic algorithms for least-cost design of water distribution networks." *J. Water Resour. Plann. Manage.*, 123(2), 67–77.

Sechi, G. M., and Zuddas, P. (2008). "Multiperiod hypergraph models for water resources systems optimization." *Water Resources Manage.*, 22, 307–320.

Shamir, U. (1974). "Optimal design and operation of water distribution systems." *Water Resour. Res.*, 10(1), 27–36.

Shamir, U., and Howard, C. D. D. (1981). "Water supply reliability theory." *J. Am. Water Works Associ.*, 73(7), 379–384.

Simpson, A. R., Dandy, G. C., and Murphy, L. J. (1994). "Genetic algorithms compared to other techniques for pipe optimization." *J. Water Resour. Plann. Manage.*, 120(4), 423–443.

Su, Y.-C., Mays, L. W., Duan, N., and Lansey, K. E. (1987). "Reliability-based optimization model for water distribution systems." *J. Hydraul. Eng.*, 113(12), 1539–1556.

Taher, S. A., and Labadie, J. W. (1996). "Optimal design of water-distribution networks with GIS." *J. Water Resour. Plann. Manage.*, 122(4), 301–311.

Templeman, A. B. (1982). "Discussion of 'Optimization of looped water distribution systems.'" *J. Environ. Eng. Div.*, 108(3), 599–602.

Templeman, A. B. (1992). "Entropy and civil engineering optimization." In *Optimization and artificial intelligence in civil and structural engineering*, Vol. 1, Kluwer Academic, Dordrecht, The Netherlands, 87–105.

Templeman, A. B., and Yates, D. F. (1984). "Mathematical similarities in engineering network analysis." *Civil Eng. Syst.*, 1(1), 114–122.

Walski, T. M., Brill, E. D., Gessler, J., Goulter, I., Jeppson, R. M., Lansey, K. et al. (1987). "Battle of network models: Epilogue." *J. Water Resour. Plann. Manage.*, 113(2), 191–203.

Watanada, T. (1973). "Least-cost design of water distribution systems." *J. Hydraul. Div.*, 99(9), 1497–1513.

Wood, D. J., and Charles, C. O. A. (1972). "Hydraulic network analysis using linear theory." *J. Hydraul. Div.*, 98(7), 1157–1170.

Wu, Z. Y., and Walski, T. (2005). "Self-adaptive penalty approach compared with other constraint-handling techniques for pipeline optimization." *J. Water Resour. Plann. Manage.*, 131(3), 181–192.

Yang, S.-L., Hsu, N.-S., Louie, P. W. F., and Yeh, W. W.-G. (1996a). "Water distribution network reliability: Connectivity analysis." *J. Infrastruct. Syst.*, 2(2), 54–64.

Yang, S.-L., Hsu, N.-S., Louie, P. W. F., and Yeh, W. W.-G. (1996b). "Water distribution network reliability: Stochastic simulation." *J. Infrastruct. Syst.*, 2(2), 65–72.

Zemel, E. (1982). "Polynomial algorithms for estimating network reliability." *Networks*, 12, 439–452.

This page intentionally left blank

Chapter 17

Evaluation of Water Quality and Wastewater Treatment Systems

Environmental pollution is caused by the discharge of material—biological, chemical, and physical materials, gaseous substances, and heat—into the environment, which is composed of water, air, and soil. The discharge occurs in everyday activities of consumption and production. For example, water is used for such things as drinking, cooling, washing, energy production, waste disposal, transportation, recreation, and agricultural production. These activities and uses release compounds that pollute water through dissolution and diffusion. In a similar vein, when a hydrocarbon is transformed to a more usable form of energy through a series of conversions to heat, mechanical work, and finally to electricity, a substantial part (about 60%) of the chemical energy originally present in the hydrocarbon is wasted as heat. The sulfur contained in the liquid fuel is released to the environment and causes air pollution. Today's agriculture uses a lot of chemical fertilizers. Only a small portion of chemical fertilizer is used up by plants, and the rest goes to pollute soil and water resources.

When a chemical compound is added to water, the compound is likely to dissolve, diffuse, and result in an increase in pollution. Dissolution and diffusion of contaminants involve mixing, disordering, and randomization, and they increase entropy. Thus, an increase in pollution translates into an increase in entropy. This statement suggests that entropy can be used as a measure of water pollution. To purify polluted water, energy is required to remove pollutants and, in turn, decrease entropy. This chapter discusses entropy as a measure of water quality assessment and water quality improvement through the process of water treatment.

17.1 Diversity Index

The diversity index (DI) has been used as an indicator of diversity of species of organisms in water and, in turn, as an indicator of water pollution. In general, as the degree of pollution increases, the number of species decreases, meaning that there is a low diversity index. Of course, the exception is pure or unpolluted water that also has a low diversity index. It has been suggested by Routledge (1979) that the admissible diversity indexes belong to the Hill family of indexes (Hill 1973) expressed as

$$\mathrm{DI}_k = \left[\sum_{i=1}^{N} p_i^k\right]^{1/(1-k)} \tag{17.1a}$$

where k is a coefficient and p_i is the relative abundance of species i in a sample of N species. DI_1 is concave everywhere. Two important special cases of the Hill family are the Shannon–Weiner diversity index (Pielou 1966; Spellerberg and Fedor 2003) and the Simpson concentration (Simpson 1949; May 1975). The Shannon–Weiner index is based on the Boltzmann–Gibbs–Shannon entropic form, in which the diversity index, DI, can, with the Boltzmann constant as unity, be calculated as

$$\mathrm{DI} = -\sum_{i=1}^{N} p_i \ln p_i \tag{17.1b}$$

where p_i represents the number of organisms of species i divided by the total number N of organisms present in the water. DI, as a barometer of health, can also be used to compare the health of one body of water with another.

The Simpson concentration can be written as

$$\psi = \sum_{i=1}^{N} p_i^2 \tag{17.2}$$

where $1 - \psi$ denotes the Gini coefficient or the Simpson diversity (Lande 1996), is concave everywhere, and can be interpreted as a variance: ψ has an advantage in that it converges rapidly to the limit value of diversity for small sample sizes (Lande et al. 2000). Comparison of equation (17.1) with equation (17.2) shows that in equation (17.1) the expectation is over $\log(1/p_i)$, whereas in equation (17.2), it is over p_i itself.

17.2 Evaluation of Water Quality Using the Diversity Index

Eutrophication corresponds to high productivity of lakes and streams by premature enrichment. Usually, DI drops as bloom occurs. For example, eutrophication

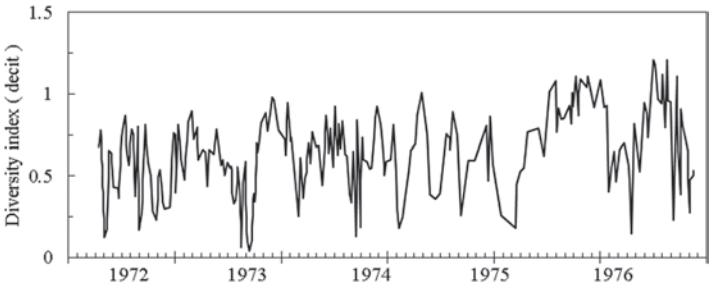

Figure 17-1 *Variation of diversity index for phytoplankton in Lake Kasumigaura. Source: Tai and Goda (1980). Reproduced with permission from S. Tai.*

is most serious in summer months, and a drop in DI becomes evident, because there is a decrease in the number of organisms and different species. When lakes and streams receive nutrients, such as nitrogen and phosphorus, from point and nonpoint sources of pollution, these nutrients promote the growth of populations of phytoplankton during warm months, resulting in algal bloom and depletion of oxygen, and consequently degradation of water quality. One can examine the variations of the phytoplankton community of a lake, then compute the diversity index for phytoplankton using equation (17.1), and plot it as a function of time. Tai and Goda (1980) examined the phytoplankton of Lake Kasumigaura in Ibaraki, Japan, for a period of six years from 1972 to 1977 and computed DI, as shown in Fig. 17-1, which shows that as DI decreases, entropy increases, as shown by equation (17.1). One can also examine the variation of DI with chemical oxygen demand (COD) for different lakes or water bodies. The diversity of phytoplankton species reaches a maximum when nutrient concentration is moderate. Tai and Goda (1980) computed DI for phytoplankton communities of five lakes in Japan—Chuzenji, Kasumigaura, Motosu, Shikotsu, and Yunoko—and plotted against measured COD, as shown in Fig. 17-2. They reported that DI dropped in oligotrophic lakes, such as Lake Kasumigaura; increased in mesotrophic lakes, such as Lake Motosu and Lake Yunoko; and reached a maximum in the case of moderate nutrient concentration, such as Lake Chuzenji.

17.3 Evaluation of Water Treatment Systems

Energy is required to remove pollutants and purify water, that is, to decrease the entropy of the solution. A water treatment system generally requires and dissipates a large amount of energy for removing pollutants from solution. Conversely, there is generation of entropy internally by the irreversibility of the treatment system. It can then be reasoned that the thermodynamic efficiency of a treatment system can be evaluated by the rate of decrease of entropy of feedwater and the rate of internal entropy production. Entropy makes it possible to evaluate both the unusable energy and the environmental pollution.

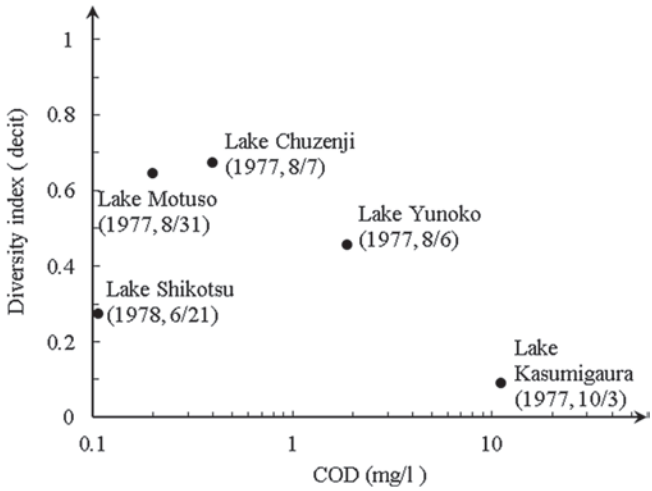

Figure 17-2 *Relation between COD and diversity index for phytoplankton. Source: Tai and Goda (1980). Reproduced with permission from S. Tai.*

Consider a wastewater treatment system, as shown in Fig. 17-3, wherein polluted water is treated with reverse osmosis (RO) and solutes (salts) are separated from a solution of raw water by a continuous separating plant; that is, the water separation system, such as RO, includes flows of material, energy, and entropy. The system is enclosed, permitting an exchange of both matter and energy with the surroundings. There is entropy of raw water, and there is internal entropy production caused by irreversible processes occurring in the system. Because of the removal of pollutants, the entropy of raw water decreases, but the entropy of the whole system increases because of the irreversibility of the system at a definite rate (internal entropy production). This phenomenon indicates that the decrease in entropy of raw water, ΔS, is smaller than the internal entropy production, dS_i.

The flows of matter, energy, and change in entropy in a water treatment system are shown in Fig. 17-3. Let Q denote the flow rate with concentration C. The flow consists of raw water, (Q_r), with concentration C_r, effluent (Q_e) with concentration C_e, and concentrate (or sludge) (Q_s) with concentration C_s. Let E denote energy flow and E_h denote heat energy flow. The energy flow consists of energy flow E_r associated with raw water and heat energy E_{hr}, energy associated with effluent E_e and heat energy E_{he}, and energy associated with concentrate (or sludge) E_s and heat energy E_{hs}. Then one can write the mass balance as

$$C_r Q_r = C_e Q_e + C_s Q_s \tag{17.3a}$$

and energy balance as

$$E_r = E_e + E_{he} + E_s + E_{hs} \tag{17.3b}$$

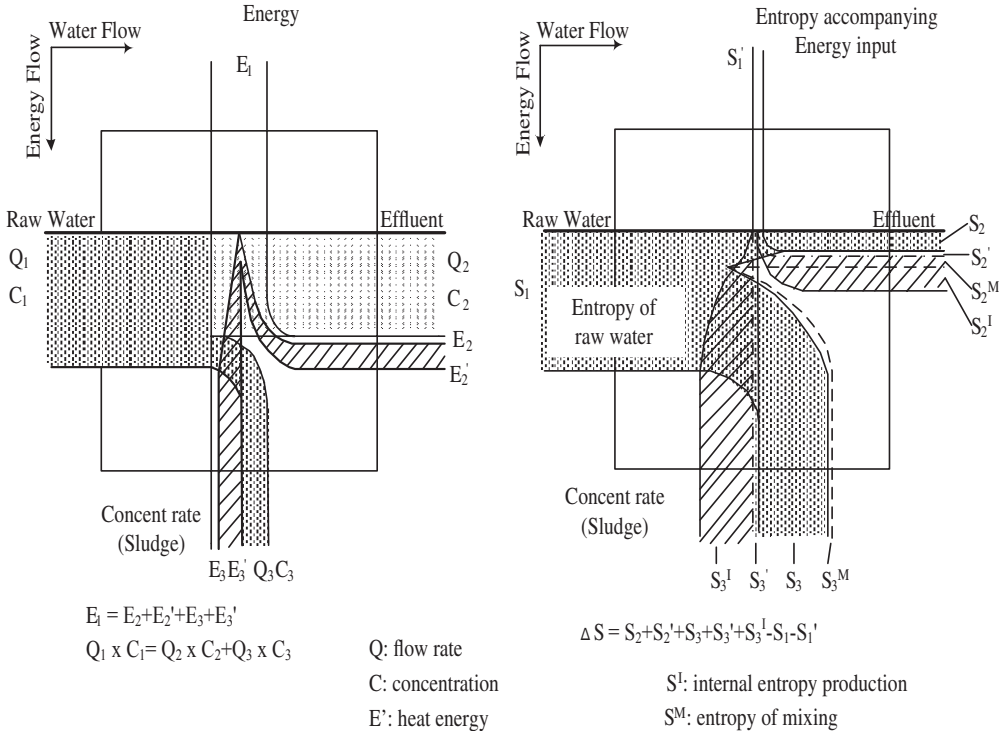

Figure 17-3 *Flow of matter and energy, and the change in entropy. Source: Tai and Goda (1980). Reproduced with permission from S. Tai.*

In a similar manner, one can consider the entropy of water flow and energy flow. Let S denote the entropy, which consists of the entropy of mixing, S^M, and the internal entropy production, S^I. Then, S_r denotes the entropy of raw water, and the entropy associated with its heat energy is S_r^h. S_e denotes the entropy of effluent, consisting of internal entropy production, S_e^I, and entropy associated with its heat energy, S_e^h. S_s denotes the sludge entropy, consisting of the internal entropy production, S_s^I, and entropy associated with its heat energy, S_s^h. The change in entropy can be written as

$$\Delta S = S_e + S_e^I + S_e^h + S_s + S_s^I + S_s^h - S_r - S_r^h \tag{17.4}$$

Thus, there are three types of water for consideration: polluted water, treated water, and wastewater. When raw water is fed into the treatment plant, concentrate (sludge) and effluent (clean water) are produced by treatment, and heat is dissipated by the operating pressure. The mixture is made up of substances, each with a molar fraction with respect to substances N_i. Entropy per mole of ideal solution and dilute real solution (raw or polluted water) S (g cm^2/s^2 K) can be expressed (Tai and Goda 1985) as

$$S = -R\sum x_i \ln x_i + \sum x_i s_i \tag{17.5}$$

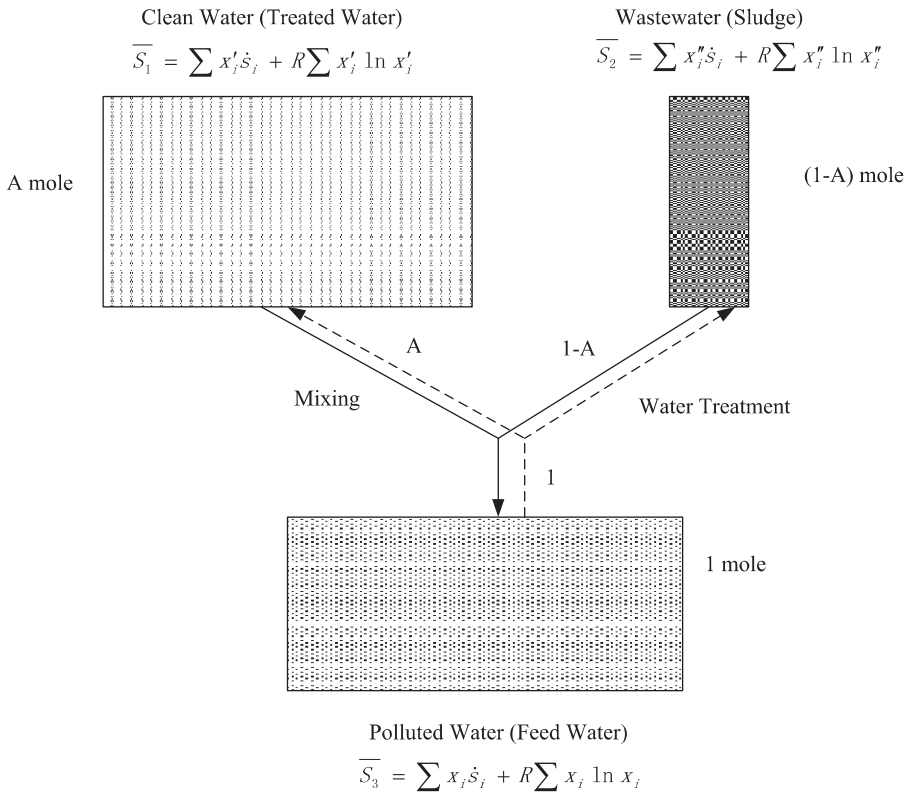

Figure 17-4 *Entropy change in mixing and water or wastewater treatment. Source: Tai and Goda (1985). Reproduced with permission from Taylor and Francis.*

where R is the gas constant (g cm^2/s^2 mol K, 8.134×10^7 g cm^2/s mol K), x_i is the mole fraction of component (substance) i, and s_i is the standard or thermodynamic entropy from the third law of entropy of component i (g cm^2/s^2 K), and K is the absolute temperature. In equation (17.5), the first term represents "entropy mixing" per mole of ideal or real solution, ΔS^M, and the second term represents "standard entropy" per mole of solution.

Entropy changes as a result of mixing. One can compute the entropy of treated water, wastewater, and polluted water, as well as compute internal entropy production. To that end, one can consider $(1 - A)$ moles of wastewater (sludge) mixed with A moles of clean water (treated water), as shown in Fig. 17-4. Entropy of the effluent (clean) water per mole S_e can be expressed as

$$S_e = -R\sum x_i^{Me} \ln x_i^{Me} + \sum x_i^{Me} s_i^e \tag{17.6}$$

where x_i^{Me} is the mole fraction of component i of effluent (clean) water.

Entropy per mole of sludge S_s can be written as

$$S_s = -R\sum x_i^{Ms} \ln x_i^{Ms} + \sum x_i^{Ms} s_i^s \tag{17.7}$$

where x_i^{Ms} is the mole fraction of component i of the concentrate or sludge.

Entropy per mole of the raw (polluted) water S_r can be written as

$$S_r = -R\sum x_i^{Mr} \ln x_i^{Mr} + \sum x_i^{Mr} s_i^r \tag{17.8}$$

where x_i^{Mr} is the mole fraction of component i of the raw water.

The entropy decrease of a molar raw water in a water treatment system ΔS can be expressed as

$$\Delta \bar{S} = AS_e + (1-A)S_s - S_r \tag{17.9}$$

where A is the molar ratio of effluent flow to raw water flow.

Assuming that there is no chemical reaction, the absolute entropy term is deleted, and entropy caused by the mixing is retained. Substituting equations (17.6) to (17.8) in equation (17.9), the result is

$$\Delta \bar{S} = R\left[\sum x_i^{Mr} \ln x_i^{Mr} - A\sum x_i^{Me} \ln x_i^{Me} - (1-A)\sum x_i^{Ms} \ln x_i^{Ms}\right] \tag{17.10}$$

As an example, if one mole of feedwater is 18 cm^3, the rate of entropy decrease of feedwater in the reverse osmosis system is given as

$$\frac{\Delta S}{\Delta t} = \Delta \bar{S} \frac{Q_r}{18} \tag{17.11}$$

where Q_r is the feedwater flow rate, and $\Delta \bar{S}$ is given by equation (17.8) or (17.9).

17.3.1 Internal Entropy Production

Natural water bodies, including rivers, canals, lakes, and estuaries, as well as some artificial flow systems, such as water treatment systems, are open systems. In such systems, there occurs an exchange of material and energy between the system and its external environment or surroundings. The total change in entropy of an open system ΔS is the sum of change in entropy of the inflowing flux ΔS_e and the entropy created irreversibly in the system ΔS_I. The increase in entropy in an open system can be expressed as

$$\Delta S = \Delta S_e + \Delta S_I \tag{17.12}$$

The local entropy production per unit time and volume, σ, is related to the rate of internal entropy production within the system $\Delta S_I/\Delta t$ (cal/K, g/s^3K) by the volume integral. Thus, this relation for a system in steady state can be written as

$$\frac{\Delta S_I}{\Delta t} = \frac{1}{T}\int_V \sigma dV \tag{17.13}$$

where σ is the entropy production rate, V is the volume (cm^3), and T is the absolute temperature. The term $(\Delta S_I/\Delta t)T$ is often referred to as the dissipative function Φ:

$$\Phi = T\frac{\Delta S_I}{\Delta t} \tag{17.14}$$

The local entropy production rate σ can be expressed as a sum of flows with conjugate forces. Important conjugate fluxes and forces in nonequilibrium thermodynamics for various processes (Tai and Goda 1985) are given in Table 17-1.

If the system is mechanical by virtue of a series of analytical procedures for irreversible thermodynamic processes, then the local entropy production rate can be expressed as

$$\sigma = \frac{J_s}{T}\text{grad}(-T) + \frac{J_{ch}}{T}A + \sum\frac{J_i}{T}\text{grad}(-\mu_i) \tag{17.15}$$

where J_s is the entropy flux (vector), J_i is the flux of component i, μ_i is the chemical potential of component i, J_{ch} is the rate of chemical change per unit volume, A is the affinity of chemical reaction, and T is the temperature of the system. (Symbols are also defined in Table 17-1). Equation (17.13) can now be expressed as

$$\frac{dS_I}{dt} = \int_V \frac{1}{T}\left[J_s\text{grad}(-T) + J_{ch}A + \sum J_i\text{grad}(-\mu_i)\right]dV \tag{17.16}$$

Equation (17.16) expresses the local entropy production rate as a sum of products of fluxes and their conjugate forces.

Table 17-1 *Conjugate fluxes and forces in nonequilibrium thermodynamics.*

Processes	Flux	Conjugate force	Power
Chemical reaction	Reaction rate per unit volume, $\boldsymbol{J_{ch}}$	Chemical affinity, $\boldsymbol{A}$	$\boldsymbol{J_{ch}} \times \boldsymbol{A}$
Flow of electric current	Electric current, $\boldsymbol{I}$	Electrical potential, $\boldsymbol{E}$	$\boldsymbol{I} \times \boldsymbol{E}$
Diffusive flow of nonelectrolytes	Flux of nonelectrolytes, $\boldsymbol{J_i}$	Chemical potential gradient, grad $(-\mu_i)$	$\boldsymbol{J_i} \times \text{grad}(-\mu_i)$
Diffusive flow of electrolytes	Flux of electrolytes, $\boldsymbol{J_i}$	Electrochemical potential gradient, grad $(-\overline{\mu_i})$	$J_i grad\left(-\overline{\mu_i}\right)$
Volumetric flow	Volumetric flow, $\boldsymbol{J_v}$	Hydrostatic pressure difference, $\Delta \boldsymbol{P}$	$\boldsymbol{J_v}\Delta \boldsymbol{P}$
Thermal flow	Flux of entropy, $\boldsymbol{J_s}$	Temperature gradient, grad$(-\boldsymbol{T})$	$J_s\text{grad}(-\boldsymbol{T})$

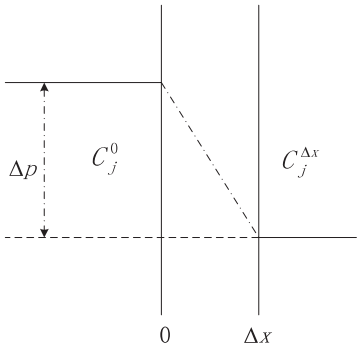

Figure 17-5 *Illustration of a membrane of thickness* Δx.

17.3.2 Evaluation of Reverse Osmosis

Reverse osmosis (RO) is a water treatment process and has been used for treatment of sewage effluents and desalination of seawater. At the National Institute of Environmental Studies in Japan, wastewater from its laboratory is treated by reverse osmosis after treatment by precipitation with alum, sand, filtration, and activated carbon adsorption for reuse as cooling water and boiled feedwater transport across a reverse osmosis membrane as shown in Fig. 17-5. The system is comprised of two compartments separated by a membrane of thickness ΔX. The compartments may contain different concentrations as well as components to which the membrane is impermeable, which causes a difference in osmotic pressure across the membrane. Pressures on the left side of the membrane are different from those on the right side, but a constant pressure difference is maintained in the system.

Let it be assumed that the system is isothermal, i.e., grad$(-T) = 0$, and that no chemical reaction takes place between them, i.e., $J_{ch} = 0$. Equation (17.16) simplifies to each chemical constituent:

$$\frac{dS_I}{dt} = \frac{1}{T}\int_V \sum J_i \text{grad}(-\mu_i) dV \tag{17.17}$$

The flows are constant in a stationary state, and, hence, equation (17.17) can be integrated across the membrane from surface 0 to ΔX and can be used to determine the rate of increase in entropy production per unit area of the membrane as a whole:

$$\begin{aligned} \frac{dS_I}{dt} &= \frac{1}{T}\int_0^{\Delta X} \left[\sum J_i \text{grad}(-\mu_i)\right] dX \\ &= \frac{1}{T}\sum J_i(\mu_i^0 - \mu_i^{\Delta x}) = \frac{1}{T}\sum J_i \Delta\mu_i \end{aligned} \tag{17.18}$$

During integration, the unknown chemical potential gradient in the membrane, grad($-\mu_i$), has been replaced by the known chemical potential difference $\Delta\mu_i$.

The rate of internal entropy production for the transport of a binary solution of nonelectrolytes across the simple membrane can be expressed as

$$\frac{dS_I}{dt} = \frac{1}{T}(J_s \Delta\mu_s + J_w \Delta\mu_w) \tag{17.19}$$

where subscripts s and w correspond to the solute and water, respectively. The chemical potentials μ_s and μ_w can be expressed as

$$\Delta\mu_w = V_w(\Delta P - P_{os}) \tag{17.20}$$

$$\Delta\mu_s = V_s\left(\Delta P + \frac{P_{os}}{\overline{C_s}}\right) \tag{17.21}$$

where V_w is the partial molar volume of water, V_s is the partial molar volume of the solute, ΔP is the difference in operating pressure across the membrane, ΔP_{os} is the original osmotic pressure, and $\overline{C_s}$ is the average concentration of solute.

Inserting equations (17.20) and (17.21) in equation (17.19), one obtains

$$\frac{dS_I}{dt} = \frac{1}{T}\left[(J_w V_w + J_s V_s)\Delta P + \left(\frac{J_s}{\overline{C_s}} - J_w V_w\right)P_{os}\right] \tag{17.22}$$

The first term within parentheses on the right side represents the total volume flux J_v across the membrane:

$$J_v = J_w V_w + J_s V_s \tag{17.23}$$

Substituting equation (17.23) in equation (17.22), one obtains

$$\frac{dS_I}{dt} = \frac{1}{T}\left[J_v(\Delta P - P_{os}) + J_s \frac{P_{os}}{\overline{C_s}}(1 + \overline{C_s} V_s)\right] \tag{17.24}$$

An order of magnitude analysis shows that $\overline{C_w} V_w >> \overline{C_s} V_s$ and $\overline{C_w} V_w \cong 1$. Equation (17.24) then simplifies to

$$\frac{dS_I}{dt} = \frac{1}{T}\left[J_v(\Delta P - P_{os}) + J_s \frac{P_{os}}{\overline{C_s}}\right] \tag{17.25}$$

For ideal solutions with small concentration differences, $\overline{C_s}$ can be taken as the numerical average of the concentrations of each side of the membrane:

$$\overline{C_s} = \frac{C_s^0 + C_s^{\Delta X}}{2} \tag{17.26}$$

The osmotic pressure across the membrane, P_{os}, can be written following van't Hoff's law for the osmotic pressure of dilute solutions as

$$P_{os} = RT(C_s^0 - C_s^{\Delta X}) \tag{17.27}$$

Substituting equations (17.26) and (17.27) in equation (17.25), the result is

$$\frac{dS_I}{dt} = \frac{1}{T}\left[J_v \Delta P - RTJ_v(C_s^0 - C_s^{\Delta X}) + 2RTJ_s \frac{C_s^0 - C_s^{\Delta X}}{C_s^0 + C_s^{\Delta x}} \right] \tag{17.28}$$

The rate of internal entropy production during the transport of solution of a single electrolyte dissociating into two ions across the membrane can be expressed as

$$\frac{dS_I}{dt} = \frac{1}{T}\left[J_v \Delta P - RTJ_v(C_s^0 - C_s^{\Delta X}) + 2RTJ_s \frac{C_s^0 - C_s^{\Delta X}}{C_s^0 + C_s^{\Delta x}} + IE \right] \tag{17.29}$$

in which E is the electric potential difference between the reversible electrodes and I is the electric current. For the case of nonelectrolytes, $E = 0$ or $I = 0$, and equation (17.29) reduces to equation (17.28). For the transport of multielectrolyte solution across a simple membrane, the rate of internal entropy production can be expressed as

$$\frac{dS_I}{dt} = \frac{1}{T}\left[J_v \Delta P - RTJ_v \sum (C_s^0 - C_s^{\Delta X}) + 2RT \sum J_s \frac{C_s^0 - C_s^{\Delta X}}{C_s^0 + C_s^{\Delta x}} + IE \right] \tag{17.30}$$

Referring to the flow diagram of a reverse osmosis system in Fig. 17-6, the points of measurements for the actual RO system are the entrance (feed) and exit (concentrate and permeate) in each vessel. Using the symbols of the figure,

$$\Delta P = \frac{P_f + P_c}{2} - P_p \tag{17.31}$$

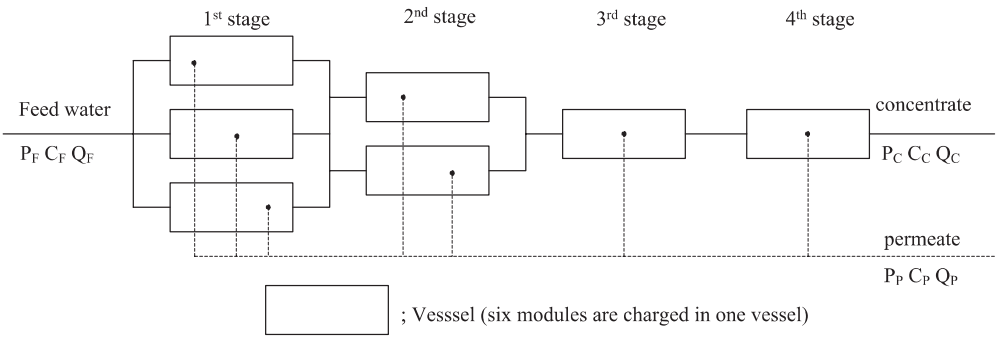

Figure 17-6 *Diagram of reverse osmosis system (spiral-wound type).*
Source: Tai and Goda (1985). Reproduced with permission from Taylor and Francis.

$$J_v = Q_p \tag{17.32}$$

$$J_i = Q_p C_{p_i} \tag{17.33}$$

$$C_i^0 = \frac{C_{fi} + C_{si}}{2} \tag{17.34}$$

$$C_i^{\Delta X} = C_{p_i} \tag{17.35}$$

where subscript f refers to the feed, C refers to the concentrate, p refers to the permeate, P_f is the hydrostatic pressure of feedwater in the RO system (g cm^{-1}s^{-2}), P_c is the hydrostatic pressure of concentrate in the RO system (g cm^{-1}s^{-2}), P_p is the hydrostatic pressure of permeate in the RO system (g cm^{-1}s^{-2}), J_v is the volume flux across a membrane (cm/s), Q_p is the flow rate of permeate in the RO system (cm/s), and J_i is the flux of component i across a membrane (g cm^{-2} s^{-1}),

$$\frac{dS_I}{dt} = \frac{1}{T}\left[\begin{aligned} &Q_p\left(\frac{P_f + P_c - 2P_p}{2}\right) - RTQ_p \sum \frac{C_{fi} + C_{ci} - 2C_{p_i}}{2} \\ &+ 2RTQ_p \sum C_{p_i} \frac{C_{fi} + C_{ci} - 2C_{p_i}}{C_{fi} + C_{ci} + 2C_{p_i}} \end{aligned}\right] \tag{17.36}$$

or

$$\begin{aligned} \Phi = {} & Q_p\left(\frac{P_f + P_c - 2P_p}{2}\right) - RTQ_p \sum \frac{C_{fi} + C_{ci} - 2C_{p_i}}{2} \\ & + 2RTQ_p \sum C_{p_i} \frac{C_{fi} + C_{ci} - 2C_{p_i}}{C_{fi} + C_{ci} + 2C_{p_i}} \end{aligned} \tag{17.37}$$

17.3.3 Thermodynamic Efficiency

Efficiency of an engineering system is generally represented by the ratio of work done to input energy. A wastewater treatment system decreases the entropy of polluted feed water. Using the reverse osmosis membrane technique separates solutes from wastewater. Fig. 17-6 shows the energy conversion in a wastewater treatment system. The input energy per unit of time $\Delta E/\Delta t$ is converted into three parts: (1) available work for removing contaminants, $-T\Delta S/\Delta t$, (2) work dissipated as unavailable work, TDS_I/dt (entropy produced within the system per unit time) or useless work, and (3) diffuse energy, $\Delta E'/\Delta t$, not converted and flowing out of the system. The input energy applied to do work can be expressed as

$$\frac{\Delta E}{\Delta t} - \frac{\Delta E'}{\Delta t} = -T\frac{\Delta S}{\Delta t} + T\frac{dS_I}{dt} \tag{17.38}$$

Efficiency of the treatment system, η, and the work done can be expressed as

$$\eta = \frac{-T\Delta S / \Delta t}{-T\Delta S / \Delta t + TdS_I / dt} \tag{17.39}$$

Example 17.1 Tai and Goda (1985) conducted an experiment on removing salts from treated wastewater by the use of the reverse osmosis facility at the National Institute for Environmental Studies at Ibaraki, Japan. They then evaluated the dissipation function and the rate of production of internal entropy for the membrane process. For each stage, entropy change, dissipation function, and internal entropy production rate are given in Table 17-2. Compute the thermodynamic efficiency for each stage in the desalination of treated wastewater by the reverse osmosis system.

Solution The thermodynamic efficiency can be computed using equation (17.39). For stage 1,

$$\eta = \frac{-(-0.932)}{51.30 - (-0.932)} \times 100 = 1.784$$

For stage 2,

$$\eta = \frac{-(-0.781)}{42.63 - (-0.781)} \times 100 = 1.80$$

For stage 3,

$$\eta = \frac{-(-1.166)}{43.63 - (-1.166)} \times 100 = 2.60$$

For stage 4,

$$\eta = \frac{-(-0.959)}{33.61 - (-0.959)} \times 100 = 2.77$$

The efficiency of removal of salts is below 3%, which is very low.

Table 17-2 *Entropy change, dissipation function, and internal entropy production rate for each stage in Example 17.1.*

Stage	$\Delta S/\Delta t$ (g/s^{3}K)	$\Phi \times 10^3$ g/s^3	dS_i/dt (g/s^{3}K)
1	–0.932	15.39	51.3
2	–0.781	12.81	42.63
3	–1.166	13.11	43.61
4	–0.959	10.11	33.61

Source: Data from Tai and Goda (1985).

Example 17.2 Using the reverse osmosis system, Tai and Goda (1985) removed salt from seawater, for which the operating conditions are given in Table 17-3. They also computed the rate of change in entropy using equation (17.10), the dissipation function using equation (17.36), and the rate of internal entropy production using equation (17.35), as shown in Table 17-4. Compute the thermodynamic efficiency.

Solution The thermodynamic entropy is computed using equation (17.38). For spiral wound, $\eta = 41.1\%$; for hollow fiber (permasep), $\eta = 40.0\%$; for hollow fiber (XFS), $\eta = 1.3\%$; and for tubular, $\eta = 44.2\%$.

Table 17-3 *Operating conditions for the reverse osmosis of salt from seawater in Example 17.2.*

Type of module	Operating condition				
	Q_f ($\times 10^{-4}$ cm/s)	Q_p ($\times 10^{-4}$ cm/s)	C_f (g/l)	C_p (g/l)	ΔP ($\times 10^7$ g/cm·s^2)
Spiral wound (ROGA-2A-TFC)	19.3	3.38	30	0.3	6.08
Hollow fiber (permasep-B-10)	2	0.33	30	0.27	5.67
Hollow fiber (XFS-416708)	1.3	0.41	30	0.3	5.67
Tubular (Nitto-NRO-A)	4.1	2.25	24	2.5	5.37

Source: Data from Tai and Goda (1985).

Table 17-4 *Rate of change in entropy, dissipation function, and rate of internal entropy production for Example 17.3.*

Type of module	Entropy change, $\Delta S/\Delta t$ (g/s^3·K)	Dissipation function Φ ($\times 10^3$ g/s^3)	Internal entropy production rate, $\Delta S_i/\Delta t$ (g/s^3·K)
Spiral wound (ROGA-2A-TFC)	–28.5	12.2	40.8
Hollow fiber (permasep-B-10)	–2.4	1.1	3.6
Hollow fiber (XFS-416708)	–0.7	1.3	4.4
Tubular (Nitto-NRO-A)	7.3	7.3	24.4

17.4 Relation to Shannon Entropy

The entropy of mixing per molar solution for ideal solution and dilute solution is

$$\Delta S^M = -R\sum x_i \ln x_i \tag{17.40}$$

Introducing equation (17.9) in equation (17.40), one obtains the decrease of entropy of raw water:

$$\Delta S = A\Delta S_e^M + (1-A)\Delta S_s^M - \Delta S_r^M \tag{17.41}$$

where ΔS_e^M is the entropy of mixing per mole of effluent, ΔS_s^M is the entropy of mixing per mole of concentrate, and ΔS_r^M is the entropy of mixing per mole of raw water.

Here is the Shannon discrete entropy:

$$H = -\sum p_i \ln p_i \tag{17.42}$$

Comparing equation (17.42) with equation (17.40), one gets

$$\Delta S^M = RH \tag{17.43}$$

In a similar manner,

$$\Delta S = R\Delta H \tag{17.44}$$

where ΔH represents the change in entropy of discrete information in raw water and can be determined by the use of conditional entropy of discrete information. The entropy of mixing per ideal solutions can be computed by multiplying the entropy of discrete information by the gas constant. Similarly, the change in entropy when separating solutes from solution can be computed by multiplying the change in entropy of discrete information by the gas constant. Information can be equated to the decrease of entropy.

17.5 Environmental Performance of Waste Treatment Systems

Waste treatment yields a variety of products, organic and inorganic. Emissions of these products into the environment, including the atmosphere, the hydrosphere, the pedosphere (land), and the lithosphere, does not follow uniform standards throughout the world. In countries with high standards of waste management, the emissions are limited by stringent environmental protection regulations. The products or resources have both pollution (toxic) and resource

(recyclable) potential. Some of the products can be used for recycling or landfilling. It may be desired to analyze the partitioning of substances during waste treatment.

There are many treatment systems available—for example, thermal and mechanical, and their application may depend on the type of waste. A treatment system may be a simple process or a combination of processes. If the goals of a waste treatment system are environmental protection and resource conservation, then the question arises, Which treatment best satisfies these goals? Total emissions and residues of the treatment system must be minimized or optimized.

In general, gaseous and aqueous emissions from waste management should contain low concentrations of metals. As these cannot be destroyed, they must be transferred into solid outputs of waste treatment systems. There is, of course, considerable uncertainty as to the fate and the leaching potential of metals in residues over a long period of time. The optimal waste treatment system generates one or more residues with high or low concentrations of metals that can be used as a resource. The efficiency of transfer of a metal contained in a waste to a high percentage into a single output is called the substance-weighted concentrating efficiency (SCE).

The evaluation of a waste treatment system (WTS) depends on the concentrations in the outputs. For simplicity, ranges of mean concentrations of single outputs can be used for evaluating different systems using SCE. The Shannon entropy provides a measure of SCE. Let there be n number of substances to be considered and k number of n outputs of a WTS. Then the concentration of a substance j in a system output i is denoted as C_{ij}. One can write

$$C_j = \sum_{i=1}^{k} C_{ij}, \quad j = 1, 2, \ldots, n \tag{17.45}$$

Interpreting C_{ij}/C_j as a measure of probability of substance j to get into output i, that is, substance j is being fractionated into k outputs, the Shannon entropy H as a measure of SCE can be expressed as

$$H(C_{ij}) = -\sum_{i=1}^{k} \frac{C_{ij}}{C_j} \log_2 \left(\frac{C_{ij}}{C_j} \right) = \log_2 C_j - \sum_{i=1}^{k} C_{ij} \log_2 C_{ij} \tag{17.46}$$

It can be shown that $H(C_{ij})$ is indirectly a function of mass balance and transfer coefficients of substances into the WTS residues but is not a function of input concentrations of these substances.

If $C_{ij} = C_j$ for any i, then $H(C_{ij}) = 0$. This statement means that substance j is transferred into one single output fraction. Clearly, this case, although highly likely to be reality, corresponds to the optimum scenario for a WTS, because the concentration cannot be zero in any output. Conversely, if $C_{ij} = C_j/k$, $i = 1, 2, \ldots, k$, then

$$H(C_{ij}) = \log_2 k \tag{17.47}$$

This equation states that substance j is equally fractionated among k outputs, or that all outputs have the same concentration, and it corresponds to the worst-case scenario. The implication is that WTS only dilutes the input during substance transport and that no increase or decrease of concentration occurs.

The relative entropy $H_{\text{rel}}(C_{ij})$, which is dimensionless and ranges between 0 and 1, can be defined as

$$H_{\text{rel}}(C_{ij}) = \frac{H(C_{ij})}{H(C_{ij})_{\max}} = \frac{H(C_{ij})}{\log_2 k} \tag{17.48}$$

$H(C_{ij})$ can be used to assess the range of concentration of any metal in different residues. A question arises: What happens if a system has more than two solid outputs? Then the mean concentration of an output must be weighted with the frequency of occurrence of concentration (corresponding to the mass flow of the output). Let m_i denote the frequency (mass) of output i ($m_i \geq 1$), $i = 1, 2, \ldots, k$, such that

$$m = \sum_{i=1}^{k} m_i \tag{17.49}$$

Then,

$$C_j = \sum_{i=1}^{k} m_i C_{ij} \tag{17.50}$$

The Shannon entropy can be expressed as

$$H_m(C_{ij}, m_i) = \log_2 C_j - \frac{1}{C_j} \sum_{i=1}^{k} m_i C_{ij} \tag{17.51}$$

and

$$H_m(C_{ij}, m_i)_{\max} = \log_2(m) \tag{17.52}$$

The mass-weighted relative entropy can be expressed as

$$H_{m\text{rel}}(C_{ij}, m_i) = \frac{H_m(C_{ij}, m_i)}{H_m(C_{ij}, m_i)_{\max}} = \frac{H_m(C_{ij}, m_i)}{\log_2 m} \tag{17.53}$$

The SCE of a WTS for a substance j can be expressed as

$$\text{SCE}_j = H_{m\text{rel}}(C_{ij}) \tag{17.54}$$

The value of SCE_j ranges between 0 and 1; the optimum is 0.

For comparing SCE_j for different substances, the substance-specific SCE_j must be weighted. Let $H_{\text{rel}}(C_{ij})_{\text{ref}}$ be the relative entropy of substance j for its natural occurrence, which can be interpreted as a measure for a fictitious natural partitioning of substance (e.g., concentration of one mass unit of Earth's crust

and concentration of one mass unit (ore). The substance-weighted $SCE_{j,w}$ for substance j can be written, with g_j as weighting between 0 and 1 for n metals, as

$$SCE_{j,w} = g_j SCE_j \tag{17.55}$$

where

$$g_j = \frac{H_{rel}(C_{ik})_{ref\,min}}{H_{rel}(C_{ij})_{ref}} \tag{17.56}$$

The total substance-weighted concentrating efficiency (TSCE) for n substances can be expressed as

$$TSCE = \frac{\sum_{j=1}^{n} g_j SCE_j}{\sum_{j=1}^{n} g_j} = \frac{\sum_{j=1}^{n} SCE_{j,w}}{\sum_{j=1}^{n} g_j} \tag{17.57}$$

The value of TSCE ranges between 0 and 1; the optimum is 0.

Questions

Q17.1 Collect monthly data on the phytoplankton of a lake for a number of years and then compute DI. Plot the DI as a function of time, and discuss if entropy increases or decreases and why.

Q17.2 Collect monthly data on the phytoplankton and COD of several lakes for several years. Then plot the variation of DI with COD for these lakes and comment on the plot.

Q17.3 Consider a reverse osmosis (RO) system composed of, say, four stages that is used for treatment of wastewater that can then be reused. Obtain data on the operating condition and analyze the feed, permeate, and concentrate in the RO system. Then compute the rate of entropy decrease of the feedwater and the rate of internal entropy production for each stage.

Q17.4 Assume the same system as in Q17.3 for treatment of seawater or saltwater. Using similar data as in Q17.3, compute the rate of entropy decrease of the feedwater and the rate of internal entropy production for each stage.

Q17.5 Compute the ratio of the rate of internal entropy production of the feedwater to the rate of entropy decrease for each stage and discuss the result. If the difference in concentrations of the seawater and wastewater are neglected, then for what kind of water is the RO system more effective?

Q17.6 Compute the efficiency of the RO system based on the results in Q17.3 and Q17.4. The efficiency may depend on the membrane configuration.

References

Hill, M. O. (1973). "Diversity and evenness: A unifying notation and its consequences." *Ecology*, 54, 427–432.

Lande, R. (1996). "Statistics and partitioning of species diversity, and similarity among multiple communities." *Oikos*, 76, 5–13.

Lande, R., DeVries, P. J., and Wallis, T. R. (2000). "When species accumulation curves intersect: Implications for ranking diversity using small samples." *Oikos*, 89, 601–605.

May, R. M. (1975). "Patterns of species abundance and diversity." In *Ecology and evolution of communities*, M. L. Cody and J. M. Diamond, eds., Harvard University Press, Cambridge, MA, 81–200.

Pielou, E. C. (1966). "Shannon's formula as a measure of specific diversity: Its use and misuse." *Am. Nature*, 100, 463–465.

Routledge, R. D. (1979). "Diversity indices: Which ones are admissible?" *J. Theoret. Biol.*, 76, 503–515.

Simpson, E. H. (1949). "Measurement of species diversity." *Nature*, 163, 688.

Tai, S., and Goda, T. (1980). "Water quality assessment using the theory of entropy." Chapter 21 in *River pollution control*, M. J. Stiff, ed., Ellis Horwood, Chichester, UK.

Tai, S., and Goda, T. (1985). "Entropy analysis of water and wastewater treatment processes." *Int. J. Environ. Studies*, 25, 13–21.

Spellerberg, I. F., and Fedor, P. J. (2003). "A tribute to Claude Shannon (1916–2001) and a plea for more rigorous use of species richness, species diversity and the 'Shannon–Weiner' index." *Global Ecol. Biogeogr.*, 12, 177–179.

Additional Reading

Brown, J. H., Gupta, V. K., Li, B., Milne, B. T., Restrepo, C., West, G. B. (2002). "The fractal nature of nature: Power laws, ecological complexity and biodiversity." *Philos. Trans., Royal Society, Series B*, 357, 619–626.

Denisov, S. (1997). "Fractal binary sequences: Tsallis thermodynamics and the Zipf law." *Phys. Lett., A*, 235, 447–451.

Goda, T., Tai, S., and Matsushige, K. (1987). "Physico-chemical significances of TOD, TOC and COD." *Scie. Rev. Setsunan University, Series A*, 6, 41–53.

Goda, T., Tai, S., and Yamane, A. T. (1981). "Evaluation of thermodynamic efficiency of reverse osmosis process using entropy." *Water Res.*, 15, 1305–1311.

Harte, J., Kinzig, A .P., and Green, J. (1999). "Self-similarity in the distribution and abundance of species." *Science*, 284, 334–336.

Japan Water Reuse Promotion Centre (1976, 1977). "Desalination technique of sea water for reduction of energy." *Jpn. Water Reuse Promotion Centre,* Technical Reports, Tokyo.

McGill, B. J. (2003). "A test of the unified neutral theory of biodiversity." *Nature*, 422, 881–885.

Mouillot, D., and Lepretre, A. (1999). "A comparison of species diversity estimators." *Res. Popul. Ecolog.*, 41, 203–215.

Tai, S. (1979). "Evaluation and control of water quality using entropy theory." Ph.D. dissertation, Kyoto University, Kyoto, Japan.

Volkov, I., Banavar, J. R., Hubbell, S. P., and Maritan, A. (2003). "Neutral theory and relative species abundance in ecology." *Nature*, 424, 1035–1037.

Whittaker, R. H. (1972). "Evolution and measurement of species diversity." *Taxon*, 21, 213–251.

Index

Page numbers followed by *e*, *f*, and *t* indicate equations, figures, and tables, respectively.

About the Author

Vijay P. Singh, Ph.D., D.Sc., P.E., P.H., Hon. D.WRE, is a University Distinguished Professor and holds the Caroline and William N. Lehrer Distinguished Chair in Water Engineering at Texas A & M University. He currently serves as editor-in-chief of *Water Science and Engineering* and *Journal of Ground Water Research* and as associate editor of more than 20 other journals. He also serves as editor-in-chief of Springer's Water Science and Technology Library Book Series. He has won more than 65 national and international awards, including three honorary doctorates, for his technical contributions and professional service. Professor Singh has been president and senior vice-president of the American Institute of Hydrology and a member of numerous committees of ASCE, AWRA, AGU, and ICID. He is widely published in the areas of hydrology, groundwater, hydraulics, irrigation engineering, environmental engineering, and water resources, as well as stochastic and mathematical modeling.